Australian Government
Geoscience Australia

Report 2 of 5
Final Report
July 2012

BROKEN HILL MANAGED AQUIFER RECHARGE (BHMAR) PROJECT

Securing Broken Hill's Water Supply: Assessment of Conjunctive Water Supply Options Involving Managed Aquifer Recharge and/or Groundwater Extraction at Menindee Lakes

Geological and Hydrogeological Framework and Conceptual Model

Record
2012/12

GeoCat #
73820

Lawrie, K.C., Brodie R.S., Tan, K.P., Gibson, D., Magee, J., Clarke, J.D.A., Halas, L., Gow, L., Somerville, P., Apps, H.E., Smith, M, Christensen, N.B., Abraham, J., Hostetler, S. & Brodie, R.C.

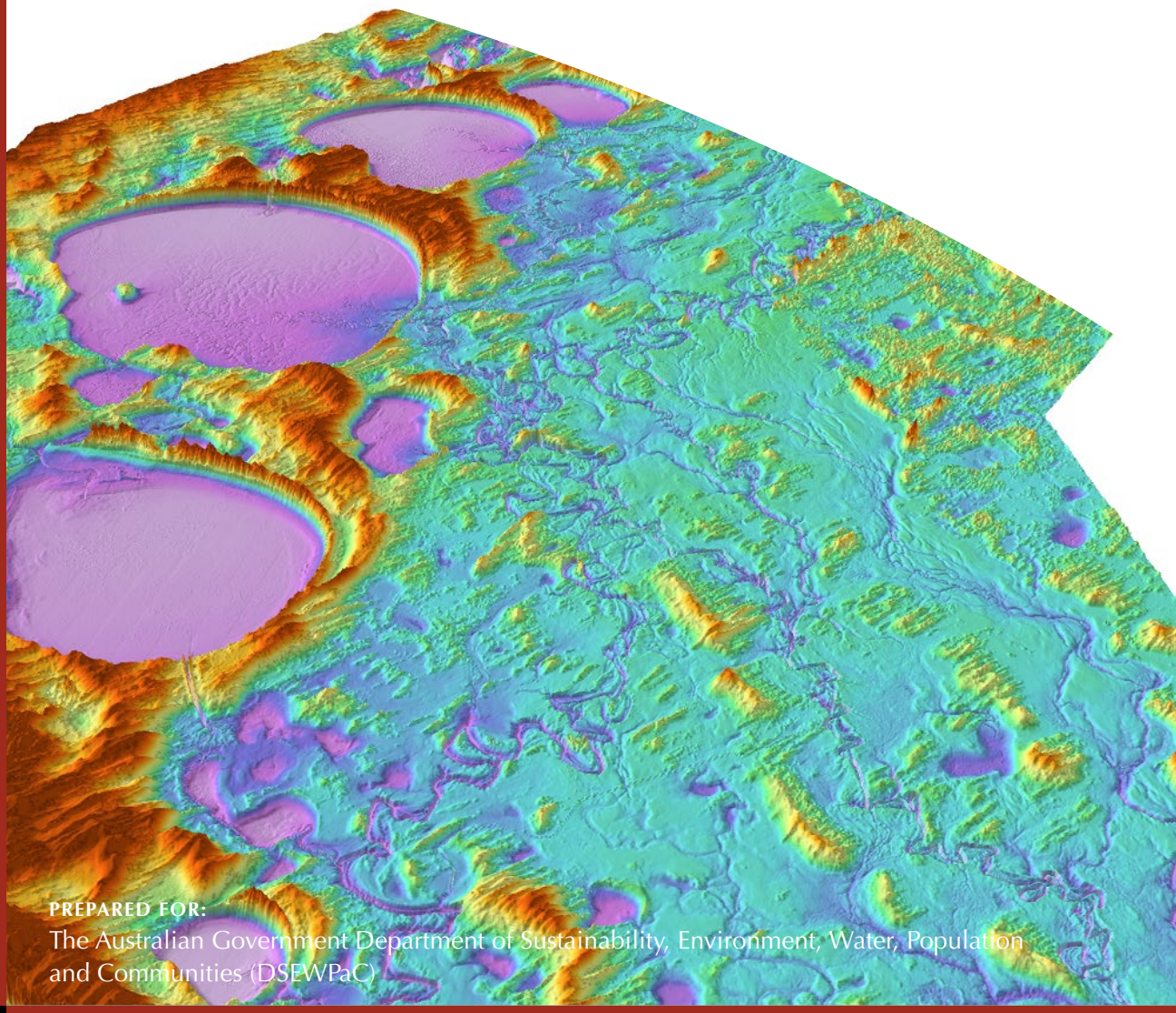

PREPARED FOR:
The Australian Government Department of Sustainability, Environment, Water, Population and Communities (DSEWPaC)

Broken Hill Managed Aquifer Recharge (BHMAR) Project

Geological and Hydrogeological Framework and Conceptual Model

GEOSCIENCE AUSTRALIA RECORD 2012/12

by

Lawrie, K.C.[1], Brodie, R.S.[1], Tan, K.P. [1], Gibson, D.[1], Magee, J.[1], Clarke, J.D.A.[1], Halas, L.[1], Gow, L.[1], Somerville, P. [1], Apps, H.E. [1], Smith, M.[1], Christensen, N.B. [2], Abraham, J. [4], Hostetler, S. [3] and Brodie, R.C.[5]



Australian Government

Geoscience Australia

[1] Groundwater Group, Environmental Geoscience Division, Geoscience Australia, Canberra ACT Australia; [2] Department of Earth Sciences, Aarhus University, Aarhus, Denmark; [3] Formerly U.S. Geological Survey, Crustal Geophysics and Geochemistry Science Center, Denver, Colorado, USA. Currently XRI Geophysics, Denver, Colorado, USA; [4] FrOG Tech, Canberra ACT Australia; [5] Minerals and Geohazards Division, Geoscience Australia, Canberra ACT Australia.

Department of Industry

Minister for Industry: The Hon Ian Macfarlane MP
Parliamentary Secretary: The Hon Bob Baldwin MP
Secretary: Ms Glenys Beauchamp PSM

Geoscience Australia

Chief Executive Officer: Dr Chris Pigram

This paper is published with the permission of the CEO, Geoscience Australia



© Commonwealth of Australia (Geoscience Australia) 2012

With the exception of the Commonwealth Coat of Arms and where otherwise noted, all material in this publication is provided under a Creative Commons Attribution 3.0 Australia Licence (http://www.creativecommons.org/licenses/by/3.0/au/)

Geoscience Australia has tried to make the information in this product as accurate as possible. However, it does not guarantee that the information is totally accurate or complete. Therefore, you should not solely rely on this information when making a commercial decision.

Please note: This version of the report replaces the version released on 12th December 2013. Inconsistent labelling of stress orientations on structural diagrams have been corrected and relevant figure captions modified accordingly. Identified report formatting issues have also been resolved.

ISBN: 978-1-921954-91-7
ISSN 14482177

GeoCat #: 73820

Geoscience Australia acknowledges funding of this project by the Australian Government Department of the Environment.

Bibliographic reference: Lawrie, K.C. , Brodie, R.S. , Tan, K.P. , Gibson, D., Magee, J., Clarke, J.D.A., Halas, L., Gow, L., Somerville, P., Apps, H.E., Smith, M., Christensen, N.B., Abraham, J., Hostetler, S. and Brodie, R.C., 2012. *BHMAR Project: Geological and hydrogeological framework and conceptual model.* Geoscience Australia Record 2012/12. Geocat 73820. 687 p.

EXECUTIVE SUMMARY

PROJECT BACKGROUND

In the southern half of Australia, recent droughts and predictions of a drier future under a number of climate change scenarios have led to the search for innovative strategies to identify more secure water supplies for regional communities and industries, while also delivering environmental benefits to threatened river systems. These issues are of particular concern in the Murray-Darling Basin (the Basin), where the recent Millennium Drought (late 1990's - 2010) adversely affected many communities, industries and the environment. While subsequent heavy rains and flooding associated with La Niña cycles broke the drought in late 2010-2012, there is general acknowledgement that longer-term strategic solutions are needed to protect communities against future droughts and to achieve a healthier working Basin.

It has long been recognised that one of the areas with the greatest potential to contribute water savings in the Basin is at the Menindee Lakes Storages (MLS), located on the lower section of the Darling River in far western New South Wales. The MLS provide the main (up to 2,050 GL) water supply storage in the lower Murray-Darling River system, and play a significant role in meeting South Australia's water requirements. The MLS are also the principal water supply storage for the City of Broken Hill, which is supplied via a 110 km pipeline. The shallow nature of the Lakes, which are located in a hot, windy, semi-arid environment, results in the evaporation of a significant amount of water.

Changing the management of the MLS to provide enhanced water security for Broken Hill and reduce these evaporative losses is possible, but Broken Hill's water supply would first need to become less reliant on the MLS. To address these issues, in 2008 the Australian Government confirmed its 2007 election policy commitment to invest up to $400 million to reduce evaporation and improve water efficiency at the MLS, secure Broken Hill's water supply, protect the local environment and heritage, and return up to 200 GL to the Basin. As part of a broader suite of scientific and technical investigations, the Broken Hill Managed Aquifer Recharge (BHMAR) project was tasked with assessing the viability of Managed Aquifer Recharge (MAR) and/or groundwater extraction options to provide improved drought security for Broken Hill. An initial scoping study assessed options within a 150 km radius of Broken Hill, while Phase 1 of the BHMAR project narrowed the search to an area of the Darling Floodplain near Menindee. Based on the findings of these scoping studies, the BHMAR project was subsequently tasked with identifying and assessing:

- Alternative groundwater-related water supply options for Broken Hill that could provide enhanced drought security for periods up to 3 years (~30 GL), within 20 km of existing water and energy infrastructure at Menindee.
- Potential MAR opportunities and groundwater resources that could provide enhanced drought security and promote regional development for communities and industries (e.g. agriculture and mining) across a larger area (~7,500 km^2) of the Darling Floodplain.

This report documents the scientific findings from multi-disciplinary investigations that have substantially revised the geological and hydrogeological framework and evolution of the BHMAR study area. These new findings underpin a new hydrogeological conceptual model for the Darling River floodplain. Additional data and sub-contractor reports are included in fifteen accompanying appendix volumes, and in the BHMAR project GIS (Apps *et al*., 2012h). 3D models of the data are also contained in the project GIS. The data and interpretations in these final reports supersede all previous interpretations contained in earlier interim reports (Lawrie *et al*., 2008; 2009; 2010a, 2011).

The final project reports have been reviewed internally by scientific experts within Geoscience Australia (GA) and the Commonwealth Scientific and Industrial Research Organisation (CSIRO); externally reviewed by independent consultants within Australia, as well as by an expert panel from the United States Geological Survey (USGS). The project was guided by a Steering Committee with representatives from the Australian and New South Wales governments. The project is managed by the Australian Government Department of the Environment, previously the Department of Sustainability, Environment, Water, Population and Communities (SEWPaC).

KEY SCIENTIFIC FINDINGS IN THE BHMAR STUDY AREA

1. Scientific investigations in the BHMAR project have completely revised our understanding of the age, stratigraphy and depositional mode of the Darling Floodplain surficial sediments, and the hydrostratigraphy, hydrogeology, and history of geological and landscape evolution of the Cenozoic Murray Geological Basin in the project area.
    i. Details of the depositional mode, mineralogy, and characteristics of the stratigraphic units have been invaluable in guiding interpretation of the AEM data, and in characterising and evaluating the identified groundwater resources.
    ii. The revised 3D frameworks and details of internal geological and hydrogeological characteristics are also essential for the identification and assessment of MAR options. Table A summarises a revised stratigraphic column based on the BHMAR project investigations.
    iii. These revisions have important implications for understanding hydrological and hydrochemical processes, and for understanding recharge and inter-aquifer leakage leading to the localisation of groundwater resources.
    iv. This new knowledge has practical implications for assessing groundwater resources and MAR options in the BHMAR project area, and regionally.
2. Airborne electromagnetics (AEM) and remote sensing data (LiDAR and Landsat), validated by ground and borehole geophysics, and laboratory data from a drilling program, have been used to map key functional elements of the hydrological system
    i. Surface geomorphology, and the multi-layered sequence of aquitards and aquifers have been mapped at high-resolution to produce a new 3D map of the hydrostratigraphy in the top 100 m of the Lower Darling Floodplain.
    ii. The Blanchetown Clay occurs throughout most of the study area, providing an upper confining aquitard to key Pliocene aquifers (Calivil Formation and Loxton-Parilla Sands), and potential MAR(and groundwater extraction) options. Mapped ‘holes’ and fault offsets in the Blanchetown Clay provide potential recharge windows and inter-aquifer leakage pathways to the underlying target Pliocene aquifers.
    iii. The thickness, extent and salinity distribution of the Pliocene aquifers have been mapped in 3D. Multi-scale surveys combined with drilling data have revealed significant aquifer heterogeneity at regional and borefield scales. These data enabled identification of palaeochannels with favourable hydraulic properties and low salinities in the Pliocene aquifers, greatly assisting with the identification and prioritisation of groundwater resources and MAR targets.
3. There is evidence of significant Neogene-to-Present tectonics in the study area.
    i. Extensive Neogene-to-Present faulting, tilting and warping of the Lower Darling Valley sediments is evident from multiple independent lines of evidence including AEM, airborne magnetic, regional gravity, seismic reflection and borehole datasets. These faults appear to be largely formed through reactivation of basement faults mapped in the underlying Darling Geological Basin.
    ii. The Blanchetown Clay is warped and tilted at a range of scales, and is locally sharply offset by faults with up to 20 m vertical offset. Overall, the Blanchetown Clay top surface varies in elevation by 60 m across the study area. Many of the faults controlling this deformation are reactivated basement faults mapped in magnetic, gravity and seismic datasets.
    iii. Neogene faults that offset the Blanchetown Clay horizon and localise inter-aquifer leakage are more numerous than surficial Neotectonic structures.
    iv. The palaeo-stress orientations of Neogene structures interpreted from faults mapped in the AEM data suggest a similar stress field to present day conditions, but with rotation of the maximal principal stress field within two trans-tensional strike slip fault zones (the Menindee and Talyawalka Fault Systems).
    v. The shallow Coonambidgal and Menindee Formation aquifers are also largely structurally controlled with deeper deposition localised in small fault-controlled trans-tensional basins (half graben and grabens).
    vi. The target Pliocene aquifers are deposited in broad, structurally-controlled palaeovalleys.

vii. There is no evidence to suggest that Neogene-to-Present structures that control the Pliocene and younger sediments, had any influence on the palaeogeography or facies distribution of upper Renmark Group sediments.

viii. The present-day courses of Talyawalka Creek and the Darling River are largely structurally controlled, with straight-line segments and box-like drainage patterns controlled by intersecting faults mapped in LiDAR, AEM, airborne magnetic and regional gravity datasets.

a. These faults provide important recharge pathways to underlying aquifers where they intersect the river and adjacent flush zones.

b. Other evidence for neotectonics includes lake tilting (crossing shorelines); while a number of surface scarps and linear topographic highs are coincident with faults and horst blocks mapped in the underlying geology.

4. A completely new conceptual model for the Darling Floodplain hydrological system (including the Lower Darling Alluvium and Western Murray Porous Rock Groundwater Management Units) has been developed.

i. The mounding of groundwater levels near the river indicates the regional significance of losing river conditions. Groundwater chemistry and stable isotope data show that recharge is episodic and linked to high-flow flood events rather than river leakage being continuous. Critically, rapid and significant groundwater level responses were measured during flood events. Continuation of rising trends after the flood peak receded suggests that this is an actual recharge response rather than hydraulic loading, with rapid recharge facilitated by structural disruption of the aquitards.

ii. Mud veneers and mineral precipitates are evident along much of the Darling River channel bank when river flows are low. During low-flow conditions these act as impediments to river leakage. During floods, high-flow velocities scour these deposits, revealing lateral-accretion surfaces in the shallow scroll-plain sediments. This scouring allows lateral bank recharge to the shallow aquifer.

iii. Recharge to the underlying Pliocene aquifer occurs via erosional 'holes' in the confining aquitard, and in areas where vertical fault offsets enable inter-aquifer leakage through the juxtaposition of the unconfined Menindee and Coonambidgal Formation aquifers and the Pliocene aquifers. Mapped depressions in the river bed ('cod holes'), are floored by indurated clays, and do not provide preferential connectivity to the underlying aquifer.

iv. Such flow-dependent recharge has implications for groundwater assessment and management. For example, an analysis of historic river flows suggests that active recharge to the groundwater system would only occur for about 17% of the time when flow exceeds about 9,000 ML/d. Recharge would be negligible with groundwater extraction during low-flow conditions.

v. Diffuse recharge from rainfall to the Pliocene aquifers is interpreted to be insignificant, due to the combination of low average rainfall, high evaporation, minor irrigation and the presence of thick, extensive aquitards over most of the study area. This conclusion is supported by recharge estimates using the chloride mass balance approach.

5. The results of scientific investigations into MAR/groundwater options to secure Broken Hill's water supply, are reported separately (Lawrie *et al*., 2012c). This includes the science findings associated with carrying out maximal and residual risk assessments for MAR options at a priority site (Jimargil), and three other potential borefield sites. This includes more detailed descriptions of the local geology and hydrogeology.

6. The results of scientific investigations into regional MAR/groundwater options more broadly in 14 targets across the Darling Floodplain, are reported in Lawrie *et al*. (2012d). This includes a more detailed description and assessment of the geology and hydrogeology of each target.

Table A. *Stratigraphic column showing the relationships between geological units, their age, dominant lithologies and hydrogeological properties.*

Lithostratigraphy	Age	Lithology	Hydrostratigraphy	
Coonambidgal Formation (Qa)	Holocene To younger Pleistocene 0 - ?40 ka	Near-surface mud drape	Aquitard, typically unsaturated to partially saturated	
		Sandy base	Shallow unconfined aquifer near leakage, otherwise unsaturated	
Menindee Formation (Qam)	Younger Pleistocene ?50 ka - >150 ka	Muddy top	Thin aquitard, typically unsaturated	
		Sandy base	Shallow unconfined aquifer near leakage, otherwise unsaturated	
Willotia beds (Qaw)	>150 ka - ?500 ka	Mostly sand	Perched or shallow unconfined aquifer near leakage, otherwise unsaturated	
Woorinen Formation (Qdw)	Middle Pleistocene 0 - ?500 ka	Muddy top	Thin unsaturated aquitard	
		Sandy base	Shallow unsaturated sands	
Blanchetown Clay (Qpc)	Older Pleistocene ?500 ka - 2.5 Ma	Mud	Regional confining aquitard, partially to fully saturated	
Chowilla Formation (Tpcs)	?2.5-?2.6 Ma	Sand	Very localised semi-confined aquifer	
Calivil Formation (Tpc)	Pliocene 2.6 - 5.3 Ma	Local muddy top	Locally confining aquitard, typically saturated	
		Predominantly sandy with local muddy units	Regional aquifer, mostly semi-confined to confined. Unconfined marginal to leakage areas.	
Loxton-Parilla Sands (Tps)	Pliocene 2.6 - 5.3 Ma	Fine to medium sands	Regional semi-confined to confined aquifer. Unconfined marginal to leakage areas. Underlying to laterally equivalent to Calivil Formation, southern part of project area only	
Renmark Group (Ter)	Tertiary (Paleocene to Miocene)	Upper Renmark Group- Muds with sandy channels	Local semi-confined to confined aquifer	Aquitard base to overlying Calivil Formation target aquifer
		Middle Renmark Group - Mud with minor sand	Regional aquitard	
		Lower Renmark Group – Sands, silt and lignite	Confined aquifer in regional troughs	
Paleozoic (Devonian)	Paleozoic >251 Ma	Metasediments	Fractured and weathered rock aquifer	

REVISED GEOLOGICAL AND HYDROGEOLOGICAL FRAMEWORK

1. Renmark Group Sediments

   i. Regionally, the Renmark Group comprises the non-marine Paleocene to Miocene sediments of the Murray Geological Basin. Deposition of the Renmark Group in the project area is controlled by the Menindee Trough, a northeast-southwest trending Paleozoic structural basin. The basal Renmark Group sequence tends to be limited to the Menindee Trough, with the upper part of the Renmark Group occurring across the whole project area. The latter is also likely to be influenced by the underlying Menindee Trough, possibly as a sag basin.

   ii. The upper part of the Renmark Group is a widespread non-marine succession of Miocene age in the Murray Geological Basin. Unlithified and nowhere exposed, it is a poorly understood. It is inferred from drilling to be deposited on a low-relief sedimentary plain dominated by anastomosing fixed-channel streams, flowing southward into a complex low-energy coastal plain with numerous lagoons and bays. In 90% of the BHMAR holes drilled, the upper Renmark Group is represented by fine-grained muds.

   iii. The upper Renmark Group sequence mostly acts as an underlying aquitard to important aquifers in the overlying Calivil Formation succession. Hydraulic connection between the Calivil Formation and Renmark Group tends to be limited, except where Renmark Group channel sands immediately underlie the Calivil Formation. In these areas there can be a distinct salinity gradient.

2. Pliocene Aquifers (Calivil Formation and Loxton-Parilla Sands)

   i. The Pliocene aquifers are the main focus of investigations in this study. In the project area, the Pliocene aquifers predominantly comprise the fluvial Calivil Formation, with the shoreline and shallow marine Loxton-Parilla Sands restricted to the southernmost part of the area. Post-depositional warping, tilting and discrete offsets associated with tectonic activity have influenced the thickness, extent and preservation of the Pliocene aquifers. AEM mapping validated by drilling has enabled the lateral extents and thickness of the Pliocene aquifers to be identified.

   ii. Facies analysis indicates the Calivil Formation was deposited in deep braided streams across a dissected sedimentary landscape. Overall, the sequence is fining-upwards, with evidence that the rivers that deposited the Calivil Formation prograded over the Loxton-Parilla Sands. Channel fill materials comprise gravels and sands, and local fine-grained units represent abandoned channel fills and local floodplain sediments. Integration of textural and hydraulic testing data has revealed there are five hydraulic classes (coarse to very coarse sand and gravel, medium sand, fine sand, muddy sand, and mud) within the Calivil Formation. At a local scale (10s to 100s of metres), there is considerable lithological heterogeneity, however at a regional scale (km), sands and gravels are widely distributed with particularly good aquifers developed in palaeochannels and at the confluence of palaeo-river systems.

   iii. The Calivil Formation aquifer varies significantly in thickness (0-70 m) over the project area. This variability results from (1) in-filling of broad (structurally-controlled) palaeovalleys in an undulating palaeo-landscape, with relief of up to 40 m from valley bottoms to hill tops; and (2) post-depositional tectonic effects that include movement on discrete faults, as well as warping and tilting of the landscape. The effect of tectonic inversion along reactivated faults has been erosion and local thinning of the Calivil Formation sequence prior to deposition of the overlying lacustrine Blanchetown Clay. In some narrow fault zones, the Calivil Formation appears to have been completely eroded. Tectonic activity after deposition of the Blanchetown Clay has resulted in further warping, tilting and faulting of the Calivil Formation.

   iv. The lower bounding surface of the formation is marked by an erosional contact with Renmark Group sediments. There is a 10m year hiatus between deposition of the Renmark Group and the Calivil Formation. Beneath this erosional surface, the Renmark Group sediments show evidence of significant weathering, particularly where preserved on local palaeo-highs. The upper surface of the Calivil Formation is irregular, with up to 16 m of relief evident. This relief is due to the channel and bar topography in the upper Calivil Formation at the time of inundation by Lake Bungunnia (and commencement of Blanchetown Clay deposition) combined with post Calivil Formation tectonic warping and faulting.

v. The semi-confined to confined Calivil Formation aquifer is the principal target aquifer for MAR and groundwater extraction in the study area. The level of confinement of the aquifer is defined by the presence, thickness, lithology and structural integrity of the overlying Blanchetown Clay. In places, a fine-grained upper part of the Calivil Formation sequence can also act as an upper confining layer for the Calivil Formation aquifer proper. In localised areas away from the groundwater mounding associated with the modern drainage, the standing water level may locally lie beneath the upper confining aquitard, and in these areas, the Calivil Formation aquifer becomes unconfined.

vi. The Loxton-Parilla Sands were deposited as marginal marine and beach-barrier deposits during a major Miocene-Pliocene marine regression. In this study, drilling has demonstrated the presence of Loxton-Parilla sands in the south of the area, with stranded dunes also present about 30 km southeast of Lake Menindee. Drilling has also demonstrated that the Calivil Formation locally overlies the Loxton-Parilla Sands. In the south of the area, the latter form a good aquifer approximately 40 m thick.

3. Blanchetown Clay

i. This study has mapped the near-ubiquitous presence of relatively thin (~10 m) Blanchetown Clay deposited in palaeo-megalake Bungunnia throughout the project area. An integrated mapping approach has revealed variations in Blanchetown Clay aquitard extent and thickness, with a complex sub-surface distribution observed (Figure A). Variations in the elevation of the top of the Blanchetown Clay (20-80 m AHD) are attributed mainly to tectonic activity.

ii. The aquitard properties of the Blanchetown Clay are demonstrated by hydrograph responses in overlying and underlying aquifers, by wetting profiles observed in drill core, moisture data obtained from cores, nuclear magnetic resonance (NMR) and gamma logging, laboratory permeameter measurements on cores, and hydrogeochemical data. The study has also confirmed that the aquitard forms a major barrier to recharge and discharge.

iii. Recharge and inter-aquifer leakage to the underlying Pliocene aquifers is localised where the Blanchetown Clay is either absent (through erosion by the Darling River system, non-deposition, or facies change to fluvial sand), and/or where fault offsets juxtapose the Menindee and Coonambidgal Formation unconfined aquifers with the Pliocene aquifers. This has resulted in previously unrecognised resources of fresh to slightly brackish water in the underlying semi-confined aquifer. Where present, the Blanchetown Clay could form an effective confining aquitard for MAR schemes.

4. Quaternary fluvial units and geomorphology, Lower Darling Valley.

i. The Lower Darling Valley is a laterally confined valley, which widens southwards into the Murray Geological Basin from a constriction at Wilcannia

ii. The surficial Quaternary fluvial (river-deposited) sediments of the valley form a complex group of units which vary in their distribution, character and geomorphic expression through the BHMAR project area. Two new units, the Willotia beds and the Menindee Formation have been designated for the older fluvial units, while the previously defined Coonambidgal Formation is retained for the youngest unit.

iii. All three fluvial units were deposited by active meandering lateral-migration phases apparently separated by phases of incision or channel stability, as occurs at present.

iv. Over time, continued mud deposition on floodplains buried and obscured scroll-plain morphology, and soil formation and precipitation of secondary minerals such as carbonate altered the sediment character and reduced the effectiveness of the surficial aquifers.

v. The location of the active river tract has changed through time, almost certainly controlled by neotectonic structural movements.

5. Willotia beds.

i. The new term ‘Willotia beds’ is here used for a suite of river to lake sediments that are not sufficiently well known to give them full formation status. They overlie the Blanchetown Clay at higher elevations bounding the Darling Floodplain.

ii. The stratigraphy and sedimentology of the unit (from project cores and cliff exposures) is similar to other surficial fluvial units and is typically 10-20 m in thickness with basal fine to coarse sands and an upper fine-grained overbank muddy facies.

iii. The Willotia beds are virtually always overlain by aeolian sediments, and occur outside the Darling floodplain margins and underlie large areas of aeolian sediment within the floodplain.

iv. The heavily modified overbank muds form an effective vertical infiltration barrier and precipitation of secondary minerals in the lower sand probably reduces groundwater movement.

6. Menindee Formation. The newly defined Menindee Formation replaces the former use of Shepparton Formation in the Lower Darling Valley.

i. Morphologically the Menindee Formation floodplain is highly variable and ranges from upper rarely flooded floodplain with thin patches of aeolian (wind-deposited) cover to lower floodplain with channels scoured by floods. The average thickness is about 14 m with basal fine to coarse sands (6.5 m average thickness) overlain by overbank muds (7.7 m average thickness).

ii. Lateral-migration phases were active at 85 thousand years ago (ka) and >150 ka and many more phases almost certainly occurred, but have not yet been dated.

iii. The overbank mud unit is widespread and is part of the near-surface aquitard, forming an effective barrier to vertical infiltration. The basal sands represent a shallow unconfined aquifer in the river corridor.

iv. Secondary mineralisation in the sands, especially of carbonate, probably becomes better developed with age and reduces aquifer transmissivity. In particular, banks of the Darling River cut into Menindee Formation lower sands are often impregnated with secondary carbonate which is very likely to impede lateral infiltration.

7. Coonambidgal Formation

i. The Coonambidgal Formation consists of inactive scroll-plain tracts (river deposits with preserved traces of meander migration), formed by episodic lateral-migration phases that are incised into the Menindee Formation floodplain.

ii. Four cross-cutting scroll-plain phases have been dated at 2-6 ka, 17-22 ka and 25-30 ka and 45-50 ka are designated Coonambidgal Formation Phases 1-4. Stratigraphically and sedimentologically, Coonambidgal Formation sediments are essentially identical to the Menindee Formation with an average thickness of 14 m and basal fine to coarse sands (7.3 m average thickness) overlain by overbank muds (7.5 m average thickness).

iii. Morphologically, the scroll-plain meander dimensions vary, apparently due to variations in river discharge while the lateral migration phases were active. Preservation of scroll morphology becomes less distinct with increasing age.

iv. As for the Menindee Formation, the overbank mud unit is widespread and is part of the near-surface aquitard, forming an effective barrier to vertical infiltration. However, secondary mineralisation in the lower sands is much less developed than the Menindee Formation and provides minimal impediment to lateral infiltration. As the Coonambidgal Formation is the youngest Quaternary fluvial unit, it is the shallow unconfined aquifer with the closest hydraulic connection with the Darling River and its anabranch channels.

8. Tectonic Activity

i. Evidence for significant Neogene-to-Present tectonic activity is evident in AEM and LiDAR data, and validated by drilling and surface mapping. The AEM data in particular reveals that the unconsolidated alluvial sediments in the study area are significantly affected by tectonic activity, with evidence of widespread faulting, warping and regional tilting of sub-surface stratigraphy due to deformation within regional shear zones, and due to basin subsidence or margin uplift. For example, the Blanchetown Clay shows considerable modification, with up to 60 m difference in elevation largely as a result of post-depositional faulting, tilting and warping of these lacustrine deposits. Vertical fault offsets of up to 20 m are mapped at the Blanchetown Clay horizon in the AEM data (Figure A and Figure B).

ii. Faults mapped in the AEM and LiDAR datasets are coincident with faults and lineaments mapped independently in the geological basement using other geophysical datasets including

regional gravity, airborne magnetics, and seismic datasets in the basement. Major faults appear to be linked to long-lived basement faults that control the location of underlying Devonian Basins (Figure B).

iii. Reactivation of these basement faults appears to be a factor in controlling deposition of the Pliocene aquifers, the overlying Blanchetown Clay, and Pleistocene aquifers. There is evidence for tectonic inversion on several of these structures. Examples include horst structures during or post-Calivil Formation and Blanchetown Clay deposition becoming graben structures in the Pleistocene.

iv. Most faults do not appear to offset near-surface Pleistocene mud aquitards, with only a few more recent fault scarps evident in LiDAR data. However, the Talyawalka Creek and Darling River follow long-lived structural corridors. There is also evidence of recent tilting, with crossing shorelines observed at Lake Mindona, and a few up-warped areas observed to be associated with local landscape highs, suggesting relatively recent movement.

v. Vertical offsets of the upper confining aquitard (Blanchetown Clay) up to ~20 m have been mapped, although vertical displacements are generally less than 5 m. No faults were intersected during drilling, however there is substantial indirect evidence of a link between aquifer recharge and fault distribution, with inter-aquifer leakage across faulted stratigraphic offsets postulated as a principal recharge (inter-aquifer leakage) mechanism in many of the key groundwater resource targets. In particular, fast response rates (days) observed in bore hydrographs lateral to the river are taken as evidence of hydraulic connection via discrete structures, or through inter-aquifer leakage where faults have juxtaposed the Coonambidgal Formation and Menindee Formations and the Calivil Formation. Figure C is a representative cross section through the central project area showing the relationships between hydrostratigraphy, tectonic activity, and groundwater flow.

vi. Overall, tectonics appears to have played a significant role in development of the sedimentary system since the Pliocene, and strongly influence groundwater flow and recharge dynamics.

Summary of Geological and Landscape Evolution

The geomorphic/geological history for the Menindee area as determined by this project can be summarised as:

1. Complex history of pre-Palaeozoic deformation and metamorphism in Proterozoic basement rocks. Several E-W shear zones mapped in the Darling Geological Basin basement are reactivated in Neogene times (e.g. Talyawalka Fault System);
2. Formation of Palaeozoic-Mesozoic Basins (e.g. Menindee, Wentworth and Blantyre Troughs) as part of the Darling Geological Basin. Deposition of a thick (several km) sequence of clastic sediments within extensional fault-bounded basins is interrupted episodically by structural inversion along these structures (e.g. in Carboniferous). Several of these structures appear to have been reactivated in Neogene times;
3. Formation of the Murray Geological Basin, with deposition of Renmark Group clastic sediments by rivers flowing southward towards a shallow sea to the south of the BHMAR project area in the Palaeocene to Miocene;
4. Depositional hiatus in the Miocene with weathering and local erosion of the Renmark Group sediments;
5. In the south of the study area, deposition of marginal marine sands and shoreline dunes (Loxton-Parilla Sands) in shallow water at the northern margin of a marine basin. Pene-contemporaneous with this was deposition of fluvial Calivil Formation sediments by the palaeo-Darling River and its tributaries in the Pliocene. The Calivil Formation sediments locally overlie the Loxton-Parilla Sands in the study area;
6. Damming of the palaeo-Murray River and its tributaries, including the palaeo-Darling River, with Blanchetown Clay deposition in palaeo-Lake Bungunnia in the Late Pliocene to Pleistocene;

7. Pliocene regression, and the drying up of Lake Bungunnia, due to a combination of lowering of the sill of the dam that initiated the lake (McLaren *et al*., 2012) and the onset of a dryer climate;
8. Continued fluvial and local lacustrine deposition, with sediment derived from the northwest (Broken Hill area) and the north (palaeo-Darling River, which passed through a gap in basement hills at Wilcannia at the edge of the Murray Basin). These Willotia bed sediments may be also partly a time equivalent of the upper part of the Blanchetown Clay deposited further south in Lake Bungunnia;
9. Incision of a trench into the Blanchetown Clay to form the modern course of the Murray River (Murray Gorge). This trench propagated headwards up the Darling Valley by nickpoint retreat, incising the Willotia beds but generally not the Blanchetown Clay in the Menindee area;
10. Deposition of fluvial sediments of the Menindee Formation and subsequently Coonambidgal Formation within the eroded trench by the Darling River and its distributaries;
11. Concurrent with 8, 9 and 10, formation of the lake basins around Menindee, with local wave erosion and shoreline deposition; and
12. Concurrent with 8, 9 and 10, deposition and preservation of aeolian sand across much of the area, particularly where not flooded and reworked in the trunk river valley.
13. There are multiple lines of evidence to show that the area has been tectonically active in the Neogene-to-present day, as evidenced by a number of scarps, lineaments, and drainage alignments that are coincident with underlying faults. There is also evidence of neotectonics from some lake tilting in the south of the project area.

As the project area sits astride the Darling Fault Lineament, a continental-scale structural feature, it is perhaps not surprising that tectonic activity has played a major role in shaping the landscape in the project area. The Darling River Lineament itself may be a much younger structure than commonly thought.

Tectonics appears to have influenced the distribution of the major Pliocene and younger aquifers and aquitards. Although the data appear to show that tectonic activity has waned significantly since the Pleistocene, with only a few structures apparent in the modern landscape, tectonics still influence the location of the major drainage elements.

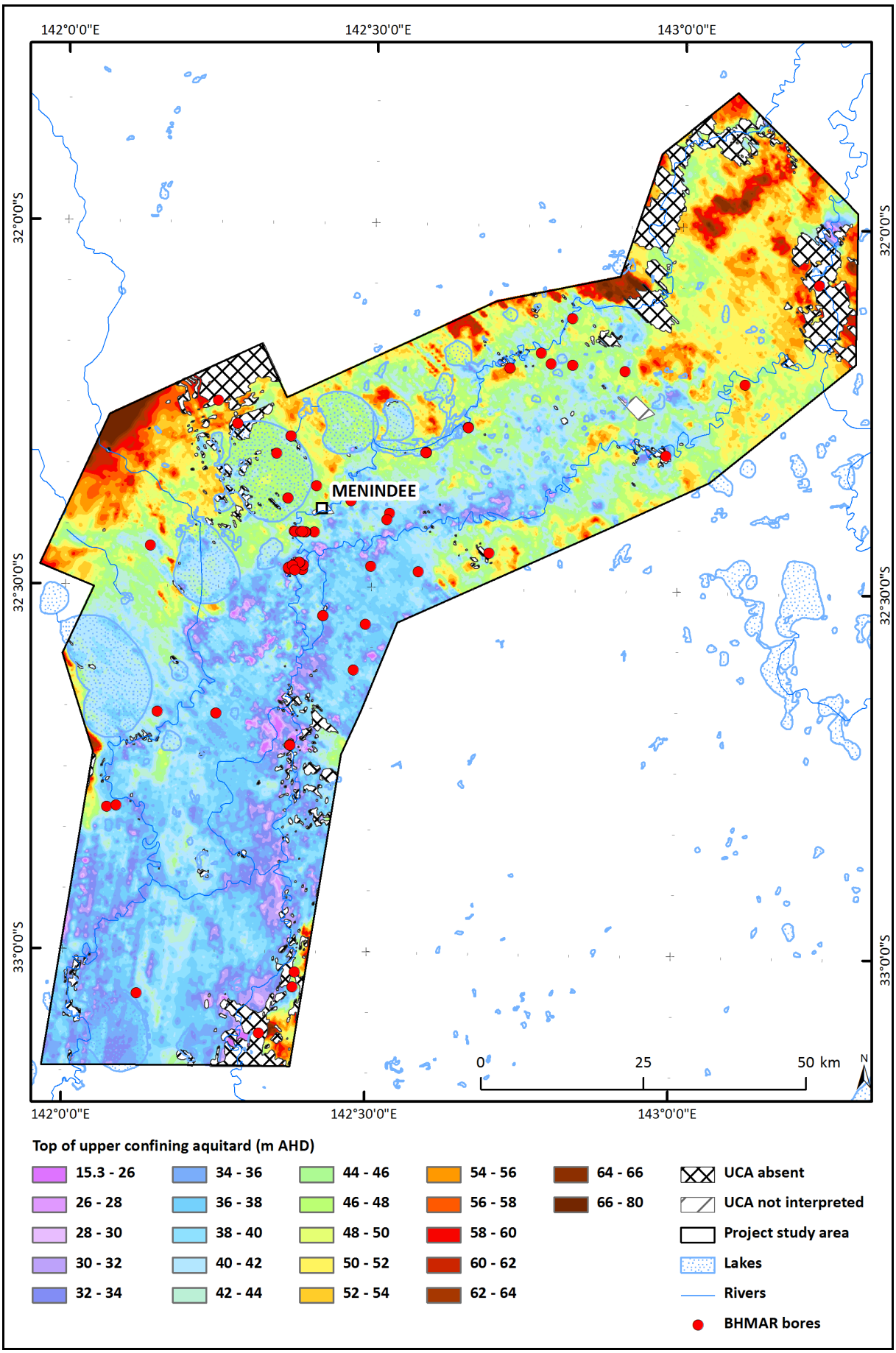

Figure A. *Top of the upper confining aquitard (predominantly Blanchetown Clay) in metres AHD. Significant elevation differences (~50 m) are apparent, with greater depths shown in purple and shallower depths in brown.*

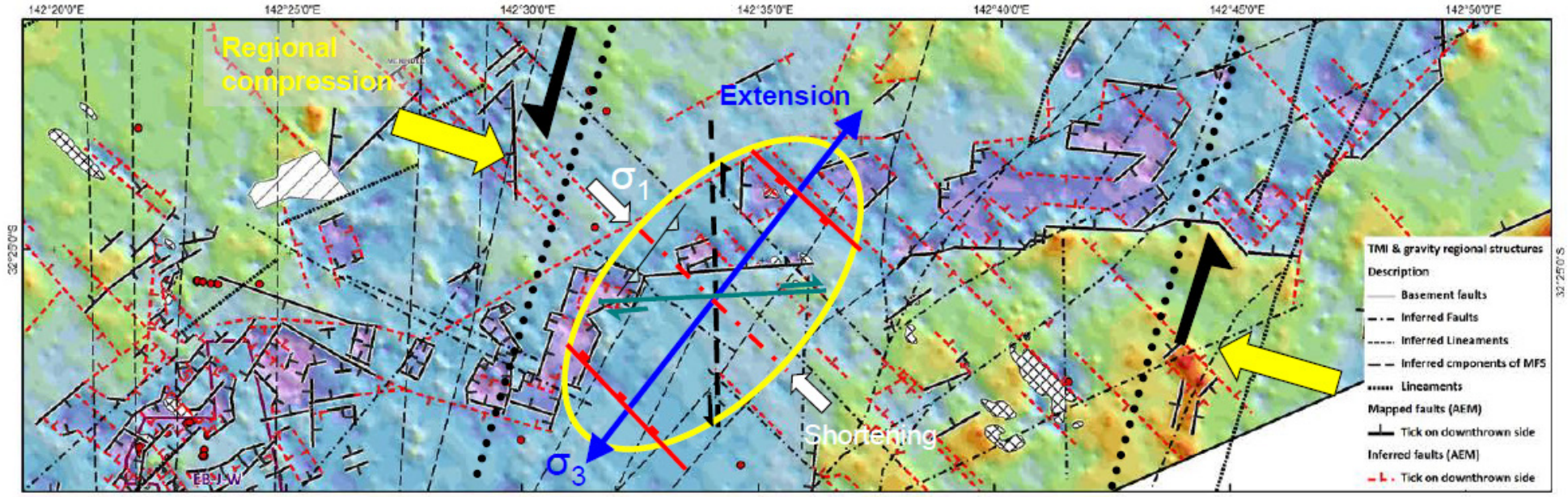

Figure B. *This image shows the depth to the top of the Blanchetown Clay aquitard in an area where the Talyawalka and Menindee Fault Systems link. The Talyawalka Fault zone is oriented approximately E-W in the centre right of each image, and has a fault trace of over 160km to the east. The purple colours are depositional lows filled with Coonambidgal Formation sands. In both images, the purple areas are delineated by faults that are mapped across several AEM flight lines (black lines), with inferred faults (parallel to flight lines), in red. Faults and lineaments identified in magnetics data are also plotted. In image b, the strain ellipse (yellow) and arrows represent the interpreted stress field under which the faults formed. N-S and NNE-SSW trending sinistral strike-slip faults form at an oblique angle in response to regional WNW-WSE shortening (yellow arrows). Within the shear zones, extension in a NE-SW orientation (blue line and arrows), is typically denoted by normal faults (red) that define grabens and half-grabens. ENE-WSW antithetic faults zones are also observed to form in this stress system, and provide important linkages between these extensional structures. Minor reverse faults (black line with pale blue-green triangles) and associated horst blocks are formed by NW-SE shortening within the shear zones. The structures mapped are consistent with models of simple shear couples within strike-slip fault systems and consistent with broader regional Neogene-and present day crustal stresses for this region of Australia. The orientation of the Talyawalka Fault System is consistent with dominant antithetic strike-slip movement in this shear zone system, with significant influence from pre-existing, underlying basement structures.*

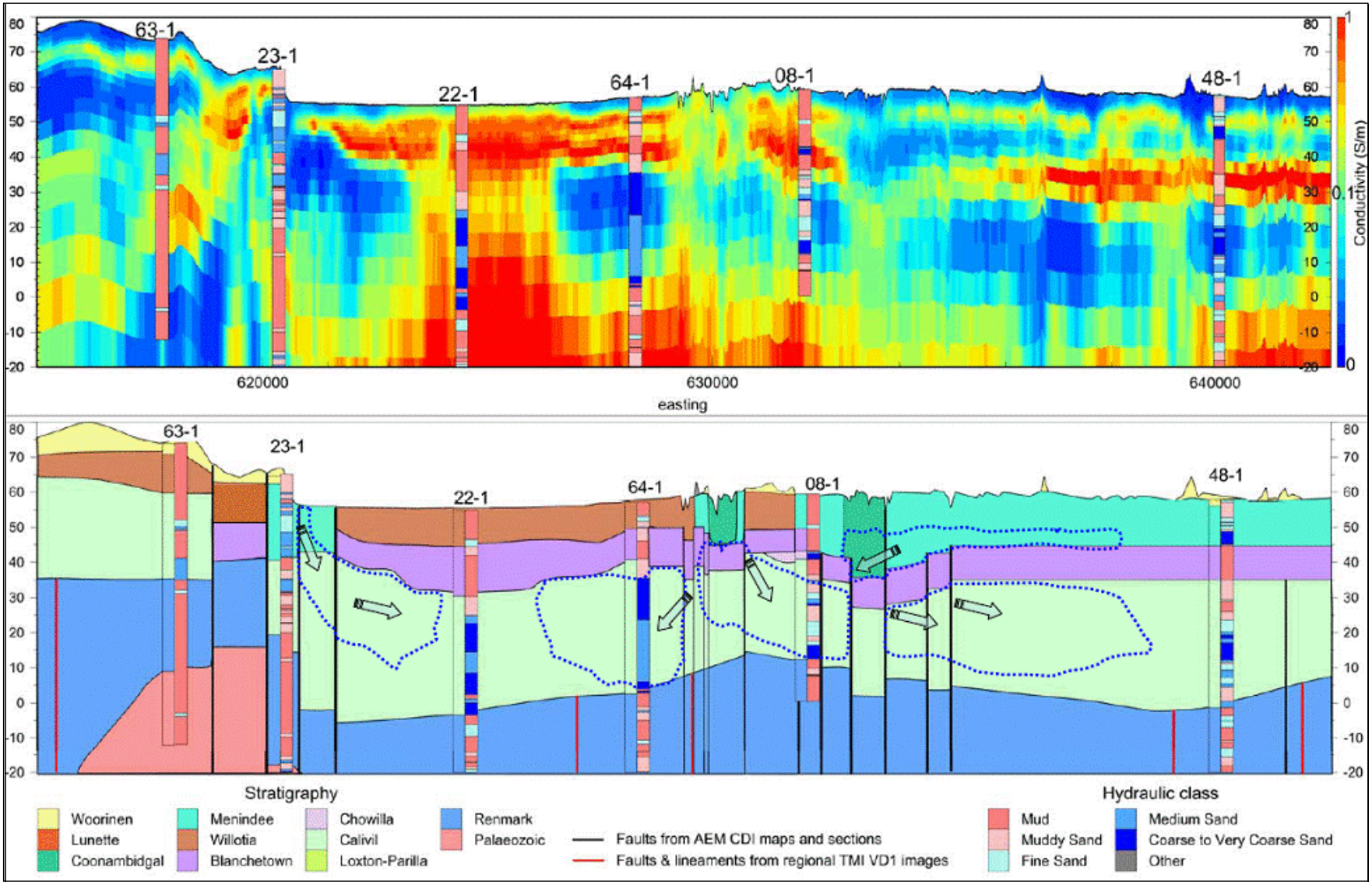

Figure C. *Geological cross-section NNW-SSE across the project area from north of Lake Menindee to Larloona Station. The top panel is an AEM conductivity depth section, with blue representing low electrical conductivity and red being high. The geological interpretation of the section is in the panel below. Boreholes are also displayed. Arrows in the lower panel denote schematic recharge pathways to fresh groundwater resources.*

NEW HYDROGEOLOGICAL CONCEPTUAL MODEL

Figure D summarises the conceptual model showing the configuration of aquifers and aquitards within the sediments of the Lower Darling Floodplain. It also shows the recharge dynamics associated with leakage from the Darling River. The importance of river (and lake) leakage in recharging the shallow unconfined aquifers and Calivil Formation target aquifer is inferred from different lines of evidence, including:

- Interpolation of groundwater salinities based on a relationship between the AEM and pore fluid chemistry showed freshening near the river and also in particular leakage sites associated with the Menindee Lakes.
- Watertable contours interpreted for the shallow aquifer show significant mounding near the Darling River and the MLS. The interpreted groundwater levels for the underlying Calivil Formation aquifer have a broadly similar pattern suggesting the influence of river leakage. The dominant hydraulic gradient near the river is downwards, reflecting greater opportunity for river leakage (rather than groundwater discharge to the river).
- The majority of shallow groundwaters have a chemistry dominated by sodium, calcium, magnesium and bicarbonate, which is similar to the Darling River samples. In contrast, local rainfall samples are more enriched in calcium and potassium, suggesting that recharge from rainfall is not as important as river (or lake) leakage. A mixing trend is evident between the surface waters and shallow groundwaters, and the more saline and evolved Calivil Formation and Renmark Group regional groundwaters.
- The stable isotopes of water (oxygen-18 and deuterium) in rainfall, river, lake and groundwater samples show that the Darling River recharges the unconfined and semi-confined near-surface aquifers. The fresh Calivil Formation groundwaters have a stable isotope signature similar to Darling River samples collected during high flows. This would support recharge into the Calivil Formation being linked to high-flow events, rather than continual river leakage. The tight clustering of the Calivil Formation stable isotope samples suggests that recharge is relatively rapid. The contrast in the isotopic signature of the fresh Calivil Formation groundwaters and that of the shallow groundwaters, suggests that recharge to the Calivil Formation occurs near-river, rather than via infiltration through the shallow aquifer in the floodplain.
- The fresh near-river shallow groundwater typically has a modern carbon signature, further supporting river leakage under current climatic conditions as being the dominant recharge process. There is a decrease in the proportion of modern carbon as the Calivil Formation groundwaters progressively become more saline and less influenced by modern recharge.
- Data from monitoring bores screened in the unconfined, Calivil Formation and upper Renmark Group aquifers show rises in groundwater levels associated with high flow events in the Darling River. Overbank flow is not necessary for such recharge to occur. The continuation of rising trends in the Calivil Formation monitoring bores after the flood peak recedes suggests that this is an actual recharge response rather than hydraulic loading. Simple Darcian vertical infiltration cannot explain the rapid response. Faulting and vertical structural offsets of formations near the river could result in pathways for such by-pass flow.

In summary, during low-flow conditions (Figure Da) there is no recharge as a mud veneer and also mineral precipitates along the river bed and banks act as an effective seal. Under no-flow conditions, the deep holes in the river bed can be windows to the watertable and act as critical drought refuges for the aquatic ecosystem.

During high-flow conditions (Figure Db), the riverbanks and bed are scoured and the mud veneer seal is removed. This allows recharge to occur predominantly by lateral bank recharge through the sandy sequences in the shallow aquifer as well as bypass flow via faulted offsets. The high river stage level facilitates lateral and downward leakage. Overbank flow is not a pre-requisite for recharge but can provide other localised recharge pathways in the floodplain. Structural features and gaps in the Blanchetown Clay confining layer provide flow paths to the Calivil Formation aquifer. During flood recession, there may be some drain-back from bank storage in the unconfined aquifers encouraging carbonate precipitation at the riverbanks. The mud veneer is also redeposited with declining river stage and flow velocities. Over time, the system returns to relatively low-flow conditions with the channel mud veneer again constraining river leakage.

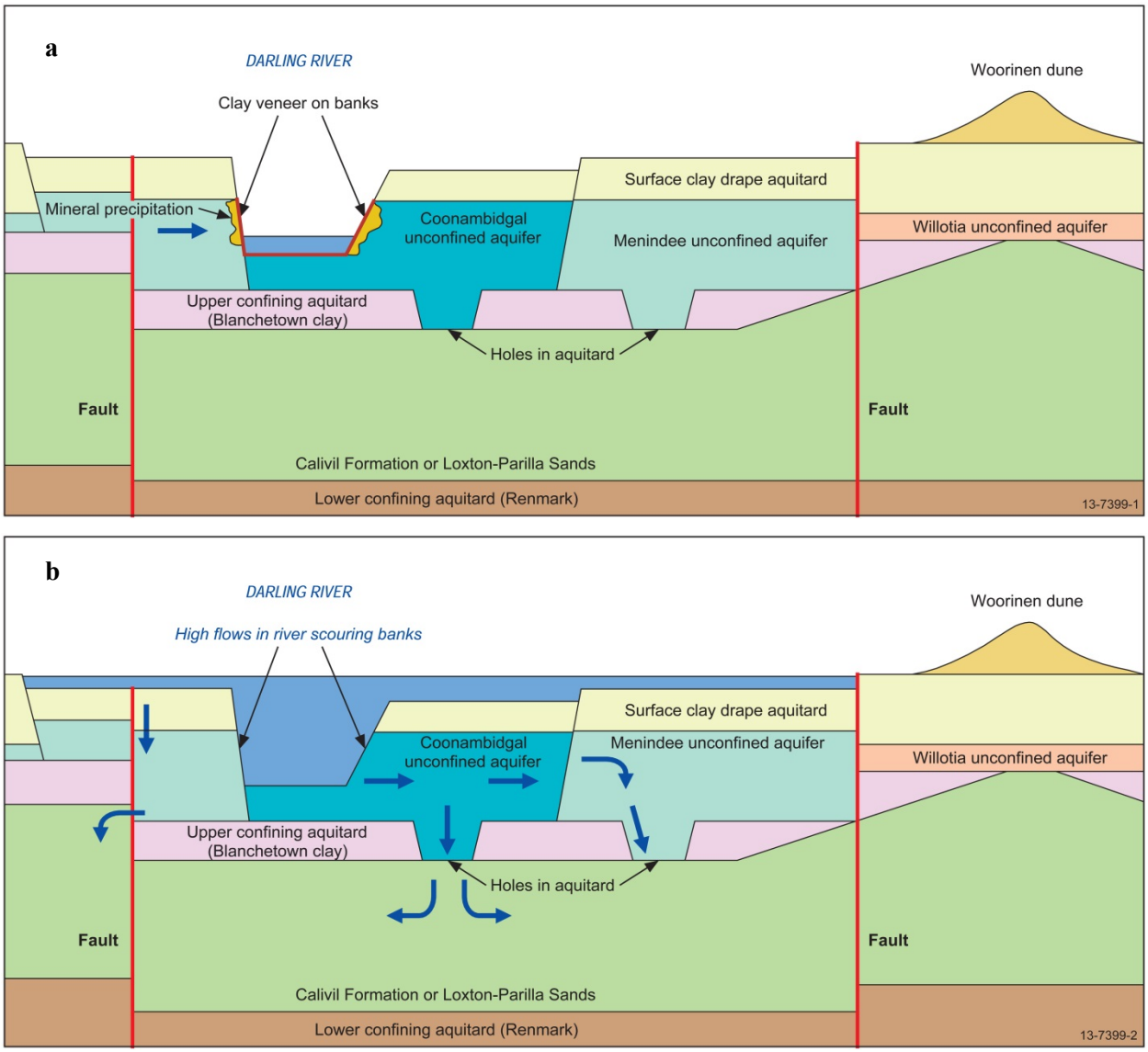

Figure D. *Conceptual model for groundwater recharge in the Lower Darling Floodplain alluvial sediments. In the top image (a), low flow conditions are illustrated. In the bottom image (b), high flow conditions are illustrated.*

BROADER SCIENTIFIC FINDINGS

1. A new, multi-scale methodology was developed to estimate groundwater quality and storage volumes, and applied to the Pliocene aquifers. This methodology is a significant improvement on previous approaches that rely upon extrapolation from limited borehole data.
   i. Salinity thresholds were estimated by comparing the downhole pore fluid data with the AEM response at a borehole scale. Bulk volumes for each water quality class in a target were then calculated using these thresholds on an AEM depth slice basis, which had been mapped into textural classes. An effective porosity range for each textural class was developed by integrating borehole nuclear magnetic resonance (NMR) data and laboratory porosity data (from Lexan-encapsulated core samples). These effective porosity ranges were used to convert the depth-slice bulk volume estimates to stored groundwater volumes.
   ii. Sensitivity analysis revealed that there are still significant uncertainties in volume estimates using this approach. There can be order-of-magnitude differences in the volume calculations depending on the AEM technology, inversions and constraints used. Significant variations were also found when different AEM conductivity thresholds were used to map groundwater salinity. Various estimates of effective porosity were used to represent the geological heterogeneity.

iii. Due to this uncertainty, the groundwater storage volumes should only be considered as indicative estimates. The estimates are still useful in a relative sense, as a tool to prioritise the groundwater targets and to scope the potential aquifer storage capacity for MAR options.

2. This study has demonstrated the importance of selecting the most appropriate AEM system and optimizing the AEM inversions for generating a wide range of customized interpretation products.
   i. New inversion code (WANDA) has been developed for rapid inversion of the AEM data.
   ii. A lateral correlation procedure was developed to correlate AEM data strictly horizontally.
   iii. New Fiduciary (FID)-point borehole correlation procedures were developed to assess AEM inversions.
   iv. Bayesian inference via a reversible jump Markov Chain Monte Carlo (RJ-McMC) inversion for selected AEM data sets provided useful (quantitative) assessment of the final inversion models.
3. A new methodology, integrating fuzzy-k means (FCM) cluster analysis with conventional hydrochemical and hydrodynamic analysis provides invaluable new insights into groundwater processes.
4. Fundamental vertical accuracy (at 95% confidence level) of the LiDAR 5 m DEM dataset was found to be 0.52 m, due to inherent inaccuracies of the methodology, insufficient ground control points and cumulative errors including the ellipsoid-geoid transformations and resampling procedures. These vertical inaccuracies need to be factored in to flood modelling, and in utilisation of LiDAR datasets as an absolute height datum. Even considering this factor, flood inundation extent mapping of the central project area has a 93% compatibility with corresponding Landsat TM 5 imagery.
5. Critical to successful completion of the study was development of a trans-disciplinary research methodology. This approach enabled the team to recognise fundamental problems in discipline approaches, helped identify critical data gaps, and led to significant innovation across discipline boundaries. This research methodology was vital in the development of the hydrogeological conceptual model that underpinned MAR assessment.
6. It is our understanding that this is the first use of AEM for MAR identification and assessment. The project has developed trans-disciplinary methodologies and workflows that provide a template for future hydrogeological investigations and MAR assessments.

RECOMMENDATIONS

BHMAR Project Area Specific Science Recommendations

1. If an alternative water supply option for Broken Hill involving MAR or groundwater extraction is pursued at the Jimargil site, then it is recommended that the following steps be taken to characterise this site from a geological and hydrogeological perspective:
    i. Additional drilling, sampling and ground geophysics is required to validate the interpretation of aquifer properties and groundwater quality, particularly in the central part of the Jimargil potential borefield target area where existing data is limited. Understanding the heterogeneity of the hydrogeological system at the borefield scale is essential for optimising borefield design.
    ii. Long-term aquifer pump tests to (1) derive key aquifer hydraulic parameters for the target Calivil Formation, (2) assess leakage between the Calivil Formation aquifer and the overlying Quaternary aquifers, including the potential impact on the shallow watertable and (3) assess the potential for ingress of more saline or lower quality groundwater into the pumped aquifer, either laterally from within the Calivil Formation or vertically, particularly from the underlying upper Renmark Group.
    iii. Construction of a borefield scale GOCAD mesh model is required to integrate hydrostratigraphic mapping and geological faults in 3D. This is essential if full use is to be made of project datasets in numerical groundwater models. This is also essential for understanding recharge, interaquifer leakage and groundwater flow paths.
    iv. Ground geophysical (electrical) surveys are recommended to characterise potential pump test sites at high resolution.
    v. It is recommended that the AEM data be re-inverted to incorporate new drilling, ground and borehole geophysical data, to maximise the value of all existing project borehole data.
    vi. Geochemical and geophysical (resistivity) monitoring of the borefield site should be undertaken in conjunction with aquifer pump tests to map any spatial changes in groundwater salinity.
    vii. In the BHMAR study, recharge to the Pliocene aquifers is dominated by episodic leakage during high river flows and via structurally controlled disruptions to the regional overlying aquitards. This results in significant variations in recharge rates in both space and time, resulting in significant challenges in terms of extrapolating point-based recharge estimates. To address this spatial and temporal variability in recharge, it is recommended that a calibrated, transient numerical groundwater flow and solute transport model be constructed. This will also help optimise borefield design and assess potential negative impacts, regardless of the option selected at the Jimargil site.
    viii. If Aquifer Storage and Recovery (ASR) is further contemplated at this site, additional science investigative and modelling steps have been outlined in Lawrie *et al*. (2012c).
2. If any of the other regional MAR/groundwater resource targets are to be developed, then a similar program to that outlined above for the Jimargil site will be required to characterise the sites from a geological and hydrogeological perspective.
    i. Currently, very few of these regional targets are characterised using more than one borehole. If groundwater extraction is to be considered at these targets, a significant additional program of drilling, sampling and analysis would be required.
    ii. Establishing baseline groundwater-level monitoring is important, particularly in the context of understanding the aquifer response to episodic flood events.
    iii. Groundwater sampling is required to better define and understand potential water-quality issues.
    iv. Tracers or isotopes (such as radiocarbon) are required to help define the extent to which modern recharge is occurring in a target.
    v. Calibrated, transient numerical groundwater flow models would be required to determine the recharge, environmental impacts and acceptable groundwater extraction limits for the individual targets for all potential development options.

vi. It is recommended that solute transport modelling is also incorporated, considering the possibility of saline ingress.

vii. At present, only entry-level MAR assessments have been carried out on most of the regional targets. If MAR is to be considered at any of the regional sites, then a substantive program of scientific investigations, similar to that undertaken in Phase 3 of the BHMAR study, would be required to address issues in the maximal and residual risk assessment process.

3. Structural analysis has revealed a complex history of Neogene-to-Present tectonics in the study area. Further analysis is required to:

   i. Systematically classify faults based on the amount of vertical displacement, with a particular emphasis on identifying those faults which completely offset the confining aquitards. This is required to assess the potential for recharge and inter-aquifer leakage.

   ii. Classify faults based on their relative age of movement. This could be accomplished based on their AEM and geomorphic (and LiDAR) expression, noting subsequent erosion history. Identifying faults that have a more recent neotectonic expression in the landscape will assist with understanding recharge processes and broader evaluation of seismic risk in the area.

   iii. Trenching and age dating of potential fault scarps is recommended to conclusively demonstrate that the lineaments observed in the LiDAR data have a tectonic origin. The data obtained would also provide invaluable information on regional tectonic models and earthquake risk.

4. It is recommended that further detailed studies be undertaken at an individual target scale to integrate hydrogeochemical, geomorphic, hydrostratigraphic and structural data to map recharge, inter-aquifer leakage and groundwater flow pathways at a target scale. This would best be accomplished in 3D, using an appropriate GOCAD mesh model which could then provide a basis for numerical groundwater models.

5. It is recommended that detailed geomorphic mapping be finalised across the entire BHMAR study area. More broadly, in areas where the trend in the floodplain dictates, it is recommended that the regional digital elevation model be levelled prior to geomorphic mapping. This will then facilitate the generation of both rapid and highly detailed geomorphic mapping of the floodplain using a semi-automated contouring tool. More detailed mapping will be particularly important in regional targets where MAR involving enhanced infiltration options may be considered.

6. Recommendations relating to hydrographic Monitoring and analysis include:

   i. Continue to collect time-series groundwater-level and barometric data from the existing project monitoring network. The monitoring of the groundwater response to flood events of varying magnitude is required to better quantify recharge dynamics.

   ii. Trial the installation of additional logger technologies in the monitoring bores to collect time-series data of complimentary parameters (such as groundwater electrical conductivity or temperature).

7. Recommendations with respect to the use of tracers and age dating include:

   i. Trials should be conducted into alternative groundwater age-dating techniques (such as sulfur hexafluoride SF_6) to test and extend the interpretations based on the use of carbon-14 and chlorofluorocarbon analyses.

   ii. Using chlorofluorocarbon as a tracer tool, analysis of CFC-113 is recommended in addition to the conventional analysis of CFC-11 and CFC-12. This would improve evaluation of groundwater mixing fractions between the fresh river leakage and the saline regional groundwaters.

   iii. Investigations should be carried out into the use of heat as a tracer for interactions between the river (or lakes) and the shallow unconfined aquifer. This can include the installation of infrastructure to monitor temperature in the river and also within the near-river sediments.

Broader Regional Scientific Recommendations

1. The revised understanding of the age, stratigraphy, mode of deposition and tectonic history of the Lower Darling Valley floodplain sediments has broader implications for the hydrogeology of the Western Murray Porous Rock Aquifer and Lower Darling Alluvium Groundwater Management Units

(GMUs). It is recommended that further geological and hydrogeological studies be undertaken to up-date the hydrogeological conceptual models underpinning groundwater management in these two GMUs.

2. Based on the conceptual understanding of key groundwater processes from this study, it is recommended that similar scientific investigations be carried out in the Basin (and nationally), to identify other river reaches where the hydrogeological conceptual models may require up-dating based on the new knowledge generated in the BHMAR study. This new knowledge and the datasets generated, could be used to assess the potential for additional MAR options and/or groundwater resources across the Basin (and nationally). Studies should include the Upper Darling River between Bourke and Wilcannia.
3. Identification of significant Neogene tectonics (and neotectonics) in the BHMAR study area most likely has broader regional (and national) implications. It is recommended that regional studies utilising similar mapping methodologies be used to assess the extent and significant of tectonics in the Murray-Darling Basin (and Australia more generally).
    i. Reconnaissance mapping of the area covering the Western Murray Porous Rock Aquifer, utilising regional gravity, airborne magnetics and high resolution DEMs, has identified regionally significant lineaments that may play an important role in recharge and inter-aquifer leakage processes. However, further work is recommended to characterise these lineaments and assess their significance, if any, for groundwater processes.
    ii. Similar studies are required in the Basin and more broadly, prioritised to areas where connectivity between surface water and key aquifers, or where inter-aquifer leakage, has been identified as a key factor in water management.
    iii. It is also recommended that future hydrogeological and MAR studies should consider tectonic studies as an integral part of future investigations and assessments.
4. The project provides the opportunity to develop a Darling Floodplain strategic science site. The BHMAR project area is the most data-rich site in Australia from a hydrology-hydrogeology-geomorphology-neotectonics perspective. A groundwater observation network (40 bores) has been established, and sites established for the trialling of new geophysical and remote sensing technologies.
    i. It is recommended this site be recognised as a strategic science site for the trialling of a range of new geophysical, remote sensing technologies, and science methods.
    ii. More specifically, it is recommended that a number of monitoring sites (e.g. tiltmeters, microseismic monitoring stations, GNSS reference station) be established at strategic locations within this area to provide baseline stations for future technology and science trials.
    iii. It is also recommended that inSAR techniques be trialled in the BHMAR study area to assess the degree of floodplain breathing as a consequence of episodic flooding.
    iv. It is also recommended that inSAR techniques be trialled in the BHMAR study area to assess the capability of InSAR techniques for mapping watertable fluctuations in unconfined aquifers under Australian landscape conditions.

Broader Scientific Recommendations

1. The BHMAR study has demonstrated that a trans-disciplinary systems science approach, utilising modern investigative mapping, characterisation and assessment technologies, can provide substantive new insights into the hydrogeology of Australia's unique near-surface landscapes. Similar methodologies and technologies are recommended for future groundwater investigations in Australia, particularly in shallow sedimentary systems. These methods provide the integrative framework required to address the many inter-related issues encountered in assessing MAR options and groundwater extraction, particularly in hydrogeologically and hydrogeochemically complex areas.
2. Future assessments and models of surface-groundwater interaction in similar environments in the Murray-Darling Basin need to take into account possible linkages between high-volume floods and episodic recharge events. Physically based hydraulic modelling could also be undertaken to better understand the relationship between river-flow rates, groundwater-infiltration rates, sediment scouring and deposition. Based on the conceptual understanding of key groundwater processes from this study, it is recommended that a broader assessment be carried out in the Basin to identify other river reaches

where additional groundwater resources may exist, and/or MAR options may provide enhanced drought security and regional-development opportunities.

3. Future assessments of groundwater quality for ASR and/or a groundwater extraction schemes in Australia need to pay particular attention to hydrogeochemical processes relating to groundwater salinity, clay dispersion and acidification, in addition to redox-sensitive trace metal processes. The hydrological (and recharging) conditions can be highly variable under the alternating drought and flood periods which are so characteristic of the hydrology in Australia. These changing conditions can in turn affect water quality by saturation of oxidised/reduced materials via changes in aquifer watertable height and also by inter-aquifer mixing of groundwater with variable water quality.
4. Studies of Neogene-to-Recent intraplate deformation are recommended nationally to identify and characterise key structures that might play an important role in recharge and inter-aquifer leakage processes, and to refine models of present-day and neotectonic palaeostress trends and partitioning.
5. A number of recommendations are made about the use of AEM technology for the high-resolution mapping of near-surface hydrogeological systems and the identification and assessment of MAR targets:
    i. AEM data acquisition should be considered as part of any data-acquisition strategy in data-poor areas. These data can map large near-surface areas rapidly, maximising the likelihood of identifying multiple MAR targets.
    ii. The mapping and assessment of MAR targets often requires high-resolution geophysical data to resolve the complexities of the hydrogeological system. Traditional derivative analysis approaches for AEM technology selection are inadequate for assessing the ability of candidate systems to map MAR targets. A comparative analysis of candidate systems, consisting of both theoretical considerations and field studies including test lines over representative hydrostratigraphic targets is recommended.
    iii. Optimisation of AEM data for MAR investigations should also involve careful consideration of AEM data-acquisition strategy, AEM system calibration, and validation and inversion methods.
    iv. It is recommended that a phased approach to AEM data acquisition be trialled to decrease the costs of acquiring AEM data for MAR target mapping. Depending on the nature of the target and the size of the area of investigation, initial reconnaissance mapping of MAR targets could utilise wide line-spaced data to identify potential MAR targets in Australia's major river basins.
        a. As shown in this study, one risk of using this phased approach is that wide line-spacing data may identify targets that on closer inspection may not pass assessments. To minimise these risks, a swath-mapping approach, with 3-5 closely-spaced (e.g. 200 m) flight lines separated by wider line spaced data (e.g. 1-2 km), could be trialled to give more opportunity for key elements of the hydrogeological system to be mapped and assessed.
        b. It should be noted however, that for logistic reasons, it is not always possible to acquire data in phased approaches, however the potential benefits of using such an approach for MAR mapping and assessment should be investigated in future investigations.
        c. The area surveyed should be sufficient to allow for assessment of multiple targets, given the likelihood of failure of some targets on hydrogeological, economic, environmental or social factors.
        d. Depending on the hydrogeological system, it is likely that high-density line spacing and/or follow up high-resolution ground geophysics would be required to provide sufficient data to resolve the complexities of many Australian hydrogeological systems.
6. The key learnings and recommendations from applying various methods to estimate recharge are outlined below.
    i. There are many different methods for estimating groundwater recharge. Some of these provide estimates of potential recharge or deep drainage, which is the flux below the root zone that has the potential to reach the watertable over varying periods of time. Other methods focus on groundwater responses where recharge accessions have actually reached the watertable. Many of these methods apply only to the unconfined aquifer and cannot be extrapolated to estimating groundwater recharge to confined or semi-confined aquifers. An understanding of the geometry and structure of the hydrostratigraphy, including any overlying aquitards is recommended to ensure that the recharge-estimation method is appropriate.

ii. It is important to understand the assumptions inherent in any recharge-estimation method and the implications of these on method suitability. This is important to ensure that the recharge method is appropriate to the conceptual model developed for the groundwater system. For example, the groundwater chloride mass-balance method assumes that the chloride in groundwater originates from rainfall, with no other subsurface chloride sources. It also assumes that surface-water leakage to the aquifer is absent. With river/lake leakage interpreted as the dominant recharge mechanism, these assumptions are not met for the BHMAR study area so the derived potential recharge estimates are not valid. A verification of the underlying assumptions of the recharge method against the conceptual model is recommended in future investigations.

7. A significant number of additional recommendations that follow from the specific science methodologies used in the BHMAR project are made in Lawrie *et al*. (2012a). The reader is referred to the latter report for the details of specific science methodology recommendations.

CONTENTS

Executive Summary i

Contents xxi

List of Figures xxv

List of Tables xxxv

1. Introduction 1
   - 1.1 Background 1
   - 1.2 Recent Research into Securing Broken Hill's Water Supply and Identifying Significant Water Savings 2
     - 1.2.1 Hydrology and Evaporation Studies 3
     - 1.2.2 Geoscience Australia Hydrogeological Investigations 4
   - 1.3 Purpose and Scope of this Report 7

2. Regional Setting 9
   - 2.1 Study Area 9
   - 2.2 Darling River and Floodplain Hydrology 9
     - 2.2.1 Darling River Hydrology 9
     - 2.2.2 Menindee Lakes Storages (MLS) 12
     - 2.2.3 Evaporation 13
   - 2.3 Climate, Climate Variability and Predicted Climate Change 23
     - 2.3.1 Present-day Climate 23
     - 2.3.2 Palaeo-climate and Implications for Streamflows and Recharge 23
     - 2.3.3 Predicted Climate Change 25
   - 2.4 Land Use and Cultural Heritage 25

3. Project Data Acquisition 26
   - 3.1 New Data Acquisition 26

4. Regional Geology 30
   - 4.1 Geological Basement 30
   - 4.2 Darling Geological Basin 30
     - 4.2.1 Bancannia Trough 31
     - 4.2.2 Menindee Trough 31
     - 4.2.3 Blantyre Trough 32
     - 4.2.4 Pondie Range Trough 32
   - 4.3 Murray Geological Basin 35
     - 4.3.1 Regional Geology 35
     - 4.3.2 Regional Hydrogeology 39

5. Stratigraphy and Evolution of the Murray Geological Basin Sediments within the Darling Valley 47
   - 5.1 Renmark Group 47
     - 5.1.1 Project Area 47
     - 5.1.2 Architecture 52
     - 5.1.3 Palynology 72
     - 5.1.4 Analogues 73
     - 5.1.5 Hydrological Implications 78
   - 5.2 Pliocene Units 79
     - 5.2.1 Introduction 79
     - 5.2.2 Distribution 80
     - 5.2.3 Thickness and Relationships 83
     - 5.2.4 Age and Environment 93
     - 5.2.5 Lithostratigraphy 93

5.2.6 Architecture 104
5.2.7 Depositional Conceptual Model 109
5.2.8 Cements 112
5.2.9 Diagenetic Conceptual Model 115
5.2.10 Outcrop Analogues 119
5.2.11 Modern Analogues 122
5.2.12 Hydrogeological Implications 122
5.3 Blanchetown Clay and Chowilla Sand 122
5.3.1 Blanchetown Clay in the Menindee Area 126
5.3.2 Stratigraphic Relationships and Depositional History 130
5.3.3 "Holes" in the Blanchetown Clay 137
5.4 Quaternary Units 152
5.4.1 Quaternary Fluvial Units and Geomorphology, Lower Darling Valley 152
5.4.2 Quaternary Lacustrine Units 203
5.4.3 Quaternary Aeolian Woorinen Formation 211
5.5 Landscape and Geological Evolution in the Study Area 223
6. Tectonic Framework 225
6.1 Tectonics in the BHMAR Project Area 225
6.2 Evidence for Tectonics in the Unconsolidated Alluvial Sediments 225
6.3 Deformation of the Blanchetown Clay 226
6.3.1 Previous Investigations 226
6.3.2 BHMAR Investigations 227
6.4 The Menindee and Talyawalka Fault Systems 230
6.5 Evidence for Neotectonics 231
6.6 Deformation Model for the BHMAR study area 243
6.6.1 The Role of Faults in the Hydrogeological Conceptual Model 247
7. Hydrogeology 249
7.1 Lower Aquitard (Renmark Group) 249
7.1.1 Hydrogeology 249
7.1.2 Groundwater Flow and Dynamics 255
7.2 Pliocene Sands Aquifer 256
7.2.1 Hydrogeology 256
7.2.2 Groundwater Flow and Dynamics 271
7.2.3 Groundwater Quality 274
7.3 Upper Confining Aquitard 277
7.3.1 Hydrogeology 277
7.3.2 Upper Confining Aquitard Diffusion 286
7.4 Shallow Unconfined Quaternary Aquifer 293
7.4.1 Hydrogeology 293
7.4.2 Groundwater Flow and Dynamics 306
7.4.3 Groundwater Quality 313
7.5 Near Surface Aquitard 313
8. Hydrochemistry 328
8.1 Major Ion Chemistry 328
8.2 Fuzzy k-means Analysis 347
8.3 Stable Isotope Analysis 364
8.4 Radiocarbon Analysis 371
8.5 Chlorofluorocarbons 381
8.6 Radon 388
8.7 Strontium Isotopes 393
9. Recharge and Hydrogeological Conceptual Model 394
9.1 Previous Recharge Studies 394

9.2 Recharge Estimation 395
9.2.1 Watertable Fluctuation Method 395
9.2.2 Hydraulic Loading 400
9.2.3 Temperature Monitoring 400
9.2.4 Darcian Seepage Velocities 402
9.2.5 Groundwater Mounding 404
9.2.6 Flood Frequency Analysis 406
9.2.7 Radiocarbon Depth Models 408
9.2.8 Chloride Mass Balance Method 408
9.2.9 Comparison of Recharge Methods 410
9.3 Palaeorecharge 413
9.3.1 Continental-scale Climate and Catchment Setting 413
9.3.2 Glacial-interglacial Climate Cycles 413
9.3.3 Lower Darling Fluvial Activity Phases 415
9.3.4 Recharge Implications of Long-term Palaeoclimatic and Palaeoenvironmental Changes 418
9.4 Conceptual Hydrogeological Model 421
9.4.1 Recharge Impedance During Low-flow Conditions 423
9.4.2 Field Observations During Flooding 432
9.4.3 Direct Connectivity Between River Channel and Semi-Confined Aquifer 443
9.4.4 Recharge Potential of GWR Targets 446
10. Vegetation Assessment 448
10.1 Introduction 448
10.1.1 Why is it Important to Investigate the Health of Vegetation in this Area? 448
10.1.2 Why Use Remote Sensing Over Field Studies? 448
10.1.3 What are the Key Questions Being Addressed in this Study? 449
10.2 Background 449
10.2.1 Rainfall 449
10.2.2 Lake Water 450
10.2.3 River Water 454
10.2.4 Flood Waters 459
10.2.5 Groundwater 461
10.2.6 Vegetation Dynamics 466
10.3 Method Summary 471
10.3.1 How are Vegetation Dynamics Being Assessed? 471
10.3.2 Specific Drought Analysis 474
10.3.3 Interpreting Landsat Time Series Profiles 476
10.4 Analysis 477
10.4.1 Impacts of Regulation on Menindee Lakes Woody Vegetation 477
10.4.2 Importance of River Flow and Flooding to Vegetation Function 530
10.4.3 Vulnerability of Vegetation to Potential Groundwater Extraction and MAR Schemes 581
10.5 Conclusions 583
10.5.1 Lake-Fringing Vegetation 583
10.5.2 Riparian and Floodplain Vegetation 584
10.6 Recommendations 584
11. BHMAR Hydrogeological Investigations- Broader Implications 585
11.1 Existing Regional and Basin Groundwater Management Plans 585
11.2 Groundwater Management Implications of BHMAR Project 587
11.3 Upper Darling Alluvial Groundwater Resource Potential 595
12. Discussion 599
12.1 Using AEM to Map MAR and Groundwater Resource Targets 599
12.1.1 3D Mapping of Hydrostratigraphy, Structure and Groundwater Salinity 600
12.2 Characteristics of Australian Rivers 601

12.2.1 Comparing Menindee Area with Tucson Basin 602
13. Conclusions 604
13.1 Key Scientific Findings in the BHMAR Study Area 604
13.2 Revised Geological and Hydrogeological Framework 606
13.3 Summary of Geology and Landscape Evolution 609
13.4 New Hydrogeological Conceptual Model 610
13.5 Broader Scientific Findings 611
14. Recommendations 613
15. References 618
Acknowledgements 639
Glossary 643

LIST OF FIGURES

Figure A. Oblique map view of the top of the Upper Confining Aquitard x
Figure B. Depth to top of Blanchetown Clay where Talyawalka and Menindee Fault Systems link xi
Figure C. Geological cross-section NNW-SSE across the project area from north of Lake Menindee to Larloona Station. xii
Figure D. Conceptual model for groundwater recharge in the Lower Darling Floodplain alluvial sediments xiv
Figure 1-1. Location of the BHMAR study area in relation to the Murray-Darling Drainage Basin 1
Figure 2-1. Map showing the location of BHMAR study area relative to Menindee and Broken Hill 10
Figure 2-2. Map showing the location of the Menindee Lakes 11
Figure 2-3. Mean annual lake evaporation across USA 22
Figure 2-4. Average monthly percent capacity for three Menindee Lakes and Average Return Interval for Class C flows. 24
Figure 3-1. Datasets acquired during the project, grouped by theme 28
Figure 3-2. Simplified project workflow 29
Figure 4-1. Map of regional gravity data 33
Figure 4-2. Generalised stratigraphic profile of Darling Geological Basin 34
Figure 4-3. Seismic reflection profile from survey line C99/01 34
Figure 4-4. Location of the Murray and Darling Geological Basins 35
Figure 4-5. Structural contours for the base of the Murray Geological Basin sediments 37
Figure 4-6. Interpreted cross section through part of northwestern Murray Geological Basin 38
Figure 4-7. Stratigraphic chart for Cenozoic formations in the Murray Geological Basin 39
Figure 4-8. Areas of downward head gradient and significant recharge in northwest Murray Geological Basin 42
Figure 4-9. Areas of upward head gradient and significant discharge in the northwest Murray Geological Basin 43
Figure 4-10. 1-second SRTM image for Western Murray Porous Rock aquifer area 44
Figure 4-11. Regional salinity-yield mapping for the Pliocene Sands aquifer 45
Figure 4-12. Regional gravity image for the Western Murray Porous Rock aquifer 46
Figure 5-1. Histogram distribution of bed thickness in Renmark Group 53
Figure 5-2. Schematic diagram of representative plugged channel dimensions 55
Figure 5-3. Interpreted lithostratigraphy for 61.0-72.3 m depth slice 57
Figure 5-4. Anastomosing pattern in the distribution of fine-grained and muddy sands in the Renmark Group 58
Figure 5-5. Woody horizon in coarse channel sands, Renmark Group 59
Figure 5-6. Reworked mud clasts and woody debris at base of channel, Renmark Group 60
Figure 5-7. Organic-rich channel plug, Renmark Group 61
Figure 5-8. Green floodplain muds, Renmark Group 62
Figure 5-9. Dark floodplain muds and oxidised palaeosols, Renmark Group 63
Figure 5-10. Interclasts on soil surface, Renmark Group 64
Figure 5-11. Insect nest, Renmark Group 64
Figure 5-12. Goethitic root impressions in carbonaceous mud, Renmark Group 65
Figure 5-13. Lignite interval, Renmark Group 66
Figure 5-14. Crevasse splay deposit, Renmark Group 67
Figure 5-15. Sapropel of interpreted floodplain pond infilled by crevasse splay, Renmark Group 68
Figure 5-16. Levee bank sediments, Renmark Group 69
Figure 5-17. Interdistributary bay deposits of laminated carbonaceous muds, Renmark Group 70
Figure 5-18. Weathered Renmark Group 71
Figure 5-19. Exhumed inverted low sinuosity channel, Brushy Basin Member, Utah 73
Figure 5-20. Individual channels of Brushy Basin Member 74
Figure 5-21. Cross section through a small, multistorey fixed channel, Brushy Basin Member 74
Figure 5-22. Magdalena River floodplain showing numerous fixed channels forming an anastomosing network of well developed levees 76
Figure 5-23. Magdalena River floodplain, showing well-developed levees, crevasse splays and an inundated floodplain 77

Figure 5-24. Astronaut photograph of Mississippi Delta 78
Figure 5-25. Regional cross section F-F1 showing possible palaeovalley features in the Calivil Formation 81
Figure 5-26. Sonic core at BHMAR64, showing Calivil Formation overlying Upper Renmark Group 84
Figure 5-27: Composite image of sonic core showing contact between Calivil Formation gravels and Renmark Group clays in BHMAR33 84
Figure 5-28: Schematic diagram of Calivil Formation deposits over the irregular topography of the Renmark Group 85
Figure 5-29: Cross section G-G1 87
Figure 5-30. Local geological cross section through the northern end of the Jimargil site. 89
Figure 5-31: Cross section V-V1 91
Figure 5-32. Histogram of hydraulic sediment classes in the Calivil Formation 95
Figure 5-33. Textural pie diagrams for sonic bores in the Calivil Formation – northern project area 96
Figure 5-34. Textural pie diagrams for sonic bores in the Calivil Formation – central project area 97
Figure 5-35. Textural pie diagrams for sonic bores in the Calivil Formation – southern project area 98
Figure 5-36. Composite image of sonic core showing fine-grained (silty) lithologies and coarser-grained (sandy) lithologies in the Calivil Formation 99
Figure 5-37. Localised gravel sheet in the river bed at Shaw River, Western Australia 100
Figure 5-38. Very localised gravels derived from lateral debris flows at Shaw River, Western Australia .. 100
Figure 5-39. Photomicrograph of goethite-cemented coarse-grained sandy gravel 103
Figure 5-40. Photomicrograph of goethite-cemented coarse sandy gravel 103
Figure 5-41. Channel hierarchy of the braided Braphaputra River system, Bangladesh 104
Figure 5-42. Channel hierarchy of the braided Rakaia River system, New Zealand 105
Figure 5-43. Channel hierarchy of the braided Burdekin River system, Australia 105
Figure 5-44. Frequency histogram of channel unit thickness within the Calivil Formation 106
Figure 5-45. Braided river pattern defined by medium-grained sand units in 43.5 to 51.5 m depth slice ... 108
Figure 5-46. Depositional conceptual model showing channel architecture of a deep braided river system 111
Figure 5-47. Typical fluvial lithofacies associated with deep braided perennial rivers 111
Figure 5-48. Photomicrograph of dark meniscus goethite forming a thin skin on sand grains 112
Figure 5-49. Photomicrograph showing meniscus cementation 113
Figure 5-50. Photomicrograph showing carbonate cementation 113
Figure 5-51. Photomicrograph of microquartz and chalcedony cement 114
Figure 5-52. Photomicrograph showing opal and chalcedony cement 114
Figure 5-53. Composite image of sonic core showing lower contact between reduced and oxidised lithologies in Calivil Formation 116
Figure 5-54. Semi-permanent pool along the Gilbert River channel 117
Figure 5-55. Semi-permanent pool along the Mitchell River 117
Figure 5-56. Conceptual model of river bed diagenesis, specifically irregularities in dry river bed detrital accumulation 118
Figure 5-57. Conceptual model of river bed diagenesis, specifically partial flooding of depressions leading to the development of deep pools 118
Figure 5-58. Conceptual model of river bed diagenesis, specifically river flooding leading to burial of former pools and bars 118
Figure 5-59. Conceptual model of river bed diagenesis, specifically falling water levels resulting in formation of new deep pools and exposed bars 119
Figure 5-60. Bedding plane exposure of trough cross beds in the Salt Wash Member, Utah 120
Figure 5-61. Parallel bedded red siltstone, shale and fine-grained sandstones forming overbank facies of the Salt Wash Member, Utah 121
Figure 5-62: Abandoned shale-filled channel of the Salt Wash Member, Utah 121
Figure 5-63. Elevation of top of the upper confining aquitard 124
Figure 5-64. Evolution of reconstructions of Lake Bungunnia 126
Figure 5-65. Location of Viewmont riverbank cliff section 127
Figure 5-66. Viewmont riverbank cliff section showing topographically high Blanchetown Clay under thin aeolian sand 128
Figure 5-67. AEM flight line 21100, showing highly conductive Blanchetown Clay 128

Figure 5-68. AEM cross section showing the Blanchetown Clay conductor extending horizontally westward from below Redbank Creek scroll plain to BHMAR1A-1 129
Figure 5-69. AEM cross section showing the Blanchetown Clay conductor extending horizontally northward from below the Great Darling Anabranch scroll plain 130
Figure 5-70. BHMAR19-1 core photos showing contact between medium-grained sand in the Willotia beds and clay-rich Blanchetown Clay..... 131
Figure 5-71. BHMAR06-1 core photographs showing Blanchetown Clay..... 134
Figure 5-72. BHMAR06-1 core photographs showing laminated Blanchetown Clay, sharp contact with Calivil Formation and absence of the Karooda surface 135
Figure 5-73. BHMAR88-3 core photographs showing Chowilla Sands underlying Blanchetown Clay 136
Figure 5-74. Double conductivity peaks in induction logs of BHMAR43-1 and BHMAR99-1 136
Figure 5-75. Gamma logs for Blanchetown Clay at BHMAR99-1 and BHMAR21-1 137
Figure 5-76. AEM cross section showing conductive Blanchetown Clay pinching out over a strongly resistive Palaeozoic basement high..... 138
Figure 5-77. AEM cross sections showing conductive Blanchetown Clay apparently thinning towards a hole..... 139
Figure 5-78. AEM cross sections showing Blanchetown Clay conductivity anomaly at 30-60 m AHD, with interpreted warping and faulting..... 140
Figure 5-79. Depth to top of upper confining aquitard at Jimargil..... 141
Figure 5-80. Elevation of top of Blanchetown Clay aquitard in m AHD for the area northeast of Jimargil, including detailed structural interpretation 142
Figure 5-81. Cross Section S-S1..... 146
Figure 5-82. AEM cross sections showing the Blanchetown Clay as a thin unit with low conductivity at Lake Menindee..... 147
Figure 5-83. Two apparent holes in the Blanchetown Clay conductivity anomaly..... 148
Figure 5-84. Residual of the Darling River channel DEM and depth to the top of the upper confining aquitard. 149
Figure 5-85. Map of the residual of the Darling River channel DEM and depth to the top of the upper confining aquitard for a reach of Darling River at Jimargil..... 150
Figure 5-86. Map of the residual of the Darling River channel DEM and depth to the top of the upper confining aquitard for the Darling River in the northern part of Jimargil..... 151
Figure 5-87. Schematic diagram of the stratigraphic relationship between Quaternary fluvial units in the Darling River tract of the project area 157
Figure 5-88. Schematic diagram of the stratigraphic relationship between Quaternary fluvial units in the Talyawalka-Anabranch tract of the Lower Darling in the project area..... 157
Figure 5-89. Surface landforms mapped at a regional scale in the BHMAR study area..... 158
Figure 5-90. Location of natural exposures of Willotia beds and Blanchetown Clay in the BHMAR study area 160
Figure 5-91. Photograph of Redbank Creek cliff section 162
Figure 5-92. Location of Redbank Creek cliff section 162
Figure 5-93. Stratigraphy of Redbank Creek cliff section..... 163
Figure 5-94. Photographs of weathering features within the Redbank Creek cliff section 163
Figure 5-95. Cross section through Redbank Creek cliff section..... 164
Figure 5-96. Section exposure of Willotia beds at Cawndilla outlet channel..... 165
Figure 5-97. Location of Great Darling Anabranch cliff section exposure 166
Figure 5-98. Stratigraphy of the Great Darling Anabranch cliff section 167
Figure 5-99. Photographs of Willotia bed mud and gypsum efflorescence at the Great Darling Anabranch cliff section 167
Figure 5-100. Block diagram of the morphology and depositional elements of a meander river 168
Figure 5-101. Menindee Formation overbank mud, Three Mile Creek..... 170
Figure 5-102. Coonambidgal Formation overbank mud, Darling River scroll plain 170
Figure 5-103. Coonambidgal Formation ripple cross-laminations, Talyawalka Creek..... 171
Figure 5-104. BHMAR66 core photographs of medium- to coarse-grained Menindee Formation sands.... 171
Figure 5-105. BHMAR80A-2 core photographs of medium- to coarse-grained Coonambidgal Formation sands..... 172
Figure 5-106. Standard meander and scroll geometry parameters measured in the Coonambidgal Formation lateral phase deposits..... 175

Figure 5-107. BHMAR23 core photographs of medium- to coarse-grained Menindee Formation equivalent lateral-valley sands 178
Figure 5-108. Location map of Yampoola Corridor 179
Figure 5-109. Elevation map of Yampoola Corridor in the south of the BHMAR study area 180
Figure 5-110. Location of Quaternary fluvial unit dating sites 184
Figure 5-111. Location of OSL sample sites at Menindee Common 185
Figure 5-112. Stratigraphy of tracer trench DR01, including OSL dating results 185
Figure 5-113. Stratigraphy of hand auger hole DR01A, including OSL dating results 186
Figure 5-114. Location of OSL sample sites at Chalky Well Station 187
Figure 5-115. Stratigraphy of hand auger hole CHW01, including OSL dating results 187
Figure 5-116. Location of BHMAR75-8 and BHMAR79A-2 at Menindee Common 188
Figure 5-117. Stratigraphy of BHMAR79A-2, including radiocarbon dating results 188
Figure 5-118. Location of OSL sample sites on Appin Station 190
Figure 5-119. Stratigraphy of tractor trench TAL02, including OSL dating results 191
Figure 5-120. Stratigraphy of tractor trench TAL03, including OSL dating results 191
Figure 5-121. Stratigraphy of tractor trench TAL04, including OSL dating results 192
Figure 5-122. Location of OSL sample site on Tandou Station 193
Figure 5-123. Stratigraphy of hand-auger hole TAN01, including OSL dating results 193
Figure 5-124. Location of OSL sample sites on Cuthero Station 194
Figure 5-125. Stratigraphy of hand auger hole CUTH01, including OSL dating results 194
Figure 5-126. Location of OSL sample site on Larloona Station 195
Figure 5-127. Stratigraphy of hand auger hole LAR01, including OSL dating results 196
Figure 5-128. Stratigraphy of tractor trench DR02, including OSL dating results 197
Figure 5-129. Stratigraphy of tractor trench DR03, including OSL dating results 197
Figure 5-130. Stratigraphy of hand auger hole DR06, including OSL dating results 198
Figure 5-131. Stratigraphy of hand auger hole CHW02, including OSL dating results 198
Figure 5-132. Stratigraphy of BHMAR75-8, including OSL dating results 199
Figure 5-133. Location of OSL sample site MN01 200
Figure 5-134. Stratigraphy of hand-auger holes MN01-3 at north-western end of Lake Menindee, including OSL dating results 200
Figure 5-135. Location of tractor trench 3MC06 201
Figure 5-136. Stratigraphy of tractor trench 3MC06 on Appin Station, including OSL dating results 201
Figure 5-137. Radial plot of OSL samples 3MC06 and 3MC10 202
Figure 5-138. System of overflow lakes on the Teryaweynya Creek 205
Figure 5-139. SPOT and elevation images of Stephens Creek 206
Figure 5-140. Elevation information for the southern portion of the BHMAR study area 207
Figure 5-141. Modelled natural storage volume for Lake Cawndilla 210
Figure 5-142. Modelled natural storage volume for Lake Pamamaroo 210
Figure 5-143. Modelled natural storage volume for Lake Menindee 211
Figure 5-144. Location of relict aeolian features shown on a LiDAR DEM 213
Figure 5-145. Area of discontinuous aeolian sediments on the relict Menindee Formation floodplain 214
Figure 5-146. Within-valley aeolian sediments on Viewmont Station 215
Figure 5-147. Location of 3MC06 tractor trench profile and hand auger holes 3MC01 and WS03 216
Figure 5-148. LiDAR image showing location of 3MC01, 3MC06 and WS03 217
Figure 5-149. Lithological profile of auger hole 3MC01 218
Figure 5-150. Recovered sediment samples from augering of 3MC01 218
Figure 5-151. Lithological profile of auger hole WS03 219
Figure 5-152. Aeolian deposit at WS03 auger site 219
Figure 5-153. Lithological profile of tractor trench 3MC06, including OSL dating results 220
Figure 5-154: The Talyawalka Creek scroll plain demonstrating scroll-plain dunes types 222
Figure 5-155. Talyawalka scroll plain marginal aeolian deposit on Menindee Formation floodplain 222
Figure 5-156. Aeolian deposit on Coonambidgal Formation Phase 2 scroll plain 223
Figure 6-1 Map showing location of the major geological basement features relative to the BHMAR project area. 229
Figure 6-2 Blanchetown Clay surface (m AHD) for an area NE of Jimargil, including mapped structural features 232

Figure 6-3. Tiled conductivity depth sections with 200 m spacing between flight lines for an area near Menindee 233
Figure 6-4. Depth to top of upper confining aquitard including structural features and stress fields south of the Jimargil borefield 235
Figure 6-5. Elevation of top of Blanchetown Clay aquitard in m AHD for the area northeast of Jimargil, including detailed structural interpretation 237
Figure 6-6. Maps of first vertical derivative of total magnetic intensity and regional gravity, with major faults delineated. 239
Figure 6-7. Structural features shown on the LiDAR DEM including Talyawalka Scarp 241
Figure 6-8. LiDAR DEM image of the Darling River near Bootingee showing unusual drainage patterns, including straight line segments and box-like patterns. 241
Figure 6-9. Lineaments evident on the LiDAR and magnetic TMI 242
Figure 6-10. Mean stress orientations within Australian stress provinces 244
Figure 6-11. A diagrammatic representation of the structural strain pattern produced by a sinistral shear couple, as occurs within the Menindee Fault System (MFS) 245
Figure 6-12. Ductile deformation in basement lithologies to east of BHMAR study area 246
Figure 6-13. Blanchetown Clay surface and associated structural features for the northern portion of Jimargil 248
Figure 7-1. Textural composition of the Renmark Group 250
Figure 7-2. Map with pie chart textural composition information about the Renmark Group 251
Figure 7-3. Indicative lithology of Renmark Group for 61.0-72.3 m AEM depth slice 252
Figure 7-4. Box and whisker plots of aquifer properties based on slug testing of BHMAR monitoring bores 254
Figure 7-5. Box and whisker plots of aquifer properties based on NMR logging intervals of BHMAR monitoring bores 254
Figure 7-6. Box and whisker plots of aquifer properties based on formation aggregates of NMR logging intervals in BHMAR monitoring bores 255
Figure 7-7. Hydrograph of BHMAR79A-2 screened in the Renmark Group at Menindee Common 255
Figure 7-8. Interpreted extent and stratigraphic thickness of the semi-confined aquifer (only Calivil Formation and Loxton-Parilla Sands) 260
Figure 7-9. Interpreted extent and stratigraphic thickness of the semi-confined aquifer 261
Figure 7-10. Interpreted thickness of the Calivil Formation in central part BHMAR study area 262
Figure 7-11. Interpreted thickness of the Loxton-Parilla Sands 263
Figure 7-12. Textural composition of the Calivil Formation and Loxton-Parilla Sands 264
Figure 7-13. Map with pie chart textural composition information about the Loxton-Parilla Sands 265
Figure 7-14. Indicative lithology of semi-confined aquifer for 36.7-43.5 m AEM depth slice 266
Figure 7-15. Indicative lithology of semi-confined aquifer for 43.5-51.5 m AEM depth slice 267
Figure 7-16. Indicative lithology of semi-confined aquifer and lower aquitard for 51.5-61.0 m AEM depth slice 268
Figure 7-17. Lower estimate of transmissivity of the semi-confined aquifer 269
Figure 7-18. Upper estimate of transmissivity of the semi-confined aquifer 270
Figure 7-19. Interpreted elevation of semi-confined aquifer potentiometric surface 272
Figure 7-20. Hydrographs for bores BHMAR80A-2, 80A-7 and 80B-2 screened in the Calivil Formation at East Bootingee 273
Figure 7-21. Hydrograph of BHMAR23-2 screened in Calivil Formation at Lake Menindee 274
Figure 7-22. Predicted groundwater salinity in the Pliocene aquifer for 43.5-51.5 m depth slice 275
Figure 7-23. Distribution of groundwater resource targets in the Pliocene aquifer 276
Figure 7-24. Textural composition of the Blanchetown Clay and Calivil Formation 278
Figure 7-25. Map with pie chart textural composition information about the Blanchetown Clay 279
Figure 7-26. Map with pie chart textural composition information about the Calivil Formation 280
Figure 7-27. Indicative lithology for 18.1-22.0 m depth slice 281
Figure 7-28. Indicative lithology of sediments for the 22.0-26.1 m AEM depth slice 282
Figure 7-29. Indicative lithology of sediments for the 26.1-30.9 m AEM depth slice 283
Figure 7-30. Indicative lithology of sediments for the 30.9-36.7 m AEM depth slice 284
Figure 7-31. Interpreted thickness of upper confining aquitard 285
Figure 7-32. Relationship between power exponent and effective dispersion coefficient for various porosities 287

Figure 7-33. Box and whisker plot of salinity of Blanchetown Clay pore fluids 287
Figure 7-34. Diffusion distance over different time frames for the upper confining aquitard 289
Figure 7-35. Plots of diffusion distance against diffusion time for the upper confining aquitard 289
Figure 7-36. Time required for upper confining aquitard diffusion – high estimate 290
Figure 7-37. Time required for upper confining aquitard diffusion – low estimate 291
Figure 7-38. Interpreted extent and stratigraphic thickness of Coonambidgal Formation 296
Figure 7-39. Interpreted extent and stratigraphic thickness of Menindee Formation 297
Figure 7-40. Interpreted extent and stratigraphic thickness of Willotia beds 298
Figure 7-41. Indicative lithology of shallow sediments for the 9.2-11.0 m AEM depth slice 299
Figure 7-42. Indicative lithology of shallow sediments for the 11.0-13.1 m AEM depth slice 300
Figure 7-43. Indicative lithology of shallow sediments for the 13.1-15.6 m AEM depth slice 301
Figure 7-44. Indicative lithology of shallow sediments for the 15.6-18.1 m AEM depth slice 302
Figure 7-45. Interpreted extent and stratigraphic thickness of the shallow unconfined aquifer 303
Figure 7-46. Lower estimate of transmissivity of the shallow unconfined aquifer 304
Figure 7-47. Upper estimate of transmissivity of the shallow unconfined aquifer 305
Figure 7-48. Interpreted elevation (m AHD) of the watertable surface 308
Figure 7-49. Depth to watertable 309
Figure 7-50. Saturated thickness of the shallow unconfined aquifer 310
Figure 7-51. Saturated thickness of the shallow unconfined aquifer 311
Figure 7-52. Hydrographs of BHMAR84-3 and 84-4 screened in the Coonambidgal Formation at Jimargil 312
Figure 7-53. Hydrographs for bores BHMAR77-3 and BHMAR92-2 screened in Menindee Formation at East Bootingee 312
Figure 7-54. Textural composition of the Coonambidgal Formation, Menindee Formation and Willotia beds 314
Figure 7-55. Map with pie chart textural composition of the Menindee and Coonambidgal Formations 315
Figure 7-56. Map with pie chart textural composition for the Willotia beds 316
Figure 7-57. Indicative lithology of shallow sediments for the 0-1.6 m AEM depth slice 317
Figure 7-58. Indicative lithology of shallow sediments for the 1.6-2.2 m AEM depth slice 318
Figure 7-59. Indicative lithology of shallow sediments for the 2.2-2.8 m AEM depth slice 319
Figure 7-60. Indicative lithology of shallow sediments for the 2.8-3.5 m AEM depth slice 320
Figure 7-61. Indicative lithology of shallow sediments for the 3.5-4.4 m AEM depth slice 321
Figure 7-62. Indicative lithology of shallow sediments for the 4.4-5.3 m AEM depth slice 322
Figure 7-63. Indicative lithology of shallow sediments for the 5.3-6.4 m AEM depth slice 323
Figure 7-64. Indicative lithology of shallow sediments for the 6.4-7.7 m AEM depth slice 324
Figure 7-65. Indicative lithology of 7.7-9.2 m AEM depth slice 325
Figure 7-66. Thickness of near-surface aquitard 326
Figure 7-67. Percentage thickness of near-surface aquitard from the ground surface to the base of the Darling River 327
Figure 8-1. Piper diagram of major ion analyses of rainfall, surface water and groundwater samples 330
Figure 8-2. Piper diagram of major ion analyses of pore fluid samples 330
Figure 8-3. Scatter plots of EC and TDS for BHMAR water samples 333
Figure 8-4. Scatter plots of Cl and Na for BHMAR water samples 336
Figure 8-5. Scatter plots of Na and HCO_3 in mmol/L for BHMAR water samples 337
Figure 8-6. Scatter plots of Na + K and Ca + Mg in mmol/L for BHMAR water samples 339
Figure 8-7. Scatter plots of Cl and (Ca + Mg)/HCO_3 ratio in mmol/L for BHMAR water samples 340
Figure 8-8. Scatter plots of SO_4 and Ca + Mg in mmol/L for BHMAR water samples 341
Figure 8-9. Scatter plots of Ca + Mg and Na + K normalised to Cl in mmol/L for BHMAR water samples 342
Figure 8-10. Scatter plots of SO_4 + HCO_3 and Ca + Mg in meq/L for BHMAR water samples 343
Figure 8-11. Scatter plots of Na and K in mmol/L for BHMAR water samples 344
Figure 8-12. Piper diagram of Darling River surface water samples grouped by river flow 345
Figure 8-13. Scatter plots of Cl and Br/Cl ratio in mmol/L for BHMAR water samples 346
Figure 8-14. Scatter plots of analytes for Darling River surface water samples grouped into fuzzy k-means classes 348
Figure 8-15. Piper diagram of major ion analyses of BHMAR surface waters and groundwaters grouped by fuzzy k-means classes 349

Figure 8-16. Piper diagram of major ion analyses of BHMAR pore fluids classified by fuzzy k-means 349
Figure 8-17. Map of fuzzy k-means classification of shallow groundwater samples..... 351
Figure 8-18. Map of fuzzy-k means classification of Calivil Formation and Loxton-Parilla Sands groundwater samples 352
Figure 8-19. Fuzzy k-means classification of Renmark Group groundwater samples..... 353
Figure 8-20. Downhole plots of fuzzy k-means classification of pore fluids. 355
Figure 8-21. Map showing least evolved fuzzy k-means pore fluid class within the Calivil Formation. 357
Figure 8-22. Map showing least evolved fuzzy k-means pore fluid class within the Blanchetown Clay. ... 358
Figure 8-23. Downhole fuzzy class recharge index for a transect of Menindee Common BHMAR bores. 359
Figure 8-24. Map showing the maximum recharge index defined by pore fluid fuzzy-k mean classes for Calivil Formation interval in BHMAR sonic holes. 360
Figure 8-25. Map showing the maximum recharge index defined by pore fluid fuzzy-k mean classes for Blanchetown Clay interval in BHMAR sonic holes. 361
Figure 8-26. Map showing relative influence of lateral and vertical recharge processes..... 362
Figure 8-27. Scatter plot of maximum recharge index for Calivil Formation pore fluids against maximum recharge index for Blanchetown Clay pore fluids 363
Figure 8-28. Stable isotope plots from Hughes et al. (2009)..... 365
Figure 8-29. Stable isotope plot of $\delta^{18}O$ and $\delta^{2}H$ for BHMAR rain water and surface water samples..... 366
Figure 8-30. Scatter plot of $\delta^{18}O$ and $\delta^{2}H$ for BHMAR groundwater samples 367
Figure 8-31 Scatter plots of $\delta^{18}O$ and $\delta^{2}H$ for BHMAR groundwater samples..... 368
Figure 8-32. Scatter plot of $\delta^{2}H$ and Cl for BHMAR groundwater samples..... 369
Figure 8-33. Plot of Darling River discharge at Weir 32 and corresponding $\delta^{2}H$ values measured at sites along the river. 370
Figure 8-34. Rating curve for Darling River gauging station at Weir 32..... 370
Figure 8-35. pMC scatter plots for BHMAR groundwater samples..... 373
Figure 8-36. Map showing pMC of sampled groundwaters in the shallow unconfined aquifer. 375
Figure 8-37. Map showing pMC of sampled groundwaters in the Calivil Formation aquifer. 376
Figure 8-38. Map showing pMC of sampled groundwaters in the Renmark Group. 377
Figure 8-39. pMC scatter plots with other carbon analytes for BHMAR groundwater samples..... 379
Figure 8-40. $\delta^{13}C$ scatter plots for BHMAR groundwater samples..... 380
Figure 8-41. Comparison of uncorrected ^{14}C age with corrected ^{14}C age by Fontes & Garnier (F-G) method. 381
Figure 8-42. Scatter plots of CFC-11 and CFC-12 ages and concentrations for BHMAR groundwaters.... 383
Figure 8-43. Scatter plots of CFC-12 and sample depth for BHMAR groundwaters 384
Figure 8-44. Scatter plots of pMC and CFC-12 for BHMAR groundwaters 384
Figure 8-45. Map of showing pMC and CFC-12 ages of sampled groundwaters in the shallow unconfined aquifer 385
Figure 8-46. Map showing pMC and CFC-12 ages of sampled groundwaters in the Calivil Formation aquifer 386
Figure 8-47. Map showing pMC and CFC-12 ages of sampled groundwaters in the Renmark Group..... 387
Figure 8-48. ^{222}Rn scatter plots for BHMAR groundwaters..... 389
Figure 8-49. Map showing groundwater ^{222}Rn (Bq/L) in the shallow unconfined aquifer 390
Figure 8-50. Map showing groundwater ^{222}Rn (Bq/L) in the Calivil Formation aquifer 391
Figure 8-51. Map showing groundwater ^{222}Rn (Bq/L) in the Renmark Group 392
Figure 8-52. Scatter plots of $^{87}Sr/^{86}Sr$ ratio for BHMAR groundwaters..... 393
Figure 9-1. Location of groundwater level monitoring network in the BHMAR project area..... 396
Figure 9-2. Temperature recordings from the Darling River 401
Figure 9-3. Seasonal groundwater temperature variation in BHMAR84-3..... 401
Figure 9-4. Time series monitoring of groundwater elevation and temperature for BHMAR80A-2..... 402
Figure 9-5. Section showing geometry and parameters for calculating groundwater mound (from Bouwer, 2002)..... 404
Figure 9-6. Number and proportion of flow events exceeding flow thresholds for Darling River at Weir 32 flow record. 407
Figure 9-7. Stable isotope plot of oxygen-18 and deuterium for BHMAR groundwater samples 419
Figure 9-8. Radiocarbon ages of BHMAR groundwater samples plotted against sample depth and classified by formation..... 420

Figure 9-9. Radiocarbon ages of BHMAR groundwater samples plotted against sample depth and classified by distance to surface water 420
Figure 9-10. Conceptual model for groundwater recharge in the Darling Floodplain alluvial sediments. .. 423
Figure 9-11. Location of surface sample site on Menindee Common 425
Figure 9-12. Menindee Common sample collection point, looking southwest 425
Figure 9-13. Muddy slope mantle covering river bank 426
Figure 9-14 View northwest across the Darling River showing dark muddy slope deposits 426
Figure 9-15. Pre and post flood photographs of Darling River bank 427
Figure 9-16. East bank of Darling River downstream of East Bootingee showing variable but strong erosion. 428
Figure 9-17. East bank of Darling River downstream of East Bootingee showing downslope transport 428
Figure 9-18. Menindee Formation overbank muds overlying carbonate-cemented lateral-accretion sands 429
Figure 9-19. Closer view of carbonate-cemented sands. 430
Figure 9-20. Menindee Formation lateral accretion sands in BHMAR77-2 430
Figure 9-21. Oblique aerial photographs of flood observation site on 18 March, 2011. 433
Figure 9-22. Images of area of flood observations. 434
Figure 9-23. Topographic profile of flood observation site. 434
Figure 9-24. Pre-flood view from point 4 435
Figure 9-25. Flood processes on October 2010. 436
Figure 9-26. Flood processes on October 2010 (continued) 437
Figure 9-27. Post flood photographs on September 2011. 440
Figure 9-28. Post flood photographs on September 2011 (continued). 441
Figure 9-29. In-river survey single beam echo sounder data draped over the LiDAR dataset 444
Figure 9-30. Photograph of the Darling River bed during drought, including perennial waterhole 444
Figure 9-31. Comparison between river channel elevation and top of the upper confining aquitard 445
Figure 9-32 Predictive assessment of modern recharge potential and dominant recharge pathways 447
Figure 10-1. Monthly rainfall data for Menindee Post Office. 450
Figure 10-2. Lake levels for Lakes Pamamaroo, Cawndilla and Wetherell 453
Figure 10-3. Murray-Darling Basin including the Darling River and tributaries 454
Figure 10-4. Rivers and creeks in the BHMAR study area 456
Figure 10-5. River flow data for Wilcannia, Weir 32 and Burtundy 458
Figure 10-6. River level data for Wilcannia, Weir 32 and Burtundy 458
Figure 10-7. Images of the Menindee region during flooding in March 2011 460
Figure 10-8. Conceptual model of connectivity between Calivil Formation and shallow aquifer 462
Figure 10-9. Depth to top of the upper confining aquitard 463
Figure 10-10. Upper confining aquitard thickness map 464
Figure 10-11. Depth to the watertable 465
Figure 10-12. Pre-existing Landsat derived vegetation species mapping 466
Figure 10-13. Photos of River Red Gum and Black Box 467
Figure 10-14. Photos of woody vegetation subject to too much and too little water 470
Figure 10-15. Spatial distribution of vegetation structural classes as defined by Landsat imagery 472
Figure 10-16. Discretization of the study area into different geomorphic populations 473
Figure 10-17. Graphical representation of the generation and amalgamation of statistics for Landsat temporal analysis 474
Figure 10-18. Example of an annual Landsat time series profile 477
Figure 10-19. Lake Menindee LiDAR DEM 479
Figure 10-20. 1945 aerial photographs of Lake Menindee 480
Figure 10-21. 2009 LiDAR vegetation structural mapping at Lake Menindee 481
Figure 10-22. NDVI values for lake-fringing woody vegetation in 2009 at Lake Menindee 483
Figure 10-23. Comparison between vegetation condition in 2009 with respect to 2004 at Lake Menindee 484
Figure 10-24. Variation in lake-fringing vegetation condition during the drought at Lake Menindee 485
Figure 10-25. Depth to top of the upper confining aquitard for Lake Menindee 486
Figure 10-26. Hydrographic response in Calivil Formation at Lake Menindee 487
Figure 10-27. Depth to watertable at Lake Menindee 488
Figure 10-28. Lake Cawndilla LiDAR 490
Figure 10-29. 1945 aerial photographs of Lake Cawndilla 491
Figure 10-30. 2009 LiDAR vegetation structural mapping at Lake Cawndilla 492

Figure 10-31. NDVI values for lake-fringing woody vegetation in 2009 at Lake Cawndilla 493
Figure 10-32. Comparison between vegetation condition in 2009 and in 2004 at Lake Cawndilla 494
Figure 10-33. Variation in lake-fringing vegetation condition during the drought at Lake Cawndilla 495
Figure 10-34. Relative reliance of lake-fringing vegetation on groundwater and surface water at Lake Cawndilla 496
Figure 10-35. Depth to watertable at Lake Cawndilla 497
Figure 10-36. Lake Pamamaroo LiDAR DEM 498
Figure 10-37. 1945 aerial photographs of Lake Pamamaroo 499
Figure 10-38. 2009 LiDAR vegetation structural mapping at Lake Pamamaroo 500
Figure 10-39. Location of Lake Wetherell in relation to nearby lakes 501
Figure 10-40. Vegetation habitat mapping in associated with Lakes Wetherell and Tandure 502
Figure 10-41. Lake Tandou LiDAR DEM 503
Figure 10-42. 1945 aerial photographs of Lake Tandou 504
Figure 10-43. 2009 LiDAR vegetation structural mapping at Lake Tandou 505
Figure 10-44. NDVI values for lake-fringing woody vegetation in 2009 at Lake Tandou 507
Figure 10-45. Comparison between vegetation condition in 2009 with respect to 2004 at Lake Tandou 508
Figure 10-46. Variation in lake-fringing vegetation condition during the drought at Lake Tandou 509
Figure 10-47. Relative reliance of lake-fringing vegetation on groundwater and surface water 510
Figure 10-48. Extent and distribution of woody vegetation within the three flood elevation zones 512
Figure 10-49. Landsat time series analysis for open forest, woodland and open woodland vegetation fringing Lake Pamamaroo 513
Figure 10-50. Landsat time series analysis for open forest, woodland and open woodland vegetation fringing Lakes Menindee and Cawndilla 514
Figure 10-51. Black Box vegetation at Lake Speculation 515
Figure 10-52. Landsat time series analysis for Black Box and open forest vegetation fringing Lake Speculation 516
Figure 10-53. Analysis of different vegetation structural classes with regards to condition pre- and post-2002 518
Figure 10-54. NDVI values for lake-fringing woody vegetation in 2009 521
Figure 10-55. Comparison between vegetation condition in 2009 with respect to 2004 523
Figure 10-56. Variation in lake-fringing vegetation condition during the drought 525
Figure 10-57. Relative reliance of lake-fringing woody vegetation on groundwater and surface water 528
Figure 10-58. Analysis of different vegetation structural classes with regards to condition pre- and post-2002 533
Figure 10-59. Hydrographic data for BHMAR84-4 535
Figure 10-60. Time series vegetation condition analysis for Darling River A 536
Figure 10-61. Reliability of source water at Darling River A 537
Figure 10-62. Depth to top of the upper confining aquitard for Darling River A 538
Figure 10-63. Depth to watertable at Darling River A 539
Figure 10-64. Hydrographic data for BHMAR34 540
Figure 10-65. Depth to top of the upper confining aquitard for Darling River B 541
Figure 10-66. Time series vegetation condition analysis for Darling River B 543
Figure 10-67. Reliability of source water at Darling River B 544
Figure 10-68. Depth to watertable at Darling River B 545
Figure 10-69. Time series vegetation condition analysis for Darling River C 547
Figure 10-70. Reliability of source water at Darling River C 548
Figure 10-71. Depth to watertable at Darling River C 549
Figure 10-72. Time series vegetation condition analysis for Darling River D 551
Figure 10-73. Reliability of source water at Darling River D 552
Figure 10-74. Depth to watertable at Darling River D 553
Figure 10-75. Depth to top of the upper confining aquitard for Darling River D 554
Figure 10-76. Time series vegetation condition analysis for Talyawalka Creek 556
Figure 10-77. Depth to watertable at Talyawalka Creek 557
Figure 10-78. Saturated thickness of the shallow unconfined aquifer along Talyawalka Creek 558
Figure 10-79. Percentage thickness of near-surface aquitard along Talyawalka Creek 559
Figure 10-80. Depth to top of the upper confining aquitard around Talyawalka Creek 560
Figure 10-81. Time series vegetation condition analysis for Seven and Nine Mile Creeks 561

Figure 10-82. Reliability of source water at Seven and Nine Mile Creeks 562
Figure 10-83. Depth to watertable at Seven and Nine Mile Creeks 563
Figure 10-84. Percentage thickness of near-surface aquitard along Seven and Nine Mile Creeks 564
Figure 10-85. Time series vegetation condition analysis for Three Mile Creek 565
Figure 10-86. Depth to watertable at Three Mile Creek..... 566
Figure 10-87. Time series vegetation condition analysis for Tandou Creek, Redbank Creek and Darling Anabranch..... 569
Figure 10-88. Reliability of source water at Tandou Creek, Redbank Creek and Darling Anabranch 571
Figure 10-89. Depth to watertable at Tandou Creek, Redbank Creek and Darling Anabranch 572
Figure 10-90. Depth to top of the upper confining aquitard for Tandou Creek, Redbank Creek and Darling Anabranch..... 573
Figure 10-91. Time series vegetation condition analysis for Charlie Stones Creek and Yampoola Creek.. 575
Figure 10-92. Reliability of source water at Charlie Stones Creek and Yampoola Creek 576
Figure 10-93. Depth to watertable at Charlie Stones Creek and Yampoola Creek 577
Figure 10-94. Time series vegetation condition analysis for Coonalhugga Creek..... 578
Figure 10-95. Depth to watertable at Coonalhugga Creek 579
Figure 10-96. Reliability of source water at Coonalhugga Creek 580
Figure 11-1. Regional salinity-yield mapping for the Pliocene Sands aquifer. 591
Figure 11-2. Regional distribution of average rainfall. 592
Figure 11-3. Regional distribution of vegetation and cropping/pasture. 593
Figure 11-4. Regional aeromagnetics, Pliocene Sands salinity-yield mapping and extent of Blanchetown Clay. 594
Figure 11-5. Image showing the upper reaches of the Darling River, marked to show the gaining and losing reaches. 598
Figure 12-1. Perspective view of BHMAR Project AEM 3D conductivity model 601

LIST OF TABLES

Table A. Stratigraphic column showing the relationships between geological units iv
Table 2-1. Elevations, depths, areas and capacities of MLS lakes 13
Table 2-2. Mass-balance evaporation estimates for Lakes Wetherell and Pamamaroo 19
Table 2-3. SEBAL 2009 evaporation estimates for Lakes Wetherell and Pamamaroo 20
Table 5-1. BHMAR sonic bores with significant thicknesses of Renmark Group 48
Table 5-2. All sonic bores that intersected the Renmark Group 50
Table 5-3. BHMAR boreholes with problematic contacts between the Renmark Group and Calivil Formation 51
Table 5-4. Renmark Group sand bed thickness 52
Table 5-5. Renmark Group lithology on contact with the Calivil Formation in all BHMAR holes 54
Table 5-6. Renmark Group lithology on contact with the Calivil Formation in Jimargil boreholes 54
Table 5-7. Murray Basin pollen zones 72
Table 5-8. Comparison between inferred features of the Renmark Group and its modern analogue, the Magdalena River 75
Table 5-9. Distribution of Calivil Formation and Loxton-Parilla Sands in the southernmost project bores 85
Table 5-10. Compositional information about the Calivil Formation based on thin section analysis 102
Table 5-11. Percentage and abundance of different grain types within the Calivil Formation based on thin section analysis 102
Table 5-12. Interpreted channel widths 107
Table 5-13. Gravel bed river facies models 110
Table 5-14. Bedload-dominant sand river facies models 110
Table 5-15. Cement stratigraphy 115
Table 5-16. Stratigraphic column showing the relationships between geological units 154
Table 5-17. Stratigraphic description of Willotia beds in BHMAR boreholes 161
Table 5-18. Quaternary fluvial formations recognised in the lower Darling Valley 172
Table 5-19. Meander geometry of lower Darling Coonambidgal Formation lateral migration phases 173
Table 5-20. Mud and sand-facies and total thickness of Quaternary lateral-migration fluvial units measured in BHMAR boreholes 176
Table 5-21. Mud facies and total thickness of Quaternary lateral-migration fluvial units measured in BHMAR boreholes 177
Table 5-22. Summary table of OSL samples, location and ages dating results 182
Table 5-23. OSL results categorised by formation 183
Table 5-24. Radiocarbon dating for different pre-treatment regimes 183
Table 5-25. Radiocarbon dating results for a wood sample at BHMAR79A-2 using different pre-treatment regimes 189
Table 7-1. Characteristics of the Calivil Formation aquifer in the BHMAR study area 257
Table 7-2. Summary statistics for salinity of Blanchetown Clay pore fluids 288
Table 7-3. Combinations of D_e and C/C_o used to derive diffusion distances in the upper confining aquitard 289
Table 7-4. Characteristics of the shallow Quaternary aquifer in the BHMAR study area 294
Table 8-1. Summary of BHMAR hydrochemical analyses 328
Table 8-2. Analytical averages for the classification of BHMAR water samples using fuzzy k-means 347
Table 8-3. Classification of BHMAR water samples using fuzzy k-means 347
Table 8-4. Assumptions used in correction models for radiocarbon ages 378
Table 9-1. Summary of groundwater response in BHMAR bores with onset of flood from 14/10/2010 398
Table 9-2. Recharge estimates for unconfined aquifers based on watertable fluctuation method 399
Table 9-3. Summary of input parameters for travel time estimates through Blanchetown Clay profile 403
Table 9-4. Sensitivity analysis of travel time through Blanchetown Clay profile 403
Table 9-5. Summary of estimates of infiltration rates using Bouwer (2002) groundwater mounding equation 405
Table 9-6. Summary of events exceeding flow thresholds for the Darling River at Weir 32 gauge record (1974-2012) 406
Table 9-7. Summary statistics of diffuse recharge rates using groundwater chloride mass balance 409
Table 9-8. Summary of radiocarbon recharge estimates for selected Jimargil bores 411

Table 9-9. Comparison of recharge estimates using different methods for sites at Jimargil 412
Table 9-10. Distribution of NMR free and bound water in vadose zone of inundated floodplain areas 438
Table 10-1. Natural sill levels and artificial full supply and surcharge levels for the Menindee Lakes 451
Table 10-2. Minimum monthly flow requirements for the Darling River 457
Table 10-3. Maximum river gauge levels for five of the largest historic floods within the Barwon-Darling catchment 459
Table 10-4. General water regime specifications and tolerances for maintenance of mature River Red Gums 470
Table 10-5. General water regime specifications and tolerances for maintenance of mature Black Box 471
Table 10-6. Classification of vegetation condition in terms of overall trend in behaviour and comparison between start and finish of the drought 475
Table 10-7. Classification of vegetation condition at the conclusion of the drought 475
Table 10-8. Different water level conditions for each lake 478
Table 11-1. Summary of the Western Murray Porous Rock Groundwater Source. 586
Table 11-2. Diversion Limits for BHMAR groundwater resource units under the Basin Plan 587
Table 11-3. Water balances using river system modelling and monthly accounting approaches for two Darling River reaches 596
Table 11-4. Comparison of Darling River main stem inflows and outflows for specific wet years 597
Table 12-1. Comparison between the sediments of the Tucson Basin and the Menindee project area 603

1. Introduction

1.1 BACKGROUND

Recent periods of prolonged drought and predictions of a drier future for the southern half of Australia under a number of climate change scenarios (Barron *et al*., 2011) have led to the search for innovative strategies to identify more secure water supplies for regional communities and industries, while also delivering environmental benefits to threatened river systems. These issues are particularly pressing in the Murray-Darling Basin (the Basin), where the recent Millennium Drought (late 1990's - 2010) adversely affected many communities, industries and the environment (MDBA, 2010a, b). While subsequent heavy rains and flooding associated with La Niña cycles broke the drought in late 2010-2012, there is general recognition of the need to provide longer-term strategic solutions to achieve a healthier working Basin (MDBA, 2010b; 2011; 2012b).

It has long been recognised that one of the areas with the greatest potential to contribute water savings in the Basin is at the Menindee Lakes Storages (MLS), located on the lower section of the Darling River in far western New South Wales, adjacent to the township of Menindee (Figure 1-1). The MLS provide the main water supply storage (up to 2,100 gigalitres, GL) in the lower Murray-Darling River system, and play a significant role in meeting South Australia's water requirements. The MLS are also the principal water supply storage for the City of Broken Hill, which is supplied via a 110 km pipeline (Figure 2-1). The MLS also provide water locally near Menindee for irrigators and stock and domestic use.

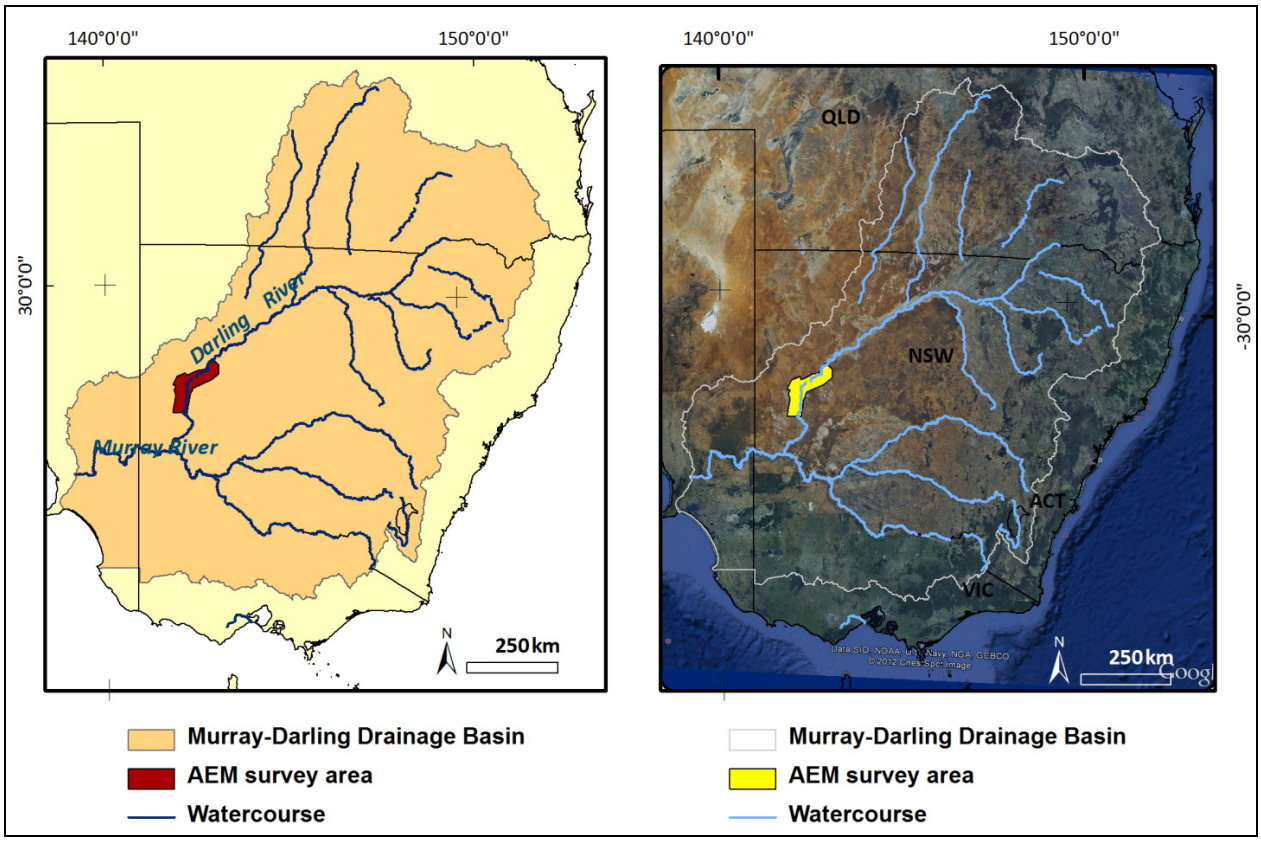

Figure 1-1. *Location of the BHMAR study area in relation to the Murray-Darling Drainage Basin in south-eastern Australia.*

The shallow nature of the lakes in this hot and windy semi-arid environment results in significant evaporation (Evans *et al*., 2009; MDBA, 2010a; Chiew *et al.*, 2002). It is estimated that the average evaporation loss for the MLS as a whole is in the order of 420 GL per year, and a nominal market value of some $420 m. This quantity is nearly 10 % of the entire surface water diversion in the Basin for the last three years (MDBA, 2010a), and is similar to the 500 GL/yr figure identified for recovery under the Living Murray Program (MDBA, 2010a). Moreover, evaporative losses increase to approximately 700 GL/yr when the Lakes are full (Maunsell, 2007). The opportunity cost of this water evaporating each year is realised by downstream irrigators, communities and ecosystems.

Currently, management of the MLS aims to maintain a minimum storage of 300 GL in order to secure Broken Hill's water requirements (of <10 GL/yr) in times of drought. This volume is estimated to guarantee a 21 month supply, and when the supply is depleted to 18 months the upper river intakes are managed to attempt to regain the 21 month supply. However, during the recent Millennium Drought even this storage has proven insufficient to provide a secure supply of suitable quality water to Broken Hill. For example, in 2002-2003, reservoirs at Broken Hill were empty, and there was insufficient storage in Lake Wetherell in the MLS (Country Water, pers. comm., 2009). This led to sourcing of water from the residual pool of water at Lake Menindee. This water was of poor quality (2,300 EC), yet was supplied to the residents of Broken Hill, despite being significantly above the 1500 EC limit deemed acceptable for human consumption (Country Water, pers. comm., 2009). With even that source in danger of running dry, plans were made to bring in water supplies by train at significant cost, while a Reverse Osmosis (RO) plant was constructed (but never commissioned). The situation was only saved when floodwaters came down the Darling River (Country Water, pers. comm., 2009).

Changing the management of the MLS to provide enhanced water security for Broken Hill, reduce these evaporative losses, and provide downstream economic and environmental benefits is possible, but Broken Hill's water supply would first need to become less reliant on the MLS. To address these issues, in 2008 the Australian Government confirmed its 2007 election policy commitment to "invest in water saving infrastructure from the National Plan for Water Security and to invest up to $400 million to reduce evaporation and improve water efficiency at Menindee Lakes on the Darling River in Western New South Wales, secure Broken Hill's water supply, protect the local environment and heritage and return up to 200 billion litres to the Murray Darling Basin". This included a commitment to work with the New South Wales (NSW) Government and the local community to improve the Menindee Lakes water storage system.

1.2 RECENT RESEARCH INTO SECURING BROKEN HILL'S WATER SUPPLY AND IDENTIFYING SIGNIFICANT WATER SAVINGS

In 2006, Australian and NSW Governments jointly funded investigations (Maunsell, 2007; SKM, 2009a, 2010) to identify opportunities for substantial water savings in the Darling River System, including the Menindee Lakes. The outcome was to be a 20-year Strategic Plan for water savings, based on an integrated approach of structural works, river and storage operating strategies and water market activities. The study was organised in two parts:

- Part A, aimed at generating and broadly screening a large number of options and then compiling from these a manageable number of alternate, integrated water saving schemes.
- Part B, developing the Darling River System Strategic Plan. This was to follow a benefit/cost analysis of short-listed schemes and a preliminary environmental assessment.

In April 2007, Part A of the feasibility study entitled 'Darling River Water Savings Project (DRWSP)' was published (Maunsell, 2007). The Part A study modelled a number of options from which the most promising were used to develop six different integrated water saving schemes. These were considered to be core options for reconfiguration of the MLS to reduce evaporative losses and achieve significant water savings. It was on the basis of the Part A findings that the 2007 Australian Government funding commitment was made.

Following the November 2007 election, the DRWSP Part B study was jointly funded by the Australian and NSW governments to provide detailed information and analysis needed to assess the technical feasibility and further development of the proposed water saving schemes. The Part B study further refined the basic options identified in the Part A Report, in particular, focusing more on storage management options rather

than engineering solutions such as partitioning the Lakes. Extensive hydrological modelling was undertaken across some 90 options to evaluate the impact of different infrastructure and operational rules. The Part B Final Report, completed in March 2010 (SKM, 2009a, 2010), focussed on six options ranging from minimal changes to significant change, and generating a wide range of water savings at Menindee Lakes.

In July 2010, following completion of the DRWSP, the NSW and Australian Governments signed a Memorandum of Understanding (MOU) to guide cooperative investigation and subsequent implementation of key water reform initiatives in NSW, including for Broken Hill's water supply and Menindee Lakes' operational arrangements. The MOU committed the two governments to a program of joint work up to the end of 2010 including:

- Additional technical investigations to establish the feasibility (and cost) of using local aquifers to secure Broken Hill's water supply in drought periods;
- Further analysis (including modelling) of infrastructure and operational changes at Menindee Lakes to deliver substantial water savings, while protecting the local environment and heritage, and ensuring no directly attributable adverse impact on water entitlement security of irrigators at Menindee Lakes, and in the Lower Darling and Murray Rivers.
- Public consultation on changed arrangements at Menindee Lakes and the proposal for Broken Hill's water supply to be made less reliant on supplies from Menindee Lakes.

1.2.1 Hydrology and Evaporation Studies

1.2.1.1 MLS Evaporation Estimation

In hot, windy, semi-arid environments like the Darling River floodplain, evaporation from shallow reservoirs like the MLS is often a significant component of the water balance, although accurate quantification is often limited. Estimating the amount of evaporation from the MLS has been a particularly contentious issue, given the debate about possible changes to the MLS operating regime to reduce evaporative losses.

Several methods exist to estimate evaporation from reservoirs, however, these are often data intensive and not considered cost-effective. In the Broken Hill region, the pan coefficient method, which is considered to be the least accurate of these methods (Evans *et al*., 2009), has traditionally been used to measure evaporation at the MLS and other local reservoirs (Country Water, pers. comm., 2010).

There have been several previous studies that have attempted to estimate evaporative losses from the MLS. Estimates are often reported but poorly justified. These studies are discussed in more detail in Section 2.2.3. The obvious exception to this is the work done by Sinclair Knight Merz (Evans *et al*., 2009). The SEBAL (Surface Energy Balance Algorithm for Land) method, which was initially developed for estimating evapotranspiration from land at large scales using satellite imagery (Bastiaanssen *et al.,* 1998), was trialled to estimate evaporation from the MLS system (Evans *et al.,* 2009). The trial application, funded by the Australian Government's National Water Commission, examined data for the 2004/05 period, when water remained in only two of the lakes (Lake Wetherell and Lake Pamamaroo). The other lakes had been dry since 2002.

The SEBAL estimates of evaporation from the MLS were compared with local pan evaporation data. The study found that, based on 2004/05 data, and using a uniform pan factor of 0.7 across the year, would result in winter evaporation being overestimated by up to 20% and summer evaporation being underestimated by up to 10 % (Evans *et al*., 2009). The SEBAL 2009 measurements of evaporation were then compared to estimates of evaporation calculated using a traditional water balance method. The results of this comparison, show that provided the appropriate water depth assessment method is selected, the SEBAL method was able to produce accurate estimates of evaporation from water storages (Evans *et al*., 2009). More details about the study can be found in Section 2.2.3.

Using this method, it was determined that 133 GL of water evaporated from Lake Wetherell, and 118 GL from Lake Pamamaroo in 2004/05. This represents 63.7% of the maximum storage capacity of Lake Wetherell (209 GL) and 42.5% of the maximum storage capacity of Lake Pamamaroo (277 GL). The

evaporation rates are actually similar, with the differences largely due to the larger surface area to volume ratio within Lake Wetherell.

Overall, the SEBAL study would appear to confirm the very significant contribution that evaporation losses make to the water balance in the MLS (Evans *et al*., 2009). It also confirms that the current strategy of retaining a minimum of 300 GL supply in the MLS would not provide much more than 21 months supply for Broken Hill without augmentation by diversion of additional river flows. As demonstrated in the 2002-2005 period, this strategy fails if additional flows are not available for diversion. Overall, given historical flow and climate records for the past century, it would seem prudent to provide additional drought security for Broken Hill by putting in place alternative supply options that anticipate future droughts and negligible river flows lasting for periods greater than 21 months. The prudence of planning for such droughts is only reinforced by projections of drier climates forecast by many climate change models (Barron *et al.,* 2011).

1.2.1.2 Surface Hydrological Modelling

There have been a number of studies of the hydrology of the Darling River (e.g. CSIRO, 2008a, b, Barma, 2010, SKM, 2010; and reviewed in Podger, 2010). However, as part of the process of identifying a preferred option for a Menindee Lakes Project, the Australian Government engaged the Commonwealth Scientific and Industrial Research Organisation (CSIRO), in conjunction with the Murray-Darling Basin Authority (MDBA), to report on hydrological modelling of different management options for the Menindee Lakes.

This work was undertaken to determine the potential volume of water savings that could be transferred to the Commonwealth Environmental Water Holder. This work took into account climate change scenarios and scenarios projecting no adverse impacts on the water entitlement holders at Menindee Lakes, the Lower Darling River or the Murray River (Podger, 2010, 2011) The hydrological modelling took account of a range of stakeholder concerns, and assessed potential changes to the operational rules for the MLS that could have a positive impact on all indicators (Podger, 2011).

In response to these requirements, CSIRO identified an option that was predicted under conditions of adopting a more natural filling regime in Lakes Menindee and Cawndilla; a 185/185 operating rule to replace the existing 640/480 rule; the Lake Menindee outlet being increased to 14,400 ML/day; and Broken Hill's water supply being secured (Podger, 2010).

There were a number of positive impacts predicted for the proposed option including (1) increased flows in the lower reaches of the Darling and Murray Rivers (including the Lower Lakes and Coorong); (2) improved allocations in dry years; (3) South Australian water restrictions would be reduced on average; and (4) improved allocations would be available in the Lower Darling and Victoria. The study also projected that there would be some minor downstream impacts, all of which were either within the error of the model or could be offset; for example the NSW Murray November allocations might decrease on average by 1% (which was considered to be within the model error) but would be recovered by June. However, these savings are dependent upon implementation of conjunctive use options involving groundwater extraction or MAR to secure Broken Hill (and Menindee's) water supply during droughts.

1.2.2 Geoscience Australia Hydrogeological Investigations

Central to the plan to realise water savings from the MLS is the identification of alternative water supply options to ensure Broken Hill's water supply during periods of prolonged drought. To this end, in 2008 the Department of Sustainability, Environment, Water, Population and Communities (SEWPaC) initially funded a regional groundwater assessment project (the Broken Hill Groundwater Assessment (BHGA) project).

1.2.2.1 BHGA Project

The BHGA Project (Lewis *et al.,* 2008), found that the opportunity existed to develop an integrated water supply strategy to secure Broken Hill's water supply and allow for significant amounts of water currently stored at Menindee Lakes to be returned to the environment by developing Managed Aquifer Recharge (MAR) options. The study concluded that this could be achieved by integrating the existing surface water operations at the Menindee Lakes Storages and the Stephens Creek and Umberumberka Reservoirs with groundwater options.

Lewis *et al.* (2008) identified nine potential areas for further groundwater investigation in the Broken Hill region, although subsequent considerations of the hydrogeology and infrastructure costs reduced this to five priority areas (Lawrie *et al*., 2009a). Among the measures suggested was the purposeful recharge of water to aquifers for subsequent recovery and/or environmental benefit (Managed Aquifer Recharge (MAR)). MAR encompasses a wide variety of methods usually adapted to local situations which are governed by water quality, the type of aquifer available, topography, land use, and the intended uses of the recovered water (Dillon *et al.,* 2009). Other options identified included the direct extraction of groundwater resources, and/or desalinisation of brackish groundwater (Lewis *et al.,* 2008).

The BHGA study also concluded that the quality and extent of groundwater in the Broken Hill area is poorly understood, and the potential for sourcing significant quantities of previously unallocated fresh and brackish groundwater is thought to be relatively high (Lewis *et al*., 2008). The BHGA study recognised that any future investigations would necessarily entail significant new hydrogeological investigations. A future work plan was identified to assess the potential for MAR and groundwater resource options in the region, and SEWPaC commissioned Geoscience Australia to undertake further scientific investigations (the Broken Hill Managed Aquifer Recharge (BHMAR) project).

1.2.2.2 The BHMAR Project

The primary objective of the Broken Hill Managed Aquifer Recharge (BHMAR) project was to identify potential MAR and/or groundwater resource options to provide a more secure alternative water supply for Broken Hill during droughts. This would reduce the amount of water required to be stored in the MLS, and identify water-saving measures for the Darling River system. The options assessed include MAR schemes such as infiltration basins, Aquifer Storage and Recovery (ASR), Aquifer Storage, Transport and Recovery (ATSR), bank infiltration, as well as groundwater extraction (Lawrie *et al*., 2012c). Any new option would involve retaining a (reduced) capacity within the MLS, with water supply arrangements operating as a conjunctive use scheme with MAR and/or groundwater extraction providing a vital drought-security component. A secondary objective of the project was the identification of other groundwater resources and MAR targets in the Darling Floodplain region to provide improved drought security for local communities and industries (e.g. agriculture and mining; Lawrie *et al*., 2012d).

The boundary of the BHMAR project area relative to the major drainage features including the Menindee Lakes System (MLS) is shown in Figure 2-1. The project area covered 7,541.5 km^2 and was defined primarily by the groundwater salinity-yield mapping from previous investigations (Lewis *et al.,* 2008; Lawrie *et al*., 2008, 2009a,b). While the search for alternative water supply options for Broken Hill was initially on an area within 50 km of Menindee, a relatively larger project area was scoped to identify additional groundwater resources and MAR options to underpin regional development (for agriculture and mining) as well as enhanced water security for regional communities (Lawrie *et al*., 2012d). The size of the project area was also determined by the need to consider the groundwater system holistically, including the broader regional hydrogeological impacts of groundwater use and replenishment on environmental assets. Scientific, technical and logistic considerations and limitations were also taken into consideration, with the project area reduced in size at the end of preliminary assessments (Phase 1), given the short timeframe to complete scientific investigations and interpretation to high confidence levels in such a data-poor area.

For the MAR assessment component of the project (Lawrie *et al*., 2012c, d), investigations have adhered to the stringent assessment framework set out in the Australian Guidelines for Managed Aquifer Recharge

(NRMMC–EPHC–NHMRC, 2009) and Water Recycling: Augmentation of Drinking Water Supplies (NRMMC–EPHC–NHMRC, 2008). The BHMAR project was the first project in Australia to apply these new guidelines, with the assessment framework reflected in a 5-phase work plan designed in accordance with the MAR guidelines:

- Phase 1 (Oct. 2008 - Feb. 2009): Study area finalisation and technical risk assessment / AEM technology selection exercise for six potential project areas for MAR options near Broken Hill;
- Phase 2 (Apr. 2009- Mar. 2012): Acquisition of baseline hydrogeological and geological data to derive a new conceptual groundwater model and identify potential MAR and groundwater resource targets and options across the project area;
- Phase 3a (Jul. 2010- May 2012): Acquisition of additional hydrogeological and geoscientific data to assess the feasibility of MAR and groundwater extraction options at a priority borefield target within 20 km of Menindee, and assess groundwater extraction-only options;
- Phase 3b: Carry out the necessary groundwater modelling and engineering design to optimise borefield design;
- Phase 4: Implement and test preferred groundwater extraction and storage options at a small operational scale;
- Phase 5: Construct and operate groundwater extraction/storage option.

Phase 1 of the project recognised the Darling Floodplain as the area most likely to yield groundwater resource and/or MAR storage options (Lawrie *et al*., 2009a). Phase 2 of the BHMAR project involved a major new data acquisition phase, including an airborne electromagnetics (AEM) survey (32,000 line km); a light detection and ranging (LiDAR) survey (20 cm vertical resolution), a drilling program of 44 sonic and rotary mud holes; borehole geophysics (EM and gamma logging); field mapping, and field and laboratory hydrogeochemical investigations. The Phase 2 study identified a large number of potential MAR targets, and an excellent aquifer (the Calivil Formation), on which subsequent investigations focussed.

Phase 3a of the project commenced in mid-July 2010, with the specific aim of determining, with a defined level of confidence, whether at least 3 years water supply (~30 GL), at a similar salinity to that already available for Broken Hill would be available at all times through new groundwater-related arrangements. While a number of targets were identified (Lawrie *et al*., 2009a, 2010a), ranking of targets led investigations to focus on a single priority target (GWR1), south of Menindee township. The target was the semi-confined to leaky-confined Pliocene Calivil Formation aquifer at depths of 30-80 m below surface.

Investigations initially focussed on two small sub-areas (Jimargil and Menindee Common) within this target (Lawrie *et al*., 2010a). These sub-areas were chosen to address bank filtration, basin infiltration and ASR options, and contain two end members of the hydrogeological system within the aquifer. Both sites were considered representative of potential future borefield sites. Subsequently, work focussed primarily on the Jimargil site, with the Menindee Common site found to be less suitable (Lawrie *et al*., 2011). The Jimargil site (and surrounding area), has the appropriate hydrostratigraphy, significant native fresh groundwater, and was accessible in the project timeframes. The interim findings of these investigations have previously been reported (Lawrie *et al.,* 2010a, 2011).

Phase 3a investigations have involved detailed characterisation of the hydrogeological system at a limited number of sites. This was achieved through the drilling of 56 new boreholes (Appendix 1, Halas *et al*., 2012), groundwater pump tests (Appendix 6, Somerville *et al*., 2012; Appendix 13, Apps *et al*., 2012g), hydrogeological, hydrogeophysical (ground and borehole geophysics including borehole NMR; Appendix 10, Apps *et al*., 2012d; Appendix 3, Apps *et al*., 2012f; Appendix 1, Halas *et al.*, 2012), hydrogeochemical sampling and analysis (Appendix 3, Apps *et al*., 2012f), modelling and interpretation. The Phase 3a study assessed a range of possible MAR options including injection, passive or enhanced recharge, and/or conjunctive use involving a combination of surface, groundwater extraction and/or MAR options (Lawrie *et al*., 2012c, d). Pre-commissioning maximal and residual risk assessments have also been undertaken in accordance with national MAR guidelines (NRMMC–EPHC–NHMRC, 2009). This includes accounting for human health risks in water supply, and environmental risks in relation to surface water-groundwater interaction and sustaining groundwater-dependent vegetation.

In the second half of 2011, the emphasis on investigations shifted somewhat, with a request from SEWPaC to explore a greater range of water supply options including assessment of a greater range of MAR options (including a re-examination of infiltration options), as well as groundwater extraction-only options (Lawrie *et al*., 2012c, d). In 2012, a further request was made to include assessment of drought security options over shorter time periods (3 months and up to 3 years). Estimates of groundwater resources across the whole project area were also requested (Lawrie *et al*., 2012d).

Any water savings generated by a Menindee Lakes Project have the potential to make a substantial contribution towards the environmental water needs of the Basin and act as an offset such that less water is required for the shared reduction amount for the southern Basin zone or the Murray and Lower Darling, identified under the Basin Plan (MDBA, 2012b).

1.3 PURPOSE AND SCOPE OF THIS REPORT

This report details the results from geological, hydrogeological and hydrogeochemical investigations, and sets out 3D geological and hydrogeological frameworks and a new hydrogeological conceptual model for the area. The report draws on the detailed findings previously presented in a number of interim reports (Lawrie *et al.,* 2008, 2009a, 2010a, 2011), and the project results presented in accompanying scientific and technical reports (Lawrie *et al.,* 2012a, c, d). The accompanying reports and supporting appendices and digital data are listed below. The full BHMAR study findings are summarised in Lawrie *et al*. (2012e). Overall, the final reports are:

- Final Report 1: Lawrie *et al*. (2012a). BHMAR Project: Data Acquisition, processing, analysis and interpretation methods. This report details the substantive new data investigative program undertaken as part of this project, and includes details of the data acquisition, processing analysis and interpretation methods.
- Final Report 2 (this report): Lawrie *et al*. (2012b). BHMAR Project: Geological and Hydrogeological Framework and Conceptual Model**.** This report details the results from geological, hydrogeological and hydrogeochemical investigations, and sets out 3D geological and hydrogeological frameworks and new hydrogeological conceptual model for the area.
- Final Report 3: Lawrie *et al*. (2012c). BHMAR Project: Securing Broken Hill's Water Supply: Assessment of Conjunctive Water Supply Options Involving Managed Aquifer Recharge Options at Menindee Lakes. This report details the findings of investigations into finding groundwater-related water supply options for Broken Hill within a 20 km radius of Menindee. These options include groundwater extraction and MAR.
- Final Report 4: Lawrie *et al*. (2012d). BHMAR Project: Assessment of Potential Groundwater Resources and Underground Storage Options in the Darling Floodplain. This report details the results of investigations to identify groundwater resources potential MAR options in the greater BHMAR study area within the Darling Floodplain
- Final Report 5: Lawrie *et al*. (2012e). BHMAR Project: Assessment of Conjunctive Water Supply Options to Enhance the Drought Security of Broken Hill, Regional Communities and Industries-Summary Report. This report summarises the results from the BHMAR study.

All the supporting data, analytical, interpretation and product generation methods are included in fifteen accompanying appendix volumes, and all project data and products are available in the BHMAR project GIS (Gow *et al*., 2012a). All ancillary publications are listed below:

- Appendix 1: Halas, *et al*. (2012). Graphical display of borehole geological and geophysical logs and hydrogeochemical data
- Appendix 2: Spulak *et al*. (2012). Core photographs
- Appendix 3: Apps *et al*. (2012f). Borehole geophysical and geological data
- Appendix 4: Apps *et al*. (2012c). AEM data: acquisition reports, inversion and calibration, FiD comparisons, and basic conductivity map and cross-section products
- Appendix 5: Apps *et al*. (2012b). AEM-based interpretation products: maps and cross-sections

- Appendix 6: Somerville, *et al*. (2012). Hydrological, climate, hydrochemical and hydrodynamic data
- Appendix 7: Apps *et al*. (2012e). Age dating.
- Appendix 8: Apps *et al*. (2012a). Recharge models and data
- Appendix 9: Gow *et al*. (2012). Remote sensing /vegetation health analysis background data and intermediate products
- Appendix 10: Apps *et al*. (2012d). Ground and in-river geophysics and supporting data
- Appendix 11: Apps & Lawrie (2012). CSIRO MAR reports
- Appendix 12: Apps & Gibson (2012). Drilling construction, location and remediation data and reports
- Appendix 13: Apps *et al*. (2012g). Borehole Hydraulic Data (contractor reports)
- Appendix 14: Lawrie *et al*. (2012f). LIDAR acquisition and processing contractor reports
- Appendix 15: Magee *et al*. (2012). Cultural Heritage and environmental clearance surveys

Other final products include:

- Halas *et al*. (2012b). Broken Hill Managed Aquifer Recharge Project 3D GoCAD Model.
- De Hoog *et al*. (2012). Broken Hill Managed Aquifer Recharge Project WORLDWIND virtual globe model.
- Caldwell *et al*. (2012). Broken Hill Managed Aquifer Recharge Project. Fly-through movie.

2. Regional Setting

2.1 STUDY AREA

The BHMAR study area is located approximately 100 km south-east of Broken Hill, in the Murray-Darling Drainage Basin within New South Wales (Figure 2-1). The project area covers approximately 7,500 km^2 of the Lower Darling Valley (LDV), a single fluvial system, with multiple channels and distributaries, in a laterally confined, wide, funnel-shaped valley form. The LDV widens southwards into the Murray Geological Basin from about 8 km width at a constriction 25 km upstream of the study area at Wilcannia to about 30 km width some 200 km downstream at the southern boundary of the study area. The LDV is characterized by a very low-gradient fluvial plain with abundant shallow ephemeral lunette lakes. Topography in the area varies only by ~60 m, with a fall in floodplain elevation of about 20 m between the northern and southern extremities of the project area, over a distance of about 175 km. The principal rivers in the floodplain are the Darling River, the Talyawalka and the (Darling) Anabranch. The study area is approximately 100 km upstream of the confluence of the Darling and Murray rivers at the town of Wentworth.

Within the study area, the Menindee Lakes are the most prominent surface water bodies, comprising a group of shallow lakes adjacent to the lower Darling River. The largest lakes are Lakes Menindee, Cawndilla, and Pamamaroo, with smaller lakes including Tandure, Speculation, Spectacle, Bijiji, Balaka, Malta, Eurobili and Emu (Taylor-Wood *et al*., 2001; Figure 2-2). Other lakes include Lakes Kangaroo, Packers and Tandou, which fill from the Tandou Creek anabranch, with Lakes Mindona and Yartla in the south of the area.

2.2 DARLING RIVER AND FLOODPLAIN HYDROLOGY

2.2.1 Darling River Hydrology

The Darling River is typical of rivers in semi-arid regions, displaying a high degree of hydrological variability linked to the extremes of climate cycles expressed as episodic floods and drought. Under natural flow conditions, prior to regulation, reaches of the Darling River have periodically dried out. The longest period of zero flow ever recorded was 362 days in 1902/03. The principal tributaries are the Paroo, Warrego, Culgoa, Moonie, Macintyre, Gwydir, Namoi, Castlereagh and Macquarie Rivers. Analysis of stream flow data shows that floods are mainly sourced from the Culgoa, Macintyre and Namoi catchments, and occasionally the Bogan and Warrego. Flooding occurs episodically, although the largest floods tend to occur between January and March. River level and flow data recorded at Wilcannia, Weir 32 and Burtundy are reported in Appendix 6 (Somerville *et al*., 2012).

The Darling has been substantially modified by regulation and diversions for irrigation and urban water supplies, with substantive reductions in river flow over the past 100 years, particularly since the 1960's. Thoms & Sheldon (2000) have estimated a reduction in median annual discharge of the Darling River by up to 73 % at Wilcannia, with diversions from the river in 1997/98 accounting for 87 % of the long-term mean-annual flow. Overall, water resource development has contributed to more than tripling the average period between flooding of the Lower Darling River and the Darling Anabranch Lakes. Prior to large-scale development flooding occurred on average once in less than 3 years, while post-development this interval has increased to occurring only once in more than 8 years. At the same time, flood volumes have also been greatly reduced such that the average annual flood volume is only a fifth of the volume under pre-development conditions (CSIRO, 2008a, b). The maximum period between floods is now nearly 23 years (CSIRO, 2008a, b).

Flows and river heights within the Lower Darling are highly regulated throughout the late spring, summer and autumn each year, with water inflows captured and stored in Menindee Lakes and subsequently released. Despite the clear evidence of significant changes to flow regime, river model evaluation suggests that the Darling River system remains one of the least well understood parts of the Murray-Darling System, with a relatively complicated anabranching river network and incomplete gauging (CSIRO, 2008a, b; Podger, 2010). These changes in hydrologic regime are likely to have impacted significantly on the river and its associated floodplain, wetlands and lakes, with implications also for recharge dynamics.

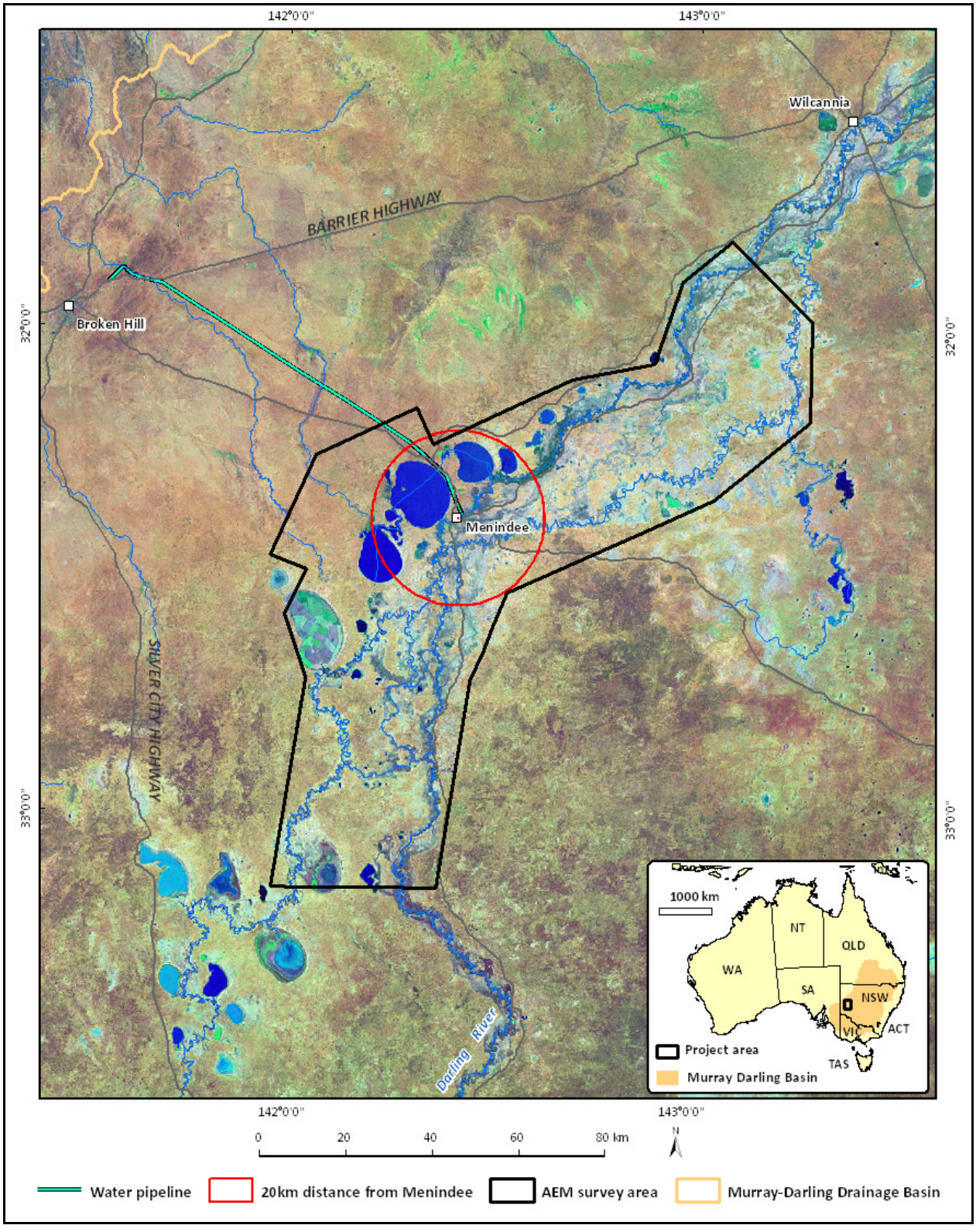

Figure 2-1. *Map showing the location of BHMAR study area relative to Menindee and Broken Hill.*

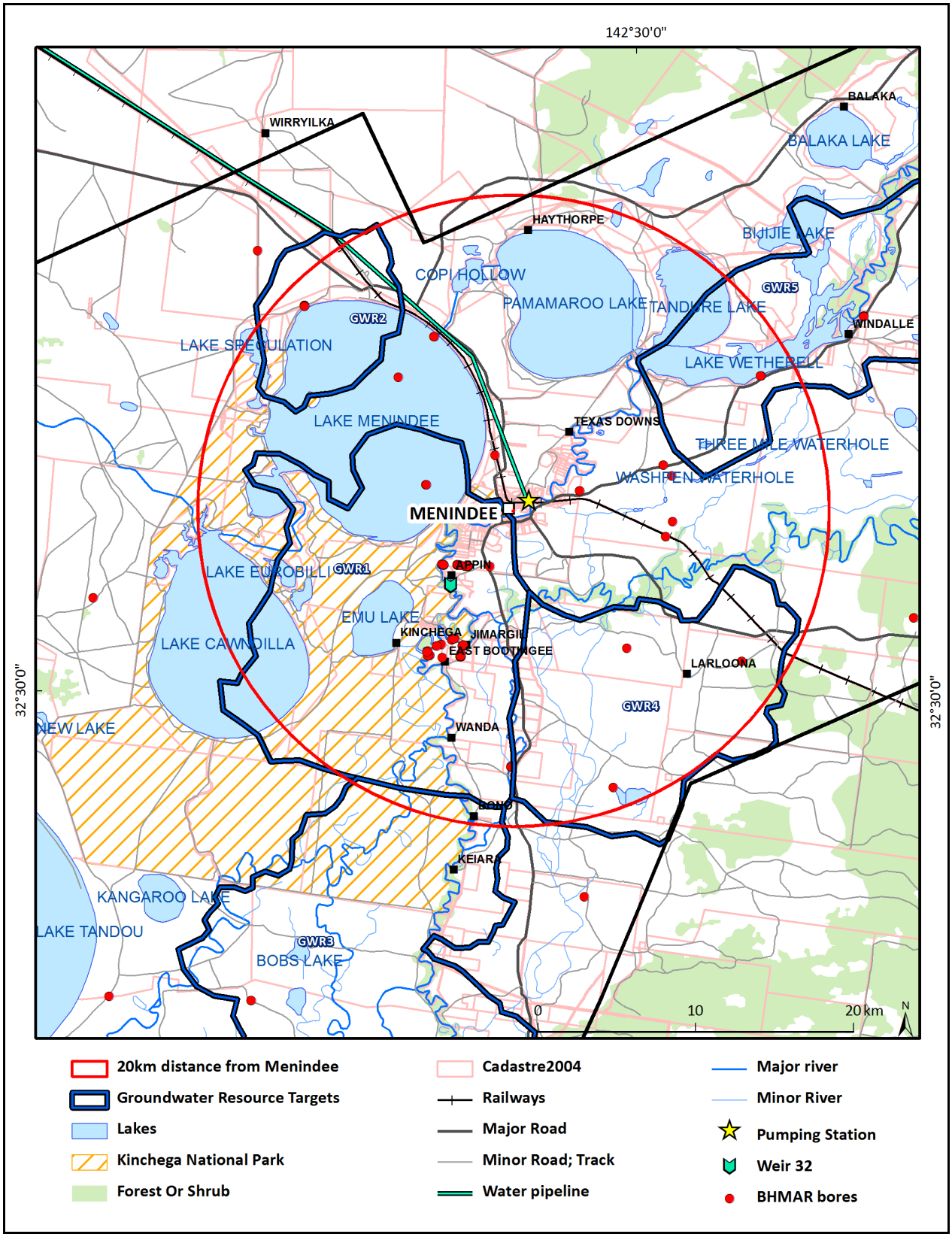

Figure 2-2. *Map showing the location of the Menindee Lakes. The red circle denotes an area within 20 km radius of the township of Menindee.*

Prior studies of the groundwater system (Brodie, 1994; Kellett, 1994) have shown that vertical groundwater head gradients are downward for much of the Darling River floodplain between Menindee and Wilcannia, with significant volumes of fresh to brackish groundwater stored in shallow floodplain alluvium. Recent hydrologic modelling has also demonstrated that the Darling River from Wilcannia to the Anabranch Lakes is a losing reach (CSIRO, 2008a, b). A reduction in flood volumes and extent due to increased diversions is likely to have some impact on recharging of aquifers, particularly on perched aquifers and surface-groundwater interactions across areas of the floodplain that are less frequently flooded or not influenced by lateral bank infiltration.

2.2.2 Menindee Lakes Storages (MLS)

Construction of the MLS was initiated in 1949 and completed by 1960, with some upgrades occurring in 1968. The MLS have a combined surface area of 463 km^2 and a total storage capacity of 1750 GL (Table 2-1), although this can be increased to 2050 GL under certain flow conditions, when the lakes are surcharged. Under the current Murray-Darling Basin Agreement, operational management of the lakes moves to the Murray-Darling Basin Authority (MDBA) when the combined volume of the lakes exceeds 640 GL during a filling phase and water is released to the Lower Darling River as requested by the MDBA. During a draw-down phase, management reverts to NSW when the combined volume falls below 480 GL. This regime is referred to as the 640/480 Rule.

The combination of small dams, weirs, regulators, canals and levees was designed to capture and retain Darling River floodwaters with the original intention of:

- Providing Broken Hill with a reliable water supply;
- Providing water for South Australia during dry periods and thereby making additional Upper Murray water available for irrigation;
- Providing water for irrigation between Menindee and Wentworth;
- Meeting stock and domestic water needs for landholders on the Great Darling Anabranch.

Although not designed specifically for the purpose, the scheme also provides for some flood mitigation downstream of Menindee by a pre-release strategy to manage the height and duration of floods. However, the MLS was designed and operated to maximise water storage and supply with filling and draining operational regimes focussed on water-supply efficiency and effectiveness without consideration of the environmental quality of the lakes. Historic lake level data for Lakes Wetherell/Tandure, Pamamaroo and Menindee/Cawndilla are provided in Appendix 6 (Somerville *et al*., 2012).

The artificial channels and inlet and outlet regulators of the MLS have effectively turned part of the Menindee Lakes into an artificial overflow and storage system whereby Lake Pamamaroo overflows via Copi Hollow to Lake Menindee which then overflows to Lake Cawndilla. There are outlet regulators at Lake Pamamaroo and Lake Menindee to release water back into the Darling River and an outlet regulator at Lake Cawndilla to release water into Tandou Creek.

While meeting essential water supply needs for communities and irrigators, a number of environmentally adverse outcomes from the operation of the MLS have been recognised (Auld & Denham, 2001; Kingsford *et al*., 2002; Nicol, 2004; Kingsford *et al*., 2004; Kingsford & Porter, 2006). Although more than 99% of the wetlands that comprise the lakes and floodplain of the MLS are degraded by too much or too little flooding (SKM, 2010), the MLS are still identified as an important environmental asset in a semi-arid environment (Kingsford *et al*., 2002). Despite being a water supply storage facility, and despite significant periods when many of the main lakes are largely dry, the MLS are listed on the Directory of Important Wetlands. Several waterbird species that are reported to occupy habitats at Lake Menindee, Lake Cawndilla and Morton Boolka are listed under the Commonwealth Environment Protection and Biodiversity Conservation Act 1999, with six listed under the NSW Threatened Species Conservation Act 1995 (SKM, 2010). The lakes are also culturally important for the local aboriginal people, with many burial and other sacred sites. Economically, the Menindee Lakes are a focal point for regional tourism and recreational activities, and also support irrigated agricultural enterprises.

A detailed operational scheme to achieve significant environmental benefits for the MLS has been set out by the MDBA (2010a). However, it is difficult to see how any operational scheme for the lakes that successfully matches the natural flooding and drying regime can also achieve the current water storage and supply requirements of the system.

Table 2-1. *Elevations, depths, areas and capacities of MLS lakes.*

Lake	Lake floor level (m AHD)	Lake surface area (ha)	Full supply level (m AHD)	Full supply depth (m)	Full supply capacity (ML)	Original surcharge level (m AHD)	Surcharge lake depth (m)
Malta	60.14	300	61.67	1.53	3,000	62.68	2.54
Balaka	59.23	1,200	61.67	2.44	18,000	62.68	3.45
Bijiji	58.62	1,000	61.67	3.05	20,000	62.68	4.06
Tandure	55.88	2,100	61.67	5.79	88,000	62.68	6.80
Wetherell	49.60	9,500	61.67	12.07	209,000	62.68	13.08
Pamamaroo	55.27	6,900	60.45	5.18	270,000	61.97	6.70
Menindee	54.35	15,900	59.84	5.49	595,000	61.36	7.01
Cawndilla	52.68	9,400	59.84	7.16	547,000	61.36	8.68

Although the record is complex, filling of the MLS tends to occur primarily during Class C flows, defined as above 12,000 ML/day (Figure 2-4). On average, Class C flows occur in the Darling River at Menindee every 1.6 years, regardless of the month. However, as indicated in Figure 2-4, the intervening periods between Class C flows are highly variable; for time series river and lake level data, refer to Appendix 6 (Somerville *et al*., 2012). For example, there were no Class C flows between 2002 and 2007 during the Millennium Drought, necessitating the replenishment of the MLS using lower magnitude flood flows. The average return interval (ARI) on a monthly basis varies – the ARI for Class C flows occurring in April is 3.4 years, whilst the ARI for Class C flows occurring in December is 6.1 years.

2.2.3 Evaporation

2.2.3.1 Introduction

Evaporative loss of significant quantities of water annually from the large and shallow Menindee Lakes located in a hot semi-arid environment is widely recognised as a major issue. Estimating the amount of evaporation from the Menindee Lakes Storage (MLS) has been a particularly contentious issue, given the debate about possible changes to the MLS operating regime to reduce evaporative losses. The BHMAR project is the latest in a number of investigations, since 1995, designed to identify options for improving the Menindee Lakes water storage system operational efficiency, namely by reducing evaporative losses. However, there are a variety of different estimates of annual evaporation losses from the Menindee Lakes in published sources and reports. This section examines evaporation from lakes and methodology for its measurement or estimation and also summarises available results from the Menindee Lakes as well as providing a comparison to sites in similar climatic regions elsewhere.

Evaporation is the process whereby a liquid changes its state to a gas by molecular transfer or loosening the bonds between adjacent molecules by thermal vibrations. Condensation is the reverse process. When evaporation from the liquid is balanced by condensation from atmosphere the liquid is said to be at *saturation vapour pressure*, which increases with temperature. However, equilibrium rarely occurs as air and the adjacent water are usually at different temperatures and have different vapour pressures. Net evaporation is then the difference between the flow of water vapour from the area of lower vapour pressure and greater flow from the area of higher vapour pressure (Linacre & Hobbs, 1977). Therefore the rate of evaporation from a water body is directly dependent on the surface area of the water, and the relative difference between the equilibrium vapour pressure of the water and the vapour pressure of the air. However, the instrumental measurement and estimation of evaporation for a natural water body are complicated by a number of factors, which are summarised below from Jensen (2010) and Finch & Calver (2008).

- The temperature of the water body is generally dependant on the incident solar radiation and the surface area of the water body but is reduced by the albedo or reflectance of the water surface which increases with low angle solar radiation (higher latitudes and morning and evening), waves and water turbidity.
- Salinity is important as dissolved salts result in a lower equilibrium vapour pressure than pure water at the same temperature, resulting in reduced evaporation. There is approximately a 1% decrease in evaporation for each 1% increase in salinity. Additionally, crystallising salts can increase albedo but the greater optical density of brines can increase solar radiation absorbance.
- Water depth is important for allowing solar radiation penetration and absorbance. Deep water bodies with large volume can transfer and distribute heat within the water column, thereby reducing or delaying evaporation. Energy stored in the water column can result in a lag in evaporation relative to received net solar radiation and reduced evaporation overall. Stratification of the water body can be an important factor.
- Wind is important for disturbing and removing a layer of air at saturation vapour pressure from close to the water surface, which would otherwise insulate the water body from further evaporation. By this process wind removes water vapour and energy (stored as latent heat of vaporisation) to other areas. Wind is also important in increasing the rate of water vapour transfer to the air by producing waves, foam and spray which increase the surface area of the water body.

2.2.3.2 Methods for estimating evaporation from lakes

A number of techniques have been used to estimate lake evaporation from available climatic data and recent reviews of methods include Jensen (2010) and Finch & Calver (2008). Commonly used techniques are summarised below from those sources:

Pan evaporation coefficient

The most common method of directly measuring evaporation is by recording losses from an open pan of water filled to a specified level and adjusted for additions by rainfall. This method results in an evaporation record in mm/day directly relatable to rainfall but is considered to be the least accurate of the methods available for estimating evaporation (Evans *et al*., 2009). The most commonly used pan is the US Class-A Evaporation Pan which is a galvanised iron cylindrical tank with a diameter of 120.7 cm and a depth of 25.4 cm with the pan filled to 5 cm from the pan lip. The pan rests 15 cm above ground on a leveled, wooden slatted base and the top is normally enclosed by a mesh screen to prevent birds and animals drinking from it. While these standardised dimensions allow comparison of evaporation measurements between sites, many pan characteristics cause difficulties in relating pan evaporation measurements to evaporation from natural water bodies. Most notably, the metallic pan sides and base are efficient collectors of additional solar energy, resulting in increased evaporation. The standard bird/animal mesh guard interrupts normal airflow across the water surface and also affects evaporation. A number of different designs and sizes of evaporation pans have also been used including buried and floating pans but all have different energy absorbance and micrometeorological characteristics to natural water bodies and require some conversion to estimate evaporation from a natural water body. The nature of the fetch upwind of the pan, whether dry or wet and how vegetated, can also be important (Jensen, 2010)

A number of published studies have reviewed and experimentally investigated the question of pan coefficients to convert pan evaporation measurements to evaporation from lakes including Roher (1931), Kohler *et al*. (1955, 1958), Hounam (1973), Garrett & Hoy (1978), Linacre (1994), Finch & Calver (2008) and Jensen (2010). Coefficients tend to range from 0.65 to 0.85; are higher under humid conditions than arid conditions; and vary seasonally with the highest pan evaporation usually preceding evaporation from deeper lakes in an annual cycle. A general coefficient of 0.7 is often used both because it falls near the middle of the range of most measured values and because it is the applicable value where water and air temperatures are approximately equal.

Lowe *et al*. (2009) used Bayesian statistics and Monte Carlo simulation to assess sources of errors associated with pan coefficients. They examined uncertainty in data measurements from pan evaporators and bird guard adjustment factors and errors in the factor application due to spatial variability between sites and temporal and other variability in the pan coefficient itself. They found that the 95% probability intervals surrounding

estimates from pan coefficients were as much as ± 40% of the best estimate. The spatial extrapolation of pan evaporation measurements and uncertainties of the coefficient itself were the most important sources of error and the single easiest way to reduce uncertainty was to locate a well maintained evaporation pan at the lake itself.

Mass Balance or water budget

The mass balance method of measuring lake evaporation is simple in concept but often difficult in practice due to uncertainties in quantifying some of the terms (Finch & Calver, 2008; Jensen, 2010). Evaporation is calculated as the residual loss of water volume after all other inflows (precipitation, surface water inflow, and groundwater inflow) and outflows (surface outflow, groundwater outflow) are quantified and summed. Precipitation and lake surface area are usually easily measured although multiple rain gauges may be required where lakes are very large or occur in complex topographic settings. Surface outflow is usually spatially restricted and also relatively easy to quantify. Surface and groundwater inflows and groundwater outflow are much more difficult to quantify. Therefore results obtained from this method become more uncertain when inflow and groundwater outflow quantities are significant and uncertainties of their estimation are of the same order as the evaporation.

Energy balance

The total energy required for evaporation consists of the heat necessary to convert liquid water to water vapour plus the energy carried away from the water body (advection) by the water vapour molecules (Finch & Calver, 2008). In this method, evaporation from a lake is estimated from the residual energy component that is presumed to have resulted in evaporation, which remains when all the other components of the water body energy budget are known and summed (Finch & Calver, 2008; Jensen, 2010). A complexity of inputs and outputs are required including incident short- and long-wave solar radiation and their albedo, long-wave radiative loss from the water, temperature of the evaporated water, energy used in warming the atmosphere in contact with the water (sensible heat radiated upwards), water inflow and outflow heat fluxes and the conduction heat flux between the water and substrate. The method requires measurement or estimation of these terms and works best where inflows and outflows are small compared to the lake volume rendering those values less important. The large number of measurements required and their difficulty of measurement is the major disadvantage of this method. The importance of net radiation in the energy budget requires accurate measurement or estimation of that component (Finch & Calver, 2008)

Equilibrium temperature

This is a variation of an energy balance approach that considers heat transfer processes at the surface of a water body. The concept of equilibrium temperature is used for estimating energy storage and it is calculated from meteorological data from nearby stations. The model calculates an equilibrium time constant and an equilibrium temperature when the net rate of energy exchange is zero; it assumes that the water is well mixed and the bottom heat flux is negligible (Jensen, 2010). The equilibrium temperature of a well-mixed body of water is a function of time and water depth and can be used to estimate heat storage, evaporative and sensible heat flux and the long wave radiative loss from the water (Finch & Calver, 2008).

Bulk or mass transfer

This method estimates evaporation using a derivation of the bulk transfer equation that relates a mass transfer coefficient to wind speed and the difference between the saturated vapour pressure of the air and the vapour pressure of the air (Finch & Calver, 2007). The mass transfer coefficient is the total drag coefficient and is a combination of the skin friction and a force resulting from deceleration of the wind in the direction of flow; it is calculated from theory as a function of atmospheric stability and surface roughness (Finch & Calver, 2008). The transfer coefficient depends on lake size due to enhanced efficiency of turbulent transfer as water surface roughness increases.

Combination equations or the Penman-Monteith equation

Penman (1948) combined the aerodynamic mass transfer and energy balance approaches and derived an equation to estimate lake evaporation that eliminated the requirement for surface temperature. However, the open-water form of the equation did not allow for heat storage and was therefore not applicable to deep water bodies or advected energy (Finch & Calver, 2008). A number of variations were derived to deal more

effectively with the energy balance component of the equation, including the issues of stored energy, and Monteith (1956) derived a modified version, the Penman-Monteith equation, which does not contain empirical calibration factors of the Penman wind function and incorporates heat storage, net advected energy, aerodynamic resistance, surface roughness, water body size and atmospheric stability. It is therefore often considered to be the best description of the evaporation process, provided the necessary input parameters are available (Finch & Calver, 2008). Linacre (1993) derived a simplified version of the Penman equation that required fewer input parameters, just air temperature, wind speed and dew-point data.

Uncertainties of evaporation estimates are larger for deeper lakes, because of the larger heat-storage component and this is further complicated by water-body stratification. Systematic uncertainty can also occur due to changes in aerodynamic conditions due to different surroundings to a water body such as vegetation density and type (Finch & Calver, 2008).

SEBAL remote sensing

SEBAL (Surface Energy Balance Algorithm for Land) is a remote sensing method of estimating evapotranspiration at regional or catchment scales using satellite thermal infrared imagery (SKM, 2009b). The technique is relatively new and has been developed since the late 1990s (Bastiaanssen *et al.*, 1998). The SEBAL method is essentially a variant of the energy balance method whereby the input data are remotely sensed. The use of remote sensing has the advantage of acquiring data from the entire area of interest rather than requiring extrapolation from point-based measurements, such as meteorological stations. For every individual image pixel, SEBAL calculates a complete radiation and energy balance as well as the heat and water vapour transport. Different processing is required for water bodies than over land. Pixels identified as open water, by an unsupervised classification (whereby pixels of negative Normalised Difference Vegetation Index (NDVI) are classified as water) are processed by an alternative calculation routine derived from the Penman-Monteith equation (SKM, 2009b).

2.2.3.3 Evaporation estimates from the Menindee Lakes

The Menindee Lakes are subject to high evaporation losses due to a combination of their shallow depths, large surface areas and location in an area with a hot semi-arid climate. A number of the above-listed methods have been used to estimate evaporation losses from the Menindee Lakes and these are detailed below. Some of the reported values have scant detail concerning the methodology used; others have gone to considerable lengths to provide the best possible estimates. However, there is general agreement between the derived estimates.

Pan coefficient method

DLWC (1998) determined a very high annual evaporation loss of 754 GL from the Menindee Lakes system, which is cited in a number of subsequent publications. This estimate was presumably derived by a pan coefficient method but the original report has been unobtainable and no details of the methodology are provided by subsequent reports.

Moore (2000), in a detailed introduction to the Menindee Lakes Sustainable Development (MLESD) Project Report, suggested that previous attempts to estimate evaporation from the Menindee Lakes using pan coefficients did not take into account evaporation at the capillary fringe of the wetted perimeter outside the lake in addition to evaporation from the water surface. Additionally, Moore (2000) suggested that there was likely to be a higher than normal pan coefficient for the Menindee Lakes, due to their large and shallow nature and the impact of high temperatures. Moore (2000) suggested that when these two factors were combined, the true pan coefficient for the Menindee Lakes could be 1.0 or even higher and that detailed investigation of this issue, including derivation of an appropriate pan coefficient would be part of the MLESD Project. However, no such section appears in the lengthy collection of consultant reports from the project.

Webb McKeown (2007) used a pan coefficient method to derive a figure for the whole Menindee Lakes System of 393 GL/yr net evaporation loss (i.e. evaporation minus rainfall), but the methodology and coefficient used are not detailed.

SKM (2009b) provide the most detailed and well documented example of using the pan coefficient method to estimate evaporation from two of the Menindee Lakes, Pamamaroo and Wetherell, in order to compare the results to a test of the SEBAL 2009 methodology. They adopted a pan coefficient figure of 0.71 based on a specific estimate for Lake Pamamaroo determined by Hoy (1977, cited in Grayson *et al*., 1996) from a study that compared pan evaporation to evaporation estimates from water mass balance and energy balance methods in 13 Australian lakes. This pan factor contained an adjustment for having a bird guard fitted and the same coefficient was adopted for the adjacent Lake Wetherell as Hoy (1977) had given no specific factor for Wetherell. SKM (2009b) also estimated the uncertainty of the pan coefficient for Lakes Wetherell and Pamamaroo using methods devised by Lowe *et al*. (2009), outlined above. Using the pan coefficient of 0.71, annual evaporation was estimated for Lake Wetherell as 131.1 GL and for Lake Pamamaroo as 120.4 GL. As indicated above, the pan coefficient method should only be applied on an annual basis because it assumes no net change in heat storage across the calculation period. Studies that have investigated seasonal or monthly pan coefficients have found significant intra-annual variation. SKM (2009b) used comparison between measured pan evaporation and SEBAL derived lake evaporation rates for Lakes Wetherell and Pamamaroo to derive annual, quarterly and monthly pan coefficients for those lakes. They found that the derived annual values of 0.72 for Wetherell and 0.7 for Pamamaroo were very similar to the previously recommended coefficient of 0.71 for the Menindee Lakes but the monthly and quarterly coefficients varied considerably, from 0.83 to 0.46 for Lake Wetherell and from 0.86 to 0.52 for Lake Pamamaroo. However, these factors are derived from only one year of SEBAL evaporation estimates and must be considered preliminary.

SKM (2009b) estimated a combined total 251.8 for Lakes Wetherell and Pamamaroo, which represent 39.3% of the area of the total Menindee Lakes system. If the estimate is scaled up to include the whole lake system surface area it is equivalent to 640.8 GL.

Mass balance method

Maunsell (2007) report an estimate of average annual evaporation loss from the Menindee Lakes system of 426 GL/yr which can increase to approximately 700 GL/yr when the Lakes are full. These estimates have been cited widely but minimal details of modelling methodology or inputs are provided other than a statement that the estimates are based on more than 100 years of modelled inflow data.

In addition to their pan coefficient study, SKM (2009b) also provided the most detailed and well documented example of using the mass balance method to estimate evaporation from Lakes Pamamaroo and Wetherell, again in order to compare the results to a test of the SEBAL 2009 methodology, on comparable annual, quarterly, monthly and daily timescales. Because the Menindee Lakes have minimal surface inflow in addition to the regulated Darling inflow and no unregulated surface outflow they have good potential for the mass balance method. Potential gains and losses to groundwater provide the main uncertainty, with additional uncertainty provided by the abundance of River Red Gums on much of the former floodplain portions of Lake Wetherell.

Lake Wetherell is an artificial impoundment behind the Main Weir of the Menindee Lakes Scheme across the Darling River near the former Lake Pamamaroo natural inlet/outlet channel. The impoundment consists of the Darling River channel, portions of the floodplain and a number of smaller floodout lakes (Tandure, Bijiji, Balaka and Malta) on the northern side of the floodplain. Much of the upstream portion of Lake Wetherell is constrained within the incised Darling River channel and the deepest parts of the lake (12.1 m) occur in the Darling channel at the weir. Therefore the channel represents a significant proportion of the total lake volume and only the downstream portion of the lake extends onto the floodplain where water levels are less than 2 metres in depth and where the rising and falling of water levels has encouraged lush growth, particularly of red gums. The smaller lakes linked to Lake Wetherell are slightly deeper (3-4 m) and lack all but fringing vegetation. Because of this complexity, the area/volume details of Lake Wetherell were originally poorly known and the volume was significantly overestimated by the original surveys at the time of construction as 267 GL at Full Supply Level (61.67 m AHD) and 343 GL at Surcharge Level (62.28 m AHD). Recent more accurate surveying by bathymetry and LiDAR (Theiss Services, 2002) has indicated respective volumes of 209 GL and 262 GL. Lake Wetherell inflows were derived from gauging at Wilcannia

(150 km upstream) with an assumed travel time of 5 days and associated river losses of 60 ML/day, based on NSW Office of Water data (supplied to SKM, 2009b). River water outflows from Lake Wetherell and inflows and outflows from Lake Pamamaroo were as measured through the flow-control regulators. Assumptions for other unquantified components included a loss of 1 mm/day to groundwater and gain from an assumed local catchment area of 75 km^2 with a runoff efficiency of 40%, for each lake.

The annual, quarterly and monthly results from the mass-balance evaporation estimation for the period July 2004 to June 2005 for Lakes Wetherell and Lake Pamamaroo (SKM, 2009b) are summarised in Table 2-2.

More recent data gathered during the BHMAR Project provides additional information about groundwater processes with relevance to these estimates. Most of the project area, including Lakes Pamamaroo and Wetherell, is underlain by the regional Upper Confining Aquitard which dominantly consists of early Quaternary Blanchetown Clay lacustrine clay and sandy mud. The naturally occurring Lake Pamamaroo has lacustrine sandy-mud lake-floor sediments overlying continuous Blanchetown Clay and the opportunity for groundwater recharge from Pamamaroo is very limited. This conclusion is supported by the Airborne Electromagnetic (AEM) data which show minimal indications of relatively fresh flush zones beneath the lake. In contrast, the floodplain portion of Lake Wetherell consist of Late Quaternary fluvial Coonambidgal Formation and Menindee Formation which comprise a lower lateral-accretion sand aquifer below the near-surface overbank-mud aquitard. Groundwater recharge to this upper unconfined regional aquifer can occur, particularly through lateral leakage via the lower channel banks. Additionally, lithology mapping from the AEM inversions indicates that a significant hole in the Upper Confining Aquitard occurs under Lake Wetherell, potentially allowing vertical leakage to the underlying regional semi-confined, Calivil-Formation aquifer. Enhanced hydraulic heads due to inundation of the floodplain by the lake is highly likely to favour both these groundwater recharge processes, and the AEM data demonstrates a substantial flush zone of relatively fresh water beneath Lake Wetherell extending into the Calivil-Formation aquifer. It is therefore highly likely that the loss to groundwater is considerably higher for Lake Wetherell than Lake Pamamaroo, though as yet unquantified, and that the mass-balance evaporation estimate derived by SKM (2009b) for Lake Wetherell is an overestimation.

An additional complicating factor for Lake Wetherell is the lush red-gum dominated vegetation which grows over much of the shallow former floodplain portion of the lake floor. Red gums are known to freely transpire when water is available (Roberts & Matson, 2011) so there might be enhanced evapotranspiration from lake Wetherell compared to Lake Pamamaroo. However, it might also be possible that reduced wind flow across the water surface in the areas with red gums will reduce evaporation from the water surface, compensating for the increased transpiration losses. This issue is complex and would require a detailed specific study to resolve.

Table 2-2. *Mass-balance evaporation estimates (Jul, 2004 to June 2005) for Lakes Wetherell and Pamamaroo (SKM, 2009b). Figures in bold indicate months when inflows and outflows are minimal and evaporation is likely to be the predominant factor affecting the lake volume. January 2005 estimate for Lake Pamamaroo was not provided for reasons not specified by SKM (2009b).*

Assessment period	Lake Wetherell		Lake Pamamaroo	
	Evap. (GL)	% Volume	Evap. (GL)	% Volume
Annual Jul 2004-Jun 2005	125.8	60.2	132.4	47.6
Quarterly July 2004-Sept 2004	18.8	9.0	11.3	4.1
Quarterly Oct 2004-Dec 2004	49.3	23.6	26.9	9.7
Quarterly Jan 2005-Mar 2005	38.6	18.5	N/A	
Quarterly Apr 2005-Jun 2005	19.0	9.1	20.9	7.5
Monthly Jul 2004	2.7	1.3	**3.2**	**1.2**
Monthly Aug 2004	8.6	4.1	**4.2**	**1.5**
Monthly Sept 2004	**7.6**	**3.6**	**3.9**	**1.4**
Monthly Oct 2004	**13.5**	**6.5**	**4.2**	**1.5**
Monthly Nov 2004	16.8	8.0	**9.1**	**3.3**
Monthly Dec 2004	19.0	9.1	**13.6**	**4.9**
Monthly Jan 2005	**14.4**	**6.9**	N/A	
Monthly Feb 2005	16.8	8.0	17.1	6.2
Monthly Mar 2005	7.5	3.6	12.7	4.6
Monthly Apr 2005	7.2	3.4	**8.4**	**3.0**
Monthly May 2005	6.4	3.1	**6.3**	**2.3**
Monthly Jun 2005	**5.4**	**2.6**	**6.2**	**2.2**

Penman-Monteith combination equation method

As part of the CSIRO Murray Darling Basin Sustainable Yields (MDBSY) Project, McJannet *et al*. (2008) assessed methods of estimation of evaporation from open water surfaces which would be most suitable for use in the Murray Darling Basin (MDB). They briefly reviewed available methods and concluded that the Penman-Monteith combination equation method was the most accurate, applicable method. They then developed a model based on the Penman-Monteith equations and tested it against other estimates from seven locations in the MDB and concluded that the model requires only readily available datasets and could produce reliable estimates of evaporation from a range of water body sizes across the MDB. Unfortunately the Menindee Lakes were not one of the model test areas but McJannet *et al*. (2008) specifically state that the model was developed for estimating evaporation from open water surfaces in the MDB as part of the MDBSY Project.

In the MDBSY Project regional report that included the Menindee Lakes system (CSIRO, 2008a, b), estimates of annual evaporation losses are provided for the Menindee Lakes (355.4 GL) and for individual lakes as well (Lake Menindee: 125.4 GL; Lake Cawndilla: 92.9 GL; Lake Pamamaroo: 80.6 GL; Lake Wetherell: 56.5 GL). Though it is not specifically stated, these estimates are presumed to be derived from the MDBSY Project methodology developed by McJannet *et al.* (2008).

SEBAL 2009 method

The SEBAL 2009 method was used by SKM (2009b) to estimate evaporation from two of the Menindee Lakes, Pamamaroo and Wetherell, using Landsat and MODIS satellite imagery from 2004/2005 when the downstream large lakes, Menindee and Cawndilla were dry and drought conditions prevailed. SKM (2009b) used the shallow-lake model of SEBAL 2009 which estimates evaporation using the Penman-Monteith equation based on daily climate data (temperature, wind speed, humidity and solar radiation) and water-body energy fluxes from sinusoidal functions for the diurnal and annual water temperature. The SEBAL 2009

assessment for Lakes Pamamaroo and Wetherell was performed on daily, monthly, quarterly and annual time steps according to the available data. Twenty two instantaneous MODIS images (250 m resolution), evenly distributed throughout the year, were integrated to determine monthly, quarterly and annual evaporation using a relationship between the evaporative fraction (ratio of actual evapotranspiration to available energy) calculated for each image and measured daily climate and radiation data. Four evenly distributed Landsat images (30 m resolution) were used to derive moderate resolution daily products that enabled sharpening of the coarser resolution images.

The annual, quarterly and monthly results from the SEBAL 2009 evaporation estimation for the period July 2004 to June 2005 for Lakes Wetherell and Pamamaroo (SKM, 2009b) are summarised in Table 2-3. Using this method, it was determined that 133 GL of water evaporated from Lake Wetherell, and 118 GL from Lake Pamamaroo in 2004/05. This represents 63.7 % of the maximum storage capacity of Lake Wetherell (209 GL) and 42.5 % of the maximum storage capacity of Lake Pamamaroo (277 GL). The evaporation rates (in mm/year, Table 2-3) are actually similar, with the differences largely due to the larger surface area to volume ratio within Lake Wetherell.

Table 2-3. *SEBAL 2009 evaporation estimates (July 2004 to June 2005) for Lakes Wetherell and Pamamaroo (SKM, 2009b).*

Assessment period	Lake Wetherell			Lake Pamamaroo		
	Evap. (mm)	Evap. (GL)	% Volume	Evap. (mm)	Evap. (GL)	% Volume
Annual Jul 2004-Jun 2005	1,839	133.1	63.7	1,780	118.1	42.5
Quarterly July 2004-Sept 2004	256	23.7	11.3	270	17.4	6.3
Quarterly Sept 2004-Dec 2004	630	49.3	23.6	592	37.0	13.3
Quarterly Jan 2005-Mar 2005	650	51.4	24.6	674	45.9	16.5
Quarterly Mar 2005-Jun 2005	221	8.7	4.2	254	18.1	6.5
Monthly Jul 2004	36	3.4	1.6	38.1	2.5	0.9
Monthly Aug 2004	96	8.9	4.3	102.2	6.6	2.4
Monthly Sept 2004	125.2	11.4	5.6	129.6	8.3	3.0
Monthly Oct 2004	180.5	15.3	7.3	169.1	10.8	3.9
Monthly Nov 2004	189.4	14.9	7.1	176.3	11.1	4.0
Monthly Dec 2004	267.2	19.1	9.1	249.0	15.2	5.5
Monthly Jan 2005	267.7	25.2	12.1	284.9	17.6	6.3
Monthly Feb 2005	193.8	15.8	7.6	214.3	15.2	5.5
Monthly Mar 2005	168.3	10.4	5.0	182.2	13.1	4.7
Monthly Apr 2005	109.9	5.3	2.5	137.5	9.8	3.5
Monthly May 2005	64.3	2.4	1.1	77.8	5.5	2.0
Monthly Jun 2005	31.9	1.1	0.5	38.4	2.7	1.0

Summary of Menindee Lakes evaporation estimates

The estimates for annual evaporation from the Menindee Lakes system presented above vary from 355 to 700 GL/year, which is equivalent to a range of 20-40% of the total system volume of 1750 GL at full supply level. The most detailed and well documented study by SKM (2009b) used three different methods to derive estimates from two of the Menindee Lakes with good agreement which scale up to about 640 GL/year or 36.6% of the total system volume at full supply level.

Evaporation from lakes is essentially dependant on their surface areas. The estimate of evaporation from the Menindee Lakes is a relatively large percentage of their volume because they are very shallow. An annual evaporation rate of 1800 mm will remove half the volume of a 3.6 m deep lake, about a third the volume of a 5.4 m deep lake, but only 5% of the volume if the lake was 36 m deep; the same amount of water will have been removed in each instance.

2.2.3.4 Comparison of Menindee evaporation estimates to other sites

The high evaporation loss figures from the Menindee Lakes, as both GL/yr and percent volume amounts, used for the BHMAR reports, can be compared to evaporation losses estimated from other sites with similar climatic settings. For instance, anomalously small volume losses of about 5% have been reported from aquifer recharge infiltration basins in southern Arizona, which have a similar climatic setting and similar water depths to the Menindee Lakes (Thompson, Pers. Comm., 2012).

Tucson in southern Arizona is at about the same latitude as Menindee (~32º) and has a similar semi-arid climate with rainfall of ~280 mm/year (~230 in Menindee), hot summers and high potential evaporation, but is at considerably higher altitude (~730 m versus 61 m for Menindee). In common with much of central and southern Arizona, competition between growing urban centres and irrigated agriculture for water supply sourced mainly from groundwater led to declining groundwater levels and quality. This resulted in construction of the Central Arizona Project (CAP) to supply water from the Colorado River to both urban centres and for irrigation in central and southern Arizona. CAP has the capacity to transfer 1850 GL of Colorado River water per year from Lake Havasu via a 600 km aqueduct, rising about 730 m in elevation through fourteen pumping plants. The CAP was the largest and most expensive water transfer project ever constructed in the US with construction completed late in 1992, at a cost approaching US$5 billion (Hanneman, 2002). Unviable water supply economics for irrigation and unacceptable water quality for urban use have resulted in much of the CAP quota for the Tucson region being used to recharge aquifers and being banked for later use.

A number of recharge areas have been developed including the Pima Mine Road Recharge Project (PMRRP) on the Santa Cruz River flood plain about 27 km south of Tucson. Five infiltration basins at PMRRP cover a total of 15 hectares and are excavated to as much as 4 m in depth to just above coarse sand and gravel levels. Annual maintenance includes scraping and ripping of the basin floor to remove accumulated fines and biological crusts and infiltration rates vary from 0.6 to 1.8 m/day with the highest rates occurring after full profile wetting has occurred immediately following maintenance. Annual losses to evaporation are very low at 5% of volume (Thompson, Pers. Comm. 2012) due to a management regime designed to minimise evaporative losses. The ponds are not operated during the hottest part of the year and the very high infiltration rates promoted by the maintenance regime result in a brief residence time of water in the pond and minimal opportunity for absorbed solar radiation to be converted to evaporation. The system must effectively transfer absorbed solar energy in the form of higher water temperatures to the groundwater reservoir.

This very effective minimisation of evaporation by the management regime of the infiltration ponds, due to the high cost of CAP water, is the explanation for the highly discrepant percent volume losses between The Menindee Lakes and the southern Arizona recharge basins, such as PMRRP, which have similar water depths and potential evaporation. The similarity of potential evaporation in the Tucson area to Menindee is demonstrated by regional studies of lake evaporation in the semi-arid western US where very high rates, similar to those estimated for the Menindee Lakes are recorded (Meyers & Nordenson, 1962; Hanson, 1991). The map of lake evaporation provided by Hanson (1991; Figure 2-3) indicates a value of about 1778 mm near Tucson.

A specific example of lake evaporation in the region is provided by Sahuarita Lake which is located within 4 km of the PMRRP infiltration facility. Sahuarita Lake is an artificial recreation lake in the town of Sahuarita, with a surface area of 4.05 Ha, a 1.6 km perimeter, a maximum depth of 3.0 m, an average depth of 2.13 m and holds approximately 86 ML of water (J. Harlan Glenn Associates, 2001). The lake is carefully managed for recreation and water quality is maintained by forced vertical mixing by injection of air through diffusers on the lake bottom to maintain a uniform water column and to sustain stocked fish. Mass water balance estimates of evaporation indicate an annual loss to evaporation of 71 GL and an annual loss due to seepage to groundwater of 12 ML. These losses represent 83% and 14 % of the total volume respectively and the lake level is maintained by pumping from a nearby well in the Upper Santa Cruz Valley aquifer.

As for the nearby PMRRP infiltration basins, the nearby Sahuarita Lake has a similar climatic setting and water depth to the Menindee Lakes but Sahuarita has extremely high evaporative losses, even higher than those estimated from the Menindee Lakes. This is probably due to the forced mixing by aeration which

would maximise both the water-body temperature mixing as well as the air/water surface area. While not designed as such, this effectively constitutes management that maximises evaporation in sharp contrast to the infiltration basin management which minimises evaporation.

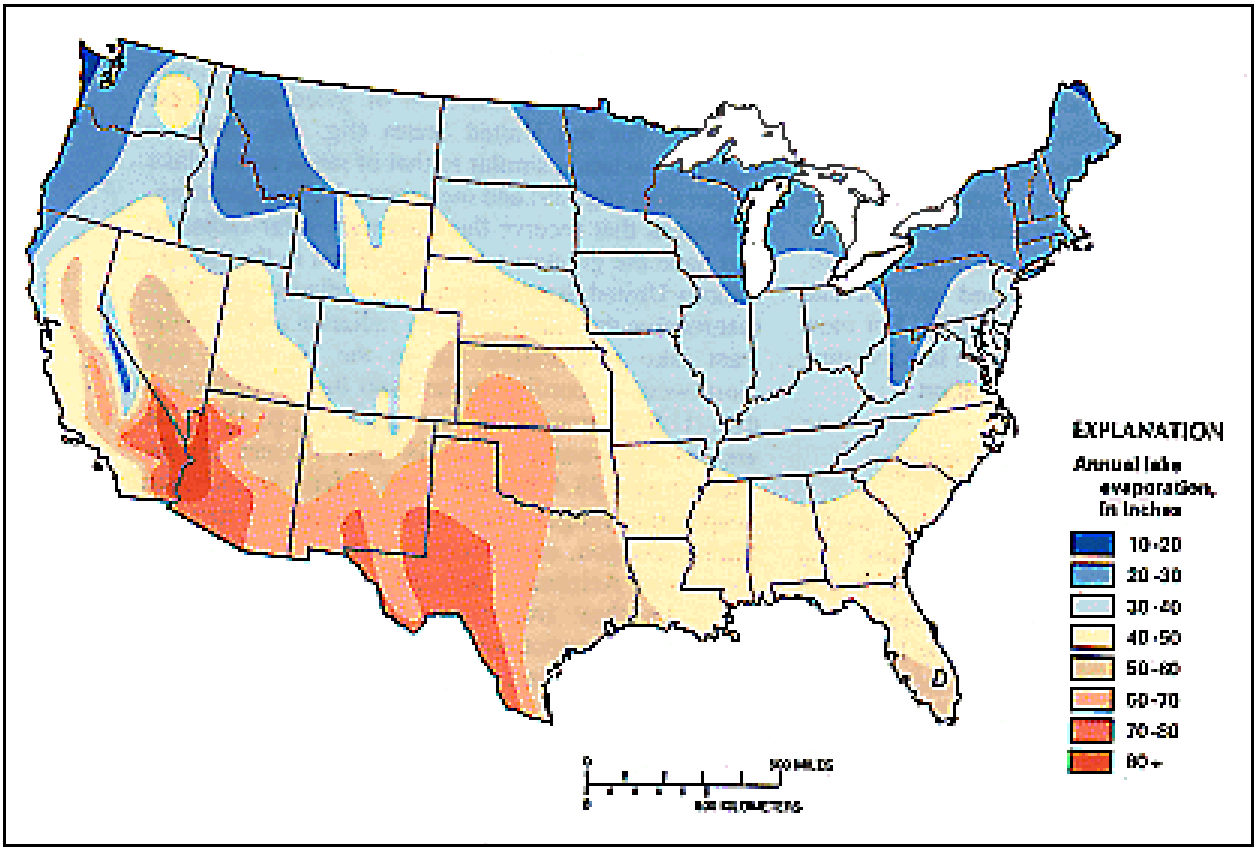

Figure 2-3. *Mean annual lake evaporation in the conterminous United States, 1946-55, from Hanson (1991). Lake evaporation in southern Arizona near Tucson is about 70 inches or 1778 mm per annum.*

2.3 CLIMATE, CLIMATE VARIABILITY AND PREDICTED CLIMATE CHANGE

2.3.1 Present-day Climate

The climate in the BHMAR study area is semi-arid. The area lies within a zone of uniform seasonal distribution of precipitation. Overall, annual rainfall is low with an average of between 200-250 mm/year, with high rates of evaporation exceeding 2400 mm/year[1]. Daily and monthly rainfall data measured at Menindee Post Office are available in Appendix 6 (Somerville *et al*., 2012). The BoM climate data record[2] indicates a mean daily maximum temperature at Menindee of 26°C and a mean daily minimum of 11°C. Summer maxima are commonly in excess of 35° C and temperatures may drop below zero during winter.

The tributaries of the Darling River have a large and complex catchment on the western side of the Eastern Highlands and the western slopes and plains of northern NSW and southern Queensland, situated mostly in a weakly summer-dominant rainfall zone. Many of the contributing catchments are arid to semi-arid with significant areas contributing no runoff (Thoms *et al*., 1996). However, winter-westerly rainfall events can be significant, especially in the southernmost NSW portion of the catchment. Additionally east-coast lows can occasionally deliver significant precipitation to the headwater catchments. These events can bring intense precipitation to eastern coastal regions which can occasionally penetrate beyond the rainfall divide and impact westerly-flowing Darling catchment streams.

2.3.2 Palaeo-climate and Implications for Streamflows and Recharge

Global climate has varied markedly at long-term timescales (10s to 100s of thousands of years) with the glacial-interglacial climate cycles. Though only a trivial part of mainland Australia around the highest mountain, Mt Kosciuszko in the south east, was actually glaciated, the impact of lowered temperatures, lowered sea level, low sea-surface temperatures and widespread periglacial activity in highland catchments have profoundly modified precipitation, temperatures, evaporation and runoff across much of the continent. Variations in precipitation and runoff over the entire Darling catchment are particularly important for variations in recharge of the aquifers of the BHMAR Project area.

Unfortunately, there are sparse palaeo-climate records for the Darling catchment and no continuous long-term records. However, groundwater chemistry from the region suggests that river leakage is by far the dominant recharge mechanism with rainfall recharge insignificant (see Section 8). Therefore, variations in river flow due to palaeo-climatic changes in the catchment are likely to be most relevant for changes in recharge and these can be addressed by continental-scale and catchment-region palaeo-climate records. Additionally, this can be complemented by reconstruction of variations in fluvial activity and discharge from geomorphic, stratigraphic and geochronological studies of the Quaternary fluvial deposits of the study region.

[1] http://www.bom.gov.au/climate/averages/tables/cw_047031.shtml

[2] http://www.bom.gov.au/climate/averages/tables/cw_047019.shtml

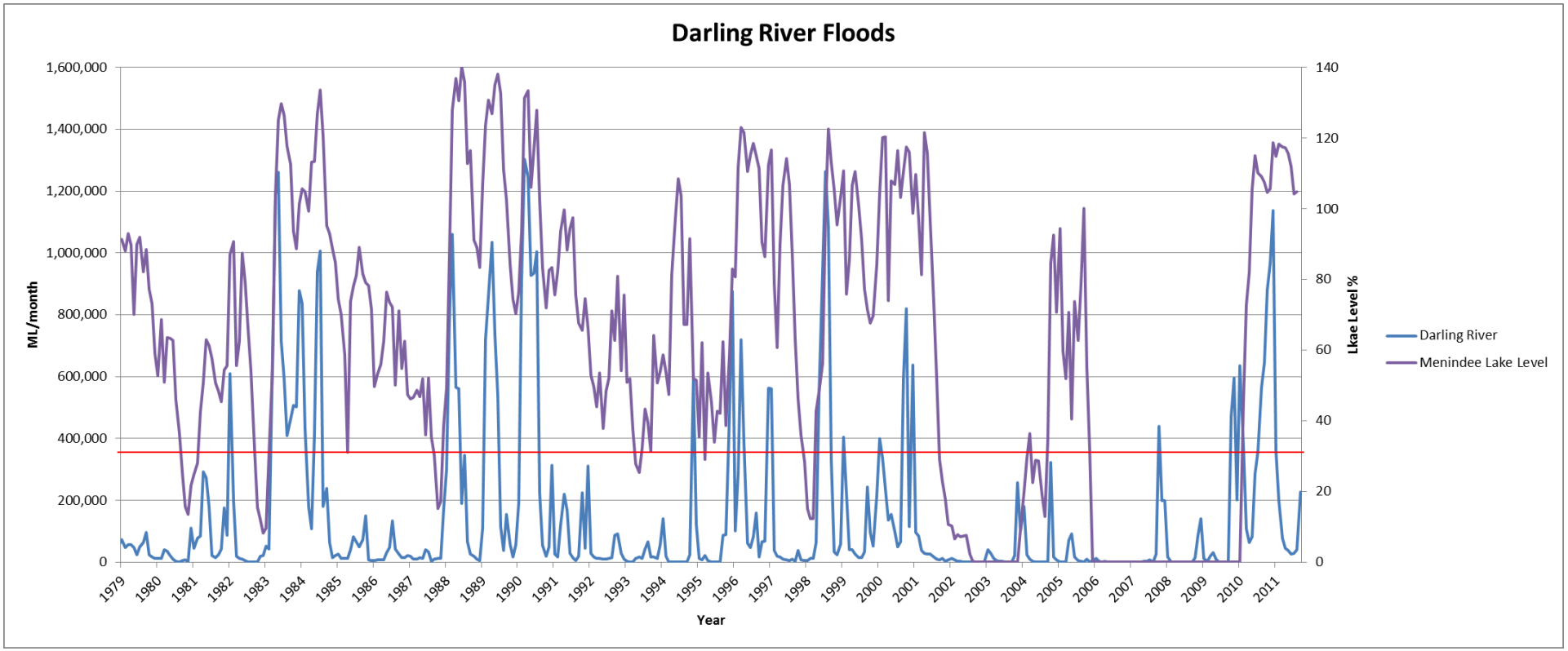

Month	Jan.	Feb.	March	April	May	June	July	August	Sep.	Oct.	Nov.	Dec.
ARI (years)	4.9	4.5	3.6	3.4	4.7	5.8	4.6	3.6	3.6	4.3	6.4	6.1

Figure 2-4. *(Top) Average monthly percent capacity for three Menindee Lakes (Cawndilla, Menindee and Pamamaroo) compared to monthly streamflow of the Darling River at Wilcannia. Class C flow (360,000 ML/month) is shown by the red line. (Bottom) Average Return Interval (ARI) for Class C flow (> 12,000 ML/day) of the Darling River at Wilcannia for each month (streamflow and lake level information from http://waterinfo.nsw.gov.au/.*

2.3.3 Predicted Climate Change

Drought conditions in much of inland eastern Australia over the past 8 years in particular have seen marked declines in river flows in the Darling River system. While recent good rains have led to significant floods (March 2010), rainfall-runoff modelling with climate-change projections from global climate models indicates that future runoff in the region is more likely to decrease than increase (CSIRO, 2008a, b; Barron *et al*., 2011). About three-quarters of the modelling results show a decrease in runoff and about one-quarter of the results show an increase in runoff for the region.

Under the best estimate (median) 2030 climate modelling, average annual runoff within the region would be reduced by 10 %. The extreme estimates (from the high global warming scenario) range from a 37 % reduction to a 7 % increase in average annual runoff. The results from the low global warming scenario range from a 12 % reduction to a 2 % increase in average annual runoff for the region (CSIRO, 2008a, b).

2.4 LAND USE AND CULTURAL HERITAGE

The BHMAR project area is one of great cultural sensitivity to the local Indigenous Community (Martin, 2001; Witter, 2009), with a large number of culturally significant sites identified during this project (Lawrie *et al*., 2010a; Magee *et al*., 2012). The importance of local Indigenous cultural beliefs and traditions was recognised at the commencement as a crucial aspect of the project, and all team members were made aware of these issues and asked to respect these values. For the fieldwork component of this study, the local Indigenous community were consulted about the process of carrying out assessments for field investigations and drilling activities. Consequently, detailed cultural assessments were undertaken by specialists with the assistance of members of the local Indigenous community employed through the Menindee Local Aboriginal Land Council (MLALC). In accordance with the wishes of the local Indigenous community, and to obtain permissions from the NSW Lands Dept., cultural heritage assessments were conducted at each proposed drilling site.

Members of the local Indigenous Community were also employed to assist with monitoring any potential site disturbance during drilling activities, and to assist geologists on-site with core recovery. From Geoscience Australia's perspective, the employment of members of the local Indigenous Community was extremely successful, under arduous conditions both day and night. A similar arrangement was put in place for augering and the digging of pits for shallow geomorphic investigations. Reports on cultural heritage at each proposed drilling site were submitted along with other technical information to the NSW Lands Department as part of the drilling approval process. A number of sites deemed too sensitive were not drilled, and alternative sites identified. A similar process has been identified for obtaining approvals for disposal of groundwater associated with 7-day pump tests. Potential cultural heritage sensitivities with regards to the various groundwater-related targets and options have also been assessed and discussed in Lawrie *et al*. (2012c, d).

3. Project Data Acquisition

The BHMAR project has involved the acquisition, processing, integration and interpretation of significant new geological, hydrogeological, hydrogeophysical and hydrochemical datasets. The project is the largest single hydrogeological investigation project undertaken by the Australian Government over the past 30 years. Details of data acquisition, data processing, analysis, integration and assessment methods, and product generation, can be found in Lawrie *et al*. (2012a). Ancillary data and contractor reports can be found in 15 accompanying appendices and in the project database and GIS (Gow *et al.,* 2012a). These final reports supersede earlier reporting of data acquisition and assessment methods (Lawrie *et al.,* 2009a; 2010a, b; 2011).

3.1 NEW DATA ACQUISITION

Data acquisition in the BHMAR Project involved a phased approach, with investigations initially at a regional scale, with subsequent investigations at more local scales as potential groundwater resource and MAR targets were identified and assessed. Data acquisition strategies were guided by national guidelines for drinking water and MAR (NRMMC–EPHC–NHMRC, 2008, 2009; NHMRC-NRMMC, 2011).

The datasets acquired in BHMAR phases 1-3, and a simplified project workflow showing the relationship of datasets are summarised in Figure 3-1and Figure 3-2 respectively. Data acquisition utilised a phased approach, and was guided by the two main project objectives, and the requirement to address very specific questions embedded with the national MAR guidelines.

In summary, the BHMAR Project has acquired the following key datasets:

- A 31,834 line km airborne electromagnetic (AEM) survey using the SkyTEM heliTEM system.
- A high resolution LiDAR digital elevation survey (20 cm vertical resolution) over the ~7,500 km^2 project area.
- 100 bores in a 7.5 km drilling program, including 60 sonic bores.
- Construction of a piezometer network, including installation of automated data loggers in 40 bores, with groundwater levels manually checked every 3-4 months.
- A hydrochemical sampling program of surface water, groundwater and pore fluids. This entailed analysis of about 1600 hydrochemical samples (25 analytes and including trace metals).
- Stable isotopic characterisation of river, lake and groundwater.
- A program of groundwater age dating using radiocarbon (^{14}C) and chlorofluorocarbon (CFC) tracers.
- Limited (7-day) pump tests, and more extensive aquifer slug tests.
- Ground resistivity and IP surveys of potential borefield sites, including time lapse-monitoring of the effects of pumping operations in the target aquifer.
- In-river mapping of the Darling River bed using multi-beam sonar (echo sounder) and sub-bottom profiler methods to map river bed bathymetry and composition.
- Borehole geophysics including gamma, induction and nuclear magnetic resonance (NMR) logging.
- Age dating of geological materials with optical stimulated luminescence (OSL), radiocarbon and palynology.
- Laboratory column tests to assess aquifer storage and recovery (ASR) clogging potential.
- Laboratory permeameter and porosity testing of drill core materials.
- Geochemical analysis (major and trace elements and trace metals) of drill core materials.
- Scanning electron microscopy (SEM), x-ray diffraction (XRD), portable infrared mineral analyser (PIMA) and Hylogging multi-spectral analysis of drill core materials for mineralogical analysis.
- Limited groundwater and water-rock interaction modelling.
- Surface geomorphic mapping, trenching and hand augering.
- Mapping of Indigenous cultural heritage sites.

The acquisition, processing, and interpretation of such large, varied and complex datasets has involved a multi-disciplinary approach involving a core team of 10 scientists within Geoscience Australia, and with an additional 20 staff and 40+ contractors involved at various stages in data acquisition and processing. Data processing, analysis and assessment methods are documented in detail in Lawrie *et al.* (2102a).

In summary, a multi-disciplinary 3D hydrogeological systems mapping approach has been developed in this project to guide development of new geological and hydrogeological conceptual models, and to provide a framework for understanding complex hydrogeological and hydrogeochemical processes. Integration of the 3D mapping with hydrochemical and hydrodynamic data provides critical new insights into surface-groundwater interactions and groundwater flow. Using this approach, it has been possible to develop a new understanding of recharge processes, and identify potential recharge and groundwater flow pathways which is important for the assessment of groundwater-related targets (Lawrie *et al*., 2012c, d).

The new datasets, knowledge and hydrogeological conceptual models generated in the project have provided a reliable basis for the identification, characterisation and initial assessment of groundwater resources and MAR options (Lawrie *et al*., 2012c, d). The products and knowledge generated will also provide important inputs to assist with the parameterisation of groundwater and solute transport models that are critical to the next steps in the assessment of MAR and groundwater extraction options in the area.

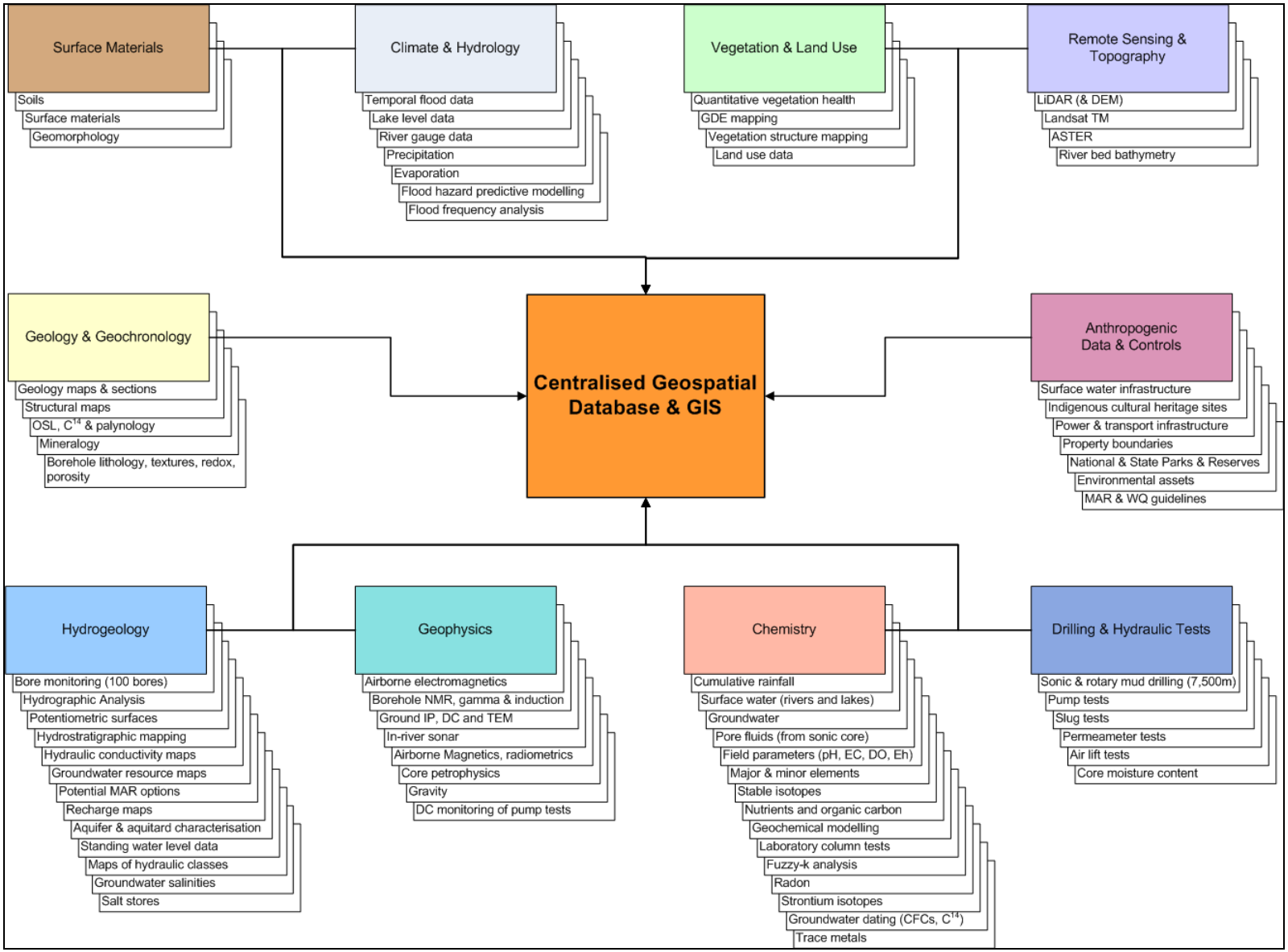

Figure 3-1. *Datasets acquired during the project, grouped by theme.*

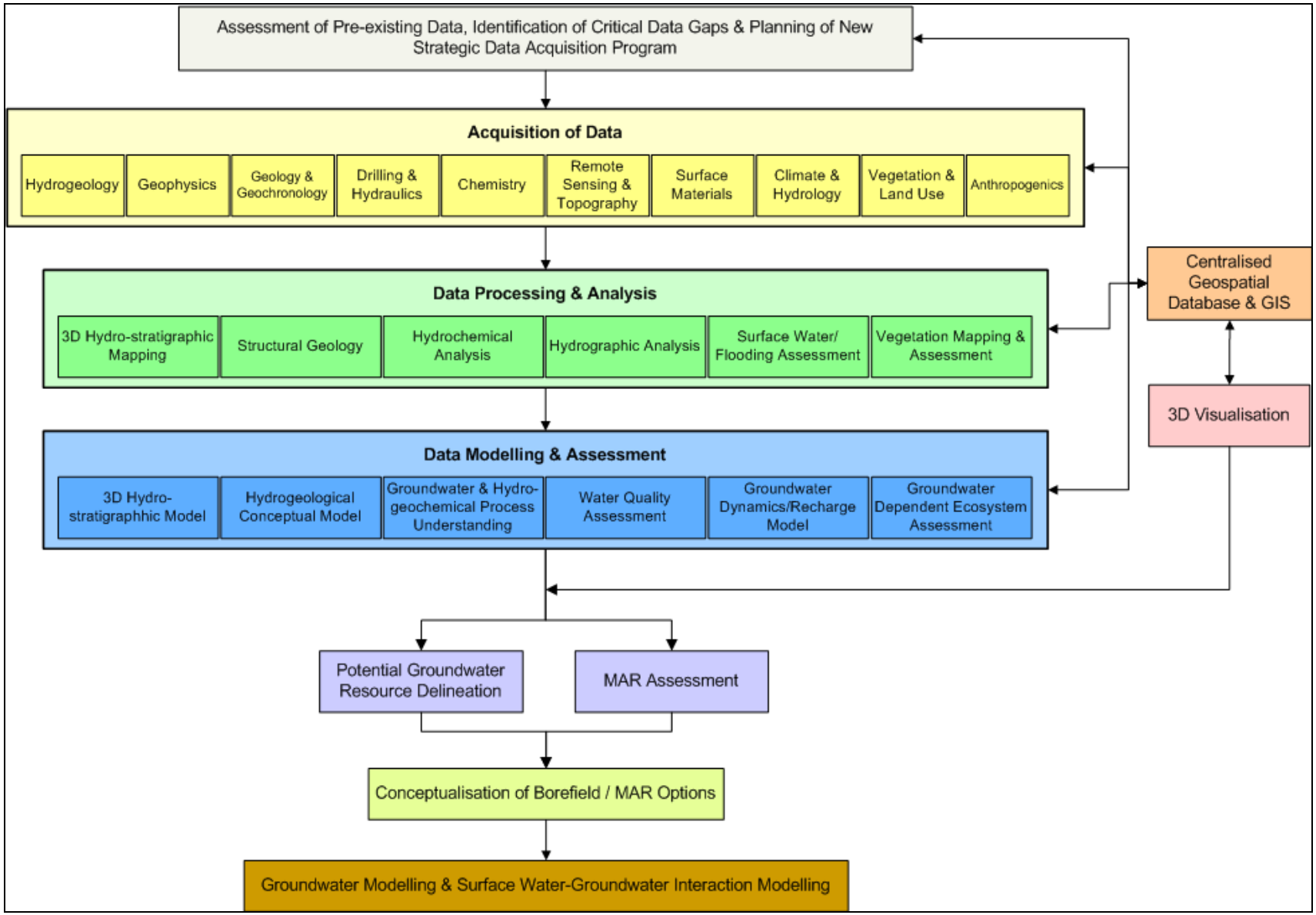

Figure 3-2. *Simplified project workflow. Those themes listed under acquisition of data relate to Figure 3-1.*

4. Regional Geology

4.1 GEOLOGICAL BASEMENT

The geological basement to the BHMAR study area probably consists of rocks of many ages and lithology. However, it is expected that these will be almost entirely sedimentary, mostly of Palaeozoic age. The Murray Basin in the survey area overlies several depocentres of the Palaeozoic Darling Geological Basin, including the Menindee, Wentworth and Blantyre Troughs (Brown & Stephenson, 1991). The petroleum exploration well Blantyre 1, drilled in the northeast of the survey area in the latter, intersected a veneer of early Permian and possibly Carboniferous sediments underlain by >1700 m of late Devonian fluvial and lacustrine sandstone and shale (Brown & Stephenson, 1991). Further north (between the survey area and Wilcannia), possible Cretaceous shales have been identified in deep water bores (Mike Williams, written communication, 2009). The nearest outcropping basement is in the Scopes Range and Dolo Hills where deformed Cambrian, Ordovician and Devonian rocks have been mapped. Unpublished data (David Gibson, Geoscience Australia) suggests that there are also younger undeformed rocks locally present in these areas, possibly Permian or Mesozoic in age.

In the BHMAR study area, two basement highs have been recognised in the AEM data, both of which have been penetrated by project drilling. A basement high extending south from the southeastern corner of the Scopes Range just to the north of Lake Menindee was intersected by BHMAR 63 and BHMAR23. Lithologies intersected are weakly cemented shale, sandstone and conglomerate. These are almost certainly rocks of Palaeozoic age. A piezometer in sandstone and conglomerate in BHMAR23 yielded 3.5 l/s of brackish water (5000uS/cm), indicating that the rocks form an aquifer in their own right. However, the low conductivity of these rocks in downhole geophysical logs and AEM data (generally <100 mS/m) suggest that porosity is low. A second basement high was intersected in BHMAR14 in the north of the survey area (at Christmas Rocks). The lithology here is weathered mudstone, almost certainly of Palaeozoic age.

It is expected that Proterozoic metamorphic basement as exposed in the Broken Hill Block will only be present at considerable depth beneath Palaeozoic rocks.

4.2 DARLING GEOLOGICAL BASIN

The Darling Geological Basin (DGB) is one of the largest on-shore sedimentary basins in Australia, occupying ~90,000 km^2 of western New South Wales (Figure 4-1; Neef, 2012). The DGB is bounded to the south by the Cenozoic Murray Geological Basin (MGB). The basin is variably infilled with over 8,000 m (up to 12,000 m?) of mainly Devonian sedimentary rocks formed in a wide range of depositional environments, ranging from alluvial to marine (Moffitt &Weatherall, 2004). The basin overlies regional basement structures coinciding with boundaries between the Late Palaeozoic Kanmantoo, Lachlan and Southern Thomson Fold Belts (Moffitt & Weatherall, 2004; Cooney & Mantaring, 2007). The DGB consists of seven smaller sub-basins. Within the BHMAR study area these are mainly the Bancannia Trough and the Menindee Trough, although minor parts of the Blantyre and Pondie Range Troughs also occur (Figure 4-1).

The Darling Geological Basin comprises a number of discrete sedimentary troughs which formed in areas of maximum tectonic extension. These include the Ivanhoe, Blantyre, Pondie Range, Nelyambo, Neckarboo, Bancannia and Menindee Troughs, as well as the Poopelloe Lake complex (Kingham, 1998; Moffitt & Weatherall, 2004). These north-west and north-east-trending infrabasins underlie the Cenozoic sediments of the Murray Geological Basin, and have been identified using a combination of regional aeromagnetic and gravity surveys and petroleum exploration drilling, (Brodie, 1994; Lewis *et al*., 2008). The general spatial variation in sedimentary facies across the basin (fluvial sandstones in the western troughs to submarine fan facies in the eastern troughs) suggests that many troughs of the greater Darling Geological Basin were probably interconnected during prolonged depositional periods (Cooney & Mantaring, 2007). Key elements of the DGB that lie within the BHMAR study area include the Menindee Trough, the Blantyre Trough, and the Mount Wintlow High. These are covered by the younger sediments of the Murray Geological Basin, and do not outcrop.

The Darling Geological Basin contains sedimentary formations deposited from the Late Silurian to the Early Carboniferous (Figure 4-2). Outcrops of these Palaeozoic rocks are sparsely distributed across the basin; consequently, most of our geological understanding has been derived from sub-surface petroleum exploration drilling and geophysical surveys. The most common sedimentary rocks are Late Silurian to Early Devonian fossiliferous marine shales and Early Devonian to Early Carboniferous fluvial quartz-rich sandstones (Willcox *et al*., 2003).

In the Broken Hill region, the Menindee and Bancannia Troughs unconformably overlie Proterozoic and Lower Palaeozoic basement rocks of the Broken Hill Domain and Wonominta Blocks. In contrast, the eastern sub-basins, e.g., the Pondie Range Trough, onlap deformed and metamorphosed Lower Palaeozoic rocks of the Lachlan Fold Belt. The northern extent of the Darling Geological Basin is concealed by Mesozoic sedimentary rocks of the Eromanga Basin (part of the Great Artesian Basin (GAB)). To the south and west a relatively thin composite veneer of Upper Carboniferous, Permian and Cretaceous rocks, and Cenozoic sediments of the Murray Geological Basin, also cover the Darling Basin (Brown *et al*., 1982; Moffitt & Weatherall, 2004).

Major crustal extension in the Devonian, caused by reactivation of older fault systems, led to the formation of the Darling Geological Basin. At the end of the Ordovician Period, a major tectonic change altered the palaeogeographic distribution of south-eastern Australia, from a marginal marine sea to a series of deep troughs and basins (Cooney & Mantaring, 2007). The relative movement of rigid basement blocks, combined with reactivation of faults, determined the ultimate form and subsidence history of these sedimentary troughs during the Late Silurian and Early Devonian (Cooney & Mantaring, 2007). Seismic reflection surveys have confirmed the presence of major faults which form the eastern and western margins of many sub-basins (e.g. Figure 4-3).

4.2.1 Bancannia Trough

The Bancannia Trough separates the basement provinces of the Broken Hill Domain and the Wonominta Blocks. The trough is 25 km-wide and about 100 km-long, trending north-west, and corresponds to a major regional gravity low, (Figure 4-1; Moffitt & Weatherall, 2004; Blevin *et al*., 2007). Gravity-derived depth-to-basement estimates (confirmed by seismic data) suggest that the thickness of the sedimentary sequence exceeds 8 km, particularly in the east (Figure 4-3). Three petroleum wells have previously been drilled in the Bancannia Trough: Bancannia North-1, Bancannia South-1 and Jupiter-1. Drilling records provide the most comprehensive data on the nature and composition of the sedimentary rocks.

Well completion reports have documented thick sequences of Palaeozoic sedimentary rocks in the Bancannia Trough. The basal unit is commonly a marine, fossiliferous Cambrian to Ordovician sequence, overlain by Devonian continental sandstones and ‘red-bed’ sequences. Basement rocks of unknown age comprise dacite, andesite, and muscovite-bearing schist and phyllite (Lewis *et al*., 2008).

Petroleum exploration drilling has shown that the porosity and permeability of the Devonian rocks in the Bancannia Trough range from poor to fair, with the highest porosities in the Upper Devonian sandstones. These rocks are relatively friable and were easy to drill, although the underlying Devonian rocks (Lower to Mid-Devonian) down to basement depths have poor of low porosity. No significant petroleum shows were reported in any wells drilled in the Bancannia Trough.

4.2.2 Menindee Trough

The Menindee Trough occurs south of Broken Hill (Figure 4-1), forming a north-east trending depositional sub-basin. A series of north-east master faults and north-trending sinistral normal faults are the dominant structural features. The Menindee Trough is of similar dimensions to the Bancannia Trough, with regional gravity and magnetic data suggesting that the underlying basement rocks are related to the nearby Broken Hill Domain and Curnamona Province.

Seven petroleum wells have been drilled into the central part of the Menindee Trough: Nulla Nulla-1, Tararra-1, Ennis Vale-1, Kopi Plain-1, Ironstone Tank-1, Avery-1 and Popiltah-1 (Lewis *et al*., 2008). The sedimentary profile is variably developed across the Menindee Trough, and includes near-surface sediments of the Quaternary Wunghnu Group, underlain by parts of the Miocene Murray Group, the Eocene Renmark Group, the Cretaceous Millewa Group (including the Meretti and Pyap Members), the Permo-Carboniferous Cape Jervis Beds, and the Devonian to Early Carboniferous Mulga Downs Group (Lewis *et al*., 2008).

The Murray Group has relatively poor porosity due to the dispersive clay matrix. Moderate to good porosity (visual estimates only) occurs in the Cape Jervis Beds, some parts of the Renmark Group (except for clay-rich lenses) and the Pyap Member. The Devonian sandstones have variable porosity; some sections have good aquifer characteristics, i.e., porosity and permeability which would make them potential targets for investigating deep groundwater resources.

4.2.3 Blantyre Trough

The Blantyre Trough (Figure 4-1) contains the thickest sedimentary section in the Darling Geological Basin, with up to 12,000 metres of mostly Devonian age rocks (Moffitt & Weatherall, 2004). The only petroleum exploration well, Blantyre-1, drilled about 2,000 m of Late Devonian and Early Carboniferous rocks overlain by younger Permian and Cenozoic sequences which were poorly consolidated or unconsolidated (Lewis *et al*., 2008). These rocks were covered by a relatively thin veneer of Quaternary alluvium and dune sands. Early Devonian units were absent, suggesting that the well was terminated above the geological basement (Moffitt & Weatherall, 2004).

4.2.4 Pondie Range Trough

The Pondie Range Trough is located east of the Wonominta Block (Figure 4-1), and has an estimated sedimentary thickness in excess of 8,000 m (Moffitt and Weatherall, 2004). Three petroleum wells have previously been drilled in the trough; Booligal Creek-1, Gnalta-1 and Pondie Range-1. Based on results of petroleum well drilling the Pondie Range Trough contains shallow sub-cropping Devonian rocks which unconformably underlie Cenozoic sediments of variable thickness (Lewis *et al*., 2008). For example, the Booligal Creek-1 well encountered Devonian sandstones with excellent porosity characteristics at about 240 m depth, whereas Pondie Range-1 drilled similar rocks at 80 m. Gnalta 1 was sited from surface in outcropping Devonian sandstones.

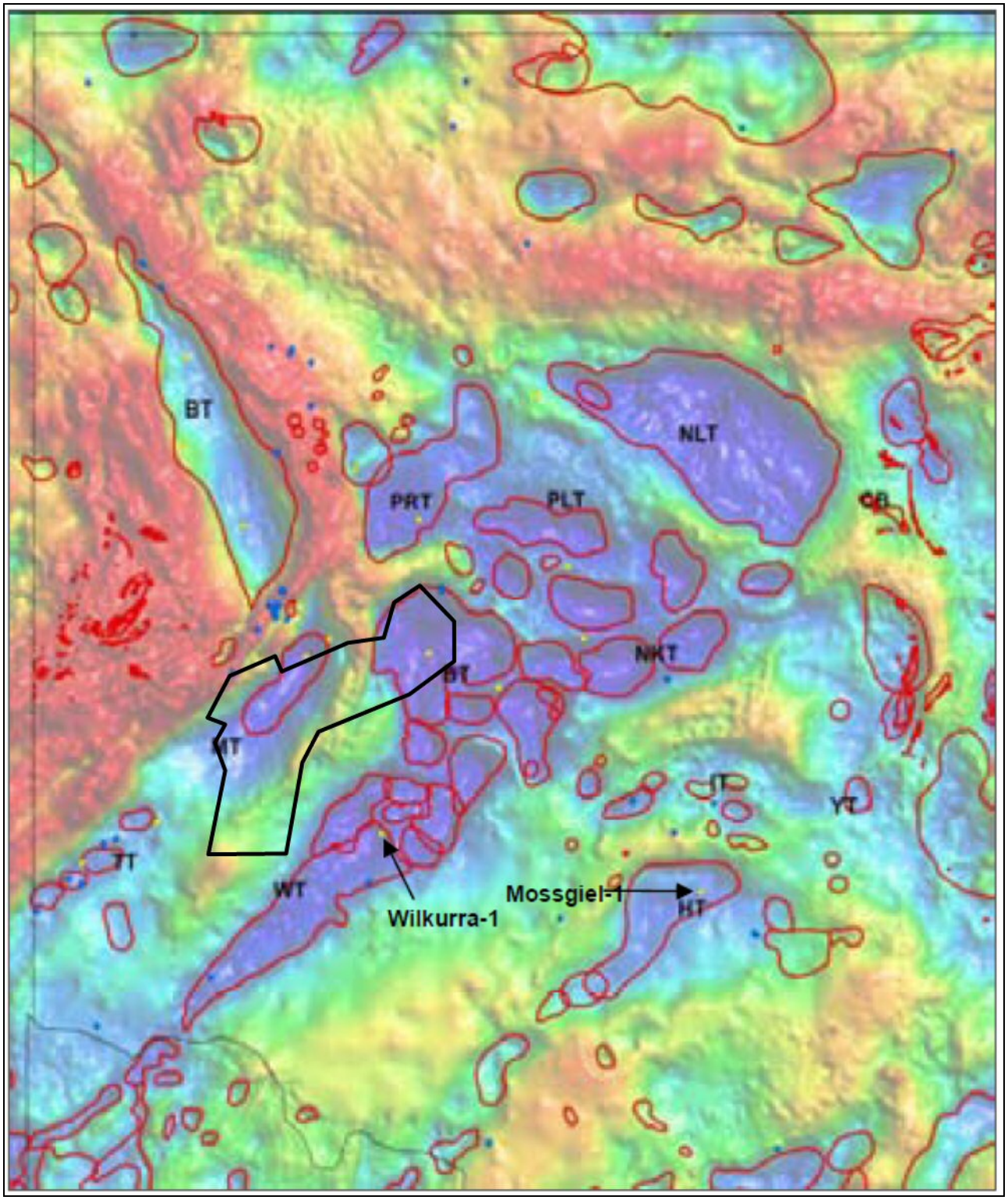

Figure 4-1. *A map of regional gravity data. Gravity lows (dark blue) are considered to be Silurian granites that underlie the Devonian extensional troughs. The granites are thought to have stabilised the crust (Blevin et al., 2007). Subsequent tectonic reactivation has largely focussed on the granite and basin margins, with little internal deformation of the Palaeozoic sedimentary basin materials. The main sub-basins of the Darling Geological Basin which occur within 150 km of Broken Hill include the Bancannia Trough which lies to the north of the Blantyre Trough (BT), the Wentworth Trough (WT), and the Menindee Trough (MT). The Mount Wintlow High is the gravity high to the south of the Menindee Trough, partially within the BHMAR study area. The DGB elements are overlain by a variable thickness of younger sediments belonging to the Murray Geological Basin. The BHMAR study area is also outlined. Figure adapted from Blevin et al. (2007).*

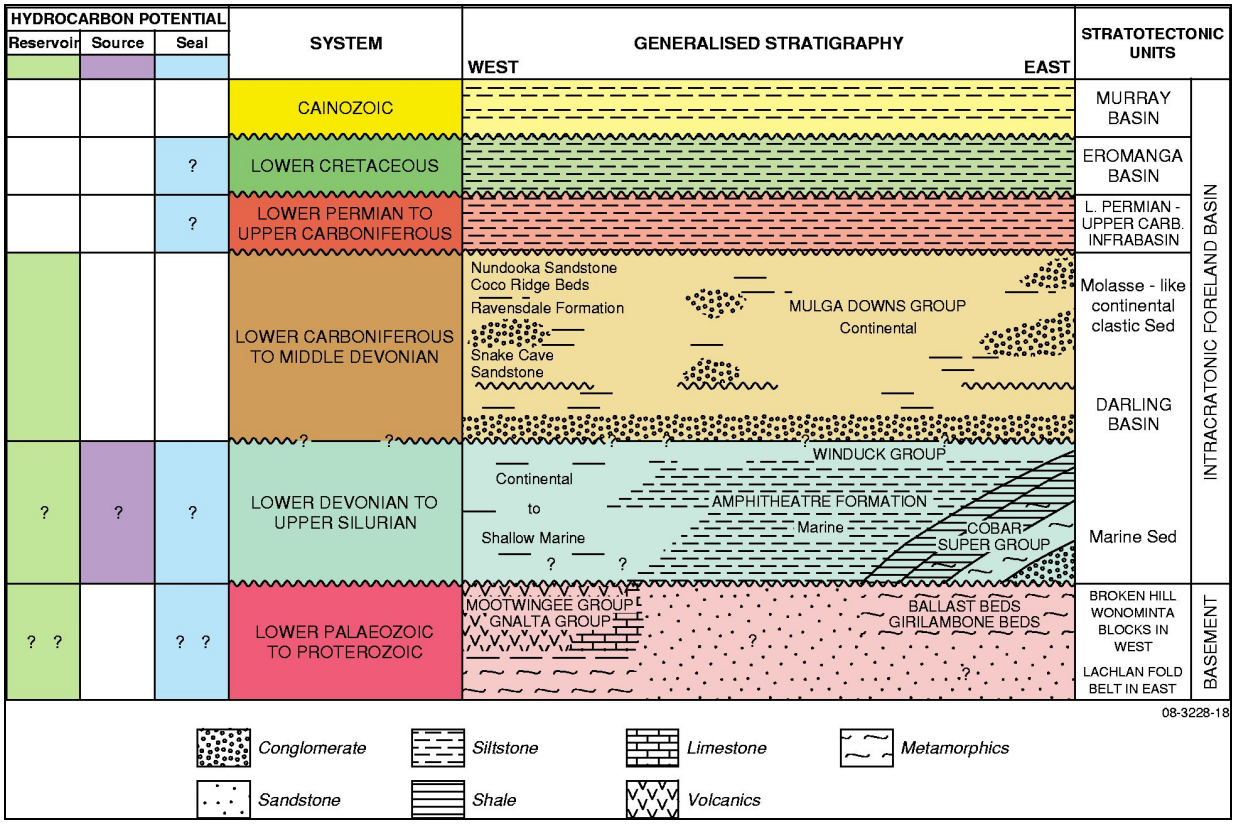

Figure 4-2. *Generalised stratigraphic profile for the Darling Geological Basin, also showing older and younger rock formations in the region. Most sedimentary rocks of the Darling Geological Basin were formed in the Devonian Period.*

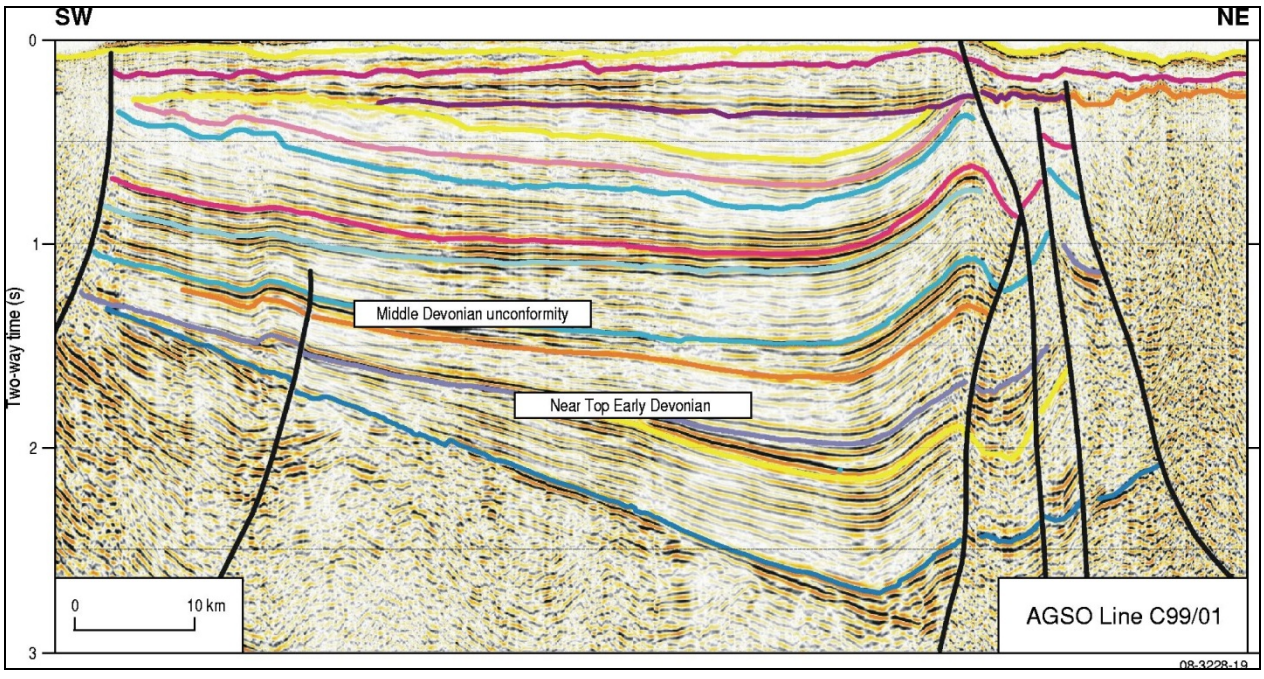

Figure 4-3. *Seismic reflection profile from survey line C99/01 conducted by the Australian Geological Survey Organisation across the central part of the Bancannia Trough. Up to 8,000 m of relatively flat-lying Devonian sedimentary rocks within the Bancannia Trough (interpreted horizons marked by various coloured lines on this image) occur between major sub-vertical faults which form the eastern and western margins of the sub-basin (data from Geoscience Australia). Importantly, the interpretation shows that there is significant evidence of tectonic inversion on basin bounding and within-basin structures. This is consistent with tectonic inversion recognised by Neef (2012).*

4.3 MURRAY GEOLOGICAL BASIN

The Murray Geological Basin is a large but relatively shallow Cenozoic sedimentary basin, extending over 300,000 km^2 of south-eastern Australia (Figure 4-4). Contours for the base of the Cenozoic sediment deposits within the basin show a dominant north-east trend, synonymous with the underlying infrabasins of the Tarrara, Menindee and Wentworth Troughs (Figure 4-1). These are embayments to the main depositional centre for the Murray Geological Basin, the Renmark Trough, where over 600 metres of Cenozoic sediment has accumulated (Figure 4-5). The Renmark Trough is bounded to the west by the Hamley Fault, separating it from a smaller depression, called the Canegrass Lobe (Figure 4-5). Smaller north-east trending depressions also separate structural highs, such as the Redan Embayment between the Broken Hill Block and Scopes Range as well as the Bunnerungee Trough between the buried basement ridges of the Lake Victoria and Lake Wintlow Highs (Brodie, 1994). The Neckarboo Ridge, to the east of the Darling River, is a basement high that is traceable on the land surface by elevated dune fields, 10–20 km across.

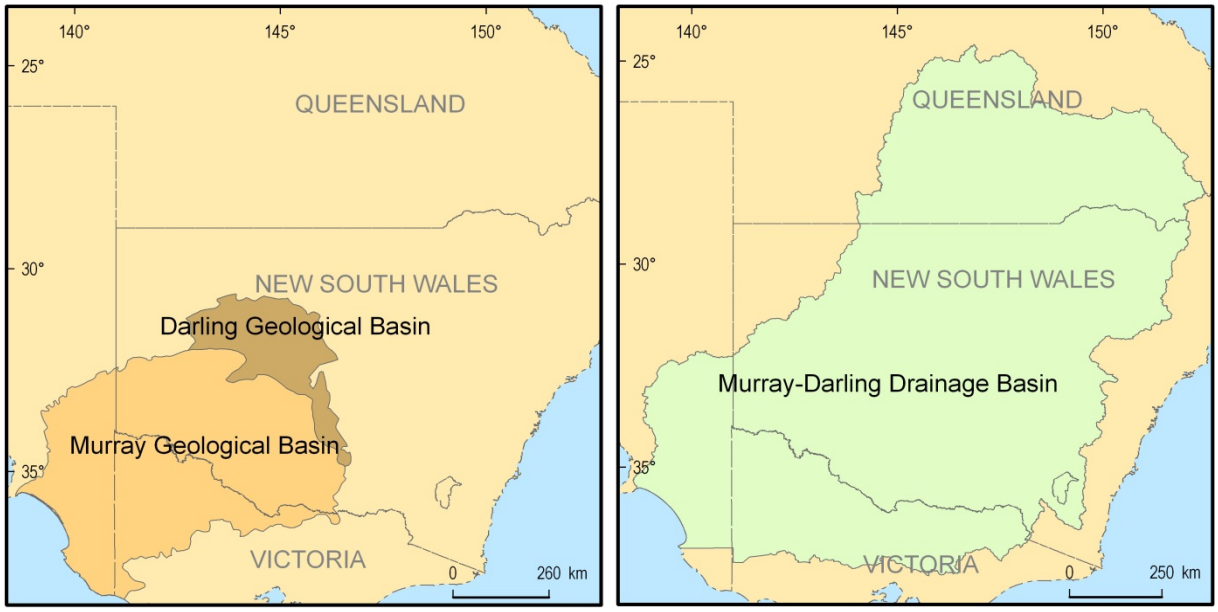

Figure 4-4. *Location of the Murray Geological Basin and Darling Geological Basin in south-eastern Australia (left-hand panel) compared with the present-day Murray-Darling (surface water) Drainage Basin (right-hand panel.*

The focus of geological investigations in the BHMAR study has been the shallow sediments of the Cenozoic Murray Geological Basin, at its northern juncture with the Darling River Basin. These basins, which have different geological and hydrogeological characteristics and histories, lie largely within the Murray-Darling Drainage Basin (defined by the present surface water catchment).

Prior to this study, there was only a very broad regional understanding of the large-scale sedimentary features, tectonic history, geomorphology, and groundwater systems of the north-western portion of the Cenozoic Murray Basin (Bowler & Magee, 1978; Brown, 1989; Brown & Stephenson, 1991; Brodie, 1994; Lewis *et al*., 2008). In general, more was known about the geology of the deeper sedimentary basins underlying the study area, largely on account of their oil and gas prospectivity (Blevin *et al*., 2007).

4.3.1 Regional Geology

The Murray Geological Basin contains sedimentary sequences formed in aeolian, fluvial, marine and marginal marine depositional environments. Towards the north-west basin margin, in the area of interest for this study (Mallee region of western NSW and South Australia) sediment fill is mostly of fluvio-lacustrine origin and contains extensive sand bodies which are capable of storing and transmitting significant quantities of groundwater (Figure 4-6). These aquifers are separated from limestone aquifers further to the south by marginal marine clays and marls.

Tectonic disruption during the Cenozoic is generally considered to be limited to minor differential subsidence, so that the depositional history of the basin tends to relate more to sea-level fluctuations. The area has had an enduring low-lying and subdued topographic expression that was periodically flooded by shallow epicontinental seas throughout the Cenozoic. Episodes of fluvio-deltaic, paralic and shallow marine sedimentation within the stratigraphic record correspond to periods of relatively high global sea level. This contrasts with erosion and non-deposition during periods of low global sea level. Based on recognition of major depositional and non-depositional events, the Cenozoic sediments of the basin are chronologically divided into three main sequences (Brown, 1989; Brown and Stephenson, 1991):

1. A **Palaeocene to Lower Oligocene sequence**, including the deep fluvio-lacustrine sand, carbonaceous silt and clays of the *Warina Sand* and *Lower Renmark* aquifers;
2. An **Oligocene to Middle Miocene sequence**, where a marine transgression deposited the *Murray Group* platform limestone aquifer, as well as various marginal marine clay aquitards such as the *Ettrick Formation, Winnambool Formation* and *Geera Clay*. Up-basin, fluvial deposition formed sand, silt and lignite deposits of the *Middle Renmark* and *Upper Renmark*; and
3. An **Upper Miocene to Pliocene sequence**, where the sand plain and beach ridges of the *Loxton-Parilla Sands* formed with the retreat of the sea following a short-lived marine transgression. The *Calivil Formation* is the fluvial equivalent found closer to the basin margins, consisting of fine- to coarse-grained quartz sand.

Figure 4-7 summarises the stratigraphic relationships within the Murray Geological Basin. The overlying veneer of Quaternary sediments includes aeolian, fluvial, lacustrine and colluvial deposits. These include the Shepparton Formation and Coonambidgal Formation aquifers associated with the Murray-Darling River system (Lewis *et al*., 2008).

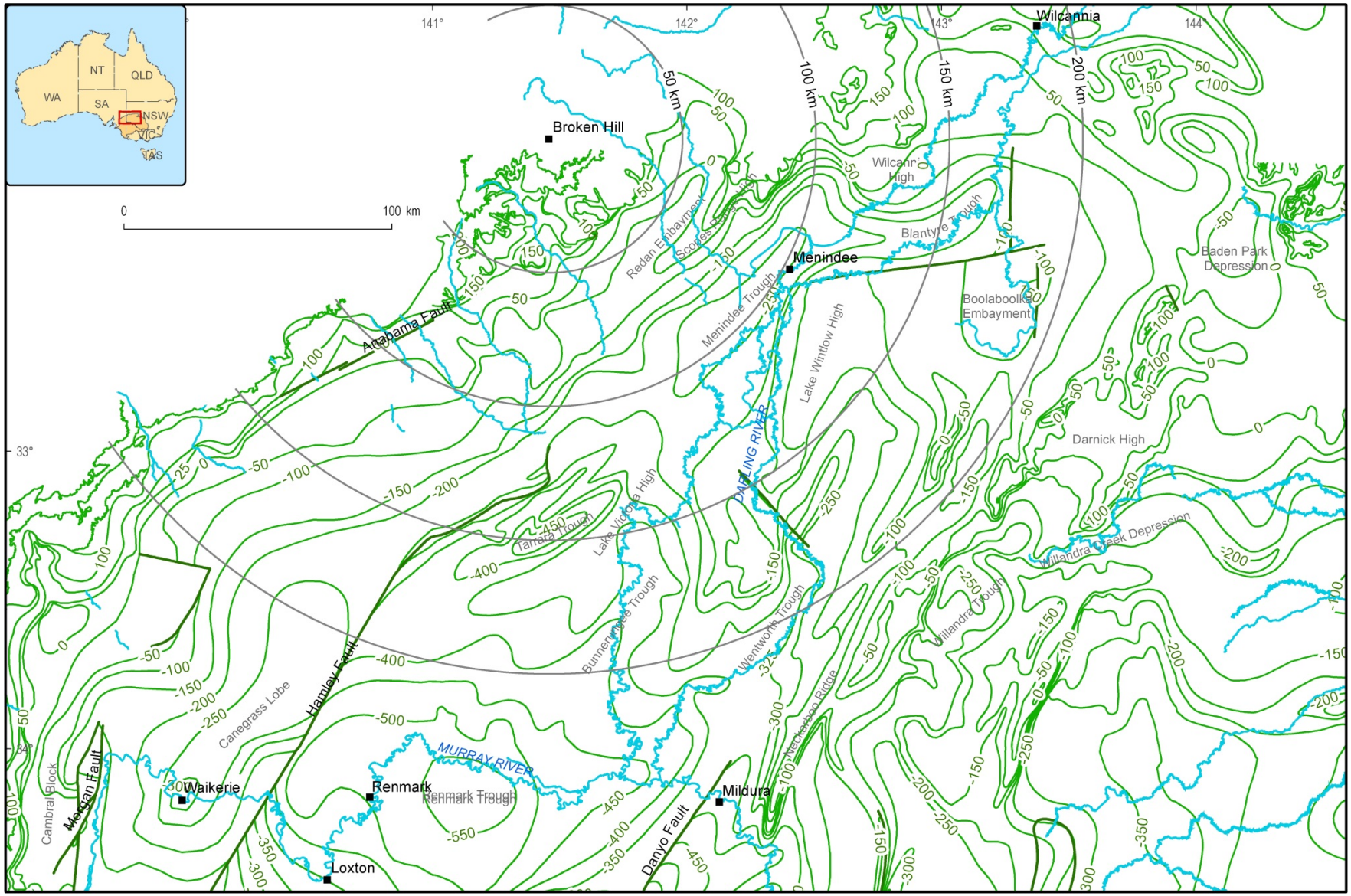

***Figure 4-5**. Structural contours for the base of Murray Geological Basin (MGB) sediments, and locations of underlying infrabasins such as the Menindee Trough. These contours show the variable thickness of sediments in the MGB, and that the north-west margin of the basin abuts the Proterozoic Broken Hill Domain (after Brodie, 1994).*

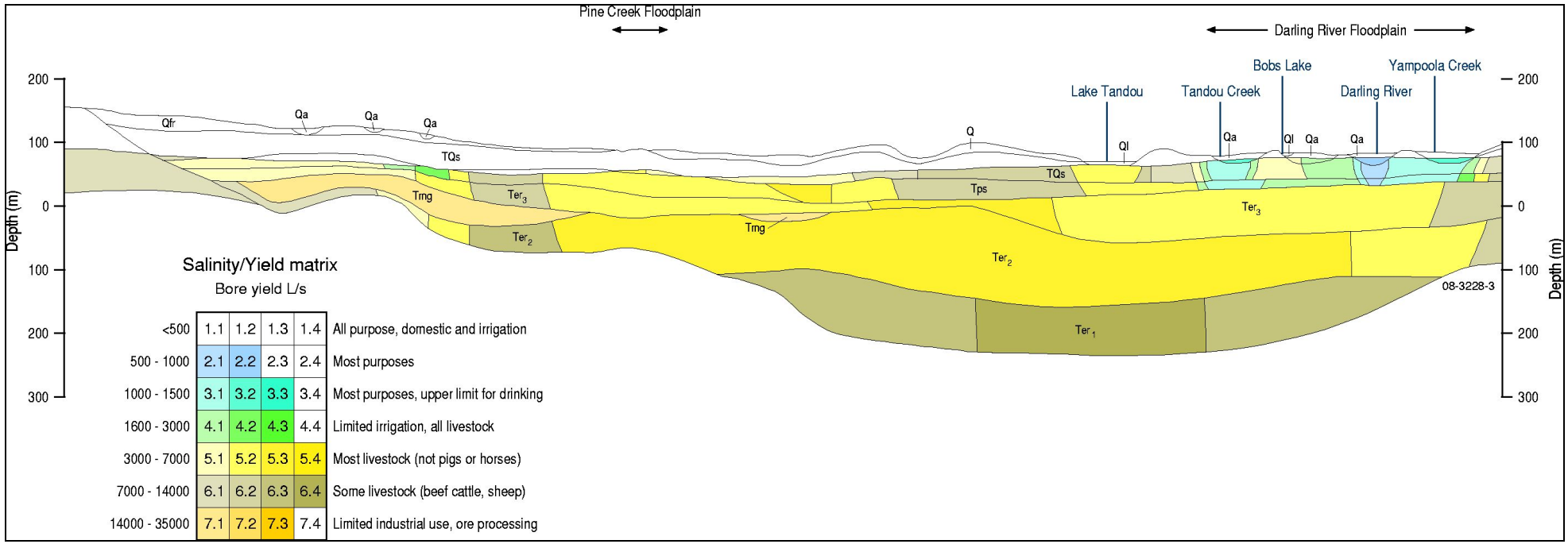

***Figure 4-6**. Interpreted cross-section (east-west) through part of the north-western Murray Geological Basin, showing the distribution of the main Cenozoic aquifers in the vicinity of the Menindee Lakes. The west side of the section (left-hand edge) shows the Murray Geological Basin thinning-out as it abuts the Proterozoic basement rocks of the Broken Hill Domain, whereas the eastern side (right-hand edge) shows multiple stacked aquifers of varying groundwater quality and yield in the Menindee area (aquifer symbols are: Ter1 – Lower Renmark Group; Ter2 – Middle Renmark Group; Ter3 – Upper Renmark Group; Tmg – Murray Group; Tps – Pliocene Sands; TQs – Shepparton Formation; Qs – Quaternary Alluvial deposits; Ql – Quaternary lake deposits). This section is based on the hydrogeological mapping of Brodie, 1994.*

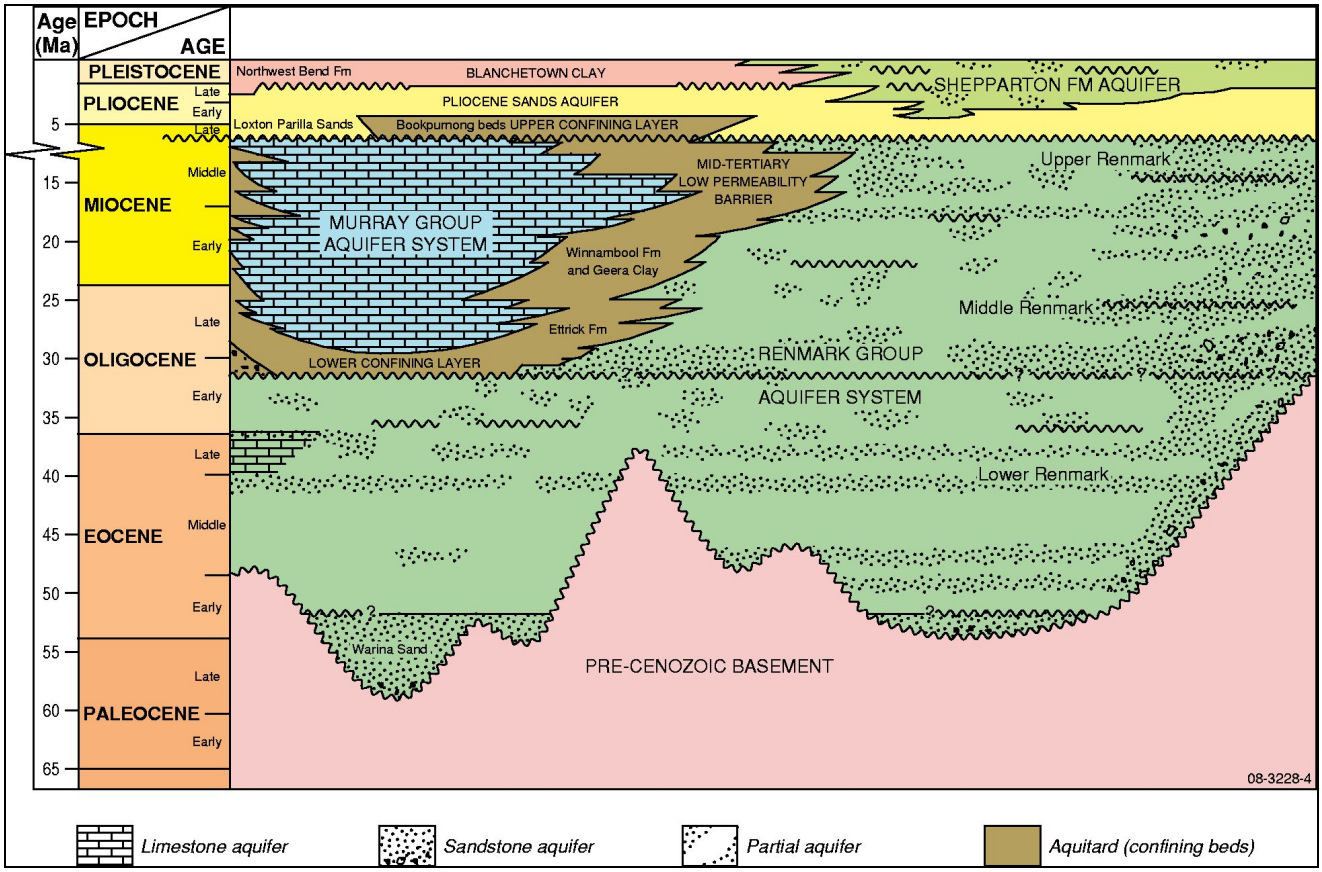

Figure 4-7. *Schematic stratigraphic chart showing temporal and spatial relationships of the various Cenozoic age formations in the Murray Geological Basin. The left-hand side represents the generalised western side of the basin, and the right-hand side shows the eastern side of the basin (after Brown & Stephenson, 1991).*

4.3.2 Regional Hydrogeology

4.3.2.1 Regional Groundwater Recharge Processes

Groundwater systems within the layered sequence of aquifers in the Murray Geological Basin generally flow from the basin margins and structural highs to the basin depocentre, in the vicinity of Renmark. The basin margins are therefore important sites of aquifer recharge. Along a 20–50 km-wide zone parallel to the north-west basin margin the shallow watertable is higher than the head in the deepest aquifer. As shown in Figure 4-8, this is indicated by a negative head difference which commonly exceeds -10 m after correction for density effects due to salinity and temperature. Thus, the potential vertical flow direction is downward. The vertical hydraulic conductivity of the sediments largely determines the extent of recharge.

The elevated basement ranges surrounding the basin are relatively impermeable and a significant component of a large rainfall event becomes surface run-off. This is channelled by small dendritic streams for 40–60 km into the sand plain of the Murray Basin, typically draining into terminal lakes. Some of the streams, such as Stephens Creek, Pine Creek and Turkey Plain Creek, have significant channels with a sandy bed and thus represent losing streams (to the water table) when they flow. Adjacent to the Broken Hill Block and Scopes Range, the shallow sediments are fluvial and sand-dominated, allowing rapid infiltration which reduces evaporative losses. The drainage off the surrounding basement supplements the direct infiltration of rainfall in the area. The extent of this recharge mechanism is reflected in the relatively low salinities (3,500–5,000 mg/L) found in a corridor bordering the basement highs (Figure 4-8). Isotopic data provides evidence of recharge from surface water flow following summer thunderstorms (Evans & Kellett, 1989).

Further to the south-west and in South Australia, the shallow sediments adjacent to the Benda Range are mostly marginal marine and clay-dominant. Here, infiltration is not as pronounced, and groundwater in the shallow aquifer is saline (> 14,000 mg/L). The equivalent freshwater head difference is also negative over

the Lake Wintlow High near Pooncarie. Here, recharge is concentrated at the apices of two alluvial fans developed over the structural high.

4.3.2.2 Local Recharge Processes

Further into the basin, recharge also occurs at the local scale. For example, sandy swales can be sites of internal drainage, receiving localised run-off after significant storm events. Rapid infiltration maintains a thin freshwater lens buoyed over the saline regional groundwater. Groundwater mounds developed under irrigation districts are extreme examples of enhanced recharge in this environment.

Recharge studies in the Mallee region have been used to establish links between clearing of native vegetation, enhancement of recharge, watertable rise and salinisation. Field measurements of recharge under native vegetation, including the mallee, belah-rosewood and pine woodland assemblages, indicate very low rates of < 0.3 mm/yr, or about 0.1 % of mean annual rainfall (Cook *et al.*, 1996). Potential recharge can increase dramatically following agricultural development. The magnitude of the change is largely dictated by the land-use and soil type. Where mallee vegetation has been cleared for cropping or annual pastures, recharge through sandy soils (<10 % clay) have been measured at 20–40 mm/yr (Cook *et al.*, 1996). The recharge is typically less than 5 mm/yr in areas where the clay content of the soil exceeds 20 %. However, recharge rates seem not to diminish linearly with further increases in clay content (Kennett-Smith *et al*., 1994). This is due to percolation between peds, cracks or root channels in clay soils. The magnitude of recharge may also depend on the amount of rainfall. Field data suggests that potential recharge of <1 mm/yr exists for non-cropped sites with mean annual rainfall <250 mm/yr (regardless of soil type) (Kennett-Smith *et al*., 1994). The threshold for cropped lands is lower.

Another important recharge mechanism is river leakage, e.g., on the Darling River floodplain. Downstream of Menindee, regulation of flow has effectively increased the average river stage, altering the interaction between the river and the underlying fluvial aquifer. A series of piezometer transects indicate that the river is losing water to the shallow aquifer (Stannard, 1981). A dilution aureole is found along most of the river, where shallow groundwater salinities range from 400–4,000 mg/L (Figure 4-8). This contrasts with typical salinities of about 20,000 mg/L in the shallow aquifer away from the lower reach of the river. Downhole conductivity logging (electro-magnetic method) of piezometers indicates a distinct interface between an upper freshwater lens and underlying saline regional groundwater (Williams & Beckham, 1995). The system appears to be dynamic, with the interface moving both laterally and vertically in response to changes in river level (Jewell, 1993).

There is evidence that the groundwater dilution aureole occurred along parts of the floodplain and lake system before the onset of river regulation. Mulholland (1940) recorded water wells obtaining fresh to brackish groundwater flanking river channels and floodplain lakes in the Talyawalka system. Large flood events allow overflow via Teryaweynya Creek into a chain of lakes to the south of the Talyawalka Creek. This resulted in freshening of groundwater (<2,000 mg/L) in the shallow aquifer underlying these lakes (Kellett, 1994). Significantly, water discharging from the Darling River at Wentworth is bicarbonate-dominant rather than chloride-dominant (major anion species), implying relatively low levels of groundwater accessions (Mackay & Eastburn, 1990).

The hydrological regime for the Darling Anabranch is also reflected in the underlying groundwater system. The groundwater salinity in the shallow fluvial aquifer of the Anabranch floodplain progressively degrades downstream from <1,500 mg/L to over 5,000 mg/L (Brodie, 1994). This reflects only sporadic major flood events reaching and hence recharging the bed of the lower reaches. At the turn of the century, numerous soakage wells were sunk along the main channel (Withers, 1994) to access this resource. These wells were typically 6–9 metres deep and were mostly used as a drought reserve. Likewise, the sediments of the upper floodplain lakes (e.g., Mindona and Travellers Lakes) contain better quality groundwater due to the greater frequency of flooding. Recharge from advancing floods is mainly via deep cracks developed in the dry heavy clay of the lake bed.

The use of the Menindee Lakes as water storages has had a significant impact on the underlying groundwater system. A groundwater mound is evident over the lake system, creating a density-corrected head difference between the shallow aquifer and the deepest Tertiary aquifer of over ten metres (Brodie, 1992). Downward

leakage is indicated by the level of dilution apparent in the deeper aquifers. There is potential for the watertable within depressions down-gradient from the storages (such as Emu Lake and Lake Tandou) to rise and cause salinisation problems (Bish & Salotti, 1996).

4.3.2.3 Regional Groundwater Discharge Processes

Groundwater flows from the basin margins to the regional discharge zone located near Renmark. Here, the potential vertical groundwater flow is upwards, driven by high heads in the deeper aquifers. This is defined by a positive equivalent freshwater head difference which progressively increases down the flow path (Figure 4-9). The head in the basal Lower Renmark aquifer is up to 20 m higher than the head in the shallow Murray Group Limestone aquifer. Near Waikerie, bores located in topographic lows which tap the confined Lower Renmark aquifer are commonly artesian.

Regional groundwater discharge is expressed as numerous salinas entrenched into the sand plain. These are particularly evident in a ~50 km-wide corridor north of Lake Victoria to Lake Popiltah and bounded to the east by the Darling Anabranch (Figure 4-9). This low-lying region overlies the regional depocentres of the Renmark and Tarrara Troughs, which were focal zones for tectonic subsidence and differential compaction. The control on the distribution of salt lakes in this area is two-fold. Firstly, they are located in depressions within swale and ridge systems. This reflects deposition during the Pliocene of Loxton-Parilla Sand beach ridges, separated by broad swales and local palaeochannels. In these lows, the regional watertable intersects the land surface and discharge conditions prevail. Secondly, the discharge zones tend to occur near the basin-ward edge of the marginal marine deposits. Here, the Geera Clay and Winnambool Formation are thinner, allowing greater opportunity for upward leakage from the pressurised basal aquifer.

Prominent NE-trending ridges evident in SRTM (and LiDAR) data (Figure 4-10 and Figure 4-11), are tectonic horst blocks related to reactivation of underlying basement faults mapped in magnetics and gravity data (Figure 4-12). The influence of topography (and underlying geology) is evident on maps of salinity yield for the aquifer (Figure 4-11).

4.3.2.4 Local Groundwater Discharge Processes

Local geological structures facilitate upward leakage of groundwater. Nulla Spring Lake, for example, is fault-bounded to the west with the underlying Blanchetown Clay displaced by nearly 10 m (Ferguson & Radke, 1992). The Scotia complex is located on the up-thrown side of the Hamley Fault where the upwarped Parilla Sand and Blanchetown Clay are relatively thin.

The Murray River traverses the regional discharge zone and mostly gains saline groundwater. River regulation, irrigation development and the practice of maintaining off-river storages in adjoining riverine lakes have resulted in significant changes to flow dynamics. Irrigation around Mildura caused the shallow watertable to rise by over 10 metres, resulting in significant displacement of saline groundwater into the river (Rural Water Commission, 1991). A series of interception bores along both sides of the river now operate to reduce the salt impact. Similar groundwater mounds have developed under the irrigation districts in South Australia (Barnett, 1991). An average daily salt return to the river is estimated at 104 tonnes at Waikerie/Golden Heights, 146 tonnes at Berri/Cobdogla and 80 tonnes at Loxton (Smith & Watkins, 1993). Hydraulic loads, causing displacement of saline groundwater, are also imposed by water storages (e.g., Lake Victoria), river locks and evaporation basins located within or near the floodplain.

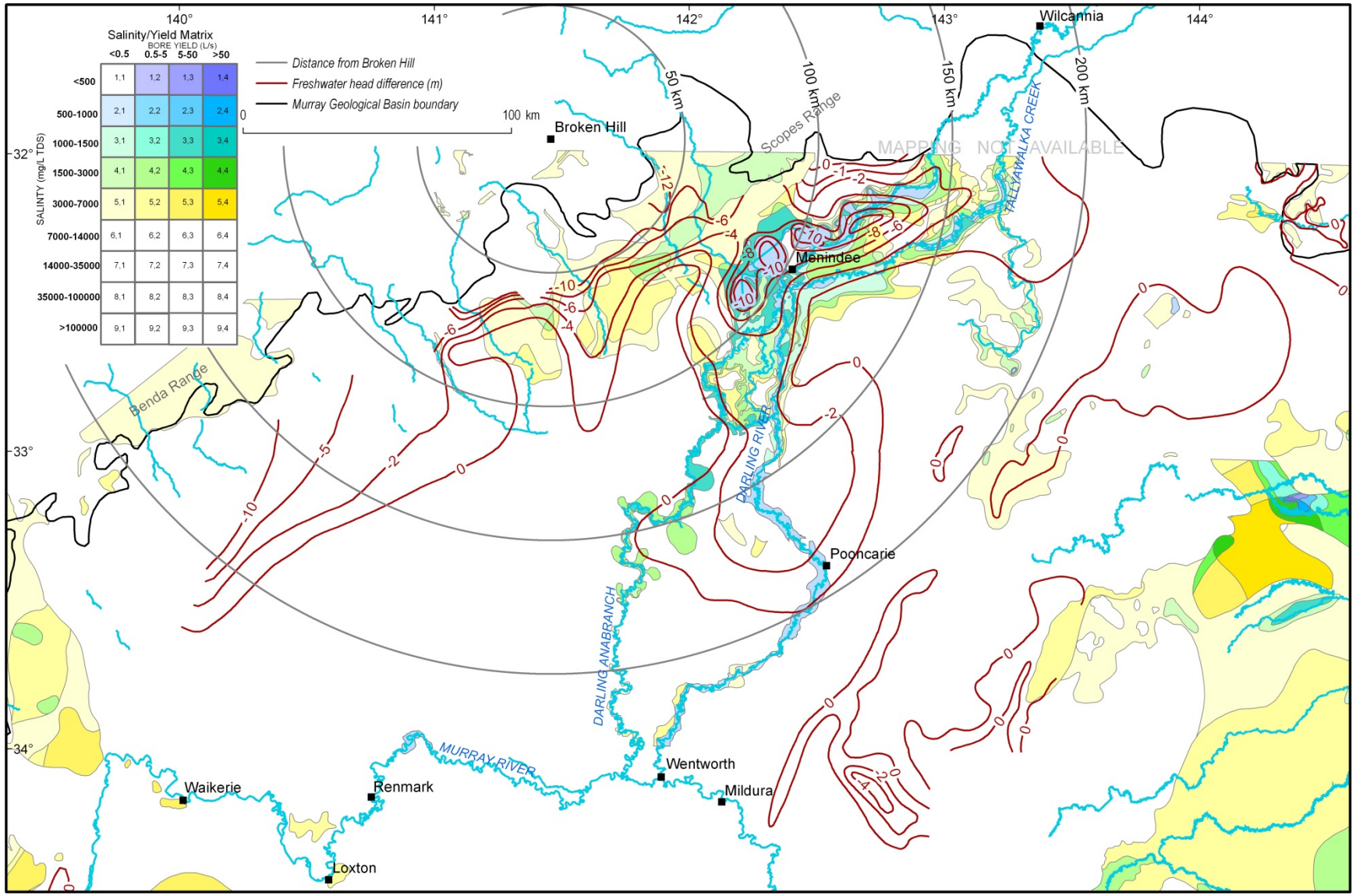

Figure 4-8. *Areas of downward head gradient and significant recharge in the north-west Murray Geological Basin. The areas of negative head difference(shown by contours) mean that the shallow unconfined (water table) aquifer is at a higher level than the confined head of the deepest aquifer, and hence vertical groundwater flow is directed downwards (hydrogeological mapping after Brodie, 1994 shows variations in groundwater salinity and yield*).

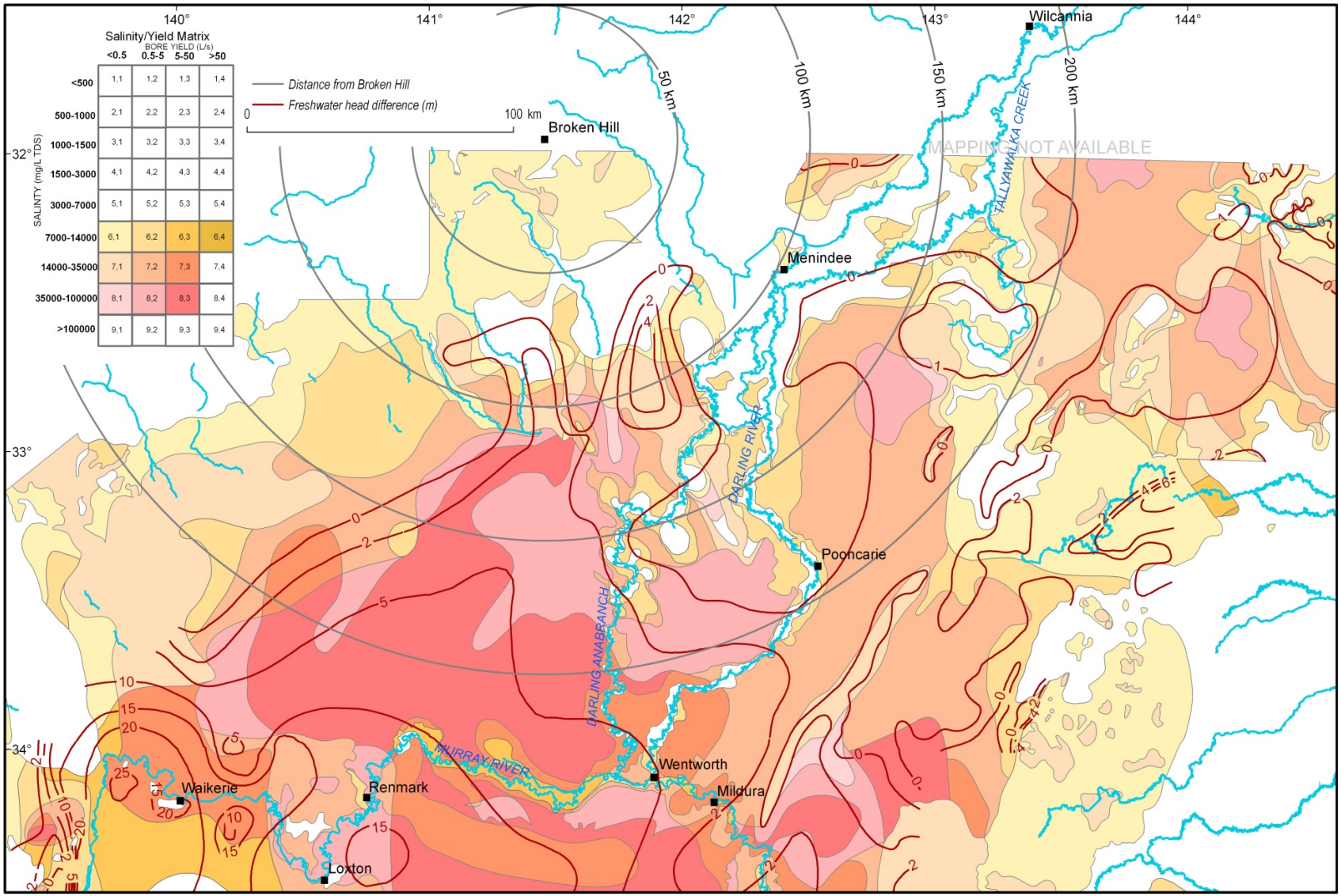

Figure 4-9. *Areas of upward head gradient and significant discharge in the north-west Murray Geological Basin Major discharge sites are defined here by the areas of greatest groundwater head difference (shown by the contour lines), e.g., up to 20 m variation around Waikerie. In the Broken Hill area the greatest head difference is <5 m (hydrogeological mapping showing variations in groundwater salinity and yield after Brodie, 1994).*

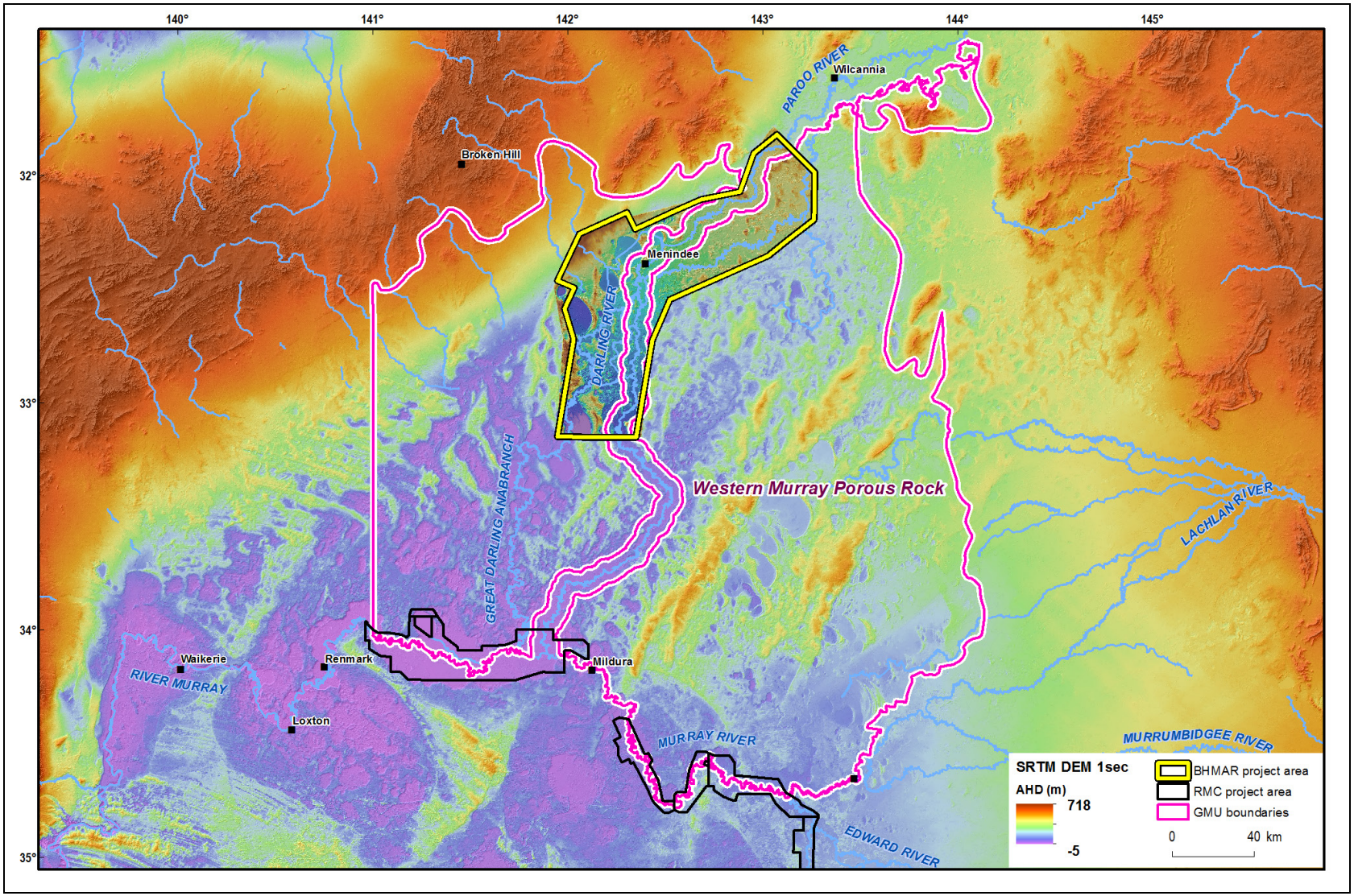

Figure 4-10. *A 1 Second SRTM DEM image showing landscape elevation over the Western Murray Porous Rock Aquifer. Prominent NE-trending ridges are tectonic horst blocks related to reactivation of underlying basement faults mapped in magnetics and gravity data.*

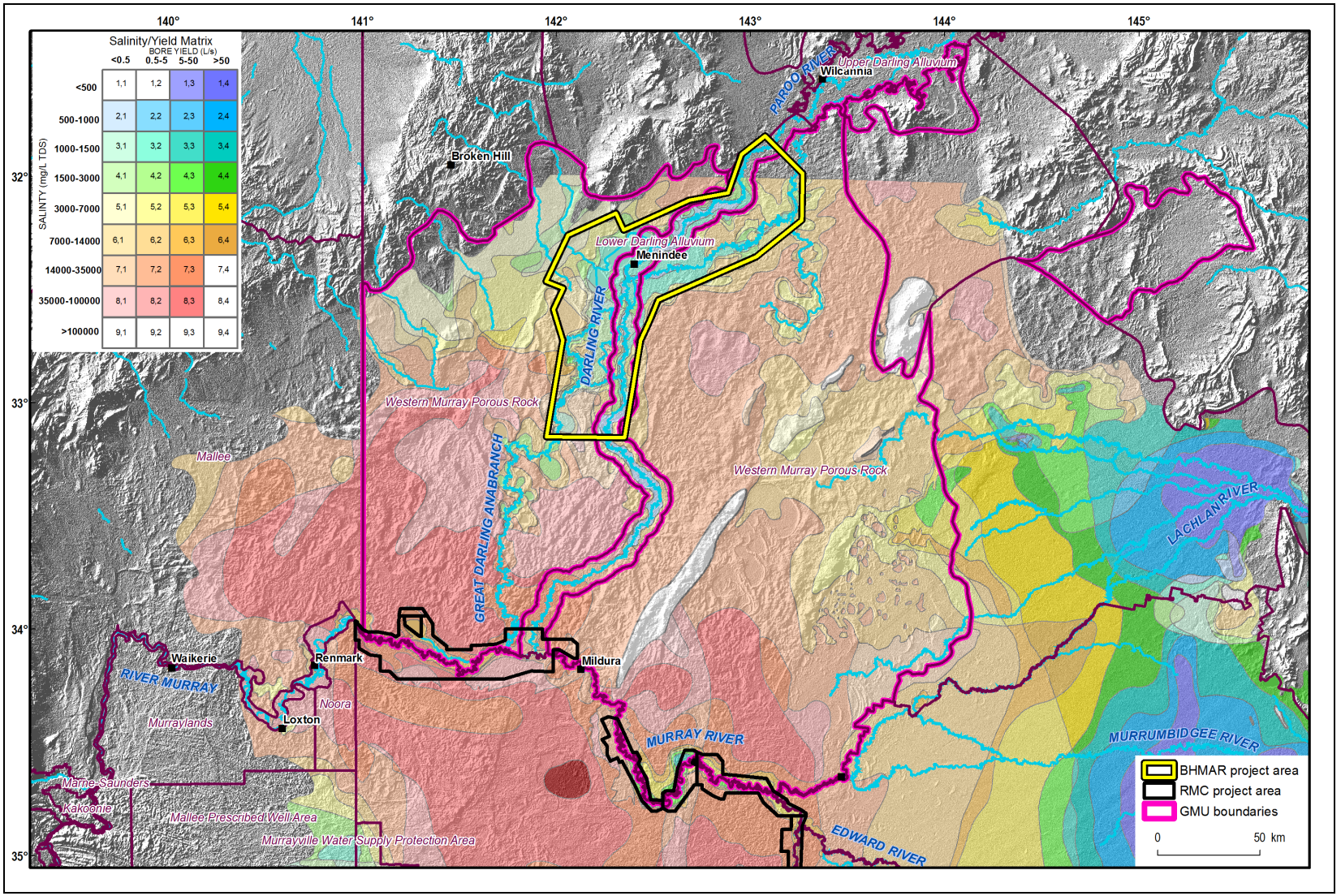

***Figure 4-11**. Regional salinity-yield mapping for the Pliocene Sands (Calivil Formation and Loxton-Parilla Sands) aquifer from the 1:250,000 scale Murray Basin Hydrogeological Map Series. The mapping is underlain by the regional DEM. The BHMAR project and groundwater management unit (GMU) boundaries are also shown.*

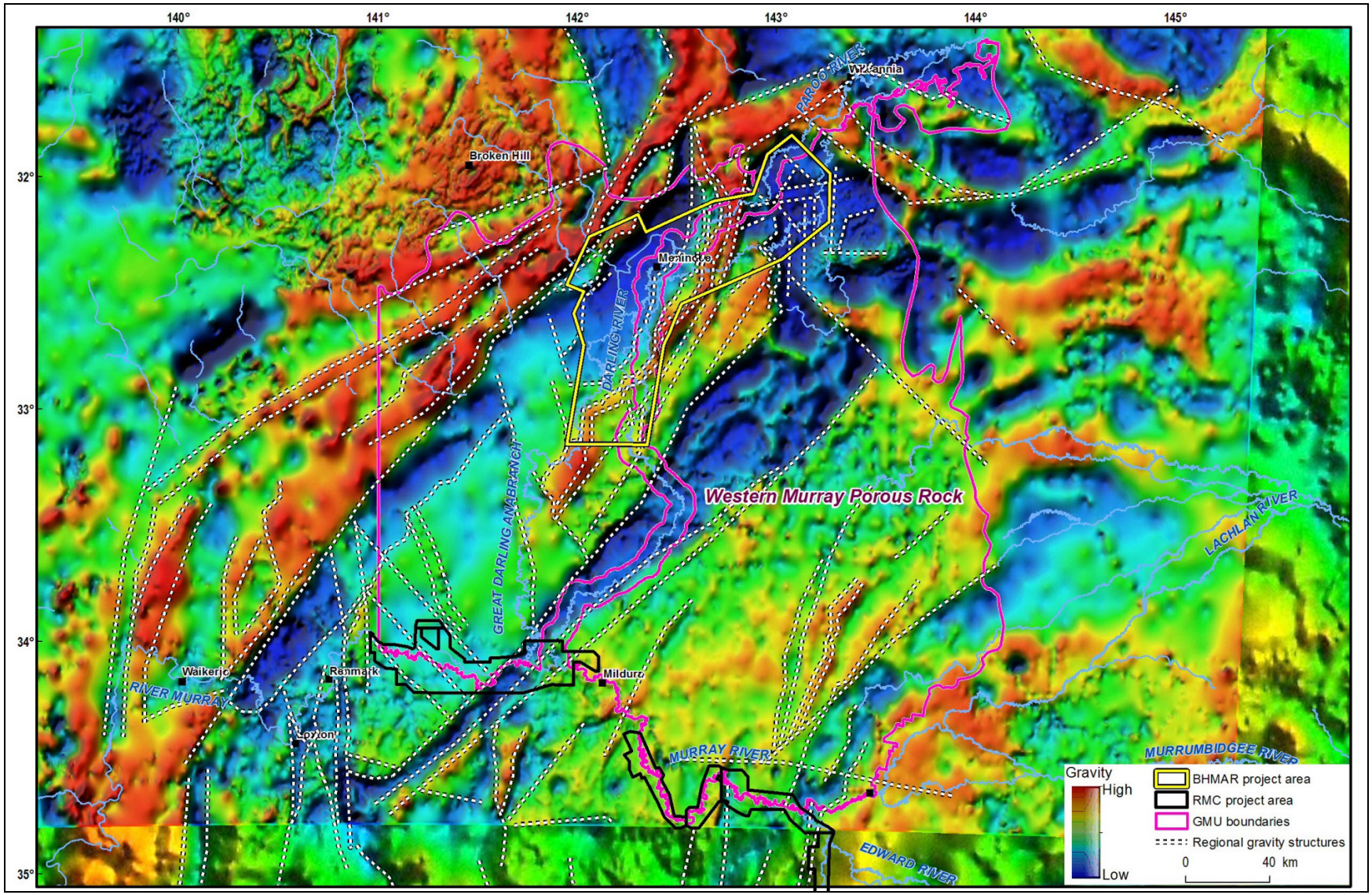

***Figure 4-12**. An image showing variations in regional gravity over the Western Murray Porous Rock Aquifer. Many of the lineaments mapped are coincident with magnetic lineaments. Several of the major lineaments correspond with features in the SRTM DEM. (Figure 4-10).*

5. Stratigraphy and Evolution of the Murray Geological Basin Sediments within the Darling Valley

The focus of geological investigations in the BHMAR study has been the shallow sediments of the Cenozoic Murray Geological Basin, at its northern juncture with the Darling River Basin. These basins, which have different geological and hydrogeological characteristics and histories, lie largely within the Murray-Darling Drainage Basin (defined by the present surface water catchment).

Prior to this study, there was only a very broad regional understanding of the large-scale sedimentary features, tectonic history, geomorphology, and groundwater systems of the north-western portion of the Cenozoic Murray Basin (Bowler & Magee, 1978; Brown, 1989; Brown & Stephenson, 1991; Brodie, 1994; Brodie, 1998; Lewis *et al*., 2008). In general, more was known about the geology of the deeper sedimentary basins underlying the study area, largely on account of their oil and gas prospectivity (Blevin *et al*., 2007). The new geological framework, geomorphology and landscape evolution is discussed in this section. The key stratigraphic units of relevance are shown in Table 5-16.

5.1 RENMARK GROUP

The lower aquitard in the project area consists of the Renmark Group or, where present, Palaeozoic basement. In the study area, the Palaeozoic basement is limited in occurrence and was only encountered in three sonic holes.

Regionally, the Renmark Group comprises the non-marine Palaeocene to Miocene sediments of the Murray Geological Basin (Brown & Stephenson, 1991). The sediments are in part laterally equivalent to the Oligo-Miocene Murray Group marine deposits. Basin-ward, the Renmark Group passes into the marginal marine to shallow marine Geera Clay Formation. This formation, with its diagnostic marine microfauna and thin carbonate beds does not occur in the project area

Deposition of the Renmark Group in the project area is controlled by the Menindee Trough (Lawrie *et al.,* 2009a, and references therein), a north-east to south-west trending structural basin that limits the lower Renmark Group and influences the thickness of the middle and upper Renmark Group. The Menindee Trough is somewhat narrower overall than the project area, widens to the south-west and narrows to the north-east. The upper part of the Renmark Group occurs across the whole project area. It too is probably controlled by the underlying Menindee Trough, possibly as a sag basin.

The upper Renmark Group is a widespread non-marine succession of Miocene age in the Murray Basin. Unlithified and nowhere exposed, it is poorly understood. It is inferred from drilling to be deposited on a low relief sedimentary plain dominated by anastomosing fixed channel streams, flowing southward into a complex low energy coastal plain with numerous lagoons and bays. In 90% of the holes drilled, the upper Renmark Group is represented by muds.

The upper Renmark Group sequence acts as an underlying aquitard to important aquifers in the overlying Calivil Formation succession. Hydraulic connection between the Calivil Formation and Renmark Group tends to be limited, except where Renmark Group channel sands immediately underlie the Calivil Formation. In these areas there can be a distinct salinity gradient from the Calivil Formation down into the Renmark Group, indicating groundwater mixing (Table 5-16; Figure 5-87).

5.1.1 Project Area

The Renmark Group disconformably underlies the Calivil Formation everywhere in the project area except where bedrock highs rise through the succession into the Calivil Formation. The full succession in the area

was intersected in only one historic borehole (GW036838), a log of which is available in Lawrie *et al.* (2010b). Bedrock was encountered at a depth of 310 m. Other historic boreholes with significant thickness of Renmark Group are T2:0702 (TD 235 m), GW036881 (TD 164 m), GW036881 (TD 183 m), and GW036840 (TD 150 m).

Renmark Group sediments and/or basement were encountered in most BHMAR project bores, with the exception of a relatively small number of shallow monitoring bores. However many boreholes only had a narrow interval of Renmark Group in them. Boreholes with extensive thicknesses of Renmark Group (>20 m) and/or basement are shown in Table 5-1, and all boreholes that intersected the Renmark Group are shown in Table 5-2. The top Renmark Group lithology, where it is in contact with the Calivil Formation aquifer, is also shown. These boreholes were largely used for the more detailed facies analysis discussed below. Sampled Renmark Group contained Oligocene (presumably late Oligocene) through to Early and Middle Miocene spores and pollen (Macphail, 2010), representing the middle to upper part of the Renmark Group, mostly likely the Olney Formation equivalent (c.f. Brown & Stephenson 1991).

Table 5-1. *BHMAR sonic bores with significant thicknesses of Renmark Group. Bores are listed in decreasing order of Renmark Group thickness.*

Borehole	Thickness of Renmark (m)	Comments
BHMAR33-1	147.0	Thickest Renmark Group drilled in project. Lowest 24.15 m is sand and excluded from analysis in this section as it may be a lower stratigraphic unit.
BHMAR04	78.9	
BHMAR61	70.55	Thick sand (17-18 m thick)
BHMAR35	54.4	Sand unit 12-13 m thick
BHMAR34	53.8	
BHMAR16	50.58	
BHMAR64	45.9	Sand 15-16 m thick
BHMAR66	39.15	
BHMAR06	38.5	
BHMAR23	37.3	Lowest proportion of sand (4.4%)
BHMAR18	36.0	Sand 14-15 m thick
BHMAR05	33.77	
BHMAR21	30.1	Thick sand (5-6 m thick) on contact
BHMAR22	30.0	
BHMAR43	28.7	
BHMAR03B	27.9	Highest sand content (78.7%)
BHMAR65	25.25	
BHMAR19	24.0	
BHMAR57	24	
BHMAR36	23.4	Sandiest hole (87%) 18.25 m coarse to very coarse sand
BHMAR48	23.13	
BHMAR31	21.35	

Table 5-2 includes four problematic holes drilled during Phase3a, BHMAR79A-2, 79A-6, 88-3 and 88-7 (Table 5-3), which are located on the Menindee Common. These specific holes are problematic as they are interpreted as having very thick sand units underlying the Calivil Formation with only subtle differentiation between the two units. The lower part of the thick sand in these holes is both reduced and also increases in conductivity with depth. There are two possible explanations for these observations as summarised in Table 5-3. Option 1: the observed sand unit is a thick channel deposit in the Renmark Group that coincidently underlies Calivil Formation. Option 2: the sand is an unusually thick section of Calivil Formation that has been stratified both with respect to salinity and redox. Of the two explanations, Option 1, that there is coincidently a thick Renmark Group channel immediately beneath the Calivil Formation, is considered most likely as it best explains the observations. Hydrologically, the implications of both models are the same, that excessive pumping in these holes may result in up-coning of the saline and reduced water into the main aquifer.

The two southernmost sonic holes, BHMAR29 and 31, show very distinctive facies in the Renmark Group. They are composed of well laminated very dark brown muds and sandy muds. These sediments contain marine dinoflagellates of Oligocene to Middle Miocene area. This suggests that this unit is laterally equivalent to the Geera Clay, although these holes lack the characteristic marl beds and marine faunas of that formation (c.f. Brown & Stephenson, 1991).

Table 5-2. *All BHMAR sonic bores that intersected the Renmark Group.*

Hole	Thickness m	Top Lithology	Comments
BHMAR03B	27.9	Mud	
BHMAR04-1	78.9	Mud	
BHMAR05	33.77	Mud	
BHMAR06	38.5	Mud	
BHMAR08-1	12.0	Mud	weathered upper Renmark
BHMAR16-1	50.58	Sandy mud	
BHMAR17-1	16.38	Mud	
BHMAR18-1	36.0	Mud	Weathered upper Renmark
BHMAR19-1	24.0	Mud	
BHMAR21-1	30.1	30.1 m of mostly sand	
BHMAR22-1	30.0	Mud	
BHMAR23-1	37.3	Mud	
BHMAR29-1	12.0	Mud	Transitional to Geera Clay
BHMAR31-1	21.35	Sub-metre scale interbedded mud and sand	Transitional to Geera Clay
BHMAR33-1	147.0	Mud	
BHMAR33-5	6.8	Thin (1.57 m) sand over mud	
BHMAR33-6	6.43	Sub-metre scale interbedded mud and sand	
BHMAR33-7	5.0	Mud	
BHMAR33-8	13.58	Mud	
BHMAR33-9	5.5	Mud	
BHMAR 34-1	53.8	Sub-metre scale interbedded mud and sand	
BHMAR35-1	54.4	Mud	
BHMAR36-1	23.4	18.25 m coarse to very coarse sand on contact	
BHMAR41-1	22.75	Mud	
BHMAR43-1	28.7	Sub-metre scale interbedded mud and sand	
BHMAR48-1	24.0	Mud	
BHMAR57-1	24.0	Sandy mud	
BHMAR58-1	16.65	Mud	
BHMAR61-1	70.55	Mud	Lignite bed
BHMAR64-1	45.9	Mud	
BHMAR65-1	25.25	Mud	
BHMAR66-1	39.15	Mud	
BHMAR71-3	15.39	Mud	
BHMAR75-3	7.13	Mud	Lignite beds
BHMAR75-7	10.5	Mud	
BHMAR75-8	2.9	Mud	
BHMAR77-2	8.2	Mud	
BHMAR79A-2	19	5.97 m of sand and muddy sand	May be partly Calivil Formation
BHMAR79A-6	8.2	>8 m medium to coarse sand	May be partly Calivil Formation
BHMAR80A-2	3.22	Mud	
BHMAR80B-2	10.4	Mud	
BHMAR83-2	4.12	3.7 m fine to medium sand, some muddy	
BHMAR84-2	7.25	Mud	
BHMAR88-3	21.1	Sand	May be partly Calivil Formation
BHMAR88-7	32.65	Sand	May be partly Calivil Formation
BHMAR92-1	13.5	12.3 m of fine to medium sand, some muddy	
BHMAR99-1	6	Mud	

Table 5-3. BHMAR boreholes with problematic contacts between the Renmark Group and Calivil Formation.

Borehole	Option	Thickness Renmark	Thickness Renmark Group sand	Comments
BHMAR79A-2	1	19 m	13.95 m[1]	Sand on contact, picked on colour change in sand and rising conductivity
BHMAR79A-2	2	4.9 m	1.1 m	Base thick sand, all over-lying sand in Calivil Formation
BHMAR79A-6	1	7.99 m	7.99 m[1]	Picked on colour change in sand and mud content
BHMAR79A-6	2	0 m	0 m	Calivil Formation to end of hole, base not exposed, redox & salinity stratified aquifer in Calivil Formation
BHMAR88.3	1	16.64 m[1]	16.64 m[1]	Sand on contact, picked on colour change in sand and rising conductivity
BHMAR88-3	2	0 m	0 m	Calivil Formation (sand) to end of hole, base not exposed
BHMAR88-7	1	32.65 m	21.6 m[2]	Calivil Formation to 50.35 (picked on first appearance of mud, and rising conductivity)
BHMAR88-7	2	4.4 m	1.15 m	Calivil Formation to 78.6 (picked on colour change and start of muddy lithology)

[1] Within known thickness of Renmark Group sand bodies in other holes.

[2] ~3 m thicker than next thickest amalgamated channel complex.

5.1.2 Architecture

5.1.2.1 Architectural elements

The logged lithologies of the Renmark Group consist of two main elements: sands and muds. Amongst the 47 drillholes that intersected Renmark Group sediment, a total of 216 individual sand beds have been identified in the drill cores. Plotting the number of sand beds in the holes with significant thicknesses of Renmark Group (Table 5-1) against thickness of those beds in one metre increments gives Table 5-4. Represented in graphical form (Figure 5-1) three main groups are observed - thin units (01, 1-2 and 2-3 m), medium units (3-4, 4-5, and 5-6 m) and thick units (7-22 m).

Table 5-4. *Renmark Group sand bed thickness distribution.*

Thickness	Total beds	% of total individual sand beds present in drill cores (N = 216)
0-1	108	50
1-2	45	20.8
2-3	30	13.9
3-4	10	4.6
4-5	8	3.7
5-6	3	1.4
6-7		
7-8	1	0.5
8-9	1	0.4
9-10	1	0.5
10-11	1	0.5
11-12	1	0.4
12-13	1	0.5
13-14	1	0.5
14-15	1	0.4
15-16	1	0.5
16-17		
17-18		
18-19	2	0.9
19-20		
20-21		
21-22	1	0.5

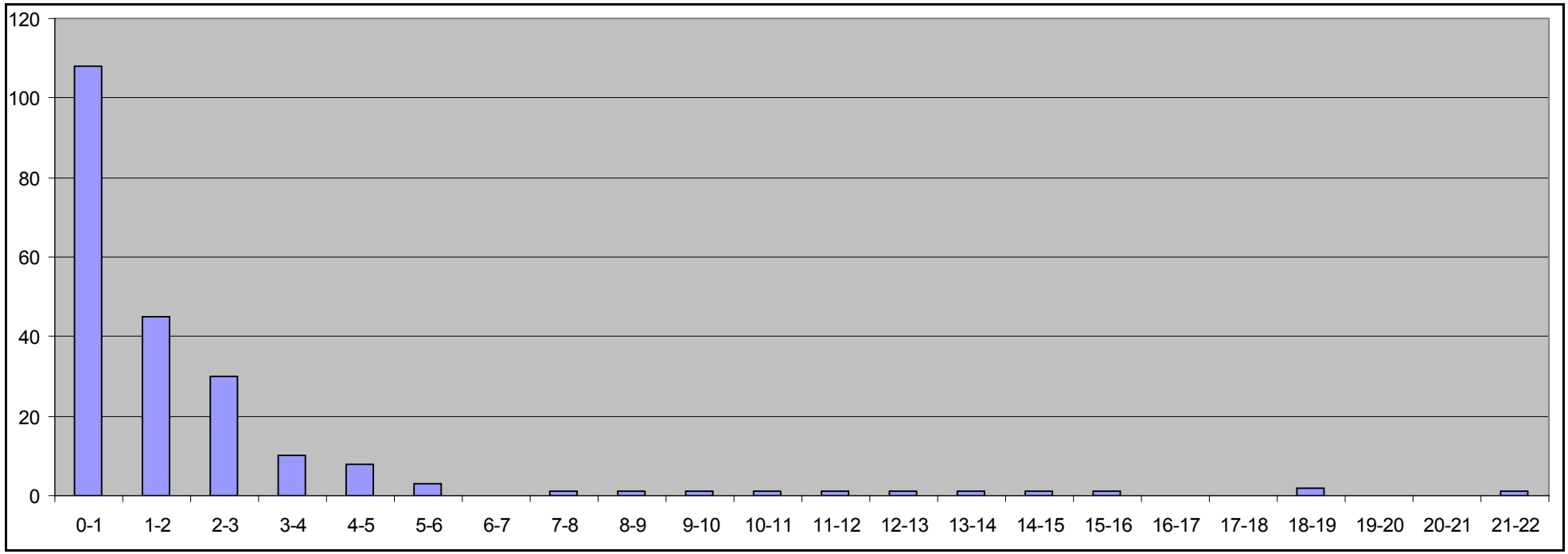

Figure 5-1. *Histogram of number of beds of specified thickness in Renmark Group. Beds 1-3 m thick are interpreted as levee bank and crevasse splay deposits, those 3-6 m thick single storey channel deposits, and those greater than 7 m multistorey stacked channels.*

Only a small percentage (12.7%) of the area of Renmark Group is composed of thick (>3 m) sand (Table 1 5). Mud deposits make up more than three quarters of the area (76.7%) while thinly interbedded muds and sands make up the remainder (10.6%). At Jimargil the proportion of sand is somewhat higher (19.1%; Table 1 6) due to the presence of muddy sand in a number of holes. The aquitard properties remain unaffected, however, because of the lower hydraulic conductivities found in these lithologies due to the muddy matrix.

Table 5-5. *Renmark Group lithology on contact with the Calivil Formation observed in all BHMAR holes.*

Lithology	Number	Percent	comments
Mud or sandy mud	36	76.7	Floodplain
Sub metre interbedded sand and mud	5	10.6	Levee or splay (near channel)
Sand and muddy sand	6	12.7	Channel
Total	47	100.0	

Table 5-6. *Renmark Group lithology on contact with the Calivil Formation in Jimargil boreholes.*

Lithology	Number	Percent	Comments
Mud or sandy mud	15	71.4	Floodplain
Sub metre interbedded sand and mud	2	9.5	Levee or splay (near channel)
Sand and muddy sand	4	19.1	Channel
Total	21	100	

5.1.2.2 Interpreted depositional environments

Sands (including minor gravels) are interpreted as being deposited in three environments:

- Channels: fine- to coarse-grained sands, gravels, muddy sands;
- Crevasse splays: fine to medium sands, sometimes muddy, very rare gravel; and
- Levees: fine sand and silty sand.

As shown by Figure 5-3, the data falls into three main groups. The majority of units (84.7%) are thin <3 m), and are interpreted as thin crevasse splays and levee deposits. The much smaller number (9.7%) of medium thickness units (3-6 m) are interpreted as thicker crevasse splay deposits. Thick (>7 m) units are interpreted as channels, and are often composed of multistorey units separated by thin muddy beds. They comprise only a small proportion of the overall number (4.6%) but make up a significant part of the total thickness.

Table 1-5 shows that only a small proportion of the area of Renmark Group (12.7%) exposed along the contact with the Calivil Formation is composed of thick (>3 m) sand associated with channels, the remainder is composed either of impermeable floodplain deposits (76.7%) or levee and splay deposits of limited permeability and extent. The presence of thick Renmark Group sands in contact with the Calivil Formation as observed at the BHMAR79A and 88 series of holes is unusual. Due to their relatively close proximity to one another it is concluded that these holes have probably intersected the same sand body.

The small area of channel deposits compared to the floodplain deposits suggests a fixed channel fluvial system while the relatively large number of individual channel units suggests an anastomosing system. This is consistent with the scarcity of thick successions of thinly interbedded medium- to fine-grained sands and silts that would indicate meandering channel depositional systems (unlike those encountered in the Coonambidgal, and Menindee Formations and the Willotia beds.

Approximate channel widths can be calculated using thickness to width ratios appropriate for fixed channels (Gibling, 2006). Fixed channels have width:depth ratios of 5:15. The narrowest channel units therefore are estimated to be 15-45 m wide, the widest 110-330 m.

An additional insight into channel dimensions can be obtained from the thickness of black muddy units overlying some channel deposits. These are interpreted as mud plugs deposited in flooded abandoned channels. The channel bank height above the basal sands can be estimated from the thickness of the clay plug (Figure 5-2). Based on this principal, channel banks were in some cases up to 7 m high with maximum sand channel thickness of 6 m. The sand units with reported thickness of greater than 6 m (Figure 5-2 and Table 5-4) represent channels that were completely filled by sand, without space for a plug to form.

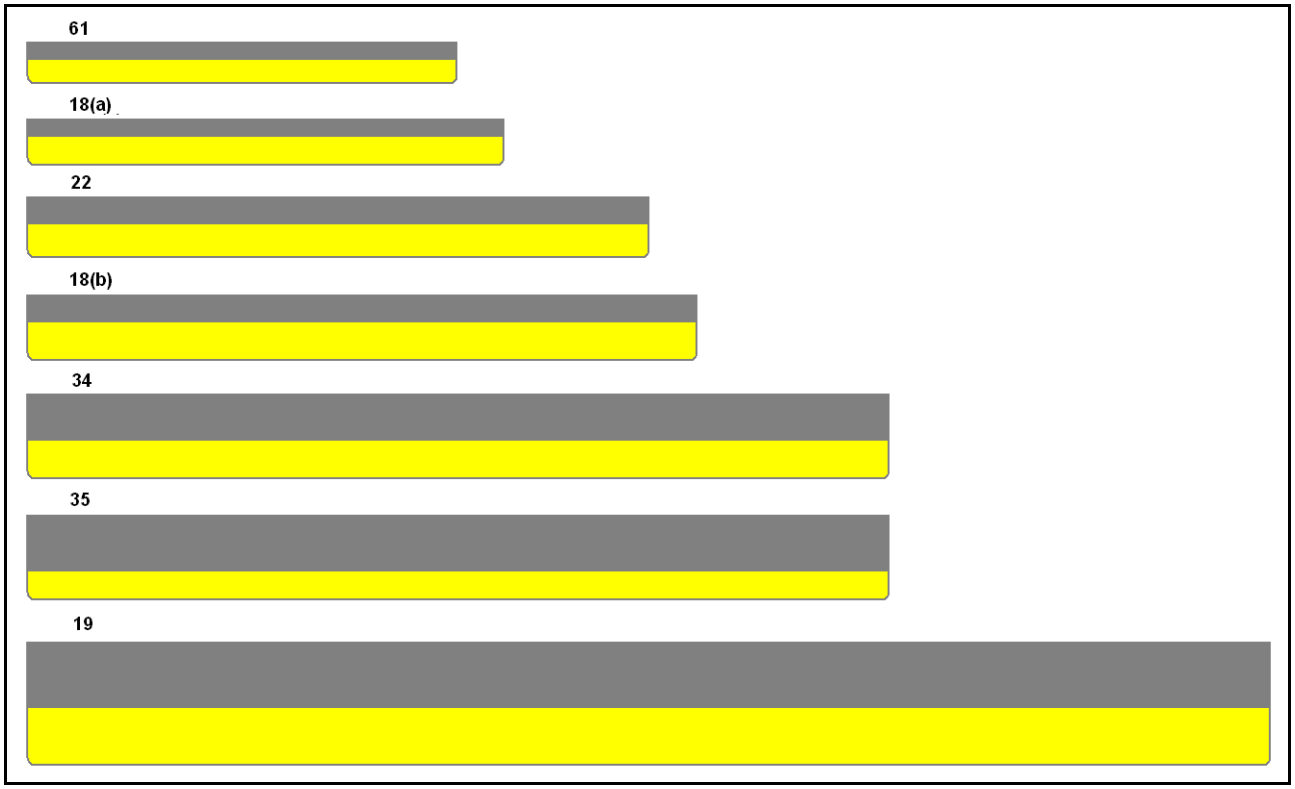

Figure 5-2. *Schematic diagram of representative plugged channel dimensions for different bores intersecting the Renmark Group, assuming a 1:10 depth to width ratio. Grey represents organic-rich plug, yellow represents sands. Thicknesses and depth rounded to nearest 0.5 m. BHMAR61 80-84.5 m, channel 4.5 x 45 m, plug 2 m, sand 2.5 m. BHMAR18, example (a) 82.5-87.5 m, channel 5 x 50 m, plug 2 m, sand 3 m. BHMAR22 58.5-65 m, channel 6.5 x 65 m, plug 3 m, sand 3.5 m. BHMAR18 example (b) 74-81 m, channel 7 X 70 m, plug 3 m, sand 4 m, BHMAR34 87-96 m, channel 9 x 90 m, plug 5 m, sand 4 m. BHMAR35 46.5-55.5 m, channel 9 x 90 m, plug 6 m, sand 3 m, BHMAR19 63.5-76.5, channel 13 x 130 m, plug 7 m, sand 6 m.*

Levees (raised banks along the edges of fixed channels) and splays (sediment lobes formed when river channels break through the levees) are both composed of interbedded sands and muds. Levees in particular are composed of fine-grained sands and silts, while splays may be composed of coarse-grained sands through to muds.

Muds (silt, clay, and sandy muds) are interpreted as overbank deposits, including floodplains, lakes, swamps, levees, and abandoned channel fills. Associated with these deposits are lignites and rare textures interpreted as palaeosols and insect nests, most probably ants or termites (see Hasiotis (2004) for comparisons). But for the most part, the floodplain sediments are clay-rich muds either organic-rich or strongly gleyed, with colours dominated by grey, black, green and dark brown. Rootlet horizons are bright yellow, indicating localised oxidation. These features suggest that the floodplain was commonly inundated and, even when not, was subject to a very high watertable.

Not all floodplain deposits are reduced or rich in organic carbon. At some locations, possibly associated with palaeo-highs, the Renmark Group has been variably weathered. Examples include sites BHMAR08 and BHMAR35. White to very light grey floodplain deposits also found in BHMAR35, although there is weathering observed from the cores, it is likely that the clays were originally very low in organic matter.

Similar white to very light grey, but still reduced, clay deposits occur in Eocene palaeovalley fills in Western Australia (Clarke, 1994).

Very dark brown muds, well laminated, with thin sand laminae and marine dinoflagellates in BHMAR29 and 31 are interpreted as inter distributary bay fills in a delta environments (see Coleman & Prior, 1982). The absence of macroscopic marine indicators, such as shelly material, suggests that a marine influence is either low or brief. Liners of trocospiral foraminifera were found in two samples from BHMAR31-1 at depths of 65.6-65.7 m and 66.95-97.05 m (Macphail, 2010). These deposits pass laterally into the mid-Tertiary permeability barrier of the Geera Clay (Brown & Radke, 1989). These results are comparable with those of Radke (1990) who inferred deposition on a lower coastal plain to estuarine environment in the Hatfield 1 bore, some 200 km south-east of Menindee. Radke (1990) reported a much greater abundance of marine indicators in his samples, consistent with a setting closer to the palaeoshoreline than the BHMAR project area.

Distributary channels in such deltaic systems function analogously to those on anastomosing floodplains (Miall, 1996), with similar channel thickness to width ratios (Gibling, 2006). The main differences arise from the nature of the flooding between the channels. On a wet anastomosing floodplain inundation is associated with river flooding and rainfall, with consequent fresh water dominance. In inter-distributary bays the flooding is from the sea, the salinity depending on the position of the freshwater/seawater interface. In addition, bays may show tidal influence.

In support of the facies interpretation from drill cores, lithostratigraphic mapping based on borehole lithological information and AEM depth slices revealed extensive presence of fine textured sediment. For example, at depth interval 61.0 m – 72.3 m, Renmark Group is present across two-thirds of the study area and the textures are dominantly mud and muddy sand (Figure 5-3). The sand in the central area, which includes GWR1, GWR3, GWR4 and GWR6) is part of the Calivil formation overlying on predominantly Renmark Group muds.

Due to the narrow width of the channels, the relatively thin sand and muddy sand (mostly <6 m), and the relatively thick (> 10 m) AEM depth slices at depths >50 m, it is difficult to observe any distinct morphology associated with anastomosing channels, levees and splays from the AEM. Broad zones of texture classes such as mud and muddy sand were mapped instead, and the overall patterns may show certain geomorphic feature. For example, textural classification of sediments in the AEM depth slices (51.5 m – 6 1.0 m) locally reveal an anastomosing pattern, although the channels are often too small to show up clearly. The best examples is found in target GWR14 (Figure 5-4), where the palaeochannels and the flow directions can be interpreted.

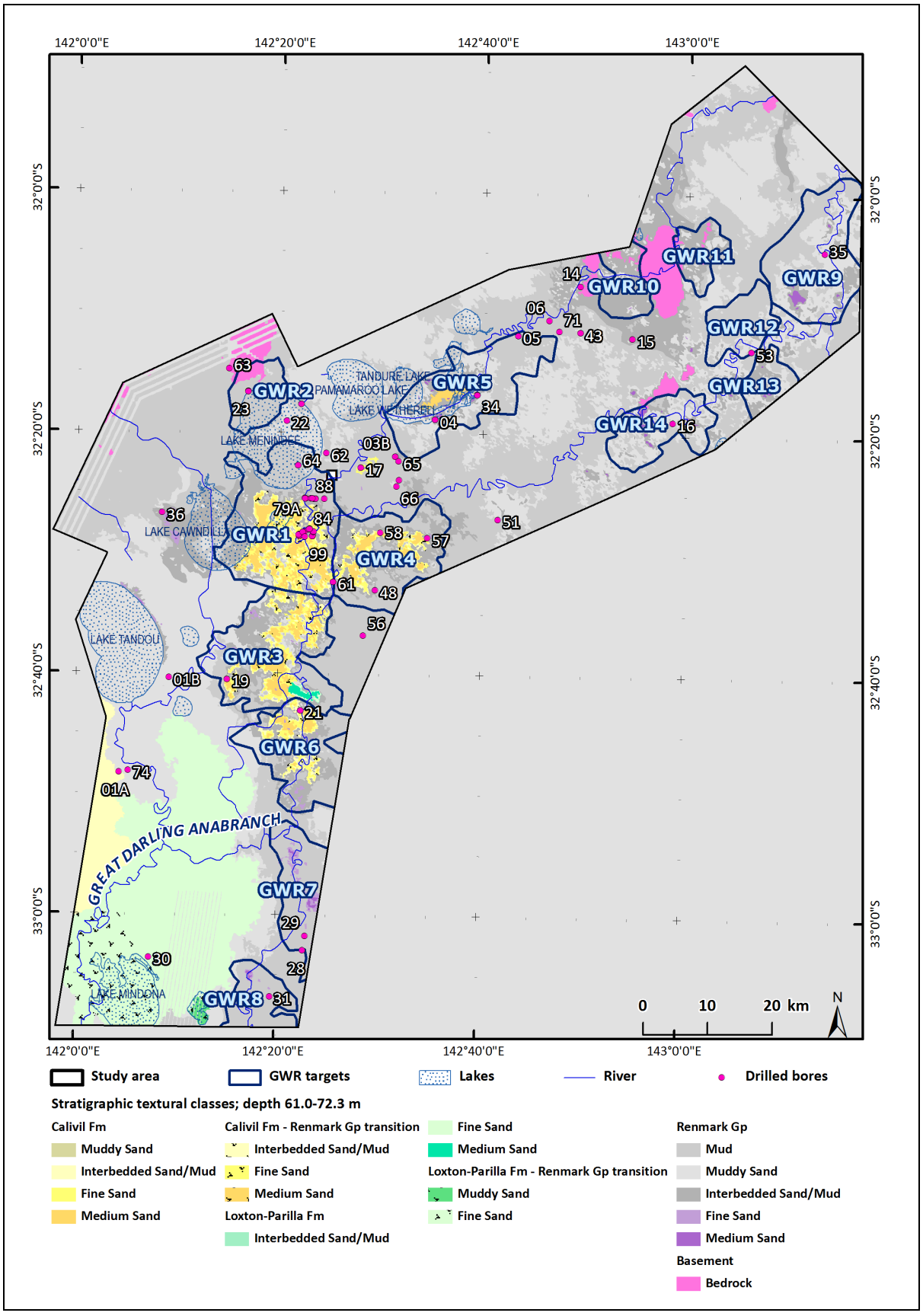

Figure 5-3. *Map of lithostratigraphy interpreted from AEM data (depth interval 61.0 m – 72.3 m), validated using borehole lithostratigraphic information.*

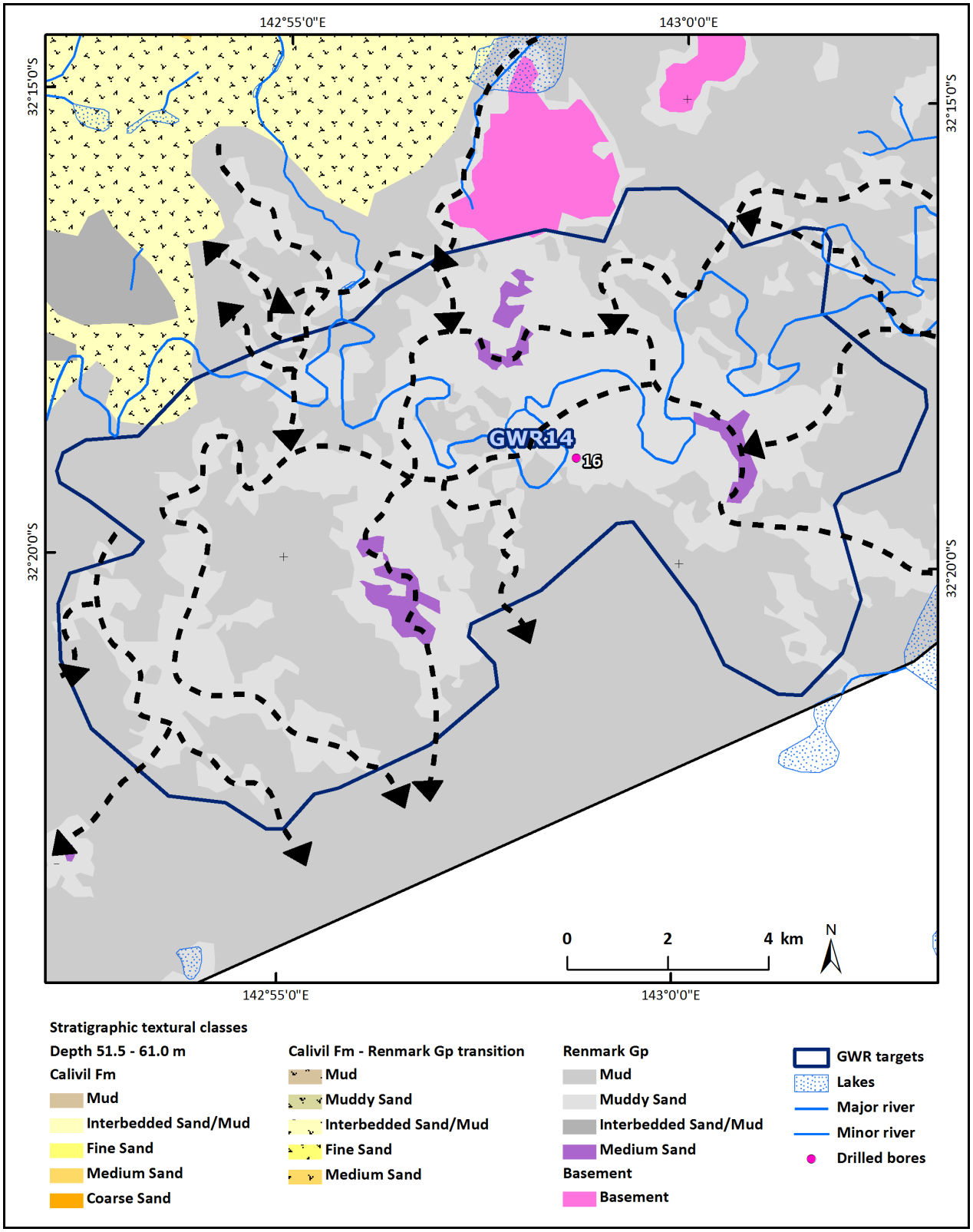

Figure 5-4. *Anastomosing pattern in the distribution of fine and muddy sands in the Renmark Group at 51.5-61.0 m depth for target GWR14. Possible channel courses indicated.*

5.1.2.3 Core lithologies

Channel sands (Figure 5-5 and Figure 5-6) range from medium- to coarse-grained, and are very rarely gravelly. Locally they may contain intraclasts and woody debris, especially at the base of channels.



Figure 5-5. *Woody horizon in coarse channel sands, arrow point downhole, cores from left to right, Renmark Group, BHMAR79A-61 62.11 m (top left) - 164.34 m (bottom right. Note oxidation of sands in this unit, which is in contact with the Calivil Formation aquifer.*

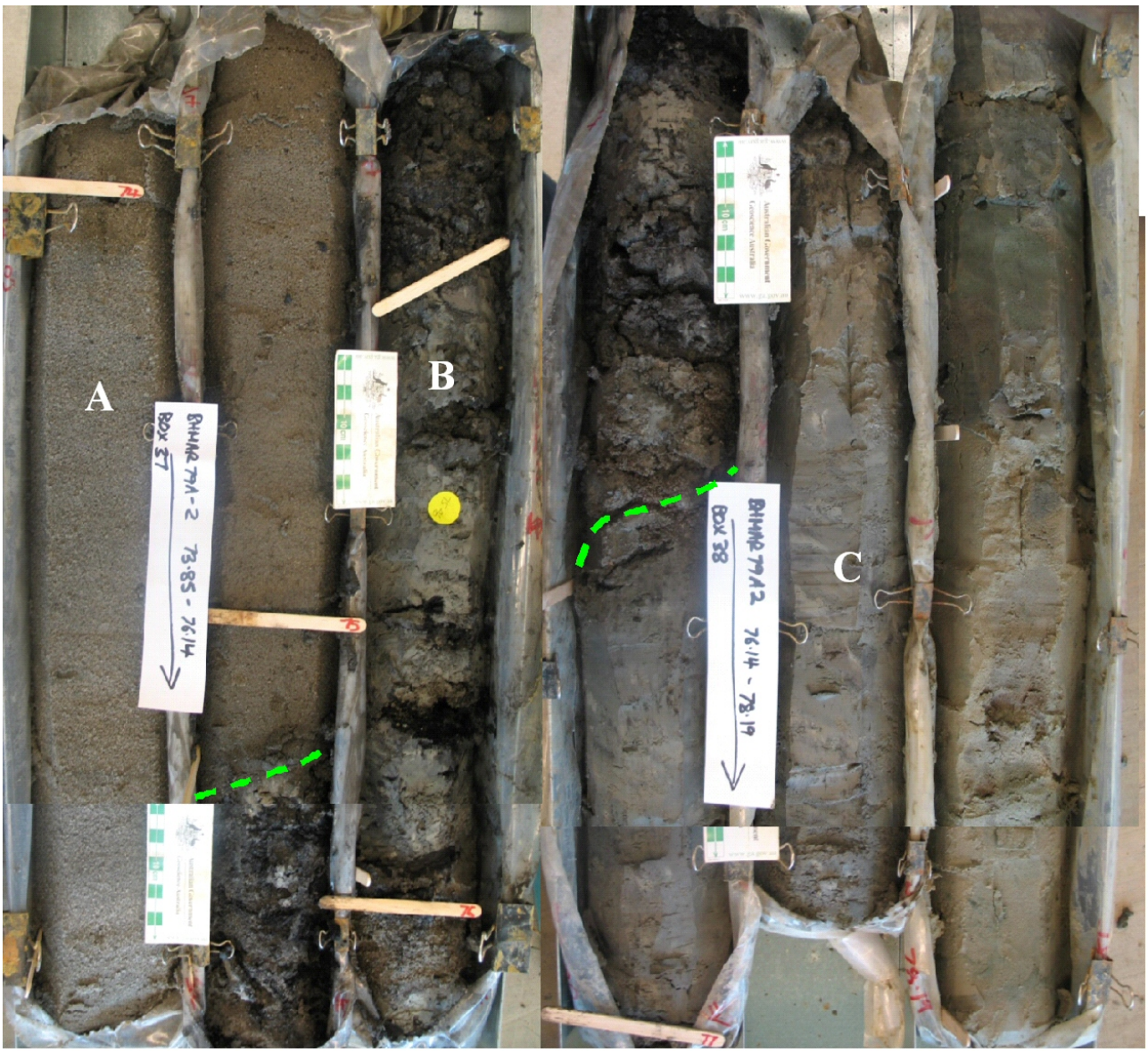

Figure 5-6. *Reworked mud clasts and woody debris at base of channel, Renmark Group, BHMAR79A-2 74.85 m (top left) – 78.19 m (bottom right). A = clean, well sorted coarse channel sand. B = mixed muddy intraclasts and woody debris at base of channel. C = floodplain lithologies (silts, clays, and thin sands).*

Anastomosing channels are fixed, rather than meandering. They can still shift position through avulsion, usually associated with major flood events breaching levees and diverting flow into a new channel. Unlike meandering systems the old channel is not immediately abandoned, resulting number of simultaneously active fixed channels. Eventually, however old channels are blocked, either because they fill with sand (giving rise to thick, multistorey channel sand bodies), or through development of levees across the ends of the channel (Miall, 1996). In this second case the channel will remain as a deep abandoned channel or billabong, gradually filling up with fine-grained and organic rich sediments, and forming a distinctive plug.

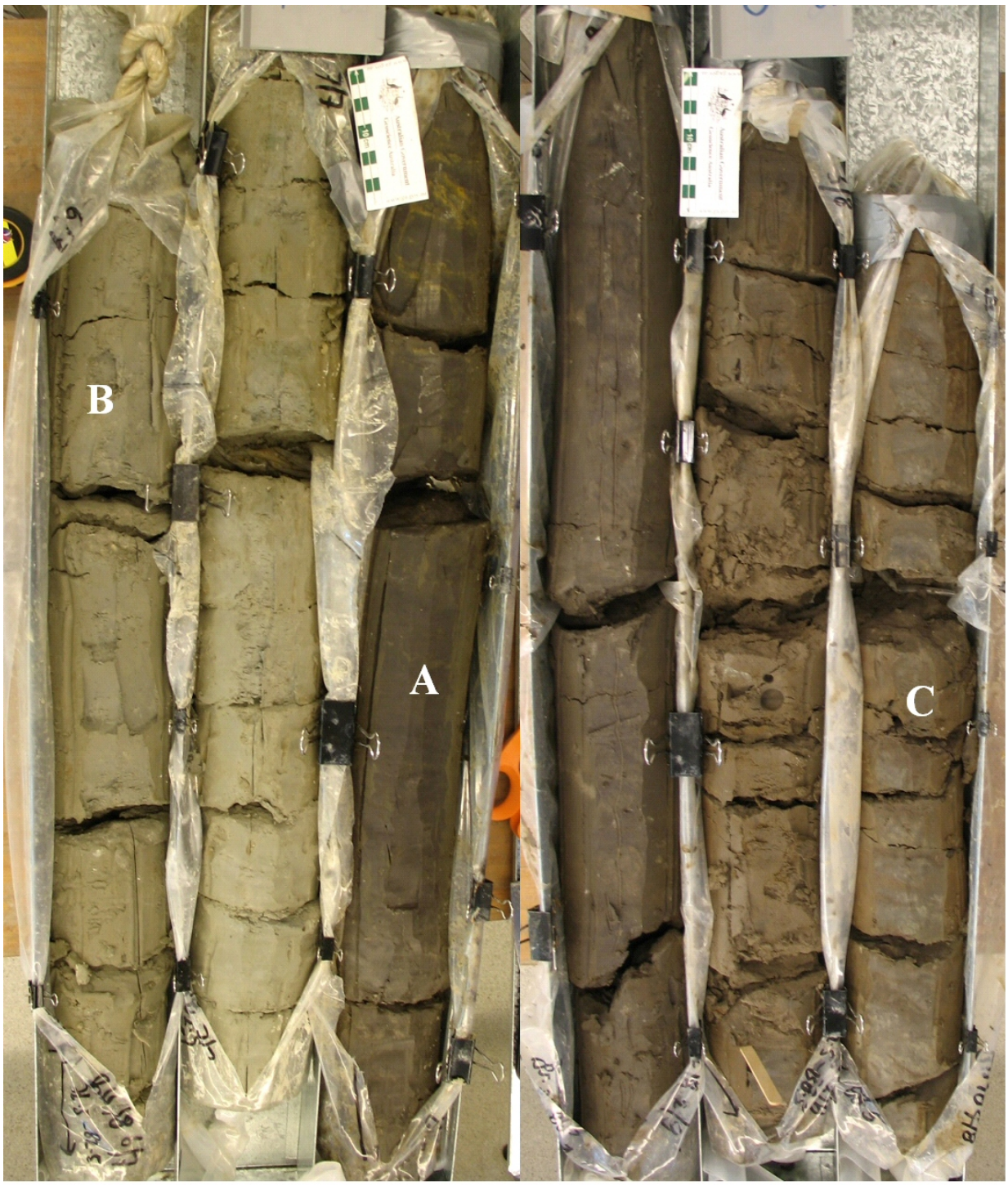

Figure 5-7. *Organic-rich channel plug (A), Renmark Group, BHMAR18, 80.8 m (top left) -86.0 m (bottom right). B = green floodplain clays overlying organic-rich plug filling abandoned channel, C = muddy sands of channel.*

Floodplain muds make up the bulk of the Renmark Group in terms of both stratigraphic thickness and area.

The two most common lithologies seen in core are green muds (Figure 5-8) and grey or chocolate organic rich muds (Figure 5-9). The green muds are interpreted as being formed in wet but not inundated floodplains. Wet, because the green colour comes from Fe^{2+} minerals, and not inundated, because organic matter is not accumulating. The presence of rare palaeosols (Figure 5-9, Figure 5-10) and insect nests (Figure 5-11), most probably ants or termites (c.f. those of Hasiotis, 2004) supports wet, but not inundated soils. The grey and chocolate muds are interpreted as inundated floodplain deposits, such as mineral-rich swamps, where organic material can accumulate. Common root impressions (Figure 5-12) and loss of fine-sedimentary structures such as laminate indicate that both environments supported vegetation and infaunal biota.

Minor floodplain lithologies include light coloured muds, lignites, and sapropels. Light-coloured clays (Figure 5-12) are found in significant thicknesses only in BHMAR 34, and are associated with goethitic staining and goethitic root impressions. These very light grey muds may be a result of weathering of formerly more carbonaceous sediments, but equally may present relatively reduced sediments that lack organic matter, by comparison with Eocene palaeovalley sediments from western Australia that were almost white but none the less contained reduced, as indicated by well-preserved spores and pollen and the presence of pyrite framboids (Clarke, 1994). Lignites form from environments that support abundant vegetation, are permanently inundated, and have low mineral input. Lignites in the project area (Figure 5-13) are thin, relatively rare (found only in BHMAR61 and 75-3), and are mostly likely formed in swamps distal from channels. Sapropels are fine grained organic rich and mineral poor deposits dominated by algae such as *Botrycoccus*, they form in open water environments distal from any mineral input. Like lignites they are rare in the project area.



Figure 5-8. *Green floodplain muds (reduced iron, organic poor), Renmark Group, BHMAR33-1, 102.1-104.17 m. Arrow points downhole, top left is youngest, bottom right oldest. Small white flecks are filled burrows of soil invertebrates.*

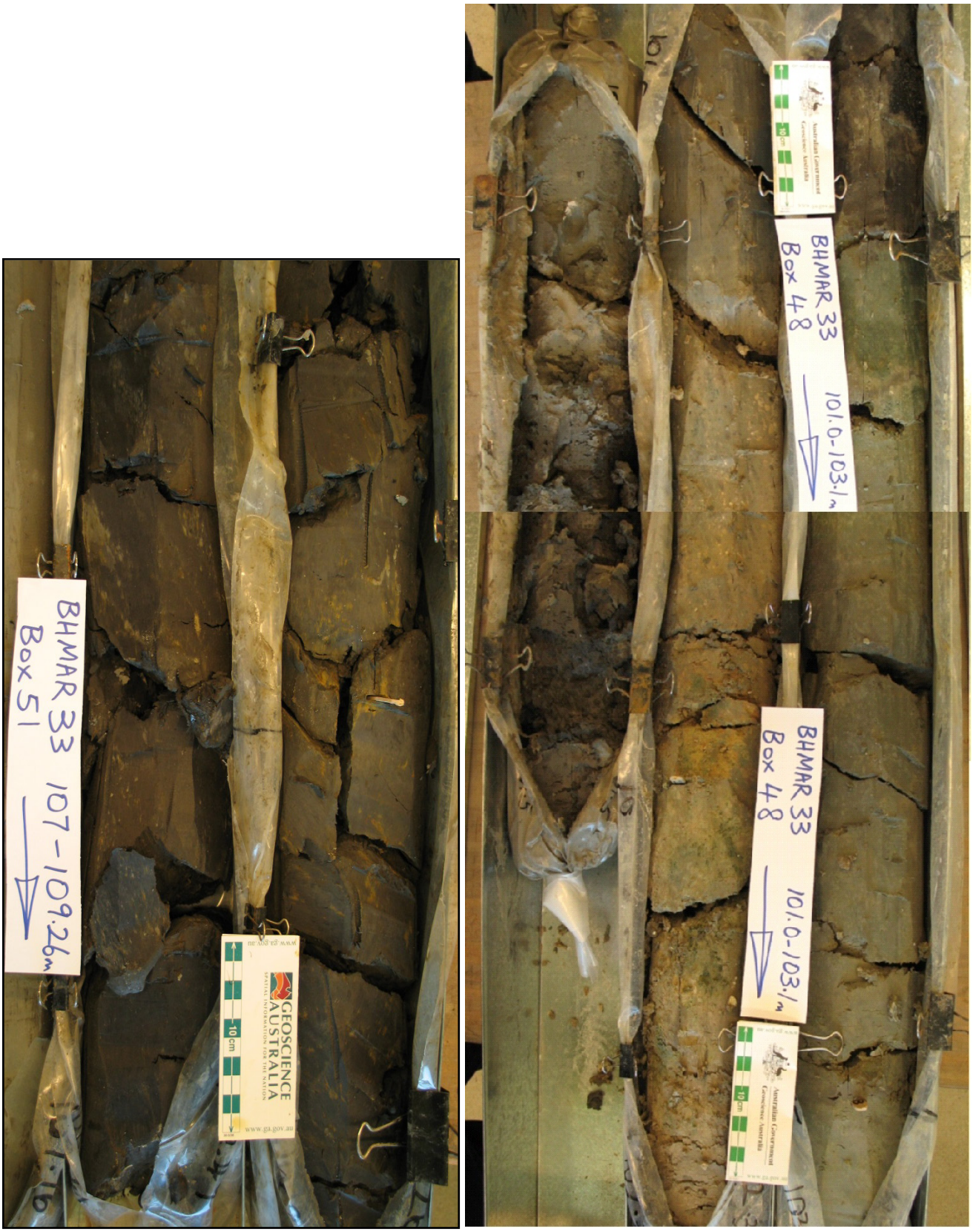

Figure 5-9. *Left: dark floodplain muds (reduced, organic-rich) formed in inundated environment, Renmark Group, BHMAR33-1, 107.0-109.26 m. Arrow points downhole, top left is youngest, bottom right oldest. Yellow streaks are interpreted as goethite-stained root impressions. Right: oxidised palaeosol (yellow) in floodplain clays, overlain by green clays and underlain by grey clays.*



Figure 5-10. *Intraclasts on soil surface (looking up) Renmark Group, BHMAR33-1, 163.65 m.*



Figure 5-11. *Insect nest, most probably built by termites or ants in palaeosol, Renmark Group, BHMAR33-1 163.65 - 163.85 m. Arrow points downhole.*

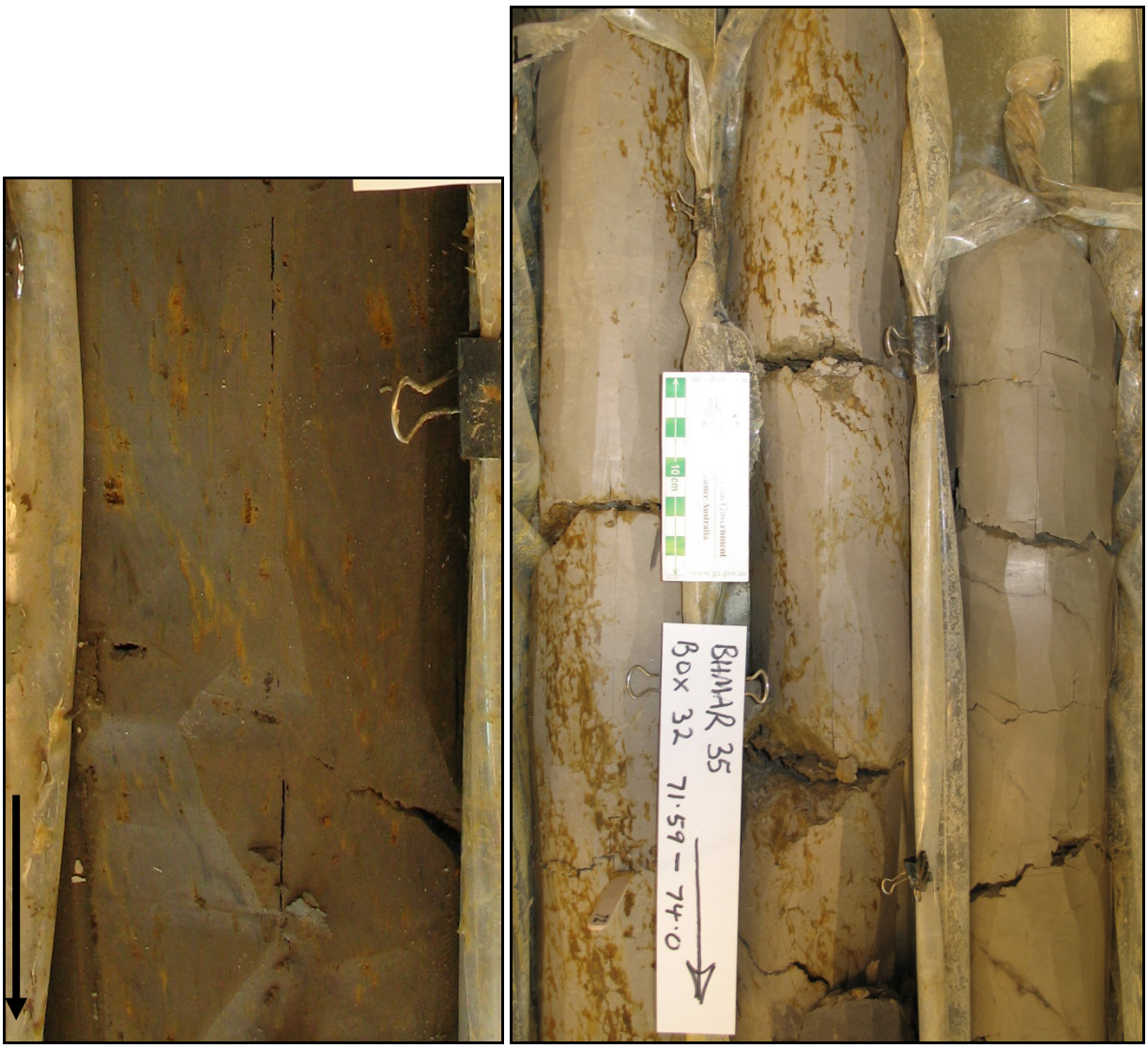

Figure 5-12. *Renmark Group in BHMAR34 at approximately 35 m. Left: goethitic root impressions in carbonaceous mud, and right: Light coloured floodplains muds. Arrow points downhole.*



Figure 5-13. *Lignite interval (A) in Renmark Group, BHMAR 61 underlain by organic-rich mud (B) and overlain by channel sand (C) with intraclastic base.*

Crevasse splays deposits are sheets of relatively thin sand, occasionally coarse to gravelly, overlain by mud, formed when levees rupture during flood and sands are deposited as lobes and small distributary channels on the floodplain. The levee is then built up over the breech, resulting in a thin sand sheet in the floodplain succession (see Miall, 1996), including environments both temporarily and permanently flooded. Examples of thin sand deposits interpreted as splays are shown in Figure 5-14 and Figure 5-15.

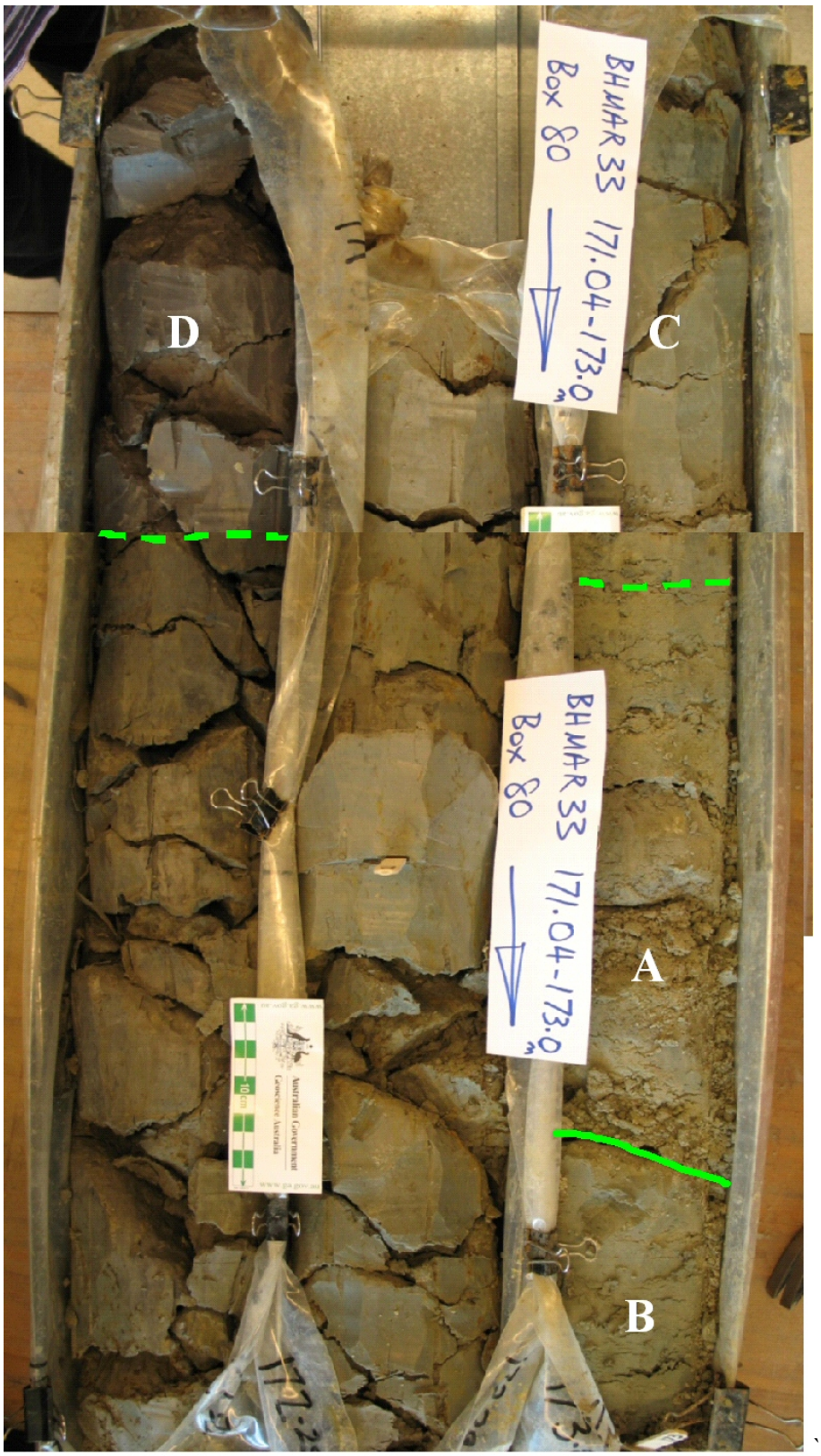

Figure 5-14. *Crevasse splay deposit (A) in Renmark Group, BHMAR33-1 171.04 m (top left) to 173.0 m (bottom right). B = underlying green clay (wet floodplain deposit), C = overlying green clay (wet floodplain deposit), which grades up into D = organic-rich floodplain lake deposit.*

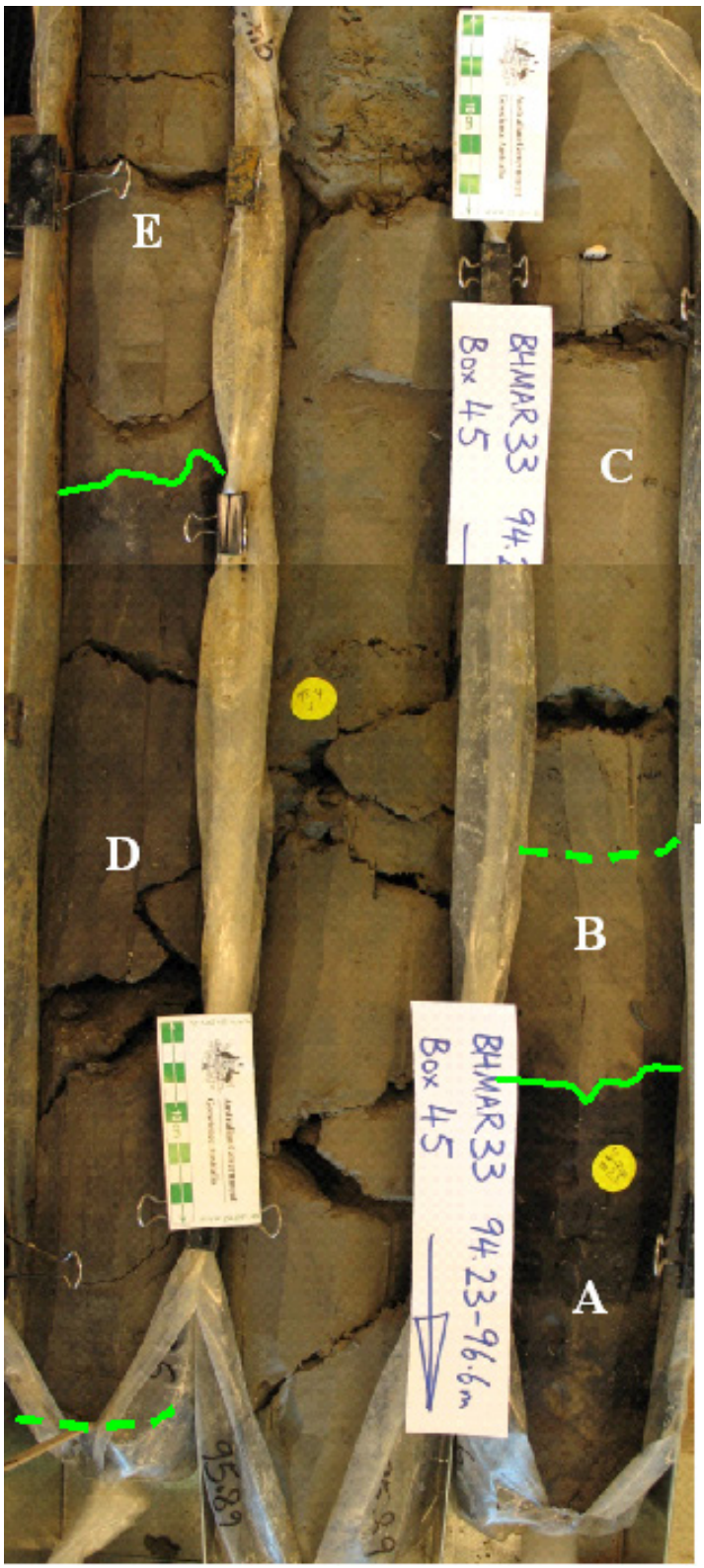

Figure 5-15. *Sapropel of interpreted floodplain pond (A) infilled by crevasse splay (B), Renmark Group, BHMAR33-1, 94.23 m (top left) – 96.6 m (bottom right). C = green (wet) floodplain formed by infill of pond, with eventual re-establishment (D) of organic rich clays (return to inundated conditions).*

Levees are natural raised banks to channels formed by deposition during floods occurring most rapidly near the channel. They are composed of interbedded fine sands and silts, commonly rippled, with thin mud drapes deposited in the final phases of the flood. An example of an interpreted levee bank deposit is shown in Figure 5-16.



Figure 5-16. *Levee bank sediments, Renmark Group, BHMAR33-1 ~64 m. Sediment is composed of interbedded fine yellowish sands and greyish silts. Arrow indicates down-hole direction.*

Inter-distributary deposits are equivalent to floodplain deposits except they form in the inter-distributary bays between channel levees in deltas (Coleman & Prior, 1982). In the Renmark Group they are transitional to the Geera Clay, and marine dinoflagellates. The inter-distributary bay deposits are laminated organic-rich mud (Figure 5-17) and are found only in BHMAR29 and 31, the two southernmost sonic bores in the project area.



Figure 5-17. *Inter-distributary bay deposits of laminated carbonaceous mud, Renmark Group, BHMAR29. Arrow on card indicates downhole direction, youngest strata at top left, oldest at bottom right.*

Locally weathered Renmark Group is present in a few holes associated with higher parts of the pre-Calivil Formation topography. The weathering is therefore interpreted as being pre-Calivil Formation in age. The best developed examples are in BHMAR8 (Figure 5-18) and BHMAR35. Weathering consists of the destruction of organic matter, oxidation of Fe^{2+} to Fe^{3+}, and some secondary iron precipitation. Original depositional textures such as bedding and root impressions are generally well preserved.



Figure 5-18. *Weathered Renmark Group in BHMAR08, ~47 m. Arrow indicates down-hole direction.*

5.1.3 Palynology

Macphail (2010) using the modified zonations of Macphail (1999), identified the Renmark Group in the project area as being from the Late Oligocene to Middle Miocene (Table 5-7) which corresponds to between 23.03 and 13.65 Ma, a period of 9.38 million years.

Table 5-7. *Murray Basin pollen zones and the Renmark Group at Menindee.*

Era	Zone	Distribution
Late Pliocene to Pleistocene	*Tubulifloridites pleistocenicus*	Calivil
Late Miocene to Early Pliocene	*Monotocidites galeatus*	Calivil
Late Early to Middle Miocene	*Canthiumidites bellus*	Renmark
late Oligocene-late Early Miocene	*Proteacidites tuberculatus*	Renmark
Early Oligocene	Upper *Nothofagidites asperus*	reworked elements
Late Eocene	Middle *Nothofagidites asperus*	reworked elements
Middle Eocene	Lower *Nothofagidites asperus*	reworked elements
Early Eocene	*Malvacipollis diversus*	Not found

Macphail (2007) divided the Cenozoic into five time slices for palaeoclimatic interpretation. The Renmark Group in the project area corresponds to Time Slice T-4 (Oligocene-Middle Miocene, 33.7-11.2 Ma). Using microfloras from the Murray Basin, rainfall gradients across the basin appear to have been similar in direction (but not volume) to those of the present-day. Climates in the western and central Murray Basin (which includes the project area) were interpreted by Macphail (2007) as being suboptimal for the extensive development of *Nothofagus* (temperate) or *Araucaria* (subtropical) rainforest in the Oligocene, although conditions remained seasonally wetter (humid) and warmer (mesotherm range) than at present.

Trends in the rare preserved thermophilic taxa suggest mean air temperatures reached maximum values during the late Early to Middle Miocene, whilst diminishing *Araucaria* and *Lagarostrobos* values imply that climates also became effectively drier at about the same time. Marine flooding appears to have allowed grass communities to form around the margins of the basin at a time when grasses were uncommon or absent in drier, interfluve habitats. Further towards the central Murray Basin conditions were initially more equable in terms of rainfall and mean temperatures but became more strongly seasonal during the Miocene. Marine transgression helped to maintain high humidity across the basin during the Early Oligocene and Late Oligocene-Middle Miocene. The replacement of *Nothofagus* (*Brassospora*)-dominated rainforest (Oligocene) by communities successively dominated by *Araucariaceae* (~Early Miocene) and then *Casuarinaceae* and *Myrtaceae* (~Middle Miocene), is reliable evidence that conditions became effectively drier and increasingly seasonal.

Spores and pollen in the project area drill core (Macphail, 2010) indicate that Oligocene-late Early Miocene climates were wet but possibly cooler and/or more uniform than those that came later, based on the higher relative abundance of *Nothofagus* (*Brassospora*) sp. in the Myrtaceae-dominated coastal vegetation. By the Late Early to Middle Miocene climates were probably warmer and rainfall less seasonal than in the Early Pliocene. These conditions supported complex rainforest communities dominated by (1) *Nothofagus* (*Brassospora*) spp. and gymnosperms on floodplains inland of the palaeoshoreline, or (2) Myrtaceae (*Syzygium*-type) and unidentified angiosperms in areas subjected to a marine influence. Casuarinaceae and *Proteaceae* species are common.

Individual samples from floodplain facies contained numerous taxa indicating freshwater swamp to lake conditions, including the algae *Botryococcus* and *Pediastrum*. Sedges, rushes, and ferns are also present. The inter-distributary bay facies contained *Botryococcus* and *Pediastrum* and a minimum of eight dinoflagellate taxa (Macphail, 2010).

5.1.4 Analogues

Analogues are helpful in conceptualising the architecture of the Renmark Group. Two are given in this report, the well-studied Brushy Basin Member, which is particularly helpful due to excellent outcrop exposure, showing architectural elements; and the Magdalena River, which appears to be a modern counterpart to the river systems that deposited the Renmark Group. The classic inter-distributary bay fills of the lower Mississippi Delta provide an analogue for the carbonaceous laminated muds in the southernmost part of the project area.

5.1.4.1 Brushy Basin Member

The Brushy Basin Member of the Morrison Formation is a Jurassic-age anastomosing fluvial succession in Utah and adjacent areas of the United States. Clarke & Stoker (2011) described Brushy Basin low sinuosity anastomosing fixed channels with widths of 20-100 m and 2-15 m thickness, composed of medium-grained sand to conglomerate (Figure 5-19, Figure 5-20, Figure 5-21). Splays in the same area were 10 cm to 2 m thick, with lateral extents varying from less than 10 m to hundreds of metres which are within the range for the unit reported by Demko *et al.* (2004) and Kjemperud *et al.* (2008). Furthermore, many of the trace fossil assemblages associated with vegetation growth and soil invertebrates, as documented by Hasiotis (2004) are similar to the Renmark Group. Outcrops of the channels and splays within the Brushy Basin Member give a good visual impression of what those in the Renmark Group might look like, albeit the Brushy Basin Member is dominated by oxidised facies, rather than the reduced facies, as is the Renmark Group.



Figure 5-19. *Exhumed inverted low sinuosity channel, Brushy Basin Member, Morrison Formation, Utah. Channel is surrounded by floodplain sediments, showing the relatively small proportion of the area that is composed of channels. Ridge height ~20 m.*

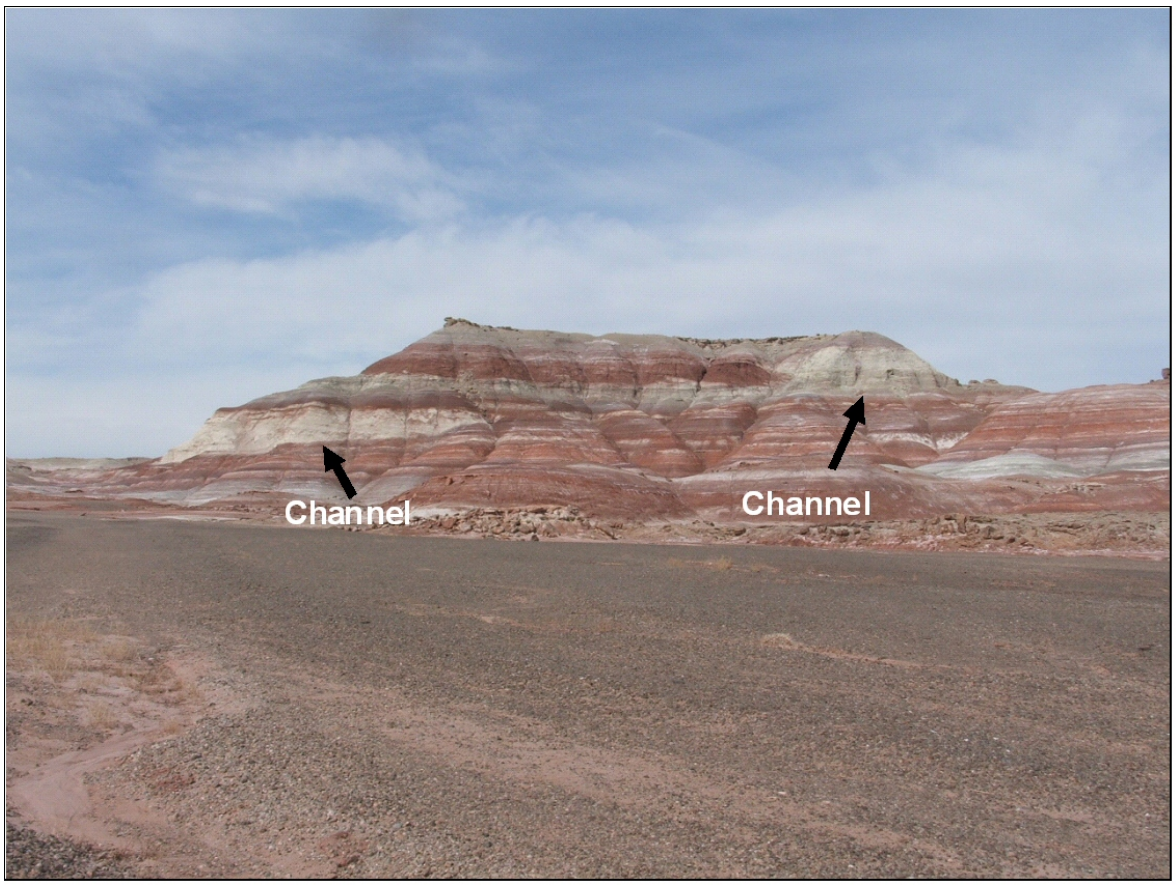

Figure 5-20. *Individual channels in the Brushy Basin Member ~20 m thick and 200 m wide. Reddish-brown units are floodplain clays and thin white beds crevasse splay deposits.*

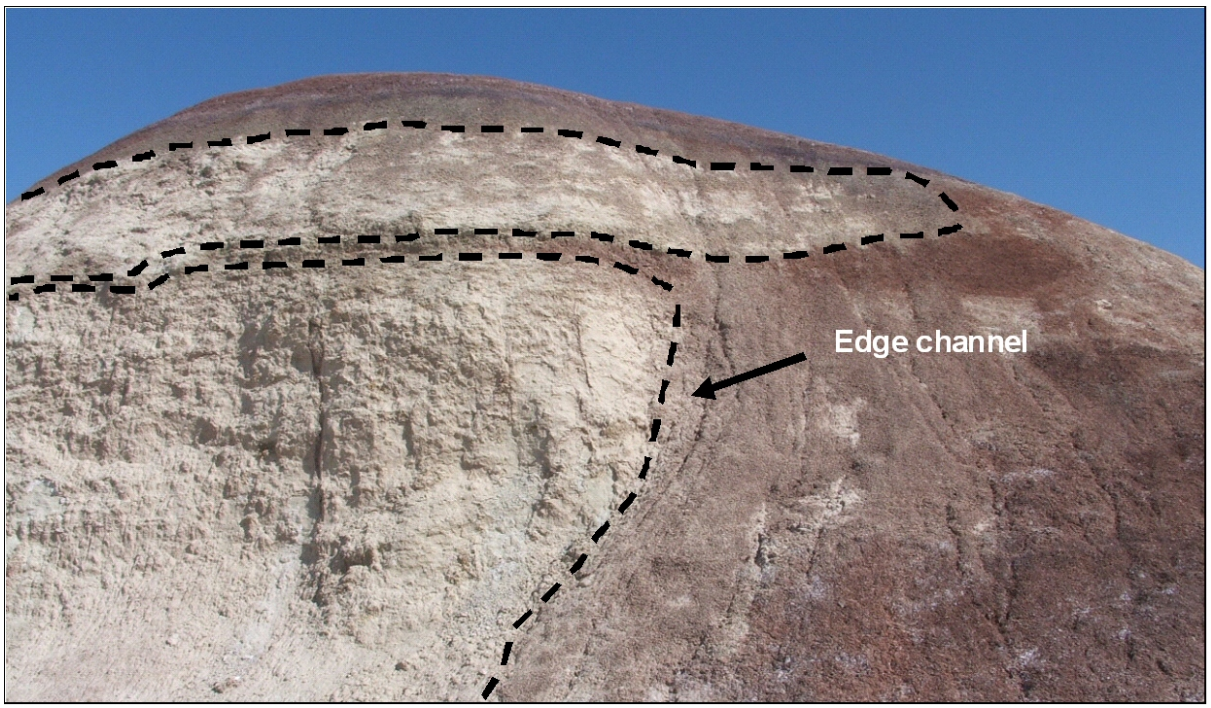

Figure 5-21. *Cross section through a small, multistorey fixed channel in the Brushy Basin Member of the Morrison Formation (Jurassic, Utah), showing lower and upper channel fills with shard terminations, separated by thin channel plug of clay, all encases by red clay-rich floodplain deposits. Outcrop height ~6 m.*

5.1.4.2 Magdalena River

An even closer analogue is provided by the present-day Magdalena River in Columbia, South America (Smith, 1986). The Magdalena River is a major anastomosing river system in a high rainfall area characterised by a mostly inundated floodplain. Levees and crevasse splay channels form the highest points in the largely flooded landscape, as shown by Figure 5-22 and Figure 5-23. Table 5-8 compares the measured characterises of the Renmark Group in the project area with those of the Magdalena River. It shows a remarkable correspondence between the two depositional systems with respect to lithology, architecture, and scale.

Table 5-8. *Comparison between inferred features of the Renmark Group and its modern analogue, the Magdalena River.*

Parameter	Renmark Group (this study)	Magdalena River (from Smith, 1986)
Floodplain sediments	Clayey mud, organic mud, lignite	Clayey mud, organic mud, peat
Proportion of area	77%	80-90%
Environment	Wet floodplain, lake, marsh, peat bog	Wet floodplain, lake, marsh, peat bog
Lake depth	unknown	2 m
Billabong depths	Up to 7 m	Up to 13 m
Levee sediments	Silt, mud, fine sand	Silt, mud, fine sand
Levee width	unknown	100 m – 4 km
Crevasse splays	Coarse to fine sands and muds	Up to 2.6 m
Splay channel width	<75 m	8-100 m
Splay channel depth	<3 m	<2.5 m
Splay thickness	Up to 3 m	Up to 2.6 m
Channel sediments	Medium to coarse sand	Coarse to fine sand
Channel width	to 330 m	250-600 m
Channel depth	Up to 8 m	Up to 16 m
Channel thickness	3-21.6 m	5-30.5 m (average 15 m)



Figure 5-22. *Google Earth image of part of the Magdalena River floodplain, Columbia. Numerous fixed channels form an anastomosing network with well-developed levees and a largely inundated floodplain. The largest channel is ~300 m across.*



Figure 5-23. *Google Earth image of part of the Magdalena River floodplain, Columbia. Fixed channel ~30 m across with well-developed levees, crevasse splays and an inundated floodplain.*

5.1.4.3 Mississippi, Magdalena and Sinu deltas

The Mississippi Delta (Coleman, 1988; Coleman & Prior, 1982) and the upstream alluvial plain are among the most heavily documented fluvial systems on Earth. The delta is river-dominated with a complex "bird foot" geometry. It is characterised by leveed distributaries and sheltered inter-distributary bays (Figure 5-24) with fresh to marine waters; salinity depending on the balance between sea water and river water inflows. The absence of bioturbation and marine shelly fauna indicates that the examples cored in holes BHMAR29 and 31 are probably at the fresher end of the water quality spectrum.

Less well documented but similar inter-distributary bay and lake deposits are associated with the deltas of the Magdalena and Sinu Rivers of Colombia. Unlike those of the Mississippi River, which are associated with a river-dominated birdfoot delta, the Magdalena and Sinu River deltas are wave dominated (Suarez, 2004) with a well-developed barrier and lagoon, the latter being filled by a complex of anastomosing channels with inter channel bays and lagoons (Restrepo & Lopez 2008, Suarez 2004).

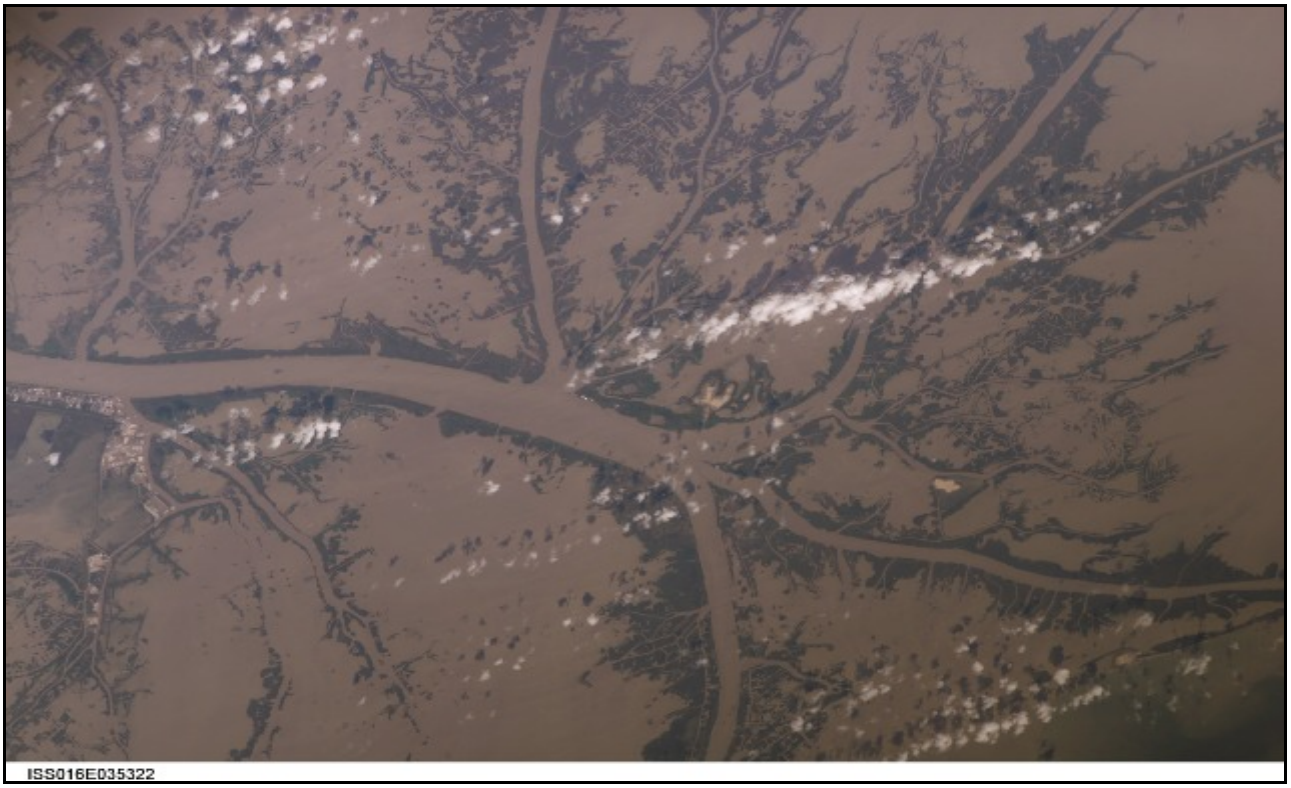

Figure 5-24. *Astronaut photograph of part of Mississippi Delta, showing inter-distributary bays (NASA image ISS016-E-35322).*

5.1.5 Hydrological Implications

In summary the Renmark Group in the project area consists of:

- Numerous thick (up to ~20 m) but relatively narrow (a few hundred metres) medium-grained sand bodies.
- Sand bodies are flanked by levee and crevasse splay deposits of similar extent containing mostly thin beds of fine-grained sand interbedded with silt and clay.
- The bulk of the Renmark Group is composed of clay-rich muds. In general the Renmark Group contains disseminated pyrite and organic matter, and, more locally lignite beds and pyrite nodules.

In general, there is a low likelihood (12.7%) of a Renmark Group channel sand units being greater than 3 m thick on contact with the Calivil Formation aquifer (Table 5-5). However on a local scale, as observed at Jimargil, Renmark Group channel features are encountered. Hydrologically, these channels are essentially shoestring features. Connectivity with other channel units will be poor, occurring only at the channels ends as individual channel segments may be tens of kilometres in length. If water is pumped out of the sand bodies, flow will occur from both ends of the channel, with only limited movement across it. Relatively little flow from the Calivil Formation is expected under current conditions or during artificial recharge because the Renmark Group channels are confined aquifers, fully saturated and, because they are more saline than those of the Calivil Formation, are density-stratified. In the relatively remote possibility that a production bore sites over the small number of places where a Renmark Group channel is in direct contact with the Calivil Formation, over-pumping of the Calivil Formation may cause up-coning of the more saline, acidic and reduced Renmark Group water into the Calivil Formation aquifer in a manner analogous to sea water intrusion in coastal zones. The one dimensional nature of the shoestring sand aquifers in the Renmark Group may mean, however, that the extent of up-coning could be much less than would be the case if the Renmark Group aquifers were laterally extensive, more like those in the Calivil Formation.

The sands in the levees and crevasse splays are adjacent to the main channels and therefore will increase the size of the aquifer. However, their area (from Table 5-5) is smaller than that of the channels themselves, and

their aggregate thickness is much less. Therefore their storage capacity is much less than of the channels. Because the sands are predominantly fine-grained, and thinly interbedded with silts and muds, their transmissivity is also expected to be less. While they may add to the storage capacity and the volume of influence of the channels, their significance is likely to be low.

The floodplain sediments make up the bulk of the Renmark Group by thickness and area. They are the main component of the basal aquitard to the Calivil Formation aquifer, and the main impedance to flow from the saline water in the Renmark Group channel sands up into the Calivil Formation aquifer, except where those sands directly underlying the Calivil.

5.2 PLIOCENE UNITS

5.2.1 Introduction

The Pliocene sediments in the study area dominantly comprise the fluvial Calivil Formation, with the shallow marine Loxton-Parilla Sands restricted to the southernmost part of the area. Post-depositional warping, tilting and discrete offsets associated with neotectonics are also recognised. AEM mapping validated by drilling has enabled the lateral extents and thickness of the Pliocene aquifers – Calivil Formation and Loxton-Parilla Sands - to be identified.

The Calivil Formation was originally defined as the Calivil Formation by Macumber (1973), but subsequently modified to Calivil Sand (Lawrence, 1975). The name reverted to Calivil Formation in the paper of Tickell & Humphreys (1980). The current definition used is that of Brown & Stephenson (1991), with the caveat that it should no longer be regarded as part of the Wunghnu Group[1].

In addition, the Calivil Formation, as defined, occurs along the southern and eastern margin of the Murray Basin, often in buried palaeovalleys or "deep leads" (Brown & Stephenson, 1991). However, some caution must be exercised regarding the extension of the term to units some 500 km away from the original location. As a regional unit, the Calivil Formation occurs across the BHMAR project area and beyond its boundaries (Lawrie *et al.,* 2009a).

Facies analysis indicates the Calivil Formation was deposited in deep braided streams across a dissected sedimentary landscape. Overall, the sequence is fining-upwards, with evidence for progradation over the Loxton-Parilla Sands. Channel fill materials comprise gravels and sands, and local fine-grained units represent abandoned channels and local floodplain sediments. Integration of textural and hydraulic testing data has revealed there are five hydraulic classes within the Calivil Formation (mud, muddy sand, fine sand, medium sand, and coarse sand to gravel). At a local scale (10s to 100s of metres), there is considerable lithological heterogeneity, however at a regional scale (km), sands and gravels are widely distributed with particularly good aquifers developed in palaeochannels and at the confluence of palaeo-river systems.

The lower bounding surface of the formation is marked by a distinctly erosional contact with Renmark Group sediment. There is a 10 m year hiatus between deposition of the Renmark Group and Calivil Formation. Beneath this erosional surface, the Renmark Group sediments show evidence of significant weathering, particularly where preserved on the palaeo-highs. The upper surface of the Calivil Formation is irregular, with up to 16 m of relief evident. This relief is due in to depositional filling of channel and bar topography in the upper Calivil Formation.

Aquifer testing has revealed Calivil Formation is the principal target aquifer for MAR and groundwater extraction in the study area. The level of confinement of the aquifer (confined-semi-confined-unconfined) is defined by the presence, thickness, lithology and structural integrity of the overlying Blanchetown Clay. In places, a fine-grained upper part of the Calivil Formation sequence can also act as an upper confining layer for the Calivil Formation aquifer proper. The aquifer becomes unconfined away from the groundwater mounding associated with the modern drainage. Aquifer thickness and transmissivities vary across the study

[1] GA stratigraphic names web site, address when accessed 28/11/11
http://dbforms.ga.gov.au/pls/www/geodx.strat_units.sch_full?wher=stratno=3322

area. However, the AEM survey has enabled targeting of sites where subsequent drilling has identified the Calivil Formation as having excellent aquifer properties. For example, pump tests at the Jimargil site inferred locally very high transmissivities (300-900 m^2/d; Table 5-16). Integration of the AEM data with borehole geophysical data (gamma, induction and nuclear magnetic resonance) and textural and pore fluid data has enabled maps of aquifer properties including groundwater salinity, porosity, storage and hydraulic conductivity to be derived.

The Loxton-Parilla Sands (Brown & Stephenson, 1991) were deposited as marginal marine and beach-barrier deposits during a major Miocene-Pliocene marine regression. This unit contains heavy mineral concentrations which have been actively explored for to the south of the study area. In the agricultural regions of the Murray-Darling Basin the Loxton-Parilla Sands are a major saline regional aquifer of considerable significance with connections to lakes and rivers. Prior to this study, palaeogeographic compilations (Kotsonis, 1999; Roy & Whitehouse, 2003) demonstrated that strandline patterns that define the Loxton-Parilla Sands are present 50 km to the south of the Menindee Lakes. In this study, drilling has demonstrated the presence of Loxton-Parilla Sands in the south of the area, with stranded dunes present about 30 km SE of Lake Menindee. Drilling has also demonstrated that the Calivil Formation locally overlies the Loxton-Parilla Sands. In the south of the area, the latter form a good aquifer approximately 40 m thick. Owing to the limited bore intersections of this formation in the BHMAR project area and the largely saline groundwater hosted by this formation we will not discuss its sedimentology in detail in this report.

5.2.2 Distribution

Fault offsets at the base of the Blanchetown Clay, visible in cross sections and in planar maps of the depth to the bottom of the Blanchetown Clay, indicate movement along discrete faults as well as warping and tilting. Up to 50 m of offset has occurred as a result of post-depositional tectonic processes across the area, creating further offsets of 10-20 m in the top of the Calivil Formation. These offset features are not as clearly evident in the base of the Calivil Formation, suggesting structural inversion occurred during and after deposition of the Calivil Formation.

Regional cross sections (refer to Lawrie *et al*., 2012d) show that deposition of the Calivil Formation appears to have been party controlled by syn-sedimentary tectonics. Inversion along the fault lines has obscured the original depositional architecture but on some cross sections, e.g. section F-F1 (Figure 5-25) the outlines of a broad palaeovalley can be seen. It is not known whether this palaeovalley was formed by sag, or erosion, or a combination of both processes.

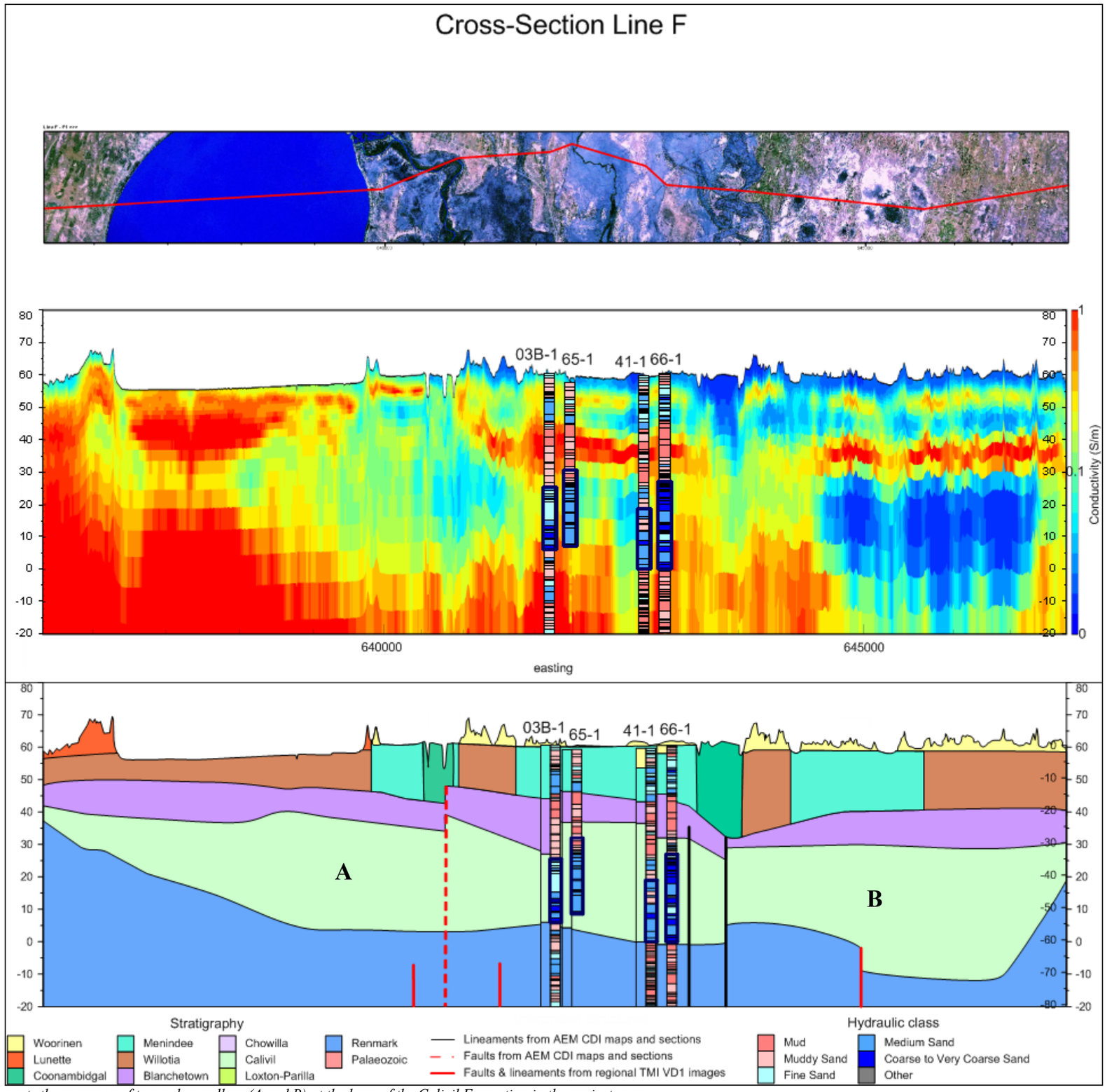

Figure 5-25. *Cross section F-F1, which suggests the presence of two palaeovalleys (A and B) at the base of the Calivil Formation in the project area.*

5.2.3 Thickness and Relationships

The Calivil Formation varies significantly in thickness (0-70 m) over the project area. This variability results from:

- In-filling of broad (structurally-controlled) palaeovalleys in an undulating palaeo-landscape, with relief of up to 40 m from valley bottoms to hill tops; and
- Post-depositional tectonic effects that include structural inversion on faults, as well as warping and tilting of the landscape.

Tectonic inversion along reactivated faults has resulted in erosion and local thinning of the Calivil Formation sequence prior to deposition of the overlying lacustrine Blanchetown Clay. Faulting is most noticeable along the western side of the Menindee Lakes, where significant vertical offsets (>10 m) are observed in the overlying Blanchetown Clay, as shown in cross sections G-G1 (Figure 5-29). In some narrow fault zones the Calivil Formation has been completely eroded. Tectonic activity post-deposition of the Blanchetown Clay has resulted in further warping, tilting and faulting of the Calivil Formation.

The upper surface of the Calivil Formation is irregular, with up to 16 m of local relief. This is observed between BHMAR33-1 and BHMAR33-8. A 6 m offset is evident, which is likely a result of erosion, although some of this offset may also be due to depositional filling of channel and bar topography in the upper Calivil Formation. The lower surface is marked by a distinctly erosional contact with the Renmark Group. Strong weathering is locally present on the Renmark Group highs (e.g. in BHMAR08-1 and BHMAR64-1, see Figure 5-26.) and while this weathering was probably more widespread is has since been removed by erosion in the majority of bore locations (Figure 5-27). The basal contact appears to be marked by incised channels. Careful interpretation of the AEM data was required to determine their orientation.

Regional cross sections (Appendix 5a, Apps *et al*., 2012b) show considerable variation in the elevation of the base of the Calivil Formation, typically between 30 and 45 m AHD, but occasionally up to 70 m AHD. We interpret the variability as primarily palaeotopography associated with the top of the Renmark Group (and occasionally older bedrock). The slopes on the variations in the base of the Calivil Formation are gentle extending over several kilometres, suggesting the most likely palaeotopographic process was fluvial incision leading to formation of palaeovalleys.

Two palaeovalleys appear to trend northeast-southwest across the northern and central part of project area, consistent with the regional tilt of the basal surface. This is approximately normal to the trends of the Loxton-Parilla Sands strand lines in the extreme south of the project area. The orientation is similar to that determined for the underlying Menindee Trough that controls the Renmark Group distribution (Lawrie *et al.,* 2009a), suggesting shared control by the same sag basin. It is suggested that subsequent tectonic movement, especially uplift along the western sides of the lakes, have resulted in the late Quaternary drainage occurring in a more north-south direction. A single palaeovalley, possibly north-south in orientation occurs in the southern half of the project area.

The presence of incised channels at the base of the Calivil Formation has a number of implications for the large scale architecture of this formation and the subsequent stratigraphy. The inferred relief at the base of the Calivil Formation is of the order of 30 m, about half the maximum thickness of the unit. During deposition of the Calivil Formation the coarse-grained fluvial sediments would have been initially confined to between the incised highs of weathered Renmark Group sediments. Once these highs were overtopped by continued sedimentation the Calivil Formation, sediments would have spread out in a largely unconfined alluvial plain. Similar depositional architecture was observed in the Lower Balonne (in sediments that are probable lateral equivalents to the Calivil Formation, see Clarke & Riesz, 2004) and in the lower Ord River (Lawrie *et al.,* 2010c).

Sediments within the incised valleys are almost entirely coarse-grained, dominated by sand or gravel. Once the substrate interfluves are buried, the depositional architecture changes to a series of channel belts separated by fine-grained floodplain lithologies. This is consistent with what is observes in the Calivil Formation, with coarse-grained lithologies near ubiquitous in the lower part of the succession and finer-grained units, specifically thick muddy units probably related to floodplain environments, occurring in the middle to upper part of the Calivil Formation. While coarse channel belt lithologies are not entirely absent

from the upper part of Calivil Formation, they are likely to be partly isolated from other channel sediments by intervening muddy floodplain lithologies. This is shown schematically in Figure 5-28. Consequently, the lower Calivil Formation channel sands and gravels are more likely to be hydrologically connected than those in the upper part. Groundwater flow in both the lower and the upper parts of the Calivil Formation is controlled by channel orientation; in the lower part this is constrained by the palaeotopography, while the upper part is constrained by regional slope.



Figure 5-26. *Sonic core for BHMAR64. Note the strongly oxidised coarse, gravelly sand of the Calivil Formation (bottom and centre core) overlying strongly oxidised bedded clays of upper Renmark Group (top core). Top of the hole is to the left.*



Figure 5-27. *Composite image of sonic core showing contact between gravels of Calivil Formation (yellow) and clays (dark grey) of upper Renmark Group in BHMAR33-1. Note complete absence on oxidation along erosional contact between the two. Arrow points downhole.*

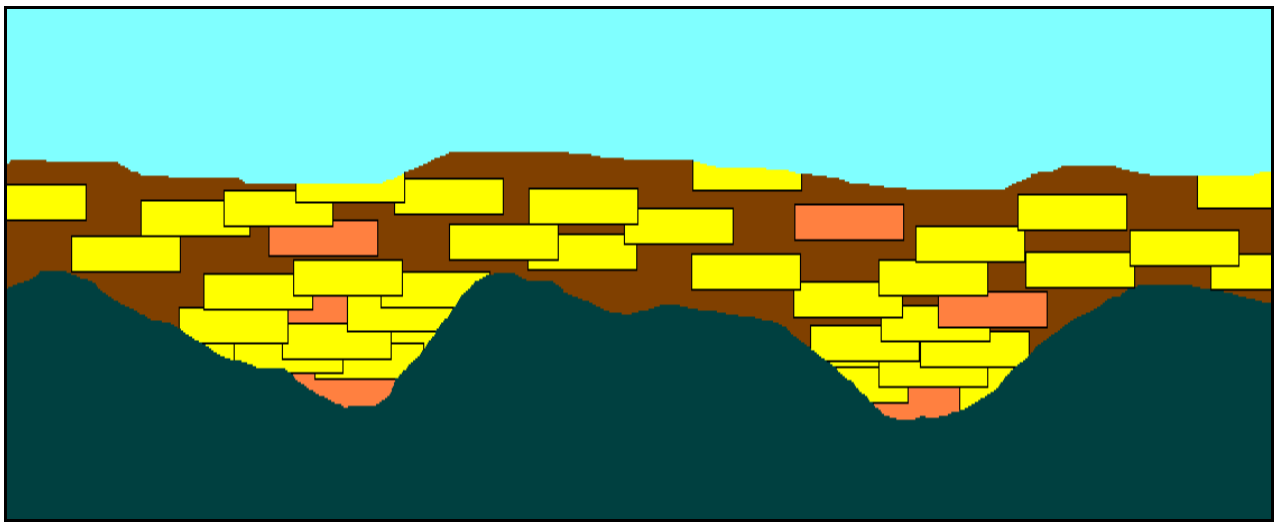

Figure 5-28. *Schematic diagram showing sand (yellow) and gravel (orange) channel and floodplain (brown) Calivil Formation deposits over an irregular topography of Renmark Group (green-grey). Diagram shows the eroded top of the Calivil Formation prior to deposition of Blanchetown Clay. Within the incised basal topography the Calivil Formation consists almost entirely of coarse-grained lithologies, once the topography is buried, both floodplain and channel deposits are present.*

There are no pre-existing formal subdivisions of the Calivil Formation, nor are there any recognisable informal units in the BHMAR study area. However, in the East-Bootingee-Jimargil area, a 3-10 m thick muddy unit is present over a distance of at least 1.4 km and at a depth of 25-35 m. This unit subdivides the upper and lower sandy parts of the Calivil Formation. Its thickness and extent suggests that it is a floodplain unit on the interfluve between two channels, rather than a mud-filled abandoned channel.

Laterally the Calivil Formation progrades over the marine Loxton-Parilla Sands towards the down-valley margin of the study area (Figure 5-31). The Loxton-Parilla Sands is much better sorted and finer-grained than the Calivil. It was encountered in several holes at the south-easternmost part of the project area (BHMAR28, 29 and 31) but not in BHMAR30 in the south-western margin. These holes clearly show the complex interfingering relationship between the two formations (Table 5-9).

Table 5-9. *Distribution of Calivil Formation and Loxton-Parilla Sands in southernmost project bores.*

Borehole	BHMAR 28	BHMAR 29	BHMAR 30	BHMAR 31
Stratigraphy	All Loxton-Parilla	Calivil Formation over Loxton-Parilla	All Calivil	All Loxton-Parilla
Thickness Calivil		30 m	40 m	
Thickness Loxton-Parilla	13 m	6 m		41 m

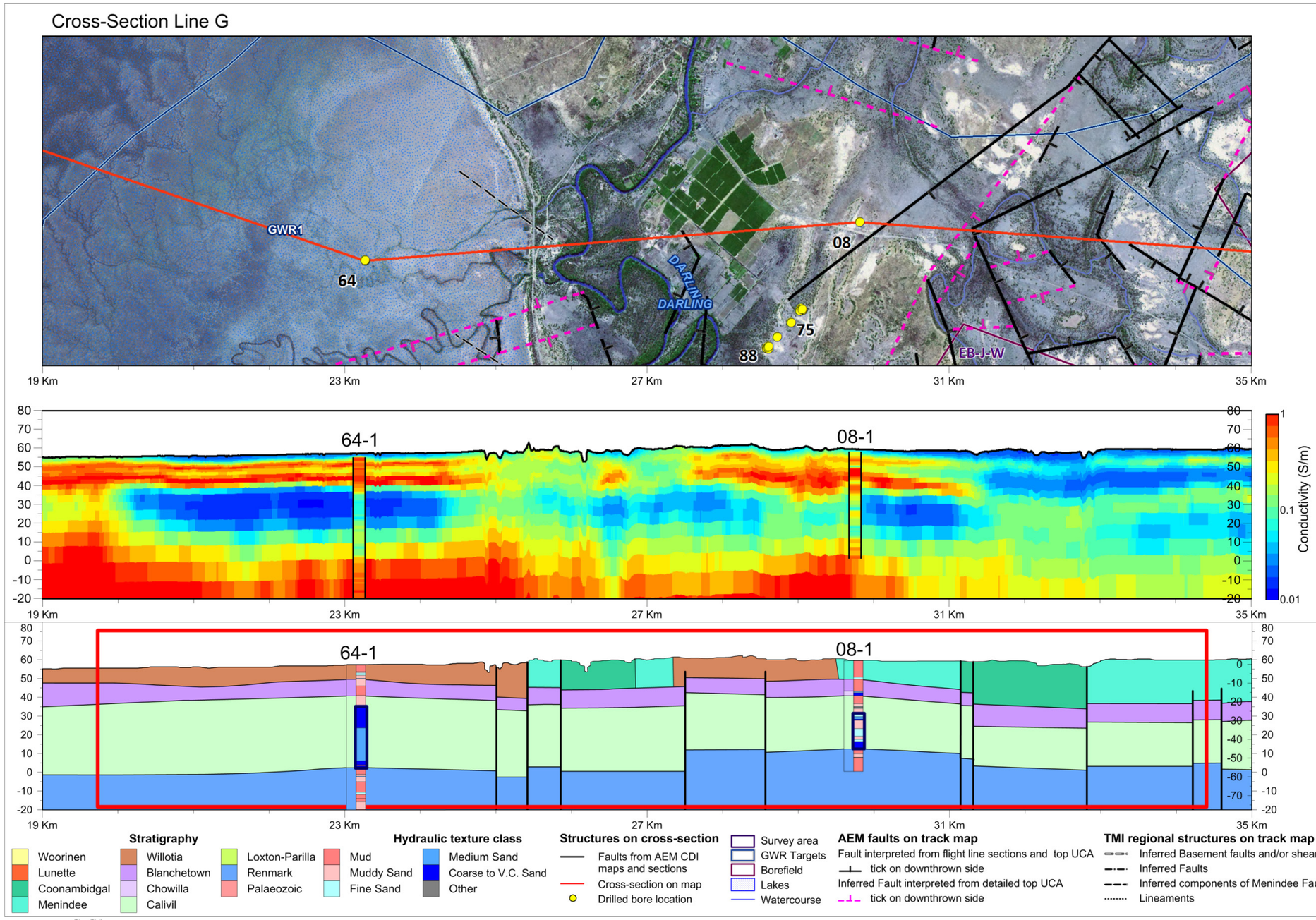

Figure 5-29. *Cross section G-G1.*

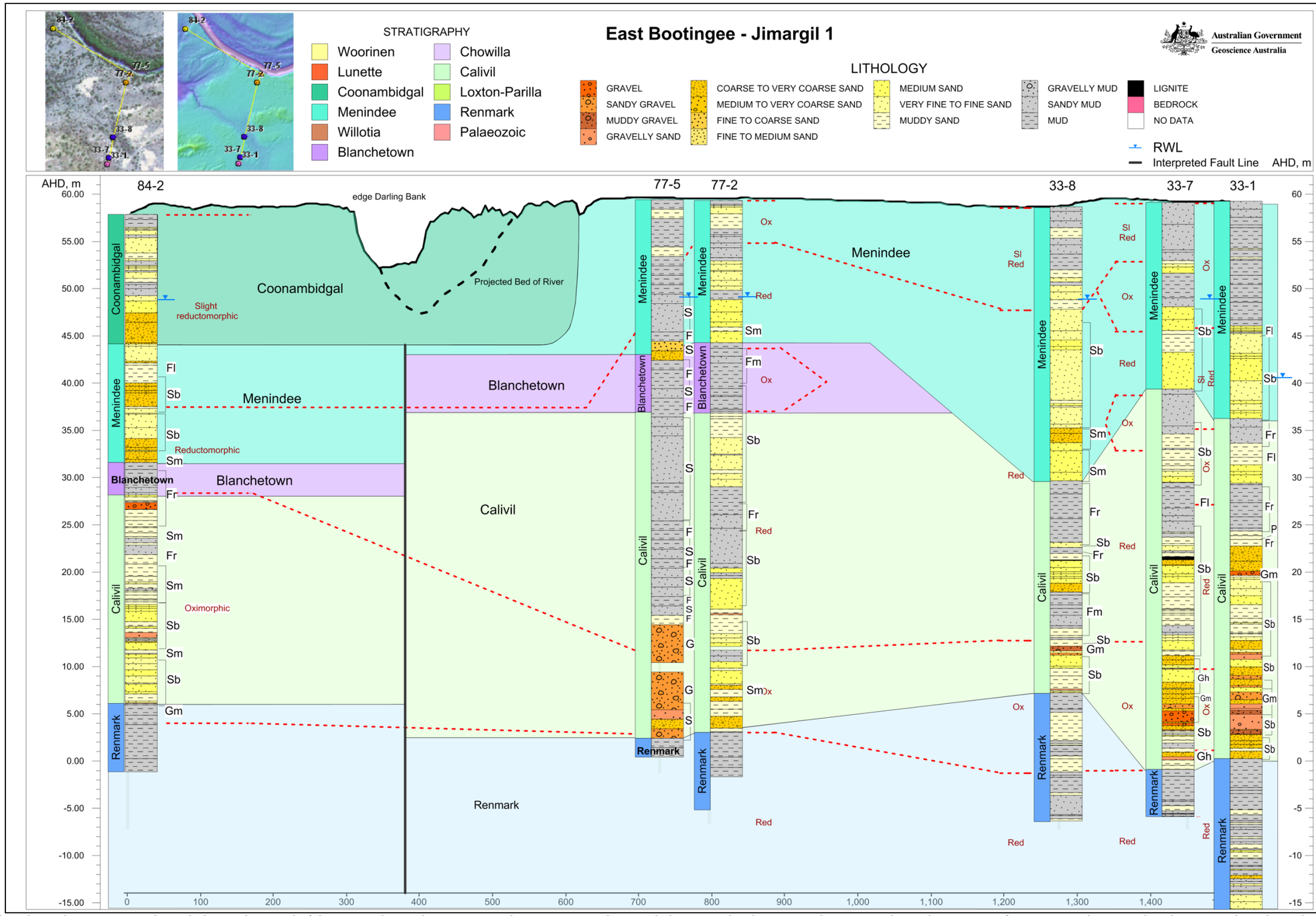

Figure 5-30. *Local geological cross section through the northern end of the Jimargil site, showing mapped Formations and textural classes, and redox zones. This section shows the upper confining aquitard marginal to the main palaeochannel.*

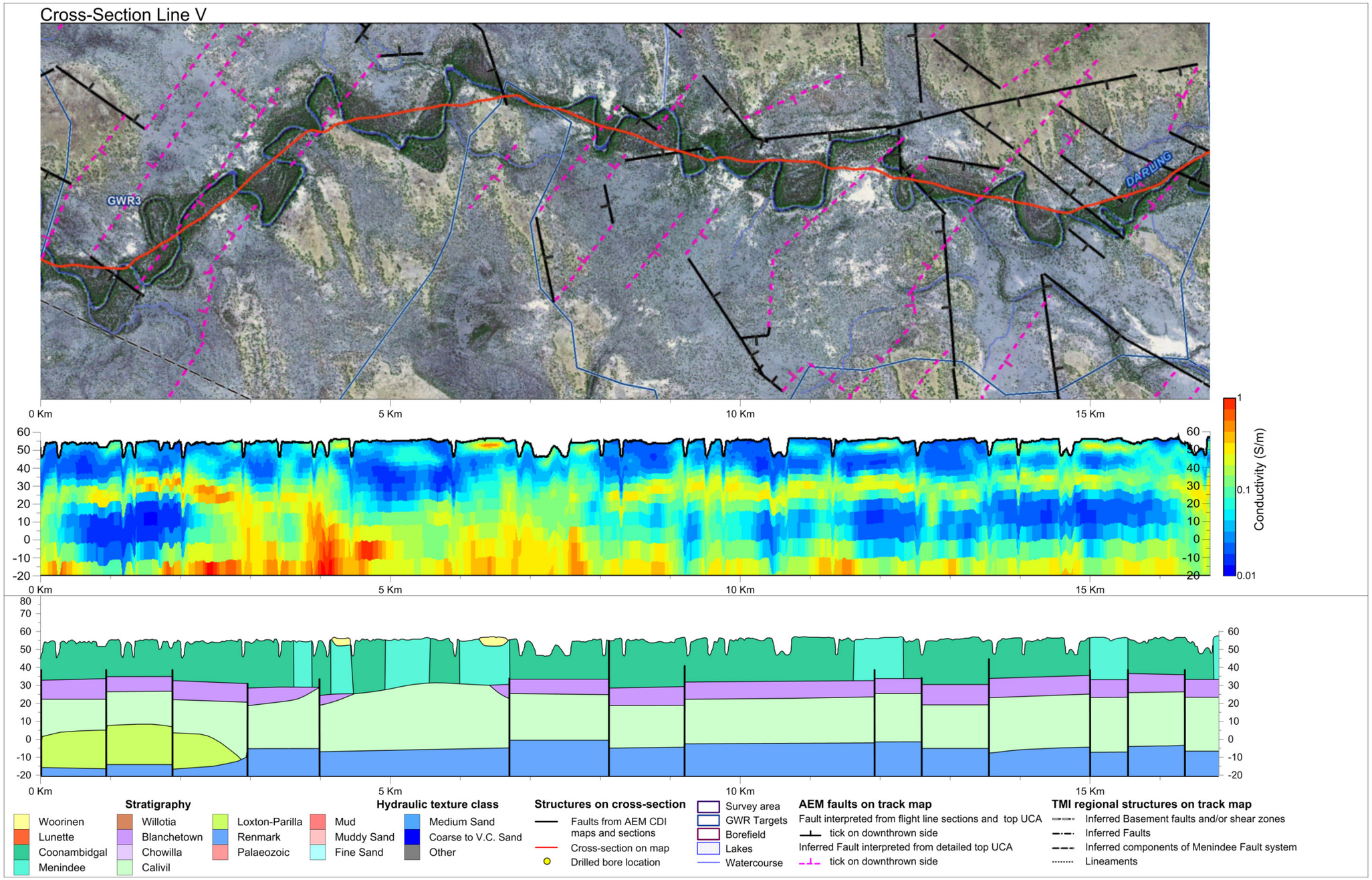

Figure 5-31.*Cross section V-V1.*

5.2.4 Age and Environment

Age control on the Calivil Formation, provided by palynology (Macphail, 2010; Appendix 7, Apps *et al*., 2012e), indicates a range from Early to Late Pliocene. The palynological age range actually extends down into the latest Miocene and up into the earliest Pleistocene, however this most likely represents the continental-scale age ranges of the indicator species rather than the age of the unit itself.

Macphail (2010) also identified several Oligo-Miocene taxa which were interpreted as reworked from the underlying Renmark Group. This is consistent with several tens of metres of erosion observed at the top of the Renmark Group in the project area.

A revised late Early to Middle Miocene age for the Calivil Formation based on palynology from cuttings from the Boga-1, Boga-317 and Buderim West-1 boreholes in the Kerang area of northern Victoria (Birch, 2003) is inconsistent with ages in the BHMAR Project area. To resolve this question, Macphail (2013; Appendix 7, Apps *et al*., 2012e) examined palynological samples from the Calivil Formation type section in the Calivil-2 borehole and a representative section of the Calivil Formation in Marma-1 borehole at the southern margin of the Murray Basin. Macphail (2013) found that the Calivil Formation in both these boreholes accumulated during the Pliocene, following marine regression from the basin and that any older Oligo-Miocene palynomorphs were reworked from exposures of the Renmark Group Olney Formation elsewhere in the basin. Macphail considers it likely that the older palynomorphs from borehole cuttings attributed to the Calivil Formation in the Kerang district are also contamination reworked from the Olney Formation.

Aquatic depositional environments indicated by the palynoflora varied from a freshwater pond or lake supporting abundant remains of the alga *Pediastrum* to sub-saline ponds supporting the halophytic dinocyst *Cobricoperidinium (*Macphail, 2010). This is consistent with marked seasonality. Mangrove-type pollen (*Zonocostites*) present in BHMAR3B indicates estuarine or at least brackish conditions with biological connection to the sea (some 70-80 km distant).

The non-aquatic vegetation shows two assemblages, an earlier (Miocene- Early Pliocene) assemblage indicative of effectively wetter (humid-subhumid) climates, and a second (Late Pliocene-Middle Pleistocene) assemblage indicative of drier climates, but semi-arid rather than arid. The earlier assemblage contains remnants of the Tertiary rainforest flora (*Araucaria*, *Podocarpus-Prumnopitys*), most likely survived as galleries along streams whilst more xerophytic shrublands dominated by *Chenopodiaceae, Casuarinaceae* and *Asteraceae* occupied the drier floodplains *(*Macphail, 2010).

The later assemblage contains temperate mesophytic taxa such as *Cyathea* and *Nothofagus* (*Brassospora*) spp., possibly as gallery woodlands along rivers. Plant communities occupying interfluve areas and floodplains appear to have been shrublands dominated by *Asteraceae* and *Eucalyptus*.

5.2.5 Lithostratigraphy

5.2.5.1 Data sources in the Menindee area

Lithostratigraphic understanding of the Calivil Formation comes from multiple sources:

- Lithological field and lab logs of sonic core. Due to uncertainties in measurement of depth of recovered core intervals, precision of interpreted lithological boundaries is ~ 10 cm. Detailed lab logs were supplemented by in-situ measurements (rock strength, pH and EC measurements), analyses (mineralogy, bulk-sediment geochemistry, pore fluid geochemistry, granulometry), and photographic record (see Appendix 2, Spulak *et al*., 2012).
- Lithological field logs of rotary mud chips. Due to the sampling recovery using this method, lithological boundary interpretation is at best accurate to ~1 m and is often worse than this. Accuracy

in identification of lithology is further affected by contamination by drill mud and time lags during the drilling process. No sedimentary structure information was preserved.

- Downhole gamma logs. Major inflections in gamma signature can be used to identify stratigraphic boundaries, while trends within units reflect features such as upward fining and upward coarsening. Low gamma signatures generally indicate sand-rich units while stronger gamma signatures occur in muddier units. Uncertainties exist due to heavy mineral bands, for example monazite and thorium enrichment associated with goethite. Some (but not all) bentonite seals used in bore construction also show gamma peaks. In addition, gamma cannot differentiate between gravel and sand.
- Downhole conductivity logs. These logs are generally less spiky than gamma curves, but the influence of water salinity can overwhelm the conductivity signature associated with lithology. Overall, major inflections represent stratigraphic boundaries, while trends within units reflect features such as upward fining and upward coarsening units. Where not overwhelmed by water quality issues, low conductivity signatures generally indicate sand-rich units while stronger gamma signatures occur in muddier units. As was the case with downhole gamma logging, gravels cannot be differentiated from sand. Trends within aquifer layers may indicate salinity density stratified groundwater.
- Nuclear Magnetic Resonance (NMR) logs. This technique measures the amount of bound and unbound water in the country formation. The method readily detects the watertable and wetting fronts. The logs show good correlation with lithology, with aquifers containing less bound and more free water and aquitards the reverse. There is also a generally good visual correlation with other geophysical logs and geological observations. As with other geophysical logging methods, gravels cannot be readily differentiated from sand.
- HyLogger data. Limited HyLogger data was available, covering most of two holes and small portions of two others. HyLogger maps the distribution of mineral phases, in particular clays, sulphates, carbonates, iron oxides and oxy-hydroxides, micas, quartz, and feldspar on the basis of spectroscopy. In addition to spectral data, HyLogger also produces core images.

5.2.5.2 Facies

The Calivil Formation is dominated by medium-grained facies, namely medium- to coarse-grained sand, with muddy and gravelly facies less common as shown in Figure 5-32. This figure indicates that more than half the Calivil Formation is composed of medium- to very coarse-grained sand. Muddy units make up less than a quarter of the total intervals, and fine-grained sand is the least common class.

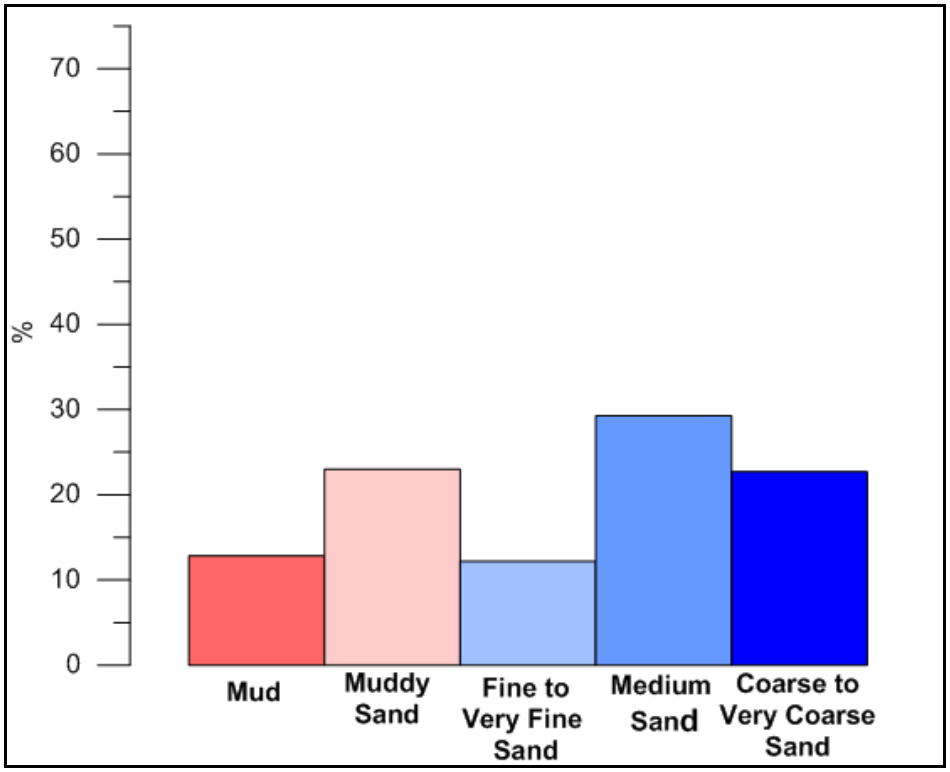

Figure 5-32. *Histogram showing abundance of all five hydraulic sediment classes in the Calivil Formation in sonic cores.*

Pie diagrams showing the abundance of the five hydrological texture classes (mud,, muddy sand, fine to very fine sand, medium sand, and coarse to very coarse sand) are shown in Figure 5-33, Figure 5-34 and Figure 5-35 for the northern, central and southern parts of the project area respectively. They are projected on the 30.9-51.5 m AEM depth slice for comparison. Some correlation between conductivity and the texture class can be observed. For example in some cases, predominantly sandy holes are associated with resistive zones and muddier holes with conductive zones. This associate is however not widespread, suggesting that while some of the AEM conductivity patterning can be attributed to sediment texture, it is also influenced and in some case overridden by water quality. The correlation appears better in the southern part of the area, but the small number of holes makes such comparisons statistically suspect.

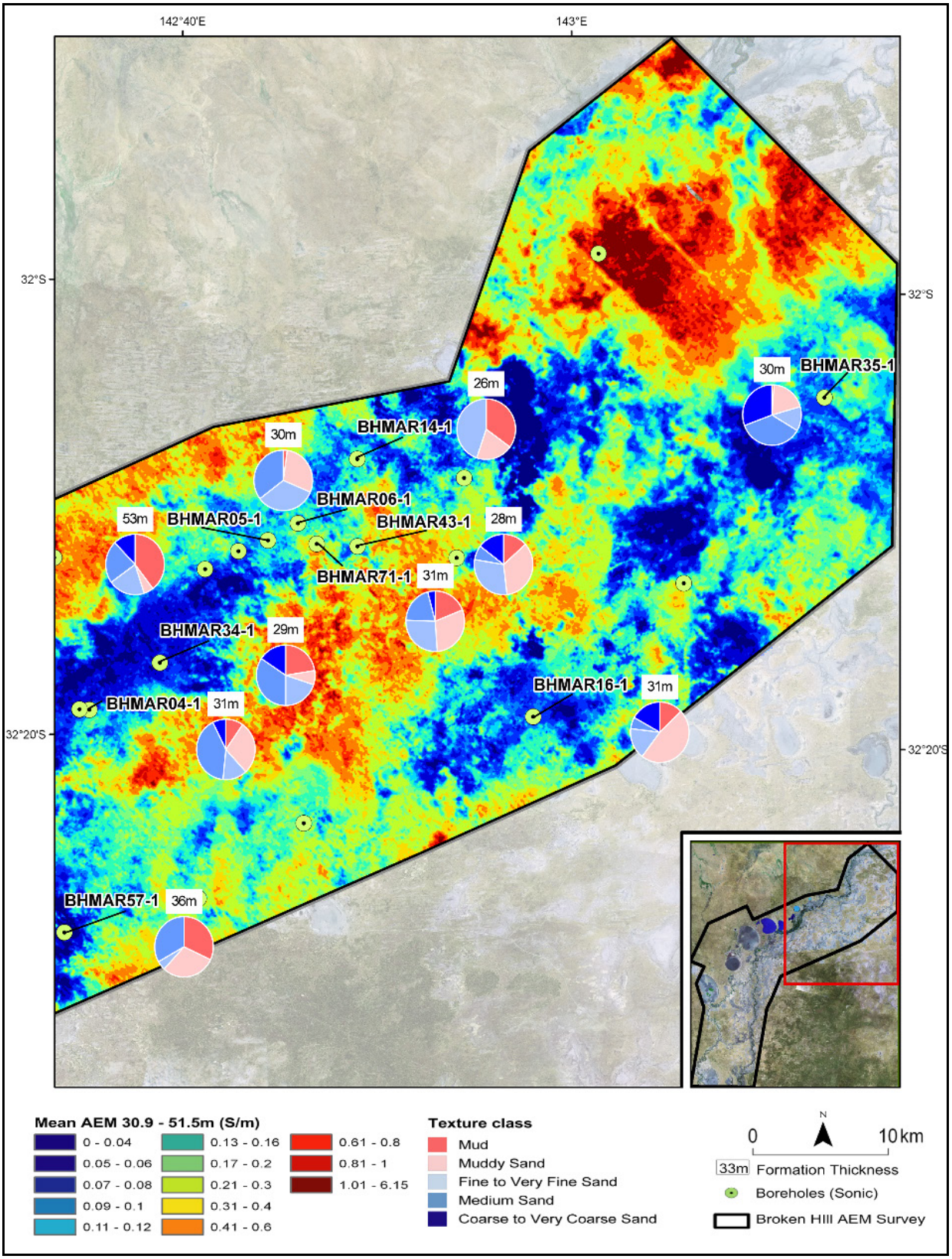

Figure 5-33. *Pie diagrams for sonic bores within the Calivil Formation in the northern part of the project area, overlaid on the 30.9-51.5 m depth slice. Some holes with high sand show good correlation with resistive Calivil Formation, such as BHMAR35-1 which encountered coarse-grained sand with only moderate amounts of muddy lithologies. Similarly, BHMAR14-1 shows a good correlation between high mud percent and conductivity. Other bores do not show such a correlation; BHMAR57-1 contains over 50% muddy lithology and no coarse sand but occurs in a strongly resistive zone, while BHMAR35-1 is located in only a moderately resistive zone, despite abundant coarse sand and low mud content. These results suggest the influence of water quality on conductivity signatures.*

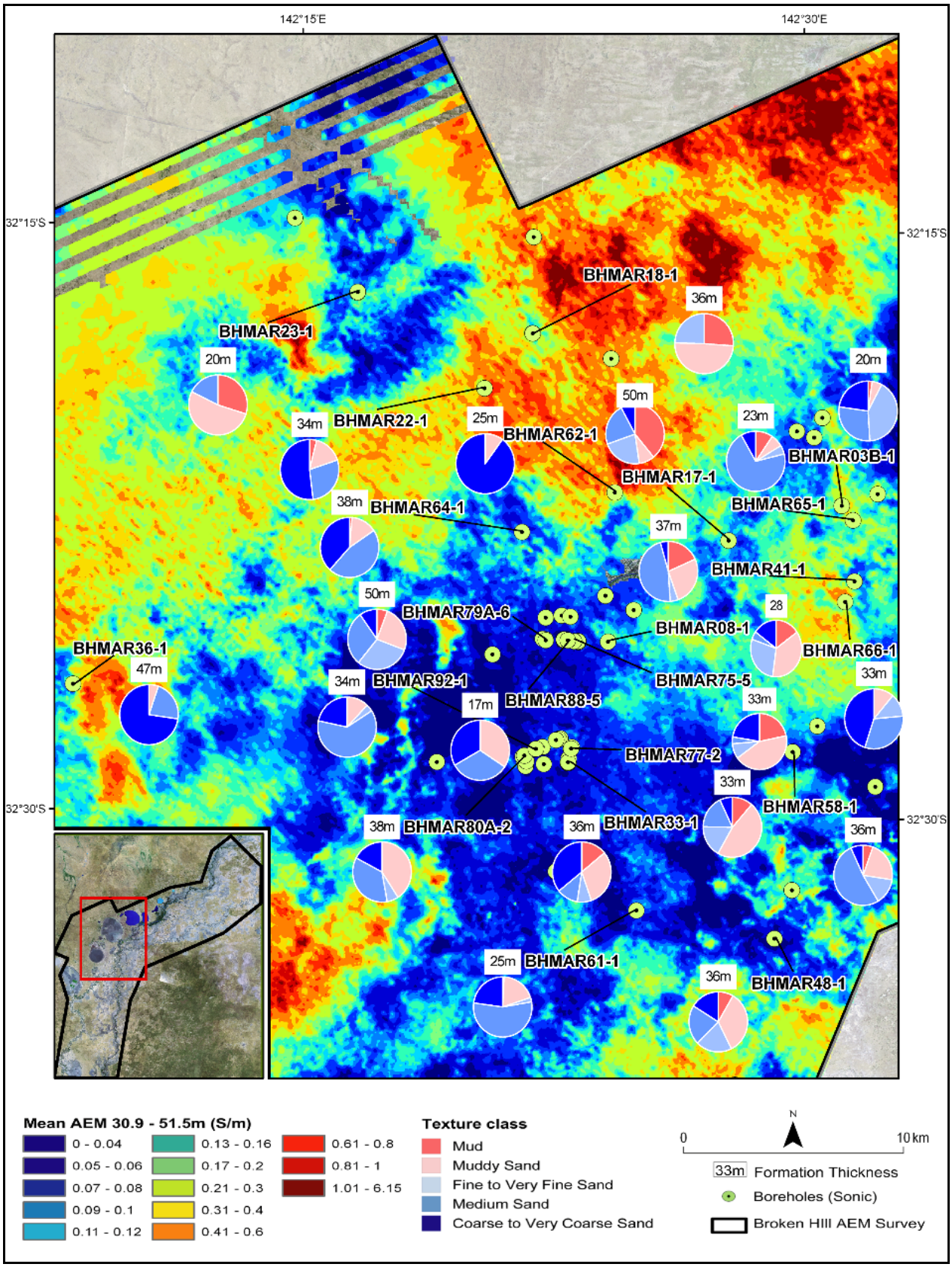

Figure 5-34. *Pie diagrams for sonic bores within the Calivil Formation in the central part of the project area, overlaid on the 30.9-51.5 m depth slice. Some holes with high sand show good correlation with resistive Calivil Formation in the 30.9-51.5 m depth slice (e.g. BHMAR61-1), as do some with high mud and conductive areas (e.g. BHMAR18-1). Others do not, BHMAR36-1 contains very little in the way of muddy lithologies but is on the edge of a conductive zone, and BHMAR48-1 is in the middle of a strongly resistive zone and BHMAR77-2 is quite muddy in a resistive zone.*

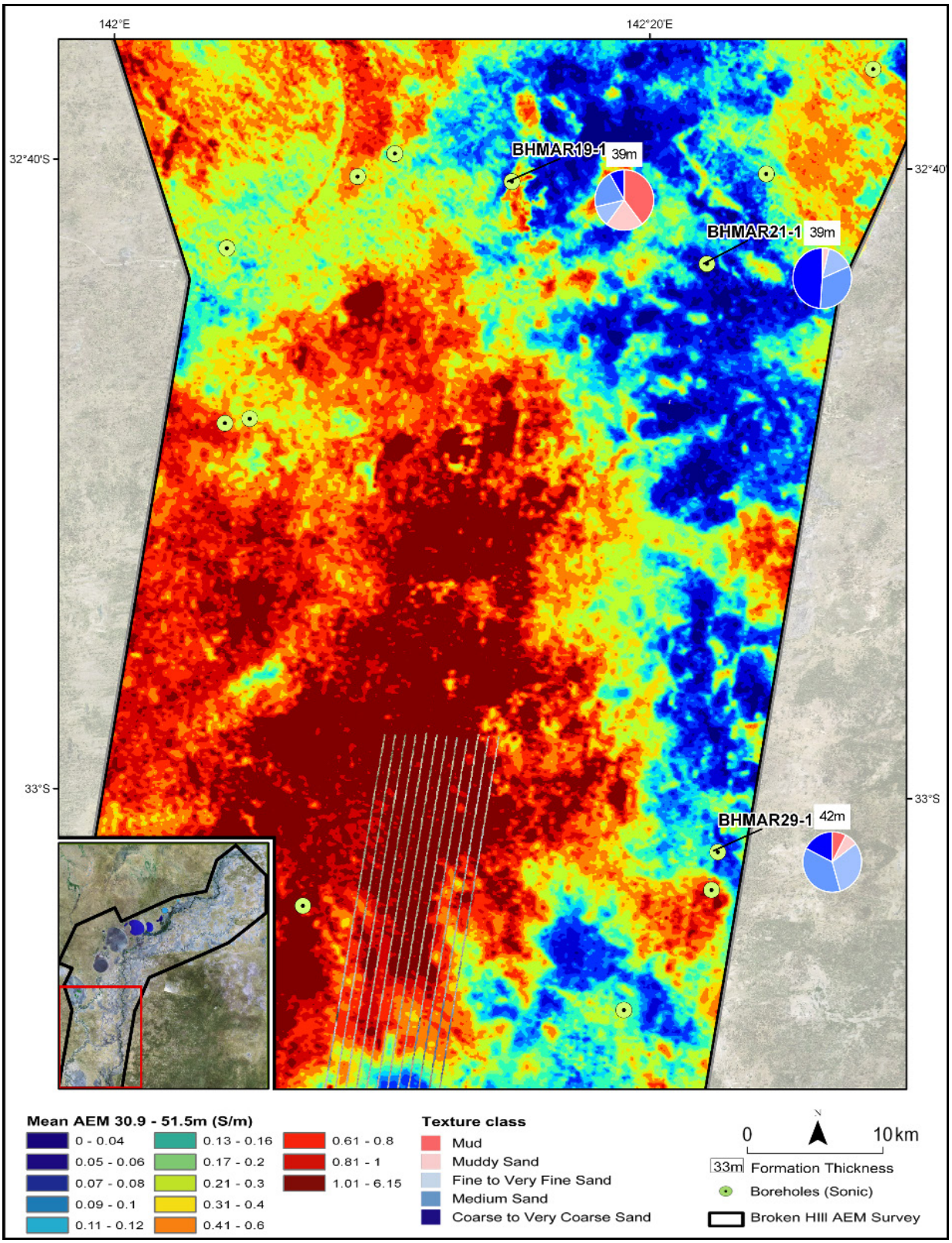

Figure 5-35. *Pie diagrams for sonic bores within the Calivil Formation in the southern part of the project area, overlaid on the 30.9-51.5 m depth slice. Data is limited to only three bore, but holes BHMAR21-1 and 29-1 are sand dominant and correspond with resistive AEM signatures in the 30.9-51.5 m depth slice.*

Sands (Figure 5-36) are composed of sub-rounded, fine- to very coarse-grained quartz. Grain roundness increases with grainsize. Some of the sand matrix in the gravelly facies is very angular, suggesting very local derivation from fragmenting silcreted outcrop. The sands are typically well sorted, with the coarsest units least well sorted. Plant material is not uncommon, occurring as wood and leaf fragments. Leafy debris is most common in finer sands, especially muddier units, with woody material in coarse sands.

Beds are typically massive to normally graded, and sometimes well bedded; the well bedded units are probably cross bedded. Individual beds generally cannot be correlated over distances as close as tens of metres. This suggests they were deposited by individual channel bars. The exception to this are the medium- to coarse-grained sands in the upper part of BHMAR88-2 and 88-7 (see Appendix 1, Halas *et al*., 2012a for stratigraphic logs of each borehole), which appear juxtaposed. However even here they do not match directly but simply present a limited lateral continuity between similar lithologies, probably amalgamated medium- to coarse-grained channel bar units.

Gravels in the Calivil Formation are composed of well polished, well rounded quartz "pea gravels" and are associated with medium- to coarse-grained sands (Figure 5-36). Gravel lenses are usually less than 2 m thick and are of limited extent (metres to tens of metres). This is consistent with the distribution of gravels in modern rivers, such as the Shaw River (Pilbara region, Western Australia) which are dominated by medium- to coarse-grained sand (Figure 5-37, Figure 5-38). Some gravels are matrix supported, floating granules to pebbles supported by sand or muddy sand, suggesting debris flow processes. Clean gravels are present, but are minor. Gravels are most common near the base of the Calivil Formation and occur more rarely higher up. Beds are massive to weakly graded. Wood debris is occasionally present, and in one case bone was observed. Wood (and bone) occurs most commonly near the base of channel units.

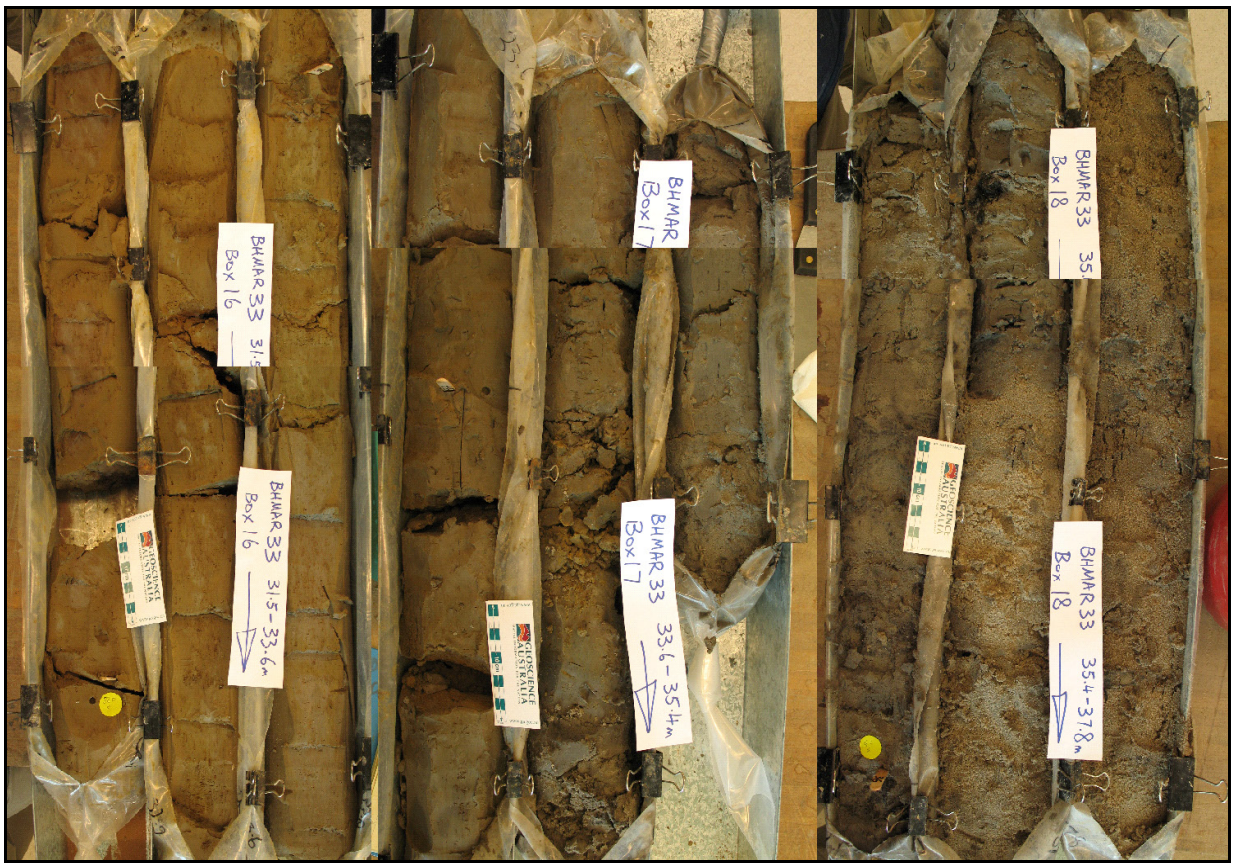

Figure 5-36. *Composite image of sonic core BHMAR 33-1 showing muddy oxidised lithologies (left) and coarser-grained (sandy) more organic-rich lithologies (right) in the Calivil Formation. Arrow points downhole.*



Figure 5-37. *Photograph of a localised gravel sheet in river bed (Shaw River, WA).*



Figure 5-38. *Photograph of very localised gravels probably derived from lateral debris flows from valley sides at Shaw River, WA.*

Muddy units range from clay to muddy sands and sandy muds and are typically bedded (Figure 5-36). In colour they are typically yellow, brown, grey or khaki and are often mottled. Thinner units tend to be silty or contain fine-grained sand while thicker units often contain root casts of carbonate and common manganese dendrites.

These muddy units are interpreted as being either local floodplain accumulations (hundreds to thousands of metres extent), or plugged channels (tens to hundreds of metres). From first principles, plugged channels are more generally sandier, and have upward fining successions. Floodplains are likewise more likely to have root casts than channel lugs owing to the greater prevalence of long-lasting vegetation (Lynds & Hajek, 2006).

In most cases these muddy units cannot be correlated over distances of tens to hundreds of metres, and are therefore thought to be abandoned channel fills. The exception is a 5-10 m thick muddy unit that extends through the East Bootingee-Jimargil area with the boreholes BHMAR84-2, 77-5, 77-2, 33-8, 33-7 and 33-1. This could be a down axis section through a channel fill, but is more likely to be a floodplain deposit. It only occurs in part of East Bootingee-Jimargil area and not at all at Menindee Common.

An exception to the above generalisation occurs in BHMAR19 in the Tandou area, where in a succession ~39 m thick, two ~ 8 m successions of muddy lithologies, separated by ~3 m of fine-grained sand, occur in the upper part of the stratigraphy. Two relatively thin (6-7 m) coarse-grained sandy units, separated by ~5 m of muddy lithologies, occur in the lower part of the hole. The nearest project bore is BHMAR1B (~9 km away) where, in a 36 m Calivil Formation succession, only the basal 3 m appears to be of coarse-grained sand, the remainder being muddy. Lithological identification in this hole is, however, more uncertain than for BHMAR19, because it was drilled by the rotary mud method, as opposed to sonic. These thicker muddy units are thought to represent genuine floodplain facies.

Similar thick, muddy units were reported prior to this project at the Menindee pumping station in drilling in hole T2:701 (Jewell, 2007). The poor quality of the rotary mud logs and the absence of geophysical logging makes interpretation of the data very difficult. However, the lack of water inflow into this hole confirms its muddy nature.

5.2.5.3 Provenance

Eight thin sections were prepared of indurated sands and gravels, such as nodules and thin beds, from the Calivil Formation. Cemented sediments were selected for ease of thin section making and to better determine the nature of cements. It is unlikely that provenance varies from indurated to non-indurated material, and a similar range of grainsize is present in both.

The composition of grains in the various thin sections is shown in Table 5-10 with grain percentages in Table 5-11. The outstanding characteristic of these sediments is their extremely quartzose nature - over 99% overall (Figure 5-39). Their provenance is predominantly igneous and metamorphic, indicated by the abundance of coarse, weakly to strongly undulose quartz grains, vein quartz, often rich in fluid inclusions, and polycrystalline quartz grains. These are interpreted as being eroded from deeply weathered rocks of the Willyama complex to the west and Palaeozoic outcrops to the northwest (see Gibson, 1999).

In drill samples pinkish grains are not uncommon, these were described as lithics, or feldspars during logging. In thin section these proved to be silcrete (Figure 5-40), indicating deep weathering of the source areas. The inferred deep weathering is consistent with the very low feldspar abundances and also with a component of recycled quartz out of older sedimentary successions such as those of the Scopes Range, and further upstream along the Darling River (Gibson, 1999).

Table 5-10. *Compositional information about the Calivil Formation based on thin section analysis.*

Sample	# grains	Quartz	Feldspar	Other	Comments
BHMAR 21 47.1 m	244	Vein/intrusive: 227 Metamorphic: 7 Silcrete: 9 Total : 243	k-spar plag total	Haematite-cemented clay pellet: 1	Ox. cemented zone in red. aquifer
BHMAR 21 47.6 m	240	Vein/intrusive: 216 Metamorphic: 6 Silcrete: 15 Total: 237	k-spar : 2 plag: 1 total: 3		Ox. cemented zone in red. aquifer
BHMAR 33 56.45 m	205	Vein/intrusive: 195 Metamorphic: 1 Silcrete: 8 Total: 204	k-spar plag total	Ferruginised wood: 1	Cemented zone in ox. aquifer
BHMAR 64 24.5 m	180	Vein/intrusive: 174 Metamorphic Silcrete: 5 Total: 179	k-spar plag total		Cemented zone in ox. aquifer
BHMAR 64 40.3 m	108	Vein/intrusive: 99 Metamorphic: 5 Silcrete: 3 Total: 107	k-spar: 1 plag total: 1		Cemented zone in ox. aquifer
BHMAR 65 50.74 m	312	Vein/intrusive: 303 Metamorphic: 2 Silcrete: 5 Total: 310	k-spar plag total	Zircon: 2	Cemented zone in red. aquifer
BHMAR 83-2 59.84 m	124	Vein/intrusive: 123 Metamorphic: 1 Silcrete Total: 124	k-spar plag total		Near base unit
BHMAR 83-2 60.85 m	152	Vein/intrusive: 148 Metamorphic: 2 Silcrete: 2 Total: 152	k-spar plag total		Very base of unit

Table 5-11. *Percentage and abundance of different grain types within the Calivil Formation based on thin section analysis.*

Grain type	Grain No.	Grain %
Vein/intrusive quartz	1485	94.71
Metamorphic quartz	24	1.53
Silcrete	47	3.0
Total quartz	1556	99.23
K-spar	4	0.26
Plagioclase	2	0.13
Total feldspar	6	0.39
Zircon	4	0.26
Clay pellet	1	0.06
Wood fragments	1	0.06
Total	1568	100.01

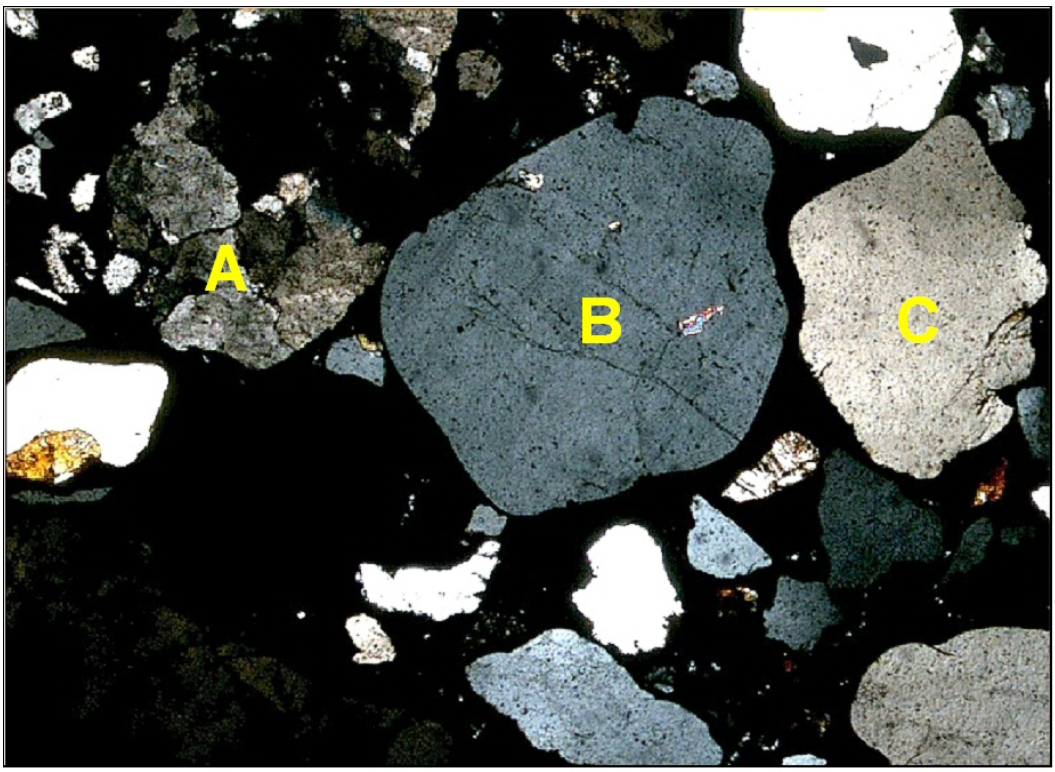

Figure 5-39. *Photomicrograph of goethite-cemented coarse-grained sandy gravel, BHMAR33-1, 56.45 m, field of view 2.5 m, crossed polars. A = Polycrystalline metamorphic quartz, B = fluid inclusion-rich vein quartz, C = intrusive quartz.*

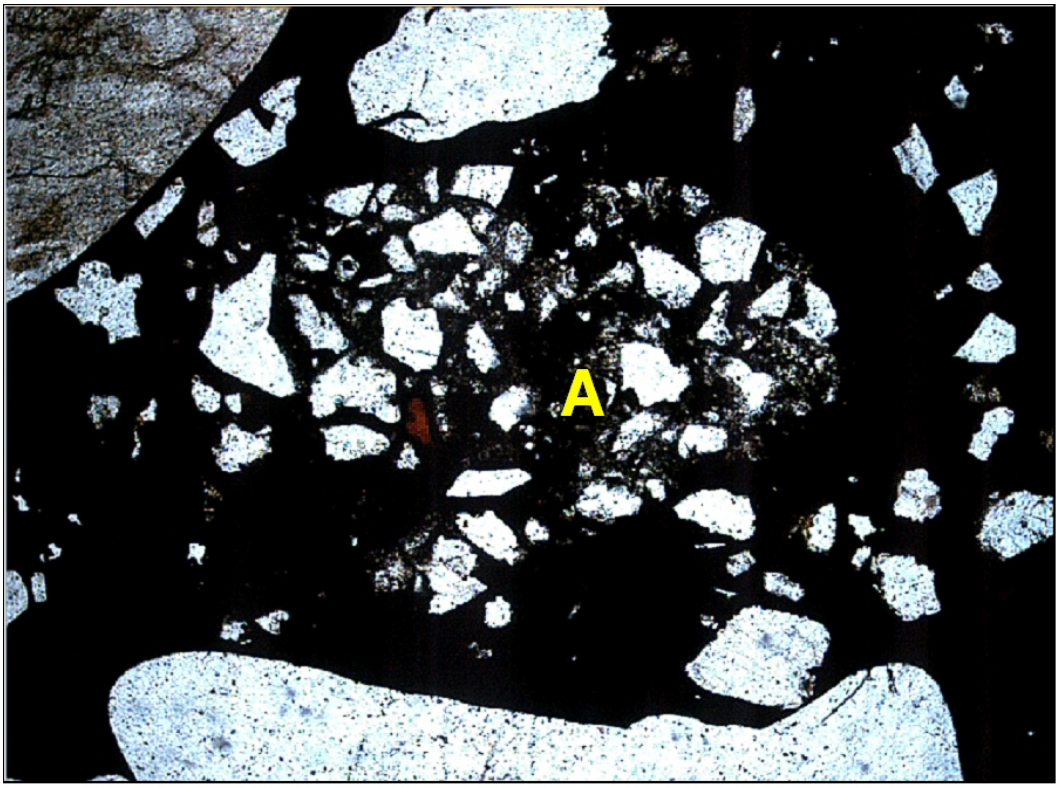

Figure 5-40. *Micrograph of goethite-cemented coarse sandy gravel, BHMAR 33-1, 56.45 m, field of view 2.5 m, crossed polars. A = silcrete fragment.*

5.2.6 Architecture

5.2.6.1 Channel hierarchy

Braided systems have a hierarchy of channels, here termed primary secondary and tertiary. The hierarchy is scale independent, as shown by three examples separated by two orders of magnitude in Figure 5-41, Figure 5-42 and Figure 5-43. The braided rivers that deposited the Calivil Formation would therefore have similar architectural features.

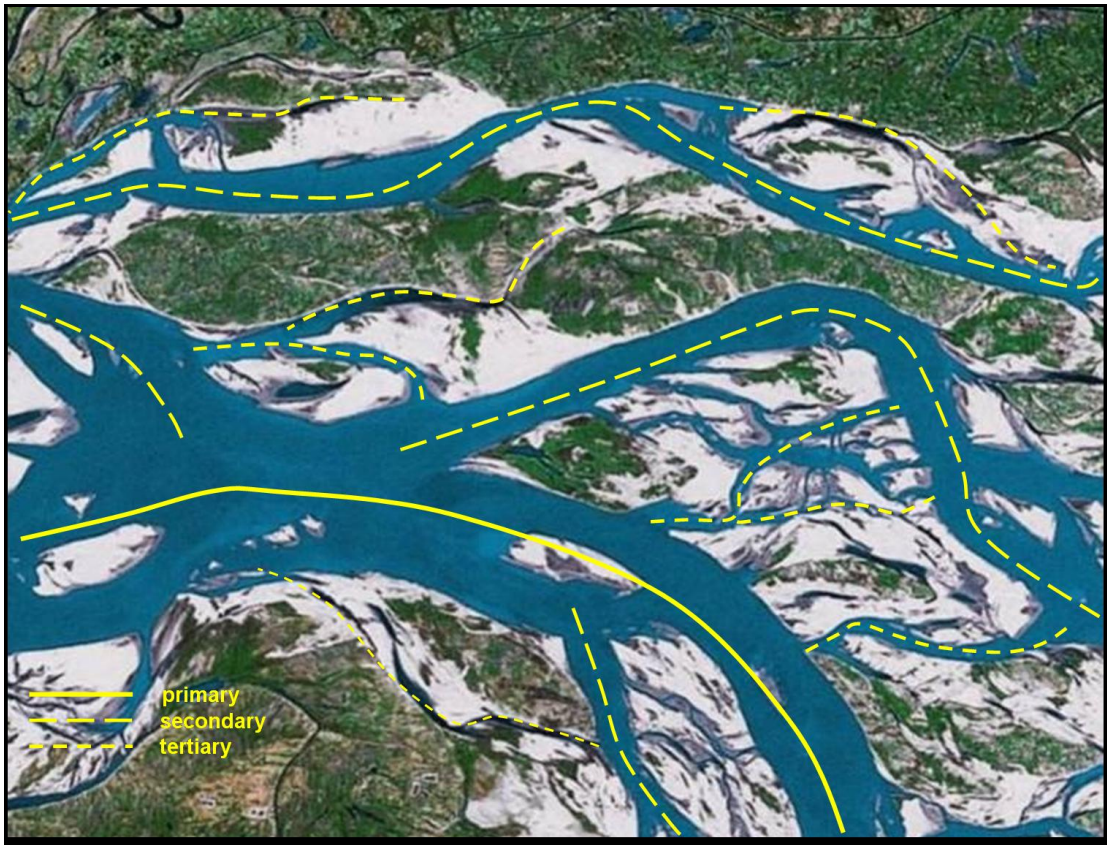

Figure 5-41. *Channel hierarchy of the braided Brahmaputra River system, Bangladesh as shown in Google Earth image. Note the channel belt width is approximately 10 km. The rivers responsible for the deposition of the Calivil Formation would have shown similar architecture.*

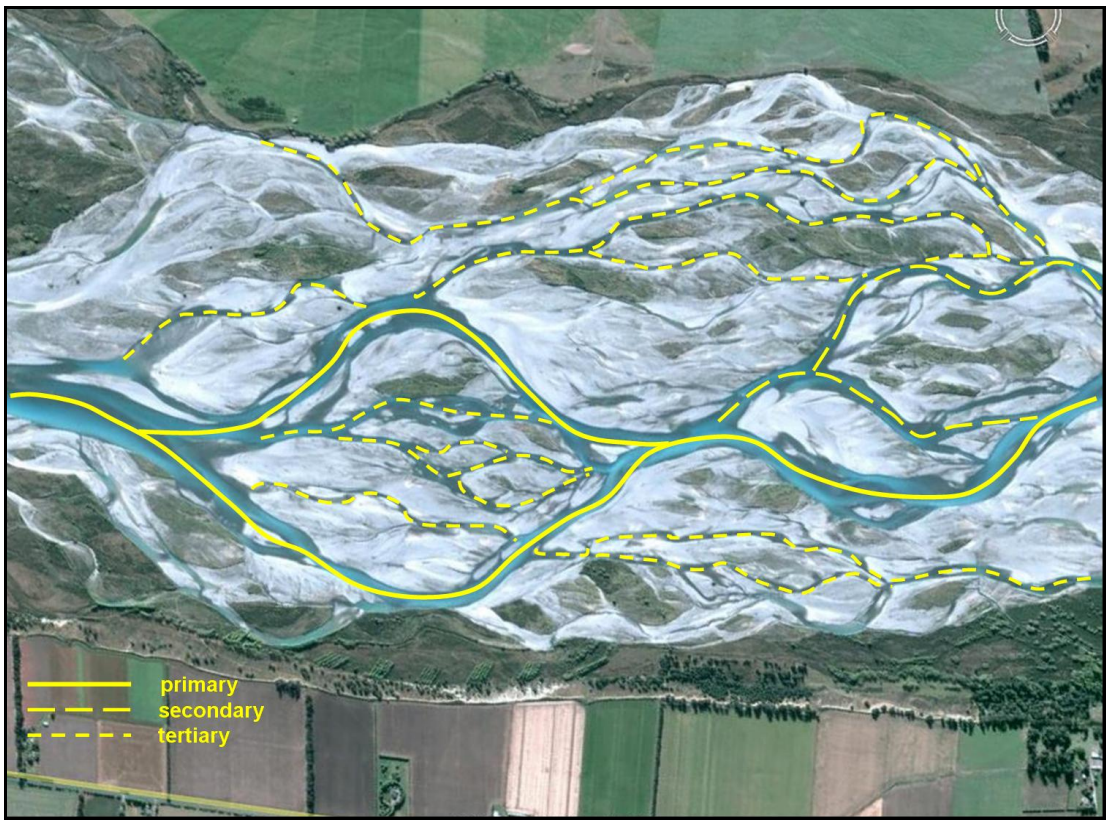

Figure 5-42. *Channel hierarchy of the braided Rakaia River system, New Zealand as shown in Google Earth image. Note the channel belt width is approximately 1 km. The rivers responsible for the deposition of the Calivil Formation would have shown similar architecture.*

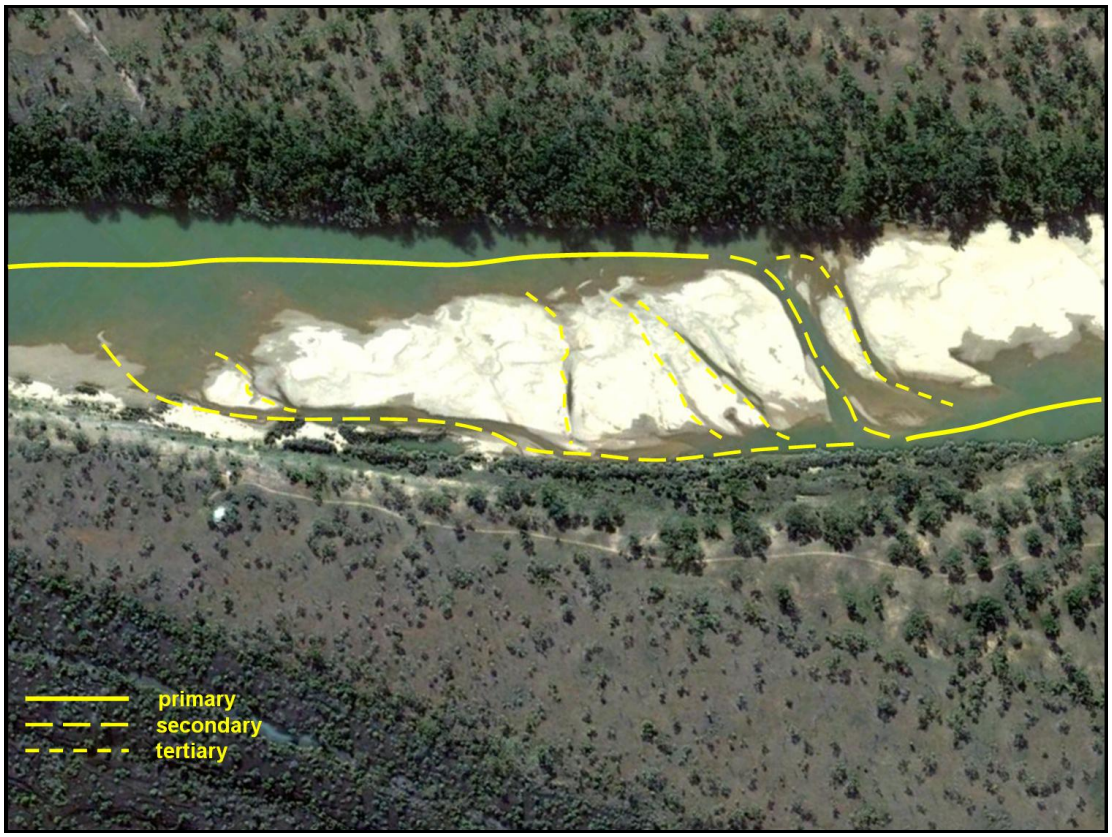

Figure 5-43. *Channel hierarchy of the braided Burdekin River system, Australia as shown in Google Earth image. Channel belt width is approximately 200 m. Note similar architecture despite an order of magnitude difference in scale. The rivers responsible for the deposition of the Calivil Formation would have shown similar architecture.*

5.2.6.2 Channel depths

Channel depths for the Calivil Formation have been estimated following the methodology of Bridge & Tye (2000) which is based on the thickness of fining upwards units in gamma logs (with assistance from conductivity logs where the patterns were doubtful). The unit thicknesses correspond to bank-full channel depth. It is important note that this method uses only geophysical logs, particularly gamma. Cycle depths are not directly comparable (without much more detailed work and checking against core data). Bore, and cannot be meaningfully compared at all with rotary mud drilling results.

For the whole project area, 64 bores with complete sections through the Calivil Formation were used, with a total of 355 channel units. Boreholes with partial Calivil Formation or Loxton-Parilla Sands were excluded. The results are plotted in Figure 5-44. As shown, upward-fining units varied in thickness from 0.5-18 m. There are three main peaks in the histogram, corresponding to thickness of 4-5, 7-8 and 10-11 m. These are interpreted as representing the tertiary, secondary and primary channel depths in the braided system, respectively. A weak 4th peak is present for unit thicknesses of 15-16 m, with 10 examples present. Thicker units, corresponding to deeper channels are interpreted as being due to locally deepened parts of the channel. Note that scours can be up to 4 times the average channel depth with scours associated with channel confluences, tight bends, and woody debris (Eilertsen & Hansen 2008). The number of cycles per hole ranged from 1-15, with 4-5 cycles being the most common.

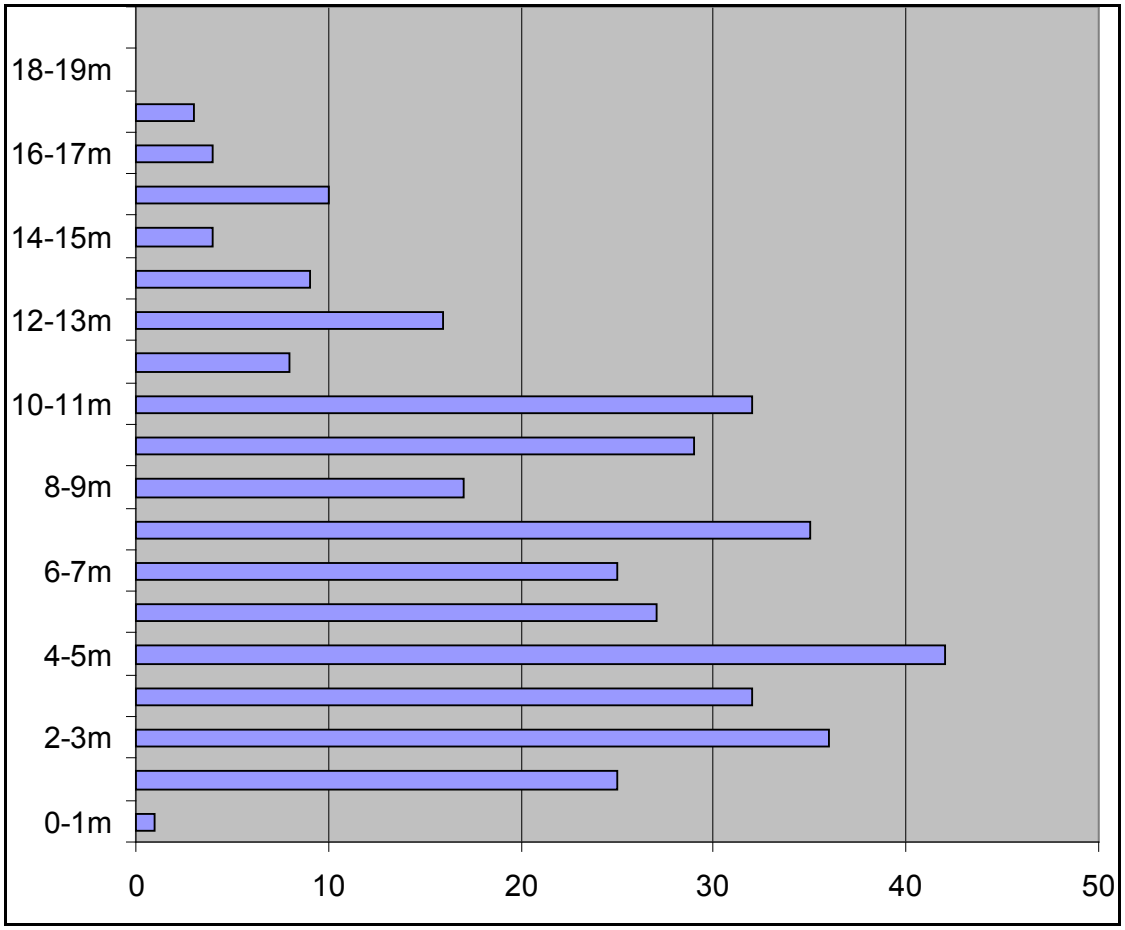

Figure 5-44. *Frequency histogram of channel unit thickness in the BHMAR study area derived from gamma logs within the Calivil Formation.*

5.2.6.3 Channel width

Channel widths are much more difficult to assess from borehole data than channel depths. This is because it is most readily determined (except in cases of very dense drilling) from channel body width/thickness ratios. These ratios are highly variable, on the scale of several orders of magnitude. For braided streams Gibling (2006) suggests that a common range is 50-1000. The possible ranges that result from this are shown in Table 5-12.

Table 5-12. *Interpreted channel widths.*

Channel rank	Depth	Width range	Minimum	Maximum
Primary	10-11 m	x50-x1000	500-550 m	10 -11 km
Secondary	7-8 m	x50-1x000	350-400 m	7 – 8 km
Tertiary	4-5 m	x50-x1000	200-250 m	4 – 5 km

The apparent variability in the Calivil Formation between borehole clusters is such that the lower value is suggested, with perhaps 1000 m a typical width for a primary channel, 700-800 m for a secondary channel, and 400-500 m for a tertiary channel. This is borne out by the mapping of aquifer textural classes from AEM data (Figure 5-45) which locally shows well-defined braided patterns from the distribution of medium- and coarse-grained sand bodies.

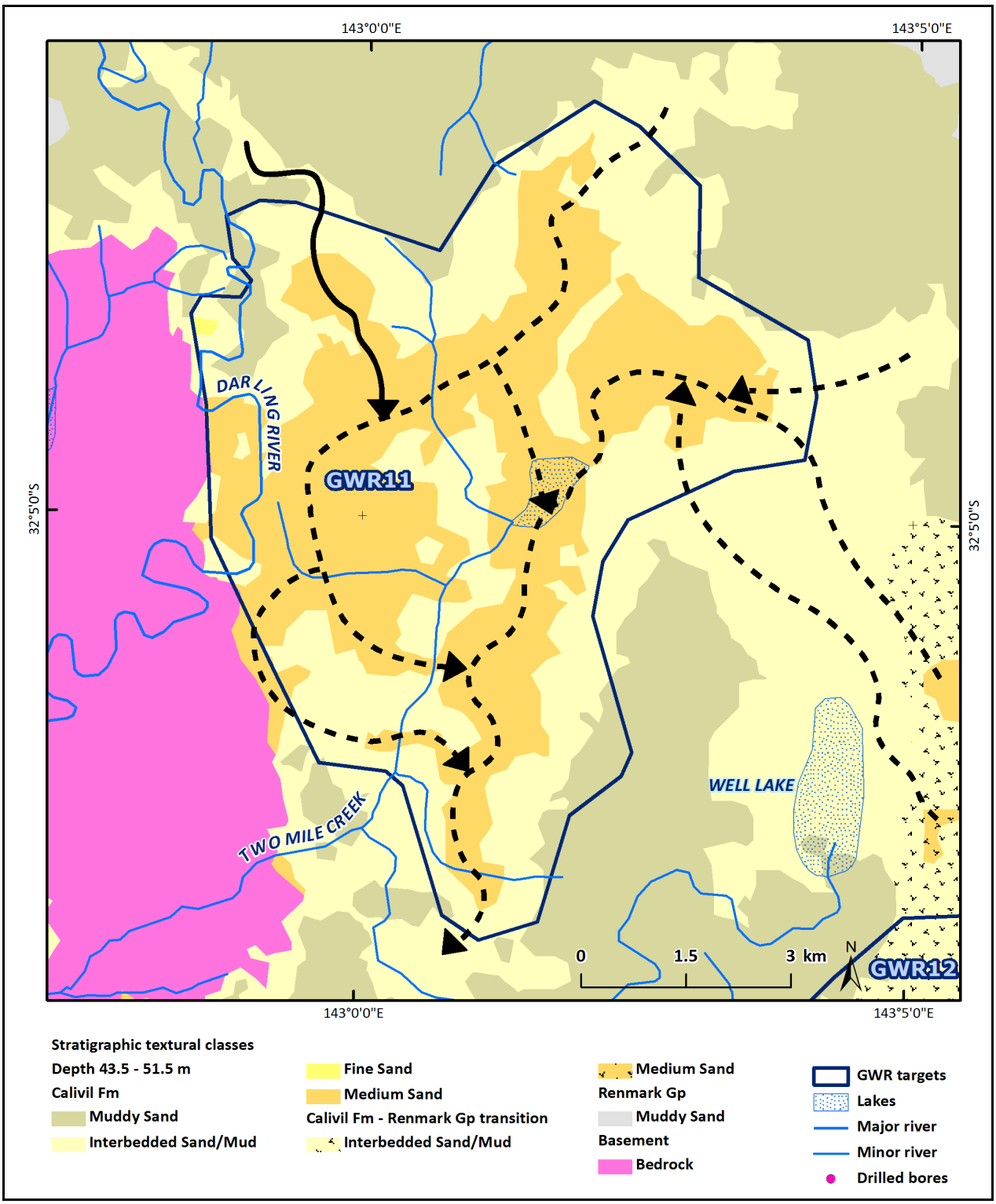

Figure 5-45. *Braided pattern defined by medium-grained sand units in the 43.5-51.5 m depth slice at the GWR11 target. Interpreted primary channels shown.*

5.2.7 Depositional Conceptual Model

The Calivil Formation is composed mostly of coarse-grained sand and gravel (some matrix supported). This is consistent with bedload dominant depositional systems (Miall 1996, Gibling 2006, Bridge & Tye 2000).

Miall (1996) classified bedload-dominant sand- and gravel-rich fluvial systems into eleven architectural models (Table 5-13, Table 5-14). Of these, seven can be excluded from applicability to the Calivil Formation because they are:

- Too coarse-grained;
- Associated with an inappropriate setting; or
- Too ephemeral.

Of the remaining four models, the sand-gravel meandering river and the high-energy sand-bed braided rivers cannot be readily differentiated from other models in drill core. However it seems unlikely that relatively slow-moving, meandering rivers would have been able to transport significant coarse-grained material over the distance that the BHMAR study area is from the possible source regions.

The remaining two models are the deep and shallow perennial braided rivers. Three lines of evidence point towards a deep channel system (Figure 5-46 and Figure 5-47):

- The 10-11 m depth of the primary channels, which sometimes locally reach 15-16 m, is most consistent with a deep river.
- The multi-storey nature of the Calivil Formation depositional units.
- Preservation of organic matter in original facies consistent with deep perennial braided stream rather than shallow ephemeral braided stream where wood is likely to be oxidised.

These data support the previous deep braided perennial river interpretation of Lawrie *et al.* (2010a, b). The indicators of both lesser and great salinity in the aquatic vegetation and xerophytic elements in the terrestrial communities, along with the carbonate and manganese in the floodplain and abandoned channel facies all indicate a strongly seasonal climate and flow regime.

Thin, localised muddy units are interpreted as overbank deposits in channels abandoned through individual channel avulsions. Thin fine-grained sand units interbedded with these are interpreted as crevasse splays. More extensive muddy units accumulated as floodplain deposits formed by channel belt avulsions.

Integrating the general deep braided stream model with the palynology data suggests that the organic matter was derived mostly from gallery woodlands. Indicators of salinity in the aquatic vegetation and seasonality in the terrestrial vegetation (Macphail, 2010), together with the secondary carbonate and dendritic manganese in the floodplain and abandoned channel facies, suggest that the flow in these rivers was probably strongly seasonal. Flow probably stagnated into the deeper parts of the channel or may even have been reduced to scattered pools during low-flow phases. This is also consistent with the local preservation of organic matter, and may explain the development of goethitic cements and early oxidation (discussed in more detail in Section 5.2.8).

Counterparts of such a system in the modern Australian landscape are rare, and none are of the right scale. The closest partial analogues would be several rivers in northern Queensland, in particular the Burdekin (Fielding *et al.,* 2009), Gilbert (Nanson *et al.,* 2005) and Mitchell Rivers.

In contrast with that reported in Phase 2 Report (Lawrie *et al.,* 2010b), there does not appear to be signs for meandering facies in the BHMAR study area. That earlier interpretation was based on thinly interbedded fine-grained sand and silt units overlying medium- to coarse-grained channel sands, interpreted as lateral accretion units of scroll bars. Re-examination of the evidence suggests that these units were too thin to be lateral accretion units and are more likely to abandoned channel fills by splay deposits.

Table 5-13. *Gravel bed river facies model (after Miall, 1996).*

	Gravel bed braided river with gravity flows	Shallow gravel bed braided river	Deep gravel bed braided river	Gravel bed wandering river	Gravel bed meandering river	Sand-gravel meandering river
Dominant processes	Gravity flows	Traction currents	Traction currents	Traction currents	Traction currents	Traction currents, suspension
Dominant architectural elements	Gravel bedforms, sandy bedforms	Gravel bedforms	Gravel bedforms, sandy bedforms, channel plugs	Gravel bedforms, downstream accretion macroforms, lateral accretion macroforms	Channels, channel plugs, lateral accretion macroforms	lateral accretion macroforms, crevasse deposits, abandoned channel
Dominant sediment types	Gravel	Gravel	Gravel	Gravel	Gravel	Gravel, sand
Minor sediment types	Sand, mud	Sand, mud	Sand, mud	Sand, mud	Sand, mud	Mud
Modern examples	Alluvial fans	Fluvio-glacial outwash deposits outwash	Mountain hinterlands	Mountain hinterlands	Mountain hinterlands	Lowlands
Comments relative to Calivil	Wrong setting, too gravelly	Wrong setting, too gravelly	Wrong setting, too gravelly	Wrong setting, too gravelly	Wrong setting, too gravelly	Difficult to determine from braided systems from core

Table 5-14. *Bedload-dominant sand bed river facies models (after Miall, 1996).*

	Shallow, perennial, sand bed braided river	Deep, perennial, sand bed braided river	High energy, sand bed braided river	Distal sheetflood sand bed river	Flashy, ephemeral sheetflood sand bed river
Dominant processes	Traction currents, suspension	Traction currents, suspension	Traction currents, deep scour, suspension	Traction currents,	Traction currents,
Dominant architectural elements	Sandy bedforms, downstream accretion macroforms	Sandy bedforms, downstream accretion macroforms	Hollows, lateral accretion macroforms	Sandy bedforms	Sandy bedforms, laminated sand
Dominant sediment types	Sand	Sand	Sand	Sand	Sand
Minor sediment types	Gravel, mud	Gravel, mud	Gravel, mud	Gravel, mud	Gravel
Modern examples	Lowlands	Lowlands	No known examples	Lowlands	Lowlands
Comments relative to Calivil	Simple macroforms, often tabular	Compound macroforms	Possible, unlikely to be recognised in core Slopes too low for high energy?	Contrary to evidence of waterlogging	Too sandy, contrary to evidence of waterlogging

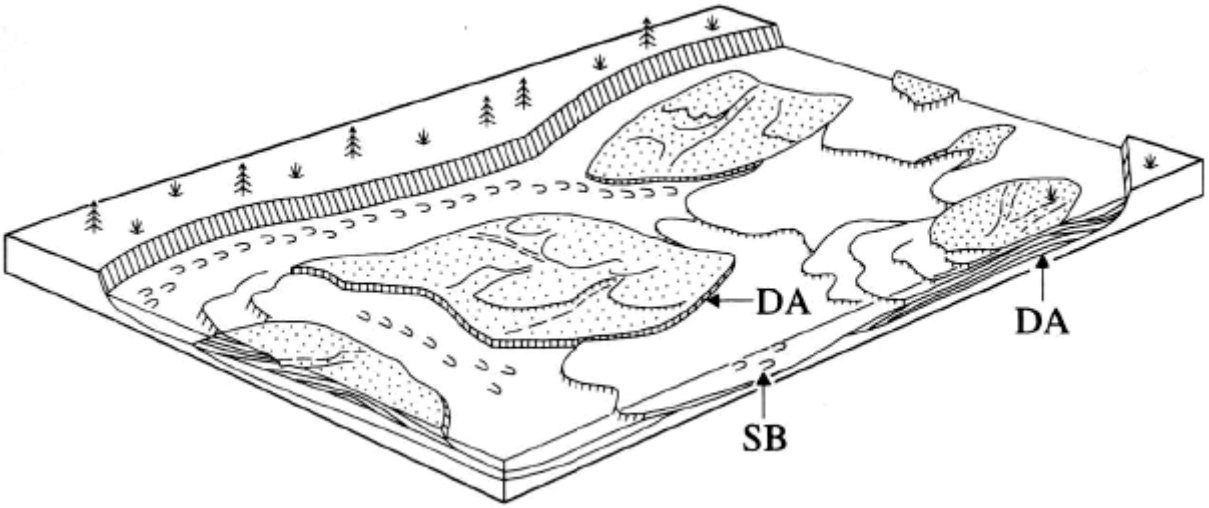

Figure 5-46. *Depositional conceptual model showing the channel architecture of a deep braided river system. From Miall (1996). SB = sandy bedforms, DA =downstream accretion macroform.*

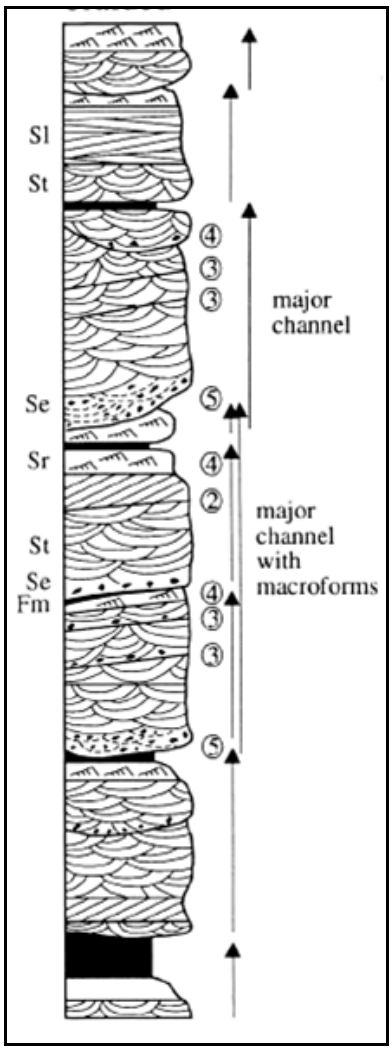

Figure 5-47. *Typical fluvial lithofacies associated with deep braided perennial rivers, from Miall (1996). Vertical arrows show direction of fining and bed thinning in cyclic successions. The numbers indicate the order of the bounding surfaces. Letters indicate facies: Sl = sand, sometimes pebbly, with low angle cross beds. St = sand, sometimes pebbly, with trough cross beds. Se = conglomeratic sands, Sr = sand, with rippled cross lamination. Fm = overbank mud.*

5.2.8 Cements

5.2.8.1 Cement types

Several types of cement are present in the Calivil Formation. In decreasing order of abundance these are goethite, clays, carbonate and silica. Goethite and goethitic or haematitic stained clays are nearly ubiquitous; other cements occur discontinuously as nodules and cemented bands.

Goethite occurs through most of the Calivil Formation, ranging from negligible grain coatings to massive cement (Figure 5-48 and Figure 5-49). It is only absent in the cleanest of sands and gravels, and in reduced zones.

Clays, both iron-stained and non-iron-stained, occur as clay skins on grains and as patchily distributed infill. XRD and HyLogger data indicate that both smectites and kaolinite cements are present. The ways these clays are distributed, as skins, and as patchy infill post-dating earlier cements, clearly indicates that they are not matrix.

Pedogenic carbonate is present in the muddy floodplain facies, typically forming rhizomorphs, and is associated with manganese dendrites. Primary carbonate cement is also present as bladed dolomite cement in reduced zones (Figure 5-50). This indication has not been confirmed by XRD.

Silica cements occur in nodules (Figure 5-51 and Figure 5-52), variably iron-stained. Three types of silica cement are observed, isopachous microquartz, isopachous opal, and cavity filling zebra chalcedony. These cements are consistent with precipitation in the phreatic zone, probably under evaporites conditions. Some rare examples of zebra chalcedony grains are reworked, indicating that the groundwater cementation was occurring at quite shallow depths and very rapidly.

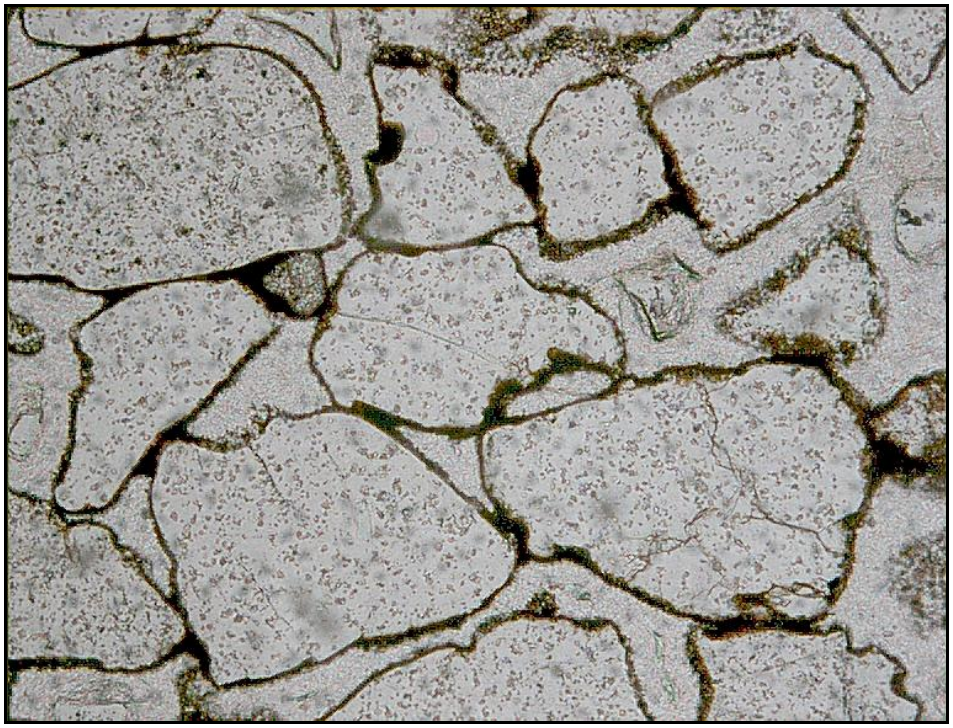

Figure 5-48. *Micrograph of medium to coarse sand, BMHAR21, 47.6 m, field of view 1.0 mm, plane light. Dark meniscus goethite forms very thin skins on grains and bridges between sand grains, indicating cementation in the vadose zone.*



Figure 5-49. *Micrograph of goethitic clay and goethitic meniscus cements on quartz grains in medium sandstone, (BHMAR83-2, 60.85 m, field of view 2.5 m, plane light. The meniscus cements indicate that the earliest phase of cementation was on the vadose zone.*

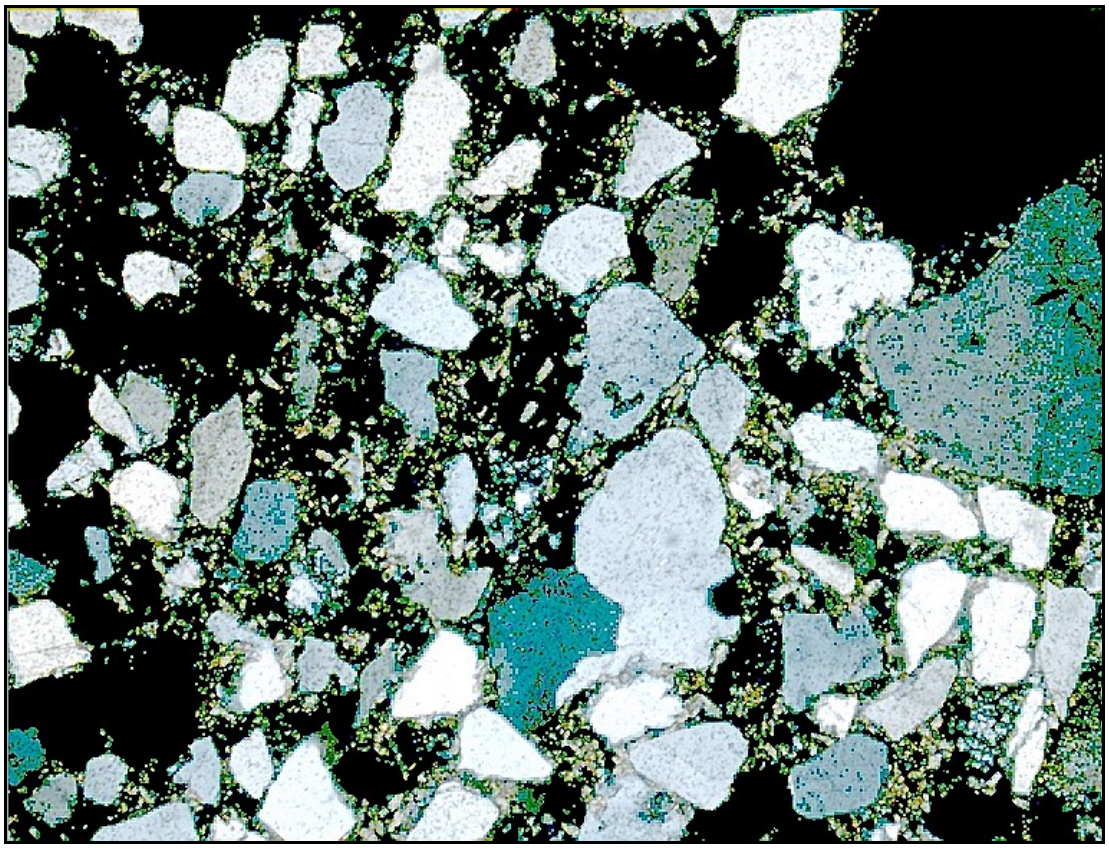

Figure 5-50. *Micrograph of carbonate cemented fine to medium sandstone, BHMAR 65, 50.74 m, field of view 2.5 mm. Cement is interpreted as phreatic in origin.*

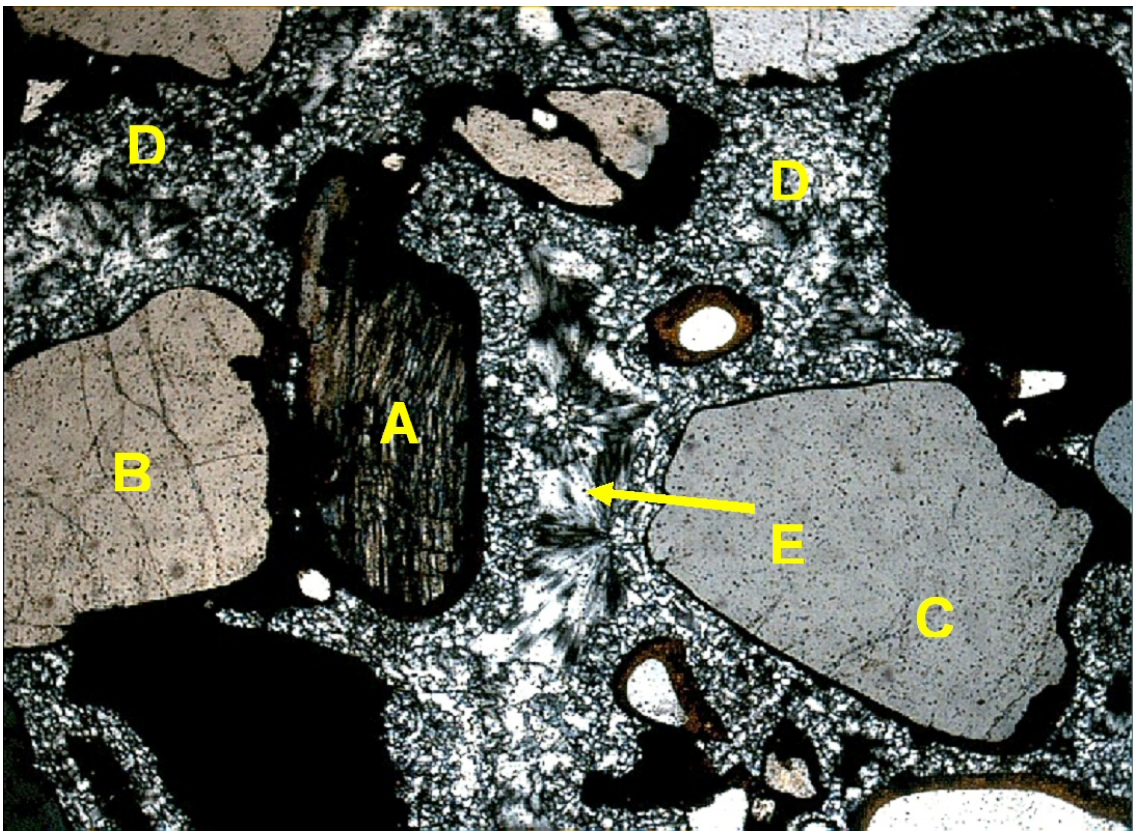

Figure 5-51. *Micrograph of microquartz and chalcedony-cement in same medium sandstone as previous Figure 5-49 (BHMAR83-2, 60.85 m), field of view 2.5 m, crossed polars. A = metamorphic quartz grain, B = vein quartz grain, C= plutonic quartz grain, D = microquartz, probably isopachous on grains, E = cavity-filling chalcedony. Both cements are phreatic and postdate early meniscus goethitic cements.*

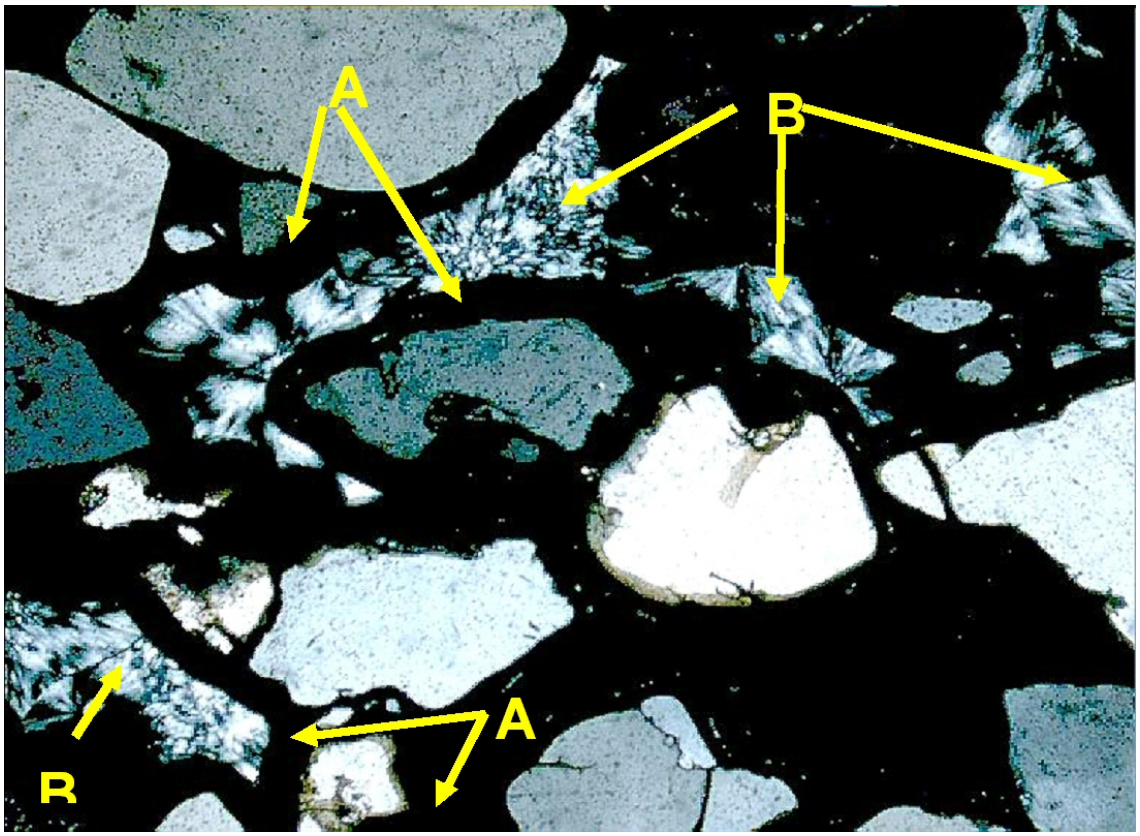

Figure 5-52. *Micrograph of opal and chalcedony-cemented medium sandstone, BHMAR83-2, 59.84 m, field of view 2.5 m, crossed polars. A = opal (isotropic) isopachous on quartz grains, B = chalcedony cavity fill, both indicating cementation in the phreatic zone.*

5.2.8.2 Cement stratigraphy

A distinctive cement stratigraphy is evident in thin sections of the cemented zones (Table 5-15). The earliest cement in the Calivil Formation is mostly meniscus goethite, goethitic clay and haematitic clay (BHMAR21 at 47.1 and 47.6 m, BHMAR64 at 24.5 m, and BHMAR65 at 40.3 m). This indicates precipitation occurred in an oxidised vadose zone. The presence of cements in all but one sample (7 out of 8) suggests that at the time of Calivil Formation deposition, most of the river bed periodically dried out, forming the coatings in the vadose zone. The goethitic concretion sample (BHMAR33 at 56.45 m) appears to be an extreme example of this type of cement. This cementation is very early, as the BHMAR21 example occurs within a larger zone with reduced features. Second generation patchy clays are locally present interstitially (e.g. BHMAR21 at 47.1 and 47.6 m, BHMAR64 at 24.5 m). Because of their patchy nature these too are also interpreted to be probably vadose zone features.

Of the three types of silica cements observed (isopachous microquartz, isopachous opal, and cavity filling zebra chalcedony), the earliest cements are either isopachous microquartz or isopachous opal, with a later cavity filling zebra chalcedony. All of which are all associated with phreatic deposition subsequent to the formation of goethitic cements in the vadose zone.

Table 5-15. *Cement stratigraphy.*

SAMPLE	CEMENT GENERATIONS			
	1ST	2ND	3RD	COMMENTS
BHMAR 21 47.1 m	Meniscus goethite	Patchy clays		Oxidised cemented zone in reduced aquifer
BHMAR 21 47.6 m	Meniscus haematitic clay	Patchy clays		Oxidised cemented zone in reduced aquifer
BHMAR 33 56.45 m	Massive goethitic clay			Cemented zone in oxidised aquifer
BHMAR 64 24.5 m	Meniscus goethite			Cemented zone in oxidised aquifer
BHMAR 64 40.3 m	Meniscus goethite	Patchy clays		Cemented zone in oxidised aquifer
BHMAR 65 50.74 m	Bladed dolomite			Cemented zone in reduced aquifer
BHMAR 83-2 59.84 m	Meniscus goethite	Isopachous opal	Cavity-filling zebra chalcedony	Near base unit
BHMAR 83-2 60.85 m	Meniscus goethite	Microcrystalline quartz	Cavity-filling zebra chalcedony	Very base of unit

5.2.9 Diagenetic Conceptual Model

The complex diagenesis of the Calivil Formation has led to a complex pattern of reductomorphic zones. These are illustrated in Figure 5-53. The diagenetic environment of the Calivil Formation consists of two contrasting styles. The first is a highly oxidised vadose zone depositing the goethite and haematite-rich meniscus cements. In some zones of the Calivil Formation this remains the dominant diagenetic environment into the phreatic zone, resulting in extensive goethite coatings and the formation of haematite and goethite nodules. This style is the most widespread. The second diagenetic style is where sands with initial vadose zone goethitic or haematitic cements have been overprinted by silica cements deposited in the phreatic zone. These appear to be associated with preserved organic matter and reduced iron minerals. This is interpreted as indicating deposition in long-lasting pools with stratified water columns conducive to the preservation of organic matter. This style is a less common. A minor diagenetic environment is represented by the muddy units with carbonate root casts and manganese dendrites. These are interpreted as forming in soil environments with fluctuating watertables and moderate evaporative concentration in the vadose zone.

This model predicts that cemented zones are likely to be discontinuous and generally strata-bound, although not strictly stratiform. An analogue for this diagenetic environment would be the Gilbert River, where there is rapid cementation of river sediments by precipitated iron and carbonate minerals (Nanson *et al.,* 2005). These are illustrated by Figure 5-54 and Figure 5-55. In this conceptual model the deep pools with their woody debris would develop stratified water columns during periods of low water. The diagenetic conceptual model is illustrated in Figure 5-56, Figure 5-57, Figure 5-58, and Figure 5-59.

The Interim Phase 2 Report (Lawrie *et al*., 2010b) concluded that since the original sediments contained organic matter the pore waters were originally reduced, along with the hosting aquifers which were subsequently partly oxidised. However the presence of meniscus goethitic and haematitic cements in thin sections indicates that reduced pore waters were not ubiquitous.

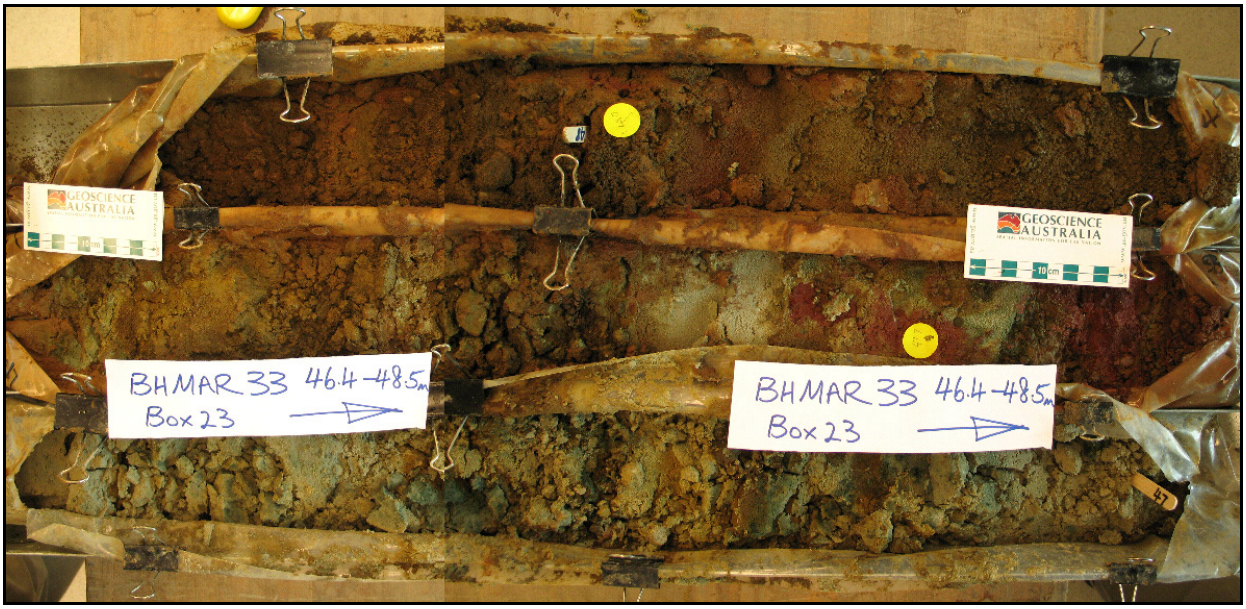

Figure 5-53. *Composite image of sonic core showing lower contact between reduced (left) and oxidised (right) lithologies in Calivil Formation in BHMAR33-1. Strong contrasting colour mottling is visible throughout. Arrow points downhole.*



Figure 5-54. *Google Earth images of semi-permanent pool along the Gilbert River, north Queensland. Note the active sand-channel belt width is approximately 600 m.*



Figure 5-55. *Google Earth images of semi-permanent pool along the Mitchell River. Note the active sand-channel belt width is approximately 1.8 km.*

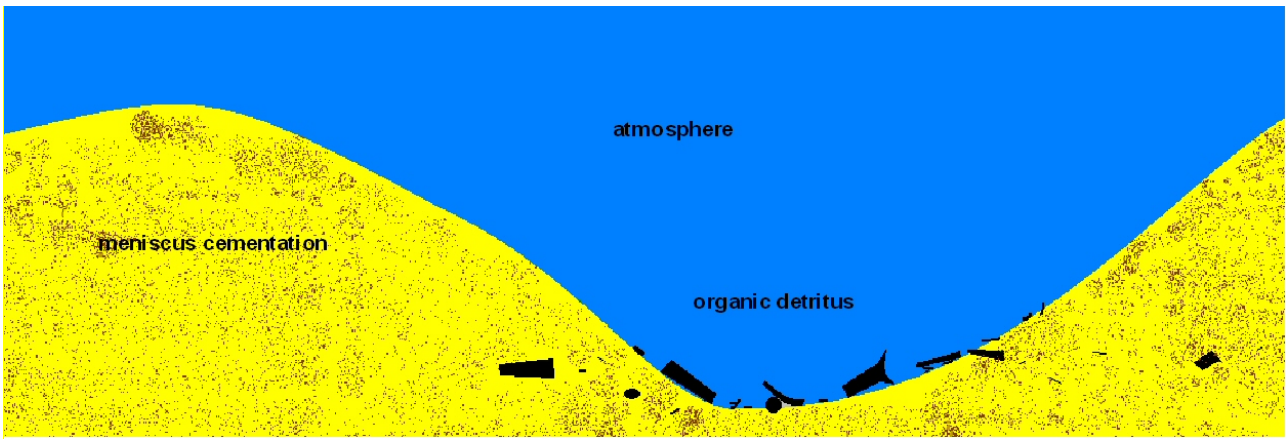

Figure 5-56. *Conceptual model showing evolution of river bed diagenetic environments, specifically irregularities in dry river bed, with organic detritus in lower parts of profile. Meniscus cementation by iron-rich phases in deep vadose zone.*

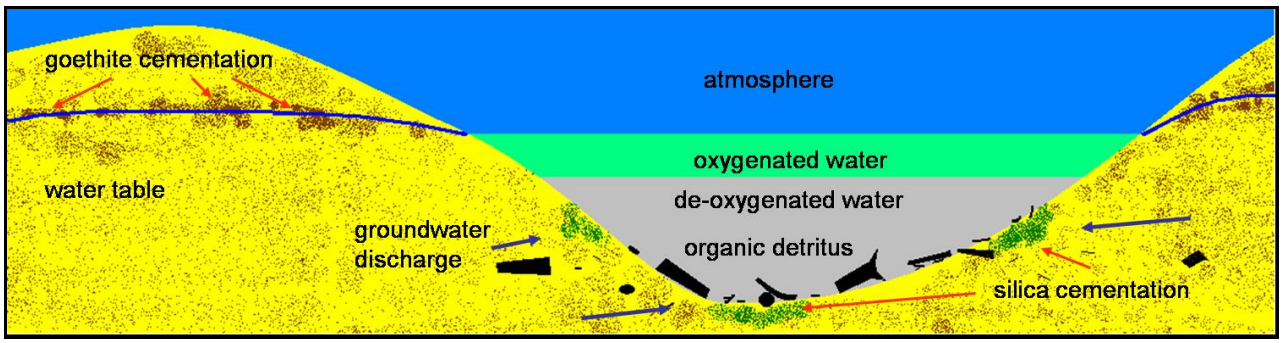

Figure 5-57. *Conceptual model showing evolution of river bed diagenetic environments, specifically partial flooding of depressions leading to deep pools in dry river bed. This leads to formation of stratified water column with oxygenated water above deoxygenated water. Discharging silica-rich groundwaters form patchy silica cements near the sediment-water interface. Conversely in the capillary fringe of the water table beneath the exposed parts goethite (and haematite) cementation is occurring in oxygenated environments.*

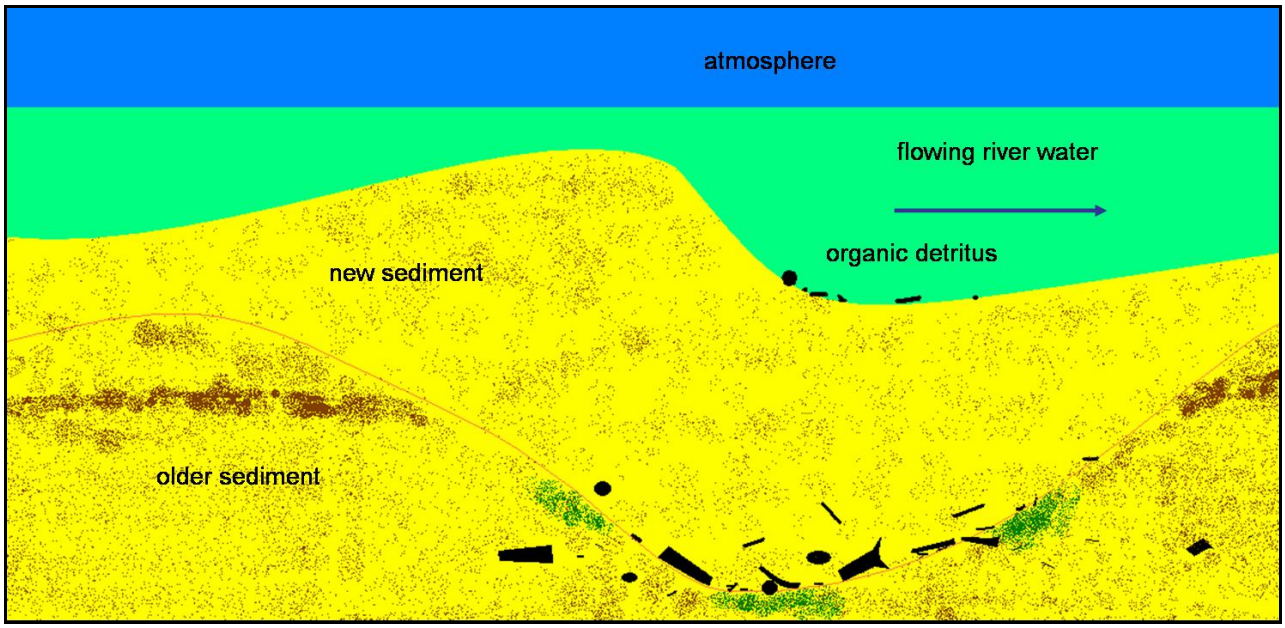

Figure 5-58. *Conceptual model showing evolution of river bed diagenetic environments, specifically river flooding leading to burial of former pools and bars beneath a new layer of sediment.*

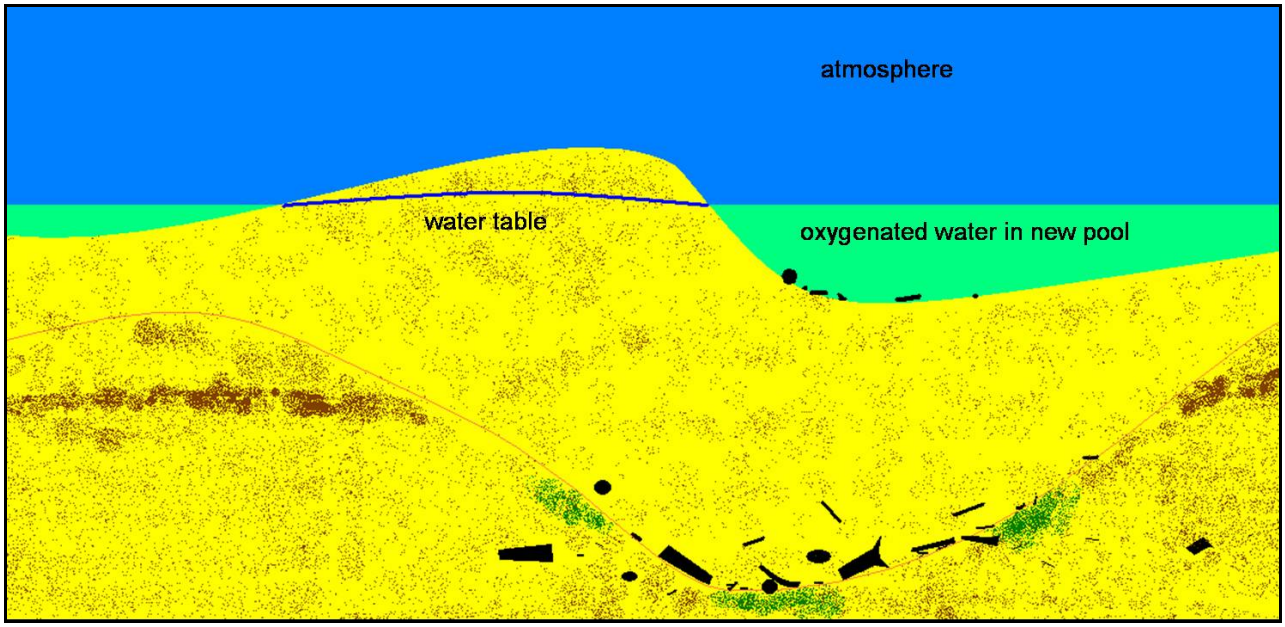

Figure 5-59. *Conceptual model showing evolution of river bed diagenetic environments, specifically falling water levels resulting in the formation of new deep pools and exposed bars. In this illustration it is still too early for cementation to have occurred or for a stratified water column to be established.*

5.2.10 Outcrop Analogues

Braided river systems in the geological record have been extensively studied (see Miall, 1996, and references therein for examples). It is not the intention to review the literature here however one example of an ancient, but well exposed analogue to the Calivil Formation is worthy of some discussion, This is the Salt Wash Member of the Morrison Formation found over much of the Colorado Plateau of the United States.

The Salt Wash Member is an extensively studied (e.g. Peterson, 1980; Robinson & McCabe, 1997, 1998; Kjemarud *et al.,* 2008) Jurassic braided stream deposit. Like the Calivil Formation, the Salt Wash Member appears to have been deposited in a savannah climate (Parrish *et al.,* 2004). Major similarities include channel scale and architecture and the presence of variable reductomorphic features. Major differences include the much greater thickness of the Salt Wash Member, lower textural maturity with abundant volcanic components, its stratigraphic context as part of a very thick basal succession many kilometres deep, and a deep burial history of several kilometres

Several photos (Figure 5-60, Figure 5-61 and Figure 5-62) of the Salt Wash Member are included to illustrate the type of geometries likely to occur within the Calivil Formation, which are difficult to visualise due to the lack of exposure.



Figure 5-60. Bedding plane exposure of trough cross beds in Salt Wash Member overlooking the Dirty Devil River near Hanksville, Utah, looking down flow. Trend lines of cross bed foresets shown. Most of the well bedded units in the Calivil Formation are almost certainly trough cross beds, although this is difficult to demonstrate from sonic core.



Figure 5-61. *Parallel bedded red siltstones, shales, and fine-grained sandstones forming overbank facies of Salt Wash Member. The extent of this outcrop, about 150 metres, and its thickness, ~4-5 m, suggests that it is probably an abandoned channel fill. Alternatively it could be a small floodplain unit between two channels. The fine-grained units in the Calivil Formation have similar lithology and extent.*

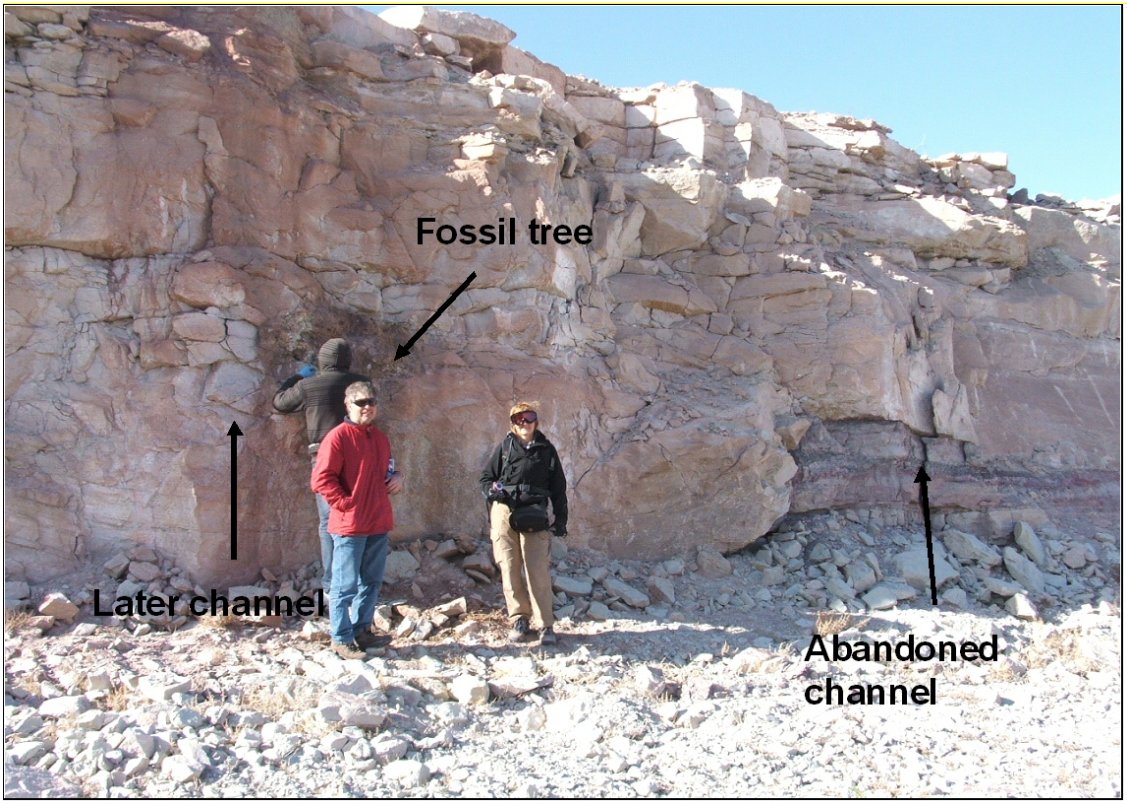

Figure 5-62. *Abandoned shale-filled channel truncated by later channel containing fossil log. The Calivil Formation has similar fossil wood material. Cut-outs such as this would allow significant cross stratal groundwater flow.*

5.2.11 Modern Analogues

Modern braided river systems have also been extensively studied, and a detailed review of their facies is beyond the scope of this report. Reference has been made to the review of Miall (1996) which developed a number of different braided channel models. A number of studies of modern braided systems which proved useful in the conceptualisation of the fluvial architecture and depositional environment of the Calivil Formation will be referred to in passing.

Braided streams are comparatively rare in modern Australian river morphologies, the best examples are perhaps the Burdekin and Gilbert Rivers mentioned previously. Although possibly more gravelly than the Calivil Formation systems, composed of less mature sediments, and with a bedrock substrate for much of its length (Alexander *et al.,* 1999; Fielding *et al.,* 2009), the Burdekin River may well illustrate the type of coarse-grained sand to gravel bed river responsible for the deposition of the Calivil Formation. The Gilbert River (Nanson *et al.,* 2005) is an example of a seasonal, partly braided fluvial system with active precipitation of cements in the sediments, including iron and carbonate. The braided Gilbert and nearby Mitchell Rivers form large, low angle fan deposits marginal to the Gulf of Carpentaria, which may also be analogous to the setting of the Calivil Formation in the BHMAR study area.

Almost all the standard reference studies on braided facies have been on non-Australian rivers. The largest and perhaps best studied examples are the conjoined massive braided deposits of the Ganges and Brahmaputra River systems (e.g. Coleman, 1968; Shukla *et al.,* 2001; Singh *et al.,* 2007). This enormous system provides numerous examples of the hierarchical nature of braided channels including clustering of interpreted channel depths proportional to the scale of depositional channels (Neton *et al.,* 1994). Considerable variability in the depositional architecture is associated with such features, nicely illustrated by the braided rivers of Nebraska (Lynds & Hajek 2006; Skelly *et al.,* 2003; Smith, 1971) and of the Canterbury Plains of New Zealand (Leckie, 2003; Browne & Niash, 2003). The strong short-range variability found in ancient systems, such as the Salt Wash Member (reviewed above) is similar to that found in these Quaternary fluvial systems and similar patterns can be inferred for the Calivil Formation.

5.2.12 Hydrogeological Implications

Our conceptual model for the Calivil Formation predicts that the formation consists of large tracts of stacked fluvial channels dominated by medium- to coarse-grained sand interconnected in three dimensions. Between the sand bodies are smaller tracts of muddier lithologies representing former floodplains. The sand bodies formed by the stacked channels are not themselves homogeneous, but include gravel lenses representing gravel bars; lenses of fine-grained sand, representing minor channels; and muddy infill units of temporarily abandoned channels. On a regional scale this results in a large aquifer with the potential for significant connectivity. The smaller scale variability (see Anderson *et al.,* 1999; Neton *et al.,* 1994) such as presence or absence of muddy channel fill and patchy cementation, which may impede flow, and gravelly units, which may increase flow, however results in significant heterogeneity at this scale. This has implications for connectivity, transmissivity and storability.

5.3 BLANCHETOWN CLAY AND CHOWILLA SAND

This study has mapped the near-ubiquitous presence of relatively thin (5-10 m) Blanchetown Clay deposits throughout the project area. The Blanchetown Clay was deposited in mega Lake Bungunnia (Firman, 1965; Bowler, 1980; Stephenson, 1986), and in the study area comprises hard brown to light grey massive to fine bedded sandy clay, with local fine calcareous and manganese cement. Sand content varies, and some thin beds of sand are included in the interpreted intersections. The aquitard properties of the Blanchetown Clay are demonstrated by hydrograph responses in overlying and underlying aquifers, by wetting profiles observed in drill core, moisture data obtained from cores, NMR and gamma logging, laboratory permeameter measurements on cores, and hydrogeochemical data. The study has also confirmed that the aquitard forms a major barrier to recharge and discharge (Table 5-16).

Prior to this study, it was generally agreed that the maximum level of lake filling was 60-65 m AHD, with the lake boundaries thought to extend as far north as Lake Pamamaroo (McLaren *et al*., 2009). However, an integrated mapping approach has revealed considerable variations in the Blanchetown Clay extent, thickness and elevation (Figure 5-63). A complex sub-surface distribution is observed, with variations in the thickness and elevation of the top of the Blanchetown Clay (20-80 m AHD) attributed in large part to tectonic activity during and post-deposition.

In the majority of the project area, the Blanchetown Clay overlies Calivil Formation fluvial sediments with little or no time gap. Only in the south of the area does it overlie coastal barrier sands (Loxton-Parilla Sands) with an appreciable time gap, during which a weathering profile developed. The Calivil Formation fluvial sediments generally fine upwards, and near the top comprise muddy overbank and channel plug deposits, as well as channel and crevasse splay sands. Therefore, in places it is difficult or impossible to place an unequivocal boundary between where clay of the Blanchetown Clay overlies clay of the Calivil Formation. In most instances, conductivity mapping cannot discriminate these units, with AEM instead mapping a combined fine-grained Calivil Formation -Blanchetown Clay aquitard, rather than individual stratigraphic units. The Blanchetown Clay is overlain by Willotia beds, Menindee Formation or Coonambidgal Formation sediments. In most cases, the latter comprise medium to coarse sands at the base, with one or two fining upward cycles. Therefore, the top of the Blanchetown Clay aquitard can be mapped in conductivity data with a greater degree of certainty. Mapping the aquitard bounding surfaces is particularly important for studies of inter-aquifer leakage, recharge and for MAR assessment.

Numerous ‘holes’ have been mapped in the Blanchetown Clay conductivity anomaly however almost all drillholes intersect a mud-rich unit. There are several possible scenarios for the origin of actual physical absence of the Blanchetown Clay, including non-deposition, facies change, faulting and erosion. Where the Blanchetown Clay is absent, local recharge has resulted in previously unrecognised resources of fresh to slightly brackish water in the underlying semi-confined aquifer. Where present, it could form an effective cap for MAR schemes.

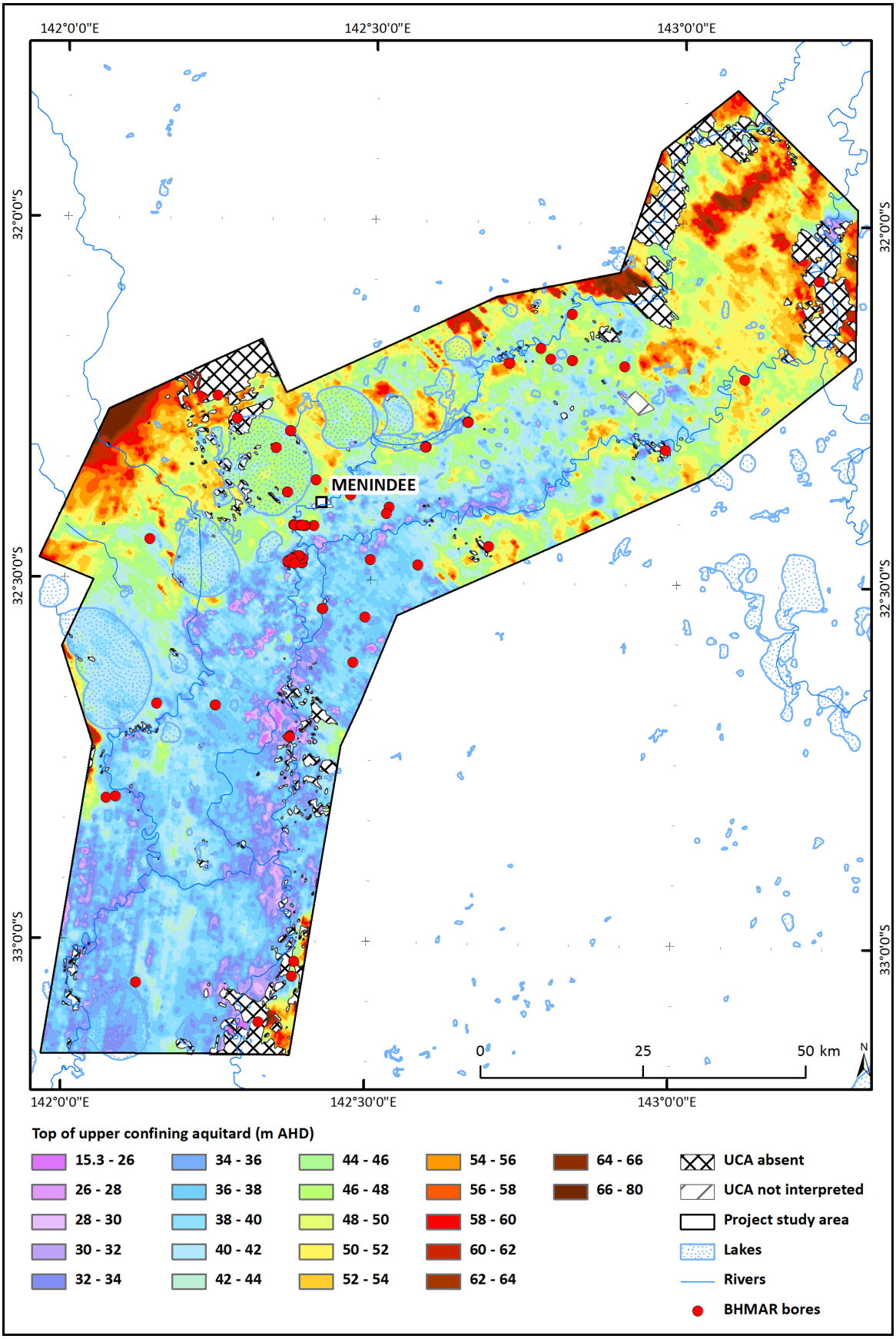

Figure 5-63. *Elevation of top of the upper confining aquitard (predominantly Blanchetown Clay). Significant elevation differences (~50 m) are apparent, with greater depths shown in purple and shallower depths in brown.*

Widespread deposition of fine-grained lacustrine sediment in the Mallee Region of the Murray Basin followed damming of the ancestral Murray River in the late stages of marine retreat from the Murray Basin in the late Pliocene. Tate (1885) was the first to identify the existence of a Quaternary palaeolake in the Murray basin, which was subsequently named Lake Nawait (Fenner, 1934; Browne, 1945). Firman (1965) renamed this feature Lake Bungunnia, and defined the Blanchetown Clay as a lacustrine unit of clay and sand deposited in this palaeolake. The lake had an irregular outline and complex stratigraphy as it filled a number of linked sub-basins, formed by tectonic deformation of the underlying Loxton-Parilla Sands. Firman examined exposures along the Murray River in South Australia, and further detailed work was carried out by Gill (1973) in the Lake Victoria-Chowilla area of south-western NSW and eastern South Australia adjacent to the Murray. Important reviews of the Blanchetown Clay and Lake Bungunnia were published by Bowler (1980), Stephenson (1986) and Brown & Stephenson (1991). More recently, Bowler *et al*. (2006) and McLaren and her associates (McLaren *et al*., 2009; McLaren & Wallace, 2010; McLaren *et al*., 2011; McLaren *et al*., 2012) have studied exposures of the Blanchetown Clay in detail. The term Chowilla Sand has been used for sand beds deposited in Lake Bungunnia, especially at the base of the section, and has been interpreted as reworked Loxton-Parilla Sands. The Geoscience Australia Stratigraphic Index shows that the Chowilla Sand has full Formation status, first used by Firman (1969, 1973) and defined by Brown & Stephenson (1991), but Gill (1973) and McLaren *et al*. (2009) have considered it a member of the Blanchetown Clay.

Most authors concur that the palaeolake resulted from tectonic uplift of the Pinnaroo Block (also termed the Padthaway High or Arch), which defeated the palaeo Murray River, although there is disagreement as to the exact course of the river. However, other mechanisms for damming have also been proposed, summarised by McLaren *et al*. (2009). It is also generally agreed that the maximum level of lake filling was to 60-65 m AHD, resulting in a lake area of around 50 000 square kilometres. Figure 5-64 shows the evolution of reconstructions of the outline and extent of Lake Bungunnia. Bowler (1980) was the first to depict general boundaries for Lake Bungunnia, extending northward to about 25 km south of Menindee. Stephenson (1986) proposed that the 60 m topographic contour approximated the extent of the lake, taking the northern extent to Menindee. Brown & Stephenson (1991) subsequently interpreted the Blanchetown Clay to comprise a core lacustrine component, which extended north to Menindee, and a peripheral fluvial component, extending further up the Darling valley to about the northeast extremity of the current project area. More recently, McLaren *et al.* (2009) extended the proposed extent of Lake Bungunnia to about Lake Pamamaroo, based on interpretation of the Shuttle Radar Topographic Mission (SRTM) DEM data.

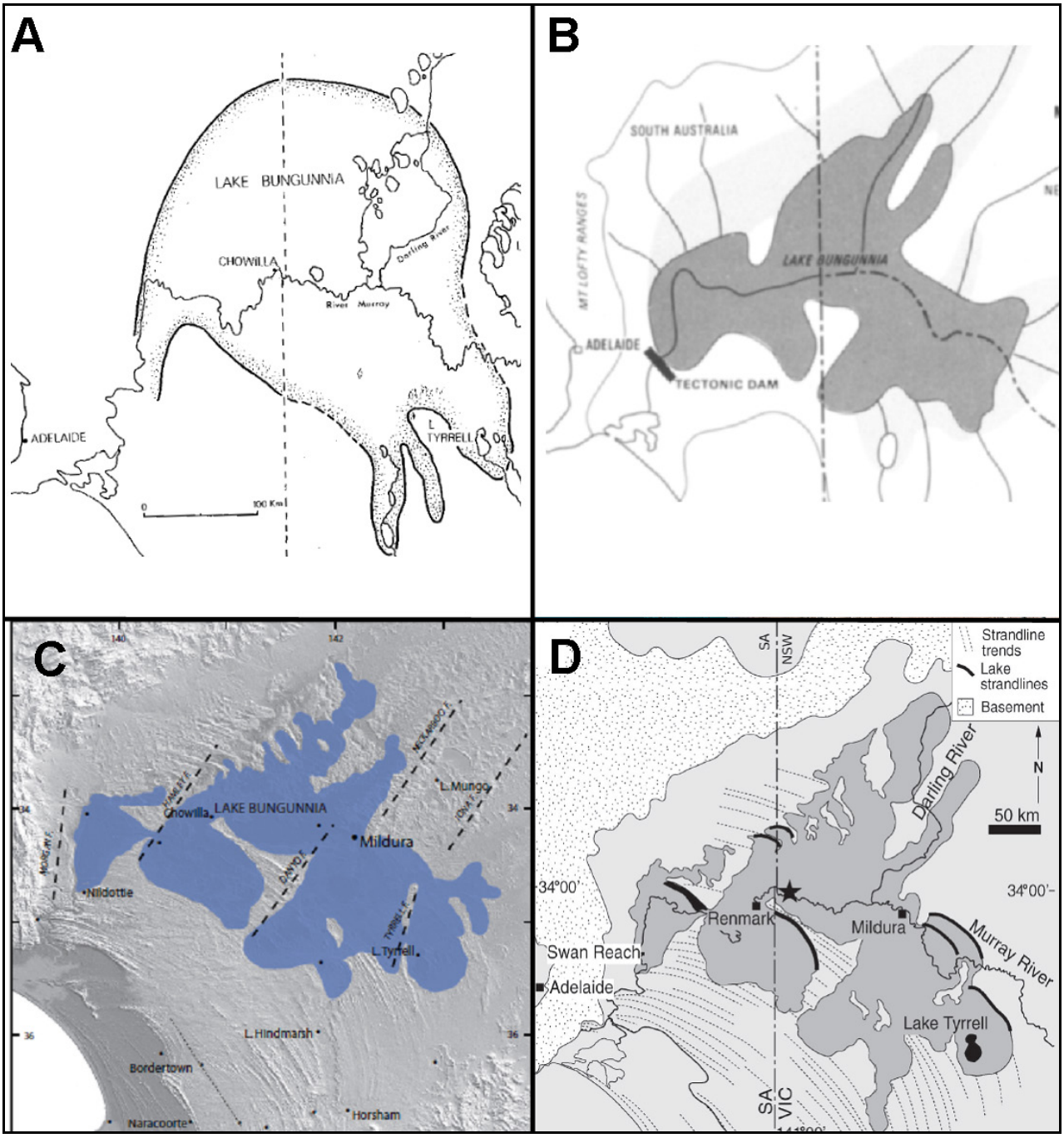

Figure 5-64. *Evolution through time of reconstructions of the outline and dimensions of Lake Bungunnia. (A: Bowler,1980; B: Stephenson, 1986; C: Bowler et al., 2006; D: McLaren et al., 2009).*

5.3.1 Blanchetown Clay in the Menindee Area

The consensus of published opinion is that the Blanchetown Clay should be present in the Menindee area. However, this is mostly based on predictive models, not hard data. Tedford (1967) reported more than 5.5 m of grey sandy silt containing unionid shells and a few thin lenses of ostracod coquina exposed in the dry Pamamaroo-Menindee canal just north of the Menindee lunette. Tedford interpreted these as (?Plio-Pleistocene) floodplain fluviatile and lacustrine sediments of the Darling River and did not recognise any lake Bungunnia sediments in the Menindee region. Though ostracod assemblages have been reported previously from some Blanchetown Clay sequences, unionids have never been reported. The degree of pedogenesis typical of the upper Blanchetown Clay is incompatible with such preservation.

Gill (1973) cites Tedford's work, but also mentions gypsiferous greenish grey clay in the Menindee Lakes area that he thought should be referred to the Blanchetown Clay. Stephenson (1986) states that lacustrine Blanchetown Clay is thought to be exposed at Lakes Tandou and Cawndilla, and Brown & Stephenson (1991) elaborate that the Lake Cawndilla occurrence is at the outlet channel. Chen (1992), who studied the geomorphology and stratigraphy of Lakes Menindee and Cawndilla for the National Parks and Wildlife Service, gave details of the Cawndilla channel exposure. There are also unpublished interpretations of Blanchetown Clay in the Menindee area made prior to the initiation of this project, including notes of an engineering geologist with NSW Department of Main Roads, who worked on the foundations for the bridges across the Darling River and Talyawalka Creek at Wilcannia (Ian Wilson, pers. comm. 2009). These notes were made available to this project, as were interpreted stratigraphy of water bores between Wilcannia and Menindee (Mike Williams, NSW Department of Water Resources, electronic communication, 2010). Additionally, O'Neil & Beckham (1995) carried out vertical electrical soundings across Lake Menindee, and included an interpreted layer of "Shepparton Formation/Blanchetown Clay" in their interpretation. However, there was no clear evidence that the interpreted occurrences of these studies were of actual Blanchetown Clay. The most northerly described exposure of Blanchetown Clay, other than from this project, appears to be in the banks of the Darling Anabranch where it is crossed by the Barrier Highway, 50 km southwest of the study area (McLaren & Wallace, 2010; McLaren *et al*., 2011).

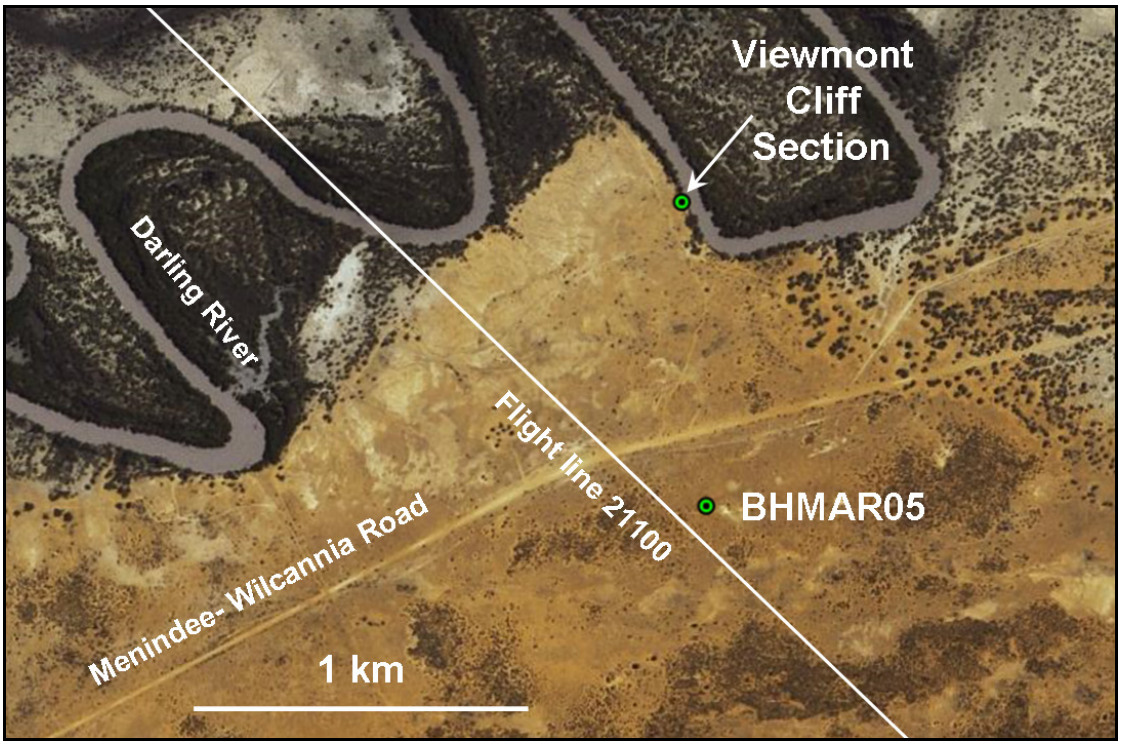

Figure 5-65. *Location of Viewmont riverbank cliff section (Figure 5-66) and BHMAR05-1 and the flight line 21100 (Figure 5-67).*

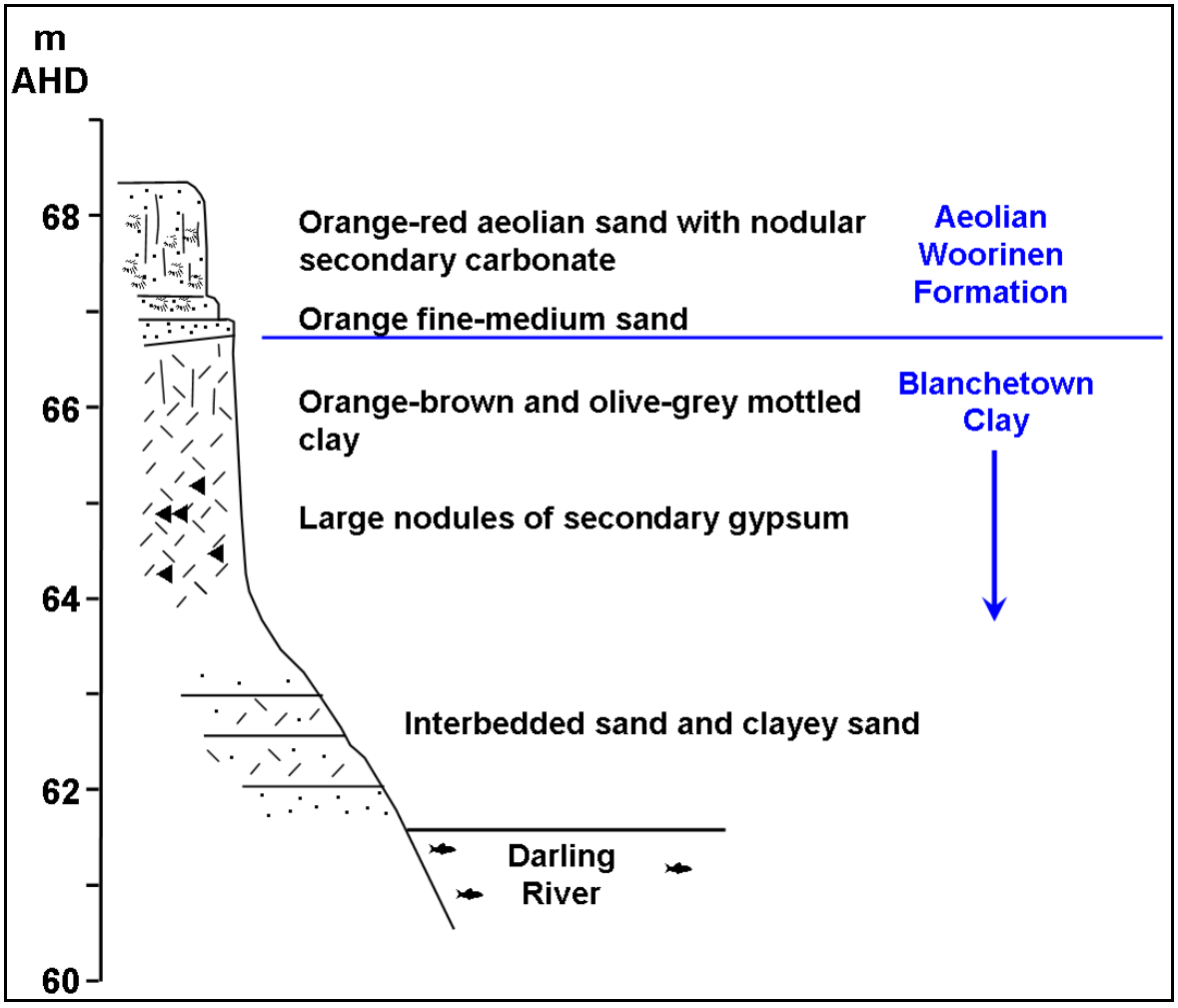

Figure 5-66. *Viewmont riverbank cliff section showing topographically high Blanchetown Clay under thin aeolian sands.*

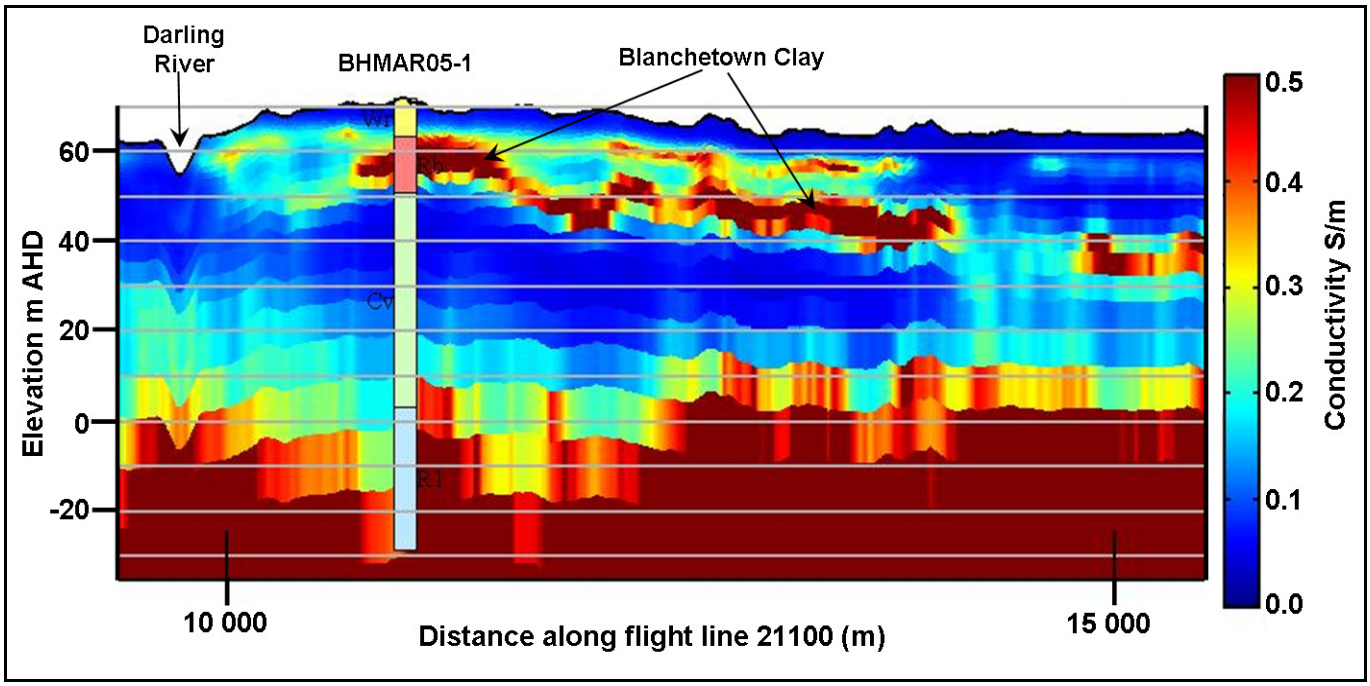

Figure 5-67. *AEM flight line 21100 showing the Blanchetown Clay as a strongly conductive layer which rises from the east and intersects BHMAR05-1 at shallow depth and is evident in river cliffs to the north.*

We have interpreted the Blanchetown Clay to be present across almost all the study area, on the basis of drillhole intersections and a near-continuous conductivity anomaly in the general range of elevations at which the Blanchetown Clay is known to occur further south. However, there is only one outcrop of the unit that we recognise (a Darling River bank cliff exposure on Viewmont Station; Figure 5-65 and Figure 5-66), as it is almost entirely buried beneath younger alluvial and lacustrine sediments. This contrasts with the situation further south, and implies that land surface elevation cannot be used to predict the shoreline of Lake Bungunnia or the distribution of the Blanchetown Clay. The presence of overlying sediments means that the Blanchetown Clay may be present beneath areas with surface elevation well in excess of 60-65 m. We have identified Chowilla Sand in one small area, on the Menindee Common where numerous drillholes intersected a thin (<3 m thick) unit of sand or muddy sand immediately below the Blanchetown Clay. Its identification as part of the Lake Bungunnia sequence and not as part of the underlying fluvial Calivil Formation is not confirmed.

Identification of the Blanchetown Clay in drillholes can also be problematic, as in some holes there are several clay-rich bands which could potentially be identified as Blanchetown Clay. This difficulty is exacerbated in rotary-mud holes, where we have found that sampling the mud cycling system with a strainer tended to indicate more mud in the cuttings than is actually present in situ. The interpretation of AEM conductivity sections through drillhole locations has helped determine which, of multiple possible clay bands, can be correctly interpreted as Blanchetown Clay. This is possible because the Blanchetown Clay forms a relative conductor which can be traced over wide areas, in contrast to clay-rich beds in a fluvial sequence, which have limited extent and are generally not visible in the AEM data.

Identification of potential outcrops of Blanchetown Clay is also assisted by interpretation of AEM sections. The river bank outcrop on the south bank of the Darling River on Viewmont station, near drill site BHMAR05 was originally thought to be too high in elevation to be Blanchetown Clay. However, AEM sections through the outcrop and drillhole BHMAR05-1 (Figure 5-67) show that the Blanchetown Clay is warped up to the north in this location, and the exposure is most probably Blanchetown Clay (see below). This contrasts with exposures on the west bank of Redbank Creek(Figure 5-91, Figure 5-92, Figure 5-93 and Figure 5-94) and the Darling Anabranch (Figure 5-97, Figure 5-98 and Figure 5-99) and in the Lake Cawndilla outlet channel (Figure 5-96), where the AEM sections (Figure 5-68 and Figure 5-69) and drillholes BHMAR1A-1 and 74-1 show that the exposed clays are above the level of the Blanchetown Clay, which remains buried at these sites (Figure 5-95). These exposures are recognised to be part of the Willotia beds (see Section 5.4.1.3).

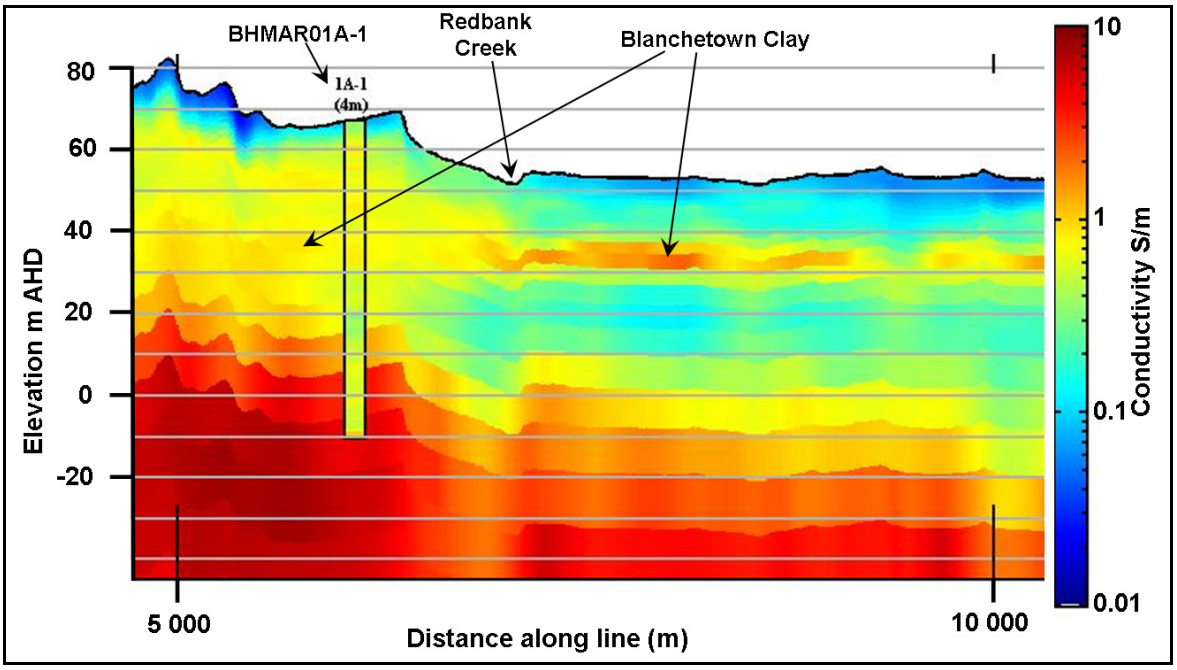

Figure 5-68. *AEM cross section showing the Blanchetown Clay conductor extending horizontally westwards from below the Redbank Creek scroll plain to BHMAR01A-1 and passing under the Redbank Cliff Section (Figure 5-91).*

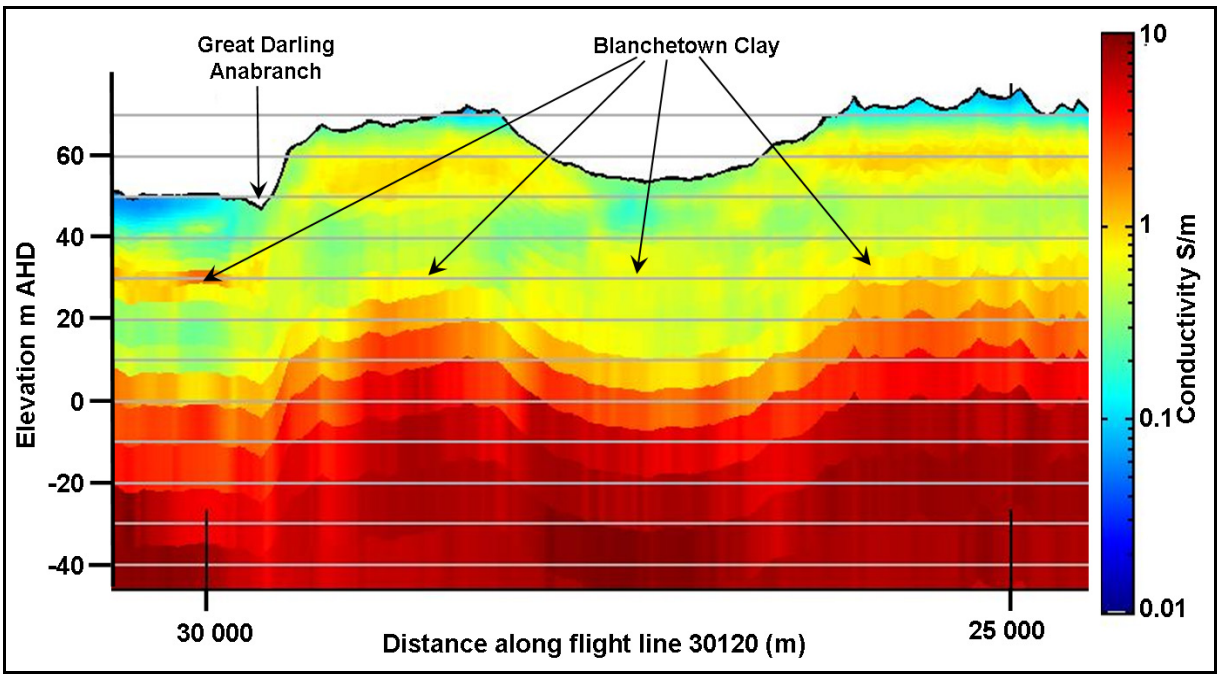

Figure 5-69. *AEM flight-line section 30120 showing the Blanchetown Clay conductor extending horizontally northwards from below the Great Darling Anabranch scroll plain and passing under the Cuthero Cliff Section (Figure 5-98).*

5.3.2 Stratigraphic Relationships and Depositional History

In the Murray River area, the Blanchetown Clay unconformably overlies the tectonically deformed Loxton-Parilla Sands which are in many places capped by the Karoonda weathering surface. There is an irregular eroded upper boundary to Quaternary aeolian sands (Woorinen Formation) and Quaternary alluvium in the river corridors. This stratigraphy is a result of the local geological and geomorphic history:

- Deposition of beach-barrier sands (Loxton-Parilla Sands) by regression of Miocene-Pliocene sea.
- Erosion and weathering of the exposed land surface (Karoonda Surface)
- Damming of the palaeo Murray to form Lake Bungunnia, and deposition of the Blanchetown Clay in the lake.
- Draining of the lake and incision of the Murray River through the Blanchetown Clay and into the Karoonda Surface, Loxton-Parilla Sands and earlier sediments.
- Erosion of the Blanchetown Clay, and deposition of windblown sand mostly in dunes (Woorinen Formation, Bunyip Sand) and younger lake clays in playa lakes, some of which may be descendents of Lake Bungunnia.

Thus in the Murray River area, there has not been continuous relatively thick regional deposition over the Blanchetown Clay, and topographic elevation has been successfully used to predict its distribution. Furthermore, McLaren & Wallace (2010) and McLaren *et al*. (2012) use SRTM DEM data to map receding shorelines of Lake Bungunnia.

The stratigraphic situation of the Blanchetown Clay in the study area contrasts markedly with that of the Murray River area to the south. In the far south of the project area, the shoreline Loxton-Parilla Sands interfinger with and are overlain by the fluvial Calivil Formation, as shown by the core in drillholes BHMAR31-1, BHMAR29-1 and BHMAR28-1. Sonic core holes BHMAR19-1 and BHMAR36-1 in particular show that the Blanchetown Clay is overlain by a fluvial to lacustrine sequence into which the Darling River floodplain has been inset, named the Willotia beds in this report (see Section 5.4.1.3; Figure 5-70) which we interpret to crop out in steep west bank sections along Redbank Creek and the Great Darling Anabranch, and in the Lake Cawndilla outlet channel. Furthermore, the Blanchetown Clay is buried by up to 25 m of younger alluvium of the Menindee and Coonambidgal Formations in the Darling floodplain area.

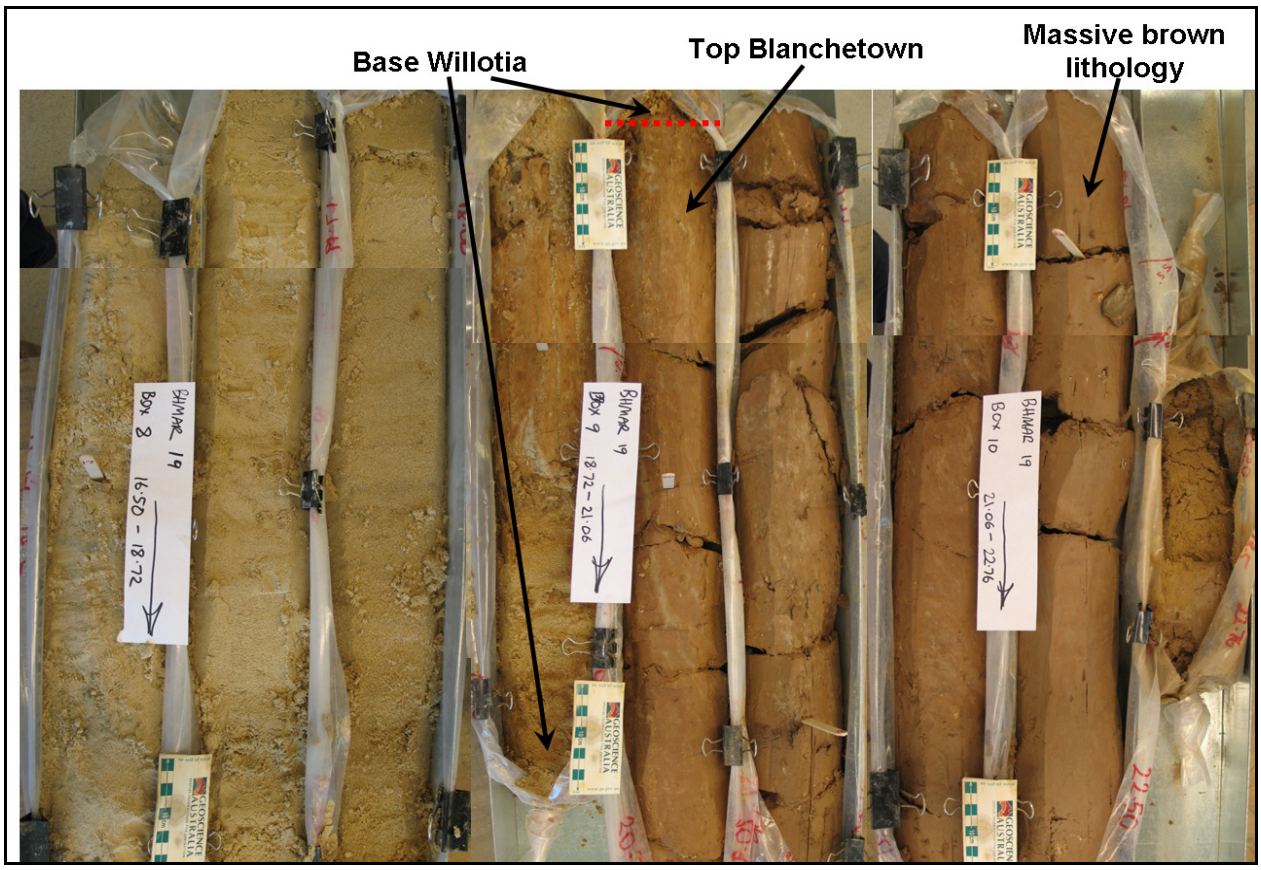

Figure 5-70. *Photographs of sonic core from BHMAR19-1 (15.5-22.76 m) showing contact between medium sand in the Willotia beds (left) and clay-rich Blanchetown Clay (right). The contact is erosional. The Blanchetown Clay in this interval is characterised by massive brown clay.*

The geomorphic/geological history for the Menindee area as determined by this project can be summarised as:

1. Complex history of pre-Palaeozoic deformation and metamorphism in Proterozic basement rocks. Several E-W shear zones mapped in the Darling Geological Basin basement are reactivated in Neogene times (e.g. Talyawalka Fault System);
2. Formation of Palaeozoic-Mesozoic Basins (e.g. Menindee, Wentworth and Blantyre Troughs) as part of the Darling Geological Basin. Deposition of a thick (several km) sequence of clastic sediments within extensional fault-bounded basins is interrupted episodically by structural inversion along these structures (e.g. in Carboniferous). Several of these structures appear to have been reactivated in Neogene times;
3. Formation of the Murray Geological Basin, with deposition of Renmark Group clastic sediments by rivers flowing southward towards a shallow sea to the south of the BHMAR project area in the Palaeocene to Miocene;
4. Depositional hiatus in the Miocene with weathering and local erosion of the Renmark Group sediments;
5. In the south of the study area, deposition of marginal marine sands and shoreline dunes (Loxton-Parilla Sands) in shallow water at the northern margin of a marine basin. Pene-contemporaneous with this was deposition of fluvial Calivil Formation sediments by the palaeo Darling River and its tributaries in the Pliocene. The Calivil Formation sediments locally overlie the Loxton-Parilla Sands in the study area;
6. Damming of the palaeo-Murray River and its tributaries, including the palaeo Darling River, with Blanchetown Clay deposition in palaeo Lake Bungunnia in the Late Pliocene to Pleistocene;

7. Pliocene regression, and the drying up of Lake Bungunnia, due to a combination of lowering of the sill of the dam that initiated the lake (McLaren *et al*., 2012) and the onset of a dryer climate;
8. Continued fluvial and local lacustrine deposition, with sediment derived from the northwest (Broken Hill area) and the north (palaeo Darling River, which passed through a gap in basement hills at Wilcannia at the edge of the Murray Basin). These Willotia bed sediments may be also partly a time equivalent of the upper part of the Blanchetown Clay deposited further south in Lake Bungunnia;
9. Incision of a trench into the Blanchetown Clay to form the modern course of the Murray River (Murray Gorge). This trench propagated headwards up the Darling Valley by nickpoint retreat, incising the Willotia beds but generally not the Blanchetown Clay in the Menindee area;
10. Deposition of fluvial sediments of the Menindee Formation and subsequently Coonambidgal Formation within the eroded trench by the Darling River and its distributaries;
11. Concurrent with 8, 9 and 10 formation of the lake basins around Menindee, with local wave erosion and shoreline deposition; and
12. Concurrent with 8, 9 and 10, deposition and preservation of aeolian sand across much of the area, particularly where not flooded and reworked in the trunk river valley.
13. There are multiple lines of evidence to show that the area has been tectonically active in the Neogene-to-present day, as evidenced by a number of scarps, lineaments, and drainage alignments that are coincident with underlying faults. There is also evidence of neotectonics from some lake tilting in the south of the project area.

This stratigraphic and geomorphic history has important consequences for the identification and distribution of the Blanchetown Clay in the Menindee area. Firstly, it overlies fluvial sediments with little or no time gap, rather than coastal-barrier sands with an appreciable time gap during which a weathering profile developed, as is the case further south. The fluvial sediments comprise muddy-overbank and channel-plug deposits, as well as channel and crevasse splay sands. Therefore in places it is difficult or impossible to place an unequivocal boundary between the two, where clay of the Blanchetown Clay overlies clay of the Calivil Formation. Secondly, the Blanchetown Clay is overlain by fluvial and lacustrine deposits. Again, these contain muds as well as sands, and the boundary may not be clear. There is an erosional hiatus where the Blanchetown Clay is overlain by Menindee or Coonambidgal Formation sediments, and in most cases there is medium or coarse sand at the base of the younger sequence, with one or two fining upward cycles. Therefore in these situations we can identify the top of the Blanchetown Clay with a greater degree of certainty. This contrasts with the Murray area, where the Blanchetown Clay is mostly overlain by aeolian sand of limited thickness.

5.3.2.1 Lithology and thickness

The Blanchetown Clay was first recognised from cliff exposures along the Murray River where it consists mainly of green-grey, red-brown or variegated, silty to sandy clay that is kaolinite and illite rich with minor smectite (Brown & Stephenson, 1991; Bowler *et al*., 2006). McLaren *et al*. (2009) performed XRD analysis on a section at Nampoo Station near the Murray River, and found that kaolinite is the dominant clay, with lesser illite, and that quartz and calcite are also present. The deposits of Lake Bungunnia have a variety of other facies. A basal sand-rich unit, the Chowilla Sand is believed to represent initial reworking of Loxton-Parilla Sands (Gill, 1973; Firman, 1973) and is probably equivalent to a similar basal sandy Irymple Member recognised further east by Lawrence (1975). Gill (1973) demonstrated that the Chowilla Sand also interdigitates with the Blanchetown Clay, and occurs at several stratigraphic levels. He interpreted this unit to be a member of the Blanchetown Clay rather than a separate formation. An upper oolitic microbial dolomitic limestone unit, the Bungunnia Limestone, occurs in the western part of the basin and probably formed in a clastic-sediment-starved regime (Brown & Stephenson, 1991). The Bungunnia Limestone has been further studied by McLaren *et al*. (2012). The silt rich Nampoo Member of the Blanchetown Clay was defined by McLaren *et al*. (2009), who interpreted it to be sourced from aeolian dust, and considered it to possibly have basin-wide extent.

Ostracod, bivalve and fish fossil assemblages in the Blanchetown Clay demonstrate an entirely non-marine, mostly freshwater depositional environment (Brown & Stephenson, 1991; Bowler *et al.*, 2006). It is locally more than 20 m thick, but mostly only a few metres thick (Brown & Stephenson, 1991). McLaren *et al*. (2009) report a total thickness including the Chowilla Sand of 34 m at Nampoo Station, but this is unusually thick.

The Chowilla Sand in the Murray area is composed of fine-to medium-grained quartz sand. It contains Diprotodontid remains (Firman 1966), and Gill (1973) and Marshall (1973) report remains of fish, marsupials, tortoises, crustaceans and ostracods. McLaren *et al*. (2009) report a thickness of 13 m at Nampoo Station, and Gill (1973) reports up to 5 m in the Chowilla area.

5.3.2.2 Age

Age-diagnostic fossils have not been reported from the Blanchetown Clay and Chowilla Sand. In addition, both outcrops and drill core samples have been found to be too weathered to have preserved microfossils. The Blanchetown Clay is constrained to a late Pliocene-Pleistocene age by palaeomagnetic reversal stratigraphy with contrasting results of from 4.0-3.4 to 0.6-0.5 Ma at Chowilla (South Australia) and Lake Tyrell (Victoria) (Bowler, 1980; An *et al.*, 1986; Bowler *et al*., 2006) and from 2.58-2.4 Ma to 1.2-0.8 Ma at Nampoo Station (northern bank of Murray River in far western NSW near the SA border) (McLaren *et al.*, 2009). Therefore a late Pliocene to Pleistocene age is indicated but a precise numeric age is equivocal.

5.3.2.3 Blanchetown Clay and Chowilla Sand in the study area

Blanchetown Clay has been identified in many BHMAR drillsites. Use of sonic drilling resulted in good core, and interpretation of the stratigraphy has been made on a combination of core lithology, wireline logs (gamma, conductivity and NMR), and AEM conductivity sections through the drill sites. Core samples are typically dense, hard brown to light grey massive to fine bedded sandy clay, with local fine calcareous and manganese cement (Figure 5-70, Figure 5-71 and Figure 5-72). Sand content varies, and some thin beds of sand are included in the interpreted intersections. The Chowilla Sand has been interpreted to underlie the Blanchetown Clay in drillholes on the Menindee Common, at sites BHMAR75 and BHMAR88 where it is composed of sand (up to medium-coarse grained) and muddy sand (Figure 5-73). It is characterised by a sharp low in gamma and conductivity logs. In almost all cases the Blanchetown Clay is represented by a single or double conductivity peak in wireline logs (Figure 5-74), but as a gamma peak only in some holes (Figure 5-75). This is attributed to a contrast in lithology between the muddy Blanchetown Clay and generally sandy beds in the lower parts of overlying units, but a lesser contrast with interbedded mud and sands in the upper Calivil Formation. In many of the rotary mud holes, recognition and differentiation from the underlying Calivil Formation and overlying units is dependent almost entirely on the wireline log character. More detailed descriptions of the Blanchetown Clay are provided below in the sections on individual targets.

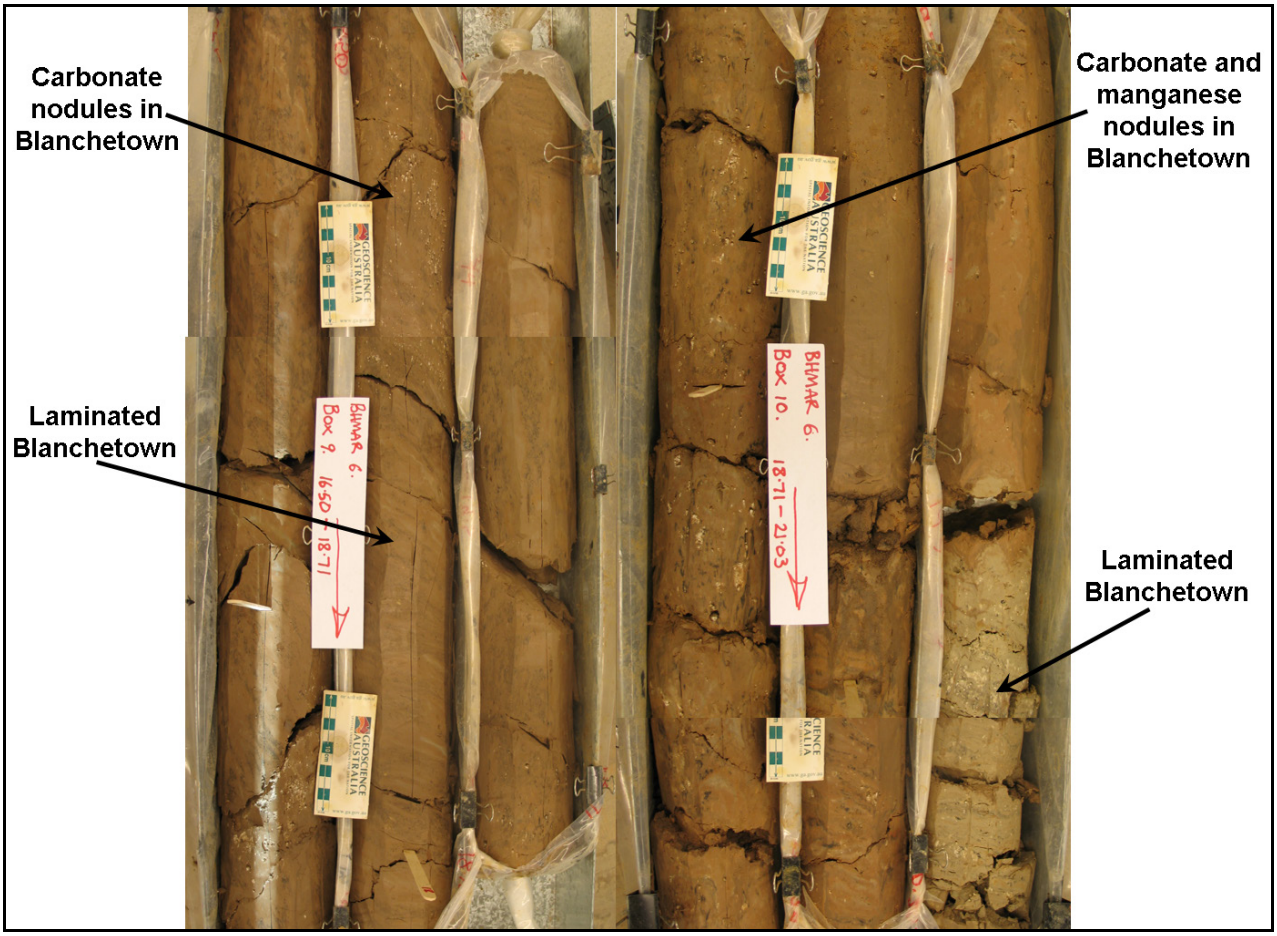

Figure 5-71. *Photographs of sonic core from BHMAR06-1 (16.5-21.03 m) showing various features of Blanchetown Clay including brown clay, light coloured silty clay, and carbonate and manganese nodules.*

Laboratory textural analyses produced some anomalous results where significant quantities of sand and even gravel abundance were reported, from Blanchetown Clay sediments that were known from laboratory logging to be mud-dominated. These anomalies were found to be due to sand-sized and gravel-sized mud aggregates which were resistant to the standard laboratory sample dispersion method. A detailed experimental study was undertaken to investigate this issue and it determined that Blanchetown Clay mud aggregates were fully disaggregated by acidification to remove cementing carbonates plus a vigorous agitation regime with chemical dispersant added (Section 11.4 of Lawrie *et al.*, 2012a). This experiment confirmed that some of the sand and all of the gravel abundances reported for the Blanchetown Clay were erroneous, but examination of the residual sand-sized fraction after dispersion also demonstrated the reality of sand grains in the sediments, sometimes at significant abundance levels and up to medium and coarse grain sizes. These results were considered in the interpretation of all Blanchetown Clay grainsize analysis results.

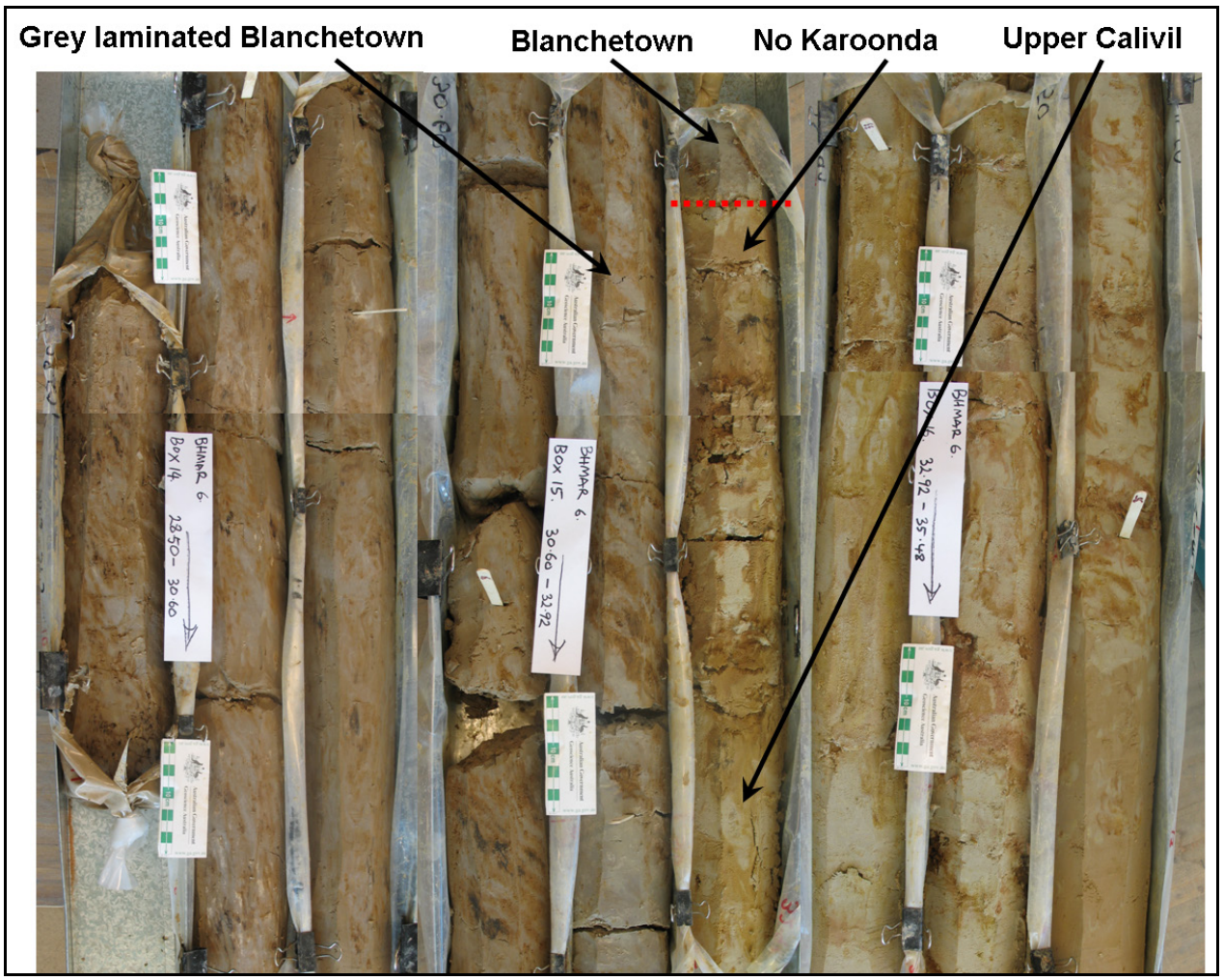

Figure 5-72. *Photographs of sonic core from BHMAR06-1 (28.5-35.48 m) showing greyish laminated Blanchetown Clay, sharp contact with underlying Calivil Formation, and the absence of the Karooda surface from the top of the Calivil Formation.*

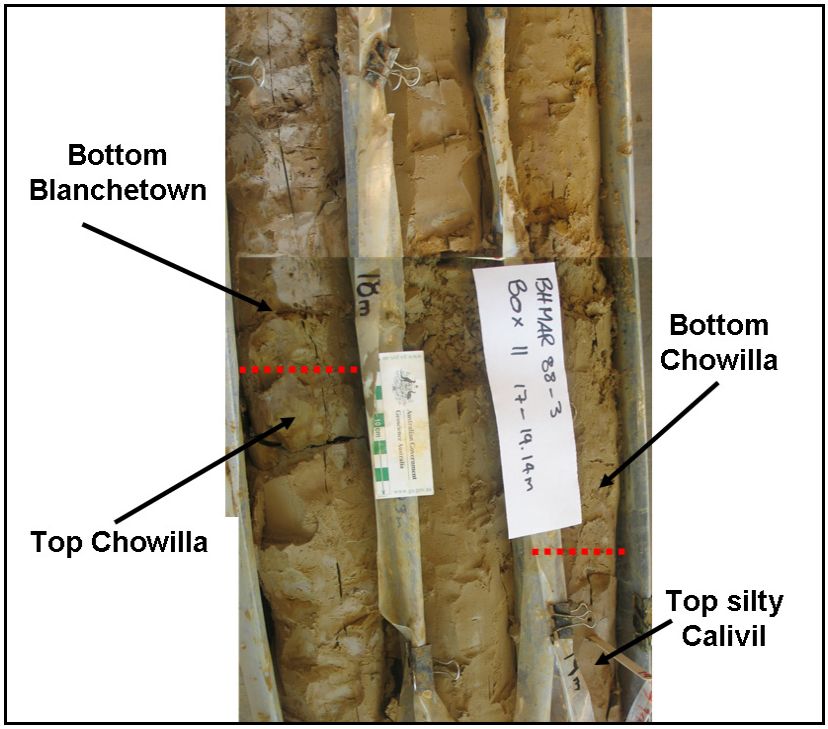

Figure 5-73. *Photographs of sonic core from BHMAR88-3 (17.0-19.14 m) showing Chowilla Sand underlying Blanchetown Clay (left) and the silty upper part of the Calivil Formation (right).*

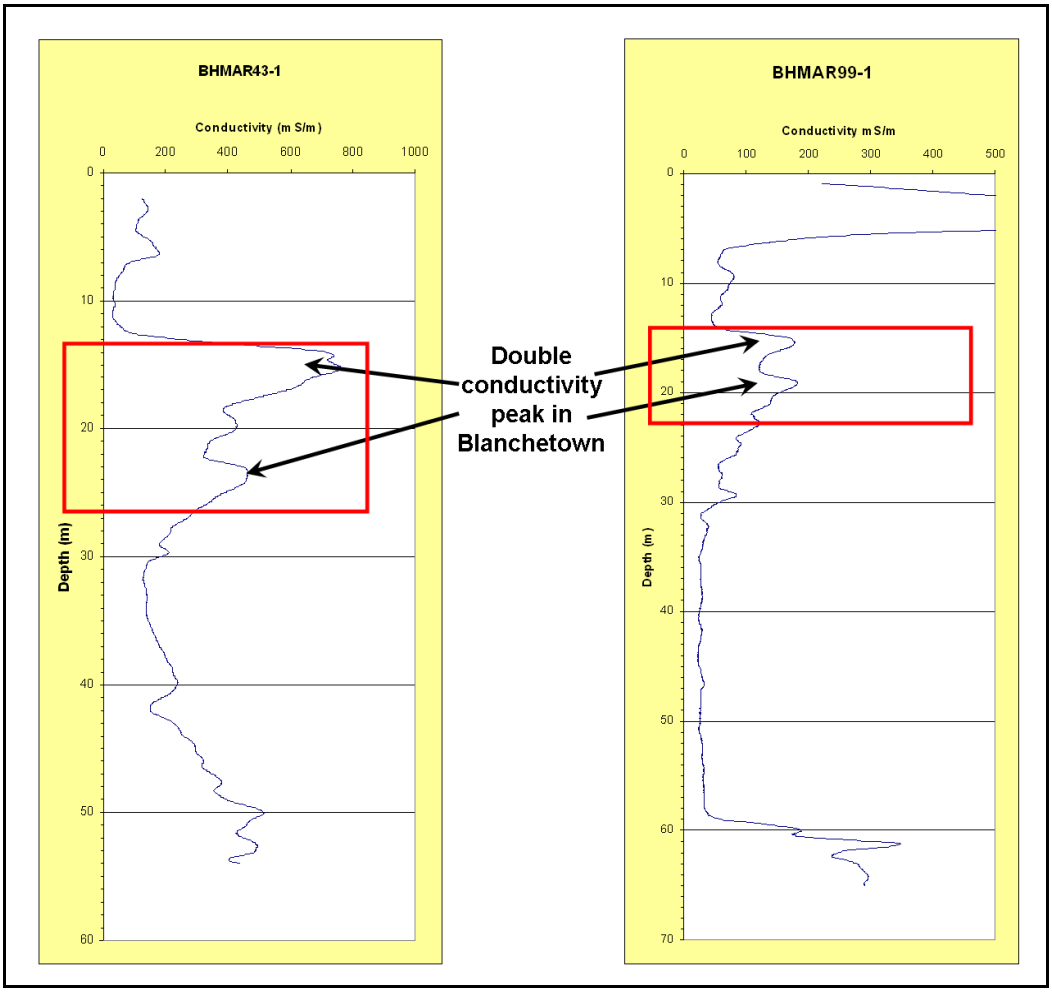

Figure 5-74. *Double conductivity peaks in induction logs of BHMAR43-1 (left) and BHMAR 99-1 (right).*

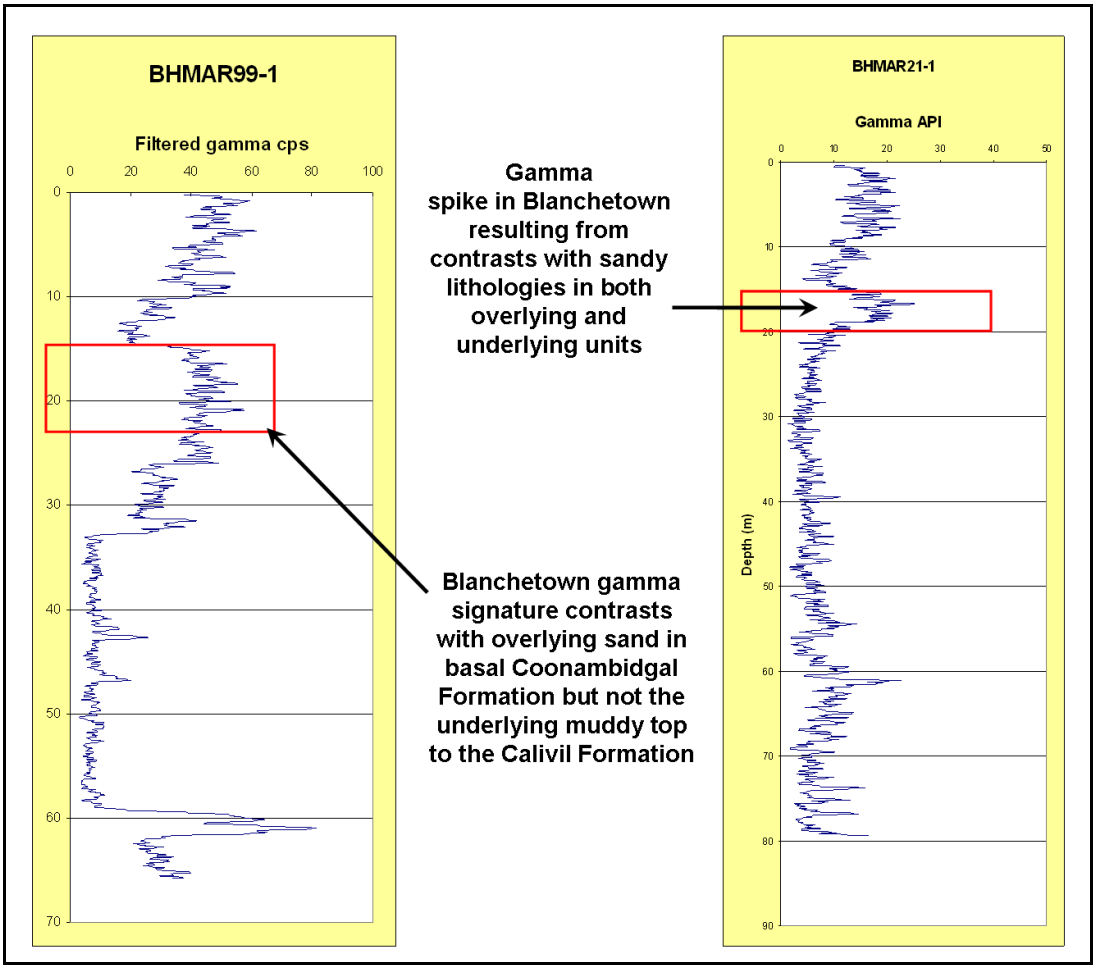

Figure 5-75. *Gamma logs of the Blanchetown Clay, showing indistinct base where underlain by muddy upper Calivil Formation (BHMAR99-1 left), but a sharp peak where the Blanchetown Clay is sandwiched between sandy units (BHMAR 21-1 right).*

5.3.3 "Holes" in the Blanchetown Clay

Numerous "holes" have been mapped in the Blanchetown Clay conductivity anomaly (refer Lawrie *et al.,* 2012a for methodology), aided by interpretation of drillhole intersections. Almost all holes intersected a clay unit that could be referred to the Blanchetown Clay, but it is interpreted to be absent from a few.

There are several possible scenarios for the origin of actual physical absence of the BC, including non-deposition, facies change, faulting and erosion. However, the mapping of "holes" has been done by interpretation of AEM conductivity data, and two further scenarios are possible: the Blanchetown Clay is present but does not have a conductivity anomaly that is detectable by the AEM system, and apparent holes may be due to misinterpretation.

5.3.3.1 Non-deposition.

The Blanchetown Clay was deposited in Lake Bungunnia. There must have been a maximum water level in the lake and shorelines at and below this level. The Blanchetown Clay could not have been deposited above this maximum elevation. Thus there is the possibility of there being islands and a maximum shoreline for the lake in the AEM area, where the Blanchetown Clay could not have been deposited. We have identified several places where this scenario is most probably present.

There is a basement high in the northern half of the project area near the boundary between AEM areas 1 and 2. It is probable that basement rocks crop out in the river at a locality named Christmas Rocks, but any outcrop was covered for the duration of the project beneath the backed up waters of Lake Wetherell. AEM sections through this area show resistive basement to within a few metres of the surface, and possible Blanchetown Clay conductivity layer pinching out against the basement (Figure 5-76). This area was most probably an island or promontory in Lake Bungunnia. Integrated interpretation of the Blanchetown Clay was not possible over much of this basement high area, and it forms an area of no interpretation.

There is a small "hole" at Kangaroo Lake near Lake Tandou where the Blanchetown Clay overlies Calivil Formation. The margins of the conductivity anomaly show thinning of the anomaly from the base upwards, suggesting that the Blanchetown Clay thins towards the "hole", suggesting that there was an island of Calivil Formation sediments (i.e. a palaeo hill before inundation) in Lake Bungunnia and that the "hole" is due to non-deposition (Figure 5-77). However, the top of the Blanchetown Clay anomaly at this locality is at about 44 m AHD, which implies a shoreline at this elevation, well below the 60-65 m maximum shoreline generally agreed on (see above).

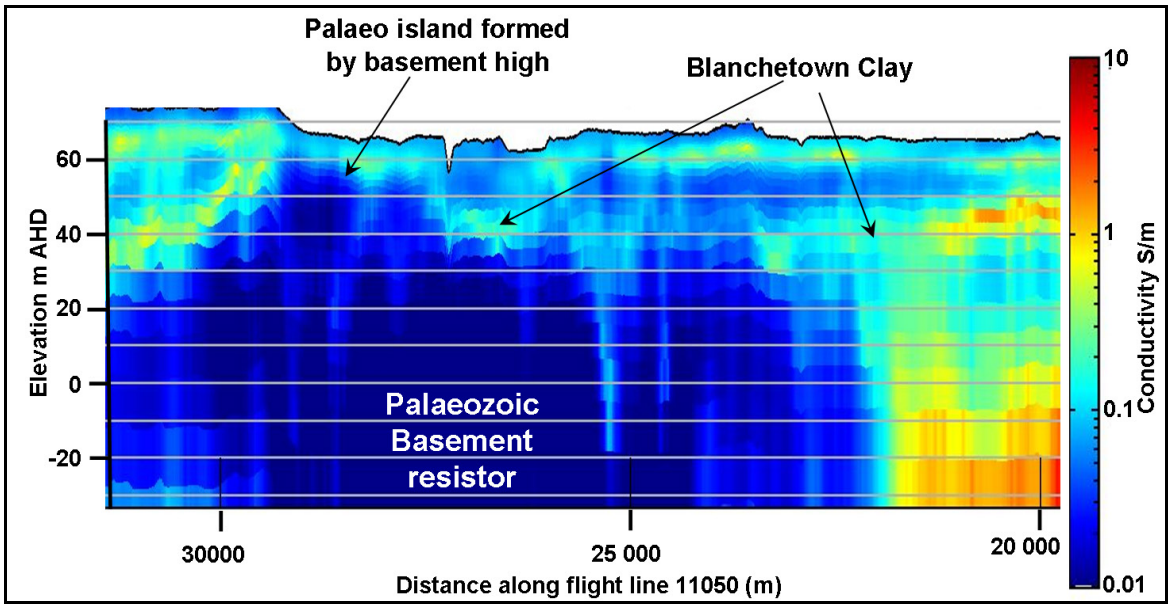

Figure 5-76. *AEM flight line 11050 showing conductive Blanchetown Clay pinching out over a strongly resistive Palaeozoic basement which reaches close to the surface at Christmas Rocks.*

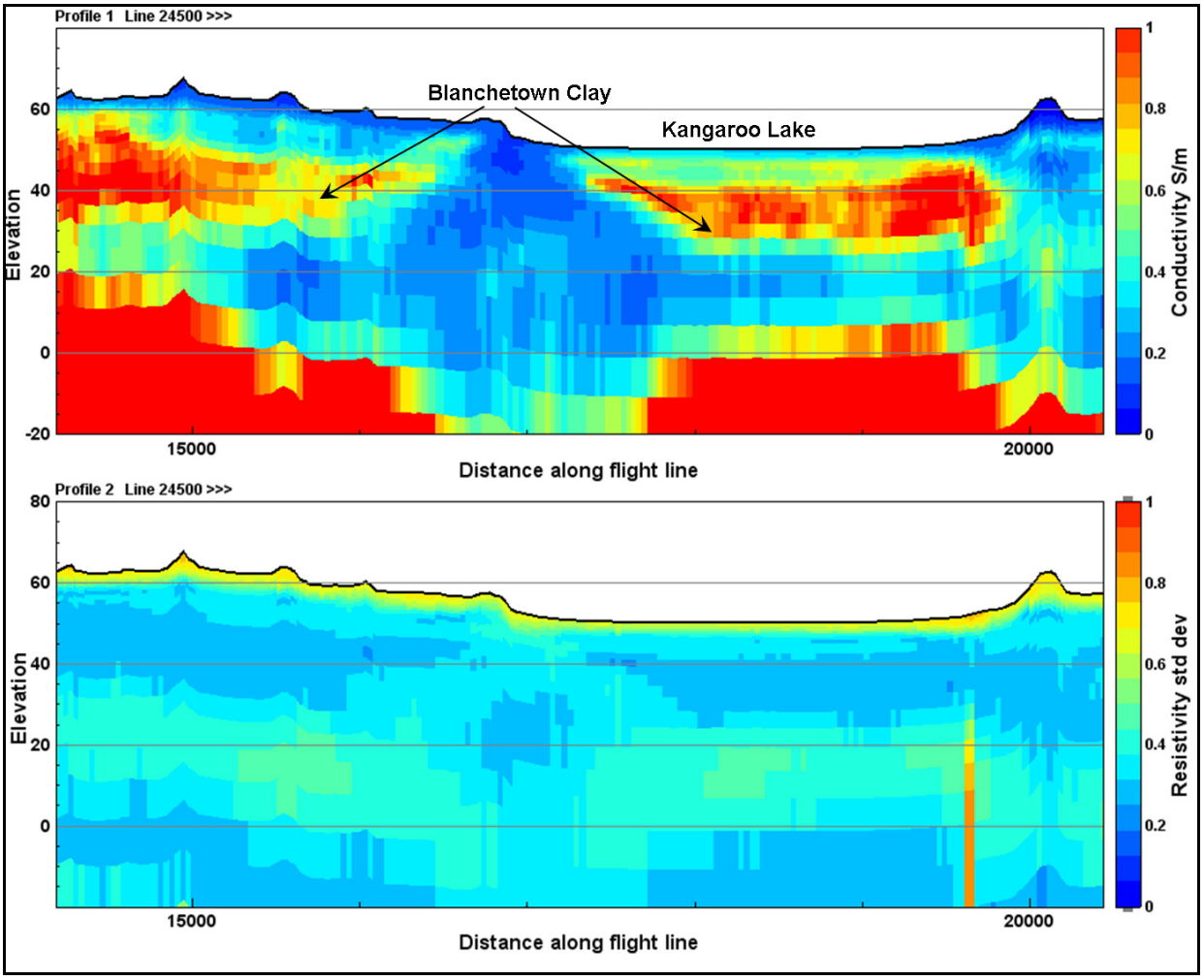

Figure 5-77. *AEM flight line 24490 through Kangaroo Lake showing conductive Blanchetown Clay apparent thinning towards a hole from the base upwards.*

5.3.3.2 Facies change

Gill (1973) demonstrated from exposures along the edge of the Murray River trench near Lake Victoria that the clay-rich lithology of the Blanchetown Clay could pass laterally into sand (his use of the term Chowilla Sand as a member of Blanchetown Clay). Other authors have also demonstrated the presence of sandy beds at the base of and within the Blanchetown Clay. From a theoretical viewpoint is it considered likely that there would be sandy deposits around the shoreline of Lake Bungunnia in the Menindee area, where sediment could be introduced by the palaeo Darling River, which flowed between basement highs at Wilcannia, and watercourses draining from the Broken Hill area. Further south, old lake shorelines are characterised by thin carbonate accumulation (McLaren *et al*., 2012), but that is in an area where little terrigenous input would be expected, distal from the palaeo watercourses draining to the lake. Thus lake deposits could become increasingly sandier in proximal areas due to wave mixing of sand and mud, or sand could be preserved in discrete palaeo-deltas into the lake.

BHMAR35-1 is considered to have intersected the most proximal part of the Blanchetown Clay. Only one sample (at 14 m) was analysed for laser grainsize, with a sand content of 30% (Appendix 3d, Apps *et al*., 2012f). However, visual examination of the core from this hole with hand lens and binocular microscope indicated that there was ~40-60% sand grains in mud for much of the Blanchetown Clay. This is higher than observed elsewhere in our drill core.

5.3.3.3 Faulting of the Blanchetown Clay

The Blanchetown Clay top surface varies in elevation by 60 m across the study area (Figure 5-63). Extensive Neogene-to-Present faulting, tilting and warping of the Lower Darling Valley sediments is evident from AEM mapping of the Blanchetown Clay. The latter is warped and tilted at a range of scales, and is locally sharply offset by faults with up to 20 m vertical offset. Neogene faults that offset the Blanchetown Clay horizon and localise inter-aquifer leakage are more numerous than surficial Neotectonic structures. Many of the faults controlling this deformation are formed through reactivation of basement faults (Figure 5-80).

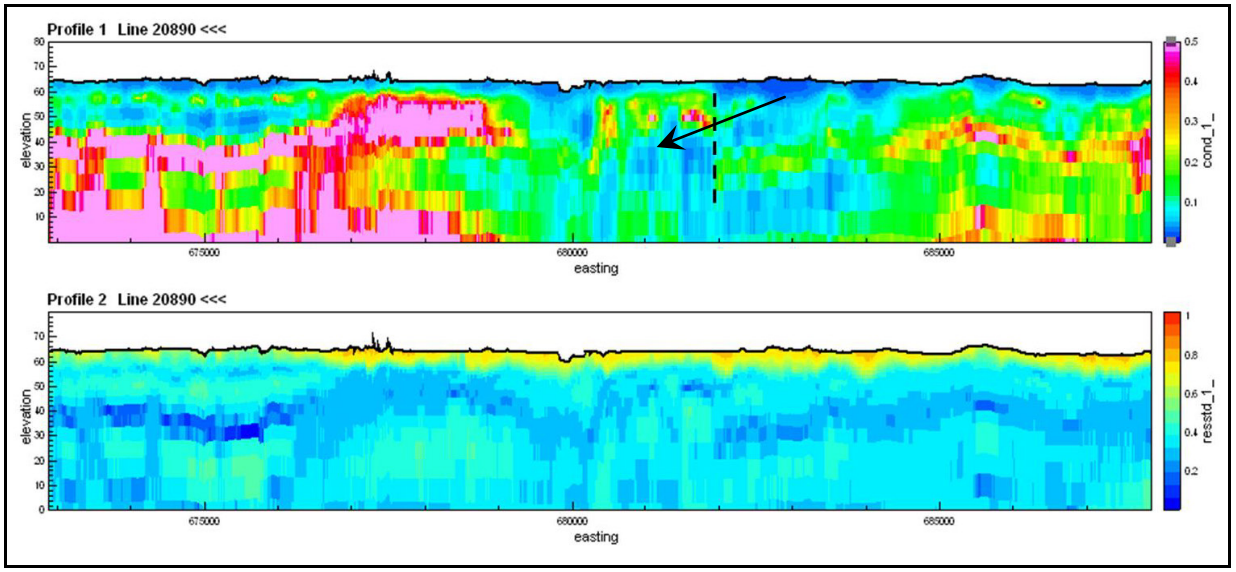

Figure 5-78. *Part of AEM flight line 20890 showing Blanchetown Clay conductivity anomaly at 30-60 m AHD, with interpreted warping and faulting (dashed line) in the centre part of the section. Arrow shows recharge pathway created by fault. Vertical scale 0-80 m AHD, horizontal distance about 21 km, linear colour scale 0-0.5 S/m conductivity and 0-1 standard deviation.*

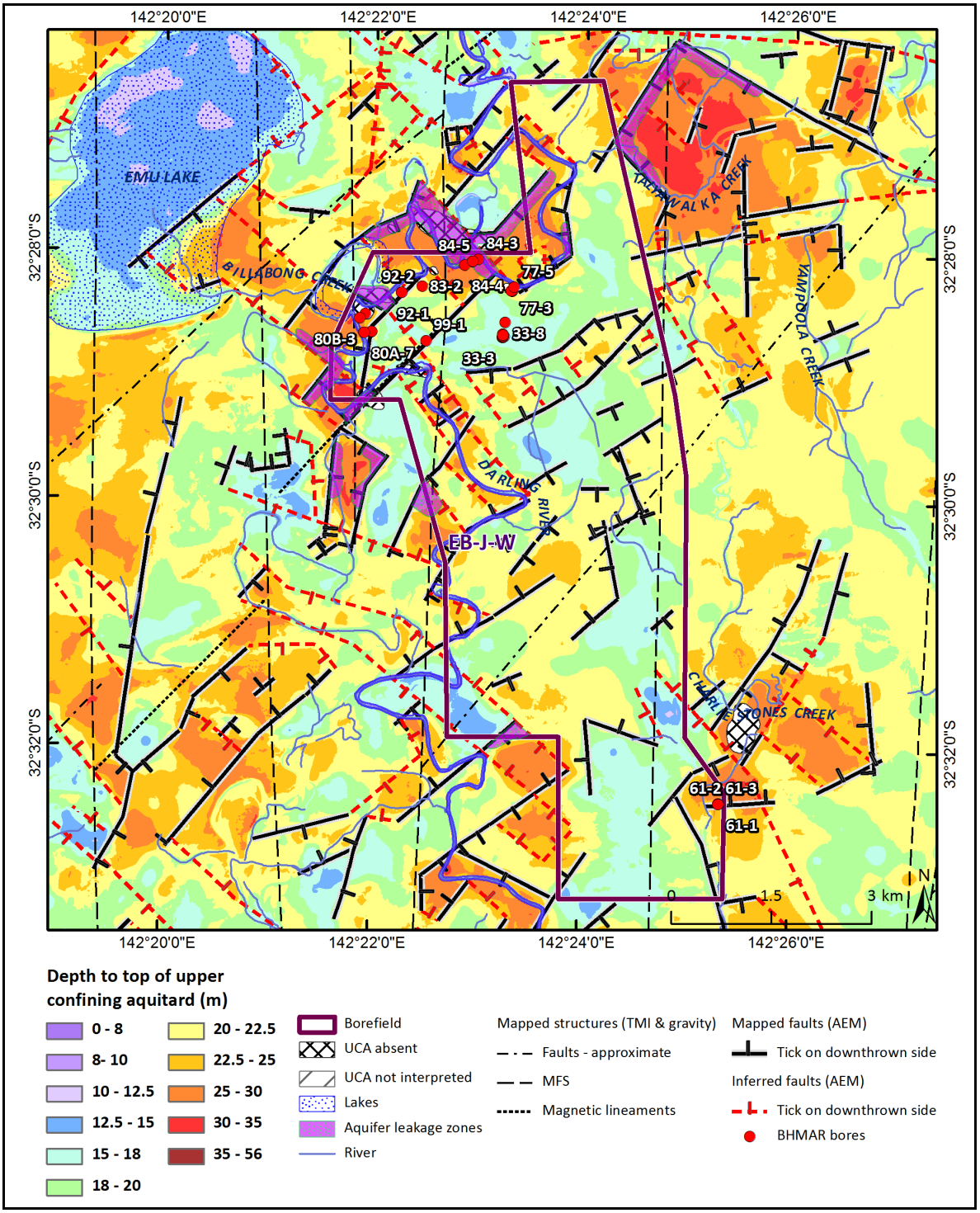

Figure 5-79. *Depth to the top of the upper confining aquitard. Holes, faults and leaky zones are also indicated.*

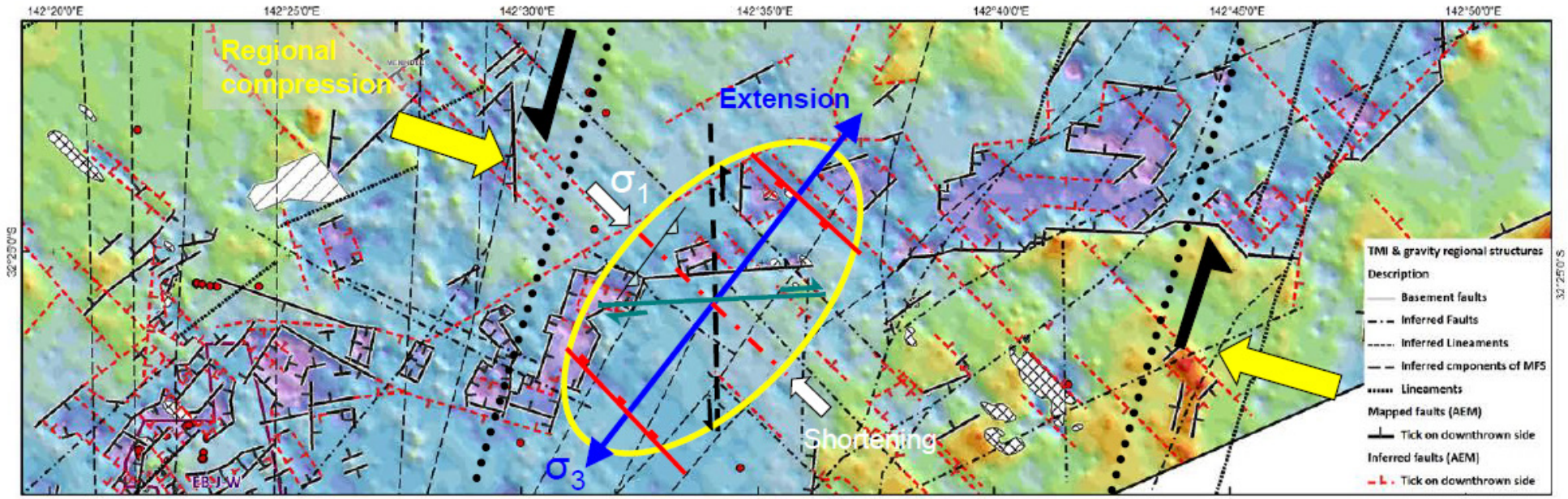

Figure 5-80. *This image shows the depth to the top of the Blanchetown Clay aquitard in an area where the Talyawalka and Menindee Fault Systems link. The Talyawalka Fault zone is oriented approximately E-W in the centre right of each image, and has a fault trace of over 160km to the east. The purple colours are depositional lows filled with Coonambidgal Formation sands. In both images, the purple areas are delineated by faults that are mapped across several AEM flight lines (black lines), with inferred faults (parallel to flight lines), in red. Faults and lineaments identified in magnetics data are also plotted. In image b, the strain ellipse (yellow) and arrows represent the interpreted stress field under which the faults formed. N-S and NNE-SSW trending sinistral strike-slip faults form at an oblique angle in response to regional WNW-WSE shortening (yellow arrows). Within the shear zones, extension in a NE-SW orientation (blue line and arrows), is typically denoted by normal faults (red) that define grabens and half-grabens. ENE-WSW antithetic faults zones are also observed to form in this stress system, and provide important linkages between these extensional structures. Minor reverse faults (black line with pale blue-green triangles) and associated horst blocks are formed by NW-SE shortening within the shear zones. The structures mapped are consistent with models of simple shear couples within strike-slip fault systems and consistent with broader regional Neogene-and present day crustal stresses for this region of Australia. The orientation of the Talyawalka Fault System is consistent with dominant antithetic strike-slip movement in this shear zone system, with significant influence from pre-existing, underlying basement structures.*

5.3.3.4 Erosion of the Blanchetown Clay

A feature of the stratigraphic history outlined above for the Menindee area is that the Willotia beds and Blanchetown Clay have been eroded to form the trench in which the Menindee and Willotia formations were deposited. In nearly all of our drillholes in the trench, Blanchetown Clay is overlain by one of these formations, and it appears that significant or widespread erosion of the clay has not occurred during erosion of the trench or lateral migration of the main river channels. This may be due either the clay forming a hard substrate that cannot be eroded by the channels, or the low natural gradient of the Darling River (the Darling falls about 25 m from Menindee to its junction with the Murray over a distance of 200 straight line kilometres, giving an overall channel gradient in the order of 50 mm per kilometre). In-river bathometric surveys obtained for this project have shown that there are scour holes in the bed of the modern river, mostly at sharp meanders. Comparison of the elevation of the base of these holes and the top of the Blanchetown Clay shows that none of the modern scour holes have eroded into the clay, but it possible that in earlier times scour holes or even the main channel may have been eroded into and through the Blanchetown Clay.

Blanchetown Clay north of BHMAR05 drill site has been warped up to outcrop in the bank of the Darling River (Figure 5-67). North of this point there is an area where the Blanchetown Clay has definitely been eroded due to its high level. Another area where the Blanchetown Clay appears to have been eroded is beneath the northern part of Lake Menindee, where it passes laterally into relatively young sands (Figure 5-107). Both these areas appear to be actively recharging aquifers from river and lake waters.

In the southern half of the project area, the Blanchetown Clay is eroded both on the crests of upfaulted horst blocks (e.g. in the southeast of the study area; Figure 5-81; Lawrie *et al*., 2012d), and in the depocentres of tectonic grabens and half-grabens, where it is eroded by Pleistocene palaeochannels (Lawrie *et al*., 2012d).

5.3.3.5 Blanchetown Clay is present without conductivity anomaly

Thin Blanchetown Clay is interpreted from core to be present BHMAR18-1, but has only low conductivity (maximum ~ 130 mS/m) when compared with the overlying Willotia beds sediments (up to 440 mS/m), and similar to the underlying Calivil Formation (80-155 mS/m). A “hole” has been interpreted in the area around this drillhole, with the AEM conductivity anomaly apparently missing (Figure 5-82). A pore fluid sample from the Blanchetown Clay at 15.3 m in this hole had EC of 674 µS/cm, not much higher than the next sample below in the Calivil Formation, 527 µS/cm. The Blanchetown Clay at this site contains water sufficiently fresh to reduce its usual conductive signature to the point where it cannot be discerned from the underlying Calivil Formation, and thus become invisible as a separate entity in the AEM data. These data suggest that although the Blanchetown Clay is predominantly an aquitard, fresh water is indeed passing through the aquitard in some locations. This may be due to discreet pathways through the clay which have not been observed in drill core, such as root zones or brittle fracture zones. If there were enough of these present, considerable leakage could occur, and pore fluid in the surrounding clay could be considerably fresher than elsewhere in the unit.

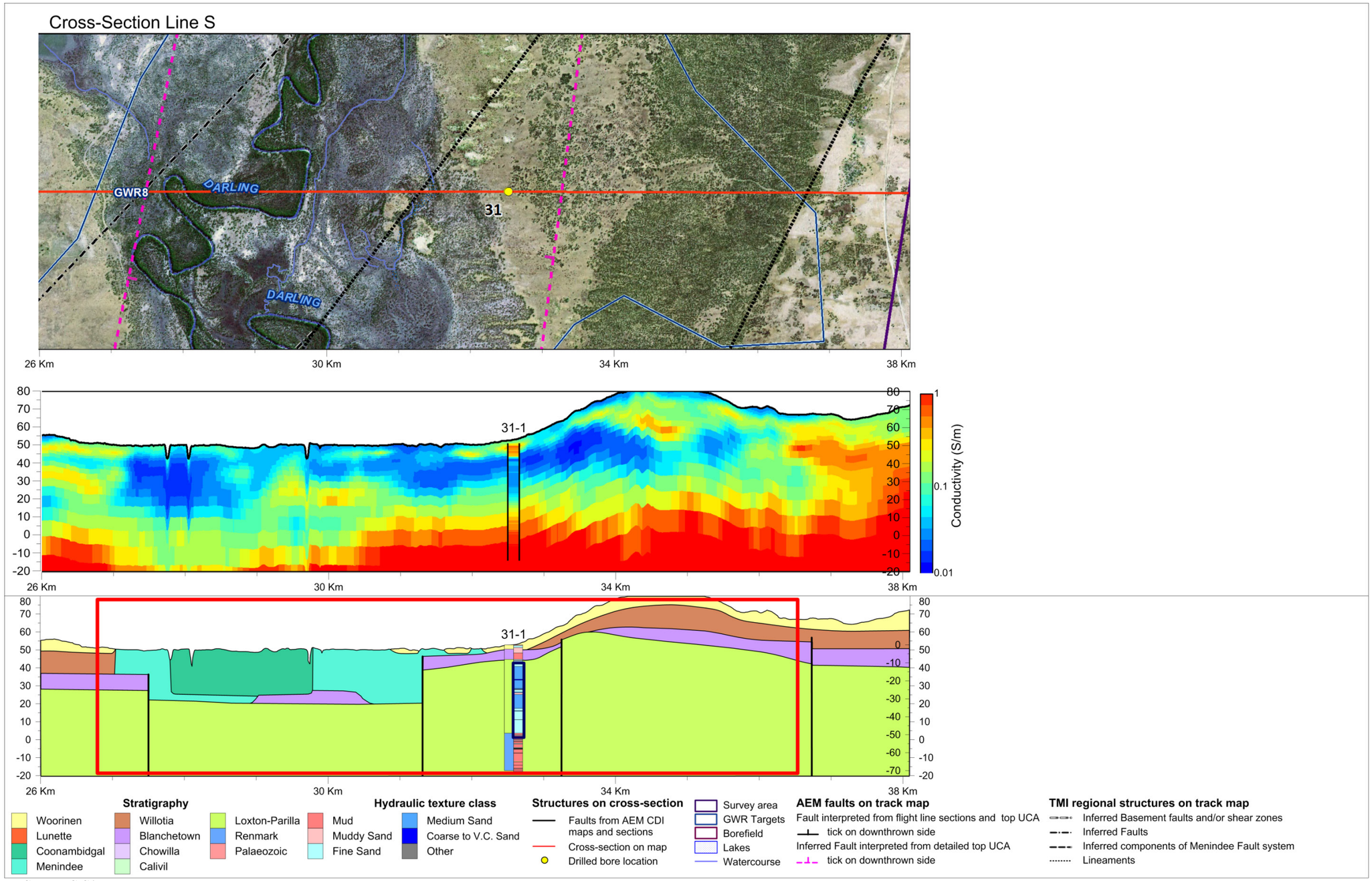

Figure 5-81. *Cross Section S-S1.*

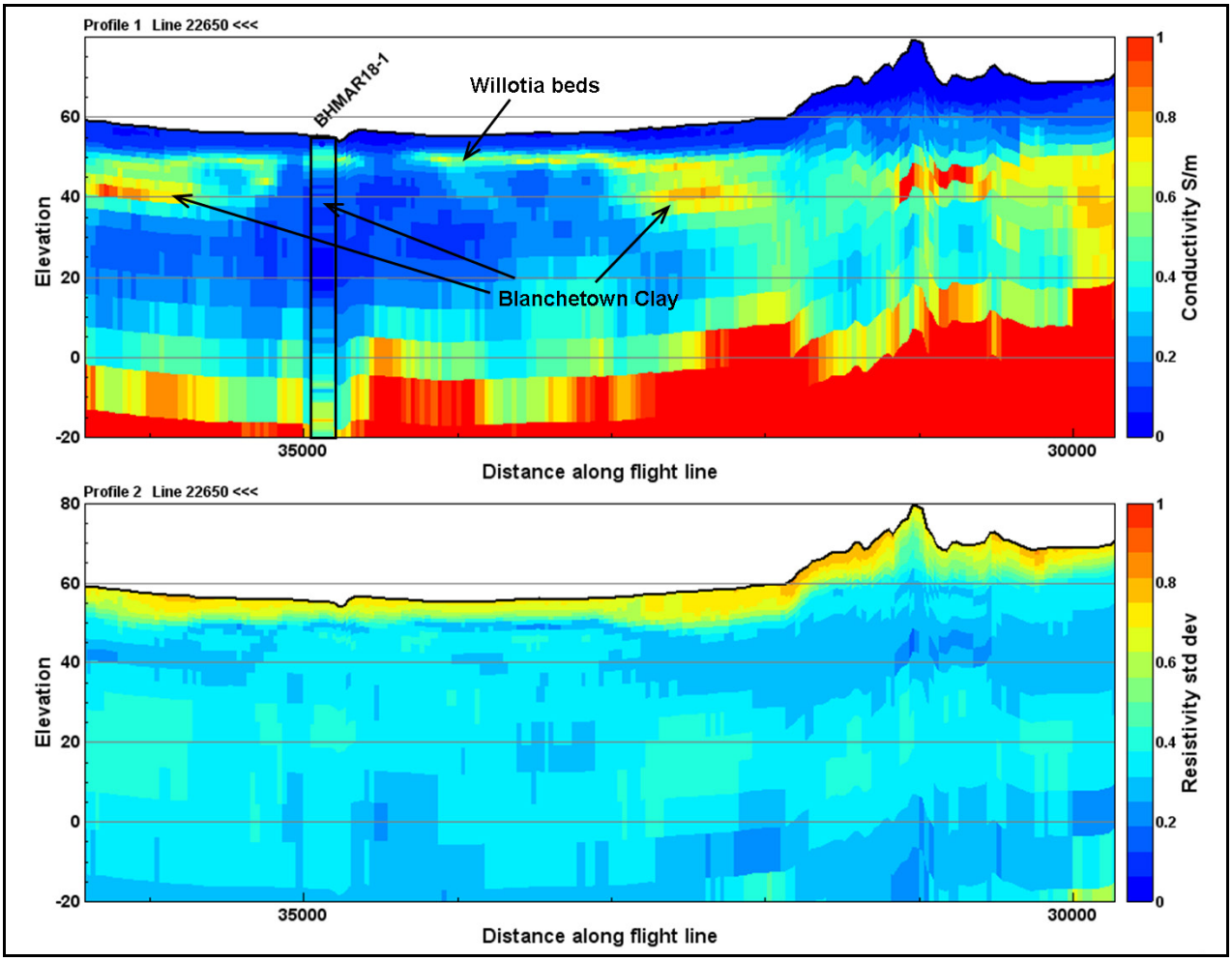

Figure 5-82. *AEM flight line 22650 through BHMAR18-1 at the eastern margin of Lake Menindee. Thin Blanchetown Clay is present in the core of BHMAR18-1, but has low conductivity (maximum ~ 130 mS/m) compared with the overlying Willotia beds sediments (up to 440 mS/m). Blanchetown Clay conductivity is similar to the underlying Calivil Formation (80-155 mS/m). With the AEM conductivity anomaly apparently missing, a "hole" has been interpreted in the area around this drillhole in conflict with Blanchetown Clay being logged as present.*

5.3.3.6 Misinterpretation

Conductivity of the Blanchetown Clay locally drops to less than 100 mS/m. Depending on the colour stretches used on sections being interpreted, this conductivity may appear the same colour as even lower conductivity sediments above and below, and thus the anomaly becomes invisible to the eye. Figure 5-83 shows an example of this type of feature.

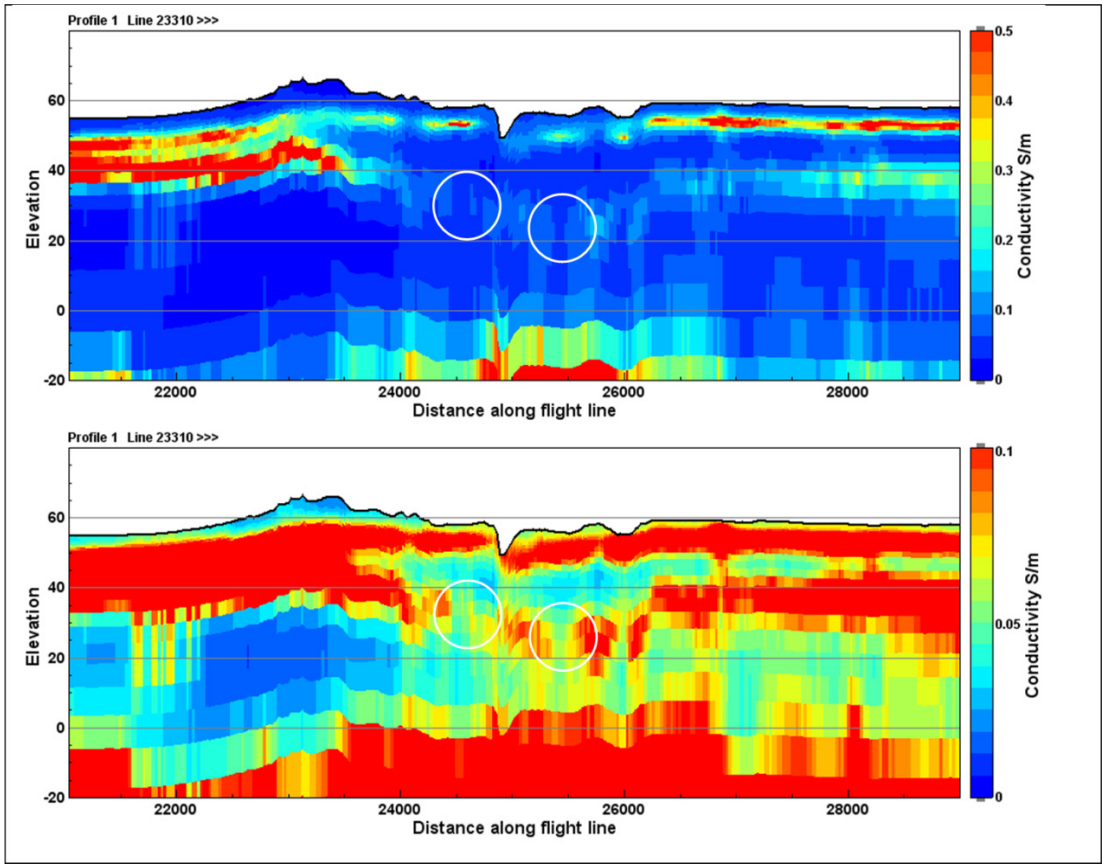

Figure 5-83. *Two apparent holes in the Blanchetown Clay conductivity anomaly (top, circled) are shown in the lower section to be zones of low conductivity which nevertheless contrast with even lower conductivity in the enclosing sediments. Although not true holes, these may be zones of leakage along features too small to be individually imaged by the AEM system.*

5.3.3.7 Recharge through the Blanchetown Clay

Vertical recharge to the Pliocene aquifers through the upper confining aquitard (Blanchetown Clay), is only likely to occur in weeks and months through and across faults that juxtapose the unconfined and underlying Pliocene aquifers, and a restricted number of erosional holes in the aquitard. A map of the residual of the Darling River channel DEM and depth to the top of the upper confining aquitard (Figure 5-84) shows that over most of its course, the Darling River channel base lies significantly above the top of the upper confining aquitard, even at cod hole locations. Only in a few locations does the thalweg of the river come within 2-3 metres of the top of the Blanchetown Clay.

A close-up of this map (Figure 5-85), shows the relationship between faults, erosional holes and inter-aquifer leakage zones for the Darling River in the northern part of the Jimargil potential borefield site. The residual height of the river channel above the Blanchetown Clay aquitard is shown (blue indicates ~2.6 m; greens ~10 m; reds ~26 m). This image shows the location of erosional 'holes' where the Blanchetown Clay is absent. The location of these holes is effectively fault-controlled (on the down-thrown side of the mapped faults). Potential inter-aquifer leakage occurs at these locations, and where there is significant vertical fault offset (>10 m) on other mapped faults that juxtapose the unconfined Coonambidgal and Menindee Formation aquifers with the underlying Calivil Formation aquifer. These potential inter-aquifer leakage zones are shown in yellow. This image also shows that the course of the Darling River is partially fault-controlled in this reach.

Further south within the Jimargil borefield, another close-up map of the residual of the Darling River channel DEM and depth to the top of the upper confining aquitard (Figure 5-86) shows a small fault-bounded horst block mapped from AEM data. The river base comes closest to the underlying aquitard between points A and

B where the horst block is located. The river course at this point is coincident with an ENE-trending fault with a downthrow to the north. These faults may provide the locus for recharge and inter-aquifer leakage.

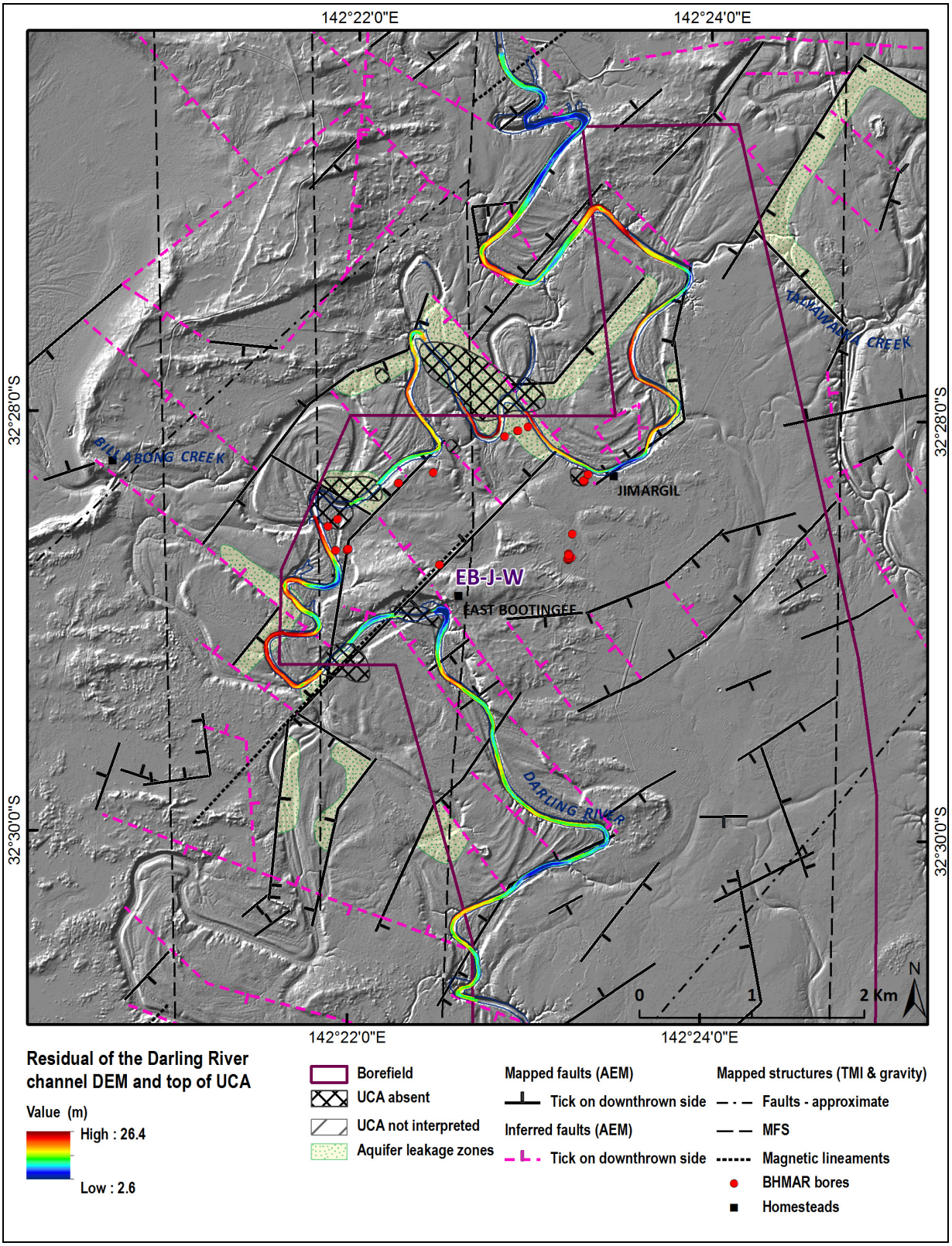

Figure 5-84. *Residual of the Darling River channel DEM and depth to the top of the upper confining aquitard. This map shows that along most of its course, the Darling River channel base (including cod holes) lies above the top of the upper confining aquitard.*

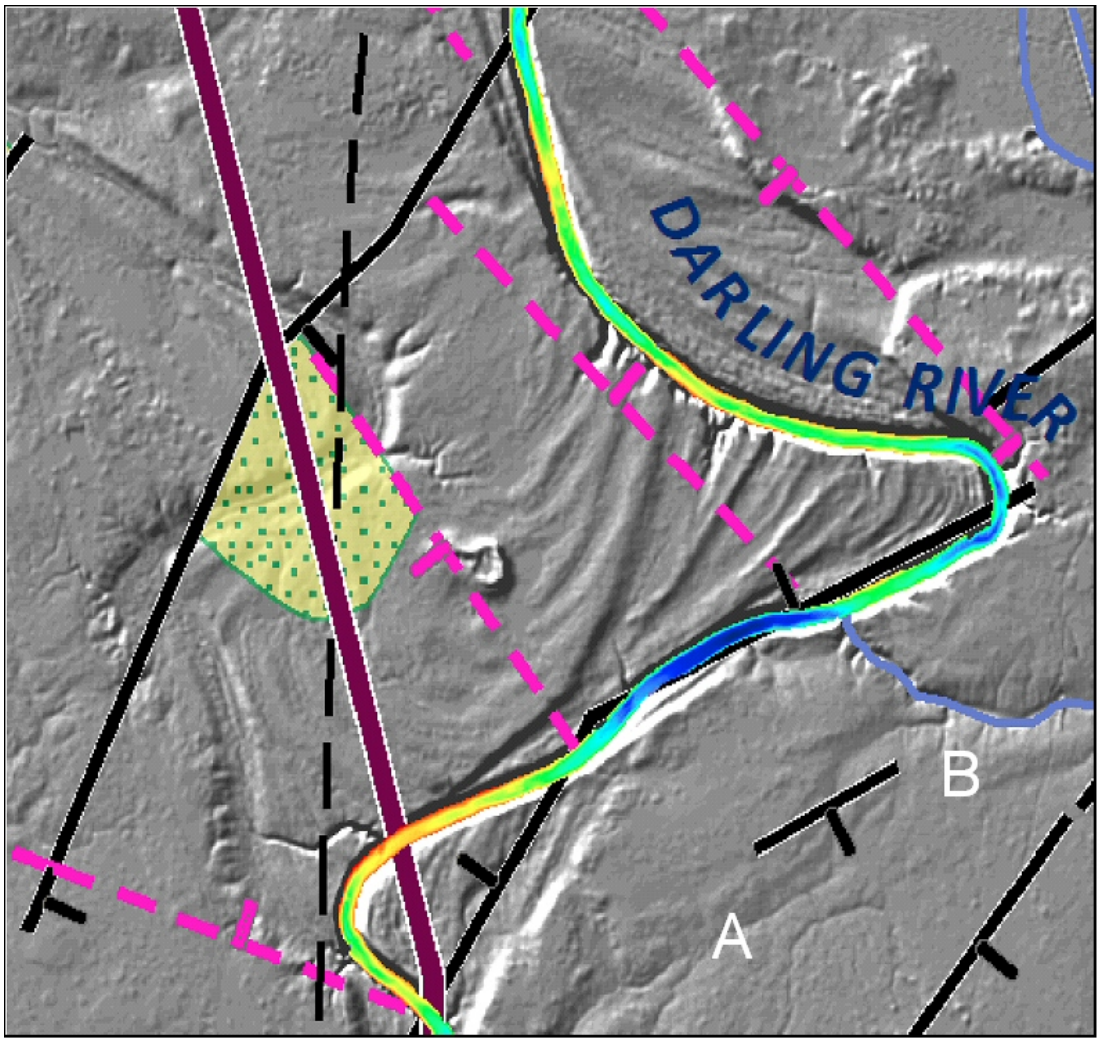

Figure 5-85. *A map of the residual of the Darling River channel DEM and depth to the top of the upper confining aquitard for a reach of* the *Darling River at the Jimargil potential borefield site. The residual height of the river channel above the Blanchetown Clay aquitard is shown (blue indicates ~2.6 m; greens ~10 m; reds ~26 m). A small fault-bounded horst block mapped from AEM data between points A and B shows where the river base comes closest to the underlying aquitard. The river course at this point is coincident with an ENE-trending fault with a downthrow to the north.*

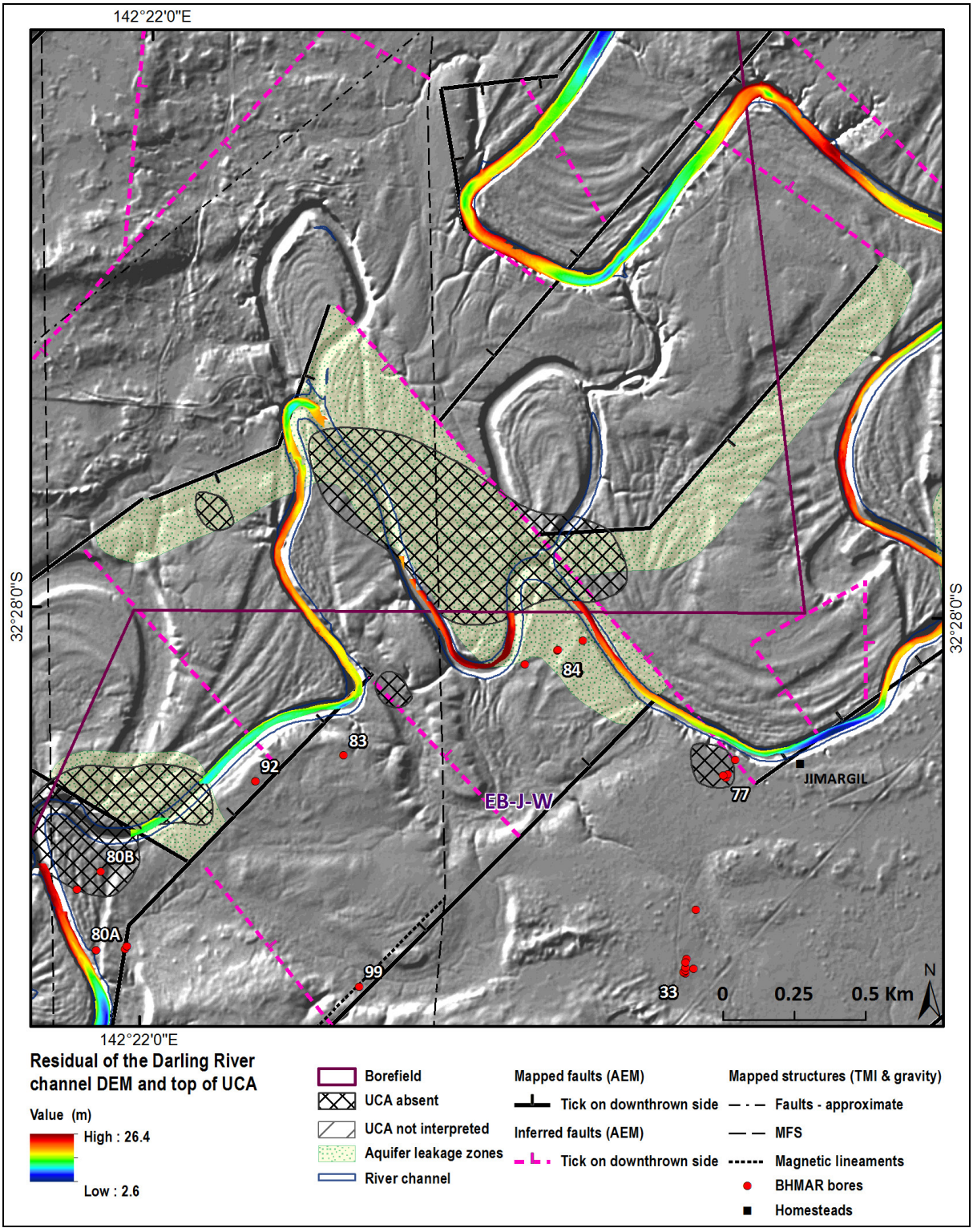

Figure 5-86. *A map of the residual of the Darling River channel DEM and depth to the top of the upper confining aquitard showing erosional holes and inter-aquifer leakage zones for a reach of the Darling River in the northern part of the Jimargil potential borefield site. The residual height of the river channel above the Blanchetown Clay aquitard is shown (blue indicates ~2.6 m; greens ~10 m; reds ~26 m). This image shows the location of erosional 'holes' where the Blanchetown Clay is absent. The location of these holes is effectively fault-controlled (on the down-thrown side of the mapped faults). Potential inter-aquifer leakage occurs at these locations, and where there is significant vertical fault offset (>10 m) on other mapped faults that juxtapose the unconfined Coonambidgal and Menindee Formation aquifers with the underlying Calivil Formation aquifer. These potential inter-aquifer leakage zones are shown in yellow. This image also shows that the course of the Darling River is partially fault-controlled in this reach.*

5.4 QUATERNARY UNITS

The Murray Geological Basin contains sedimentary sequences formed in aeolian, lacustrine, fluvial, marine and marginal marine depositional environments. Towards the north-west basin margin, in the area of interest for this study (Mallee region of western NSW and South Australia) sediment fill is mostly of fluvio-lacustrine origin.

5.4.1 Quaternary Fluvial Units and Geomorphology, Lower Darling Valley

Quaternary fluvial sediments in the Murray-Darling Basin have been studied in detail since at least the 1950s by researchers from a number of disciplines including soil scientists, geomorphologists, fluvial sedimentologists, Quaternary palaeoclimatologists and geochronologists. These studies were mainly concentrated in the Riverine Plain portion of the Murray Basin in southern NSW and northern Victoria and the outcomes of many of the early studies were summarised by Butler *et al.* (1973) and Brown & Stephenson (1991). Two main units were recognised, the Shepparton and Coonambidgal Formations, which were generalised to the whole of the Murray Basin, including the Lower Darling portion, and were used as the stratigraphic framework in the initial interim reports for this project. However, as the BHMAR Project has progressed it has become evident that the different setting of the Lower Darling River valley of the project area has resulted in a stratigraphic framework which is incompatible with elements of the Riverine Plain sequence generalised for the whole Murray Basin. There are significant differences in the depositional setting which are likely to result in contrasting depositional styles, the intra- and inter-formational relationships and the chronostratigraphy. These differences in depositional setting include:

- The Lower Darling is a single fluvial system in a laterally confined, wide, funnel-shaped valley form, which widens southwards into the Murray Basin from a constriction at Wilcannia; very different from the Riverine Plain in the eastern Murray Basin, which has been constructed by multiple fluvial systems as a series of coalescing alluvial fans with their apices at the points where the major rivers debouch from narrow bedrock-confined tracts in the highlands. The Riverine Plain has been dominantly alluvial throughout the Cenozoic history of basin sedimentation, forming a lateral equivalent to the dominantly marine sequence of the western part of the basin. As defined, the Shepparton Formation is the upper part of this thick fluvial sequence, overlying the Calivil Formation and other local units. It is a lateral equivalent of the upper part of the Pliocene marine Loxton/Parilla sands and the Quaternary lacustrine Blanchetown Clay and other Quaternary units and extends into the Late Quaternary (Brown & Stephenson, 1991). Because of the relatively confined nature of the Darling valley, fluvial deposition has probably been more effective through the latest Cenozoic than in the wide distributary fan environments of the Riverine Plain resulting in differences between the nature and relationship of Quaternary fluvial deposits in the two regions.
- A distinct contrast in catchment climate regime exists between the Darling catchment of northern New South Wales and southern Queensland, which extends well into the summer-rainfall zone, and the Riverine Plain catchments that vary from mixed-season to winter dominance from north to south. Some of the Riverine Plain catchments (especially the Murrumbidgee, Murray and Ovens) are further complicated by high-altitude seasonal effects on runoff such as winter peri-glacial conditions and spring snow-pack thaw, which were especially relevant during the cold phases of the Quaternary glacial/interglacial cycles. These factors likely ensured the Darling flow regime was always significantly different in season, regularity and magnitude by comparison with Riverine Plain rivers.
- The Lower Darling has a distal location, far from confined highland valleys.
- The Lower Darling occurs in a more arid setting than the Riverine Plain resulting in a wider variety of aeolian sediments which occur both within the valley and at its margins.
- A generally lower altitude in the Lower Darling which has three important implications, Firstly, there is a change within the valley from fluvial to marine deposition within the Pliocene sequence. In the Riverine Plain the corresponding change occurs at or beyond the western edge of the plain. The potential presence of fluvial, deltaic, barrier, lagoonal, foredune, beach and nearshore facies greatly increases the stratigraphic complexity within the valley. Secondly, in the Lower Darling the Calivil Formation is the fluvial lateral equivalent of the Loxton/Parilla marine and shoreline sands and both are overlain by the Blanchetown Clay deposited in Lake Bungunnia between the late Pliocene and the mid Pleistocene. The Blanchetown Clay extends well up the Darling Valley, as indicated by the

most recent maps of its distribution (Bowler *et al*., 2006; McLaren *et al*., 2009) and by the AEM and drilling data from this project, and it is overlain by significant fluvial deposits. In general, in the rest of the Murray Basin, Lake Bungunnia sediments are widely covered by aeolian deposits, with a relatively narrow, incised, fluvial-sediment-filled Murray River corridor. Thirdly, the impact of base-level lowering during events such as the draining of Lake Bungunnia and incision into the lake floor sediments (Bowler *et al*., 2006) is likely to have extended well up the Darling Valley. These base-level events were too distal to affect sedimentation on the Riverine Plain.

Table 5-16. *Stratigraphic column showing the relationships between geological units, their age, dominant lithologies and hydrogeological properties.*

Lithostratigraphy	Age	Lithology	Hydrostratigraphy	
Coonambidgal Formation (Qa)	Holocene To younger Pleistocene 0 - ?40 ka	Near-surface mud drape	Aquitard, typically unsaturated to partially saturated	
		Sandy base	Shallow unconfined aquifer near leakage, otherwise unsaturated	
Menindee Formation (Qam)	Younger Pleistocene ?50 ka - >150 ka	Muddy top	Thin aquitard, typically unsaturated	
		Sandy base	Shallow unconfined aquifer near leakage, otherwise unsaturated	
Willotia beds (Qaw)	>150 ka - ?500 ka	Mostly sand	Perched or shallow unconfined aquifer near leakage, otherwise unsaturated	
Woorinen Formation (Qdw)	Middle Pleistocene 0 - ?500 ka	Muddy top	Thin unsaturated aquitard	
		Sandy base	Shallow unsaturated sands	
Blanchetown Clay (Qpc)	Older Pleistocene ?500 ka - 2.5 Ma	Mud	Regional confining aquitard, partially to fully saturated	
Chowilla Formation (Tpcs)	?2.5-?2.6 Ma	Sand	Very localised semi-confined aquifer	
Calivil Formation (Tpc)	Pliocene 2.6 - 5.3 Ma	Local muddy top	Locally confining aquitard, typically saturated	
		Predominantly sandy with local muddy units	Regional aquifer, mostly semi-confined to confined. Unconfined marginal to leakage areas.	
Loxton-Parilla Sands (Tps)	Pliocene 2.6 - 5.3 Ma	Fine to medium sands	Regional semi-confined to confined aquifer. Unconfined marginal to leakage areas. Underlying to laterally equivalent to Calivil Formation, southern part of project area only	
Renmark Group (Ter)	Tertiary (Paleocene to Miocene)	Upper Renmark Group- Muds with sandy channels	Local semi-confined to confined aquifer	Aquitard base to overlying Calivil Formation target aquifer
		Middle Renmark Group - Mud with minor sand	Regional aquitard	
		Lower Renmark Group – Sands, silt and lignite	Confined aquifer in regional troughs	
Paleozoic (Devonian)	Paleozoic >251 Ma	Metasediments	Fractured and weathered rock aquifer	

5.4.1.1 Riverine Plain fluvial units

Shepparton Formation

The Shepparton Formation is defined from the eastern Murray Basin in northern Victoria (Lawrence, 1975) and the New South Wales Riverine Plain (Woolley & Williams, 1978) as fluvial and lacustrine deposition that began with the marine Pliocene regression in the west and continued through the Quaternary. It consists of a variable thickness of unconsolidated clay, silt and silty clay with lenses of fine to coarse sand and gravel, and is largely modified by pedogenesis and groundwater processes. As originally defined, it underlies the physiographic Riverine Plain and extends up the Darling Valley and highland valleys on the eastern and southern margins of the Riverine Plain. It is overlain and replaced by aeolian sands of the Mallee Region at its western margin.

The Shepparton Formation is the youngest major unit in the Riverine Plain where its surface forms an expansive flat alluvial plain formed by coalescing low-angle distributary fans on the Lachlan, Murrumbidgee, Murray, Goulburn and Loddon Rivers. Distributaries from the apices of these fans radiate across the plain as remnant traces of inactive meandering leveed palaeochannels with local aeolian source-bordering dune sands. Butler (1950, 1958) identified these distributary palaeochannels from mapped geomorphic/soil/sedimentary characteristics and called them Prior Streams.

Coonambidgal Formation

Subsequent to Butler's recognition of the distributary Prior Stream network, the Coonambidgal Formation was defined as fluvial deposition in a tributary network incised into the older distributary Prior Stream deposits. The modern rivers and an older system of Ancestral Rivers (Pels, 1964), with different channel morphology, were grouped in the Coonambidgal Formation all believed to be late Quaternary. The Coonambidgal Formation consists predominantly of unconsolidated silt, silty clay, sand and gravel with minimal pedogenic modification. Deposition occurred in fluvial channel and floodplain and fluvio-lacustrine environments.

Shepparton Formation – Coonambidgal Formation Relationship

There is an implicit age progression from Prior Streams to Ancestral Rivers to the modern rivers in the Riverine Plain fluvial sequence as originally defined. In addition, there is a morphological contrast between the low sinuosity, bedload-dominated low-leveed Prior Streams and the Ancestral Rivers which have high sinuosity, deep, non-leveed channels and are dominated by suspended load. The modern streams are similar in style to the Ancestral Rivers but with smaller dimensions and their floodplains are often set within the larger Ancestral River channel traces. Radiocarbon chronologies generally supported this scheme with different morphologies interpreted as reflecting successive Quaternary climatic phases.

Bowler (1978) questioned the separation of Ancestral Rivers and Prior Streams into genetically different categories noting that both types can occur in different reaches of the same fluvial system and that some Ancestral River channels carried similar quantities of sand and gravel to Prior Streams. Bowler (1978) suggested that Ancestral River channels might become successively more sinuous and less efficient until avulsion occurs. More recently, detailed stratigraphic studies and luminescence dating (Page & Nanson, 1996; Page *et al*., 2009; Banerjee *et al*., 2002) has demonstrated that the Prior Stream and Ancestral River distinction of chronology and mode of formation is not correct. They demonstrated that Prior Streams are mixed-load lateral accretion streams which terminate with a bedload-dominated vertical aggradation phase which they termed aggradational palaeochannels.

Ancestral Rivers are characterised by lateral migration similar to the early stages of the aggradational palaeochannels but do not progress to a terminal aggradational phase and were termed migrational palaeochannels. Aggradational and migrational palaeochannels were both characterised by larger discharges than the modern steams but importantly can occur at different times or at the same time in different reaches of the same fluvial system. Page & Nanson (1996) suggested that the shift from laterally migrating mixed-

load facies to aggrading bedload facies may be due to a non-linear channel response to threshold exceedance rather than major climatic forcing. They state that higher palaeochannel system discharges place them close to the boundary between sandy meandering and sandy braided streams with inherent instability. In this context major floods can mobilise large quantities of coarse sediment in the confined upstream reaches which cannot easily exit the Riverine Plain due to reducing competency. This stranded slug of coarse sediment initiates a shift to a bedload-aggrading phase and the stream subsequently returns to a laterally migrating, mixed-load system when bedload declines.

5.4.1.2 Quaternary fluvial units in the Lower Darling Valley

The Shepparton Formation as defined in the eastern and southern Murray Basin extends from the Pliocene to the Quaternary and is laterally equivalent to the Pliocene marine regression, the Blanchetown Clay and the mid to late Quaternary Murray-Darling fluvial system. In the Darling Valley no post-Calivil Formation fluvial sediments equivalent to the Pliocene marine regression have been recognised and Lake Bungunnia extended over the whole of the study area, except for 'holes' where Blanchetown Clay may have been eroded or not deposited on local topographic high points in the Calivil Formation. Therefore the Shepparton Formation equivalent in the study area is restricted to post-Blanchetown Clay, mid to late Quaternary fluvial deposition. Furthermore, incision due to base-level lowering after draining of Lake Bungunnia, which would not have impacted the eastern Murray Basin, has differentiated the post-Blanchetown Clay fluvial sequence in the study area into two distinct depositional units, which would not be evident in the eastern Murray Basin. This differentiation resulted in an initial fluvial unit deposited on the Blanchetown Clay followed by subsequent deposition in a lower incised valley. The older higher unit, mostly covered by aeolian sediments, is here termed the Willotia beds and the younger within-valley sediments, which are still flooded in the modern regime, are called the Menindee Formation and the Coonambidgal Formation

The discussion above about the distinction between the Shepparton and Coonambidgal Formations on the Riverine Plain, which questioned the distinction there between the chronology and mode of deposition for the Prior Streams and Ancestral Rivers, has clear implications for the study area. The original recognition and definition of the Coonambidgal and Shepparton Formations was intimately linked to the now discredited Prior Stream/Ancestral River chronological and depositional style concept. The Darling Valley has less complexity than the eastern Murray Basin, with only one fluvial system rather than coalescing fans, a distal location from confined highland valleys and a catchment dominated by summer rainfall that lacks significant higher-altitude components (with resultant snow-pack and peri-glacial runoff impacts). The major control on Darling River deposition is likely to be changes in discharge due to changes in strength or effectiveness of summer rainfall derived from the Australian monsoon. It is evident from the erosional scour channels and large floodplain bars of the northern part of the study area (close to the lateral valley constriction at Wilcannia), that very large floods occurred in the Darling system. If changes in sediment input have played a role in initiating changes in stream depositional pattern they must have been derived from local factors such as mega-flood erosion or changes in local boundary conditions. The distal location from catchment areas and confined valley tracts implies that headwater bedload sediment slugs in response to large floods are unlikely to have resulted in stream morphology shifts due to threshold exceedance as hypothesised for the eastern Murray Basin fluvial systems by Page & Nanson (1996).

It has become evident during this project that the Quaternary fluvial units in the Lower Darling valley do not represent different depositional styles as has been described for the Riverine Plain. Sediments of the Willotia beds and Menindee and Coonambidgal Formations have been deposited by a sequence of discrete lateral-migration episodes by scroll-plain tracts inset into surrounding higher and older floodplain. The youngest of these stratigraphic units, the Coonambidgal formation has been divided into four discrete phases (1-4 from youngest to oldest) which can be differentiated by their cross-cutting relationship and relative freshness of scroll traces which reflects the degree of burial by overbank mud which increases through time. The stratigraphic relationship between these units is presented schematically in Figure 5-87 and Figure 5-88, which give the framework for the more detailed analyses of the stratigraphy, sedimentology and chronology of the Quaternary fluvial units that follows in this section of the report.

The surface expression of these morphostratigraphic units has formed the basis for the recognition of geomorphic units for the regional- and local-scale geomorphic mapping (Figure 5-89 and see Lawrie *et al*., 2012a for details of geomorphic mapping).

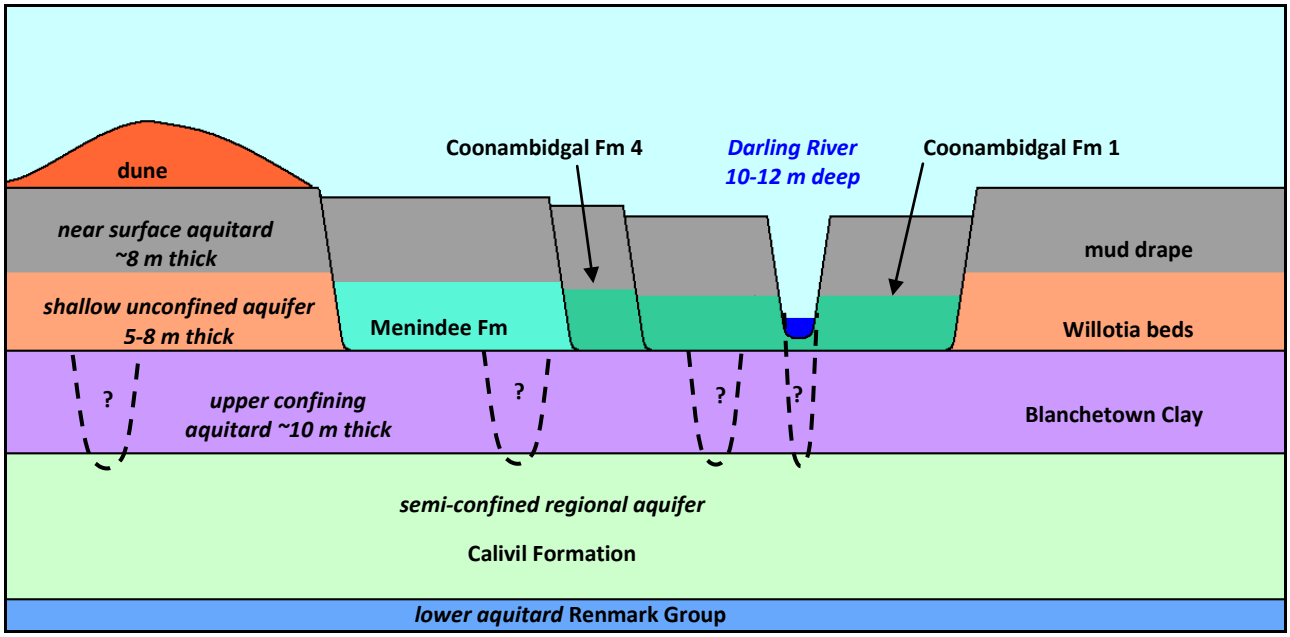

Figure 5-87. *Schematic diagram to illustrate the stratigraphic relationship between Quaternary fluvial units in the Darling River tract of the project area. Each depositional unit represents a lateral-migration phase with lateral-accretion point-bar sand and overbank mud deposition. In the modern regime, all of the Coonambidgal Formation and Menindee Formation units can be flooded and receive overbank mud deposition. Thus, scroll-plain traces are obscured in older lateral-migrational episodes of the Menindee Formation but are still evident in the Coonambidgal Formation phases. The Coonambidgal Formation 4 tract which is a relict scroll-plain adjacent to the Darling River is only drawn on one side of the Coonambidgal Formation 1 Darling River scroll plain to indicate the sparseness of its occurrence The dotted lines and question marks indicate possible deep scour holes in channels.*

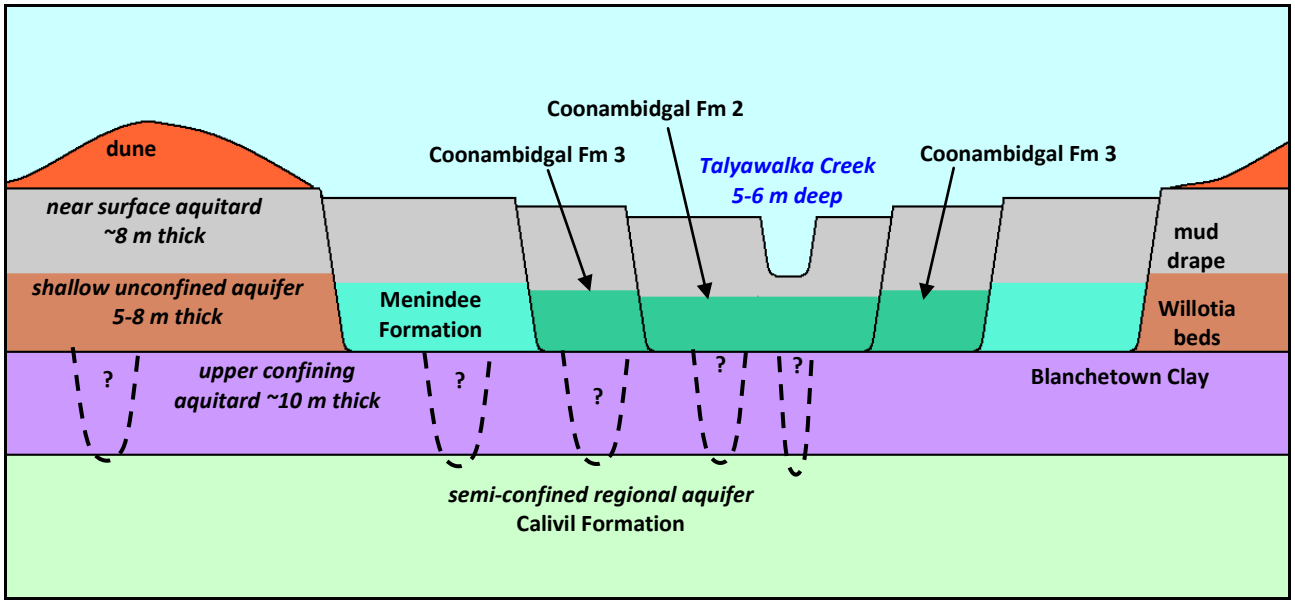

Figure 5-88. *Schematic diagram to illustrate the stratigraphic relationship between Quaternary fluvial units in the Talyawalka-Anabranch tract of the Lower Darling Valley project area. Each depositional unit represents a lateral-migration phase with lateral-accretion point-bar sand and overbank mud deposition. In the modern regime, all of the Coonambidgal and Menindee Formation units can be flooded and receive overbank mud deposition. Thus, scroll-plain traces are gradually obscured in older lateral-migrational episodes of the Menindee Formation but are still evident in the Coonambidgal Formation phases. The Coonambidgal 3 tract which is a relict scroll-plain adjacent to the Coonambidgal 2 Talyawalka-Anabranch tract is drawn on both sides to indicate its more common occurrence than the Coonambidgal 4 relict scroll plain adjacent to the Darling River (Figure 5-87). The dotted lines and question marks indicate possible deep scour holes in channels.*

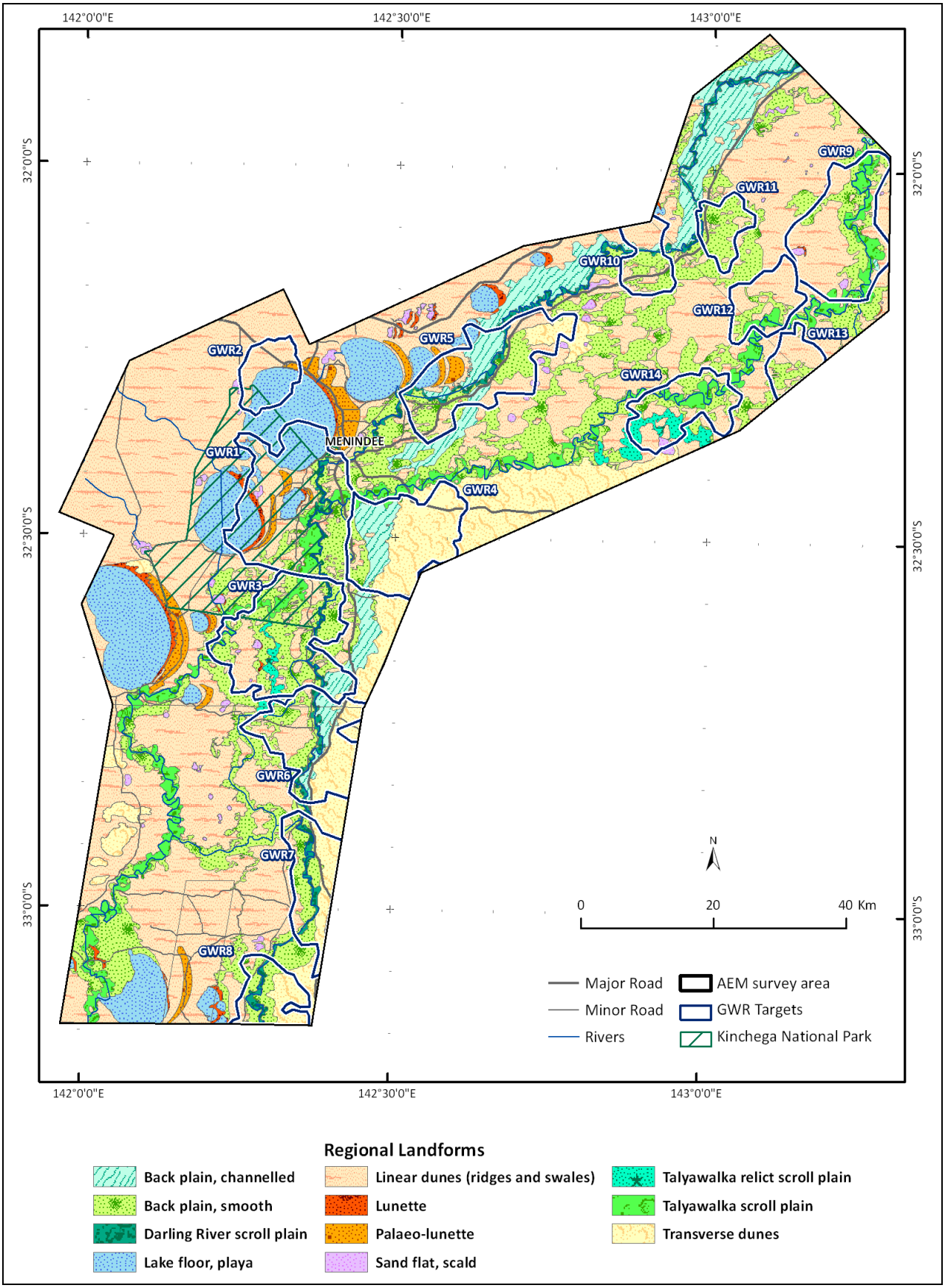

Figure 5-89. *Map of surface landforms mapped at a regional scale in the BHMAR study area. More detailed mapping was carried out at local scales to assist with recharge mapping.*

5.4.1.3 Willotia beds

The new term Willotia beds is here used for sediments not sufficiently well known to give them full formation status. In earlier interim reports for this project the informal name Redbank unit was used for these sediments with that name derived from the initial site where they were examined – a cliff exposure adjacent to the Redbank Creek on Willotia Station south of Lake Tandou. The name Redbank was later deemed as unsuitable due to multiple prior uses recorded in the Australian Stratigraphic Index at Geoscience Australia and the alternate name of Willotia beds has subsequently been approved and reserved with the Stratigraphic Index.

Tedford (1967) recognised that fluvial deposits exposed in the Pamamaroo-Menindee canal were higher than the younger sediments to the east on the Darling floodplain. Accordingly, he discussed the possible influence of base-level control on Darling flood-plain sedimentation in the Menindee area due to incision of both the lower Darling and Murray rivers into the Blanchetown Clay when Lake Bungunnia was drained by downcutting of its outlet. It is possible that deposition of the Willotia beds commenced as down-valley and lateral fluvial and deltaic units feeding into Lake Bungunnia. As the level of Lake Bungunnia lowered, later deposition of Willotia beds fluvial sediments transgressed over and/or were deposited in valleys that incised the Blanchetown Clay. Following full draining of Lake Bungunnia the lowered base level induced incision of the lower Murray into the Blanchetown Clay (Bowler *et al.*, 2006) and nick-point retreat up the Darling Valley, which would have quickly produced relatively narrow incision into the Willotia bed flood-plain deposits. After reaching base level the ancestral Darling began to laterally widen its new valley incised into the Willotia and older units and depositing the Menindee and Coonambidgal Formation fluvial sediments. Therefore the Willotia beds refers to a suite of fluvial to lacustrine sediments that overlie the Blanchetown Clay at higher elevations bounding the Darling Floodplain (where the Menindee and Coonambidgal Formations are deposited) in the Tandou-Menindee area and beneath the beds of the Menindee Lakes. It is not numerically dated, but its stratigraphic and cross-cutting relationships provide relative age constraint with respect to other stratigraphic units. It is older than the Blanchetown Clay and younger than the Menindee Formation.

The Willotia beds are thought to conformably overlie the Blanchetown Clay, i.e. with essentially continuous deposition from dominantly lacustrine muds to a combination of fluvial and lacustrine sands to muds. They were eroded by the palaeo Darling River system to form the trench in which the Menindee and Coonambidgal Formations were deposited, and thus predate these units with an erosional hiatus separating them. This relationship is evident at all sites where the Willotia beds are exposed, overlain by aeolian sediments, in cliff sections marginal to the incised floodplain sequences of younger units. Sediments overlying the Blanchetown Clay beneath the Menindee Lakes include sands as well as muds, of variable thickness as shown by the logs of holes BHMAR18-1 (13.8 m thickness), BHMAR 22-1 (10.5 m thickness) and BHMAR 64-1 (7.7 m thickness) (See Appendix 1, Halas *et al*., 2012a). These lake-floor sediments almost certainly include time equivalents of the Menindee and Coonambidgal Formation fluvial units in addition to Willotia age sediments but the lithologies of all three are identical and accurate boundaries between units cannot be determined. Therefore the whole of the post Blanchetown Clay lake-floor sediment sequence is somewhat arbitrarily referred to the Willotia beds, although it is not certain which portion of them was deposited by the same pre modern fluvial to lacustrine system that deposited the Willotia beds in higher elevation areas.

The Willotia commonly has a fine-grained muddy facies, probably mostly fluvial overbank mud but also including some lacustrine muds, which is mostly olive-green to grey but has a strong pedogenic overprint which includes red/yellow/orange mottling and secondary pedogenic or groundwater gypsum often in the form of large nodules of inter-grown selenite crystals. This lithology is also common in the Blanchetown Clay, as is evident from outcrop descriptions in Murray River banks and other sections south of the project area (Bowler *et al.*, 2006; McLaren *et al.*, 2009, 2011, 2012) and from BHMAR Project drill cores (see Section 5.3). During initial BHMAR Project investigations, deformation of the Blanchetown Clay was not recognised and a number of outcrops of this distinctive lithology close to 70 m AHD in the region were accordingly referred to the Willotia beds. These outcrops included (Figure 5-90):

- Valley-margin cliff exposures adjacent to Redbank Creek on Willotia Station south of Lake Tandou and adjacent to the Great Darling Anabranch on Cuthero Station further south

- A Darling River bank exposures on Viewmont Station
- Exposures described by Chen (1992) in the floor and walls of the Lake Cawndilla outlet canal and referred by Chen (1992) to the Blanchetown Clay.
- Weathered clay-rich sediments high in the pit walls of the Ginko and Snapper mineral sand mines just south of the study area, attributed to the Blanchetown Clay by company geologists.

Subsequent detailed section-by-section analyses of the Blanchetown Clay in the AEM inversion data has demonstrated that there are places where the Blanchetown Clay is deformed, or at least departs from its more usual uniform horizontal orientation across the study area. One such occurrence is at the Viewmont riverbank section area where the Blanchetown Clay rises from about 40 m AHD to just over 60 m AHD over about 5 km distance from south east of the Darling to the river. The elevation and thickness of the Blanchetown Clay in BHMAR 05-1 in this area verifies the reality of the AEM interpretation which identifies the muddy unit with its top at about 66.7 m AHD as the Blanchetown Clay rather than Willotia beds. Alternatively, the AEM interpretation of sections through the valley margin cliffs at Cuthero and Redbank Creek show horizontal Blanchetown Clay passing under the cliff at elevations of below 40 m AHD, an interpretation confirmed by the conductivity and gamma logs of the BHMAR mud rotary holes 1A and 74 located 280 m west and 1220 m east of the Redbank Cliff section respectively.

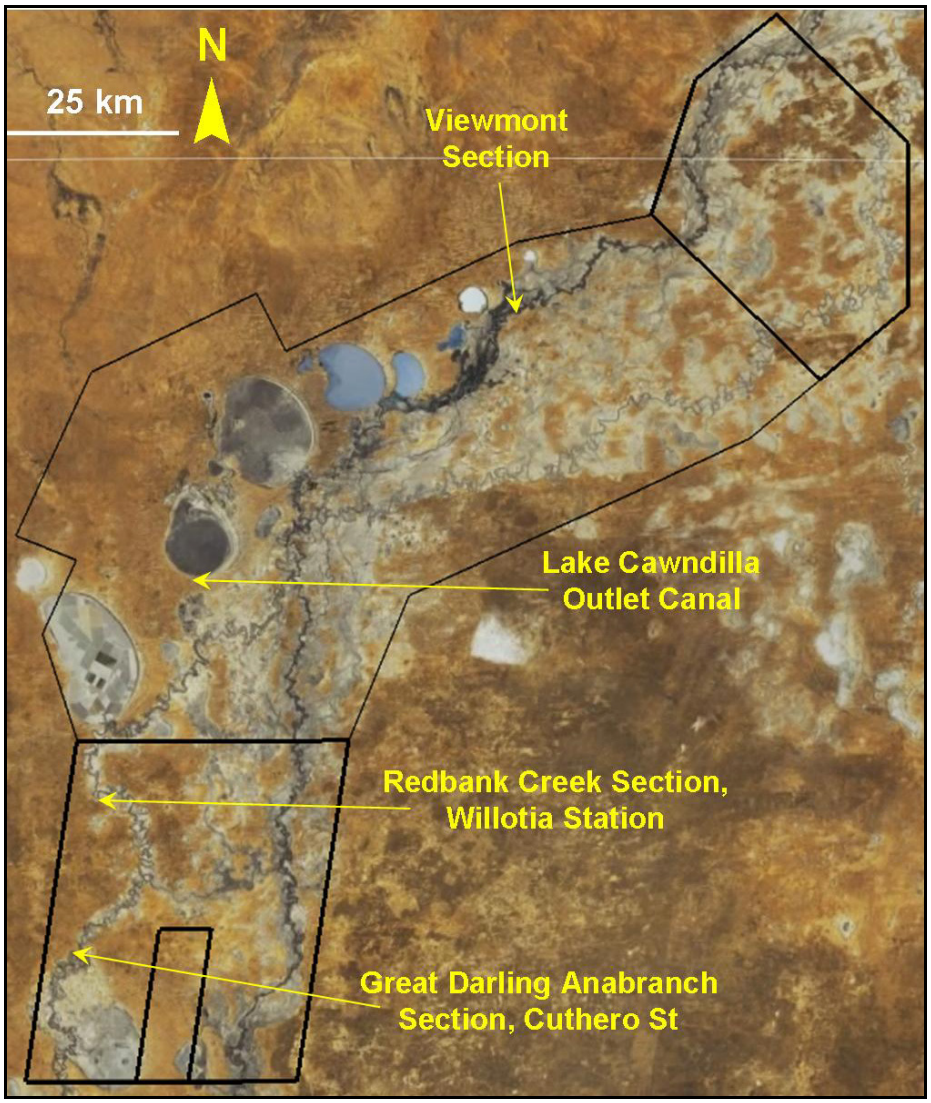

Figure 5-90. *Google Earth image showing the BHMAR project area on with the location of natural exposures of the Willotia beds and the Blanchetown Clay discussed in the text.*

Similar sediments were also recognised in some BHMAR project drillholes located at elevations close to 70 m AHD across the study area both outside the main Darling valley tract and on larger aeolian areas located within the northern Darling Valley between the Darling and Talyawalka channel tracts. Initial AEM data was equivocal as to whether the upper clay-rich unit in these areas was overlying the Blanchetown Clay or was restricted to areas where Blanchetown Clay is absent and could therefore represent laterally equivalent facies at the margins of islands of high ground during the time of Blanchetown Clay deposition. However, subsequent detailed analysis of AEM line sections and reassessment of some BHMAR drillholes clearly demonstrates Blanchetown Clay overlain by the upper clay-rich unit demonstrating that the latter is a depositional phase that is younger than or continued longer than Lake Bungunnia deposition. The upper fine-grained stratigraphic units cannot be discriminated lithologically, in an isolated exposure, drill section, geophysical down-hole log or AEM section and attribution to a specific stratigraphic unit requires multiple lines of evidence. Table 5-17 summarises the BHMAR drillholes that intersect the Willotia beds and the details are presented in the Strater™ Sections (Appendix 1, Halas *et al*., 2012a).

Table 5-17. *Summary of Willotia beds stratigraphy as intersected by BHMAR boreholes.*

BHMAR Drillhole	Willotia stratigraphy
BHMAR1A-1 BHMAR1B-1	Cuttings of the Willotia beds in these holes are mud, in part sandy. However, wireline logs indicate that sands are also present, especially towards the base. BHMAR1A was drilled in part to determine the stratigraphic relationships of the clay exposed in Redbank cliffs (see above).
BHMAR19-1 BHMAR19-2	Sonic core from BHMAR19-1 shows an 18 m thick fining up sequence above the Blanchetown Clay, with medium to coarse sand at the base, grading through fine sand to gypseous muddy sand and sandy mud, with 1 m of crystalline gypsum.
BHMAR63-1	Willotia beds are interpreted to overlie Calivil Formation directly in this hole, the Blanchetown Clay being absent. Cuttings of the interpreted interval are mud, and the wireline logs indicate that mud predominates. The underlying Calivil Formation shows predominantly sandy gamma and conductivity responses.
BHMAR36-1	Sonic core from this hole shows 14 m of fine to coarse sand, in part muddy, above the Blanchetown Clay. This interval is referred to the Willotia beds.
BHMAR51-1	30 m of mud and fine to coarse sand overlying the Blanchetown Clay in this rotary drillhole are interpreted as Willotia beds. Wireline logs indicate a considerable amount of sand in this interval.
BHMAR53-1	A 12 m sequence of mud above interpreted Blanchetown Clay is referred to the Willotia beds. Cuttings are mud, but the wireline logs suggest at basal sandier section.
BHMAR62-1	A 10 m sequence of mud above the interpreted Blanchetown Clay and beneath lunette deposits is referred to the Willotia beds in this rotary hole
BHMAR18-1, 22-1 and 64-1	These sonic core holes on the bed of Lake Menindee all intersected a fining upward sequence of sand to mud above the Blanchetown Clay. This sediment is interpreted to be part of the Willotia beds, although they may have a different genesis and age to other occurrences away from the lakes.

Redbank Cliff

The Redbank cliff section is a ~ 500 m long vertical and sub-vertical exposure up to 6-7 m in height which forms an impressive abrupt step in the local landscape (Figure 5-91, Figure 5-92). The section (Figure 5-93, Figure 5-94) has 3 m of Woorinen Formation aeolian sand with a well-developed calcareous soil and a sharp erosional contact at the base. A secondary pedogenic carbonate hardpan occurs at the base of the upper aeolian unit. Underlying the erosional break at the base of the aeolian sand is 3-4 m of Willotia beds hard dry red-brown to olive grey mottled clay, with vertical concoidal cracking, that becomes dominantly olive-grey at depth. A distinctive 10 cm thick dark band rich in secondary pedogenic manganese nodules occurs close to the top of the Willotia beds mud unit. Exposed at the toe of the slope and in front of the cliff are interbedded fluvial clayey sand and sandy clay, which was investigated in a shallow hand-auger hole. Some pedogenic gypsum nodules occur in the upper part of the interbedded fluvial sands at the toe of the slope. The Willotia beds unit is interpreted as ancient well weathered fluvial overbank mud overlying fluvial sediments and capped by dune sands of the Woorinen Formation. The nearby drillholes BHMAR 1A and BHMAR 74, on

either side of the cliff section, show that the Willotia beds unit is stratigraphically above what is interpreted as Blanchetown Clay at about 40 m AHD in both drillholes (Figure 5-95). Rotary cuttings of the interval from 40.1 to 63.6 m AHD in BHMAR1A, which is equivalent to the Willotia beds in the outcrop, are sandy mud and the conductivity log suggests some interbedded sandier beds above the interval interpreted as Blanchetown Clay.



Figure 5-91. *The Redbank Creek cliff section on Willotia Station, view north-west.*

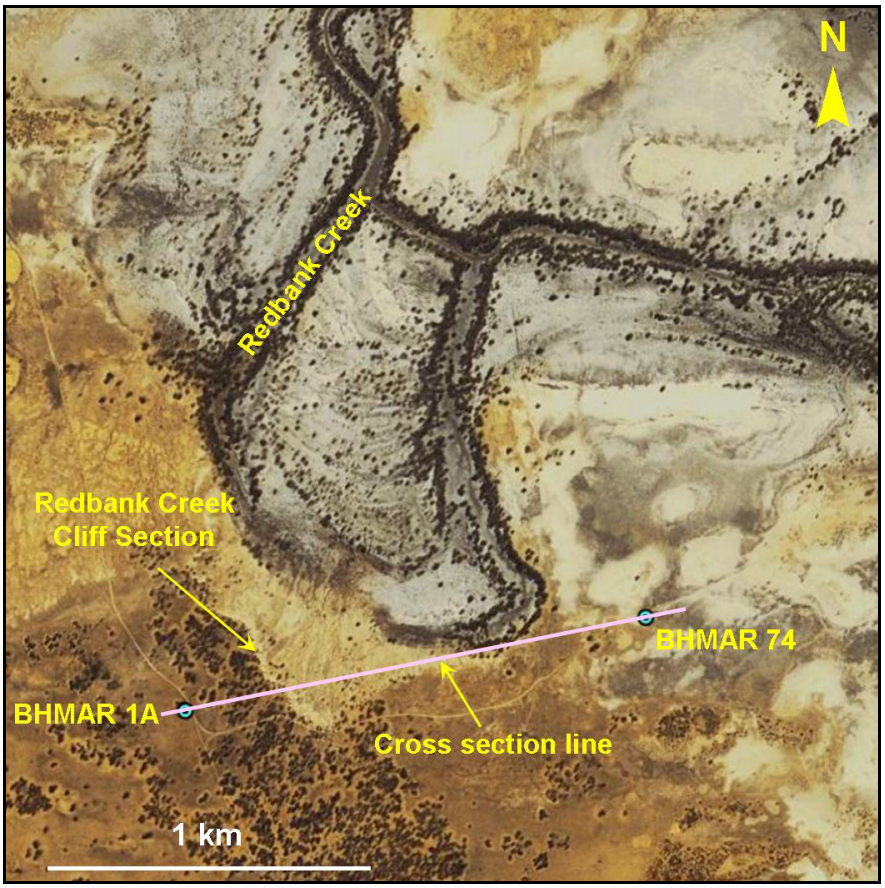

Figure 5-92. *Showing the location of the Redbank Creek cliff section (Figure 5-91) on a Google Earth image. The line of cross section marks the location of the profile in Figure 5-95.*

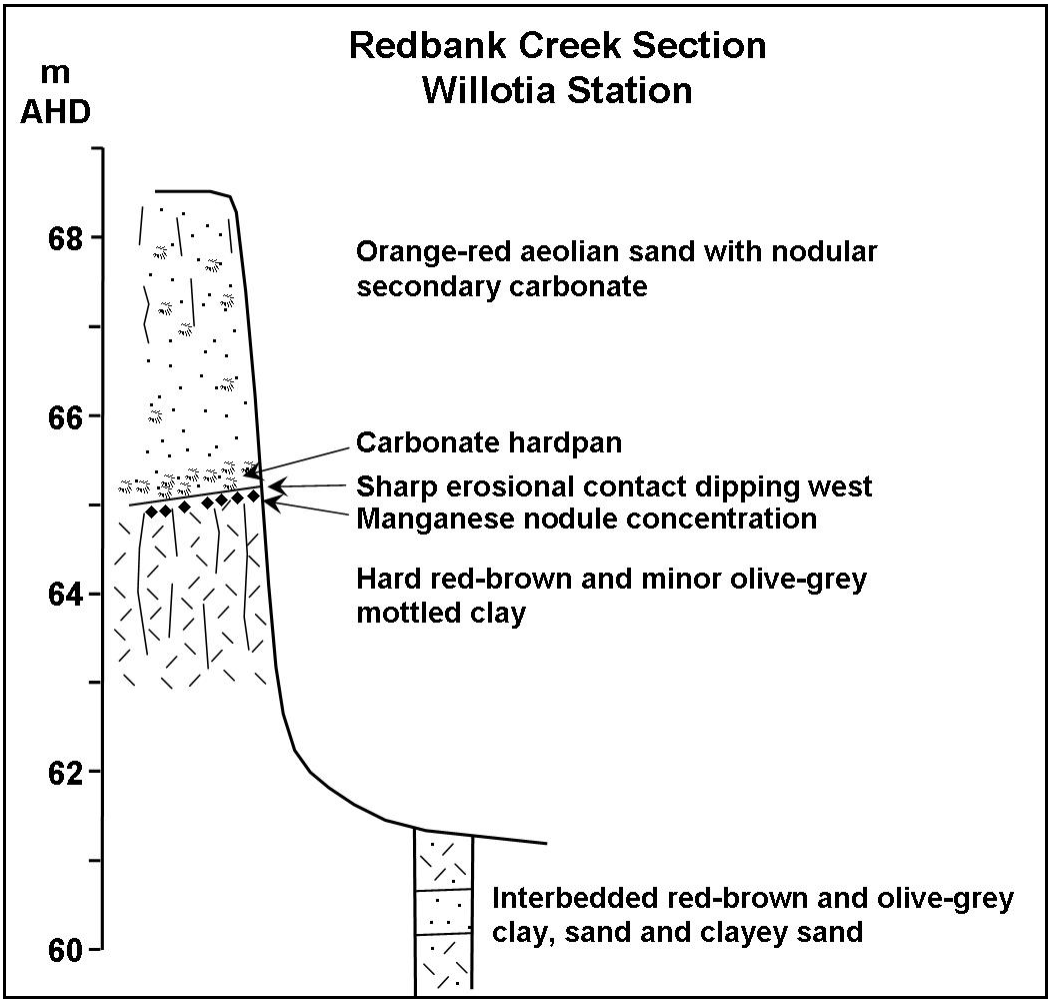

Figure 5-93. *Stratigraphy of the Redbank Creek cliff section.*

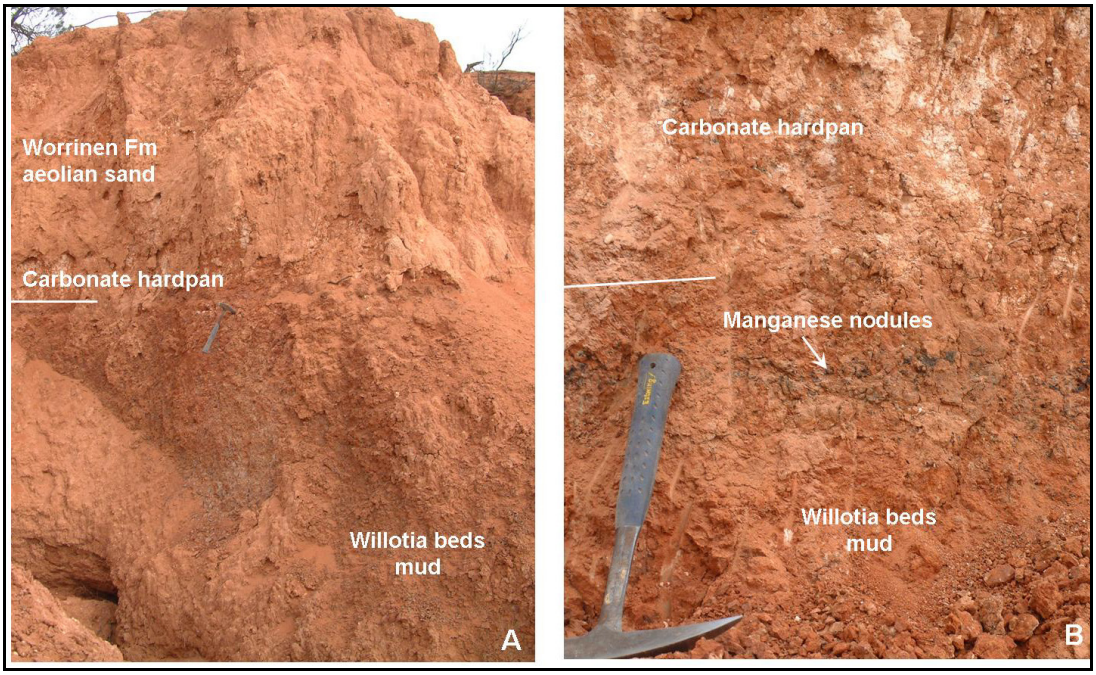

Figure 5-94. *Redbank Creek cliff section showing the aeolian sand overlying the Willotia beds mud (A) and a detailed view of the boundary (B). The white line in both A and B marks the level of the boundary.*

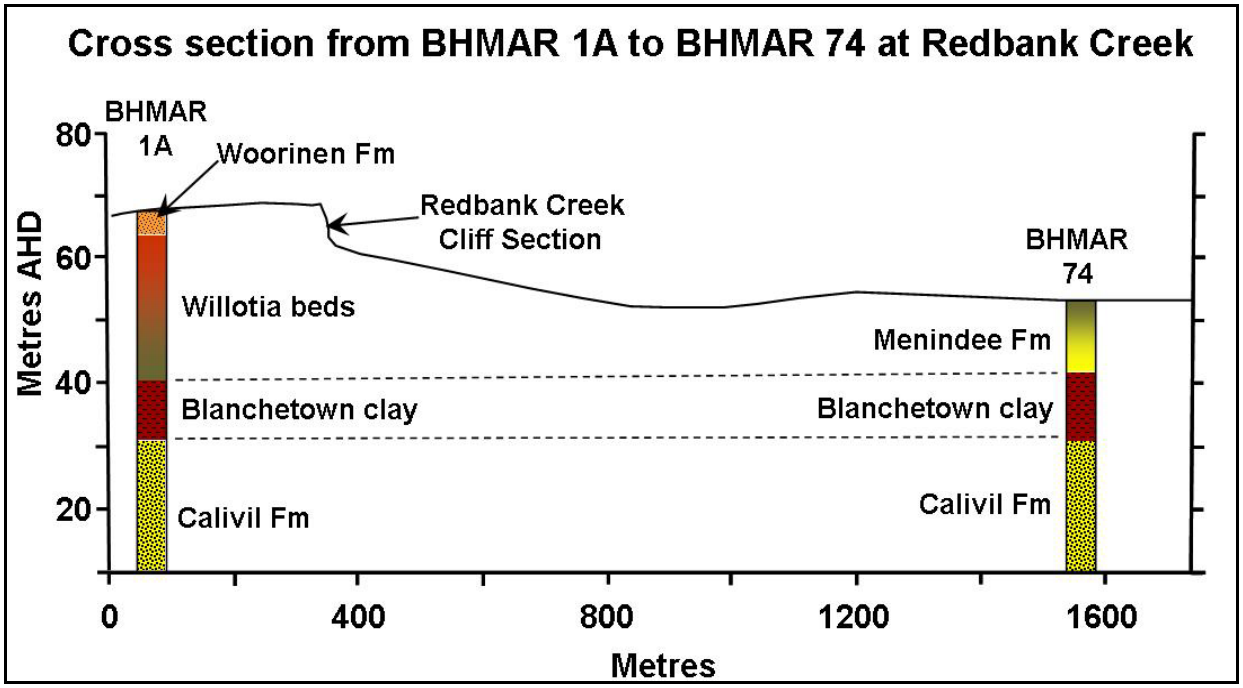

Figure 5-95. *East-west cross section from BHMAR 1A to BHMAR 74 through the Redbank Creek cliff section. The line of section is shown on Figure 5-92.*

Lake Cawndilla Outlet Channel section.

The artificial outlet channel from Lake Cawndilla (Figure 5-90) was made wider by erosion during an uncontrolled spill of the impounded water in Lakes Cawndilla and Menindee due to catastrophic failure of the embankment at the Cawndilla outlet regulator in 1964. This erosion generated vertical exposures at the channel walls for several hundred metres downstream of the outlet which expose the lunette and underlying sediments. Chen (1992) described clay with gypsum nodules exposed in the walls and identified this as possible Blanchetown Clay. Our observations down the channel show that several metres of weathered gypseous clay underlies aeolian sand at this location, and that the clay has a sharp lower contact with fine grained sand. AEM sections suggest that the Blanchetown Clay lies beneath the level of the channel floor at ~ 40 m AHD at this location, and thus the clay and the underlying sand are regarded as part of the Willotia beds Figure 5-96.

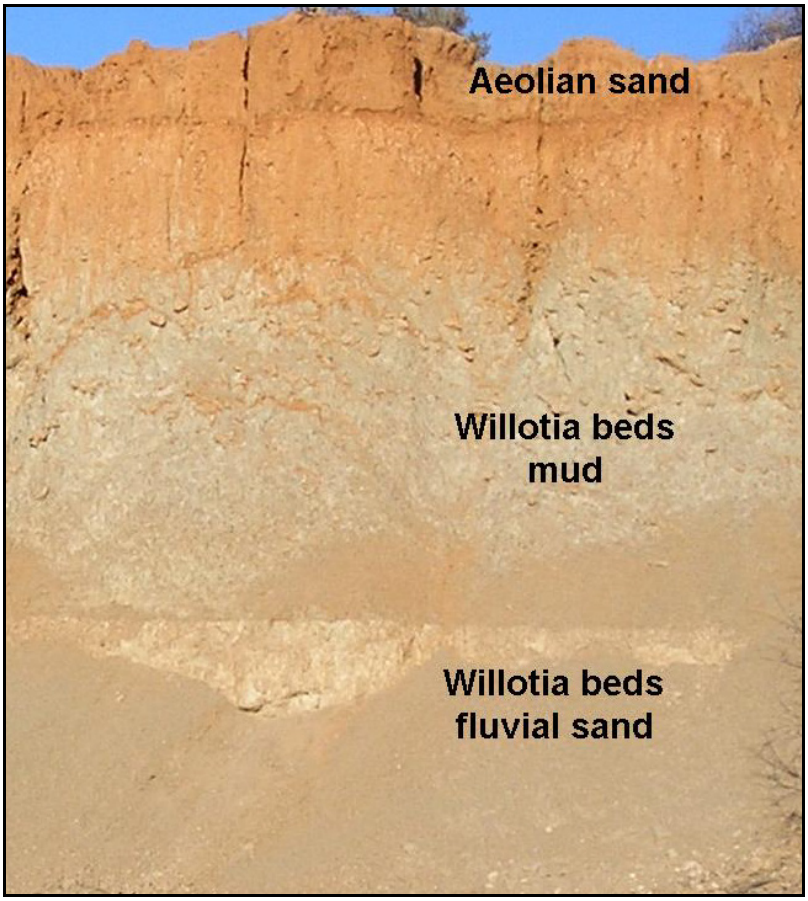

Figure 5-96. *Section exposed in the southern wall of the eroded Cawndilla outlet channel approximately 100-200 metres downstream of the outlet regulator. The section shows aeolian sand overlying mud and fluvial sand referred to the Willotia beds, the upper portion of the Willotia beds mud layer is obscured by orange sand washed down the cliff face from the overlying aeolian sand unit. The exposure is approximately 4-5 m high.*

Darling Anabranch cliff section on Cuthero Station

Another stream-marginal cliff section that forms an abrupt step in the local landscape occurs near the northern margin of Cuthero Station on the western margin of the Great Darling Anabranch at a position where outside-bend bank erosion of the steam is eroding into the western margin of the valley (Figure 5-90 and Figure 5-97). The cliff section (Figure 5-98 and Figure 5-99) exposes about 2 m of orange-red aeolian sand with nodular secondary carbonate overlying at least 8 m of mottled green-grey mud with yellow-red iron-iron-stained sandy mud patches and secondary pedogenic manganese nodules. Low in the cliff face there are large (~10 cm) nodules of intergrown selenite gypsum within the mud and a white probably gypsum efflorescence on the face of the outcrop (Figure 5-99B). The gypsum nodules have probably grown by slow displacive growth from shallow saline groundwater of meteoric origin and the efflorescence from evaporation at the cliff face from the same groundwater source.

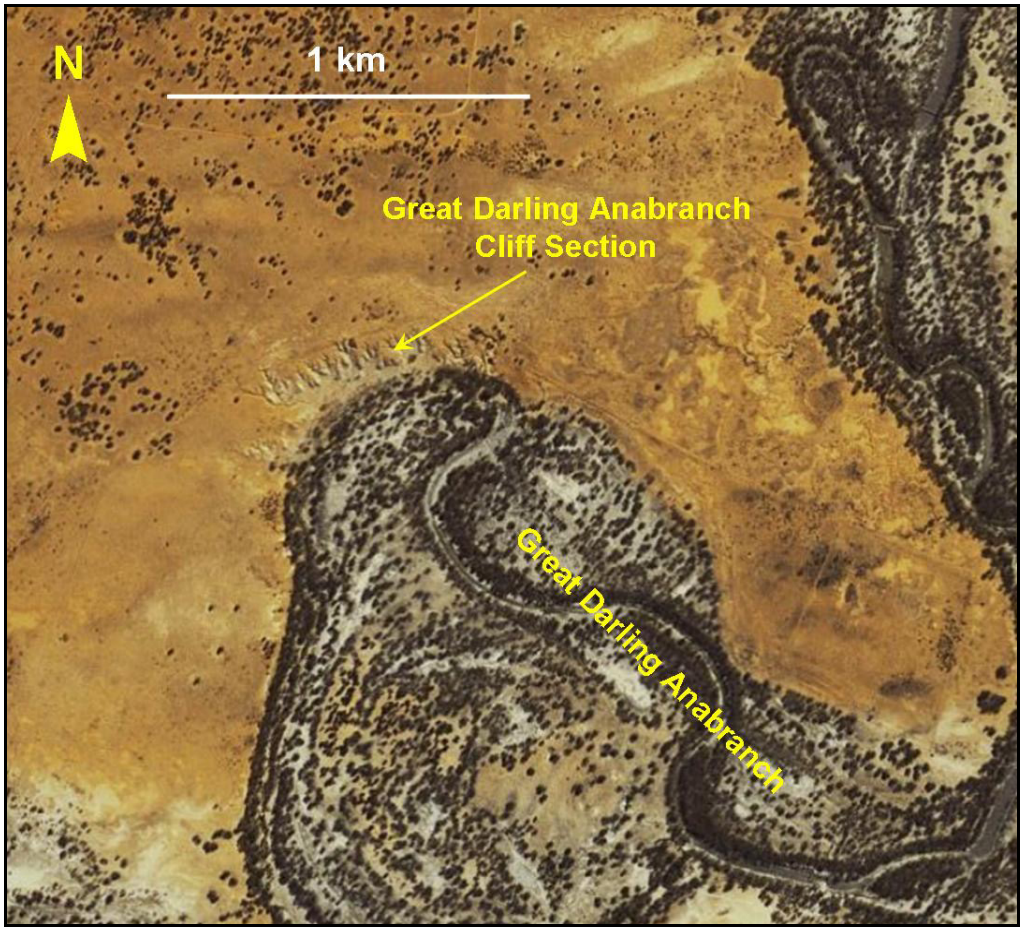

Figure 5-97. *Showing the location of the Great Darling Anabranch cliff section on Cuthero Station on a Google Earth image.*

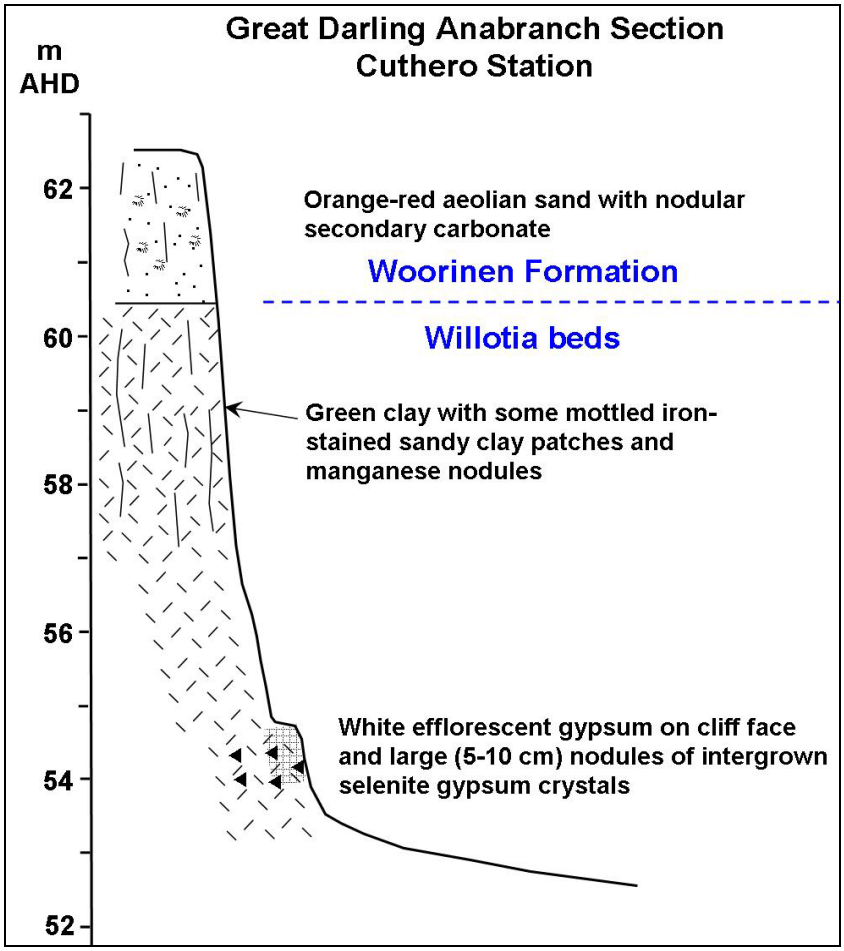

Figure 5-98. *Stratigraphy of the Great Darling Anabranch cliff section on Cuthero Station.*

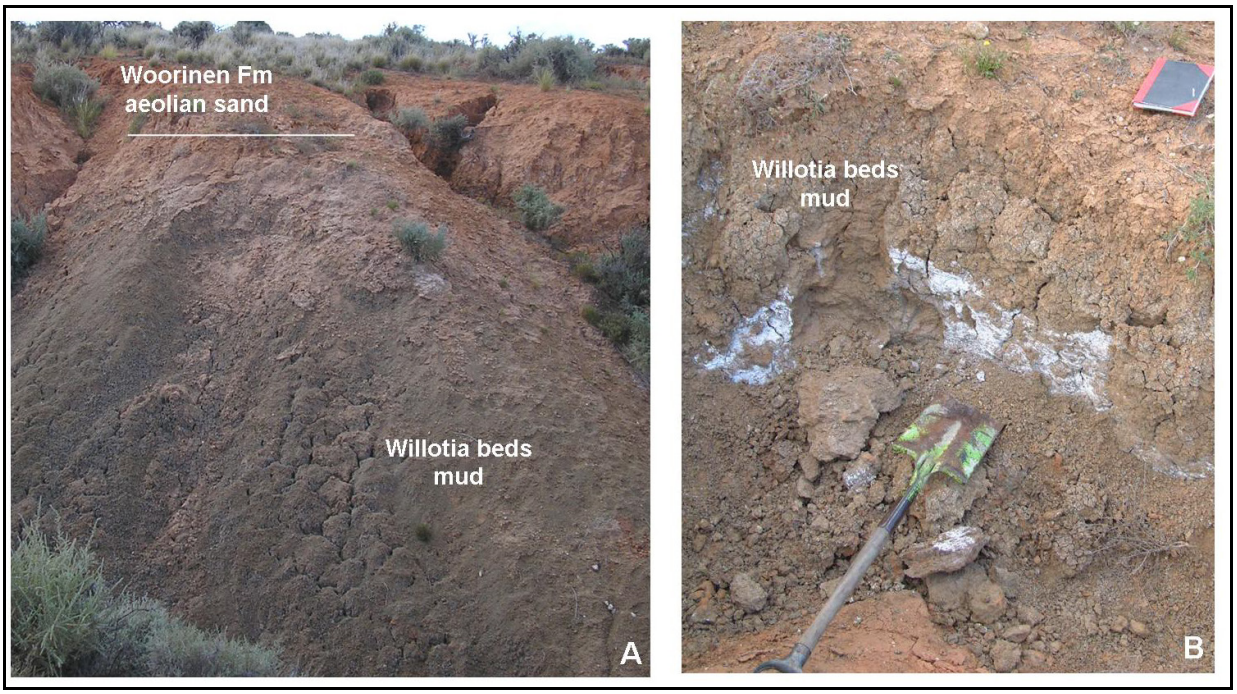

Figure 5-99. *Great Darling Anabranch cliff section photo showing Woorinen Formation aeolian sand overlying the Willotia beds mud (A). Photo B shows the white gypsum efflorescence on the surface of the mud unit near the base of the cliff.*

5.4.1.4 Menindee and Coonambidgal Formations

In the time since incision into the Willotia beds reached base level, lateral migration has widened the valley which contains the subsequent fluvial sediments, which have been deposited by a number of successive lateral-migration phases. These phases have often occurred at times of enhanced monsoon runoff but have been initiated by unknown processes. During these more active phases bank erosion and more competent down-valley transport provide sufficient bedload for mixed-load lateral-migration systems with channel and scroll-plain morphologies that reflect the discharge magnitude. Thus the Talyawalka and other anabranch systems with larger amplitude meanders, scroll radius of curvature and meander wavelengths represents significantly higher discharge than the Darling scroll plain (Bowler *et al*.,1978). Channel avulsion spatially separates different phases and deposition of overbank muds, from large flood events gradually obscures the older scroll plain deposits. Thus, unlike the Riverine Plain, All the Quaternary fluvial units in the Darling valley have the same depositional style, being deposited by successive inset lateral migration phases. As the whole flood plain can still be inundated, overbank deposition continues on all morphostratigraphic units. Thus earlier scroll plain traces are progressively obscured by burial under overbank muds. In the stratigraphic scheme adopted for this report the higher older flood plain, lacking scroll-plain traces, is referred to the new name Menindee Formation and the inset lower younger scroll-plain phases retain the name Coonambidgal Formation.

Conceptual depositional model

There is a very well developed standard depositional model for meandering rivers which deposit point bars and scroll plains by sand deposition during lateral migration and deposit overbank muds on the surrounding floodplain by vertical accretion (Walker and Cant, 1984; Miall, 1996). This model has been derived from study of a number of ancient and modern examples and Figure 5-100 illustrates the morphology and depositional elements that make up the facies model.

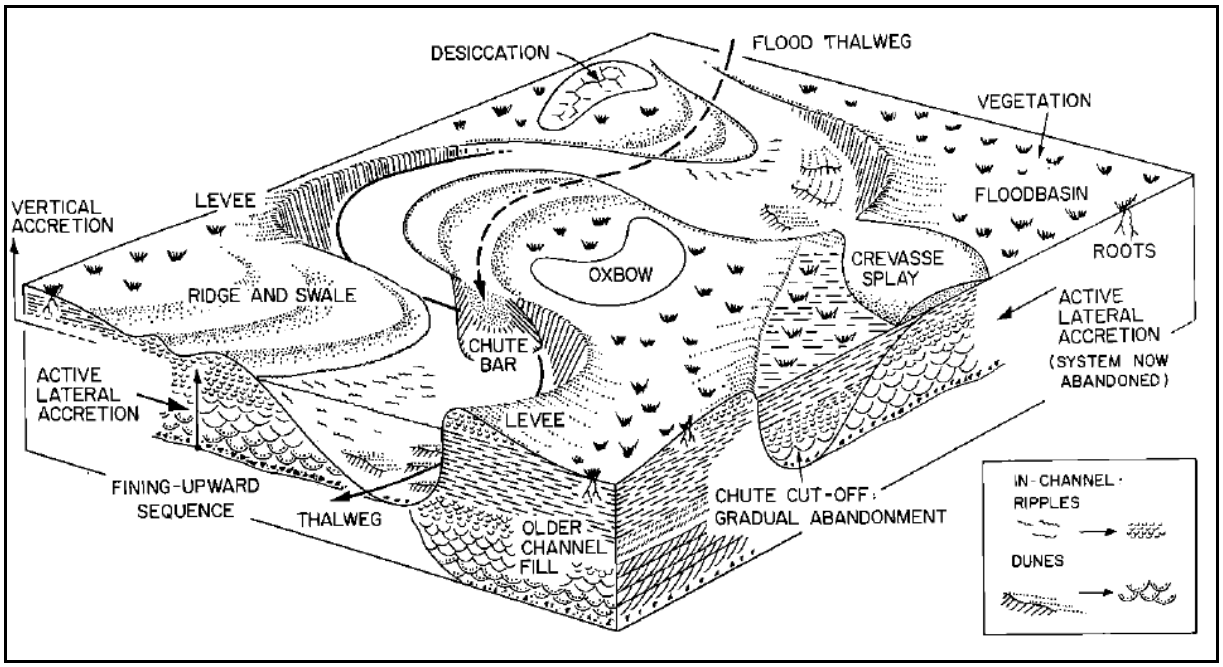

Figure 5-100. *Block diagram showing the morphology and depositional elements of a meandering river with construction of point-bar scroll plains by lateral migration and with vertical accretion of overbank muds on the surrounding floodplain (from Walker and Cant, 1984). This conceptual depositional model is applicable to the Menindee and Coonambidgal Formations.*

The channel meanders by erosion of the outer bank of the meander loop and deposition on the inner point-bar bank with a lag deposit of coarse sand and gravel on the channel floor which moves during floods. Typical sandy-channel bedforms preserved lower in the point-bar sequence, consist of trough cross bedding which passes up to ripple cross bedding in finer grained sands. Episodic lateral accretion and erosion can result in preservation of former point-bar surfaces within the sequence (lateral accretion surfaces) and a ridge and swale topography on the point-bar surface (scroll bar patterns). Erosion of the outer cut bank results in either or both lateral and downstream migration of meander loops. Lateral migration results in increased channel length, lowered slope and increased inefficiency and probably is the main driving force for meander cut-off which can occur by chute channel cut-off across point bars or by neck cut-off of whole meander loops. Both processes result in abandonment of the former channel and the formation of ox-bow lakes (most commonly called 'billabongs' in Australia) which are subsequently in-filled with mud. Outside the channel, floods deposit fine-grained sediments on the floodplain and in ox-bows and abandoned channels, which build up vertically and are therefore called vertical accretion. The coarsest silt-dominated component of this sediment is deposited as levees at the channel margins, where floods first exit the channel. On the floodplain, finer mud with abundant clay is deposited where flood flow is reduced or stagnates. Following recession of the flood these overbank mud deposits can desiccate and also be colonised by vegetation; cracking, rootcasts and soil formation are common secondary structures in these deposits. If floods breach the levees, relatively thin and laterally confined crevasse splay sand bodies can extend across the floodplain and commonly fine upwards to fine ripple cross-bedded sand.

This model ideally results in a sequence that fines upward from coarse channel-lag sand and gravel through plane-bedded and trough cross-bedded coarse to medium sand and ripple cross laminated medium to fine sands to fine overbank mud often showing desiccation cracks, vegetation traces and soil formation. However, lateral migration, particularly when contained in a confined valley tract, very commonly results in erosion and reworking of earlier deposits leading to preservation of incomplete and multi partial-episode sediment stacks.

The Menindee and Coonambidgal Formation deposits have been examined in satellite images, AEM inversion depth slices and line sections, river bank exposures, tractor-excavated pits (to 3-4 m), hand-auger holes (to 6 m) and sonic-cored and mud-rotary drillholes. They show examples of all the depositional elements illustrated in the conceptual depositional model, though many of those features are difficult to illustrate effectively in drill cores. Some examples of the depositional features are shown in Figure 5-101 to Figure 5-105. There are some features of the Darling Valley lateral-migration depositional phase deposits which are probably atypical when compared to the standard model. The channel lag deposits are generally coarse to very coarse sand and have sparse gravels. This reflects a combination of the low gradients and distal location from the highland sources. Local lateral-valley tributaries from elevated rocky terrain to the west in the Scopes and Barrier Ranges may have introduced some coarser clastics but are also characterised by low gradients as they approach the Darling. The modern Darling is a suspended-load stream with minimal bedload and no scroll-plain lateral migration currently occurring and its channel is characterised by a significant number of relatively deep holes generally ranging from 2-5 m in depth but with the deepest extending to 8 m. Most holes occur on bends where turbulence is at a maximum but typically do not conform to the standard cross-sectional morphology, with the deepest point located at the outside edge of bends, which is typical of meandering rivers. Their genesis and maintenance is attributed to scour but their exact mode of formation is equivocal. From BHMAR drillholes, the average thickness of the lateral-migration depositional phases is 14.3 m for the Coonambidgal Formation and 14.1 m for the Menindee Formation but the maximum thicknesses are 23 and 29 m respectively (Table 5-20). These extremes probably represent channel scours or holes similar to those evident in the modern Darling.

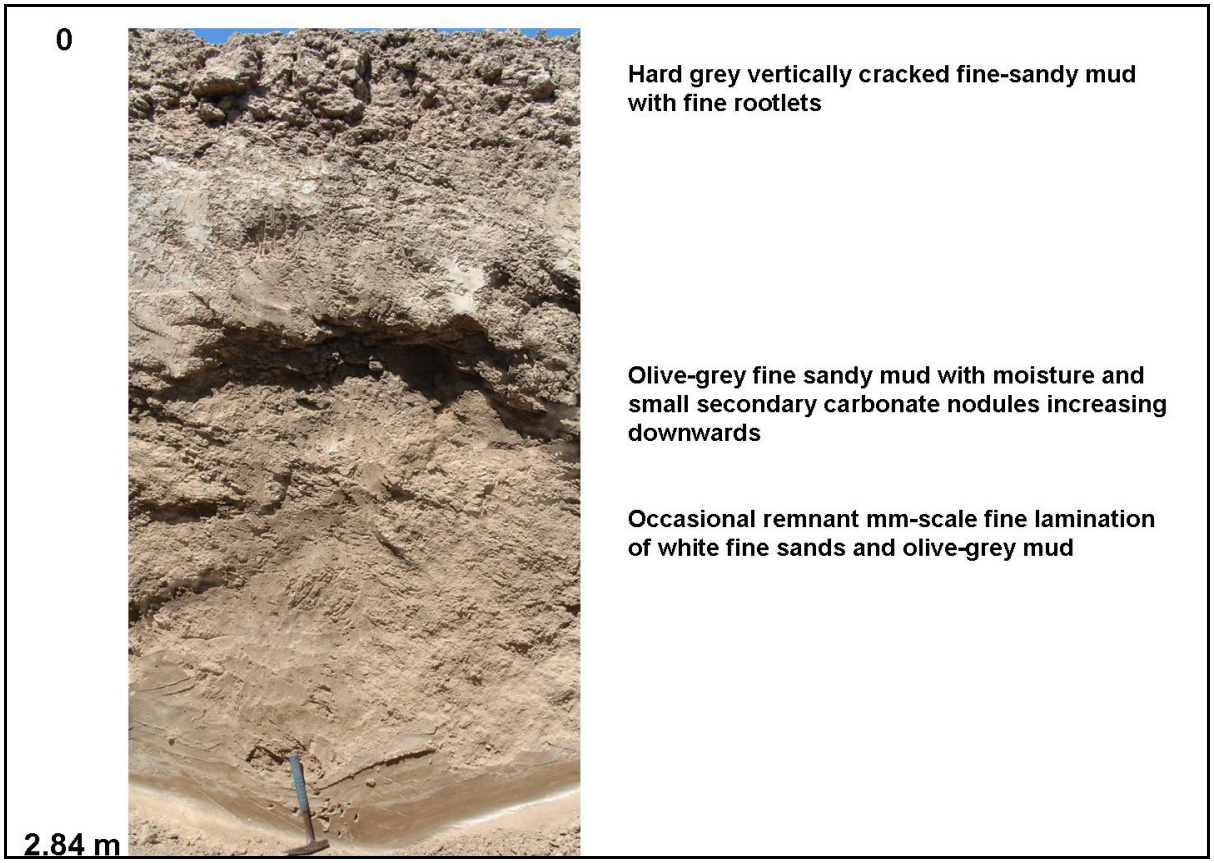

Figure 5-101. *Menindee Formation floodplain-deposited overbank mud on the Three Mile Creek floodplain.*

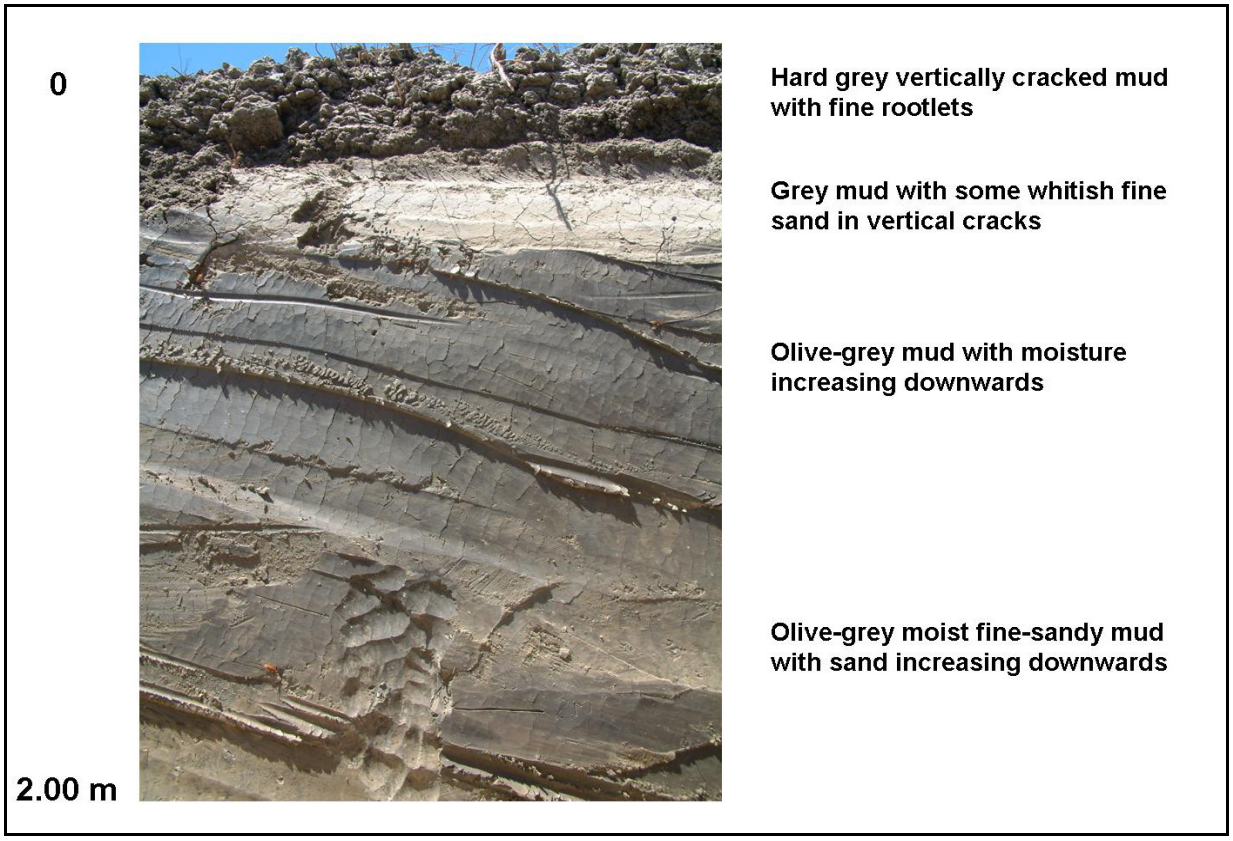

Figure 5-102. *Coonambidgal Formation overbank mud deposited on the Darling River scroll plain.*



Figure 5-103. *Coonambidgal Formation ripple cross-laminated fine to medium sand from the upper point-bar lateral accretion deposits of the Talyawalka Creek. Black circular cap is an OSL dating sample.*



Figure 5-104. *Menindee Formation medium to coarse sand from the basal point-bar lateral-accretion deposits with the arrow marking the sharp erosional contact at 15.0 m depth to the underlying Blanchetown Clay in BHMAR66. The sonic coring process does not preserve fine-scale structures in wet well sorted sands (See Section 10 in Lawrie et al., 2012a).*



Figure 5-105. *Coonambidgal Formation medium to coarse sand from the basal point-bar lateral-accretion deposits in the 11-13 m depth range in BHMAR80A-2. The sonic coring process does not preserve fine-scale structures in wet well sorted sands.*

Menindee and Coonambidgal Formation channel patterns

Landform mapping for this project has recognised four distinct phases of Coonambidgal Formation lateral migration deposition which are from youngest to oldest, The Darling River system, the Anabranch system (which includes Talyawalka Creek in the upstream of Menindee and Tandou Creek, Redbank Creek and the Great Darling Anabranch downstream of Menindee), an relict Anabranch system (associated with Talyawalka Creek upstream and with Coonalhugga Creek downstream and a relict system associated with the Darling tract. The latter relict system is sparsely exposed and has barely recognisable scroll-plain traces due to relatively thick overbank mud deposition and is of unknown age; it may be coeval with the relict Anabranch system. These phases are all inset into the Menindee Formation of the upper floodplain. These stratigraphic phases are listed from youngest to oldest in Table 5-18 and discussed below.

Table 5-18. *Quaternary fluvial formations recognised in the lower Darling Valley.*

Formation	Name, Location and associated fluvial system
Coonambidgal 1	Darling River scroll-plain tract
Coonambidgal 2	Anabranch scroll-plain tracts (Talyawalka, Tandou and Redbank Creeks and the Great Darling Anabranch)
Coonambidgal 3	Relict Anabranch scroll-plain tracts (Talyawalka and Coonalhugga Creeks)
Coonambidgal 4	Relict Darling River scroll-plain tract
Menindee	Darling Valley higher floodplain

Coonambidgal Formation 1 scroll-plain phase is associated with the present course of the Darling River. This scroll plain is narrow with relatively low channel width and meander amplitude, radius of curvature and wavelength (Table 5-19). The Darling River is the most deeply incised channel in the valley but the scroll plain is currently inactive with no lateral migration and common cementation of banks cut into Menindee Formation or older units by secondary carbonate deposition. Limited sand moves along the bed of the channel as mega-ripples or sand waves or as a thin veneer and forms rare small point bars on inside bends. The Darling scroll plain lies close to the western valley margin upstream of Menindee and at the eastern valley margin downstream of Menindee.

Coonambidgal Formation 2 scroll-plain phase is associated with various parts of the continuous anabranch tract, which consecutively downstream includes the Talyawalka, Tandou and Redbank Creeks and the Great Darling Anabranch. The anabranch scroll-plain tract is wider than the Darling with greater channel width and meander amplitude, radius of curvature and wavelength (Table 5-19). Though the anabranch channels still carry water during floods their channels are less deeply incised than the Darling and probably contain thicker clay sediment plugs. Upstream of Menindee, the Talyawalka Creek portion of the anabranch scroll-plain tract lies close to the eastern valley margin and the Tandou and Redbank Creeks and the Great Darling Anabranch downstream of Menindee are at the western valley margin. The Talyawalka trends north-south in the northern part of the wider BHMAR Project then more south westerly after divergence of the Teryaweynya Creek until it trends east-west towards Menindee abutting a prominent linear margin of the valley. The Darling River and anabranch scroll plain tracts intersect downstream of Menindee in the Jimargil/East Bootingee area of the GWR1 target. OSL dating for this project, detailed below, has demonstrated that the elements of the Coonambidgal 2 scroll-plain phase upstream and downstream of Menindee are coeval.

Table 5-19. *Meander geometry of lower Darling Coonambidgal Formation lateral- migration phases. Figures from Tilpa (*) are from Bowler et al. (1978).*

Fluvial Phase	Formation Phase	Meander Wavelength (L)	Meander Amplitude (A)	Radius of curvature of scrolls (Rc)
Darling at Tilpa*	Coonambidgal 1	1050 ± 164	575 ± 150	297 ± 94
Acres Billabong at Tilpa*	Coonambidgal 2	2190 ± 260	1620 ± 250	670 ± 210
Darling upstream of Menindee	Coonambidgal 1	970 ± 310	415 ± 135	165 ± 55
Darling downstream of Menindee	Coonambidgal 1	810 ± 350	390 ± 180	140 ± 40
Talyawalka Creek	Coonambidgal 2	1765 ± 320	1060 ± 325	370 ± 145
Tandou Creek	Coonambidgal 2	2000 ± 520	1160 ± 345	345 ± 140
Relict Talyawalka	Coonambidgal 3	1281 ± 285	1235 ± 250	425 ± 110
Relict Coonalhugga	Coonambidgal 3	1410 ± 250	975 ± 340	370 ± 120

Coonambidgal Formation 3 scroll-plain phase is older than the anabranch system with indistinct scroll-bar patterns that are also evident both upstream and downstream of Menindee. The channel and meander dimensions of the older scroll-plain tracts appear to be similar to those of the anabranch phase (Table 5-19). though the scroll traces and channel characteristics are indistinct due to a greater thickness of overbank muds. Upstream of Menindee the relict scroll-plain tract lies between the divergence of the Teryaweynya Creek and the point where the Talyawalka Creek turns east-west along the linear valley margin. Downstream of the Darling/anabranch intersection older scroll plain tracts reappear in between the Darling River and the Tandou Creek associated with the course of Coonalhugga Creek. These older, indistinct, southern scroll-plain tracts appear very similar to the upstream tracts south west of the Talyawalka Creek but cannot be mapped as continuous with them and therefore cannot be assumed to be of the same age. Though no clear evidence appears on satellite imagery, the relict scroll-plain tract must be overridden by the Talyawalka Creek tract along the east-west linear valley boundary and be intersected by both younger tracts in the Jimargil/East Bootingee Potential Borefield Area of the GWR1 area. OSL dating for this project, detailed below, has demonstrated that the elements of the Coonambidgal 3 relict scroll-plain phase upstream and downstream of Menindee are coeval.

Coonambidgal Formation 4 scroll-plain phase is sparsely evident associated with the Darling River scroll-plain tract upstream of Menindee. These relict scroll-plain traces are have similar dimensions to the Coonambidgal Formation 3 relict scroll-plain phase but are very indistinct. Most traces occur upstream of the Menindee Lakes Scheme Main Weir where they have been further obscured by sedimentation and vegetation growth due to water impounded by Lake Wetherell. Very limited indistinct traces occur between the Main Weir and the Darling River/Talyawalka Creek junction. This phase maybe coeval with or older than the Coonambidgal Formation 3 scroll-plain phase but it has not been OSL dated.

Menindee Formation floodplain is the oldest and highest of the fluvial phases and is incised by the Coonambidgal scroll-plain tracts described above. This floodplain is relatively featureless and is inundated by the highest floods of the modern regime (e.g. 1976 flood at 125 GL/day discharge at Weir 32). The Menindee Formation floodplain is incised by a number of flood scour channels which do not have scroll-plain tracts or any evidence of sand deposition or lateral migration. Upstream of Menindee, these include Two-Mile, Seven-Mile and Three-Mile Creeks between the Darling and the Talyawalka. Downstream of Menindee and east of the Darling are the Yampoola and Charlie Stones Creek scour channels. Upstream of Menindee, scour pools frequently occur where these channels pass through lateral constrictions between high-elevation, within-valley aeolian deposits demonstrating considerable stream power during high-flood flows. The Yampoola Corridor valley tract, completely lacking aeolian deposits, extends continuously along the Darling River, Three-Mile Creek and Yampoola Creek, similarly demonstrating the erosive power of high-flood events. The oldest indistinct scroll-plain tracts appear to be transitional, in terms of morphology and elevation, between the younger scroll plains and the Menindee Formation floodplain. Drill-hole stratigraphy demonstrates that the Menindee Formation flood plain was originally deposited as scroll-plain tracts during earlier lateral-migration phases that have since been buried by overbank mud deposits which have obscured the scroll traces and raised their elevation.

Bowler *et al.* (1978) demonstrated the difference in meander geometries between the modern Darling River and the Acres Billabong anabranch in the Tilpa region upstream from the project area. Meander geometries, as defined by Leopold *et al.* (1964) (Figure 5-106), of Coonambidgal Formation lateral migration phases in the project area were measured on Google Earth and presented in Table 5-19 with the values derived by Bowler *et al.* (1978) from Tilpa provided for comparison. The tracts of the Coonambidgal 3 relict Anabranch phase both north and south of Menindee were only well enough exposed for approximately 15 meander wavelengths to be measured. Accordingly, measurements of all parameters for all Coonambidgal phases in the project area were limited to 15. This relatively small number results in rather high uncertainty of the mean measurement as indicated by the standard deviations (Table 5-19). However, the results are sufficient to highlight the differences and for comparison to the results derived by Bowler *et al.* (1978). The Coonambidgal 4 phase, the relict scroll plain in the Darling River tract, is insufficiently exposed and too indistinct where it is exposed, to enable meaningful meander or scroll geometry measurements. Channel widths were not measured as the true widths of the inactive phase channels cannot be determined from the degraded channel forms. Sinuosity was also not easily measurable in the inactive phases because of the difficulty of discriminating between active and cut-off meander loops in the often overprinted scroll-plain patterns.

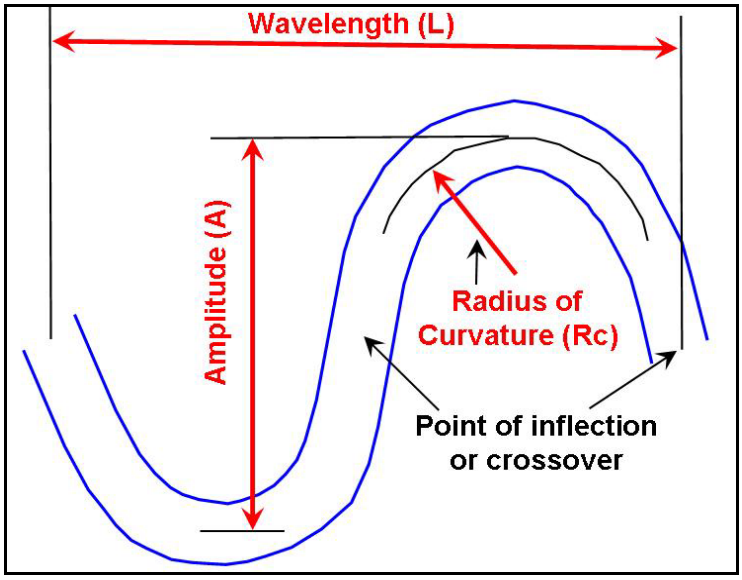

Figure 5-106. *Standard meander and scroll geometry parameters measured in the Coonambidgal Formation lateral-migration phase deposits (modified from Leopold et al., 1964).*

The meander and scroll geometry measurements (Table 5-19) demonstrate that the Darling River in the project area is similar to the Darling approximately 220 km in a straight line upstream near Tilpa, though the dimensions of all three parameters is lower in the Menindee project area. This probably reflects a downstream decline in discharge due to losses to infiltration; natural diversion to the Talyawalka Creek, the Teryaweynya Creek and lakes and to the floodplain channels; and natural diversion to the Menindee Lakes. There is also a reduction in dimensions apparent within the project area between the Darling tracts measured north and south of Menindee which similarly reflects discharge declining downstream due to the same losses. The older Coonambidgal 2 and 3 tracts in the project area have similar dimensions to the Acres Billabong tract at Tilpa, supporting the suggestion made by Bowler *et al.* (1978) that Acres Billabong is part of a former anabranch tract that includes the Talyawalka Creek and the Great Darling Anabranch. In both areas all three parameters are much larger than the modern Darling River suggesting larger discharges in the past and differences in sediment loads. As with the Darling the older tracts show an apparent decline in parameter dimensions between Tilpa and the Menindee area, probably reflecting a similar downstream decline in discharge in the past for the same reasons. Within the project area there is an interesting difference in parameter dimensions between the Coonambidgal 2 phase (Talyawalka and Tandou Creeks) and the Coonambidgal 3 phase (the relict phases at Talyawalka and Coonalhugga Creeks). The meander amplitude and radius of scroll curvature are essentially the same for all four systems but the meander wavelength of the Anabranch phase is significantly greater than for the relict phase. This difference must reflect a contrast in the discharge/sediment regime of the two phases but the more exact explanation will require a more detailed investigation of the meander geometries and sediment characteristics of the two phases. Differences in the total thickness of the morphostratigraphic units associated with these phases (Table 5-20 and Table 5-21) are also evident.

Morphostratigraphy of the Menindee and Coonambidgal Formation units.

Most BHMAR cores are located on Quaternary fluvial units and the stratigraphy of the upper units has been examined to statistically analyse the dimensions, to test the conclusion that all units share the same depositional style and to investigate infiltration potential of the fluvial sediments. There are 44 BHMAR drill sites located on the Menindee Formation higher flood plain and 22 located on the Coonambidgal Formation scroll plains. Of the latter, most are located in the East-Bootingee/Jimargil and Menindee Common areas of Target GWR1 where all scroll plain phases intersect and exact differentiation is difficult. Nine of the scroll-plain drillholes are clearly located in the Darling River Coonambidgal 1 phase and only three are clearly located in the Anabranch Coonambidgal Formation 2 phase. The remaining ten scroll-plain drillholes are

located in the East Bootingee/Jimargil area on older scroll plains that are probably equivalent to the relict anabranch Coonambidgal 3 phase. No drillholes are located on the sparsely represented relict Darling Coonambidgal 4 phase. If all units are deposited by the same style of mixed-load lateral migration fluvial system the same stratigraphic sequence will be expected to occur in each, with the possibility of variations in scale due to variations in discharge regime between different phases. The variations in scroll plain dimensions such as channel width, scroll radius of curvature, meander amplitude and meander wavelength, as discussed above, clearly reflect variations in discharge but these parameters are not detectable in core. The core does provide details of average scroll plain sequence thickness, relative thickness and nature of different scroll-plain facies and occasionally the depth of channel scours, which are all dimensions that can also reflect the magnitude of river discharge.

The analysis of fluvial facies identified in the core logs included differentiation of an upper overbank muddy zone consisting of mud and silty or fine sandy mud, a transitional zone of muddy sand and a lower scroll-bar sand-zone of fine to very coarse sand and gravel with medium sand dominant. In some cases, logs of mud-rotary drillholes were not sufficient to pride discrimination of detailed facies within the Quaternary fluvial units but total thickness can always be recognised in combination with the down–hole gamma and conductivity logs. This explains the lower numbers of bores for some facies thicknesses in Table 5-20 and Table 5-21 summarises the results. In Table 5-20 the mud-dominated upper and transitional zones are combined as together they form an effective aquitard barrier to infiltration. For all three categories analysed, the total mud, lower sand and total thickness, the number of cores analysed, the mean value and the range of values is presented. Table 5-21 presents the differentiation of the upper mud unit and the transitional unit dimensions. The number of cores from the individual scroll-plain phases is probably too low to be a representative sample, particularly for the Talyawalka/Anabranch phase. The comparison between the Menindee Formation and Coonambidgal Formation combined scroll-plain parameters shows little difference between the mean values for the total mud, lower sand and total thickness, which is consistent with the interpretation that all have been deposited by similar lateral-migration fluvial episodes. There is, however, a wider range of values for all three categories in the Menindee Formation cores which may reflect either the larger number of cores from that unit or a wider variability of discharge regimes in the lateral migration episodes preserved in the Menindee Formation.

Table 5-20. *Mud- and sand-facies and total thickness of Quaternary lateral-migration fluvial units as measured in BHMAR Project drill cores.*

Quaternary Fluvial unit	Total mud thickness (m)			Lower sand thickness (m)			Total thickness (m)		
	No.	Mean	Range	No.	Mean	Range	No.	Mean	Range
Menindee Formation highest flood plain	42	7.7	1.1-14	42	6.5	1.1-22.3	44	14.1	9.9-29
Coonambidgal Fm (All phases)	21	7.5	3.2-11	21	7.3	3-14	22	14.3	8-23
Coonambidgal Fm 1 (Darling River)	9	6.5	3.2-10	5	5.2	3-10	9 (5)	11.6	8-18
Coonambidgal Fm 2 (Talyawalka/Anabranch)	3	6.3	6.1-6.5	2	7.7	4.9-10.5	3	14.8	11-16.8
Coonambidgal Fm 3 (Relict scroll plains)	9	8.5	7-11	10	10.1	3.7-14	10 (4)	17.7	14.3-23

The dimensions of the youngest Coonambidgal 1 scroll-plain phase associated with the modern Darling River are significantly smaller than for the earlier Coonambidgal 2 anabranch and Coonambidgal 3 relict phases which is consistent with the relative meander geometry dimensions of scroll radius of curvature, meander amplitude and meander wavelength (Table 5-19) all of which suggest higher discharge in the older phases. The Relict phase has larger dimensions than the anabranch phase but the low number of cores in the latter (3) probably does not provide a statistically valid sample, though it may also reflect the apparently significant difference in meander wavelength evident in Table 5-19. Other scroll-plain planimetric dimensions of the two systems appear to be similar. The deepest dimension of total thickness is up to 29 m, nearly 15 m deeper than average for the Menindee Formation, and up 23 m, nearly 10 m deeper than

average, for the Coonambidgal Formation scroll-plain tracts. These deeper channels contain coarse sand and gravels and almost certainly represent scoured river 'holes' analogous to those mapped in the modern Darling channel by the in-river surveys. Such channels must represent important pathways for lateral and vertical groundwater movement, both within and between stratigraphic units.

Table 5-21. *Mud-facies and thickness of Quaternary lateral-migration fluvial units as measured in BHMAR Project drill cores.*

Quaternary Fluvial unit	Upper Mud			Transitional mud		
	No.	Mean	Range	No.	Mean	Range
Menindee Formation highest flood plain	40	4.8	1.1-8.8	29	4.3	0.7-11.5
Coonambidgal Fm (All phases)	21	3.8	1.3-11	19	4.1	1.2-7.8
Coonambidgal Fm 1 (Darling River)	9	3.7	2-6	8	3.2	1.2-5.5
Coonambidgal Fm 2 (Talyawalka/Anabranch)	2	1.8	1.3-2.2	2	4.5	4.1-4.8
Coonambidgal Fm 3 (Relict scroll plains)	10	4.3	1.4-11	9	4.8	1.2-7.8

Menindee Formation lateral valley fluvial sediments

At the north-western end of Lake Menindee the lake floor shows traces of an ancient channel at shallow depth. Shallow augering and AEM data indicate valley incision into the Blanchetown Clay with valley infill by lateral migration sand deposits and a clay-plugged channel (Figure 5-133, Figure 5-134). These fluvial sediments are located well away from the fluvial tracts containing the Menindee Formation and Coonambidgal Formation and when first recognised, early in the project, were correlated with lower sandy fluvial and channel-related facies of the Willotia beds unit. This correlation also related to the recognition of Willotia beds sediment overlying the Blanchetown on the Menindee lake floor south of the fluvial incision. However, subsequent investigation has resulted in a revision of this stratigraphy. An OSL date of 84.6 ± 12.5 ka from the lateral accretion sands indicates and depositional age equivalent to the Menindee Formation (see below). Analysis of the LiDAR indicates alignment of the channel on the lake floor with a now-defunct tributary valley system which can be traced north east from the lake shoreline through a distinct residual depression north of Sunset Strip and then north to the Scopes Range. To the west, the former fluvial system probably passed through Lake Speculation before heading south west. Since this Menindee Formation equivalent lateral valley was last active around 85 ka the lake has migrated over the fluvial system by the normal processes whereby lunette-lakes migrate upwind (See section on lakes/lunettes). OSL dates of around 55 ka from lunette sediments at the northern extremity of the lunette west of Sunset Strip (Cupper & Duncan, 2006), suggests that the lake was in its current position by that time, and the migration or expansion of the lake floor occurred between 85 and 55 ka.

The sonic-cored drill hole BHMAR 23 just outside the north-western Lake Menindee shoreline provides an opportunity to compare the stratigraphic facies architecture of the Menindee Formation equivalent lateral valley sequence with the characteristics of the main valley Menindee Formation units. In the upper part of the core, 2.13 metres of Woorinen Formation aeolian sand overlies 21.8 m of Quaternary fluvial sediment which extends to about 41.1 m AHD. This can be subdivided according to the scheme outlined above into 4.75 of upper mud (logged as slightly sandy clay), 4.75 m of transitional unit (logged as mostly clayey sand with thin fine sand beds) and 11.85 m of clean sands. Figure 5-107 shows the basal sands of this sequence from 18.1 to 20.8 m and demonstrates their similarity to other Quaternary basal lateral-accretion sands (Figure 5-104 and Figure 5-105). The total thickness and lower sand thickness are greater than the Menindee Formation averages (Table 5-20) but lie well within the total range of values. This similarity between the main valley and lateral valley sequences probably reflects the proximity of the site to the main valley both spatially and in elevation.



Figure 5-107. *Menindee Formation equivalent lateral-valley medium to coarse sand from the basal point-bar lateral-accretion deposits at 18.1 to 20.8 m depth in sonic drill core BHMAR 23. The sonic coring process does not preserve fine-scale structures in wet well sorted sands.*

Yampoola Corridor

The Yampoola Corridor (Figure 5-108, Figure 5-109) is a topographic feature on the Darling alluvial plain which appears to be the tract of a former trench or scroll plain of the palaeo-Darling River incised into older Menindee Formation. It is filled with younger Menindee Formation sediment, although probably not the youngest sediment of that unit. It is a zone about 3 km wide that is free of aeolian deposits, except for surface aeolian reworking of floodplain bars (see Section 5.4.3.2). The corridor laterally truncates areas of aeolian deposits (Refer to Figures 3MC floodplain), and may be locally bordered to the east by possible source-bordering dunes.

The lateral truncation of areas of aeolian deposition indicates that the Yampoola Corridor is an erosional feature, with the marginal source-bordering dunes representing sediment blown from the trench or scroll plain. Importantly, it appears that there has been no preservation of dune formation or extension over the corridor since it was formed. Various features of the modern Darling alluvial plain have been established in the corridor over its length, including the Darling and its scroll plain in the south and north, the flood-scour channels of Yampoola and Three Mile Creeks, and un-named crevasse splay channels south of Talyawalka Creek. The northern portion of the corridor has abundant floodplain bars (See Section 5.4.3.2) that extend downstream into the Three Mile Creek floodplain where the corridor diverges from the Darling River tract. The floodplain bars and the abundant flood-scour channels of the corridor are evidence that it is likely to be a preferential tract for flow during the highest overbank flood events and this probably ensures that aeolian deposits continue to be removed in the modern flood regime.

The Yampoola Corridor is crossed by Talyawalka Creek and its scroll plain, and is only partly coincident with the Darling scroll plain. Therefore it predates these features. Only one project hole (BHMAR14) has intersected the corridor. Core logging indicates a mixture of sand and clay down to the interpreted base of Menindee Formation at 13.1 m, and there is no evidence that the fill of this corridor is different from the surrounding areas of older Menindee Formation.

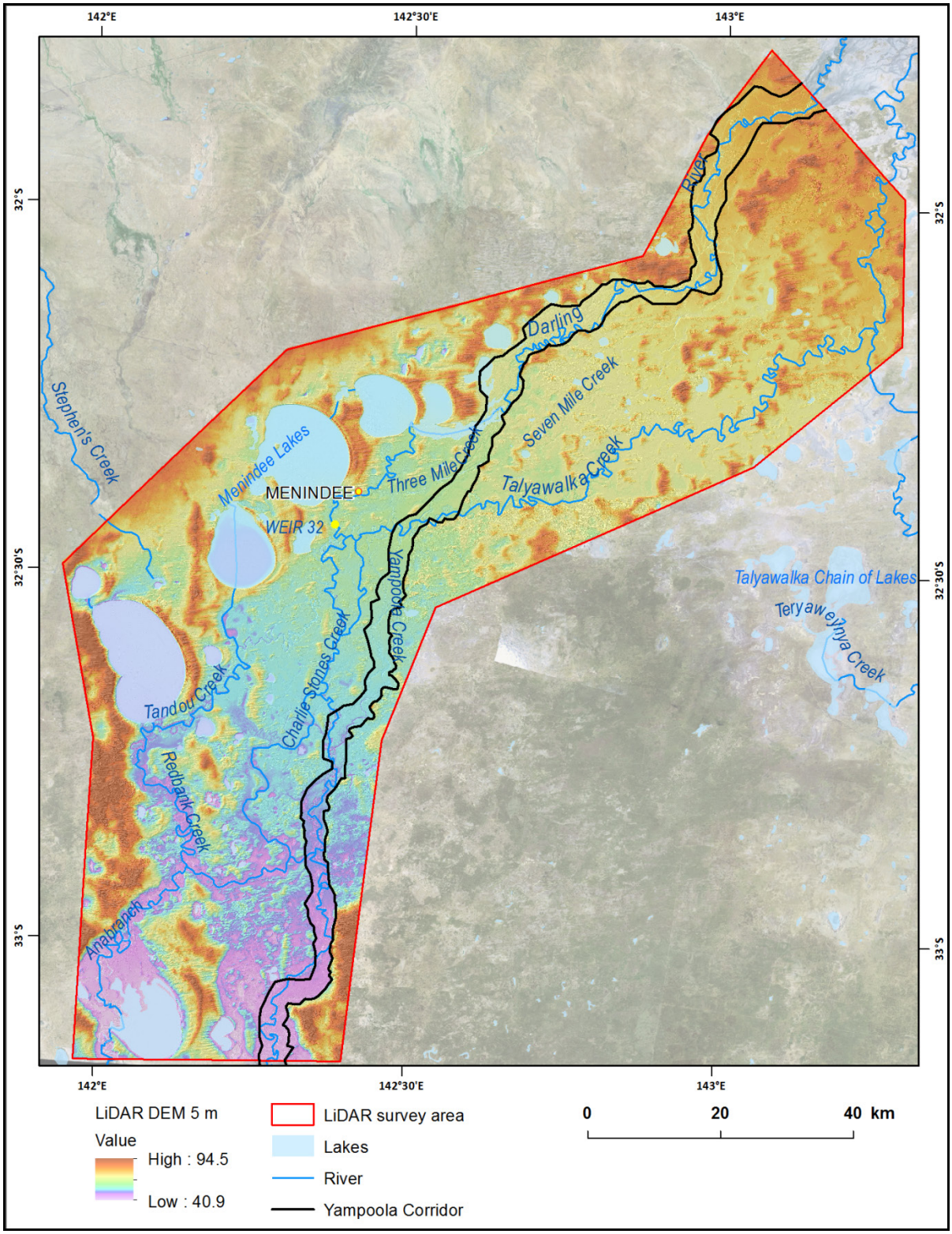

Figure 5-108 *Location of the Yampoola Corridor within the study area.*

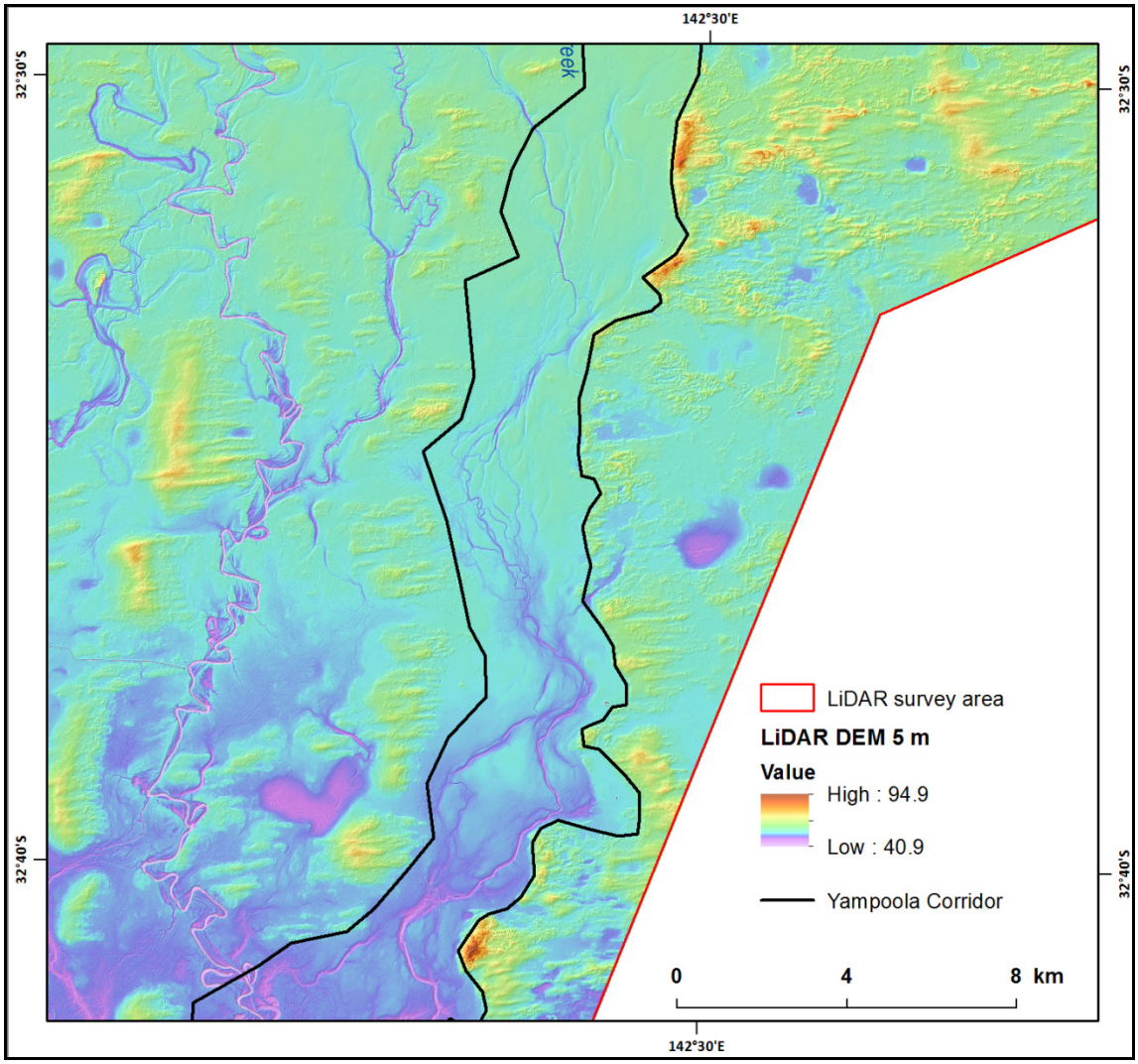

Figure 5-109 *Detail of the Yampoola corridor in the south of the study area, showing north-northeast trending dune forms along the western and eastern margins of the corridor. The western dunes may have originated as source-bordering dunes.*

5.4.1.5 Numeric dating of the Quaternary fluvial phases

Prior to this project the only numeric dating of sediments in the Darling valley was a mid-1970s conventional radiocarbon study of sediments exposed near Tilpa during excavation of the Sydney-Moomba gas pipeline (Bowler *et al.*, 1978). That study mapped similar landform associations to the BHMAR Project area with the Darling River and older anabranch (Acres Billabong) Coonambidgal Formation scroll plain tracts incised into older alluvial deposits equivalent to the Menindee Formation. Other previous numeric dating results from the Menindee region include radiocarbon, luminescence and AAR ages from the Lake Menindee and Lake Tandou lunettes (Hope *et al.*, 1983; Chen, 1992; Miller *et al.*, 1999, 2005) and radiocarbon dates on archaeological features across many landscape elements (Balme & Hope, 1990). While these latter studies provide a regional palaeoenvironmental context in terms of periods of likely relatively enhanced river activity or aridity they do not provide numeric ages for the fluvial sedimentary phases in the Darling valley discussed above. The BHMAR Project has greatly extended numeric dating of the Quaternary fluvial units with 4 radiocarbon dates and 19 OSL dates. The background to both dating techniques and the detailed methodology of their application for this project are presented in Lawrie *et al.* (2012a) and the stratigraphic context of each date is shown in Appendix 3h (Apps *et al.*, 2012f). As detailed in the Methods Section, for radiocarbon ages to be comparable to OSL dates in calendar years they require calibration for variations in the rate of ^{14}C production in the atmosphere due to temporal variations in the strength of cosmic radiation.

Radiocarbon dating of tree rings of known calendar age and cross dating of corals by both radiocarbon and U-series dating methods provide calibration datasets.

Bowler *et al.* (1978) reported radiocarbon ages that calibrate to 20-23 ka (ka = thousand years ago) from charcoal in active scroll-bar deposits of the early anabranch phase (Acres Billabong, equivalent to Coonambidgal 2). They also reported apparent waning of the anabranch phase at a calibrated age around 13 ka, which they inferred was probably close to the time of avulsion to the Darling River phase (Coonambidgal 1). Bowler *et al.* (1978) did not date the Darling scroll plain tract but presumed that it was initiated after termination of the earlier anabranch phase. Bowler *et al.* (1978) also obtained a minimum age of 23.5 ka (calibrated) from soil carbonate in older alluvium near Tilpa (Menindee Formation equivalent).

During the BHMAR Project, samples for Optically Stimulated Luminescence (OSL) dating were taken in tractor-excavated pits and from hand-auger holes from a number of Coonambidgal and Menindee Formation units in the Menindee region. OSL dating measures the amount of stored energy in the crystal lattice of quartz sand grains, due to the impact of environmental radiation from natural uranium, thorium, potassium and cosmic sources. Minimal exposure to sunlight zeroes the stored energy, which then begins to re-accumulate following shielding from sunlight by burial. The technique therefore dates the time of last exposure to sunlight which is presumed to be the time of deposition of the sand grains. OSL dating carried out during this project (Table 5-22, Table 5-23) has extended our understanding of the numeric age of the fluvial units with confirmation and additional detail provided by the 4 radiocarbon dates (Table 5-24). Dating site locations are shown in Figure 5-110.

Table 5-22. *OSL sample numbers, locations, laboratory measurement summaries and calculated ages. Samples were measured at the Luminescence Dating Laboratory, University of Adelaide. 'Wt Av dose rate (Gy/ka' = weighted average dose rate (in Grays/thousand years) calculated from two different analytical methods. 'Equivalent dose (Gy)' = the natural dose (in Grays) measured in the sample. The age of the sample in thousands of years equals the equivalent dose divided by the dose rate.*

Lab Code	Field Code	Easting	Northing	Wt Av dose rate (Gy/ka)	Equivalent dose (Gy)	Age
AdBL 10016	DR01/05	637630	6417688	2.206 ± 0.068	4.8 ± 1.2	**2.2 ± 0.6**
AdBL 10017	DR01/10	637630	6417688	2.018 ± 0.075	6.5 ± 1.5	**3.2 ± 0.8**
AdGL 11091	DR01A/1	637424	6417600	1.981 ± 0.098	7.78 ± 0.49	**3.9 ± 0.3**
AdGL 11092	CHW01/1	620640	6336406	0.962 ± 0.048	7.13 ± 0.48	**7.4 ± 0.6**
AdBL 10013	TAL02/6	641507	6410736	1.875 ± 0.088	35.1 ± 3.6	**18.7 ± 2.0**
AdBL 10014	TAL03/6	641724	6410458	1.599 ± 0.081	28.6 ± 1.4	**17.9 ± 1.6**
AdBL 10012	TAL04/9	641848	6410195	1.572 ± 0.112	33.5 ± 3.3	**21.3 ± 2.2**
AdGL 11095	TAN01/1	622732	6379787	1.768 ± 0.105	34.09 ± 2.28	**19.3 ± 1.7**
AdGL 11097	CUTH01/1	597498	6348646	2.096 ± 0.152	43.48 ± 2.84	**20.7 ± 2.0**
AdGL 11096	TAN01/5	622732	6379787	0.886 ± 0.060	28.42 ± 1.76	**32.1 ± 3.1**
AdGL 11098	LAR01/1	676353	6414981	1.352 ± 0.060	33.64 ± 2.20	**24.9 ± 2.1**
AdBL 10018	DRO2/8	637455	6417542	1.837 ± 0.081	87.0 ± 9.0	**47.4 ± 6.3**
AdBL 10019	DRO3/9	637564	6417057	1.588 ± 0.065	61.7 ± 10.2	**38.9 ± 6.5**
AdBL 10011	DRO6/6	637788	6417057	1.497 ± 0.061	127.7 ± 22.9	**85.3 ± 15.6**
AdGL 11093	CHW02/1	622077	6336297	1.593 ± 0.119	72.27 ± 6.84	**45.4 ± 5.5**
AdGL 11094	CHW02/3	622077	6336297	1.990 ± 0.145	103.29 ± 7.05	**51.9 ± 5.2**
AdGL 11099	BHMAR 75-8/2	630780	6411483	1.317 ± 0.070	>200	**>150**
AdBL 10015	3MC06/10	644153	6414823	1.756 ± 0.057	5.2 ± 1.6 13.5 ± 2.7	**3.0 ± 0.7** **7.7 ± 1.5**
AdBL 10020	MN01/8	621548	6427523	0.855 ± 0.049	72.3 ± 9.3	**84.6 ± 12.4**

Table 5-23. *OSL sample numbers, Quaternary fluvial unit sampled and calculated ages.*

Field Code	Formation	Age
DR01/05	Coonambidgal 1 Darling R scroll plain	**2.2 ± 0.6**
DR01/10	Coonambidgal 1 Darling R scroll plain	**3.2 ± 0.8**
DR01A/1	Coonambidgal 1 Darling R scroll plain	**3.9 ± 0.3**
CHW01/1	Coonambidgal 1 Darling R scroll plain	**7.4 ± 0.6**
TAL02/6	Coonambidgal 2 Talyawalka-Anabranch scroll plain	**18.7 ± 2.0**
TAL03/6	Coonambidgal 2 Talyawalka-Anabranch scroll plain	**17.9 ± 1.6**
TAL04/9	Coonambidgal 2 Talyawalka-Anabranch scroll plain	**21.3 ± 2.2**
TAN01/1	Coonambidgal 2 Talyawalka-Anabranch scroll plain	**19.3 ± 1.7**
CUTH01/1	Coonambidgal 2 Talyawalka-Anabranch scroll plain	**20.7 ± 2.0**
TAN01/5	Coonambidgal 3 relict Talyawalka-Anabranch scroll plain	**32.1 ± 3.1**
LAR01/1	Coonambidgal 3 relict Talyawalka-Anabranch scroll plain	**24.9 ± 2.1**
DRO2/8	Menindee Formation higher floodplain	**47.4 ± 6.3**
DRO3/9	Menindee Formation higher floodplain	**38.9 ± 6.5**
DRO6/6	Menindee Formation higher floodplain	**85.3 ± 15.6**
CHW02/1	Menindee Formation higher floodplain	**45.4 ± 5.5**
CHW02/3	Menindee Formation higher floodplain	**51.9 ± 5.2**
BHMAR 75-8/2	Menindee Formation higher floodplain	**>150**
3MC06/10	Floodplain bar on Menindee Formation higher floodplain	**3.0 ± 0.7** **7.7 ± 1.5**
MN01/8	Menindee Formation equivalent lateral valley sand	**84.6 ± 12.4**

Table 5-24. *Radiocarbon dating results for different pre-treatment regimes for a wood sample at 8.7 m depth in core BHMAR 79A-2.*

Laboratory code	Material dated	Radiocarbon age Years BP ± 1σ	Calibrated age Years ± 2σ	Calibrated age Ka ± 2σ
SANU18109	Cellulose	4470 ± 45	5090 ± 240	5.09 ± 0.24
OZN662	Untreated black wood	4195 ± 35	4740 ± 170	4.74 ± 0.17
OZN664	Holocellulose	4300 ± 40	4835 ± 150	4.835 ± 0.15
OZN665	ABOX pre-treatment	4235 ± 35	4775 ± 150	4.775 ± 0.15

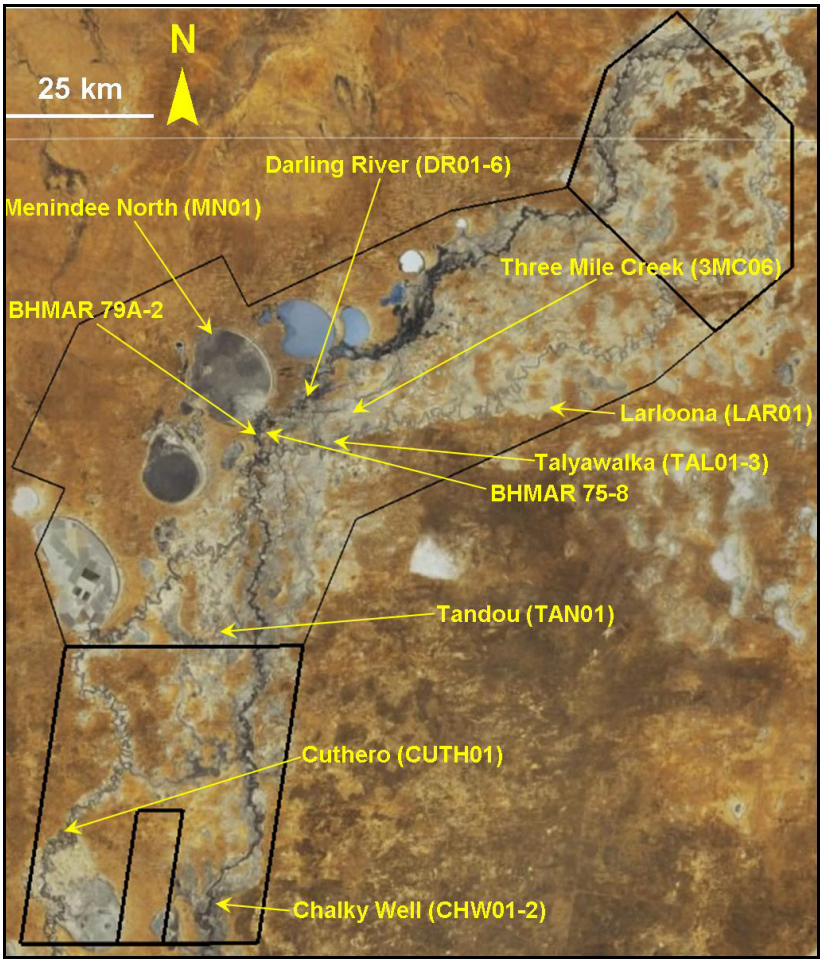

Figure 5-110. *Location of Quaternary fluvial unit dating sites.*

Coonambidgal Phase 1 Darling River scroll-plain chronology.

The initial OSL dating samples from the Coonambidgal 1 Darling-River scroll plain were taken from tractor-dug trenches on Menindee Common, upstream of Menindee (Figure 5-110, Figure 5-111). Dates marking the termination of this phase from tractor pit DR01 (Figure 5-111, Figure 5-112), at the youngest edge of the scroll plain near the river, were 2.2 ± 0.6 ka and 3.2 ± 0.8 ka at 2 and 2.34 m depth respectively.

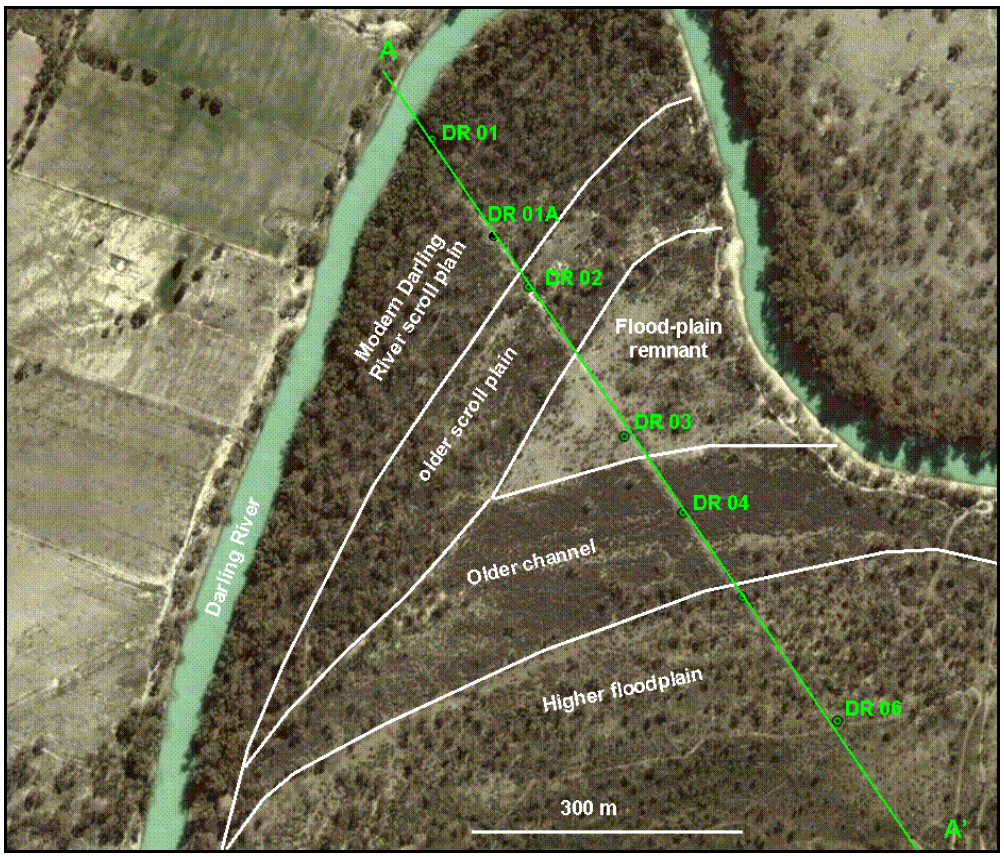

Figure 5-111. *Location of OSL sample sites at the Darling River, Menindee Common.*

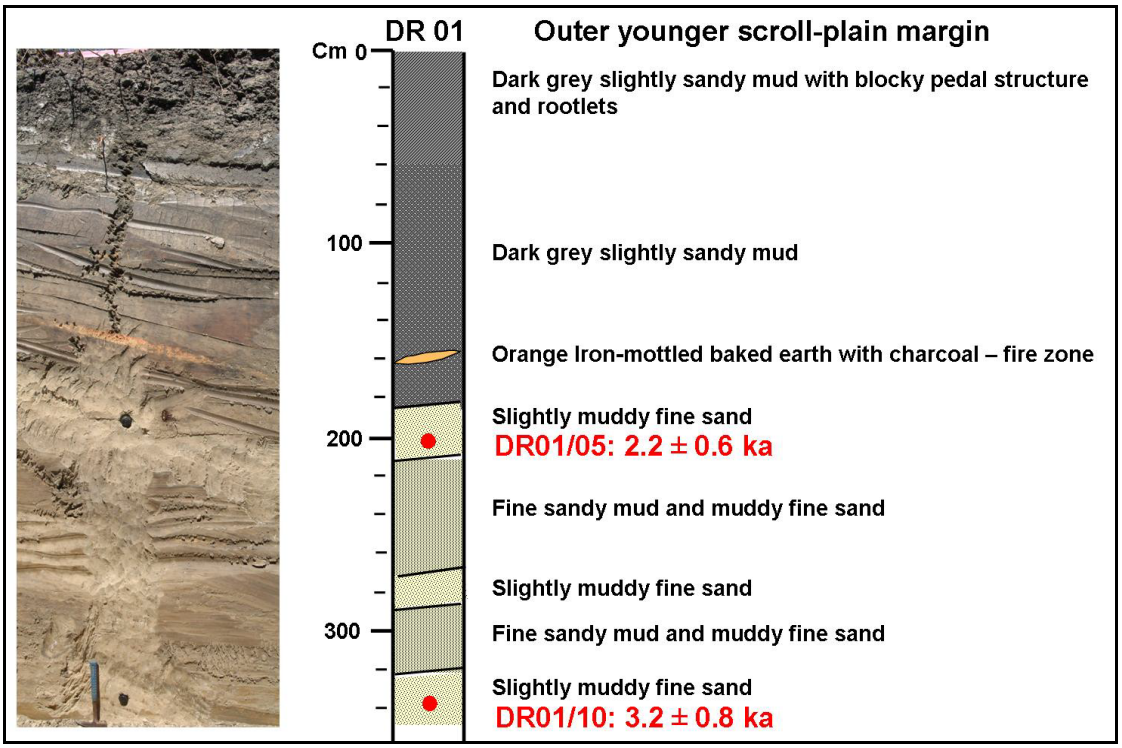

Figure 5-112. *Stratigraphy of tractor trench DR01 showing the OSL dating results in red.*

During initial satellite image analysis and field reconnaissance at this site, the 'older scroll-plain' tract marked in Figure 5-111 was thought to be part of the Coonambidgal 1 youngest scroll plain. Accordingly, tractor trench DR02 (Figure 5-128) was sited to provide an age closer to the initiation of that phase at that site. However, when the tractor-trench section was examined the sediments appeared to have possible multiple overbank mud layers and a greater degree of secondary pedogenic features in the form of secondary carbonate and manganese nodules. On the ground the scroll-plain traces (ridges and swales) were more subdued that closer to the river, the surface appeared to be slightly higher and the box woodland was less dense with a smaller average tree size. These characteristics were all consistent with an interpretation that trench DR02 was located on an older scroll plain, perhaps having a thin coating of Coonambidgal 1 overbank mud, but no lateral accretion sands of the youngest phase. This reinterpretation of the site was confirmed by a date of 47.4 ± 6.3 at 3.45 m depth in DR02. During a later phase of OSL sampling an additional sample was obtained from a hand-auger hole at DR01A (Figure 5-111, Figure 5-113) close to the true outer margin of the Coonambidgal 1 scroll-plain tract and a date of 3.9 ± 0.3 ka was obtained at a depth of 2.8-3.0 m.

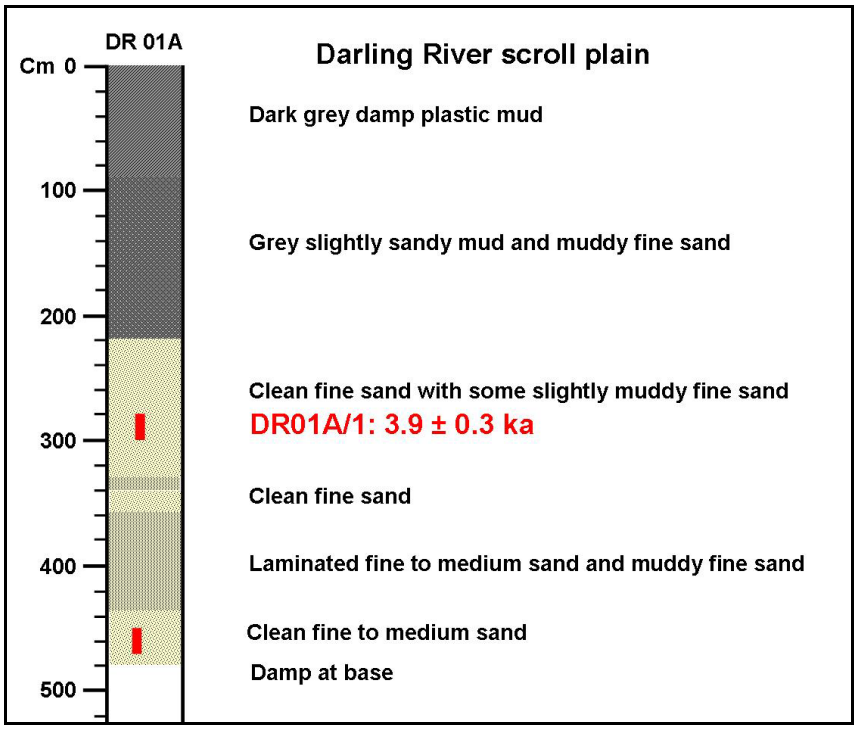

Figure 5-113. *Stratigraphy of hand-auger hole DR01A showing the OSL dating result in red.*

During the second phase of OSL sampling, a site in the southern portion of the study area on Chalky Well Station was selected to date the Coonambidgal 1 youngest scroll plain downstream of Menindee F (Figure 5-110, Figure 5-114). Access was difficult in August 2011 due to recent recession of major flooding but a hand-auger hole CHOW01 at the older inner margin of the scroll plain (Figure 5-114) provided a sample dated to 7.4 ± 0.6 ka at 2-2.14 m depth (Figure 5-115). This result is significantly older than the oldest scroll-plain date from DR01A of 3.9 ± 0.3 ka further north and also older than the calibrated radiocarbon age of 5.09 ± 0.24 ka for basal sands of this phase discussed below. Ground observations at the time of sampling definitely indicated that the auger-hole was located within the Coonambidgal 1 youngest scroll plain phase. However, when the GPS location was later plotted on LiDAR and Google Earth imagery both suggested that the location was very close to the boundary, perhaps just metres outside of it. This raises questions as to whether the date truly represents the early part of that phase or in some way represents the influence of older sands. The sediments outside the youngest scroll plain at that site are Menindee Formation and dated nearby at CHW02 to around 45-50 ka (see below). Accordingly, if the sample in CHW01 was dating the earlier sediments, that the scroll plain is incised into, it should have produced a very much older age. Additionally, the Luminescence Lab report of that sample has no indications of an anomalous age spread of the quartz grains as would be expected if the sample contained grains of mixed ages due to reworking. Therefore the age is interpreted as indicating the time of onset of the Coonambidgal 1 scroll-plain phase at the Chalky Well site.

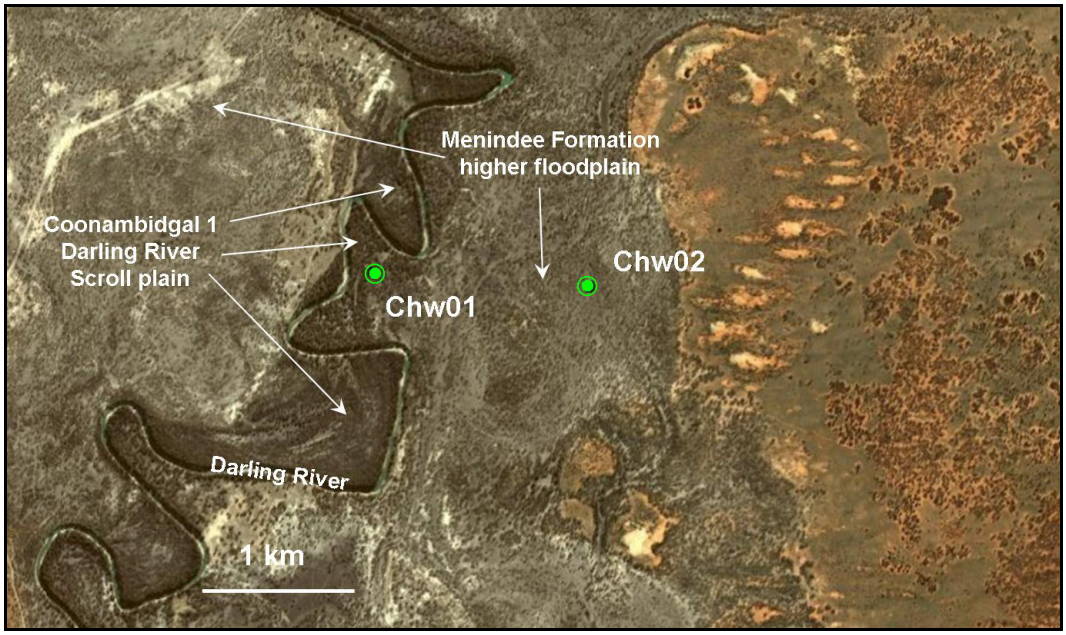

Figure 5-114. *Location of OSL sample sites close to the Darling River on Chalky Well Station in the southern part of the project area.*

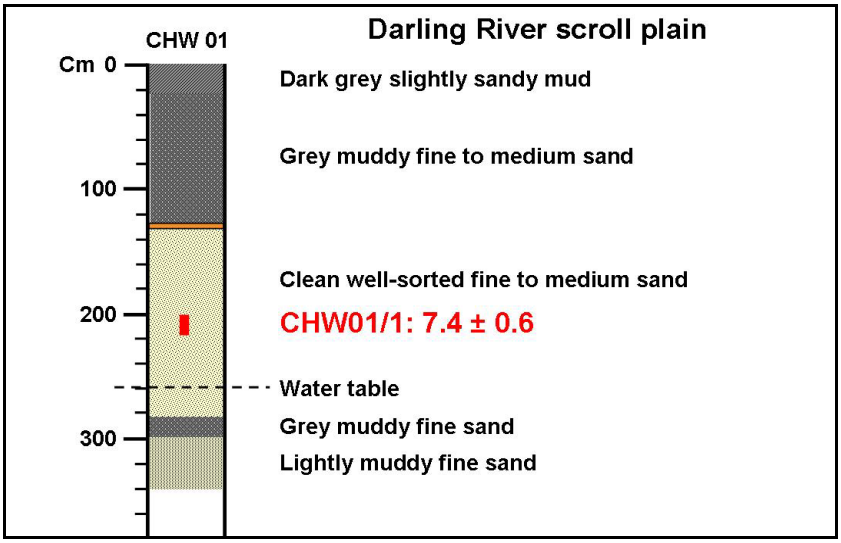

Figure 5-115. *Stratigraphy of hand-auger hole CHW01 showing the OSL dating result in red.*

The sonic-core drill site BHMAR79A-2 is located close to the outer margin of the Coonambidgal 1 Darling River scroll plain near the Menindee Common/Appin Station boundary (Figure 5-110, Figure 5-116) at 57.06 m AHD. During laboratory logging of the split core, relatively large (>5 cm scale) black fragments of apparent wood were recorded in the core in the basal scroll-plain sand at 8.7 m (Figure 5-117) and 8.9 m depth where the base of the Coonambidgal Formation was at 9.1 m. These samples were extracted from the core and the one from 8.7 m (48.36 AHD) was found to be a larger single solid mass. It seemed evident from visual and hand-lens examination that the sample had originally been wood, though it was uncertain whether it was now degraded wood blackened by absorption of humic compounds or whether it had been burnt and consisted of charcoal also probably containing post-depositional humic material.

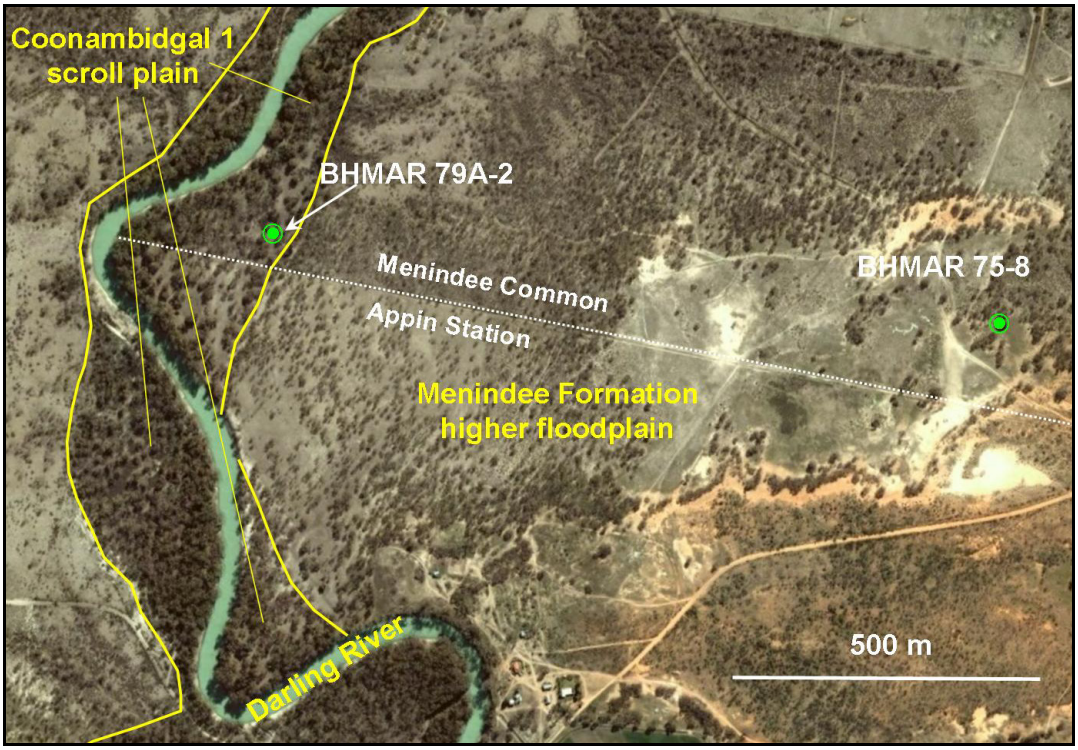

Figure 5-116. *Location of Sonic–core drillholes BHMAR 79A-2 on the Coonambidgal 1 Darling River scroll plain and BHMAR 75-8 on the Menindee Formation higher floodplain close to the southern margin of Menindee Common.*

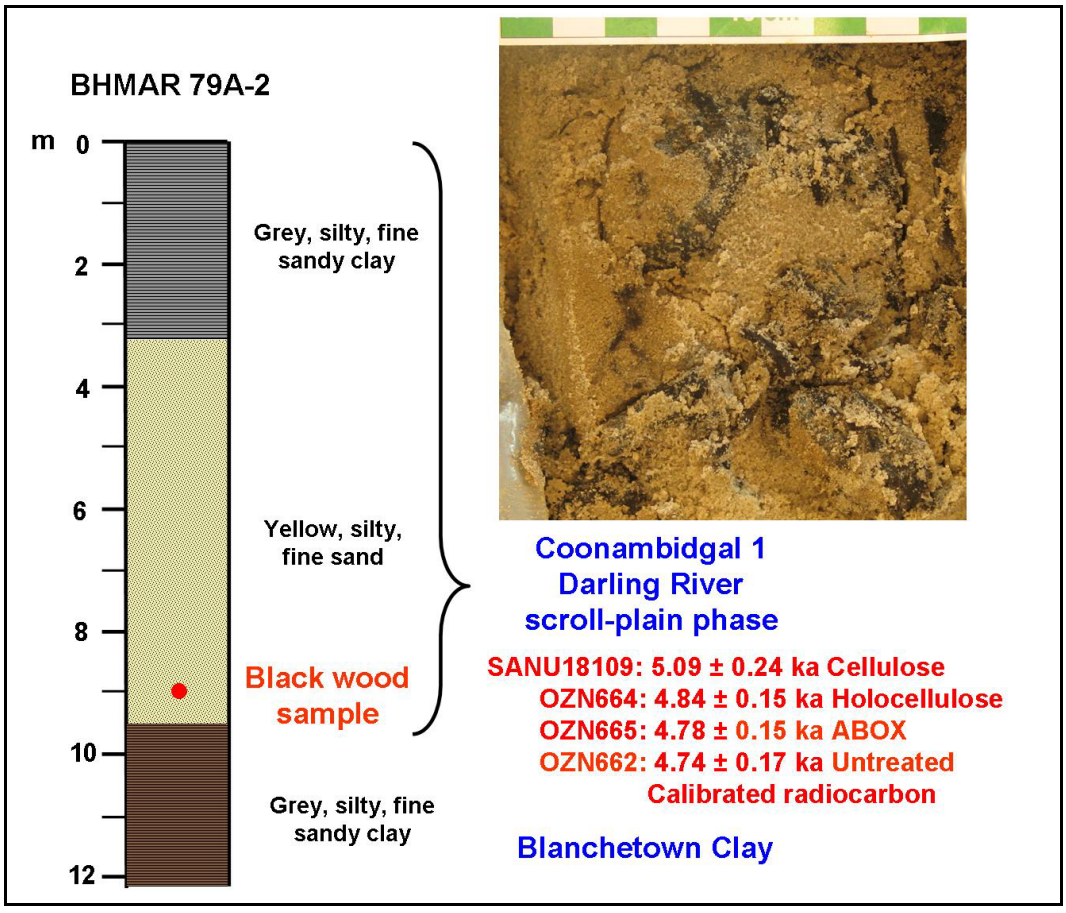

Figure 5-117. *Summary stratigraphic log of sonic-cored drillhole BHMAR 79A-2 showing the radiocarbon dating result in red. Inset at top right shows the blackened wood sample at 8.7 m in the core (1 cm bar scale units).*

Dr Richard Gillespie, a consultant radiocarbon chemist extracted cellulose, a strong crystalline polysaccharide long-chain non-branched polymer that is resistant to hydrolysis and is present in plant cell walls, from the sample for AMS radiocarbon dating. Dr Gillespie also dated other fractions to investigate the efficacy of various pre-treatment regimes in removing organic contamination of wood samples (see Lawrie *et al*., 2012a for details). Accordingly, a total of 4 samples were AMS radiocarbon dated and the results are listed in Table 5-24, showing the results of all dated fractions of the BHMAR 79A-2 sample including the pre-treatment regime and the age obtained in radiocarbon years, the calibrated age in years and the calibrated age in ka (thousands of years ago). In accordance with previously published results (Gillespie *et al.*, 2008; Stevenson *et al.*, 2010), cellulose extraction provides the oldest age, and is the pre-treatment regime that has most successfully eliminated the impact of younger radiocarbon contamination. The holocellulose sample provides the next best sample decontamination and both cellulose extractions perform better than ABOX pre-treatment (Bird *et al.*, 1999, 2002; Turney *et al.,* 2001a, 2001b), which is the current best practice standard pre-treatment regime that utilises the whole sample.

Table 5-25. *Radiocarbon dating results for different pre-treatment regimes for a wood sample at 8.7 m depth in core BHMAR 79A-2.*

Laboratory code	Material dated	Radiocarbon age Years BP ± 1σ	Calibrated age Years ± 2σ	Calibrated age Ka ± 2σ
SANU18109	Cellulose	4470 ± 45	5090 ± 240	5.09 ± 0.24
OZN662	Untreated black wood	4195 ± 35	4740 ± 170	4.74 ± 0.17
OZN664	Holocellulose	4300 ± 40	4835 ± 150	4.835 ± 0.15
OZN665	ABOX pre-treatment	4235 ± 35	4775 ± 150	4.775 ± 0.15

It is a somewhat unexpected outcome, that the ages are all so similar and close to the age of the cellulose sample, including the untreated wood sample, from which the age result includes all the organic contamination that has stained the sample black. In fact, the three non-cellulose dates (untreated, holocellulose and ABOX) are statistically the same when their uncertainties are considered and they have a pooled mean radiocarbon age of 4239±21 years BP. They are, however, significantly younger than the SANU cellulose date, reinforcing the conclusion that full cellulose extraction is the most effective pre-treatment. The relatively old age of the untreated sample, close to the true age of the wood sample, shows that all the organic contamination of the sample occurred very soon after burial, rather than occurring due to contamination beginning after deposition and continuing till the present. It is likely that organic contamination would have begun with absorption of bacterial and fungal carbon as decay of the wood sample occurred followed by absorption of soluble organic carbon compounds (especially humic compounds) supplied by vertical or lateral soil moisture or groundwater movement. The restriction to early contamination may imply either that groundwater circulation (either vertical or lateral) around the sample has been minimal or absent or that mobile groundwaters have carried little or no soluble organics.

The age of the wood sample should be slightly older than the age of deposition of the enclosing scroll-plain sands to allow some time for the age of the tree and for reworking of the wood into final deposition position. Therefore the age of sediment deposition, which is stratigraphically close to the age of initiation of the Coonambidgal 1 Darling River scroll-plain phase at this site, is likely to be slightly before 5 ka.

In summary, the age of onset of the Coonambidgal 1 Darling River scroll-plain phase has been investigated at three sites and the age of termination of the phase has been investigated at one site. Individual scroll-plain sites are unlikely to all contain sediments that date to the initiation of the lateral-accretion phase and a larger number of dated sites will be required to accurately determine that age. However, it is more likely that most sites close to the river will be close to the age of termination. Accordingly, the Coonambidgal 1 Darling River scroll-plain phase is believed to have been active between 7-5 ka and 2-3 ka, with initiation probably considerably later than the terminal Pleistocene age of 13 ka inferred by Bowler *et al.* (1978) from Tilpa.

Coonambidgal Phase 2 Talyawalka-Anabranch scroll-plain chronology.

OSL dating samples from the Coonambidgal 2 anabranch-phase scroll plain were obtained for the initial batch from tractor-dug trenches in the scroll plain of an abandoned meander of the Talyawalka Creek on Appin Station just south of the Menindee-Ivanhoe road (Figure 5-110, Figure 5-118). Across the scroll plain from youngest to oldest, dates of 18.7 ± 2 ka from 2.37 m in trench TAL02, 17.9 ± 1.6 ka from 2 m in trench TAL03 and 21.3 ± 2.2 ka from 3.19 m in trench TAL04 were obtained (Figure 5-119, Figure 5-120 and Figure 5-121).

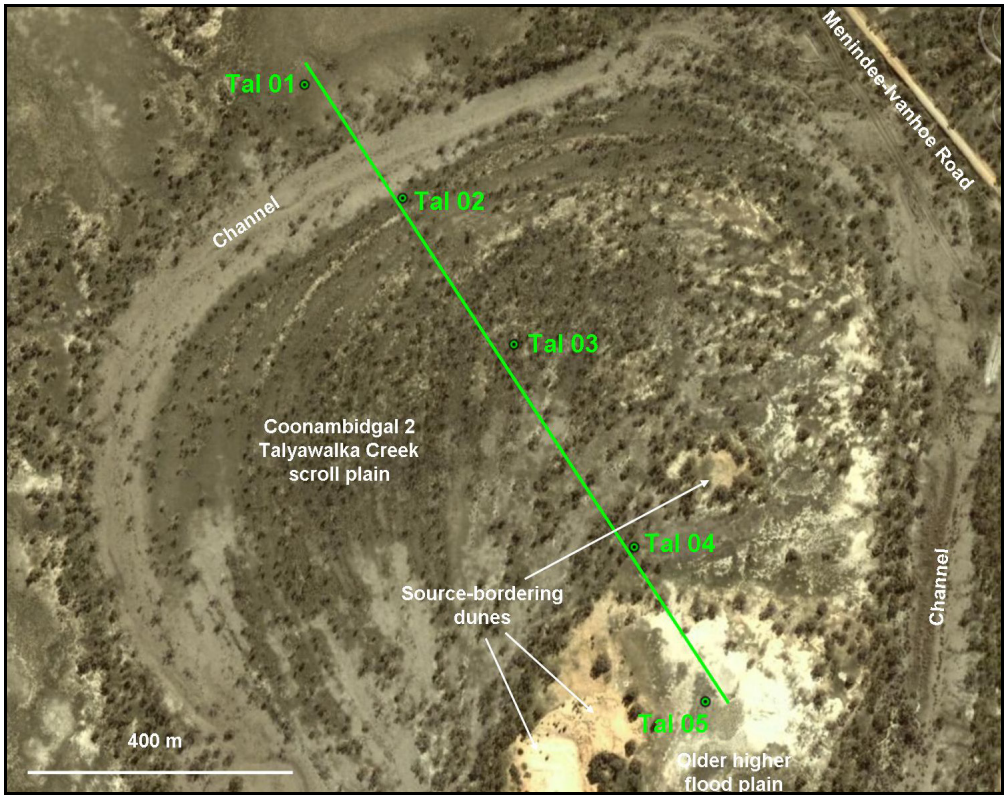

Figure 5-118. *Location of OSL sample sites on the Talyawalka Creek scroll plain on Appin Station.*

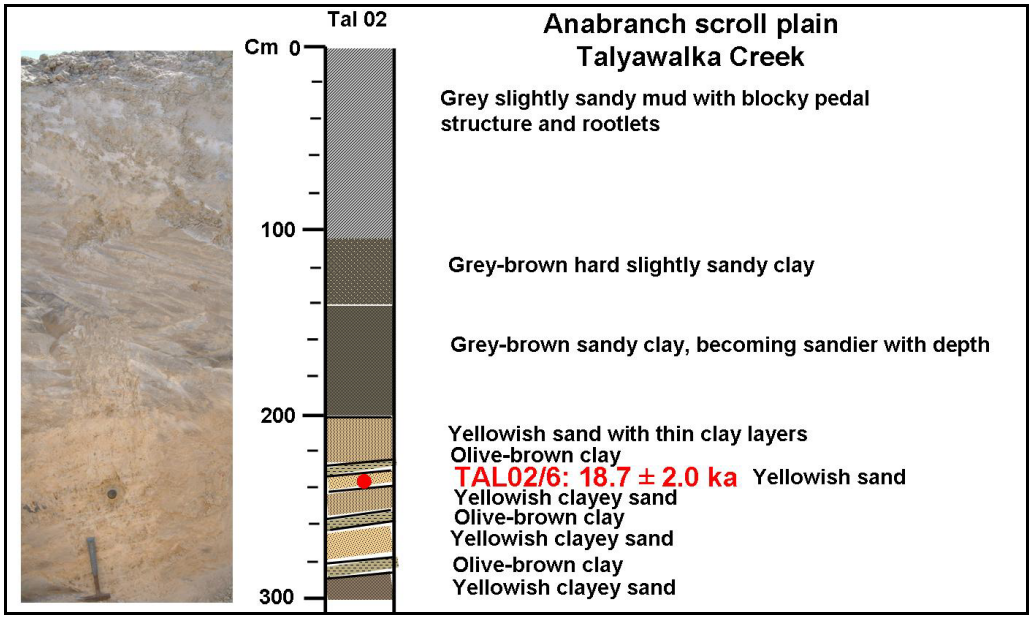

Figure 5-119. *Stratigraphy of tractor trench TAL02 showing the OSL dating result in red.*

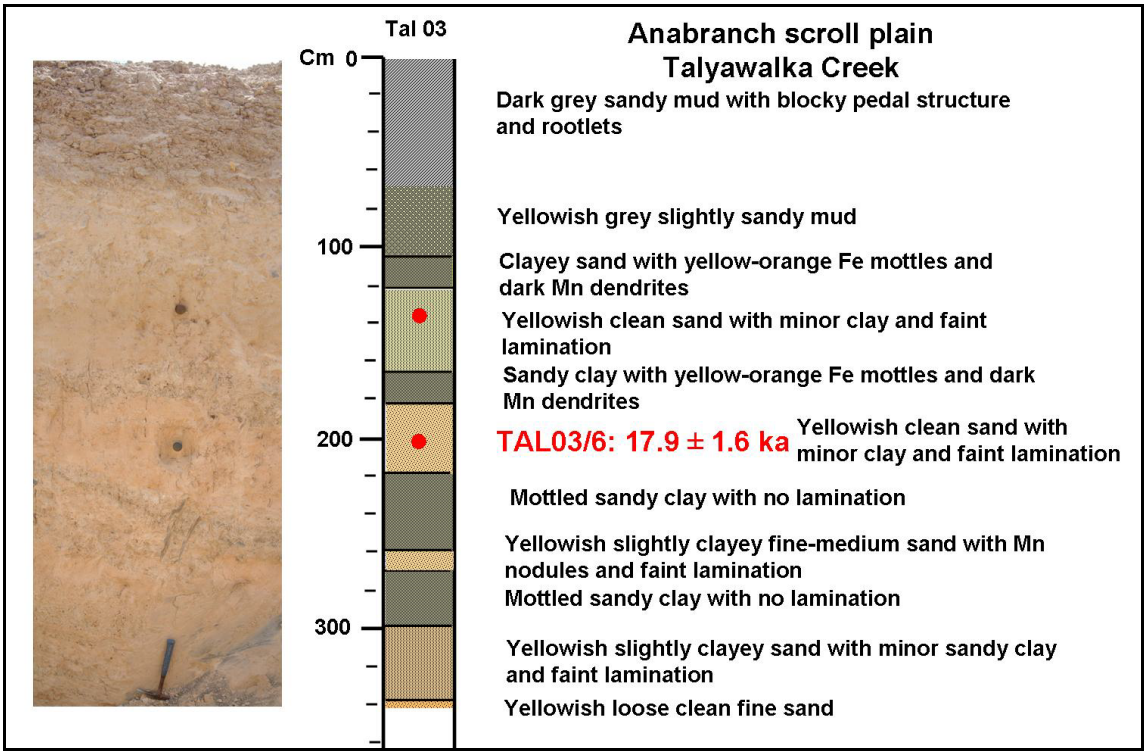

Figure 5-120. *Stratigraphy of tractor trench TAL03 showing the OSL dating result in red.*

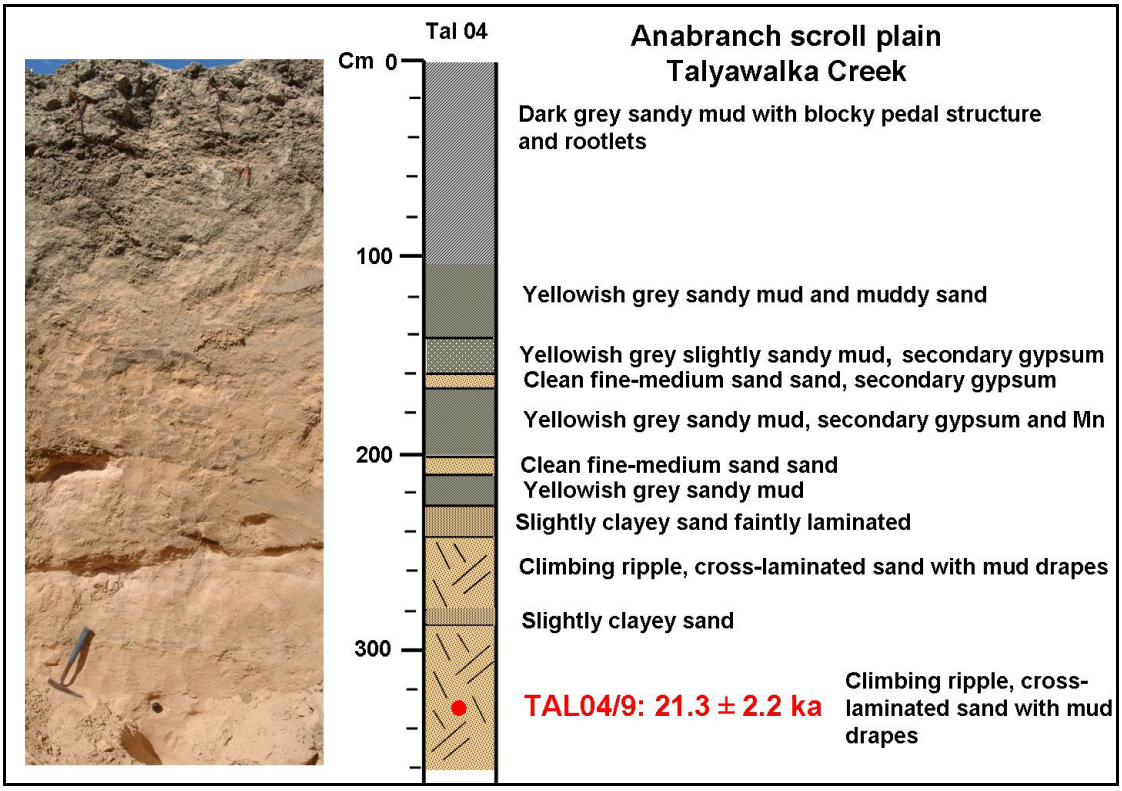

Figure 5-121. *Stratigraphy of tractor trench TAL04 showing the OSL dating result in red.*

In the second OSL dating batch, samples were targeted from two sites in the Coonambidgal 2 Talyawalka-Anabranch scroll-plain phase from the southern portion of the project area south of Menindee. The first site was located on Tandou Station (Figure 5-110) where Coonambidgal 2 lateral-accretion sands overlie the relict scroll-plain phase in the Coonalhugga Creek tract and date to 19.3 ± 1.7 ka at 2.05-2.2 m in hand-auger hole TAN01 (Figure 5-122, Figure 5-123). The second site is on the scroll plain of the Great Darling Anabranch on Cuthero Station (Figure 5-110) where Coonambidgal 2 lateral-accretion sands date to 20.7 ± 2 ka at 5.2-5.32 m in hand-auger hole CUTH01 (Figure 5-124, Figure 5-125).

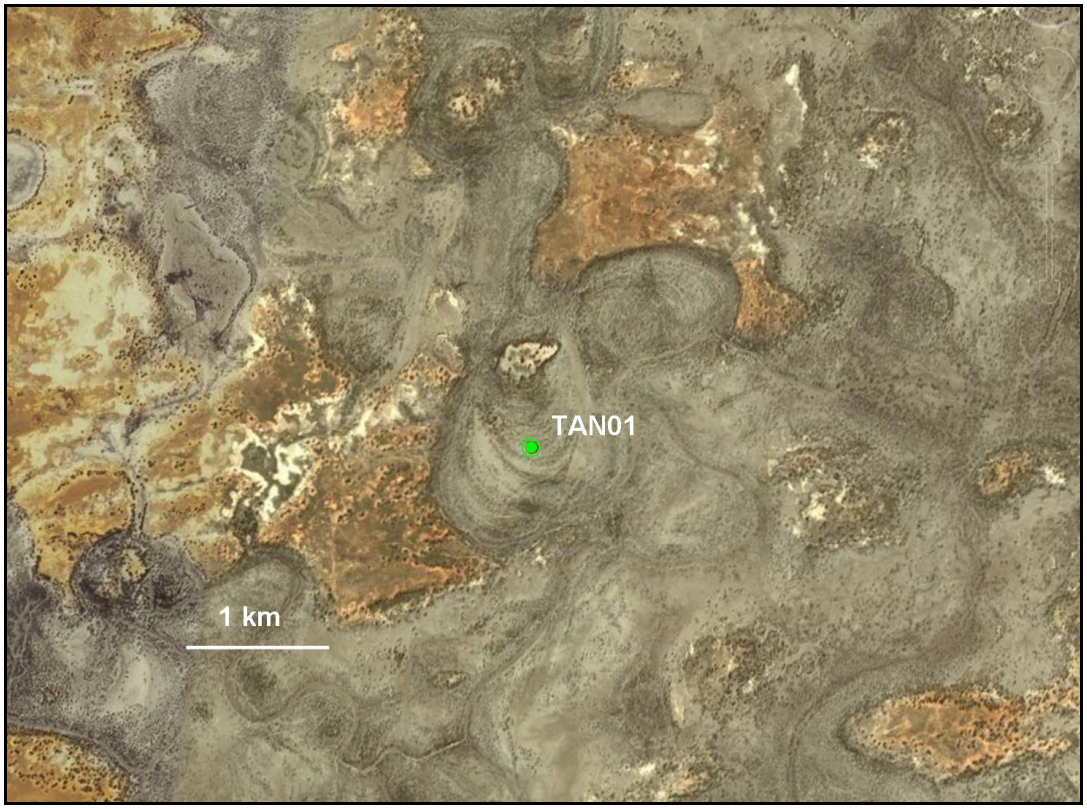

Figure 5-122. *Location of the OSL sample site on the Coonalhugga Creek scroll plain on Tandou Station.*

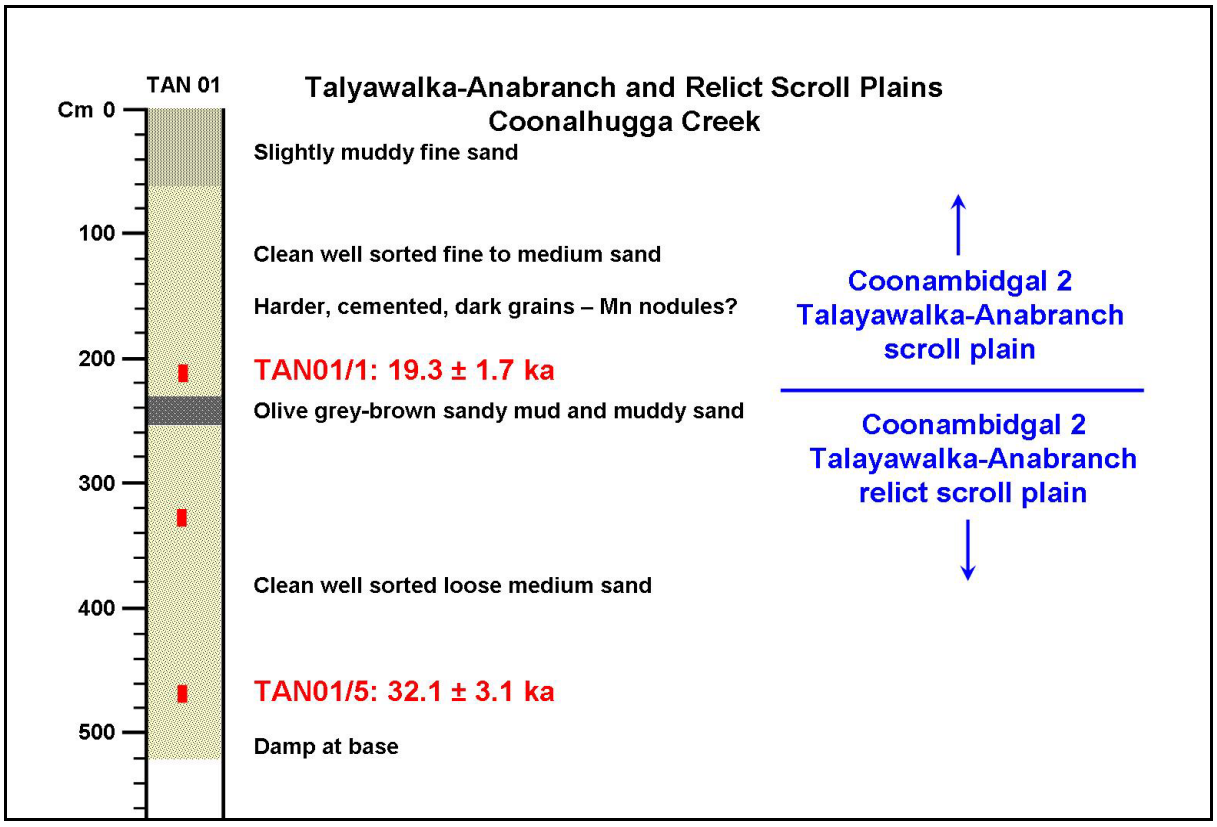

Figure 5-123. *Stratigraphy of hand-auger hole TAN01 showing the OSL dating results in red.*

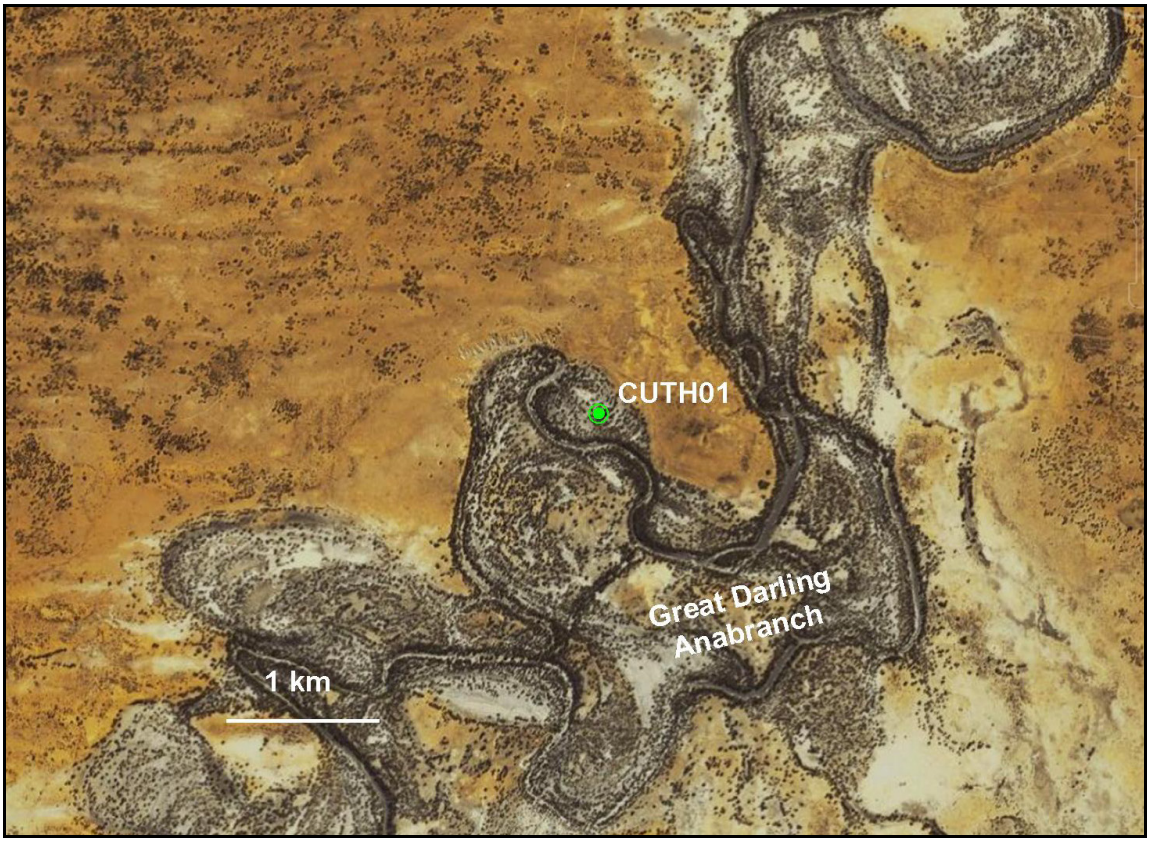

Figure 5-124. *Location of the OSL sample site on the Great Darling Anabranch scroll plain on Cuthero Station.*

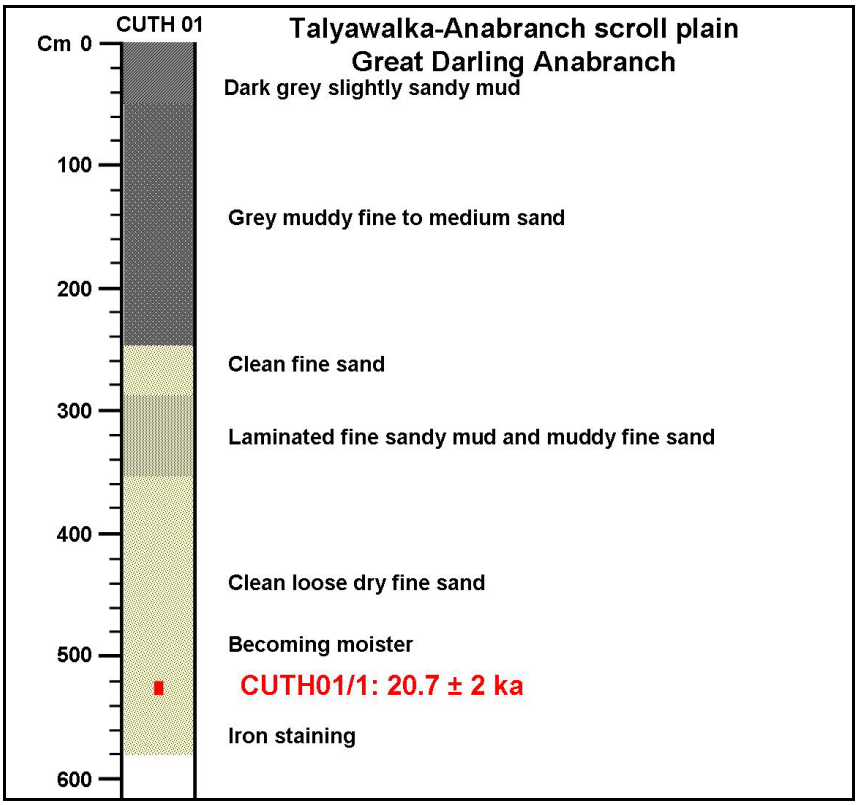

Figure 5-125. *Stratigraphy of hand-auger hole CUTH01 showing the OSL dating result in red.*

In summary all five OSL dates from the Coonambidgal 2 Talyawalka-Anabranch scroll-plain phase cluster tightly between 21.3 and 17.9 ka and therefore accord well with the calibrated radiocarbon dates (20-23 ka) obtained from Acres Billabong scroll-plain deposits near Tilpa by Bowler *et al.* (1978) and confirm deposition of this phase over only a few thousand years at time of the LGM (Last Glacial Maximum, around 20 ka).

Coonambidgal Phase 3 Relict Talyawalka-Anabranch scroll-plain chronology.

In the second OSL dating batch, samples were targeted from two sites in the Coonambidgal 3 relict Talyawalka-Anabranch scroll-plain phase from both the northern and southern portions of the project area upstream and downstream of Menindee. The first site was located on Tandou Station (Figure 5-110) where the relict scroll-plain phase in the Coonalhugga Creek tract was dated to 32.1 ± 3.1 ka at 4.5-4.65 m in hand-auger hole TAN01 (Figure 5-122, Figure 5-123). The second site is on the relict scroll plain of the Talyawalka Creek on Larloona Station (Figure 5-110) where Coonambidgal 3 lateral-accretion sands date to 24.9 ± 2.1 ka at 4.5-4.65 m in hand-auger hole LAR01 (Figure 5-126, Figure 5-127).

In summary, the two dates from widely separated sites correlated to this phase span more than 5 ka, whereas the meander morphology and preservation appears identical (Figure 5-119; Figure 5-123). More dates are required to unequivocally determine the age-span of this event.

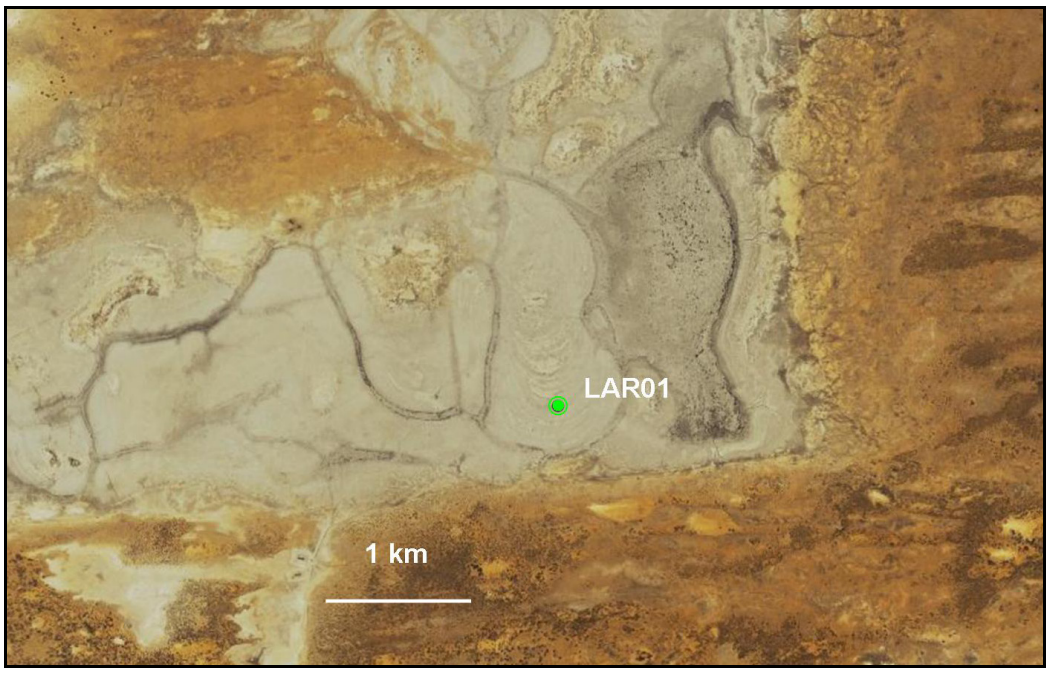

Figure 5-126. *Location of the OSL sample site on the relict Talyawalka scroll plain on Larloona Station.*

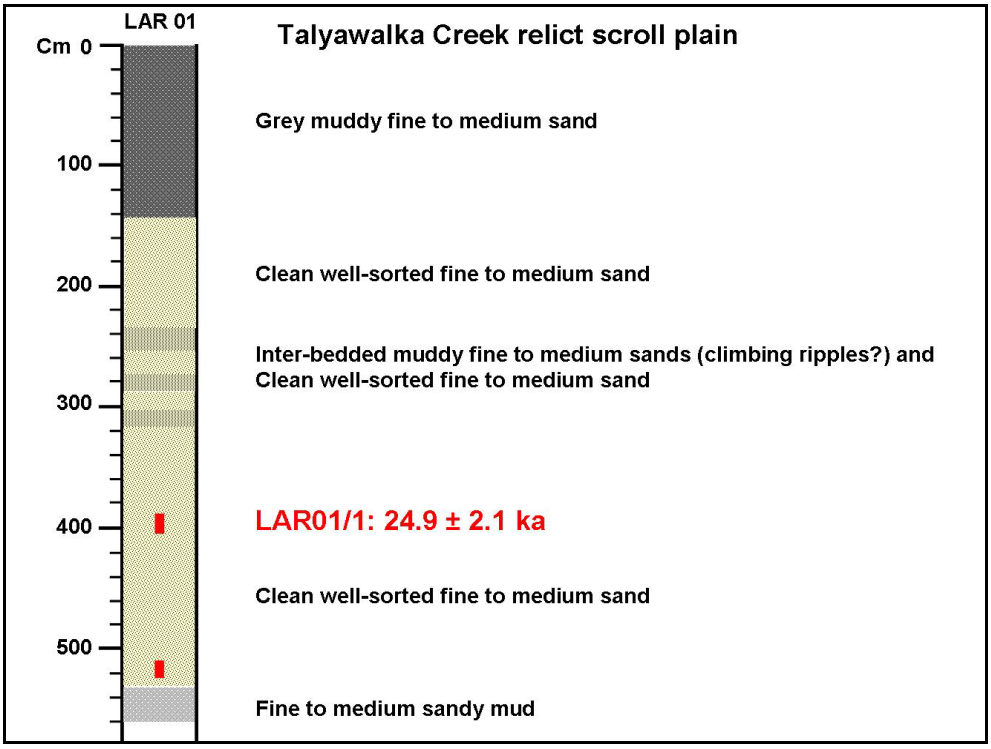

Figure 5-127. *Stratigraphy of hand-auger hole LAR01 showing the OSL dating result in red.*

Coonambidgal Phase 4 Relict Darling River scroll-plain chronology.

No samples specifically from the Coonambidgal 4 relict Darling River scroll-plain phase have been dated. However, the older scroll plain adjacent to the Coonambidgal 1 Darling River scroll plain phase at trench site DR02 (Figure 5-110, Figure 5-111, Figure 5-128), which was discussed earlier, may belong to this phase. Similarly, samples from the Menindee Formation higher floodplain at Chalky Well station (CHW02, Figure 5-110, Figure 5-114, Figure 5-131) are from a portion of the higher floodplain that shows indications of channel and possible scroll traces. Based on their location and appearance, it is possible that these two sites are equivalent in age to the Coonambidgal 4 relict Darling River scroll-plain phase. Dates from both sites are detailed in the next section and they suggest a scroll-plain phase active between 50 and 45 ka.

Menindee Formation scroll-plain phase chronology

Three OSL samples from the first dating phase at the Darling River site (Figure 5-110, Figure 5-111) dated lateral accretion sands of the Menindee Formation. These dates are 47.4 ± 6.3 ka at 3.45 m in trench DR02 in the older scroll plain of unknown affinity (Figure 5-128), 38.9 ± 6.5 ka at 4.05 m depth in trench DR03 in a floodplain remnant (Figure 5-129) and 85.3 ± 15.6 ka at 2.7—2.8 m depth in hand-auger hole DR06 on the higher floodplain at the margin of the Darling River tract (Figure 5-130). The dates from trenches DR02 and DR03 provide an inversion of the expected ages. The geomorphic interpretation (Figure 5-111) implies that the triangular piece of remnant floodplain where trench DR03 is located has been incised on two sides by the older scroll plain to the north west and the older channel to the south. Therefore the date from trench DR02 in the older scroll plain should be younger than the date in trench DR03 from the floodplain remnant. Further geomorphic investigation and dating will be required to resolve this apparent contradiction.

The age of lateral accretion in the Menindee Formation was investigated in the southern part of the area downstream of Menindee on Chalky Well Station (Figure 5-110, Figure 5-114). Dates of 45.4 ± 5.5 ka at 2.3-2.48 m depth and 51.9 ± 5.2 ka at 3.5-3.67 m depth were obtained in hand-auger hole CHW02 (Figure 5-131).

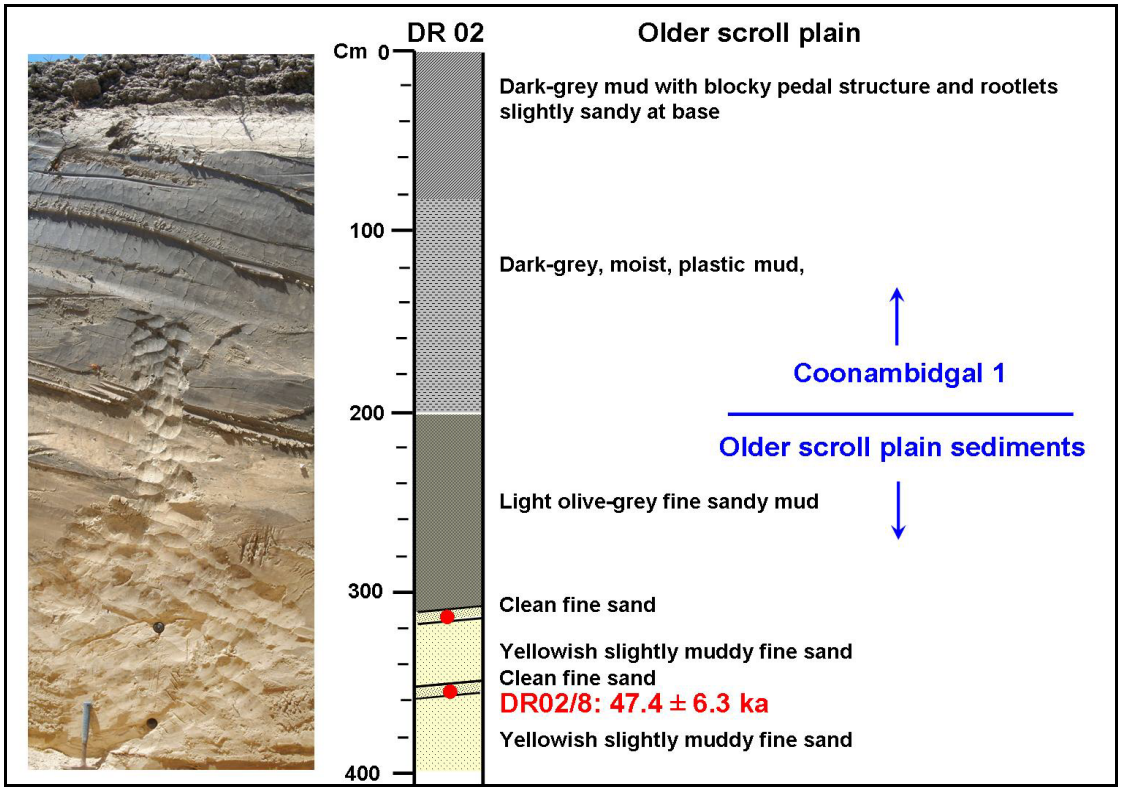

Figure 5-128. *Stratigraphy of tractor trench DR02 showing the OSL dating result in red.*

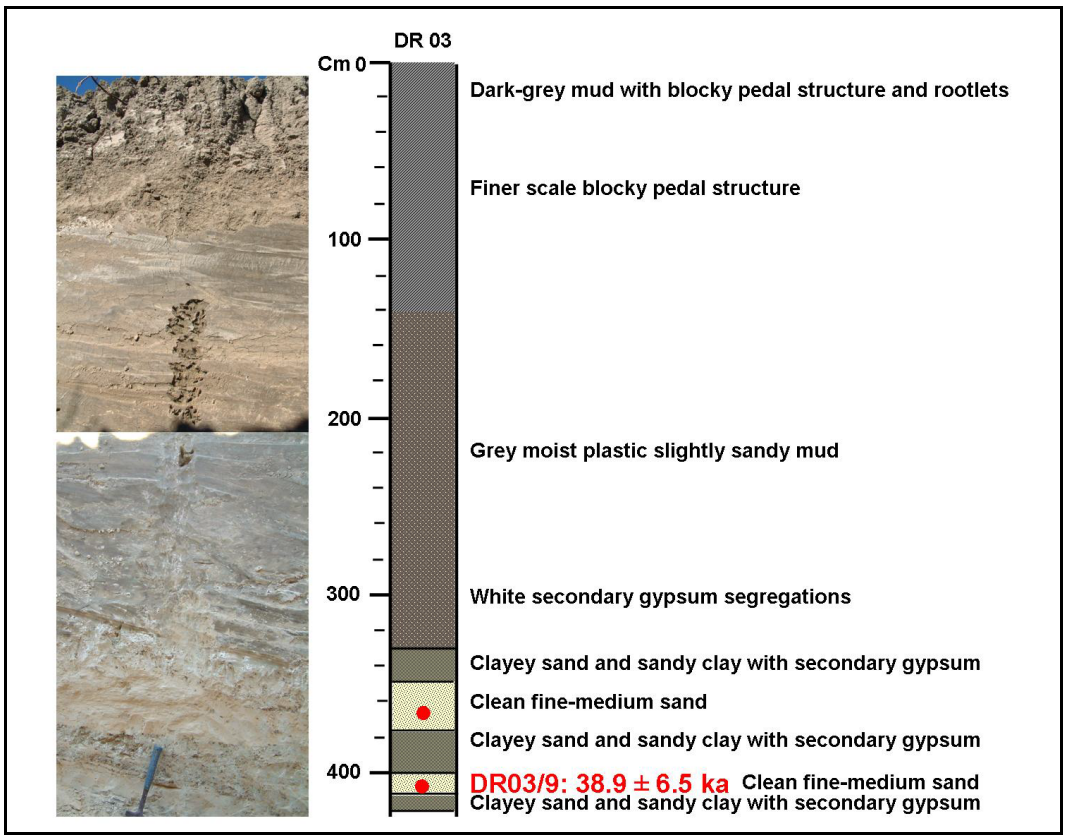

Figure 5-129. *Stratigraphy of tractor trench DR03 showing the OSL dating result in red.*

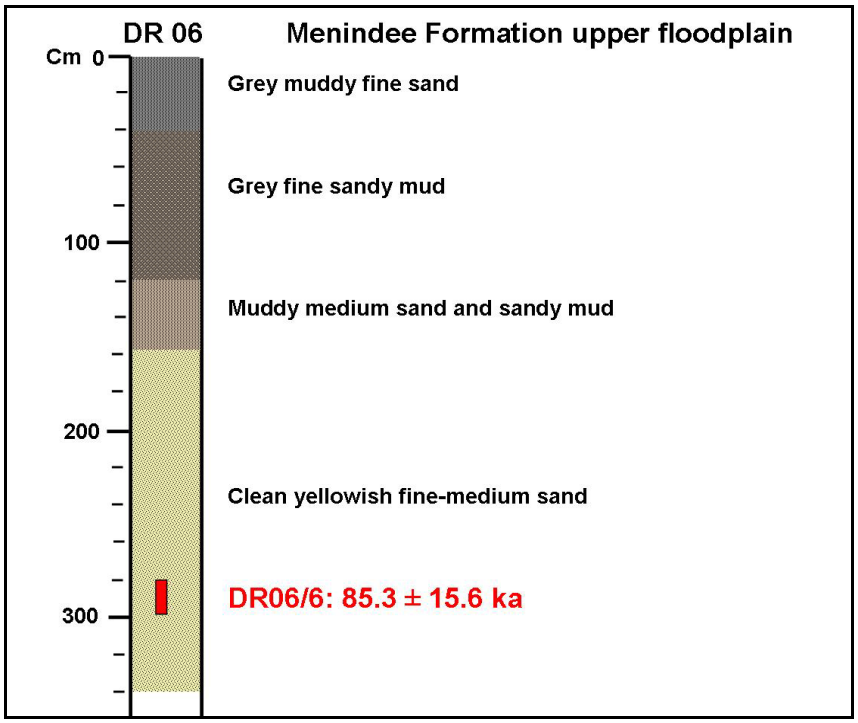

Figure 5-130. *Stratigraphy of hand-auger hole DR06 showing the OSL dating result in red.*

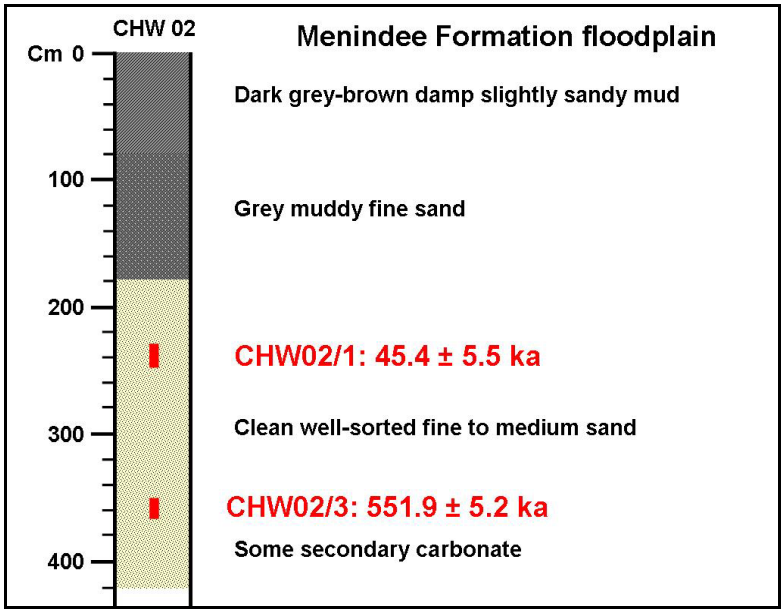

Figure 5-131. *Stratigraphy of hand-auger hole CHW02 showing the OSL dating results in red.*

In an attempt to extend back in time the ages obtained from Menindee Formation lateral-accretion sands a variation of the sonic coring technique which utilises a Lexan liner in the core barrel was successfully modified for OSL sampling (Lawrie *et al.,* 2012a). This was done in drillhole BHMAR 75-8 situated on the highest elevation floodplain at the margin of the Darling River tract on Menindee Common (Figure 5-110, Figure 5-116). A date of >150 ka was obtained from 9.8-9.95 m depth in BHMAR 75-8, close to the base of the lateral accretion sand at 11.3 m (Figure 5-132).

Two additional samples were OSL dated which have relevance for the Menindee Formation. Firstly, a sample from the lateral-accretion sands of the Menindee Formation equivalent lateral-valley deposits that underlie the north-eastern end of Lake Menindee (Figure 5-110) that were discussed above. In hand-auger hole MN01 on the lake floor an OSL date of 84.6 ± 12.4 ka was obtained from lateral-accretion sand at a

depth of 4.6-4.78 m (Figure 5-133, Figure 5-134). The relevance of this date for the Quaternary fluvial stratigraphy of the project area in the Darling Valley is discussed above in the section on Menindee Formation lateral-valley fluvial sediments.

The second OSL sample with relevance for the Menindee Formation is a date from a floodplain bar on the Three Mile Creek floodplain (Figure 5-110). These bars on the upstream portion of the Three Mile Creek flood plain where it diverges from the Darling River tract are at the downstream end of a complex pattern of very large depositional bars and intervening scour channels. These features are present in the northern part of the project area particularly upstream of the lakes where the floodplain is relatively restricted between the north–western valley margin and large areas of within-valley aeolian deposits. The Three Mile Creek flood plain bar and scour channel complex is part of the Yampoola Corridor discussed above. These bars are taken to be evidence of extremely large megafloods which have affected the Darling River in the past. Megafloods have been well documented from other Australian semi arid Central Australian river systems (Bourke, 1994; Bourke and Pickup, 1999). An equivocal date with two possible ages of 3.0 ± 0.7 ka or 7.7 ± 1.5 ka was obtained from a sample at 3 m depth in tractor trench 3MC06 (Figure 5-135, Figure 5-136).

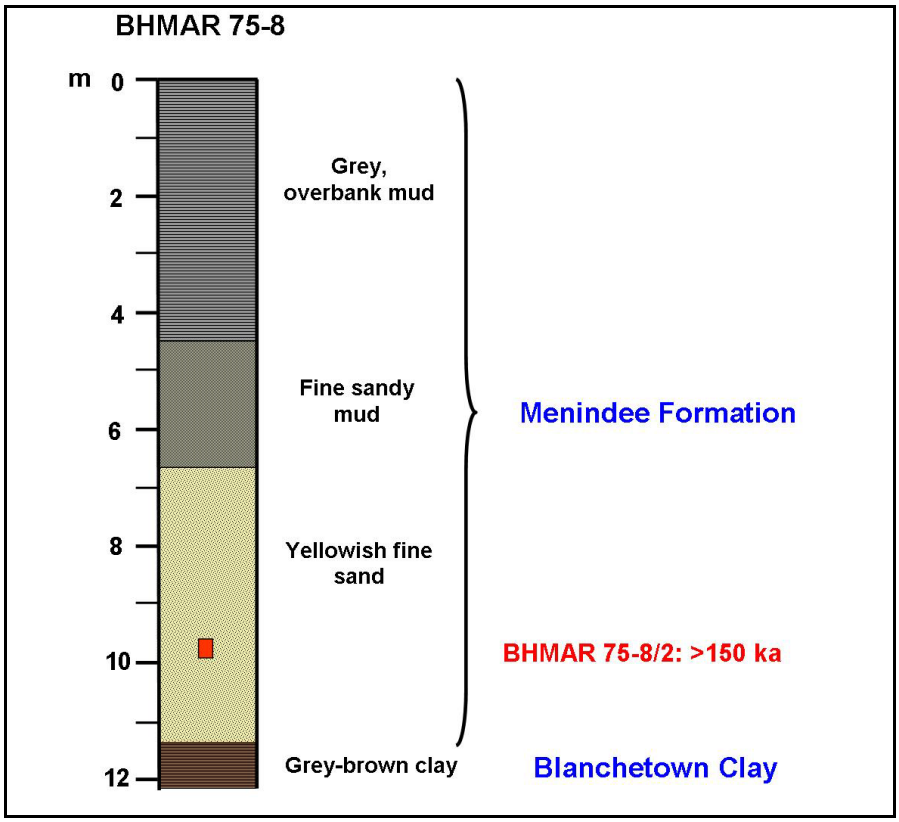

Figure 5-132. *Summary stratigraphic log of sonic-cored drillhole BHMAR 75-8 showing the OSL dating result in red.*

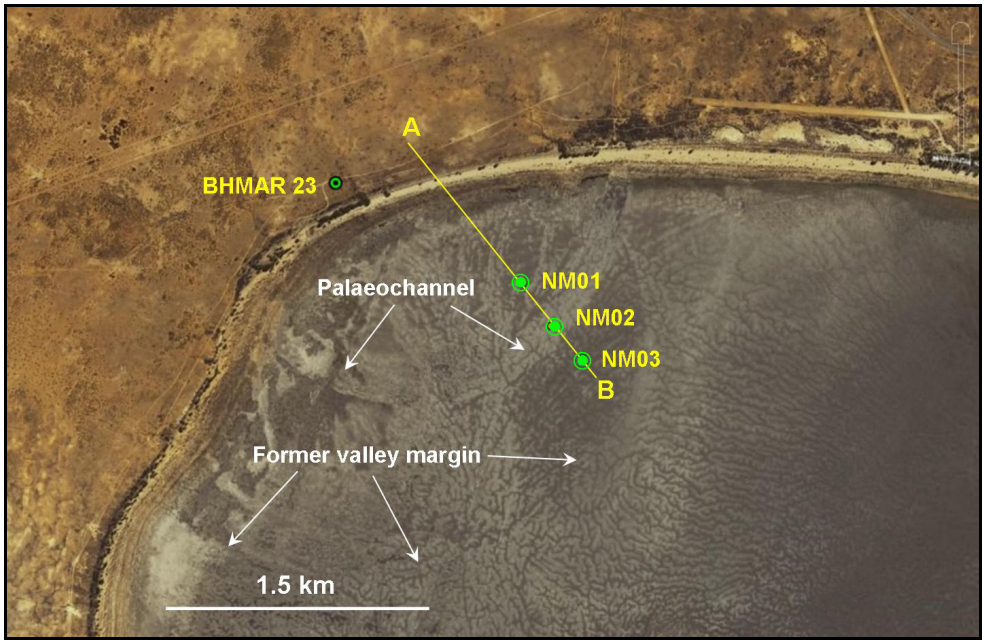

Figure 5-133. *Location of the OSL sample site in hand-auger hole MN01 on the north-western Lake Menindee floor, near the BHMAR 23 borehole. The palaeochannel and ancient valley margin now underlying the lake are marked. The line A – B marks the line of section through the hand-auger holes shown in Figure 5-134.*

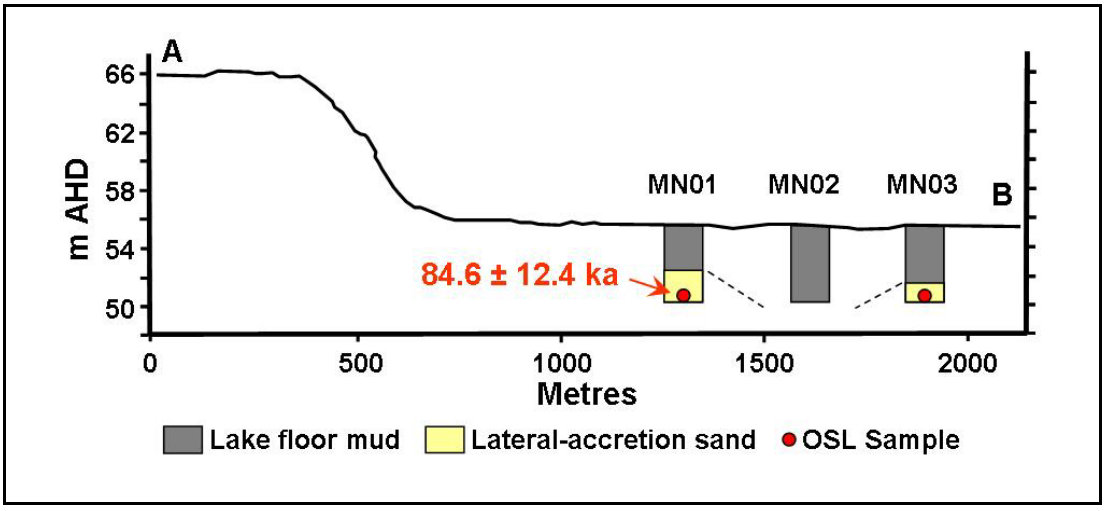

Figure 5-134. *Stratigraphy of hand-auger holes MN01-3 at the north-western end of Lake Menindee, showing the OSL dating results in red.*

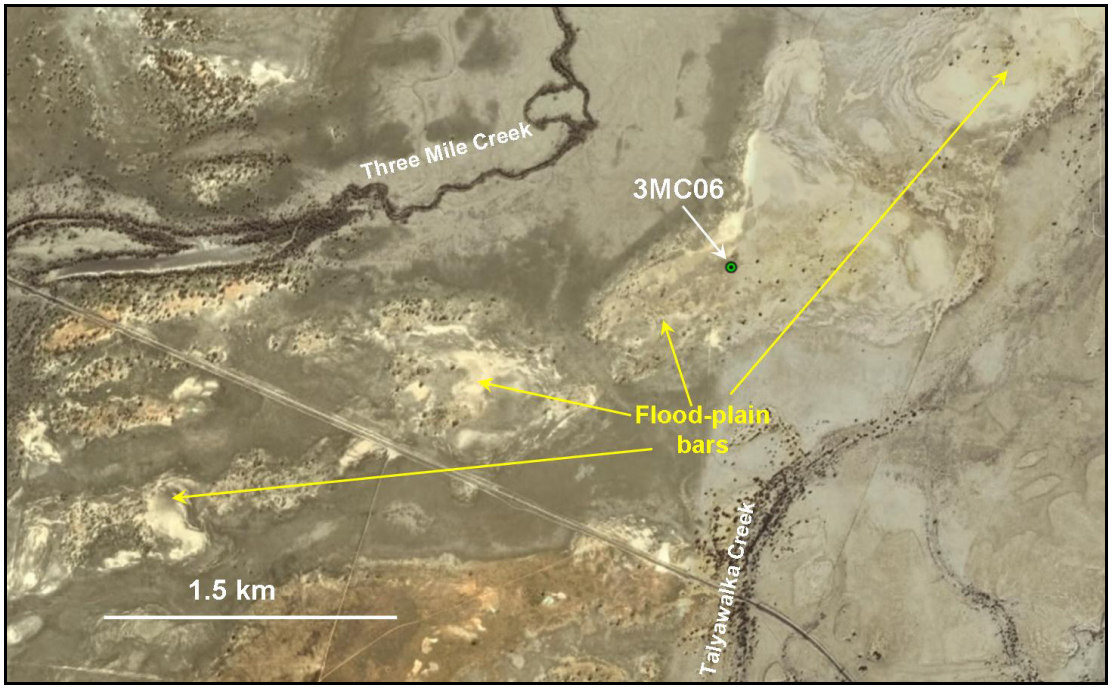

Figure 5-135. *Location of the tractor trench 3MC06 on a floodplain bar on the Three Mile Creek Menindee Formation floodplain.*

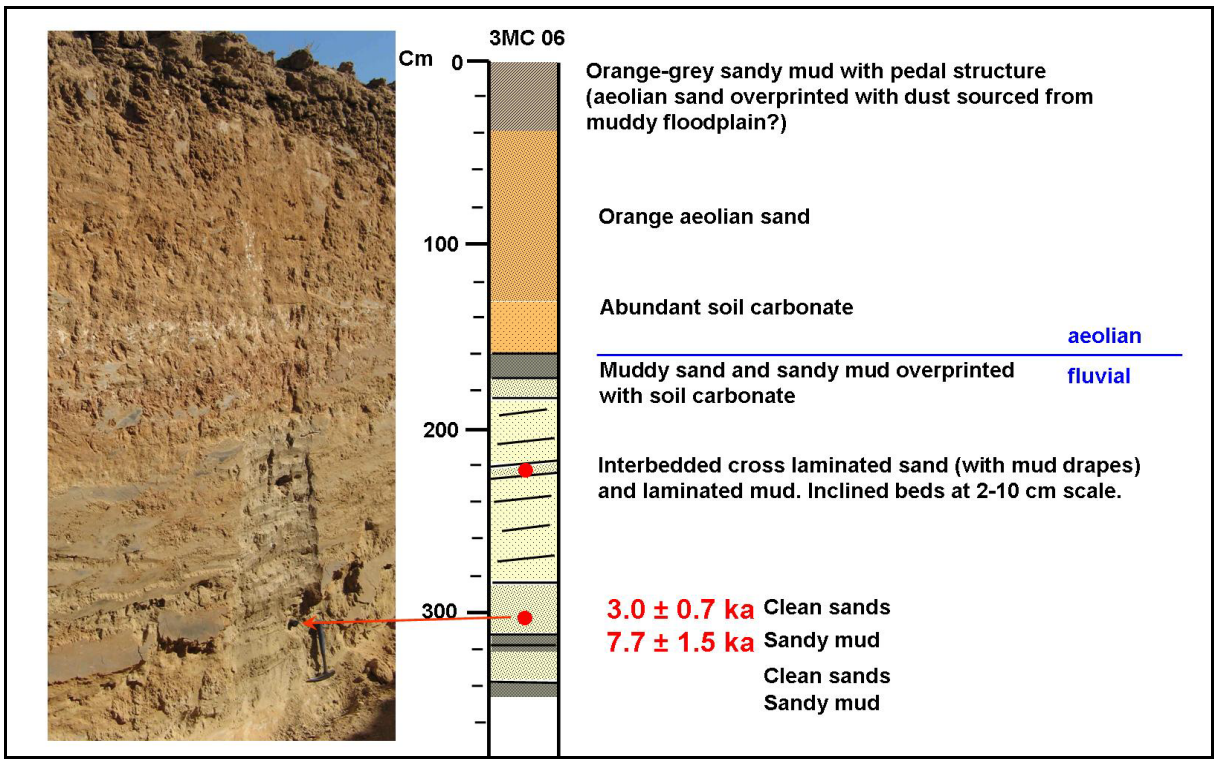

Figure 5-136. *Stratigraphy of tractor trench 3MC06 on a floodplain bar on Appin Station showing the OSL dating result in red.*

This OSL dating sample was the only one of nineteen dates which gave equivocal results. The stratigraphic sequence in the trench (Figure 5-136) consists of 1.5 m of orange aeolian sand with relatively well developed pedogenic secondary carbonate overlying fluvial interbedded sand, sandy mud and ripple cross-laminated sand. The upper bed of the fluvial sequence consists of muddy sand and sandy mud and this texture contrast has resulted in impregnation by a secondary pedogenic carbonate overprinted from the overlying aeolian sand. The initial interpretation of this sequence was of Menindee Formation aged fluvial deposition of flood bars with later aeolian reworking of the upper sands and a considerable period of time to mobilise relatively well developed pedogenic carbonate. No numeric ages had yet been derived from the project area and based on the stratigraphic interpretation reported above a pre Holocene age was expected. The OSL laboratory reported that the radial plot of natural dose results (ED) indicated that there might be two groups of grains, having distinct ages (Figure 5-137). The two groups of grains produce the two possible alternate ages for this sample of 3.0 ± 0.7 ka or 7.7 ± 1.5 ka.

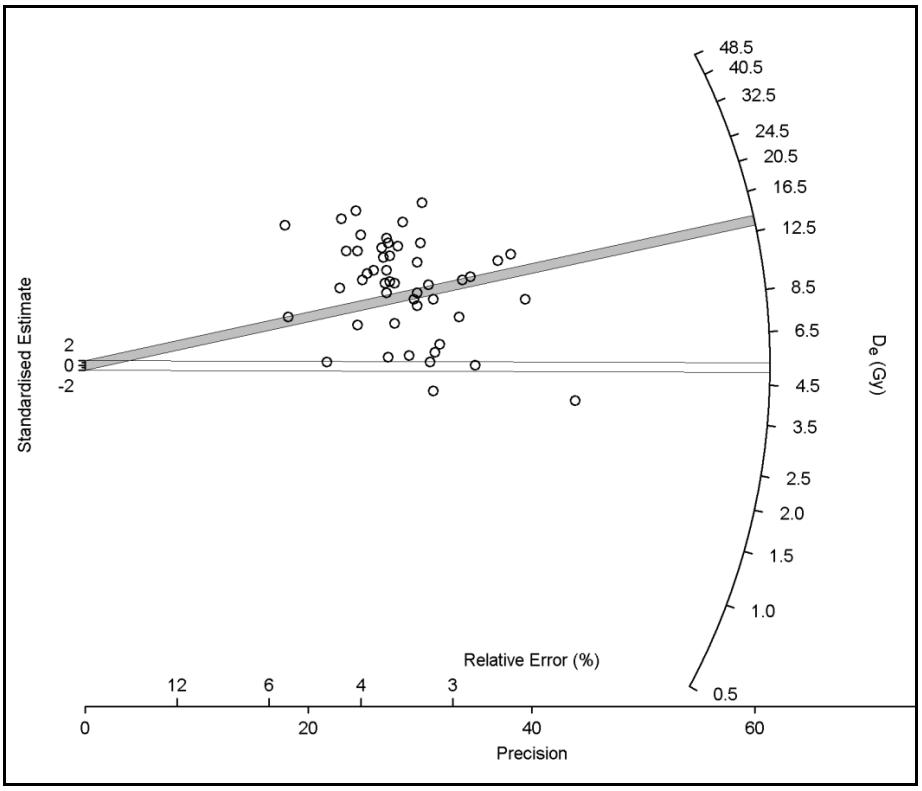

Figure 5-137. *Radial plot of OSL sample 3MC06/10 indicating two possible Equivalent Dose (ED) values: 5.19 ± 1.56 and 13.54 ± 2.72. A radial plot has ED on the curved y axis, and precision / relative error on the x axis.*

There are both post-depositional and depositional mechanisms that can explain populations of grains with mixed ages. The post-depositional mechanism involves mixing of grains up and down the profile by pedogenic or bioturbation processes. This could certainly be important if the sample came from the upper aeolian sand unit which has abundant evidence of pedogenesis. However, the sample comes from 1.5 m below the lower boundary of the aeolian sand and the pedogenic overprint of the upper portion of the fluvial unit only extends about 20 cm. The sample comes from ripple cross-laminated sands with fine mud drapes preserved, clear evidence that no post-depositional mixing has occurred.

The depositional situations that can result in populations of mixed age include various mechanisms of re-working of grains from a previous depositional event without complete bleaching or zeroing of the previous stored energy occurring due to exposure to sunlight. This might occur due to erosion and deposition occurring at night or due to high turbidity of flood waters rendering them opaque to light transition. Normally, sand grains in train in river bedload are moved in multiple depositional episodes, perhaps over months or years before they are finally buried in channel or point-bar sediments, immobilised and begin anew to accumulate OSL trapped energy. This relatively prolonged transport history gives abundant opportunity for full bleaching and zeroing of any previously accumulated OSL energy to occur. The situation

in the floodplain bars, which are only formed by extreme megaflood events, may be quite different and only involve a single depositional event, at a time of high water turbidity. Therefore a likely interpretation of the sand grain population including two age groups is either that two megaflood episodes occurred at about 7.5 ka and 3 ka or that a single megaflood at 3 ka is represented and the floodplain bar at 3MC06 contained grains locally reworked from a sand unit previously deposited about 7.5 ka.

Quaternary fluvial unit chronology summary

Stratigraphic and sedimentological analyses have demonstrated that the Quaternary fluvial units of the Lower Darling Valley, the Coonambidgal and Menindee Formations, have been deposited in mixed-load streams by a number of discrete lateral-migration phases, as lateral-accretion channel and point-bar sand and vertical accretion overbank mud. Continued overbank-mud deposition eventually buries and obscures scroll-plain traces, but up to four successive scroll-plain tracts of the Coonambidgal Formation (termed 1 to 4 from youngest to oldest) have been identified inset into the Menindee Formation higher floodplain, generally with no scroll or channel traces. In between the lateral migration phases, the river is probably similar to today – a suspended-load stream with stable, often carbonate-cemented, banks which is not laterally migrating. Meander geometry dimensions are much larger in previous lateral-migrational phases (Coonambidgal 2-4) than for the one associated with the modern Darling course (Coonambidgal 1) clearly indicating greater river discharge during past episodes.

OSL and radiocarbon dating during this project has provided the first comprehensive numeric chronology for these Quaternary fluvial episodes in the Lower Darling. Lateral migration episodes occurred from 7-5 to 3-2 ka (Coonambidgal 1), 22 to17 ka (Coonambidgal 2), 25 to 30 ka (Coonambidgal 3), 40 to 50 ka (Coonambidgal 4? or Menindee Formation), around 85 ka (Menindee Formation) and >150 ka (Menindee Formation). The chronologically well-controlled episodes back to 30 ka suggest lateral-migrational intervals of about 5 ka separated by approximately 10 ka periods of quiescence. An additional detailed geochronological investigation of the age of lateral accretion sands in the Menindee Formation would almost certainly identify a number of additional episodes.

The mechanism that controls the onset and termination of lateral-migration phases is uncertain but is probably a combination of changes in discharge and sediment regimes. The timing of episodes over the past 30 ka demonstrates activity during highly contrasting phases of the glacial-interglacial climate cycles, from full glacial conditions (20 ka) to full interglacial conditions (7-5 to 3-2 ka Holocene phase). This effectively demonstrates that the onset and termination of lateral-migration phases is not a matter of simple climate-cycle forcing (See long-term climate change section). It is possible that anomalous local production of sandy sediment by highly erosive megaflood events may play a role in the initiation of lateral migration events and possible dates of 3.0 ± 0.7 ka or 7.7 ± 1.5 ka from a floodplain bar interpreted as a megaflood deposit may indicate an association with the Holocene Coonambidgal 1 lateral-migrational phase.

5.4.2 Quaternary Lacustrine Units

5.4.2.1 Lakes in arid and semi-arid Australia

Arid and semi-arid Australia, including the Murray-Darling Basin, is characterised by low elevation, low gradients and negative water budgets and has abundant ephemeral lakes of variable size which comprise four different categories:

Flood-out lakes are the most common type and are connected by a single or multiple channels to an adjacent low-gradient fluvial system. They are filled by passing floods which exceed the feeder channel sill level then partially emptied as the flood peak passes and flow reverses in the feeder channel, until the sill level is reached. Evaporation then lowers lake level until the next flood replenishes the lake, and deflation of the bed during dry periods prevents infilling by sediment. Flood-out lakes can thus contain long but discontinuous lake-level records that reflect the flood history of the adjacent fluvial system.

Overflow lakes are less common than flood-out lakes in arid Australia; they are connected consecutively along a drainage channel and fill successively as each basin overflows to the next along the chain. Effects of

changing hydrology may be felt differentially from upstream to downstream in the system. The Willandra Lakes, east of the Darling Valley, are a classic example of an overflow system.

Terminal lakes are basins at the end of a drainage system with no surface outlet channel. Water is lost by infiltration to groundwater or by evaporation and they are frequently saline. Examples in Australia are Lakes Eyre and Tyrrell.

Groundwater discharge lakes have no connection to co-ordinated surface drainage and occur where saline groundwater discharges at the surface by evaporation. They typically have highly irregular outlines and frequent islands and the combined suite of associated landforms, including sand and gypsum/clay lunettes and islands, sand and clay plains and halite salinas, were termed *boinkas* by Macumber (1980). Lake Gairdner (South Australia) and the Raak Plain (north western Victoria) are examples of large groundwater discharge systems in Australia.

Bowler (1981, 1986) studied the hydrologic evolution and spatial variability of Australian arid-zone lakes by relating catchment area/lake area ratios to climate and runoff functions. The resulting classification illustrated both the factors controlling the palaeoclimatic sensitivity of lakes as well as the controls on sedimentary processes and the resulting sediment records. A hydrologic continuum from wet to dry was recognized to operate both through time, due to Quaternary glacial/interglacial climate cycles and spatially, as climatic zones vary across the continent. When surface water dominates, smooth shorelines are produced and quartz-rich beaches and foredunes, rich in biological carbonates, are deposited on the downwind margins by wind-induced erosion and sediment transport. As hydrological budgets become negative, groundwater and salinity dominate and salt crystallization disrupts lake-floor sediments resulting in deflation to the shoreline of sand-sized sediment aggregates and salts by the dominant wind.

Lakes of all four categories are characterized by lunette dunes on their downwind shorelines which are quartz-rich and contain biogenic carbonate when surface water dominates and are clay-rich and gypseous when groundwater dominates (Bowler, 1973, 1983; Magee, 1991). Because of the almost universal association of Australian arid-zone lakes with lunettes the lakes are often referred to as *lunette lakes*. This strong genetic association between lakes and lunettes and the consequence that lunettes are archives of their source lake's history is the reason that lunettes are here described under the heading of lacustrine rather than aeolian landforms. A predominant wind direction results in wave-eroded cliffs on the upwind margins, long-shore (when wet) or across-lake (when dry) sediment transport and deposition in beaches or lunettes on the downwind margin. In the longer term, this process results in migration of the lake basin into the dominant-wind direction.

5.4.2.2 Lakes in the Lower Darling Valley

The Lower Darling Valley is characterized by a very low-gradient fluvial plain and has abundant ephemeral lunette lakes which are mostly flood-out lakes including both the Menindee Lakes associated with the Darling River and the Anabranch Lakes associated with the Great Darling Anabranch.

Overflow lakes are rare in the Darling system with the exception of the Teryaweynya Creek anabranch, which diverges to the east from the Talyawalka Creek near the Teryawynia/Blantyre Station boundary and continues as an overflow lake system downstream of Dry Lake and Teryaweynya Lake (Figure 5-138). Within the Darling Valley proper, some of the flood-out lakes overflow to separate lake basins with examples being Lake Menindee to Lake Cawndilla, Speculation Lake and Lake Spectacle; and Lake Tandou to Lake Nettlegoe. Similar examples in the Great Anabranch Lake system are Yelta Lake to Bijiji Lake and Nitchie Lake to Lake Mikengay. Artificial canals and inlet and outlet regulators of the Menindee Lakes Storage Scheme have effectively turned part of the Menindee Lakes into an artificial overflow system whereby Lake Pamamaroo overflows via Copi Hollow to Lake Menindee which then overflows to Lake Cawndilla which then overflows back to the river system via an artificial outlet canal.

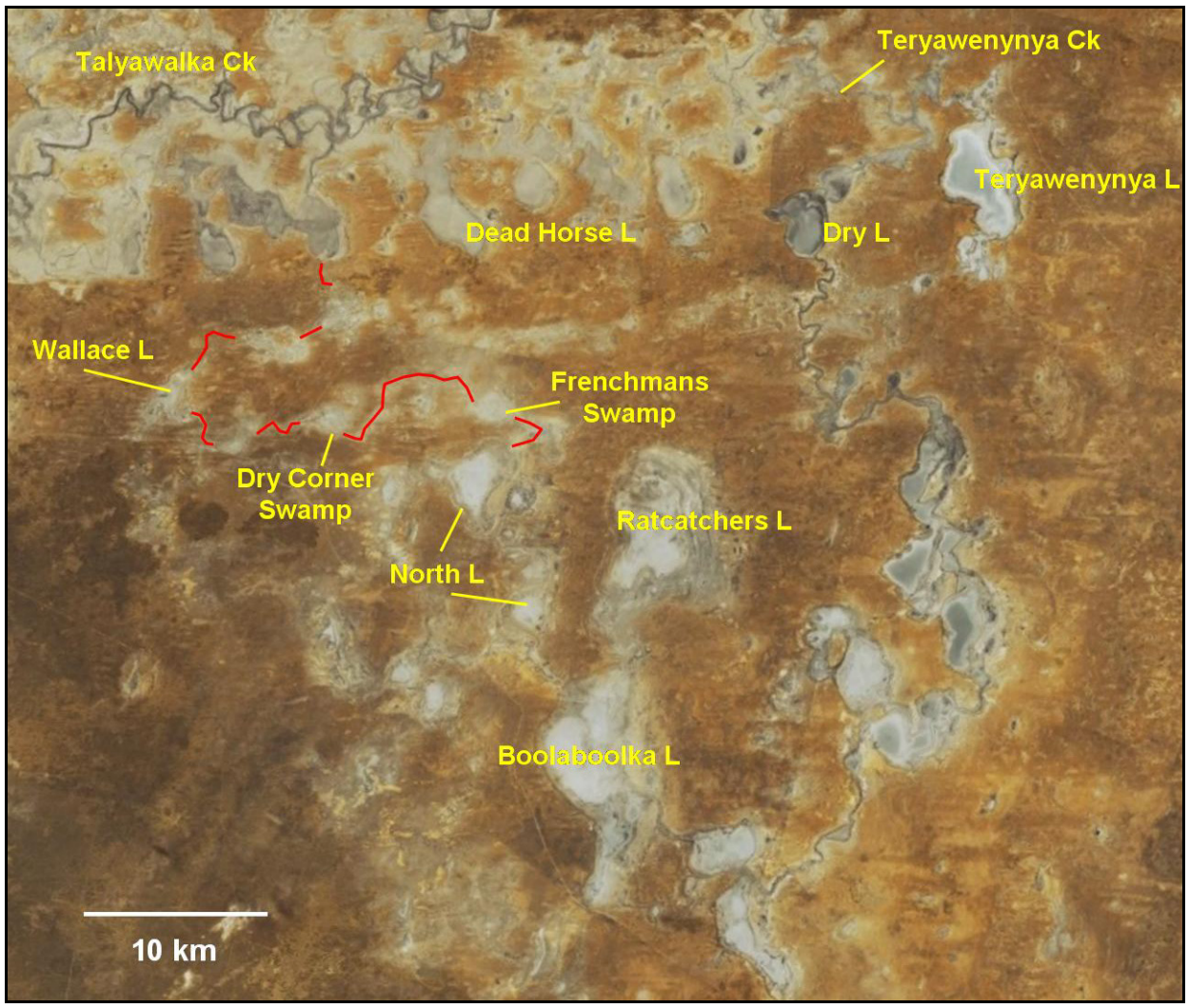

Figure 5-138. *Overflow lake system on the Teryaweynya Creek. Red lines mark the inactive overflow from the Teryaweynya system back to the Talyawalka Creek.*

Terminal Lakes are very rare in the Lower Darling system. New Lake, between Lake Cawndilla and Lake Tandou, is a small terminal lake at the end of the Stephens Creek drainage from the Broken Hill Block to the west (Figure 5-139). However, New Lake shows no evidence of higher salinity, indicating that it is probably not completely closed either for surface hydrology or groundwater leakage. The LiDAR and satellite imagery both suggest a possible overflow from New Lake to Lake Tandou (Figure 5-139) which is inactive in the current regime but probably operated in wetter climatic phases of the Quaternary. The lakes listed above (Cawndilla, Speculation, Nettlegoe, Bijiji and Milkengay) which fill by overflow from flood-out lakes closer to the river are effectively terminal lakes. However, as with New Lake, they show little evidence of increased salinity, indicating that they probably are connected to regional shallow aquifers by groundwater leakage and do not accumulate salts. In the Teryaweynya system (Figure 5-138), Ratcatchers and North Lakes are terminal lakes fed by overflow from Boolaboolka Lake. Though flooding in the historically known period, with artificially enhanced diversion from the Talyawalka to the Teryaweynya, has never extended beyond North and Ratcatchers lakes (Withers, 1996), there are indications of overflow beyond North Lake (Figure 5-138). Satellite imagery indicates now-defunct overflow connection via Frenchmans Swamp, Dry Corner Swamp, Wallace Lake (near Big Ampi homestead) and other small unnamed lakes - eventually extending to the older Talyawalka scroll-plain tract west of Dead Horse Lake. This overflow connection back to the main Darling valley has probably been active in past wetter climatic phases on glacial-interglacial timescales. Because the drainage is not occluded by dunes it is highly probable that the last phase of fluvial activity must post-date the last major dune-building phase. There is some evidence of increased salinity, in the form of complicated multiple lunettes and irregular lake morphologies, in Ratcatchers Lake and other lakes filled by overflow from North Lake. But the lack of significant salinity in the distal lakes of the Teryaweynya system reflects flushing of salts by periodic surface water throughflow to the Darling valley.

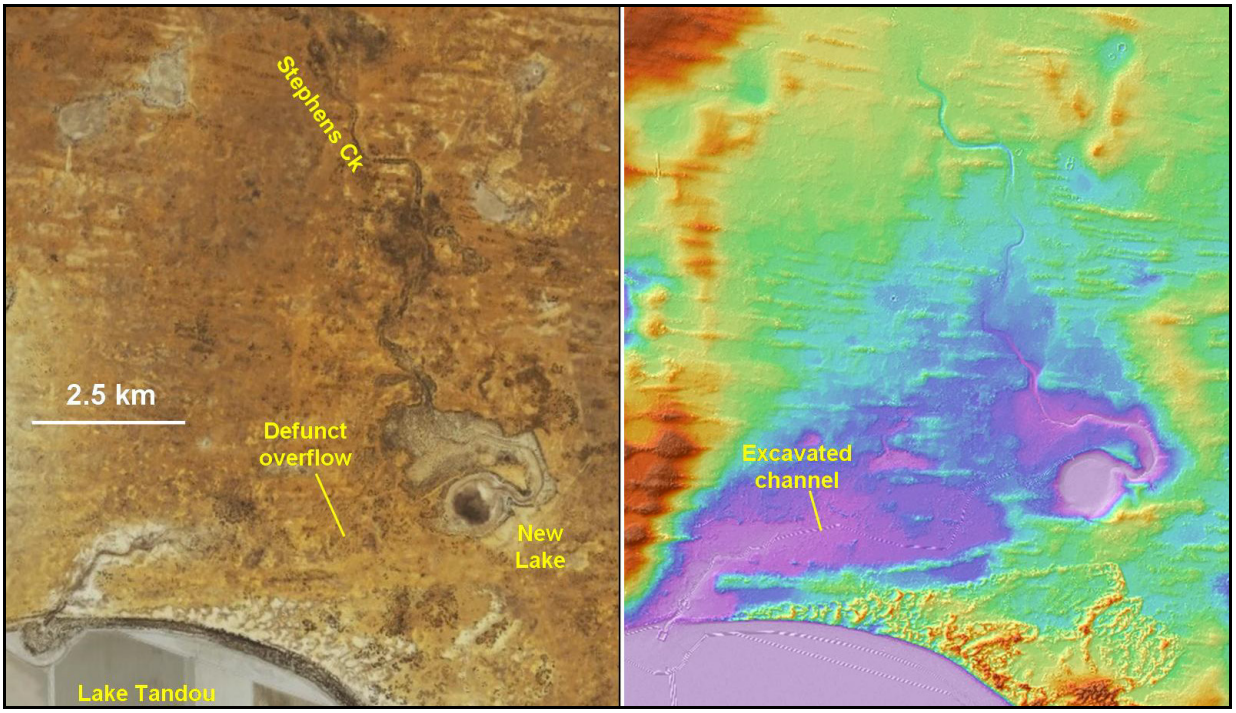

Figure 5-139. *New Lake at the terminus of Stephens Creek. LiDAR view on the right demonstrates a topographic barrier across the former inlet to Lake Tandou. An irrigation canal has been excavated between the lakes.*

Groundwater lakes in the Darling Valley south of the study area

Groundwater in the Pliocene Loxton-Parilla/Calivil Formation sand aquifer in the Darling valley generally flows south towards the Murray River and salinity increases towards the south where numerous widespread groundwater discharge zones occur (Evans & Kellett, 1989). These discharge zones include the Scotia and Nulla boinkas located north of the Murray and west of the Darling and they represent groundwater windows into the Loxton-Parilla Sands (Fergusen *et al.*, 1995, 1997). Evaporative concentration and brine refluxing mechanisms have concentrated groundwater salinity to >100,000 mg/L TDS (Evans & Kellett, 1989). The lake basins are isolated by dunefields and sand plains from fluvial input and present-day groundwater discharge occurs in smaller basins excavated into larger, higher, now-defunct groundwater basins (Cupper, 2005, 2006; Cupper *et al.*, 2000).

Darling lakes water table and the Blanchetown Clay

The Darling and Great Anabranch lakes are subtly different to lunette lakes elsewhere in the Murray-Darling Basin in that they are shallower and have significantly flatter lake floors. This difference reflects the controlling influence exerted by the Blanchetown Clay and the water table within that unit (Figure 5-140). The Late Pliocene to Middle Pleistocene lacustrine Blanchetown Clay sediments were deposited on an irregular land surface at the top of the Pliocene Calivil/Loxton-Parilla Sands. The Blanchetown Clay tends to infill the underlying topography and produce a flatter upper depositional surface. Within the modern lake basins, groundwater-controlled deflation has provided an additional mechanism for producing a horizontal upper Blanchetown Clay surface.

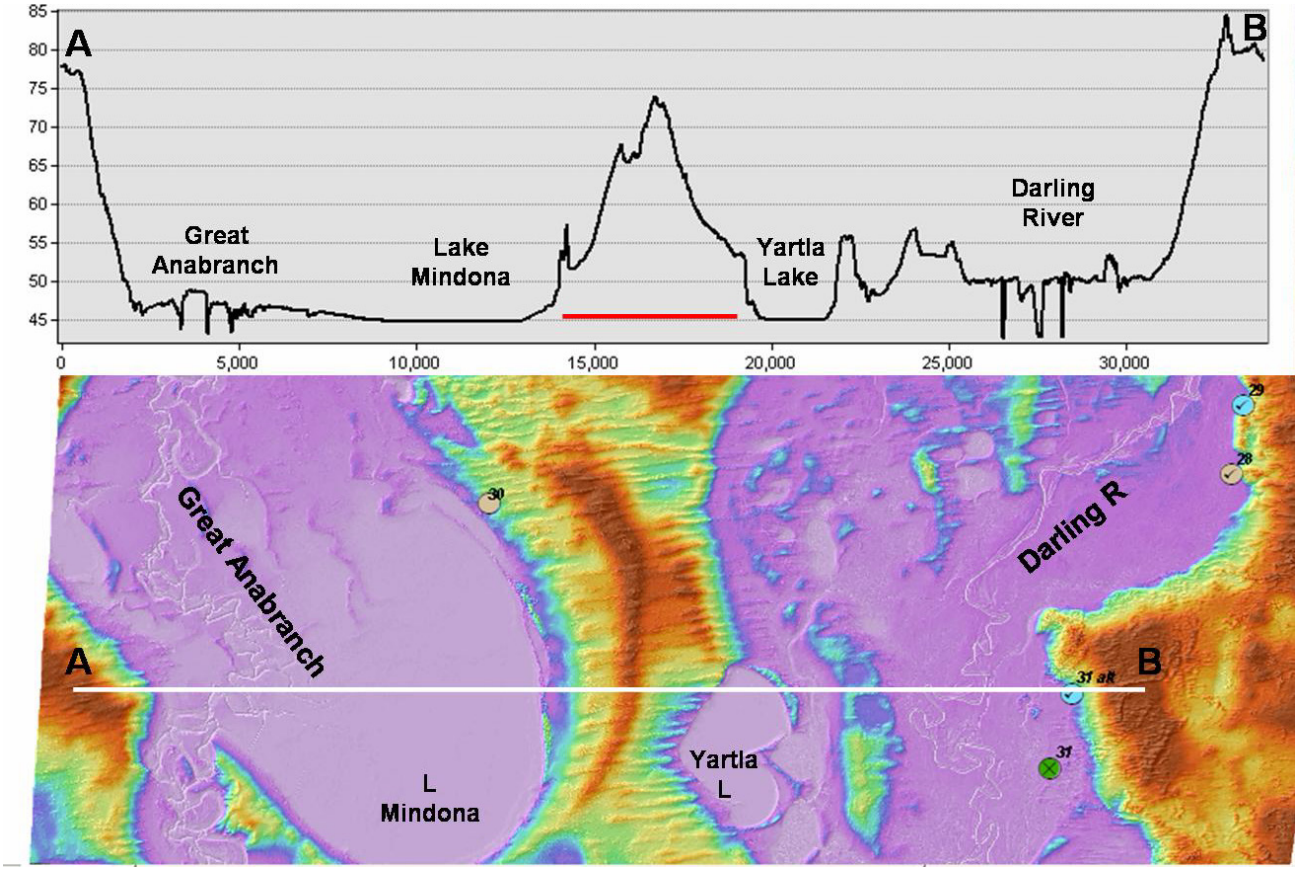

Figure 5-140. *LiDAR view of the southern portion of the BHMAR study area with a cross section (A-B) across the Darling valley showing the floors of Lakes Mindona and Yartla at the same elevation, controlled by the water table in the Blanchetown Clay. The Darling River and the Great Anabranch which feed the lakes are at different levels.*

5.4.2.3 Lunettes

In common with most Murray–Darling Basin lakes the Darling Lakes are characterized by lunettes, lee-side aeolian accumulations derived from the lake basins. These are high-quality archives of the hydrologic state of the lake, with quartz foredune sediments representing lake-full conditions, gypseous, clay pellet-rich sediments reflecting saline groundwater domination, and soils forming when deposition is not occurring. Under full freshwater conditions, wind-induced wave erosion and sediment transport produce smooth shorelines and quartz-rich beaches and foredunes on the downwind margins; sediments are terrigenous and rich in biological carbonates. When full, the lakes of the system provided rich resources for human occupation, and archaeological evidence is abundant in the lunette depositional sites adjacent to the lakes (Balme & Hope, 1990; Hope, 1981; Hope *et al.*, 1983; Hope, 1993; Pardoe & Martin, 2002; Pardoe, 2003). With negative hydrological budgets groundwater and salinity dominate. Salts (particularly gypsum, halite, and sodium sulfates) crystallize displacively in the lake sediments, disrupting them and allowing deflation of sand-sized sediment aggregates and salts by the dominant wind. Clay-rich dunes or lunettes form on the downwind shoreline, and finer dust material is spread further down basin (Bowler, 1973, 1983; Magee, 1991).

5.4.2.4 Origin of the Lower Darling Valley lake Basins

Bowler & Magee (1978) suggested that the *en echelon* arrangement, NNW-SSE alignment of the Willandra Lakes and the presence of silcrete-cemented, well sorted, beach-like sands at the western lake margins suggested that the basins formed in depressions between marine strandline ridges of the Loxton/Parilla Sands. The alignment of the Great Anabranch Lakes and the location of Loxton/Parilla beach ridges nearby

suggest that a similar origin there may be possible. However, the Menindee Lakes are unlikely to have any connection to the beach ridges as they have no suggestive arrangement or alignment and they are located up-valley from the known extent of the Loxton/Parilla marine incursion, an inference confirmed by investigations during this project. Reference is often made in the literature to the Menindee Lakes as 'deflation basins' and occasionally as having origins as abandoned meanders. This is presumably a comparison to Gill's (1973) explanation for Lake Victoria as "a giant billabong" whereby the lake basin was scoured by an ancestral Murray deflected towards the north-west. This putative and speculative origin was derived by Gill to explain specific features at Lake Victoria and it is even more speculative to transfer that mechanism to the Menindee Lakes with absolutely no supporting evidence.

Therefore at the beginning of the BHMAR Project the mechanism of initiation and origin of the Lower Darling lake basins, particularly the Menindee Lakes, was very uncertain. However, it was clear that the Lower Darling embayment of the Murray-Darling Basin is underlain by a relatively complex series of troughs and highs of the Paleozoic Darling Basin with the Menindee Trough underlying the Menindee Lakes (Lawrie *et al.*, 2010a, b). Despite burial beneath up to 300 m of Cenozoic Murray-Basin sediments, the Darling Basin structures have expression as highs and lows in the modern landscape that suggested the possibility of neotectonic warping or faulting. Recent investigations in the Murray Basin have demonstrated widespread reactivation of basement structures which have deformed the post Loxton/Parilla Sand landscape (Brown & Stephenson, 1991; Kellett, 1989; Bowler *et al.*, 2006; McLaren *et al.*, 2009) and this portion of the Lower Darling valley, where the Menindee Lakes occur, has a number of large-scale features suggestive of neotectonic control:

- A constriction of the valley width.
- Intersection of the scroll-plain tracts of the Darling River, the Talyawalka Creek and pre-Talyawalka scroll-plain phase(s).
- The Talyawalka Lineament, apparent in satellite scenes immediately south of Talyawalka Creek, which forms the boundary between floodplain and sand dune country, the southern boundary of the Menindee Formation valley in this area and probably a Lake Bungunnia shoreline (Lawrie *et al*., 2010a, b).

These features all suggested that this portion of the valley has been influenced by subtle neotectonic reactivation of basement structures which may include depression over the Menindee Trough as a controlling mechanism for the location of the Menindee Lakes. These indications have been strongly confirmed by the recognition in this project of the widespread and significant impact of neotectonics on the Blanchetown Clay, which has clearly also impacted the nature and location of the overlying fluvial units. In turn, this strongly suggests that neotectonics have also controlled the origin and location of the lakes though this has not yet been a specific focus of investigations.

However, irrespective of their origin, the cyclic combination of shoreline erosion during surface water flooding phases, lake-floor deflation during groundwater-controlled drying phases and upwind depo-centre migration provides a clear mechanism for continuation, migration and enlargement of the basins once they are established. The combination of the valley constriction in the central project area near Menindee and broad levees adjacent to the Talyawalka Creek in its east-west alignment across the valley axis between the Talyawalka Lineament and the Darling River just south of Menindee provide a valley-scale mechanism for damming of floods. This ponding effect would both raise the height of and increase the duration of floods in the Menindee area thereby enhancing deflection of water into the lakes.

5.4.2.5 Pre-regulation hydrology of the Menindee Lakes.

In common with all flood-out lakes, the pre-regulation Menindee Lakes would have commenced to fill when flood levels exceeded the sill level in the channels connecting the lakes to the Darling River. Most of the lakes have relatively symmetrical flat-floored dish morphology with fan deltas located at the channel entrance and multiple channels crossing these deltas. Menindee Creek enters south-eastern Lake Menindee, where in-washed sediment has formed a fan delta approximately 6 km wide and extending about 4 km into

the lake. However, within the lake the main channel crossing the fan continues about 4.3 km beyond the delta across the floor of the lake towards the north west until it turns south west and connects through a complex inter-lake area to the Cawndilla Creek which fills Lake Cawndilla. Deposition of sediment in wide levees associated with the channel on the lake floor have resulted in an asymmetric lake-floor profile with the south-western lake floor higher than the north-eastern lake floor where the deepest part of Lake Menindee occurs. A complex network of distributary channels radiate both south west and north east of the main channel. The artificial inlet regulator to Lake Menindee is located in the north east, adjacent to the deepest point and inflows since operation of that system have constructed a small low-elevation delta about 1.7 km wide and extending about 0.4 km into the lake.

These geomorphic characteristics combined with the height and volume of any particular flood, control the lake flooding regime. In all of the lakes but Menindee, the lakes would have commenced to fill as soon as the flood height exceeded the sill level of the inlet channel and continued to fill at a rate and to a level determined by the flood height on the flood plain. As the flood peak in the river passed and the lake level exceeded the flood height, flow would have returned to the river until the sill height in the inlet channel was reached. The residual pool in each lake below the sill level would then have been slowly reduced by a combination of evaporation and seepage. This regime would have resulted in large areas of the lake floor above the sill level being subject to relatively short-term inundation and characterised by lignum and black box perennial vegetation communities. The residual pool environment below the sill level would have been characterised by migrating zones of shallow water, mud flats and marginal aquatic ephemeral vegetation as the water body shrank. This regime resulted in a complexity of ecosystems on the lake floor and a wide variety of habitats for waterbirds. The natural flood regime resulted in a classic 'boom-bust' cycle, highly productive in terms of the vegetation seed bank and the complexity and abundance of invertebrates (Nicol, 2004; Jenkins & Boulton, 2003) which in turn supported abundant and diverse populations of aquatic fauna, waterbirds and terrestrial fauna. The situation in Lake Menindee is complicated by its overflow connection to Lake Cawndilla and its asymmetric lake-floor topography. Lake Cawndilla and the deeper north-eastern portion of Lake Menindee are the effective residual pool phases of Lake Menindee during a flooding cycle and the broad higher portion of the lake floor adjacent to the channel across the lake floor would have formed extensive mud flats after return flow to the inlet sill level.

The Menindee Lakes must have had a higher frequency of flooding compared to the Teryaweynya Lakes and the Great Anabranch Lakes due to their close connection to the better-watered Darling River. However, detailed information regarding the amount and duration of pre-regulation flooding of the Menindee Lakes is not available. Most reports and papers state anecdotally that under natural conditions, inflow to the larger lakes (Cawndilla, Menindee, Pamamaroo and Tandure) would have occurred every 1 to 2 years with the longest droughts at 4-5 years. The smaller upstream lakes (Bijiji, Balaka and Malta) had inflow about once every three years with the longest droughts about 9-11 years. This information seems to be sourced to a 1994 report by Bewsher Consulting Pty Ltd but no explanation is provided for why the flood regime should vary for the larger and smaller Menindee Lakes given that all are in close proximity and share identical close connection to the Darling River system. Unless there is a difference in sill controls, all of the Menindee Lakes should be expected to have a common response to the Darling flood regime. Detailed information on the inlet-channel sill levels combined with LiDAR data would allow detailed reconstruction of the pre-regulation flooding history of all the lakes by comparison to the long daily river gauging record. The same method would allow determination of what the natural flood regime would have been during the post-regulation period. Sill elevations for number of the lakes are provided in the large report produced by the Menindee Lakes Ecologically Sustainable Development Project (Moore & Midgley, 2002) but there are contradictions and inconsistencies in the levels provided. Modelling of the natural flood regimes of Lakes Pamamaroo, Menindee and Cawndilla were compared with artificial regimes by DLWC (Moore & Midgley, 2002) and the results (Figure 5-141, Figure 5-142, Figure 5-143) demonstrate some of the characteristics discussed above. The flattening in the Cawndilla and Pamamaroo natural volume curves at about 170 GL and 200 GL respectively represents the level at which each lake reaches sill level and return flow to the river ceases. Menindee, with its more complex topography and hydrology does not show a similar relationship.

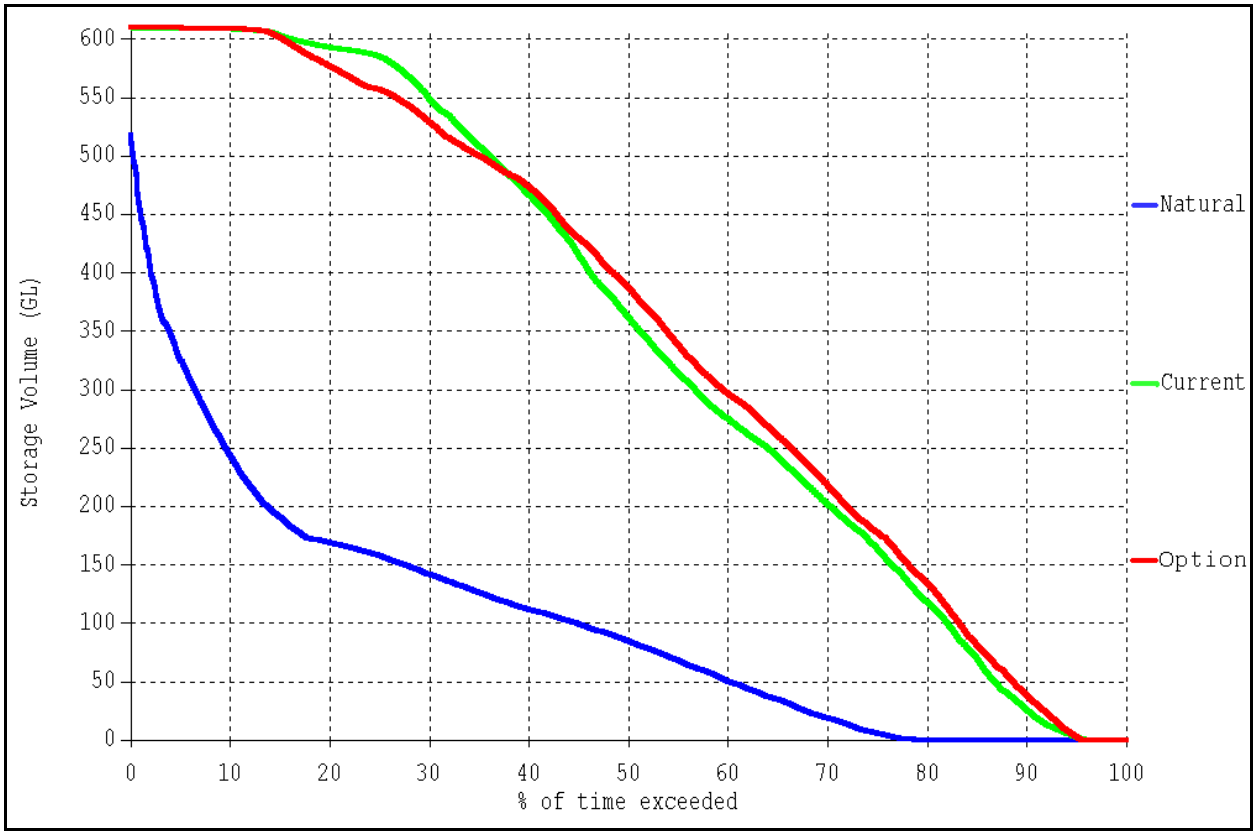

Figure 5-141 *Modelled Lake Cawndilla natural storage volume compared to different regulated regimes from Moore & Midgley (2002).*

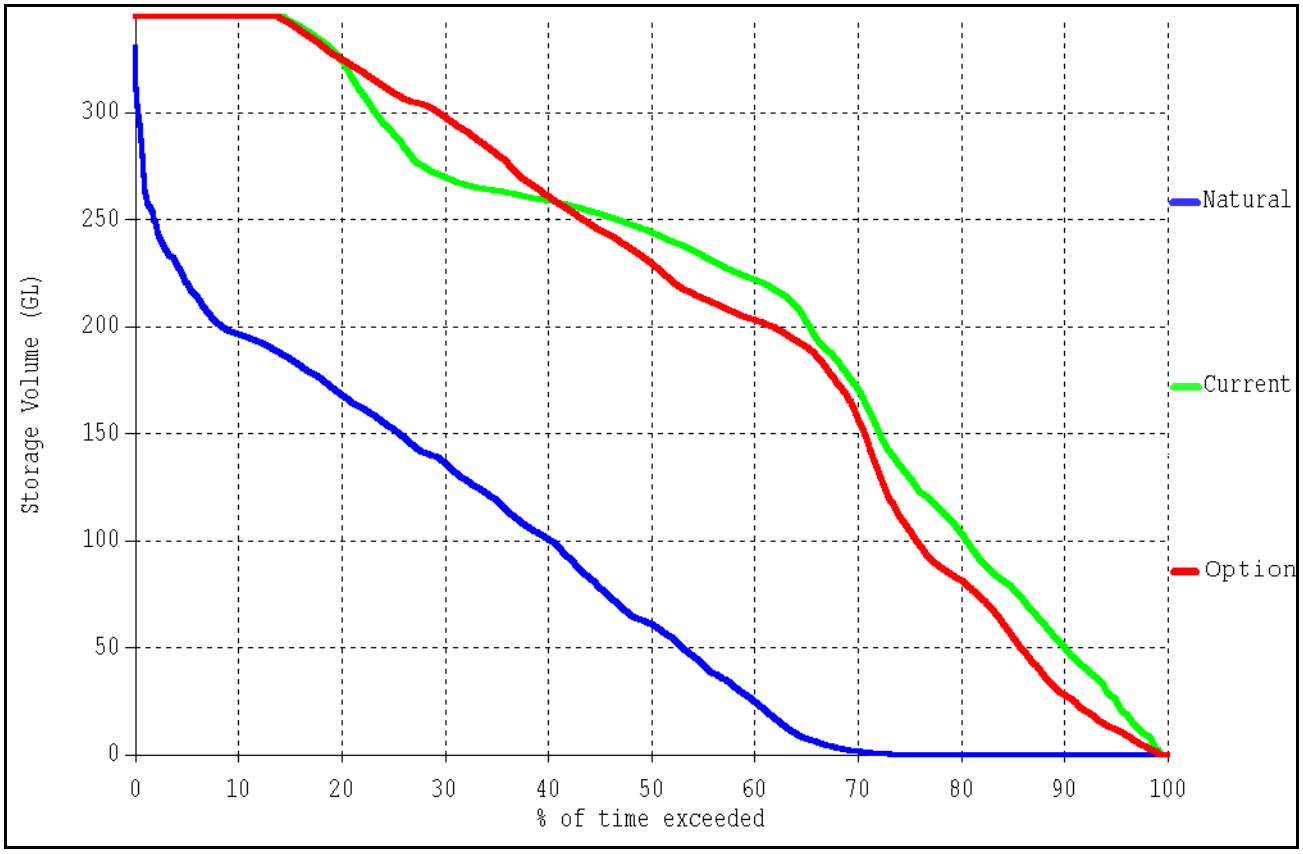

Figure 5-142. *Modelled Lake Pamamaroo natural storage volume compared to different regulated regimes from Moore & Midgley (2002).*

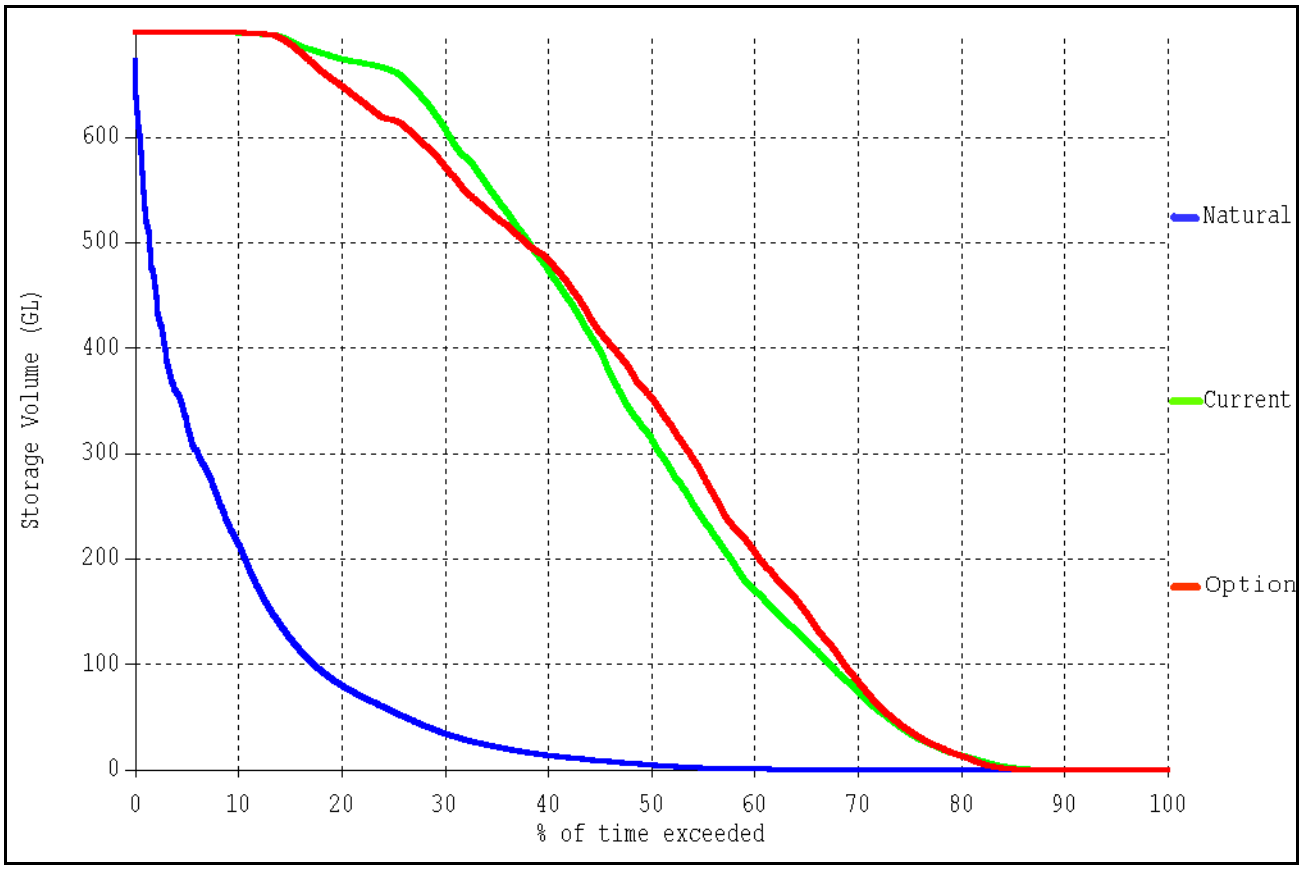

Figure 5-143. *Modelled Lake Menindee natural storage volume compared to different regulated regimes from Moore & Midgley (2002).*

5.4.3 Quaternary Aeolian Woorinen Formation

Quaternary aeolian units are widespread in the Murray Basin where a number of regional-scale stratigraphic units have been recognised (Brown & Stephenson, 1991), which include a variety of sand plains and different dune forms. Most widespread are sand plains and various longitudinal dune forms which are included in the Woorinen Formation. Bowler & Magee (1978) described the geomorphology of unusual Woorinen Formation longitudinal dunes of the Mallee Region in the Murray Basin as regular, discrete, low dunes with high clay content and wide swales. These dunes were interpreted to have a significant sediment source of pelletal clays derived from adjacent groundwater-salinised swales in a manner analogous to lunette formation. This genesis resulted in them being fixed in form and position through multiple episodes of dune activation followed by stability, in response to Quaternary glacial-interglacial climate cycles, which results in vertically stacked sediment/soil sequences. Bowler & Magee (1978) also recognised and mapped a continuum between these unusual mallee dunes and more typical higher, steeper, more closely spaced sand-rich forms which lack the clay-pellet component and multiple soil horizons. These were interpreted to represent single, more-recent dune activation with greater sand abundance and no source contribution from groundwater salinised swales. The highest levels of sand supply and dune activity result in a change from longitudinal dune forms to irregular sub-parabolic dunes, which are usually steeper, higher and lack finer-grained swales. In the Mallee dunefields of the Murray Basin large lobes of these dunes transgress across longitudinal dunefields and sand plains and are defined as different stratigraphic units such as the Molineaux-Lowan Sands and the Bunyip Sand (Brown & Stephenson, 1991).

Within the BHMAR Project area, there are a variety of aeolian landform types in both valley-marginal and within-valley settings, which range in form from sand plain to a variety of longitudinal, irregular and sub-parabolic dunes. However, the unusual mallee dune forms are rare or absent and large transgressive lobes of irregular sub-parabolic dunes, of the Molineaux-Lowan Sands type, do not occur within the project area, though Bowler & Magee (1978) mapped such features further to the east. Accordingly, within the study area, all non-lunette aeolian landforms are designated as Woorinen Formation and are described according to their

landscape setting and landform type. Within the project area the Woorinen Formation generally consists of red-brown siliceous sands and calcareous silty and clayey sand. Variable pedogenesis and secondary carbonate deposition increases with age and produces nodular and hardpan calcareous soils. Though the aeolian sediments of the formation form a widespread element of the surficial cover they generally have little impact on the hydrogeology and have not been studied extensively for this study. The distribution and nature of aeolian landforms have been mapped in detail but the sedimentology, stratigraphy and chronology of aeolian sediments have received minimal attention.

5.4.3.1 Valley-marginal aeolian sediments

Aeolian sediments occur both east and west of the main Darling Valley in the project area where they form a mostly continuous cover over Willotia beds and earlier sediments. At some places along the western upwind valley margin Woorinen Formation aeolian sediments have transgressed across lake floors and Menindee Formation floodplain. To the east of the valley there are areas where the aeolian sands are reworked into irregular sub-parabolic transverse dunes which may be due to enhanced sand supply on the downwind side of the Darling Valley. Similar irregular sub-parabolic dune forms also occur west of the valley in the southern part of the project area. As indicated above, these irregular sub-parabolic dunes do not form dunefield lobes that transgress across earlier dunefields with different morphology.

Some large higher-elevation aeolian accumulations generally east of the Darling Valley have surface reworking of sands into longitudinal dune forms (Figure 5-144). These accumulations are mainly the broad relict lunettes that lie to the east (downwind) of many of the larger lakes (outside the younger lunettes, which are at the eastern lake margins). Also included are other large aeolian non-lunette features, such as the straight north-south ridge extending along much of the western side of Lake Cawndilla, which is believed to have a structural origin. The linear dunes formed on all these systems are often broad, stabilised and very regular forms with wide intervening swales and irregular crests scalloped by minor transverse dunes.

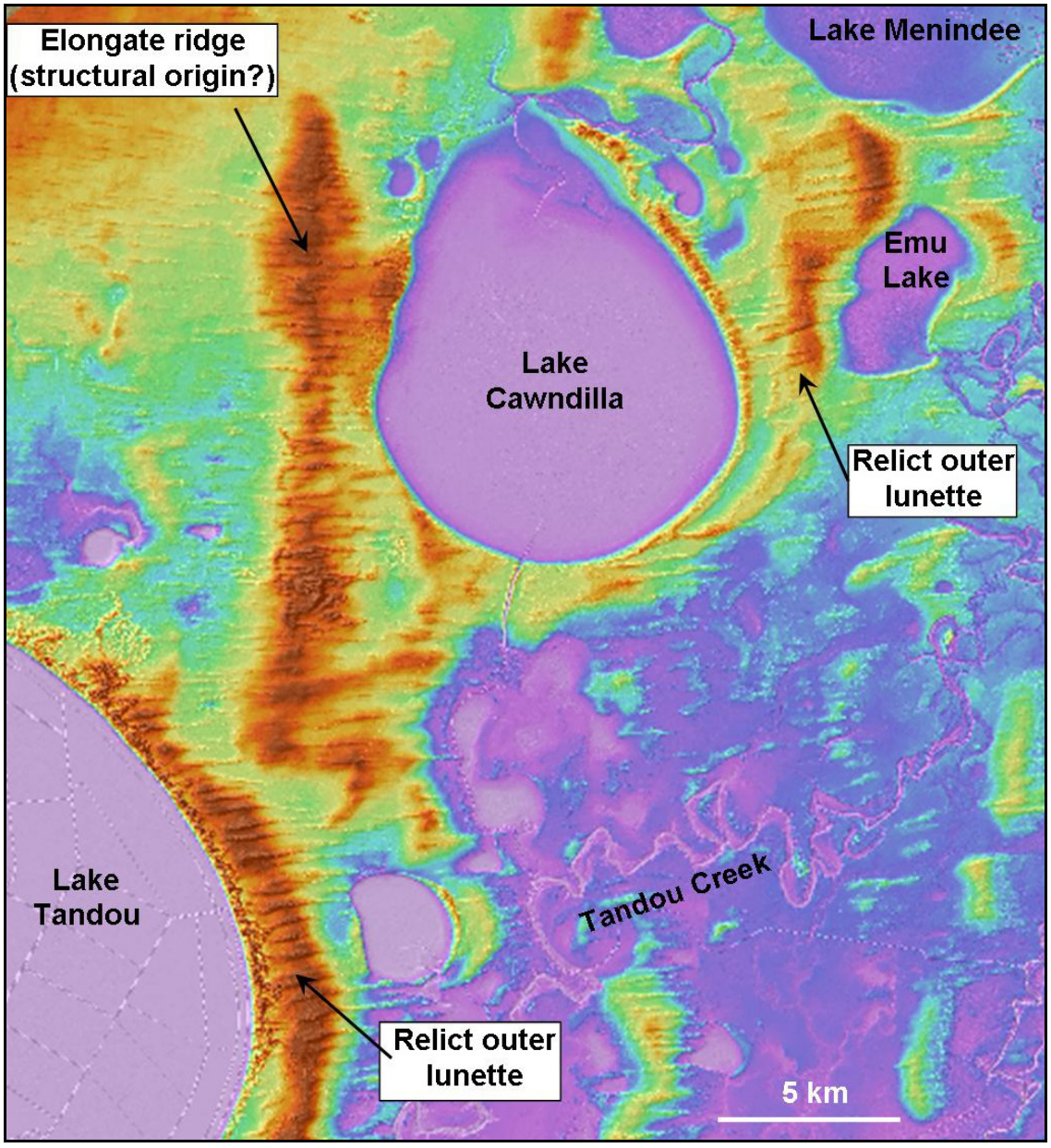

Figure 5-144. *LiDAR image illustrating linear dunes developed on relict aeolian features such as lunettes and a possible north-south structural ridge.*

5.4.3.2 Within-valley aeolian sediments

Within the valley, there are a number of types of aeolian sand deposits which vary in size, elevation and relationship to the fluvial stratigraphy. The relationship between aeolian and fluvial landforms is complex and sometimes difficult to interpret. In some places, fluvial systems are clearly eroding aeolian landforms as indicated by sharp erosional contacts at channel margins (Figure 5-147, Figure 5-148, Figure 5-152). However, away from channels, where floodplain overbank mud may be building up at the margin of an area of aeolian sediments the contact will rarely appear sharp. In other places, the aeolian sediment might be transgressing over floodplain and this will also result in very irregular contacts (Figure 5-146). In many places it is not possible to be certain which landform is growing at the expense of the other and both processes might be happening with expansion of aeolian areas during dry episodes and subsequent burial by overbank mud during large floods. The nature of contacts between aeolian and fluvial landforms will also vary from upwind to downwind locations. Satellite images and LiDAR have been relied on to differentiate and map aeolian and fluvial landform inter-relationships. BHMAR drillholes are mostly sited away from thicker aeolian sediments because of the practical difficulties of sighting a large drill rig on steep dunes, to

minimise per metre drilling costs and often due to cultural heritage issues on aeolian terrain. Therefore, subsurface information about the aeolian sediments and the underlying units has been derived from the AEM supplemented by some shallow hand-auger holes.

Discontinuous aeolian sediments on relict floodplain

On the eastern side of the valley, east of Menindee and south of Talyawalka Creek, there is a large area of aeolian sands deposited on the valley floor. These sands appear relatively continuous in satellite imagery and are highly variable with a complex mixture of sand plain, linear and irregular sub-parabolic dune forms as well as complex of channels and small lakes due to the occluded drainage (Figure 5-145). This area is interpreted to consist of Woorinen Formation aeolian sand transgressing over older Menindee Formation floodplain with some channels and lakes still active in the area during the highest floods of the modern regime. The contact between the fluvial and aeolian landforms is highly irregular. The LiDAR image (Figure 5-145) indicates that, despite the apparent continuity of aeolian sediments evident in the satellite image, the overall relief is low indicating that the aeolian sands are generally very thin. The AEM (See Regional Sections G-G1 and P-P1) and logs of BHMAR57 and BHMAR48 all confirm that this area has a relatively thin and discontinuous aeolian cover over Menindee Formation floodplain. Smaller examples of the same landforms occur in other parts of the project area particularly on the eastern valley margin in the southern half off the project area.

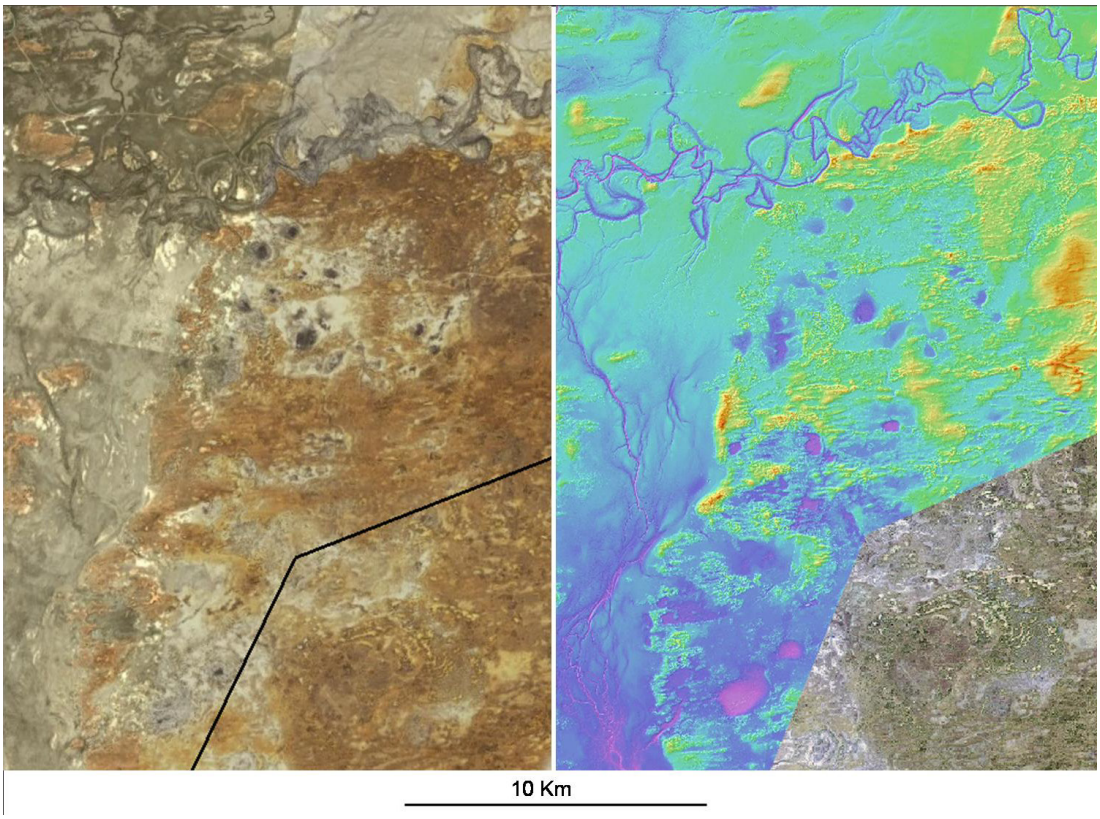

Figure 5-145. *Area of discontinuous aeolian sediments on relict Menindee Formation floodplain in the eastern central part of the project area south of Talyawalka Creek.*

Large high-relief areas of aeolian sediment

These larger areas of within-valley aeolian sediments are irregular in shape and consist of reddish-orange aeolian sand. They occur over most of the Lower Darling Valley and are larger and more abundant where the valley is widest. Where the valley width is constricted these features are virtually absent such as upstream of the project area in the valley constriction downstream of Wilcannia. At the upstream end of the BHMAR Project area, where the valley widens downstream of the Wilcannia constriction, these aeolian features

occurring between the Darling and the Talyawalka are relative large and are often dissected by multiple flood scour channels. They become smaller, more irregular and more widely spaced down valley towards the constriction in the central part of the project area near Menindee. Downstream of the Menindee constriction they are again larger especially where the Great Darling Anabranch and the Darling River are widely separated by up to 60 km of dunefield. There is a size-continuum across the project area for these aeolian sediment landforms and the boundary between large and smaller forms is arbitrarily placed at about 5 km. The larger examples are often geomorphically complex, relatively highly elevated above the floodplain (up to 65-70 m AHD) and have longitudinal dunes developed on them (Figure 5-146). Their geomorphology and sand colour is indistinguishable from valley-marginal Woorinen Formation. The boundary between the aeolian and fluvial landforms can vary from very sharp at river channel margins to irregular and diffuse on floodplains, especially on the eastern downwind margins (Figure 5-146). The aeolian sands overly Willotia beds fluvial and lacustrine sediments and are likely to have been formed by dune migration across the Willotia beds floodplain during arid periods when Woorinen Formation dunefields were regionally active. Subsequently, these areas have been left intact as erosion residuals during the post Willotia beds incision and deposition of the Menindee and Coonambidgal Formation sediments. They have well-developed, nodular and hardpan calcareous soils developed on them.



Figure 5-146. *Large irregular area of within-valley aeolian sediment south of the Darling River on Viewmont Station.*

During the time of Menindee and Coonambidgal Formation deposition, local flood-plain sand sources may have contributed additional sand to these areas. Lunettes on the downwind margin of some floodplain lakes and source-bordering transverse dune on the downwind margins of north-south scroll-plain tract reaches are examples of source areas for this process.

These aeolian features were active during phases when river activity was minimal and aridity was greater than today. In the current regime, dunes are vegetated and essentially inactive and even though none of the river channels are laterally migrating there is sufficient fluvial activity for overbank deposition on the wider floodplain during large floods which is building up over the edge of aeolian sediments. Bowler *et al.* (1978) demonstrated this stratigraphic relationship north of the BHMAR Project area in the Sydney to Moomba gas-

pipeline trench. Hand-augering in some small aeolian areas (see below) where the stratigraphic setting is similar, also demonstrated this relationship.

Small lower-relief areas of aeolian sediment

Over much of the valley are variably sized smaller (< 5 km) areas of aeolian deposits (Figure 5-147) at modest elevations (up to 60-65 m AHD) which probably have a variety of origins. Some are smaller versions of the large-area category and consist of Woorinen Formation sand plain and dunes over residual Willotia beds sediment. Others have probably developed as source-bordering features adjacent to lateral-migration channel phases during Menindee Formation and Coonambidgal Formation deposition. Where investigated, these aeolian sediments extend below the level of the Shepparton Formation floodplain and are interpreted as sourced from earlier lateral-accretion phases now buried by overbank deposition which laps onto the aeolian mounds. These deposits consist of at least 6-7 m of red-brown or orange aeolian fine to medium sands with nodular calcareous pedogenic horizons. At least two depositional episodes capped by soil formation are evident. Hand-augering in an aeolian area at site 3MC01 (Figure 5-147, Figure 5-149) and WS03 on Appin Station (Figure 5-147, Figure 5-151) demonstrates that multiple aeolian depositional units separated by pedogenic carbonate extend below the level of the adjacent Menindee Formation flood plain.

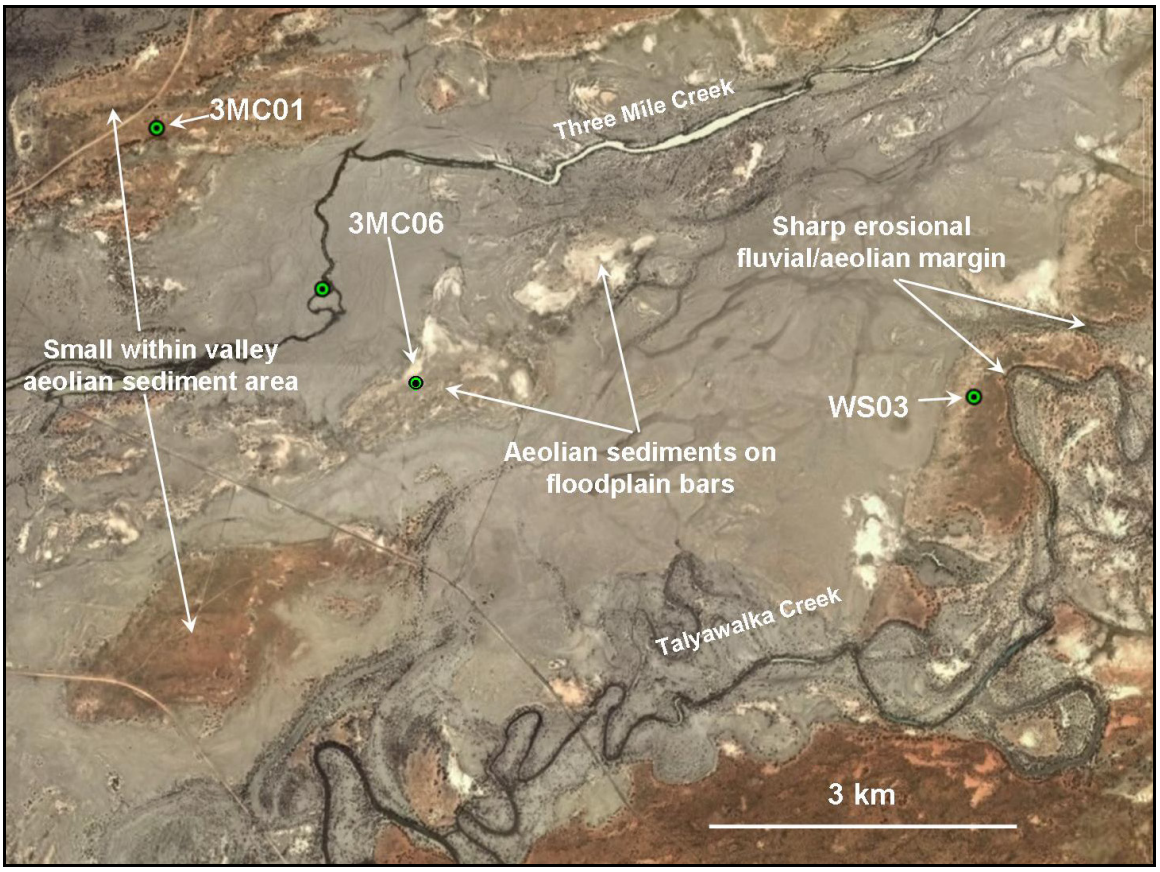

Figure 5-147. *Google image of the Three Mile Creek floodplain showing examples of within-valley aeolian sediment types and the location of the 3MC06 tractor-trench profile and hand-auger holes 3MC01 and WS03.*

Figure 5-148 shows a LiDAR image of the same area of the Three Mile Creek floodplain as shown in Figure 5-147 with topographic profiles across the western floodplain, between sites 3MC01 and 3MC06, and at the eastern floodplain margin through WS03. The LiDAR and profiles clearly show that the small-area aeolian deposits, where 3MC01 and WS03 are located, have higher elevation and relief and development of longitudinal dunes, in contrast to the floodplain-bar aeolian deposits, where 3MC06 is located. Auger hole 3MC01 demonstrates that the aeolian sediments on the NW margin of the flood plain extend to below flood plain level. In 3.4 m of section there are two aeolian depositional events separated at 2.1 m, which both consist of reddish-orange, clean, fine to medium, aeolian sands grading to paler sands with pedogenic secondary carbonate (Figure 5-149, Figure 5-150).

Hand-auger hole WS03 is located on the eastern margin of the Menindee Formation Three Mile Creek floodplain on one of a series of small areas of aeolian deposition, which were probably once one large area. These areas have a conspicuous straight western margin (Figure 5-147, Figure 5-148) which defines the eastern margin of part of the Yampoola Corridor, an ancient valley tract described above in (Section 5.4.1.4). The former larger area of aeolian deposits has been dissected by flood scour channels cut by overflow from upstream floodplain onto the Three Mile Creek floodplain. Scour pools, with waterholes, are developed in the constrictions between individual aeolian features. The lower-elevation Talyawalka Creek scroll-plain is eroding into the eastern margin of the southernmost aeolian area on which WS03 is located (Figure 5-152).

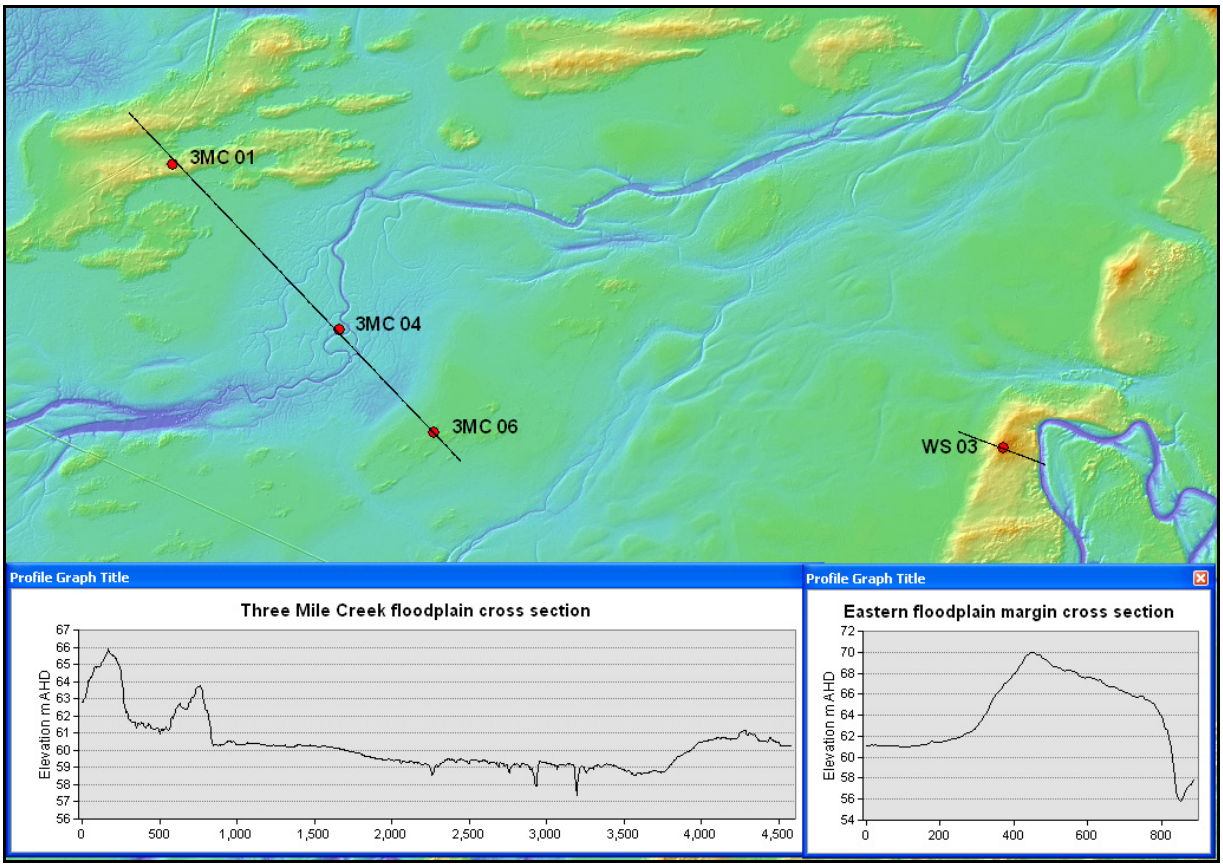

Figure 5-148. *LiDAR image of the Three Mile Creek Menindee Formation floodplain showing the location of the cross section and the Profiles 3MC01, 3MC06 and WS03 described in the text.*

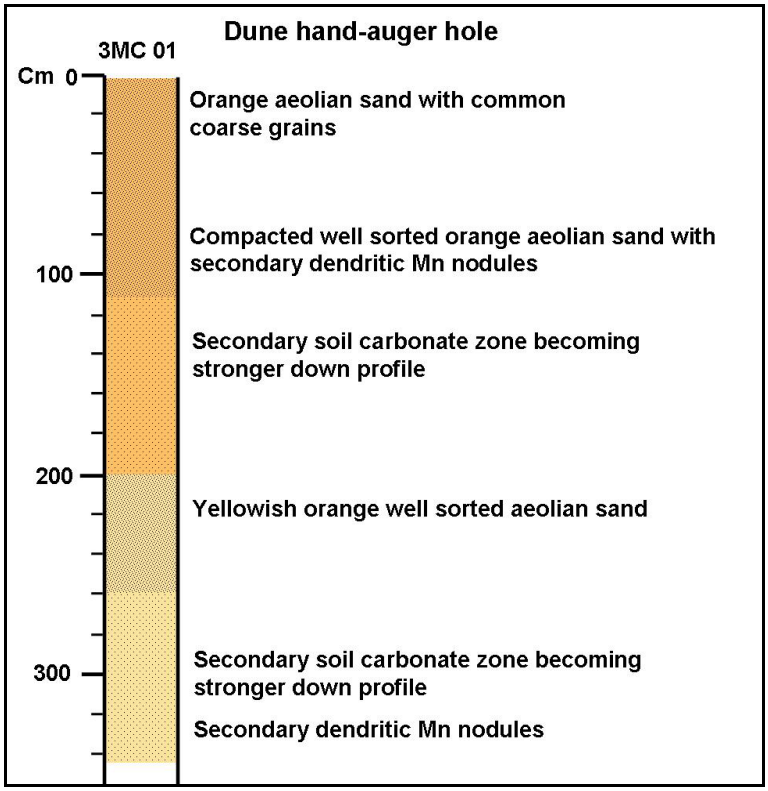

Figure 5-149. *Profile of hand-auger hole 3MC01 showing two cycles of aeolian deposition, with clean orange fine-medium aeolian sand overlying a nodular secondary-carbonate soil horizon.*



Figure 5-150. *Sediments from the 3MC01 hand-auger hole in approximately 20 cm intervals extending from the top of the hole at the bottom left to the bottom of the hole (3.45 m) at the top right. The upper sediments (bottom, left row) are orange-red aeolian fine to medium sands overlying whitish sediments containing nodular pedogenic secondary carbonate which begin in the top piles of the left hand row (~ 1.1 m depth). In the bottom piles of the right row are non-calcareous, orange, aeolian fine to medium sands of an earlier dune phase which also pass down to a nodular pedogenic secondary carbonate zone (at about 2.65 m) visible in the top few piles of the right row.*

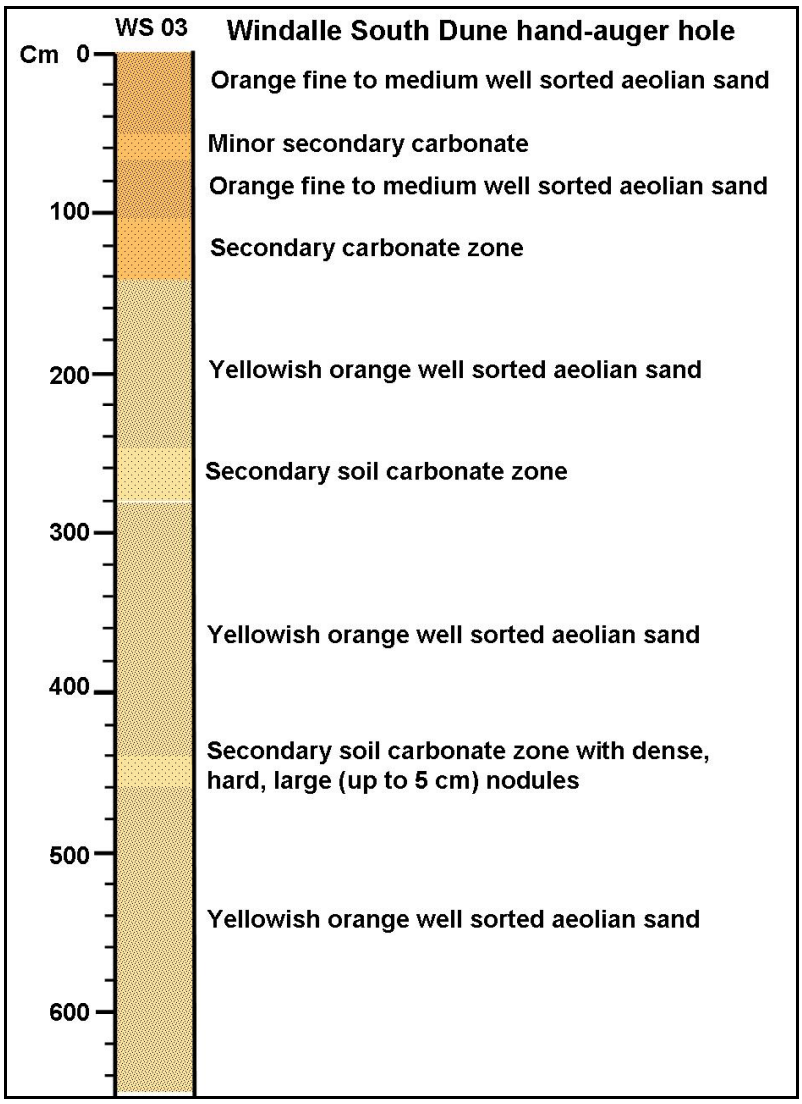

Figure 5-151. *Profile of hand-auger hole WS03 showing at least two cycles of aeolian deposition.*



Figure 5-152. *Eastern margin of the small aeolian deposit where the WS03 site occurs showing how the Talyawalka creek channel (lowest area left of centre) is eroding the margin of the aeolian sand area. Black Box trees to the left are on the Talyawalka scroll plain. Arrowed figure on dune crest indicates the scale.*

Hand-auger hole WS03 (Figure 5-151) shows 6.5 m of dry yellow-orange fine to medium aeolian sand which becomes slightly yellower with depth. Secondary pedogenic carbonate occurs over much of the interval from 0.4 to 2.8 m with denser concentrations at 1.0 to 1.4 m and 2.5 to 2.8 m. A deeper level of harder carbonate nodules occurred at 4.4 to 4.65 m. These separate levels of secondary carbonate suggest at least two episodes of dune-building followed by pedogenesis have occurred. The auger-hole penetrated to approximately the same level as the Three Mile Creek floodplain to the west so did not conclusively confirm that the aeolian

sediments extend to a deeper level and are now being buried by floodplain alluvium. However, the hole did confirm that the aeolian sediments do not sit on a relatively high (above floodplain level) plinth of older floodplain sediment, such as the Willotia beds. It is likely that the aeolian sediments represent source-bordering dune accumulation on the downwind eastern margin of a former laterally-migrating channel system in the Menindee Formation. The dunes were subsequently laterally truncated by the later Menindee Formation incision phase represented by the Yampoola Corridor and have been partially buried by overbank alluvium and further truncated by flood scour channels and the Coonambidgal Formation Talyawalka scroll-plain phase.

Aeolian sediments on flood-plain bars

In the upper part of the project area, the Darling River tract follows the Yampoola Corridor to the off-take of Three Mile Creek where the Yampoola Corridor diverges to the south. In this northern part of the project the Yampoola Corridor is characterised by landforms indicative of large-scale floods, commonly termed mega-floods, in the form of scour channels and floodplain bars. These bars have low elevation (1-2 m above the Menindee Formation floodplain) and are commonly capped by an irregular surface of aeolian reworked deposits, which generally lack longitudinal dune forms (Figure 5-147, Figure 5-148). The surface of these deposits is characterised by a variety of forms and traces with isolated scalds and small sand accumulations generally less than 1 m high. These floodplain features are interpreted as bars deposited on the floodplain by extreme flood events and later modified by aeolian reworking or additions.

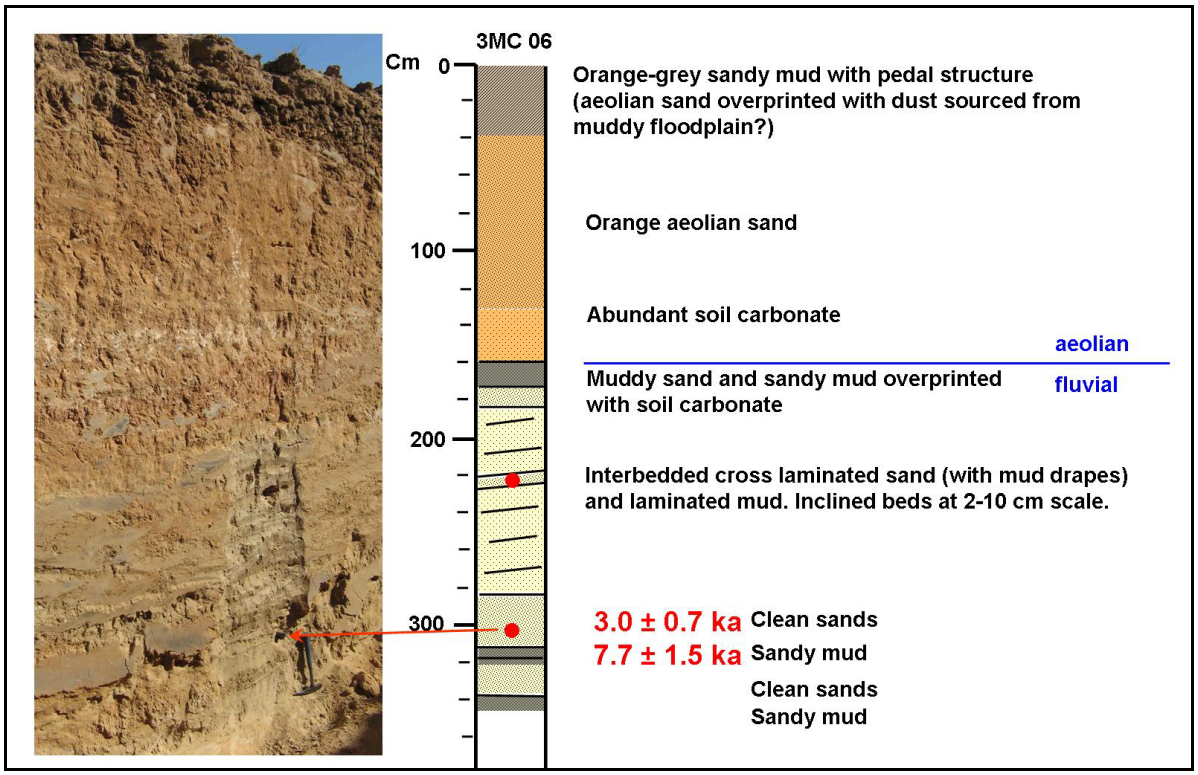

Figure 5-153. *Profile of tractor-dug trench 3MC06 showing orange aeolian sand with a secondary-carbonate soil horizon overlying fluvial sediments deposited in a floodplain bar. OSL dating results in red.*

Tractor-trench 3MC06 is located on a floodplain bar on the Three Mile Creek floodplain (Figure 5-147, Figure 5-148) and has 1.6 m of medium aeolian sand directly overlying fluvial sediments that consist of interbedded clayey sands and cross laminated sands with mud drapes, which were deposited during fluvial deposition of the bar (Figure 5-153). The upper 1.6 m aeolian sand unit consists of well-sorted, orange, medium sands with the upper 0.4 m greyer, and with a blocky pedal structure due to an overprint of mud sourced as aeolian sand-sized aggregates and dust from the floodplain upwind. The aeolian sand unit has a well-developed calcareous soil and the secondary carbonate has overprinted the upper 0.2 m of the

underlying fluvial sediments. An OSL sample from the fluvial sediments at about 3 m in 3MC06 provides a numeric age for deposition of the floodplain bar and the age of the mega flood event. As can occur with flood deposits, there were some issues with effective dose bleaching during the depositional event and two possible ages are indicated, 3.0 ± 0.7 ka and 7.7 ± 1.5 ka. This suggests a mid to later Holocene age for the mega-flood event.

Scroll-plain source-bordering aeolian sediments

Two types of irregular sand accumulations occur associated with the Coonambidgal Formation scroll-plain, lateral-accretion deposits (Figure 5-154). Both of these deposit types are only known from the earlier Coonambidgal Formation Phase 2 and Phase 3 scroll-plain tracts and are absent from the Coonambidgal Phase 1 Darling River scroll plain, which has smaller dimensions indicative of less active sand movement. The first type (Figure 5-154A) occur on the Menindee Formation floodplain but immediately adjacent to the Talyawalka scroll plain, and consist of relatively large irregular sand accumulations up to at least 6 m above the floodplain with good examples occurring close at Talyawalka scroll-plain near where the Menindee to Ivanhoe Road crosses Talyawalka Creek (Figure 5-154A). These sand deposits have been extensively deflated exposing their internal stratigraphy which consists of brown- and buff-coloured sands with a moderately well-developed calcareous soil and abundant cultural material accumulated as a deflation lag (Figure 5-155).

The second type (Figure 5-154B) are rare smaller and lower (1.5-2 m) irregular sand accumulations that occur rarely on the scroll plain itself and consist of white fine-medium sands with minimal pedogenesis. These areas generally have relatively flat featureless upper surfaces that lack dune forms (Figure 5-156). An auger hole through one example near the BHMAR99 drillhole (Figure 5-156) demonstrated that the dune directly overlies scroll plain sands with overbank mud onlapping the dune flanks.

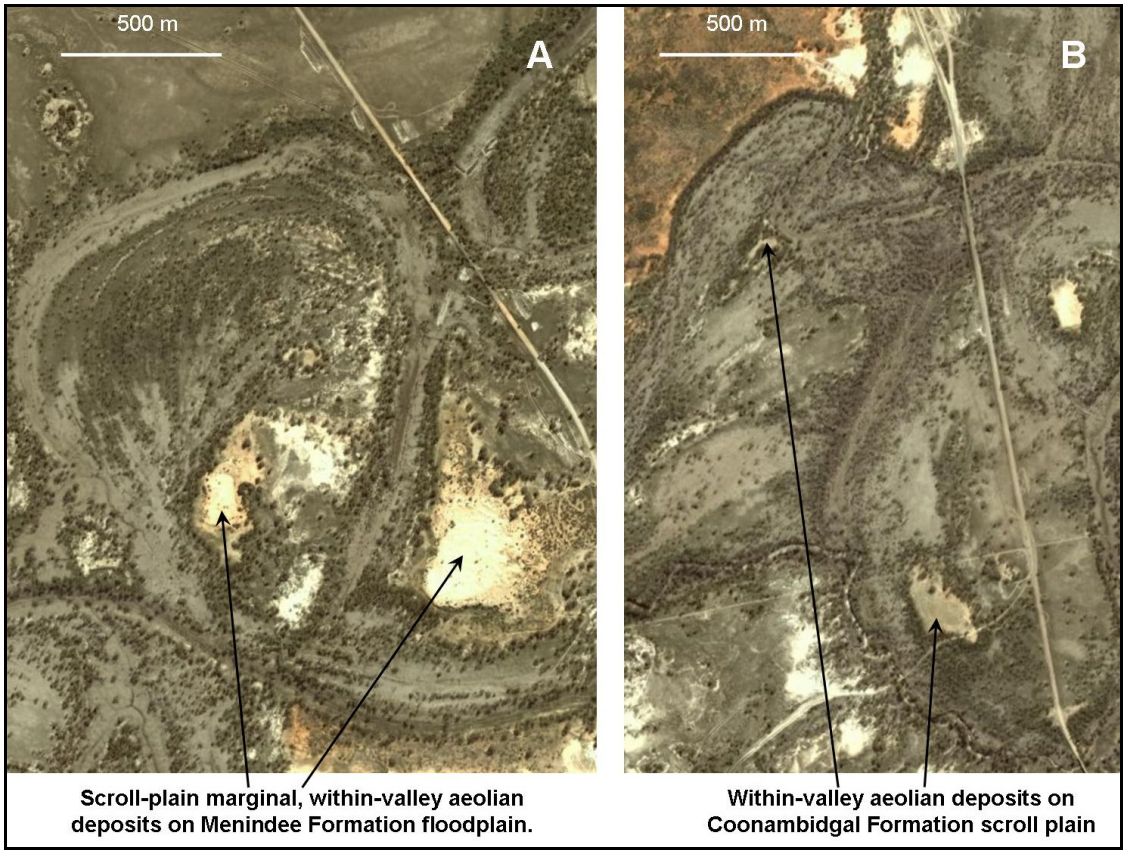

Figure 5-154. *The Talyawalka Creek scroll plain near the Menindee-Ivanhoe road (A) and the Menindee-Pooncarie road (B) demonstrating scroll-plain related dune types.*



Figure 5-155. *Talyawalka scroll-plain marginal aeolian deposit on Menindee Formation floodplain. View looking south across the larger area located in the bottom right of Figure 5-154. Deflation has exposed the core of the deposit. The Black Box trees in the background are at the channel margins.*



Figure 5-156. *Aeolian deposit on Coonambidgal Formation Phase 2 scroll-plain On East Bootingee Station north of BHMAR99. View looking west across the surface of the deposit showing its generally flat featureless nature and lack of dune forms. The channel is in the left background (with Black Box trees at the margin) and the scroll plain in the right background with Black Box trees across it.*

5.5 LANDSCAPE AND GEOLOGICAL EVOLUTION IN THE STUDY AREA

The geomorphic/geological history for the Menindee area as determined by this project can be summarised as:

1. Complex history of pre-Palaeozoic deformation and metamorphism in Proterozoic basement rocks. Several E-W shear zones mapped in the Darling Geological Basin basement are reactivated in Neogene times (e.g. Talyawalka Fault System);
2. Formation of Palaeozoic-Mesozoic Basins (e.g. Menindee, Wentworth and Blantyre Troughs) as part of the Darling Geological Basin. Deposition of a thick (several km) sequence of clastic sediments within extensional fault-bounded basins is interrupted episodically by structural inversion along these structures (e.g. in Carboniferous). Several of these structures appear to have been reactivated in Neogene times;
3. Formation of the Murray Geological Basin, with deposition of Renmark Group clastic sediments by rivers flowing southward towards a shallow sea to the south of the BHMAR project area in the Palaeocene to Miocene;
4. Depositional hiatus in the Miocene with weathering and local erosion of the Renmark Group sediments;
5. In the south of the study area, deposition of marginal marine sands and shoreline dunes (Loxton-Parilla Sands) in shallow water at the northern margin of a marine basin. Pene-contemporaneous with this was deposition of fluvial Calivil Formation sediments by the palaeo Darling River and its tributaries in the Pliocene. The Calivil Formation sediments locally overlie the Loxton-Parilla Sands in the study area;

6. Damming of the palaeo-Murray River and its tributaries, including the palaeo Darling River, with Blanchetown Clay deposition in palaeo Lake Bungunnia in the Late Pliocene to Pleistocene;
7. Pliocene regression, and the drying up of Lake Bungunnia, due to a combination of lowering of the sill of the dam that initiated the lake (McLaren *et al*., 2012) and the onset of a dryer climate;
8. Continued fluvial and local lacustrine deposition, with sediment derived from the northwest (Broken Hill area) and the north (palaeo Darling River, which passed through a gap in basement hills at Wilcannia at the edge of the Murray Basin). These Willotia bed sediments may be also partly a time equivalent of the upper part of the Blanchetown Clay deposited further south in Lake Bungunnia;
9. Incision of a trench into the Blanchetown Clay to form the modern course of the Murray River (Murray Gorge). This trench propagated headwards up the Darling Valley by nickpoint retreat, incising the Willotia beds but generally not the Blanchetown Clay in the Menindee area;
10. Deposition of fluvial sediments of the Menindee Formation and subsequently Coonambidgal Formation within the eroded trench by the Darling River and its distributaries;
11. Concurrent with 8, 9 and 10 formation of the lake basins around Menindee, with local wave erosion and shoreline deposition; and
12. Concurrent with 8, 9 and 10, deposition and preservation of aeolian sand across much of the area, particularly where not flooded and reworked in the trunk river valley.
13. There are multiple lines of evidence to show that the area has been tectonically active in the Neogene-to-present day, as evidenced by a number of scarps, lineaments, and drainage alignments that are coincident with underlying faults. There is also evidence of neotectonics from some lake tilting in the south of the project area.

As the project area sits astride the Darling Fault Lineament, a continental-scale structural feature, it is perhaps not surprising that tectonic activity has played a major role in shaping the landscape in the project area. the Darling River Lineament itself may be a much younger structure than commonly thought.

Tectonics appears to have influenced the distribution of the major Pliocene and younger aquifers and aquitards. Although the data appear to show that tectonic activity has waned significantly since the Pleistocene, with only a few structures apparent in the modern landscape, tectonics still influence the location of the major drainage elements.

6. Tectonic Framework

Many of Australia's landscapes have developed in response to active geodynamic processes, including long-wavelength continental tilting, intermediate-wavelength folding, and short-wavelength fault displacement of the surface (Sandiford & Quigley, 2009). When combined with structural and stratigraphic studies, these observations suggest that the geomorphology of parts of the Australian continent has changed dramatically in the Late Cenozoic in response to active tectonic processes (Quigley *et al*., 2010). Geological studies have more recently used high resolution Digital Elevation Models to identify several hundred faults across the Australian continent with demonstrable Pliocene and/or Quaternary displacements (Quigley *et al*., 2010). Recently, AEM studies have mapped significant faults with evidence of tectonic activity from the Miocene to the Quaternary and Recent times in the nearby Callabona Sub-Basin (Roach, 2012).

6.1 TECTONICS IN THE BHMAR PROJECT AREA

The BHMAR project area sits astride the continental scale 1000-km long northeast-southwest trending Darling River Lineament (DRL; Figure 6-1; Hills, 1955), also known as the Darling Fault (Neef, 2005). This major crustal lineament is considered to have a complex history of movement through the Palaeozoic and into the Cenozoic (O'Sullivan *et al*., 1998; Neef, 2005, 2007, 2011). The Darling River follows this feature for some 400 km between Bourke and Menindee.

Recently, studies of the underlying Darling Basin have revealed a very complex geological and tectonic history (Neef, 2012). However, despite the identification of major basement faults at depth in the BHMAR project area, the general view had been that there has been little deformation in the Darling Basin since mid-Carboniferous time (Neef, 2012). Similarly, studies of the northern Murray Basin have found limited evidence for significant neotectonic activity in this part of the Basin (Sandiford, 2003; Quigley *et al*., 2006, 2010). Exceptions are the Scopes Ranges Fault on the western margin of the project area, the Mundi-Mundi and Kantappa Faults (Quigley *et al*., 2006), and along the Mulculca Fault (Hill *et al*., 2003). These faults lay 100 and 60 km northwest of the BHMAR project area respectively. Mineral sand miners have also recognised significant fault offsets of Pliocene sands 20 km south of the BHMAR project area (Roy & Whitehouse, 2003).

Adjacent to the DRL are the Devonian to Mesozoic Menindee, Wentworth and Blantyre Troughs (Figure 6-1). These troughs are fault-bounded, and are thought to have formed as a result of transcurrent faulting on the DRL (Neef, 2012). These troughs are separated by the Lake Wintlow High (Glen *et al*., 1996; Figure 6-1). Devonian sediments in the Menindee Trough are reportedly at least 4.5 km thick (Blevin *et al*., 2007) and may be as thick as 14 km (Glen *et al.*, 1996).

Contours for the Cenozoic sediment deposits within the Murray Geological Basin show a dominant north-east trend, synonymous with the underlying Devonian to Mesozoic Infrabasins/Troughs (Lawrie *et al*., 2012b). These are embayments to the main depositional centre for the Murray Geological Basin, the Renmark Group Trough, where over 600 m of Cenozoic sediment has accumulated.

6.2 EVIDENCE FOR TECTONICS IN THE UNCONSOLIDATED ALLUVIAL SEDIMENTS

Structural analysis of AEM, airborne magnetics, regional gravity, and LiDAR, validated by drilling data and field observations, was carried out independently, with interpretations then integrated to develop structural maps and a model for tectonic evolution of the BHMAR project area. Overall, the study has revealed a complex tectono-stratigraphic history affecting not only the basement geology, but with significant neotectonic effects on the present landscape and Murray Basin sediments beneath the Darling Floodplain (Lawrie *et al*., 2012b). The faults mapped in this study play a significant role in recharge and inter-aquifer leakage (Lawrie *et al*., 2012c, d).

In this study, detailed maps showing structures mapped at the scale of individual MAR/groundwater resource targets are provided in Lawrie *et al*. (2012d). Regional and target scale cross-sections showing the

distribution of faults are also provided in Lawrie *et al.* (2012d). Borefield scale maps and cross-sections showing structures for the Jimargil. Lake Menindee, Larloona and Kinchega National Park sites are provided in Lawrie *et al*. (2012c).

6.3 DEFORMATION OF THE BLANCHETOWN CLAY

The Blanchetown Clay provides the confining aquitard to the priority Calivil Formation aquitard, and hence mapping its distribution and character across the project area was important to both MAR and groundwater resource evaluation. The Blanchetown Clay is a variably thick (0-17 m; average ~10 m), variably saturated (dry to fully saturated), stiff, often indurated, clay-rich aquitard that occurs as a distinctive lithological layer throughout most of the BHMAR study area (Lawrie *et al*., 2012b). The Blanchetown Clay was deposited in a lacustrine environment, in the regionally-extensive palaeo Lake Bungunnia (McLaren *et al*., 2009).

To the south of the study area, the Blanchetown Clay is known to be essentially flat-lying, and present at a relatively constant elevation (relative to AHD; McLaren *et al*., 2009). Where present, the top of the Blanchetown Clay should therefore be expected to provide a flat-lying marker horizon in the BHMAR study area. The BHMAR Project has mapped the extent of the Blanchetown clay across the project area in the Darling Valley by utilizing both AEM and drill core.

6.3.1 Previous Investigations

Detailed investigations of the Blanchetown Clay were critical to determining if the latter could be used as a marker horizon for deformation studies in the study area. Previous studies have shown that the Blanchetown Clay was deposited in a large tectonically dammed lake sometime in the period from later Pliocene to the middle Quaternary (Stephenson, 1986). The origin and extent of the lake and the nature of the infilling sediments has been studied extensively by a number of papers including Bowler *et al*. (2006), McLaren *et al*. (2009, 2011, 2012), McLaren & Wallace (2010) and Miranda *et al*. (2008).

Using the shoreline elevation of 60 m AHD derived by Stephenson (1986) both Bowler *et al*. (2006) and McLaren *et al*. (2009) used the regional SRTM DEM to map the extent of the lake basin. This resulted in considerable improvements on earlier reconstructions (Bowler, 1980; An *et al*., 1986; Stephenson, 1986) which had relied on the extent of known outcrop and borehole intersections. Both SRTM reconstructions resulted in similar definition of the lake with a complex tectonic separation into sub-basin depocentres along the Murray and south of that river and flooding up the Darling Valley but not the Willandra Creek Valley to the north.

However, Bowler *et al*. (2006) and McLaren *et al.* (2009) disagreed about the palaeomagnetic chronology for lake deposition and the nature and location of tectonic damming that had formed the lake. Both reconstructions showed the lake extending up the Darling Valley to about the vicinity of Lake Pamamaroo, though Bowler *et al*. (2006) did refer to difficulties of differentiating between lacustrine of fluvio-lacustrine (deltaic?) deposition in distal valley parts of the lake. Subsequent publications by the McLaren group remapped the lake extent using higher resolution SRTM DEMs combined with higher shoreline levels (65 m AHD in the west and 70 m AHD in the east, with the discrepancy attributed to post-depositional tectonics) derived from levelled outcrops. These revised maps showed the lake extending further up the Darling Valley to about the upstream end of Lake Wetherell and also up the Willandra Creek Valley to the northern side of Lake Garnpung.

Utilising a DEM combined with levels of the lake shoreline derived from outcrop to map the former extent of Lake Bungunnia is difficult because the lake sediments have been substantially covered by later Quaternary fluvial and aeolian sediments. This methodology also requires an assumption that the deposits of the lake have not been altered by post-depositional tectonics. Clearly the Cainozoic sediments of the Murray Basin have been disrupted by reactivation of basement structures and these faults have played a significant role in both damming of drainage to form Lake Bungunnia and in controlling the detailed geometry of the lake sub-basin depocentres.

Bowler *et al*. (2006) argued that coincident thickening of the Upper Miocene Bookpurnong Beds and the location of Lake Bungunnia sub-basin depocentres south of the Murray, demonstrated the longevity of pre-lake tectonic controls. Furthermore, they argued that substantial thickening of Blanchetown Clay deposition in the sub-basin depocentres demonstrated that tectonic movement and sub-basin development occurred early in the history of lake formation. However, subsequent work (MacLaren & Wallace, 2010) suggested shoreline variation from east to west from 70 to 65 m AHD due to tectonic deformation during or subsequent to deposition. The revised adoption of shoreline levels above Stephenson's (1986) original 60 m AHD also led to DEM mapping extending the lake extent into the Willandra Trough, east of the Neckarboo Ridge, where Blanchetown Clay is not known from either outcrop or core intersection (Kellett, 1989), though information is sparse. Kellett (pers. comm.) reports that Blanchetown Clay was not identified in the Willandra Trough sequence but that the rotary drilling technique employed was not ideal for Blanchetown Clay identification and its presence cannot be ruled out.

None of the SRTM DEM mapping studies (Bowler *et al*., 2006; McLaren *et al*., 2009, 2011, 2012; McLaren & Wallace, 2010) provide any detail of the extent of Lake Bungunnia or the nature of the Blanchetown Clay sediments up the Darling Valley embayment as far as the BHMAR Project area. Scant information regarding outcrop or drillhole intersections existed prior to the BHMAR Project.

6.3.2 BHMAR Investigations

Investigations of the Blanchetown Clay have resulted in a number of conclusions and inferences:

- The Blanchetown Clay was deposited on an irregular, eroded fluvial terrain of the upper surface of the Pliocene Calivil Formation, which lacked a ferruginised upper layer equivalent to the Karoonda Surface identified to the south, over most of the project area.
- In the southern part of the project area, The Blanchetown Clay overlies marginal marine, nearshore, beach, lagoonal and foredune facies of the Loxton-Parilla Sands with deposition absent on some relatively high foredune crests which would have probably been islands in Lake Bungunnia.
- Blanchetown Clay, or its fluvio-lacustrine or deltaic equivalent, extends at least to the northern limits of the project area, well north of previously mapped limits, and time-equivalent fluvial fine-grained sediments might extend well up the Darling Valley.
- The Blanchetown Clay consists dominantly of mud and sandy mud lithologies in the Darling Valley of the project area; a basal sandy member equivalent of the Chowilla Sand occurs rarely and facies equivalents of the Bungunnia Limestone and the silty Nampoo Member reported further south (McLaren *et al.,* 2009) are not recorded.
- The Blanchetown Clay can be used as a marker horizon for deformation studies.

In the BHMAR study area, mapping of the Blanchetown Clay was made possible only with the final AEM inversion (Lawrie *et al*., 2012a). Because the final inversion utilised a new lateral parameter correlation procedure and 'loose' regularization settings, a number of additional checks were made on the final AEM inversion (including assessment of data residuals), to ensure that no artefacts were created during the inversion procedure. This gave additional confidence to the mapping of units such as the Blanchetown Clay (Lawrie *et al*., 2012a).

To map the Blanchetown Clay, the top surface was identified at close intervals in every AEM flight line section across the study area (Lawrie *et al*., 2012b; Figure 6-2 and Figure 6-3). The mapped points were then used to create a contoured map of the elevation of the top of the Blanchetown Clay surface (Figure 6-2). The interpretation was confirmed by drilling data. The AEM mapping reveals that rather than being flat lying the Blanchetown Clay is warped and tilted at a range of scales, with elevation of the top surface varying by ~ 60 m in elevation across the project area (Lawrie *et al*., 2012b; Figure 6-2). These lacustrine deposits filled in an undulating palaeo-topography, and have been eroded in a number of locations and these issues partially explain variations in thickness of the unit including minor variations in the elevation of the top surface (<10 m), but not the 50-60 m differences in elevation mapped across the study area.

Furthermore, in addition to being warped and tilted of the Blanchetown Clay, the latter is sharply offset in a number of locations, with vertical displacements of up to 20 m noted (Lawrie *et al*., 2012b; Figure 6-2). Offsets were recorded during systematic interpretation of all the AEM flight line sections (Lawrie *et al*., 2012a) and a map of the offset locations combined with the contoured top Blanchetown Clay surface. The

pattern of folding and faulting mapped in the Blanchetown Clay is consistent with the faulting of similar materials used in sandbox and clay laboratory deformation experiments (McClay & Dooley, 1995).

Using this approach, individual offsets in the Blanchetown Clay were found to occur in linear zones of varying length that cross several flight line sections (Figure 6-3). These linear offset zones have been interpreted as geological faults, with vertical displacements of 5-20 m mapped across many of these structures. Interpretation of flight line sections reveals that these faults do not always terminate abruptly, with monoclinal warps mapped in zones 200-400 m beyond mapped fault offsets (Lawrie *et al*., 2012b). When the distribution of these individual faults is plotted, it is evident that a number of other, flight line-parallel faults (i.e. NW-SE in the central project area) with similar vertical displacements also present. These are mapped as 'inferred' faults, and are required to explain the sharp changes in the elevation of the Blanchetown Clay surface between flight lines (Figure 6-4a). The inferred faults have strike lengths of 2-8 km, while sidewall faults have shorter strike lengths of ~800 m. Some of the synthetic and antithetic strike-slip faults have been mapped for distances of 5-10 km (Figure 6-4). The mapped strike lengths of individual fault segments are consistent with observations of other intra-plate near-surface strike –slip zones (Sylvester, 1988; Cunningham & Mann, 2007).

In summary, the main findings about the deformation of the Blanchetown Clay are:

- At the western lateral valley margin Blanchetown Clay can be traced in AEM sections to elevations above 70 m AHD, clearly indicating tectonic uplift.
- Within the valley there is widespread evidence of tectonic displacement of the Blanchetown Clay before, during and after deposition, resulting in up to a 60 m elevation difference in the depth to the top of the unit across the project area (20-80 m AHD).
- The Blanchetown Clay within the project area is warped tilted and in places sharply offset by up to 20 m with identical thickness across offsets clearly demonstrating post-depositional movement, rather than draping of earlier structures.
- A complex array of fault geometries, the presence fault-zone corridors and indications of fault reactivation, sometimes with reversal of vertical movement, have combined to produce a highly complex Blanchetown Clay distribution. These neotectonic structures also largely control the location and nature of later Quaternary fluvial and lacustrine deposition.

All these conclusions and observations, particularly the evidence of widespread neo-tectonics, demonstrate that simplistic mapping of the extent of Lake Bungunnia and its sediments in the Darling Valley by reference to the regional SRTM DEM is not valid. The BHMAR project data will allow a comprehensive review of the extent of Lake Bungunnia in the Darling Valley as well as a major revision of the range of sedimentary facies and post-depositional structural deformation of the sediments.

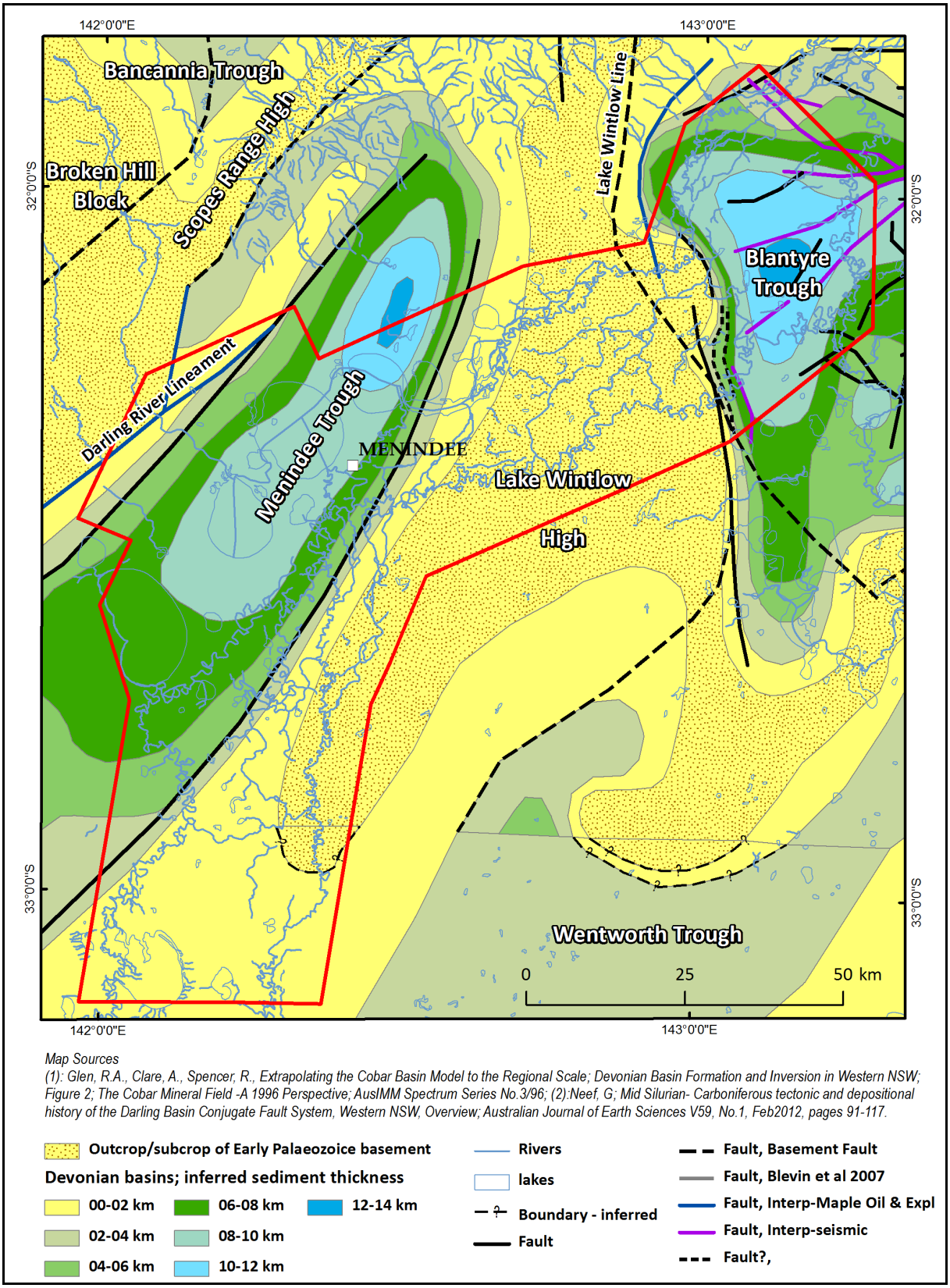

Figure 6-1. *Map showing location of the major geological basement features relative to the BHMAR project area (denoted by red line), including the approximate location of the continental-scale Darling River Lineament. Key components of the Darling Geological Basin that are shown include the underlying Menindee, Blantyre, Bancannia and Wentworth Troughs, the Lake Wintlow Basement High, and the Scopes Range High. Many of these mapped basement faults have a long geological history, with new evidence from the AEM mapping of the shallow Murray Basin sediments, and surface mapping, indicating that some of these structures have been reactivated in the Neogene-recent past.*

6.4 THE MENINDEE AND TALYAWALKA FAULT SYSTEMS

Faulting of the top Blanchetown Clay surface does not occur throughout the study area (Lawrie *et al*., 2012b), and is largely confined within a number of discrete, relatively linear corridors (Lawrie *et al*., 2012b). The two most prominent corridors are sub-parallel to the Darling River south of Menindee, and sub-parallel to the Talyawalka Creek. The structural corridor parallel to the Darling River is ~70-100 km in length and 5-15 km wide (Figure 6-4), while that associated with the Talyawalka Creek is 2-5 km wide and can be traced for >50 km to the east of where the Talyawalka intersects with the Darling River (Figure 6-5). Other mapped fault zones are discussed in more detail in Lawrie *et al*. (2012b).

In this series of reports, the structural corridor associated with the Darling River south of Menindee is referred to as the Menindee Fault System (MFS), and that associated with the Talyawalka Creek is referred to as the Talyawalka Fault System (TFS). These major fault zones change in their character along strike, largely coincident with changes in underlying basement geology, and where regional faults of different orientation intersect (Lawrie *et al*., 2012b). Major step-overs occur in association with basement heterogeneities, and between en-echelon fault segments (Lawrie *et al*., 2012b).

Within the MFS in the vicinity of the Jimargil potential borefield site, the Blanchetown Clay top surface and mapped faults define a series of rhomboidal, box-like grabens and half-grabens, that are arranged en-echelon within a broad N-S structural corridor (Figure 6-4a and b). The geometry of these grabens and half-grabens is consistent with extension within an intra-plate strike slip system formed as a consequence of reactivation of pre-existing, underlying basement faults and heterogeneities during WNW-ESE regional compression (Figure 6-4b). The grabens are linked by a smaller number of key faults with a ~N-S strike orientation which are interpreted as synthetic strike-slip faults (Harding & Lowell, 1974). Oblique-slip displacement on antithetic and synthetic strike-slip faults within the MFS is indicated by reversals of vertical displacement along the strike of these faults (Figure 6-4a and b). The overall geometry of the extensional and strike-slip faults observed within the MFS is consistent with analogue models (McClay & Dooley, 1995) and natural examples of intra-plate strike-slip zones (Cunningham & Mann, 2007).

The polarity of the half-grabens changes across the principal N-S faults, with those to the east of the fault generally with a throw down to the south, while those on the west of the fault generally have a throw down to the north (Figure 6-4). This is generally indicative of basement heterogeneity. Within the MFS, elevation changes of up to 35 m are recorded within the structural corridor, within the maximum displacement across individual faults ~20 m (e.g. Figure 6-2).

AEM sections reveal that the graben and half-graben structures form depocentres that are infilled by Coonambidgal Formation sediments (Figure 6-2 and Figure 6-3). Deposition of the Coonambidgal-Menindee Formation sediments is interpreted as syn-kinematic with faulting, with strata deposited in scroll plain deposits from rivers localised by the faulting. A number of WSW-ENE to WNW-ESE antithetic faults (Figure 6-4) provide linkages between extensional faults. Linear horst blocks are localised in compressional zones perpendicular to the maximum principal stress orientation, mainly in association with antithetic faults (Lawrie *et al*., 2012b).

Independent of the interpretation of the AEM data, structural analysis of airborne magnetic and regional gravity data, reveals that key faults mapped as major basement faults are coincident with some of the key structures observed to offset the Blanchetown Clay (Lawrie *et al*., 2012b). In airborne magnetic data, a series of N-S faults mapped in the underlying geological basement (Devonian or pre-Devonian) are coincident with faults that define the MFS corridor (Figure 6-6a). Moreover, in regional gravity data, the two key structures defining the Menindee Trough depocentre are coincident with the two main N-S faults mapped in the AEM and airborne magnetic data (Figure 6-6b).

The pattern of faulting observed at the top of the Blanchetown Clay cannot be mapped to the same degree of confidence at deeper levels using AEM data. This is because the next clay marker horizon (the upper Renmark Group clay aquitard) lies at depths near the limit of the depth of investigation of the AEM survey (~80-100 m). Also, the loss of resolution at these depths means that fault offsets only >10-15 m will be observed in the AEM conductivity depth sections. Nevertheless, a few of the major faults noted to offset the

Blanchetown Clay are observed to offset the Upper Renmark clay, particularly in areas where electrical conductivities are lower (Lawrie *et al*., 2012b).

Overall, formation of brittle faults in the Blanchetown Clay is consistent with analogue models (McClay & Dooley, 1995). In the BHMAR study area the Blanchetown Clay forms a relatively stiff, indurated layer that would have deformed very differently from the unconsolidated sands that it overlies. It is unlikely that evidence of fault planes will be preserved in the sands due to their unconsolidated nature, except if mineralised due to either de-watering and fluid mixing along faults planes. The sands are cemented in a number of locations, with iron cements (haematite-goethite) common.

6.5 EVIDENCE FOR NEOTECTONICS

Several of the major faults identified in AEM, airborne magnetics and gravity data are also identified as lineaments, scarps and topographic ridges in surface LiDAR datasets (Figure 6-7, Figure 6-8 and Figure 6-9). Figure 6-7 shows that the Talyawalka Scarp (TS), which is a prominent scarp in the present-day landscape, with a throw down to the north. This feature is coincident with a basement shear zone. It is postulated that the relief on the scarp is related to Neogene structural reactivation of the basement structure, with significant seismicity by the scale of the scarp. The Talyawalka Creek effectively follows this major lineament. En-echelon half graben structures are delineated by extensional faults mapped at the Blanchetown Clay layer also associated with extension across this basement fault, which is localised across a basement heterogeneity (Lawrie *et al*., 2012b). A number of other scarps present in the image may also be related to tectonism.

Similarly, Figure 6-8 unusual drainage patterns observed for a reach of the Darling River near Bootingee are also interpreted as fault-related. At this location, the river has numerous straight-line segments and a box-like pattern in the river course. A number of straight line scarps (A-E) that parallel the river course are observed to be coincident with mapped faults in the underlying geology. In Figure 6-8, Scarp A is coincident with faults mapped in the AEM and with lineaments in airborne magnetic data. Scarps B, D and E, are coincident with faults mapped in the AEM data, while scarp C and the river course are coincident with an underlying strike-slip fault mapped in the magnetic basement. The drainage pattern is more reminiscent of an incised upland rather than an active low gradient floodplain. The drainage pattern is attributed to neotectonics.

The coincidence of basement faults and heterogeneities with surface scarps and drainage lines is illustrated in Figure 6-9a. Scarps, drainage lines and lineaments evident in the LiDAR are mapped for a reach of the lower Yampoola Creek floodplain east of the Darling River and south of Menindee township. Figure 6-9b shows the same area with the backdrop being the TMI 1st VD draped over the LiDAR image. The lineaments from the LiDAR image are effectively coincident with faults mapped in the TMI (black lines) and regional gravity data (white dotted line). These data are interpreted as showing evidence for neotectonics in this area through reactivation of basement structures.

There is also evidence of recent tilting, with crossing shorelines observed at Lake Mindona, and a few up-warped areas observed to be associated with local landscape highs, suggesting relatively recent movement (Lawrie *et al*., 2012b). Some of the mapped structures show a complex history of tectonic inversion, with significant offsets and thickness changes across key aquifer and aquitards evident.

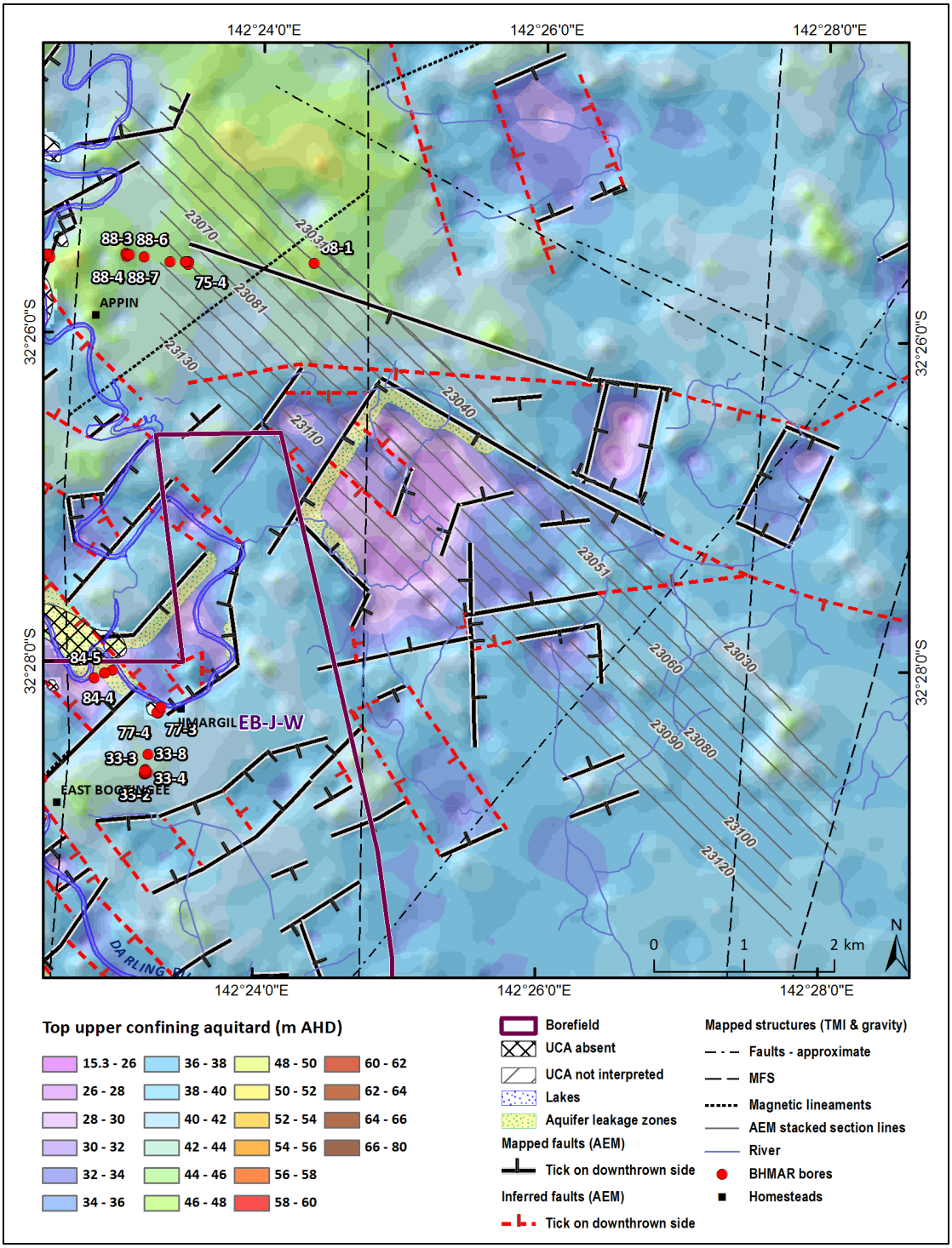

Figure 6-2. *Top Blanchetown Clay surface (m AHD) for an area NE of Jimargil, showing the location of flight line sections in Figure 6-3. The mapped faults define a half-graben structure, with linear horst-blocks evident in Figure 6-3 shown in map view. This map also shows the location of potential inter-aquifer leakage zones where the Coonambidgal and Calivil Formation aquifers are juxtaposed across extensional and sidewall faults.*

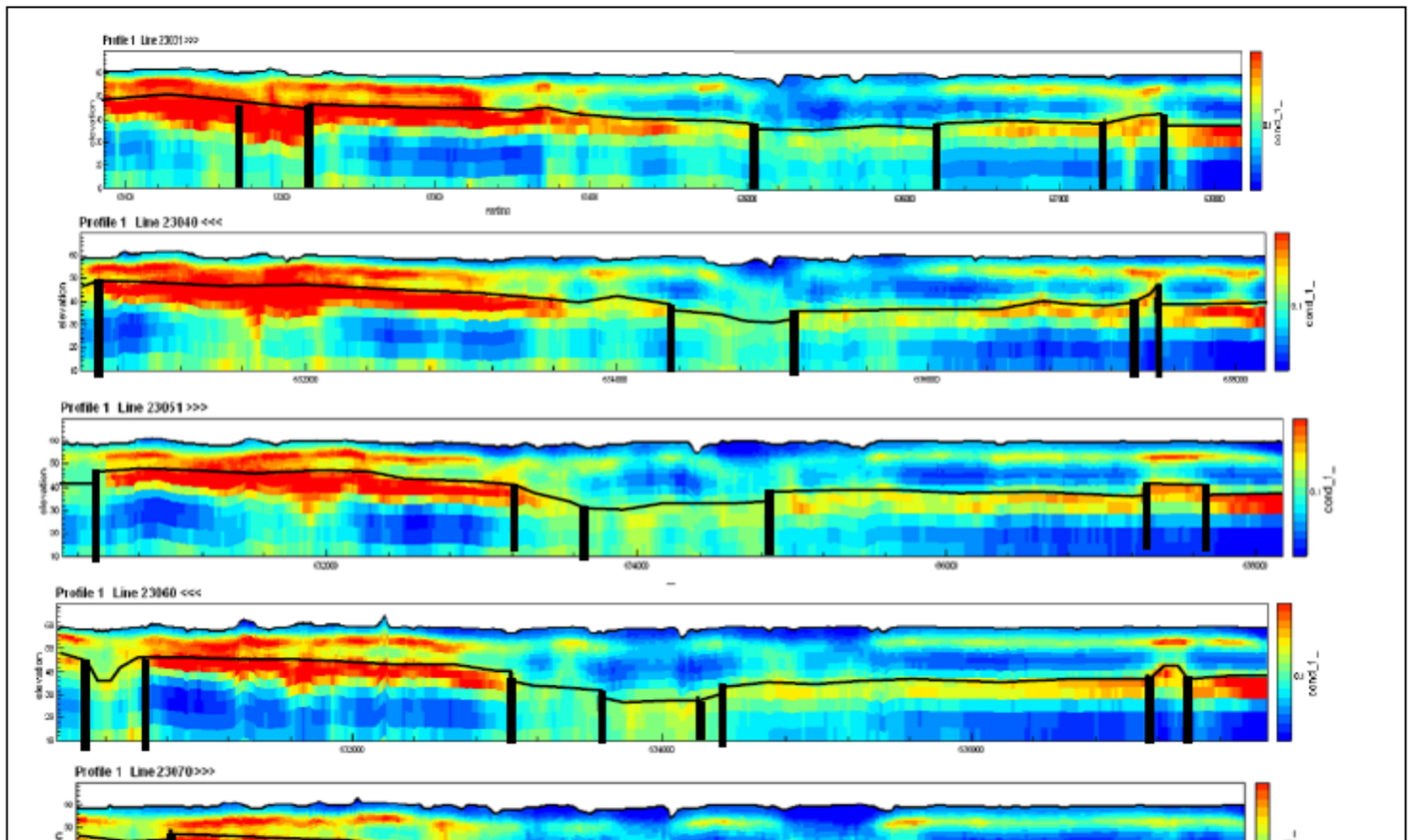

Figure 6-3. *Tiled conductivity depth sections with 200 m spacing between flight lines for an area near Menindee. Fault. Offsets of the top of the upper confining aquitard (Blanchetown Clay- shown with a thicker black line) are evident. The location of individual flight line sections relative to the mapped graben basins is shown in Figure 6-2.*

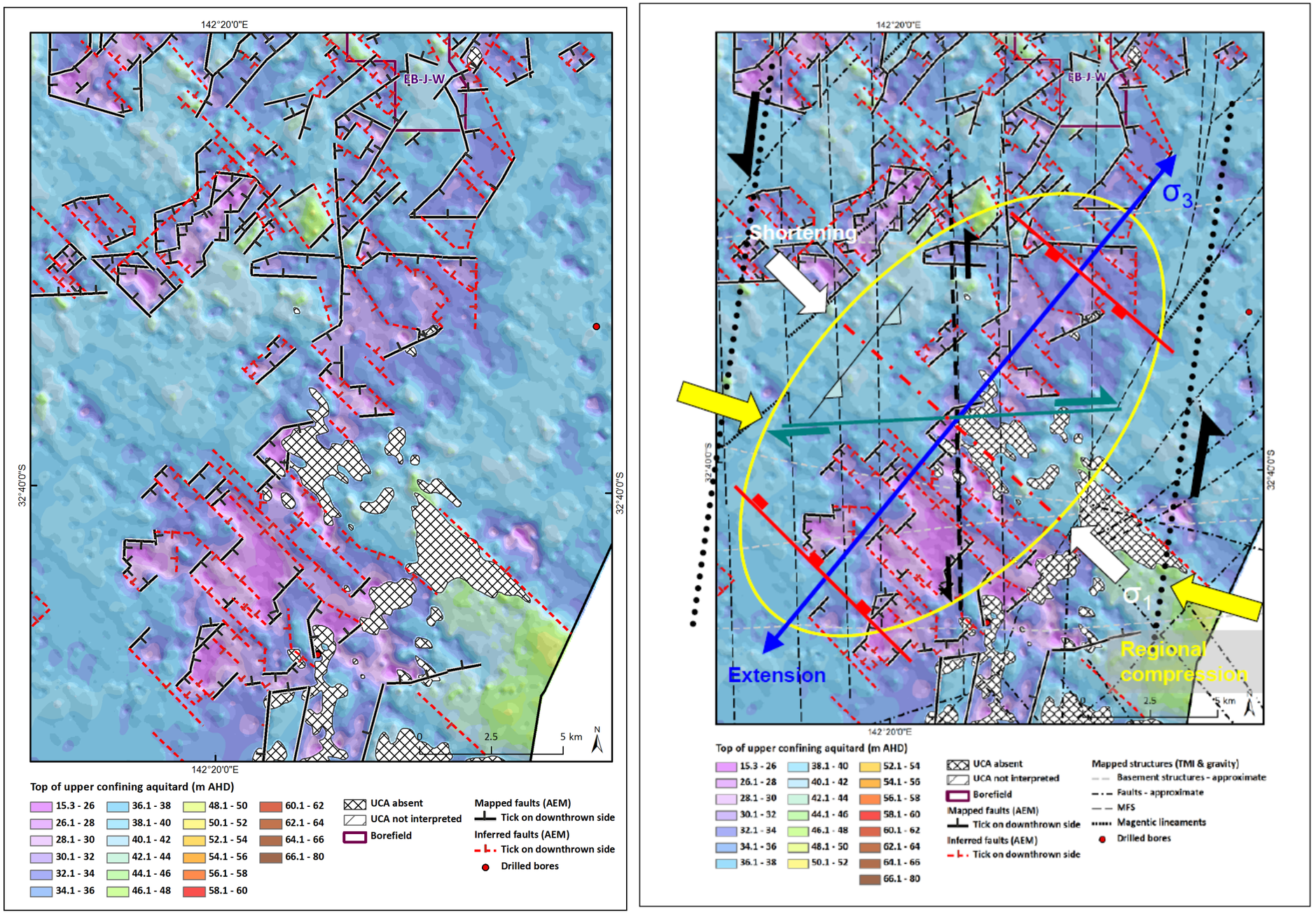

Figure 6-4. *Both images show the depths to the top of the Blanchetown Clay aquitard in an area south of Jimargil. The Darling River runs approximately N-S in the centre of each image. The purple colours are depositional lows filled with Coonambidgal Formation sands. In the left hand image (a), the purple areas are delineated by faults that are mapped across several flight lines (black lines), with inferred faults (parallel to flight lines), in red. In the right hand image (b), the faults from the regional magnetics data have been projected on the same image. The pattern of deformation is produced by regional WNW-ESE shortening (yellow arrows), and reactivation of underlying, pre-existing basement heterogeneities and faults. The black dotted lines denote the shear zone boundaries, with a sinistral sense of displacement similar to that found in the MFS. The yellow line denotes the strain ellipse. Most of the displacement within the MFS is taken up on N-S striking antithetic strike-slip faults (black broken line). Within the shear zones, extension in a NE-SW orientation (blue line and arrows), is typically denoted by normal faults (red) that define grabens and half-grabens. ENE-WSW antithetic faults zones are also observed to form in this stress system, and provide important linkages between these extensional structures. Minor reverse faults (black line with pale blue-green triangles) and associated horst blocks are formed by NW-SE shortening within the shear zones. The crustal stresses indicated are consistent with the Neogene-present day crustal stresses for this region of Australia. Inter-aquifer leakage occurs where the fault offsets juxtapose the Coonambidgal and Calivil Formation aquifers.*

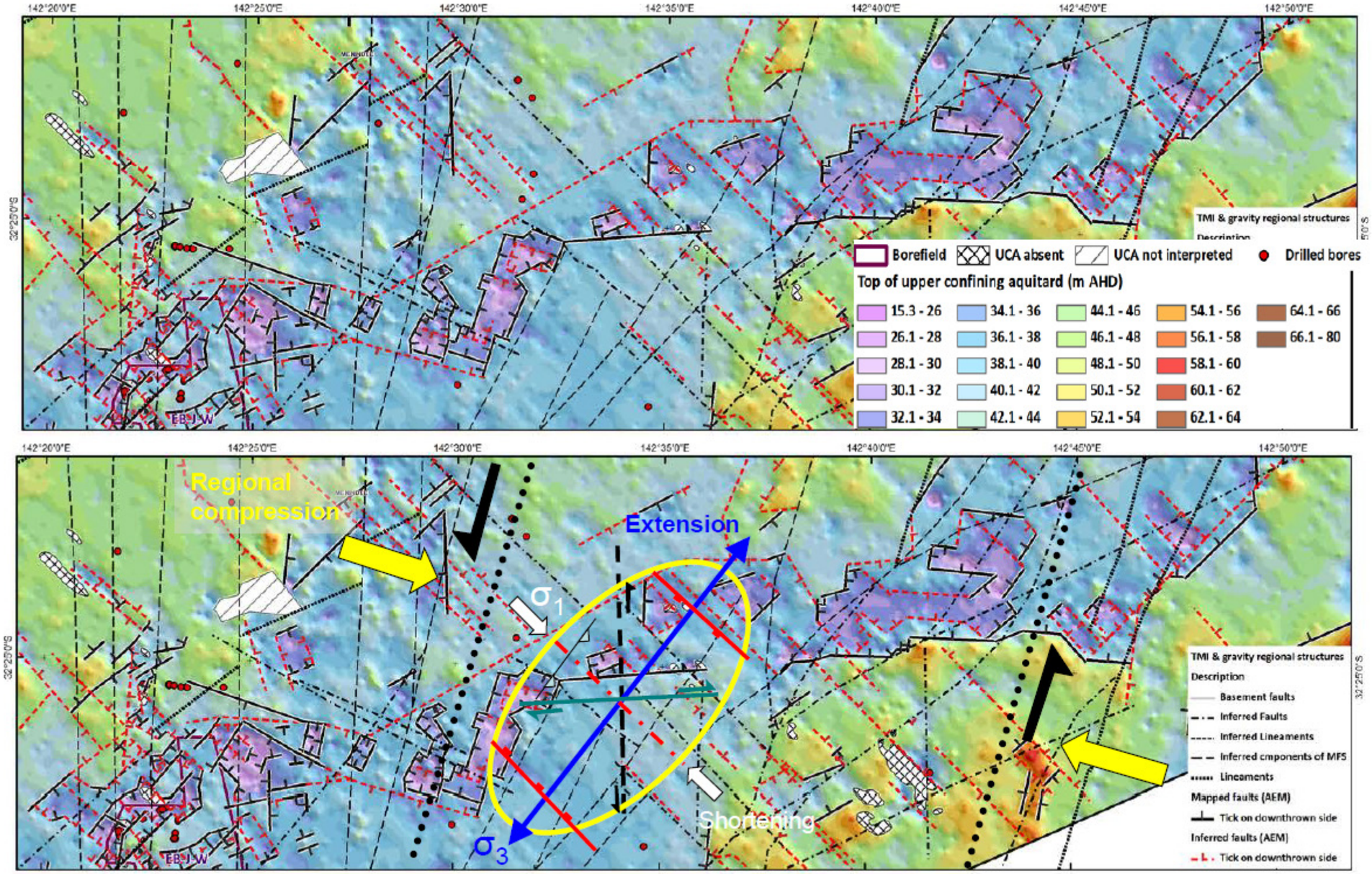

Figure 6-5. *Top and bottom images show the depths to the top of the Blanchetown Clay aquitard in an area where the Talyawalka and Menindee Fault Systems link. The Talyawalka Fault zone is oriented approximately E-W in the centre right of each image, and has a fault trace of over 160km to the east. The purple colours are depositional lows filled with Coonambidgal Formation sands. In both images, the purple areas are delineated by faults that are mapped across several AEM flight lines (black lines), with inferred faults (parallel to flight lines), in red. Faults and lineaments identified in magnetics data are also plotted. In image b, the strain ellipse (yellow) and arrows represent the interpreted stress field under which the faults formed. N-S and NNE-SSW trending sinistral strike-slip faults form at an oblique angle in response to regional WNW-WSE shortening (yellow arrows). Within the shear zones, extension in a NE-SW orientation (blue line and arrows), is typically denoted by normal faults (red) that define grabens and half-grabens. ENE-WSW antithetic faults zones are also observed to form in this stress system, and provide important linkages between these extensional structures. Minor reverse faults (black line with pale blue-green triangles) and associated horst blocks are formed by NW-SE shortening within the shear zones. The structures mapped are consistent with models of simple shear couples within strike-slip fault systems and consistent with broader regional Neogene-and present day crustal stresses for this region of Australia. The orientation of the Talyawalka Fault System is consistent with dominant antithetic strike-slip movement in this shear zone system, with significant influence from pre-existing, underlying basement structures.*

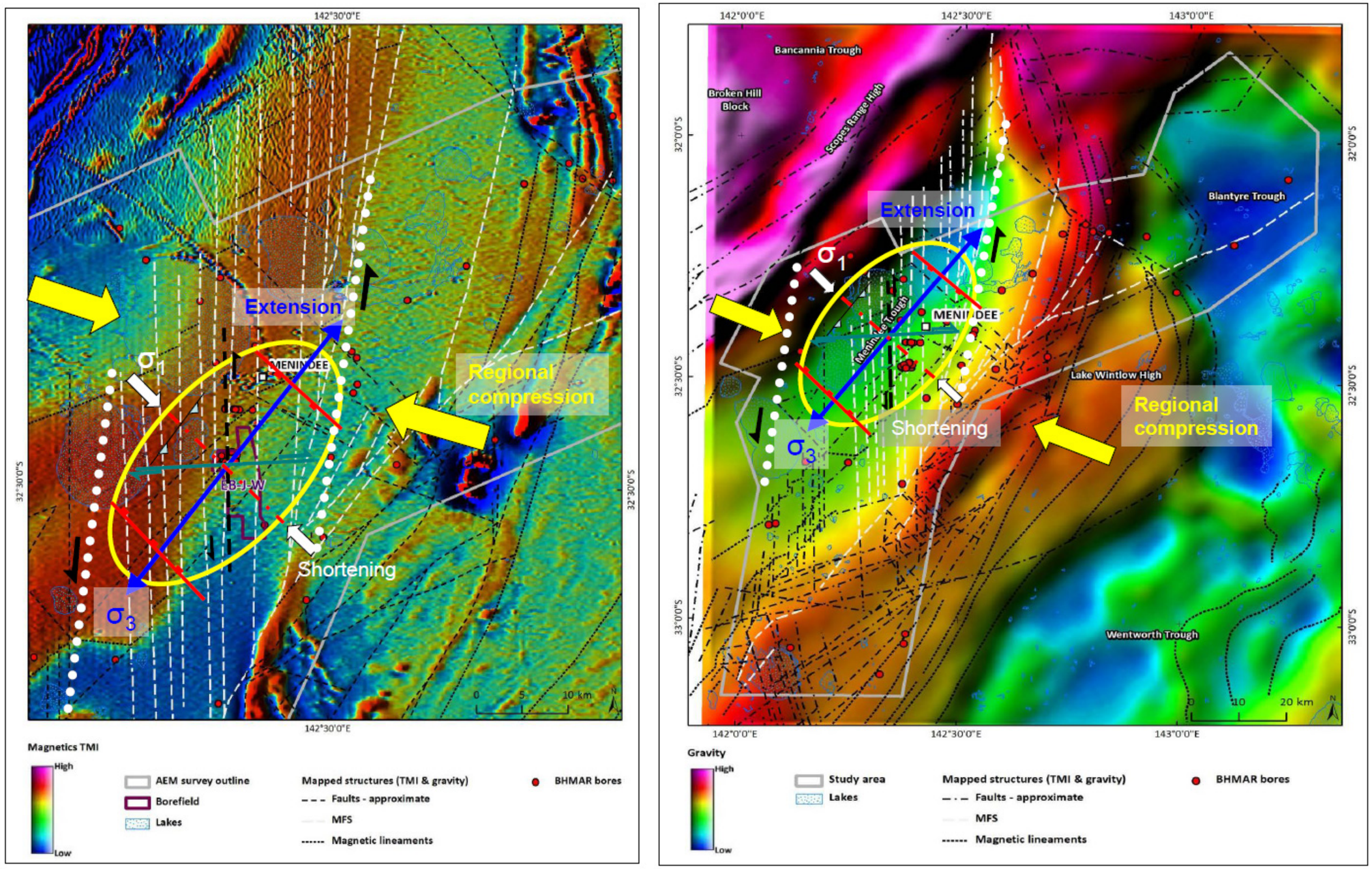

Figure 6-6. *The left hand figure (a) shows a map of first vertical derivative of total magnetic intensity (TMI) major fault zones indicated. The image on the right (b) is the regional gravity data with the same faults and lineaments mapped The local stress fields for within the DFS are shown in both figures, with the Neogene-present day maximum horizontal stress shown as yellow arrows. N-S and NNE-SSW trending sinistral strike-slip faults form at an oblique angle in response to regional WNW-WSE shortening (yellow arrows). Within the shear zones, extension in a NE-SW orientation (blue line and arrows), is typically denoted by normal faults (red) that define grabens and half-grabens. ENE-WSW antithetic faults zones are also observed to form in this stress system, and provide important linkages between these extensional structures. Minor reverse faults (black line with pale blue-green triangles) and associated horst blocks are formed by NW-SE shortening within the shear zones. The structures mapped are consistent with models of simple shear couples within strike-slip fault systems and consistent with broader regional Neogene-and present day crustal stresses for this region of Australia.*

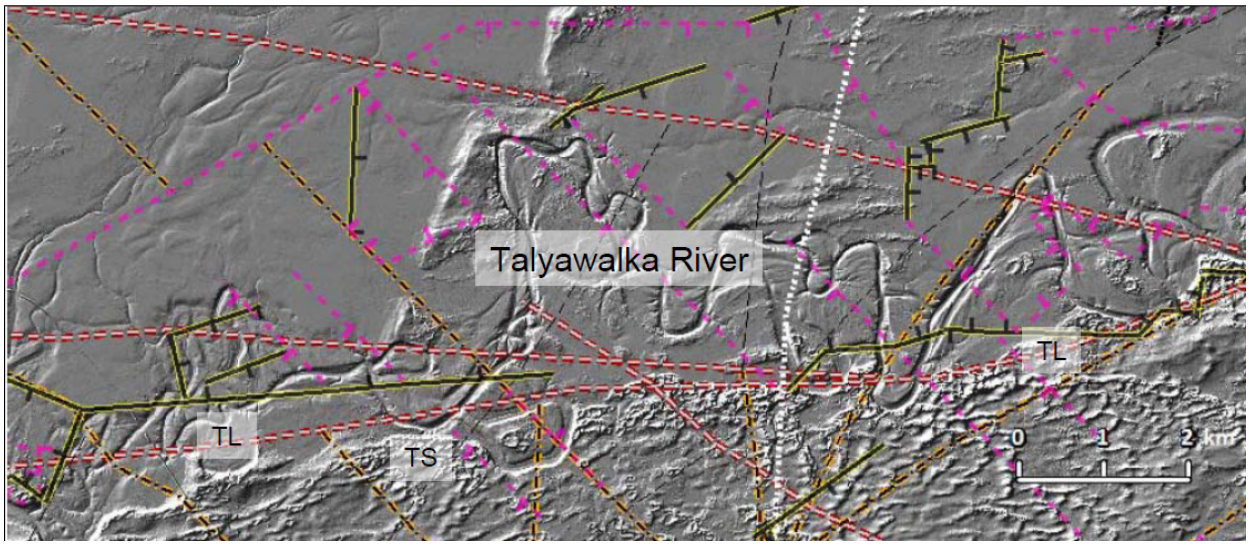

Figure 6-7. *LiDAR image showing the Talyawalka Scarp (TS) which is effectively coincident with a basement shear zone (TL – one of several sub-parallel basement shear zones (broken white lines with red border). It is postulated that the relief on the scarp is related to Neogene structural reactivation of the basement structure. The Talyawalka Creek effectively follows this major lineament. En-echelon half graben structures are delineated by extensional faults mapped at the Blanchetown Clay layer (solid black and dotted pink lines). A number of other scarps present in the image may also be related to tectonism.*

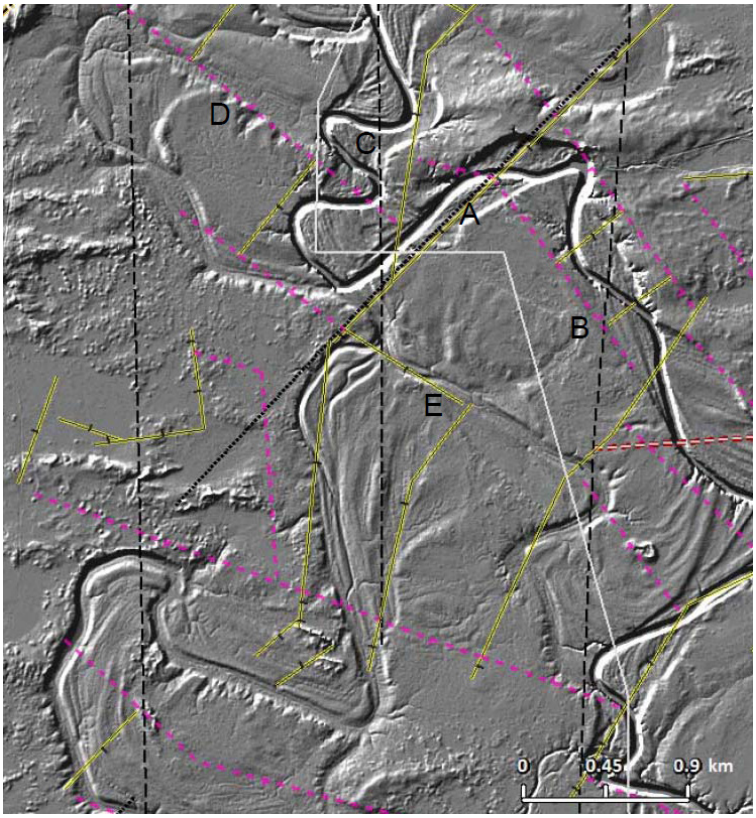

Figure 6-8. *LiDAR image of the Darling River near Bootingee showing unusual drainage pattern with numerous straight-line segments and box-like pattern in the river course. A number of straight line scarps (A-E) that parallel the river course are observed to be coincident with mapped faults in the underlying geology. Scarp A is coincident with both faults mapped in both the AEM (black with yellow border) and with lineaments in airborne magnetic data (dotted black line).Scarps B, D and E, are coincident with faults mapped in the AEM data, while scarp C and river course, are coincident with an underlying strike-slip fault mapped in the magnetic basement. The drainage pattern is more reminiscent of an incised upland rather than an active low gradient floodplain. The drainage pattern is attributed to neotectonics.*

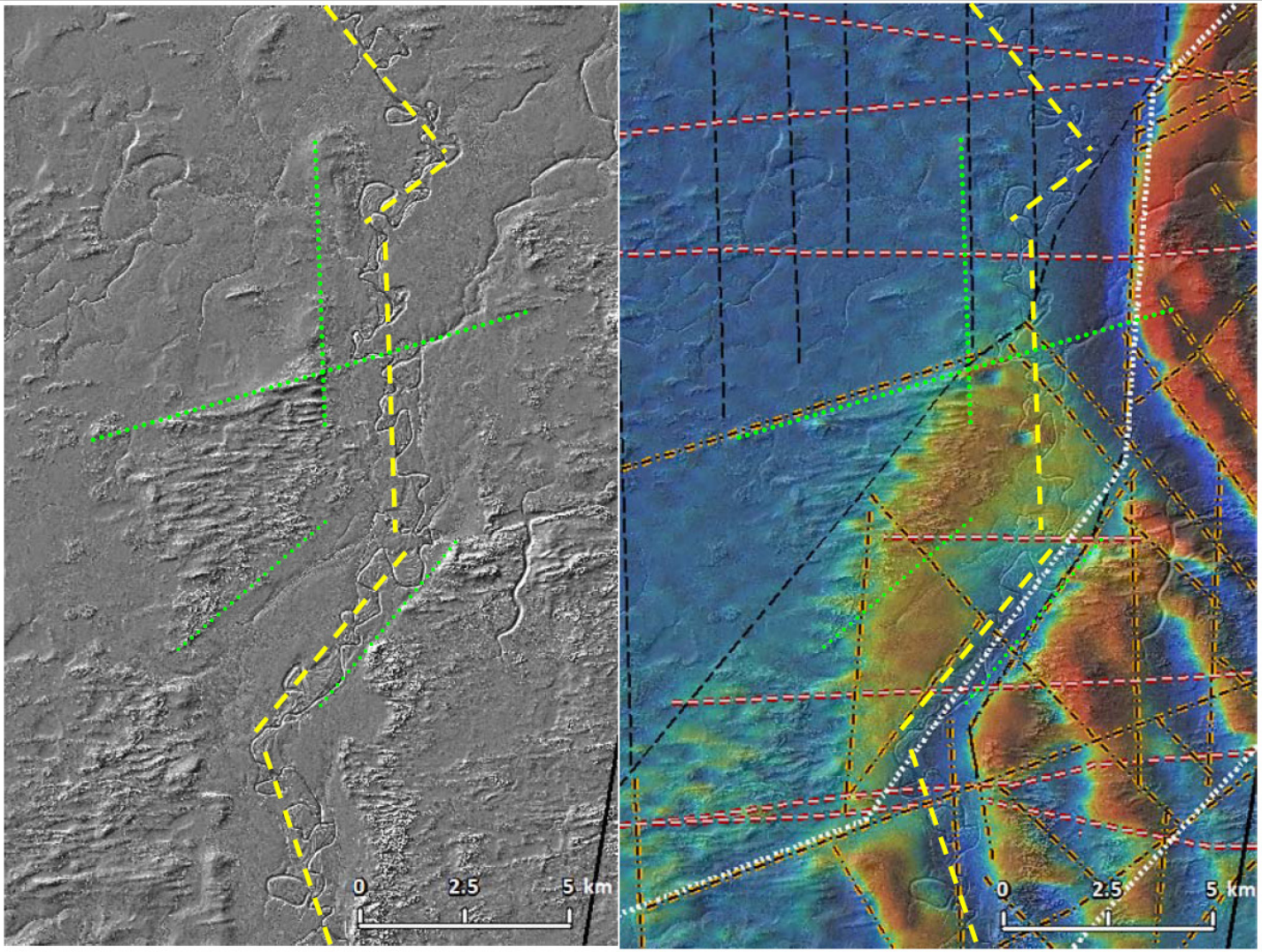

Figure 6-9. *The left hand image is a LiDAR image with lineaments mapped for a reach of the lower Yampoola Creek floodplain east of the Darling River and south of Menindee township. The green traces are surface scarps, the yellow traces are along the course of the Darling River. The right hand image shows the same area with the backdrop being the TMI 1st VD draped over the LiDAR image. The lineaments from the LiDAR image are effectively coincident with faults mapped in the TMI (black lines) and regional gravity data (white dotted line). These data are interpreted as showing evidence for neotectonics in this area through reactivation of basement structures.*

6.6 DEFORMATION MODEL FOR THE BHMAR STUDY AREA

A holistic structural model for the study area has been developed (Lawrie *et al*., 2012b). Overall, the geometry of the mapped faults in the Menindee and Talyawalka Fault Systems is consistent with releasing steps or jogs in other intra-plate strike-slip fault zones. The rhomboidal box-like basins are interpreted as zones of slip transfer between over-stepping, subparallel strike-slip faults. Releasing steps or jogs in basement strike-slip fault zones characteristically produces rhombic-shaped pull-apart basins in the overlying sedimentary section (e.g., Crowell, 1974; Aydin & Nur, 1985; Christie-Blick & Biddle, 1985; Sylvester, 1988; Cunningham & Mann, 2007). The mapped fault arrays are also consistent with laboratory analogue (clay) models (McClay & Dooley, 1995).

Figure 6-11 shows a diagrammatic representation of the structural strain pattern produced by a sinistral shear couple across the Menindee Fault System (MFS). Most of the displacement within the MFS is taken up on antithetic strike-slip faults oriented ~N-S. The pattern of deformation is produced by regional WNW-ESE shortening (yellow arrows), and reactivation of underlying, pre-existing basement heterogeneities and faults. The black dotted lines denote the shear zone boundaries, with a sinistral sense of displacement similar to that found in the MFS. The yellow line denotes the strain ellipse. Most of the displacement within the MFS is taken up on N-S striking antithetic strike-slip faults (black broken line). Within the shear zones, extension in a NE-SW orientation (blue line and arrows), is typically denoted by normal faults (red) that define grabens and half-grabens. ENE-WSW antithetic faults zones are also observed to form in this stress system, and provide important linkages between these extensional structures. Minor reverse faults (black line with pale blue-green triangles) and associated horst blocks are formed by NW-SE shortening within the shear zones.

The principal bounding faults to the MFS are coincident with basement faults that define the depocentre of the underlying Menindee Trough (Figure 6-6). These faults were initially ~N-S trending extensional faults formed in a trans-tensional regional stress regime in the Palaeozoic (Glen *et al*., 1996; Neef, 2012), although there is evidence for inversion regionally in the mid-Devonian and Carboniferous (Blevin *et al*., 2007; Neef, 2012). Evidence from the AEM mapping LiDAR data suggests that some of these basement faults have been re-activated post- Pleistocene, with some active in the Neogene to present day. Evidence from all geophysical datasets is for sinistral displacement across the major strike-slip zones at a regional scale (Figure 6-6).

The location and orientation of individual extensional faults depends on the overall stepping geometry of the strike-slip zone, the inter-relationships between adjacent en-echelon strike slip faults, and relationships to underlying basement heterogeneities (Sylvester, 1988; Christie-Blick & Biddle, 1985; Cunningham & Mann, 2007). In the BHMAR study area, the formation of rhombic grabens and half-grabens is consistent with their localisation in releasing bends, and where faults over-step (Cunningham & Mann, 2007). The formation of linear zones of compression in the hanging walls of antithetic strike-slip faults (e.g. in the TFS), and as elongate pressure ridges in zones of convergent strike-slip movement, is also consistent with laboratory (Schreurs, 1994; Naylor *et al*., 1986; McClay & Dooley, 1995) and natural examples of intra-plate strike-slip deformation (Harding & Lowell, 1974; Christie-Blick & Biddle, 1985; Cunningham & Mann, 2007).

Regional basement faults mapped from airborne magnetics are shown on a map of airborne magnetics for an area of the MFS (Figure 6-6a) and projected on a map of regional gravity data form the whole BHMAR study area (Figure 6-6b). The sinistral displacement across individual strike slip faults within the MFS are clearly evident in the airborne magnetic data (Figure 6-6a), while the association between the mapped faults and major basement features in the geology are also evident on the gravity data (Figure 6-6b).

At a regional scale, formation of the MFS is consistent with formation of this fault zone as an antithetic strike-slip zone to broadly WNW-ESE crustal shortening consistent with present-day stress maps of the Australian continent (Figure 6-10). The latter have data gaps in this region, with the maximum horizontal stress extrapolated from measurements in the nearby Cooper-Eromanga Basins (Reynolds *et al*., 2006; Hillis *et al*., 2008). While most of the mapped faults in the BHMAR study area are consistent with strike-slip deformation, a component of deformation may also be related to regional warping and tilting due to basin subsidence or margin uplift (Hillis *et al*., 2008).

The Talyawalka Fault System (TFS), and other ENE-WSW-trending faults observed in LiDAR and AEM data (Figure 6-5 and Figure 6-7), are coincident with basement structures observed in airborne magnetic data (Figure 6-12). It would appear that these basement structures, which may have been ductile shear zones, are reactivated in the Neogene-to-present. Their orientation is consistent with antithetic strike slip displacement at a low angle to the present day maximum compression ((Figure 6-10).

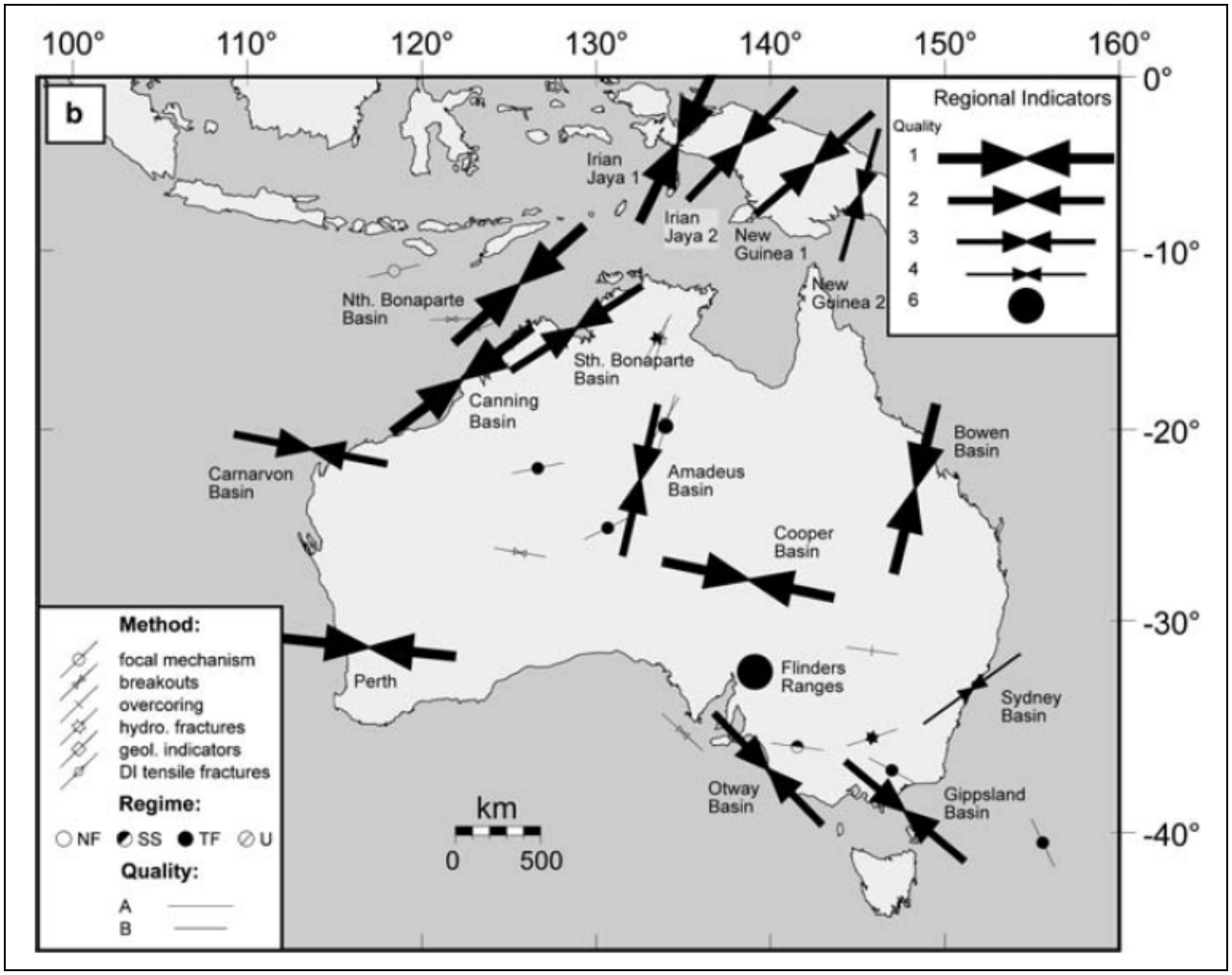

Figure 6-10. *This figure shows the mean stress orientations within Australian stress provinces. The size of the arrow indicates the consistency of stress orientations within the province. From Hillis et al. (2008).*

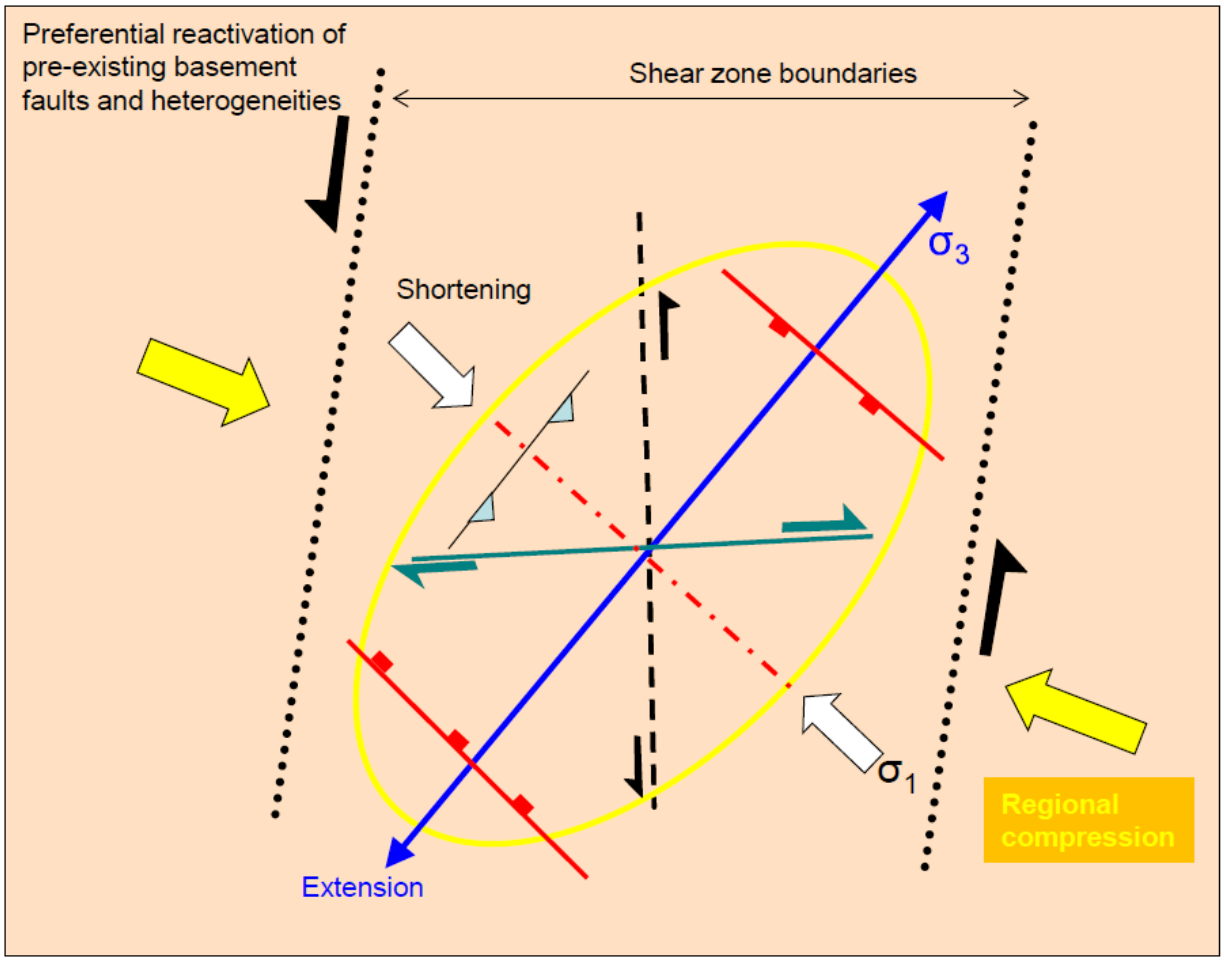

Figure 6-11. *A diagrammatic representation of the strain pattern within the MFS and TFS intra-plate shear zones. The pattern of deformation is produced by regional WNW-ESE shortening (yellow arrows), and reactivation of underlying, pre-existing basement heterogeneities and faults. The black dotted lines denote the shear zone boundaries, with a sinistral sense of displacement similar to that found in the MFS. The yellow line denotes the strain ellipse. Most of the displacement within the MFS is taken up on N-S striking antithetic strike-slip faults (black broken line). Within the shear zones, extension in a NE-SW orientation (blue line and arrows), is typically denoted by normal faults (red) that define grabens and half-grabens. ENE-WSW antithetic faults zones are also observed to form in this stress system, and provide important linkages between these extensional structures. Minor reverse faults (black line with pale blue-green triangles) and associated horst blocks are formed by NW-SE shortening within the shear zones.*

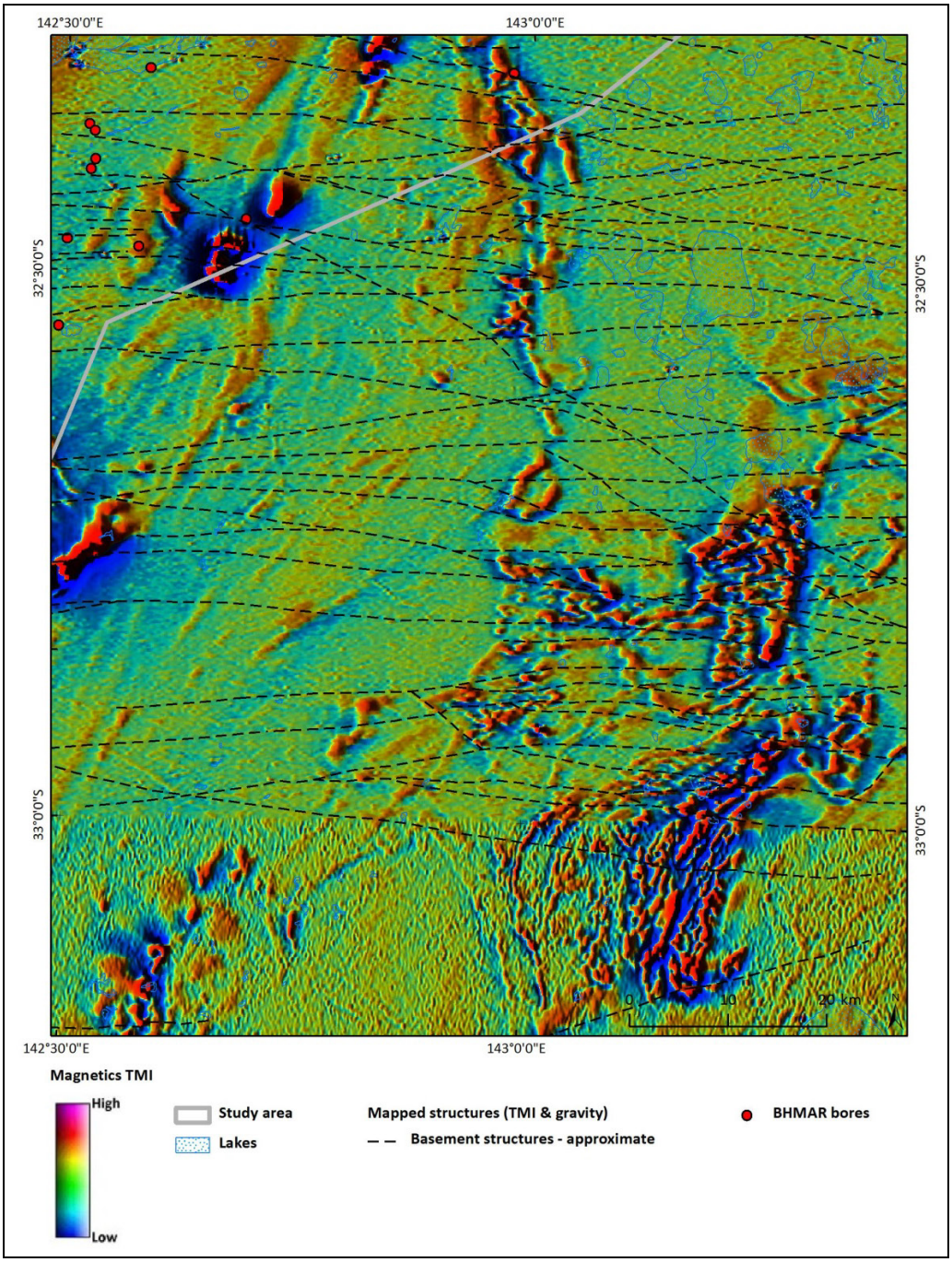

Figure 6-12. *Ductile deformation in basement lithologies immediately to the east of the BHMAR study area. The Talyawalka Fault System, and other relatively minor ENE-WSW faults observed in LiDAR data appear to be basement structures. These appear to have been reactivated in the Neogene-to-present. Their orientation is consistent with antithetic strike slip displacement at a low angle to the present day regional compression*

In summary, the geomorphic/geological history for the Menindee area as determined by this project can be summarised as:

1. Complex history of pre-Palaeozoic deformation and metamorphism in Proterozic basement rocks. Several E-W shear zones mapped in Proterozoic basement are reactivated in Neogene times (e.g. Talyawalka Fault System);
2. Formation of Palaeozoic-Mesozoic Basins (e.g. Menindee, Wentworth and Blantyre Troughs) as part of the Darling Geological Basin. Deposition of a thick (several km) sequence of clastic sediments within extensional fault-bounded basins is interrupted episodically by structural inversion along these structures (e.g. in Carboniferous). Several of these structures appear to have been reactivated in Neogene times;

3. Formation of the Murray Geological Basin, with deposition of Renmark Group clastic sediments by rivers flowing southward towards a shallow sea to the south of the BHMAR study area in the Palaeocene to Miocene;
4. Depositional hiatus in the Miocene with weathering and local erosion of the Renmark Group sediments;
5. In the south of the study area, there was deposition of marginal sands and shoreline dunes (Loxton-Parilla Sands) in shallow water at the northern margin of a marine basin. Pene-contemporaneous with this was deposition of fluvial Calivil Formation sediments by the palaeo Darling River and its tributaries in the Pliocene. The Calivil Formation sediments locally overlie the Loxton-Parilla Sands in the study area;
6. Damming of the palaeo-Murray River and its tributaries, including the palaeo Darling River, with Blanchetown Clay deposition in palaeo Lake Bungunnia in the Late Pliocene to Pleistocene;
7. Pliocene regression, and the drying up of Lake Bungunnia, due to a combination of lowering of the sill of the dam that initiated the lake (McLaren *et al*., 2012) and the onset of a dryer climate;
8. Continued fluvial and local lacustrine deposition, with sediment derived from the northwest (Broken Hill area) and the north (palaeo Darling River, which passed through a gap in basement hills at Wilcannia at the edge of the Murray Basin) to the south of the BHMAR study area. These Willotia bed sediments may be also partly a time equivalent of the upper part of the Blanchetown Clay deposited further south in Lake Bungunnia;
9. Incision of a trench into the Blanchetown Clay to form the modern course of the Murray River (Murray Gorge). This trench propagated headwards up the Darling Valley by nickpoint retreat, incising the Willotia beds but generally not the Blanchetown Clay in the Menindee area;
10. Deposition of fluvial sediments of the Menindee Formation and subsequently Coonambidgal Formation within the eroded trench by the Darling River and its anabranches;
11. Concurrent with 8, formation of the lake basins around Menindee, with local wave erosion and shoreline deposition; and
12. Concurrent with 8 and 9, deposition and preservation of aeolian sand across much of the area, particularly where not flooded and reworked in the trunk river valley.
13. There are multiple lines of evidence to show that the area has been tectonically active in the Neogene-present day, as evidenced by a number of scarps, lineaments, and drainage alignments that are coincident with underlying faults. There is also evidence of neotectonics from some lake tilting in the south of the project area.

6.6.1 The Role of Faults in the Hydrogeological Conceptual Model

The recognition of faults in multiple geophysical datasets, combined with drilling and field validation, provides increased confidence in the structural maps and interpretation that play a vital role in the hydrological conceptual model. In particular, faults with a surface landform expression, including those that control or intersect the major rivers, provide potential recharge pathways to underlying aquifers. Furthermore, juxtaposition of unconfined Coonambidgal Formation and semi-confined Calivil Formation aquifers across faults, particularly where the Coonambidgal Formation infills graben depocentres, may provide loci for inter-aquifer leakage (Figure 6-13).

The important role of faults in recharge is highlighted by the GW1 groundwater target, where hydrodynamic and hydrochemical studies show the Calivil Formation aquifer is rapidly recharged despite no direct connection between the river and the underlying aquifer, and a paucity of holes in the Blanchetown Clay and shallow aquitard (Lawrie *et al*., 2012b). In this target, bypass flow through faults is required to explain the rapid recharge (<1 week) of the Calivil Formation aquifer in bores 200-300 m lateral to the Darling River (Lawrie *et al*., 2012b).

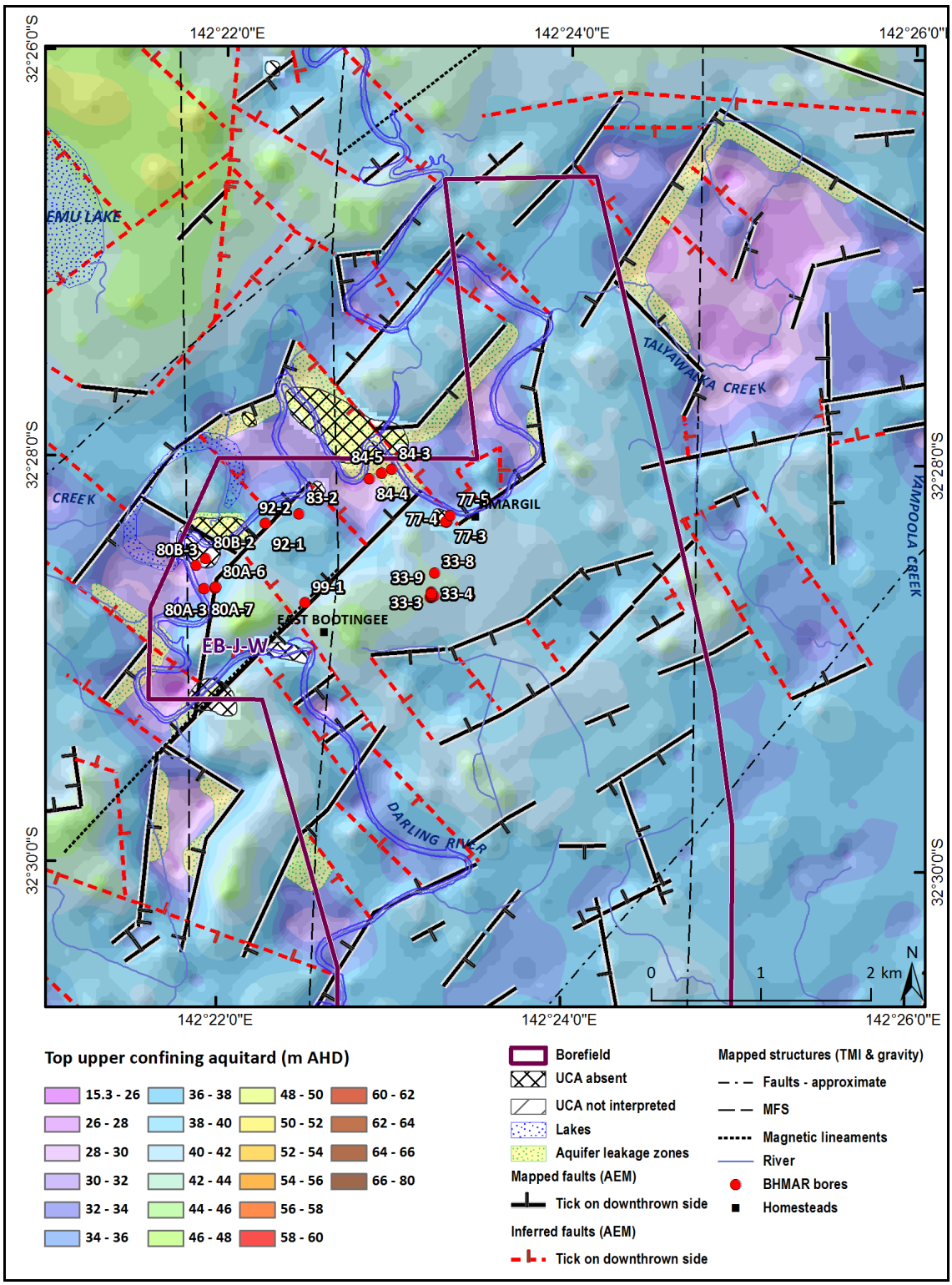

Figure 6-13. *Map of the top Blanchetown Clay surface showing contoured elevations and interpreted faults. This image also shows potential inter-aquifer leakage zones (pale yellow stipple) which occur at sites where the unconfined Coonambidgal Formation aquifer is juxtaposed against the semi-confined Calivil Formation aquifer and/or where the Blanchetown Clay has been eroded (cross-hatched pattern) on the footwall zones of some of the larger faults. Rapid recharge of the Calivil Formation is recorded in a number of the bores close to these zones.*

7. Hydrogeology

This section reframes the stratigraphy described in Section 5 from a hydrogeological perspective. The Calivil Formation and Loxton-Parilla Sands have been identified as the target aquifer for the purpose of the project objectives. Hence, the stratigraphic units (and components within) have been redefined as aquifers or aquitards, relative to the Pliocene Sands aquifer, which is dominantly the Calivil Formation in the BHMAR project area. In this way, with decreasing depth and geological age, the stratigraphy can be classified into:

- The Lower Aquitard representing the muds and muddy sands commonly found in the upper parts of the Renmark Group. Regionally, these sediments form the base to the target aquifer.
- The Pliocene Sands Aquifer consists of the sands and gravels hosted in the Calivil Formation, as well as the laterally equivalent Loxton-Parilla Sands evident in the south of the BHMAR project area. This is the primary target for groundwater resource and MAR assessment.
- The Upper Confining Aquitard which largely consists of the Blanchetown Clay that overlies and confines the Pliocene Sands aquifer. The upper sequence of the Calivil Formation can also be included in this aquitard, where it consists of muddy sands and muds.
- The Shallow Unconfined Aquifer consisting of the shallow Quaternary alluvial Coonambidgal Formation, Menindee Formation and Willotia beds that are largely separated from the Pliocene Sands Aquifer by the Blanchetown Clay. Away from modern drainage, the Quaternary sediments can become unsaturated and the watertable is within the underlying formations.

The section describes characteristics of these aquifers and aquitards, including groundwater salinity, hydraulic conductivity, transmissivity, potentiometry and groundwater dynamics.

7.1 LOWER AQUITARD (RENMARK GROUP)

7.1.1 Hydrogeology

Mud and muddy sands of the Renmark Group represent the lower aquitard that bounds the overlying regional semi-confined aquifer in the Calivil Formation and the Loxton-Parilla Sands. The lower aquitard can be characterised by the indicative lithology based on sediment textural classification for two representative depth slices. Figure 7-1 shows the textural composition of the Renmark Group and Figure 7-2 shows the spatial distribution of these textural compositions. The 51.5-61 m depth slice (Figure 7-16) is the first slice at depth with a significant proportion of Renmark Group sediments. The figure shows that the Renmark Group consists of a mosaic of predominantly muddy sediments, a combination of muddy sands, muds, and interbedded sands and muds. Rare bodies of fine sand present localised fixed anastomosing channel systems large enough to be resolved by the AEM system at these depths and conductivities.

In the 61.0-72.3 m depth slice (Figure 7-3) the sediments are composed predominantly of Renmark Group sediments except where the most deeply incised palaeochannel thalwegs filled by the Calivil Formation occur. The Renmark Group consists of a mosaic of predominantly muddy sediments, a combination of muddy sands, muds, and interbedded sands and muds. Rare bodies of fine sand present localised fixed anastomosing channel systems large enough to be resolved by the AEM system at these depths and conductivities. These details are not readily visible in maps at these scales and are discussed more fully in the report on individual groundwater targets (Lawrie *et al.,* 2012d).

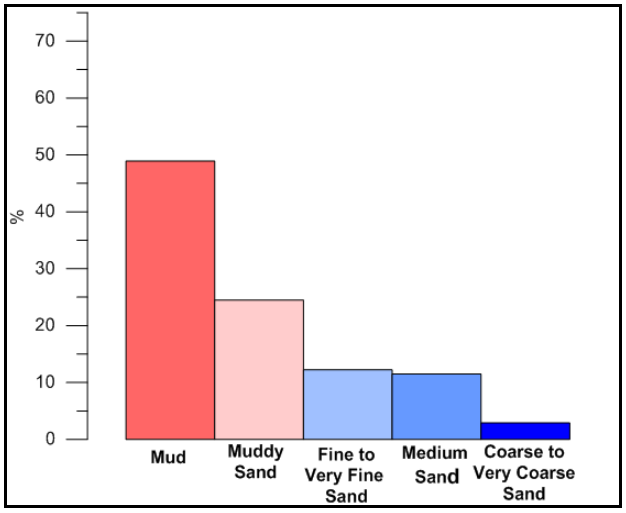

Figure 7-1. *Textural composition of Renmark Group.*

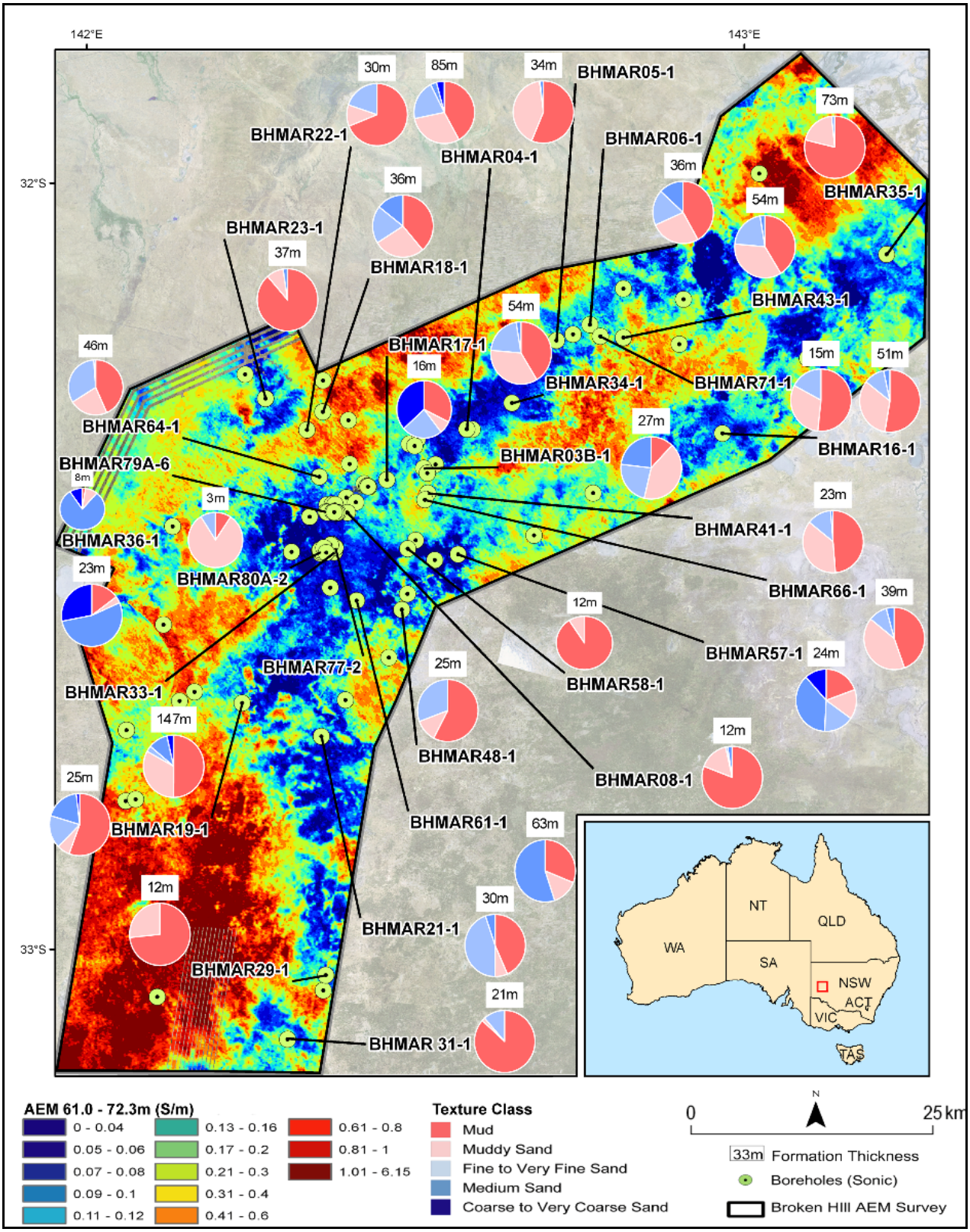

Figure 7-2. *Pie charts showing the textural composition of the Renmark Group present across the study area. Partial thicknesses of the Group intersected in drill cores are labelled.*

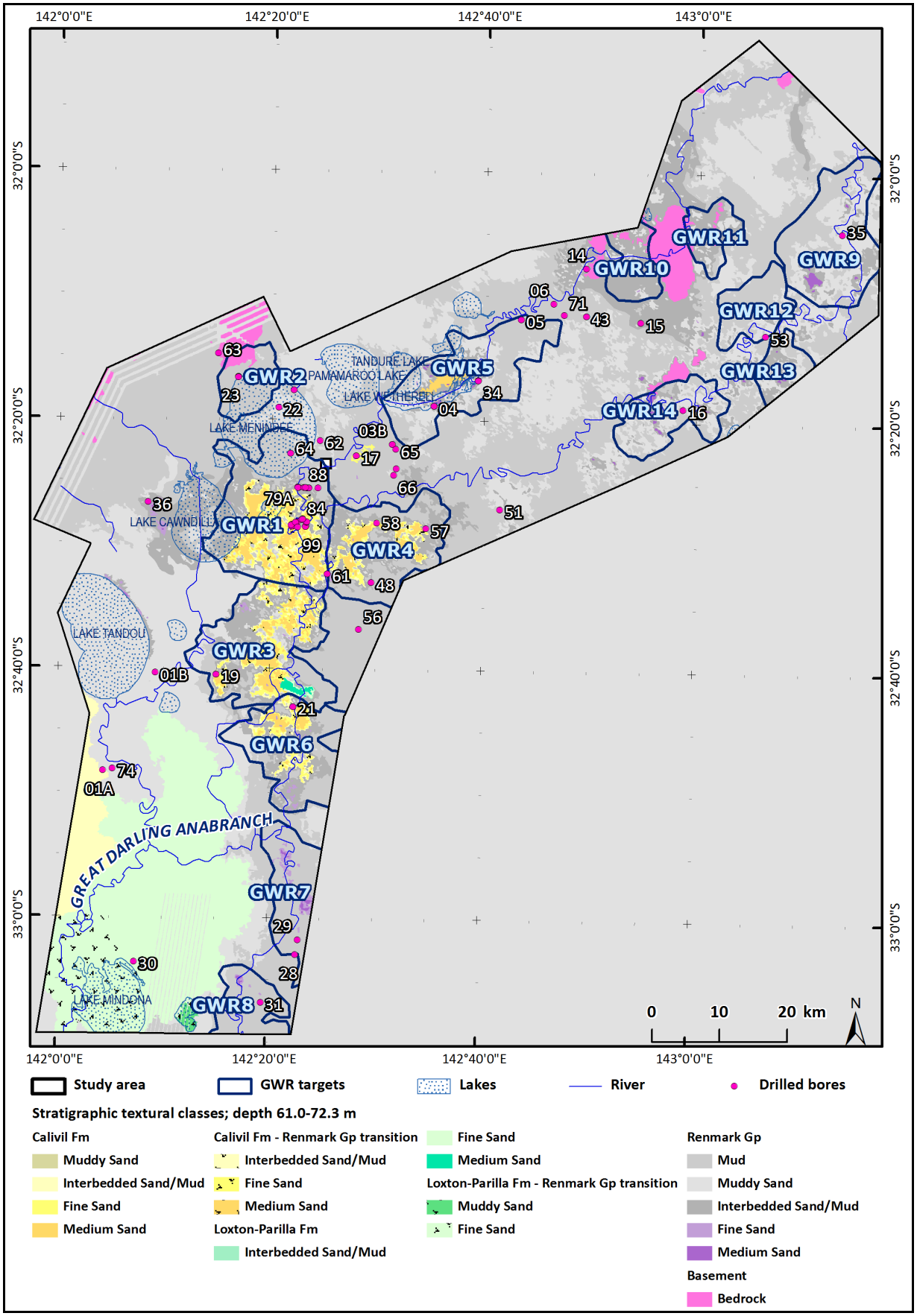

Figure 7-3. *Indicative lithology of the lower aquitard (Renmark Group) and minor semi-confined aquifer (Calivil Formation) and across the project area, based on sediment textural classification, illustrating the 61.0-72.3 m AEM depth slice.*

Slug tests of BHMAR monitoring bores provide transmissivity estimates for aquifer horizons within the stratigraphy, including the Renmark Group. This has been supplemented by hydraulic conductivity estimates derived from the nuclear magnetic resonance (NMR) logging of selected monitoring bores. One advantage of the NMR logging is that it enables characterisation of the aquitard units, including the finer-textured Renmark Group sediments, in addition to the aquifers. The methods used in data acquisition and processing are outlined in Lawrie *et al.* (2012a), as well as the identified limitations of the logging.

Figure 7-4a and b are box and whisker plots that summarise the slug test results across the aquifers screened by the monitoring bores. In these plots, the "boxes" show the central 50% of the data and the line within the box is the median (50th percentile) of the data. The "whiskers" represent the outer tails of the sample population, based on what is termed the interquartile range. The maximum value is plotted as a red dot if it is an outlier beyond the range defined by the whiskers, and the minimum is represented as a blue dot if it is an outlier. Figure 7-4a and Figure 7-4b respectively show the relative distribution of hydraulic conductivity and transmissivity values derived by slug tests for the various screened aquifer formations. These plots show that sand horizons within the Renmark Group (Ter) that have been screened in the monitoring bores have moderate hydraulic properties – relatively high hydraulic conductivities and transmissivities compared to the Coonambidgal Formation (Qac) and Menindee Formation (Qam) aquifers but relatively low compared to the Calivil Formation (Tpc) target aquifer. The slug test transmissivities for the Renmark Group aquifer horizons would be considered to be intermediate to high (Krasny, 1993).

Figure 7-5 and Figure 7-6 are box and whisker plots for various hydraulic parameters derived from the NMR logging. With data processing, hydraulic conductivity values are estimated on the basis of 0.5 m intervals down the logged hole (Lawrie *et al.,* 2012a). Figure 7-5a shows the distribution of these hydraulic conductivity values for the 0.5 m downhole intervals assigned to particular formations. Any NMR data above the watertable depth at the logging site was excluded, to ensure that the statistics related to saturated sediments. Figure 7-5a shows a broad range in hydraulic conductivity for 0.5 m intervals in the upper part of the Renmark Group (Ter) intersected in the boreholes and logged by the NMR tool. Even the more permeable zones in the Renmark Group have relatively low hydraulic conductivities compared with the Calivil Formation (Tpc)and the Loxton-Parilla Sands (Tps). Rather than being grouped by formation, Figure 7-5b plots the 0.5 m interval hydraulic conductivity data on the basis of the host lithology, whether it be a mud, muddy sand, fine sand, medium sand or coarse to very coarse sand. This shows the natural progression of increasing hydraulic conductivity with increasing grainsize.

Figure 7-6 provides a different perspective of the NMR logging. The 0.5 m downhole intervals are assigned to their relevant formation to derive statistics on the basis of the formations intersected in each borehole. A formation transmissivity was derived by summing the transmissivities of the 0.5 m intervals within the bounds of the formation. The resulting transmissivity statistics across the NMR-logged boreholes are presented in Figure 7-6b. The NMR-derived formation transmissivities for the Renmark Group are significantly lower than the slug test equivalents. This probably reflects the positive bias in the slug test data, due to the preferential screening into the more transmissive parts of these stratigraphic units. One issue with the Renmark Group transmissivities against the other formations is that the boreholes are only partially penetrating the upper part of the formation, whilst the full saturated sequence is represented for the other formations. The NMR-derived transmissivity for the Renmark Group sequences intersected downhole would be considered imperceptible to low (Krasny, 1993). The NMR hydraulic data on a formation basis (Figure 7-6a) was generated by dividing the formation transmissivity data (Figure 7-6b) by the downhole formation thickness. This shows the moderate nature of the intersected Renmark Group – it does not have the aquifer properties of the Calivil Formation or Loxton-Parilla Sands and neither the aquitards properties of the Blanchetown Clay.

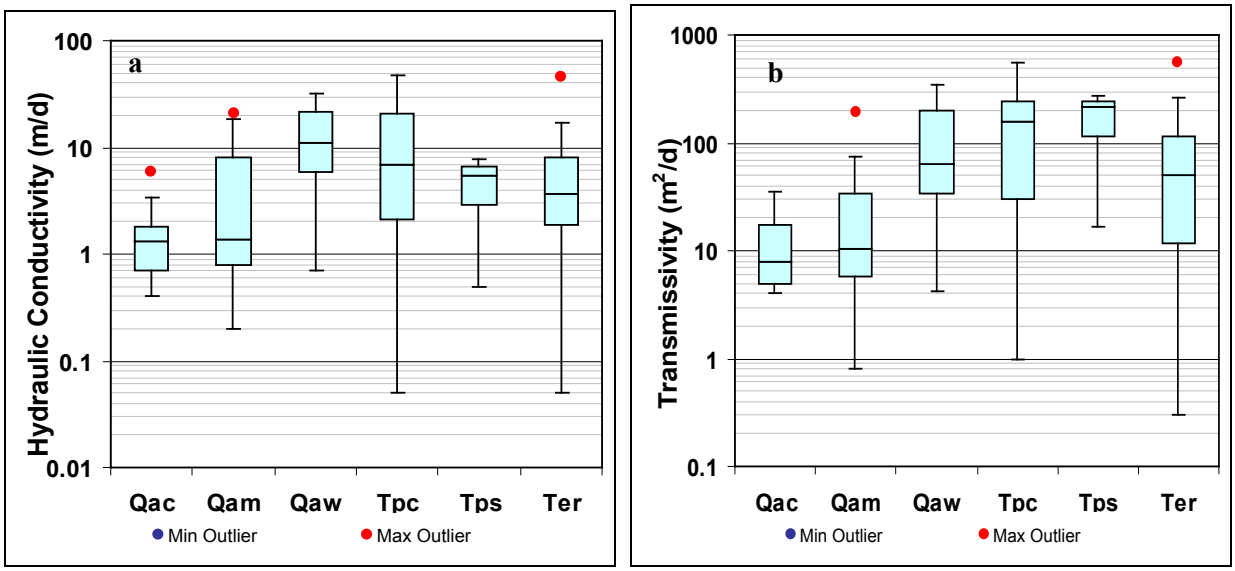

***Figure 7-4**. Box and whisker plots of aquifer properties based on slug testing of BHMAR monitoring bores (a) hydraulic conductivity (b) transmissivity. In these plots Qac = Coonambidgal Formation, Qam = Menindee Formation, Qaw = Willotia beds, Tpc = Calivil Formation, Tps = Loxton-Parilla Sands and Ter = Renmark Group.*

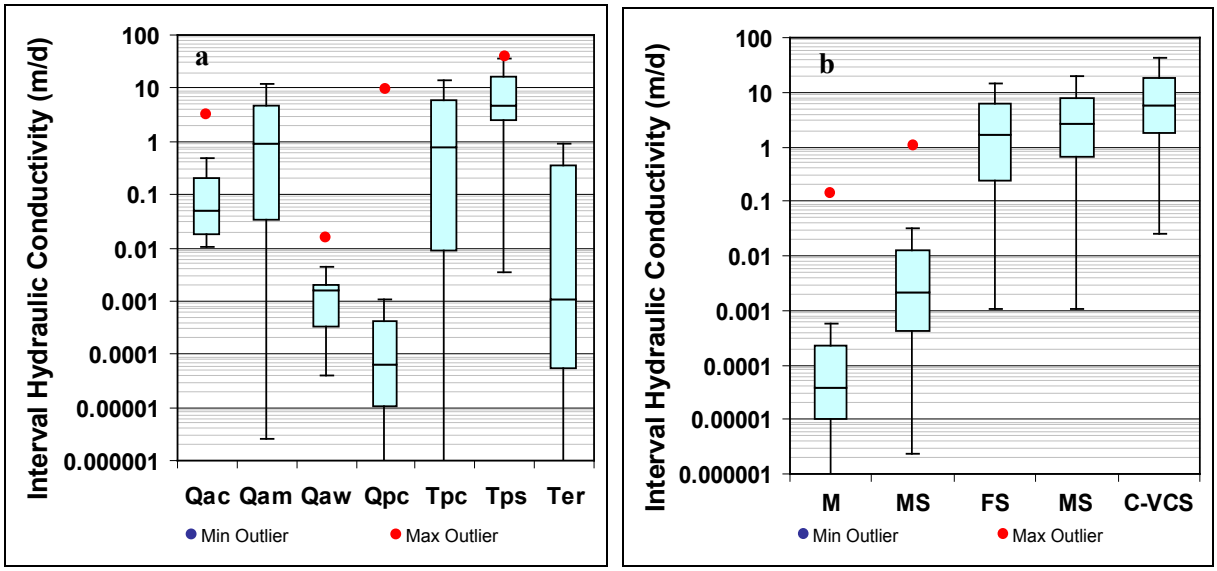

***Figure 7-5.** Box and whisker plots of aquifer properties based on NMR logging intervals of BHMAR monitoring bores (a) hydraulic conductivity of 0.5 m NMR logging intervals grouped by formation (b) hydraulic conductivity of 0.5 m NMR logging intervals grouped by lithology. In these plots Qac = Coonambidgal Formation, Qam = Menindee Formation, Qaw = Willotia beds, Tpc = Calivil Formation, Tps = Loxton-Parilla Sands, Ter = Renmark Group, M = mud, MS = muddy sand, FS = fine sand, MS = medium sand and C-VCS = coarse to very coarse sand.*

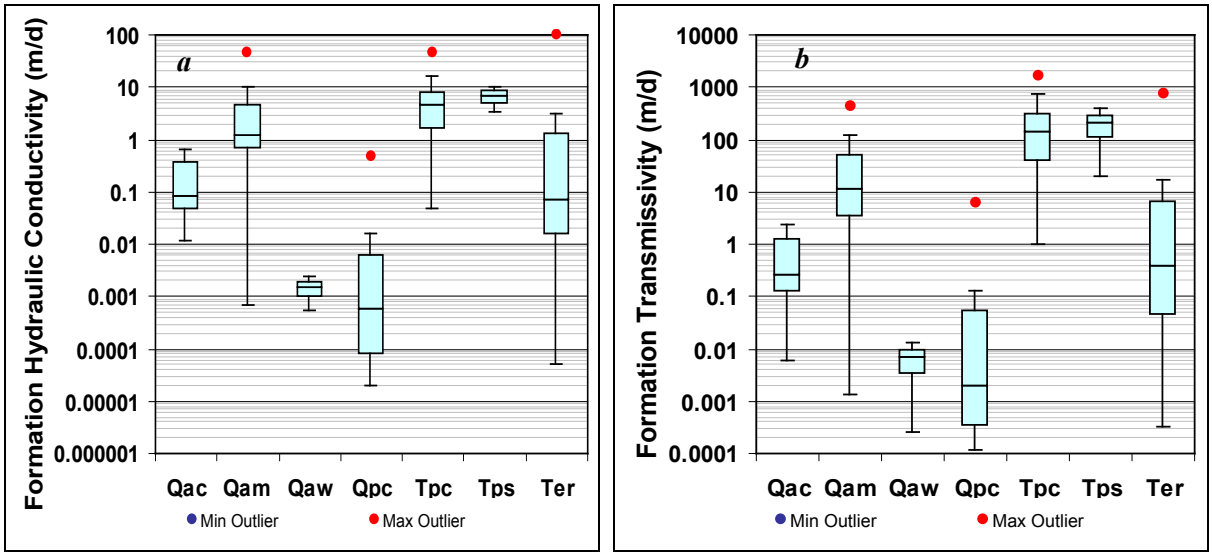

Figure 7-6. *Box and whisker plots of aquifer properties based on formation aggregates of NMR logging intervals in BHMAR monitoring bores (a) average of NMR hydraulic conductivity over formation interval (b) total NMR transmissivity of formation interval. In these plots Qac = Coonambidgal Formation, Qam = Menindee Formation, Qaw = Willotia beds, Tpc = Calivil Formation, Tps = Loxton-Parilla Sands and Ter = Renmark Group.*

7.1.2 Groundwater Flow and Dynamics

Groundwater monitoring bores have been constructed into sand horizons of the Renmark Group as part of nested piezometer sites. This provided an opportunity to measure the response of these aquifers to flooding of the Darling River. The groundwater level increases in seven bores in the Renmark Group ranged from 0.4 to 0.9 m for the period October 2010 to December 2011. As an example, the groundwater level in bore BHMAR79A-2, located at Menindee Common and 170 m from the Darling River, rose a total of 0.8 m over this period (Figure 7-7). Some hydrographs have a similar response to that observed in the overlying Calivil Formation aquifer, but typically of a smaller magnitude.

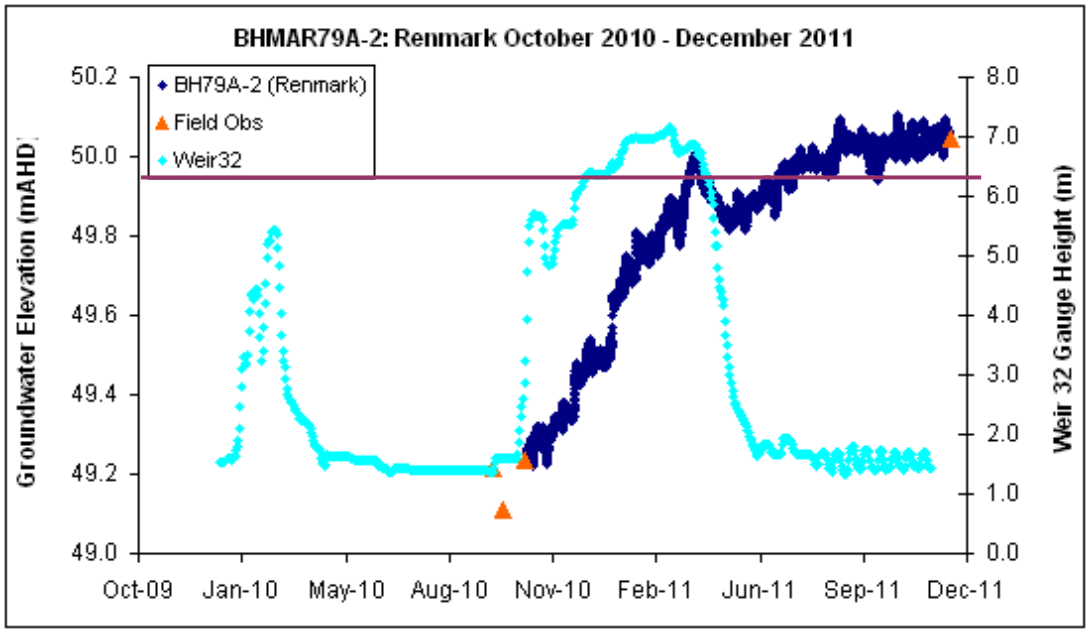

Figure 7-7. *Hydrograph of BHMAR79A-2 screened in the Renmark Group at Menindee Common. The light blue points are the Darling River stage height measurements at the Weir 32 gauge. The purple line is the Weir 32 gauge height at which overbank flow occurs. The orange triangles are manual measurements of groundwater levels in the monitoring bore as a comparison with the logger data.*

7.2 PLIOCENE SANDS AQUIFER

7.2.1 Hydrogeology

Pliocene units, dominated in the study area by the fluvial Calivil Formation with the marine Loxton-Parilla Sands evident in the southern part, are the target aquifers for groundwater resource or managed aquifer recharge (MAR) opportunities. Table 7-1 summarises the key features of the Pliocene Sands aquifer in the study area. The Blanchetown Clay represents an aquitard marker horizon over the top of the Calivil Formation. This means that the latter tends to be a confined aquifer system. However, there is evidence for leakage or bypass flow through the Blanchetown Clay, so the Calivil Formation can be locally semi-confined. Mapping of tectonic structures and areas where the Blanchetown Clay thins or is absent is provided in the Section 5.3.1. Away from the mounding associated with rivers and lakes, the groundwater level in the Calivil Formation can deepen to be below the aquifer top, indicating unconfined conditions. Hence, the aquifer type varies for the Calivil Formation, most notably with distance away from the Darling River, and also in relation to areas where the Blanchetown Clay is absent, thin or structurally disrupted. As demarcated by the base of the Blanchetown Clay, the depth to the top of the aquifer can vary between 6 and 63 m, with a mean depth of ~28 m. The sonic drilling indicates similar variability in the aquifer thickness, ranging from 4 to 51 m, with a mean of ~24 m.

***Table 7-1**. Characteristics of Calivil Formation aquifer in the BHMAR study area.*

	Description	Comments
Host formations	Calivil Formation	
Aquifer type	Confined to semi-confined to unconfined	Potential for leaky confined conditions with structural features or absences of Blanchetown Clay near Darling River. Aquifer can become unconfined away from the river in certain areas; pump tests confirm confined aquifer conditions.
Depth to top of aquifer from ground surface (m)	Range: 6-63 m Mean: 27.5 m	Based on depth to base of Blanchetown Clay surface interpreted from AEM sections and boreholes over BHMAR study area.
Aquifer thickness (m)	Range: 4-51 m Mean: 24 m	Based on sonic core logging of Calivil Formation drillhole intervals in BHMAR study area
Lithologies	Coarse to very coarse sand (23%) Medium sand (29%) Fine sand (12%) Muddy sand (23%) Mud (13%)	Based on sonic core logging of Calivil Formation drillhole intervals in BHMAR study area.
Porosity and storage coefficients	NMR mobile water P_{25}: 0.06 Mean: 0.14 P_{75}: 0.21 Aquifer pump tests Storativity: 0.002 and 0.001	25th percentile, mean and 75th percentile of the NMR mobile water for the saturated Calivil Formation intervals in NMR logged holes in the study area. NMR mobile water used as a surrogate for effective porosity. Storativity estimates from two Calivil Formation aquifer tests undertaken at the Jimargil site. Biased to the high transmissivity zones in aquifer.
Hydraulic conductivity (K, m/d) and transmissivity (T, m^2/d)	Slug Tests: Range: 0.05-137 m/d, Mean: 15 m/d Range: 1-1850 m^2/d, Mean: 200 m^2/d NMR Logs: K Range: 0.2-60 m/d, K Mean: 13 m/d T Range: 0.9-1630 m^2/d, T Mean: 370 m^2/d Aquifer pump tests: 300 and 930 m^2/d (n=2)	Range and mean of slug test results for Calivil Formation monitoring bores in BHMAR study area. Range and mean of average K and total T for Calivil Formation sections in NMR logged monitoring bores in BHMAR study area. Two aquifer tests undertaken at the Jimargil site. Biased to the high transmissivity zones in aquifer
Elevation of groundwater level	Range: 3701-56.6 m AHD Mean: 44.9 m AHD	Based on Calivil Formation potentiometric surface over BHMAR study area for December 2011, interpreted from borehole monitoring data.
Depth to groundwater level from ground surface	Range: <2 – 54 m Mean: 17 m	Based on difference grid between ground surface and interpreted Calivil Formation potentiometric surface over BHMAR study area.
Groundwater salinity (TDS, mg/L)	Range: 246-32753 mg/L Mean: 3125 mg/L	Total dissolved solids (TDS) range and average for groundwater samples from Calivil Formation monitoring bores in BHMAR study area (n=111).
Number of ADWG2011 water quality exceedances	Total dissolved solids TDS >600 mg/L (94/114) Total dissolved solids TDS >1200 mg/L (52/114) pH >8.5 (3/114) Chloride Cl >250 mg/L (56/114) Sodium Na >180 mg/L (68/114) Sulfate SO_4 >250 mg/L (35/114) Iron Fe >0.3 mg/L (39/114) Manganese Mn >0.1 mg/L (91/114) Fluoride F >1.5 mg/L (6/114) Aluminium Al >0.2 mg/L (3/114) Antimony Sb >3 µg/L (3/114) Arsenic As >10 µg/L (7/114) Boron B >4 mg/L (3/114) Molybdenum Mo >50 µg/L (26/114) Nickel Ni > 20 µg/L (3/114) Uranium U >17 µg/L (11/114) Ammonia NH_3 >0.39 mg/L-N (21/114)	Australian Drinking Water Guidelines (ADWG2011) exceedances for 114 groundwater samples from BHMAR01A-1, 01B-1, 03B-2, 04-2, 04-4, 05-2, 06-1, 08-1, 14-1, 15-1, 16-1, 17-1, 17-2, 18-2, 19-1, 21-3, 22-1, 23-2, 33-2, 33-3, 33-4, 33-5, 33-6, 33-7, 33-8, 33-9, 34-1, 34-3, 35-1, 36-1, 41-1, 43-2, 48-1, 51-1, 53-1, 56-1, 58-1, 61-2, 62-1, 63-1, 64-2, 65-1, 66-1, 74-1, 75-1, 75-2, 75-4, 75-5, 75-6, 75-7, 75-8, 77-2, 77-3, 77-4, 77-5, 79A-6, 79A-10, 79A-12, 80A-2, 80A-5, 80A-7, 80B-2, 83-2, 84-2, 88-2, 88-3, 88-4, 88-5, 88-6, 88-7, 92-1 and 99-1.

Note: The NMR data in this figure were collected in 2011 using the Javelin tool with an inter-echo spacing of 2.5 ms. Subsequent laboratory and field tests have demonstrated that this setting underestimates the free and total water content, and derived porosities, and should only be used on a semi-quantitative comparative basis. The NMR data may also be unreliable in zones where there is significant iron-(hematite) coating of quartz grains.

Figure 7-8 shows the interpreted extent and thickness of the Pliocene Sands aquifer that incorporates the coarser-textured sediments of the Calivil Formation and Loxton-Parilla Sands. Minor sandy sediments from the upper Renmark Group and lower Blanchetown Clay have also been included in the semi-confined aquifer but this do not substantially contribute to the overall thickness, as shown when Figure 7-9 is compared with Figure 7-8. An aggregate thickness for the Calivil Formation and the Loxton-Parilla Sands, regardless of texture, are shown in Figure 7-10 and Figure 7-11 respectively.

Stratigraphic thickness of the Calivil Formation (Figure 7-10) shows that the formation is thickest (over 60 m) along the northern palaeochannel from targets GWR11 southwest to GWR1, in GWR4, beneath Lake Menindee, and south from GWR1 through to GWR6. Significant thicknesses (40-45 m) of Calivil Formation have also been interpreted beneath Lake Tandou; however this interpretation is uncertain because of a lack of verification through sonic drilling. The main unit that comprises the semi-confined aquifer also indicates the positions of the palaeochannel belts picked out by the lithology maps.

Aggregate thickness of the semi-confined aquifer is shown in Figure 7-9. This shows that the thickest aquifers (35-45 m) are developed quite locally, in targets GWR1, GWR3 through to GWR6, and with a minor amount in GWR9. Many of these, specifically those in GWR1, GWR3-GWR6 occur above incised palaeovalleys at the base of the Calivil Formation, these incised valleys, with at least 20 m of relief, provide the accommodation space for thick successions to accumulate and provide the ideal environment for the preferential deposition of relatively coarse grained sediments. A wide area of thick aquifer has been interpreted in the southwestern part of the project area. Although 30 m or more in thickness, the few boreholes and the highly electrical conductivity of the stratigraphy makes this interpretation uncertain. These aquifers have been assigned to the Loxton-Parilla Sands and are also mapped separately in Figure 7-11.

The textural composition of these units (as determined from borehole data) is shown in Figure 7-12, Figure 7-26 and Figure 7-13. The aquifer has been characterised in a series of maps derived from the AEM that includes the indicative lithology based on sediment textural classification for a number of representative depths slices (Figure 7-14 *t*o Figure 7-16). Indicative lithology based on sediment textural classification for the 36.7-43.5 m depth slice (Figure 7-14) shows a system of anabranching palaeochannel belts throughout the project area. The palaeochannel belts are typically 8 km in width and defined by bodies of medium sand. The main palaeochannel belt is interpreted as having entered the project area from the northeast, near target GWR9, then bifurcated, one channel belt diverted westward, flowing around a Paleozoic bedrock high forming targets GWR11 and GWR10, then flowed southwest forming target GWR4. The second palaeochannel belt flowed southwest into target GWR12 and then bifurcated again, the southern branch forming target GWR13. These two palaeochannel belts rejoined to form GWR14 and then flowed southwest into GWR4, where it was rejoined by the northern palaeochannel belt. The re-formed single palaeochannel belt flowed west for about 10 km. The palaeochannel belt then headed south, through targets GWR3, GWR6, GWR7 and GWR8, where it then left the project area in a south-easterly direction. A poorly defined sinuous palaeochannel belt, composed most of muddy sands, with minor medium sand, may have flowed into the project area west of Lake Cawndilla and the main channel in GWR1. A belt of muddy sands from northwest of Lake Menindee trends southeast into GWR1 and may present yet another palaeochannel. Loxton-Parilla Sands are present in the southern part of the project area and target GWR8 occurs entirely within them.

The 43.5-51.5 m depth slice (Figure 7-15) shows a system of anabranching palaeochannel belts through the project area. The palaeochannel belts are typically 8 km in width and defined by bodies of medium sand and interbedded sand mud. The main palaeochannel belt is interpreted as entering the project area from the northeast, near target GWR9, it then bifurcated, one channel belt diverted westward, flowed round a Paleozoic bedrock high forming targets GWR11 and 10, then flowed southwest forming target GWR4. A small muddy sand palaeochannel belt is present in the northern part of the north-eastern corner, it also divides in two with a southern channel belt flowing south and joining the main southern channel belt, the northern branch flowing southwest into GWR11. The architecture of the main palaeochannel belts are otherwise similar to that seen in the 36.7-43.5 depth slice. Three noteworthy differences are the generally smaller amount of medium sand: a broad apron of interbedded sand and mud along the northern and western boundary of the project area that reaches the northern palaeochannel belt, this is interpreted as being distal coalesced fan deposits from the Barrier Ranges: and the first appearance of the Renmark Group, along the northern side of the north-eastern part of the project area.

The next two depth slices are composed of a mix of Renmark Group and Calivil Formation lithologies. The 51.5-61 m depth slice (Figure 7-16) shows that the Calivil Formation is beginning to be constrained at this depth to valleys, either broad valley systems in targets GWR5, GWR10 and GWR11, or more incised valleys in targets GWR1, GWR3, GWR4, GWR5, and GWR6. In target GWR7 the Calivil Formation consists of a relatively narrow channel through the Loxton Parilla Sands before leaving the project area to the southeast. The Calivil Formation is largely absent from the 61.0-72.3 m depth slice (Figure 7-3) except in GWR1, GWR3, GWR4, GWR5 and GWR6. In these targets it is limited to incised valleys.

Aquifer transmissivity has been calculated for the semi-confined aquifer using a combination of estimated hydraulic conductivity and thickness (see Lawrie *et al*., 2012a for further details). Rather than selecting a single representative hydraulic conductivity value, a lower (1st quartile) and upper (3rd quartile) estimate were used (based on physical measurements). These transmissivity estimates are shown in Figure 7-17 and Figure 7-18 respectively. Transmissivity is influenced by the aquifer thickness as well as textural composition. For example transmissivity may be very low in one location due to thinning of the aquifer, despite being composed of material of relatively high hydraulic conductivity, and in another be due to the low hydraulic conductivity of the overall sediments (i.e. interbedded mud and fine sand). Conversely, a very thick unit with only moderate hydraulic conductivity might have high transmissivity.

The low estimation resulted in the Calivil Formation palaeochannels sequences generally having low to intermediate transmissivities, with the very low to low transmissivities in the Loxton-Parilla sands (Figure 7-17). The high estimation changed these typical ranges to both intermediate to high (Figure 7-18). The mapping is useful in identifying areas with relatively higher transmissivities in the target Pliocene aquifer. This is generally the case for all of the GWR targets, in particular GWR1, GWR4, GWR6 and GWR8 and less so for GWR2, GWR5 and GWR14. The semi-confined aquifer, including this mapping, is described in greater detail at a groundwater resource target level in Lawrie *et al*. (2012d).

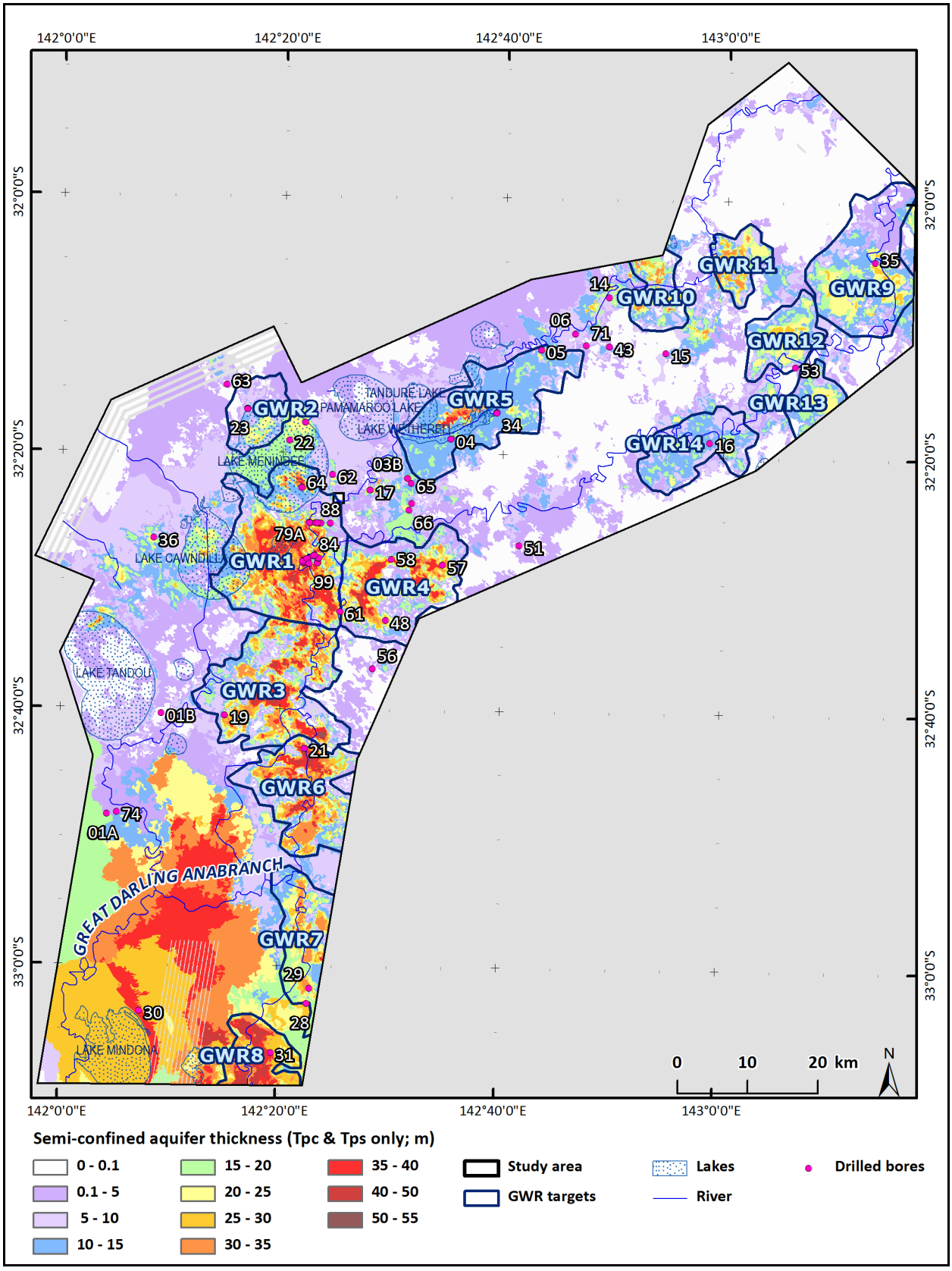

Figure 7-8. *Interpreted extent and thickness of semi-confined aquifer consisting of the Calivil Formation and Loxton-Parilla Sands only. White areas within the study extent indicate where the aquifer is absent.*

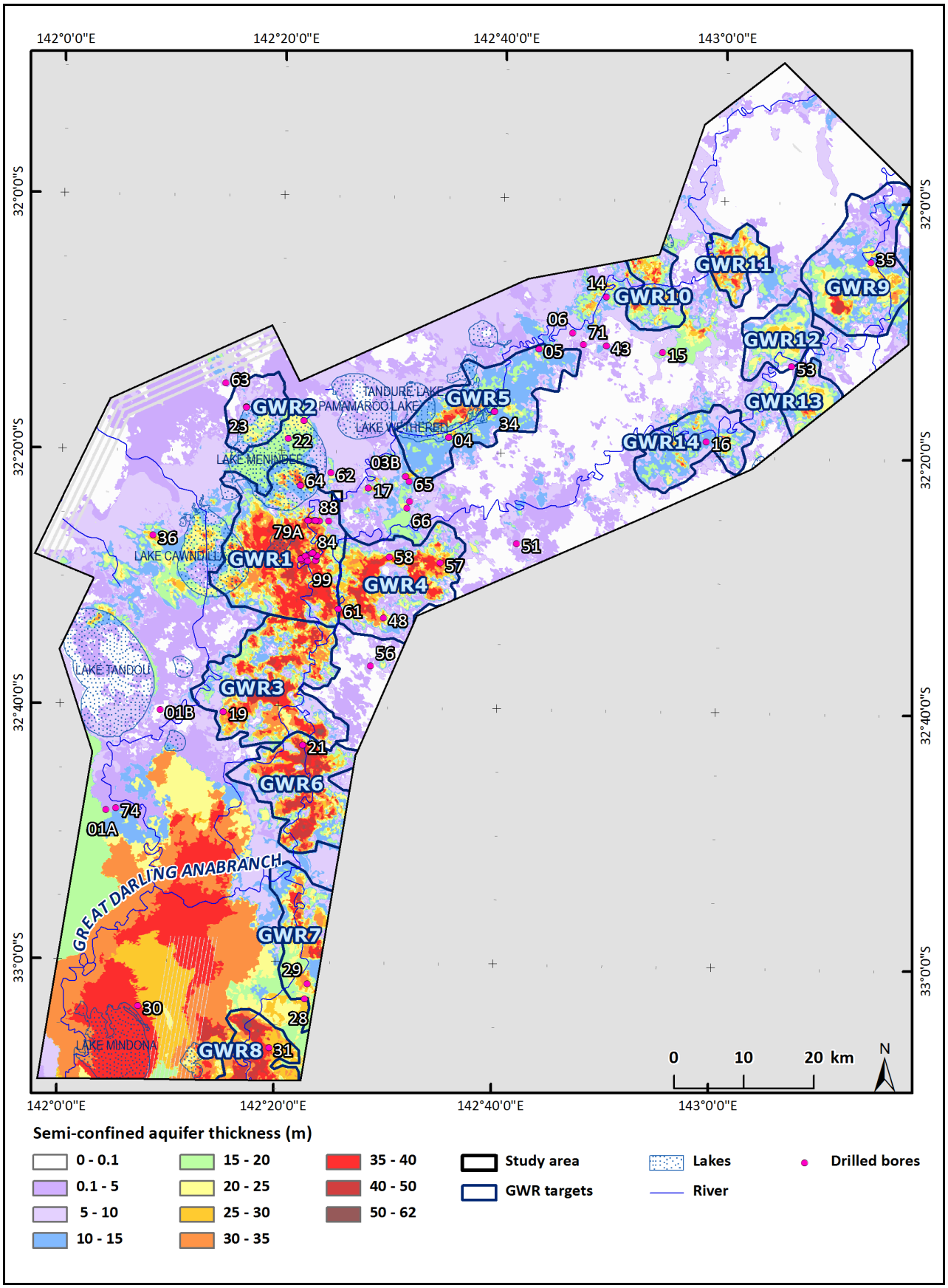

Figure 7-9. *Interpreted extent and thickness of semi-confined aquifer including sandy sediments of the Calivil Formation, Loxton-Parilla Sands, upper Renmark Group and lower Blanchetown Clay. White areas within the study extent indicate where the aquifer is absent.*

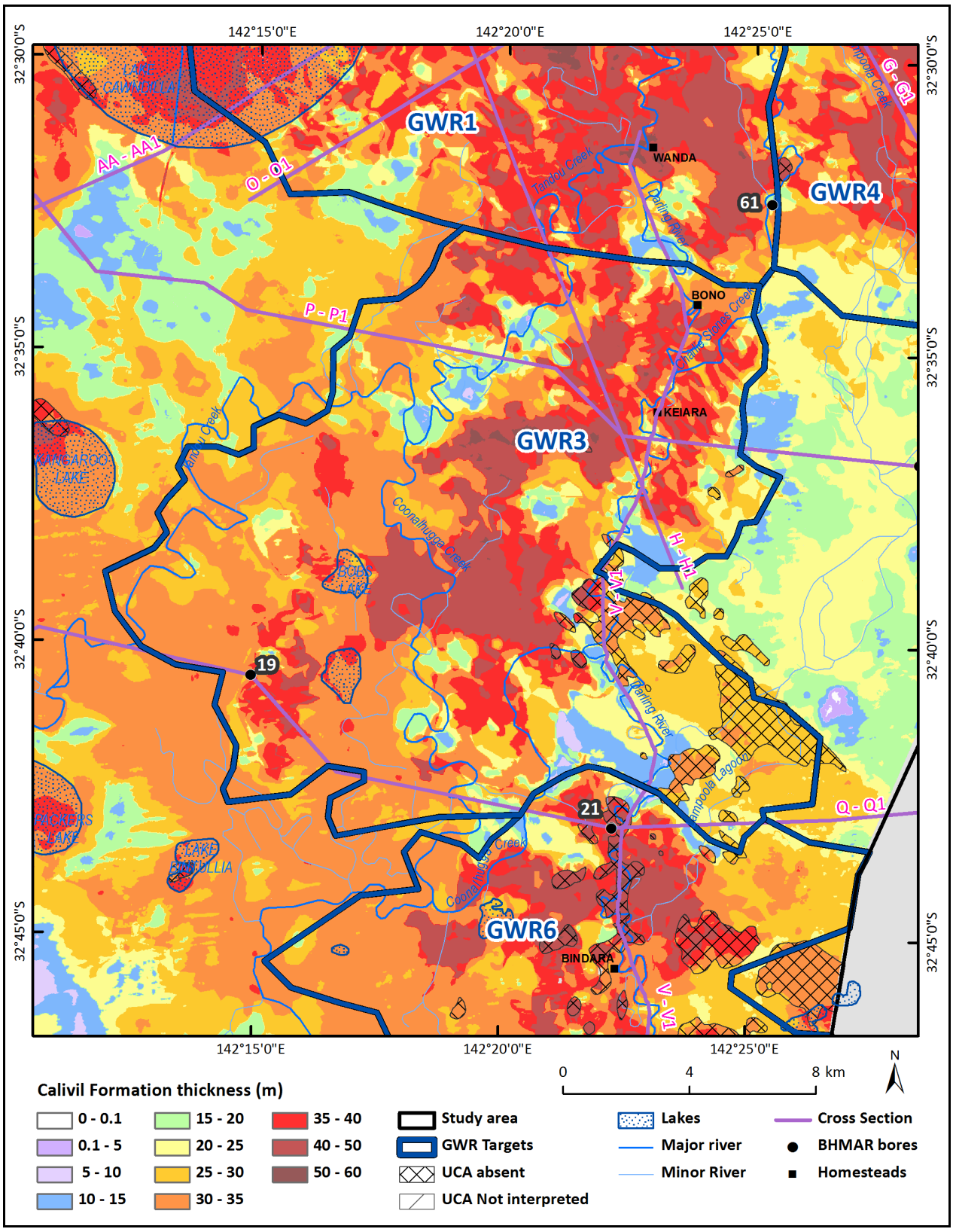

Figure 7-10. *Interpreted thickness of the Calivil Formation in the central part of the BHMAR study area.*

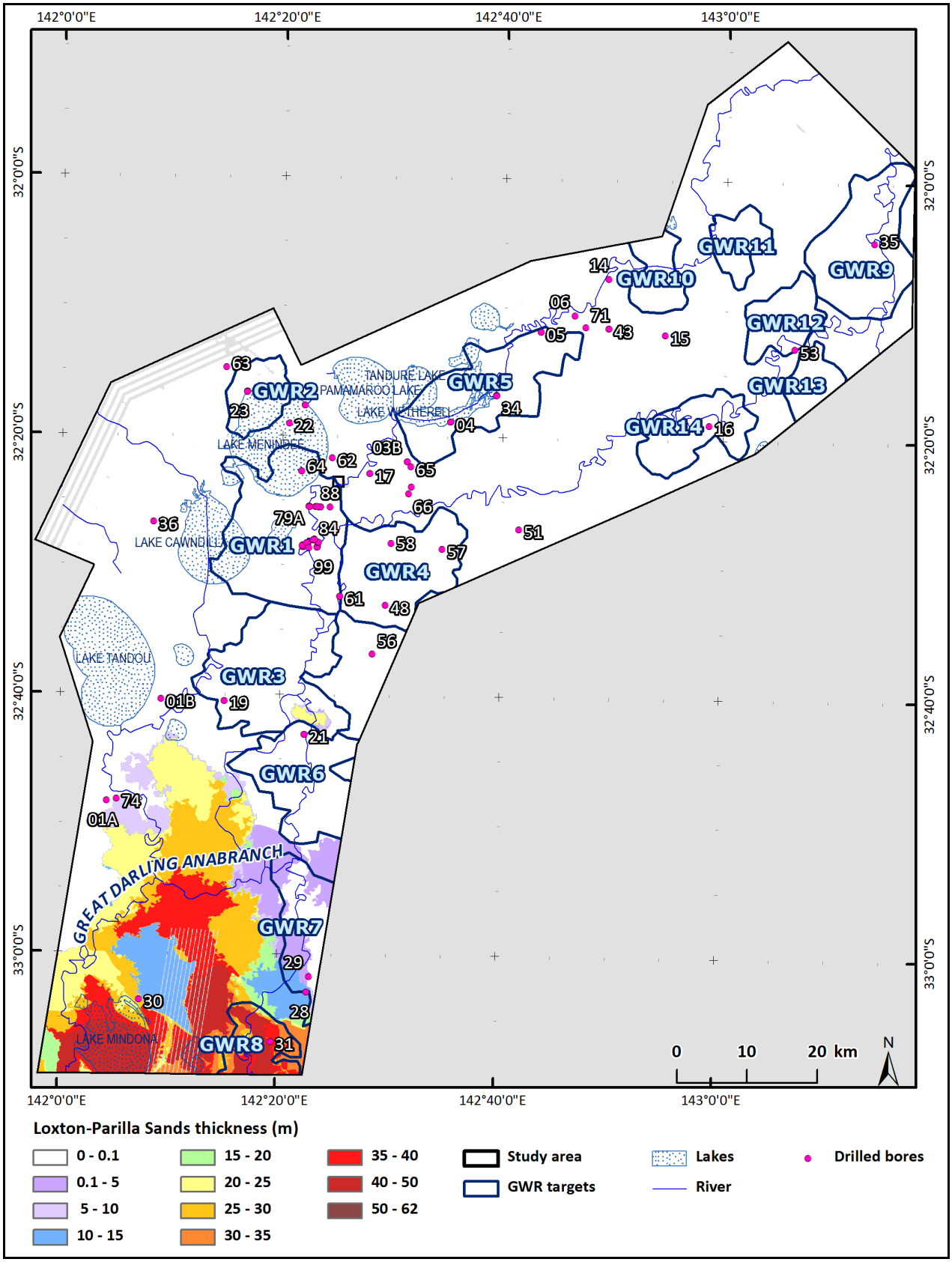

Figure 7-11. *Interpreted thickness of Loxton-Parilla Sands.*

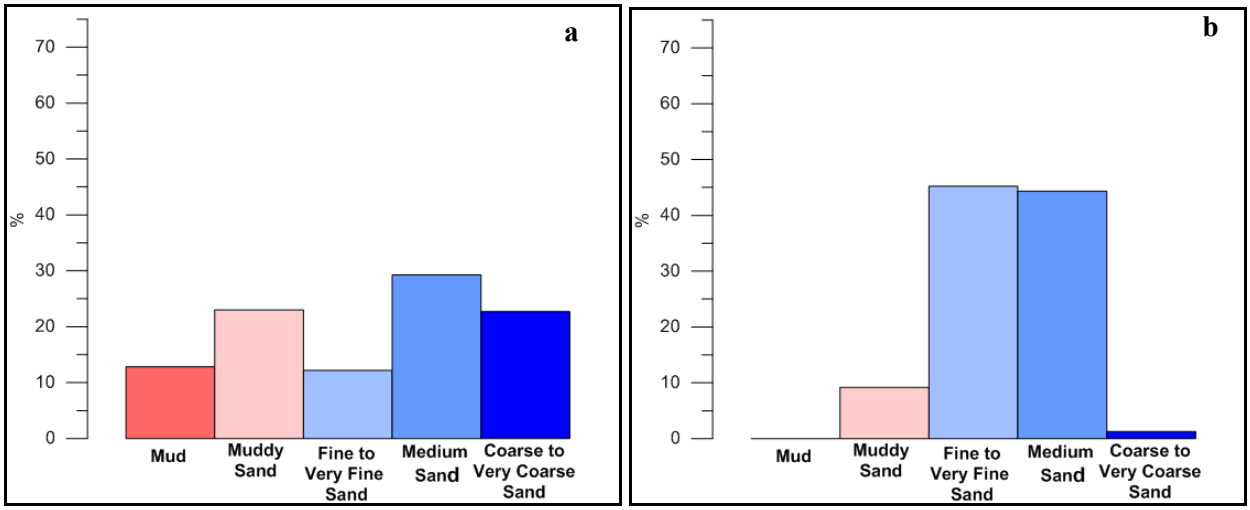

Figure 7-12. *Textural composition of a) Calivil Formation and b) Loxton-Parilla Sands.*

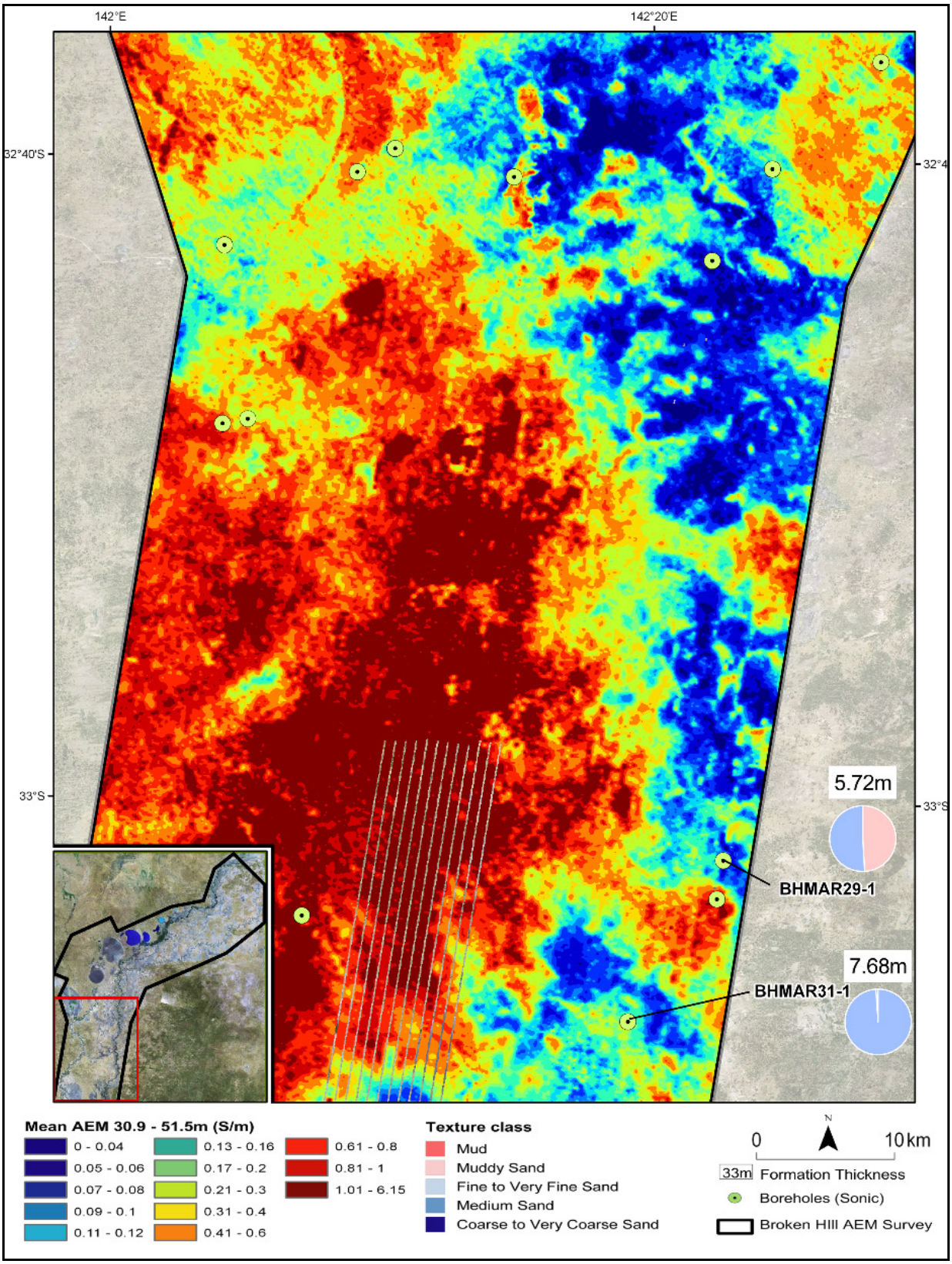

Figure 7-13. *Pie charts showing the textural composition of Loxton-Parilla Sands only encountered at two bores in the southern area. Overall thicknesses of the Formation are labelled.*

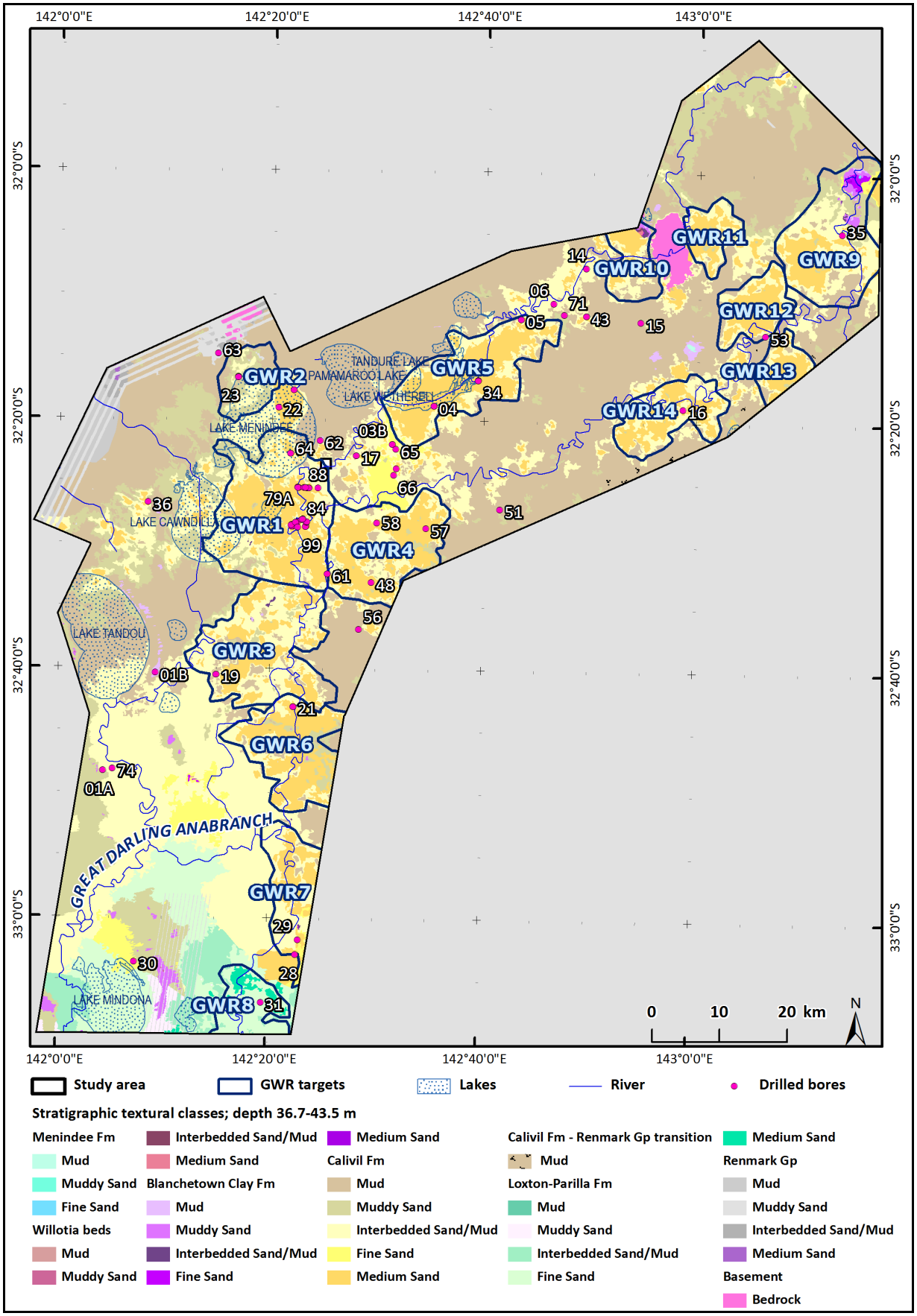

Figure 7-14. *Indicative lithology of semi-confined aquifer across the project area, based on sediment textural classification, illustrating the 36.7-43.5 m AEM depth slice.*

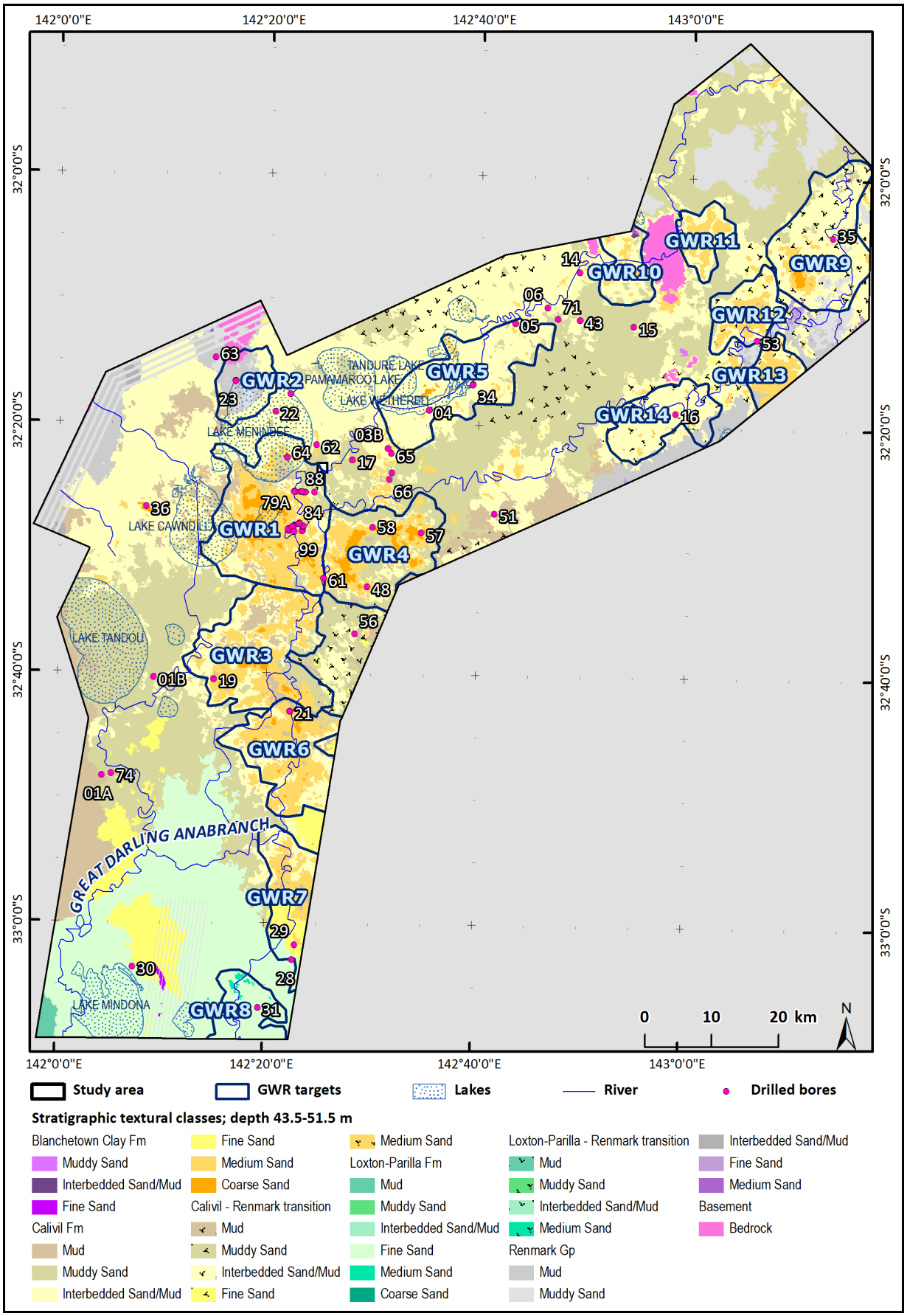

Figure 7-15. *Indicative lithology of semi-confined aquifer across the project area, based on sediment textural classification, illustrating the 43.5-51.5 m AEM depth slice. Note that the first signs of the Renmark Group lithologies also appear in this slice, on the southern side of the north-eastern part of the project area.*

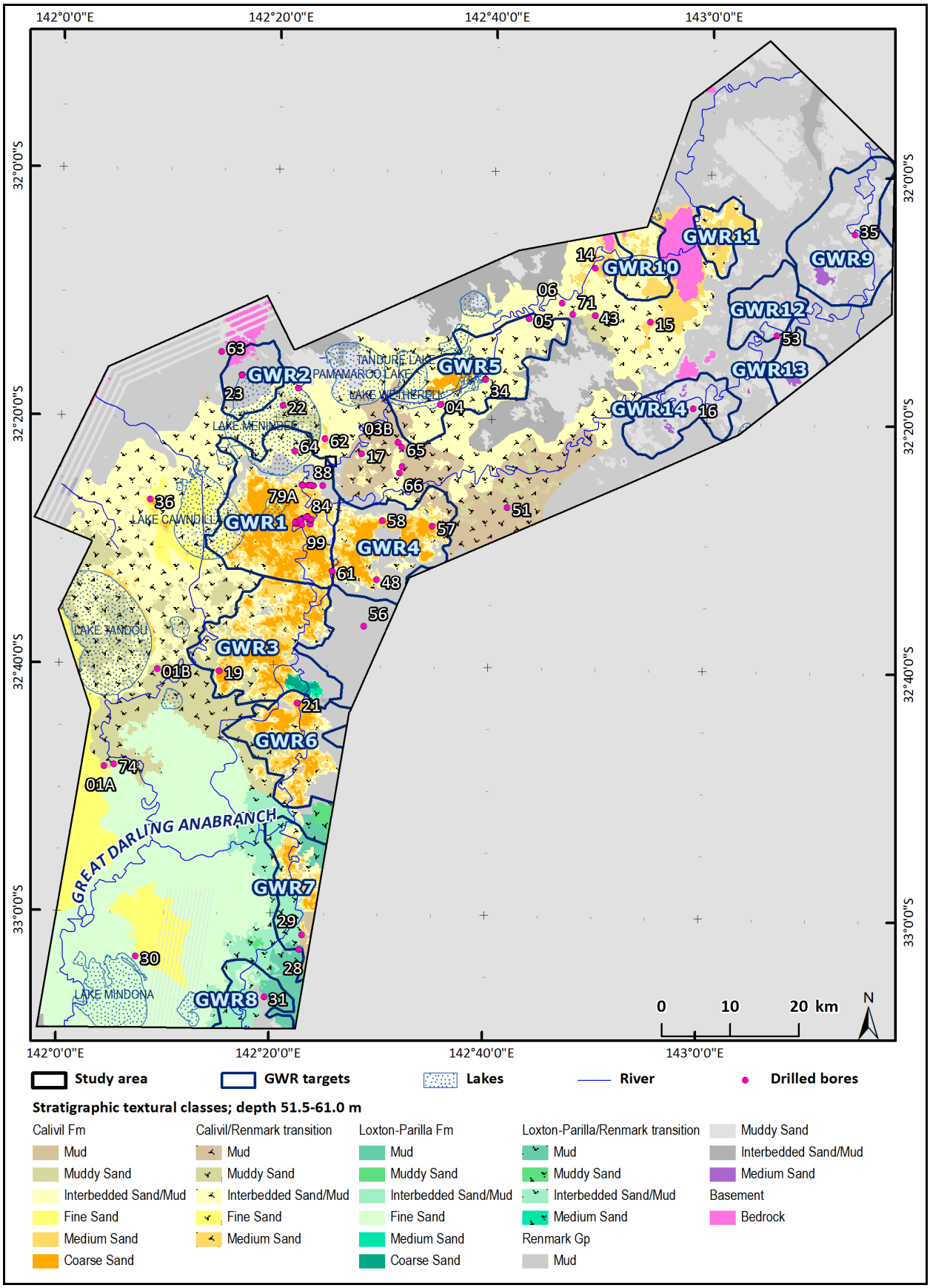

Figure 7-16. *Indicative lithology of semi-confined aquifer and the lower aquitard (Renmark Group) across the project area, based on sediment textural classification, illustrating the 51.5-61.0 m AEM depth slice.*

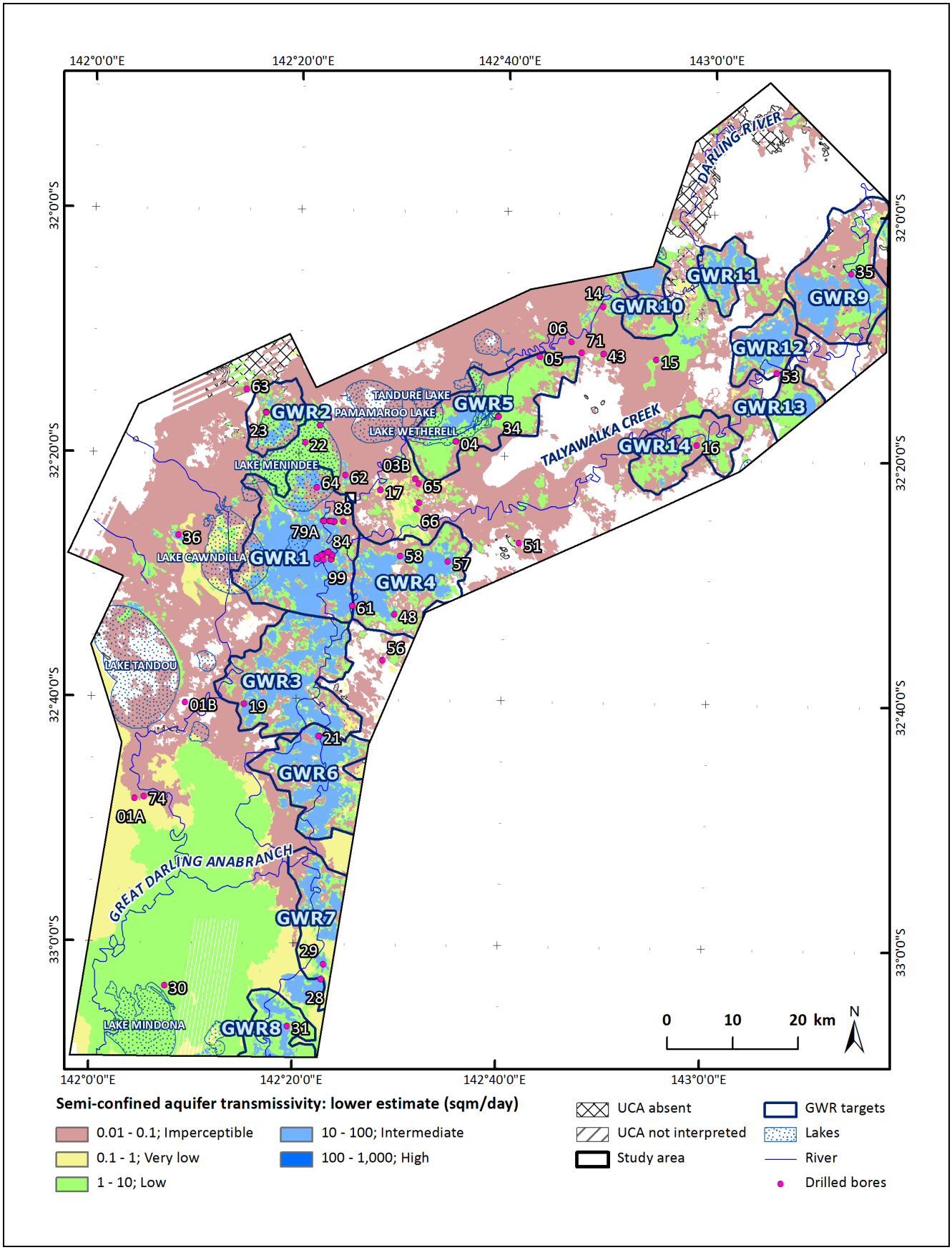

Figure 7-17. *Lower estimate of transmissivity of the semi-confined aquifer. White areas within the study extent indicate where the aquifer is absent.*

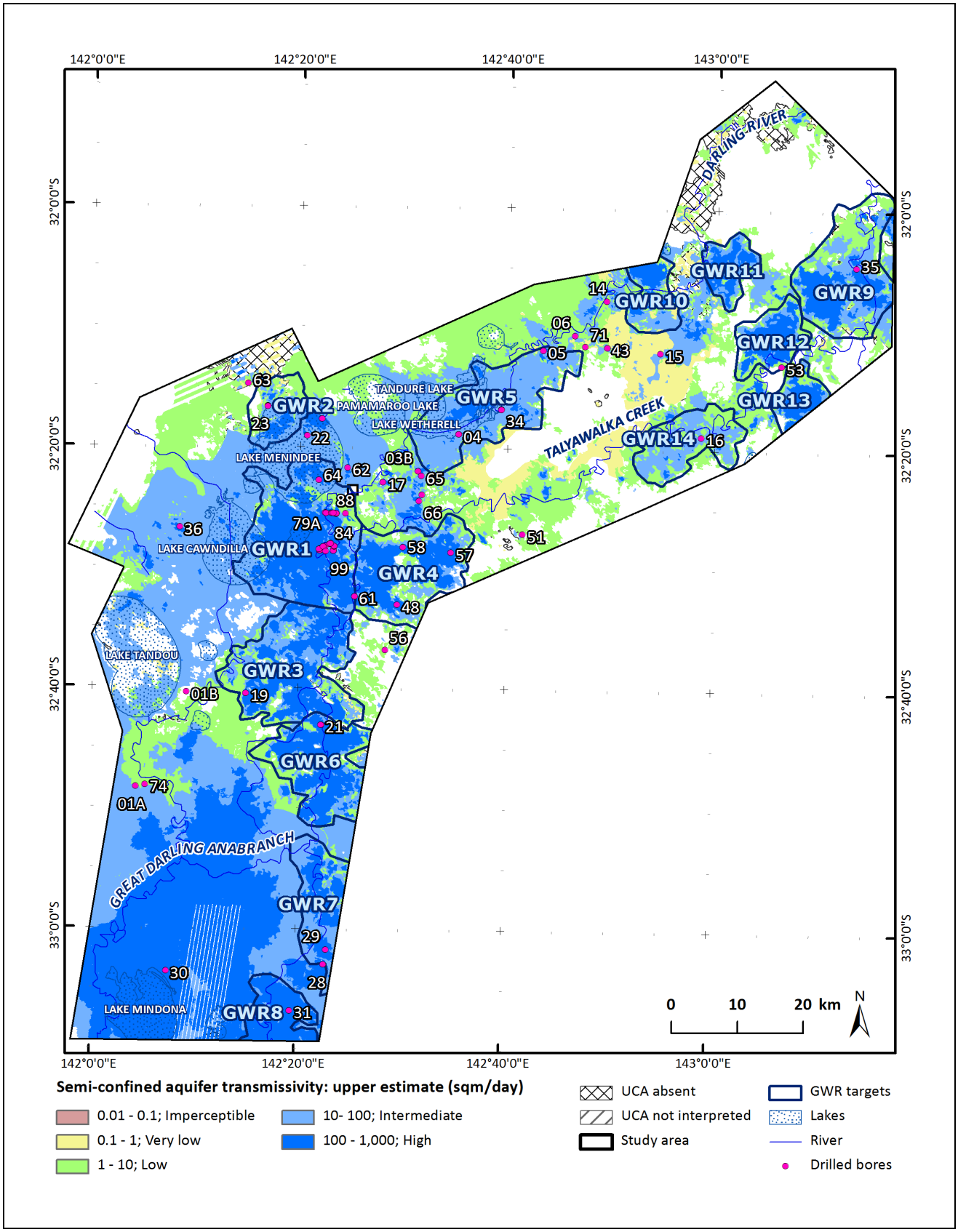

Figure 7-18. *Upper estimate of transmissivity of the semi-confined aquifer. White areas within the study extent indicate where the aquifer is absent.*

The typical lithologies of the Calivil Formation are based on descriptive logging of the sonic core. This shows a strong contrast with the shallow Quaternary sediments, with over half of the drilled intervals being medium, coarse to very coarse sands. Muddy sands and muds make up about a third of the drilled intervals into the Calivil Formation. The underlying Renmark Group mud and muddy sand tend to form a basal aquitard, but the Calivil Formation can sometimes be in hydraulic connection with the Renmark Group sands. The coarser grained lithologies in the Calivil Formation are also reflected in the estimates of hydraulic conductivity, with the average from slug tests (15 m/d) being consistent with the average from the NMR logging (13 m/d). Coupled with the reasonable aquifer thicknesses, the average aquifer transmissivity from these two methods (200 and 370 m^2/d respectively) is considered high (Krasny, 1993). Transmissivity estimates of 300 and 930 m^2/d were estimated from the two pumping tests undertaken at the Jimargil site (Lawrie *et al.,* 2012c).

Figure 7-4a and Figure 7-4b respectively show the relative distribution of hydraulic conductivity and transmissivity values derived by slug tests for the various screened aquifer formations. The slug test transmissivities in particular confirm that the Loxton-Parilla Sands (Tps) and Calivil Formation (Tpc) are the best aquifer targets in terms of hydraulic properties, with median transmissivities in the high range (217 and 115 m^2/d respectively). However, the box and whiskers for the Calivil Formation reflects its internal lithological variability, when compared with the relatively homogeneous marine Loxton-Parilla Sands. Figure 7-5 and Figure 7-6 are box and whisker plots for various hydraulic parameters derived from the NMR logging. Like the slug test data, the Calivil Formation (Tpc) and Loxton-Parilla Sands (Tps) have the better hydraulic conductivity based on the NMR data, compared with the overlying Quaternary aquifers and the underlying Renmark Group. The NMR-derived transmissivities of these formations would be considered to be intermediate to high (Krasny, 1993).

7.2.2 Groundwater Flow and Dynamics

Regional mapping by Brodie (1994) and Kellett (1994) of the shallow watertable and the potentiometric surface for the Pliocene Sands aquifer was updated for the study area, largely based on the sonic drilling program and the project monitoring bores (Lawrie *et al*., 2012a; Appendix 5, Apps *et al*., 2012b). In the absence of project data, these water level contours were based on the historic mapping (Brodie 1994, Kellett, 1994) supported by any historical groundwater level measurements recorded in State agency databases. Due to the large spacing between monitoring bores, these groundwater level contours are speculative in nature.

The potentiometric surface interpreted for the semi-confined aquifer is mapped in Figure 7-19, and shows a mounding effect associated with surface water leakage. This would suggest that the aquifer is influenced by recharge from, and is in part hydraulically connected with, the rivers and lake storages, Lake Wetherell and Lake Menindee in particular. The influence of leakage from the Darling River is particularly evident south of Menindee. The mounding disrupts the flow towards the regional discharge zone 150 km to the southwest, along the South Australian reach of the River Murray. The mounding results in a regional gradient defined by a potentiometric surface elevation of ~57 m AHD near Lake Menindee to ~37 m AHD in the southwest corner of the study area. The regional hydraulic gradient in the semi-confined aquifer is relatively low, in the order of 0.35-0.5 m/km. The average potentiometric surface elevation in the Calivil Formation is ~45 m AHD. The depth to the potentiometric surface from the ground surface is also variable, from <2 m to >50 m, the latter associated with unconfined conditions away from the effects of river or lake leakage. The average depth to the potentiometric surface is ~17 m.

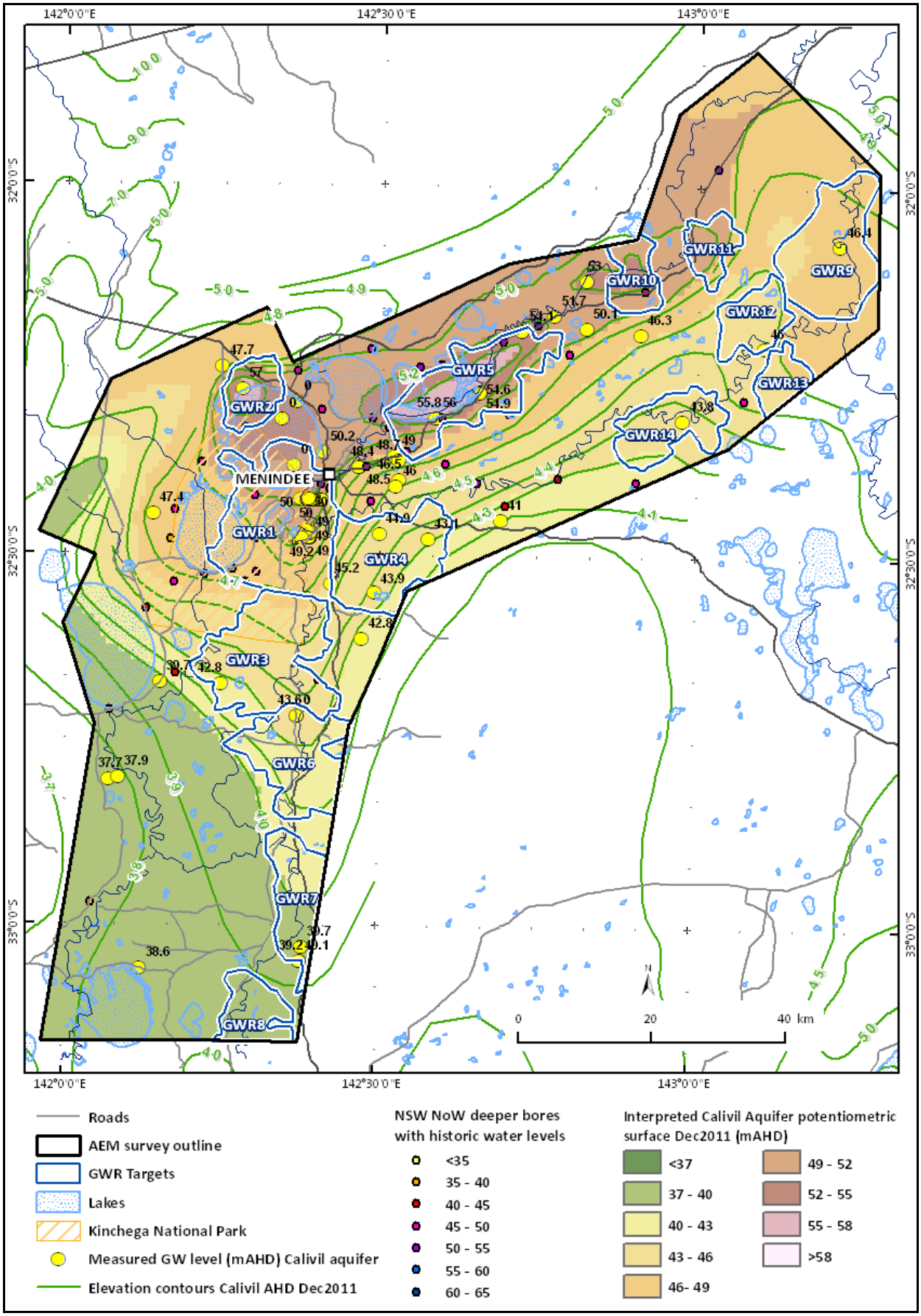

Figure 7-19. *Interpreted elevation (m AHD) of the semi-confined aquifer potentiometric surface in the BHMAR study area for December 2011. In the absence of groundwater level measurements from BHMAR project bores, historical data from NSW Office of Water (NOW) and previous hydrogeological mapping (Brodie, 1994; Kellett, 1994) were used.*

Groundwater level monitoring in the semi-confined aquifer was undertaken in 19 bores distributed along the Darling River floodplain corridor. For hydrographic data refer to Appendix 6 (Somerville *et al.*, 2012). During the 2010/11 flood event, the change in groundwater level in these bores ranged from 0.03 m to 1.40 m. The larger responses (>1 m) adjacent to the Darling River were at three sites - at BHMAR04-2 at Lake Wetherell, BHMAR17-1 and 17-2 near Menindee township and BHMAR33-8 at the Jimargil target.

Figure 7-20 plots the hydrographs of three Calivil Formation monitoring bores within 200 m of the river at East Bootingee. These show an increase in groundwater levels after the onset of high flows in October 2010. Like the shallow aquifer, groundwater response occurs prior to the onset of overbank flow. In these bores, the groundwater levels fluctuate with river levels until about May 2011. From this time, the river level began to recede but the groundwater level in these Calivil Formation bores either stabilised or continued to rise.

This maintenance or continual rise in Calivil Formation groundwater levels after the flood peak had passed suggests recharge to the deeper aquifer. If transient hydraulic loading caused by increased overlying surface and shallow groundwater storage is the dominant mechanism for the groundwater level response, then the Calivil Formation hydrograph should mirror that of the river stage or the shallow watertable. In contrast to the Calivil Formation response, the shallow watertable in the Coonambidgal Formation shows a rapid decline coincident with flow recession (Figure 7-52).

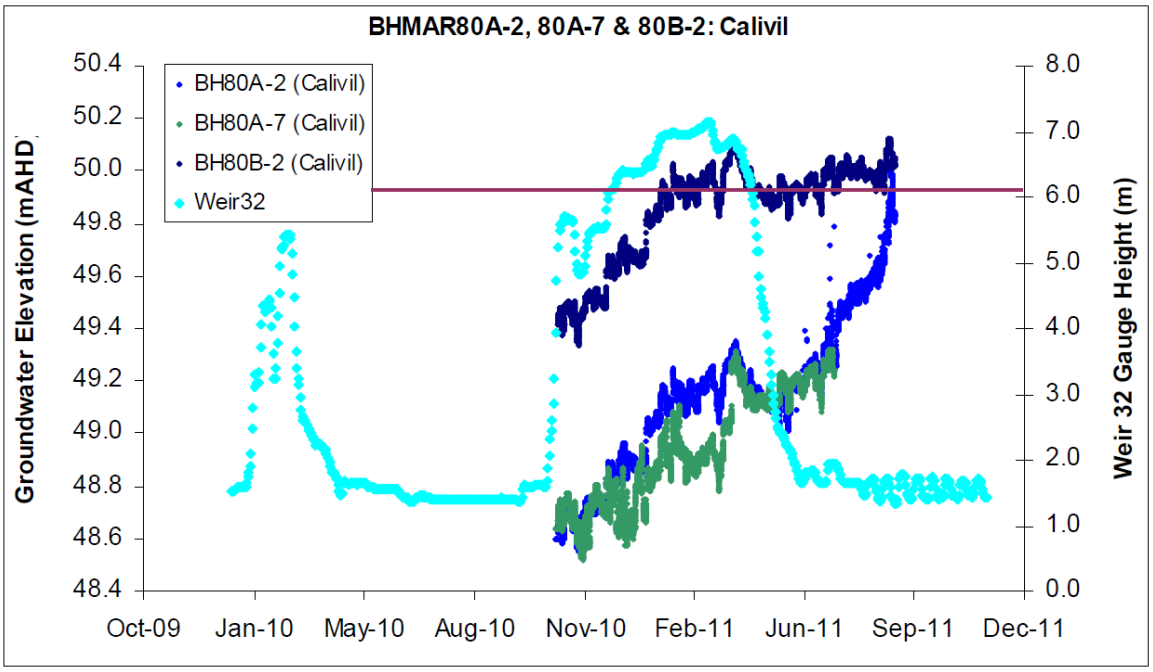

Figure 7-20. *Hydrographs for bores BHMAR80A-2, BHMAR80A-7 and BHMAR80B-2 screened in the Calivil Formation aquifer at East Bootingee. The light blue points are the Darling River stage height measurements at the Weir 32 gauge. The purple line is the Weir 32 gauge height at which overbank flow occurs.*

Groundwater level monitoring in the Calivil Formation at the northwest margin of Lake Menindee, show a monotonic 4.0 m rise from the onset of refilling of the lake (Figure 7-21). Despite the fluctuating lake levels due to water releases, the groundwater level rose continuously from the start of monitoring.

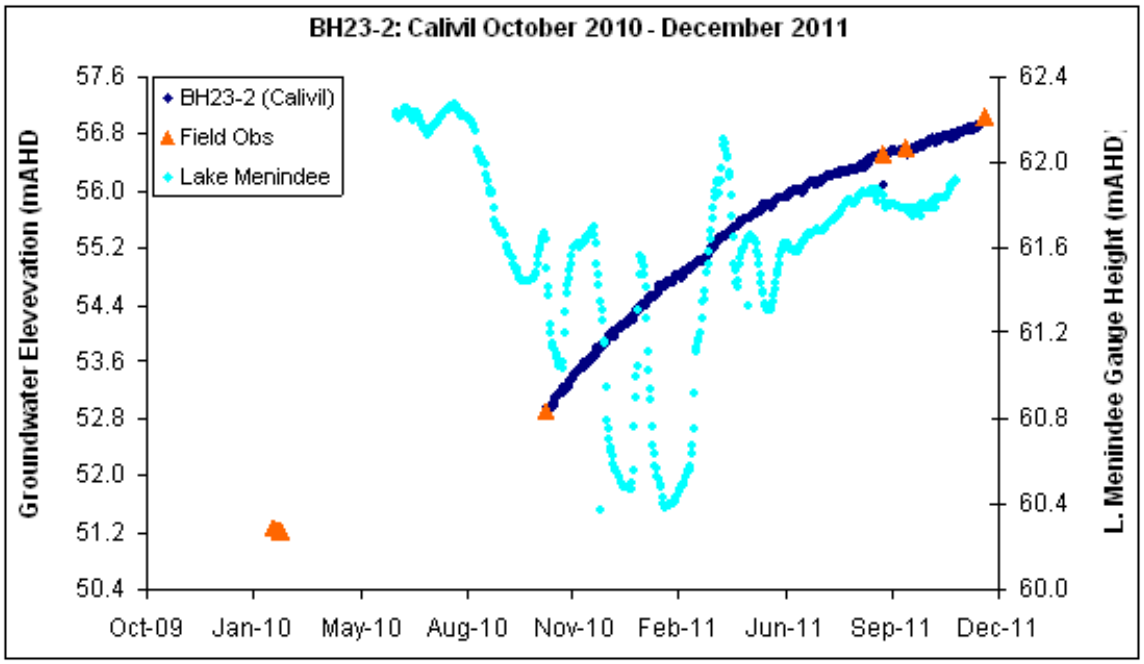

Figure 7-21. *Hydrograph of BHMAR23-2 screened in Calivil Formation aquifer and located on northwest margin of Lake Menindee. The light blue points are the stage elevation measurements for the Lake Menindee gauge. The orange triangles are manual measurements of groundwater levels in the monitoring bore as a comparison with the logger data.*

7.2.3 Groundwater Quality

Salinity is a critical water quality parameter defining the suitability of extracted groundwater to proposed uses, such as municipal, irrigation or stock and domestic. Equally, salinity is important from a MAR perspective because zones of fresh groundwater are targeted for their potential for high MAR recovery efficiencies. Hence, salinity is a fundamental dataset for identifying targets for both groundwater extraction and MAR options (Lawrie *et al*., 2012c, d).

A prominent feature of the AEM depth slices (Appendix 4, Apps *et al.,* 2012c) is the mapping of low-conductivity zones along the river corridor. The integration of pore fluid salinity (Appendix 6, Somerville *et al.,* 2012) and nuclear magnetic resonance (NMR) data (Appendix 3, Apps *et al.,* 2012f) was used to develop indicative groundwater salinity mapping on an AEM depth slice basis (Lawrie *et al.,* 2012a). Figure 7-22 is an example of this groundwater salinity mapping for a particular depth slice in the target semi-confined aquifer, showing the predicted distribution of fresh (<600 mg/L), acceptable (600-1,200 mg/L) and brackish (1,200-3,000 mg/L) groundwater. The depth slice interpretations of groundwater salinity in the semi-confined aquifer were combined to provide a perspective of the key areas with fresh groundwater resources across the study area. The approach taken is documented in Lawrie *et al.* (2012a). As indicated in Figure 7-23, this enabled the identification of 14 regional target areas (GWR1-14). The boundaries marked are the maximum spatial extent of the aquifer with predicted salinities <3000 mg/L. The regional groundwater resource targets are described in detail in Lawrie *et al.* (2012d). Targets were also identified at the borefield scale, particularly within the GWR1 resource located near Menindee. These borefield targets are described in detail in Lawrie *et al*. (2012c). The distribution of fresh groundwater resource targets largely along the Darling River and Talyawalka Creek floodplains provide compelling evidence for the fundamental importance of surface water leakage to groundwater recharge. There are also indications of groundwater freshening due to leakage from the MLS, specifically Lakes Wetherell and Menindee.

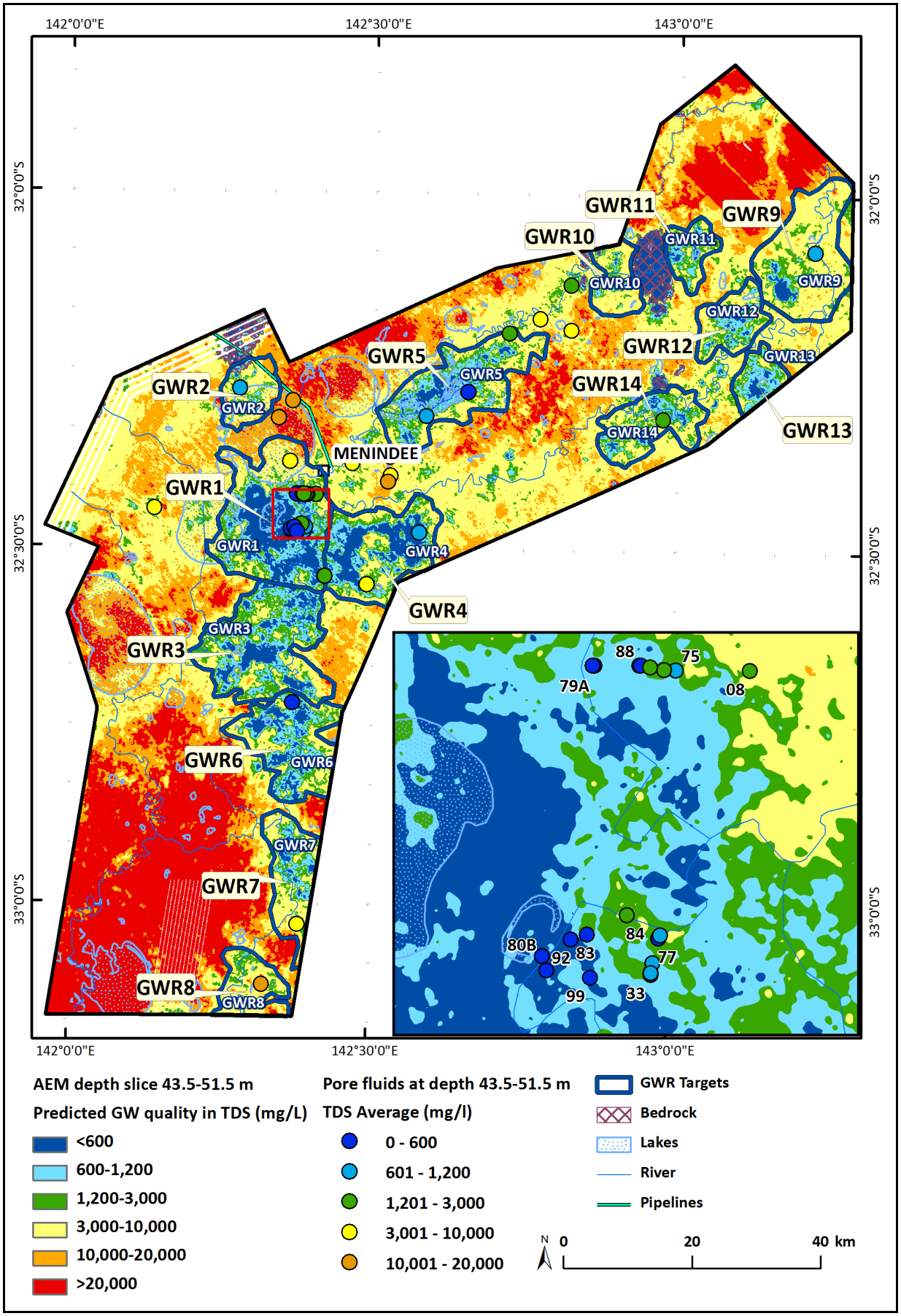

Figure 7-22. *Predicted groundwater salinity in the Pliocene aquifer (AEM CDI 43.5- 51.5 m).*

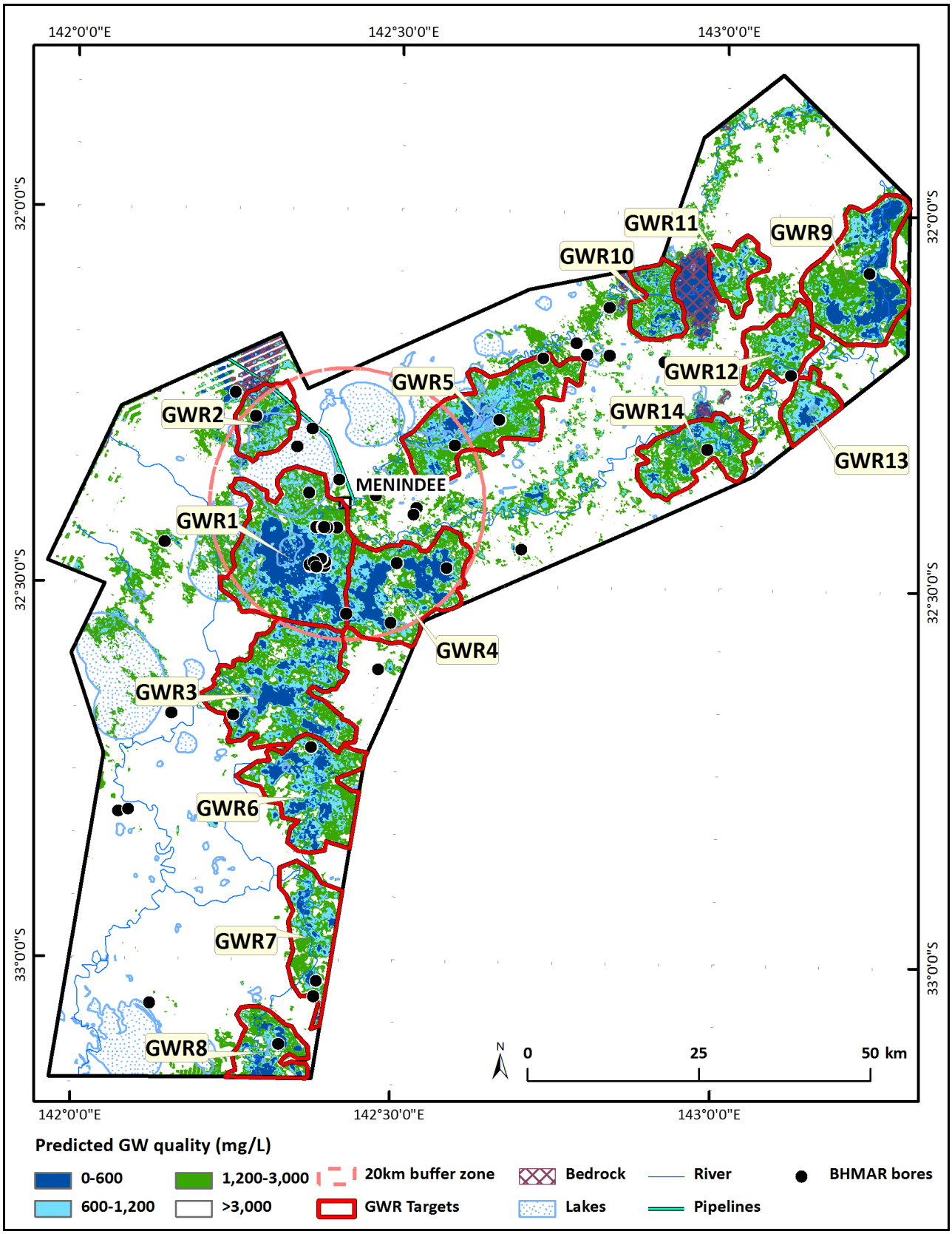

Figure 7-23. *Map of the BHMAR project area showing the distribution of groundwater resource targets (GWR1-14) in the Pliocene (Calivil and Loxton-Parilla Sand Formation) aquifers. The boundaries marked are the maximum spatial extent of the aquifer with predicted salinities <3000 mg/L.*

Sampling from monitoring bores in the Calivil Formation highlights the huge variability in groundwater salinity, ranging from fresh good quality (~250 mg/L) to near seawater concentrations (~33,000 mg/L). Due to the presence of saline groundwater, there can be ADWG2011 exceedances relating to chloride, sodium and sulfate. Elevated manganese is a common water quality issue, as well as iron to a lesser extent. Incidences of ADWG2011 exceedances relating to arsenic, molybdenum, uranium and ammonia in particular, probably reflect redox processes within the aquifer. There are also some occurrences of elevated fluoride, aluminium, antimony, boron and nickel. More detailed water quality assessments have been undertaken for the Calivil Formation aquifer at the target scale (Lawrie *et al*., 2012d) and the potential borefield scale (Lawrie *et al.,* 2012c).

7.3 UPPER CONFINING AQUITARD

7.3.1 Hydrogeology

The Blanchetown Clay forms an upper confining aquitard for underlying aquifers found in the Calivil Formation and the Loxton-Parilla Sands. The Calivil Formation can contain an upper sequence of muddy sands and muds, which can contribute to the thickness and efficacy of this aquitard. Hence, these finer grained sediments can impede vertical leakage between the unconfined aquifer hosted in the Quaternary fluvial sequences and the deeper Pliocene aquifer hosted in the Calivil Formation and Loxton-Parilla Sands. Figure 7-24 shows the textural composition of the Blanchetown Clay and Calivil Formation and Figure 7-25 and Figure 7-26 show this spatial distribution of different textural compositions from borehole data. Sandy sediments within the upper Blanchetown Clay (<18 m) have been allocated to the shallow unconfined aquifer while sandy sediments towards the base of the Blanchetown Clay (>18 m) have been allocated to the semi-confined aquifer that largely consists of the Calivil Formation and Loxton-Parilla Sands. The approach taken to derive these plots is discussed in more detail in Lawrie *et al*. (2012a).

The AEM depth slice interpretations of stratigraphy and lithology relevant to the upper confining aquitard range from depths of about 18 m (Figure 7-27) to about 37 m (Figure 7-30). The Blanchetown Clay does occur at shallower depths, particularly in isolated structural highs (Figure 7-44). Blanchetown Clay muds are a common feature across the study area at a depth of about 18 m (Figure 7-27). However, Menindee Formation sediments can occur at this depth along the southern reach of Talyawalka Creek continuing downstream into the Darling River. There can also be localised extents of upper Calivil Formation muddy and fine sands, notably within GWR2 near Lake Menindee, GWR5 at Lake Wetherell, GWR10 further upstream on the Darling River, GWR9 on Talyawalka Creek. Similar situations occur in the targets downstream of Menindee, notably GWR3, GWR6 and GWR8 (the latter associated with Loxton-Parilla Sands). These windows in the Blanchetown Clay become more obvious with depth (Figure 7-28) and partly explain the existence of fresher groundwater in these target areas. The Blanchetown Clay also transitions into upper Calivil Formation muds with depth. By a depth of about 31 m, the Blanchetown Clay is largely absent across the study area (Figure 7-30).

These depth slice interpretations have been integrated to derive a thickness map for the upper confining aquitard as shown in Figure 7-31. This map not only shows the thickness of the unit, but also various interpreted structural features, and the holes where the aquitard is either very thin or absent. The map shows that overall the upper confining aquitard has been mapped as being 8-10 m thick. It is thickest in a small area between Lakes Cawndilla and Tandou where it can exceed 20 m in thickness. The widely scattered holes in the upper aquitard correspond with areas of strong structural activity.

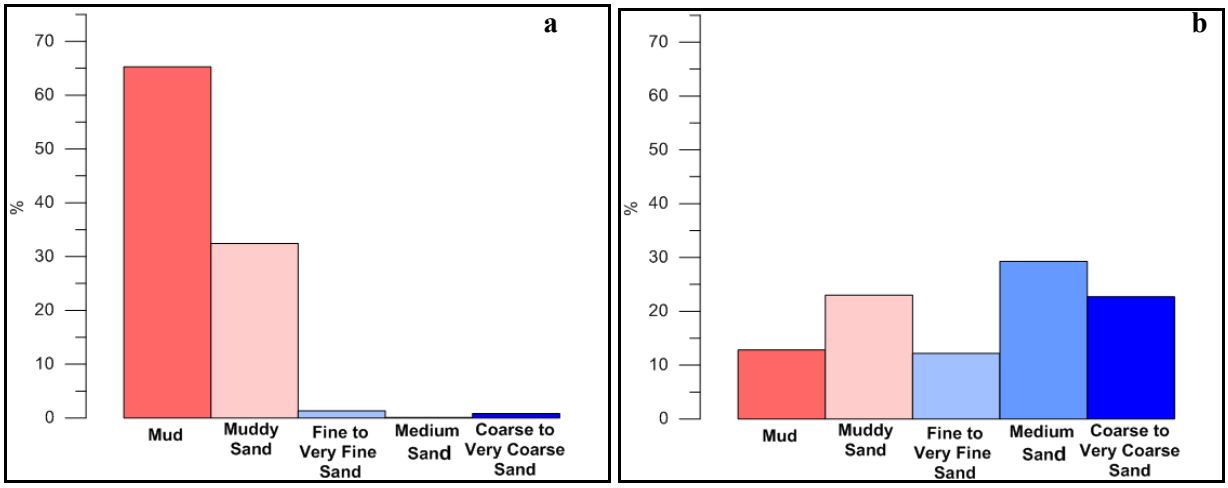

Figure 7-24. *Textural composition of a) Blanchetown Clay and b) Calivil Formation.*

Figure 7-4 to Figure 7-6 are box and whisker plots for various hydraulic parameters derived from the slug tests and the NMR logging. Being a regional aquitard, there are no monitoring bores screened in the Blanchetown Clay, reflected in the absence of slug test interpretations. However, the Blanchetown Clay (Qpc) consistently has the lowest NMR-derived hydraulic conductivities, reflecting its capacity as a regional aquitard (Figure 7-5 and Figure 7-6).

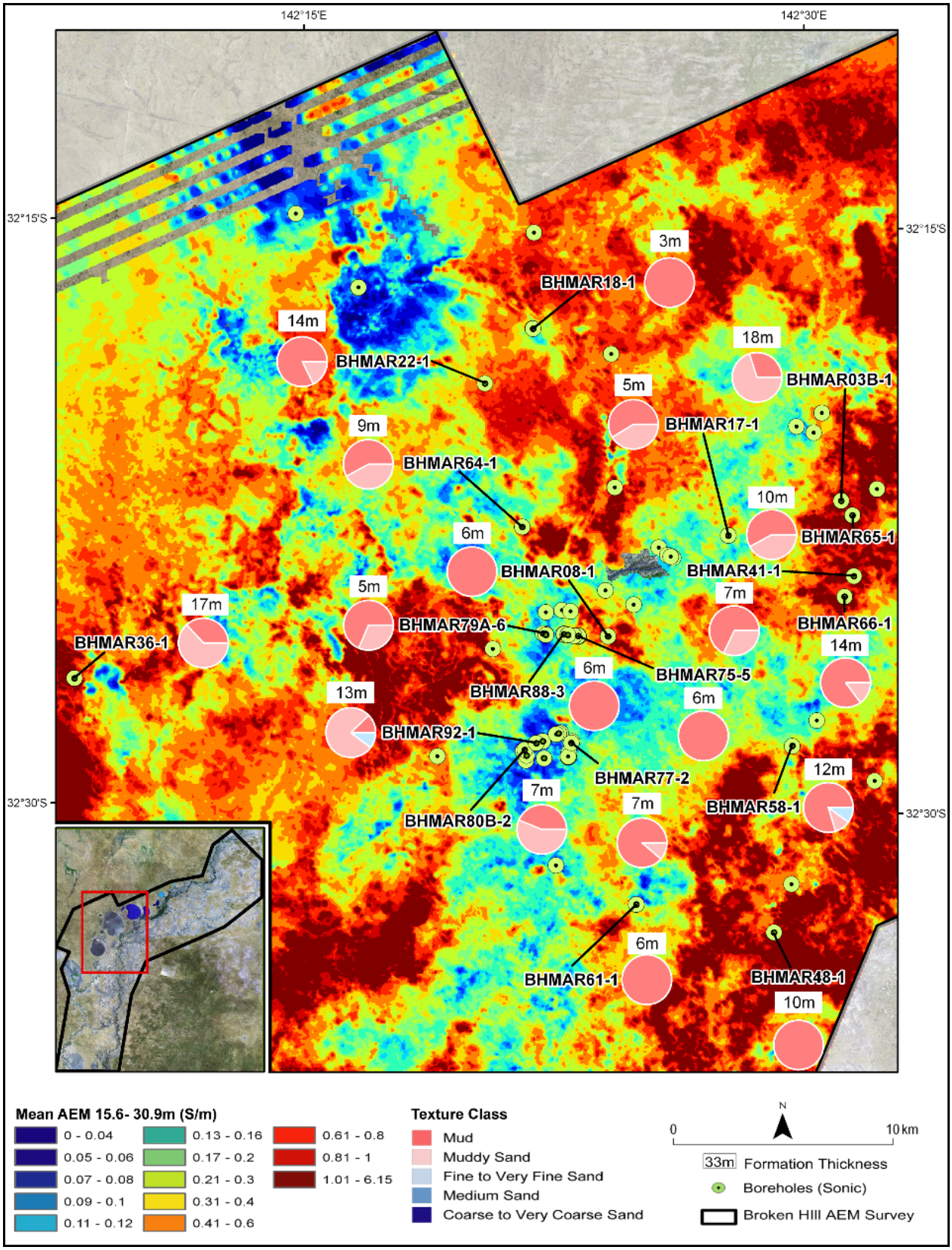

Figure 7-25. *Pie charts showing the variation in textural composition of Blanchetown Clay present across the central area. Overall thicknesses of the Formation are labelled.*

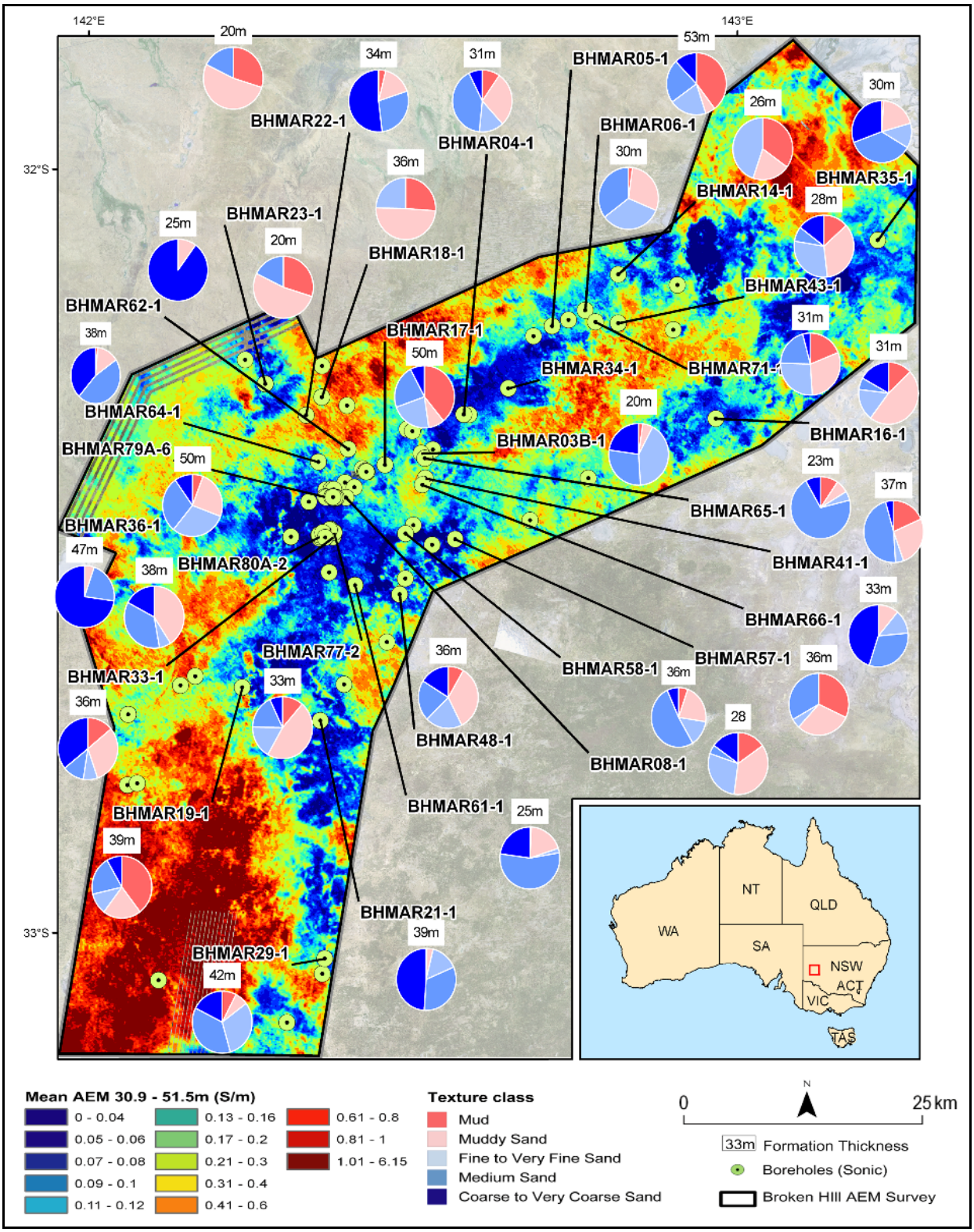

Figure 7-26. *Pie charts showing the textural composition of Calivil Formation present across the central area. Overall thicknesses of the Formation are labelled.*

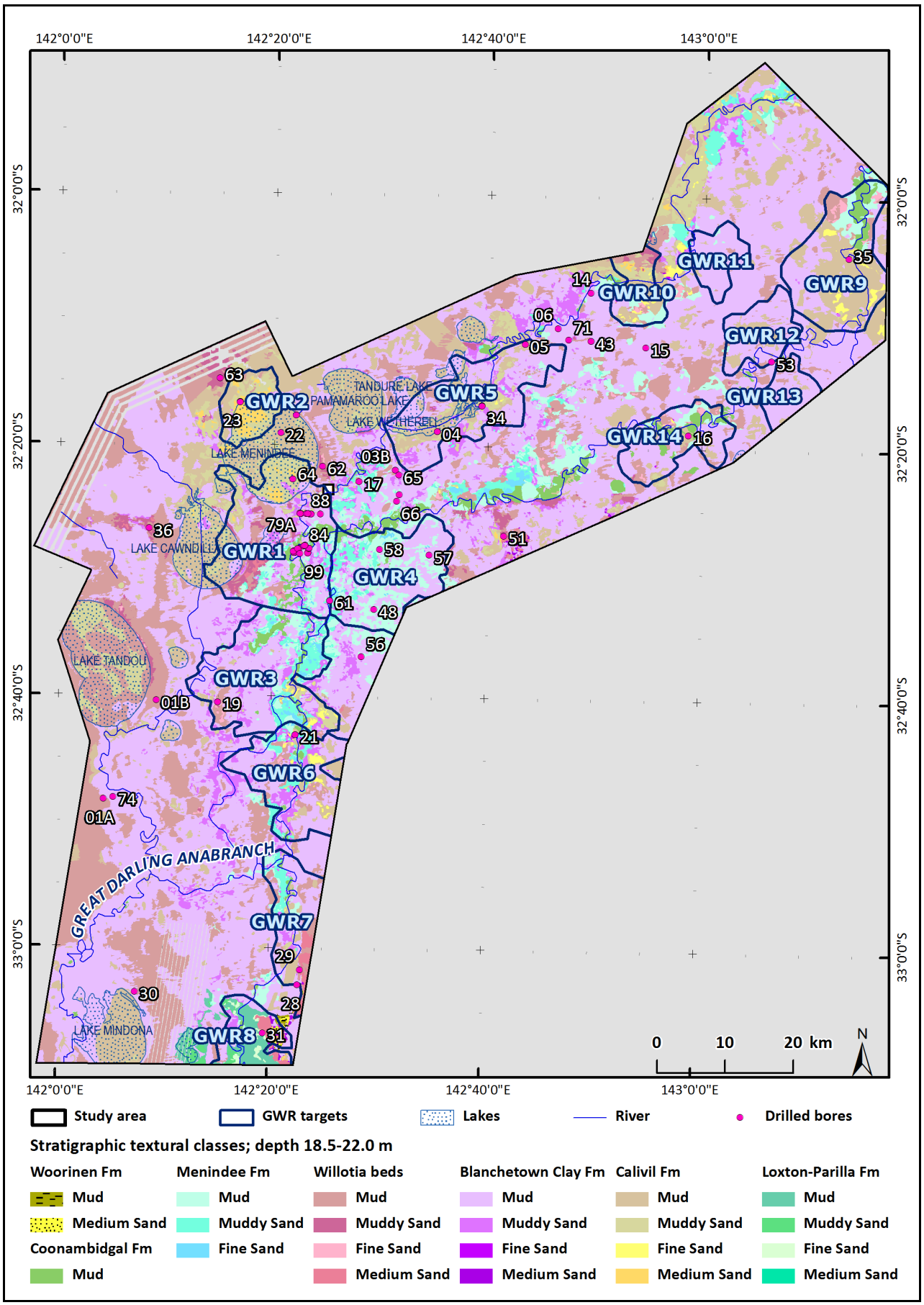

Figure 7-27. *Indicative lithology of sediments including the upper confining aquitard across the project area, based on sediment textural classification, illustrating the 18.1-22.0 m AEM depth slice.*

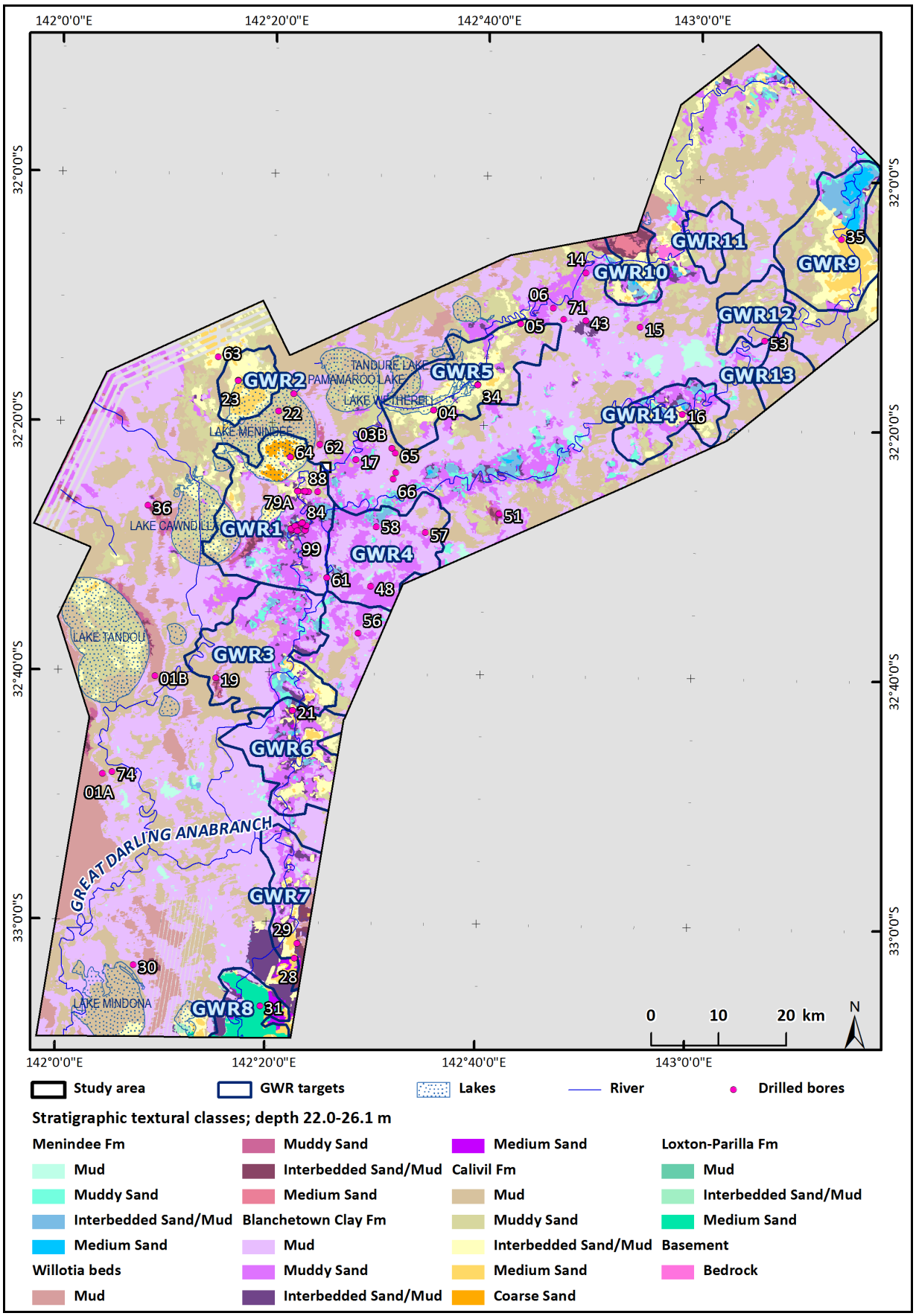

Figure 7-28. *Indicative lithology of sediments including the upper confining aquitard across the project area, based on sediment textural classification, illustrating the 22.0-26.1 m AEM depth slice.*

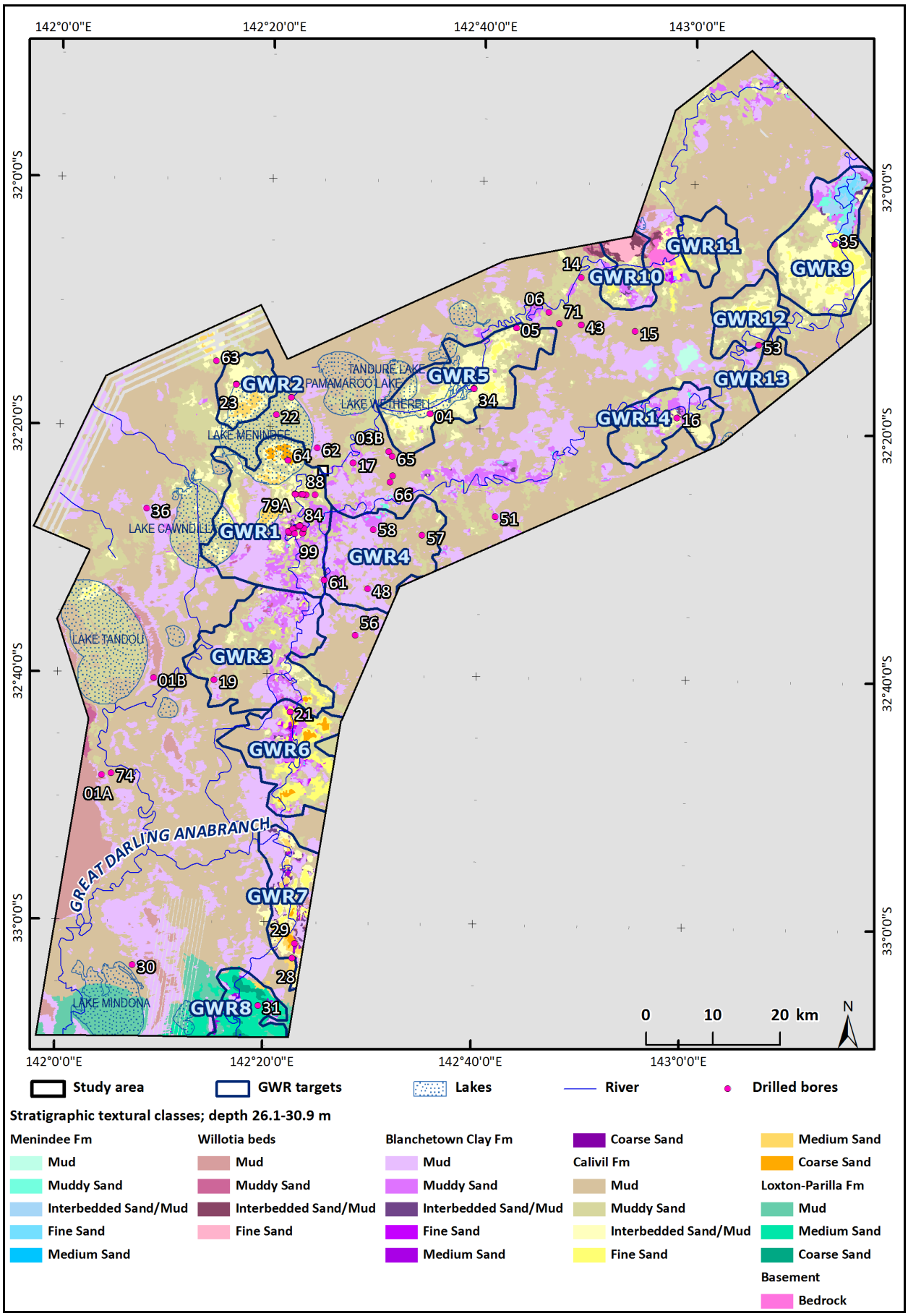

Figure 7-29. *Indicative lithology of sediments including the upper confining aquitard across the project area, based on sediment textural classification, illustrating the 26.1-30.9 m AEM depth slice.*

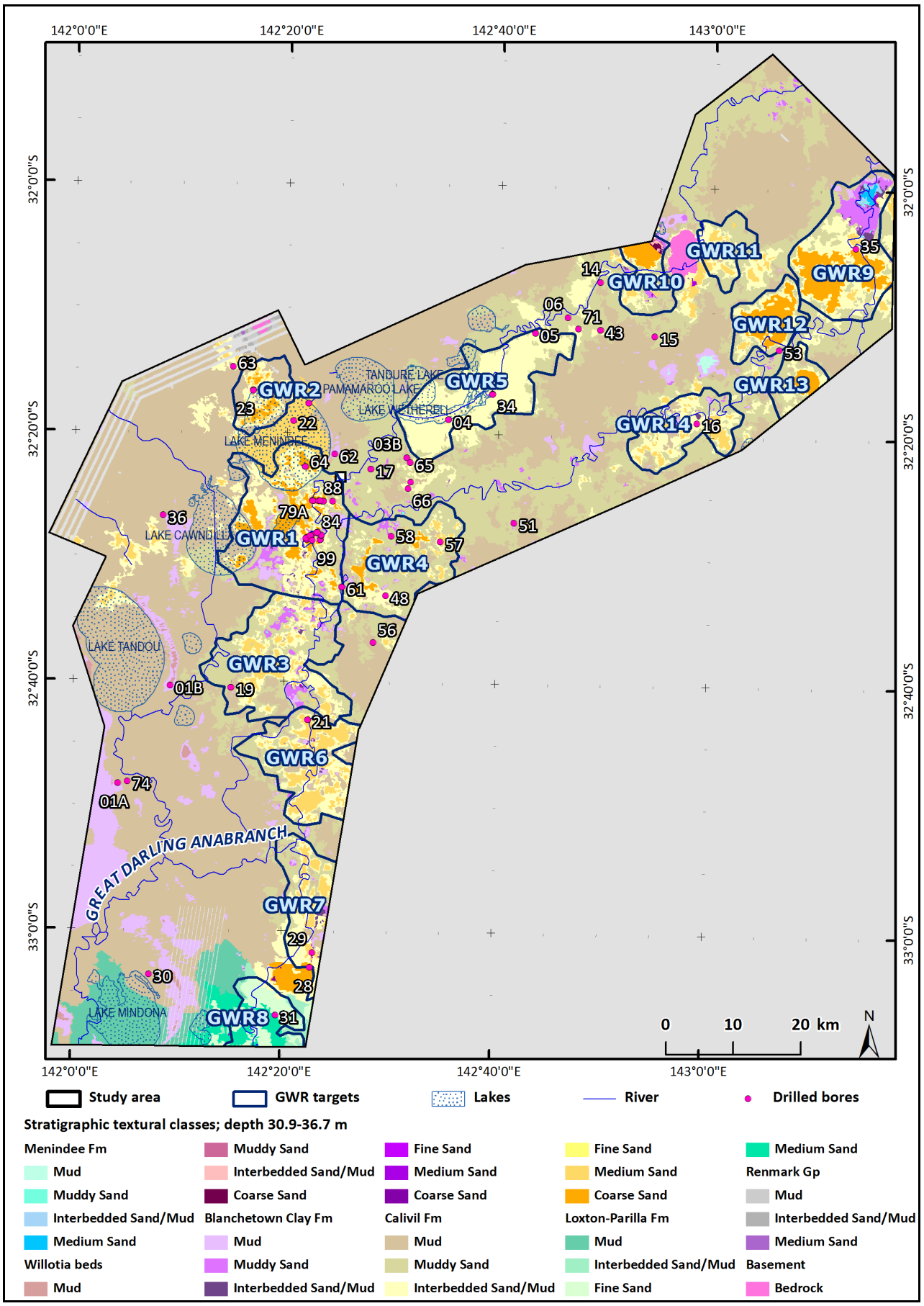

Figure 7-30. *Indicative lithology of sediments including the upper confining aquitard and semi-confined aquifer across the project area, based on sediment textural classification, illustrating the 30.9-36.7 m AEM depth slice.*

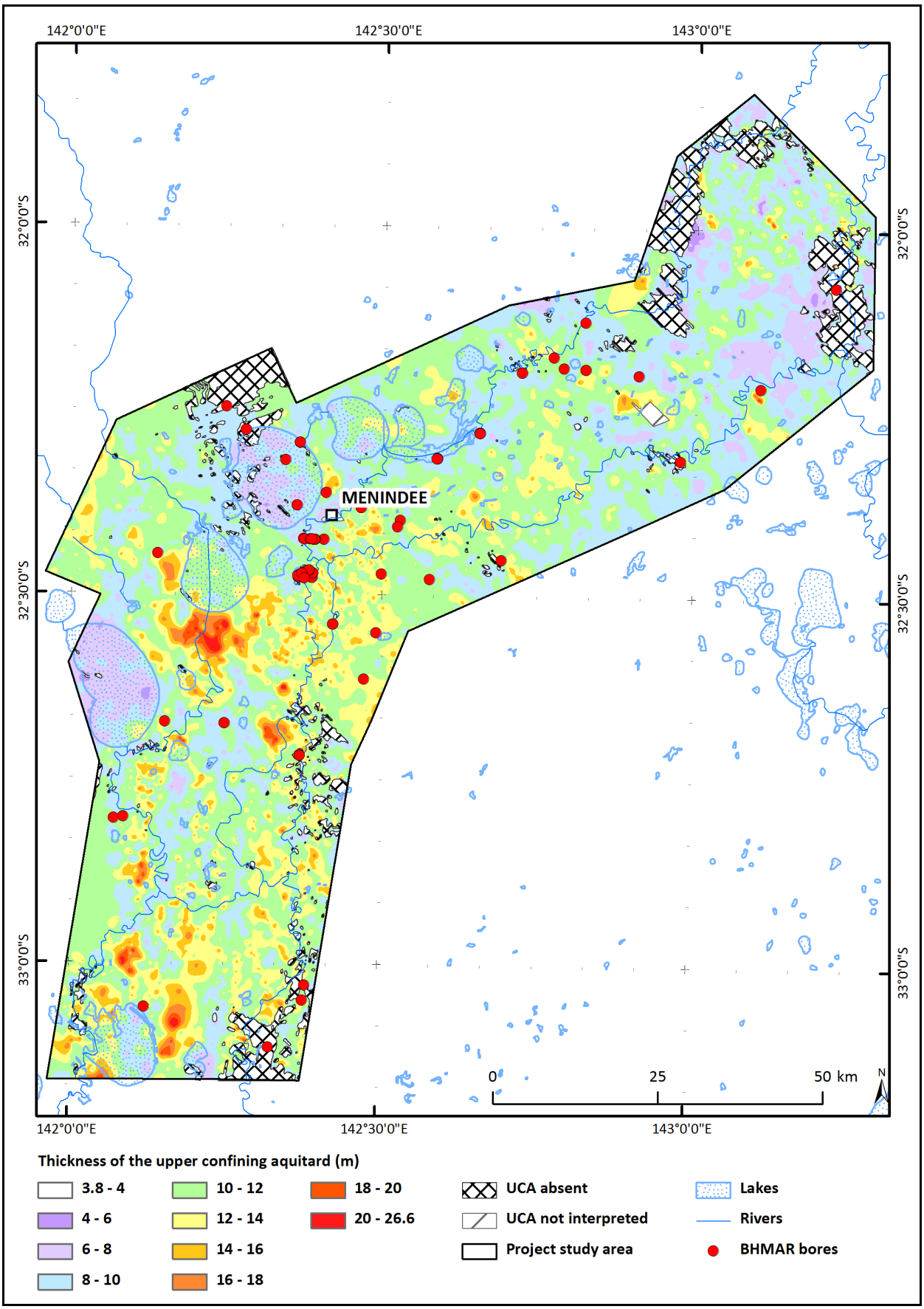

Figure 7-31. *Interpreted thickness of upper confining aquitard (the Blanchetown Clay and mud-rich upper Calivil Formation.*

7.3.2 Upper Confining Aquitard Diffusion

7.3.2.1 Aquitard Diffusion Theory

AEM profiles show that the upper confining aquitard sequence can become relatively resistive, particularly underlying modern drainage. This is in contrast with the aquitard being a distinctive and mappable conductive marker horizon. The maintenance of a zone of fresh shallow groundwater due to river leakage may induce a persistent salinity gradient for diffusion of salt from the upper confining aquitard sequence to be maintained. Hence, an understanding of possible diffusion rates in the context of the geological timeframes relating to the various river migration phases is required. The diffusion of solute through water under steady state conditions is defined by Fick's first law:

$F = -D\, dC/dx$

Equation 1

Where F is the mass flux of solute per unit area per unit time ($m^3/m^2/s$), D is the diffusion coefficient (m^2/s), C is solute concentration (g/m^3), dC/dx is the concentration gradient ($g/m^3/m$). The negative sign indicates movement from greater to lesser solute concentrations (Fetter, 2001). For major ions, D ranges between $1x10^{-9}$ and $2x10^{-9}$ m^2/s at 25 ºC. Li & Gregory (1974) report a value of $1.2x10^{-9}$ m^2/s for seawater diffusing into distilled water. An effective diffusion coefficient (D_e) is used to translate to diffusion through porous media, rather than only through a liquid phase:

$De=\omega D$

Equation 2

Where ω is an empirical coefficient, with typical values ranging 0.01-0.5 inferred from laboratory studies (Freeze & Cherry, 1979). Using the seawater diffusion coefficient of Li & Gregory (1974) as a reference, this would equate to a range of D_e of $1.2x10^{-11}$ to $6x10^{-10}$. To derive a reasonable effective diffusion coefficient, the most commonly used is the empirical relationship with porosity $ø$ (Groen *et al.*, 2000):

$D_e = D ø^m$

Equation 3

Across a number of studies, values for D_e range between $5x10^{-10}$ and $13x10^{-10}$ m^2/s (Groen *et al.*, 2000). In compacted clays, m is relatively high. For example m~2 was used for clay-rich tills, with porosities ranging 0.3-0.35 resulting in D_e/D ratios of ~0.1 (Remenda *et al.*, 1996). The m exponent is closer to unity in less consolidated clays (Appelo & Postma, 1993). Diffusion depends on the relative concentration gradient (C/C_0) of the solute and diffusion time (t) can be derived from:

$$\frac{C}{C_0} = erfc\left(\frac{x}{2\sqrt{D_e t}}\right)$$

Equation 4

Where *erfc* is the complementary error function and x is distance (Crank, 1956). Equation 4 forms the basis for estimating diffusion rates through the upper confining aquitard sequence. In this context, the relative concentration gradient (C/C_0) relate to end member salinities within the upper confining aquitard and x is the vertical distance within the profile where diffusion has occurred during time, t.

Equation 3 was used as the basis to derive a reasonable estimate of the effective diffusion coefficient D_e. Figure 7-32 summarises a sensitivity analysis undertaken by varying the power exponent m for various porosity $ø$ values, the latter ranging between 0.3 and 0.7. This would suggest that a range in D_e of between $2x10^{-10}$ and $8x10^{-10}$ m^2/s (with an average of $5x10^{-10}$ m^2/s) would be reasonable as an initial estimate, in the absence of field data.

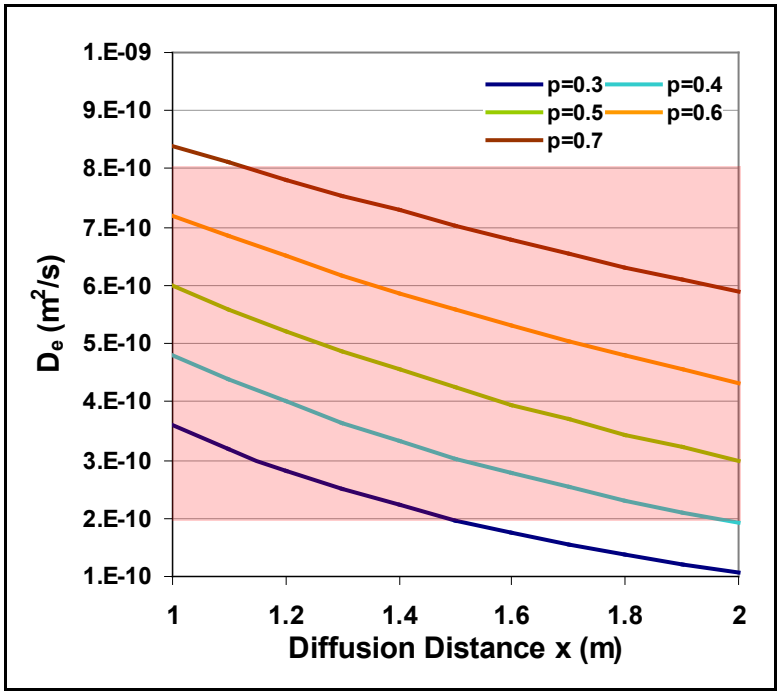

Figure 7-32. *Relationship between power exponent (m) and effective dispersion coefficient (D_e) for various porosities ranging from 0.3 to 0.7. Red shaded area is the D_e range between $2x10^{-10}$ and $8x10^{-10}$.*

The pore fluid data can be used to estimate the relative concentration gradient (C/C_0). Figure 7-33 is a box and whisker plot for pore fluid salinity (TDS, mg/L) for samples obtained from the Blanchetown Clay formation. These have been grouped, in conjunction with the available groundwater, surface water and rainfall samples, into classes defined by fuzzy k-means (refer Section 8.2). Table 7-2 provides a statistical summary for these groupings of pore fluids. Of these classes, 8e is the freshest and has the closest affinity with river leakage, and 8f is the most saline and representative of regional evolved groundwaters which tend to occur at depth or peripheral to modern drainage. The statistics for these two classes were used to define the relative concentration gradient. For example, the median salinity for the fresh end-member (Group 8e, 152 mg/L) and the saline end-member (Group 8f, 20860 mg/L) derived a relative concentration gradient of 0.007 (Table 7-2).

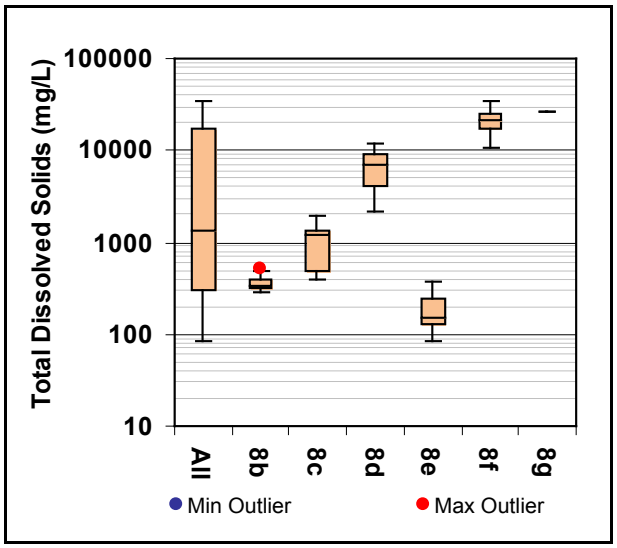

Figure 7-33. *Box and whisker plot of salinity (mg/L) of Blanchetown Clay pore fluids, classified by fuzzy k-means.*

Table 7-2. *Summary statistics for salinity of Blanchetown Clay pore fluids classified by fuzzy k-means.*

	All	8b	8c	8d	8e	8f	8g	8e/8f
Count	87	10	13	8	17	26	1	
Minimum	84	283	385	2110	84	10541	26953	
Q_1	300	312	497	3993	127	17090	26953	.005
Median	1314	344	1184	6885	152	20860	26953	.007
Q_3	17058	386	1314	9311	245	25580	26953	.014
Maximum	35033	526	1935	11868	369	35033	26953	

Figure 7-34 plots the results of Equation 4 using an effective diffusion coefficient D_e of $5x10^{-10}$ m^2/s. The diffusion distance over varying time frames from 100 years to 1 million years is shown in Figure 7-34a. Also plotted is the expected range of relative concentration gradient (C/C_0) based on the first quartile, median and third quartile statistics for the fresh and saline end members of the Blanchetown Clay pore fluids (Table 7-2). This plot suggests that over 1000 years the diffusion distance in the upper confining aquitard profile is about 5 m and over 100,000 years is about 17 m.

Figure 7-34b uses the same equation and parameters, but relates to timeframes ascribed to the Coonambidgal lateral migration phases (refer Section 5.4.1.5), to provide some hydrogeological context. The age ranges for these phases are:

- Coonambidgal 1: 6-2 ka
- Coonambidgal 2: 22-17 ka
- Coonambidgal 3: 30-25 ka
- Coonambidgal 4: 50-45 ka

The onset of the migration phase (i.e. the oldest age) is used in this analysis. Figure 7-34b would suggest that diffusion associated with leakage from river reaches where only the Coonambidgal 1 phase occurs would be in the order of about 7 m, in contrast with about 15 m in reaches where the geomorphological history goes back to the Coonambidgal 4 migration phase.

Equation 4 is also used to generate Figure 7-35 which plots diffusion distance against diffusion time. In this case, different combinations of D_e and C/C_0 were used to derive a likely range for the upper confining aquitard. These combinations are reported in Table 7-3. The low estimate corresponds to a power trend of $t=2.554x^4$ and the high estimate of $t=1.087x^4$ where t is diffusion time (years) and x is the diffusion distance (m). These power trends have been applied to the mapped thickness of the upper confining aquitard to generate an estimate of diffusion rates spatially across the study area (Figure 7-36 and Figure 7-37).

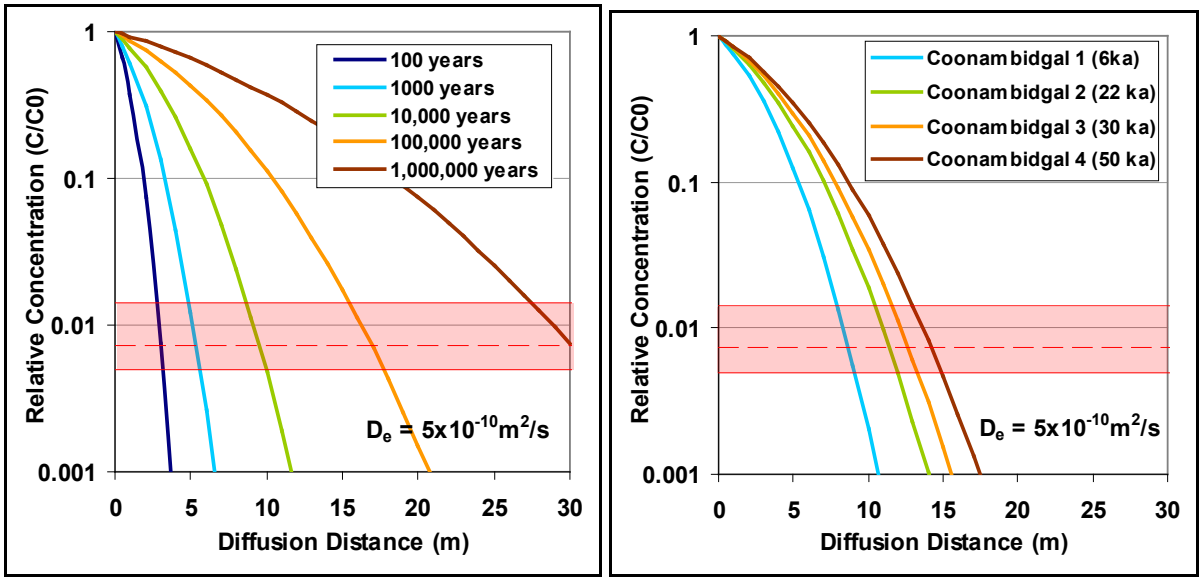

Figure 7-34. *Diffusion distance over different time frames for the upper confining aquitard (a) 100 years to 1 million years (b) timeframes relating to Coonambidgal Formation lateral migration phases. The red shaded area represents the expected range of concentration gradient (C/C_0) based on the pore fluid statistics in Table 7-2).*

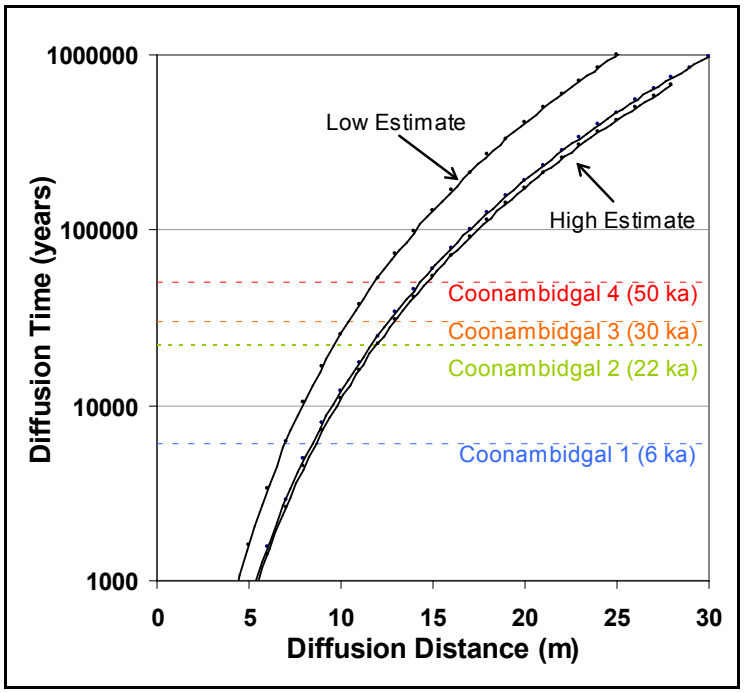

Figure 7-35. *Plots of diffusion distance against diffusion time for the upper confining aquitard.*

Table 7-3. *Combinations of D_e and C/C_0 used to derive diffusion distances in the upper confining aquitard.*

	D_e	C/C_0
Low	$2x10^{-10}$	0.005
Average	$5x10^{-10}$	0.007
High	$8x10^{-10}$	0.014

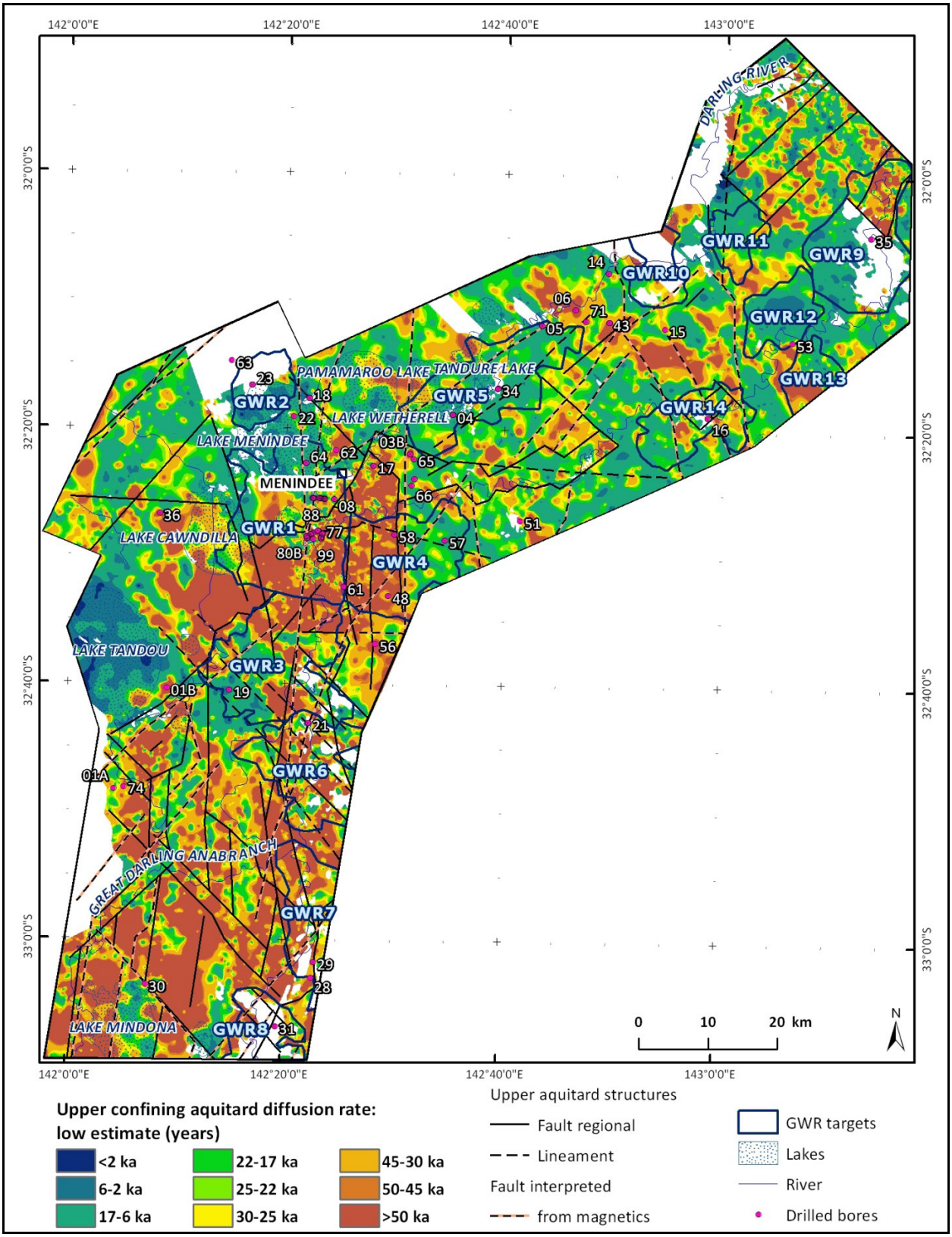

Figure 7-36. *Time required for complete diffusion of the upper confining aquitard using low estimates of effective diffusion coefficient and concentration gradient. Diffusion time have been classified into periods corresponding with the different Coonambidgal Phases.*

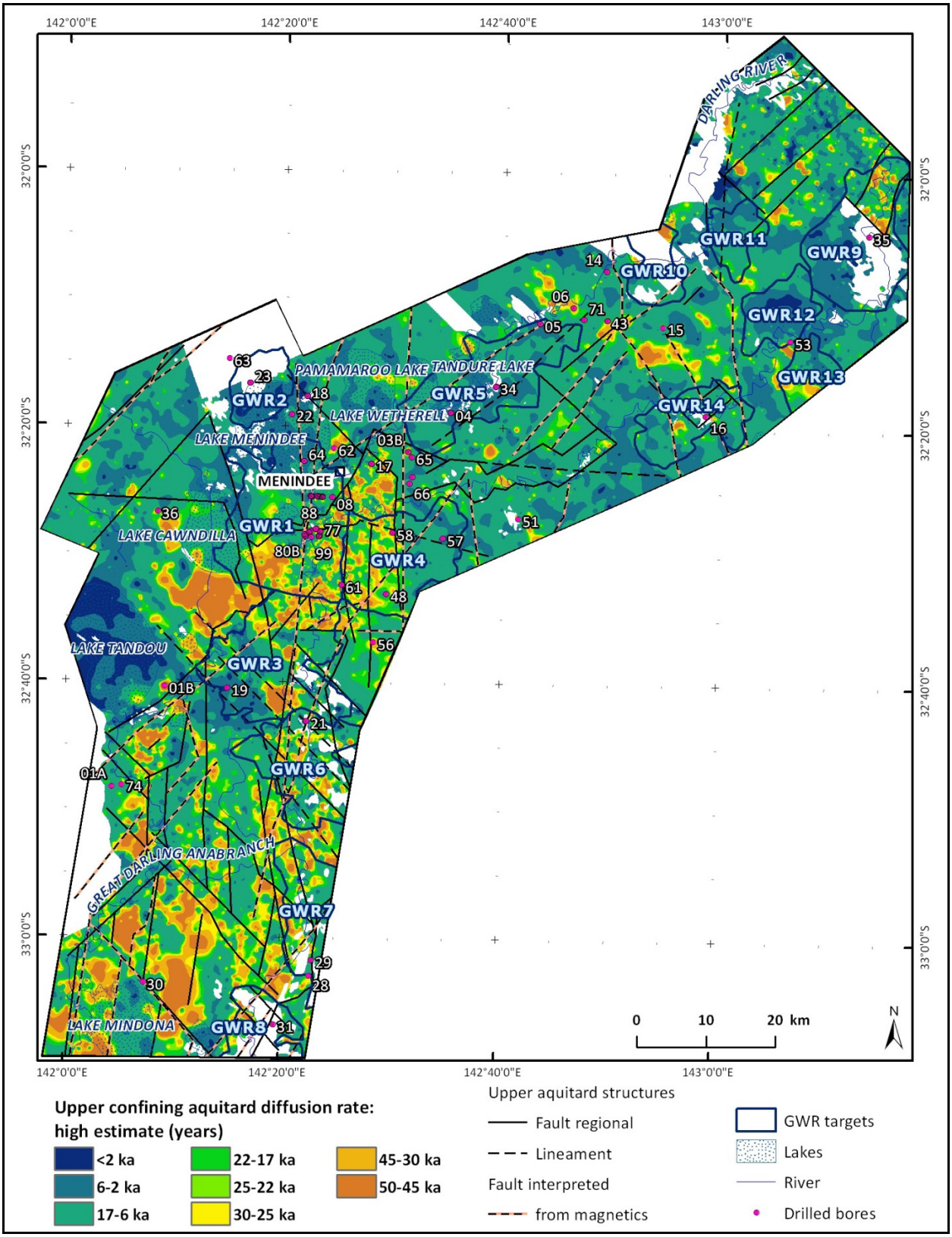

Figure 7-37. *Time required for complete diffusion of the upper confining aquitard using high estimates of effective diffusion coefficient and concentration gradient. Rates of diffusion have been classified into periods corresponding with the different Coonambidgal Phases.*

7.3.2.2 Aquitard Resistivity Interpretation

Typically the upper confining aquitard appears highly conductive in AEM data, however it is observed to be relatively resistive in some areas, particularly underlying modern drainage. There are a couple of possible explanations for these observations.

- Option 1: The aquitard is absent due to erosion associated with tectonic uplift or depositional conditions were such that it was not deposited in the first place. In these instances the resistive zone is either the shallow unconfined or semi-confined aquifer.
- Option 2: The aquitard is leaky, with fresh groundwater moving through the aquitard to adjacent aquifers. While this is typically a function of lithological characteristics of the aquitard, it can also be enhanced by faulting. In this instance the resistive zone corresponds with a sequence of upper confining aquitard that has been freshened due to physical fluid flow.
- Option 3: The aquitard has been subject to diffusion. This is a slow process and requires the aquitard to be in contact with fresh groundwater (either above or below) for long periods of time. As in the previous example, the resistive zone corresponds with a sequence of upper confining aquitard that has been freshened however this is driven by chemical processes not physical fluid flow.

Overall hydraulic conductivity of the unit is very low which suggests that the aquitard is not leaky despite the presence of resistive zones. Faults have however been mapped at a number of locations and are believed to be one of the primary mechanisms for recharge to both the shallow unconfined aquifer and the semi-confined aquifer. Any associated freshening of the aquitard would however be fairly localised.

There are some examples where the aquitard is known to be absent and an associated resistive zone corresponds with the aquifer. An example of this is at GWR8 where an elevated feature in the landscape prevented the deposition of the Blanchetown Clay. Consequently the shallow unconfined aquifer and the semi-confined aquifer are in direct connectivity here, both of which appear as highly resistive. The northern section of Lake Menindee is another example. In this case, the Blanchetown Clay was eroded by a palaeochannel that intersected the lake prior to its formation. In both these instances, resistive zones are observed throughout the profile (beginning at quite shallow depth) as they correspond with sandier sediments containing relatively fresh groundwater. Two other resistive areas are apparent. These correspond with GWR5 and GWR9.

In the case of GWR9, resistive zones are observed throughout the profile (beginning at quite shallow depth). As opposed to Lake Menindee, borehole logging data (from BHMAR35) report a 4 m thick, sandy mud/muddy sand section of Blanchetown Clay which overlies a mud-rich section of the Calivil Formation. This data clearly indicates the upper confining aquitard is present at BHMAR35, if not more broadly within the GWR9 target which supports the occurrence of diffusion. There are a number of conditions that may have combined to make this area uniquely susceptible to diffusion processes: 1) the aquitard is slightly sandier (muddy sand/sandy mud) which would increase the rate of diffusion and 2) this section of Talyawalka Creek has been exposed to stream flows more continuous and of greater volume than any other section of Talyawalka Creek. The modern Talyawalka Creek correlates with Coonambidgal Phase 2 which was reportedly active between 21-17 ka. The thickness of the upper confining aquitard and associated diffusion rates would suggest that full diffusion of the profile at this location is possible.

GWR5 corresponds with modern-day Lake Wetherell which is an artificial lake resulting from regulation of the Darling River in the 1960s. Resistive zones are observed within two AEM depth slices (26.1-30.9 m and 30.9-36.7 m). The upper confining aquitard is interpreted to occur at depth of approximately 13-35 m. High resistivity is not observed at depths shallower than 26.1 m, suggesting downwards diffusion has not yet occurred. This is in keeping with estimated diffusion rates for the upper confining aquitard. Upwards diffusion however appears to be plausible at this location and potentially others within the study area. Several resistive areas appear in the AEM depth slice 30.9-36.7 m which roughly corresponds with the base of the upper confining aquitard. These resistivity areas decrease in area upwards, suggesting the influence of upward diffusion is not extensive.

This analysis suggests that freshening of the upper confining aquitard, as identified in the AEM should not be used as an indicator leakiness of the aquitard.

7.4 SHALLOW UNCONFINED QUATERNARY AQUIFER

7.4.1 Hydrogeology

The Quaternary fluvial sediments of the Coonambidgal and Menindee Formations as well as the Willotia beds combine to form the shallow unconfined aquifer system. This is particularly the case near surface drainage features such as the Darling River, Talyawalka Creek and the Menindee Lakes, where episodic leakage has elevated the shallow watertable. The watertable deepens away from the influence of modern drainage, so much so that these Quaternary sediments can become unsaturated in the peripheral dunefield areas. Table 7-4 summarises the key features of this shallow unconfined aquifer in the Quaternary sediments.

The Blanchetown Clay acts as an aquitard base to these sequences of fluvial sands and muds. Due to its conductivity contrast, the Blanchetown Clay is an excellent marker horizon and the top surface has been mapped based on the AEM sections (Lawrie *et al.,* 2012a). Due to structural control, this top surface can vary considerably, as described in more detail in Section 6. Hence, thickness of the Quaternary sediments can vary from zero where the Blanchetown Clay crops out, to exceeding 50 m. On average, the Quaternary sediment thickness is about 17 m.

The coarser grained sediments within the Quaternary Coonambidgal Formation, the Menindee Formation, the Willotia beds (Figure 7-54) and the Blanchetown Clay (typically at depths of less than 18 m; see Lawrie *et al*., 2012b for additional information) are components of the shallow unconfined aquifer. This is particularly the case in areas with a relatively shallow watertable, most notably along the Darling River and in the vicinity of the Menindee Lakes (Figure 7-55 and Figure 7-56). The extent and thickness of the predominant stratigraphic units that constitute the Quaternary fluvial aquifer system, the Coonambidgal Formation, Menindee Formation and Willotia beds, are shown in Figure 7-38, Figure 7-39 and Figure 7-40, respectively. The watertable deepens away from the river and lakes to such an extent that the Quaternary sediments can become unsaturated and the watertable occurs in deeper parts of the hydrostratigraphy, such as the Blanchetown Clay or the Calivil Formation.

This mapping highlights the restricted distribution of the Coonambidgal Formation along to the modern Darling River (Figure 7-38). The formation appears to better developed along the Talyawalka – Anabranch drainage relative to the Darling River. In contrast, the Menindee Formation is distributed across a broad swath of the Darling River floodplain (Figure 7-39). Sediment thickness is variable, with the thickest occurring in the GWR9 target along Talyawalka Creek. The Willotia beds are in the outer periphery of the floodplain, particularly along the western margin of the BHMAR study area (Figure 7-40).

Figure 7-41 to Figure 7-44 are the stratigraphic and lithological interpretations for AEM depth slices between 9.2 m and 18.1 m depth, selected to best represent the Quaternary fluvial sediments hosting the unconfined aquifer. The best distribution of sand is evident at a depth of about 13-16 m (Figure 7-43). This shows a co-location of a corridor of sandy material with modern drainage in the southern reach of the Talyawalka Creek continuing downstream into the Darling River, to about the GWR6 target area.

These depth slice lithological interpretations have been combined to provide unconfined aquifer thickness (Figure 7-45). As this combination does not account for the watertable surface, this thickness includes both unsaturated and saturated components. Lunettes and sediments of the Woorinen Formation are not considered part of the shallow unconfined aquifer as these generally occur well above the water table and the near-surface aquitard. On these depth slice interpretations, they typically correspond with the white areas within the study area extent. Overall, the remainder of the landscape is generally associated with aquifer thickness of greater than 5 m. Greater aquifer thickness is associated with the Darling River and Talyawalka Creek. Aquifer thickness appears to be particularly thick in GWR9 however the watertable is quite deep here therefore saturated thickness is minimal.

Table 7-4. *Characteristics of the shallow Quaternary aquifer in the BHMAR study area.*

	Description	Comments
Host formations	Coonambidgal Formation, Menindee Formation and Willotia beds	Generations of Quaternary fluvial deposits of Darling River floodplain.
Aquifer type	Unconfined to unsaturated	Shallow unconfined aquifer due to groundwater mounding near surface water features. Quaternary fluvial sediments may be completely unsaturated away from the influence of river/lakes.
Depth to base of aquifer from ground surface (m)	Range:0-52 m Mean: 17 m	Based on depth to top of Blanchetown Clay surface interpreted from AEM sections and borehole data over target area.
Saturated thickness (m)	Range: 0 - 28 m Mean: 5 m	Based difference grid between watertable surface and top of Blanchetown Clay surface over entire study area.
Lithologies	Coarse to very coarse sand (4%) Medium sand (18%) Fine sand (25%) Muddy sand (28%) Mud (25%)	Based on sonic core logging of Quaternary fluvial intervals in bores in BHMAR study area.
Porosity and storage coefficients	NMR mobile water P_{25}: 0.02 Mean: 0.11 P_{75}: 0.19	25th percentile, mean and 75th percentile of the NMR free water for the saturated Quaternary intervals in NMR logged holes in the study area. NMR mobile water used as a surrogate for effective porosity. No pump tests undertaken in the shallow aquifer to estimate storage coefficients.
Hydraulic conductivity (K, m/d) and transmissivity (T, m^2/d)	Slug Tests: K Range: 0.2-32 m/d K Mean: 4.7 m/d T Range: 1-343 m^2/d T Mean: 38 m^2/d Nuclear Magnetic Resonance K : K Range: <0.001-27 m/d K Mean: 2.5 m/d T Range: <0.1 – 191 m^2/d T Mean: 23 m^2/d	Range and mean of slug test results for shallow monitoring bores in BHMAR study area. Range and mean of average K and total T for Quaternary fluvial sections in NMR logged monitoring bores in BHMAR study area.
Elevation of watertable (m AHD)	Range: 35.8 – 57.8 m AHD Mean: 44.9 m AHD	Based on the watertable surface over target area for December 2011 interpreted from borehole monitoring data.
Depth to watertable from ground surface (m)	Range: <2 – 58 m Mean: 18 m	Based on difference grid between ground surface and interpreted watertable surface over BHMAR study area.
Groundwater salinity (TDS, mg/L)	Range: 138-4813 mg/L Mean: 615 mg/L	Total dissolved solids (TDS) range and average of groundwater sampling from shallow monitoring bores in target area (n=25).
ADWG2011 water quality exceedances	Total Dissolved Solids TDS >600 mg/L (7/22) Total Dissolved Solids TDS >1200 mg/L (1/22) Chloride Cl >250 mg/L (2/22) Sodium Na >180 mg/L (3/22) Sulfate SO_4 >250 mg/L (1/22) Iron Fe >0.3 mg/L (14/22) Manganese Mn >0.1 mg/L (20/22) Antimony Sb >3 µg/L (1/22) Arsenic As >10 µg/L (3/22) Uranium U >17 µg/L (1/22) Ammonia NH_3 >0.39 mg/L-N (11/22)	Australian Drinking Water Guidelines (ADWG2011) exceedances for 22 groundwater samples from BHMAR04-3, 21-2, 23-3, 23-4, 34-2, 61-3, 79A-5, 80A-3, 80A-4, 80B-3, 84-3, 84-4, 84-5 and 92-2.

Note: The NMR data in this figure were collected in 2011 using the Javelin tool with an inter-echo spacing of 2.5 ms. Subsequent laboratory and field tests have demonstrated that this setting underestimates the free and total water content, and derived porosities, and should only be used on a semi-quantitative comparative basis. The NMR data may also be unreliable in zones where there is significant iron-(hematite) coating of quartz grains.

The transmissivity of the shallow unconfined aquifer have been generated from classified depth slices of estimated hydraulic conductivity (see Lawrie *et al*., 2012a for further details). Rather than selecting a single representative hydraulic conductivity value, a lower (1st quartile) and upper (3rd quartile) estimate was used (based on physical measurements). The resulting estimates are shown in Figure 7-46 and Figure 7-47 respectively. Transmissivity is influenced by the thickness of the aquifer as well as textural composition. The low estimate of transmissivity varies from very low to low across almost the whole area (Figure 7-46). Using the upper quartiles, the transmissivity is typically in the low to intermediate range. It is suggested that the most likely values fall between these two estimates. Regardless, the mapping is a useful guide to the relative distribution of transmissivity for the shallow unconfined aquifer. The mapping highlights the overall coarsening of the sequence (as reflected in Figure 7-41 to Figure 7-44) and increasing thickness to a less extent (Figure 7-45) with proximity to the modern drainage. Palaeochannel features with relatively high transmissivities can also be identified, most notably between the Darling River and Talyawalka Creek in the northern half of the BHMAR study area. Zones classified as having high transmissivity have been mapped in targets GWR4 and GWR6 marginal to the modern drainage (Figure 7-47). The shallow unconfined aquifer is described in greater detail at a groundwater resource target level in Lawrie *et al*. (2012d).

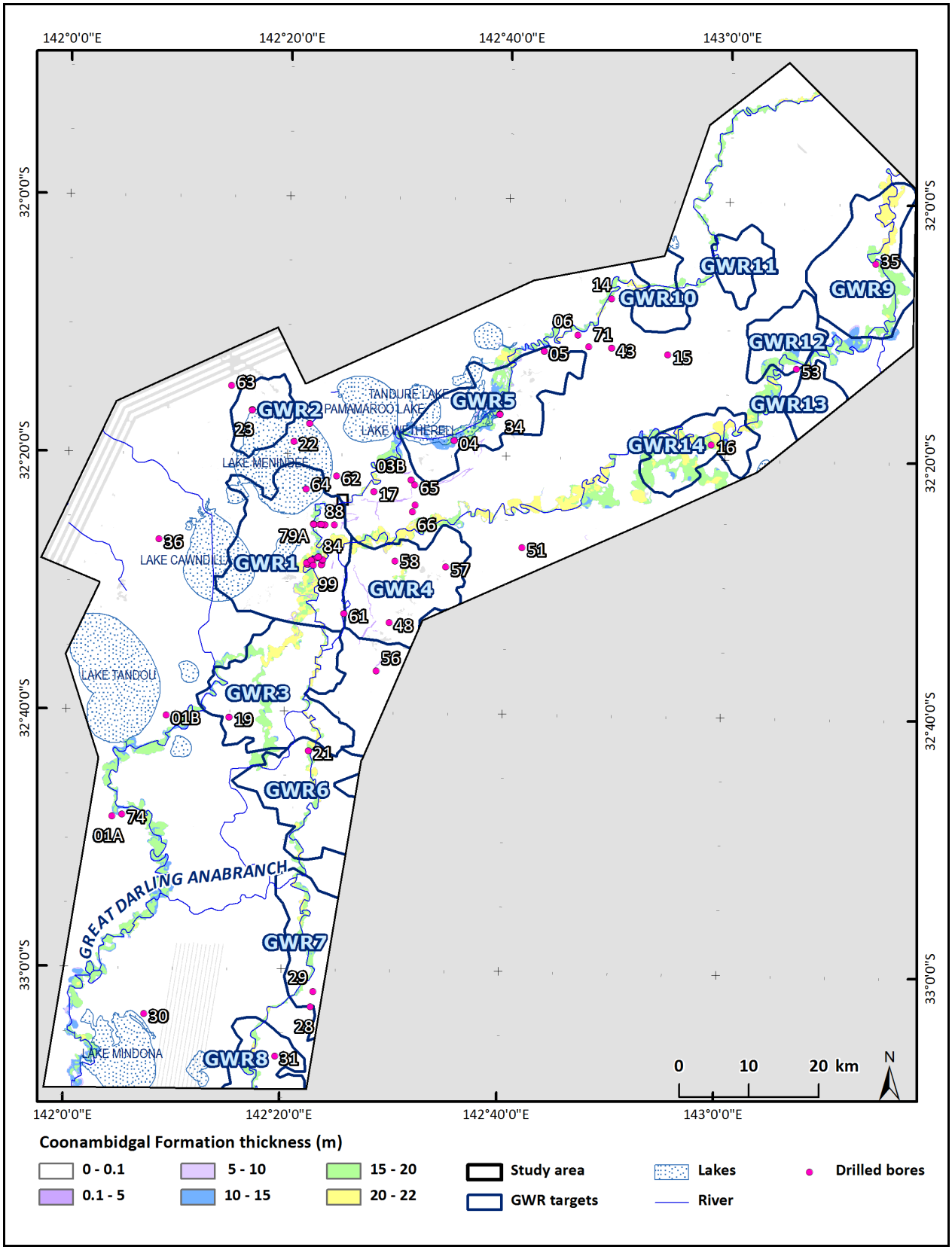

Figure 7-38. *Interpreted extent and stratigraphic thickness of Coonambidgal Formation.*

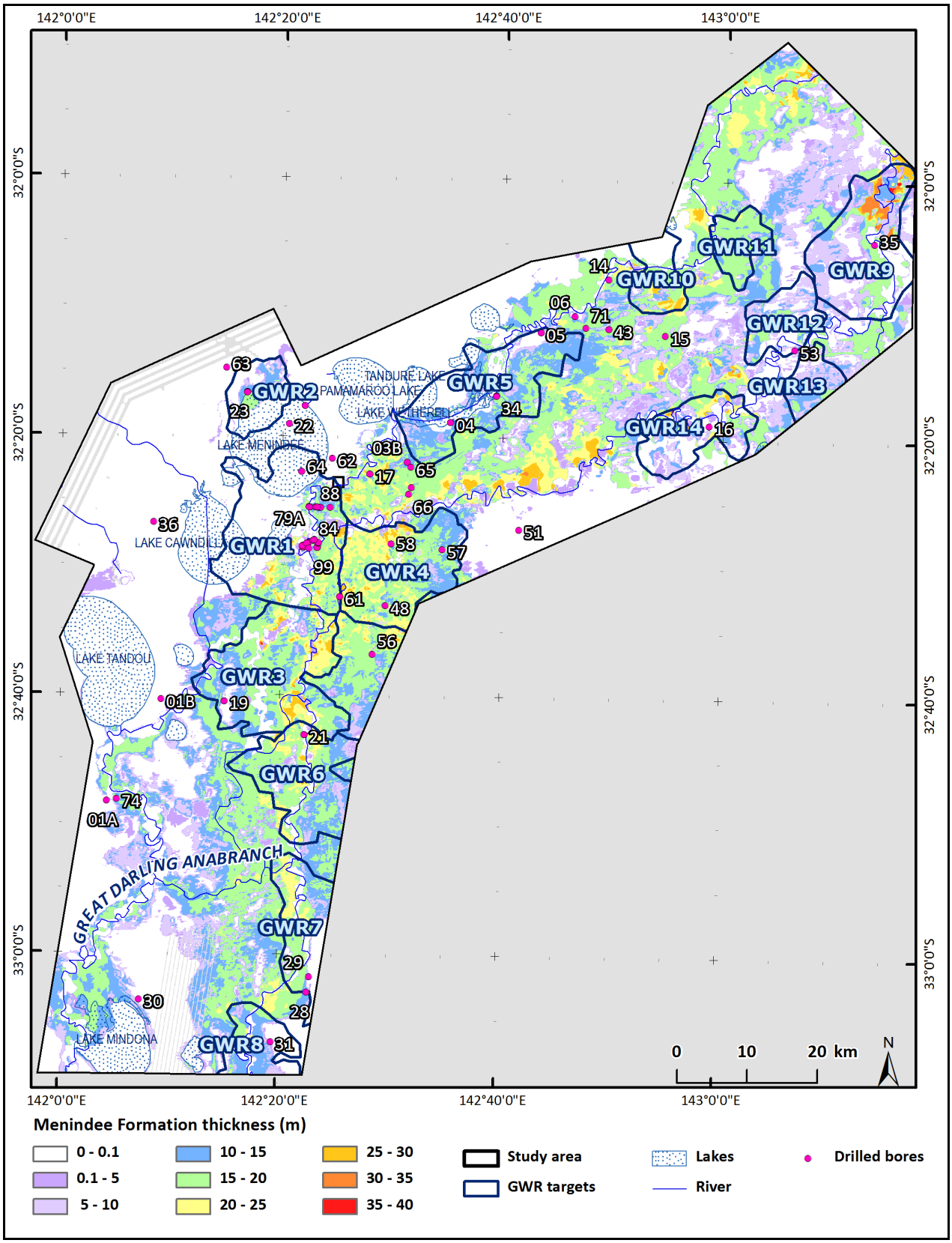

Figure 7-39. *Interpreted extent and stratigraphic thickness of Menindee Formation.*

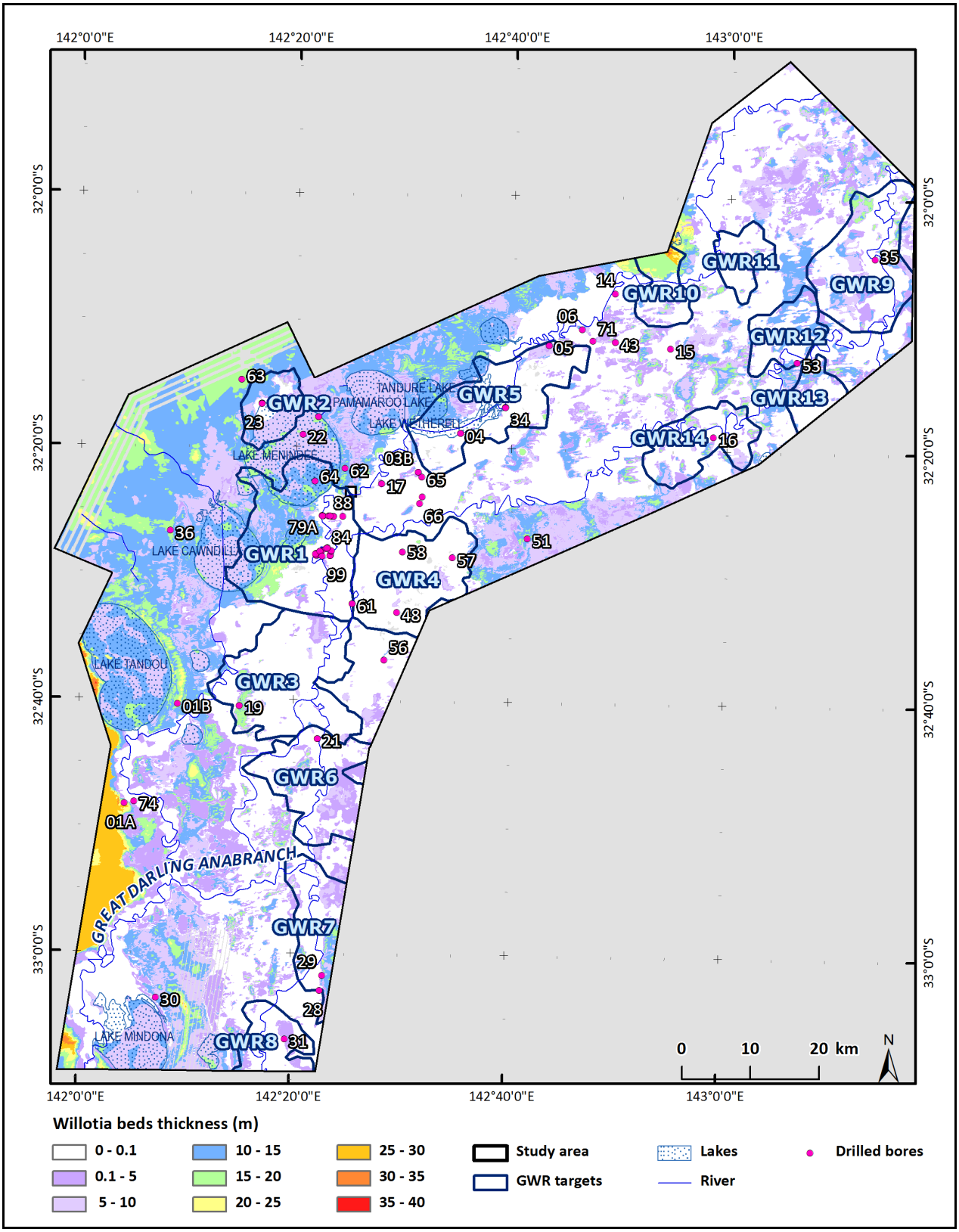

Figure 7-40. *Interpreted extent and stratigraphic thickness of Willotia beds.*

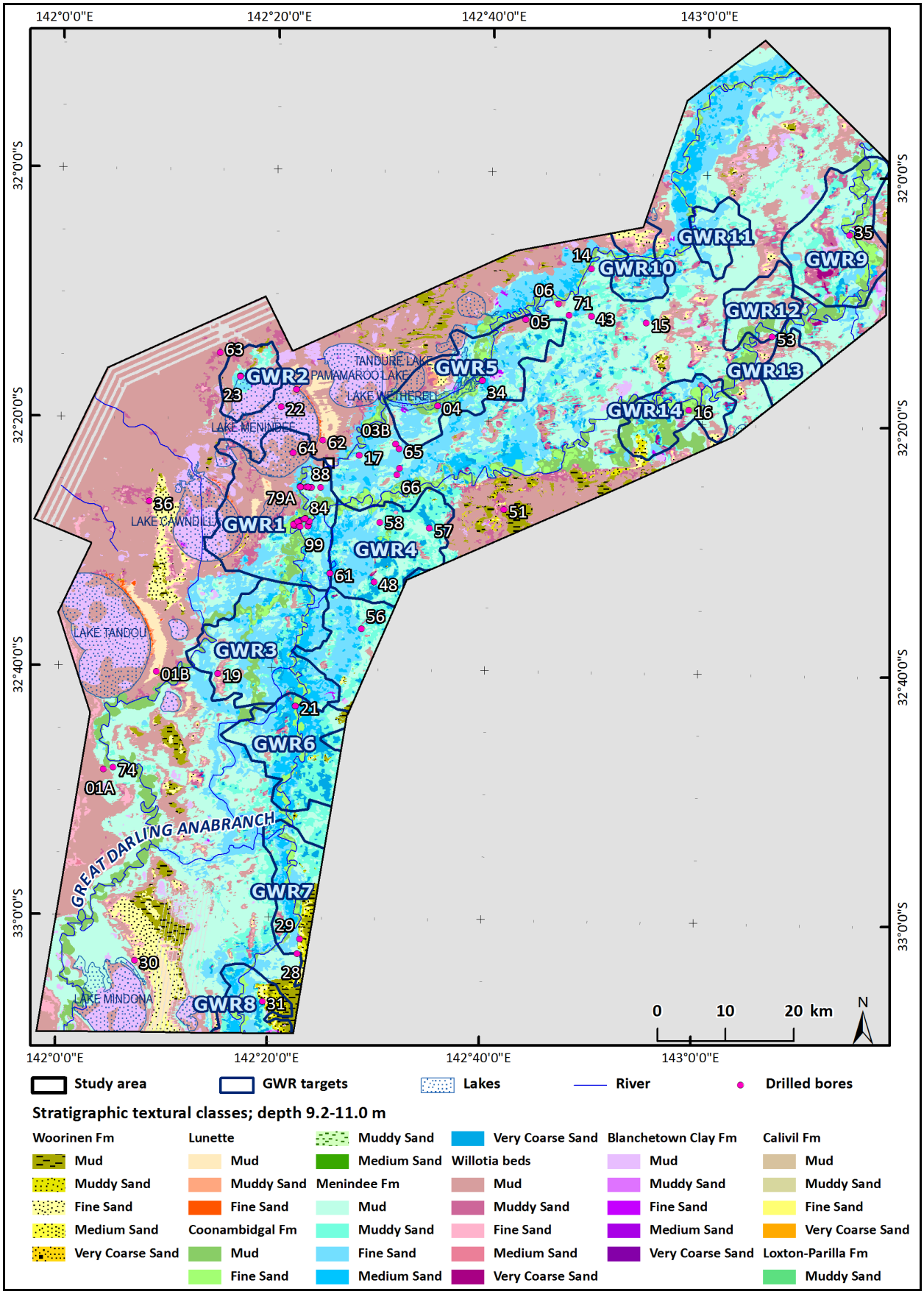

Figure 7-41. *Indicative lithology of shallow sediments including the unconfined aquifer across the project area, based on sediment textural classification, illustrating the 9.2-11.0 m AEM depth slice.*

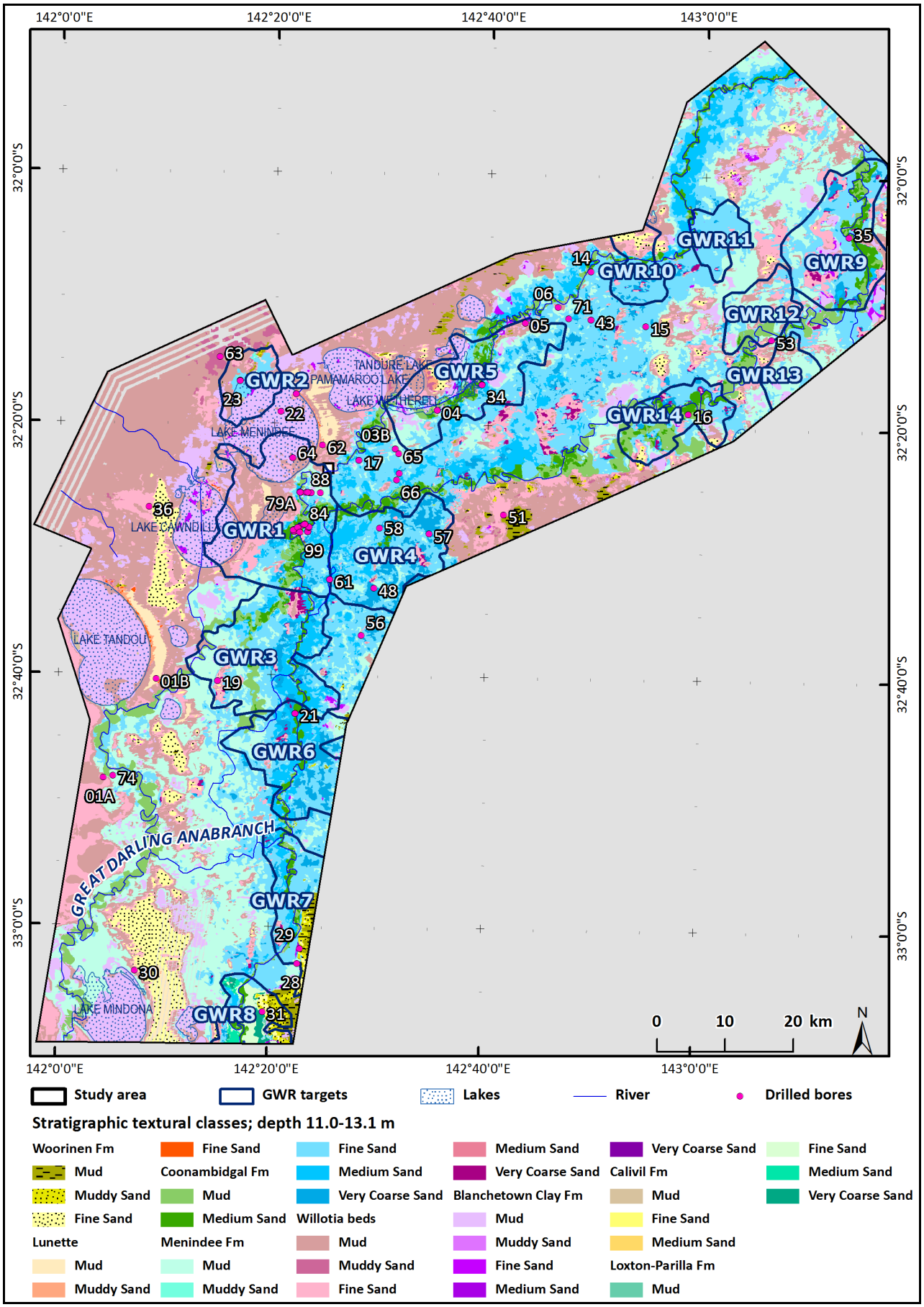

Figure 7-42. *Indicative lithology of shallow sediments including the unconfined aquifer across the project area, based on sediment textural classification, illustrating the 11.0-13.1 m AEM depth slice.*

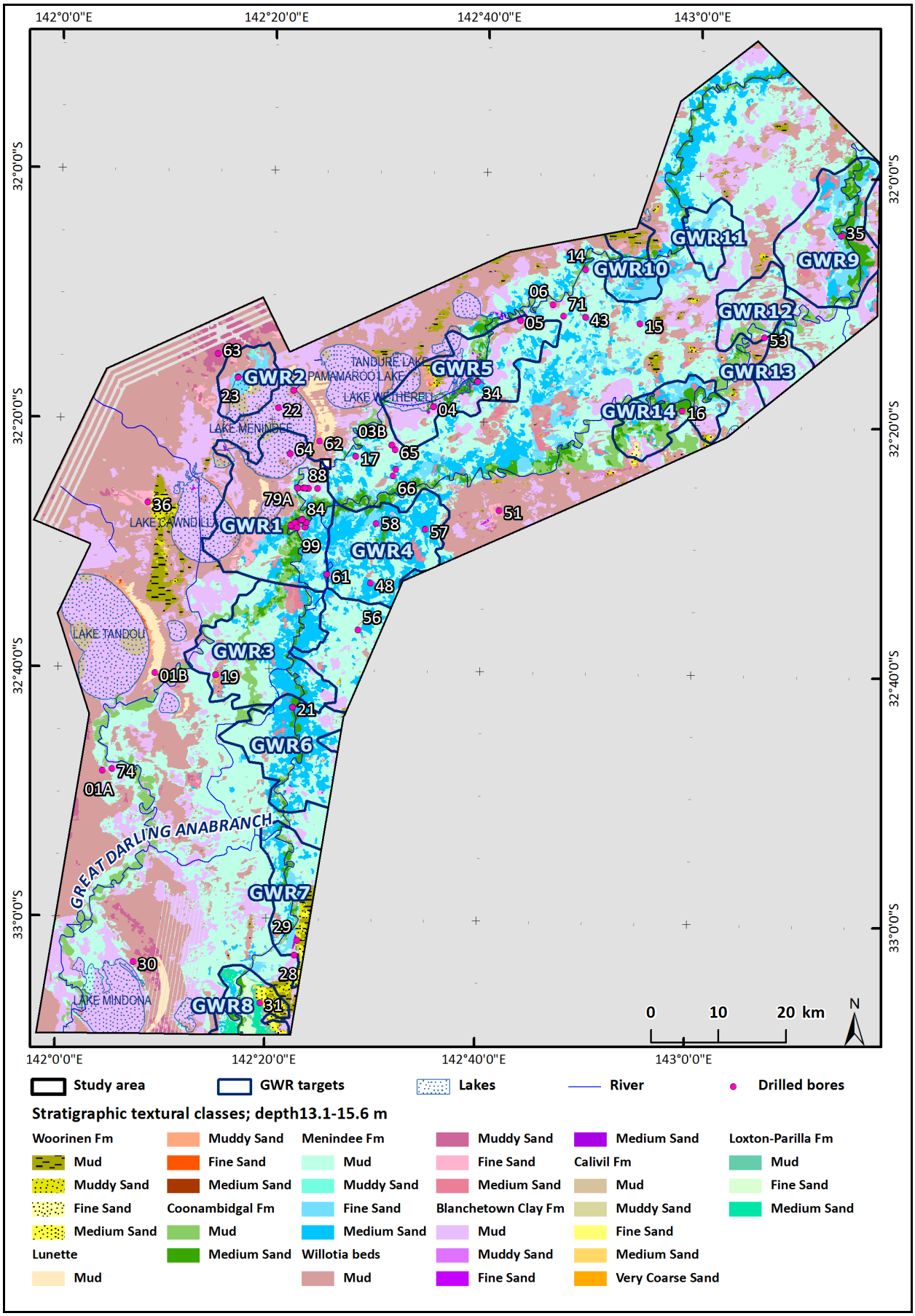

Figure 7-43. *Indicative lithology of shallow sediments including the unconfined aquifer across the project area, based on sediment textural classification, illustrating the 13.1-15.6 m AEM depth slice.*

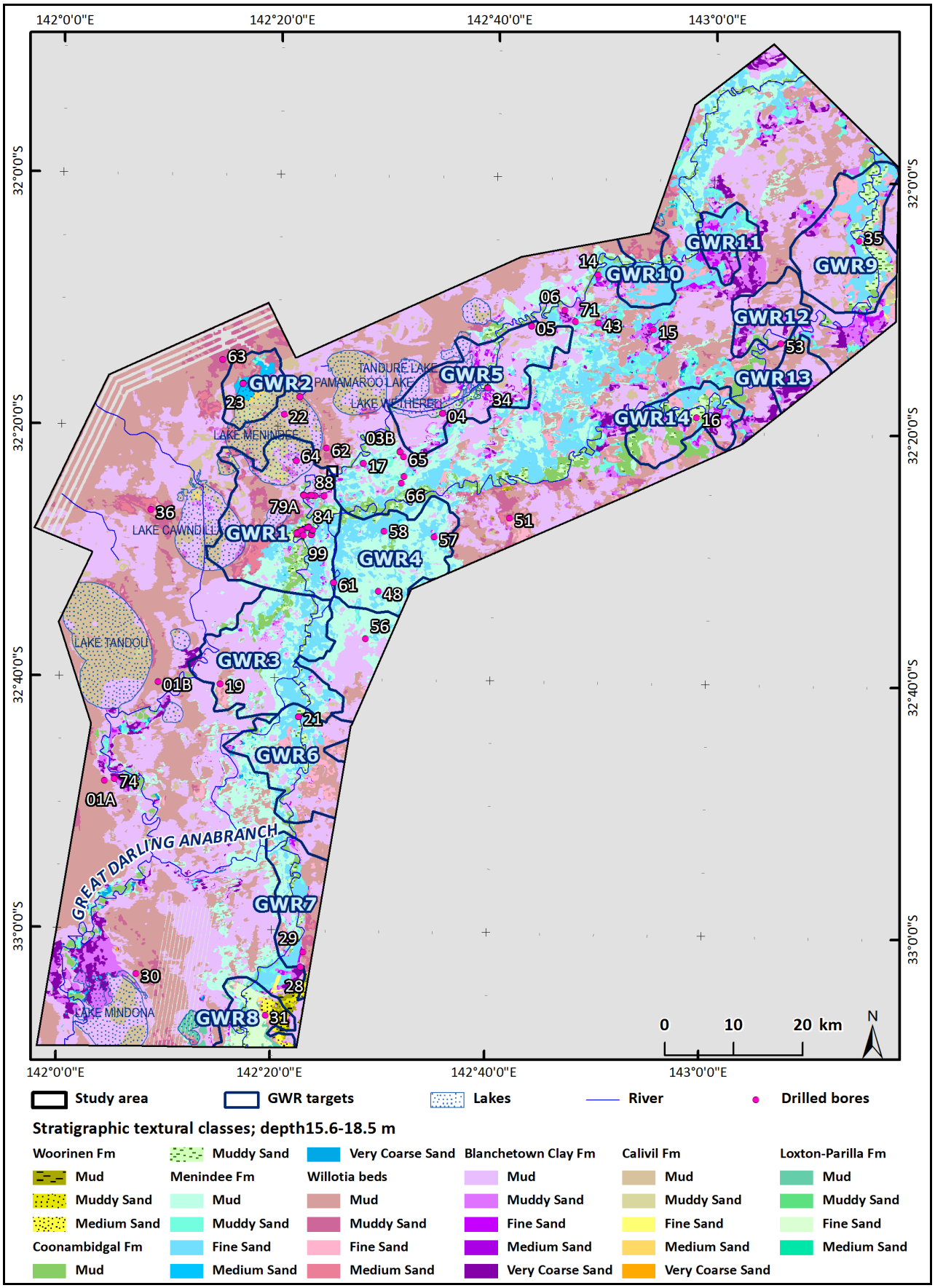

Figure 7-44. *Indicative lithology of shallow sediments including the unconfined aquifer across the project area, based on sediment textural classification, illustrating the 15.6-18.1 m AEM depth slice.*

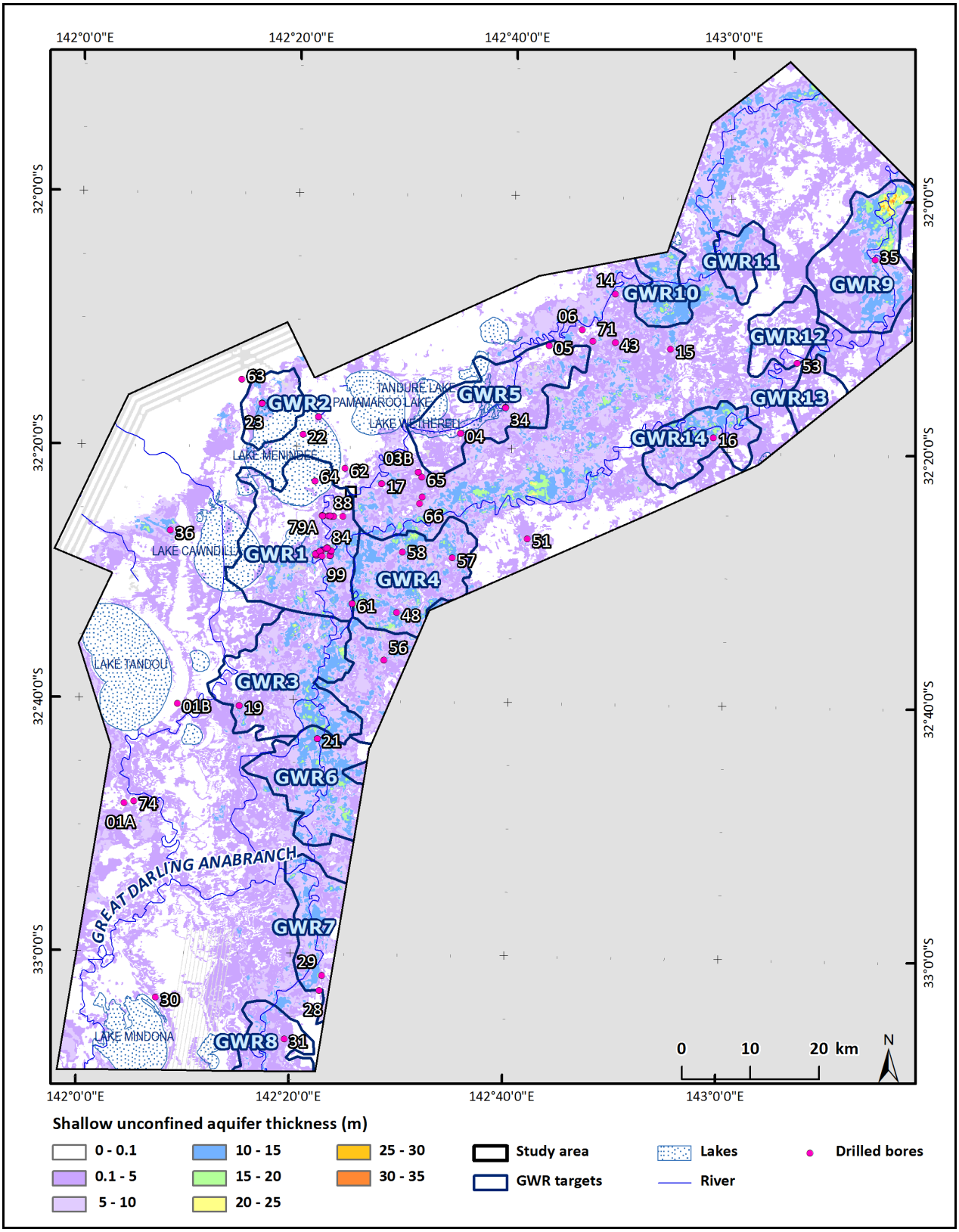

Figure 7-45. *Interpreted extent and thickness of the shallow unconfined aquifer. White areas within the study extent indicate where the aquifer is absent.*

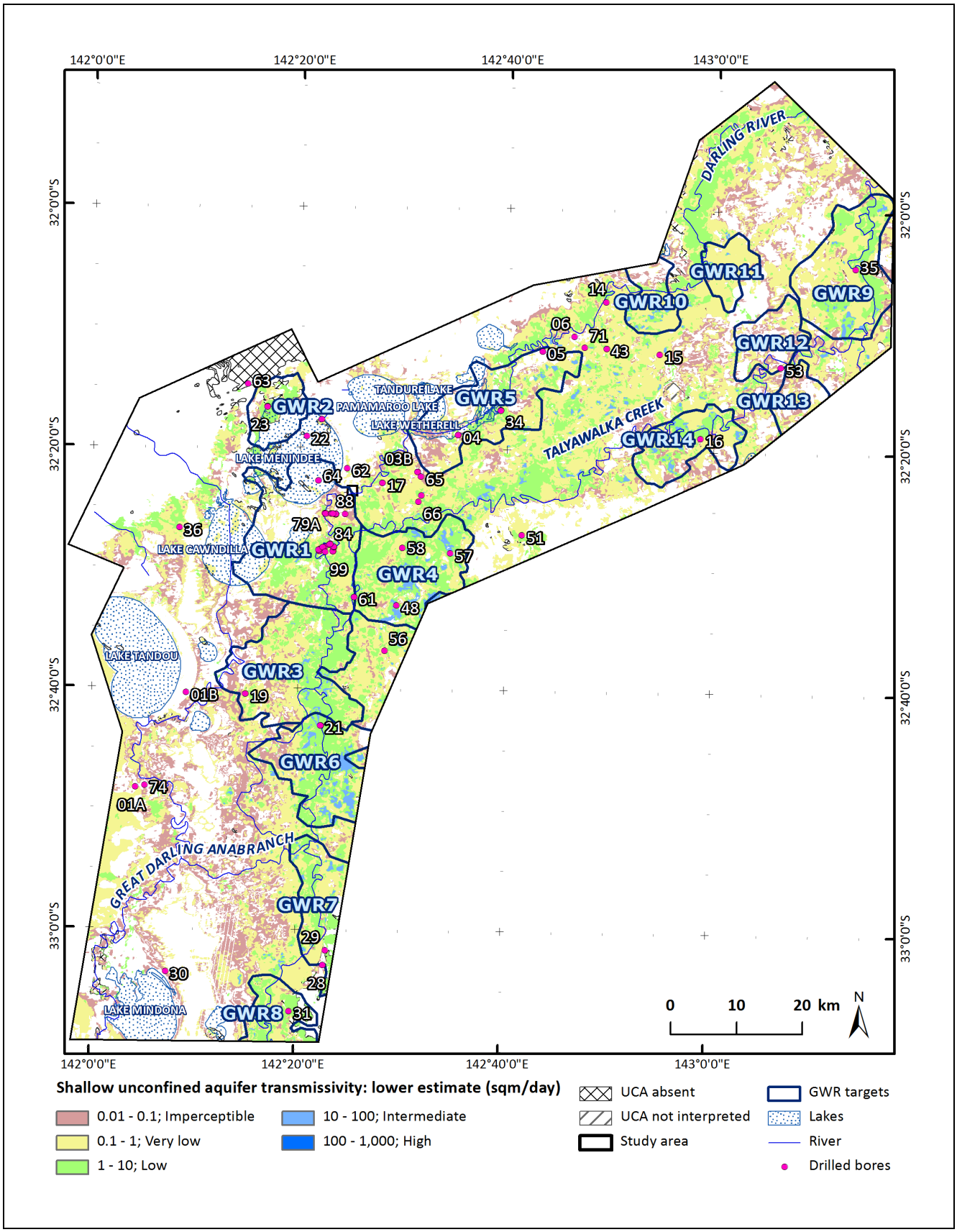

Figure 7-46. *Lower estimate of transmissivity of the shallow unconfined aquifer. White areas within the study extent indicate where the aquifer is absent.*

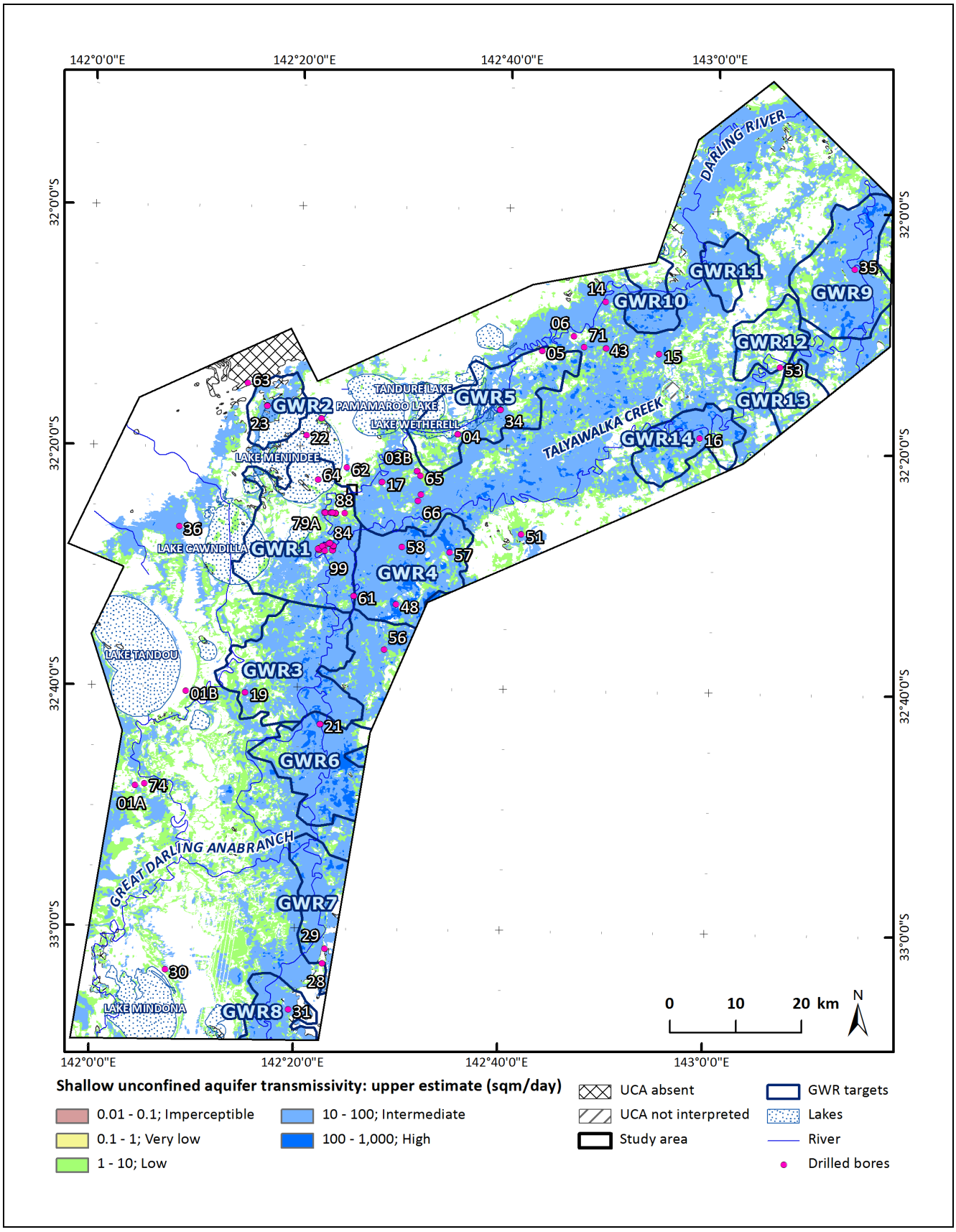

Figure 7-47. *Upper estimate of transmissivity of the shallow unconfined aquifer. White areas within the study extent indicate where the aquifer is absent.*

The sonic core provides an overview of the lithologies making up the package of shallow Quaternary fluvial units. The sonic drilling technique is described in Lawrie *et al.* (2012a). Overall averages for the drilled intervals indicate the predominance of finer-grained material, with over half being mud or muddy sand, and another quarter being fine sand (Table 7-4). The occurrence of coarse to very coarse sands is relatively minor (<5%).

Slug testing of monitoring bores screened in the coarser grained intervals indicate on average hydraulic conductivities of ~5 m/d are considered moderate. The NMR logging provides similar hydraulic conductivity statistics (Table 7-4), as they are in part derived from the slug test estimates (Lawrie *et al.,* 2012a). Due to the relatively small saturated thicknesses, the overall range in aquifer transmissivity (2-40 m^2/d) would be considered to be low to intermediate (Krasny, 1993).

Figure 7-4a and Figure 7-4b respectively show the relative distribution of hydraulic conductivity and transmissivity values derived by slug tests for the various screened aquifer formations. These results suggest that there is a general increasing trend through the generations of Quaternary fluvial sedimentation, with the youngest Coonambidgal Formation (Qac) being the least transmissive and the oldest Willotia beds being the most transmissive. Figure 7-5 and Figure 7-6 are box and whisker plots for various hydraulic parameters derived from the NMR logging. The trend seen in the slug test data for the Quaternary aquifers (Qac, Qam, Qaw) is not apparent in this dataset. One reason for the relatively low hydraulic conductivities for the Willotia beds (Qaw) could be that there tends to be greater weathering and cementation evident in these older fluvial deposits. Like the slug test data, the Calivil Formation (Tpc) and Loxton-Parilla Sands (Tps) have the better hydraulic conductivity based on the NMR data, compared with the overlying Quaternary shallow unconfined aquifers.

7.4.2 Groundwater Flow and Dynamics

The interpreted watertable surface is mapped in Figure 7-48. The approach used in mapping the watertable is described in Lawrie *et al*. (2012a). The watertable surface shows a regional south to southwest groundwater flow trend disrupted by watertable mounding associated with the river system and lake storages. This confirms the importance of river and lake leakage as being the primary mechanism for groundwater recharge, rather than diffuse recharge from rainfall. The most significant mounding is associated with leakage under Lake Wetherell in the Darling floodplain and also lake leakage near the northwest edge of Lake Menindee. Groundwater mounding is also mapped along the Darling River corridor south of Menindee as well as along Talyawalka Creek. These are losing drainage features that form local groundwater divides. High watertable elevations along the Darling River in the northeast part of the study area relate to topographic effects associated with buried basement highs, as well as the effects of river-related recharge. The mounding has created a 20 m head difference ranging from ~57 m AHD elevation near Lake Menindee to ~37 m AHD along the western boundary of the study area, over a distance of about 55 km. This equates to a gradient of ~0.4 m/km. The average watertable elevation is ~ 45 m AHD.

Depth to the watertable, as presented in Figure 7-49, was mapped as the difference between the watertable elevation and the elevation of the land surface. The dominant feature of this mapping is the relatively shallow watertable along the Darling River corridor and in particular underlying the Menindee Lakes. This reflects the mounding effect due to leakage, combined with the incision of the river channel and lake beds into the landscape. In comparison, the effect of leakage from Talyawalka Creek is muted. The watertable can exceed a depth of 50 m, in areas away from the modern drainage and where the Quaternary sediments become largely unsaturated and the underlying Calivil Formation aquifer can become unconfined. The average watertable depth is ~18 m.

The top surface of the Blanchetown Clay represents the base of the Quaternary fluvial sediments. Hence, the difference between the watertable surface and the Blanchetown Clay top surface indicates the saturated thickness of the shallow Quaternary sediments (Figure 7-50). This can vary from unsaturated conditions to a maximum saturated thickness of 28 m, with an average of 5 m of saturation. The map highlights the overwhelming influence of river leakage on the shallow unconfined aquifer in the Quaternary alluvial sequence. It shows the saturated conditions along the river corridor and under the lakes. Along Talyawalka Creek, watertable mounding in the Quaternary sediments is more localised and related to structural features.

Groundwater level measurements from bores accessing different aquifers at the same site provide insights into the vertical head gradient and therefore the direction of potential vertical groundwater flow. Actual vertical flow of groundwater between aquifers is determined by the presence and effectiveness of intervening aquitards, such as the Blanchetown Clay. Figure 7-51 maps the head difference between the shallow watertable surface (Figure 7-48) and the potentiometric surface of the Calivil Formation aquifer (Figure 7-19). Although there is no correction for density differences, particularly relating to contrasts in groundwater salinity, this does provide information on potential vertical groundwater flow direction. Areas of positive difference are where the shallow watertable is higher than the Calivil Formation groundwater level, indicating downward hydraulic gradients. These relate to the watertable mounding associated with river and lake leakage. Peripheral to the river corridor, Calivil Formation heads tend to be higher than the shallow watertable. This is because the mounding effect from leakage extends further away from the river in the semi-confined and more transmissive Pliocene aquifer, compared with the Quaternary sediment aquifers.

Monitoring bores have also been installed into the various shallow Quaternary alluvial aquifers. The groundwater response in the Coonambidgal Formation aquifer to the Darling River flood of 2010-11 can be observed in bores BHMAR84-3 and BHMAR84-4 at Jimargil (Figure 7-52). Here, the watertable within the Coonambidgal Formation rose between 2.7 m to 5.4 m over 160 to 200 days, commencing October, 2010. The watertable peaks reflect the peak river flows in March 2011. There was a synchronous response to the rising and falling water levels in the Darling River at Weir 32 (Figure 7-52). Also plotted on Figure 7-52 is the stage height (6.15 m) representing the onset of overbank flow (19,000 ML/d) at Weir 32. This height was reached in December 2010 and remained above this height for 124 days. Watertable rise prior to overbank flow suggests that these conditions are not a pre-requisite for shallow groundwater recharge. Watertable decline concomitant with the river stage receding is inferred to be due to bank storage drainage and other losses. Watertable decline can reflect shallow lateral groundwater movement away from the river corridor as well as localised vertical movement into the underlying Calivil Formation aquifer.

The eight bores in the Menindee Formation aquifer are distributed along the Darling River corridor. The watertable level change from the start of monitoring to peak river flow ranged between 0.4 m and 1.7 m. The bores generally show a steady watertable rise in response to rising river stage. The largest response occurred in the bores within 100 m of the river. Bore BHMAR77-3 (Figure 7-53) illustrates the synchronous response in groundwater height after the onset of floods in October 2010. An almost identical hydrograph profile was observed at bore BHMAR92-2 at East Bootingee (Figure 7-53). The change in groundwater height from low flow to peak was 1.2 m and 1.7 m in BHMAR77-3 and BHMAR92-2, respectively.

Groundwater levels in the unconfined aquifers that are highly responsive to rising (and falling) water levels in the Darling River (or adjacent lakes) indicate high hydraulic connectivity between shallow groundwater and surface water during high flows. Watertable response is highest in bores within 200 m of the Darling River in the target areas at Jimargil and East Bootingee, with a slower response observed at greater distances from the surface water source.

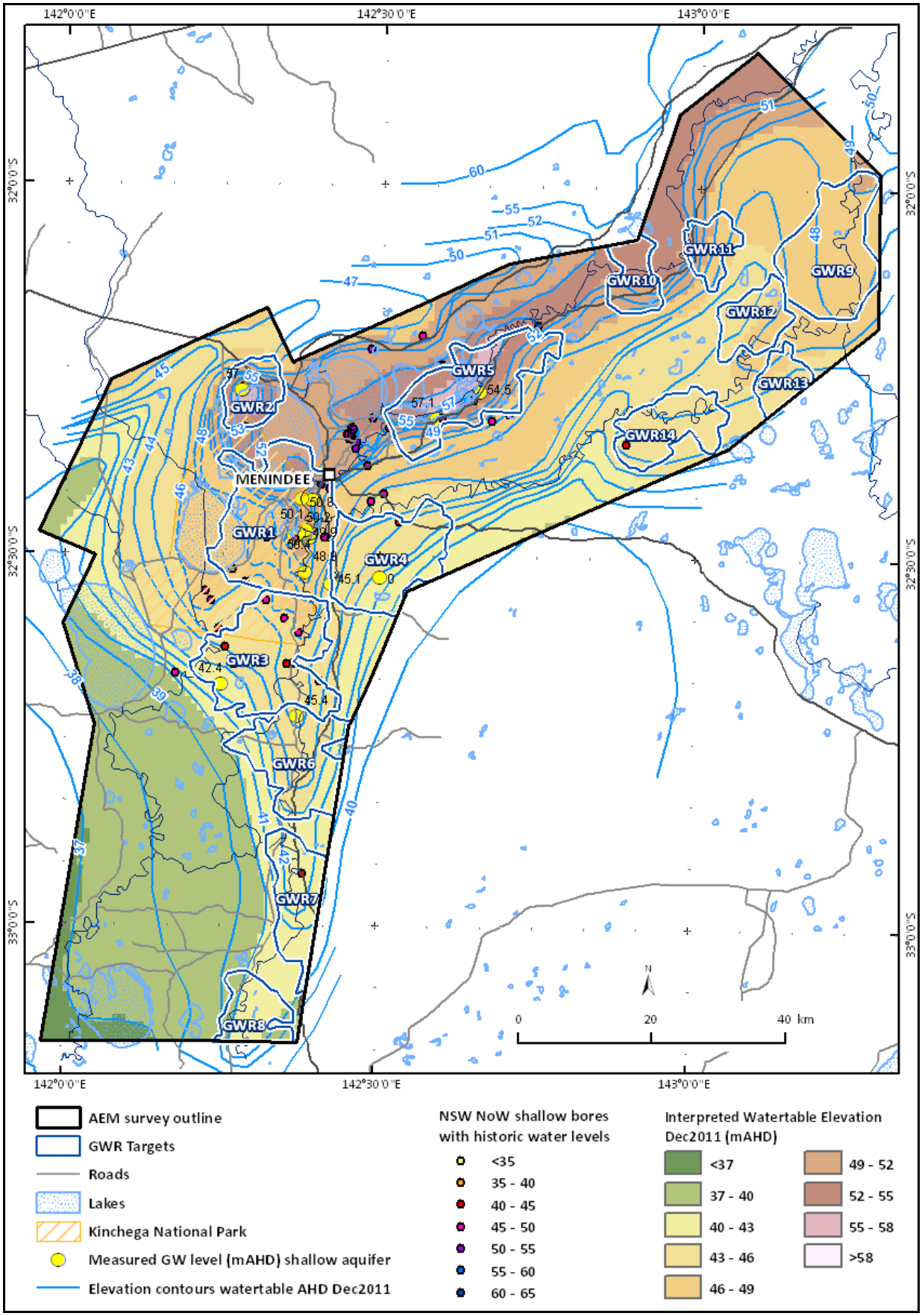

Figure 7-48. *Interpreted elevation (m AHD) of the watertable surface in the BHMAR study area for December 2011. In the absence of groundwater level measurements from BHMAR project bores, historical data from NSW Office of Water (NOW) and previous hydrogeological mapping (Brodie, 1994; Kellett, 1994) were used to interpret the watertable contours.*

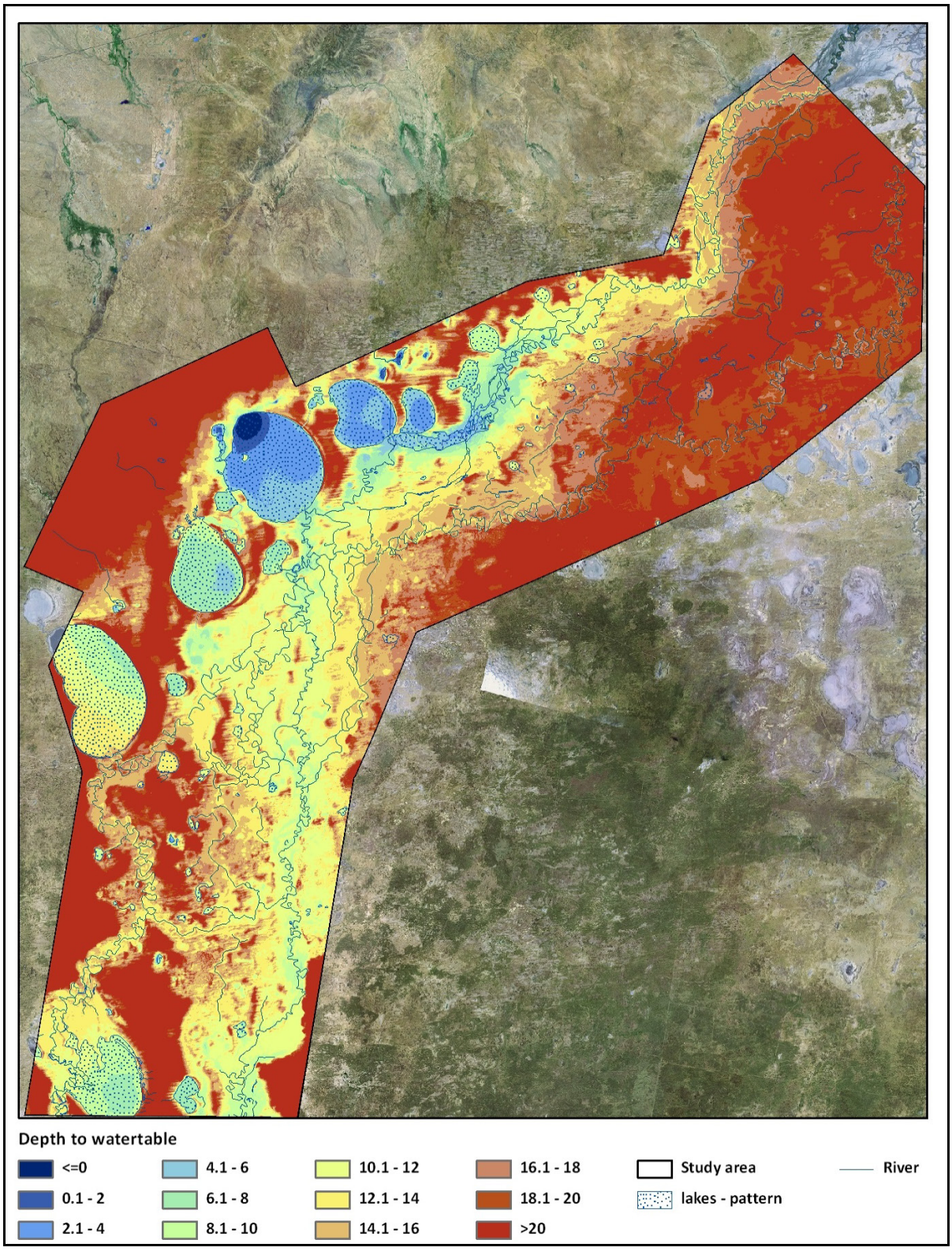

Figure 7-49. *Depth to the watertable across the BHMAR study area. This surface was computed as the difference between the potentiometric surface of the surficial aquifer and the topography. These values reflect the depth to which the rooting systems of vegetation must travel to encounter the watertable. Values of zero or less indicate the occurrence of groundwater discharge. River linework was produced for a 1:250,000 usable scale, hence there is some discrepancy between this dataset and the watertable surface.*

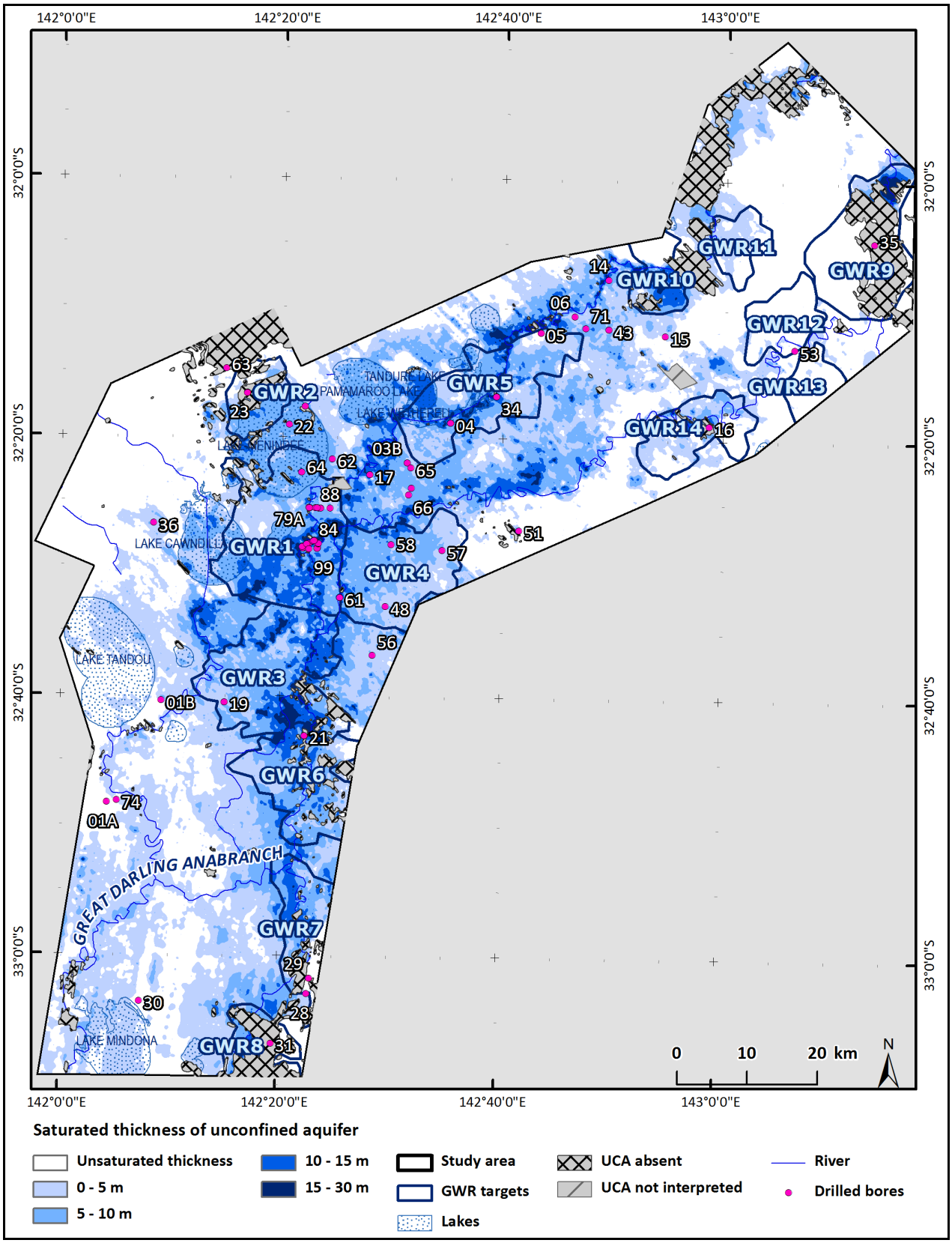

Figure 7-50. *Saturated thickness of the shallow unconfined aquifer for the BHMAR study area. This surface was computed as the difference between the watertable surface and the depth to the top of the upper confining aquitard. Where holes exist in the upper confining aquitard, saturated thickness is not shown. Away from modern drainage, the Quaternary sediments can become unsaturated and the watertable is within the underlying Calivil Formation or Loxton-Parilla Sands.*

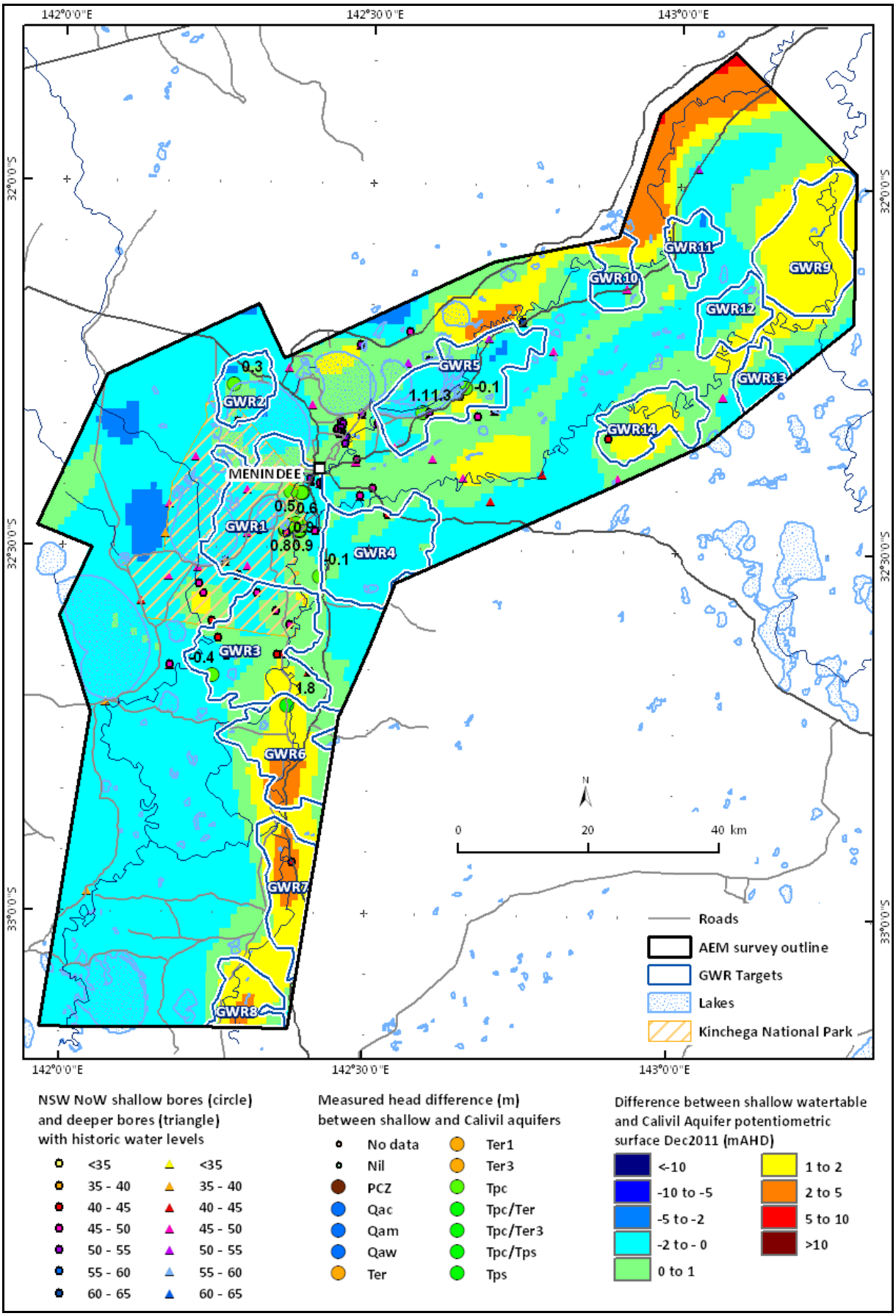

Figure 7-51. *Interpreted head difference between groundwater levels in the shallow aquifer and the Semi-confined aquifer in the BHMAR study area for December 2011. Due to the low density of monitoring bores in much of the study area, this mapping is indicative only.*

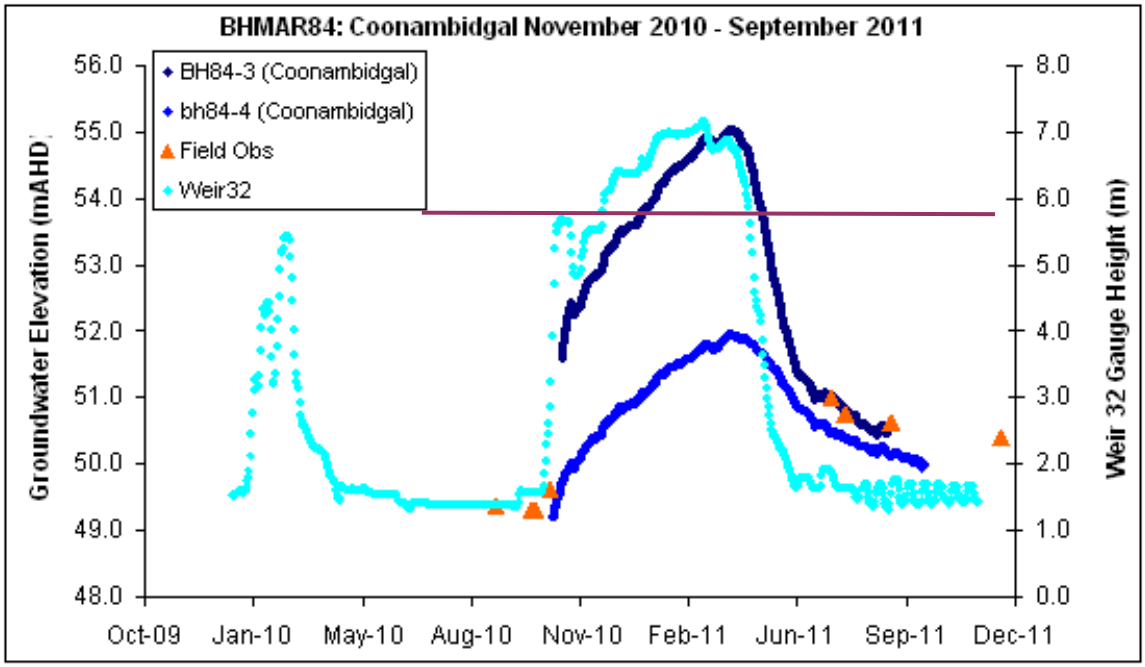

Figure 7-52. *Hydrographs of BHMAR84-3 and BHMAR84-4 screened in the Coonambidgal Formation aquifer at Jimargil. The light blue points are the Darling River stage height measurements at the Weir 32 gauge. The purple line is the Weir 32 gauge height at which overbank flow occurs. The orange triangles are manual measurements of groundwater levels in the monitoring bore as a comparison with the logger data.*

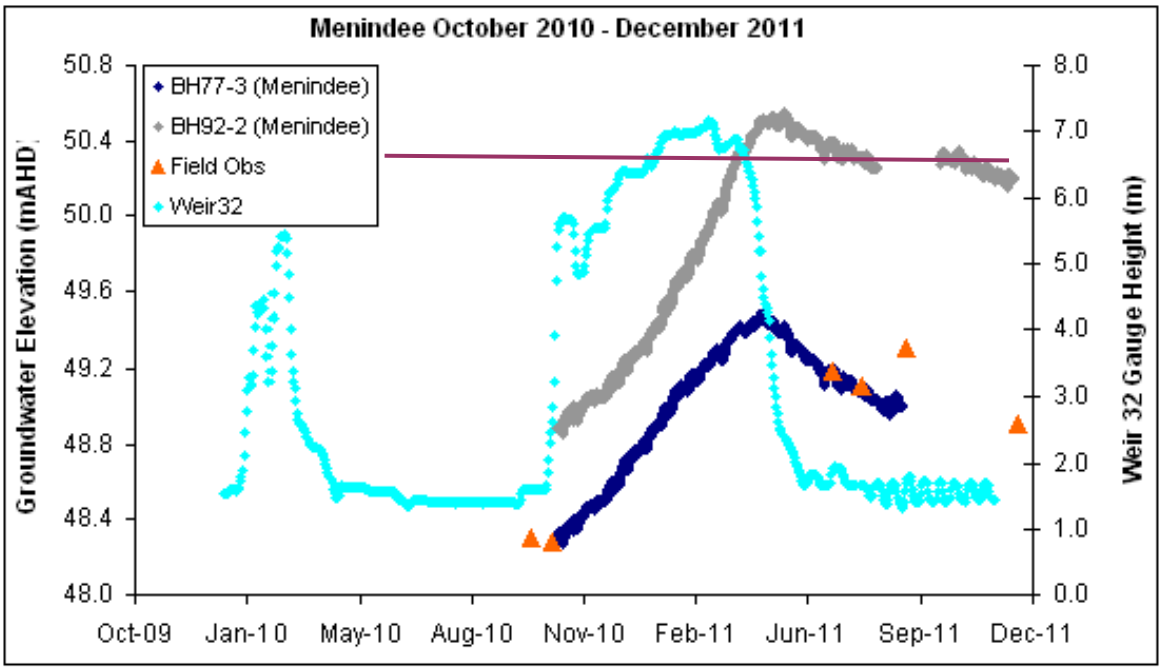

Figure 7-53. *Hydrographs for bores BHMAR77-3 and BHMAR92-2 screened in the Menindee Formation aquifer at East Bootingee. The light blue points are the Darling River stage height measurements at the Weir 32 gauge. The purple line is the Weir 32 gauge height at which overbank flow occurs. The orange triangles are manual measurements of groundwater levels in the monitoring bore as a comparison with the logger data.*

7.4.3 Groundwater Quality

Groundwater sampling from the shallow monitoring bores indicate fresh to brackish groundwater conditions (Table 7-4), with an average salinity of 615 m/L marginally above the Australian Drinking Water Guideline (ADWG2011) value for good quality water (NHMRC-NRMMC, 2011) from a salinity perspective. However, this is not representative of the shallow unconfined aquifer in its entirety across the study area, as the drilling has focused on the fresher resource targets close to the rivers and lakes. More saline shallow groundwaters can be found peripheral to the floodplain areas. Additional water quality analysis shows ADWG 2011 exceedances relating to salinity include chloride, sodium and sulfate (Table 7-4). Elevated iron and particularly manganese are the most pervasive water quality issues. ADWG2011 exceedances of redox-sensitive species, in particular ammonia, also include antimony, arsenic and uranium to a lesser degree. Water quality assessments have been made at a groundwater resource target scale (Lawrie *et al*., 2012d) as well as for the priority borefield targets (Lawrie *et al.,* 2012c).

7.5 NEAR SURFACE AQUITARD

Surficial Quaternary fluvial sediments form a complex geomorphology and near-surface hydrostratigraphy across the Darling River floodplain (Section 5.4.1). The three stratigraphic units of the Coonambidgal Formation, Menindee Formation and Willotia beds were deposited by active meandering lateral-migration phases. A feature evident in the AEM profiles and validated by drilling is near-surface deposition of overbank muds, which have buried the coarser-grained alluvial material. Figure 7-54 shows the textural composition of the Coonambidgal Formation, Menindee Formation and Willotia beds while Figure 7-55 and Figure 7-56 show the spatial distribution of different textural compositions. Secondary carbonate and illuviated-clay soil horizons can also occur in the more elevated dunefield areas. The result is a near-surface aquitard that can impede vertical infiltration in the Darling River floodplain.

Stratigraphic and lithological mapping has been undertaken for the nine depth slices within 10 m depth from land surface. These interpreted mapped are contained in entirety in Appendix 5 (Apps *et al*., 2012b) however a selection are provided here as examples of the lithostratigraphic spatial variability. Woorinen Formation fine sand, muddy sand and mud prevail within 3-4 m depth in the dunefield areas peripheral to the modern drainage (Figure 7-57 to Figure 7-60). There is a tendency for these aeolian deposits to become finer-grained with depth. Menindee Formation mud and muddy sand is dominant along the floodplain corridors, with similar Coonambidgal Formation lithologies occurring within inset corridors closest to the river. Mapping of fine sand, particularly south of Menindee, indicate areas where potential infiltration is greater. From about 5 m depth (Figure 7-61), mud and muddy sand of the Willotia beds become more apparent in the upland areas along the western margin of the BHMAR study area. This is also the case for the shallow sediments underlying the lakes. To the east, in the Talyawalka system, the fine sand to mud of the Woorinen Formation still persist to about a depth of 6.5 m (Figure 7-63). The Menindee Formation tends to become broader and more continuous with depth. Coarser sandy material can be found in the Menindee Formation along Talyawalka Creek, such as at the GWR9 target. There is also an elongate zone of sands south of Talyawalka Creek, parallel and close to the eastern boundary of the study area, most apparent in Figure 7-65. This is inferred to be a shallow Menindee Formation palaeochannel, transecting the GWR4, GWR6 and GWR7 targets.

A perspective of the near-surface aquitard can be gained by combining the shallow AEM depth slice interpretations. Figure 7-66 indicates the thickness of this hydrostratigraphic unit. Figure 7-67 is the percentage thickness of mud from surface to 9 m. The threshold thickness of 9 m was used as it approximates an average depth to the base of the Darling River from the floodplain land surface. This mapping provides a guide to near-surface infiltration potential across the study area. For example, the predominance of shallow muds in the vicinity of Lake Wetherell is likely to impede downward leakage, even if the deeper Blanchetown Clay aquitard is thin or absent at depth. This mapping is described at the groundwater resource target scale (GWR1-14) in Lawrie *et al.* (2012d).

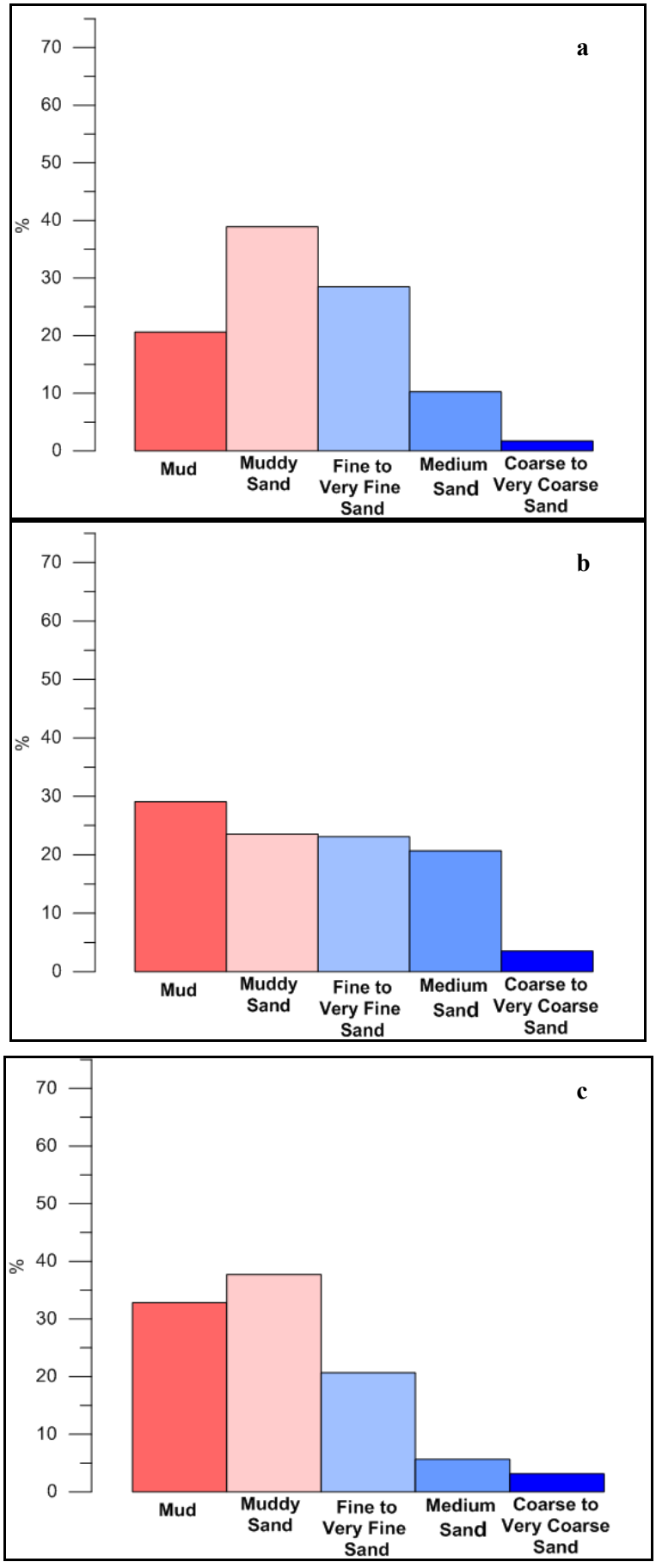

Figure 7-54. *Textural composition of a) Coonambidgal Formation, b) Menindee Formation and c) Willotia beds.*

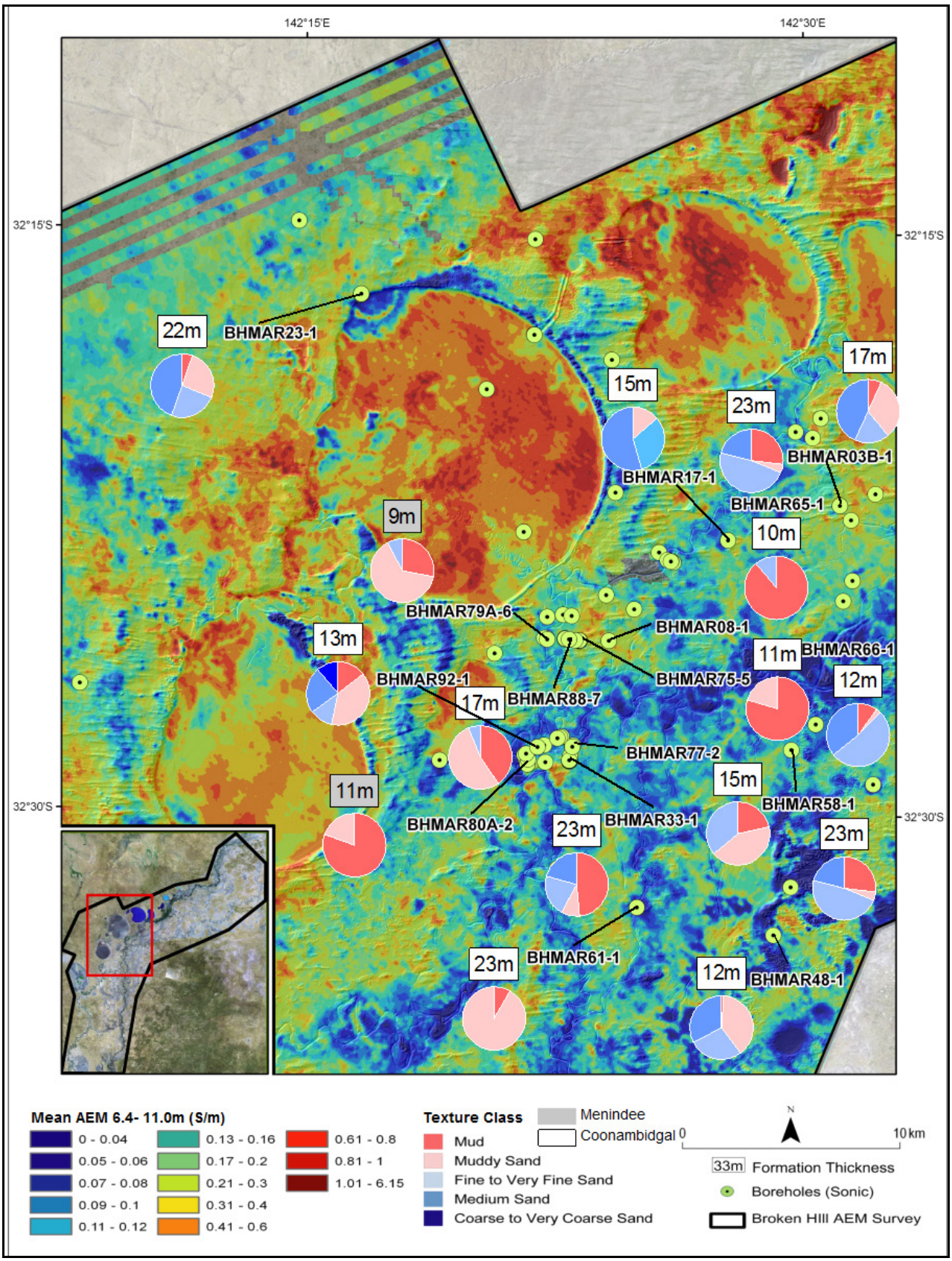

Figure 7-55. *Pie charts showing the textural composition of the Menindee and Coonambidgal Formations at several bore locations. Overall thicknesses of the formations are labelled.*

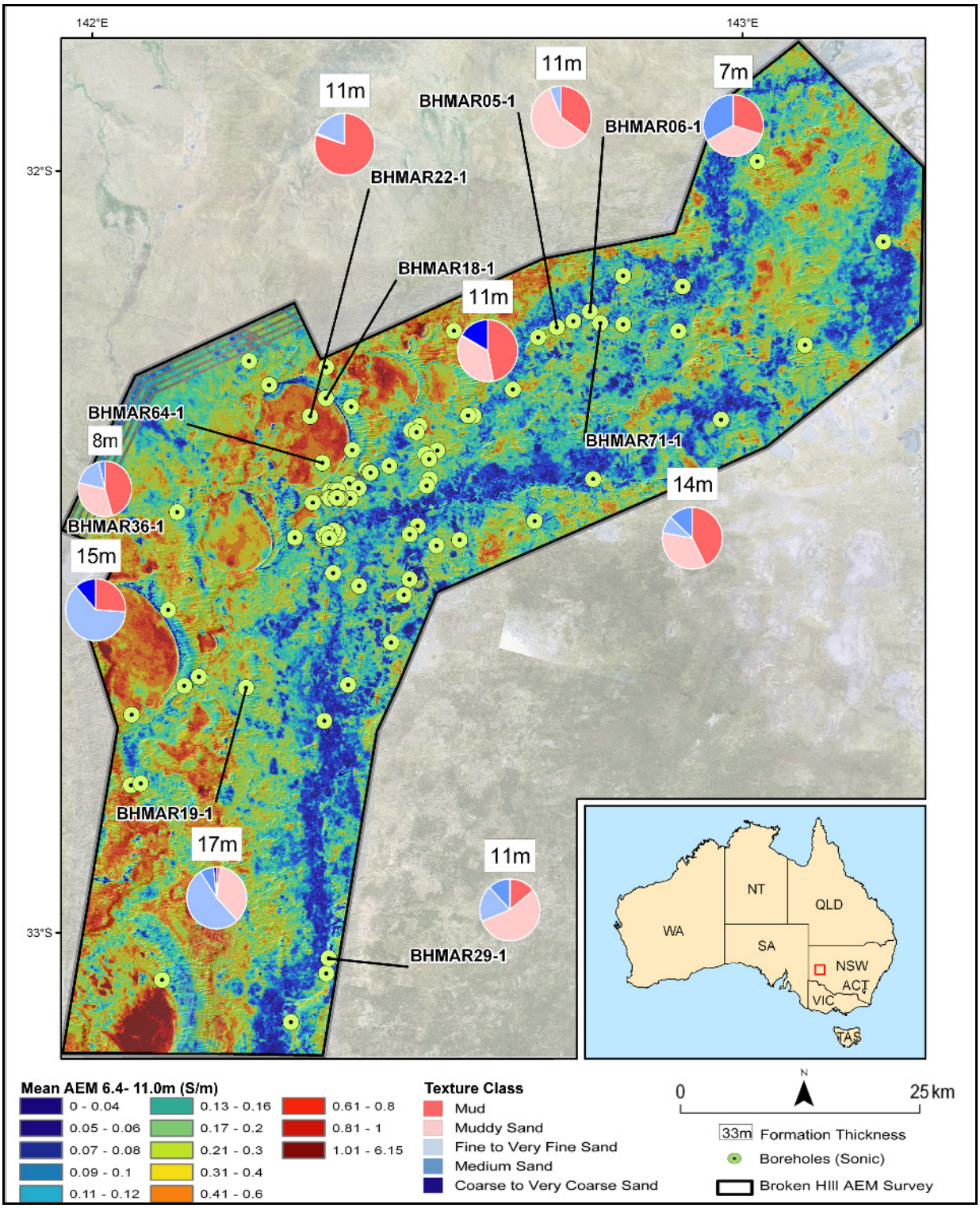

Figure 7-56. *Pie charts showing the textural composition of the Willotia beds present at several bore locations. Overall thicknesses of the unit are labelled.*

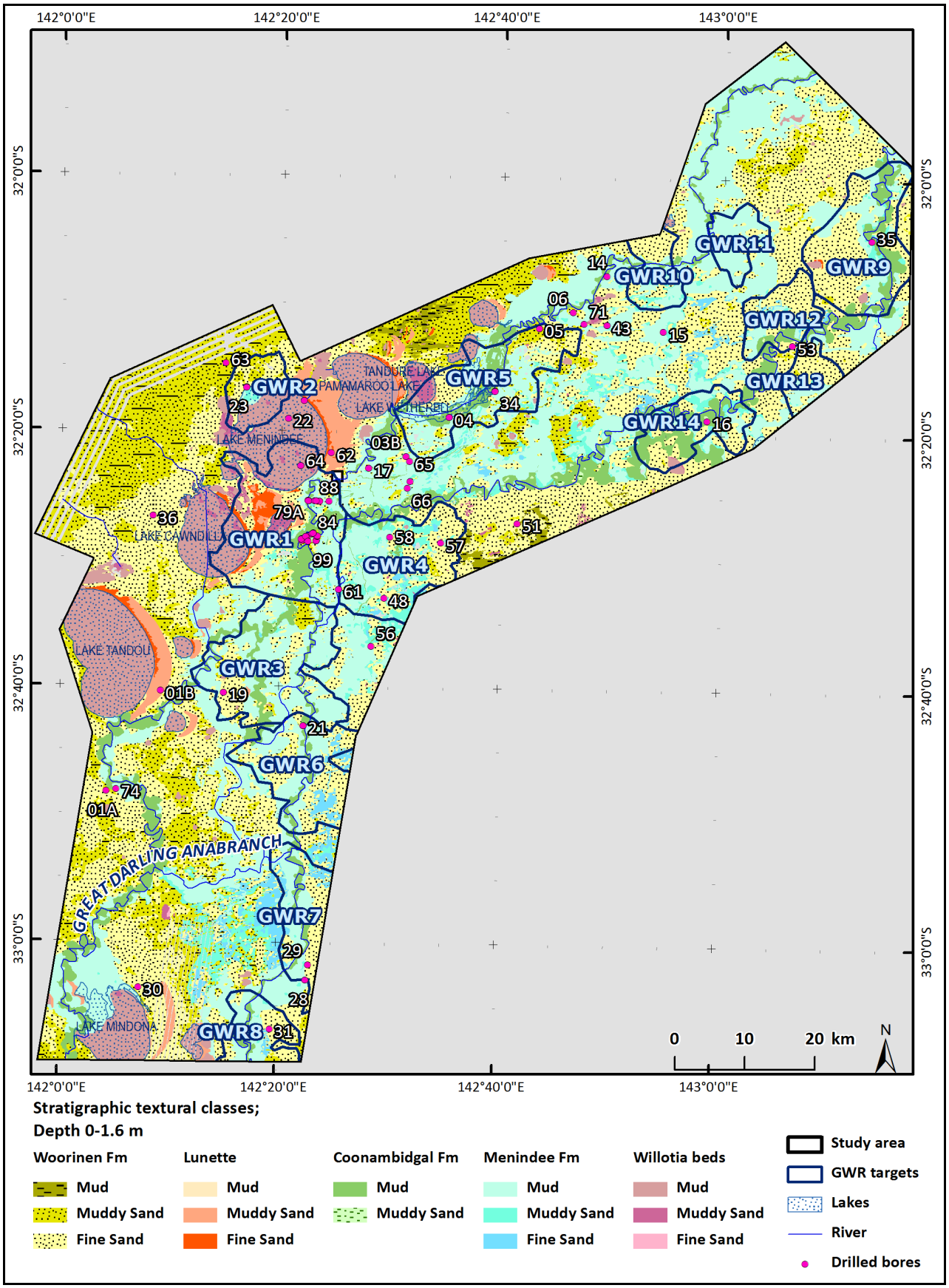

Figure 7-57. *Indicative lithology of shallow sediments including the near-surface aquitard across the project area, based on sediment textural classification, illustrating the 0-1.6 m AEM depth slice.*

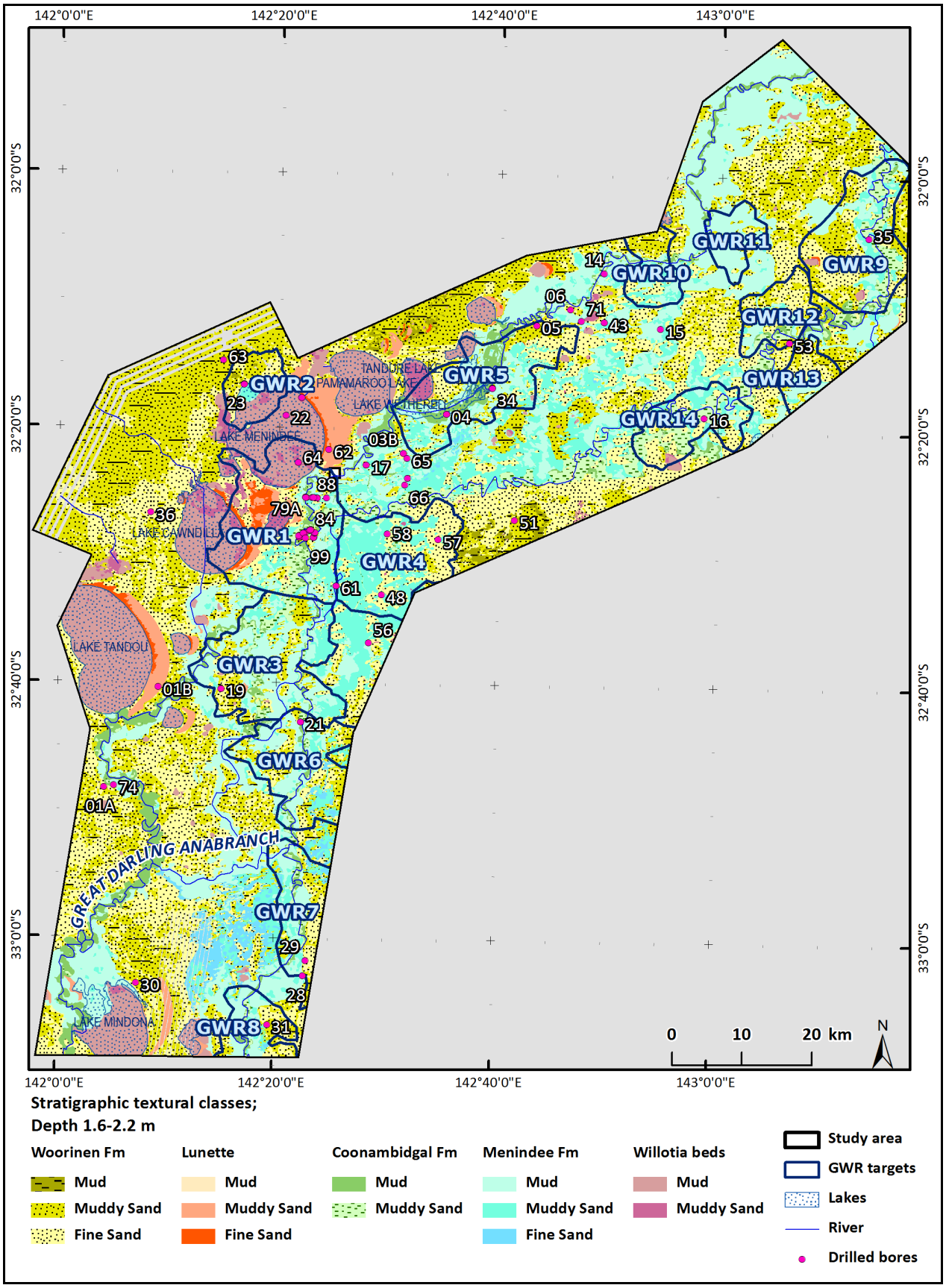

Figure 7-58. *Indicative lithology of shallow sediments including the near-surface aquitard across the project area, based on sediment textural classification, illustrating the 1.6-2.2 m AEM depth slice.*

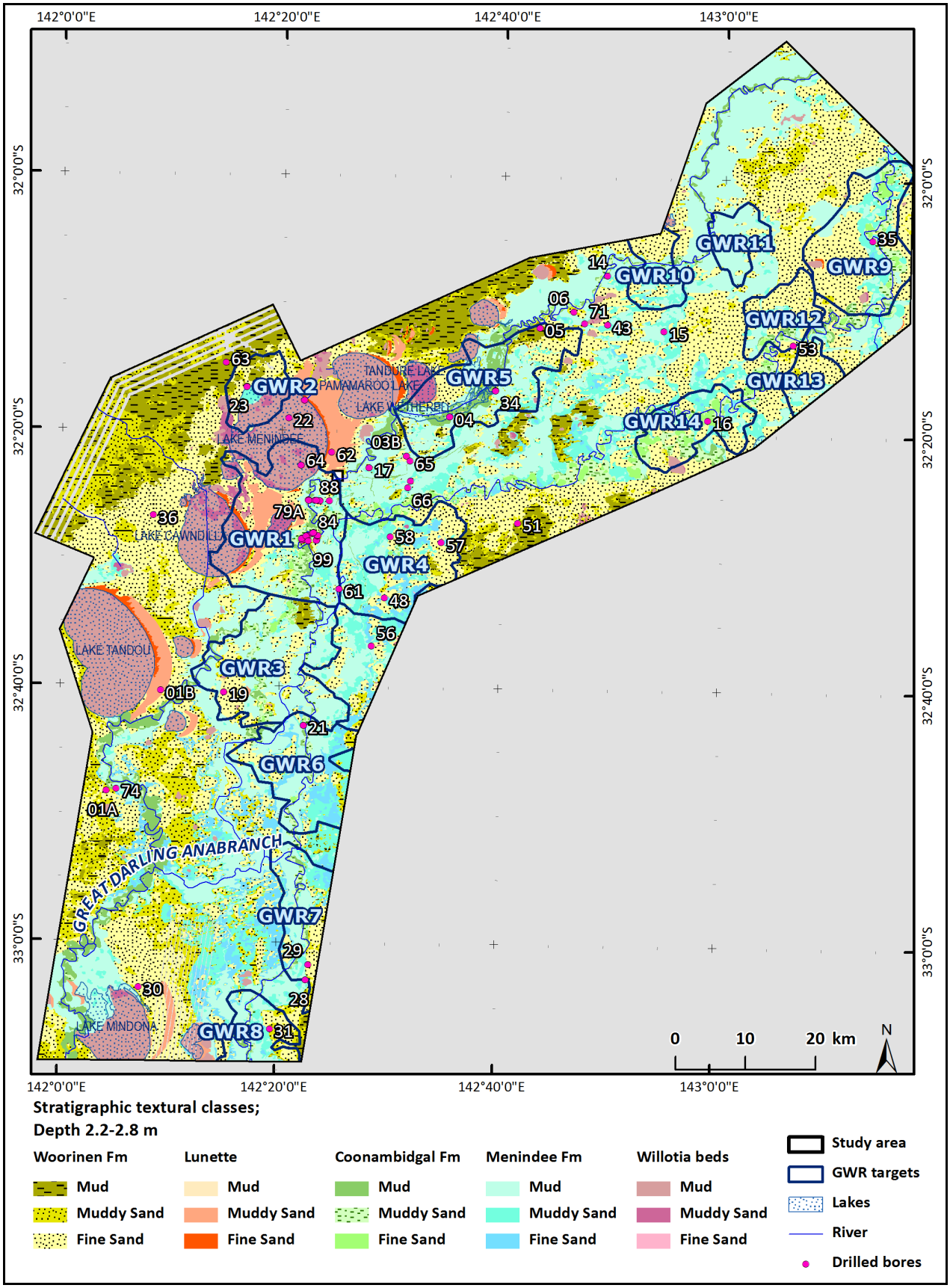

Figure 7-59. *Indicative lithology of shallow sediments including the near-surface aquitard across the project area, based on sediment textural classification, illustrating the 2.2-2.8 m AEM depth slice.*

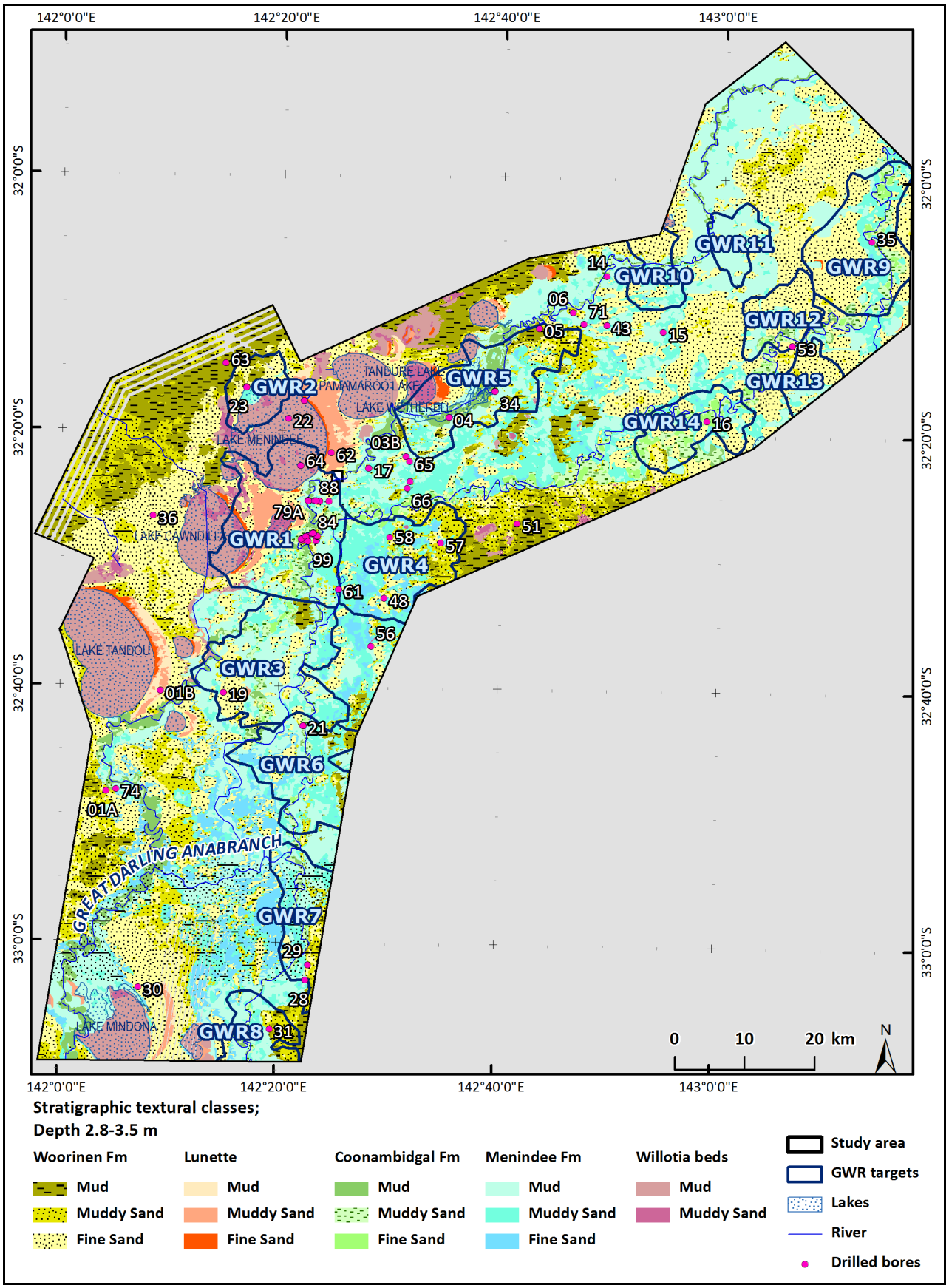

Figure 7-60. *Indicative lithology of shallow sediments including the near-surface aquitard across the project area, based on sediment textural classification, illustrating the 2.8-3.5 m AEM depth slice.*

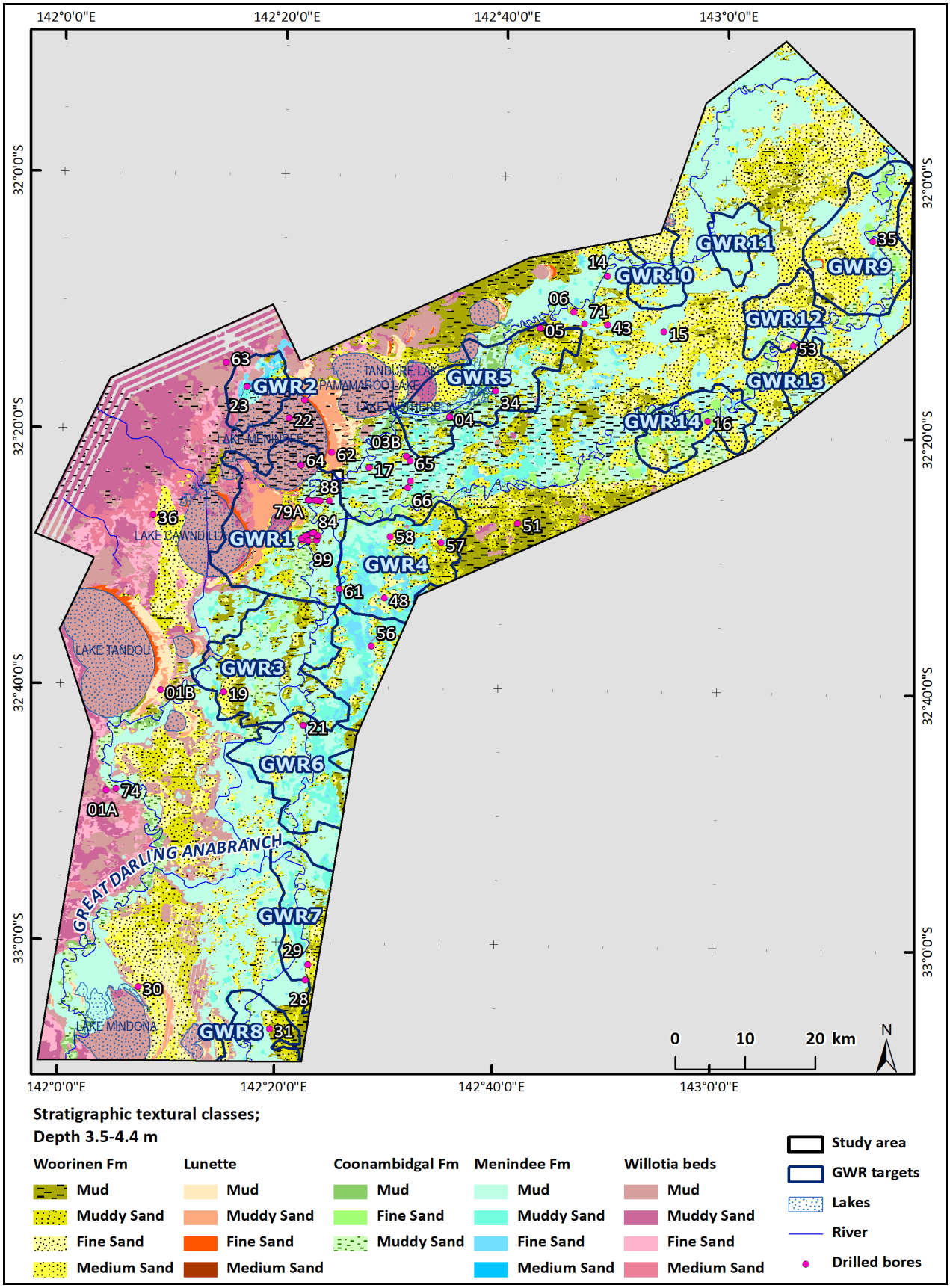

Figure 7-61. *Indicative lithology of shallow sediments including the near-surface aquitard across the project area, based on sediment textural classification, illustrating the 3.5-4.4 m AEM depth slice.*

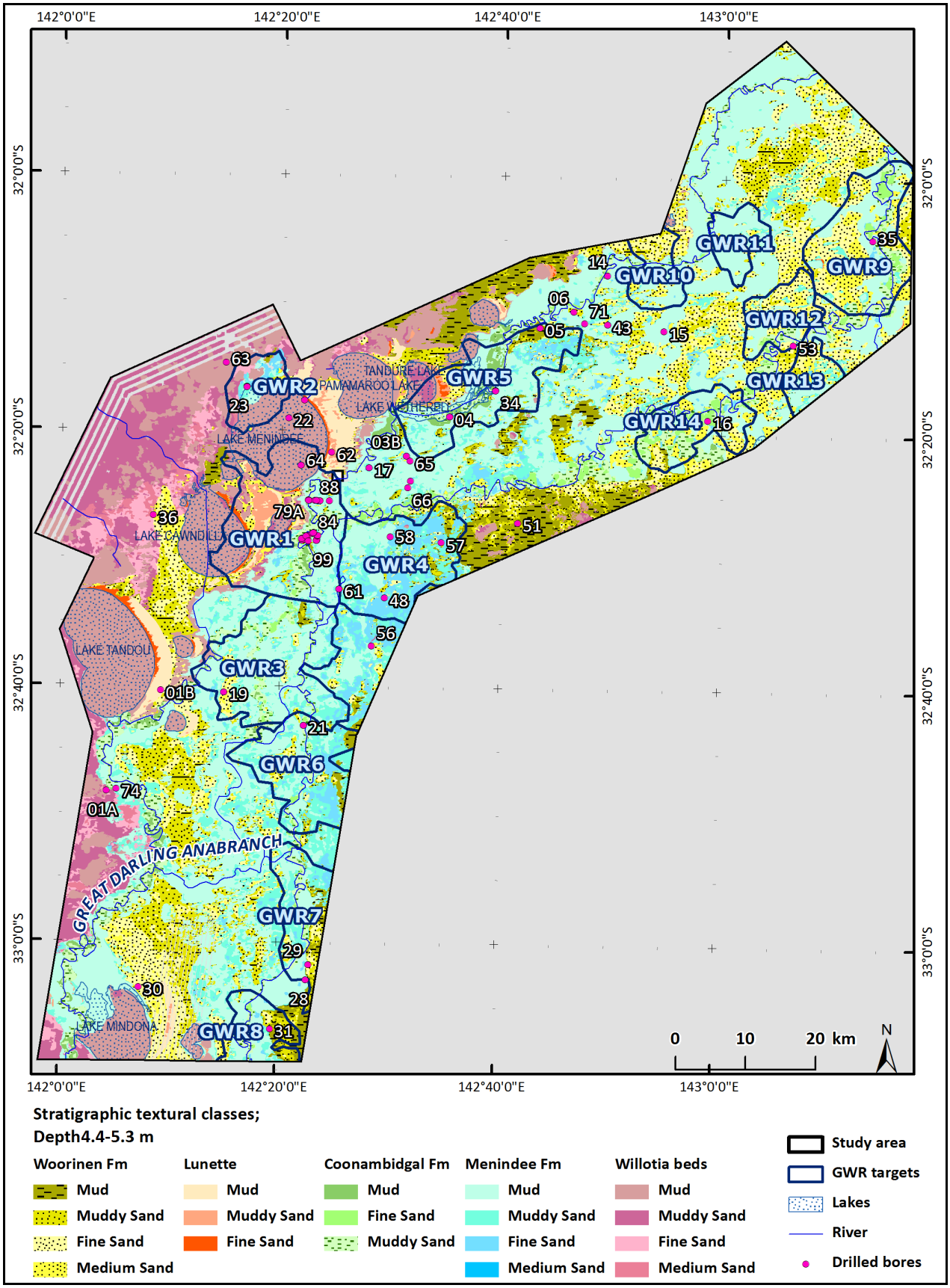

Figure 7-62. *Indicative lithology of shallow sediments including the near-surface aquitard across the project area, based on sediment textural classification, illustrating the 4.4-5.3 m AEM depth slice.*

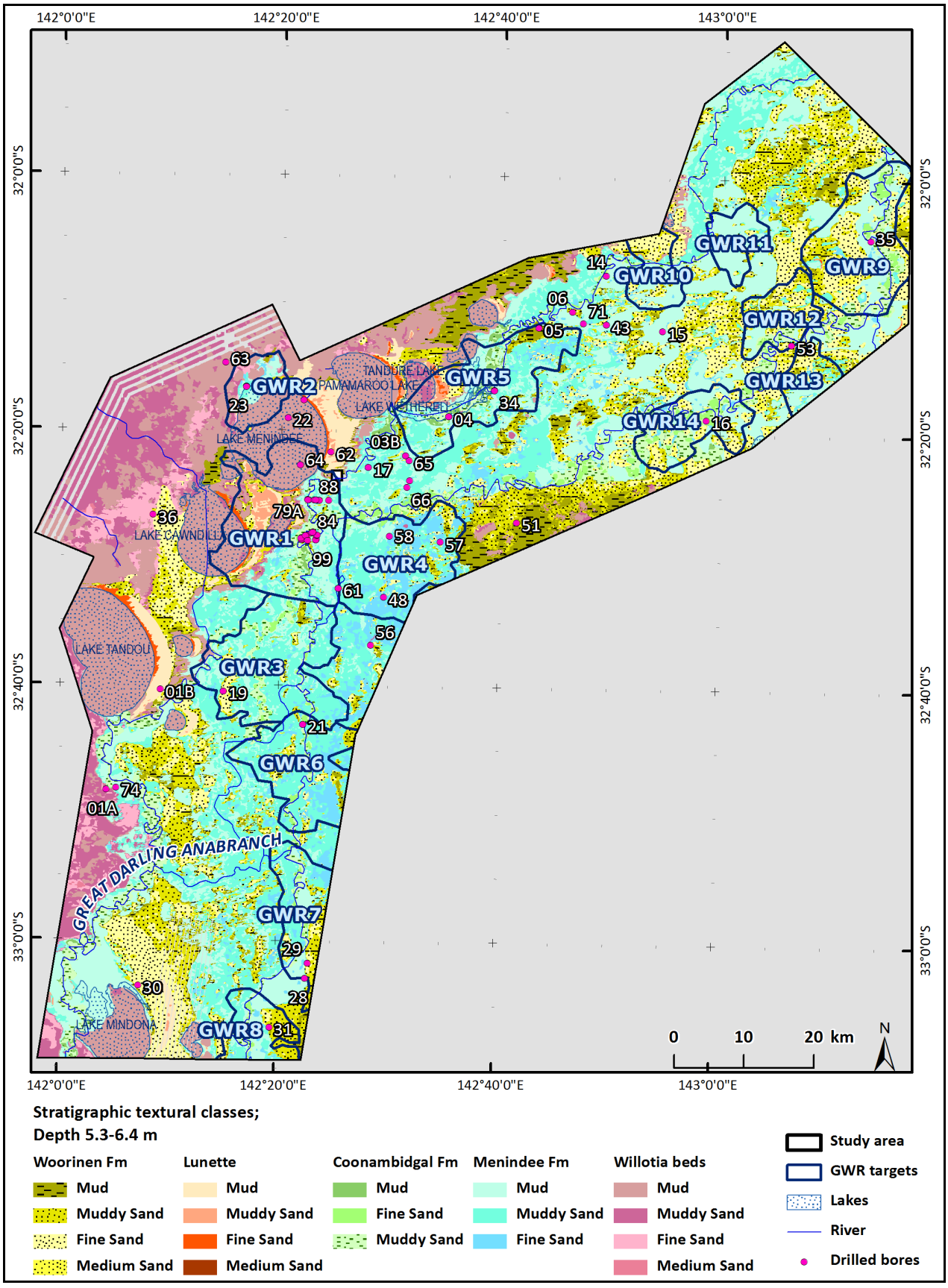

Figure 7-63. *Indicative lithology of shallow sediments including the near-surface aquitard across the project area, based on sediment textual classification, illustrating the 5.3-6.4 m AEM depth slice.*

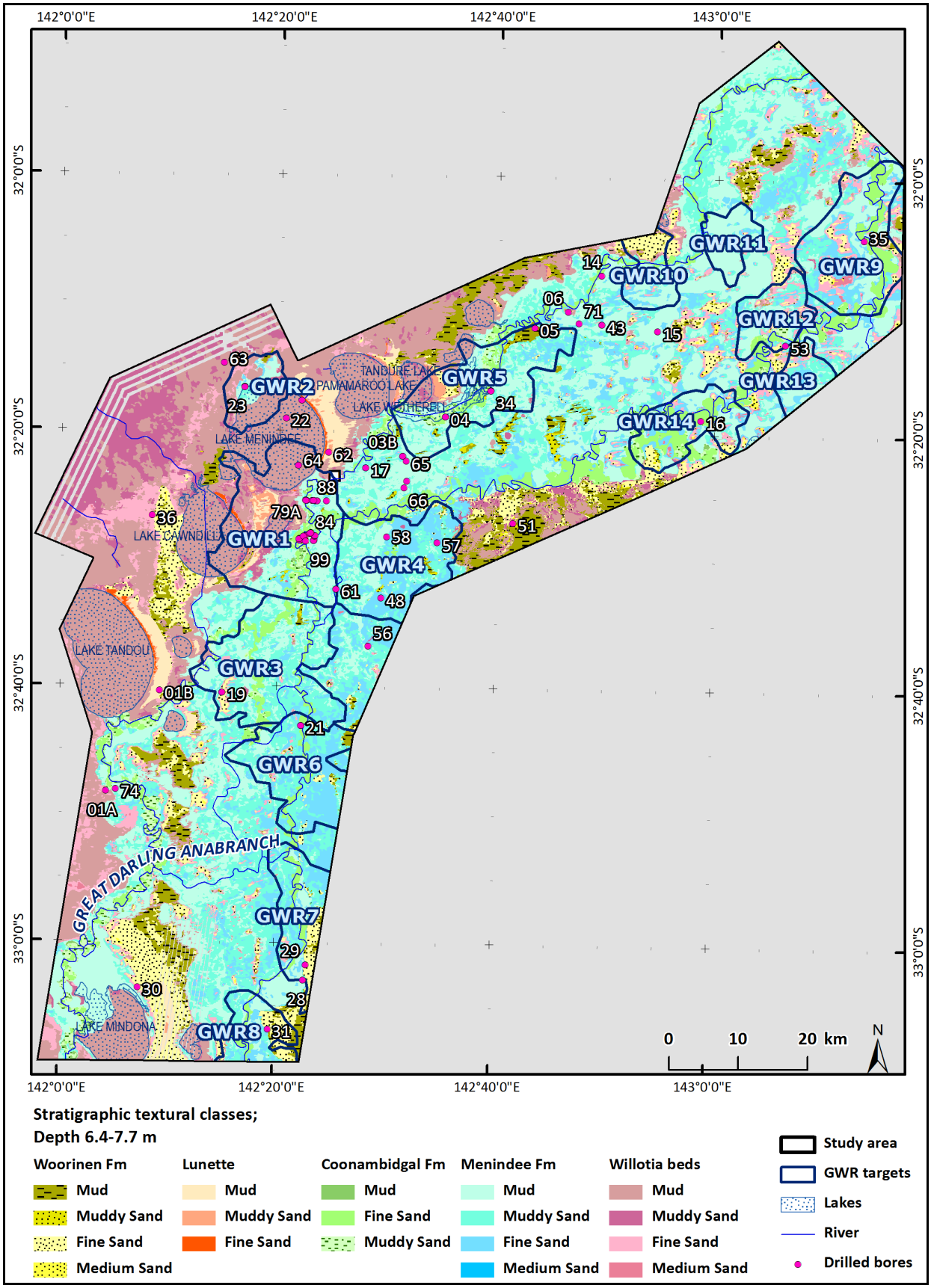

Figure 7-64. *Indicative lithology of shallow sediments including the near-surface aquitard across the project area, based on sediment textural classification, illustrating the 6.4-7.7 m AEM depth slice.*

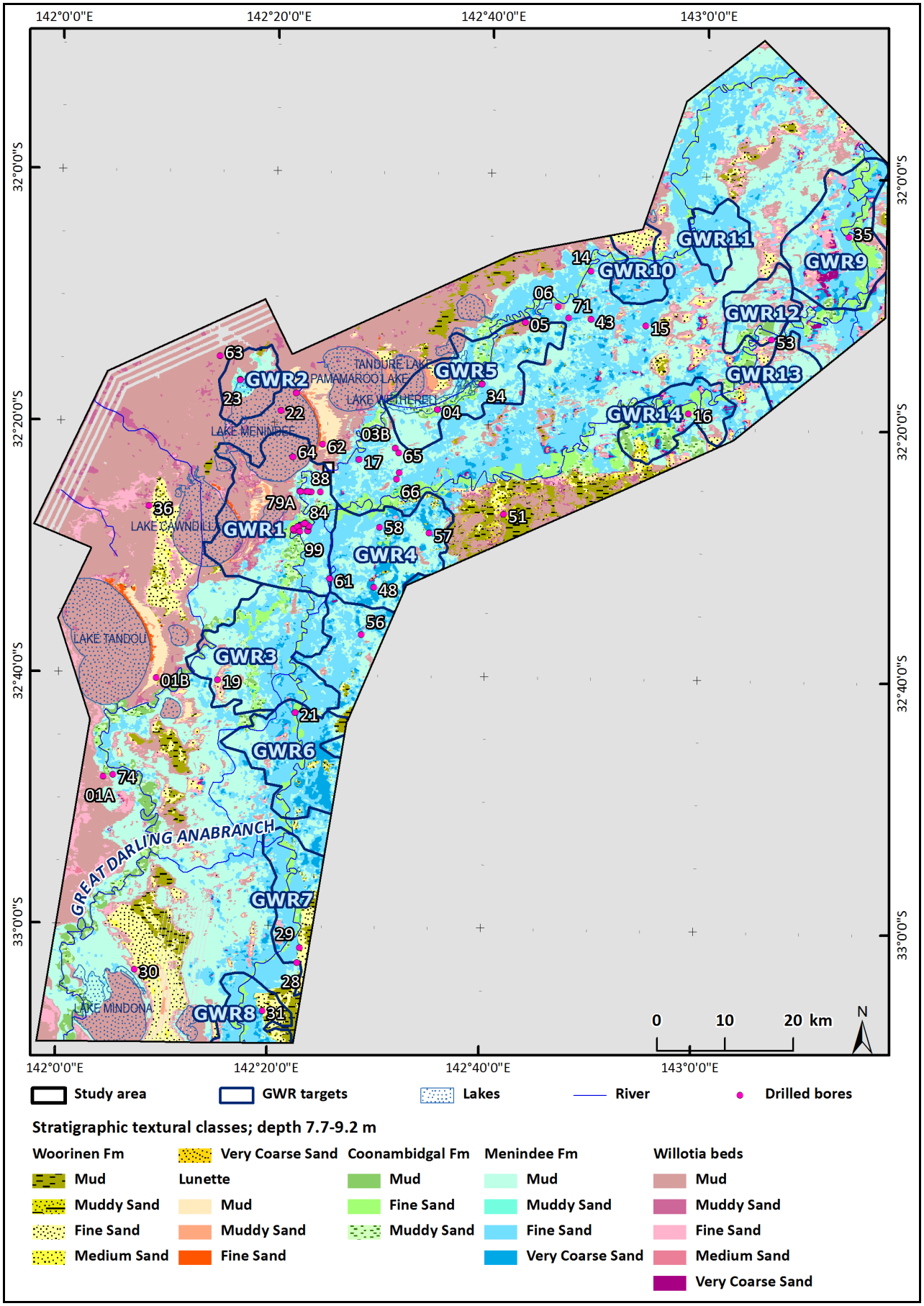

Figure 7-65. *Indicative lithology of shallow sediments including the near-surface aquitard across the project area, based on sediment textural classification, illustrating the 7.7-9.2 m AEM depth slice.*

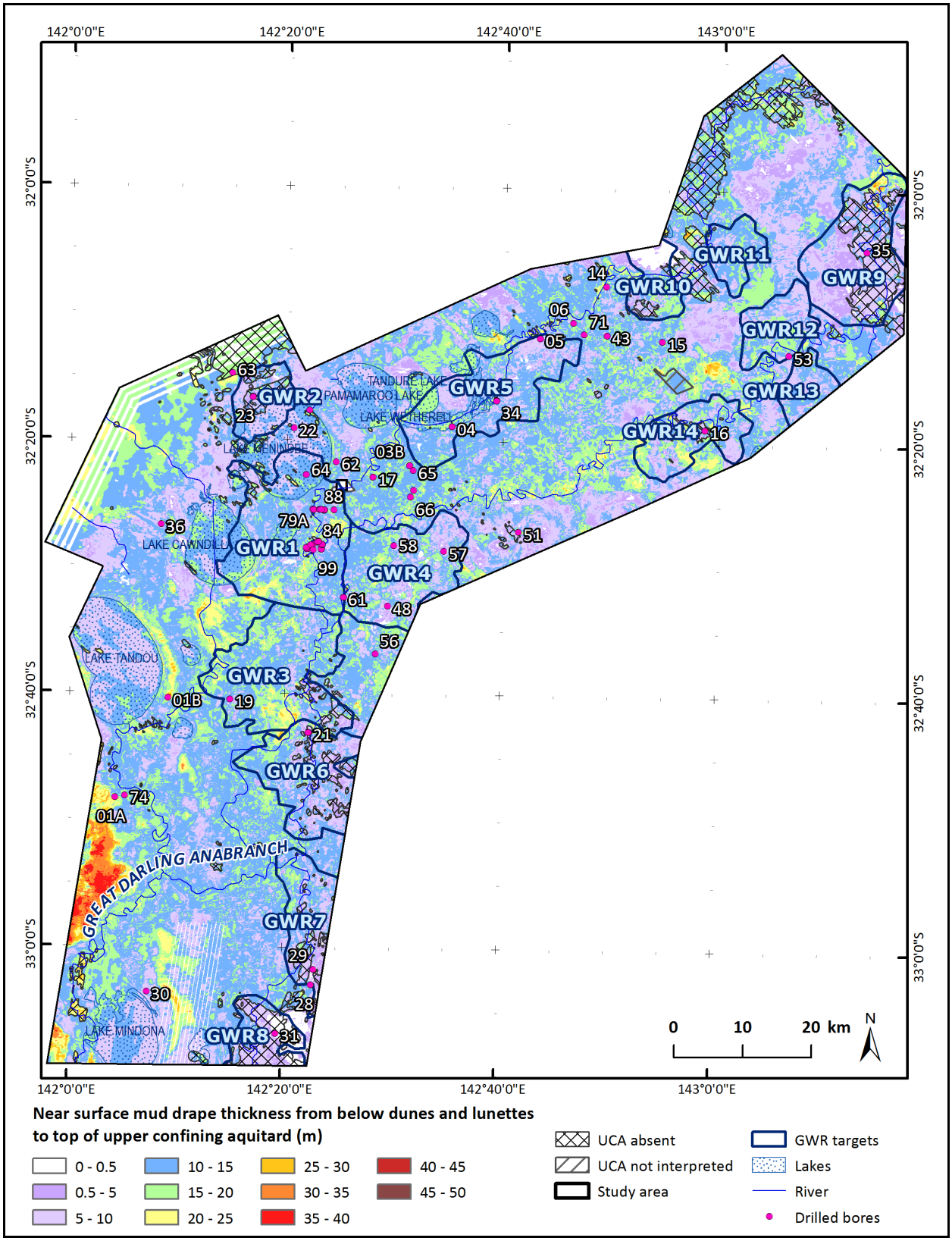

Figure 7-66. *Thickness of near-surface (mud) aquitard. River linework was produced for a 1:250,000 usable scale, hence there is some discrepancy between this dataset and the near-surface aquitard mapping.*

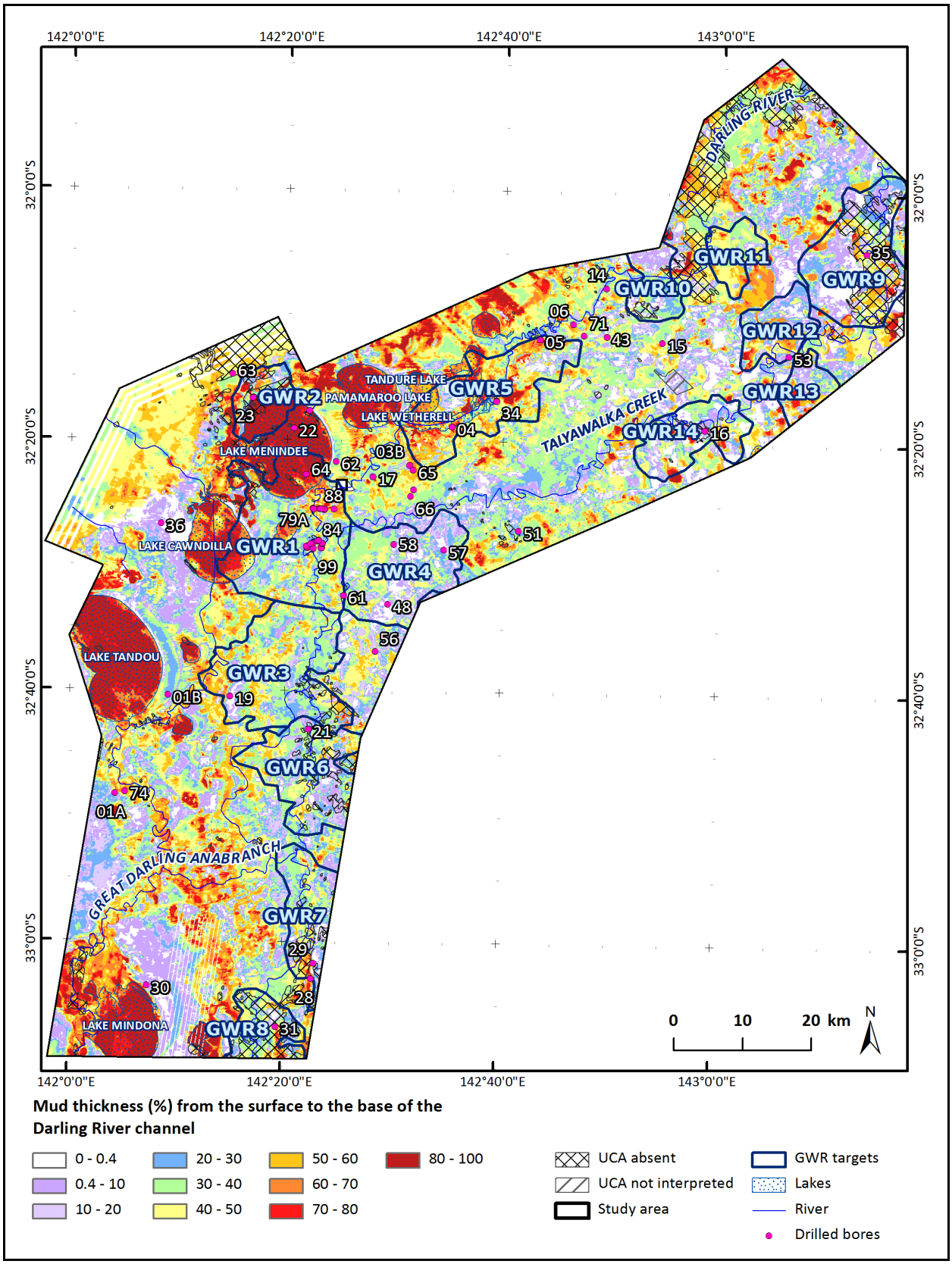

Figure 7-67. *Percentage thickness of near-surface (mud) aquitard from ground surface to the base of the Darling River (~9 m depth). River linework was produced for a 1:250,000 usable scale, hence there is some discrepancy between this dataset and the near-surface aquitard mapping.*

8. Hydrochemistry

A comprehensive water sampling program, as summarised in Table 8-1, was undertaken to assess potential water quality issues associated with possible MAR and groundwater extraction options. The sampling and analytical methods are documented in Lawrie *et al.* (2012a). Measured field parameters included electrical conductivity, pH, dissolved oxygen, Eh, turbidity, temperature, total alkalinity and specific ions (sulfide, ferrous iron and total iron). Typically, major ions and trace metal analyses were undertaken as well as nutrients, organic carbon and stable isotopes. Other analysis focussed on tracers such as radon, chlorofluorocarbons, radiocarbon and strontium isotopes Overall, 184 groundwaters from 104 bores, 1144 pore fluids from 49 cored holes, 56 surface waters from 27 sites and 10 rainfall samples were collected and analysed (Table 8-1). This project data was supplemented by historic water quality monitoring for the area available from NSW State Water and NSW Office of Water.

Table 8-1. *Summary of BHMAR hydrochemical analyses. Raw data is available in Appendix 6 (Somerville et al., 2012).*

Sample Type	Number of Sites	Number of Samples
Cumulative Rainfall	1	10
Lake Storage	17	17
River or stream	10	32
Treated water supply	3	7
Groundwater	104	184
Pore Fluids	49	1144

More complete assessment of the hydrochemistry from a MAR perspective is reported in Lawrie *et al*. (2012c), with consideration of groundwater characterisation and hydrochemical processes from a groundwater resource perspective in Lawrie *et al*. (2012d). The data are available in full in Appendix 6 (Somerville *et al*., 2012).

8.1 MAJOR ION CHEMISTRY

The major ion chemistry for groundwater and surface water samples (Figure 8-1) and pore fluid samples (Figure 8-2) provide important insights into hydrological processes, as well for the assessment of potential water quality issues associated with MAR operations or groundwater extraction.

Piper diagrams are designed to summarise the significant hydrochemical relationships between the water samples. Figure 8-1 is the Piper diagram for the rainfall, surface water and groundwater samples and Figure 8-2 is the equivalent for the pore fluid samples. Some key points from these plots are:

1. Many of the shallow unconfined Coonambidgal Formation, Menindee Formation and Willotia beds groundwaters have a Na-Ca-Mg-HCO_3 type chemistry, similar to that of the surface water samples (Figure 8-1). This indicates that river (and/or lake) leakage is important for recharge to the shallow aquifer.

– Local rainfall samples have distinctive major ion compositions, and are relatively enriched in calcium and depleted in magnesium (Figure 8-1). The groundwater samples that have the closest affinity with the rainfall samples are in the very shallow unconfined Willotia beds or Coonambidgal Formation (Figure 8-1). However, an overall lack of affinity between groundwater and rainfall samples suggests that diffuse rainfall recharge to the shallow aquifer is not significant in comparison with leakage from the rivers and lakes. This is consistent with observations of significant ponding in the landscape for many months after heavy rainfall events, and estimates of very low recharge (<1 mm/yr) calculated using the chloride mass balance rainfall recharge estimation methodology (Harrington *et al*., 2011; Lawrie *et al*., 2012a).

- The groundwaters can be loosely placed into two groups (Figure 8-1). A saline 'evolved' group with a Na-Cl-SO_4 signature plotting along the right hand margin of the Piper diagram can be differentiated from the fresher 'leakage' sample group with the surface water affinity (Figure 8-1). These 'evolved' groundwater samples are located away from the present day rivers or at depth within semi-confined (Calivil Formation) to confined (Renmark Group and Paleozoic) aquifers. Groundwater samples plotting intermediate between the surface water and saline evolved end-members, notably in the Calivil Formation aquifer, are interpreted as a product of mixing.
- The Piper diagram for the pore fluids shows a similar but broader distribution in water types (Figure 8-2). Although there is considerably more scatter, the two broad groups (evolved and leakage) are recognisable. The greater scatter in pore fluid chemistry reflects the broader sampling of the hydrostratigraphy, whilst the groundwater samples only sample the more transmissive units. The deeper pore fluids in the Renmark Group and Paleozoic are dominantly the evolved Na-Cl-SO_4 water type. The pore fluids in the shallow unconfined aquifers (Woorinen, Coonambidgal and Menindee Formations, and Willotia beds) plot across the leakage and evolved groups, reflecting the spatial variability of recharge associated with river leakage and also the potential for evapotranspirative processes to drive near-surface salinisation (Figure 8-1). For the semi-confined Calivil Formation aquifer, the pore fluids are also spread across the two groups. The Na-(Ca-Mg)-HCO_3-Cl water type can be found within a few kilometres of the river.
- The hydrochemical evolution of the groundwater in the Calivil Formation aquifer appears to occur in two main stages. In the cation ternary diagram of the Piper diagram (Figure 8-1) the initial trend from the signature of the shallow aquifer and surface waters is that of enrichment of sodium at the expense of calcium. There is then a progressive enrichment of sodium, relative to both magnesium and calcium. This is inferred to be due to ion exchange, initially calcium by sodium and progressing to calcium and magnesium exchange by sodium. In the anion ternary diagram, the overall trend is a progressive enrichment of chloride, relative to bicarbonate. The second phase of the hydrochemical trend also involves a relative addition of sulfate.
- The upper confining (predominantly Blanchetown Clay) aquitard varies significantly in moisture content and pore fluid composition, with a mixed 'leakage' signature also evident in some Blanchetown Clay pore fluids (Figure 8-2). Samples showing this 'leakage' signature are within a couple of kilometres of the major rivers and where the mud is particularly thin and/or in proximity to faults with significant offsets or where tectonics have caused sharp 'warps' in the aquitard. This suggests that the Blanchetown Clay is an aquitard of varying effectiveness across the project area.

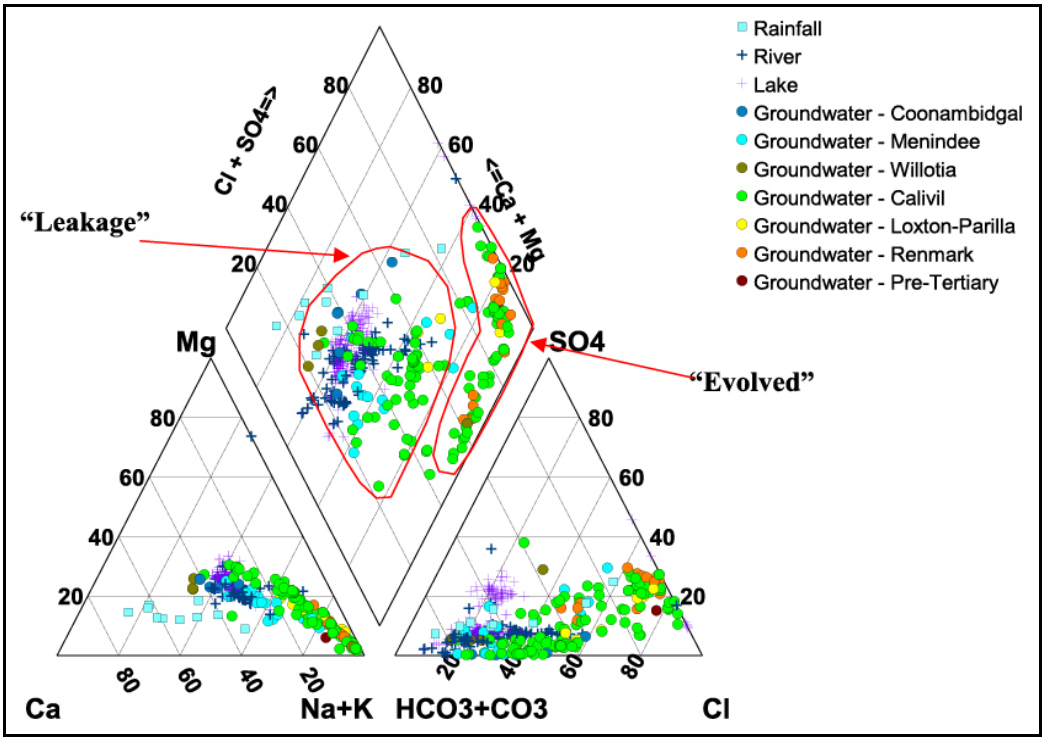

Figure 8-1. *Piper diagram of major ion analyses of rainfall, surface water and groundwater samples.*

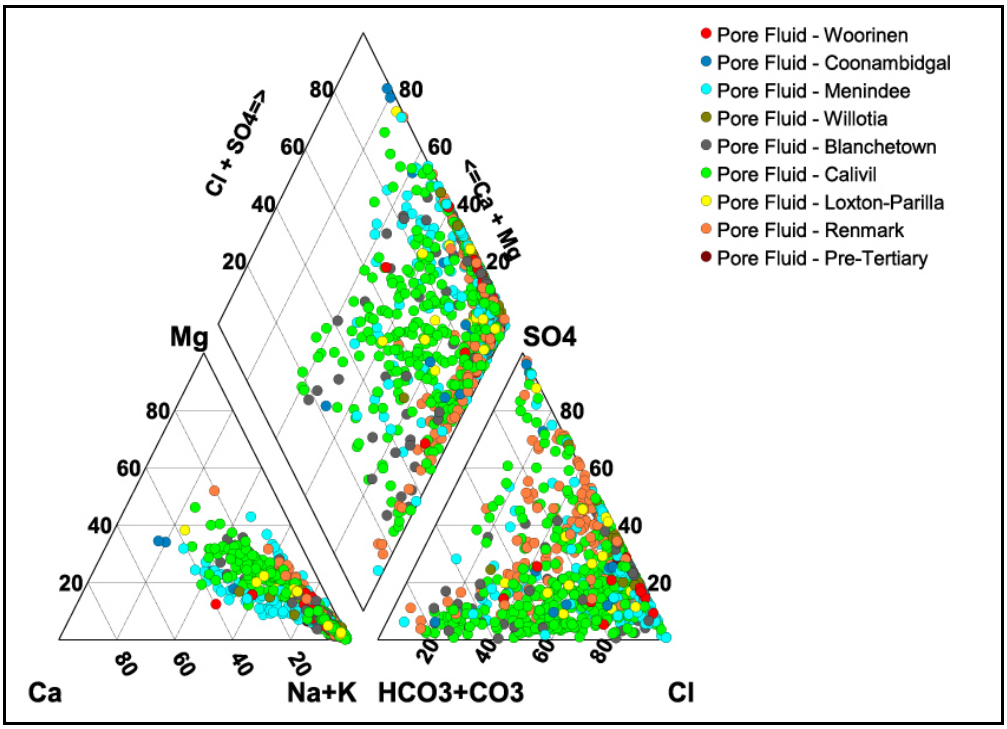

Figure 8-2. *Piper diagram of major ion analyses of pore fluid samples.*

These trends are explored further in scatter plots of salinity and major ions. The relationship between electrical conductivity (EC) and total dissolved solids (TDS) are explored in Figure 8-3a-d. As expected, there is a strong positive correlation, with the overall relationship being EC=0.68TDS (R^2>0.99) for the combined groundwaters, surface waters and rainfall samples (Figure 8-3a). However, there are differences in the TDS/EC ratio between fresh-brackish and saline groundwaters. For the former (<10,000 EC), the ratio is lower with EC=0.58TDS with R^2~ 0.99 (Figure 8-3c). This difference is interpreted to be due to the variation in dominant ions with groundwater evolution, with fresh groundwaters being typically Na-Ca-Mg-HCO_3 and saline being a Na-Cl water type. The TDS-EC relationship for the pore fluids is also strongly linear (Figure 8-3b), but has a higher proportionality (0.72) than that for the groundwaters (0.68). This is most likely due to the difference in the data populations between these two datasets, with the pore fluids having a much greater representation of saline waters (Figure 8-3b) than the groundwater samples (Figure 8-3a). The TDS/EC ratio is also lower for the fresh to brackish pore fluids (<10,000 EC) with a value of 0.65 (Figure 8-3d).

The Na and Na/Cl plots also reflect the general increase in salinity from rainfall, surface waters, shallow groundwaters, Calivil Formation groundwaters to the deeper Renmark Group groundwaters (Figure 8-4a). However, there are exceptions to the general trend, as groundwater salinity will also be a function of distance from the river as well as aquifer depth. A similar transition of increasing salinity from the Calivil Formation to the Renmark Group is also evident for the pore fluids (Figure 8-4b). The difference is that there are pore fluids in the shallow units (such as Menindee Formation and Willotia beds) which have very high salinities, inferred to be due to evapotranspirative concentration, particularly in areas of shallow watertable. This is also evident in the EC-TDS plot (Figure 8-3b). In both plots, most samples plot above the Na:Cl equivalence line. This is inferred to be due to relative enrichment of sodium by processes such as ion exchange. In Figure 8-4c, the progression towards a Na-Cl water type with increasing salinity is indicated by a merging toward the Na:Cl equivalence line, notably for the river, lake and Renmark Group samples. Although there is much greater scatter, this trend is also the case for the pore fluids, particularly for the Renmark Group samples (Figure 8-4d).

The Na-HCO_3 plot (Figure 8-5a) also shows the relative changes in bicarbonate with groundwater salinity. For river, lake and fresh groundwaters there is a dominance of sodium bicarbonate. For the deeper Na-Cl type groundwaters, the bicarbonate levels plateau with higher salinity. In contrast, the pore fluids tend to be in the higher salinity range where there is limited relationship between sodium and bicarbonate (Figure 8-5b).

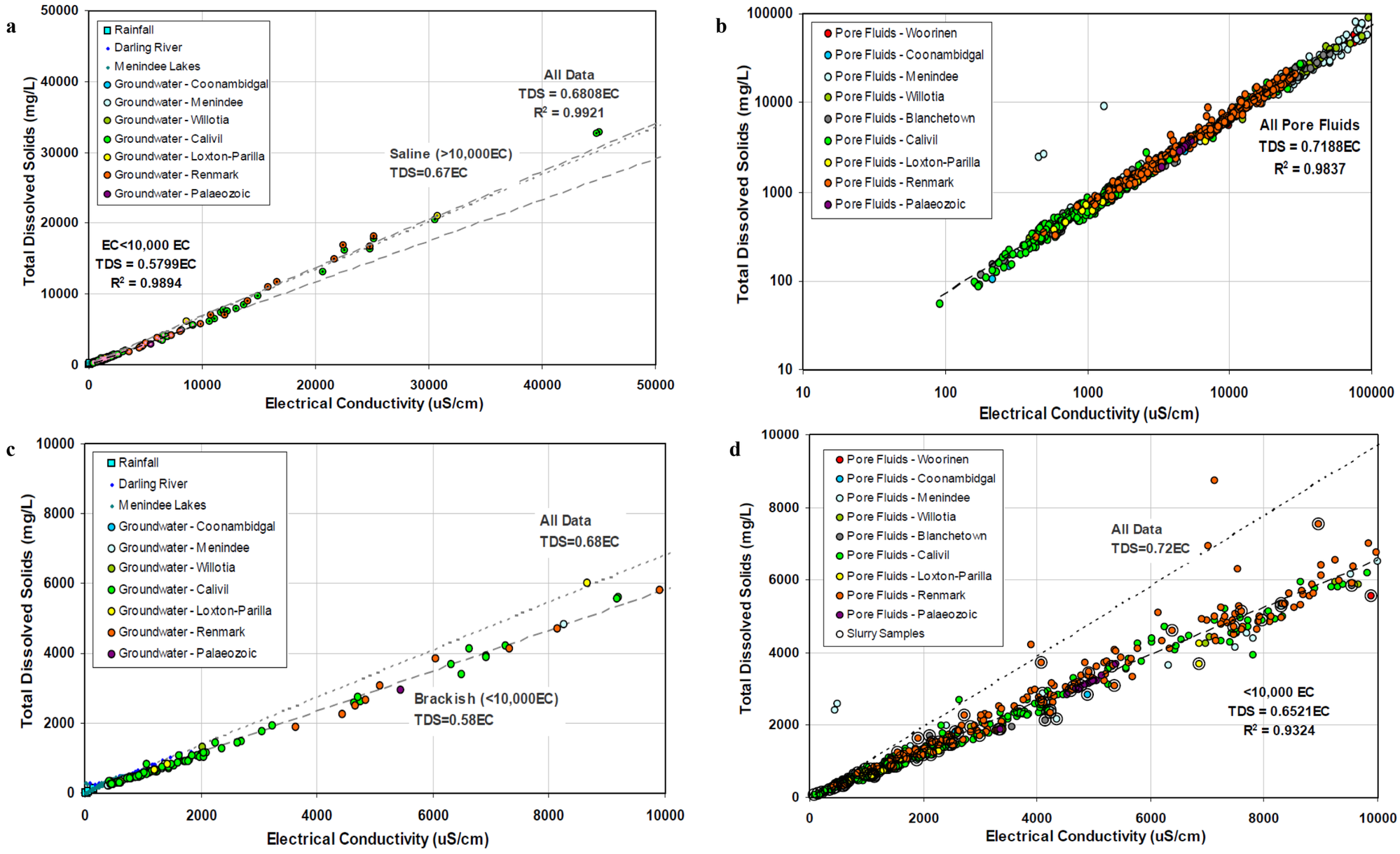

Figure 8-3. *Scatter plots of electrical conductivity and total dissolved solids for BHMAR water samples (a) electrical conductivity and total dissolved solids for groundwater and surface water samples (b) electrical conductivity and total dissolved solids for pore fluid samples (c) electrical conductivity and total dissolved solids for groundwater and surface water samples (d) electrical conductivity and total dissolved solids for pore fluid samples.*

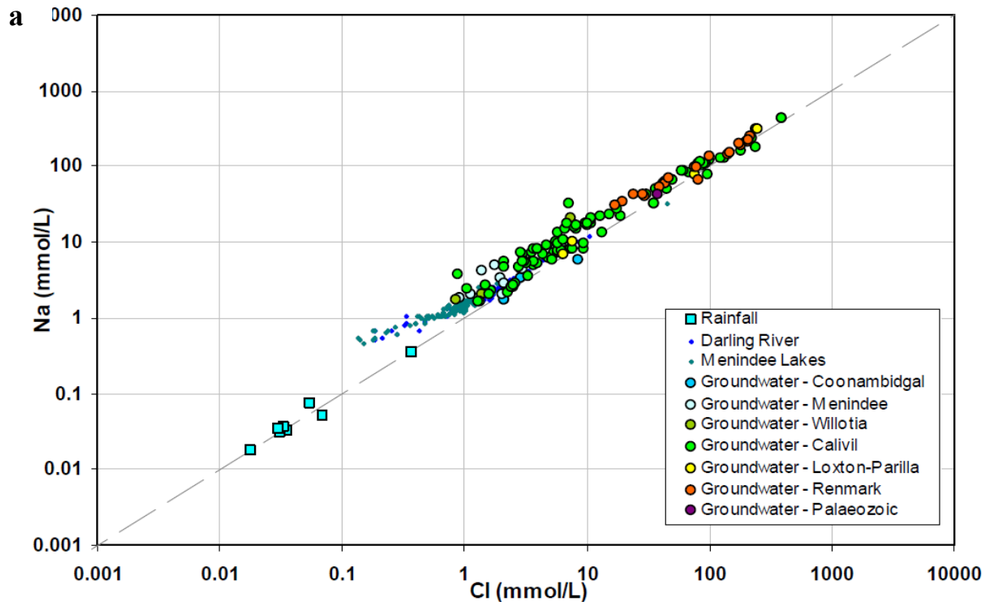

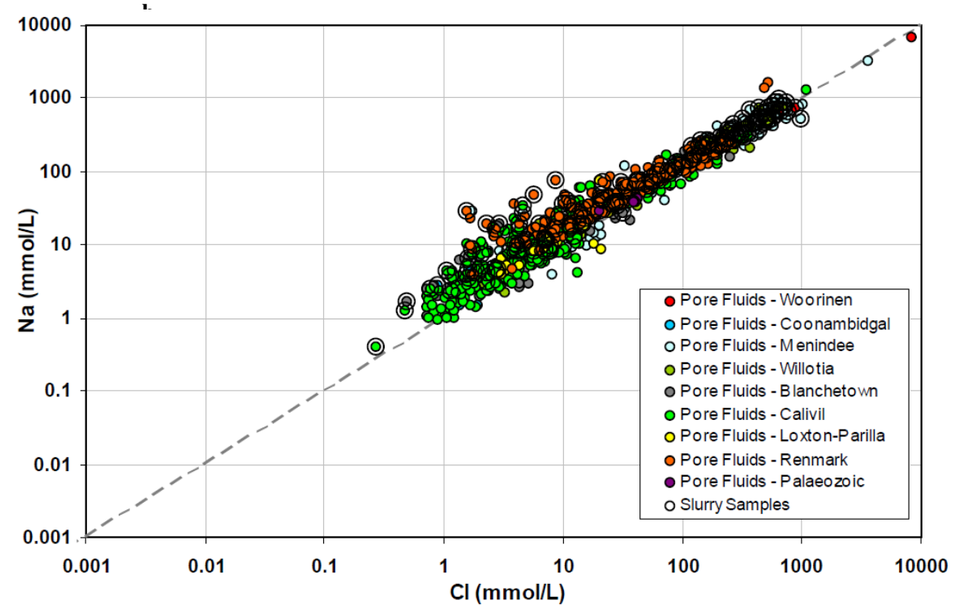

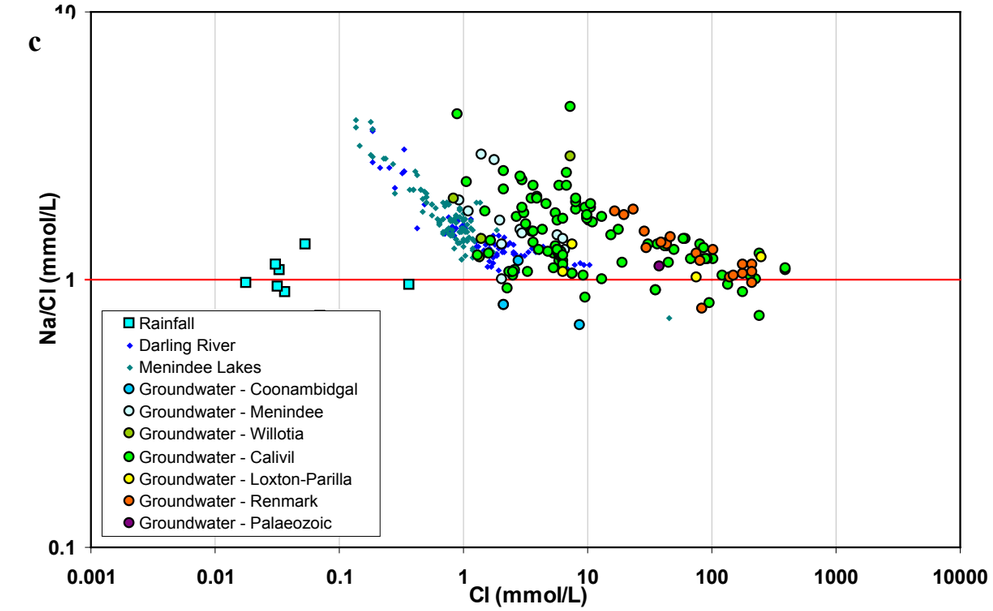

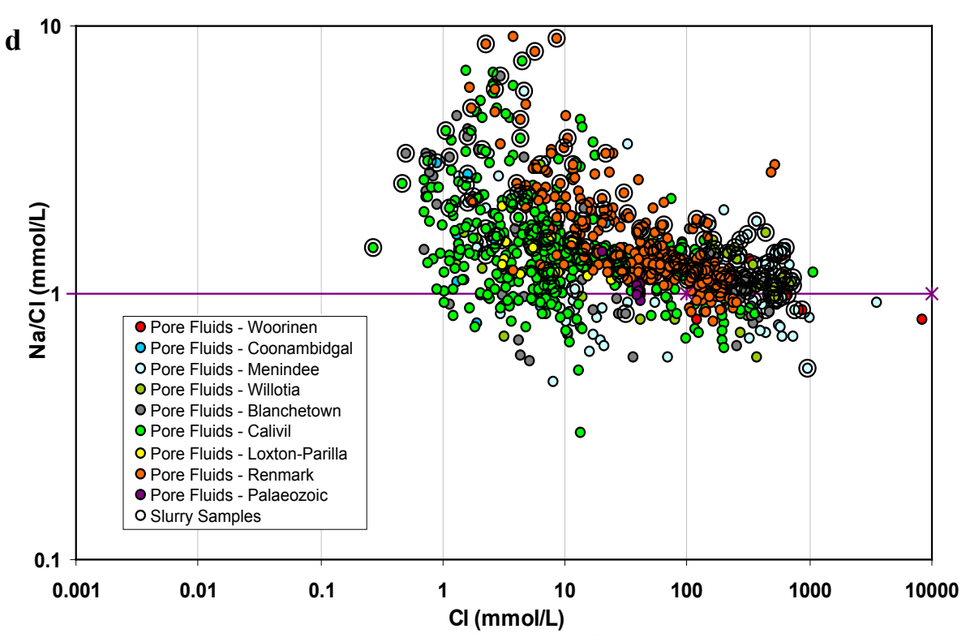

Figure 8-4. *Scatter plots of chloride and sodium for BHMAR water samples. (a) chloride and sodium in mmol/L for groundwater and surface water samples (b) chloride and sodium in mmol/L for pore fluid samples (c) chloride and sodium/chloride ratio in mmol/L for groundwater and surface water samples (d) chloride and sodium/chloride ratio in mmol/L for pore fluid samples.*

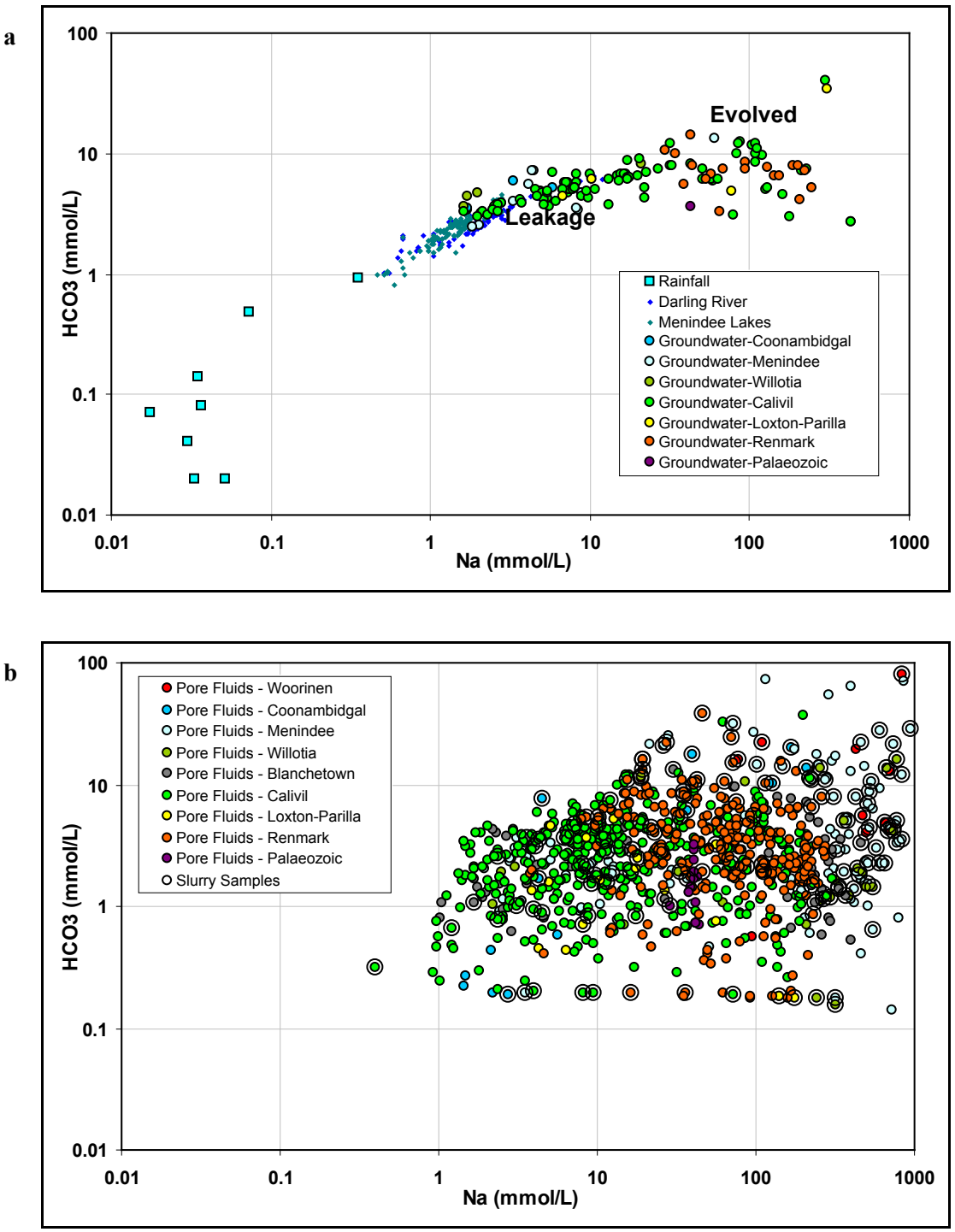

Figure 8-5. *Scatter plots of sodium and bicarbonate in mmol/L for (a) surface water and groundwater samples (b) for pore fluid samples.*

The two broad groundwater groups (evolved and leakage) identified by the Piper diagrams are also evident in the plots of the relationship between Na+K and Ca+Mg (Figure 8-6). The cluster of fresh to brackish Calivil Formation groundwater samples with the shallow groundwaters and surface waters is interpreted to be associated with leakage and mixing (Figure 8-6a). The more saline Calivil Formation groundwater samples linked with the Renmark Group samples are interpreted to be not influenced by river leakage, but represent regional evolved groundwater dominated by other processes (such as mineral dissolution or cation exchange). The two groups are further accentuated in the equivalent plot for the pore fluids (Figure 8-6b). The plot of the ratio of $(Ca+Mg)/HCO_3$ against Cl was also used to successfully differentiate these broad groundwater groups (Figure 8-7a). The equivalent plot for pore fluids had greater scatter (Figure 8-7b). This may reflect issues associated with the alkalinity titrations, particularly for the near-surface slurry samples.

The SO_4-(Ca+Mg) plot (Figure 8-8a) provides a similar perspective, with the more saline evolved groundwaters having higher sulfate concentrations than the fresher groundwaters associated with river leakage. This is also the case in the equivalent plot for the pore fluids (Figure 8-8b).

Figure 8-9 further investigates the relationships between the monovalent and divalent cations, by normalising Na and Ca+Mg to Cl. Based on ion ratios, this plot indicates that most groundwaters are influenced by ion exchange processes where, due to water-clay interactions, the divalent cations in the groundwater are progressively being replaced by monovalent cations (Figure 8-9a). As depicted in the Piper diagram (Figure 8-1), the deeper groundwaters tend to be influenced by Ca+Mg ion exchange by Na. Groundwaters where Ca exchange is dominant tend to be from the Calivil Formation aquifer. The plot also shows the influence of evaporation on the surface waters. The plot for the pore fluids (Figure 8-9b) shows a similar data distribution to that of the groundwaters, the main difference being a greater spread for the Renmark Group samples.

Figure 8-10 is the relationship between SO_4+HCO_3 and Ca+Mg and also shows the influence of ion exchange processes. Most groundwaters show a relative deficit in the divalent cations and therefore plot below the equivalence line (Figure 8-10a). This is also the case for the pore fluid samples (Figure 8-10b). Maclean & Jankowski (2003) interpreted such a deficit as reflecting ion exchange processes, with relative enrichment of groundwater Na^+, by exchange of Ca^{2+} and Mg^{2+} with clays.

A comparison of the two monovalent ions (Na and K) is presented in Figure 8-11. The plot suggests that potassium concentrations are relatively static for fresh to brackish groundwaters (<5000 EC) but increases at greater salinities (Figure 8-11a), possibly due to ion exchange. Figure 8-11a is interesting from a surface water perspective, with the river samples showing a progressive enrichment in potassium. This is explored further in Figure 8-11c, where the river water samples are categorised in terms of measured flow. This shows that Na and K progressively increase as the flow decreases, due to evaporative concentration. There is a coincidence between the high flow river samples (>10000 ML/d) that have a low potassium signature with that of the shallow groundwater samples. This would suggest that recharge by river leakage is not a continual process occurring during all flow conditions, but is specific to high flow conditions. Many of the lake samples (Figure 8-11c) are also coincident with the higher flow river samples, as the lake storages are replenished during these flood events. Other lake samples follow a similar evaporative trend to that of the lower flow river samples. The relationship between Na and K for the pore fluids is presented in Figure 8-11b. It shows a similar general grouping to that of the groundwaters but with a much greater data scatter.

The broader relationship between river chemistry and river flow is summarised by the Piper diagram of Figure 8-12. Although not entirely consistent, there is a general evolution towards Na-Cl dominance at the expense of Ca-HCO_3, as the river flow decreases. The samples contrary to this trend are likely to reflect releases from the Menindee Lakes Storages into the Darling River.

a

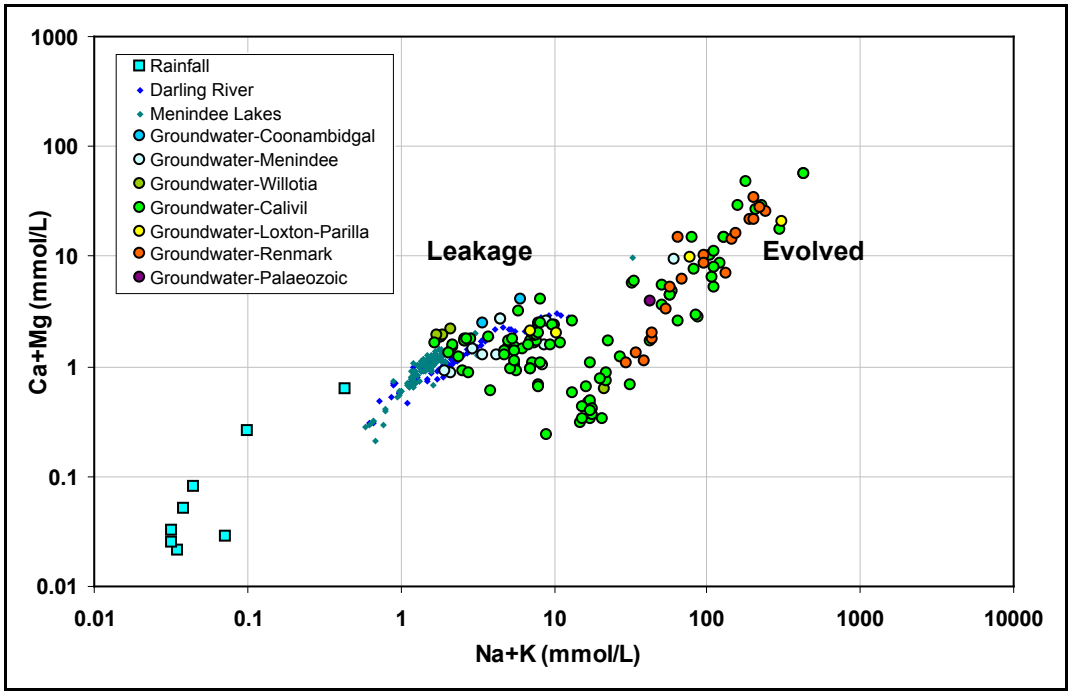

b

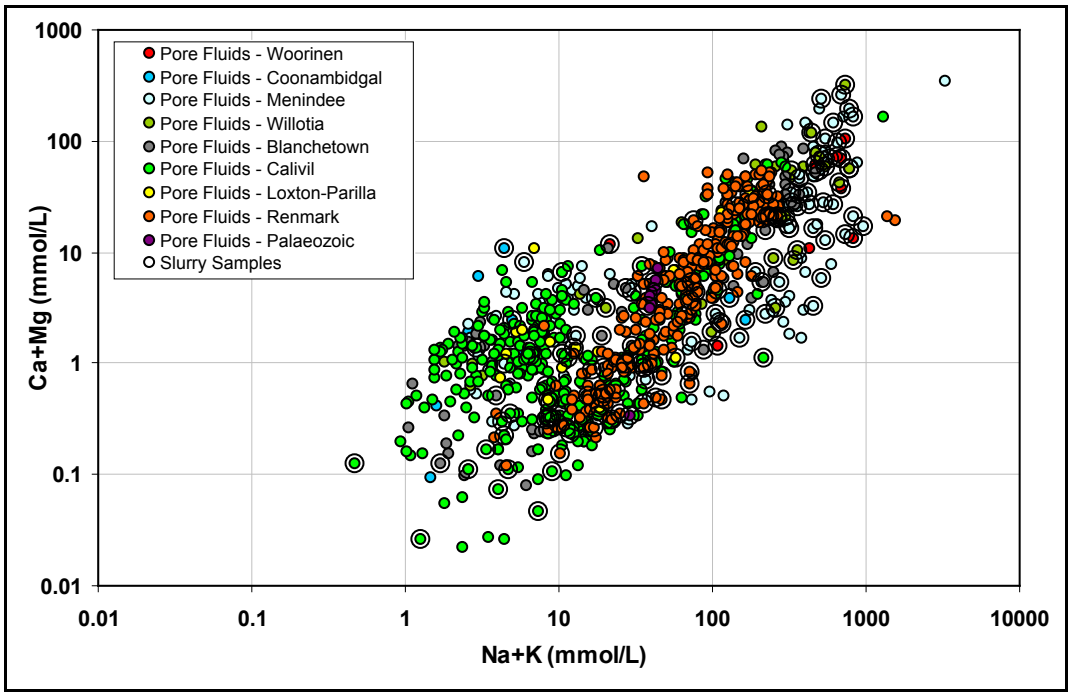

Figure 8-6. *Scatter plots of sodium + potassium and calcium + magnesium in mmol/L for (a) surface water and groundwater samples and (b) pore fluid samples.*

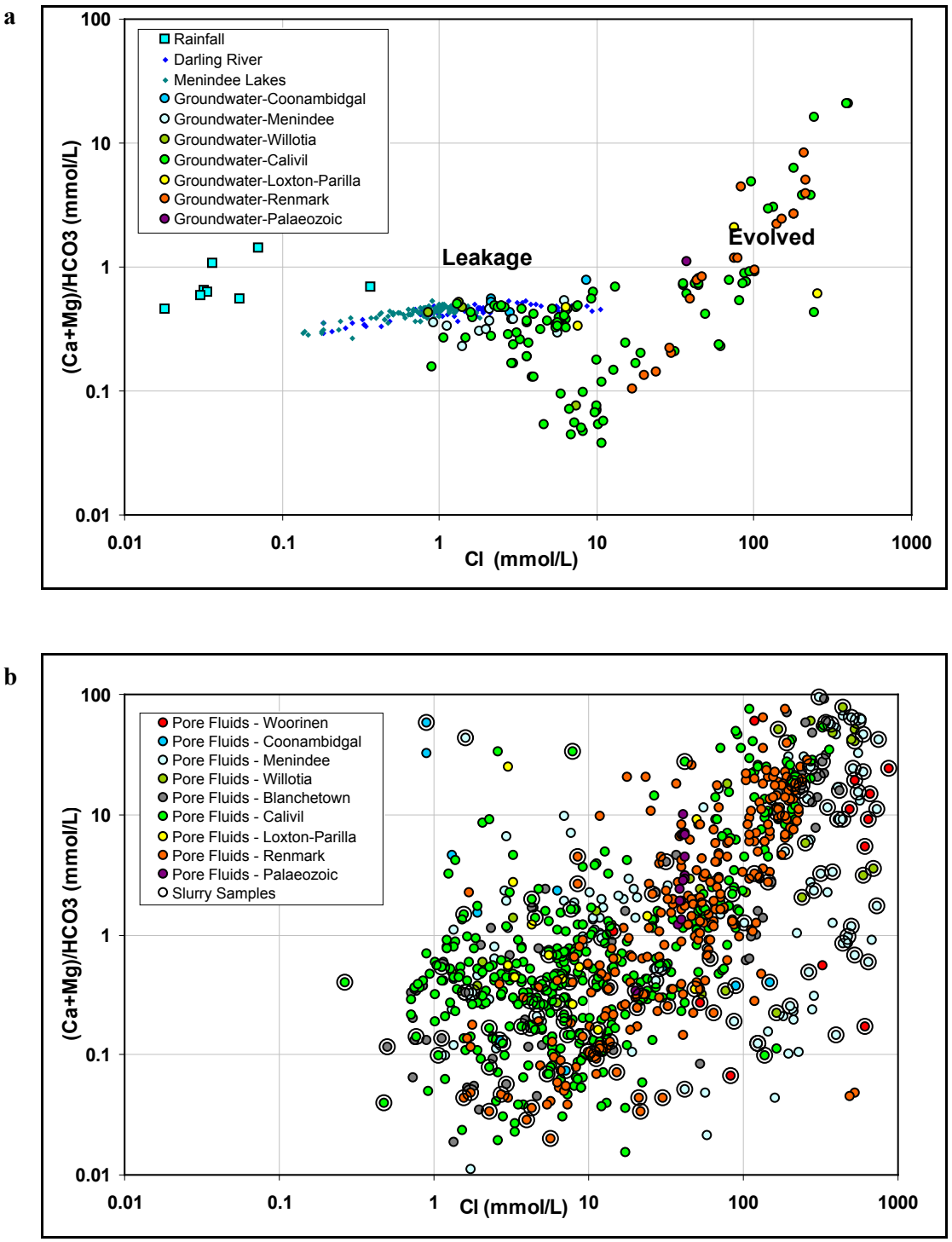

Figure 8-7. *Scatter plots of chloride and (calcium + magnesium)/bicarbonate ratio in mmol/L for (a) surface water and groundwater samples and (b) for pore fluid samples.*

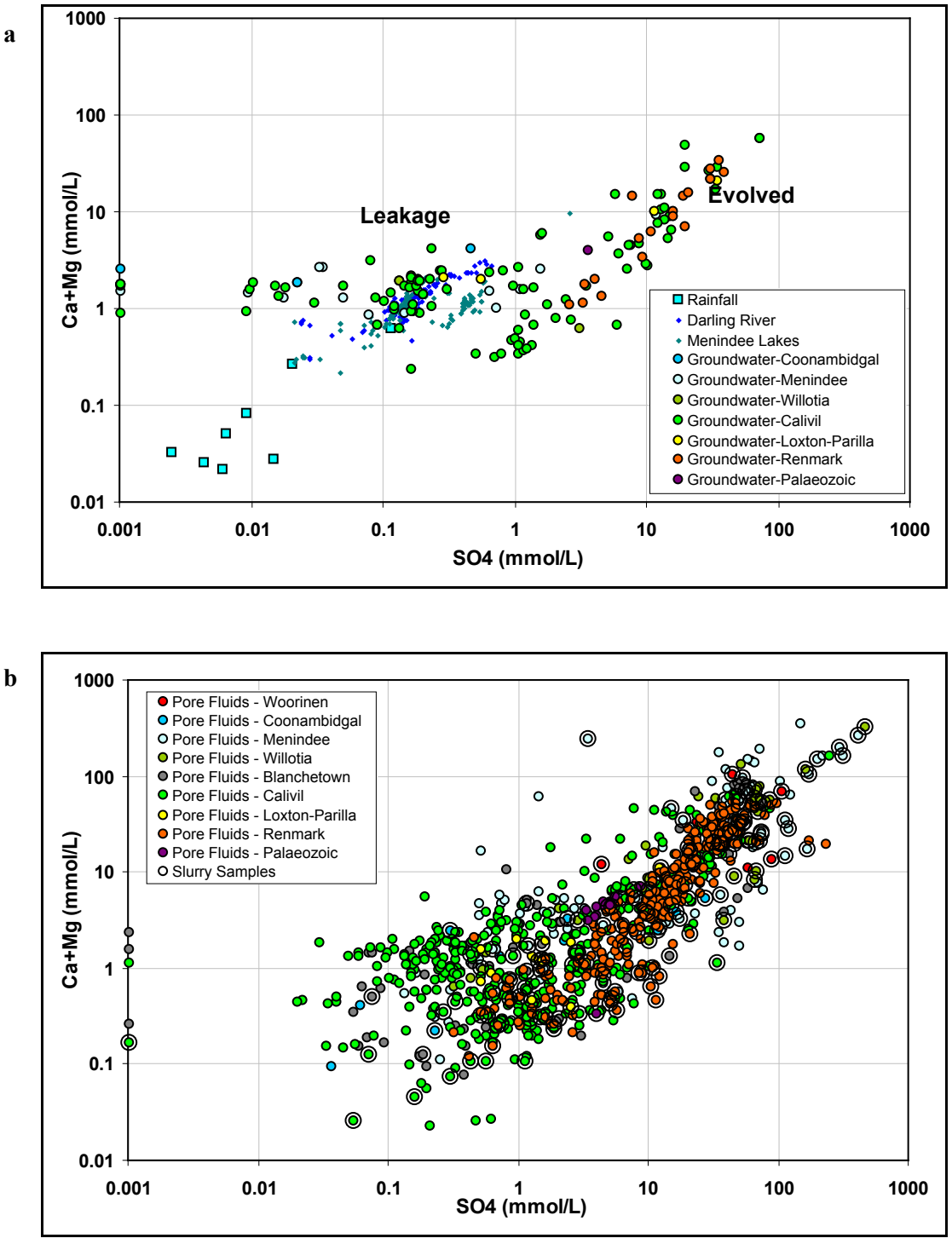

Figure 8-8. *Scatter plots of sulfate and calcium + magnesium in mmol/L(a) for surface water and groundwater samples (b) for pore fluids.*

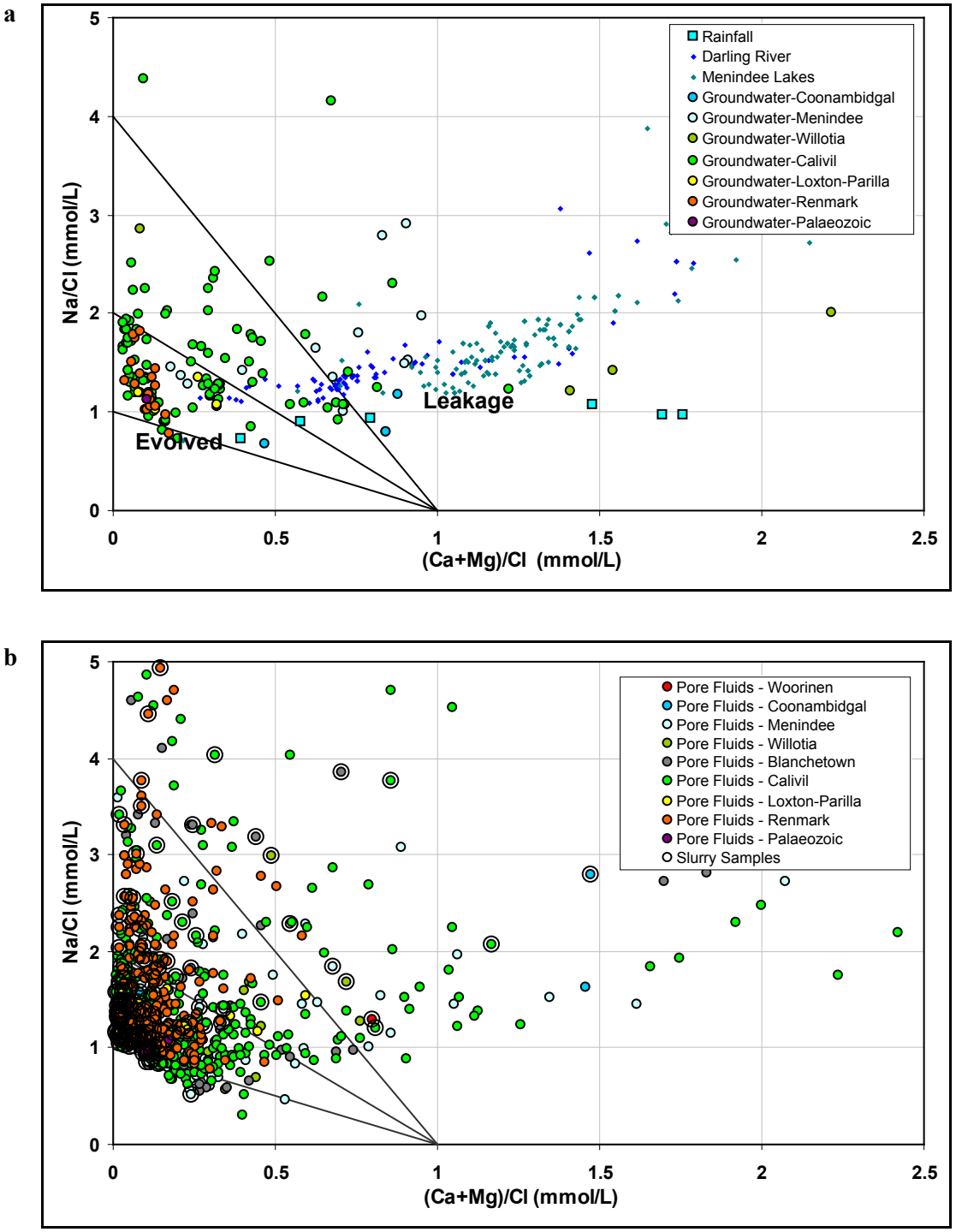

Figure 8-9. *Scatter plots of calcium + magnesium and sodium + potassium normalised to chloride in mmol/L (a) for surface water and groundwater samples (b) for pore fluids.*

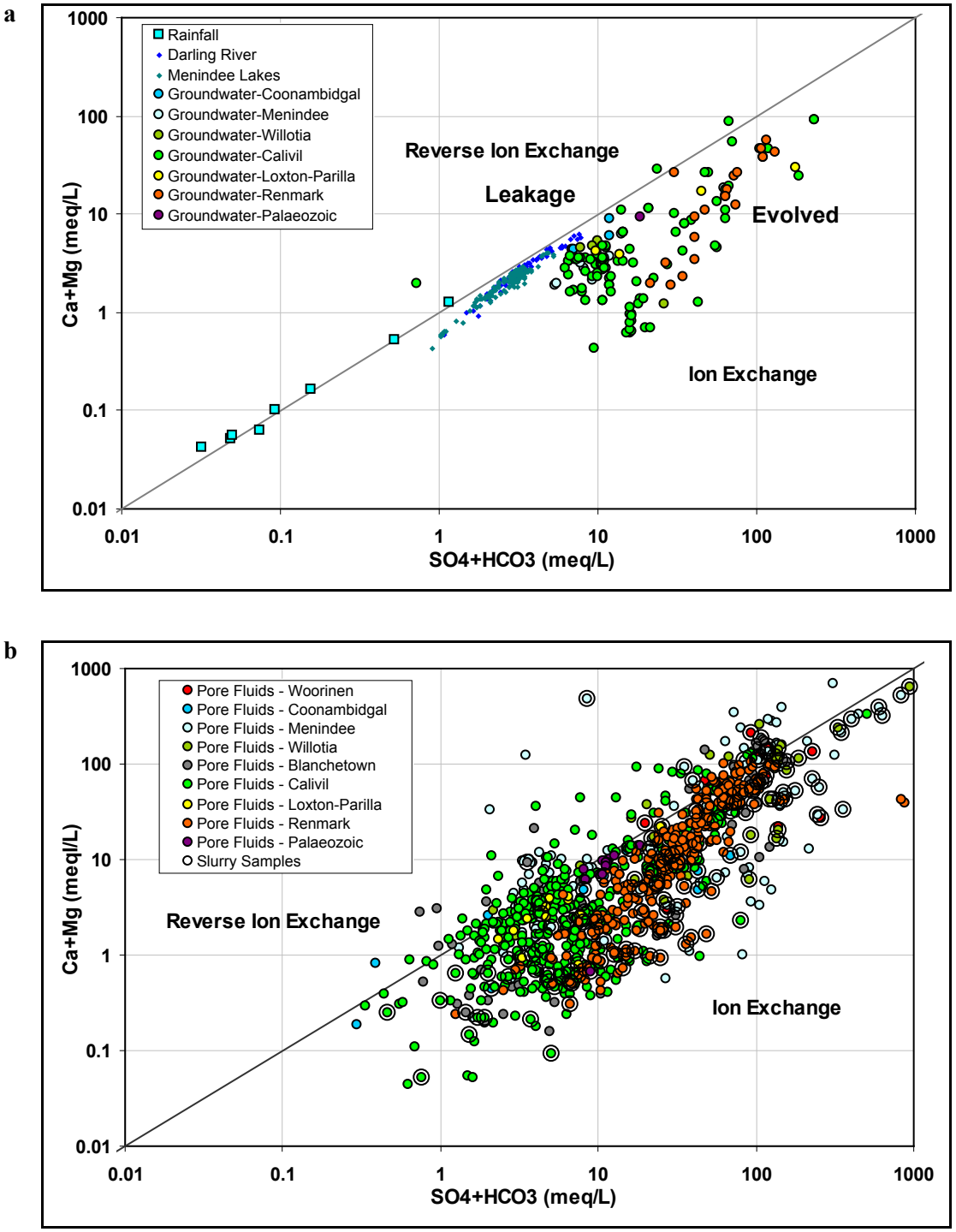

Figure 8-10. *Scatter plots of sulfate + bicarbonate and calcium + magnesium in meq/L (a) for surface water and groundwater samples (b) for pore fluids.*

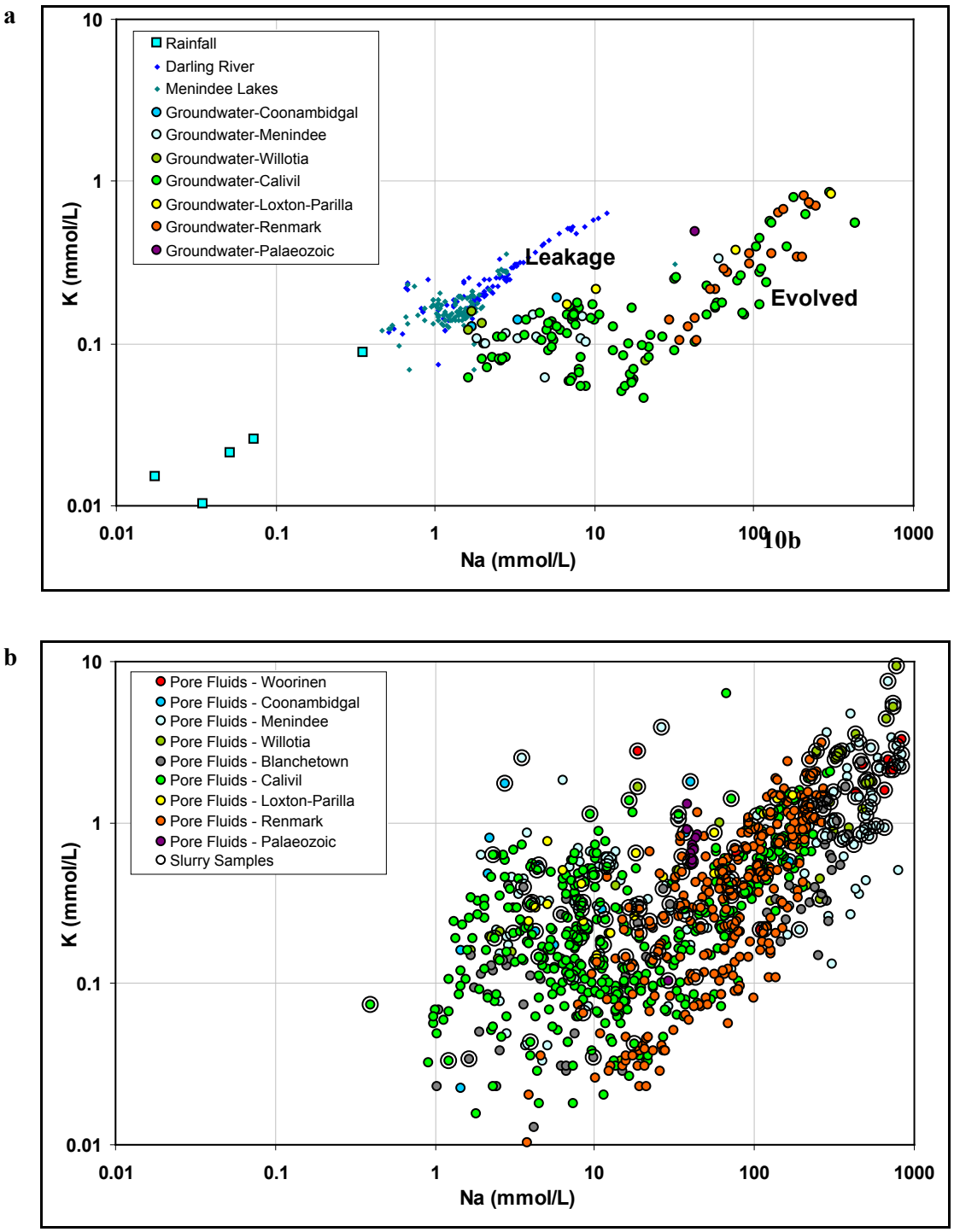

Figure 8-11. *Scatter plots of sodium and potassium in mmol/L (a) for surface water and groundwater samples (b) for pore fluids.*

c

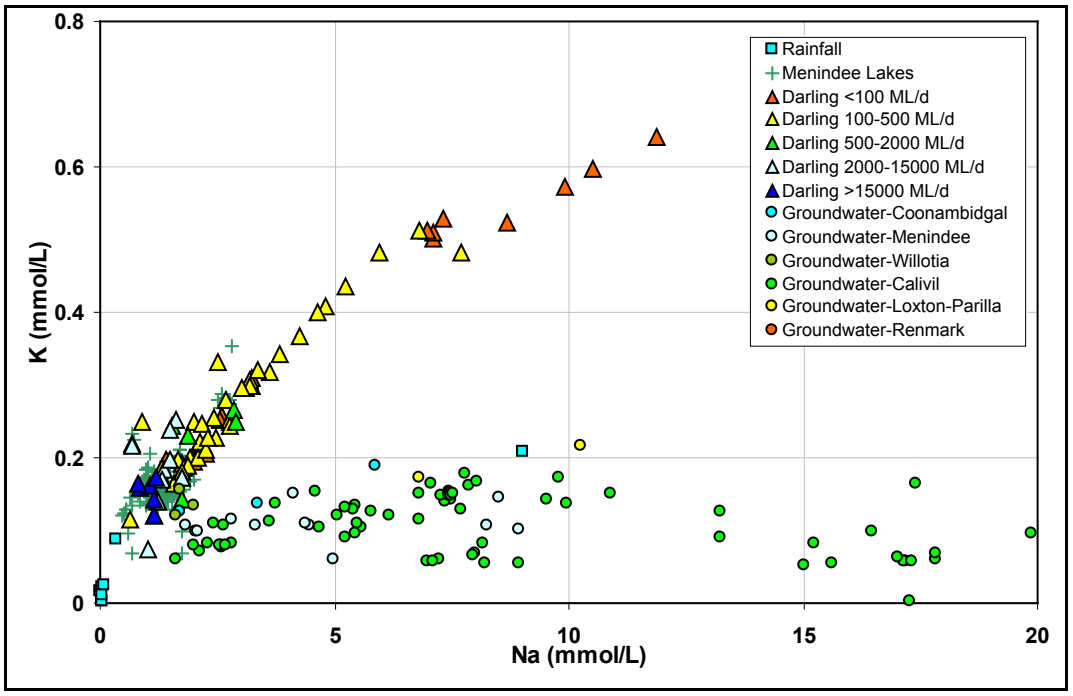

Figure 8-11 *(cont). Scatter plots of sodium and potassium in mmol/L (c) for fresh surface water and ground water samples.*

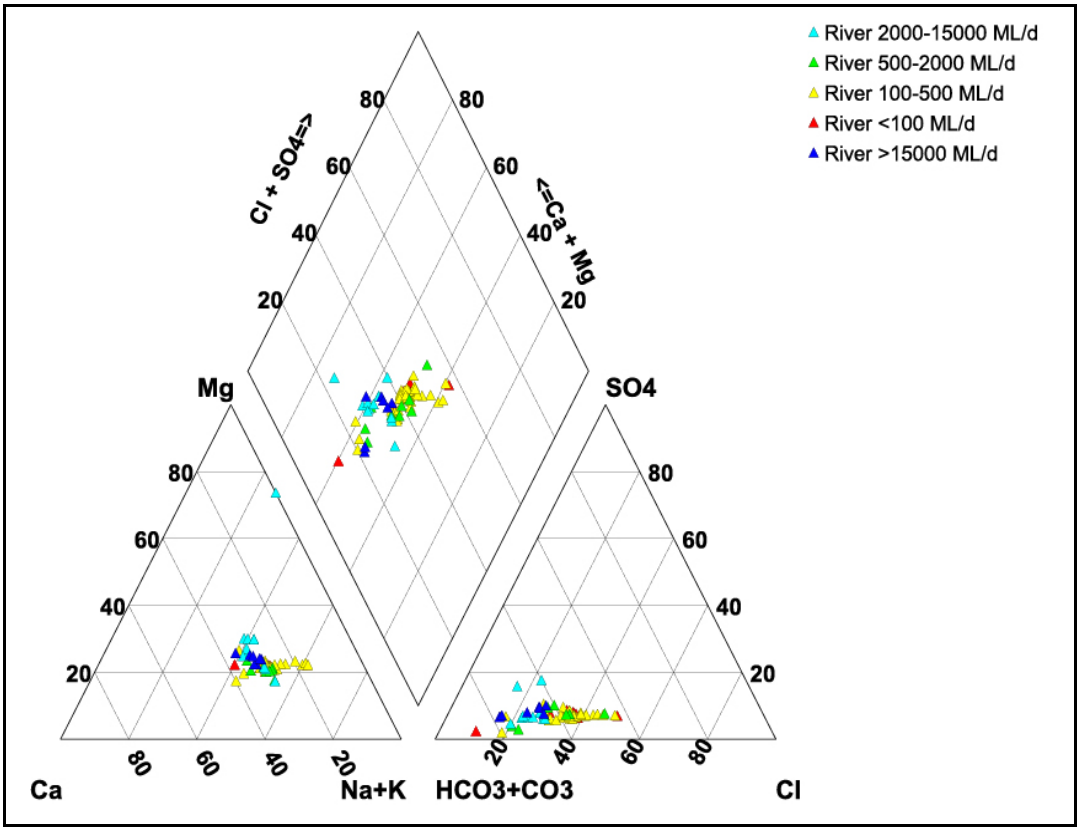

Figure 8-12. *Piper diagram of Darling River surface water samples grouped by river flow.*

Bromide is a useful conservative tracer and the molar ratio with chloride is used to help identify the origin of salinity in aquifers (e.g. Alcala & Custodio, 2008). This is plotted for the groundwater samples and surface water samples in Figure 8-13a. The limited Br analyses for the river samples suggest relative enrichment (Br/Cl ~ 0.0035) compared to the groundwater samples which plot around the seawater ratio (Br/Cl ~ 0.0015). In the equivalent plot for pore fluids (Figure 8-13b), the relatively fresher Calivil Formation pore fluids tend to plot in a broad trend between the river water ratio and the seawater ratio. This supports the influence of river leakage on groundwater recharge but would need to be confirmed by additional bromide analyses of surface waters. The deeper, more saline groundwaters and pore fluids tend to plot slightly below the conventional seawater Br/Cl ratio, Figure 8-13a and Figure 8-13b respectively. This may represent the partial role of halite dissolution in the groundwater evolution, as such dissolution produces a decrease in the Br/Cl ratio (Kloppman *et al*., 2001).

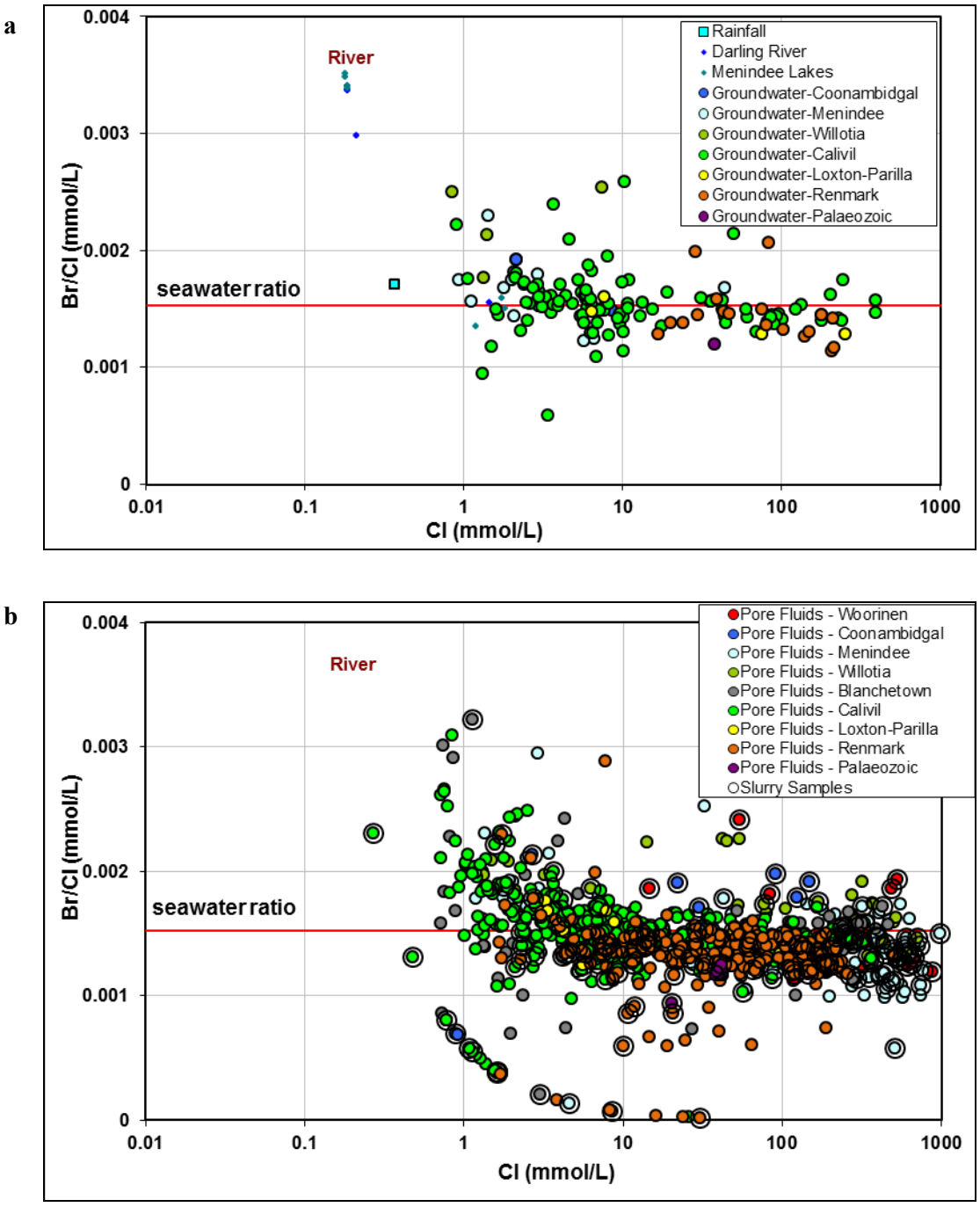

Figure 8-13. *Scatter plots of chloride and bromide/chloride ratio in mmol/L (a) for groundwater and surface water samples (b) for pore fluids.*

8.2 FUZZY K-MEANS ANALYSIS

A fuzzy k-means approach (Lawrie *et al*., 2012a) was used in a cluster analysis of the hydrochemistry dataset consisting of rainfall, river, lake, groundwater and pore fluid samples. As discussed in more detail in Lawrie *et al*. (2012a), a fuzzy k-means cluster analysis approach using the program 'FuzMe' was used. This cluster analysis resulted in the samples being assigned across eight classes (8a-8h), as well as an index (0-1) of how well the sample belongs to each of these classes. Table 8-2 summarises the averages of key analytes for the eight fuzzy classes. The issue of pore fluid contamination occurring as a result of drilling processes has been explored in Lawrie *et al*. (2012a) and found to be very minor in nature, with only 0.6% of samples being potentially affected.

Table 8-2: *Analytical averages for the classification of BHMAR water samples using fuzzy k-means.*

Fuzzy Class	EC (µS/cm)	TDS	Na	Cl	Ca	Mg	Sr	HCO_3	K	pH	SO_4	SiO_2
8a	389	323	45	46	25	13	27.4	152.9	7.1	7.69	24	18.3
8b	1059	691	138	171	40	25	0.6	209.7	10.8	8.08	90	12.9
8c	2419	1572	503	445	16	12	0.3	310.9	6.6	8.29	264	29.6
8d	8592	5756	1786	2182	107	113	2.3	290.8	20.2	8.07	1225	21.3
8e	399	236	57	53	9	5	0.1	79.7	4.8	7.55	22	20.1
8f	42773	29595	8558	12571	1013	742	18.2	621.0	69.4	7.91	5881	77.4
8g	17639	14984	2584	2880	558	441	11.2	2.8	46.5	4.13	8061	53.6
8h	597	428	69	80	30	16	0.4	184.1	10.8	8.10	21	13.6

Table 8-3 shows the distribution of the various sample types across the eight fuzzy classes. The surface water samples have the greatest affinity with the fuzzy classes 8a, 8e and 8h (and minor 8b). In contrast, the majority of the groundwater samples are in classes 8b, 8c and 8d. Importantly, there are subsets of groundwater samples that are within the classes that also have surface water samples (8a, 8e and 8h). The saturation extracts and slurries are variants of the pore fluid sampling. Collectively, the pore fluids are distributed across the fuzzy classes, with the exceptions of classes 8a and 8h, which are river and lake dominant.

Table 8-3: *Classification of BHMAR water samples using fuzzy k-means.*

	Rainfall	River	Lake	Groundwater	Pore Fluid	Saturation Extract	Slurry
8a	1	126	186	9	0	0	0
8b	0	1	1	72	171	2	12
8c	0	0	0	26	196	10	45
8d	0	0	0	35	227	8	28
8e	9	29	17	6	72	7	17
8f	0	0	0	14	125	30	60
8g	0	0	0	0	68	3	8
8h	0	56	0	1	0	0	0

Figure 8-14a to c are scatter plots exploring the differences between the fuzzy classes dominated by surface water (8a, 8e, 8h). River waters of relatively high salinities (EC >500 µS/cm) during low-flow conditions (Q< 1000 ML/d) are predominantly in the 8h class (Figure 8-14a). This is reflected in the progressive enrichment of potassium for this class of river waters (Figure 8-14b). Class 8a and 8e waters are similar in salinity and major ions such as Na, Cl, SO_4 and SiO_2 (Table 8-2). However, class 8a surface waters tend to be relatively enriched in species related to alkalinity such as HCO_3, Ca, Mg and Sr (Table 8-3, Figure 8-14c).

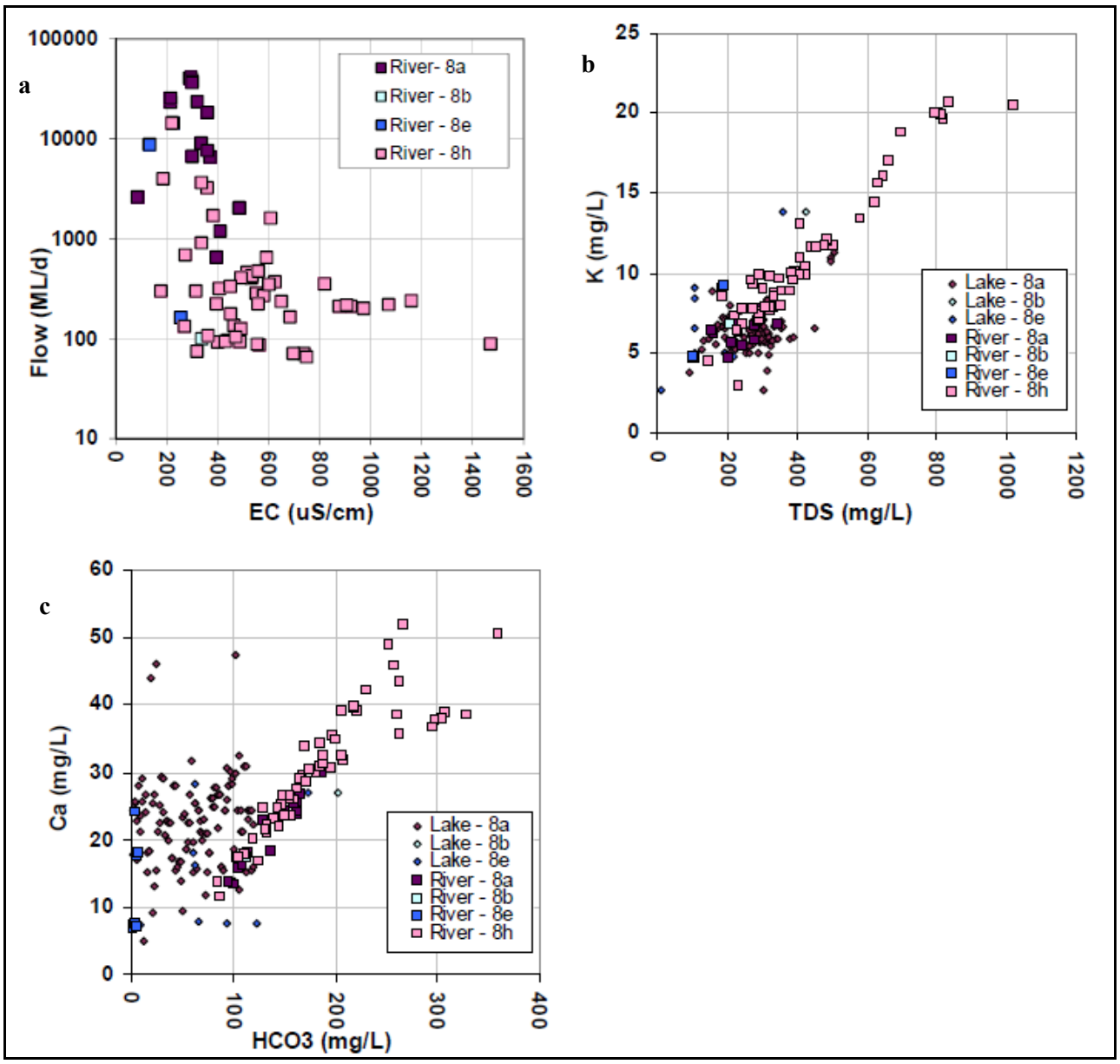

Figure 8-14. *Scatter plots of analytes for Darling River surface water samples grouped into fuzzy k-means classes (a) electrical conductivity and river flow (b) total dissolved solids and potassium (c) bicarbonate and calcium.*

Figure 8-15 and Figure 8-16 are Piper diagrams of these fuzzy classes for the water samples and the pore fluid samples, respectively. The fuzzy classes have been effective in mapping the groundwaters that have been influenced by surface water leakage, such as classes 8a, 8e and 8h, and to a lesser extent 8b. Classes 8c, 8d and 8f make up the evolved group of groundwaters that plot along the right hand margin of the Piper diagram (Figure 8-15). Class 8c is relatively bicarbonate-enriched (and less evolved) compared with classes 8d and 8f, which also have higher sulfate.

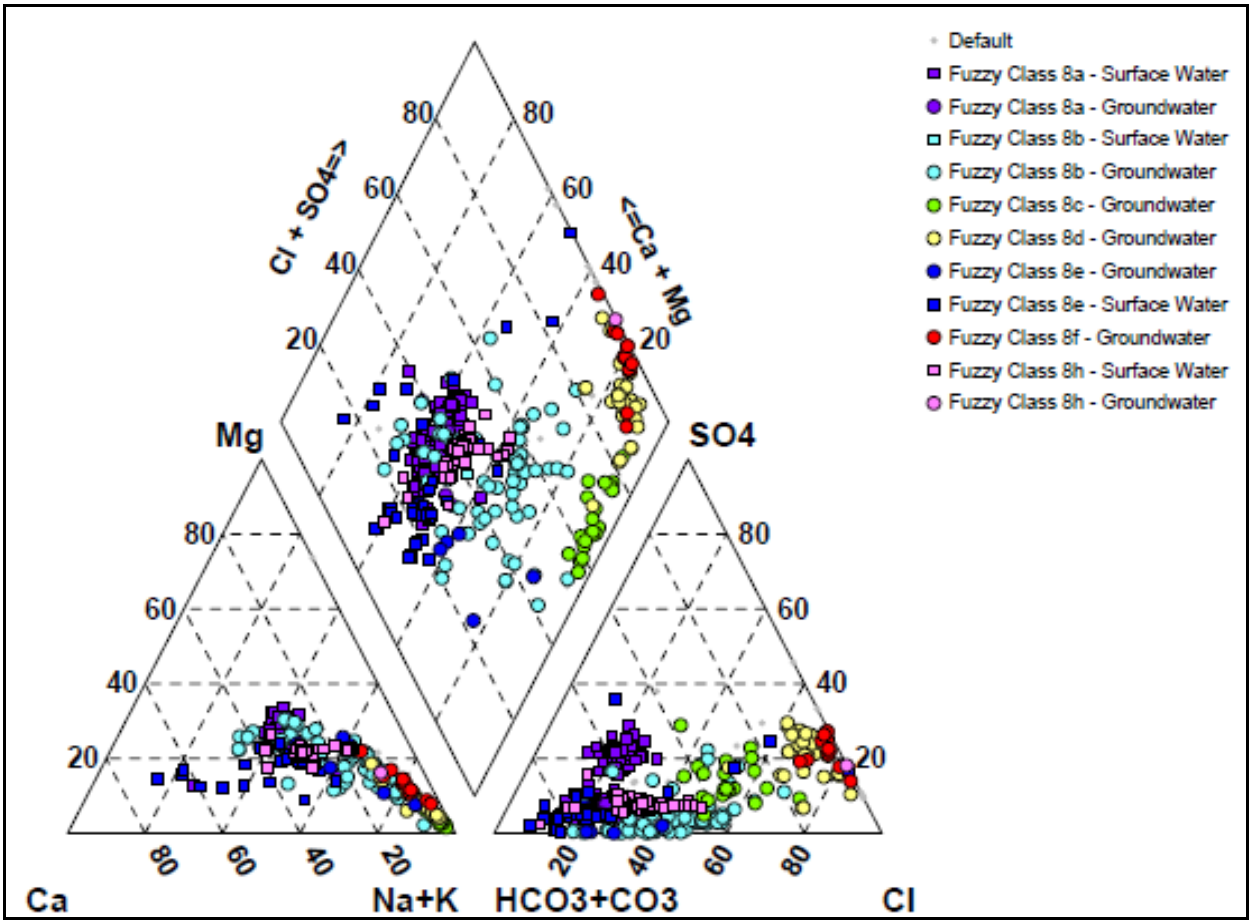

Figure 8-15. *Piper diagram of major ion analyses of BHMAR surface waters and groundwaters grouped by fuzzy k-means classes.*

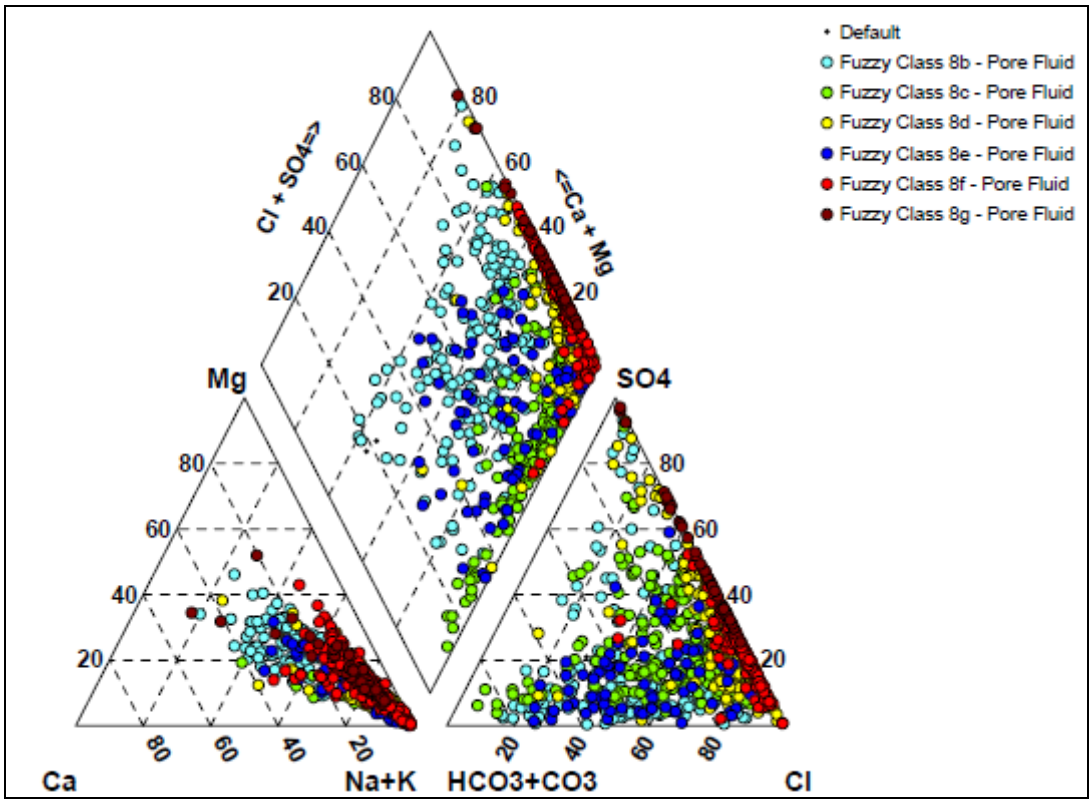

Figure 8-16. *Piper diagram of major ion analyses of BHMAR pore fluids classified by fuzzy k-means.*

Although there is a greater data spread, the Piper diagram for the pore fluids also shows that the fuzzy-k means analysis has provided meaningful clustering (Figure 8-16). The pore fluids assigned to classes 8e and 8b are interpreted to have been influenced by surface water leakage, as river and lake samples have also been assigned to these classes. There are no pore fluids (and only one groundwater) assigned to class 8h, linked to low-flow river conditions. This would support the hypothesis that groundwater recharge is associated with high flow events. The remaining classes (8c, 8d, 8f, 8g) are variants of the evolved Na-Cl-(HCO_3)-SO_4 water types. Of these classes, 8c has the lowest salinity with an average EC of 2419 µS/cm, followed by 8d (8592 µS/cm), 8g (17639 µS/cm) and 8f (42773 µS/cm), refer Table 8-2. Class 8g is unique to the pore fluids and are Na-Cl waters with relatively high sulfate levels (Table 8-2). In the eight classes defined, SO_4 ranges from 10.6 mg/L in class 8h to 4376 mg/L in class 8g. The high values of SO_4, particularly in the Renmark Group pore fluids, may indicate the presence of pyrite or other sulfides that have been oxidised during the sample extraction process. This is reflected in the average pH for class 8g pore fluids being also relatively low (Table 8-2).

Figure 8-17 maps the fuzzy k-means classification of the shallow groundwater samples in the Coonambidgal Formation, Menindee Formation and Willotia beds across the BHMAR study area. This shows the association of classes 8a and 8b in particular with river and lake leakage zones. This is better represented in the map for the Calivil Formation and Loxton-Parilla Sands groundwater samples (Figure 8-18), where classes 8b and 8e plot within the leakage zones, with the more evolved classes 8d and 8f being peripheral. The Renmark Group groundwater samples tend to have more evolved signatures (classes 8f, 8d and 8c to a lesser extent), suggesting limited active recharge to this deeper aquifer (Figure 8-19).

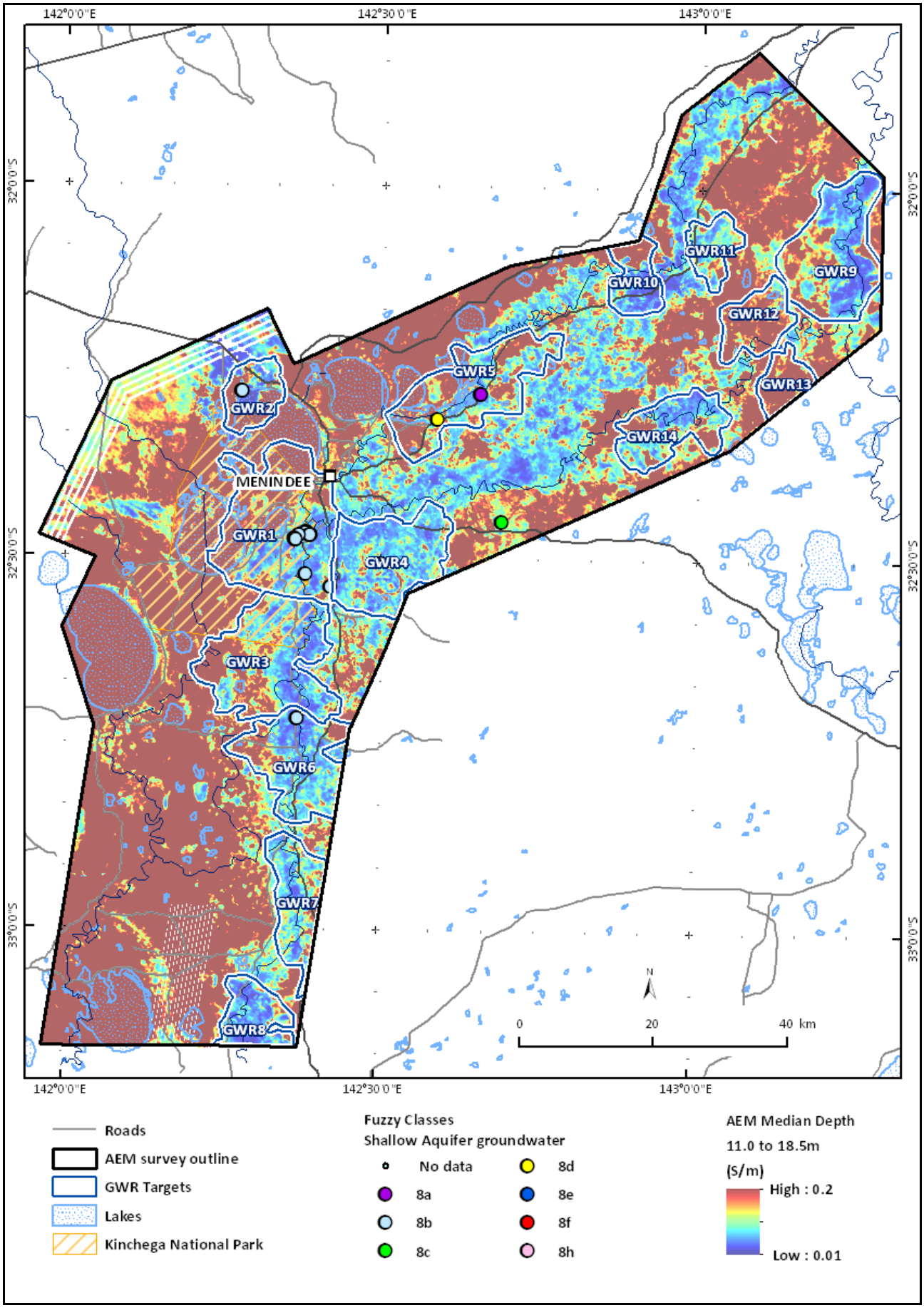

Figure 8-17. *Map of BHMAR study area with fuzzy-k means classification of shallow groundwater samples.*

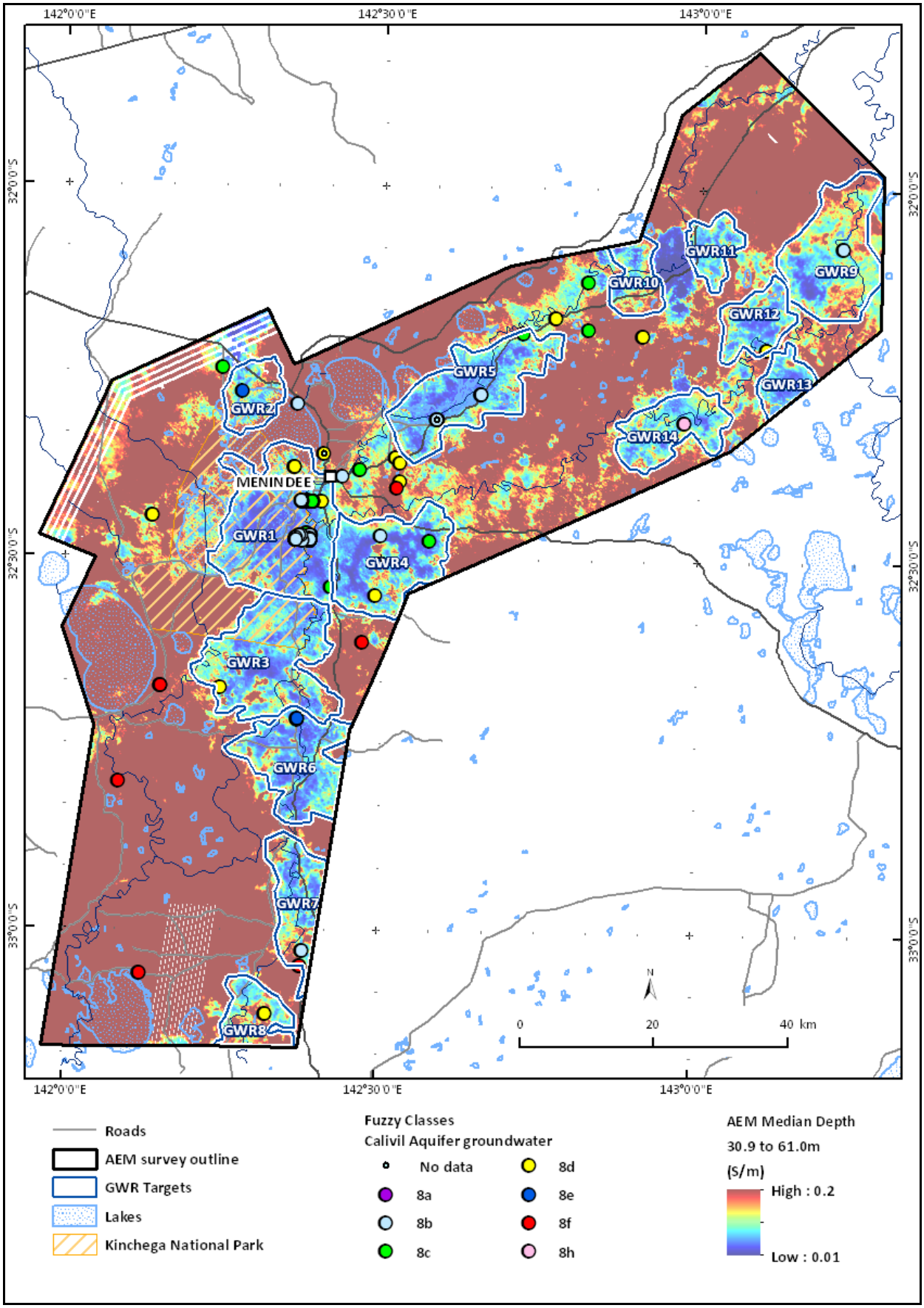

Figure 8-18. *Map of BHMAR study area with fuzzy-k means classification of Calivil Formation and Loxton-Parilla Sands groundwater samples.*

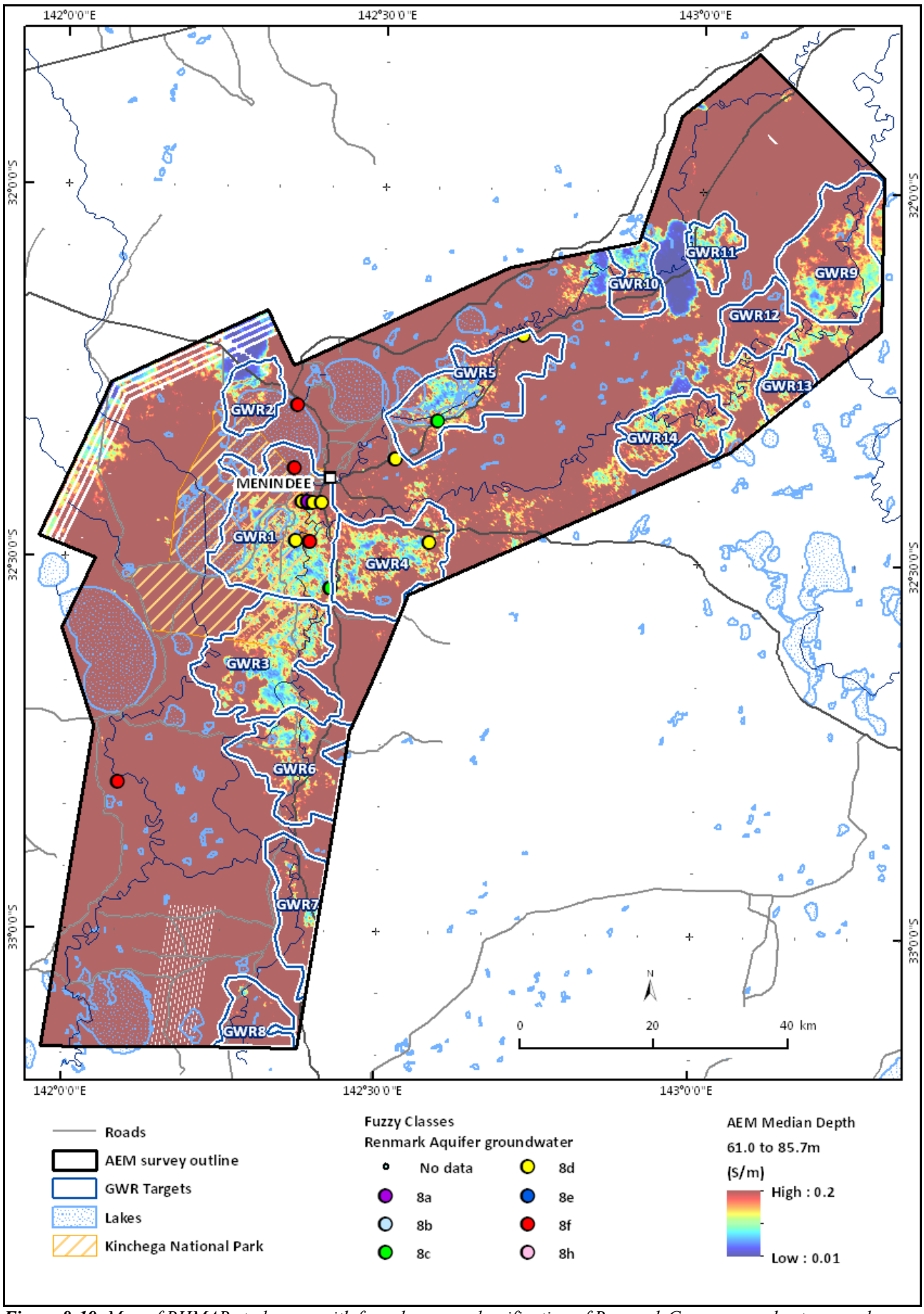

Figure 8-19. *Map of BHMAR study area with fuzzy k-means classification of Renmark Group groundwater samples.*

By linking groundwater and pore fluid samples with surface water samples, this cluster analysis was particularly useful in mapping the extent of river leakage and groundwater mixing. The most meaningful way to represent the fuzzy classification of the pore fluid data is by downhole profiles. Figure 8-20 plots the downhole profile of pore fluid fuzzy classes for selected BHMAR sonic cored holes on the basis of measured fluid electrical conductivity (EC), with downhole gamma and induction logging and the stratigraphic interpretation to provide context. In these plots, the slurry samples are differentiated from the pore fluid samples as they have a lower analytical reliability. The following observations can be made:

- The fuzzy classes most linked with the surface water samples (8e and 8b) are fresh pore fluids, mostly in the Calivil Formation (Tpc) and the shallow unconfined aquifers of the Coonambidgal Formation (Qa) and Menindee Formation (Qam). The vertical distribution of these classes represents the extent of active recharge in these aquifers. In some bores, such as BHMAR23-1 (Figure 8-20d), BHMAR34-1 (Figure 8-20e) and BHMAR80A-2 (Figure 8-20j), most of the Calivil Formation thickness contains fresh pore fluids of these classes. In others, such zones are limited to the top of the aquifer, BHMAR 18-1 (Figure 8-20c) being a good example. In some cases, such recharge is evident for the entire Calivil Formation sequence (Figure 8-20a), or in the lower section (Figure 8-20b) or the upper section (Figure 8-20c).
- These fresh recharged zones tend to be surrounded, above and/or below, by class 8c pore fluids, which are in turn transitional to class 8d pore fluids. This is best depicted in Figure 8-20c. This is inferred to represent mixing or diffusion between the actively recharged zones and the more saline and evolved regional groundwaters.
- The evolved saline pore fluids are represented by classes 8f and 8g and are located at the base of the Calivil Formation and the underlying Renmark Group (Figure 8-20b, c and i). In some bores such as BHMAR18-1 (Figure 8-20c) and BHMAR64-1 (Figure 8-20i), the profile in the Renmark Group appear to be consistently saline. Other bores, such as BHMAR61-1 (Figure 8-20h) and BHMAR41-1 (Figure 8-20f) have transitional class 8c and 8d pore fluids, suggesting greater hydraulic connection with the overlying Calivil Formation aquifer.
- As best indicated in Figure 8-20b, the saline evolved pore fluid classes are also found at the near-surface (<10 m) and these are inferred to represent evapotranspirative salt concentration.
- There are variable pore fluid classes within the Blanchetown Clay overlying the Calivil Formation target aquifer. The fresh pore fluids (classes 8b and 8e) in some bores, such as BHMAR18-1 (Figure 8-20c) and BHMAR80A-2 (Figure 8-20j), suggest either a degree of leakage and flushing through the clay sequence or diffusion (see Section 7.3.2 for more details pertaining to diffusion processes). Bores with saline pore fluids in the Blanchetown Clay, such as BHMAR41-1 (Figure 8-20f) and BHMAR64-1 (Figure 8-20i), would suggest limited vertical leakage.

These plots show that the fuzzy k-means classes define the groundwater mixing or evolution path from fresh recharged groundwater to saline regional groundwater by the order 8e-8b-8c-8d-8g-8f. On this basis, the least evolved (freshest) fuzzy class for the pore fluids within the Calivil Formation interval could be selected for each sampled hole. Figure 8-21 shows the results of this selection, showing the distribution of holes with active recharge into the target aquifer. Figure 8-22 is the equivalent mapping for the Blanchetown Clay, in terms of the least evolved fuzzy class for the pore fluids within the stratigraphic interval. This map shows whether Blanchetown Clay has been identified downhole and also where Blanchetown Clay pore fluids are fresh and have an affinity with the surface waters, inferred to be where vertical leakage (or diffusion) is occurring. In other areas, the pore fluids are saline and evolved, supporting limited vertical leakage (or diffusion) through the Blanchetown Clay.

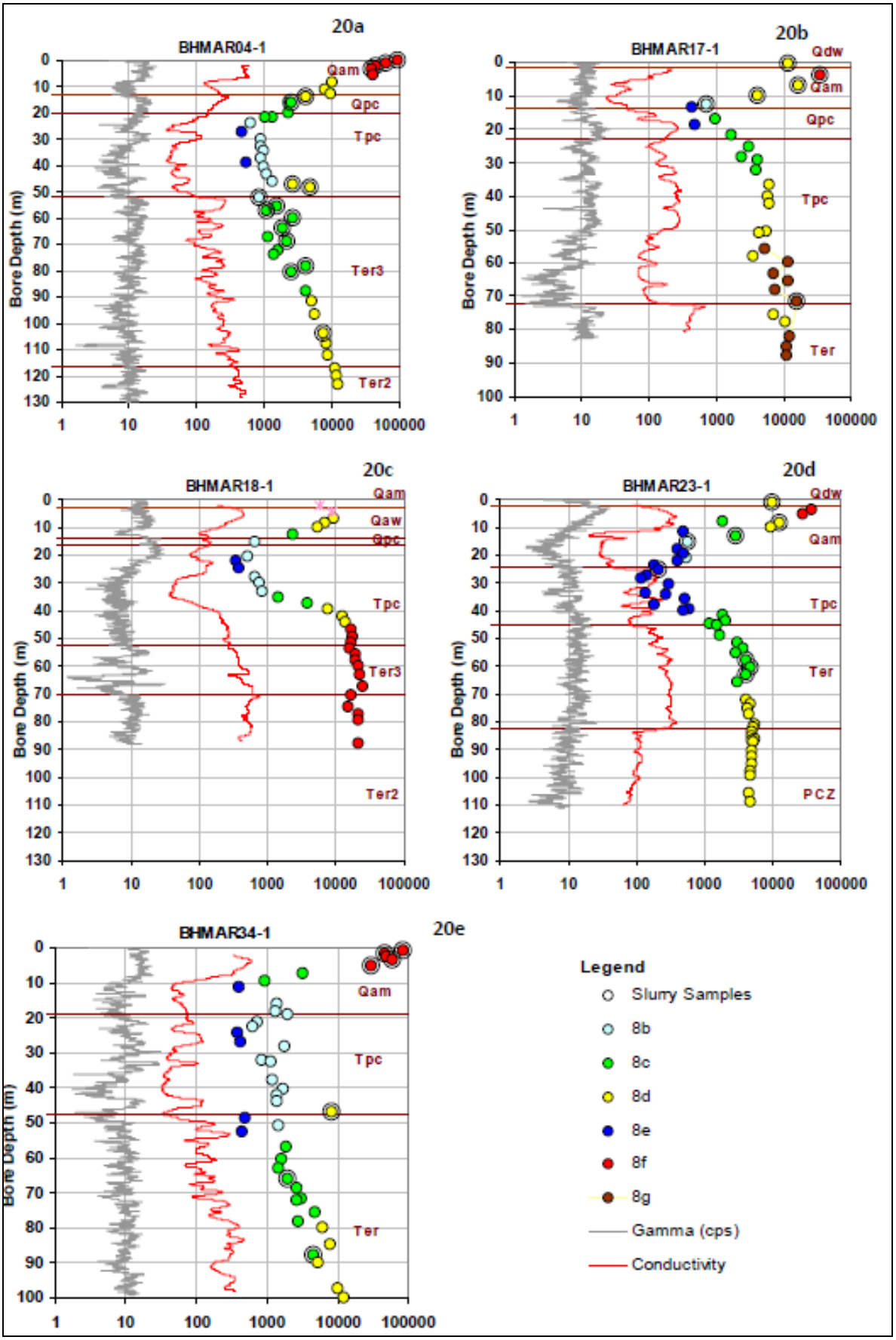

Figure 8-20. *Downhole plots of fuzzy k-means classification (8b-8g) of pore fluids for selected BHMAR boreholes. In these plots Qam = Menindee Formation, Qaw = Willotia beds, Qpc = Blanchetown Clay, Tpc = Calivil Formation, Ter3 = upper Renmark Group, Ter2 = Middle Renmark Group.*

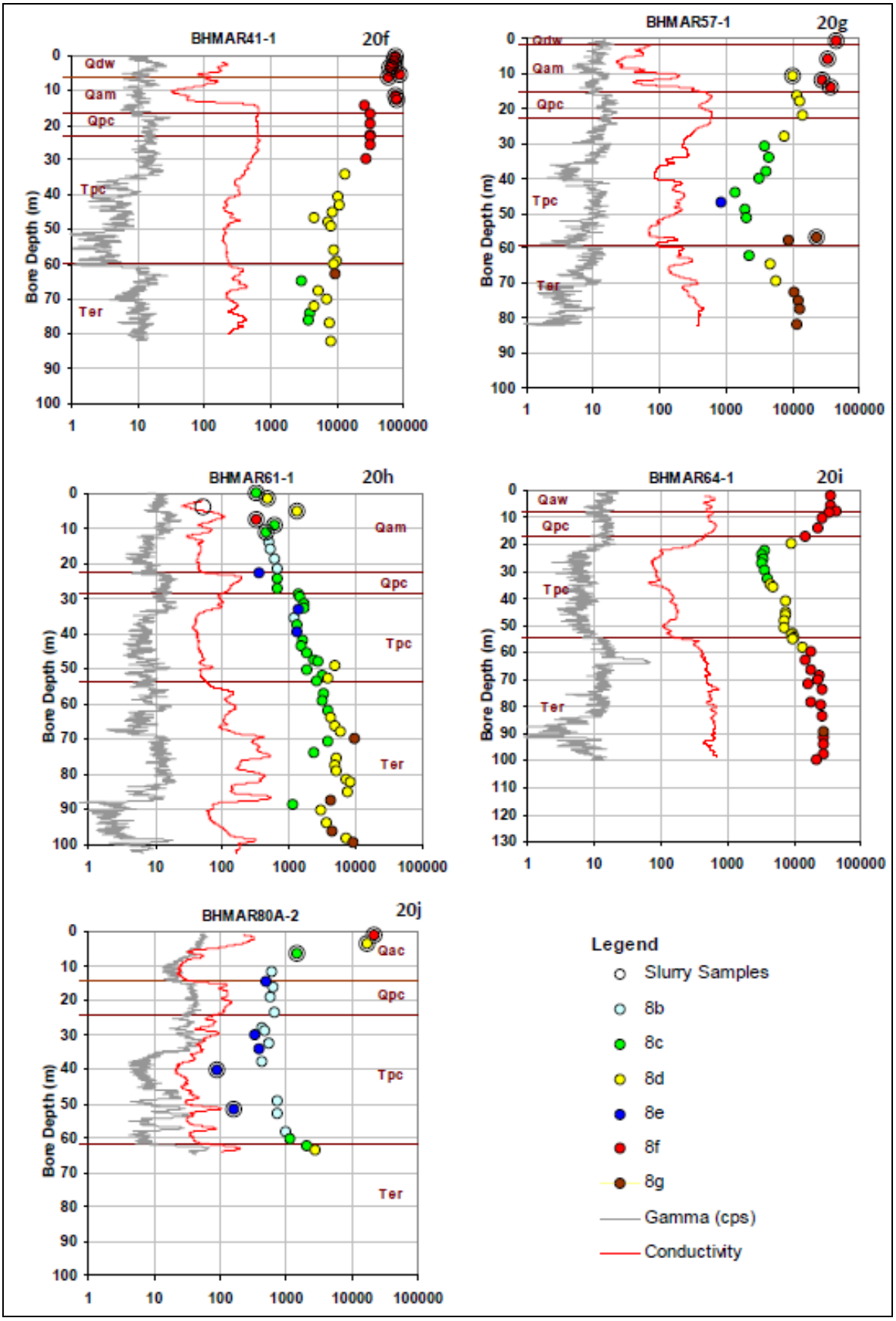

Figure 8-20 (cont). *Downhole plots of fuzzy k-means classification of pore fluids*

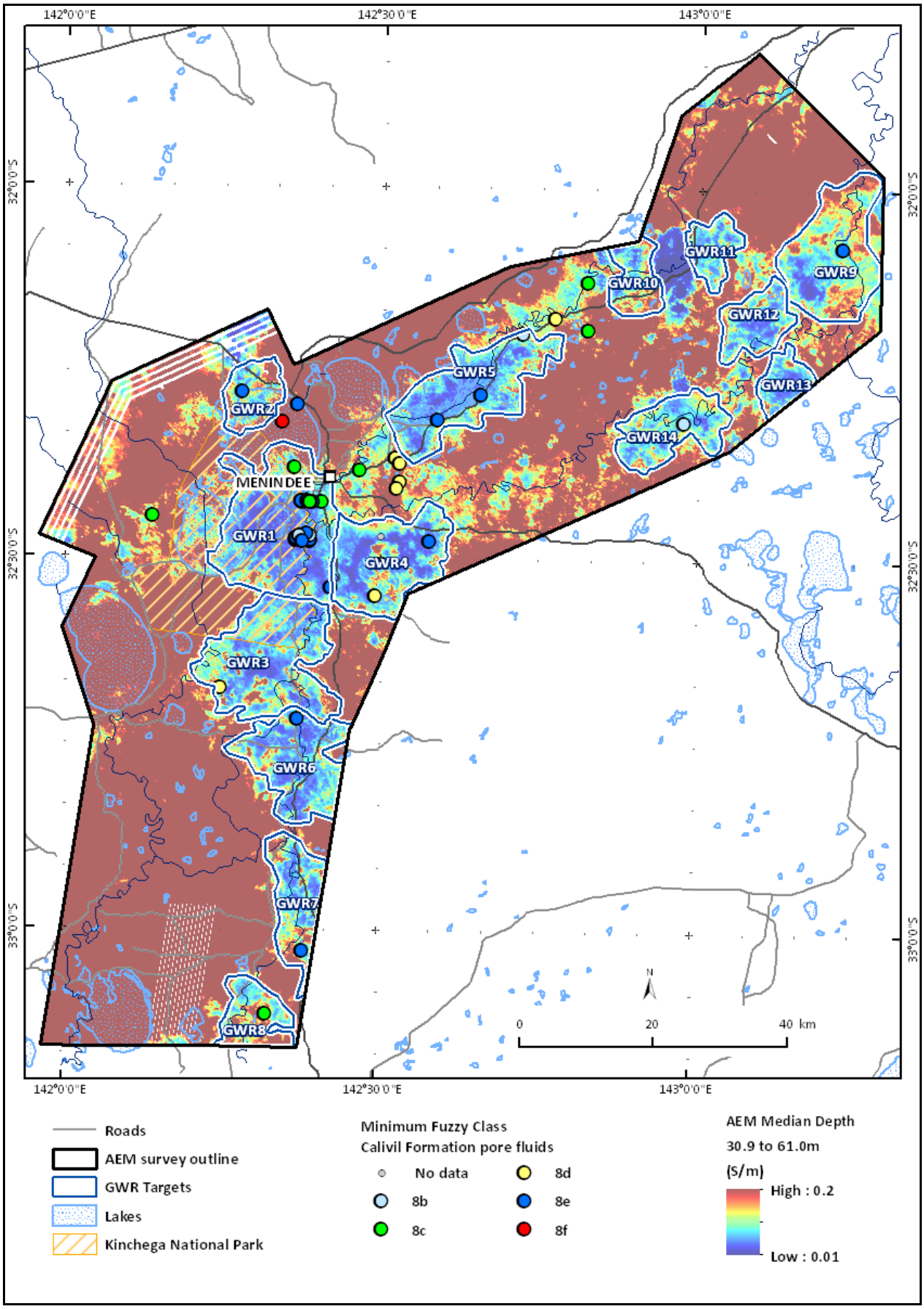

Figure 8-21. *Map of BHMAR study area showing least evolved fuzzy k-means pore fluid class within the Calivil Formation interval in BHMAR sonic holes.*

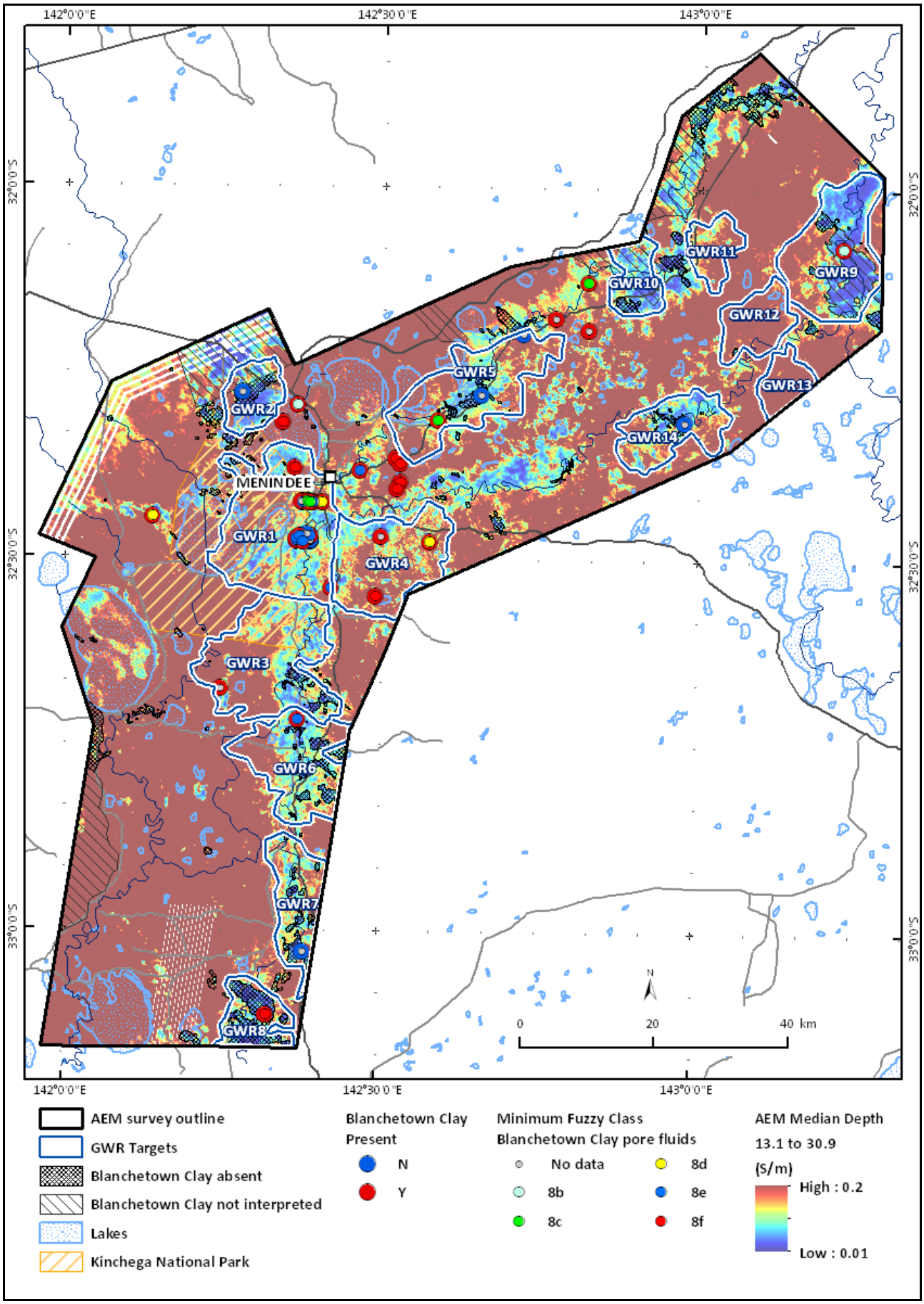

Figure 8-22. *Map of BHMAR study area showing least evolved fuzzy k-means pore fluid class within the Blanchetown Clay interval in BHMAR sonic holes.*

Recognising the significance of the two fresh pore fluid classes (8b and 8e) as a representation of zones of active recharge, a simple empirical recharge index was calculated using the statistics for these two classes. The fuzzy indices representing the goodness of fit for these classes (FI_{8b} and FI_{8e}) were combined by Equation 5:

$$(2*FI_{8e}+FI_{8b})/2$$

Equation 5

This equation incorporates a greater weighting for the class 8e index, being the freshest and having the greater affinity with the surface water samples (Table 8-2). The maximum value for the combination of these two fuzzy indices is 2, so this was used to normalise the index to between 0 (low recharge) and 1 (high recharge). The index provides a representation of the recharge zones down the sonic holes. Note that this is a relative index to highlight zones of preferential recharge and does not equate to actual estimates of recharge rates. Figure 8-23 shows a transect of these holes at Menindee Common, starting about 0.2 km from the river at BHMAR79A-2 to BHMAR08-1, located about 2.4 km out into the floodplain. This summarises the influence of river leakage on recharge into the Calivil Formation target aquifer. Figure 8-24 plots the BHMAR sonic-cored holes on the basis of the maximum recharge index for pore fluids within the Calivil Formation interval, with Figure 8-25 the equivalent map for the Blanchetown Clay.

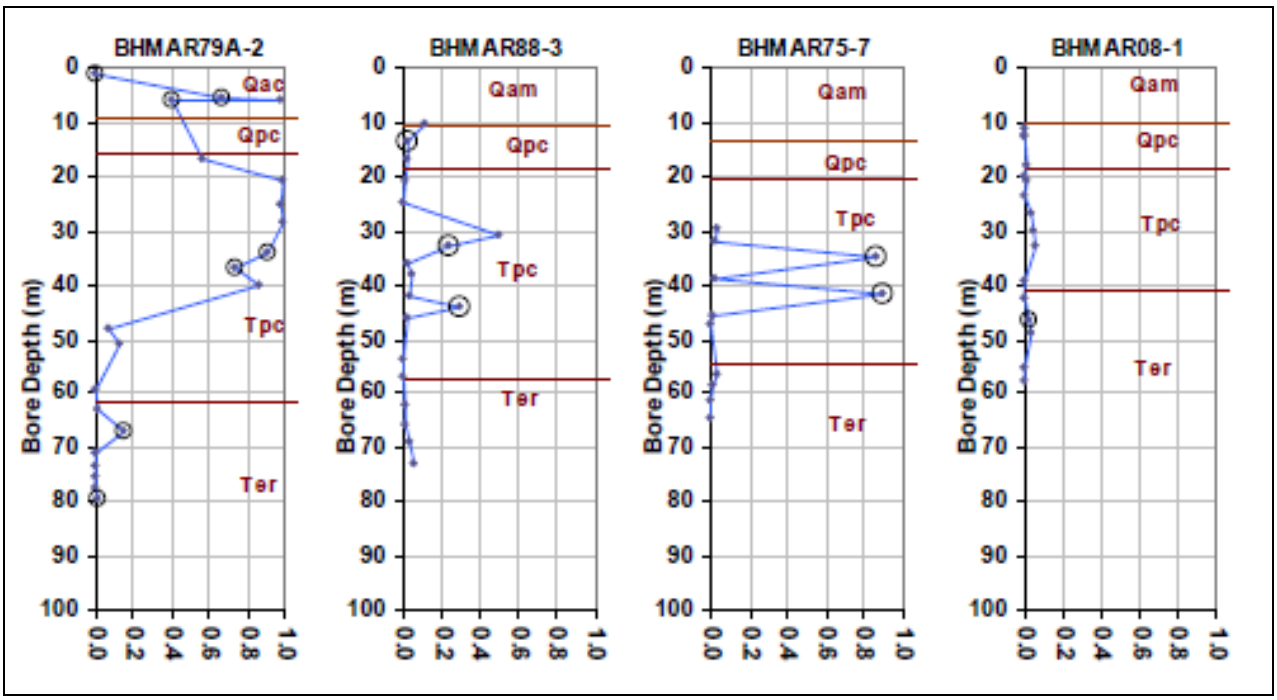

Figure 8-23. *Downhole fuzzy class recharge index for a transect of Menindee Common BHMAR bores.*

An assessment of the relative influences of lateral and vertical recharge processes was undertaken by comparing the assigned fuzzy classes for the pore fluids in the Calivil Formation aquifer with those of the overlying Blanchetown Clay. For example, high vertical leakage is a possibility where the Blanchetown Clay pore fluids are relative fresh, generating a high maximum recharge index. High lateral leakage applies if the Calivil Formation pore fluids have a high maximum recharge index, but the overlying Blanchetown Clay pore fluids have a low maximum recharge index. On this basis, the potential lateral and vertical leakage components were ranked as being high, medium or low. Figure 8-26 maps the results of this assessment across the BHMAR study area. This highlights the influence of both vertical and lateral leakage in the Jimargil-East Bootingee borefield target and the GWR2, GWR5 and GWR6 targets. Such leakage is not as apparent in sonic-cored bores in other targets such as GWR4, GWR7, GWR8 and GWR14.

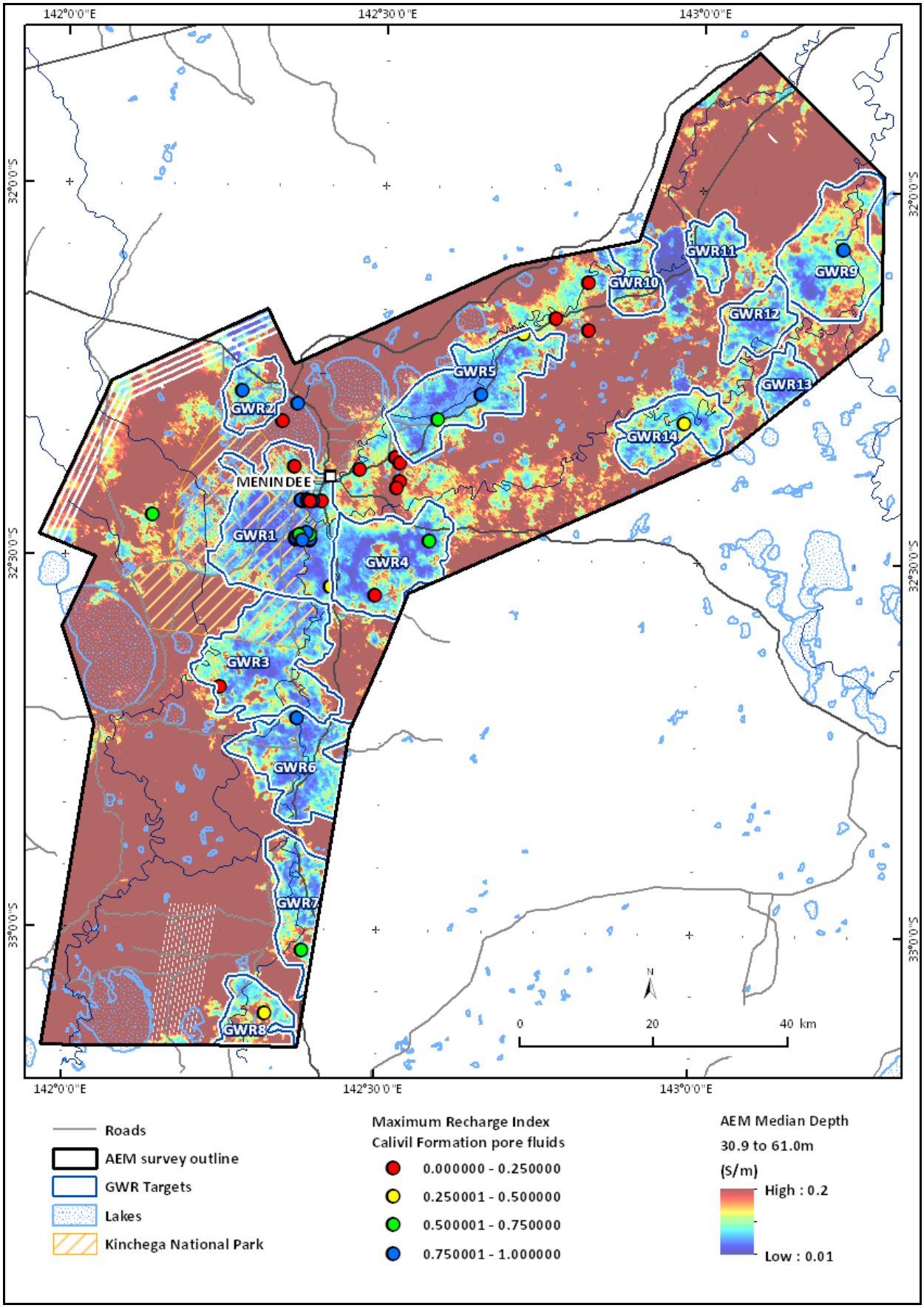

Figure 8-24. *Map of BHMAR study area showing the maximum recharge index defined by pore fluid fuzzy-k mean classes for Calivil Formation interval in BHMAR sonic holes.*

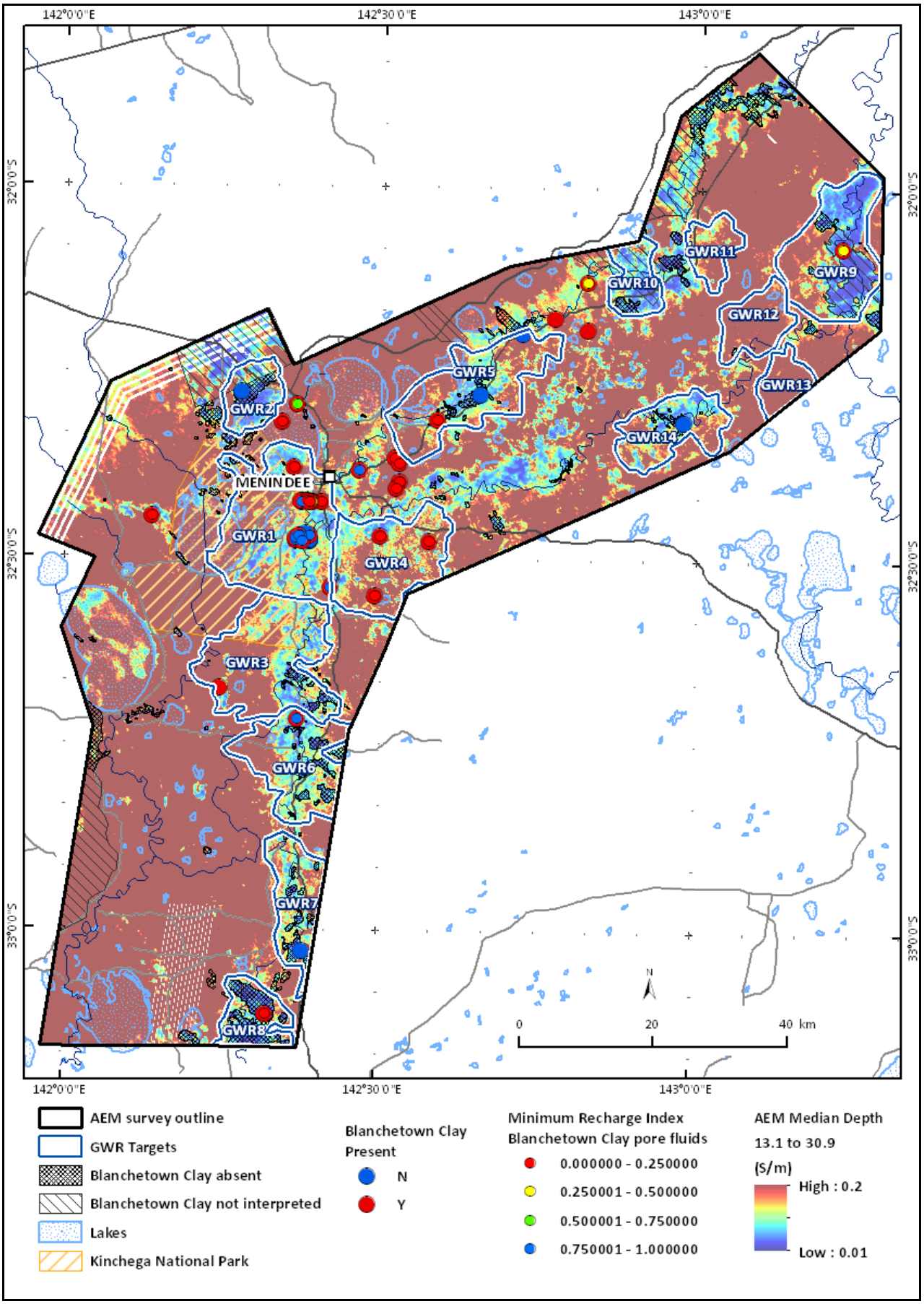

Figure 8-25. *Map of BHMAR study area showing the maximum recharge index defined by pore fluid fuzzy-k mean classes for the Blanchetown Clay interval in BHMAR sonic holes.*

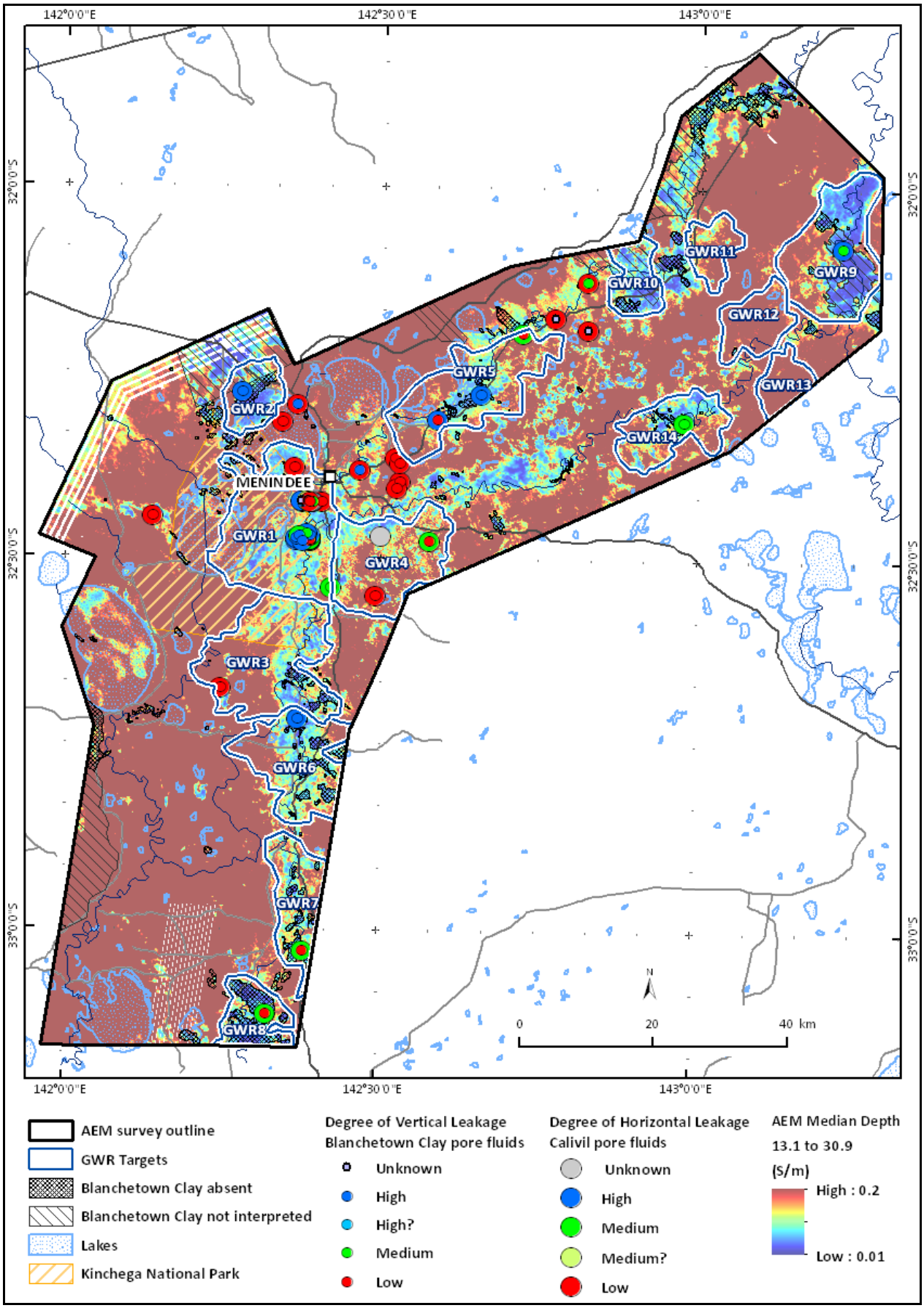

Figure 8-26. *Map of BHMAR study area showing the relative influence of lateral and vertical recharge processes based on pore fluid fuzzy-k mean classes in BHMAR sonic holes.*

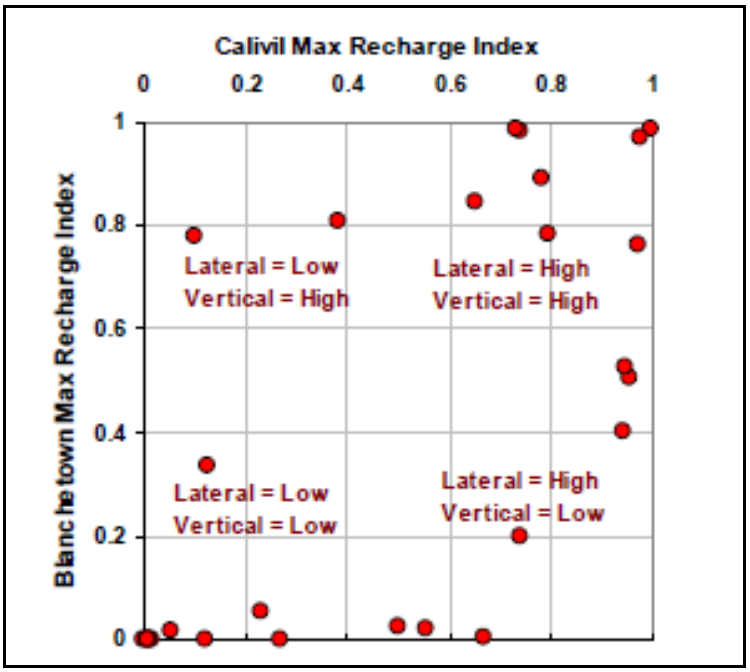

Figure 8-27. *Scatter plot of maximum recharge index for Calivil Formation pore fluids against maximum recharge index for Blanchetown Clay pore fluids, for sampled BHMAR sonic-cored holes.*

Relatively fresh pore fluids in the Blanchetown Clay can also reflect diffusion processes rather than vertical advection through the profile. The maintenance of fresh groundwater due to episodic river leakage can induce a persistent salinity gradient to enable diffusion processes in the aquitards. This can result in freshening of the pore fluids in the upper part of the aquitard because of low-salinity groundwater in the overlying Coonambidgal or Menindee Formation aquifers, or freshening in the lower part because of low-salinity groundwater in the underlying Calivil Formation.

Various estimates of the effective diffusion coefficient and relative concentration gradient were used to characterise potential diffusion through the aquitard sequence. The approach used and the underlying equations are documented in Lawrie *et al.* (2012a). By using the mapped thickness of the upper confining aquitard, a low estimate and a high estimate of the time required for complete diffusion of the aquitard profile could be mapped. Figure 7-36 is a low estimate of the required diffusion time using a high estimate for both the effective diffusion coefficient and relative concentration gradient. In contrast, Figure 7-37 is a high estimate of the required diffusion time using a low estimate for both the effective diffusion coefficient and relative concentration gradient.

These estimates have been classified on the basis of the age ranges estimated for the four phases identified for the Coonambidgal Formation. The age dating of these phases is described in Section 5.4.1.5. In this way, the potential for freshening of the aquitard due to diffusion can be compared with the likely duration of river leakage. For example, leakage from river reaches where only the Coonambidgal 1 phase occurs (such as near Menindee) is likely to have only occurred over the past 5,000 to 7,000 years. Where the geomorphological history goes back to the Coonambidgal Phase 4 migration phase (as evident in the GWR1 target area), then river leakage is likely to have persisted over a longer time frame, in the order of 40,000 to 50,000 years.

Therefore, the diffusion time maps (Figure 7-36 and Figure 7-37) give insights into the likelihood of concentration gradients being maintained due to river leakage and resulting in freshening of the aquitard pore fluid by diffusion. For example, for the GWR5 target at Lake Wetherell, even though this river reach is relatively modern (Coonambidgal Phase 1), the timeframe for complete diffusion of the aquitard profile is also relatively short. In parts of the GWR1 target, the coincidence of the Coonambidgal Phases infers that concentration gradients driving diffusion has persisted for 50,000 years. As indicated by the mapping, there are near-river zones where it would be possible for diffusion to completely freshen the aquitards profile within this timeframe.

On this basis, it should be noted that fresh pore fluids in the Blanchetown Clay may not necessarily reflect vertical advection processes, but relate to diffusion over longer time frames.

To summarise the fuzzy k-means analysis, the interpretation of the eight fuzzy classes is that:

- Class 8a consists of mostly fresh lake and river samples, the latter relating to relatively high flow conditions. These surface waters have similar salinities to class 8e surface waters but have a greater HCO_3-Ca-Mg signature. There are no groundwaters (nor pore fluids) with this association, suggesting recharge with these waters is limited.
- Class 8b are mostly fresh to brackish groundwaters and pore fluids relating to the mixing zone between river leakage and saline regional groundwaters. At depth, pore fluids in this class surround the fresher class 8e pore fluids.
- Classes 8c and 8d are groundwaters (and pore fluids) representing intermediate steps in mixing between river leakage (classes 8e and 8b) and regional saline evolved groundwaters (classes 8f and 8g).
- Class 8e contain all water types and so is inferred to be related to the dominant recharge processes. The class contains rainfall samples, river and lake samples and the freshest groundwaters, mostly in the shallow and Calivil Formation aquifers. The groundwaters (and pore fluids) in this class are the best indicator of active recharge both spatially and at depth.
- Class 8f groundwaters (and pore fluids) are the most saline and evolved Na-Cl water types typically found at shallow depths (associated with evapotranspirative processes), the Blanchetown Clay and the deeper Renmark Group.
- Class 8g are saline evolved pore fluids with relatively high sulfate and low pH, possibly indicating oxidation of sulfides during the sample extraction process;
- Class 8h are predominately river samples that are relatively saline (average EC ~600 µS/cm) and associated with moderate to low flow conditions (<4000 ML/d). There is only one groundwater (and no pore fluids) assigned to this class, suggesting that leakage and recharge to the shallow aquifer and the Calivil Formation aquifer during these river conditions is limited.

8.3 STABLE ISOTOPE ANALYSIS

Samples of rainfall, surface water and groundwater have been collected during the BHMAR project for the analysis of the stable water isotopes oxygen-18 ($\delta^{18}O$) and deuterium ($\delta^{2}H$). Data interpretation also incorporates the findings of previous stable isotope investigations for the Darling River such as the work of Gibson *et al*. (2008), Meredith *et al*. (2009) and Hughes *et al*. (2009). In particular, Hughes *et al.* (2009) reported on the monthly collection of stable water isotopes at nine stations along the Darling River, from Mungindi near the Queensland border, downstream to Burtundy near the confluence with the River Murray. Although individual flow events in the Darling River were isotopically distinct, subsequent evaporation resulted in the local evaporation lines (LEL) for these events to have a similar slope. An overall Darling River LEL was defined by the relationship $\delta^{2}H = 4.86\delta^{18}O - 4.85$ ($R^2=0.97$, n=325). The shallow slope compared to the Global Meteoric Water Line (GMWL) highlights the significance of evaporation for the Darling River (Figure 8-28a). High flow events marked the input of isotopically depleted fresh water to the river (Figure 8-28b). This was followed by progressive salinity increases and isotopic enrichment during low-flow periods. This means that the river isotope data plots further along the Darling LEL (and away from the GMWL) with reducing flow due to evaporative loss. The arrow in Figure 8-28a depicts this trend associated with decreasing river flow.

The data envelope and the Darling River LEL of Hughes *et al.* (2009) provides context for the rainfall, lake and river samples collected by the BHMAR project (Figure 8-29). The nine cumulative rainfall samples were collected from the Menindee weather station site between December 2009 and October 2010. The $\delta^{18}O$ values were in the range -7 to -2 $^{o}/_{oo}$ and the $\delta^{2}H$ values were in the range -50 to -9 $^{o}/_{oo}$. The local meteoric water line (LMWL) at Menindee derived from these isotope values is $\delta^{2}H = 7.91\ \delta^{18}O + 11$. This is similar to the LMWL relationship of $\delta^{2}H = 6.9\ \delta^{18}O + 9$ at Alice Springs (Liu *et al.,* 2010) which is based on a longer term sampling record, and could be used as a surrogate for the long-term rainfall stable isotope trend at Menindee. The Menindee LMWL is also consistent with the Global Meteoric Water Line (GMWL) relationship of $\delta^{2}H = 8\ \delta^{18}O + 10$ (Craig, 1961). The Menindee rainfall stable isotope samples and the LMWL trends for Menindee and Alice Springs are plotted in Figure 8-29.

Surface waters were collected in September 2009, January -February 2010, June-July 2010, September-October 2010 and March 2011. This involved sampling from various sites along the Darling River and from the Menindee Lake Storages. The river and lake storage samples generally plot within the data envelope of the existing stable water isotope monitoring for the Darling River (Figure 8-29).

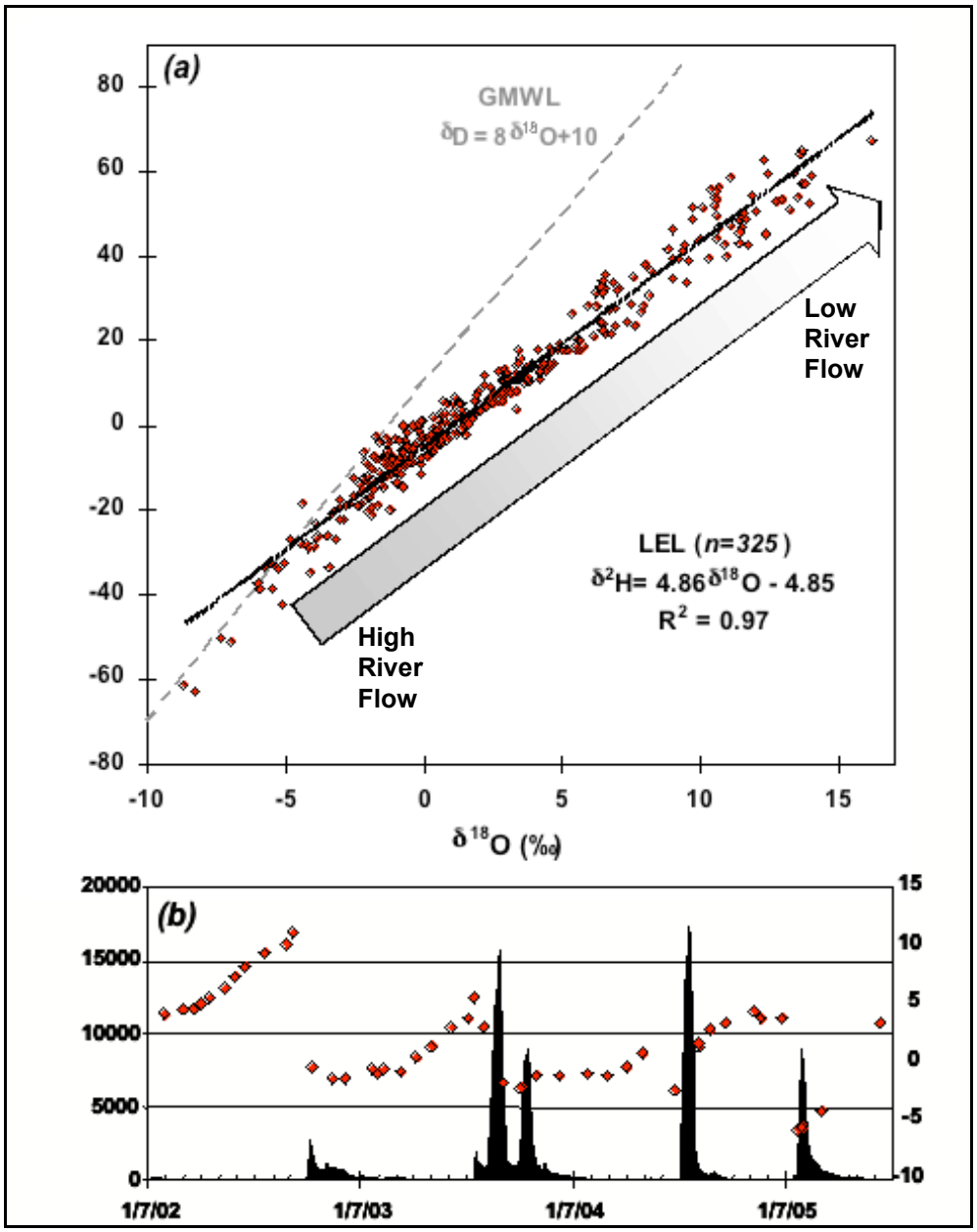

Figure 8-28. *Stable isotope plots from Hughes et al. (2009) showing (a) bivariate plot of δ^2H vs $\delta^{18}O$ for nine Darling River stations from Mungindi to Burtundy from 2002 to 2006 and (b) daily discharge and monthly $\delta^{18}O$ for Wilcannia from July 2002 to January 2006.*

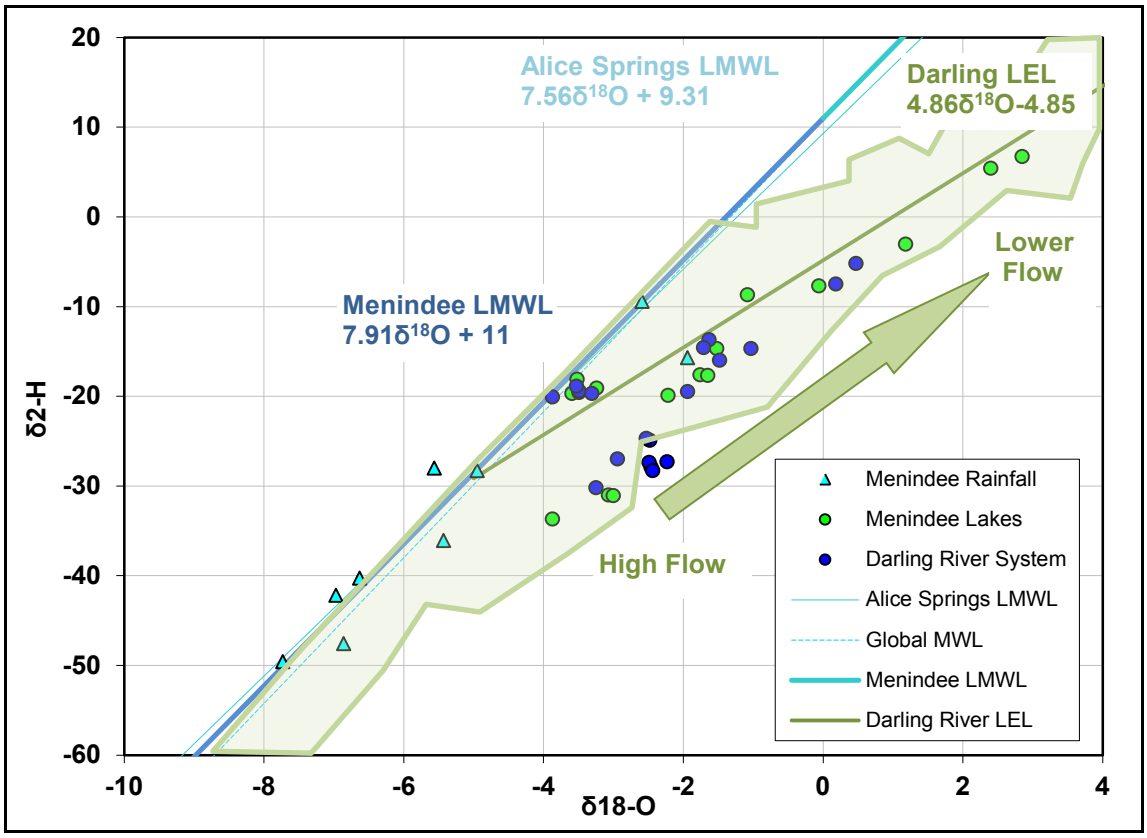

Figure 8-29. *Stable isotope plot of oxygen-18 ($\delta^{18}O$) and deuterium ($\delta^{2}H$) for BHMAR rain water and surface water samples. Data envelope and LEL trend for Darling River stable water isotope monitoring from Hughes et al. (2009) also plotted.*

The stable water isotope analyses for the suite of BHMAR groundwater samples are plotted in Figure 8-30 and are available in Appendix 6 (Somerville *et al*., 2012). The data envelope and Darling River LEL from Hughes *et al.* (2009) are also plotted. The isotope values for the Loxton-Parilla Sands (n = 4) and the Renmark Group (n = 20) groundwater samples are co-located with the bulk of the Calivil Formation samples (n = 87). This cluster is also co-located with Darling River samples with a relatively depleted signature characteristic of high river flows (Figure 8-29). In contrast, the Willotia beds (n = 3), Menindee Formation (n=11), Coonambidgal Formation (n=3) and some of the Calivil Formation (n=6) groundwater samples are isotopically heavier and plot further along the Darling River LEL. The one Paleozoic groundwater sample is anomalously depleted and plots in the lower range of the Darling River LEL. This sample is deeper and distant from the river, so its position on the plot suggests a contrast in hydrologic processes, such as palaeorecharge during previous wetter climate regimes.

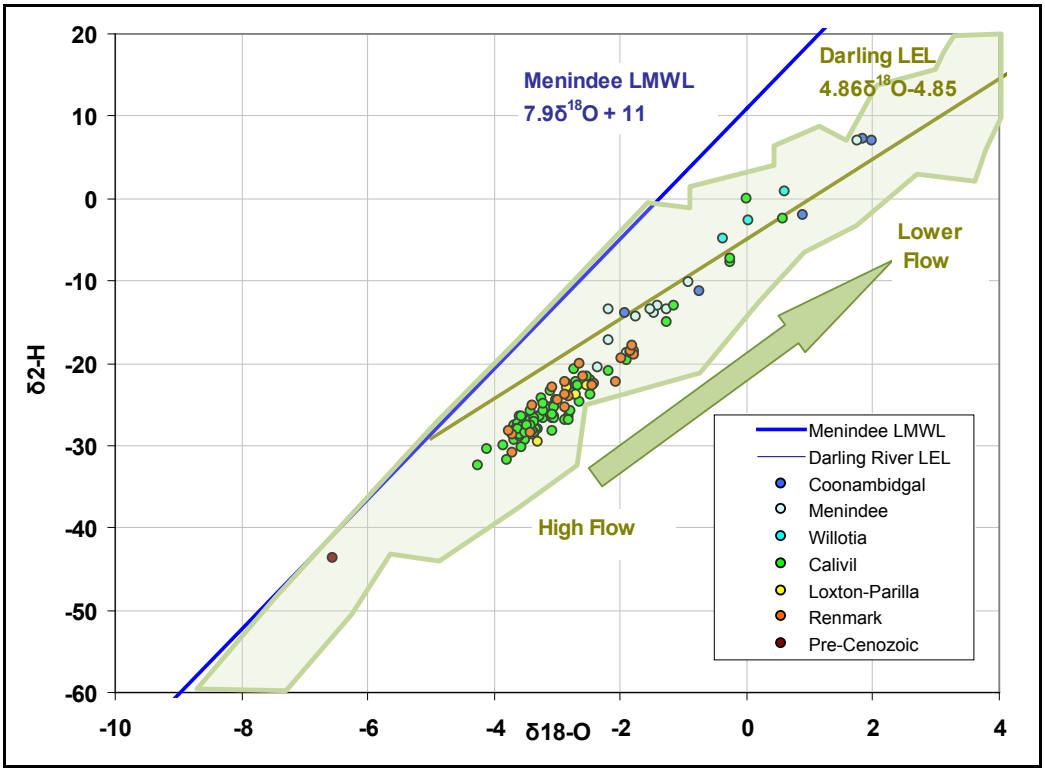

Figure 8-30. *Scatter plot of $\delta^{18}O$ and $\delta^{2}H$ for BHMAR groundwater samples. Data envelope for Darling River stable water isotope monitoring from Hughes et al. (2009) also plotted.*

Figure 8-31 provides a different perspective by plotting the groundwaters on the basis of the fuzzy k-means classes. The relatively depleted cluster with $\delta^{18}O$ values of -2 to -4 $^{o}/_{oo}$ and $\delta^{2}H$ values of -32 to -20 $^{o}/_{oo}$, dominated by Renmark Group and Calivil Formation groundwaters, cover the broad spectrum of fuzzy classes (Figure 8-31a). Focusing on the classes linked to active recharge (Classes 8a, 8b and 8e) shows the segregation between the fresh Calivil Formation (Tpc) groundwaters from the shallow aquifer (Q) groundwaters (Figure 8-31b). The fresh Calivil Formation groundwaters are part of the cluster near the base of the Darling River LEL associated with high flows and a more meteoric signature. Such tight clustering suggests that recharge is relatively rapid involving high river flow events and limited evaporative processes. In contrast, if recharge to the Calivil Formation is due to continual river leakage regardless of river flow, then the Calivil Formation samples should also extend further along the Darling River LEL. The two exceptions to this cluster (BHMAR23-2 and BHMAR18-1) are associated with leakage from Lake Menindee rather than the Darling River. These have a more enriched and evaporated signature that reflects lake conditions at the time of recharge. The fresh shallow aquifer groundwaters plot further along the Darling River LEL and have a broader range. This suggests two potential processes linked to shallow aquifer recharge of (1) lower Darling River flows than that associated with Calivil Formation recharge and/or (2) evaporative processes. For example, an evaporative signal may reflect recharge following the inundation of low-lying floodplain areas by the flood event.

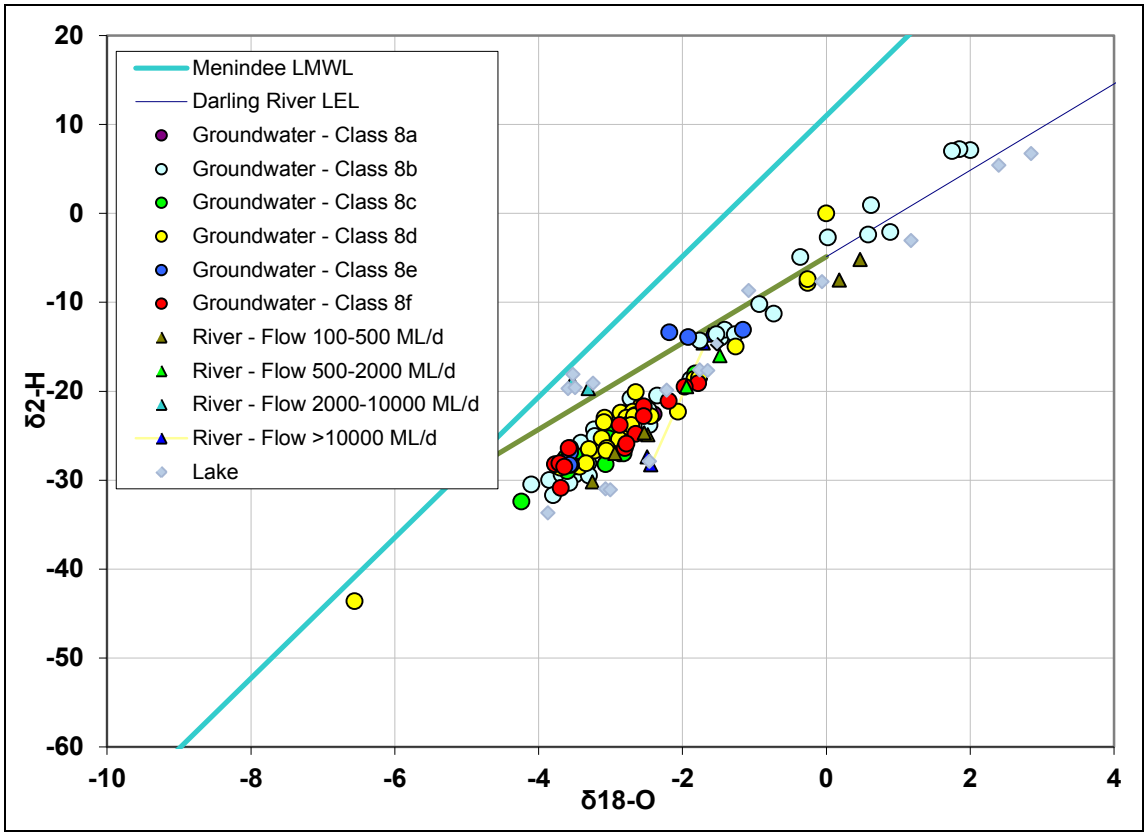

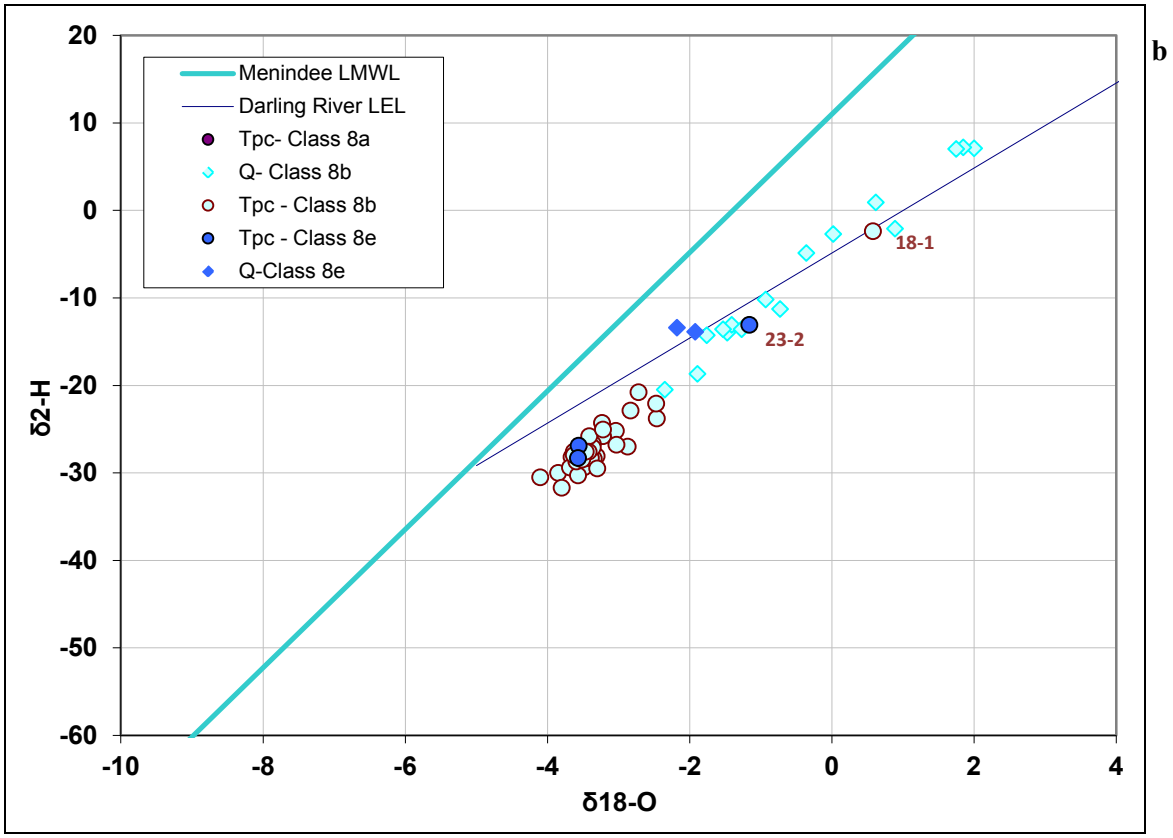

Figure 8-31. *Scatter plots of $\delta^{18}O$ and $\delta^{2}H$ for BHMAR groundwater sample, classified by fuzzy k-means.*

Figure 8-32 plots the fuzzy classes on the basis of deuterium δ^2H and chloride, as an indicator of salinity. This shows the progressive δ^2H enrichment of the river and lake samples with increasing salinity due to evaporative processes. The figure also shows the contrast between the deeper groundwater samples that have a relatively narrow and depleted δ^2H signature and the shallow groundwaters which have a broader and relatively enriched δ^2H signature. The deep groundwater exceptions to these trends are identified in the plot. These samples are related to leakage associated with Lake Menindee that would also have an evaporative signature, rather than the Darling River.

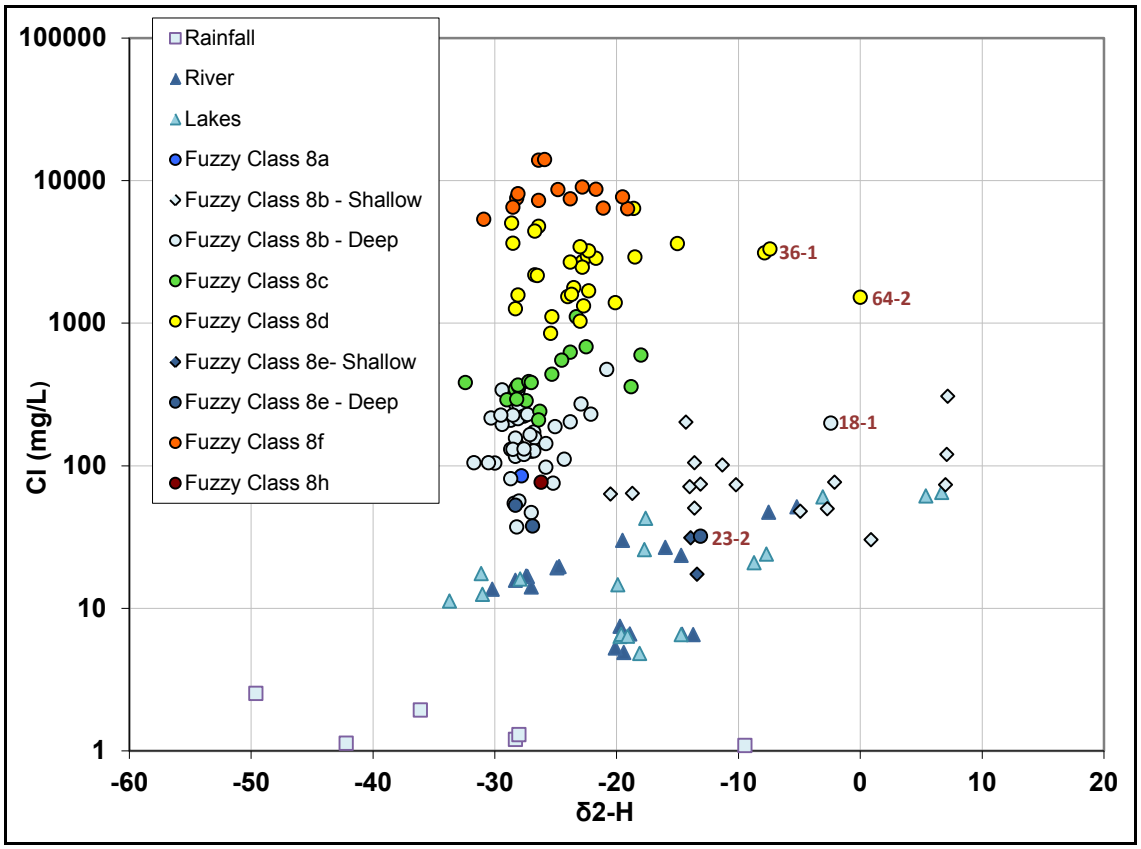

Figure 8-32. *Scatter plot of δ^2H and chloride for BHMAR groundwater sample, classified by fuzzy k-means.*

The Darling River deuterium values for the collection periods are plotted against river flow (ML/d) at Weir 32 (Figure 8-33). The two samples collected in September 2009 are isotopically enriched (δ^2H -5.2 and -7.55 $^{o}/_{oo}$) and plot in the more evaporated part of the Darling River LEL (Figure 8-29). This reflects the extended dry and low flow conditions at the time. Following catchment rainfall, samples collected in January and February, 2010 have a more depleted signal (δ^2H -13.7 to -19.7 $^{o}/_{oo}$). This isotopic depletion is the persistent pattern bought about by larger and fresher river flows in the river (Figure 8-28b). The subsequent low flows from April 2010 onwards are dominated by releases from the Menindee Lakes Storages which still have the relatively enriched signature that is associated with the previous high flow event. These releases tend to mask the progressive isotopic depletion of the river water due to evaporation (Figure 8-28b). In October 2010, another flooding event commenced. This was more significant as in December 2010 it exceeded the Weir 32 gauge height (6.15 m) associated with overbank flooding. This threshold is evident as a change in slope in the gauge rating curve and equates to a river flow of 19000 ML/d (Figure 8-34). The river samples of March 2011 are even more depleted (δ^2H -27.4 and -28.3 $^{o}/_{oo}$). These river samples are in the same location in the $\delta^{18}O$- $\delta^{2}H$ plot as the cluster of Calivil Formation samples, particularly the fresher ones associated with river leakage (Figure 8-31b). This would suggest that high river flows associated with overbank flooding is the key driver for recharge to the Calivil Formation target aquifer. This is consistent with the inference made from using potassium as a tracer (Figure 8-11 and Figure 8-12).

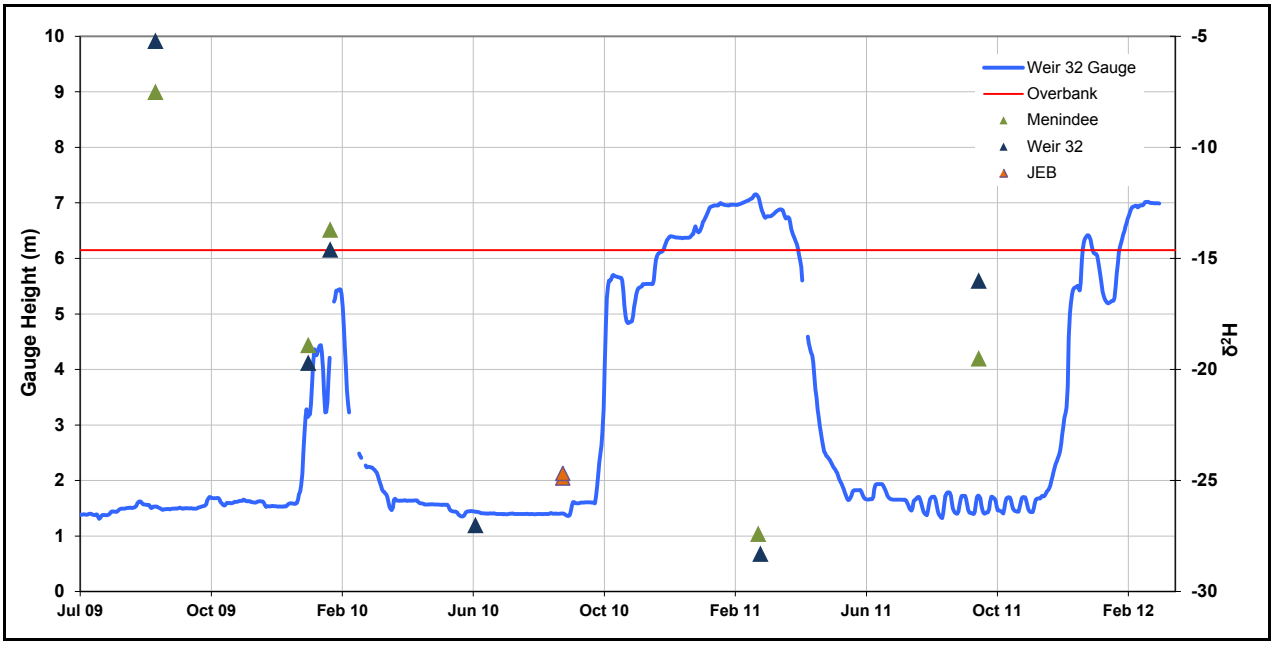

Figure 8-33. *Plot of Darling River discharge at Weir 32 for July2009 to March 2011 and corresponding δ^2H values measured at sites along the river.*

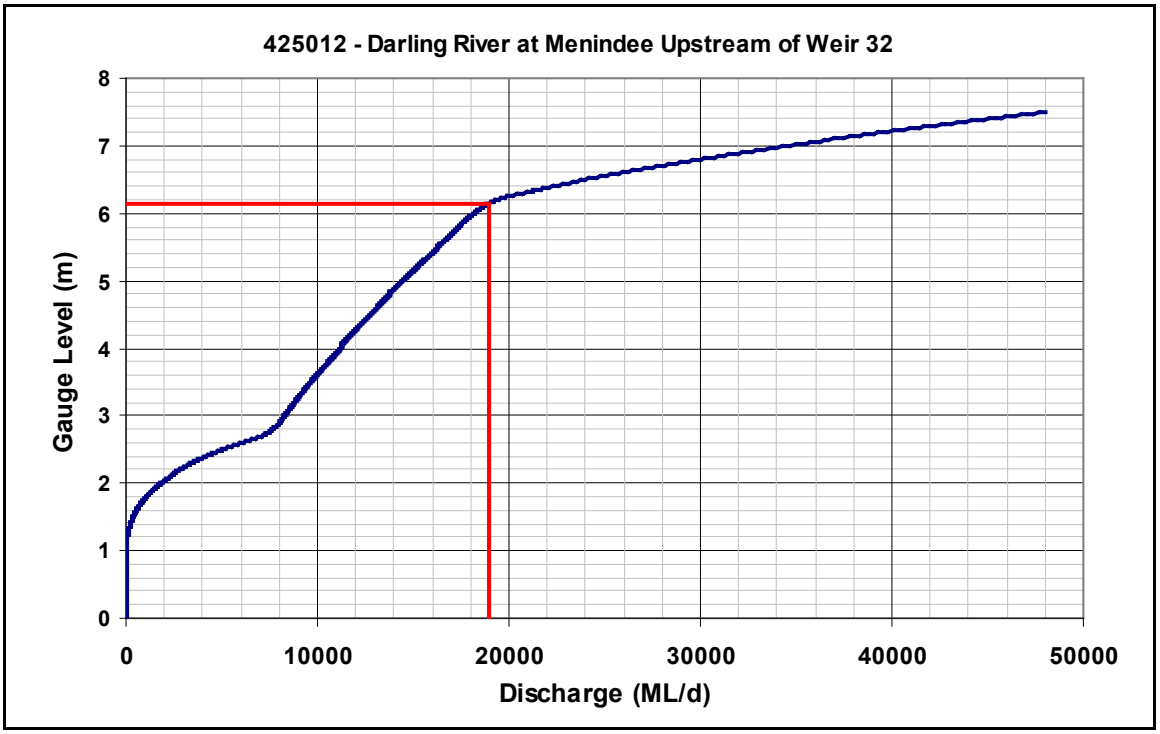

Figure 8-34. *Rating curve for Darling River gauging station at Weir 32 showing changed flow relationship at 19000 ML/d.*

In summary, a Menindee local meteoric water line (LMWL) based on cumulative rainfall samples is similar to the longer term Alice Springs rainfall LMWL and also the global meteoric line (GMWL). The regional stable isotope record for the Darling River (Hughes *et al.*, 2009) shows a significant evaporative signal compared to rainfall, as indicated by the shallow slope of the Darling River local evaporation line (LEL). The isotopic signature of Menindee surface waters collected between September 2009 and March 2011 shows the effects of variable flow conditions and regulated storage releases. The Menindee surface water and groundwater samples tend to be constrained along similar local evaporation lines, suggesting that river leakage (or lake leakage in certain cases) is the dominant recharge process. The isotopic signature for fresh

Calivil Formation samples suggests that recharge is relatively rapid and occurs during high-flow events, rather than continual river leakage. In particular, comparison with the river record suggests that recharge to the Calivil Formation is linked to the episodic high flow events. The shallow groundwater samples are isotopically heavier and have a greater evaporative trend.

8.4 RADIOCARBON ANALYSIS

Groundwater samples from the BHMAR monitoring bores were submitted for radiocarbon analysis to help estimate groundwater ages and understand recharge dynamics. Carbon-14 (^{14}C) is a widely applied dating technique for regional aquifers (Edmunds, 2009) because of its age range (up to 30,000 years) and the ubiquitous presence of dissolved inorganic carbon (DIC) in groundwater.

Figure 8-35 are scatter plots using percent modern carbon (pMC) as an initial surrogate for groundwater residence time. There is a reasonable relationship with chloride which is used as a conservative ion to map groundwater evolution (Figure 8-35a). Most of the fresh shallow groundwaters hosted within the Coonambidgal Formation, Menindee Formation or Willotia beds aquifers essentially have a modern carbon signature (pMC ≥ 99%). Values exceeding 100% pMC imply a recharge component during or since the atmospheric nuclear tests in the 1950s. This provides further evidence for surface water leakage (or diffuse rainfall) under current climate conditions being a dominant recharge process for the shallow aquifer. The shallow groundwater sampling was focused within the groundwater resource targets identified by the AEM geophysics and sonic drilling. Hence, shallow groundwater pMC is expected to decrease with increasing salinity away from these targets. The fresh Calivil Formation groundwaters have pMC values that are less than that measured for the shallow groundwaters with similar salinities, in the range 56-94% for Cl < 100 mg/L (Figure 8-35a). The Calivil Formation groundwaters become less influenced by modern recharge with progressive increase in salinity. This process continues to the saline (and old) Renmark Group and Paleozoic groundwater end members. Figure 8-35b is the pMC-Cl plot with the groundwaters plotted on the basis of the fuzzy k-means classes. This shows that fresh groundwaters with modern pMC values (pMC ≥ 99%) have all been assigned to the fuzzy classes with surface water linkages (8e and 8b in particular). The plot shows the overall decrease in pMC with increasing salinity, in the groundwater evolution sequence defined by the fuzzy classes, namely 8e-8b-8c-8d-(8g)-8f. Based on the Piper diagram, the bicarbonate/sulfate ratio was plotted against pMC, and this is also useful in mapping groundwater evolution (Figure 8-35c). With some exceptions, using the fuzzy classes defined the mixing facies between fresh shallow groundwaters and the deeper evolved groundwaters (Figure 8-35d).

Figure 8-35e plots on an aquifer basis the relationship between pMC and the distance of the sampled bore from the nearest surface water feature. Although there is a general inverse relationship, there is significant scatter. This is because there are groundwater samples from the deeper Renmark Group and Paleozoic aquifers that are relatively close to the river (or lake) but have low pMC values indicating limited influence of modern recharge. The variability in the Calivil Formation groundwaters suggests that geological heterogeneity, such as the presence or absence of the upper confining aquitard, also influences modern recharge. Figure 8-35f is the same plot as Figure 8-35e but is based on the fuzzy classes. It summarises the relationship between pMC and surface water distance better, showing the influence of surface water leakage typically within a kilometre of the river (or lake).

Plotting pMC with sample depth highlights the vertical extent for leakage in the shallow aquifer (Figure 8-35 g). It shows the shallow nature (<25 m) of the groundwaters with the modern carbon signature (pMC > 99%) in the Coonambidgal Formation, Menindee Formation and Willotia beds aquifers. Figure 8-35h also shows the broad trend in groundwater evolution with sample depth, as defined by the fuzzy classes. The mixing zone influenced by surface water leakage can be readily distinguished from the older regional groundwaters. Using class 8b as guide for the mixing zone would suggest that the limit of any significant influence of modern recharge is about 60 m depth, typically the base of the Calivil Formation aquifer.

Figure 8-36 to Figure 8-38 map the spatial distribution of groundwater pMC across the BHMAR study area. The shallow groundwaters sampled all have a modern recharge signature with pMC values typically exceeding 100% (Figure 8-36). This includes the fresh shallow groundwaters in GWR2 associated with leakage from Lake Menindee, as well as along the Darling River corridor in GWR1, GWR5 and GWR6.

High pMC values for the Calivil Formation aquifer (Figure 8-37) are notably near the Darling River at Menindee Common and Jimargil-East Bootingee in GWR1, as well as along the river corridor in GWR6, GWR7 and GWR8. In comparison, the pMC values for Calivil Formation groundwaters sampled in the groundwater resource targets along the Talyawalka (GWR9 and GWR13) have lower pMC values, in the order of 55-66%. This may be due to greater episodicity of the flow regime for the Talyawalka when compared with the Darling River, reflected in lesser recharge opportunities. In the GWR4 target, samples from the three Calivil Formation monitoring bores have pMC values of 20-28%. With also a modern recharge source yet to be identified, these low values would suggest a relict palaeochannel groundwater resource for this particular target. The measured pMC values for the Renmark Group samples are typically in the range 1-25%, reflecting limited modern recharge to this deeper groundwater system (Figure 8-38). The two Renmark Group samples with pMC>40% are for BHMAR08-1 and BHMAR61-1, where some hydraulic connection with the overlying Calivil Formation is inferred.

Corrections are typically required to obtain plausible ^{14}C groundwater ages, to take into account any potential input of old ^{14}C-free carbon dissolved into the groundwater. Such input can be due to (1) dissolution of carbonate minerals or organic material in the sediment sequence; (2) the input of deep-seated CO_2 from volcanic activity or limestone metamorphism, (3) methanogenesis or (4) oxidation of organic material within the sediments sequence or (4) carbon diffusion from low-porosity layers (Cartwright, 2009).

Figure 8-39 compares the pMC values against other carbon-related analyses to help assess the significance of these processes, in particular carbonate dissolution and methanogenesis. Although the relationships are poor, there is a subtle increase in bicarbonate from shallow to deep aquifers (Figure 8-39a) as well as for dissolved inorganic carbon (DIC), refer Figure 8-39b. Hence, processes such as carbonate mineral dissolution may be a factor, particularly for the deeper Calivil Formation and Renmark Group aquifers. In Figure 8-39c, there is a high degree of scatter but total organic carbon (TOC) appears to broadly decrease, as pMC decreases from a modern signature (>100% pMC) to about 60% pMC, before slightly rising again as pMC reduces to zero. Figure 8-39d is the same plot with groundwaters as fuzzy k-means classes, showing that the initial TOC decrease relates to the mixing zone induced by surface water leakage. The relationship between dissolved organic carbon (DOC) and pMC is similar (Figure 8-39e).

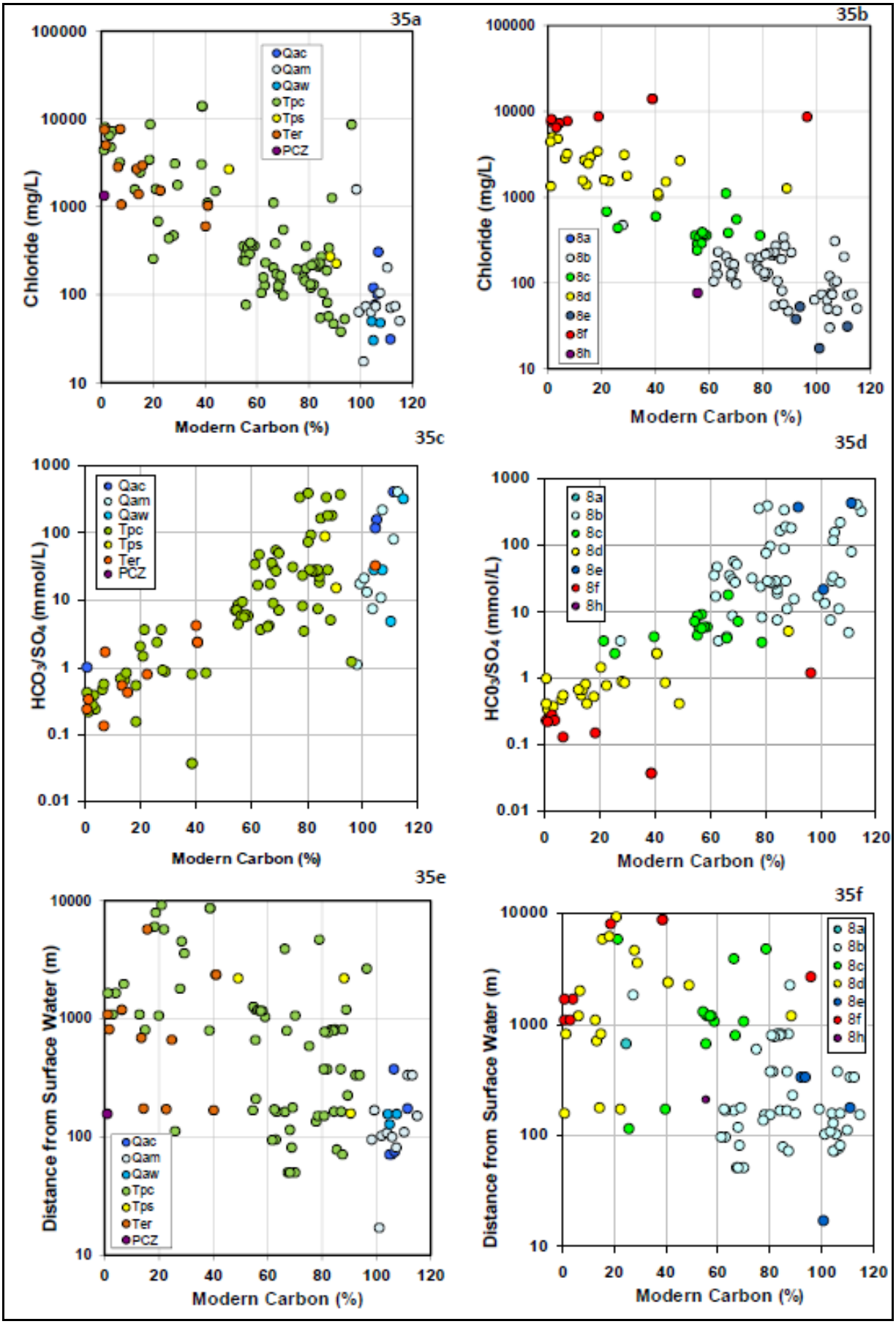

Figure 8-35. *Percent modern carbon (pMC) scatter plots for BHMAR groundwater samples.*

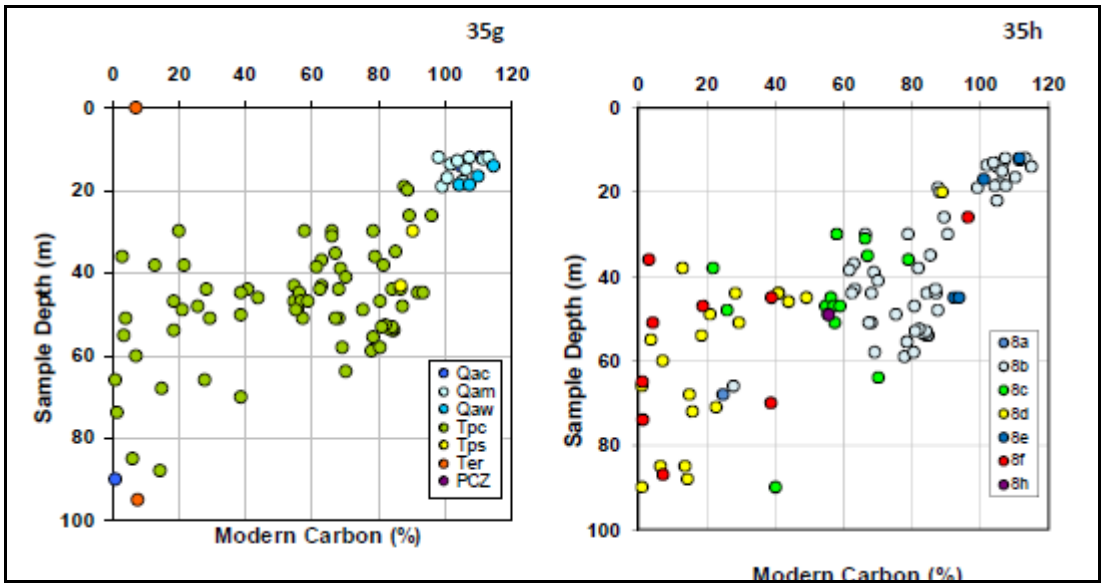

Figure 8-35. (cont.) *Percent modern carbon (pMC) scatter plots for BHMAR groundwater samples.*

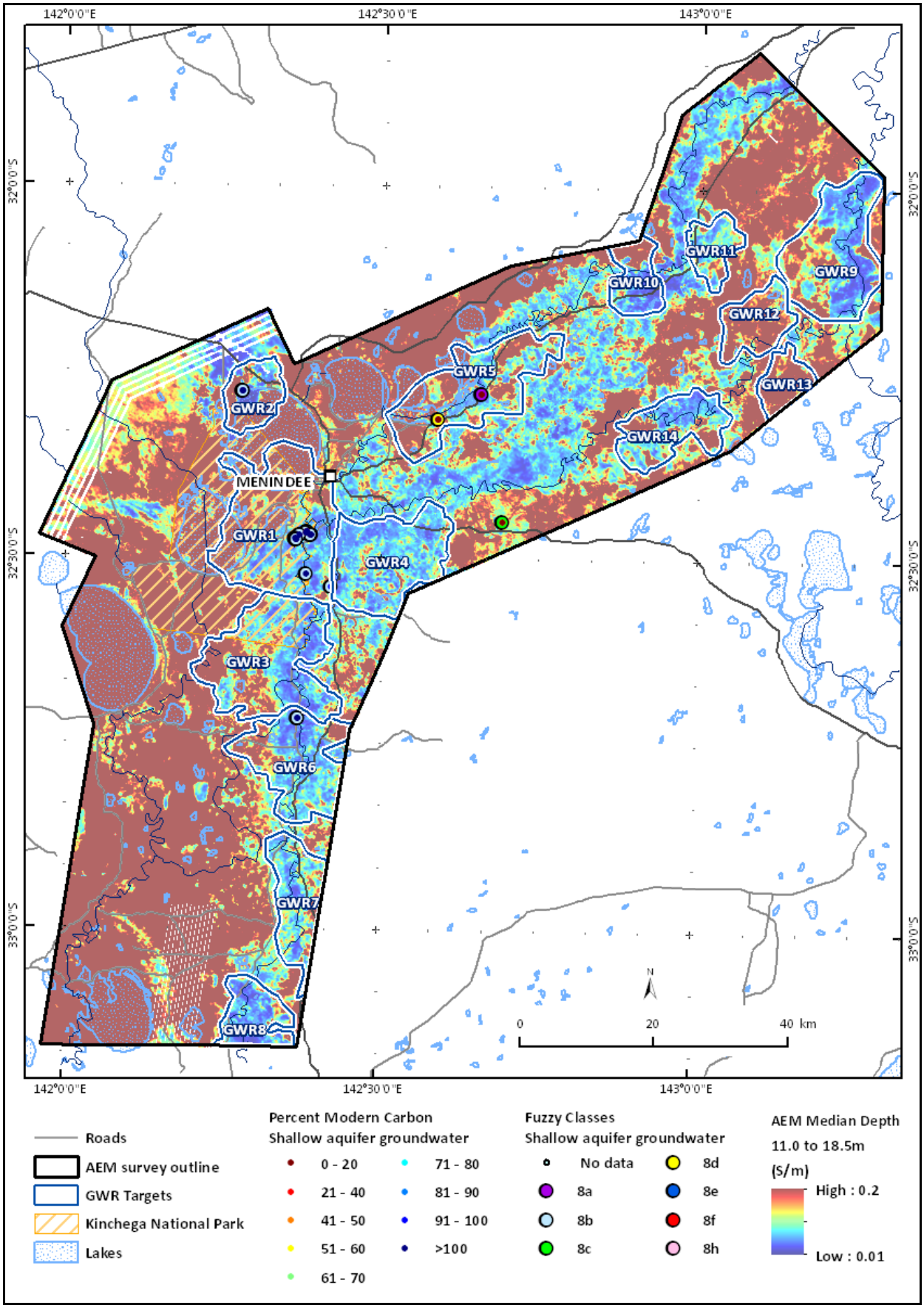

Figure 8-36. *Map of BHMAR project area showing percent modern carbon (pMC) of sampled groundwaters in the shallow unconfined aquifer.*

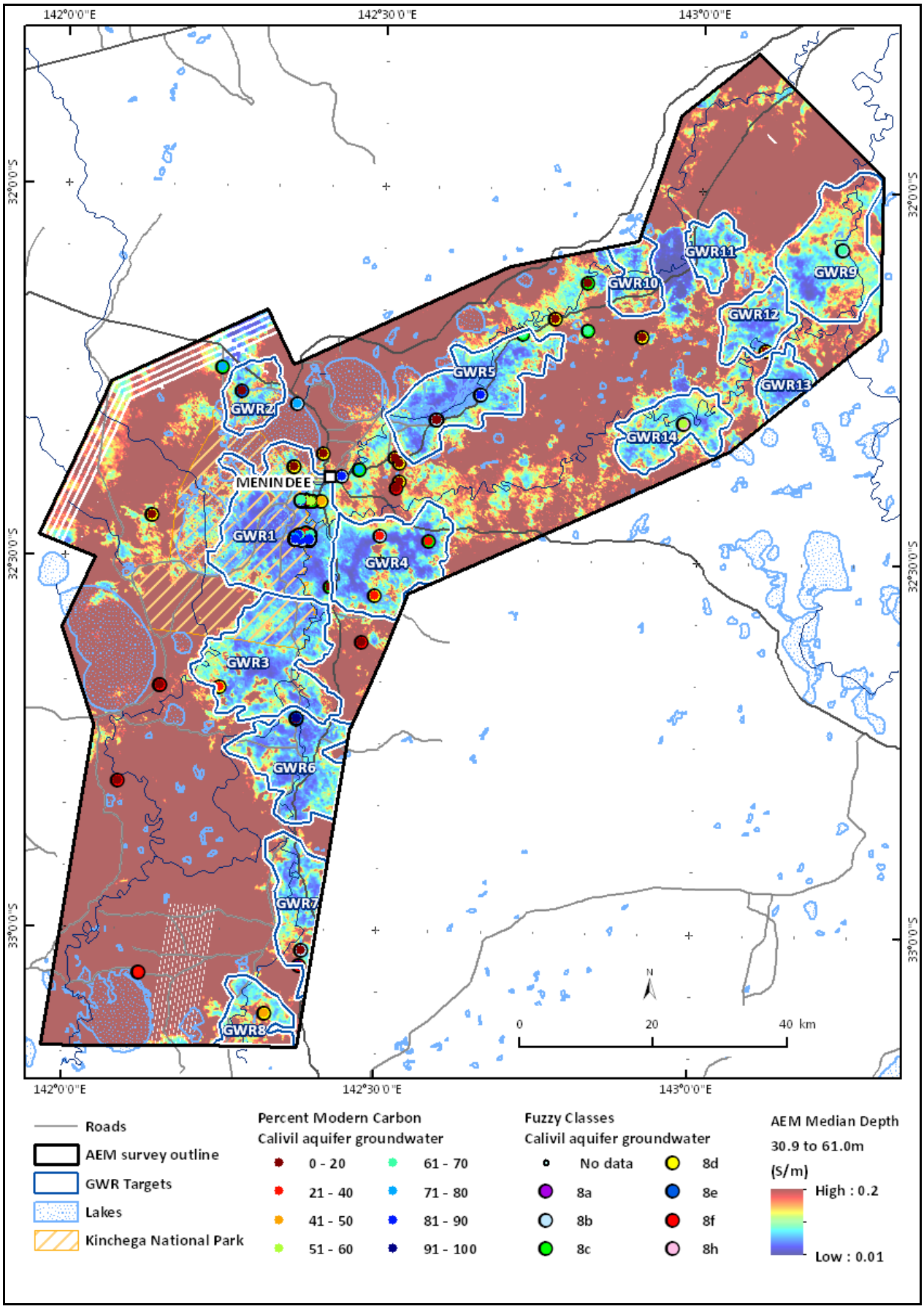

Figure 8-37. *Map of BHMAR project area showing percent modern carbon (pMC) of sampled groundwaters in the Calivil Formation aquifer.*

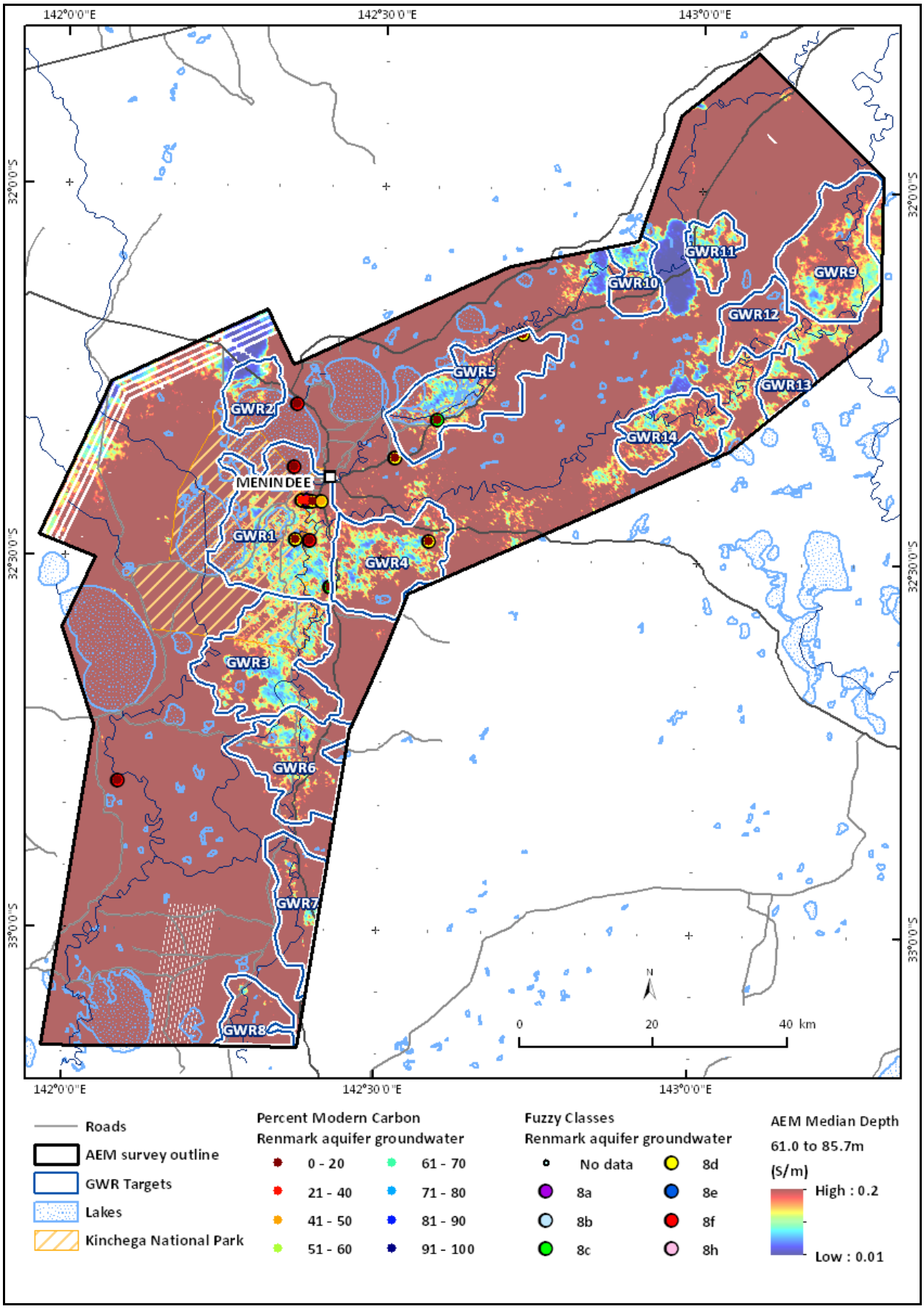

Figure 8-38. *Map of BHMAR project area showing percent modern carbon (pMC) of sampled groundwaters in the Renmark Group.*

In terms of $\delta^{13}C$, there is relatively greater scatter for the shallow aquifer (Figure 8-39f). This is explored further in Figure 8-40a and b which plot the relationship between $\delta^{13}C$ and DIC. Many of the Calivil Formation and Renmark Group samples plot along a positive trend with groundwater evolution, inferred by Cartwright (2009) to relate to calcite dissolution and/or methanogenesis by acetate fermentation. Other samples showing preferential $\delta^{13}C$ enrichment relative to static DIC concentrations can be linked to cation exchange processes. Trends in the Ca- $\delta^{13}C$ plot (Figure 8-40c-d) and SO_4- $\delta^{13}C$ plot (Figure 8-40e) have also been identified with key processes (Coetsiers & Walraevens, 2009). On this basis, methanogenesis and cation exchange are inferred to be dominant for low calcium groundwaters (<50 mg/L Ca). For intermediate groundwaters (Ca<150 mg/L), calcite dissolution drives a positive relation between Ca and $\delta^{13}C$. For more saline groundwaters (Ca>150 mg/L) other processes (possibly gypsum dissolution) cause calcium levels to rise without any change in $\delta^{13}C$. Both calcrete and gypsum have been observed in the sonic core, particularly in the shallow formations.

The geochemical correction models of Tamers (1975), Ingerson & Pearson (1964) and Fontes & Garnier (1979) were applied to the radiocarbon data. The Tamers method uses a carbon mass balance approach to consider only simple carbonate dissolution by soil CO_2. The Fontes & Garnier (F-G) method accounts for isotopic exchange with carbonate minerals in both the unsaturated and saturated zone, as well as carbonate dissolution with CO_2, so would be the preferred option. Table 8-4 summarises the input parameters and rationale used in these correction models.

Table 8-4. *Assumptions used in correction models for radiocarbon ages.*

Parameter	Value	Rationale
$\delta^{13}C$ (carbonate)	-2 ‰	Maximum measured $\delta^{13}C$ groundwater value
A (carbonate)	0 pMC	^{14}C-depleted carbonate input
$\delta^{13}C$ (CO_2 gas)	-18 ‰	Least fractionated groundwater sample – BHMAR34-2 from the shallow Menindee Formation aquifer
A (CO_2 gas)	110 pMC	Equilibration with modern atmospheric conditions

As indicated in Figure 8-41, correction using the Fontes & Garnier (F-G) method (as well as the other methods applied) consistently reduced the radiocarbon ages. This resulted in most of the shallow groundwaters having negative radiocarbon ages, as well as a subset of the Calivil Formation and Loxton-Parilla Sands groundwaters. As indicated by Figure 8-40, there is evidence for an interplay of processes such as calcite dissolution, methanogenesis and cation exchange, so simple correction models are likely to be inadequate. For example, Cartwright (2009) argued that for the analogous sediments in the Campaspe Valley in Victoria, the uncorrected radiocarbon ages were the better estimate of groundwater residence times than corrected ones. This was attributed to the dominance of methanogenesis resulting in variability in $\delta^{13}C$, with calcite dissolution a minor process.

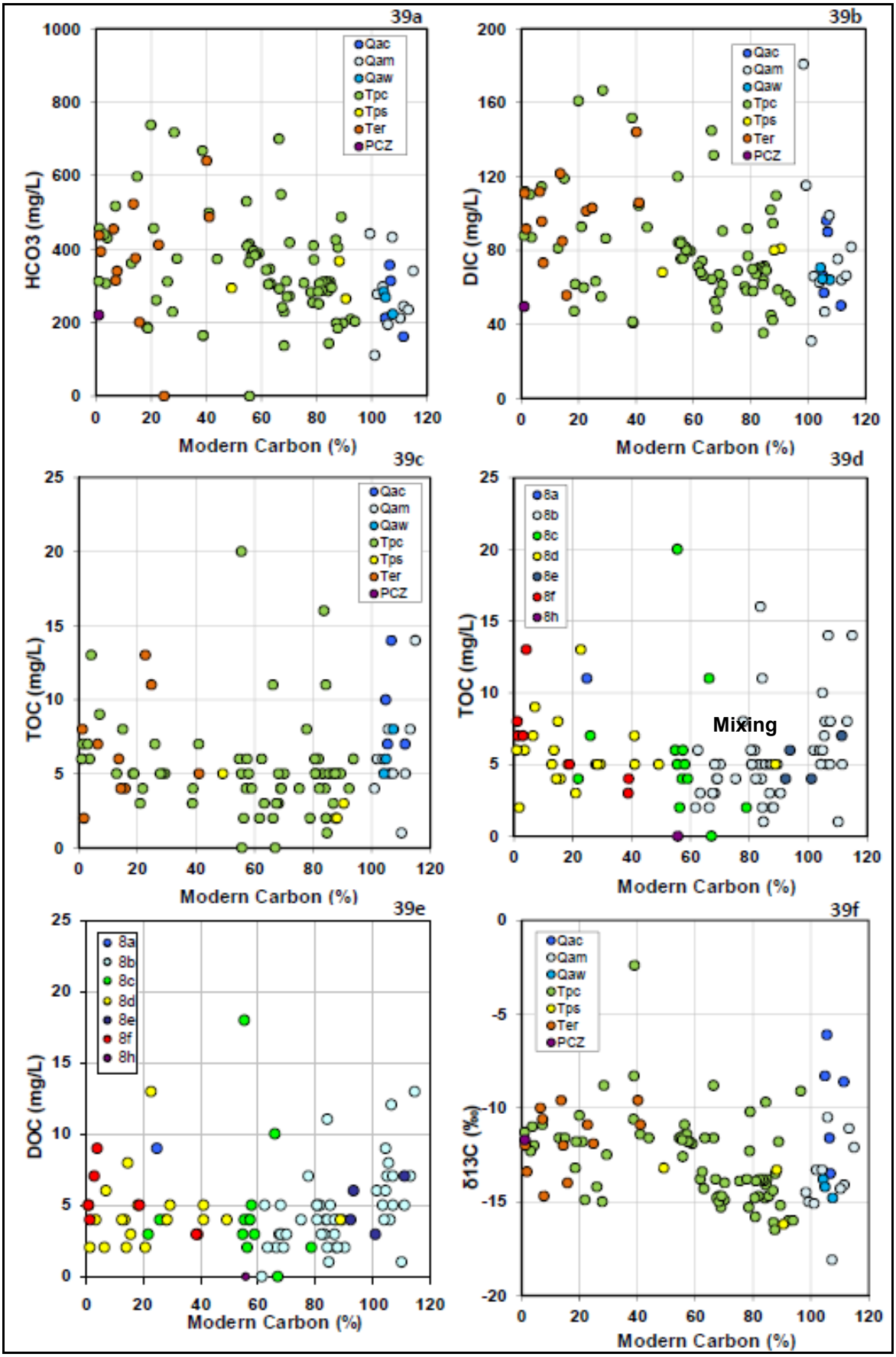

Figure 8-39. *Percent modern carbon (pMC) scatter plots with other carbon analytes for BHMAR groundwater samples.*

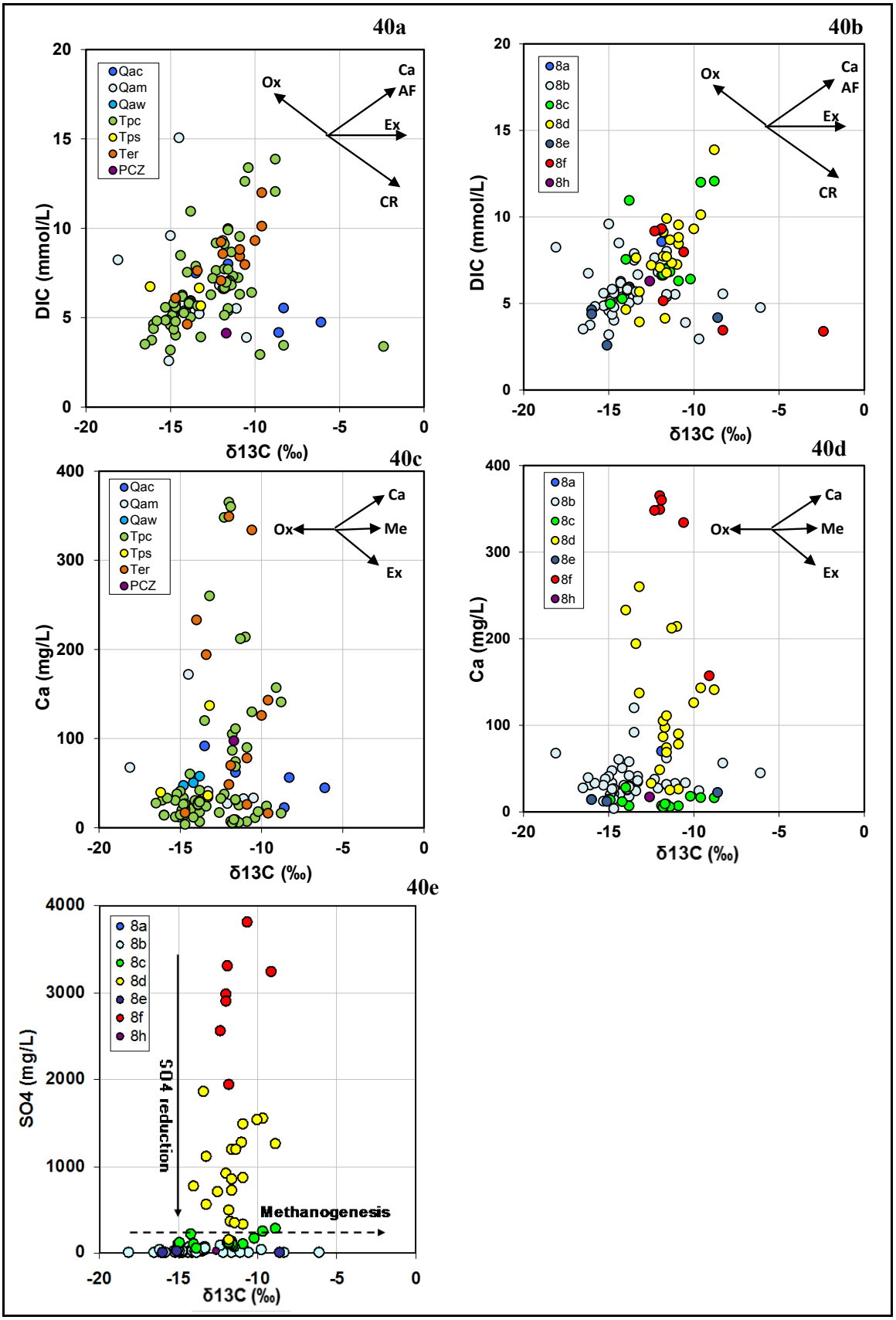

Figure 8-40. *$\delta^{13}C$ scatter plots for BHMAR groundwater samples. Note: Ox=oxidation of organic matter; Ca = calcite dissolution; Me = methanogenesis; AF = methanogenesis by acetate fermentation; CR = methanogenesis by carbon reduction; Ex = cation exchange, (after Cartwright 2009, Coetsiers & Walraevens, 2009).*

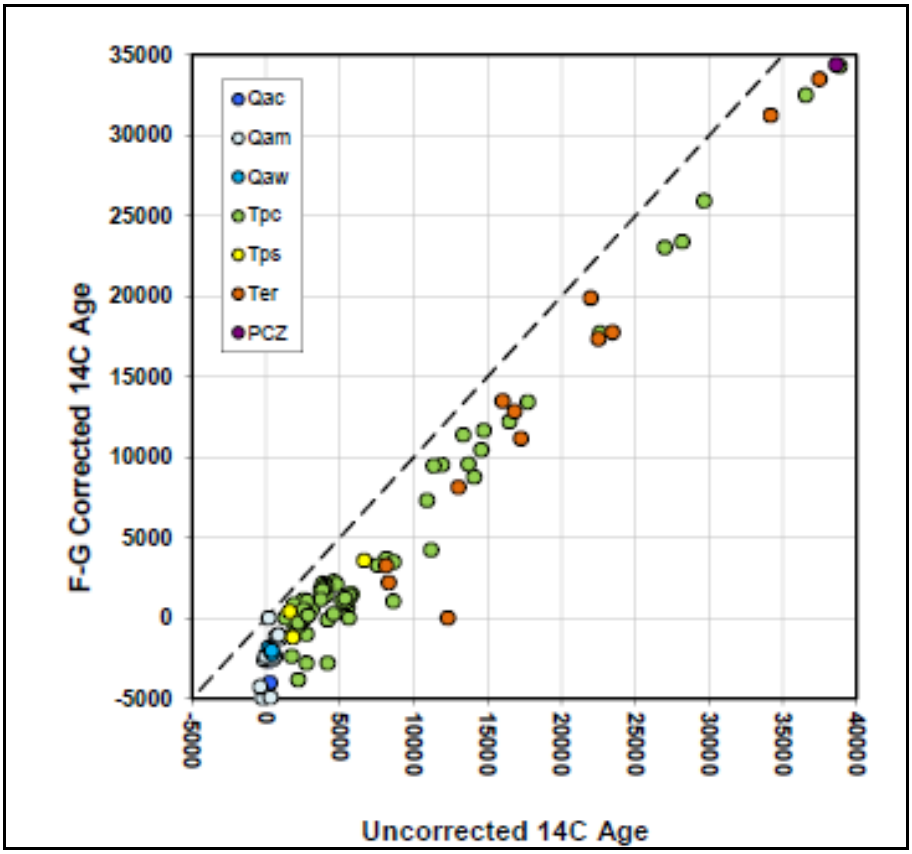

Figure 8-41. *Comparison of uncorrected ^{14}C age with corrected ^{14}C age by Fontes & Garnier (F-G) method.*

8.5 CHLOROFLUOROCARBONS

Groundwater samples were also analysed for chlorofluorocarbons (CFC-11 and CFC-12) to support the ^{14}C age dating and the understanding of recharge dynamics. Figure 8-42a and b show the poor equivalence between the CFC-11 and CFC-12 apparent ages, with the CFC-11 age tending to be less than the CFC-12 age. Figure 8-42b plots the samples using the fuzzy k-means classes and indicates that the samples with a good age correlation are the fresh (class 8b) and the saline (class 8f) end-members of groundwater evolution. The samples with an age mismatch are commonly the intermediate classes associated with mixing (classes 8c and 8d). Figure 8-42c and d indicate that the depletion of CFC-11 relative to CFC-12 can be related to either CFC-11 degradation or CFC-12 contamination. CFC-11 degradation due to the mixing between surface water leakage and saline regional groundwater would be the more plausible option. For example, Plummer *et al.* (1998a, b) noted that leakage of TOC-rich river water into the Upper Floridan aquifer (Georgia, USA) had created anaerobic zones characterised by CFC-11 degradation. On this basis, the CFC-12 ages have been interpreted to be the more reliable. Figure 8-43 plots the CFC-12 concentrations on the basis of sample depth, classified in terms of host formation (Figure 8-43a) and fuzzy k-means class (Figure 8-43b). There is significantly more variability when compared to the analogous pMC plots (Figure 8-35g and h).

The plotting of pMC and CFC-12 concentration provides a comparison between the two age-dating techniques (Figure 8-44a and b). Although there are major differences in the age range and uncertainties associated with the two techniques, the plots are still useful in illustrating some apparent inconsistencies. The lack of consistency is not surprising considering the timescales relevant to pMC (up to 40,000 years) is vastly different to that for CFC-12 (up to 50 years). Exploiting the difference in timeframes for these age tracers can be useful in understanding overall age distribution. For example, there are shallow aquifer groundwater samples that have the combination of elevated CFC-12 and pMC exceeding 100%, both consistent with modern recharge. However, there are other shallow groundwaters that also have pMC>100% but have low CFC-12, perhaps suggesting slightly older groundwater ages Inconsistencies are evident for the deeper Calivil Formation and Renmark Group groundwaters – there are samples with low pMC values (<20

pMC) indicating old groundwater ages (apparent ^{14}C ages > 12 ka) but have elevated CFC-12 indicating post-1960's recharge.

These inconsistencies are attributed to mixing between fresh modern-recharged groundwaters as one end-member and the saline evolved regional groundwaters as the other end-member. Such significant discrepancies in apparent ages can occur in heterogeneous environments due to mixing of water of different ages (Newman *et al.,* 2010). This reflects the geological heterogeneity of the complex fluvial sediment architecture of the BHMAR project area. This also recognises, in general, that a groundwater sample can be a mix of waters that have resided in the subsurface for varying lengths of time (Bethke & Johnson, 2008). Hence, the sample can have a distribution of ages, rather than a single value that is based on an assumption of piston flow. Other factors, such as possible atmospheric contamination during the CFC sampling, cannot be ruled out.

Figure 8-45 to Figure 8-47 provide the spatial context for the comparison between the two indicators of groundwater residence time, pMC and CFC-12 apparent age. For the shallow aquifer, there are sites where there is a combination of pMC indicating modern recharge (pMC>100%) and a pre-1965 CFC-12 apparent age (Figure 8-45). This is the case for the Jimargil-East Bootingee borefield. For other targets also with a modern bomb pulse signature in the shallow aquifer (such as GWR2 and GWR6) the CFC-12 ages are more recent. Figure 8-46 is the equivalent map for the target Calivil Formation aquifer. There are sites with modern (post-1965) CFC-12 ages that correspond with relatively high pMC values. For example, at Jimargil-East Bootingee, many of the Calivil Formation bores close to the river have post-1965 dates and relatively high pMC (>80%). The bores at the BHMAR33 site further away from the river consistently have the combination of high pMC values (>80%) and pre-1965 apparent CFC-12 ages. Such areas with an age combination of relatively high pMC values and pre-1965 CFC-12 ages could reflect recharge that may have occurred in the order of hundreds or thousands or years ago. For the near-river bores at Menindee Common (BHMAR79A site), the combination tends to be pMC <70% and a pre-1965 CFC-12 age. On this basis, river leakage is inferred to be less than what is evident at Jimargil-East Bootingee. The bores in the vicinity of Lake Menindee tend to have post-1965 CFC-12 ages which is another line of evidence for lake leakage associated with these sites. Conversely, there are sites that have both pre-1965 CFC-12 ages and low pMC values. In general, the regional Calivil Formation bores distant from the river (or lakes) tend to have saline evolved groundwaters and low pMC values. However, some also have post-1965 CFC-12 ages. Figure 8-47 is the comparison for the Renmark Group monitoring bores. At Jimargil-East Bootingee (and other targets such as GWR4 and GWR5) there is a consistency between low pMC values and pre-1965 CFC-12 ages. However, this is not the case for Menindee Common.

An understanding of groundwater age distribution is useful from a MAR or groundwater resource site assessment perspectives. Calivil Formation targets (such as Jimargil) that have modern (post-1960s) CFC ages and high pMC would indicate a degree of modern recharge and opportunity for natural replenishment via episodic leakage during flood events. Low salinity targets within the Calivil Formation that have indicators of pre-1965 CFC-12 ages and low pMC (such as GWR4) suggests that these are isolated from modern recharge mechanisms. Such constraints on modern recharge would be an issue for groundwater extraction for these targets, however may be seen as an advantage from a MAR perspective. In these targets dominated by palaeorecharge, lack of hydraulic connection with the shallow aquifer or surface water features would be an advantage for potential ASR operations.

In general, CFC contamination during sampling, as well as CFC-12 degradation cannot be discounted. Also there is greater uncertainty with the CFC-12 dating technique at its lower age limits (<1965) due to the lower atmospheric CFC-12 concentrations during this time period. Hence, the use of an alternative isotope tracing technique (such as CFC-113 and sulfur hexafluoride, SF_6) is recommended to resolve these ambiguous results.

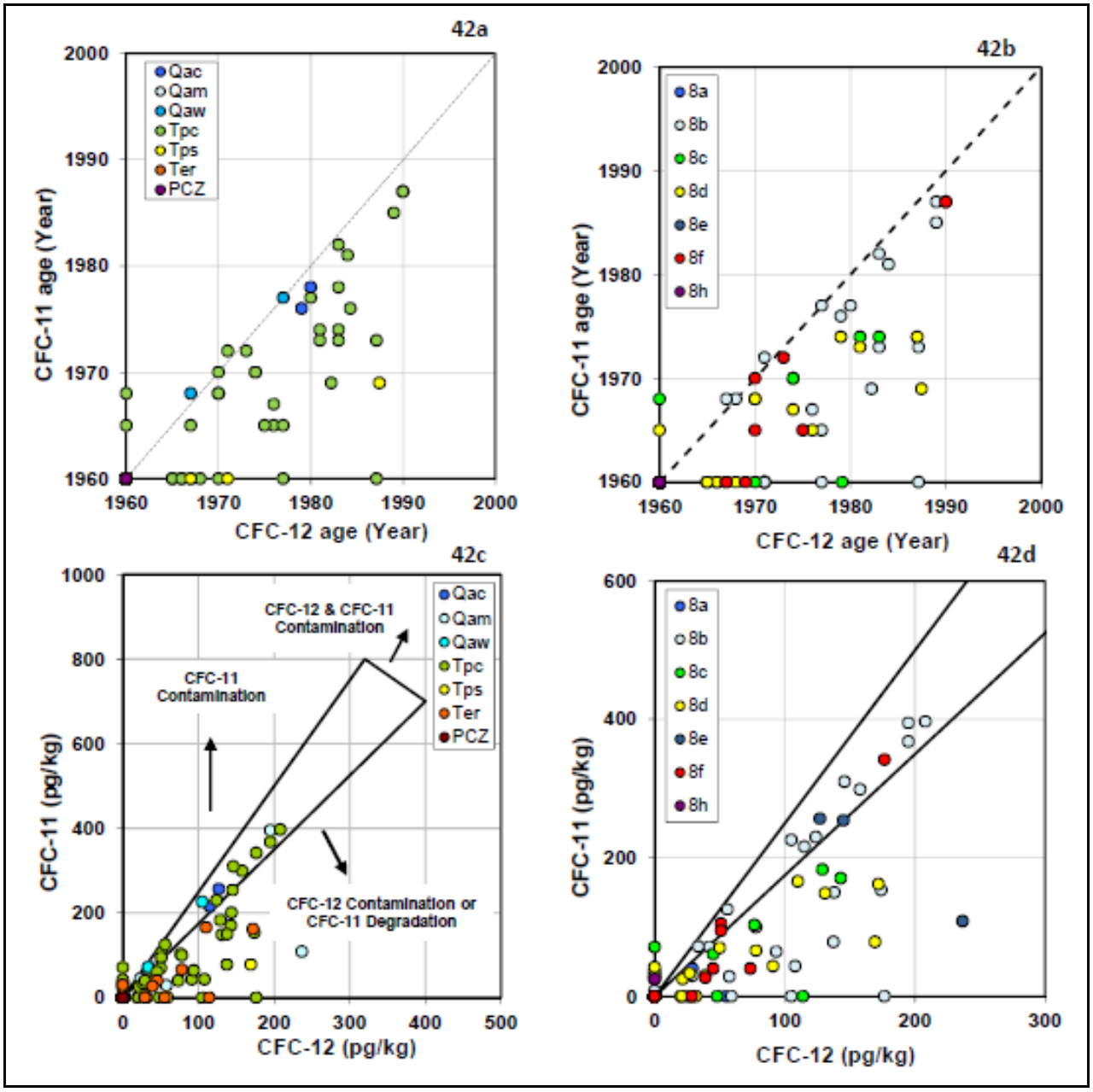

Figure 8-42. *Scatter plots of CFC-11 and CFC-12 ages and concentrations for BHMAR groundwaters.*

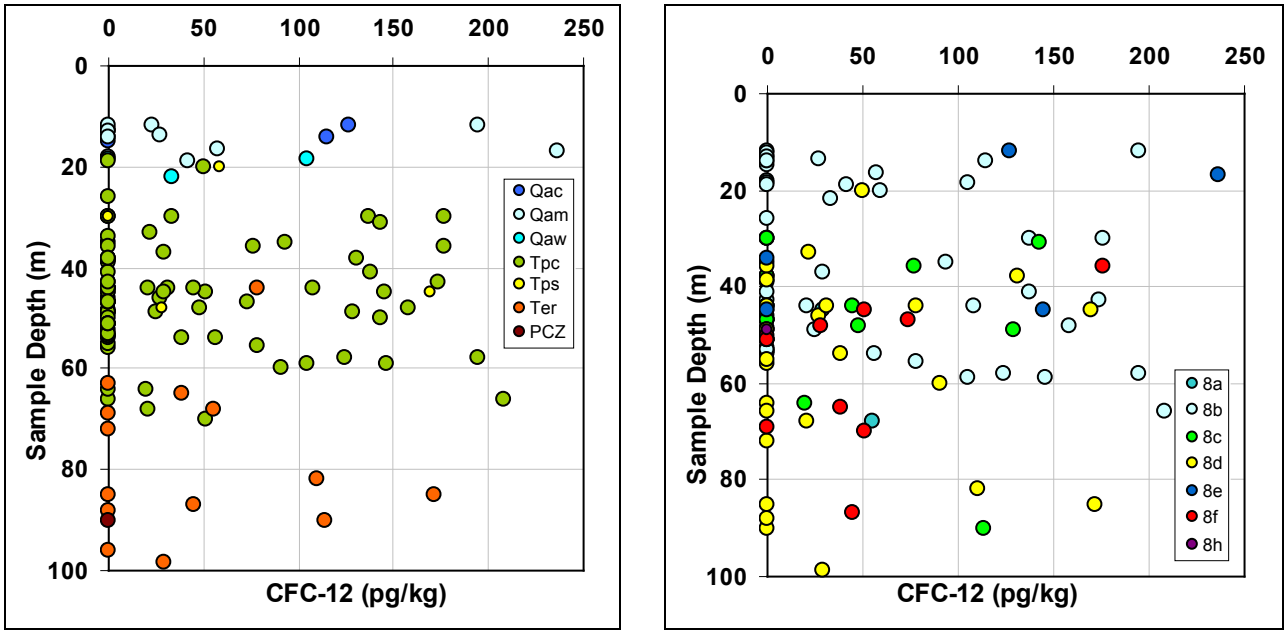

Figure 8-43. *Scatter plots of CFC-12 concentrations and sample depth for BHMAR groundwaters.*

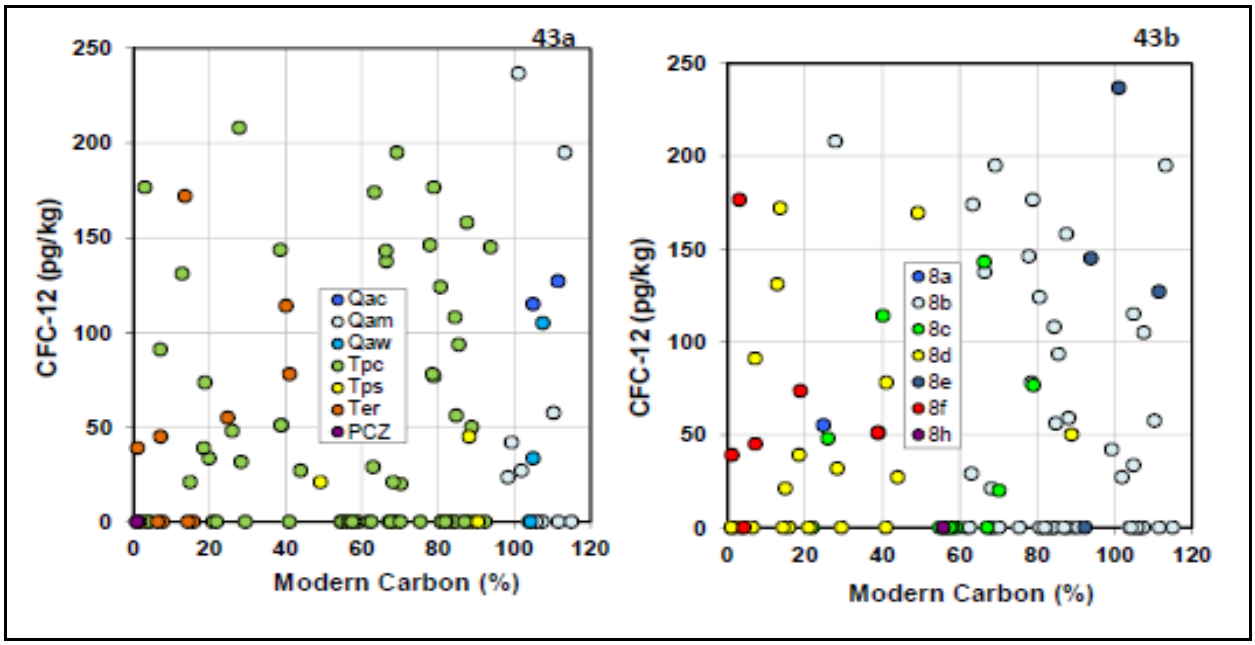

Figure 8-44. *Scatter plots of percent modern carbon (pMC) and CFC-12 concentrations for BHMAR groundwaters.*

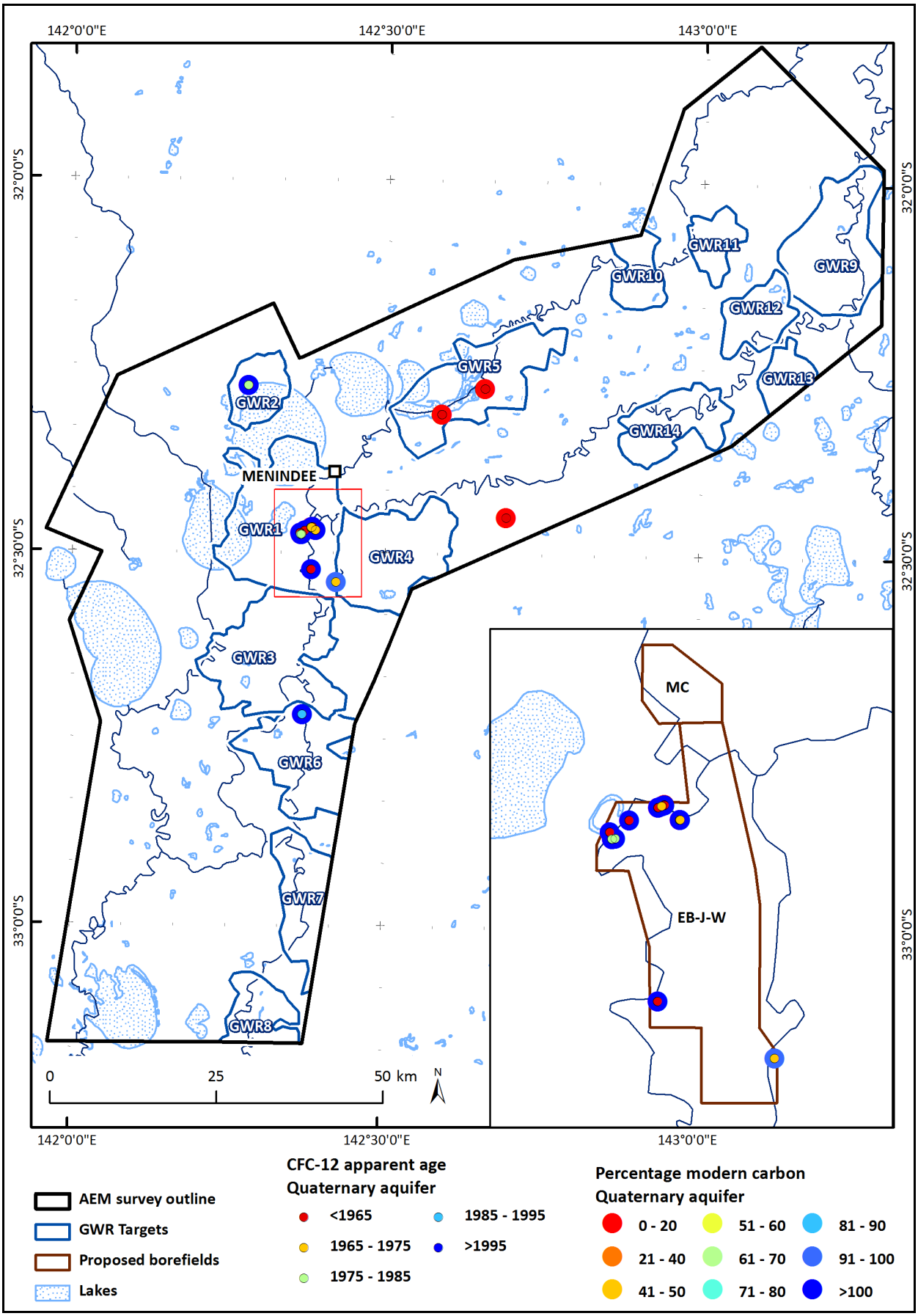

Figure 8-45. *Map of BHMAR project area showing percent modern carbon (pMC) and CFC-12 ages of sampled groundwaters in the shallow unconfined aquifer.*

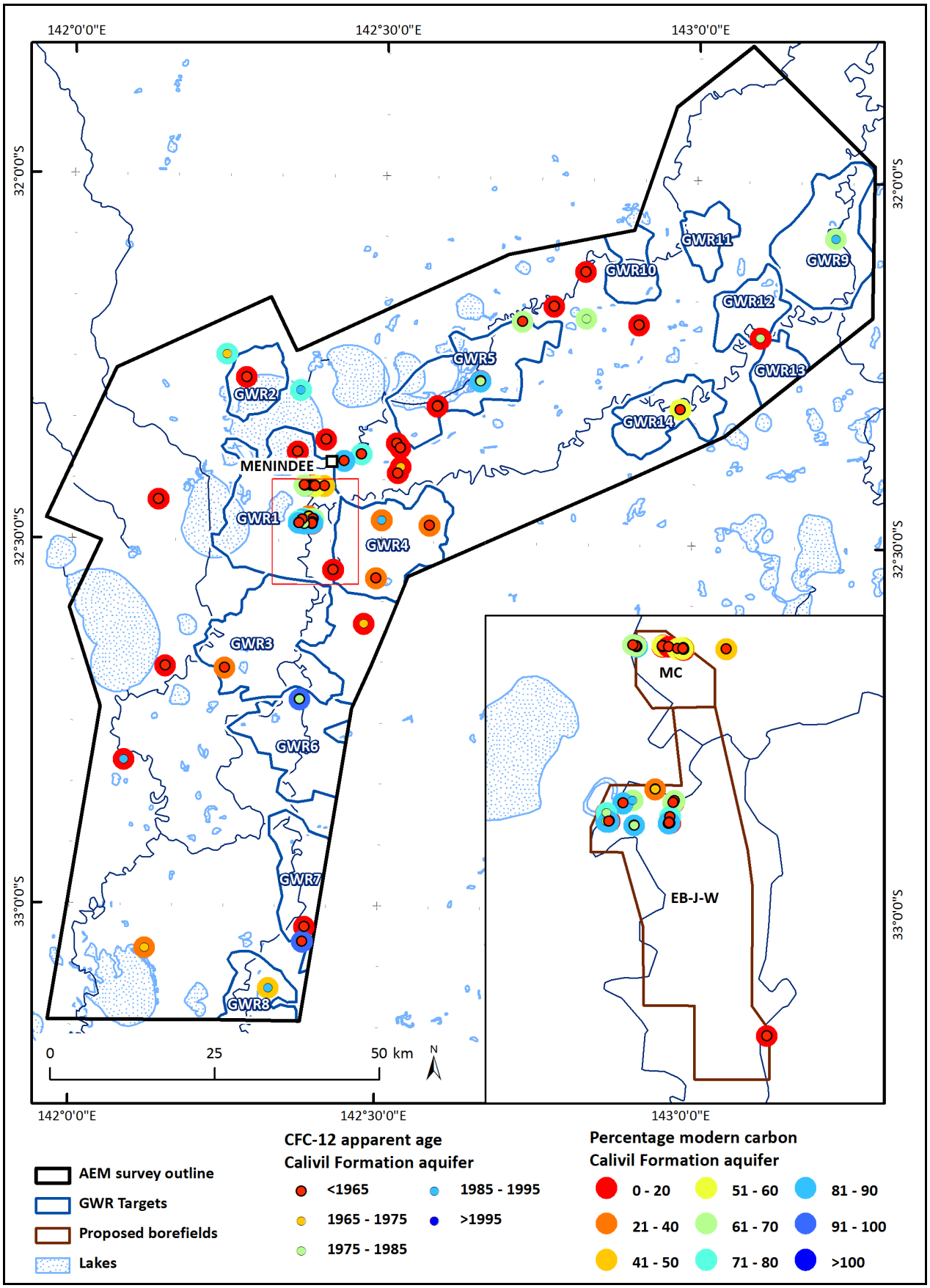

Figure 8-46. *Map of BHMAR project area showing percent modern carbon (pMC) and CFC-12 ages of sampled groundwaters in the Calivil Formation aquifer.*

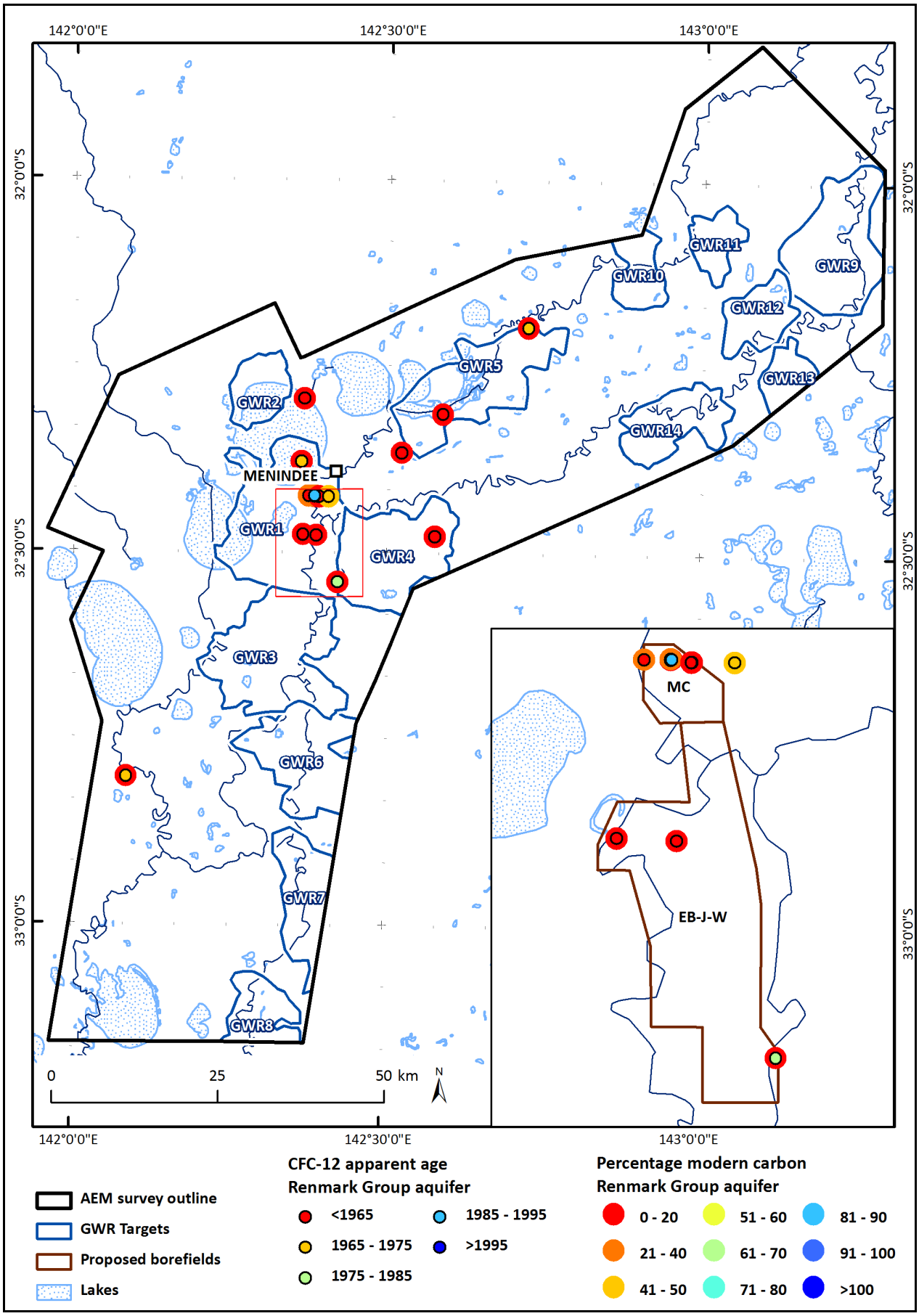

Figure 8-47. *Map of BHMAR project area showing percent modern carbon (pMC) and CFC-12 ages of sampled groundwaters in the Renmark Group.*

8.6 RADON

Radon-222 (^{222}Rn) is a radioactive isotope that has a half-life of 3.8 days and is a product of the radioactive decay of radium-226 (^{226}Ra) in uranium-bearing rocks and sediments. Radon concentrations in groundwater depends on the presence of these radioactive isotopes in the aquifer matrix, and can vary from <2 Bq/L within clastic sediments to >200 Bq/L in igneous and metamorphic rocks (Lee & Hollyday, 1993). In the BHMAR study, groundwater samples were analysed for radon-222, principally to evaluate water quality suitability against national drinking water guidelines (NHMRC-NRMMC, 2011). Combined with analyses for surface water features, radon-222 can also be used as a tracer to understand stream-aquifer connectivity. Several studies (Ellins *et al*., 1990; Crandall *et al*., 1999; Cook *et al*., 2003) have demonstrated that radon can be used to identify locations of significant groundwater input to a stream. Radon was also used in a study in France to determine stream water loss to groundwater as a result of groundwater withdrawals (Bertin & Bourg, 1994). Katz *et al.* (1998) used ^{222}Rn to quantify mixing between river water and groundwater resulting from a recharge pulse from a sinking stream in the carbonate Floridan aquifer.

In general, radon levels in the groundwaters of the study area are relatively low (<20 Bq/L), below the ADWG2011 guideline for safe drinking water of 100 Bq/L. Figure 8-48a-d plot the relationship between ^{222}Rn and other key parameters. These plots were used to explore the possible influence of river/lake leakage on groundwater radon distribution There is no consistent relationship between ^{222}Rn and chloride (Figure 8-48a) or with sample depth (Figure 8-48b). However, the plots with pMC (Figure 8-48c-d) shows that the ^{222}Rn average (5.1 Bq/L) and range (2-8 Bq/L) for the shallow groundwaters is significantly less than for the other deeper aquifers, namely the Calivil Formation (average 6.6 Bq/L, range 0-47 Bq/) and Renmark Group (average 6.6 Bq/L, 1-18 Bq/L). This could be due to the mixing and dilution effect of river leakage, but it also may reflect that uranium or thorium content of the shallow aquifer material is low, relative to the deeper formations.

Figure 8-49 to Figure 8-51 plot the groundwater radon values for the shallow, Calivil Formation and Renmark Group aquifers, respectively. At Jimargil-East Bootingee, many of the Calivil Formation bores close to the river tend have low radon values (< 5 Bq/L), with sites BHMAR80A and BHMAR77 slightly higher (5-8 Bq/L), refer Figure 8-50. The BHMAR33 Calivil Formation bores have even higher values (6-14 Bq/L). A similar situation applies for Menindee Common, where the Calivil Formation groundwater samples from the near-river bores (BHMAR79A site) typically have low radon levels (<2 Bq/L). At the BHMAR75 site, about 1.7 km from the river, dissolved radon in the Calivil Formation groundwaters is in the range 4-12 Bq/L. At Menindee Common, the radon in the Renmark Group groundwaters has a similar range of 4-18 Bq/L (Figure 8-51). Overall, these patterns are consistent with dilution of groundwater radon due to river leakage.

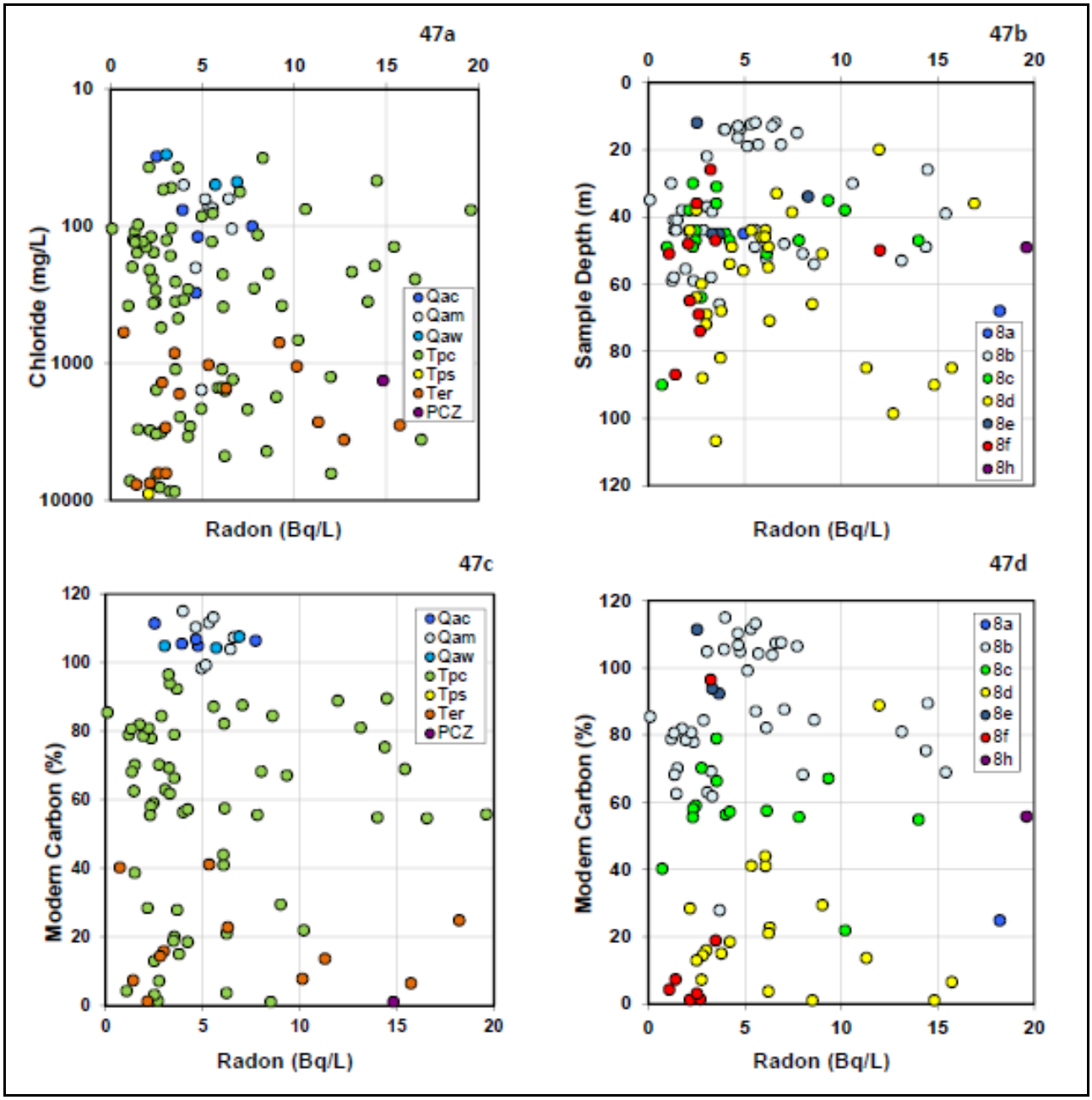

Figure 8-48. *Radon-222 scatter plots for BHMAR groundwaters.*

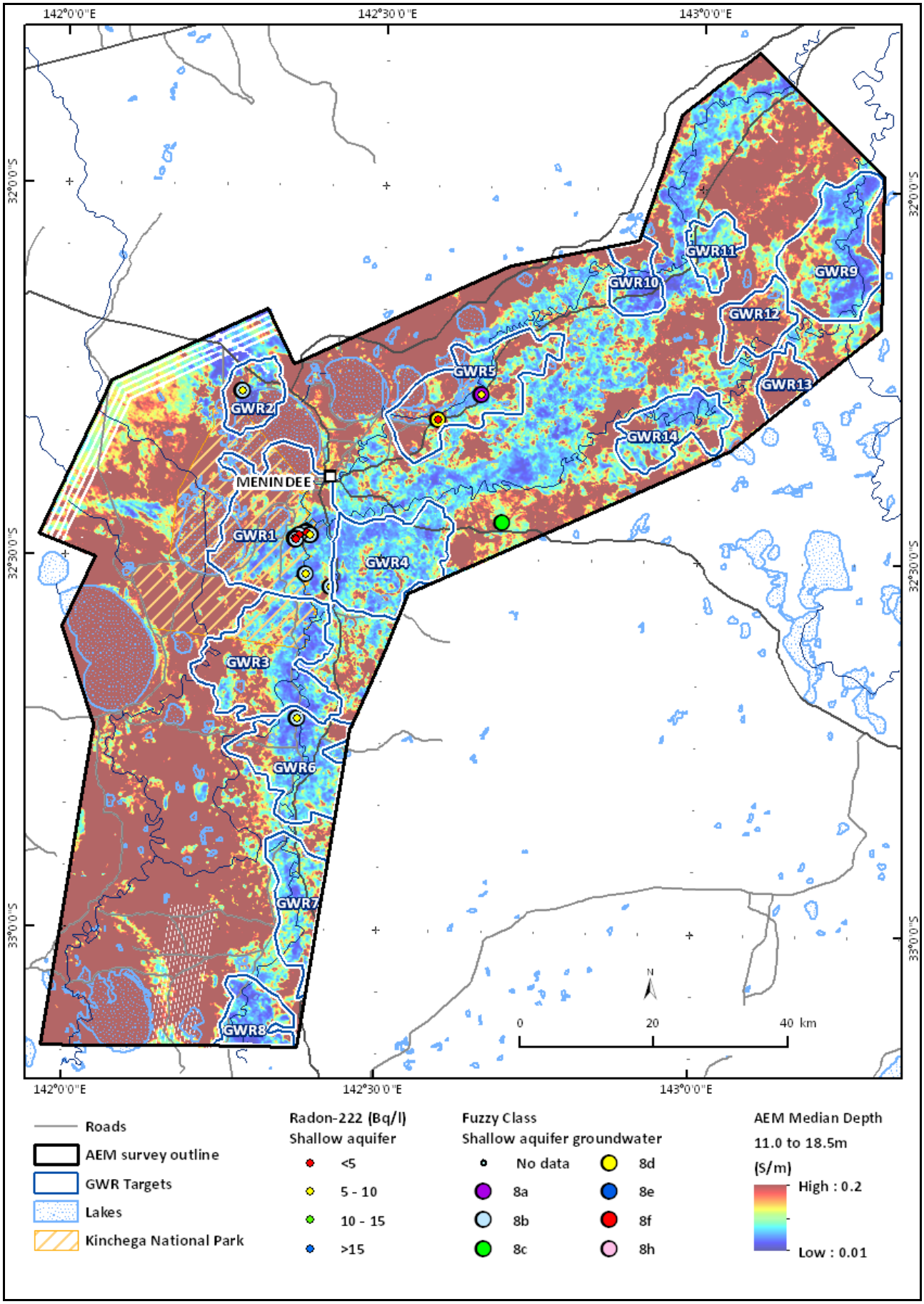

Figure 8-49. *Map of BHMAR project area showing radon-222 concentrations (Bq/L) of sampled groundwaters in the shallow unconfined aquifer.*

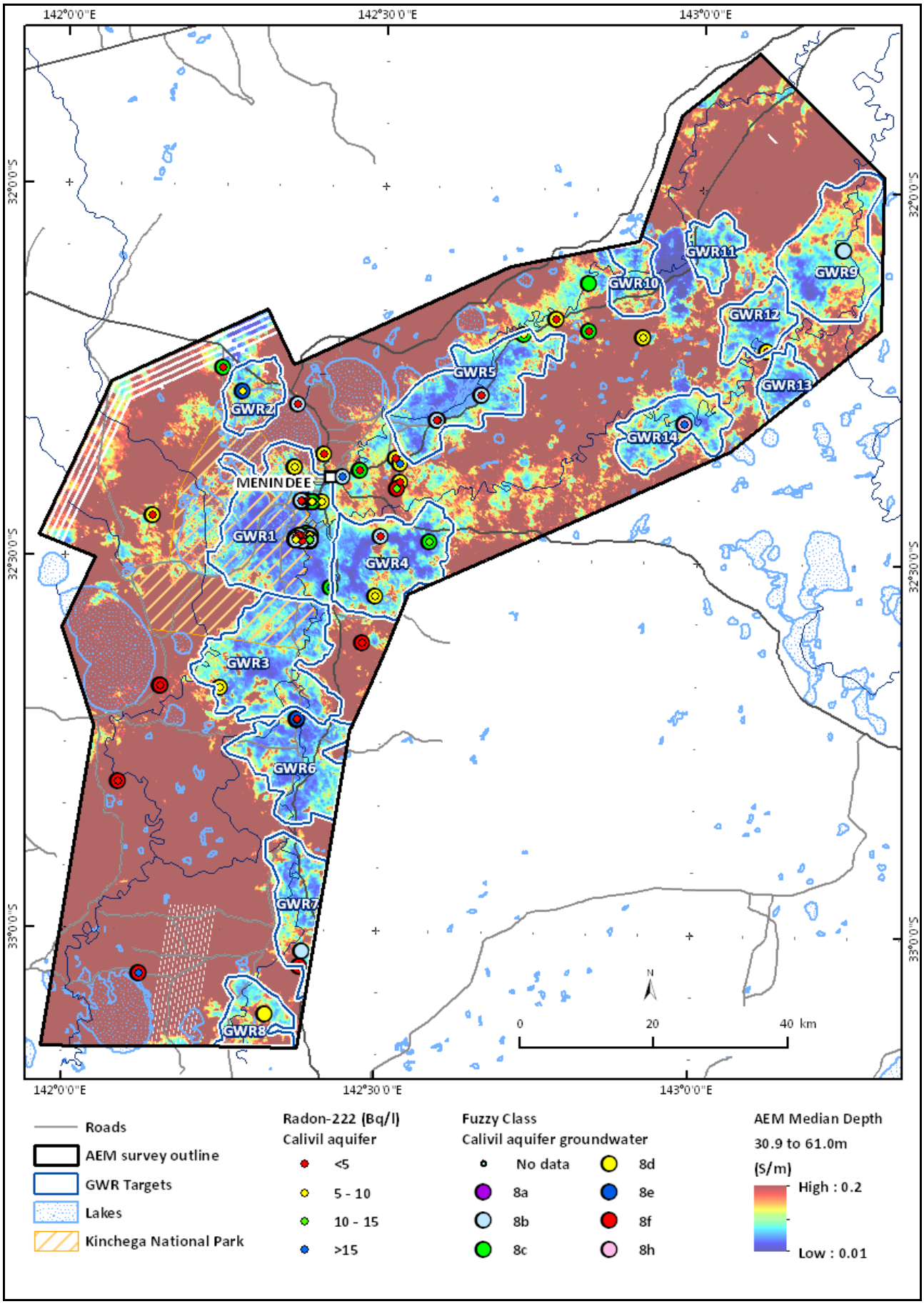

Figure 8-50. *Map of BHMAR project area showing radon-222 concentrations (Bq/L) of sampled groundwaters in the Calivil Formation aquifer.*

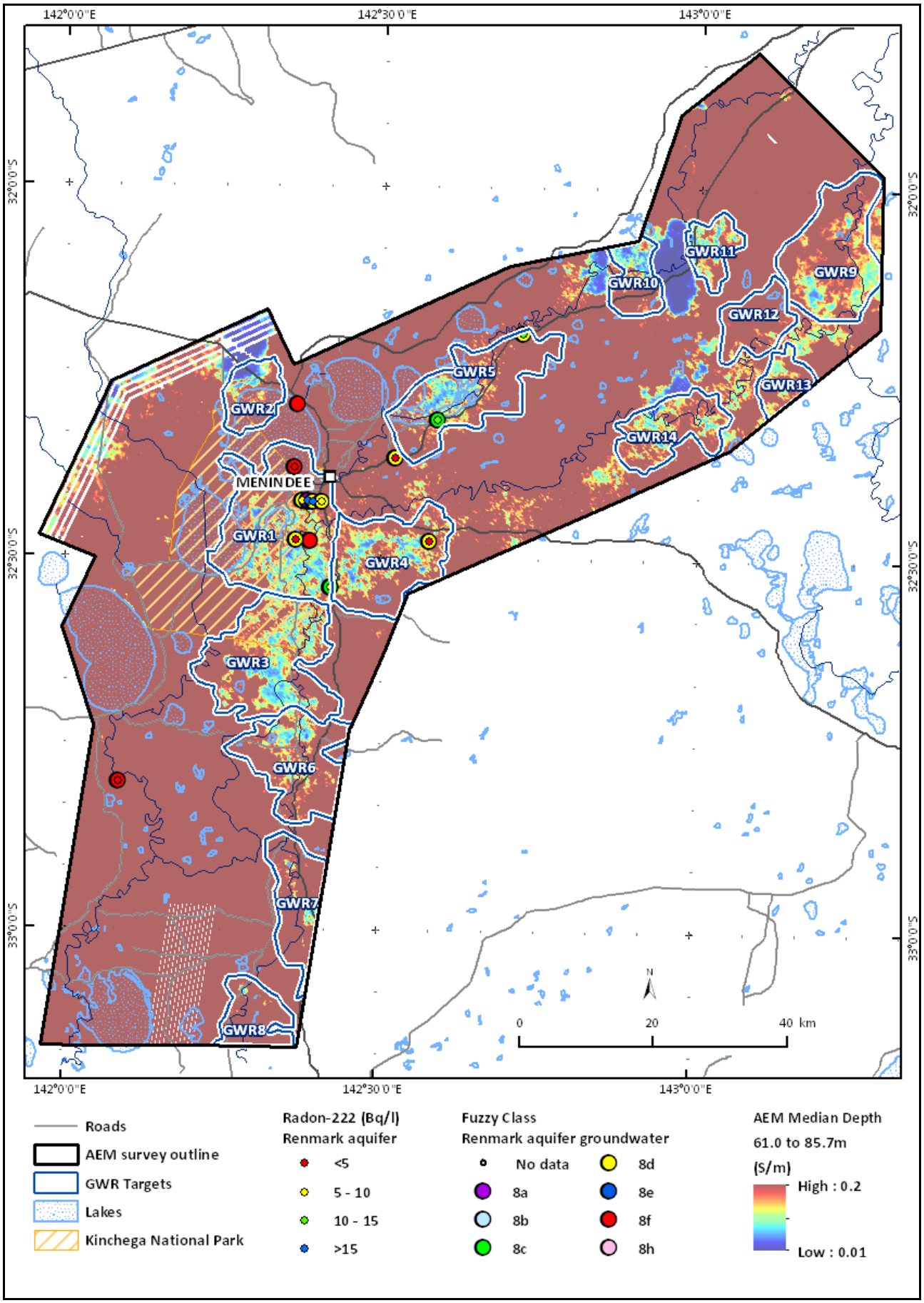

Figure 8-51. *Map of BHMAR project area showing radon-222 concentrations (Bq/L) of sampled groundwaters in the Renmark Group.*

8.7 STRONTIUM ISOTOPES

The strontium isotope ratio $^{87}Sr/^{86}Sr$ was analysed for 16 monitoring bores to help determine the provenance of groundwaters. Figure 8-52 plots $^{87}Sr/^{86}Sr$ with chloride, both on an aquifer and a fuzzy class basis. Most of the fresh to brackish groundwaters sampled in the Darling River floodplain that are influenced by river leakage have $^{87}Sr/^{86}Sr$ ratios of 0.707-0.710. These are in the Menindee Formation, Calivil Formation and Renmark Group aquifers. More saline and evolved groundwater samples in the Renmark Group aquifer have higher values (0.710-.711). The BHMAR23 samples with $^{87}Sr/^{86}Sr$ >0.712 are associated with the leakage site on the northwest margin of Lake Menindee. This contrast in the $^{87}Sr/^{86}Sr$ ratio is inferred to be due to aquifer sediments being derived from erosion of the Broken Hill block to the northwest, in contrast with regional sediment deposition from the north for the Darling Floodplain. The landscape evolution and sediment history of the study area is outlined in Section 5 of this report.

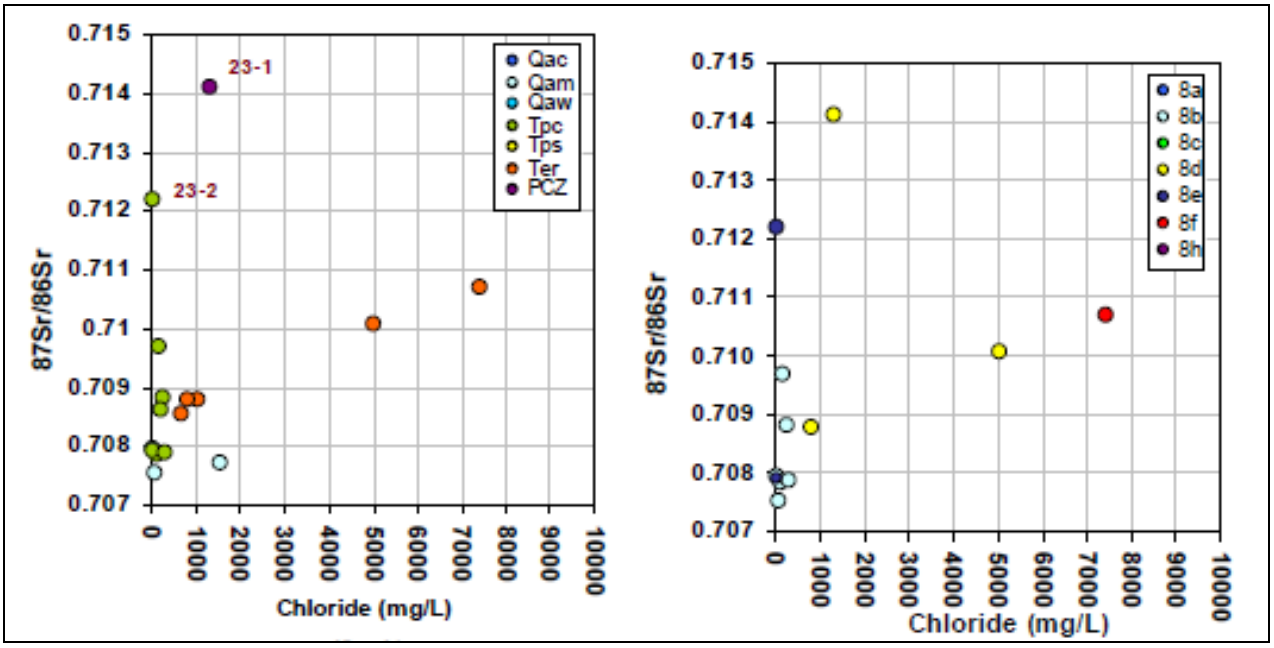

Figure 8-52. *Scatter plots of $^{87}Sr/^{86}Sr$ ratio for BHMAR groundwaters.*

9. Recharge and Hydrogeological Conceptual Model

Significant volumes of fresh groundwater have been identified in targets along the Darling and Talyawalka floodplains. Long-term extraction of these resources is predicated on reducing to acceptable limits any potential negative impacts such as groundwater level decline, saline water ingress or reduced ecosystem health. As well as groundwater storage, this requires an understanding of aquifer replenishment. In fact, long-term groundwater extraction limits tend to be based on the quantification of recharge, rather than storage. To this end, different approaches were applied to better understand the magnitude and dynamics of groundwater recharge. Integrating these recharge studies with other datasets was used to develop a conceptual hydrogeological model for the Darling River sediments.

9.1 PREVIOUS RECHARGE STUDIES

Previous recharge studies in western NSW have focussed on diffuse rainfall recharge, particularly assessing the potential impact on the groundwater balance due to clearing of native vegetation and land use change. Field recharge measurements under native vegetation, including mallee, belah-rosewood and pine woodlands, inferred very low recharge rates to the unconfined aquifer of <0.3 mm/yr or about 0.1% of mean annual rainfall (Cook *et al*., 1996). Kennett-Smith *et al.* (1991) reported deep drainage under native vegetation of 0.1-0.2 mm/yr near Pooncarie, to the southeast of the BHMAR study area. In such a semi-arid environment, the native woodland species are very efficient at intercepting infiltrated water before it reaches the regional watertable.

Land clearing and cropping can significantly alter the recharge regime in the Mallee zone. In areas of sandy soils (<10% clay), relatively high rainfall (>250 mm/yr) and where native vegetation has been cleared for cropping, potential recharge rates of 20-40 mm have been estimated (Cook *et al.,* 1996). At cleared and cropped sites near Balranald and Euston to the southeast of the BHMAR study area, Cook & Walker (1989) estimated potential recharge rates of 5.6 mm/yr and 6.9 mm/yr (or 1.7% and 2.2% of average rainfall), respectively. At the Pooncarie site, Kennett-Smith *et al.* (1991) reported a maximum potential recharge rate with clearing and grazing of 1.5 mm/yr or 0.6% of average annual rainfall. Where clay content in the soil profile exceeded 20%, the measured potential recharge from rainfall was typically less than 5 mm/yr upon clearing (Cook *et al.,* 1996). Field data also suggest that for cleared but non-cropped areas with mean annual rainfall <250 mm/yr, potential recharge was < 1 mm/yr regardless of soil type (Kennett-Smith *et al.,* 1994). Wohling *et al.* (2012) concluded that the combination of annual average rainfall and clay content of the soil profile (0-2 m depth) were useful predictors of deep drainage.

Regional steady-state groundwater flow modelling in western NSW (Kellett, 1997; Brodie, 1998) used variable recharge rates depending on the extent of native vegetation, rainfall and soil type. For the NSW Mallee region east of the Darling River, Kellett (1997) used a uniform recharge rate of 0.1 mm/yr for areas with undisturbed native vegetation. Where clearing had occurred, a recharge rate based on 1% of rainfall was applied. For the NSW Mallee area west of the Darling River, Brodie (1998) used 0.05% as the proportion of average rainfall for recharge under native vegetation. For cleared areas, different proportions of average rainfall were used (0.05-5%), depending on an estimate of sand percentage of the soil profile, using land systems mapping.

Based on these previous studies, a low diffuse recharge rate by rainfall of <1 mm/yr would be anticipated over much of the BHMAR study area. This is based on a number of characteristics of the study area (1) the average annual rainfall between 200 and 250 mm/yr, less than the threshold of Kennett-Smith *et al*. (1994), (2) the common occurrence of fine-textured soils and near-surface aquitards that impede infiltration and (3) only limited areas of cropping which could potentially enhance rainfall accessions. Infiltration to the Calivil Formation aquifer is further constrained by the extensive distribution of the overlying Blanchetown Clay aquitard, albeit structurally disrupted. There are several lines of evidence that support episodic leakage during high flows as the dominant recharge mechanism, rather than diffuse recharge from rainfall.

9.2 RECHARGE ESTIMATION

Different approaches were taken to better understand and to estimate groundwater recharge. This included applying the chloride mass balance method (Crosbie *et al*., 2010), the watertable fluctuation method (Healy & Cook, 2002), the steady state groundwater mounding equation of Bouwer (2002) and radiocarbon depth models for unconfined and confined aquifers (Cook & Bohlke, 2000). Flood frequency and associated recharge was also investigated. Each of these methods is also discussed in Lawrie *et al*. (2012a).

9.2.1 Watertable Fluctuation Method

Data loggers in a network of 40 monitoring bores, augmented by manual groundwater level measurements, enabled the groundwater response to flooding during 2010-2011 to be measured in the shallow unconfined (Coonambidgal and Menindee Formations), semi-confined (Calivil Formation) and the confined (Renmark Group) aquifers at several target sites (Figure 9-1). This allowed the opportunity to apply the watertable fluctuation method to help quantify recharge to the shallow unconfined aquifer.

The watertable fluctuation (WTF) method is a simple approach to estimating recharge using groundwater level data (Healy & Cook, 2002). The approach has a long history of application in groundwater resource studies (e.g. Meinzer, 1923; White, 1932; Rasmussen & Andreasen, 1959). The assumption is made that any rises in groundwater levels in an unconfined aquifer are due to percolating waters reaching the watertable. On this basis, the equation to calculate the recharge rate (R) is:

$$R = S_y \frac{\Delta h}{\Delta t}$$

Equation 6

where S_y is the specific yield of the unconfined aquifer, Δh is the rise (m) in the elevation of the groundwater level and Δt is the duration (d) of the recharge event.

Recharge is equated to the volume of water stored in the incremental volume of aquifer defined by the watertable rise. This assumes that other components of the water budget such as baseflow, pumping, inter-aquifer leakage or evapotranspiration are effectively zero during the time of recharge. The method is independent of the actual mechanism of recharge, whether it is piston flow though the unsaturated zone, via preferential pathways such as fractures, or from leakage of surface water features.

There are limitations to its application (Healy & Cook, 2002). The method can only applied to unconfined aquifers and works better for shallow dynamic systems where the watertable response to rainfall is rapid and strong. It becomes difficult to reconcile groundwater fluctuations with recharge episodes for aquifers with deep watertables due to the time lag associated with downward infiltration through the unsaturated zone. It is assumed that the pre-recharge groundwater level recession can be extrapolated as part of calculating Δh. Constant rates of recharge cannot be distinguished as the method relies on the short-term response to rainfall or flood events. Other mechanisms for watertable fluctuations need to be accounted for, including diurnal evapotranspiration cycles, ocean tides and transmission of changes to atmospheric pressure. The method only estimates recharge at the site of the bore, so may be representative for only a small area of the catchment. Results can also be influenced by the frequency of the groundwater level measurements used in the analysis. By resampling groundwater monitoring data, Delin *et al.* (2007) concluded that it is necessary to collect groundwater level measurements on at least a weekly basis. In the BHMAR study, the use of downhole loggers allowed such data to be recorded at a 15-minute interval.

As indicated in Equation 6, a reliable estimate of specific yield (S_y) is required to quantify recharge. This is typically defined as the volume of water that an unconfined aquifer releases from storage per unit surface area of aquifer per unit decline in the watertable (Freeze & Cherry, 1979). In the context of recharge calculations, this relates to the volume of water added to the aquifer per unit rise in the watertable. In the absence of direct measurements for the Coonambidgal Formation, Menindee Formation and Willotia beds aquifers, a nominal S_y range of 0.05-0.10 was used in the calculations. This represents the greatest uncertainty in the resulting recharge estimates. S_y in reality varies as a function of depth to the watertable (Childs, 1960). It also varies over time in response to the wetting and draining history. If multiple rises occur

closely spaced in time, the sediments may not fully drain between rises. In theory, it would be appropriate to assign different values of S_y to different rises. In practice, however, the information and resources required to make these accommodations are rarely available.

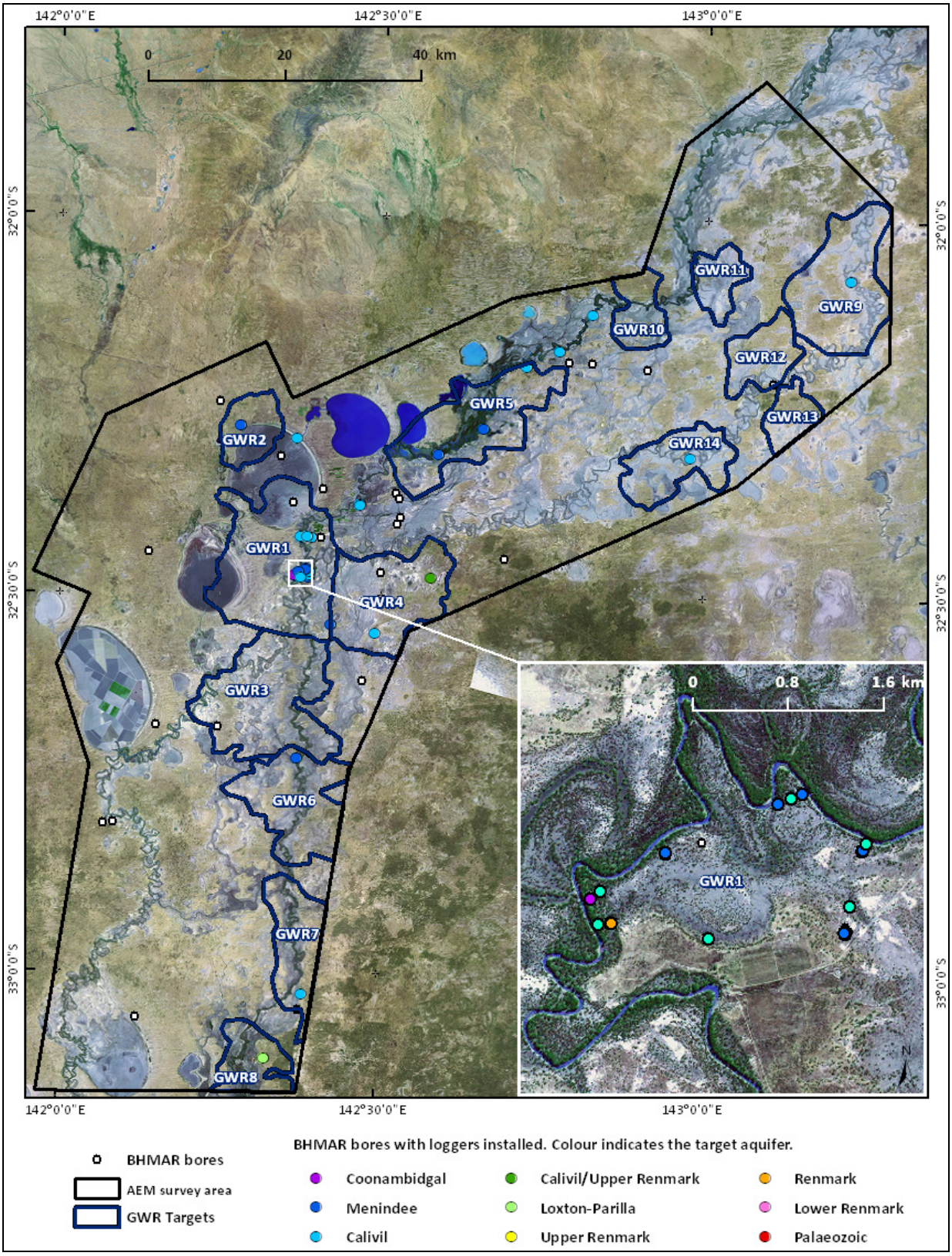

Figure 9-1. *Location of groundwater level monitoring network in the BHMAR project area.*

Table 9-1 summarises the groundwater response to the 2010/11 flood event. Where the initial response was monitored, groundwater levels generally rose within 10 days of the start of flooding. The table also reports the number of days from the onset of flooding in October, 2010 to the peak in the groundwater level.

Results of applying the watertable fluctuation method for the bores in the shallow unconfined aquifer are summarised in Table 9-2. The recharge along the Darling River corridor for the flood event period varies by at least an order of magnitude (19-543 mm) but is highly significant compared to recharge estimates based on diffuse rainfall (<1 mm/yr). This flood event represents a groundwater recharge volume of 19-543 ML per kilometre square of aquifer receiving recharge along the river corridor. In the north near Lake Wetherell (BHMAR34-2) the average daily recharge during the event was ~0.06 mm/d; in the Jimargil area (BHMAR77-3, BHMAR84-4, BHMAR92-2 and BHMAR33-3) the average daily recharge ranged 0.07-1.3 mm/d; and further south at Tandou (BHMAR21-2) recharge was ~0.2 mm/d. At the northwest margin of Lake Menindee (BHMAR23-2) recharge from lake leakage was ~0.7 mm/d, equating to ~300 ML per kilometre square of aquifer over the time period.

Table 9-1. *Summary of groundwater response in BHMAR bores with onset of flood from 14/10/2010.*

BHMAR Bore	Target	Aquifer	Screened Interval (m below land surface)	Distance from River/Lake (m)	No. of days to peak groundwater level	Event ΔRWL (m)	Initial Time Lag in Groundwater Response (d)
Shallow Unconfined							
34-2	GWR5	Menindee Formation	8-20	81	680	0.56	
84-3	GWR1	Coonambidgal Formation	10-23	17	307	5.43	10
84-4	GWR1	Coonambidgal Formation	12-23	100	341	2.74	
04-3	GWR5	Menindee Formation	8-14	95	571	1.71	
77-3	GWR1	Menindee Formation	11-16	115	307	1.17	6
33-3	GWR1	Menindee Formation	14-23	813	407	0.38	7
92-2	GWR1	Menindee Formation	12-16	151	407	1.67	10
21-2	GWR6	Menindee Formation	10.5-23.5	334	677	1.51	
61-3	GWR1	Menindee Formation	12.5-22.5	168	642	0.74	
23-2	GWR2	Calivil Formation	29-47	157	407	4.01	
Calivil Formation							
16-1	GWR14	Calivil Formation	12-52	210	626	0.07	
35-1	GWR5	Calivil Formation	16-46	163	576	0.03	
75-2	GWR1	Chowilla/Calivil Formation	18-23	1195	407	0.16	
14-1		Calivil Formation	41-59	201	566	0.56	
04-2	GWR5	Calivil Formation	34-52	95	575	1.17	
17-2		Calivil Formation	22.5-34.5	1063	521	0.86	
17-1		Calivil Formation	54-72	1063	580	1.20	
34-1	GWR5	Calivil Formation	27-51	81	680	0.98	
05-2	GWR5	Calivil Formation	28-40	794	568	0.29	
06-1		Calivil Formation	30-60	820	194	0.30	
57-1	GWR4	Calivil Formation/Upper Renmark Group	34.5-82.5	5731	349	0.32	
75-5	GWR1	Calivil Formation	40-52	1185	369	0.20	48
88-5	GWR1	Calivil Formation	35-41	672	307	0.75	10
92-1	GWR1	Calivil Formation	32-62	151	407	0.75	7
80A-7	GWR1	Calivil Formation	42-54	71	251	0.68	10
80A-2	GWR1	Calivil Formation	35-53	164	773	0.86	10
80B-2	GWR1	Calivil Formation	53-65	135	307	0.74	10
99-1	GWR1	Calivil Formation	33-57	375	309	0.71	
61-2	GWR1	Calivil Formation	36-66	168	642	0.43	
21-1	GWR6	Calivil Formation/Upper Renmark Group	20-74	334	676	0.49	
Loxton-Parilla Sands							
29-1	GWR7	Calivil Formation/Loxton-Parilla	17-53	158	576	0.77	
31-1	GWR8	Loxton-Parilla	11-51	2204	573	0.21	
Renmark Group							
88-3	GWR1	Upper Renmark Group	65-71	663	379	0.77	10
79A-2	GWR1	Upper Renmark Group	65-77	172	773	0.86	10
80A-6	GWR1	Upper Renmark Group	84-102	174	307	0.76	
61-1	GWR1	Upper Renmark Group	86-116	168	578	0.47	
04-1	GWR5	Upper Renmark Group	90-102	95	575	0.74	
05-1	GWR5	Upper Renmark Group	94.5-100.5	794	265	0.35	
33-1	GWR1	Lower Renmark Group	182-206	813	407	0.38	

Notes: ΔRWL is the maximum rise (peak) in groundwater level in the bore, from the start of flood event

Table 9-2. *Recharge estimates for unconfined aquifers based on watertable fluctuation method.*

BHMAR	Aquifer	Screened Interval (m below land surface)	Location	ΔRWL (m): Start to PEAK	Peak: days	Event Recharge (mm)	Daily Recharge (mm/d)	Recharge Source	Distance to Source (m)	Confidence
84-3	Coonambidgal	10-23	East Bootingee	5.43	162	272-543	1.7-3.4	Darling River	17	Moderate
84-4	Coonambidgal	12-23	East Bootingee	2.74	162	137-274	0.9-1.7	Darling River	100	Moderate
04-3	Menindee	8-14	Lake Wetherell	1.71	571	86-171	0.1-0.3	Lake Wetherell	95	High
77-3	Menindee	11-16	Jimargil	1.17	182	59-117	0.3-0.6	Darling River	115	Moderate
33-3	Menindee	14-23	Jimargil	0.38	358	19-38	0.05-0.1	Darling River	813	High
92-2	Menindee	12-16	East Bootingee	1.67	203	83-167	0.4-0.8	Darling River	151	Moderate
34-2	Menindee	8-20	Lake Wetherell	0.56	680	28-56	0.04-0.08	Lake Wetherell	81	Moderate
21-2	Menindee	10.5-23.5	Tandou	1.51	595	76-151	0.13-0.25	Darling River	334	Moderate
61-3	Menindee	12.5-22.5	Wanda	0.74	486	37-74	0.08-0.15	Charlie Stones Creek	168	Moderate
23-2	Menindee/ Calivil	29-47	Lake Menindee	4.01	407	200-401	0.5-1.0	Lake Menindee	157	High

Notes: ΔRWL is the maximum rise (peak) in groundwater level in the bore from the start of flood event

.

9.2.2 Hydraulic Loading

Hydraulic loading can be a component of an observed groundwater level rise. The impact of hydraulic loading on a confined aquifer in terms of a groundwater level response (ΔSWL) is a proportion of the observed watertable fluctuation (Δh) in the overlying unconfined aquifer, with that proportion being the combination of the unconfined aquifer specific yield (S_y) and the loading efficiency (γ) of the confined aquifer (Harrington & Cook, 2011), represented by:

$$\Delta SWL = \Delta h.\gamma.S_y$$

Equation 7

This equation was used in a sensitivity analysis to determine the likely magnitude of hydraulic loading associated with the 2010/11 flood event. The average measured watertable response to the flood peak at Jimargil was used as a representative value for Δh (=2.2 m), a range of 0.5-0.9 was used for the loading efficiency based on published data (Harrington & Cook, 2011) and a range of 0.05-0.1 was used for the specific yield of the unconfined aquifer. This yields a quantum of the potential impacts of hydraulic loading associated with the flood peak on the order of a 0.05-0.2 m rise in Calivil Formation groundwater levels. As indicated in Figure 7-20, the observed rises in Calivil Formation groundwater levels are significantly higher than this, on the order of 0.6-1.6 m. Hydraulic loading may be a component of the response in the Calivil Formation groundwater levels during the flood phase, but does not fully explain the full magnitude of the observed responses. Hydraulic loading also would not explain the post-flood maintenance (or rise) of Calivil Formation groundwater levels whilst river stage (and the shallow watertable) subsequently receded.

The relatively short timeframe (in the order of days) for groundwater levels in the Calivil Formation aquifer to respond to high-flow conditions in the river is typical for semi-confined aquifers in this setting. Vekerfy & Meijerink (1998) investigated the lag between river stage for the river Danube and bore hydrographs in unconfined and semi-confined parts of the adjoining alluvial aquifer. These lags ranged from 1-85 days, with the tendency for lag times increasing with distance away from the river. Lag times were shorter under semi-confined conditions than under unconfined conditions, due to the efficiency for which head changes could be propagated, in the order of several kilometres per day. Moench & Barlow (2000) developed analytical models for the interaction of confined, semi-confined and unconfined aquifers with an adjoining stream. The application of these models at two field sites simulated groundwater responses to stream flood pulses in both unconfined and confined aquifers in the order of 1-2 days (Barlow *et al.,* 2000).

On this basis, it is interpreted that the initial responses in the Calivil Formation bores do not necessarily represent actual recharge at the borehole site at this time, but most likely reflect propagation of head changes from locations where there is hydraulic connection between the Calivil Formation, via structural pathways or aquitards gaps, to the shallow aquifer system and the river. In addition to the short-term responses, there are persistent groundwater level rises observed in Calivil Formation bores over the timeframe of months following the flood event. The hydrographs for bores BHMAR80A-2 and 80A-7 (Figure 7-20) are good examples. The hydrograph for BHMAR23-2 (Figure 7-21) shows a steady recharge response over similar timeframes due to leakage from Lake Menindee. These longer-term post-flood responses are interpreted to be indicators of actual recharge to the Calivil Formation, as opposed to the initial head propagation during the actual flood.

9.2.3 Temperature Monitoring

To ascertain whether observed changes in head were related to groundwater recharge, or due to other processes such as hydraulic loading, the groundwater temperature data was also assessed. Temperature can be used as a natural tracer to identify surface water infiltration, flow through fractures and flow patterns in the groundwater system (Anderson, 2005). Many authors have utilised temperature as a tracer of groundwater-surface water interactions, as discussed in the two review papers (Anderson, 2005; Kalbus *et al*., 2006), although these studies typically focus on interactions within the streambed (e.g. Baskaran *et al*., 2009; Rau *et al*., 2010).

The basic principle being that within the surficial zone (<1.5 m below surface), temperature is influenced by seasonal heating and cooling of the land surface (Silliman & Booth, 1993) with groundwater temperatures typically ~1-2°C higher than the mean annual surface temperature (Freeze & Cherry, 1979). Within the subsurface, groundwater temperature normally follows the geothermal gradient (increase temperature by 1°C every 20-40 m depth) unless perturbed by groundwater flow (Parsons, 1970). In both the surficial and subsurface zones, an injection of warmer or cooler surface water would result in an associated rise or fall (beyond ambient fluctuations) in groundwater temperature.

Surface water temperatures were recorded at two different times – summer (January 2010) and winter – August 2012). River water temperatures ranged from 26.1-28.8°C in summer to 12-13.4°C in winter with a diurnal trend of temperature peaks in the afternoon and troughs in the early morning (Figure 9-2). Groundwater temperatures were much less varied. Only a 0.2°C seasonal temperature change was observed from a shallow bore (10-23 m screen interval) close to the river (~17 m; Figure 9-3).

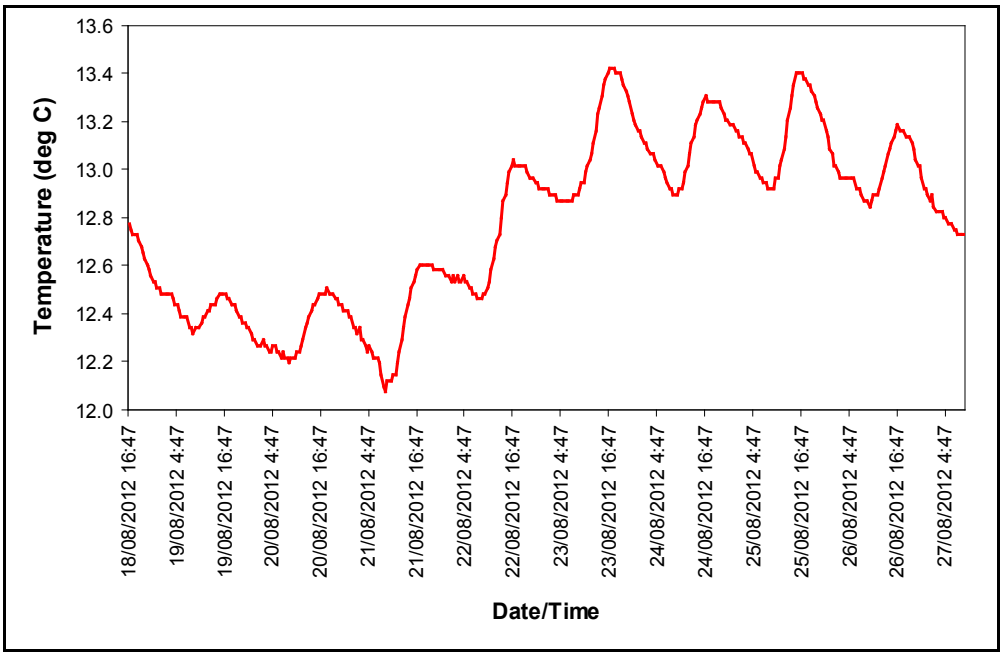

Figure 9-2. *Temperature recordings from the Darling River (18/08/12-27/08/12). Note the diurnal trend, with peaks in the afternoon and troughs in the early morning.*

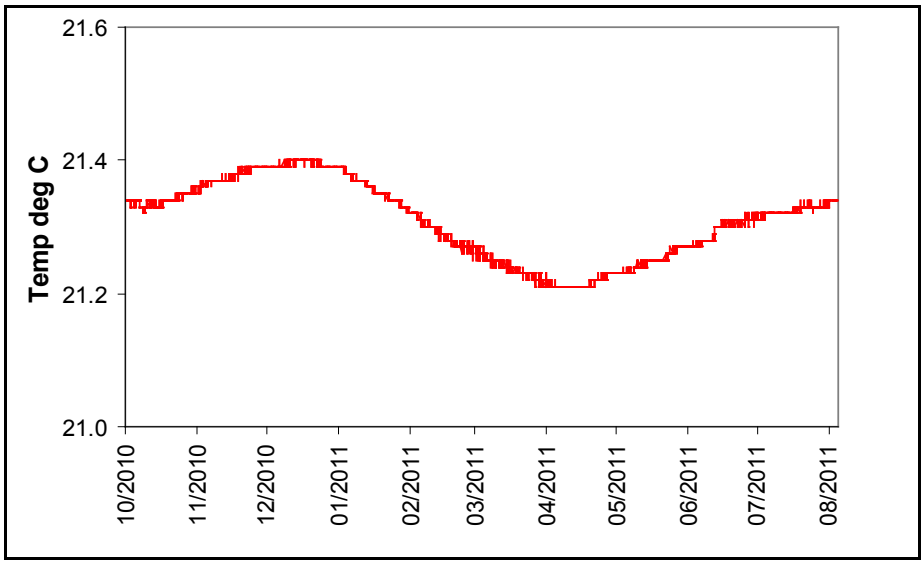

Figure 9-3. *Temperature data for BHMAR84-3, screened within the Menindee Formation aquifer. Note the 0.2℃ variation in temperature.*

Figure 9-4 plots the Calivil Formation groundwater levels in BHMAR80A-2 with monitoring of groundwater temperature during the 2010/11 flood event. This shows a steady groundwater temperature of 21 ºC that is punctuated by a rapid rise of about a degree followed by fluctuating temperature conditions. This suggests that heat may be a useful tracer for the measurement of relatively rapid by-pass flow during high river flow conditions. This requires further analysis of existing monitoring of groundwater temperature associated with the installed pressure transducers. There is also an opportunity to supplement the existing monitoring by higher resolution temperature sensors in both the bores and at river gauging sites.

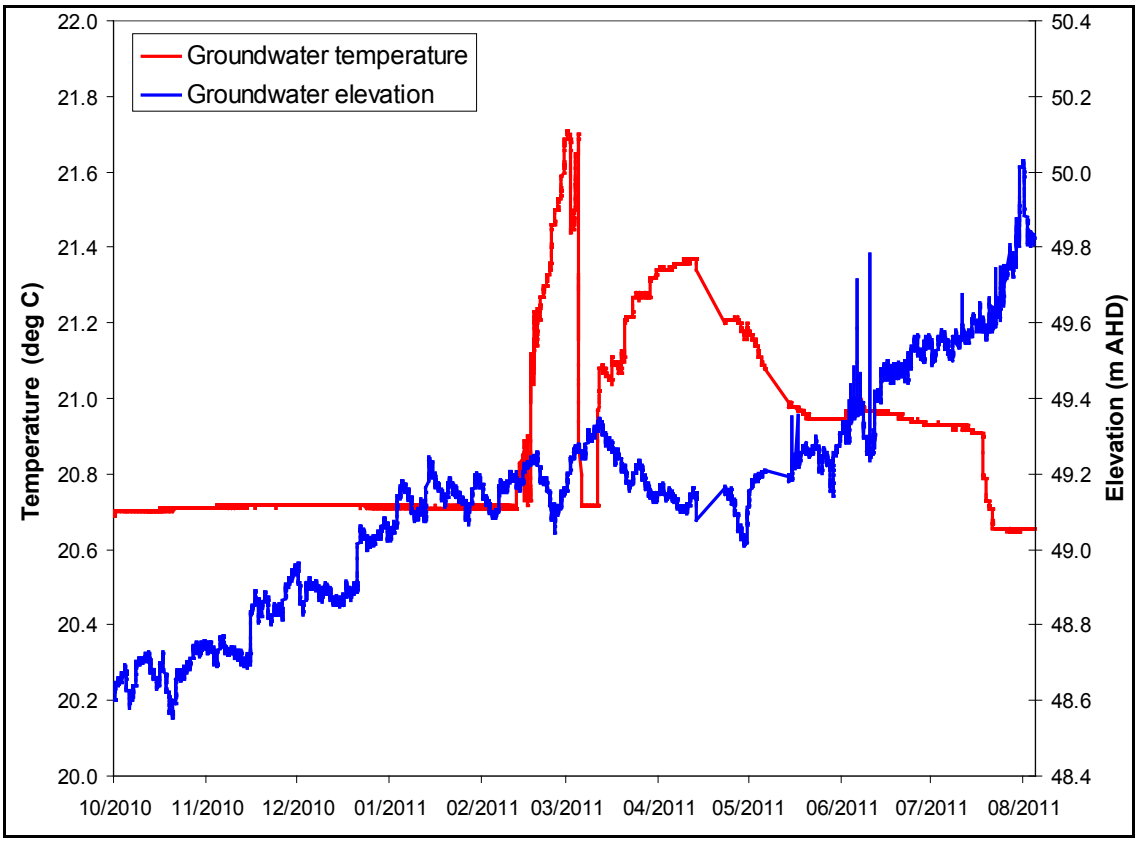

Figure 9-4. *Time series monitoring of groundwater elevation and temperature for bore BHMAR80A-2 screened in the Calivil Formation aquifer at East Bootingee.*

Unfortunately the temperature data obtained from the pressure transducer loggers were in many instances either highly erratic or showed no response despite changes in groundwater levels. Two possible explanations for these observations are firstly that the data loggers were faulty (Schlumberger pers. comm. 2012) or not sensitive enough to detect sub-degree changes in water temperature; or secondly that the temperature pulse associated with groundwater recharge had dissipated before encountering the temperature loggers. In a study undertake by Baskaran *et al*. (2009), the authors were only typically able to detect temperature fluctuations 25 cm below the streambed. Groundwater temperature data obtained in this study are at distances of between 17 m and approximately 2 km and at depths of 8 to approximately 200 m. The relative low hydraulic conductivity of the heterogeneous aquifer sediments is likely to be insufficient to allow for rapid groundwater flow resulting in groundwater temperature fluctuation at measurement sites. Consequently, little could be concluded from the groundwater temperature measurements collected.

9.2.4 Darcian Seepage Velocities

The response time in the order of months for the Calivil Formation and Renmark Group aquifers to the 2010-11 flood event suggests that there are alternative pathways through the shallow and Blanchetown Clay aquitards. By way of comparison, the seepage velocity (v) through the Blanchetown Clay aquitard separating the shallow Quaternary aquifer and the underlying Calivil Formation aquifer can be estimated assuming Darcian flow without dispersion using Equation 8.

$$v = -\frac{Kdh}{n_e L}$$

Equation 8

Where K is the vertical hydraulic conductivity of the Blanchetown Clay aquitard, dh is the head difference between the shallow Quaternary aquifer and the underlying Calivil Formation aquifer, n_e is the effective porosity of the Blanchetown Clay and L is the Blanchetown Clay thickness. A sensitivity analysis of seepage velocity was undertaken using low, typical and high estimates of these input parameters (Table 9-3). This analysis derived travel times through a typical Blanchetown Clay thickness ($L=8$ *m*) ranging between years to millennia, and typically being in the order of centuries (Table 9-4). Hence, vertical infiltration through the overlying Blanchetown Clay aquitard is not a reasonable explanation of the recharge response of the Calivil Formation and Renmark Group aquifers being in the timeframe of months. Faulting, vertical structural offsets of formations or gaps in the Blanchetown Clay near the river could result in much quicker pathways to the Calivil Formation.

Table 9-3. *Summary of input parameters for travel time estimates through Blanchetown Clay profile.*

Parameter	Low Estimate	Typical Estimate	High Estimate	Comments
Vertical hydraulic conductivity of Blanchetown Clay (K, m/s)	1E-12	1E-10	1E-09	Based on lab centrifuge tests on Blanchetown Clay core samples
Head difference between shallow aquifer and Calivil Formation aquifer (dh, m)	1	3	5	Based on mapping of groundwater levels using borehole monitoring in both aquifers
Thickness of Blanchetown Clay (L, m)	3	8	14	Based on thickness mapping using AEM profiles and borehole data
Effective porosity of Blanchetown Clay (ne)	0.01	0.06	0.18	Based on representative porosity values for clay (McWhorter & Sunada, 1977)

Table 9-4. *Sensitivity analysis of travel time through Blanchetown Clay.*

Estimate	Seepage Velocity (m/s)	Seepage Velocity (m/yr)	Travel Time (L=8 m) (yr)
Low	4E-13	1E-05	640,000
Typical	6E-10	0.02	400
High	2E-07	5	1.5

9.2.5 Groundwater Mounding

Hantush (1967) developed analytical equations to estimate steady-state groundwater mounding associated with uniform percolation. Bouwer (2002) applied these in the context of artificial recharge investigations to estimate infiltration from long strip basins using Equation 9:

$$H_c - H_n = \frac{iW}{2T}\left(\frac{W}{4} + L_n\right)$$

Equation 9

where H_c is the height of the groundwater mound in the centre of the recharge area, H_n is the height at the watertable at a control site away from the recharge area, W is the width of the recharge area, L_n is the distance between the edge of the recharge area and the control site, T is the aquifer transmissivity and i is the average infiltration rate (Figure 9-5).

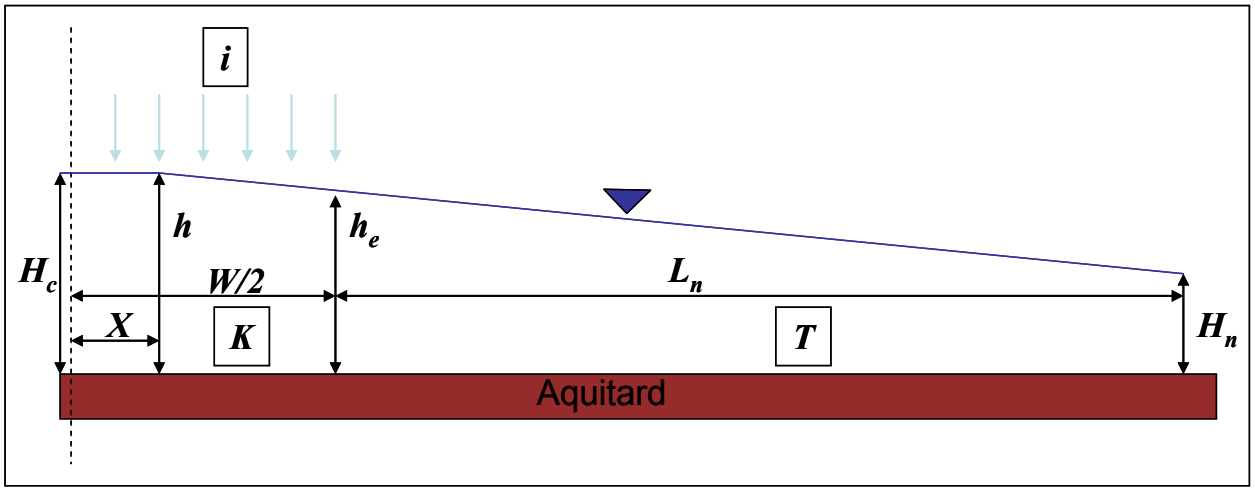

Figure 9-5. *Section showing geometry and parameters for calculating the groundwater mound below a long infiltration area (strip) of width W (adapted from Bouwer, 2002).*

The steady state equation assumes that the recharge feature has a length of at least five times the width (W). On this basis, Equation 9 was used to estimate the infiltration rate from the Darling River, based on the geometry of the resulting watertable mound. Table 9-2 summarises the application of this equation using selected bores at Jimargil as control sites.

Table 9-5. *Summary of estimates of infiltration rates using Bouwer (2002) groundwater mounding equation.*

Parameter (from Equation 2)	Value	Rationale
Control Site BHMAR 80A-3		
H_c (m)	8.1	Aquifer base (42.4 m AHD) from BHMAR80A-2 log and RWL (50.4 m AHD) interpolated from measured RWL at BHMAR80A-4
H_n (m)	7.9	Aquifer base (42.4 m AHD) from BHMAR80A-2 log and measured RWL (50.3 m AHD) at BHMAR80A-4
W (m)	80	width (m) of Darling River bank full
T (m^2/d)	4.8	sum of NMR transmissivity values for saturated part of watertable aquifer in BHMAR80A-2
L_n (m)	125	Distance from river edge to BHMAR80A-2
Infiltration rate i (mm/d)	**0.17**	
Infiltration rate i (mm/yr)	**60**	
Control Site BHMAR99-2		
H_c (m)	7.4	Aquifer base (43 m AHD) from BHMAR99-1 log and RWL (50.4 m AHD) interpolated from measured RWL at BHMAR80A-4
H_n (m)	6.5	Aquifer base (43 m AHD) from BHMAR99-1 log and RWL (49.5 m AHD) interpolated from December 2011 watertable contours
W (m)	80	width (m) of Darling River bank full
T (m^2/d)	13.1	Sum of NMR transmissivity values for saturated part of watertable aquifer in BHMAR99-1
L_n (m)	1005	Distance from river edge to BHMAR99-1
Infiltration rate i (mm/d)	**0.29**	
Infiltration rate i (mm/yr)	**105**	
Control Site BHMAR92-2		
H_c (m)	8.3	Aquifer base (42 m AHD) from BHMAR92-1 log and RWL (50.3) interpolated from measured RWL from BHMAR92-2
H_n (m)	8.2	Aquifer base (42 m AHD) from BHMAR92-1 log and measured RWL (50.2 m AHD) from BHMAR92-2
W (m)	80	width of Darling River bank full
T (m^2/d)	10	NMR T values for saturated part of watertable aquifer in BHMAR92-1
L_n (m)	85	Distance from river edge to BHMAR92-1
Infiltration rate i (mm/d)	**0.24**	
Infiltration rate i (mm/yr)	**87**	

9.2.6 Flood Frequency Analysis

Analysis of hydrographic and hydrochemical data conclude that groundwater recharge is dominated by river leakage associated with high-flow events. The recharge during high-flow events, as well as the duration and frequency of these flow events needs to be quantified. Such an analysis was undertaken using the historic stream gauging record for the Darling River at Weir 32 (425012) by:

- Checking for any gaps in the data record which spans about 38 years (1974-2012). Such gaps were minor (<1% of record) and were filled by linear interpolation between the existing bounding data.
- Defining a flow event as a continuous record of daily flows that exceeded a defined flow threshold (e.g. 10,000 ML/d). Statistics were collected such as the event duration, total event flow and maximum event flow for events where flow exceeded the particular flow threshold.
- Repeating the compilation of these event statistics using different flow thresholds.

Table 9-6 summarises these flow event statistics. The number of flow events decreased as the magnitude of the flow threshold increased (Figure 9-6a). This is also the case for the proportion of the historic record that had recorded daily flows exceeding the threshold (Figure 9-6b). About 16% of the record had flows exceeding 10,000 ML/d whilst about 4% had flows exceeding 25,000 ML/d.

These statistics (Table 9-6) are needed to derive a long-term recharge average, considering that the recharge associated with episodic high-flow events is interspersed with relatively long periods of zero recharge under low to average river flow conditions. This requires an understanding of what constitutes a reasonable flow threshold where recharge by river leakage becomes significant. Hydrographs of near-river monitoring bores screened in the Calivil Formation aquifer show a response to high flows before the onset of overbank conditions. For the Weir 32 site, responses to flows on the order of 8-10,000 ML/d were observed, which are below the gauge level corresponding to overbank flow of about 19,000 ML/d. In terms of duration, these flows represent about 16-18% of the overall historic record (Table 9-6). This means that active recharge to the groundwater system would only occur for about 17% of the time. On this basis, the recharge rate associated with the episodic high flows would need to be multiplied by this proportion (0.17) to derive a long term average recharge rate. This analysis supports the need to maintain a hydrographic network in the study area, to monitor the groundwater response to flow events of varying magnitude.

***Table 9-6**. Summary of events exceeding flow thresholds for the Darling River at Weir 32 gauge record (1974-2012).*

Flow Threshold (ML/d)	Total Days	Proportion of Record	Number of events	Minimum Duration (days)	Maximum Duration (days)	Average Duration (days)
5000	3216	0.23	38	3	360	85
8000	2573	0.18	29	5	355	89
10000	2171	0.16	22	2	342	99
15000	1728	0.12	20	9	212	86
19000	1136	0.08	18	7	181	63
25000	604	0.04	9	1	110	67

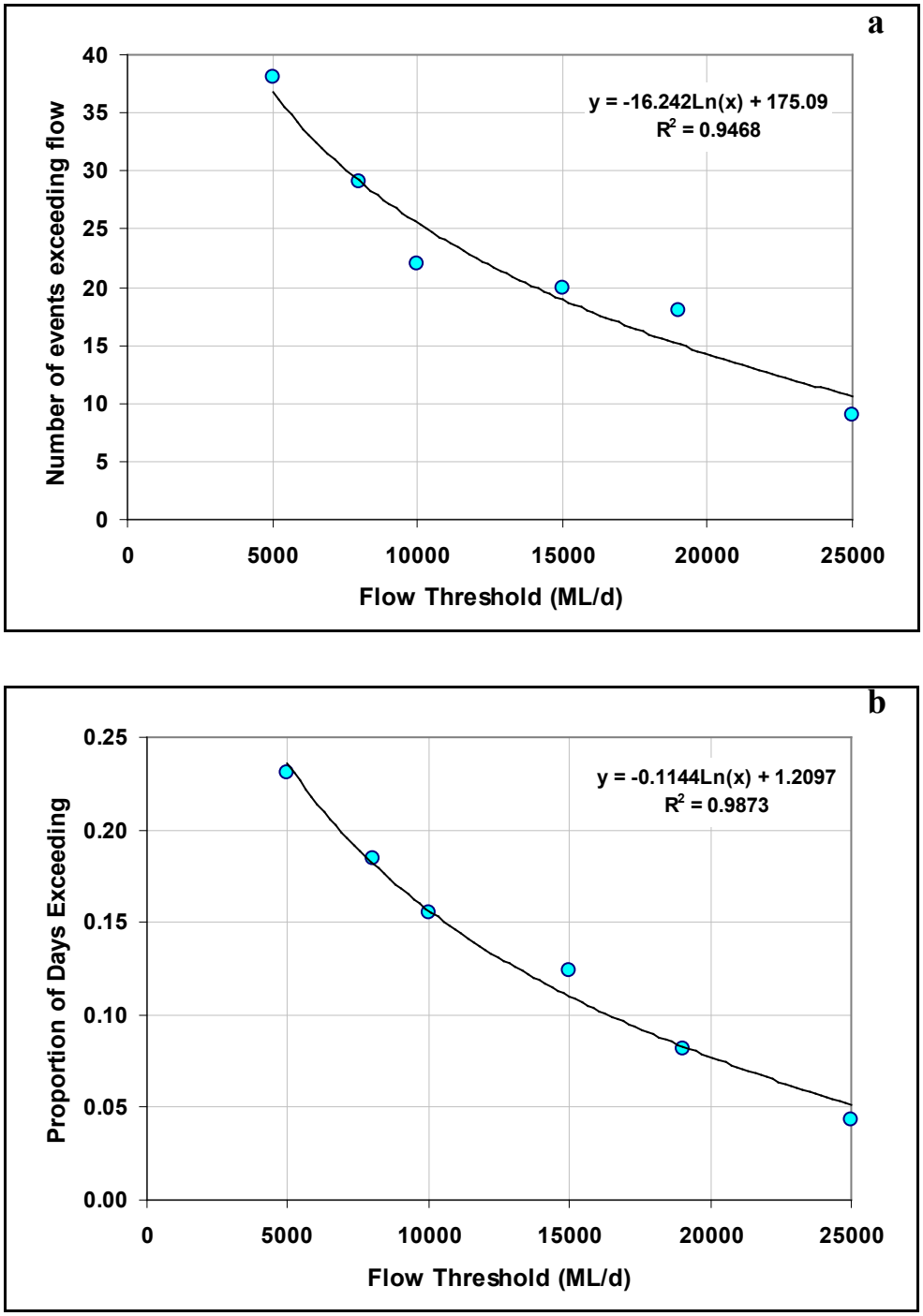

Figure 9-6. *Number (a) and proportion (b) of flow events exceeding flow thresholds for Darling River @ Weir 32 flow record.*

9.2.7 Radiocarbon Depth Models

The depth profile of radiocarbon (^{14}C) concentrations in groundwater can be used to estimate a steady state recharge rate (Vogel 1966, Walker & Cook, 1991). Equation 10 relates the ^{14}C depth profile in the absence of diffusion:

$$C = C_0\left(\frac{H}{H-z}\right)e^{-\lambda H\theta / R}$$

Equation 10

Where C_0 is the initial ^{14}C groundwater concentration at the watertable, C is the ^{14}C at depth z from the watertable, H is the depth to aquifer base, λ is the ^{14}C radioactive decay constant (1/8270 yr^{-1}), θ is aquifer porosity and R is the recharge rate. The equation considers uniform recharge of an unconfined aquifer with constant thickness and porosity and with uniform horizontal velocity with depth.

Solving for recharge (R), Equation 10 becomes:

$$R = \frac{-\lambda H\theta}{\ln(CH-z)-\ln(C_0H)}$$

Equation 11

However, the assumptions inherent in Equation 11 are invalid for the Calivil Formation target aquifer, being semi-confined rather than unconfined. Based on Cook & Bohlke (2002), the equivalent equation for a semi-confined aquifer with constant thickness in the confined part is:

$$C = C_0e^{-\lambda(z\theta / R+xH\theta / Rw)}$$

Equation 12

This equates to:

$$R = \frac{-\lambda\theta(z+wH/x)}{\ln(C)-\ln(C_0)}$$

Equation 13

Where H is the constant aquifer thickness, C is the ^{14}C at depth z from the top of the aquifer, w is the width of the recharge area and x is the horizontal distance between the site and the edge of the recharge source. Table 9-8 summarises the results of applying the unconfined recharge model (Equation 11) to the Coonambidgal and Menindee Formation radiocarbon samples, and the confined recharge model (Equation 13) to the Calivil Formation radiocarbon samples. For the Coonambidgal Formation samples, the initial C_0 concentration was set at 115 percent modern carbon (pMC) which is the maximum recorded for these shallow bores. As the equivalent for the confined model represents the ^{14}C input at the top of the Calivil Formation aquifer, a range defined by the minimum (101 pMC) and the maximum (115 pMC) for the shallow aquifer samples were used in the confined model calculations. This is the reason why the radiocarbon recharge estimates for the Calivil Formation are reported as a range.

9.2.8 Chloride Mass Balance Method

The groundwater chloride mass balance (GCMB) is the most common method used to estimate steady-state diffuse recharge from rainfall in Australia, due to its ease of use and minimal data requirements (Crosbie *et al.,* 2010). There are some limitations of this method; GCMB can only be calculated if the groundwater at the screen depth is at a steady state. If vegetation clearing has occurred, a period of time must elapse before a new steady state is reached; this period of time varies with rainfall rates and hydraulic properties of the

soil/regolith between the surface and the bore screen. There are other assumptions inherent in this methodology discussed by Leaney *et al*. (2011). For example, the chloride in groundwater is assumed to originate from precipitation. If there are other subsurface sources of chloride beside precipitation, such as halite deposits or marine-sourced formation waters, then the calculated recharge rates would be erroneously low. The bromide/chloride ratio of groundwater can be used to investigate the potential influence of halite dissolution in groundwater evolution (Davis *et al*., 1998; Wood, 1999; Kloppman *et al.,* 2001). The deeper, more saline groundwaters in the study area have a Br/Cl ratio slightly lower than for conventional seawater, suggesting some influence of halite dissolution (Section 8.1).

By way of comparison with the other recharge estimation approaches, the GCMB method was employed using pre-existing data, namely chloride in rainfall, average rainfall amount and soil classes (available via MapConnect, http://ga.gov.au/topographic-mapping/mapconnect.html) and groundwater chloride data (available from NSW Office of Water). Equation 14 was used where R is the long term recharge rate (m/d), D is the chloride deposition rate (kg/m^2/d) and C_g is the concentration of chloride in the groundwater (kg/m^3). The chloride deposition rate (D) is the combination of the average chloride concentration (kg/m^3) in rainfall and the average rainfall rate (m/d):

$$R = \frac{D}{C_g}$$

Equation 14

Preliminary diffuse recharge rates from rainfall derived from this method (using existing groundwater chloride measurements) ranged from 0.1 to 7.3 mm/yr in the BHMAR study area with an average diffuse recharge rate (n= 30; taken at differing rainfall and soil classes) of 1.2 mm/yr. As part of the BHMAR Project, a series of sonic boreholes were drilled across the study area. Pore fluid samples were extracted from the core and analysed for a suite of parameters including chloride concentrations (Lawrie *et al.,* 2012a). Table 9-7 summarises the statistics of these pore fluid estimates of diffuse recharge on a stratigraphic basis. The recharge rates derived from the 706 pore fluid samples ranged from 0 to 37 mm/yr, averaging 1.8 mm/yr (see Appendix 8, Apps *et al*., 2012a).

Table 9-7: *Summary statistics of diffuse recharge rates calculated using the groundwater chloride mass balance approach on BHMAR pore fluids.*

Unit	Stratigraphy	Count	Minimum	Mean	Maximum
All	All Units	706	0.0	1.8	37.0
Qa	Coonambidgal Formation	5	2.1	8.8	14.8
Qam	Menindee Formation	49	0.0	1.8	11.3
Qaw	Willotia beds	22	0.0	2.4	10.0
Qpc	Blanchetown Clay	50	0.0	3.5	37.0
Tpc	Calivil Formation	337	0.0	2.3	19.0
Tps	Loxton-Parilla Sands	8	0.1	0.7	2.1
Ter	Renmark Group	223	0.1	0.5	8.2

Applying the GCMB method to the pore fluid data, provides downhole profiles of estimated recharge rates The downhole variability in the recharge estimates suggests that the groundwater recharge regime is more complex than simply diffuse vertical recharge from precipitation that assumes a disconnection between surface water and groundwater. The pore fluids with relatively high estimated recharge rates (>7 mm/yr) are all associated with boreholes located close to rivers or lakes that have hydrochemical or hydrographic evidence of surface water leakage. This is most evident for the Coonambidgal Formation (Table 9-7), where the pore fluids are sampling the shallow unconfined aquifer near the Darling River.

If the dominant recharge mechanism is by river or lake leakage, then the underlying assumptions of the chloride mass balance method do not hold. This means that the derived recharge statistics, as reported in Table 9-7, are not valid.

9.2.9 Comparison of Recharge Methods

Table 9-9 compares the different approaches taken to estimate groundwater recharge, focussing on the Jimargil site due to its greater data availability. The estimates derived from the watertable fluctuation method as reported in Table 9-2 relate to a specific high flow event. Therefore, these values were multiplied with the proportion factor (0.17) estimated by the flood frequency analysis to convert to a long-term recharge rate. This takes into account that active recharge only occurs 17% of the time during high flow conditions, with recharge being effectively zero for the remaining 83% of the time.

Recharge rates derived from the watertable fluctuation method for the shallow Coonambidgal Formation and Menindee Formation aquifers are reported as ranges due to the uncertainty (and inherent variability) of the specific yield parameter used in the calculations (Table 9-9). The watertable fluctuation recharge for the Coonambidgal Formation aquifer bores tends to exceed 100 mm/yr. However, some Coonambidgal Formation bore hydrographs show rapid watertable declines with river flow recession, indicating losses by processes such as drainage of bank storage back to the river or inter-aquifer leakage. For the Menindee Formation aquifer bores, long-term recharge is more in the range of 20-60 mm/yr. The steady-state mounding equation (Bouwer, 2002) provides recharge rates of a similar magnitude for the Coonambidgal and Menindee Formation aquifers.

Recharge rates derived from the unconfined radiocarbon model (Equation 11) are significantly lower for the Coonambidgal Formation and Menindee Formation aquifers than using any other methods (Table 9-9). For the Calivil Formation aquifer bores, results using the confined radiocarbon model (Equation 13) are reported as ranges due to variations in the radiocarbon input parameter. For the Calivil Formation aquifer, the radiocarbon method suggests that relatively close to the river (as exemplified by BHMAR77-5 and BHMAR80A-7) long-term recharge may be in the order of 20-35 mm/yr, with recharge decreasing with distance away from the river source. As the analysis focuses on monitoring bores in the Jimargil target, the recharge rates reported in Table 9-9 are likely to be relatively high compared to regional averages. Such relatively high recharge is limited to the river corridor (and specific areas of lake leakage), rather than being distributed across the whole landscape, as is the case for diffuse recharge from rainfall. This makes it more difficult to derive volumetric estimates of recharge for the entire aquifer. Construction of a transient groundwater flow model calibrating the hydrographic response to a series of flood events is recommended.

Table 9-8. *Summary of radiocarbon recharge estimates for selected Jimargil bores.*

			Unconfined Model		Confined Model	
BHMAR	**Aquifer**	**Screened Interval (m below land surface)**	**Recharge (mm/d)**	**Recharge (mm/yr)**	**Recharge (mm/d)**	**Recharge (mm/yr)**
80A-3	Coonambidgal	11-17	.02	6	N/A	N/A
80A-4	Coonambidgal	10-14	.03	10	N/A	N/A
80B-3	Coonambidgal	11-16	.02	7	N/A	N/A
84-3	Coonambidgal	10-23	.01	5	N/A	N/A
84-4	Coonambidgal	12-23	.01	5	N/A	N/A
84-5	Coonambidgal	10-23	.02	8	N/A	N/A
77-3	Menindee	11-16	.02	8	N/A	N/A
77-4	Menindee	11-15	.03	10	N/A	N/A
92-2	Menindee	12-16	.05	19	N/A	N/A
77-2	Calivil	47-55	N/A	N/A	.01-.02	5-6
77-5	Calivil	46-56	N/A	N/A	.07-0.10	27-35
80A-2	Calivil	35-53	N/A	N/A	.02-.03	7-13
80A-5	Calivil	35-55.5	N/A	N/A		
80A-7	Calivil	42-54	N/A	N/A	.05-.09	18-35
80B-2	Calivil	53-65	N/A	N/A	.016-.024	6-9
83-2	Calivil	48-63	N/A	N/A	.01-.013	4-5
84-2	Calivil	45-51	N/A	N/A	.004-.005	1.6-1.7
92-1	Calivil	32-62	N/A	N/A	.01-.02	5-8

Table 9-9. *Comparison of recharge estimates using different methods for sites at Jimargil.*

				Watertable Fluctuation (Averaged)	Mounding	Radiocarbon (Unconfined)	Radiocarbon (Confined)
BHMAR	**Formation**	**Screened Interval**	**Distance to River (m)**	**Recharge (mm/yr)**	**Recharge (mm/yr)**	**Recharge (mm/yr)**	**Recharge (mm/yr)**
80A-3	Coonambidgal	11-17	71		60	6	N/A
80A-4	Coonambidgal	10-14	174			10	N/A
80B-3	Coonambidgal	11-16	75			7	N/A
84-3	Coonambidgal	10-23	17	106-212		5	N/A
84-4	Coonambidgal	12-23	100	55-106		5	N/A
84-5	Coonambidgal	10-23	110			8	N/A
77-3	Menindee	11-16	102	18-37		8	N/A
77-4	Menindee	11-15	108			10	N/A
92-2	Menindee	12-16	151	26-51	87	19	N/A
77-2	Calivil	47-55	115	N/A	N/A	N/A	5-6
77-5	Calivil	46-56	50	N/A	N/A	N/A	27-35
80A-2	Calivil	35-53	164	N/A	N/A	N/A	7-13
80A-5	Calivil	35-55.5	174	N/A	N/A	N/A	
80A-7	Calivil	42-54	71	N/A	N/A	N/A	18-35
80B-2	Calivil	53-65	135	N/A	N/A	N/A	6-9
83-2	Calivil	48-63	177	N/A	N/A	N/A	4-5
84-2	Calivil	45-51	112	N/A	N/A	N/A	1.6-1.7
92-1	Calivil	32-62	151	N/A	N/A	N/A	5-8
80A-6	Renmark	84-102	174	N/A	N/A	N/A	

9.3 PALAEORECHARGE

9.3.1 Continental-scale Climate and Catchment Setting

Global climate has varied markedly at long-term timescales (10s to 100s of thousands of years) with the glacial-interglacial climate cycles. Only a trivial part of mainland Australia around the highest mountain, Mt Kosciuszko in the south east, was actually glaciated at the LGM (last glacial maximum). However, the impact of lowered temperatures, lowered sea level, low sea-surface temperatures and widespread periglacial activity in highland catchments during glacial times profoundly modified precipitation, temperatures, evaporation and runoff across much of the continent. Variations in precipitation and runoff in the Lower Darling region are particularly important for variations in recharge of the aquifers of the BHMAR Project area.

Australia currently receives precipitation from two main sources - summer rainfall from the Australian monsoon from the north, and winter rainfall from the westerly circulation from the south. A zone of strong summer dominance (where summer rainfall is at least 3 times winter rainfall) covers at least the northern third of the continent. Narrow zones of strong winter dominance (where winter rainfall is at least 3 times summer rainfall) occur in the south-west corner of Western Australia and southern South Australia. In between these extremes, a wide zone of weak seasonal dominance (where the ratio between seasons lies between 1.3 and 3) or uniform distribution (seasonal ratios are less than 1.3) spans the continent diagonally from the Pilbara coast in the west to the south east corner (Gentilli, 1986). The Lower Darling region falls within the zone of uniform seasonal distribution of precipitation. In addition to these seasonal rainfall sources, east-coast lows can develop in any season from various synoptic situations derived from either summer-monsoonal or winter-westerly circulations. These events can bring intense precipitation to eastern coastal regions which can occasionally penetrate beyond the rainfall divide and impact westerly flowing Murray-Darling catchment streams.

The Darling River has a large and complex catchment on the western side of the Eastern Highlands, the western slopes and plains of northern NSW and southern Queensland, situated mostly in the weakly summer-dominant rainfall zone. However, winter-westerly rainfall events can be significant, especially in the southernmost NSW portion of the catchment. Additionally east-coast lows can occasionally deliver significant precipitation to the headwater catchments. Some parts of the NSW catchment headwaters are located on the Northern Tablelands at elevations up to 1,500 m. This area has cold winters today and would have undoubtedly had periglacial activity and seasonal snowpack during lowered glacial-episode temperatures, with strong implications for altered runoff regimes.

There are a number of palaeoclimatic records across the continent which provide a useful palaeoclimatic picture both at a continental scale and for some specific regions. Unfortunately, there are sparse palaeoclimate records of any type for the Lower Darling region and no continuous long-term records. However, river leakage is by far the dominant recharge mechanism with diffuse recharge from rainfall minor in comparison. Therefore variations in river discharge due to palaeoclimatic changes in the catchment are likely to be most relevant for changes in recharge and these can be addressed by continental-scale and catchment-region palaeoclimate records. Additionally, this can be complemented by reconstruction of variations in fluvial activity and discharge from geomorphic, stratigraphic and geochronological studies of the Quaternary fluvial deposits of the study region.

9.3.2 Glacial-interglacial Climate Cycles

Ice accumulation commenced in Antarctica about 20 million years ago but the Pliocene-Quaternary glacial-interglacial cycles commenced at low amplitude about 5.5 million years ago. These cycles initially showed 21,000 year (precessional) cycles until about 2.5 million years ago. When ice advance and retreat across the Northern Hemisphere continents began at 2.5 Ma, the cyclicity increased in amplitude and switched to 41,000 years (obliquity). At about 1 million years ago the cycle amplitude increased further and changed to 100,000-year (eccentricity) timescales. The earth is currently in an interglacial, which commenced about 12,000 years ago. The Australian climate has varied markedly during these Quaternary global glacial-interglacial climate cycles with major temperature lowering during glacial episodes and variations through

the cycles in the effectiveness of both winter- and summer-seasonal rainfall regimes, which have sometimes been in phase and sometimes out of phase (Hesse *et al*., 2004).

During the peak of the previous interglacial at about 125-130 thousand years ago (ka) temperatures and sea-levels were slightly higher than during the current interglacial. The summer-monsoon-rainfall regime was much more effective with monsoon-watered rivers more active and enlarged perennial mega-lakes, such as Eyre, Gregory and Woods (Magee, 2007; Nanson *et al.*, 1992; Magee *et al*., 2004, Bowler *et al.,* 2001, Bowler *et al.,* 1998). Through the last glacial cycle the records of some summer-monsoon-watered systems such as Lake Eyre (Magee, 2007; Magee *et al.,* 2004) indicate successive less-effective wet phases in Marine Isotope Stage (MIS) 5 (~130-70 ka) which are on timescales similar to the stadial-interstadial oscillations but cannot be matched exactly due to low precision of the Optically Stimulated Luminescence (OSL) dating. There is a relatively low-level wet phase in monsoon-watered systems in MIS 3 (60-40 ka) at Lake Eyre (Magee *et al.,* 2004) and the Lake Eyre basin rivers (Nanson *et al.*, 1992) though more recent shoreline dating from Lake Frome (Cohen *et al*., 2011, 2012) suggests that this may have been a stronger event. In later MIS 3 and the Last Glacial Maximum (LGM = MIS 2) the monsoon was not effective due to lowered intensity and reduced sea level. Following termination of the glacial phase and the onset of the current interglacial, the monsoon seems to have returned about 14 ka (Wyrwoll & Miller, 2001) and by 12 ka was maintaining a low-level perennial lake at Lake Eyre (Magee *et al*., 2004). However, monsoon effectiveness has never reached the levels of the previous interglacial in either the Lake Eyre record (Magee *et al.*, 2004), the Lake Eyre Basin rivers (Nanson *et al*., 1992) or other monsoon fed mega-lakes such as Lake Woods (Bowler *et al.,* 1998) or Lake Gregory (Bowler *et al.,* 2001). Monsoon intensity correlates to insolation intensity, high summer temperatures, high sea-levels and high sea surface temperatures (Kutzbach & Guetter, 1986), however, the contrast between the effective penetration of monsoon precipitation into the continent in the previous interglacial compared to the present interglacial is regarded as anomalous by some (Magee *et al.*, 2004; Miller *et al.*, 2005).

The best long-term winter-westerly precipitation records come from the Murray Basin with a detailed, well dated, lake-level record from the Willandra Lakes, fed by a Lachlan River distributary. Other Murray Basin records include fluvial activity on the Riverine Plain from the Murray, Goulburn, Murrumbidgee and Lachlan Rivers and a smaller lake basin close to the highlands, Lake Urana. These Murray basin records are somewhat out of phase with the monsoon record. Inconsistencies at the LGM between the Willandra Lakes in the western part of the basin and the fluvial records close to the highlands are probably due to complexities of runoff from higher altitudes due to low temperatures. The Willandra Lakes (Bowler, 1998; Bowler *et al.*, 2003; Bowler *et al.*, 2012) show evidence of poorly defined, enhanced lacustrine episodes in MIS 5 and earlier interglacials but have a well dated detailed stratigraphic record from early MIS 3 (60 ka) to the present. The lakes filled at 60 ka and the system was full, fresh and overflowing until the first onset of drying at about 42 ka which was followed by a sequence of alternate wet and dry phases, with the latter becoming increasingly effective, until there was a major drying phase with substantial lake-floor deflation coincident with the LGM. The Willandra Lakes have remained dry after this event throughout the Holocene to the present day. From the Riverine Plain fluvial sequence, Page *et al.* (1996) recognise a late MIS 5 wet phase (Coleambally Unit, 115-80 ka) which has no equivalent at the Willandra Lakes and occurs after the wettest monsoon phase at Lake Eyre (Magee *et al*., 2004) but is coeval with fluvial activity in the Lake Eyre Basin rivers (Nanson *et al.*, 1992). The Kerarbury Unit (50-15 ka) Riverine Plain fluvial activity identified by Page *et al.* (1996) accords approximately with the Willandra Lakes Stage 3 wet phase, but evidence from many Riverine Plain streams including the Murrumbidgee (Page *et al.*, 1996), Murray and Goulburn (Bowler, 1978) for large actively migrating sandy bedload streams at the LGM is inconsistent with records from both the Willandra Lakes and the monsoon-fed systems. Lake Urana, close to the Riverine Plain/highlands margin was also full during the LGM (Page *et al.,* 1994). At the same time, aeolian systems in the western Murray Basin and across arid central Australia – including the major Australian dunefields, were all active indicating widespread aridity at the LGM.

This conundrum, of widespread continental aridity at the LGM, including an inactive monsoon, dry lakes and active dunefields, coincident with active migrational rivers larger than their modern equivalents adjacent to the south-eastern highlands requires explanation and has implication for parts of the Darling River catchment. Temperatures in the south-eastern highlands were up to 9° C lower at the LGM (Galloway, 1965; Barrows *et al.*, 2001, 2004) and the explanation undoubtedly derives from complexities of catchment response due to widespread periglacial conditions, reduced vegetation cover and seasonal snowpack

accumulation and melting. These factors would have resulted in high seasonal flows and enhanced supply of sandy bedload sediment. Bowler (1978), Page *et al.* (1994) and Magee (2007) have all referred to this explanation for LGM fluvial records of the Goulburn, Murray and Murrumbidgee systems. Though poorly constrained by well dated palaeoclimatic records, the Northern Tablelands of NSW also have widespread areas of land up to 1500 m AHD. These areas may have been affected by the same suite of low-temperature factors influencing catchment responses during the LGM. The headwaters of some important Darling River tributaries lie in this area including the Macquarie, Namoi, Gwydir, MacIntyre and Dumaresq rivers.

In summary, the two broad climatic systems that bring precipitation to Australia, the winter westerlies and the monsoon, have both been more effective and less effective at different times during the glacial/interglacial climatic cycles of the Quaternary. These changes have almost certainly been out of phase, with enhancement of the westerlies occurring later than monsoon enhancement in MIS 5. Additionally, enhancement of the westerlies was much stronger than the monsoon in MIS 3. Despite widespread aridity across the continent during the LGM, some rivers with high-altitude catchments, showed active lateral-migration phases at the LGM due to low-temperature modifications of catchment response. Post-LGM enhancement of monsoon precipitation in the Holocene has been much less effective than during the previous interglacial episode, and it is not yet certain if this is anomalous or part of a longer-term trend (Magee, 2007).

As detailed above, the Darling catchment is currently dominated by summer-rainfall though it can more rarely receive significant precipitation from the winter westerlies and the east. That situation is likely to have also occurred during the Quaternary. It is likely that flow in the Darling would have been enhanced episodically during the glacial/interglacial cycles including during the last interglacial, both at its height (MIS 5e, 125-130 ka) in accord with maximum monsoon enhancement and during later sub stages of MIS 5 (120-70 ka) in accord with phases of both monsoon and winter-westerly enhancement. Enhanced flow from the NSW catchment is also likely during MIS 3 due to enhanced winter-westerly precipitation. In accord with monsoon catchment records, streamflow in the Darling is unlikely to have been enhanced during the LGM unless the higher altitude NSW catchments produced significant seasonal flooding due to low-temperature induced changes in catchment response or perhaps due to changes in local boundary conditions. Holocene flow regimes are also expected to be lower than the previous interglacial in accord with all other monsoon-rainfall systems.

9.3.3 Lower Darling Fluvial Activity Phases

The lower Darling Valley in the project area shows clear geomorphic evidence of episodic lateral-migration phases evident in satellite images and on the ground as at least three successive cross-cutting scroll-plain tracts (Coonambidgal Formation). These scroll-plain tracts are successively topographically higher with less distinct scroll traces due to more overbank burial and they are inset into an older higher more featureless floodplain (Menindee Formation). Cored project drillholes demonstrate that the Menindee Formation higher floodplain consists of older similar lateral-migration phases with scroll traces now obscured by deeper burial by overbank mud. The morphology of scroll traces and channel dimensions in the younger scroll-plain tracts demonstrate that steam discharges have been higher during past lateral-migration episodes than the most recent one associated with the modern Darling. The three scroll-plain tracts mappable in the valley intersect just south of Menindee township but are mostly separated upstream and downstream of that point.

Prior to this project, there was a paucity of numeric dating of fluvial episodes in the lower Darling Valley. Bowler *et al.* (1978) used conventional radiocarbon dating of charcoal obtained in the walls of the trench excavated for the Sydney to Moomba gas pipeline where it crosses the Darling at Tilpa, approximately 220 km upstream of Menindee. Bowler *et al.* (1978) established an LGM age (23-20 ka, calibrated age) for an earlier scroll-plain phase (Acres Billabong anabranch at Tilpa). Avulsion to the modern Darling was inferred to have occurred after about 13 ka (calibrated), though no datable samples were obtained from the modern Darling scroll-plain sediments. Bowler *et al.* (1978) also obtained a minimum age of 23.5 ka (calibrated) from soil carbonate in older alluvium (Menindee Formation equivalent). The scroll and channel dimensions of the LGM phase at Tilpa indicated greater discharge, more bedload sediment and lateral migration by outside bend erosion leading to increased sinuosity and lowered gradient compared to the modern Darling. The BHMAR Project has obtained 19 OSL and 4 radiocarbon dates from fluvial phases in the Menindee

region, which provide a much more extensive numeric chronology for the Late Quaternary active depositional phases in the Lower Darling Valley. The youngest, now inactive, scroll-plain phase, associated with the modern Darling River, was active in the period 6-2 ka demonstrating an initiation considerably later than the 13 ka inferred by Bowler *et al*. (1978). The previous anabranch scroll-plain phase, associated with the Talyawalka, Redbank and Tandou creeks and the Great Darling Anabranch, has LGM dates around 20 ka confirming the veracity of ages obtained by Bowler *et al*. (1978) from the morphologically similar Acres Billabong phase at Tilpa. Indistinct scroll-plain tracts older than the anabranch system, are evident both upstream and downstream of Menindee and have ages around 30 ka. Older dates of 50-45 ka, 85 ka and >150 ka have been obtained beneath the Menindee Formation floodplain from lateral migration sediments that lack visible scroll-plain traces. These ages demonstrate that episodic fluvial phases extend well back into the Late Quaternary and many more almost certainly occur, but have not yet been dated.

Comparison between the ages of these active fluvial phases and the generalised continental-scale climatic record outlined above suggests that the Lower Darling episodic fluvial phases are not primarily climatically driven. This conclusion is drawn from the observation that the three well dated scroll-plain phases occur at very different parts of the glacial-interglacial climate cycle with the oldest (30 ka) relict phase late in the MIS 3 interstadial close to the onset of the LGM, the anabranch phase at the LGM (20 ka) and the youngest Darling River phase (6-2 ka) late in the Holocene interglacial. If the Holocene phase reflected the post-glacial reinvigoration of the Australian monsoon it would have been expected to have started earlier with Wyrwoll & Miller (2001) indicating monsoon enhancement in the north west of the continent at 14 ka and the onset of lacustrine conditions occurring at 12 ka at Lake Eyre (Magee *et al.*, 2004) and at Lake Frome at 13 ka (De Deckker *et al.*, 2011; Luly, 2001; Bowler *et al.*, 1986). Therefore the timing of the onset and duration of the discrete phases of lateral accretion in the lower Darling Valley Quaternary fluvial sequence is not apparently related to precipitation changes associated with the impact of glacial-interglacial climatic cycles on the catchment. However, it is probable that the variations in river discharge, evident during different phases, in the form of variable channel and scroll parameters, reflect long-term changes in effective catchment precipitation and runoff.

The modern Darling River is a suspended-load stream with stable, often partially carbonate-cemented banks, which is not actively migrating or depositing lateral-accretion point-bar deposits. Sand in the system is restricted to mega-ripples on parts of the channel floor and occasional small benches on the inside of meander bends. A river cannot laterally migrate if it can more easily erode bedload from the inside of bends than from the cut bank on the outside of bends (Leopold *et al.*, 1964). Therefore if a river has stable silt/clay rich and/or cemented banks and lacks abundant sandy bedload to build point-bar deposits, as does the modern lower Darling River, it will not laterally migrate. Channel cross-sectional shape and dimensions and the channel and flood plain patterns are not a simple function of river discharge but are a complex function of river discharge, slope, sediment character and abundance and channel-marginal vegetation. Therefore it is not surprising that the onset and duration of lateral migration phases in the lower Darling Valley does not correlate simply with climatically-driven changes in river discharge. It has long been known that changing the sediment load can abruptly change the channel dimensions and patterns of streams (Schumm, 1960, Schumm, 1977) and Page & Nanson (1996) suggested that major abrupt changes of channel pattern in the Riverine Plain relate to large bedload-sediment slugs flushed out of the confined valleys of the lower highlands by very large floods. As these sediment slugs work through the fluvial systems on the Riverine Plain the channel pattern eventually reverts to its former state. While the lower Darling Valley is almost certainly too remote from the highlands for a similar mechanism to operate, there may be other ways to alter the sediment regime from suspended- to mixed-load types and perhaps initiate a lateral-migrational phase. Two possibilities are examined below.

The first possibility is megaflood erosion. The highest floods of the modern Darling regime inundate the whole of the floodplain and the BHMAR Project LiDAR and satellite images demonstrate geomorphic traces of some very large floods in the past. These traces include:

- The Yampoola Corridor, an approximately 3 km wide zone of flat back floodplain, characterised by aggradation of over-bank mud and often marked by the presence of straight or slightly sinuous erosional floodplain channels such as Three Mile Creek and Yampoola Creek. This corridor is thought to represent a former ancient trench or scroll plain tract of the palaeo-Darling River that is crossed by and therefore pre-dates the Talyawalka Creek and its scroll plain. It truncates dunes

indicating that it is an erosional structure and the lack of dune construction or extension over the corridor since it was formed (more than 30 ka) strongly suggests that it has probably continued to act as a preferential mega-flood corridor.
- A complex pattern of very large depositional bars and intervening scour channels which are present in the northern part of the project area particularly upstream of the lakes where the floodplain is relatively restricted between the north–western valley margin and large areas of within-valley aeolian deposits. The bar and scour channel complex extends down the Yampoola Corridor from the upstream margin of the study area and onto the upstream portion of the Three Mile Creek flood plain.
- Deep scour pools in restricted channels between larger areas of aeolian sediment in the upstream part of the study area, between the Darling and Talyawalka scroll-plain tracts. These features require floods large enough for large-scale ponding in wider flood-plain areas upstream of the restrictions to provide sufficient head for high-energy erosive flows through the restricted channels.

It is possible that these megafloods may have had sufficient erosive capacity to generate a local sand sediment slug which might have initiated a change in stream pattern to a lateral-migration phase until the sediment slug is either worked through the system and/or stabilised in modest scroll plain tracts. An OSL date from a large flood bar on the Three-Mile Creek flood plain, suggests a mid Holocene age for megaflood sand deposition, although the exact age is perhaps equivocal due to incomplete bleaching, or multiple depositional events. This age is close to the initiation of the Darling River lateral migration phase at about 5 ka. This may provide a mechanism for the initiation of the mid to later Holocene Darling River scroll-plain phase.

The second possibility is the LGM local environmental conditions. During the LGM, conditions across Australia were dry and cold with temperatures also depressed by up to 9º C in the low altitude inland parts of central Australia including the Menindee region (Miller *et al.*, 1999) as well as in higher altitude areas. Bowler (1978) and Bowler *et al.* (1978) have examined the likely impact of extreme LGM conditions on channel forms and stream patterns of the Goulburn and Murray Rivers and the Darling River at Tilpa respectively. A number of factors were identified which could have increased discharge and sandy bedload and exacerbated bank instability, potentially altering stream patterns. These included:

- Enhanced seasonal runoff due to reduced evapotranspiration, reduced catchment vegetation and periglacial activity which was highly significant for Goulburn/Murray catchments but may also have influenced the NSW Darling catchment.
- Bank failure due to rapid draw down of water level because of highly peaked seasonal flooding regimes.
- Bank failure due to high regional saline water tables as indicated by widespread active lake deflation and construction of clay-pellet and gypsum rich lunettes over much of the western Murray Basin at the LGM.
- Bank failure due to a lack of channel fringing trees due to a combination of extreme low temperatures and low CO_2 levels. Late Quaternary pollen records from the Lower Darling region are sparse with the only well-dated and studied sequences being from groundwater playa lakes in the dunefields west of the Great Darling Anabranch, south of the study region, which have a depositional gap at the LGM (Cupper, 2005; Cupper *et al.*, 2000; Cupper, 2006). However, the records there show a decline in trees through the glacial towards the LGM and a post-glacial recovery of trees, which mirrors the general trend from records in south-eastern Australia and the Murray Basin (Williams *et al*., 2006; Hesse *et al*., 2004; Hesse *et al.*, 2005; Turney *et al.*, 2006) which consistently show low tree abundance at the LGM.
- Addition of sand to the channel due to dune activity in the region. Bowler (1978) suggests that lack of channel-marginal trees in the Goulburn/Murray system was important for sand blowing from the channels to form source-bordering dunes. In contrast to this, Bowler *et al.* (1978) have suggested that widespread LGM dunefield activity in the western Murray Basin would have resulted in a net contribution of sand to the Darling River channel, a process also assisted by a lack of channel-marginal trees.

– The combination of these factors provides a possible mechanism for changes in the sediment regime of the Lower Darling at the LGM towards a mixed load and the instigation of a stream pattern change to a lateral-accretion phase.

9.3.4 Recharge Implications of Long-term Palaeoclimatic and Palaeoenvironmental Changes

The existence of fresh groundwater targets with no apparent active recharge may be linked to the regional geomorphic history. River leakage is the dominant mechanism of recharge to all aquifers studied in the Lower Darling Valley in the BHMAR Project area. River-leakage recharge is highly likely to be enhanced by change of river pattern to active phases of lateral migration, especially when accompanied by enhanced river discharges. Unlike current fluvial activity with minimal sand deposition, the lower Darling Valley shows clear geomorphic evidence of previous episodic lateral-migration phases represented by at least four successive cross-cutting scroll-plain tracts (Coonambidgal Formation Phases 1-4). The youngest scroll-plain phase, associated with the course of the modern Darling River (Coonambidgal Formation Phase 1), was active in the period 6-2 ka. The previous Talyawalka-Anabranch scroll-plain phase (Coonambidgal Formation Phase 2) has Last Glacial Maximum (LGM) dates around 22-17 ka. Indistinct scroll-plain tracts of the relict Talyawalka-Anabranch system (Coonambidgal Formation Phase 3) have ages around 30-25 ka. Another indistinct relict scroll-plain tract associated with the Darling River (Coonambidgal Formation Phase 4) is as yet poorly defined but probably has ages of 50-45 ka. Even older ages of 85 ka and >150 ka have been obtained from pre-Coonambidgal Formation lateral-migration phases beneath the Menindee Formation floodplain.

The morphology of scroll traces and channel dimensions in the earlier Coonambidgal Formation scroll-plain tracts demonstrate that there have been episodes of river discharge higher than that of the most recent Coonambidgal Phase 1 tract associated with the course of the modern Darling. The episodes of Coonambidgal Formation Phases 1 to 3 suggest lateral-migrational intervals of about 5 ka separated by approximately 10 ka periods of quiescence. The mechanism that controls the onset and termination of lateral-migration phases is uncertain but is probably a combination of changes in river discharge and sediment regimes rather than simple glacial-interglacial climate-cycle forcing.

Enhanced river discharge is likely to include higher mean flows and higher and/or more frequent floods which increase both the hydraulic heads driving river leakage as well as the opportunities for leakage to occur. Additionally, active lateral accretion enhances river leakage by maximising lateral leakage effectiveness through sandier banks and clean, well-sorted active sandy scroll plains with minimal overbank mud drapes or secondary cementation. There would also be good opportunities for connectivity with lower aquifers via contemporary, coarse-sediment bottomed, deeper, scour channels and pools.

From these conclusions, it is expected that the regional groundwater should show evidence, in chemical tracers and age dating, of enhanced recharge pulses coincident with the active lateral-accretion phases at 6-2 ka, 22-17 ka and around 30 ka and perhaps during earlier less well defined fluvial phases. Such a comparison is difficult due to the problems of ascribing accurate ages to groundwater from radiocarbon analyses and the fact that modern recharge continues to occur in many of the groundwater resource targets. However, the Larloona GWR4 target has minimal modern recharge; radiocarbon analyses there vary from 21-28 percent modern carbon, which are equivalent to calendar ages of 10,200 to 12,500 radiocarbon years BP, which calibrate to calendar years of 12–14.8 ka (CalPal, 2007). These ages are not corrected but opportunities are minimal for interaction with old carbon and the ages are most likely to be an underestimation due to contamination by modern carbon. Considering this, the results support the likelihood that the majority of recharge to the Larloona GWR4 resource occurred when the adjacent Talyawalka scroll plain was active at 22-17 ka.

Stable isotope analysis also suggests a palaeo-recharge influence. An overall Darling River Local Evaporation Line (LEL) was defined by the relationship $\delta^2H = 4.86\delta^{18}O - 4.85$. The shallower slope of the Darling River LEL compared to the Local Meteoric Water Line (LMWL; $\delta^2H = 7.9\delta^{18}O + 11$) highlights the significance of evaporation for the Darling River. However the majority of BHMAR groundwater samples plot along a third trend line with a shallow slope ($\delta^2H = 6.5\delta^{18}O - 5.4$) referred to here as the palaeo-trend line (Figure 9-7). It is likely that the observed deviation of groundwater isotopic signature from the Darling River

LEL indicates different climatic conditions at the time of groundwater recharge. In particular, Calivil Formation and Renmark Group groundwater samples are most closely aligned to the palaeo-trend line while groundwater samples obtained from shallower units (Coonambidgal and Menindee Formations and Willotia beds), which are subject to modern recharge, follow more closely the Darling River LEL which is indicative of modern evaporative processes.

Radiocarbon dating also reveals several Calivil Formation (and all Renmark Group) groundwater samples with ages of 5,000 radiocarbon years, which equates to calendar years of 5765 ka (CalPal, 2007), or greater (Figure 9-8). There are also a cluster of Calivil Formation groundwater samples that have radiocarbon ages of less than 5,000 radiocarbon years which are most likely to be an underestimation due to contamination by modern carbon. Although there is a general inverse relationship between radiocarbon age and the distance from the nearest surface water body, there is significant scatter (Figure 9-9). This is because there are groundwater samples from the deeper Renmark Group and Paleozoic aquifers that are relatively close to the river (or lake) but are relatively old indicating limited influence of modern recharge. The variability in the Calivil Formation groundwater suggests that geological heterogeneity, such as the presence or absence of the upper confining aquitard, also influences modern recharge. This is discussed in more detail in Section 8.

Evidence of a strong palaeo-recharge influence on groundwater resources within the semi-confined (Calivil Formation) aquifer has significant implications for future groundwater development. Modern day recharge processes, believed to be driven predominantly by the flooding regime, are much less than would have been experienced during the identified three 5 ka long river channel migration phases. Consequently there is risk that any future groundwater development would essentially be extracting the groundwater resources far more rapidly than could be naturally recharged.

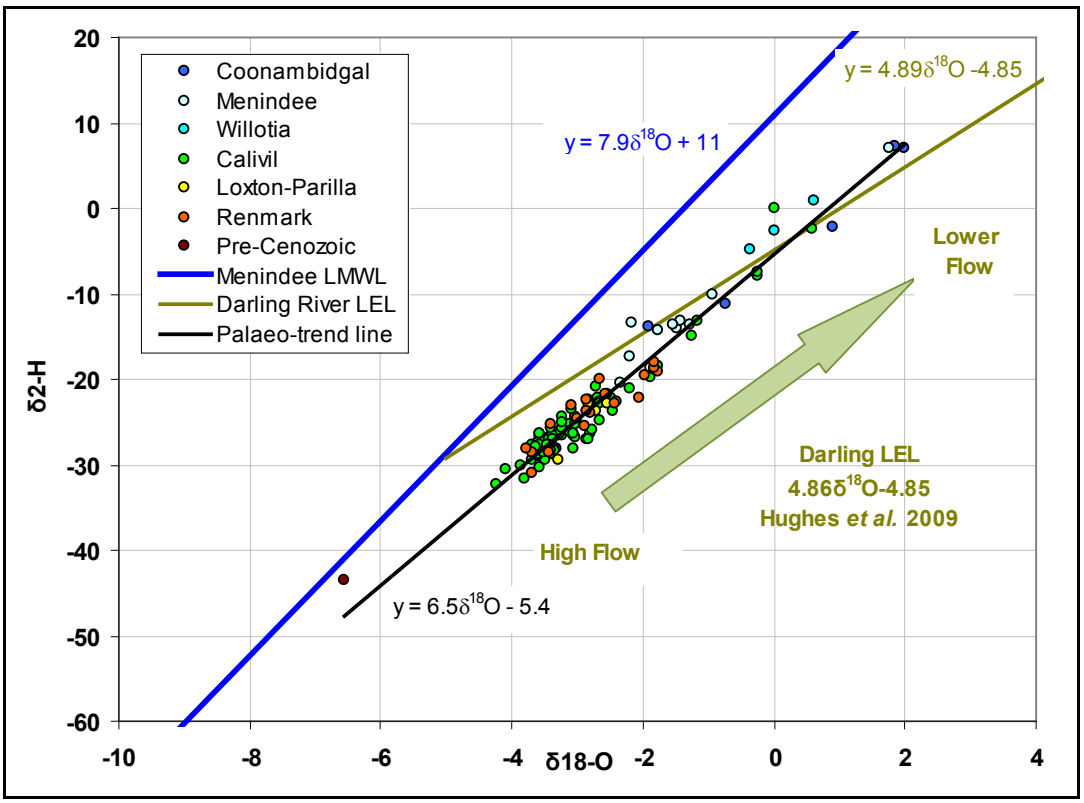

Figure 9-7. *Stable isotope plot of oxygen-18 ($\delta^{18}O$) and deuterium ($\delta^{2}H$) for BHMAR groundwater samples. Note the variation in slope of the palaeo-trend line generated from all groundwater sample data, compared with the Darling River LEL.*

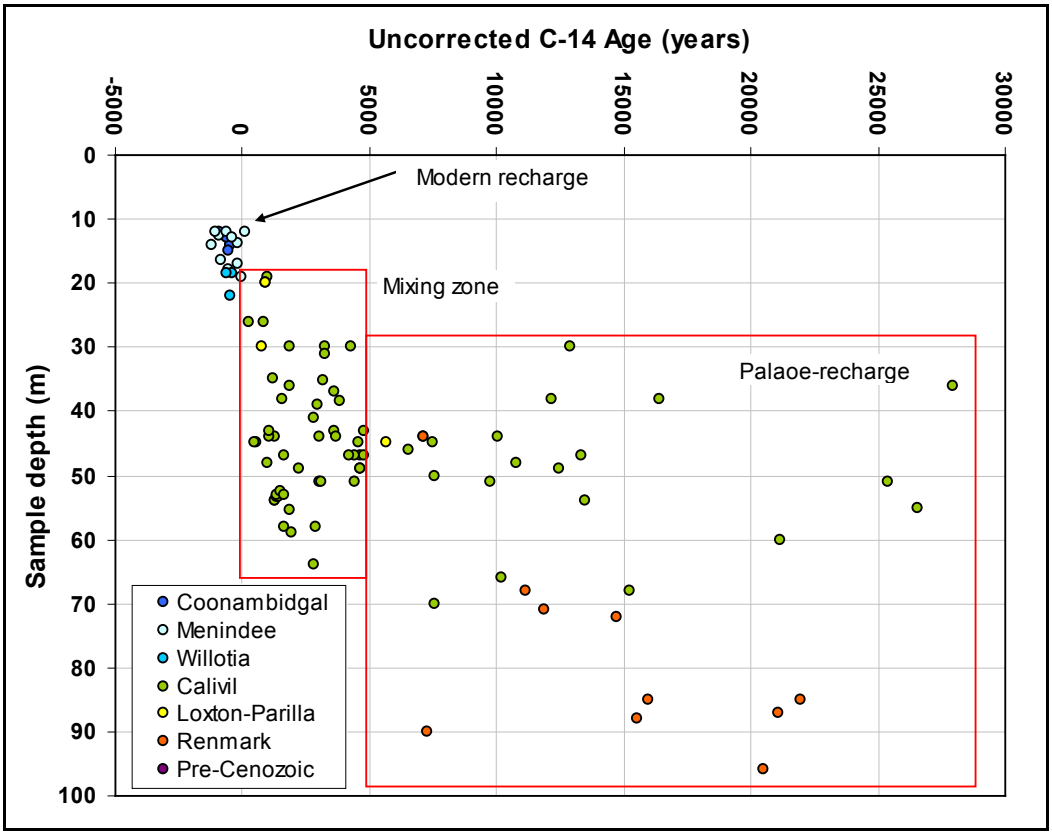

Figure 9-8. *Radiocarbon (^{14}C) ages of BHMAR groundwater samples plotted against sample depth and differentiated by formation. Three data clusters are indicated: predominantly palaeo-recharge, a mixing zone; and predominantly modern recharge.*

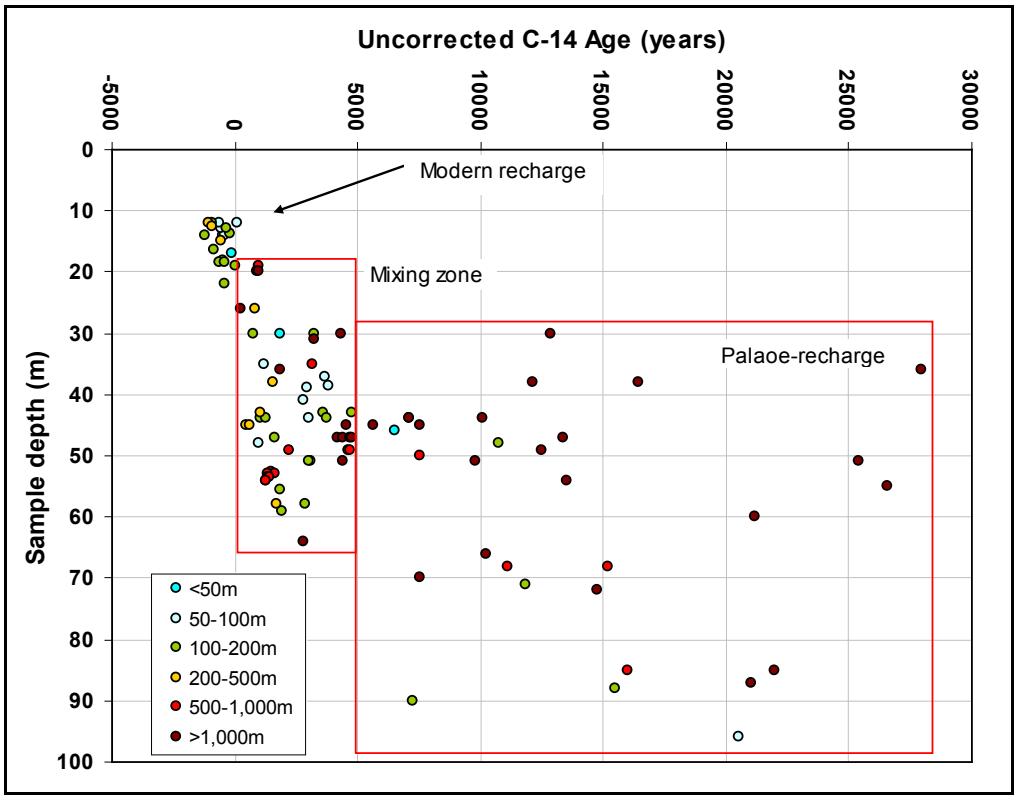

Figure 9-9. *Radiocarbon (^{14}C) ages of BHMAR groundwater samples plotted against sample depth and differentiated by distance to the nearest surface water body.*

9.4 CONCEPTUAL HYDROGEOLOGICAL MODEL

The importance of river (and lake) leakage in recharging the shallow unconfined aquifers and Calivil Formation target aquifer is inferred from different lines of evidence, including:

- Interpolation of groundwater salinities based on a relationship between the AEM and pore fluid chemistry showed freshening near the river and in particular leakage sites associated with the Menindee Lakes.
- Watertable contours interpreted for the shallow aquifer show significant mounding near the Darling River and the MLS. The interpreted groundwater levels for the underlying Calivil Formation aquifer have a broadly similar pattern suggesting the influence of river leakage, most notably in the GWR1 target area. The dominant hydraulic gradient near the river is downwards, reflecting greater opportunity for river leakage (rather than groundwater discharge to the river).
- The majority of shallow groundwater samples near the river has a chemistry dominated by sodium, calcium, magnesium and bicarbonate, which is similar to the Darling River samples. In contrast, local rainfall samples are more enriched in calcium and potassium, suggesting that recharge from rainfall is not as important as river (or lake) leakage. A mixing trend is evident between the surface waters and shallow groundwater samples, and the more saline and evolved Calivil Formation and Renmark Group regional groundwater samples.
- Stable isotopes of water (oxygen-18 and deuterium) in river, lake, rainfall and groundwater samples show that the Darling River recharges the aquifers. The fresh Calivil Formation groundwater has a stable isotope signature similar to Darling River samples collected during high flows. This would support recharge into the Calivil Formation being linked to high flow events, rather than continual river leakage. The tight clustering of the Calivil Formation stable isotope samples suggests that recharge is relatively rapid. The contrast in the isotopic signature of the fresh Calivil Formation groundwater and that of the shallow groundwater, suggests that Calivil Formation recharge occurs near-river, rather than via infiltration through the shallow aquifer in the floodplain.
- The fresh near-river shallow groundwater typically has a modern carbon signature, further supporting river leakage under current climatic conditions as being the dominant recharge process. There is a decrease in the proportion of modern carbon as the Calivil Formation groundwater progressively become more saline and less influenced by modern recharge.
- Data from monitoring bores screened in the Quaternary, Calivil Formation and Renmark Group aquifers show rises in groundwater levels associated with high flow events in the Darling River. Overbank flow is not necessary for such recharge to occur. The continuation of rising trends in the Calivil Formation monitoring bores after the flood peak recedes suggests that this is an actual recharge response rather than hydraulic loading. Simple Darcian vertical infiltration cannot explain the rapid response. Faulting and vertical structural offsets of formations near the river could result in pathways for such by-pass flow.
- Hydraulic conductivity of the upper confining aquitard is very low, and while pore fluid within the aquitard can be quite fresh, this can be explained by diffusion processes. Consequently, leakage through the upper confining aquitard is believed to be minimal unless enhanced from faulting.

A diverse range of conceptual models to explain recharge to the alluvial aquifers of the Darling River floodplain were developed over the duration of the project. Apps *et al*. (2012f) summarises these conceptual models as a series of schematic cross sections, portraying potential infiltration pathways to the target Calivil Formation aquifer. These include the scenarios of:

- Depressions ('cod holes') in the river of sufficient depth to have eroded through the Blanchetown Clay to enable direct hydraulic connection between the river and the Calivil Formation. However, sediment sampling during the in-river survey indicated that these river depressions are bedded within the aquitard. This is also supported by hydrostratigraphic cross sections developed for key near-river sites such as Jimargil (Lawrie *et al*., 2012c).
- Infiltration in the floodplain following flood inundation, preferentially via sandy sequences such as palaeo-dune sequences in the near-river Coonambidgal Formation. However, hydrographic responses in both the Quaternary and Pliocene aquifers near the river suggest that overbank flooding

is not a requisite for recharge. The stable isotope signature for the fresh Calivil Formation groundwaters shows limited effects of evaporation, which would be likely with infiltration from standing water bodies in the floodplain.

- Rainfall accessions on the floodplain, via preferential pathways such as dune sand sequences and palaeochannels deposits. Interpretation of hydrochemistry and hydrographic data in particular concludes that diffuse recharge by rainfall is limited in the study area, and this is supported by previous recharge investigations in the region (Cook & Walker, 1989; Kennett-Smith *et al*., 1991).

Figure 9-10 summarises the conceptual model showing the configuration of aquifers and aquitards and the recharge dynamics associated with the Darling River. During low flow conditions (Figure 9-10a) there is no recharge because a mud veneer (up to 20 cm thick) and mineral precipitates in and along the river banks act as an effective seal. Laboratory infiltration tests of river bank materials confirm the very low permeability of these mud veneers (Page *et al*., 2010). Under no-flow conditions, the deep holes in the river bed, which are surprisingly devoid of significant debris, can be windows to the watertable (within the shallow unconfined aquifers), and act as critical drought refuges for the aquatic ecosystem.

During high-flow conditions (Figure 9-10b), the river banks and bed are scoured and the mud veneer seal is removed, revealing accretion surfaces within the Menindee and Coonambidgal Formation scroll plain sediments. In places, there is also significant erosion of the river banks, with apparent preferential erosion of the Coonambidgal Formation, which contains less cementation than the Menindee Formation on the river banks. This allows recharge to occur predominantly by lateral bank recharge through the sandy sequences in the shallow aquifer as well as bypass flow via faults. The river channel does not appear to be in direct connection with the semi-confined aquifer. The high river stage level facilitates lateral and downward leakage. Overbank flow is not a pre-requisite for recharge but can provide other localised recharge pathways in the floodplain, particularly where the floodplain overbank mud drape is absent or thin. Structural features and gaps in the upper confining aquitard confining layer provide flow paths to the semi-confined aquifer.

During flood recession, there may be some drain-back from bank storage in the unconfined aquifers encouraging carbonate precipitation. Comparison of bank and drillhole materials also reveals that the degree of cementation in the Menindee Formation sediments increases significantly in a narrow zone near the river banks. The mud veneer also re-deposits with declining river stage and flow velocities. Over time, the system returns to relatively low-flow conditions with the channel mud veneer again constraining river leakage. The overall conclusion from our investigations is that recharge to the semi-confined aquifer is mainly due to river leakage associated with high flow events (such as major flooding) of the Darling River.

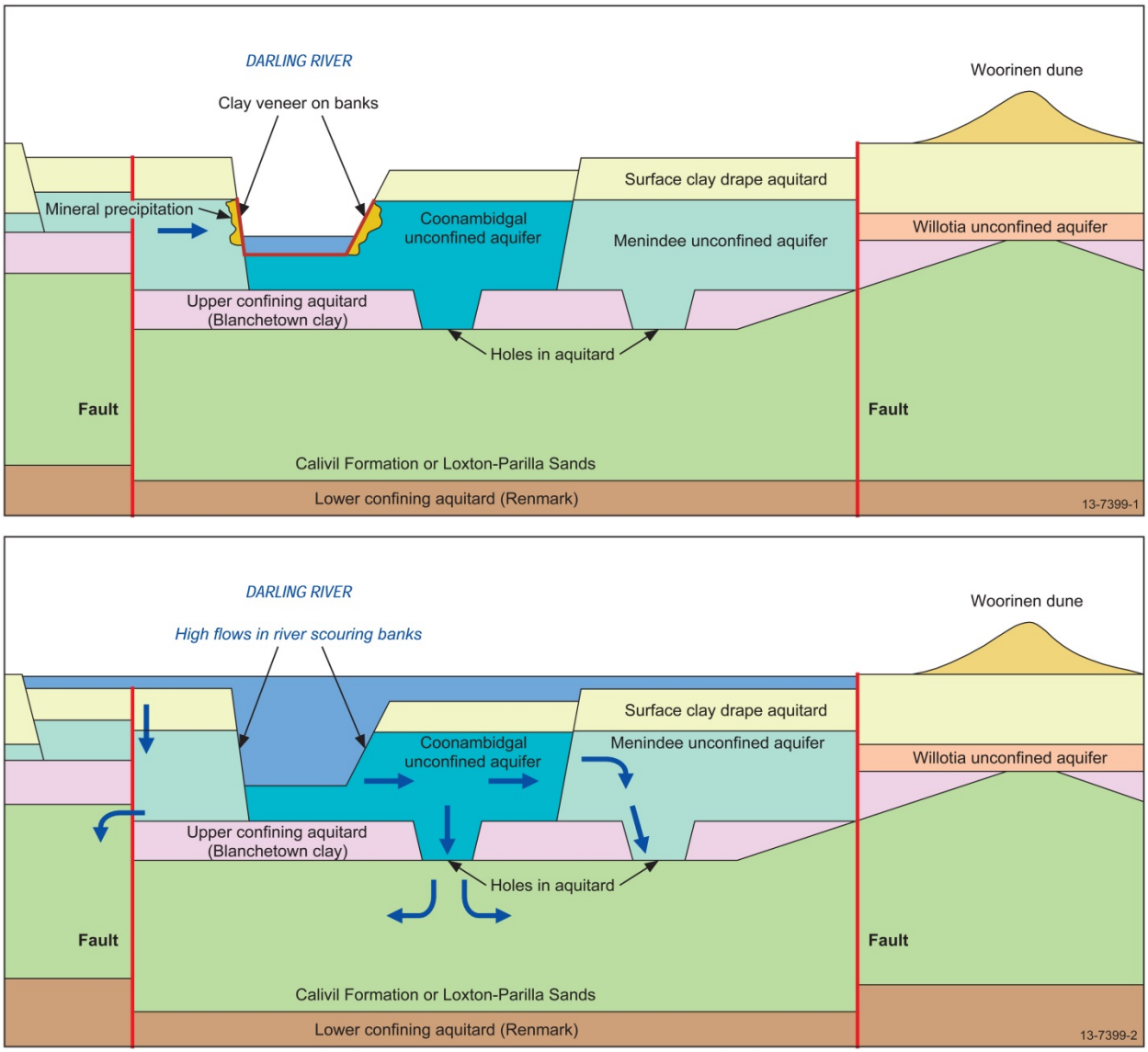

Figure 9-10. *Conceptual model for groundwater recharge in the Darling Floodplain alluvial sediments (A) during low to average flow conditions and (B) during high flow conditions.*

9.4.1 Recharge Impedance During Low-flow Conditions

Hydrographic and hydrochemical data in particular suggest relatively rapid recharge of both the shallow and semi-confined aquifers during high river flows but not during low-flow conditions. The most likely interface for direct hydraulic connection between the river and the shallow unconfined aquifer during floods is the bank and bed of the Darling River. Two potential mechanisms are proposed which impede recharge of the near-surface unconfined aquifer sands by lateral bank infiltration during low-flow conditions. These are mantling of the bank by mud-rich impervious drapes, and impregnation of the bank sediments by secondary carbonate precipitation.

These two mechanisms occur differently in the landscape and have different implications for lateral recharge by bank infiltration. The mud-rich bank mantles are almost ubiquitous over all banks irrespective of which Quaternary fluvial unit comprises the bank and they can clearly be eroded and removed under flow conditions above certain flood levels. The carbonate cementation of banks develops progressively and becomes a more effective infiltration barrier with age; it is poorly developed in the Coonambidgal Formation banks and well developed in older Menindee Formation banks. It is not eroded or reduced in effectiveness as a bank infiltration barrier by flood flow. These two barriers are discussed in detail below.

The project area had experienced a decade-long period without overbank flows prior to October 2010. During this period of low river levels, the river banks of all stratigraphic units were covered by a mantle of slope deposits. One sample was taken of the bank cover (Figure 9-11) and XRD analysis showed that it was clay-rich (Page *et al.*, 2010). These clay-rich slope deposits were formed by transferral of floodplain material down slope through a combination of sheet wash (indicated by rills), animal movement (indicated by trails), and gravity creep (inferred). The deposits were at least 20-30 cm thick, as shown by sample pits (Figure 9-12). The mantle, like the surface mud drape across the scroll and floodplains of the region, is dark in colour (Figure 9-13). This figure also shows how the basal channel sands are in the process of being masked by muds during low water periods.

Strandlines formed by plant debris with minor erosional notches were cut in this mud-rich mantle by higher flow levels, but the mantle was not removed. This is evident in Figure 9-14, which is a view across the river to the west bank in Kinchega National Park where a similar dark muddy slope deposit occurs. Also visible are strand marks of recent high water levels, composed of organic and other debris, the higher water levels have left the dark slope deposits unaffected.

The decline of river level after March 2011 enabled a number of examples of bank erosion to be documented. This showed that a hydraulic threshold was crossed when the bank was topped by floodwaters, resulting in removal of the bank-mantling muddy material. Figure 9-15 shows pre-flood and post-flood photographs of the same stretch of river bank between Jimargil and East Bootingee (just downstream from BHMAR 84-4), with evidence of Coonambidgal Formation bank cleaning having taken place during the flood event. Noteworthy in these photos is the evenness with which the mantling material has been removed.

Elsewhere the removal of the mud mantle was more uneven. Figure 9-16 shows how bank collapse during the flood has exposed the architecture of the underlying scroll bar sediments elsewhere only barely visible through the surface mantle.

The process of re-covering the bank begins almost immediately after the end of the flood. This is shown in Figure 9-17. This photograph shows how the dark surface clay deposits are already beginning to be transported down slope, only a few weeks after the end of the flood.



Figure 9-11. *Location of surface sample site (arrowed) on Menindee Common. Drilled boreholes are in red and site was described in Page et al. (2010). Google Earth Image.*



Figure 9-12. *Menindee Common sample collection point, looking southwest. Photo by CSIRO.*



Figure 9-13. *Muddy slope mantle covering river bank, looking north. Also note muddy nature of exposed river bed sediments at waters edge. Photo by CSIRO.*



Figure 9-14. *View northwest across the Darling River showing dark muddy slope deposits of opposite bank un-eroded by high river levels that did not top the bank. Photo by CSIRO.*



Figure 9-15. *(Top) Pre-flood photograph showing only gross details of bank stratigraphy visible because of obscuring surface materials, even on steep bank. (Bottom) Post flood photograph showing much cleaner bank surface and numerous details including lateral accretion surfaces.*

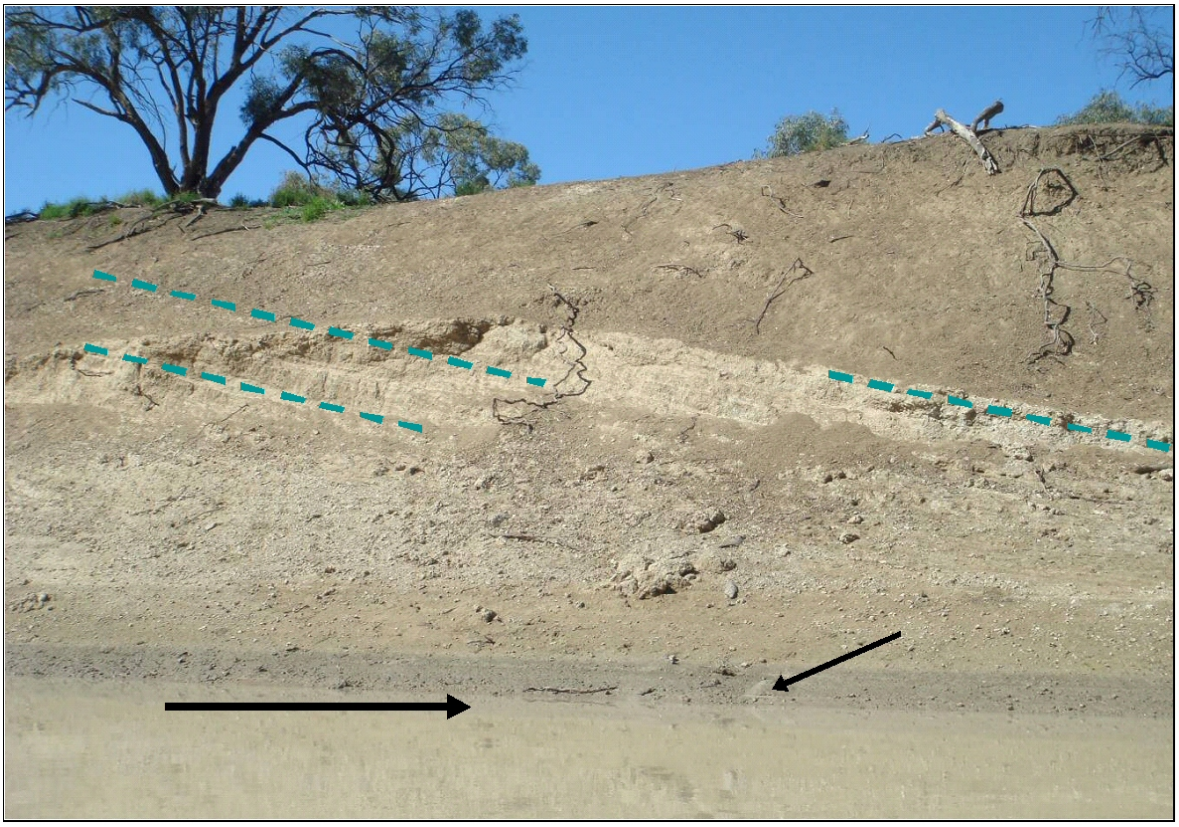

Figure 9-16. *East bank of the Darling River, downstream of East Bootingee showing variable but strong erosion following the October 2010-March 211 flood. (photo KP Tan)*



Figure 9-17. *East bank of the Darling River, downstream of East Bootingee, showing early stages of down slope transport of muddy surface material (photo KP Tan).*

Secondary carbonate cementation of Darling River banks in the Menindee Formation has been documented and photographed just downstream of Jimargil Homestead, but not quantified by detailed section logging or laboratory analysis.

The stream level in the Darling River at Jimargil is about 10-12 m below the Menindee Formation floodplain level when a regulated flow of about 200 ML/day over Weir 32 is maintained. The natural low-flow regime was almost certainly no higher than this regulated level. The Menindee Formation lateral-accretion sand shallow aquifer extends from about 5-6 m depth to 15 m in the river bank (Figure 9-18) and BHMAR 77-5 and BHMAR 77-2, which are respectively located 20 and 90 m from the river bank at this site.

The aquifer sands where they are exposed in the river bank are strongly cemented by secondary carbonate. The carbonate cementation preserves cross-bedding and other primary structures in the fluvial sands as well as rhizomorphs and results in significant reduction in pore space and permeability (Figure 9-18 and Figure 9-19). Above the lateral accretion sands, secondary soil carbonate nodules are present in the Menindee Formation overbank muds. It is probable that the carbonate cementation has resulted from lateral movement of bank storage towards the river following the flood peak, with evaporation and carbonate deposition at the river bank surface. This process is likely to happen after flood levels have temporarily raised the watertable in the shallow aquifer and reversal of flow direction occurs when the river rapidly drops to low levels. Meteoric water percolating vertically, and then discharging at the river bank, may also contribute to the carbonate precipitation process and extend it higher in the bank profile. The net result of this process is that infiltration into the shallow aquifer through Menindee Formation river banks is significantly impeded.



Figure 9-18. *Menindee Formation overbank muds overlying carbonate-cemented lateral-accretion sands exposed in the Darling River bank downstream of Jimargil Homestead.*



Figure 9-19. *Closer view of carbonate-cemented sands of Figure 9-18, showing rhizomorphs and preservation of cross bedding.*

At both the BHMAR 77-5 and BHMAR 77-2 drill sites no significant secondary carbonate occurs in the Menindee Formation shallow aquifer sands. BHMAR 77-5 (20 m from the river bank) is a mud-rotary hole with minimal sedimentological detail but only minor carbonate is reported in the field log, consistent with sparse small secondary soil carbonate nodules. BHMAR 77-2 (90 m from the river bank) is a sonic-cored hole with some nodular soil carbonate recorded in the overbank muds as well as minor carbonate cementation of thin fine sand bands in the upper mud facies. However, the upper lateral accretion sands of the unsaturated zone (Figure 9-20), equivalent to the massively cemented riverbank sands shown in Figure 9-18 and Figure 9-19, contain no secondary carbonate.



Figure 9-20. *Menindee Formation lateral accretion sands from 7.5 to 10 m depth in BHMAR 77-2 showing a paucity of secondary carbonate cementation.*

It is proposed that the process of bank sealing by mud-rich mantles during low water periods and seal removal during floods provides a plausible mechanism of lateral recharge by bank infiltration, which explains the data from hydrographs, water chemistry, and age dating:

- During normal flow periods clay-rich deposits build up on the river bank and form a surface barrier to the near-surface aquifer fluvial sands. This hydraulically isolates the river from the sandy shallow aquifers in the bank and potential transfer pathways beneath the river bed. High, but not overbank river flows are not able to effectively erode these barriers, resulting in continued isolation of both the shallow aquifer and the semi-confined aquifer from the Darling River during these conditions.
- During floods the river bed sediments are entrained by the rapid water flow. The turbulent sandy flow erodes the muddy mantle from the bank. As a result, river water is able to enter the shallow aquifers by bank infiltration under 8-10 m of hydrostatic head and then to the main Semi-confined aquifer through various pathways through the upper confining aquitard. This leads to the observed rapid hydrograph response.
- When the flood ends and the river returns to its normal low level, the bank mantle begins to re-establish itself and the sandy base is again clogged by mud. This leads to a return to the hydrological separation of the aquifers from the Darling River.
- Near surface aquifer fluvial sand banks of the older Quaternary units, Menindee Formation and Willotia beds, often have significant secondary carbonate cementation which is not eroded by any level of flood flow. Lateral recharge by bank infiltration of these elements of the near-surface aquifer is still seriously impeded even when flood flow is sufficient to remove the sealing mud mantle.

Evidence for similar processes has been reported from other studies. Brunke & Gosner (1997) reviewed exchange processes between rivers and groundwater. They found that clogging, termed as colmation, occurred during normal and low river flows, and that the clogging material was removed when the sediment was re-entrained during floods. A more detailed study of this process was made of river bed clogging along the Rhine River (Schubert 2002) and showed that only thin films of sediment are necessary for clogging to be effective. This is similar to the process envisaged for the mantling and clogging of the Darling River banks.

Major scours occur along the Cooper Creek in inland Australia (Knighton & Nanson 2000), which support semi-permanent water holes filled by fresh water. These are, however isolated from the regional saline aquifer by a water hole lining of clay-rich sediments that have settled out of suspension. Only during floods is this lining removed. During these brief events, however, significant freshwater recharge occurs from the river into the shallow aquifer (Cendón *et al.,* 2010). This illustrates how post-flood clogging can, in the Australian context, occur rapidly, isolating river water from aquifers.

In a study of Fowlers Creek, an ephemeral stream in arid inland Australia just north of Broken Hill, Dunkerley (2008) showed that high concentrations of suspended fine-grained sediments were transported during floods and deposited as mud drapes on the bed, banks and floodplain. Measurements of infiltration rates showed that these were lowest at the base of the banks and increased with elevation on the bank. This study shows that bank clogging by even thin veneers of muddy sediment can have a significant influence on infiltration. It is noted however that the process there differs somewhat from the one proposed for the Darling River, in that it occurs from sediment laden waters during the post peak flood stage, rather than sub-aerially.

Bank seals leading to reduced infiltration are also mentioned briefly by Sear *et al.* (1999) and Sophocleous (2002).

9.4.2 Field Observations During Flooding

The 2010-11 flood event for the Darling River provided the opportunity to observe near-river inundation of the floodplain. Observations during the flood were made at an inactive meander bend in the Darling River located on Menindee Common. Just upstream of the junction with Talyawalka Creek, the scroll-plain near the bend is composed of Coonambidgal Formation and was accreted against a terrace of Menindee Formation which stands approximately 2 m higher than the scroll-plain. The surface has well developed scroll bars and swales developed by the lateral accretion of the Coonambidgal Formation during migration of the river bend prior to the current stabilisation of the channel (Woodyer 1978). These are not well expressed in aerial photography (Figure 9-21) but are most visible in the LiDAR digital elevation model (Figure 9-22) and in profile (Figure 9-23) and are also very visible at ground level (Figure 9-24). The terrace surface is inundated only by the highest floods (Figure 9-21). The lowest part of the scroll-plain is adjacent to the terrace. Prior to the flood, extensive networks of surface cracks and pits formed by the collapse of subsurface pipes (known in Australia as "crab holes") were present. Crab-hole diameter ranged 1-10 cm, and cracks were typically 1-5 cm across. The polygonal blocks between cracks were about 0.5 cm-1 m across. These features were usually in the lowest part of the swales and, where measured by wire probes, the cavities extended to depths of 0.7 m beneath the surface.

The subsurface stratigraphy of the Coonambidgal Formation beneath the scroll-plain is based at the BHMAR79A site and is comprised of 8-10 m of upward-fining medium to fine silty sandy mud, the top 5-6 m of which was composed of smectite-rich silty mud. No sedimentary structures, other than crude normal grading, were observed in the fine-grained sediments in either sonic drill core or pit exposures. Large scale exposures of the Coonambidgal Formation in river banks show the presence of lateral accretion surfaces consistent with formation by scroll bars left behind by migrating meandering channels.

The scroll-plain is covered by a woodland of large River Red Gums (*Eucalyptus camaldulensis*), and black box (*Eucalyptus largiflorens*), with a partial ground cover of Lignum (*Muehlenbeckia florulenta*), saltbush (*Atriplex sp*.) and ephemerals. The terrace vegetation consists of a Lignum shrubland with common Chenopods and scattered black box (Moore 2005). Trees tend to be more common on the bars than in the swales (Figure 9-24).



Figure 9-21. *Oblique aerial photographs of study area taken on March 18 2011 from an altitude of ~300 m, at roughly peak flood. A - looking north. B – looking east. The numbers in each refer to the same features. 1 – Darling River. 2 – Scroll-plain of Coonambidgal Formation flooded to depth of ~2.5 m. 3 – Higher terrace flooded to depth of <0.5 m. 4 – point at which flood first crossed the meander. 5 – Location of sonic bore 79A-6.*

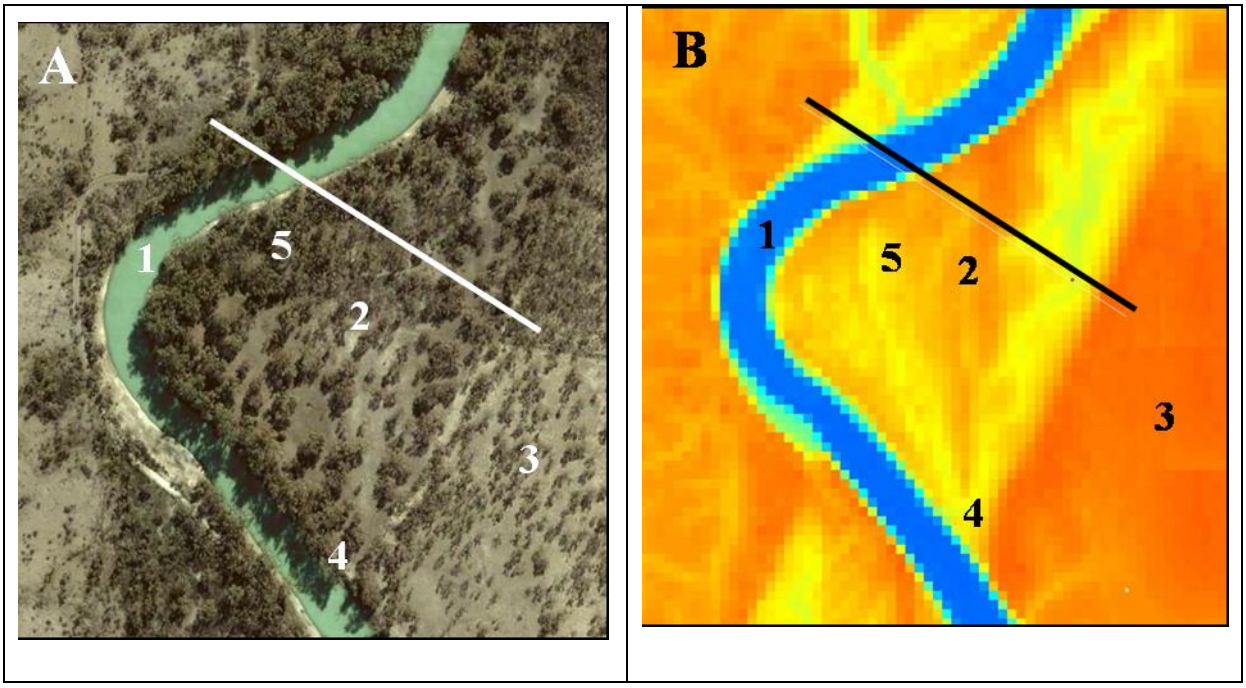

***Figure 9-22**. Images of area of flood observations A – Google Earth. B - LiDAR DEM with 5 m resolution. Line marks position of profile shown in Figure 9-23 and is 679 m long. North is at top of image, river flow is north to south. The numbers correspond to the same features as in Figure 9-21.*

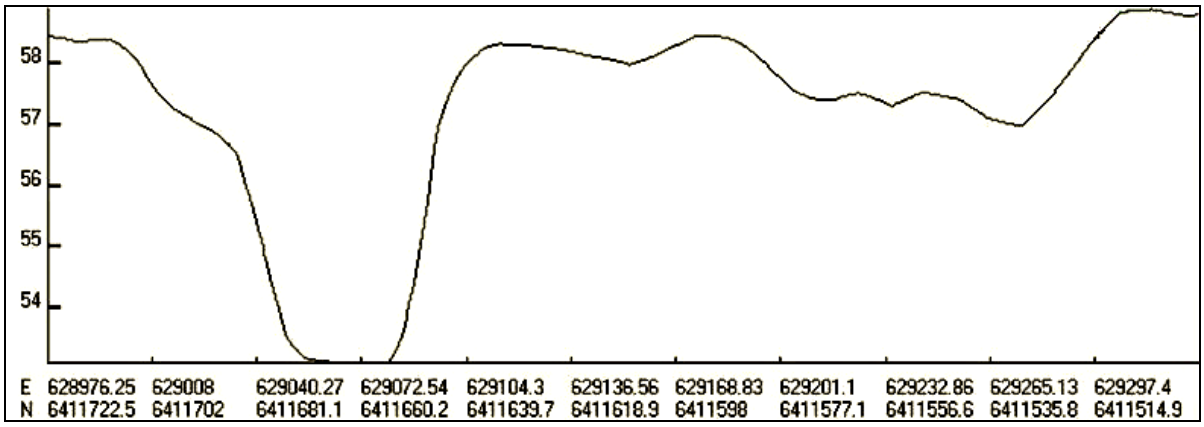

***Figure 9-23.** Topographic profile across flood observation site based on line in Figure 9-22. Line is 679 m long, coordinates are in Australian Map Grid, elevations are in metres above AHD. 1 – Darling River. 2 – Meander of Coonambidgal Formation. 3 – Older Menindee Formation terrace.*

9.4.2.1 Immediate Effects of Inundation

The rate of water rise was slow over the initial two-day period of observation in late October 2010, because of the controlled nature of the water release from the MLS, in preparation for the flood peak. At the site, water spilled over the scroll-plain from the south beginning at the lowest swale and flooded northwards (Figure 9-25A), branching out and flooding successive swales either progressively or by spilling across low points (Figure 9-25B). During the period of observation, the water level rose to a depth of ~1 m in the lowest point of the scroll-plain. The flow front was initially marked by fingers of water flow laden with plant debris (Figure 9-25C). These flowed into cracks and crab holes in the silty clay surface (Figure 9-25D). Flow was diverted into these cavities until they were filled, whereupon water spilled out and continued to flow across the surface until the next cavity was encountered. Gas bubble trains from submerged cavities still containing air were common behind the flow front (Figure 9-25E).

Water also flowed in the subsurface along cracks, causing collapse of surface material as the silty clays were slaked. As it flowed into the larger cavities, the water eroded rills into the substrate next to the hole (Figure 9-25F). The larger cavities would take up to five minutes to fill and subsurface water flow extended up to 3 m in advance of the surface flow front. Sudden collapse of the surface into water-filled cavities was

commonplace (Figure 9-27A). However, adjacent cavities less than a metre apart remained dry if they were not interconnected (Figure 9-27B).

As the flow advanced it became more turbulent, especially where it spilled over high points (Figure 9-27C), resulting in the formation of small bars and sediment ripples in small streams (Figure 9-27D). The ripples and bars were of coarse silt to very fine sand composed of quartz grains and clay pellets. The orientation of these ripple trains is determined by local microtopography and bears no relationship to larger scale gradients. The examples illustrated are orientated 180° away from the overall stream gradient. Only when the distal reaches of the swale had been flooded did the streams expand and become tranquil as the flood continued to rise (Figure 9-27E).

Small pieces of vegetation were remobilised by the advancing floodwaters, and woody debris do appear to define former flood levels (Figure 9-27F). However, most larger woody debris were not buoyant due to termite activity and large scale redistribution of plant debris appears to have been minor, at least during this flood event.

Where the flood waters were tranquil a soil wetting front up to two metres from the actual edge of flooding was established, with the distance depending on slope. This was apparently due to a capillary fringe above the perched water table even as the flood level was rising.

Water flow continued to increase following the initial inundation, peaking at 37 GL/day in March 2011. At this flow rate the entire scroll-plain at the bend was submerged to a depth of 1-2.5 m, with the shallowest parts on the high scrolls nearest the river (Figure 9-27F) and the deepest in the swale against the edge of the terrace. The flood inundated the terrace to a depth of no more than 0.5 m. During peak flow water spilled across the scroll-plain in a direction roughly parallel to the orientation of the channel belt, locally forming ripples near the bank. These later ripple trains are more reliable overall stream flow indicators than those formed earlier.

The water was highly turbid with suspended clays. Deposition of these clays is inferred to have occurred subsequent to peak flood levels. As noted, fine bed load sand and/or silt was deposited in ripples trains and small bars on the scroll-plain by traction currents. Limited scour after the flood waters subsided was observed to have occurred round trees close to the river bank.

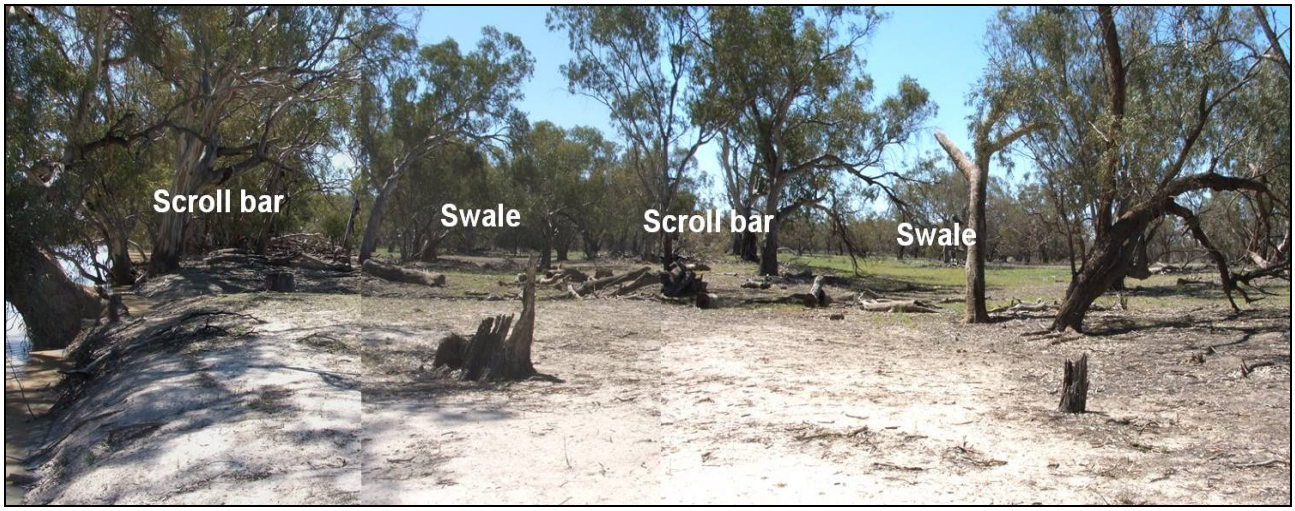

Figure 9-24. *Pre-flood view from point 4 in Figure 9-21 and Figure 9-22 looking NNW in direction of flooding and showing scroll bars and swales.*



***Figure 9-25**. Flood processes on October 2010. A – First ingress of water from the river along swale (arrowed). B – First trickle of water (~40 cm wide) across scroll from flooded swale into adjacent swale. C – Turbulent cross-country flow front ~20 cm wide. D – Flooded crack (i) and subsurface water in crack (ii) in advance of flow. Note dark wetted fringe to (i). Car keys for scale. E – Bubble train (arrowed), bubbles ~5 mm wide. F - Water going down pipe ~15 cm across and eroding small rill (arrowed) in the process.*

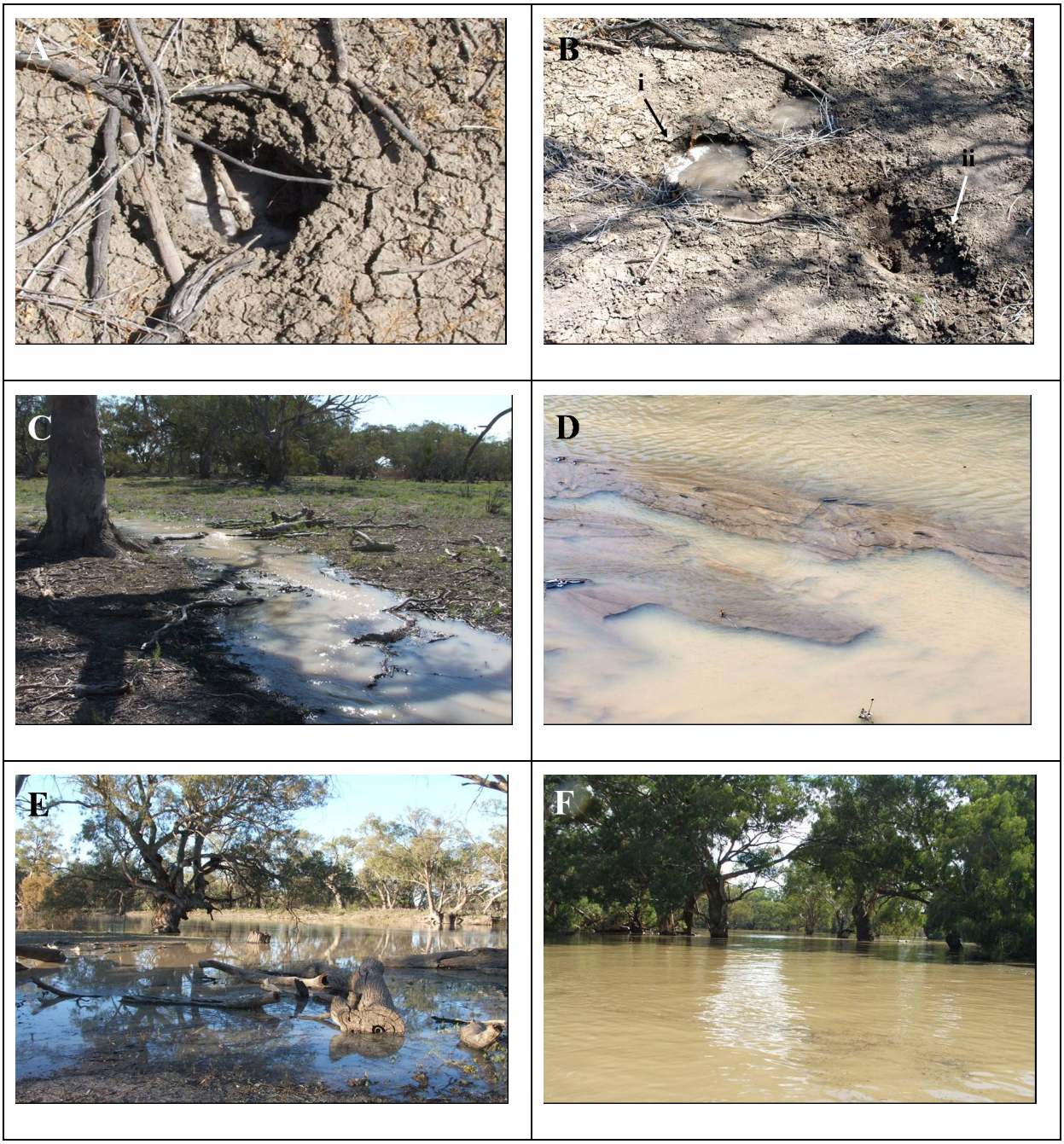

Figure 9-26. *Flood processes on October 2010 (continued). A - Collapsed pipe containing water ~30 cm below surface, pipe diameter ~20 cm. B - Adjacent collapsed pipes <1 m apart, (i) is flooded) and (ii) is dry. C- High energy stream flowing across high point where two swales join. D – Small bars and ripples formed from very fine sand to coarse silt. E – Woody debris transported by floods. F – View from river of flooded bank, water is 1.5 m deep under trees and deepening to 2.5 m in distance. Located at point 1 in Figure 9-21 and Figure 9-22.*

9.4.2.2 Post Flood Observations

The area was revisited in September 2011, six months after the flood peak. The most immediate impression was of the luxuriant vegetation growth, in particular the new growth on the eucalypts and a thick growth of clover and other ephemerals, as much as 60 cm high, across much of the scroll-plain (Figure 9-28A). Only areas that had recently dried out were still bare of vegetation. A waterline was clearly visible on trees, indicating maximum flood height (Figure 9-28B). The more flexible vegetation, in particular Lignum and grasses, was still bent by the flood flow (Figure 9-28C), which was almost at right angles to the river bank. Larger woody debris was not displaced by the flood because of the lack of buoyancy of the material. This can be seen by the unchanged position of large woody debris in Figure 9-28D when compared with the pre-flood positions in Figure 9-27A. Former areas of turbulent flow were now coated by clay-rich deposits (compare Figure 9-28E with Figure 9-28C). In several places gullies had formed on the river bank, or previous gullies had been enlarged (Figure 9-27F) by flood water draining back into the river as the water levels fell. Evidence elsewhere in the region indicates that these gullies are initiated by the collapse of piping formed by shallow subterranean flow in the clay-rich scroll-plain surface sediments.

In many places floodwaters were trapped in closed depressions after the river level fell below the level of the bank. Standing water remained in many of these depressions, formed by scroll bar swales and abandoned channels, because of the impermeable clay-rich surface seal (Figure 9-28). Clays settling out of or flocculating from suspension buried any sedimentary structures formed by the initial flooding. This is illustrated by Figure 9-28B, where smooth clay deposits had buried the ripples evident in Figure 9-26D. Water appears to be being lost from these isolated depressions purely through evaporation. As the water level gradually falls, the deposited clays are exposed as they dry out they first form shallow polygonal networks (Figure 9-28C), with the cracks penetrating no more than 5 cm into the ground, and then a crumpled surface of clay aggregates through further shrinkage of the clays (Figure 9-28D). There was no sign at this time of the formation of the larger and deeper cracking systems evident on the preflood surface. These are postulated to form through desiccation of the deeper subsoil rather than the surface layers.

Three bores inundated by the October 2010-April 2011 floods were logged by nuclear magnetic resonance (NMR). These were BHMAR 79A-6 at the Menindee Common, where the inundation observations were made, BHMAR 80A-2 and BHMAR 80B-2 in East Bootingee, and BHMAR 99-1 at Jimargil. These holes were logged in October 2011, some six months after river flow fell below the bank full level of 17 GL/day. Ponded floodwaters would have remained at some of these sites for long periods, especially at BHMAR 79A-2 and BHMAR 99-1(Stuart Oates, pers. comm.). Table 9-10 provides a summary of the NMR logging in the vadose zone of these boreholes. The NMR free and bound water profiles is plotted with other downhole data in Appendix 1 (Halas *et al.*, 2012).

Table 9-10. *Distribution of NMR free and bound water in vadose zone of inundated floodplain areas.*

Borehole	Depth to watertable (m)	NMR starting depth (m)	Free water distribution	Bound water distribution
BHMAR79-6	5	1.0	No free water above saturated zone	General decrease in bound water content down to water table
BHMAR80B-2	8	0.5	Increase in free water from 6 m	General decrease in bound water content down to water table
BHMAR99-1	9	2.0	General decrease in free water down to water table	No bound water above water table

The following observations can be made:

- Either no bound water (BHMAR 99-1) or downward decreasing bound water (BHMAR 79A-6 and BHMAR 80B-2) above the water table. This indicates that there has been either no or every limited downward percolation of floodwaters through the near surface aquitards at these bore sites.
- No free water within 5-6 m of surface for BHMAR 79A-6 and BHMAR 80B2 and downward decreasing free water in BHMAR 99-1. This indicates either no (BHMAR 79A-6 and BHMAR 80B-2) or limited (BHMAR 99-1) percolation of floodwaters through the near surface aquitards at these sites. The case of BMHAR 99-1 is noteworthy as it was located in an abandoned channel of the Darling River and water persisted here until a few weeks before NMR logging commenced (Stuart Oates, pers. comm.).

The NMR logging provides evidence that vertical infiltration in inundated areas of the floodplain plays a limited role in the recharge of the shallow aquifer, certainly in the areas of observation.

9.4.2.3 Discussion and Conclusions Based on Flood Observations

The observations of sedimentary and geomorphic processes and deposits recorded at this site give rise to a number of questions regarding their broader significance to flood-related processes along the Darling River and more generally in the Murray-Darling Basin. These include:

- What role does mineralogy, specifically the abundance of smectites and sodic soils play in micromorphology of depositional surfaces during wetting and drying, and in the development of subsurface flow?
- How does flow direction change through the course of the flooding?
- What is the relative balance between vertical flow beneath the scroll-plain and lateral flow from the bed and banks of the river play in recharging the unconfined shallow alluvial aquifer?
- What is the relative importance of surface and subsurface flow in the wetting of the scroll-plain?
- How significant is lateral transport of sediment by subsurface flow?
- What are the implications for fluvial accretion and architecture of scroll-plain sediments?

Gingele and DeDeckker (2008) showed that the clays of the Darling River system contain almost three times as much smectite as do clays in the Murray River. Odeh and Onus (2008) showed that the soils of the region were highly sodic. Taken together, these observations predict that shrink-swell and dispersive behaviour would be important processes on the areas subject to flooding along the Darling River. This prediction is confirmed by the observations of deep cracking during prolonged droughts, shallow cracking and fragmentation of clay-rich surfaces following inundation, and the formation and collapse of subsurface pipes and surface collapse features through dispersal of sodic clays. Based on these observations, it is predicted that such processes will be more prevalent on the areas subject to flooding along the Darling River than along the Murray River. This is consistent with observations along the Murray (Clarke *et al*., 2009), where surface cracking, development of piping, and dispersal of clays is far less common.

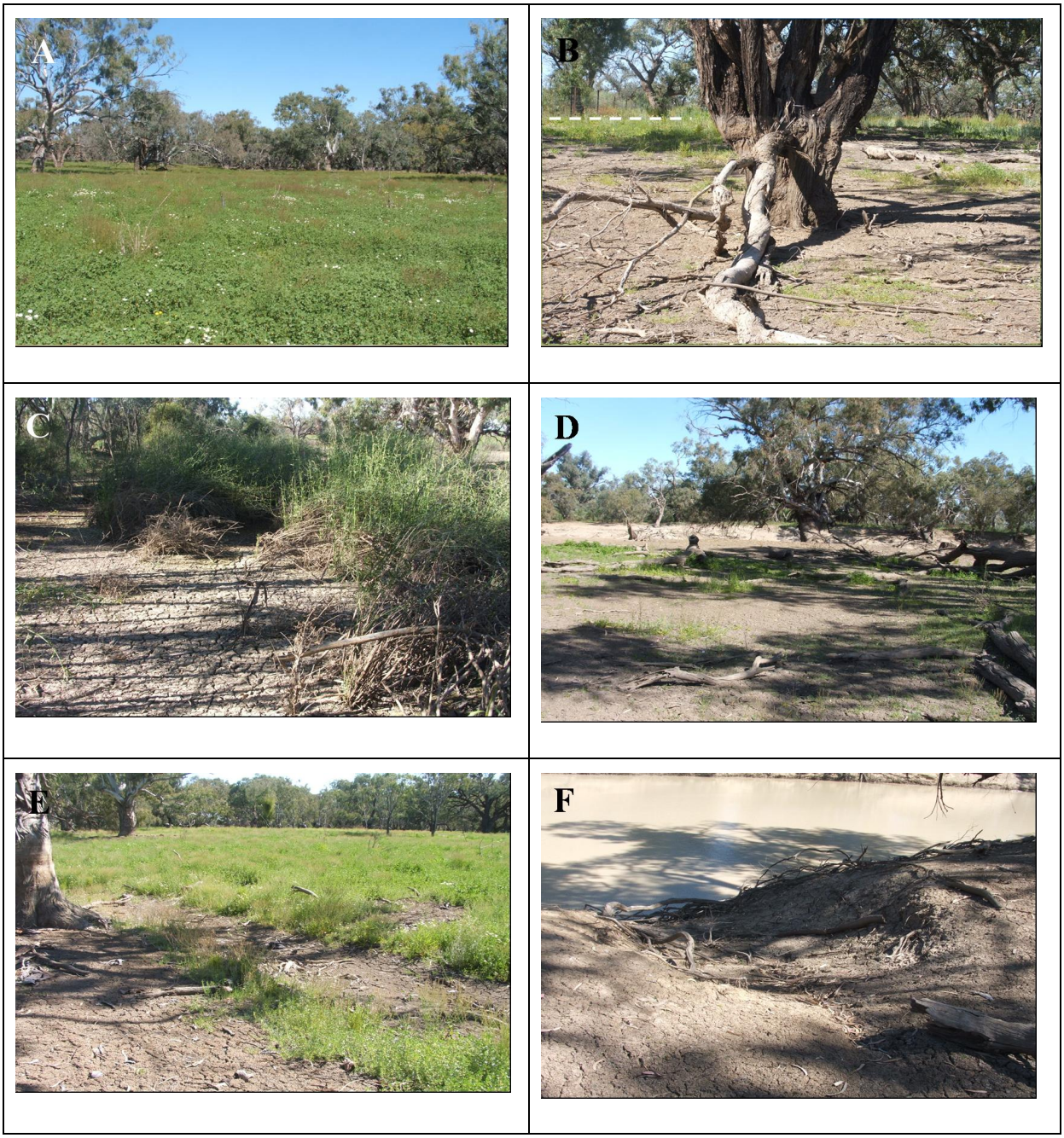

Figure 9-27. *Post flood photographs on September 2011. A - Lush ephemeral growth on floodplain post inundation, September 2011. B -Waterline on trees. Dashed line indicates height of water, note equivalence to the height of older terrace visible behind. C - Lignum on floodplain bent over by water flow from channel across floodplain (left to right). Note regrowth of Lignum in vertical orientation. D - Almost same view as Figure 9-25A, note absence of flood redistribution of woody debris. E – Almost same view as 11C, note post-flood growth of ephemeral vegetation and clay lining of former channel. F – Gully on bank enlarged by flow-back into river during waning stages of flood.*

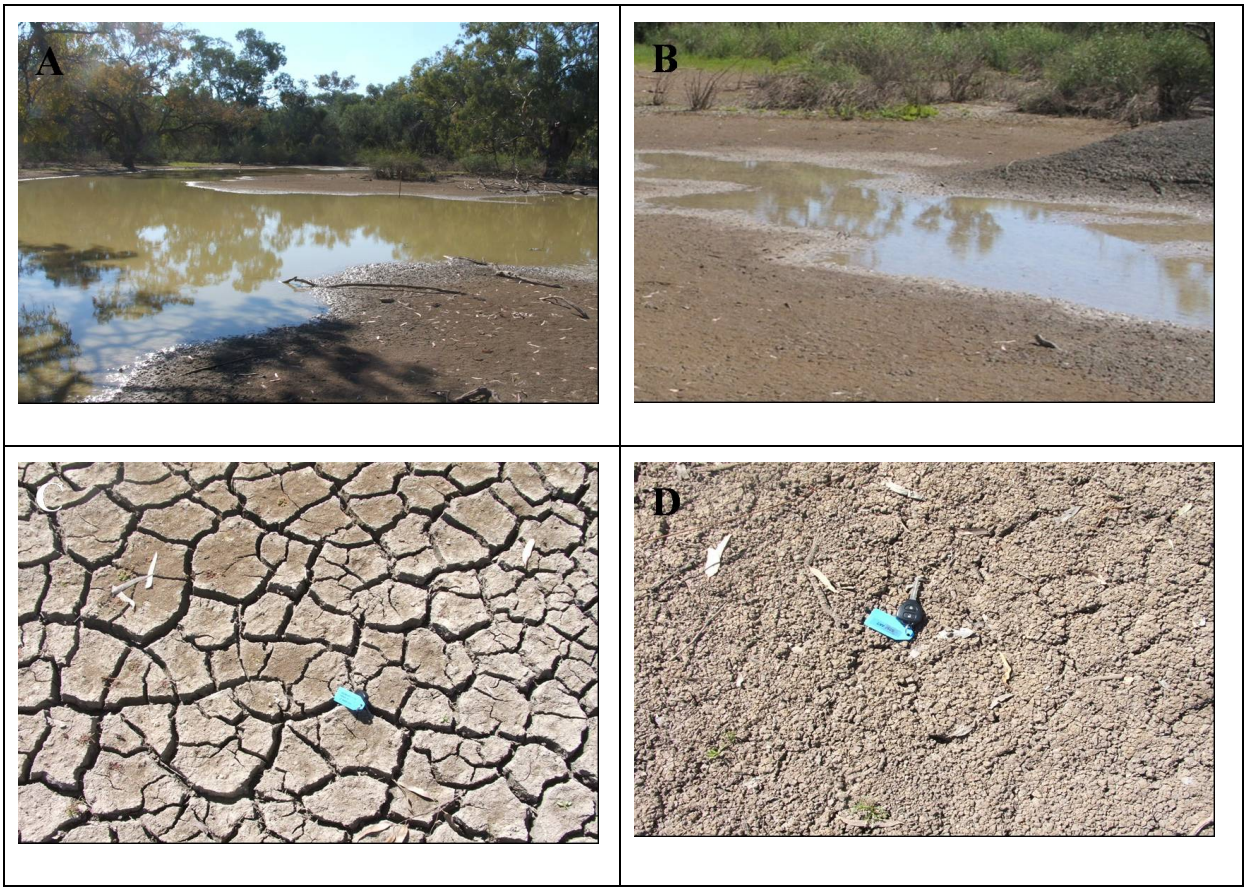

***Figure 9-28**. Post flood photographs on September 201 (continued). A – Residual flood waters still ponding in swales six months after flood recession. B - Absence of sandy bedforms in area of former flow despite their presence earlier (same general area as Figure 9-25D). C – Clay cracking of floodplain surface with evaporation of flood waters (car keys for scale). D – Crumbling of clay surface into pellets (car keys for scale).*

Initial flow directions are controlled by microrelief and can, in extreme cases, be opposite to that of the overall river. Flow directions internal to the cracks and pipes are completely independent of that of the surface. Surface flow orientation becomes parallel with the overall channel once the flood has completely topped the bank. During the waning stages of the flood flows become once again controlled by microtopography and ceased once connection to the river was lost.

The presence of relatively deep cracks and pipes in the smectite-rich profile raises the possibility that floodwaters could rapidly recharge shallow aquifers on the scroll-plain during the initial stages of a flood by bypassing the otherwise impermeable surface materials. This certainly appears to be the case in the floodplain of the Ord River in northern Western Australia (Lawrie *et al.,* 2010c). However, along the Darling River, at least at Menindee, this appears to be unlikely, given the disparity between the cracking and piping depth (~70 cm) and the thickness of the fine-grained, clay-rich surface materials (4-5 m) that makes up the near-surface aquitard. Recharge of the shallow aquifers is therefore most likely by lateral flow from the river banks.

Conversely within the uppermost metre of the fine-grained sediments on the scroll-plain, the deep cracks and piping would appear to play a significant role in wetting. This would be through greatly increasing the available surface area for wetting and allowing rapid penetration of the surface by flood waters as flooding commences. The fine-grained surface materials would therefore wet up much more rapidly than would otherwise be the case through top-down percolation of a wetting front alone. This rapid wetting would further impede access of surface water to the shallow alluvial aquifer sands at the base of the scroll-plain succession as the smectitic and sodic clays swell and disperse respectively, filling in cracks and pipes.

The extensive subsurface flow in pipes and cracks was an unexpected aspect of the flooding process, as was the degree to which the flow extended in front of the flood front. This process raises the possibility of

significant subsurface sediment transport, or lessivage (Young & Young, 2001), within the system of pipes and cracks. While well known on slopes, lessivage is less well documented on floodplains. In principle, such subsurface flow and transport might create subsurface sedimentary structures and deposits with limited laterally continuity and which might be subject to deformation and truncation with further development of cross-cutting piping and collapse. Studies of smectite-rich floodplain successions should be aware of this possibility when interpreting detailed structures and stratigraphy.

Extrapolation of these results to what might be seen in the geological record suggests that while sedimentary structures such as ripples may readily form on smectite-rich flood deposits under the appropriate flow regime, their preservation potential is poor. This is because of a range of processes operating at a range of scales including reworking of surface layers through self-mulching (Young & Young, 2001), deep cracking, dispersal on wetting, loss of identity of sand and silt sized clay aggregates on wetting and drying (as has been well documented for clay dunes and lunettes, Price 1963), piping, and collapse. These processes explain the absence of structures in fine-grained deposits at the millimetre to decimetre scales in cores through the Coonambidgal and Menindee Formations. Similar loss of primary sedimentary structures was observed in Coopers Creek (Nanson *et al.,* 1986)

Even where preserved, such ripple trains may be problematic guides to depositional conditions. Those that form earliest may have orientations significantly different to the overall stream gradient, and some may have formed in the subsurface. Mineralogically similar deposits in the geologic record, such as the bentonitic flood plain deposits of the Jurassic Brushy Basin Member of the Morrison Formation (Demko *et al.,* 2004; Kjemperud *et al*., 2008) show a similar absence of fine structure in flood deposits.

In summary, the geomorphic and sedimentary observations from this site indicate that initial flooding occurred by laminar flow and, during the earliest stages of flooding, infiltration along cracks may be as important as overland flow. These characteristics lead to the development of wetting fronts beyond the immediate extent of surface flow and local surface collapse into cracks and pipes.

Flow then became turbulent and stream-like as flooding progressed, with deposition of rippled silts and fine quartz and clay-pellet sands. Cracks and pipes are inferred to have collapsed by this stage. There was extensive reworking of small dead vegetation across the flooded area, but larger woody material was not reworked.

With expansion of the flooded area and deepening of the flood waters, flow became tranquil and suspended-load mud deposition took place. The extremely soft and waterlogged surface of the scroll-plain meant that direct observations of the depositional surface was impossible for some months after floodwater recession.

Large areas remained inundated after the flood receded as water became trapped in clay-lined depressions. It is inferred that water was lost from these areas only through evaporation as the underlying clay minimised infiltration. Recharge to shallow scroll-plain alluvial aquifers is inferred to have occurred by lateral flow from the river banks, not vertically from flood waters.

As the surface dried it was broken up through cracking at all scales. Detailed structures were lost through this self-mulching process. Deep cracks did not develop as the subsoil was still moist. The larger cracks probably developed during prolonged dry periods. Piping may develop during heavy rainfall events on deeply cracked surfaces.

The dynamic nature of the Darling River flood deposits, including self-mulching, deep cracking, piping, and dispersion, is a result of the sodium-rich soil chemistry and the smectite-dominated clay mineralogy. These features and processes lead to the obliteration of fine-to medium-scale sedimentary structures in the flood deposits of the scroll-plain observed in cores in the area and similar deposits in the geologic record.

Even where preserved, great caution must be exercised in the use of floodplain ripple orientations as palaeoflow indicators. This is especially the case for those deposited in the earliest phases of the flood where local microtopography has a stronger influence on flow than regional gradient. The possibility also exists for rippled sediments to form by lessivage through pipes. Such internal sedimentary structures may be differentiated from those formed on the surface by their much more limited lateral extent (perhaps decimetres, compared to tens to hundreds of metres).

9.4.3 Direct Connectivity Between River Channel and Semi-Confined Aquifer

In-river survey data identified a number of 'cod holes' in the river bed at bends in the river where scouring is likely to be at a maximum (Figure 9-29). These 'holes' are up to 6 m in depth below the thalweg of the river. This is a potentially important observation, as the river bed is already ~9 m below the floodplain surface, and depths of ~15 m below the current floodplain surface may result in direct connectivity between the river channel and the semi-confined (Calivil Formation) aquifer. Consequently, these 'cod holes' may be point recharge, which supports anecdotal evidence from local landholders who report these holes never dry up (e.g. Figure 9-30), and when floodwaters do come down the Darling, the river can be 'held up' for quite a few hours while floodwaters 'disappear' into these holes.

Further analysis was carried out to assess whether these holes were actually incised into the Blanchetown Clay, and hence allowing direct recharge. Elevation (m AHD) data from the in-river survey was compared with the elevation of the top of the upper confining aquitard (Figure 9-31). At no point does the river appear to have incised into the upper confining aquitard. At its deepest point, the river channel is still 2.8 m above the top of the aquitard and in some areas can be as great as 26.8 m above the aquitard. It is worth noting that only a very short stretch of river was surveyed and connection may exist elsewhere, however the presence of a large, fresh, groundwater resource at this location is not the product of direct recharge from the river straight into the Calivil Formation.

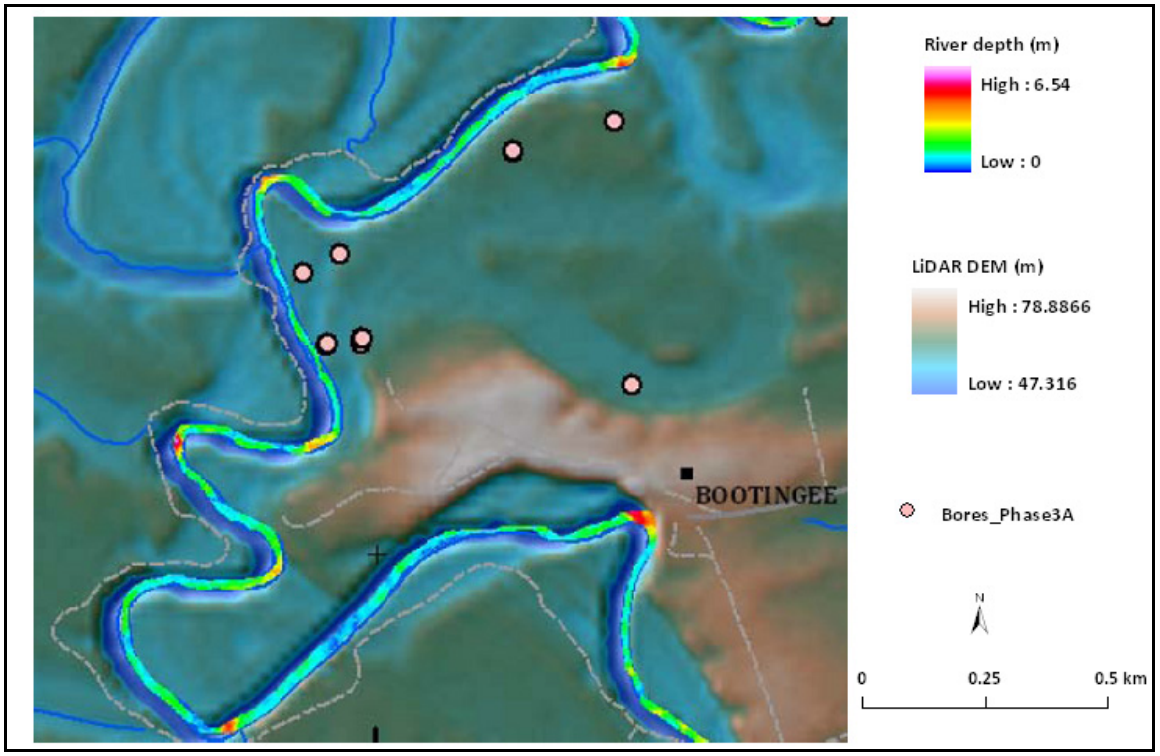

Figure 9-29. *In-river survey single beam echo sounder data draped over the LiDAR dataset. The red areas are 'holes' in the river bed up to 6 m below the river bed surface.*

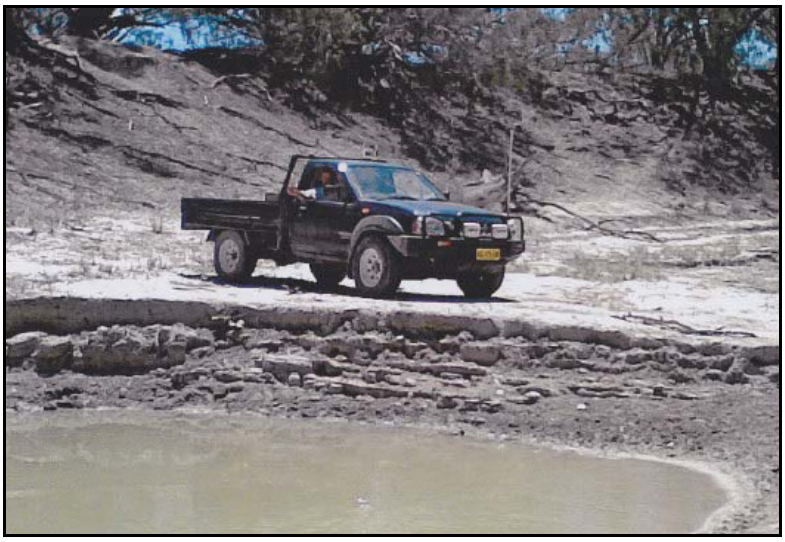

Figure 9-30. *Photograph of the Darling River bed in drought. The pool in the foreground is a perennial waterhole. The vehicle is resting on a calcrete layer in the middle of the river. Photograph courtesy of Stewart Oates, Jimargil.*

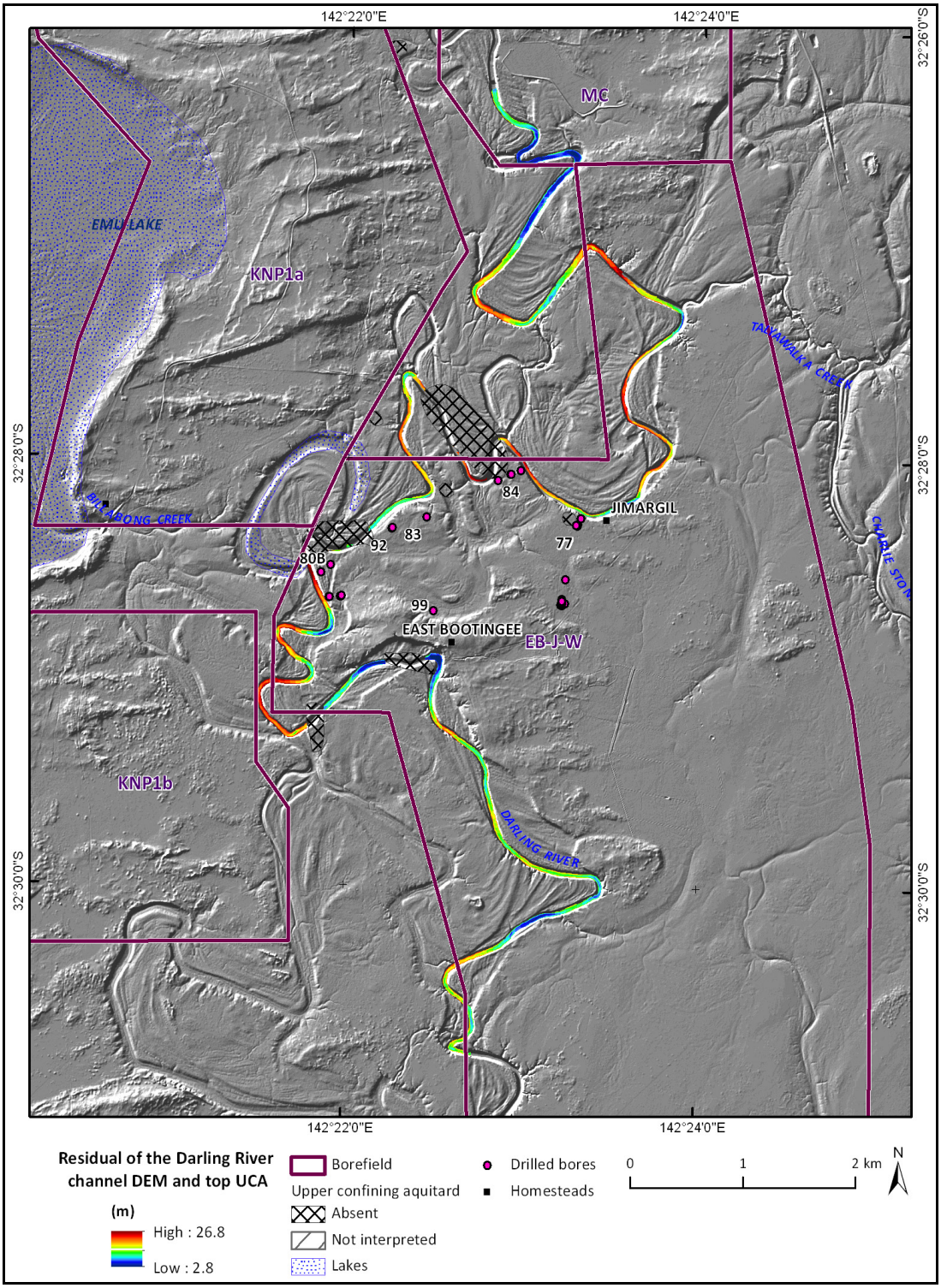

Figure 9-31. *Comparison between river channel elevation and top of upper confining aquitard (UCA). River channel elevation data was obtained from in-river survey data. At no point within the defined area is the river channel in direct contact with the UCA (i.e. 0 m) let alone the semi-confined aquifer.*

9.4.4 Recharge Potential of GWR Targets

The recharge potential for each target was assessed using a matrix approach (Lawrie *et al*., 2012a) to combine contributing factors (Figure 9-32) based on the hydrogeological conceptual model. Some groundwater resource targets are located away from modern drainage and the influence of river or lake leakage. This would suggest that such targets are largely relict resources with no obvious source of active recharge. Initially, the presence of potential surface source water and recharge pathways was assessed for each target. If either was absent, then modern recharge was inferred to be limited. GWR4 is an example of this as it lacks connectivity with surface water features and has no apparent leakage mechanism to the semi-confined aquifer. Other factors were also assessed in the matrix approach, including watertable response to flooding, leakiness of the upper confining aquitard and groundwater age dating. For example, the assessment of GWR4 was further supported by relatively old apparent radiocarbon ages for groundwater from monitoring bores in the target. Targets GWR11, 12 and 13 are also inferred to be palaeo-resources (Figure 9-32) however drilling and groundwater analysis is required to confirm this assessment. Insufficient data exists to make a determination about GWR10.

GWR9 and GWR14 are located along Talyawalka Creek and have identified recharge pathways through lateral bank recharge and vertical leakage via holes in the upper confining aquitard. Modern carbon within the Calivil Formation aquifer in these targets confirms that active recharge occurs to a degree. However, two factors limit the volume and frequency of recharge. Firstly, flows in Talyawalka Creek are limited to large flood events which occur infrequently. Secondly, the watertable is at considerable depth (>20 m) and the incision of the Talyawalka channel is relatively shallow (~ 5-6 m). Therefore, river leakage must infiltrate through a thick unsaturated zone before recharge to the watertable can occur. Slow recharge rates are confirmed by the lack of short-term response (12 month period) of the watertable to the 2010/11 flood event. These targets have been classified as possible modern recharge but at very slow rates (Figure 9-32).

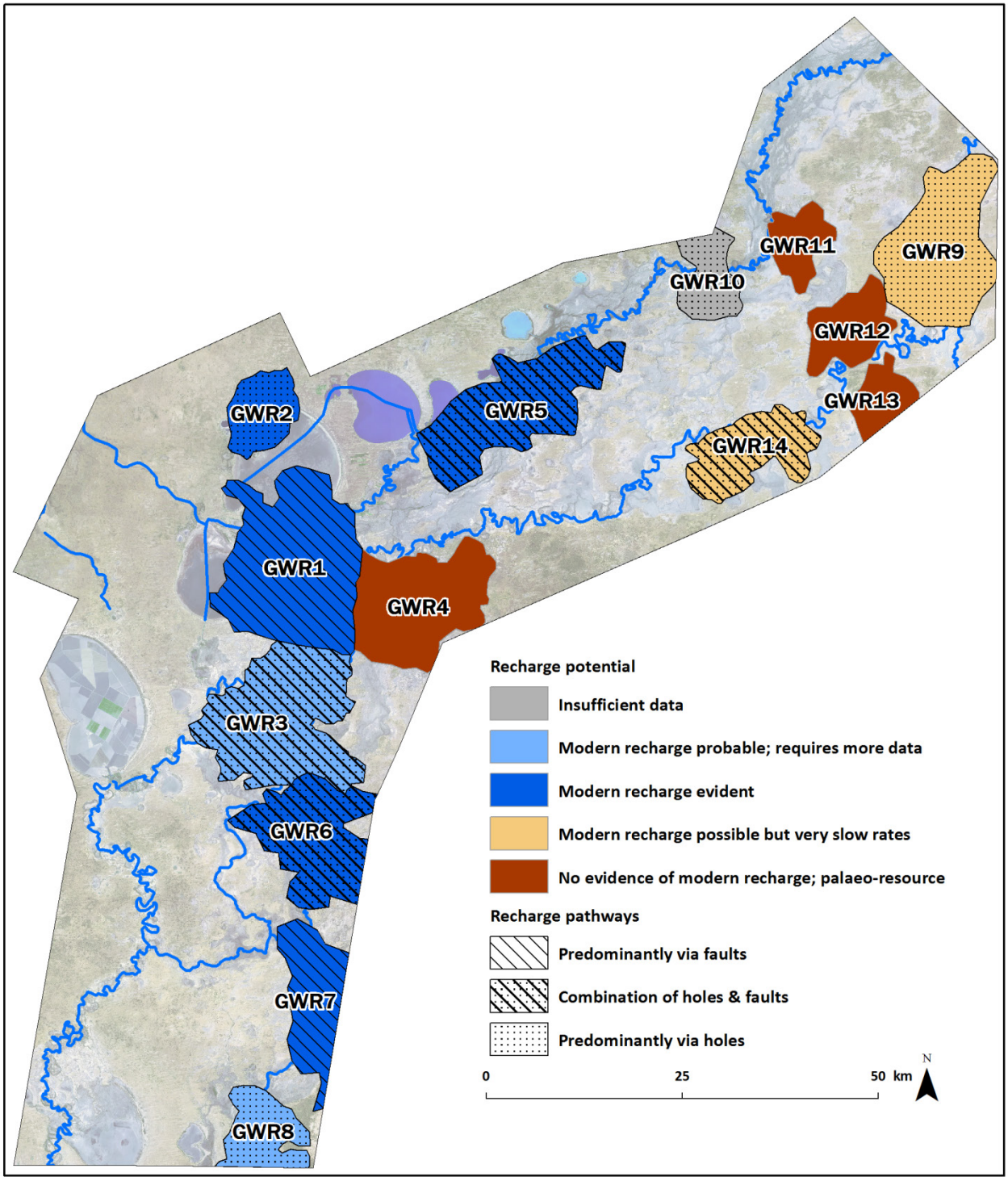

Figure 9-32. *Predictive assessment of modern recharge potential and dominant recharge pathways.*

10. Vegetation Assessment

10.1 INTRODUCTION

10.1.1 Why is it Important to Investigate the Health of Vegetation in this Area?

The Broken Hill Managed Aquifer Recharge (MAR) Project was tasked to assess whether a sustainable groundwater resource extraction approach, including MAR was a feasible option for securing Broken Hill's water supply in times of drought, instead of using surface water stored in the Menindee Lakes.

In Managed Aquifer Recharge (MAR) a water source, such as natural water from a lake or river, is used to recharge an aquifer with water under controlled conditions (Dillon *et al*., 2005; Dillon *et al*., 2009). The aquifer is used to store surplus water for later use or for environmental benefit. MAR targets are typically confined aquifers; this minimises shallow watertable fluctuations (beyond that which occurs naturally) that can have detrimental impacts on vegetation such as waterlogging, dewatering, salinisation, and acidification.

In comparison to MAR, groundwater extraction is the withdrawal of already existing groundwater resources. If the groundwater resource receives suitable recharge volumes to balance extraction, it is deemed to be sustainable. Alternatively, if more water is being extracted than what is being replaced by recharge, the groundwater resource is being 'mined'. Similar to MAR, groundwater extraction targets are typically confined aquifers, minimising lowering of the watertable and associated risks.

Consequently the two most important considerations for potential MAR and groundwater resource targets from an environmental/vegetation point of view are 1) whether vegetation is using groundwater and 2) what is the groundwater–surface water connectivity at that site? The vegetation analysis discussed later in this section provides a spatial distribution of vegetation exploiting groundwater. Coupled with temporal observations, some conclusions about the timing of groundwater use in a water availability context can also be made. Groundwater connectivity can also be qualitatively assessed using thickness and extent of the confining aquitard, hydrographic and hydrochemical data.

Under NSW legislation, any changes to the management of the lakes must consider environmental, social and economic issues. The health and condition of iconic native Australian riparian and floodplain vegetation is consequently an important consideration. Due to regulation, vegetation as it currently exists is, in reality no longer native and in a sense is managed, hence it is necessary to consider what vegetation was like prior to regulation, what the current state of vegetation is and how vegetation condition responds to different water regimes.

10.1.2 Why Use Remote Sensing Over Field Studies?

Ideally a thorough investigation of vegetation dynamics would involve detailed plot-scale vegetation surveys, visual assessment techniques (crown size, crown density, epicormic growth and dead-branch frequency; e.g. Eldridge *et al*., 1993; MDBC, 2003; Doody & Overton, 2009) and ecophysiological studies (e.g. Doody *et al*., 2009). However, due to the time constraints inherent in this project, this was not possible. Instead a GIS/remote sensing approach was developed to identify relative changes in vegetation health both spatially and temporally. While percentage canopy cover is routinely used to assess tree health in the field (e.g. Doody *et al*., 2009), it can also be obtained from LiDAR Foliage Projected Cover (FPC) and in conjunction with LiDAR Canopy DEM (CDEM) data, providing high-resolution vegetation structure information. Landsat reflective bands and Normalised Difference Vegetation Index (NDVI) have also previously been used in conjunction with other environmental predictor variables to successfully map River Red Gum health along the Murray River (Cunningham *et al*., 2007; 2009). Other authors have used minimal field study data to calibrate or validate similar remote sensing approaches (e.g. Fuller *et al*., 1997; Wagenseil & Samimi, 2007; Cunningham *et al*., 2009) including comprehensive time-series analysis for statistical assessment of temporal changes in vegetation dynamics (e.g. Hansen *et al*., 2008; Brown *et al*., 2008; Omuto, 2011; Drummond *et al*., 2012).

10.1.3 What are the Key Questions Being Addressed in this Study?

The key vegetation assessment questions/issues being addressed in this study include:

- The degree of reliance of River Red Gum and Black Box vegetation communities on different groundwater resources (e.g. lake-fill groundwater leakage, shallow river/flood-derived groundwater or deeper groundwater) during drought conditions;
- Response of River Red Gum and Black Box vegetation communities to different water regimes (e.g. drought, rainfall, river flow and flooding);
- Impacts of historical, current and potential future lake-filling regimes on fringing woody vegetation;
- What, if any, groundwater dependent vegetation exists near potential MAR sites, and whether these vegetation communities would be impacted by the development of a MAR scheme; and
- What are the vegetation characteristics of the groundwater resource targets and neighbouring National Park? Will groundwater extraction have any detrimental impacts on vegetation?

This Section addressing questions 1 through to 3, detailing both pre- and post-river regulation surface water regimes (Section 10.4.2), including rainfall, flooding and lake-filling; exploring the improved understanding of groundwater distribution and quality (Section 10.4.1); and finally looking at how vegetation responds spatially and temporally to these varying surface and groundwater resources. Points 4 and 5 are addressed in Lawrie *et al*. (2012c, d) although a summary is provided in this section.

10.2 BACKGROUND

10.2.1 Rainfall

Climate data has been measured at Menindee Post Office since 1876 and is available from the Bureau of Meteorology. Temperatures range from an average minimum of 4ºC in July to an average maximum of 34.3ºC in January. While rainfall occurs more regularly in June, highest average rainfall is observed in January. A severe rainfall deficiency occurred in November 2001 to January 2003, with a total of 115.9 mm for the 15 month period. This period represents the severest water stress the region experiences.

Monthly rainfall data is shown in Figure 10-1. This information, along with daily and annual rainfall data, is available in full in Appendix 6 (Somerville *et al*., 2012).

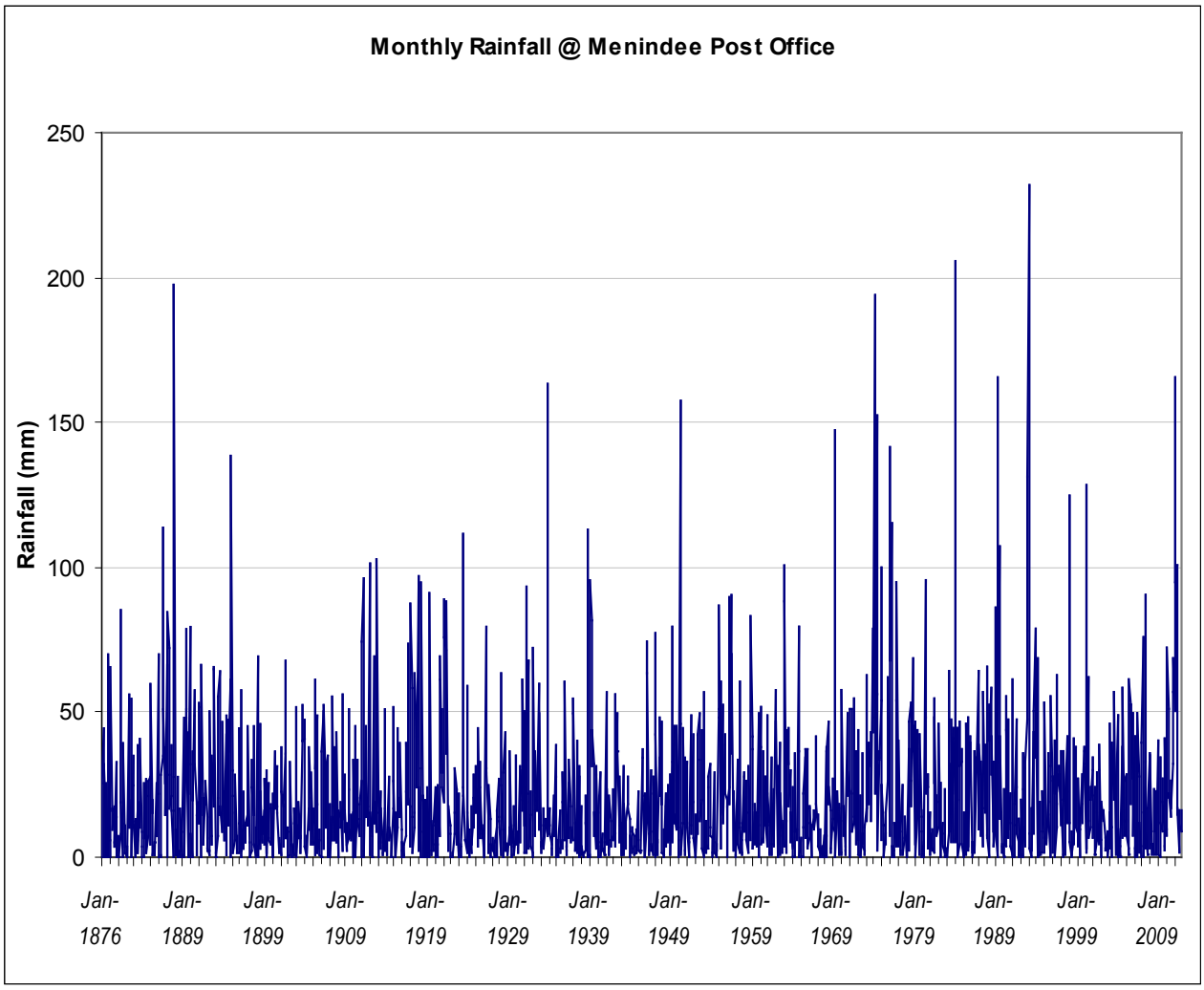

Figure 10-1. *Monthly rainfall data measured at Menindee Post Office since 1876*

10.2.2 **Lake Water**

10.2.2.1 Pre-regulation (pre-1960)

Menindee Lakes system consists of a complex series of ephemeral lakes and wetlands which form a natural storage system along the Darling River. Prior to the establishment of the Menindee Lakes Storage Scheme in 1960, ten lakes formed part of the Menindee Lakes system, with Malta, Balaka, Bijiji, Tandure, Pamamaroo and Menindee Lakes connecting directly with the Darling River, and Speculation, Eurobili, Spectacle and Cawndilla Lakes connecting to the Darling River via Menindee Lake (Taylor-Wood *et al*., 2001).

In common with all flood-out lakes, the pre-regulation Menindee Lakes (except Lake Menindee itself which is more complex) would have commenced to fill when flood levels exceeded the sill level in the channels connecting the lakes to the Darling River; and continued to fill at a rate and to a level determined by the flood height on the flood plain. Sill heights for some of the main Menindee Lakes are shown in Table 10-1. As the flood peak in the river passed and the lake level exceeded the flood height, flow would have returned to the river until the sill height in the inlet channel was reached. The residual pool in each lake below the sill level would then have been slowly reduced by a combination of evaporation and seepage. The situation in Lake Menindee is complicated by its overflow connection to Lake Cawndilla and its asymmetric lake-floor topography. Lake Cawndilla and the deeper north-eastern portion of Lake Menindee are the effective residual pool phases of Lake Menindee during a flooding cycle. The broad higher portion of the lake floor adjacent to the channel across the lake floor would have formed extensive mud flats after return flow to the inlet sill level.

Table 10-1. *Naturally occurring sill levels and artificial full supply (FSL) and surcharge levels for the Menindee Lakes.*

Lake	Sill level m AHD	FSL m AHD	Water depth (m)	Area (Ha)	Capacity (ML)	Original surcharge level	Current surcharge levels
Malta	61.85	61.67	1.5	300	3000	62.68	62.68
Balaka	59.78	61.67	2.5	1200	18 000	62.68	62.68
Bijiji	59.93	61.67	3.1	1000	20 000	62.68	62.68
Tandure	60.11	61.67	5.8	2100	88 000	62.68	62.68
Wetherell		61.67	12	9500	209 000	62.68	62.68
Pamamaroo	59.2	60.45	5	6900	270 000	61.97	61.5
Menindee	54.35	59.84	4.6	15 900	595 000	61.36	60.45
Cawndilla	54.14	59.84	5.8	9400	547 000	61.36	60.45
TOTAL					1 750 000		

With the exception of Lake Menindee, natural conditions would have resulted in large areas of the lake floor above the sill level being subject to relatively short-term inundation and characterised by Lignum and Black Box perennial vegetation communities. The residual pool environment below the sill level would have been characterised by migrating zones of shallow water, mud flats and marginal aquatic ephemeral vegetation as the water body shrank. The natural flood regime resulted in a classic 'boom-bust' cycle, highly productive in terms of the vegetation seed bank and the complexity and abundance of invertebrates (Nicol, 2004; Jenkins & Boulton, 2003) which in turn supported abundant and diverse populations of aquatic fauna, waterbirds and terrestrial fauna.

10.2.2.2 Menindee Lakes Storage Scheme (post-1960)

In the 1950s and 1960s the NSW Government constructed the Menindee Lakes water storage scheme, by connecting the natural ephemeral lakes and the Darling River by a series of weirs, regulators, channels and levees (NOW, 2010). Four weirs and 12 regulators were constructed as part of the scheme; the main weir was completed in 1960 however the entire scheme was not completed until 1968 (Taylor-Wood *et al*., 2001). As part of the water storage scheme, Lake Wetherell was created by the ponding of water behind the main weir and artificially joining Lakes Malta, Balaka, Bijiji and Tandure. In addition, man-made channels were created between Pamamaroo and Menindee Lakes and Cawndilla Lake and the Great Anabranch via Tandou Creek (Taylor-Wood *et al*., 2001) and regulators controlled flow from Wetherell to Pamamaroo and Pamamaroo to Menindee. No regulator structure exists between Menindee and Cawndilla.

Releases can be made to the Darling River through regulators from Lake Wetherell, Lake Pamamaroo and Lake Menindee, as well as from the Main Weir. Releases to the Lower Darling are measured at Weir 32. Lake Cawndilla can only drain to Lake Menindee; not directly to the Darling River. Water from Lake Cawndilla can however be released from the outlet regulator via Cawndilla Channel to Tandou Creek. Lake Tandou was banked off in 1979 and converted to irrigation thus water can then be contained by a block bank and regulator at Packers Crossing to either be diverted to Tandou Ltd water storage lakes (Lakes Kangaroo and Packers) or continue downstream to Redbank Creek before passing to the main channel of the Darling Anabranch.

The four main storage lakes - Wetherell, Pamamaroo, Menindee and Cawndilla - were originally designed with a full supply level (FSL) and a higher surcharge level at which water could be safely held for short periods of time. The difference between the FSL and surcharge levels (Table 10-1) was designed to allow for flexibility in water management. Surcharge levels for 3 of the 4 main lakes (Pamamaroo, Menindee and

Cawndilla) were lowered from original levels (Table 10-1) in response to infrastructure failure and local lake-shore erosion.

10.2.2.3 Time series lake level data

Historic lake-level data (1979 to present) was obtained from NSW Office of Water for Lakes Wetherell and Tandure, Pamamaroo, Menindee and Cawndilla and is available in full in Appendix 6 (Somerville *et al*., 2012). From this record, three lake levels were noted: fully supply level (FSL), 2010/11 flood maximum and highest recorded lake level. With the exception of Lakes Cawndilla and Menindee these values varied from lake to lake. Corresponding surface water extents were generated for each lake and each 'inundation zone', using the 5 m resolution LiDAR DEM. For more specific details on this method, refer to Lawrie *et al*. (2012a).

Historic lake level data indicates that Lakes Cawndilla and Menindee overtopped full supply levels (FSL) eight times since 1979, with controlled releases evident part-way through each of these events (Figure 10-2). Of these eight events, three went on to overtop the 2010/11 maximum and approach the historic maximum lake level. When filled, Menindee and Cawndilla effectively have the same lake level as the connecting channel is unregulated. In comparison to Lake Pamamaroo, Lakes Cawndilla and Menindee are only allocated inflows from significant flood events. The smaller flood pulses are absorbed into Lake Pamamaroo, hence greater fluctuation and more frequent overtopping of FSL observed in the Lake Pamamaroo time series (Figure 10-2b). There were two drought periods of note - March 1992 to March 1996 and August 2002 to June 2010 - when no water was present in either Lake Menindee or Cawndilla; Pamamaroo also experienced dry conditions during the second, more severe drought event (Figure 10-2).

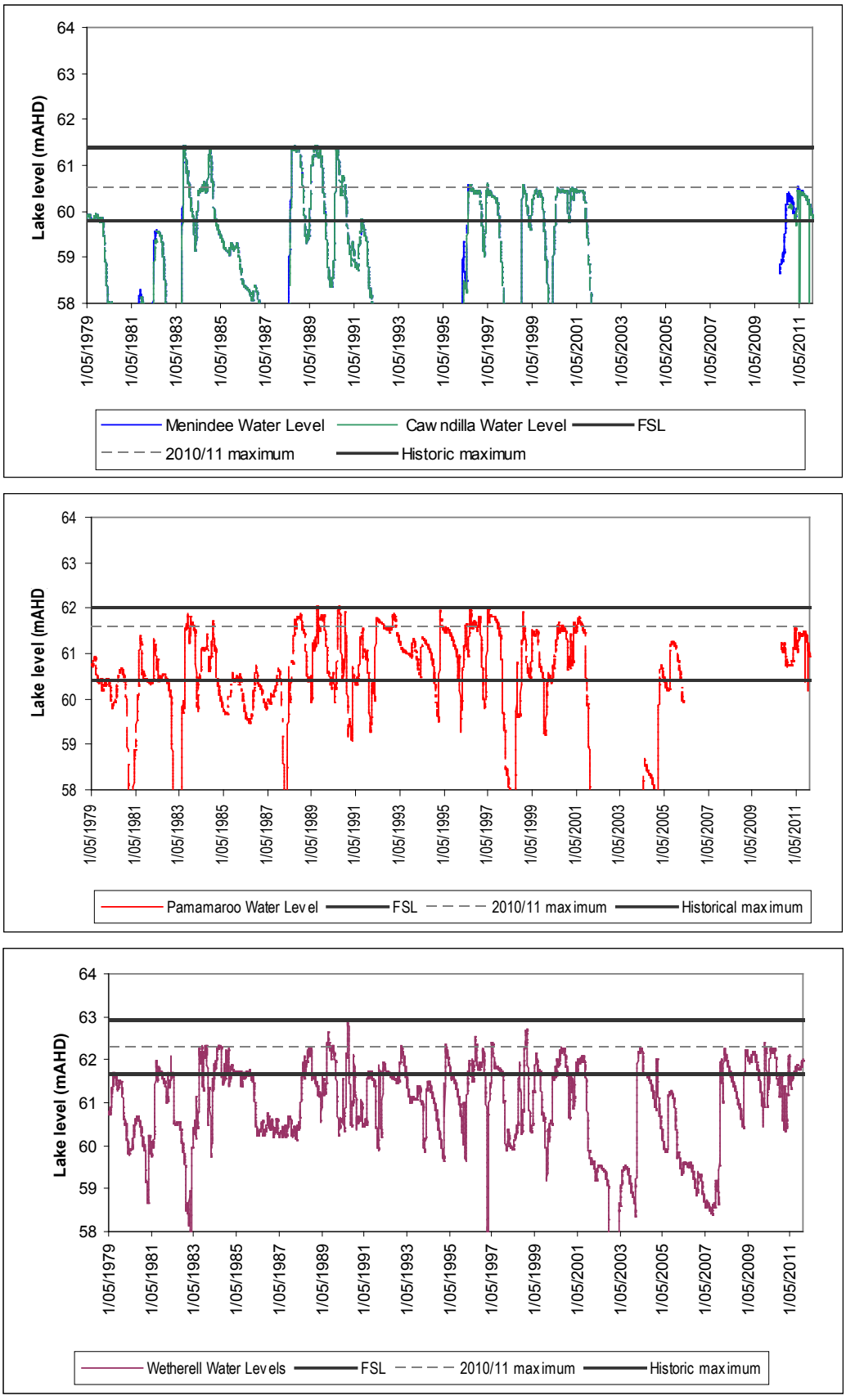

Figure 10-2. *Graphs representing lake levels at a) Lakes Cawndilla and Menindee, b) Lake Pamamaroo and c) Lakes Wetherell and Tandure. FSL (dashed line) represents full supply level, while the 2010/11 maximum and historic maximum lake levels are the lower and upper solid lines respectively.*

10.2.3 River Water

10.2.3.1 Darling River

The Darling River and its tributaries drain the north-westerly portion of the Murray-Darling Basin (Figure 10-3). Most of these tributaries drain the western margin of the Great Dividing Range and contribute relatively high runoff. Others, notably the Warrego and Paroo Rivers, have their headwaters in the more arid interior and are intermittent contributors, only providing significant runoff during intense rainfall. All tributaries join the Darling River north of Wilcannia. While technically unregulated north of the Menindee Lakes Storage Scheme, the Darling River is highly affected by headwater dams, low level weirs and water extraction. River flows generally increase downstream towards Burke but at this point, flows typically decrease due to 1) a lack of contributions from tributaries and 2) increased rates of evaporation. Consequently, while river level and flow rates are recorded at both Burke and Wilcannia, values at Wilcannia are more indicative of flows experienced in the Menindee region (Thoms *et al*., 2004).



Figure 10-3. *Murray-Darling Basin including the Darling River and its tributaries.*

The Great Anabranch of the Darling River (the Darling Anabranch) is an ancestral path of the Darling River. The Darling Anabranch is a naturally ephemeral stream which under non-regulated conditions, would only receive inflows when flows in the Darling River reached 10,000 ML/day (Campbell & Wallace, 2009) typically every 2-3 years (Gippel & Blackham, 2002). Under regulated conditions the Darling Anabranch receives flows via the southern intake and Tandou Creek when flows at Weir 32 exceed 10,000 ML/d and 20,000 ML/d respectively (Briggs & Townsend, 1993). Regulation of the Darling Anabranch has been in existence since 1869, when landholders deepened the channel by 3.6 m, enabling water to flow into the Anabranch at a lower level than previously. Banks were also built across the channels to keep floodwater from flowing into a succession of lakes until floodwaters had filled the course of the stream and a large dam further downstream (Withers, 1994). Prior to the completion of the Menindee Lakes storage scheme in 1960, the Darling Anabranch ran more frequently than Talyawalka Creek.

With the completion of the Menindee Lakes storage scheme, a nominal volume of water (50,000 ML) was released annually from Lake Cawndilla to the Darling Anabranch. Water was originally released on 1st May each year however releases were changed in 1980 to spring, better meeting demand and providing a more reliable and higher quality resource (Withers, 1994). Seasonal flow patterns consequently shifted such that high flows occurred in summer, with winter flows less variable and bank-full floods less frequent. The Menindee Lakes scheme also appeared to have resulted in the development of a flooding gradient on the Darling Anabranch floodplain such that the northern sections appeared to have reduced flooding frequency (Gippel & Blackham, 2002). Nominal flows occurred from 1960 to 2002, at which time the Darling Anabranch Pipeline scheme was proposed to return the degraded Darling Anabranch to a more natural ephemeral system through the construction of a stock and domestic water supply pipeline. This supplied landholder needs and allowed for the removal of in-stream structures. The management of flow from Lake Cawndilla was also changed to mimic more natural flow regimes.

Temporal changes to the water regimes along the Darling Anabranch have implications for vegetation analysis. Gippel & Blackham, (2002) reported that reduced flood frequency detrimentally impacted the health of riparian and floodplain vegetation. It is expected that in the absence of regulated, reliable flows (post-2002) the condition of vegetation along the Darling Anabranch is likely to further decline.

10.2.3.2 Talyawalka Creek

Talyawalka Creek is also an ephemeral anabranch of the Darling River and has only ever receives flows during high flood event; reported river levels at Wilcannia associated with flows down the Talyawalka are ~8.3 m. At Blantyre, the Talyawalka Creek branches off from the east bank and flows south during high, prolonged floods to fill a chain of 20 large and small lakes known as the Talyawalka Chain of Lakes (Figure 10-4). Typically half the floodwater goes down Teraweynya Creek into the lakes, which do not drain back after the momentum of the flood has ceased. There are only a few occasions, mostly between 1864 and 1890, when all (or almost all) the Talyawalka Chain of Lakes filled. During the 2011 floods when flows in the Talyawalka Creek reach about 18,000 ML/d, approximately one-third returns to the Darling River above Menindee and contributed to inflows, one-third continued down Talyawalka Creek, and one-third passed onto the floodplain or into the Talyawalka Chain of Lakes (NOW, 2011). The bottom end of Talyawalka Creek is connected to the Darling River by anastomosing channels, Yampoola Creek and Charlie Stones Creek (Withers, 1996).

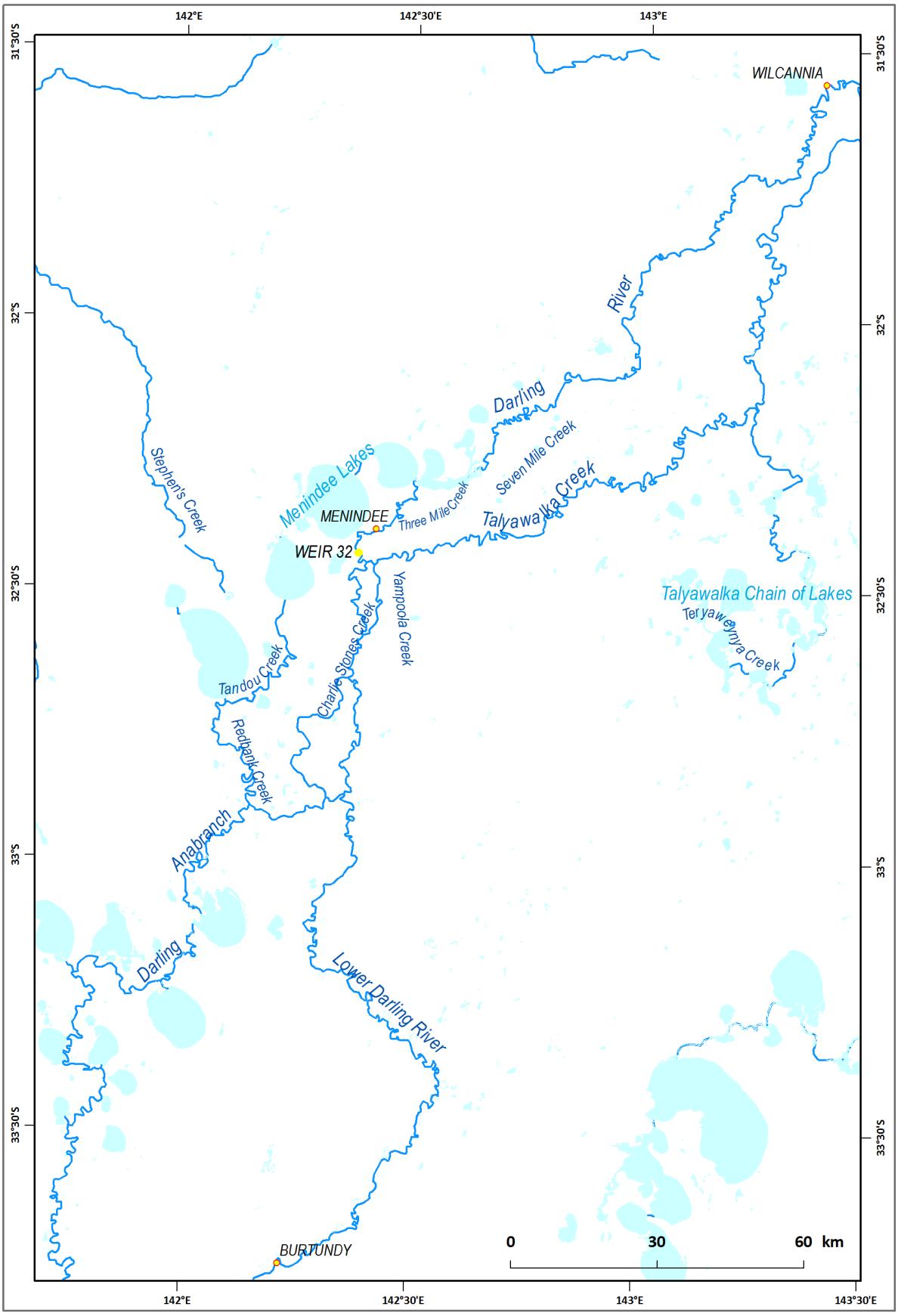

Figure 10-4. *Rivers and creeks in the BHMAR study area.*

10.2.3.3 Other creeks and streams

There are a number of other creeks within the Menindee Lakes region that receive both regulated and unregulated flows (Figure 10-4). Tandou Creek used to run in high floods and fill Tandou Lake which overflowed down Redbank Creek to the Darling Anabranch, Tandou Lake however was banked off for irrigation at the beginning of the 1974 flood. Between 1961 and 2002 (with a 3 year period (1992-1995) of no flow due to infrastructure issues) a nominal volume of water was released annually from Lake Cawndilla via Cawndilla Channel to Tandou Creek where it could be contained by a block bank and regulator at Packers Crossing. Water could then be diverted to Tandou Ltd for irrigation or passed through Packers Crossing downstream to Redbank Creek before passing to the main channel of the Darling Anabranch. Additionally, when flood flows in the Darling River reach Menindee, gates to Three Mile Creek can be opened to allow for Lake Wetherell storage water to flow through Three Mile Creek to Talyawalka Creek; an example of this was in March 1995 (Withers, 1996). Table 10-2 shows the minimal flow requirements to the Lower Darling River.

Table 10-2. *Minimum monthly flow requirements for the Darling River.*

Month	Jan	Feb	Mar	Apr	May	Jun	Jul	Aug	Sep	Oct	Nov	Dec
Flow @ Weir 32 (ML/day)	350	350	350	300	200	200	200	200	200	200	300	300

10.2.3.4 Time series river gauge data

River level and flow data have been recorded daily for Burtundy, Wilcannia and Weir 32 since 1941, 1972 and 1974 respectively. Flow data is shown in Figure 10-5. Wilcannia records unregulated flows into the Menindee Lakes Scheme, Weir 32 records flows released from Menindee Lakes while Burtundy records the remaining flows continuing down the Lower Darling River. Weir 32 and Burtundy have fairly similar flow rates with a few notable exceptions when flows reach 20,000 Ml/day at Weir 32, corresponding to reported release levels for flow to the Darling Anabranch via Tandou Creek. These releases to Tandou Creek equate to a 50% reduction is flows at Burtundy. According to Withers (1996) Wilcannia needed to record a level of 8.3 m before flood waters typically flowed down the Talyawalka. Based on the time series data for Wilcannia (Figure 10-6), Talyawalka Creek flowed approximately 18 times between 1974 and 2012.

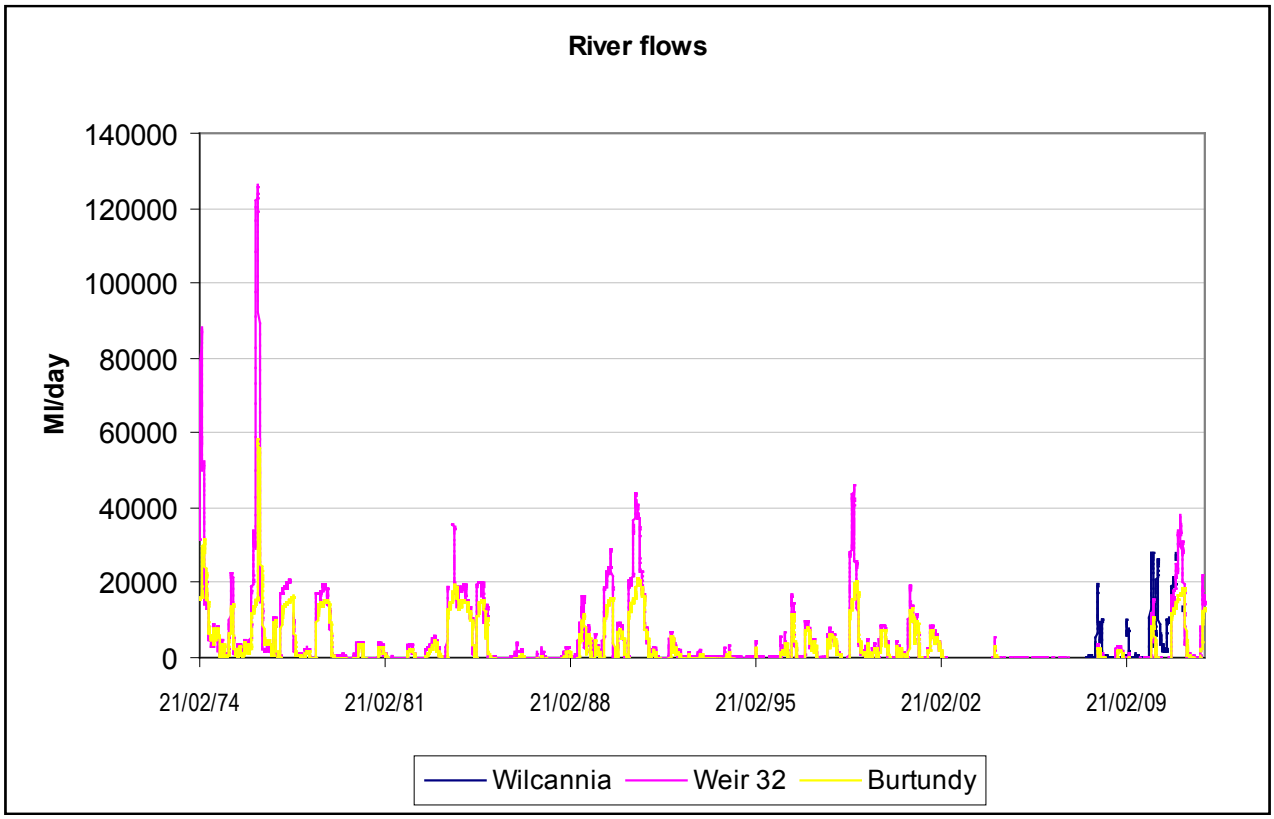

Figure 10-5. *River flow data since 1974 for Wilcannia, Weir 32 and Burtundy. Obtained from the Murray-Darling Basin Authority.*

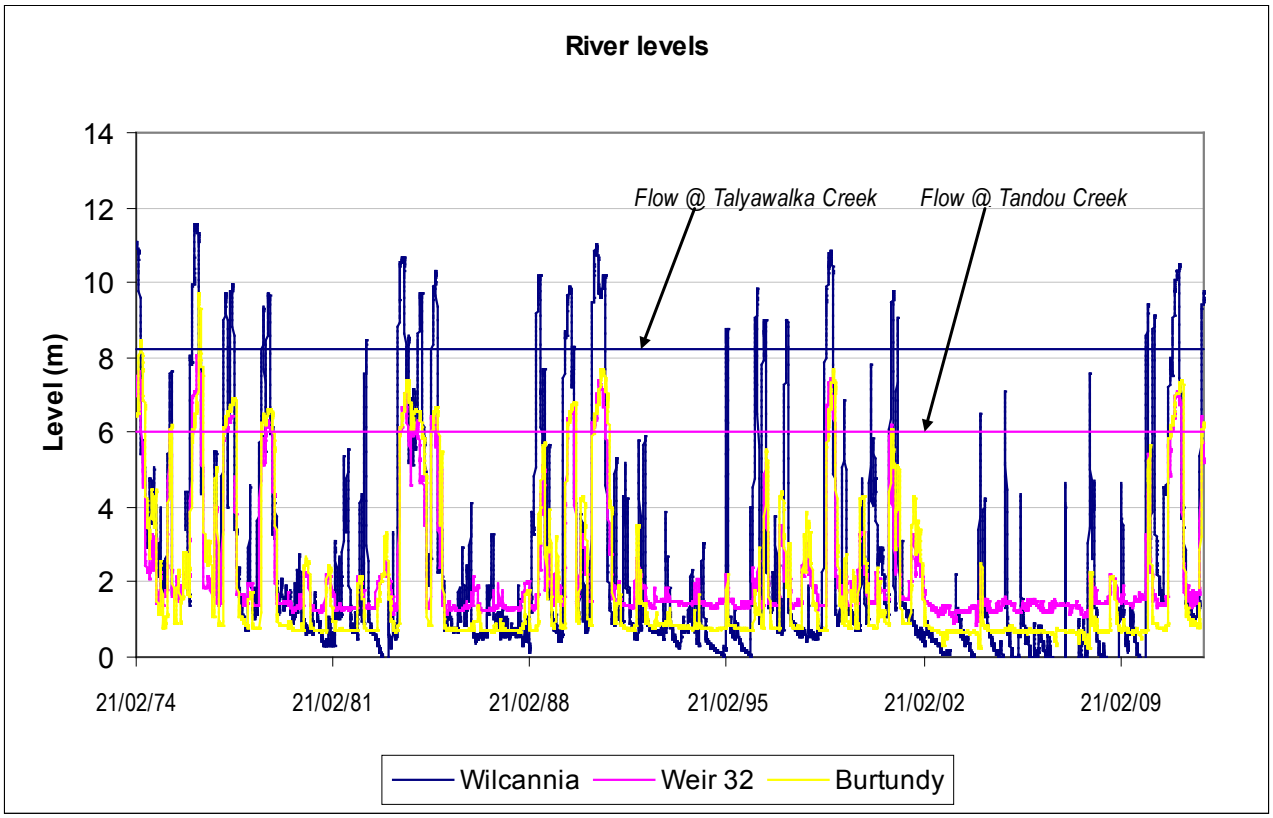

Figure 10-6. *River level data since 1974 for Wilcannia, Weir 32 and Burtundy. Obtained from the Murray-Darling Basin Authority. Note the level heights required for flows to Talyawalka and Tandou Creeks (Withers, 1994; 1996). Line colour denotes the gauge at which the level must be reached.*

10.2.4 **Flood Waters**

The severity of floods in the Menindee Lakes and the Lower Darling River is dependent on the volume, peak and duration of the floods upstream; the prior storage volume of the Lakes; the level of lake surcharge adopted during a flood event; and the capacity for the landscape to retain water.

Five of the largest flood events (over the last 25 years) are shown in Table 10-3, listed in descending order of volume as measured by the total flows at Wilcannia. Compared to previous flood events, the 2011 flood event was the third largest. Although it was much smaller than 1990 and 1998, the merging of two significant flow peaks in 2011 kept river levels at Wilcannia high for about three months. The flood peak travelled more slowly than similar-sized historical flood events presumably due to the dry floodplain and substantial transmission losses (NOW, 2011). The 1990, 2010 and 2011 floods are discussed in more detail below.

Most reports and papers state anecdotally that under natural conditions, inflow to the larger lakes (Cawndilla, Menindee, Pamamaroo and Tandure) would have occurred every 1 to 2 years with the longest drought at 4-5 years. The smaller upstream lakes (Bijiji, Balaka and Malta) had inflow about once every three years with the longest droughts about 9-11 years. According to a CSIRO study, the average period between significant inundation events has doubled to at least 3.5 years as a result of water resource development. Flood volumes have also been greatly reduced such that the average annual flood volume is now less than a quarter and in some cases only a fifth of the volume under without-development conditions for floodplains (CSIRO, 2008a).

Table 10-3. *Five largest historical floods (over the last 25 years) within the Barwon-Darling catchment. Obtained from (NOW, 2011).1990, 2010 and 2011 flood events are summarised below.*

Year	Max height at Bourke (m)	Total volume at Bourke (GL)	Max height at Wilcannia (m)	Total flows at Wilcannia (incl. Talyawalka Ck) (GL)	Max height at Weir 32 (m)
1990	12.99	9,000	11.00	8,150	7.37
1998	13.78	9,700	10.83	6,700	7.45
2011	12.56	5,800	10.50	5,000	7.10
1988	12.57	3,500	10.19	2,900	5.10
2010	10.78	2,370	9.43	2,400	5.44

10.2.4.1 1990 Flood

The 1990 April/May floods in eastern Australia covered more than one million square kilometres of Queensland and New South Wales. This substantial flood was caused by continual heavy rains in central-northern NSW and central-southern Queensland, with moderate flows in the Culgoa and Bogan Rivers and substantial flows in the upper Darling and lower Naomi Rivers by mid April (Figure 10-3; Withers, 1996). There was also localised heavy rain in Broken Hill and all parts of the north and northeast. The progress of the 1990 flood was affected by the release of water from Lake Cawndilla which preceded it, further releases down the Darling River to create flood mitigation potential in the Menindee Lakes, and the closure of the Anabranch Lakes were crops had been planted (Withers, 1994).

10.2.4.2 2010 Flood

Heavy rainfall in December 2009 and January 2010 over the lower Culgoa, Castlereagh, lower Namoi Valleys and the local Barwon River catchment around Walgett, Brewarrina and Bourke resulted in large volumes of runoff and minor to moderate flooding in the associated rivers. More heavy rainfall occurred in mid February 2010 in the Tilpa and lower Paroo areas, resulting in widespread inundation. Isolated heavy falls also occurred between Menindee and Wilcannia (NOW, 2010).

10.2.4.3 2011 Flood

Three intense rainfall events in the upper reaches of the Barwon-Darling catchment during December 2010 and January 2011 combined to produce further large inflows in the Menindee Lakes. The first of these (200 mm on 5th December 2010) occurred in central NSW in the upper reaches of the Macquarie, Castlereagh and Namoi catchments. Major flooding was experienced in the Macquarie River at Dubbo and Warren. The second significant rainfall event (>100 mm on 27th and 28th December 2010) occurred in east Queensland, with resulting runoff producing the first and largest of the two major flood peaks in the lower Condamine-Ballone system. The third rainfall event (~350 mm during the week ending 12th January 2011) was focused in south-east Queensland and northern NSW. This event caused severe flooding in southern Queensland and the Lockyer Valley, along the upper river reaches of the Condamine-Balonne and in the Border Rivers. While rainfall was intense, it was localized and high flood peaks reduced quickly as flow moved downstream. Nevertheless, rainfall on already wet catchments produced significant runoff. In the same week, heavy rainfall was also experience near Wilcannia immediately upstream of the Menindee Lakes (NOW, 2011).

After the 2010 flood, the Menindee Lakes storage scheme was surcharged at 108% after the 2010 flood. Maintaining existing release of ~16,000 ML/d was considered insufficient to keep the Lakes within capacity when confronted with the 2011 flood inflows. Hence the releases were increased to 22,000 ML/d in mid December; this resulted in some inundation downstream. Due to heavy rainfall both locally and in upstream catchments throughout December and early January 2011, releases from the Menindee Lakes were further increased in January to a maximum of ~35,000 ML/d in mid March. This resulted in extensive inundation downstream. Images taken from a light aircraft in March 2011 are shown in Figure 10-7. A decrease in flows occurred from mid-March to May when further inflows, caused by heavy rainfall in southern Queensland ensured storage levels remained above full supply level throughout winter 2011 (NOW, 2011).



Figure 10-7. *Images of the Menindee region during flooding in March 2011.*

10.2.4.4 Time-series flood extent data

As part of the vegetation assessment study a number of Landsat scenes (~300) were acquired. For the purposed of accurately assessing temporal changes in vegetation condition, inundated areas were identified and eliminated, as discussed in Lawrie *et al*. (2012a). This data was however useful in understanding where in the landscape flood waters occurred. Consequently the open water class for each scene was integrated to create surfaces showing the maximum observed inundated extent and an approximation of inundation frequency on a per year basis. Both extent and frequency are functions of the number of available cloud free scenes for that year thus they only provide a guide. This is discussed in more detail in Lawrie *et al*. (2012a). As a consequence of this inherent limitation in the Landsat inundation frequency mapping, the LiDAR DEM data was used to model inundation based on local elevation in conjunction with historic river level data.

The 1 m resolution LiDAR DEM was initially levelled to the Darling River floodplain by subtracting an interpolated floodplain elevation trend surface from the DEM. This produces a de-trended flood-plain surface. Secondly, the levelled DEM surface was adjusted to the water-level reading at the Weir 32 Darling-River gauging station at the time when the LiDAR was acquired. Potential flood extents were derived by elevation slicing of the adjusted levelled DEM between 5.5 m (the point at which overbank flow occurs at Weir 32) to 8.0 m (maximum recorded river level height). These raster surfaces were then compared with the historical record to generate a flood frequency surface per year, summarizing how many days any single Landsat pixel was inundated. There are also a number of limitations with this approach including:

- Overestimation of flood extent downstream of the gauge point;
- Underestimation of flood extent upstream of the gauge point;
- Flow volumes, losses, preferred pathways and impediments to flow were also not considered; and
- The regulated lakes (Lakes Wetherell, Tandure, Pamamaroo, Cawndilla and Menindee) were treated as unregulated lakes thus frequencies for these lakes are not truly indicative.

More detail is provided in Lawrie *et al*. (2012a). Both these datasets can however be used as a guide to predicting the extent of flood waters at different times and the approximate frequency or duration of inundation.

10.2.5 Groundwater

As discussed elsewhere in this document (Section 7), the hydrostratigraphy of the area includes (from top to bottom) a near surface, clay drape aquitard, semi-confined aquifer (Menindee and/or Coonambidgal Formation), upper confining aquitard (Blanchetown Clay, and in some cases, upper Calivil Formation), semi-confined aquifer (Calivil Formation) and lower aquitard (Renmark Group).

The semi-confined primary aquifer, the Calivil Formation consists of fluvial medium to coarse sands, combined with fine sand and sandy mud. An upper clay-rich horizon when present forms local barriers to groundwater flow. The Calivil Formation is overlain by the Blanchetown Clay aquitard which has been eroded in places by Pliocene and younger fluvial channels (Menindee and Coonambidgal Formations). The surface aquitard (clay-rich horizons) largely prevents local recharge via rainfall. Instead, recharge to the Calivil Formation is principally believed to occur during flood events when hydraulic head is high in the rivers, forcing water, via incised ‘holes’ in the Blanchetown Clay/Upper Calivil Formation aquitard into the Calivil Formation (Figure 10-8). For more information about recharge processes refer to Section 9.

Not only do these ‘holes’ in the upper confining aquitard allow for recharge to occur, they also result in localised connectivity between the shallow and Calivil Formation aquifers and different water availability for vegetation. For example, in the scenario in Figure 10-8, it is anticipated that Tree A and Tree B will exhibit different condition over time as they have access to different groundwater systems. Tree A is reliant on the watertable within the Coonambidgal Formation aquifer and localised river water while Tree B has access to the Calivil Formation aquifer via connectivity with the shallower aquifer and also directly should its root system extend that far. In the case of Tree A, were the upper confining aquitard (Blanchetown Clay) is quite thin, tree roots may be able to penetrate it to the underlying aquifer.

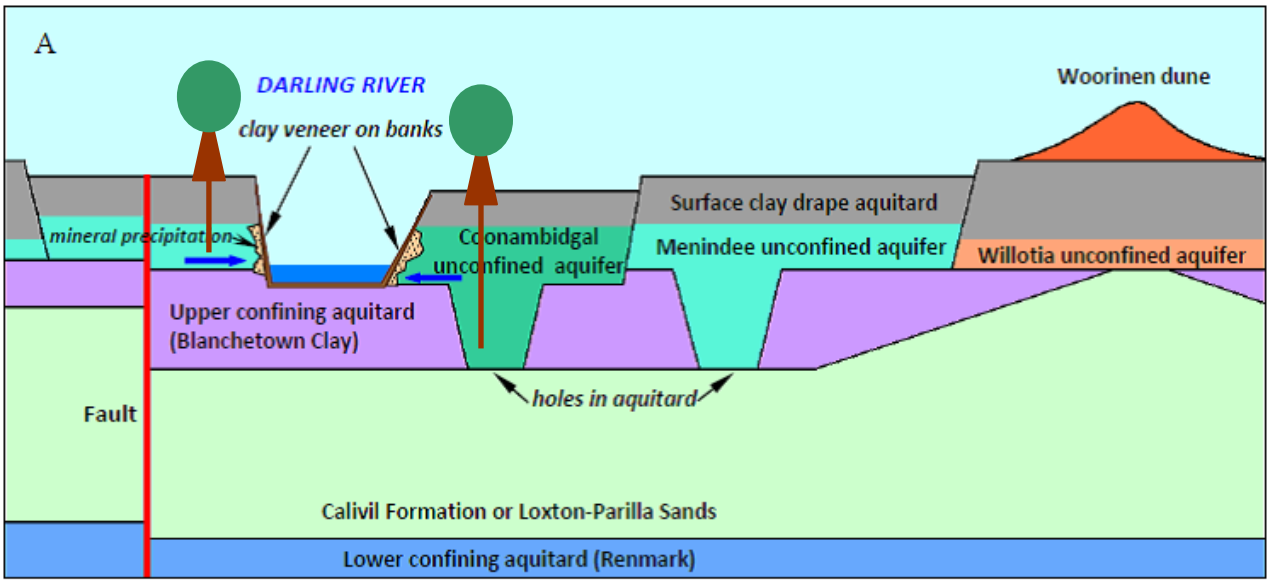

Figure 10-8. *Conceptual model of connectivity between semi-confined (Calivil Formation and Loxton-Parilla Sands) aquifer and the shallow unconfined aquifer. Tree A has limited access to groundwater due to the presence of a thick aquitard. Tree B has much greater access to groundwater as its root system corresponds with a 'hole' in the Upper Confining Aquitard.*

Consequently, in order to understand temporal and spatial vegetation dynamics, it is important to identify the distribution and thickness of the upper confining aquitard (Blanchetown Clay and Upper Calivil Formation). Such surfaces were derived from airborne electromagnetic (AEM) conductivity depth slice data and are shown in Figure 10-9 and Figure 10-10. More information about the generation of these surfaces can be found in Section 17 of Lawrie *et al*. (2012a). Potentiometric surfaces for the shallow and Calivil Formation aquifers have also been developed (Figure 10-11) based on hydrograph and borehole data (see Section 17 of Lawrie *et al*., 2012a). For more information about these surfaces, refer to Lawrie *et al*. (2012a). Potentiometric surfaces provide information about the depth to which vegetation root systems must travel to obtain groundwater resources. Surveys by Davies (1953) showed River Red Gum roots can extend to at least 10 m below the surface and the global-average rooting depths reported for sclerophyllous trees is 12.6 +/- 3.4 m (Canadell *et al*., 1996).

The quality of the groundwater resource is also important. River Red Gum and Black Box have reported salinity tolerances of ~ 30,000 and ~55,000 EC respectively (Doody & Overton, 2009). The Blanchetown Clay when saturated is typically highly saline hence is a deterrent to vegetation.

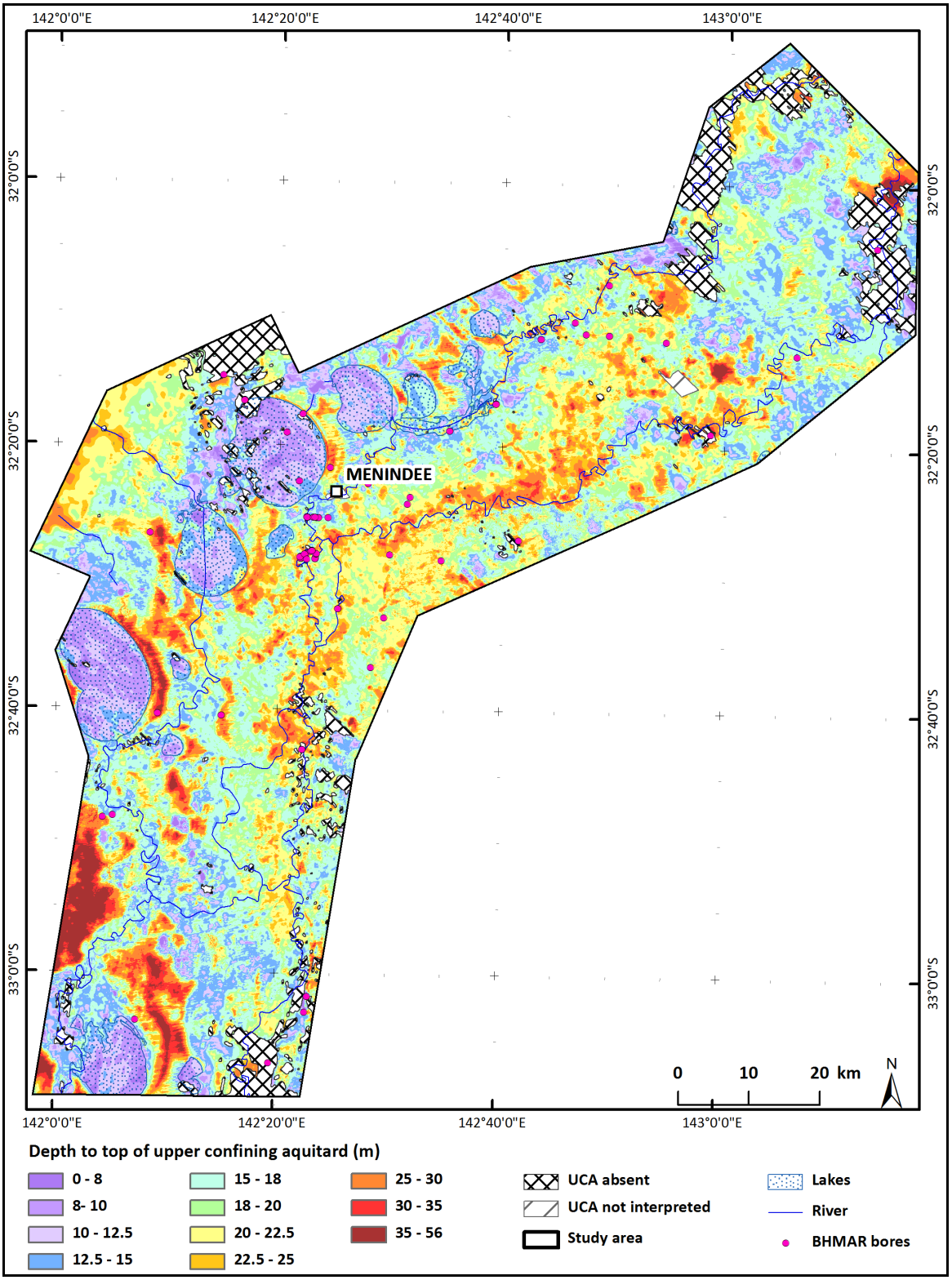

Figure 10-9. *Depth to the top of the upper confining aquitard. White areas within the AEM survey area correspond with either holes in the aquitard or an non-interpreted area.*

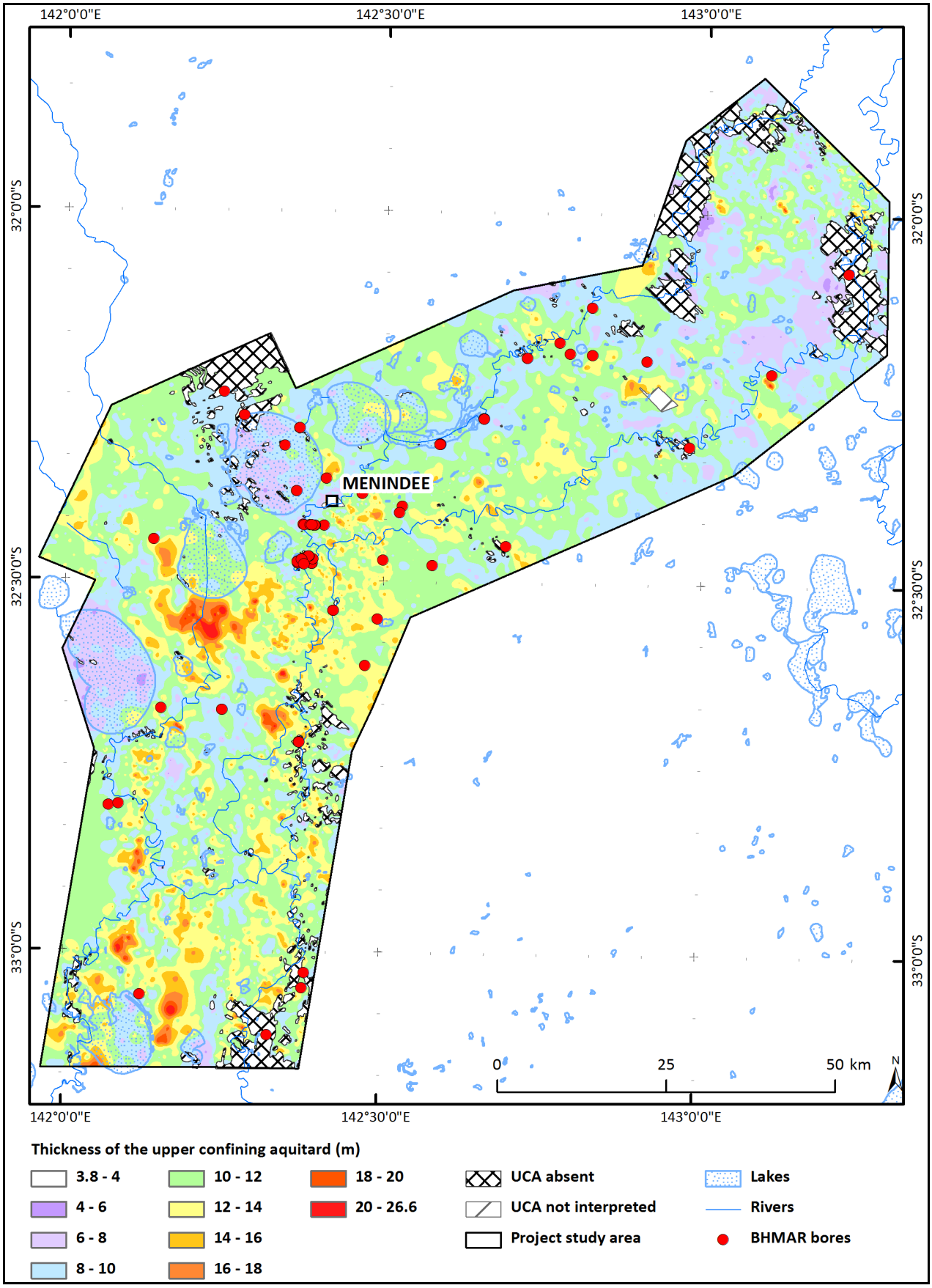

Figure 10-10. *Thickness of the upper confining aquitard.*

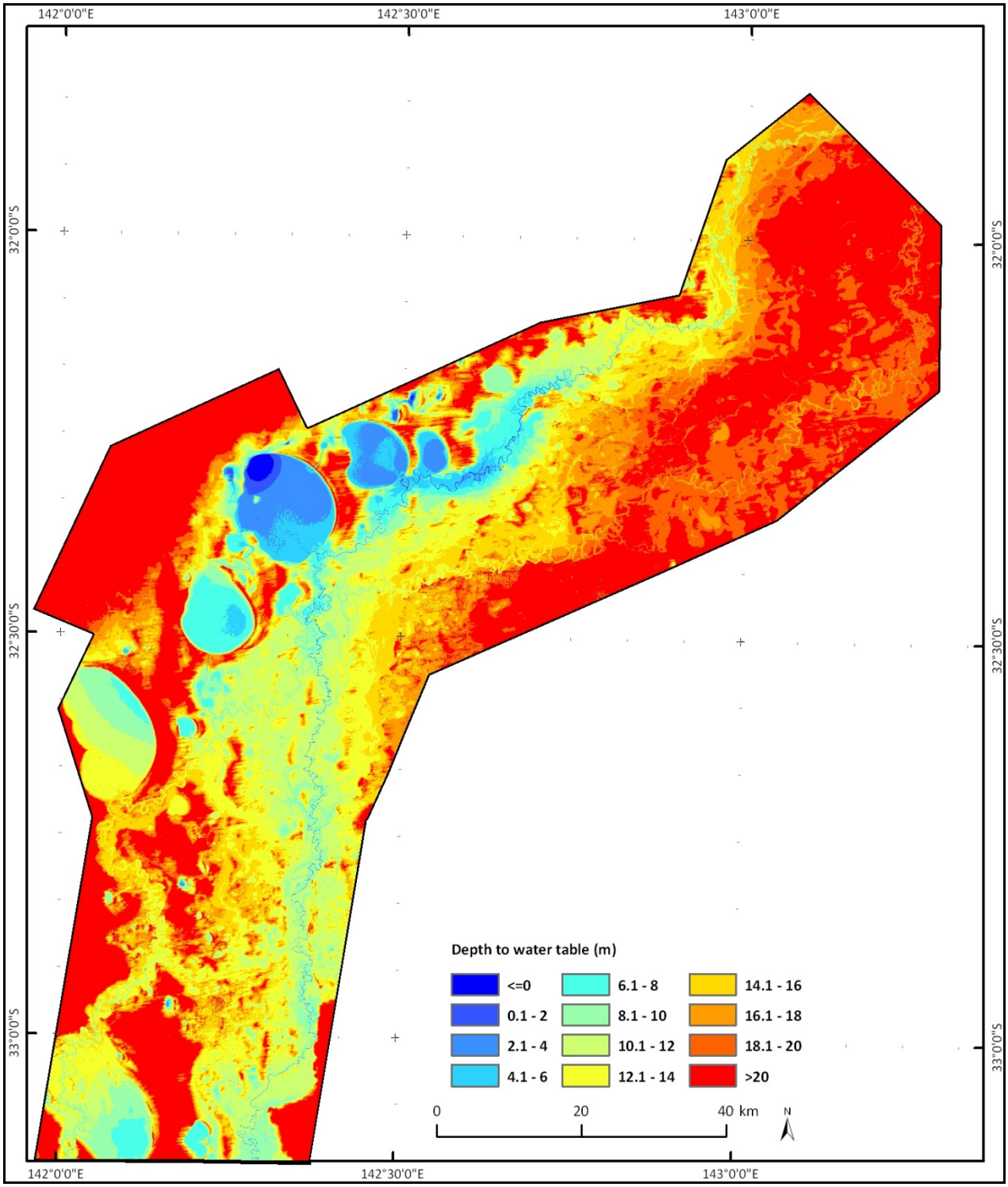

Figure 10-11. *Depth to watertable. This surface has been derived from the potentiometric surface of the surficial aquifer and topography. These values reflect the depth to which the rooting systems of vegetation must travel to encounter the watertable. Values of zero or less indicate the occurrence of groundwater discharge. Values greater than 20 m are likely to be beyond the reach of River Red Gums and Black Box in this landscape.*

10.2.6 Vegetation Dynamics

10.2.6.1 What vegetation is being investigated?

A vegetation survey in the Kinchega National Park (located within the area of study) in 2001 reported that the region predominantly consisted of riverine woodlands (Black Box - *Eucalyptus largiflorens* and River Red Gum - *E. camaldulensis*) around the lake system and on the floodplains of the Darling River and Great Darling Anabranch, with arid woodlands and shrublands on the sandplains and dunefields (Westbrooke *et al*., 2001). North of Menindee, Coolibah (*Eucalyptus coolabah*) can be mixed with Black Box; south of Menindee its distribution is quite limited (Westbrooke *et al*., 2004). Two other studies have undertaken vegetation mapping of the area: field and remote sensing based vegetation/habitat mapping around the Menindee Lakes by Taylor-Wood *et al.* (2001) and Landsat derived vegetation mapping over NSW by Ritman (1995). Figure 10-12 indicates a rough distribution of vegetation communities as mapped by (Ritman, 1995). The BHMAR Project vegetation study focuses on 'woody' vegetation, specifically River Red Gums and Black Box. While the importance of other vegetation communities is recognised, particularly wetland ecosystems, the timeframes and scope of this project were such that only tree species, specifically River Red Gums (*Eucalyptus camaldulensis*) and Black Box (*Eucalyptus largiflorens*) were investigated.

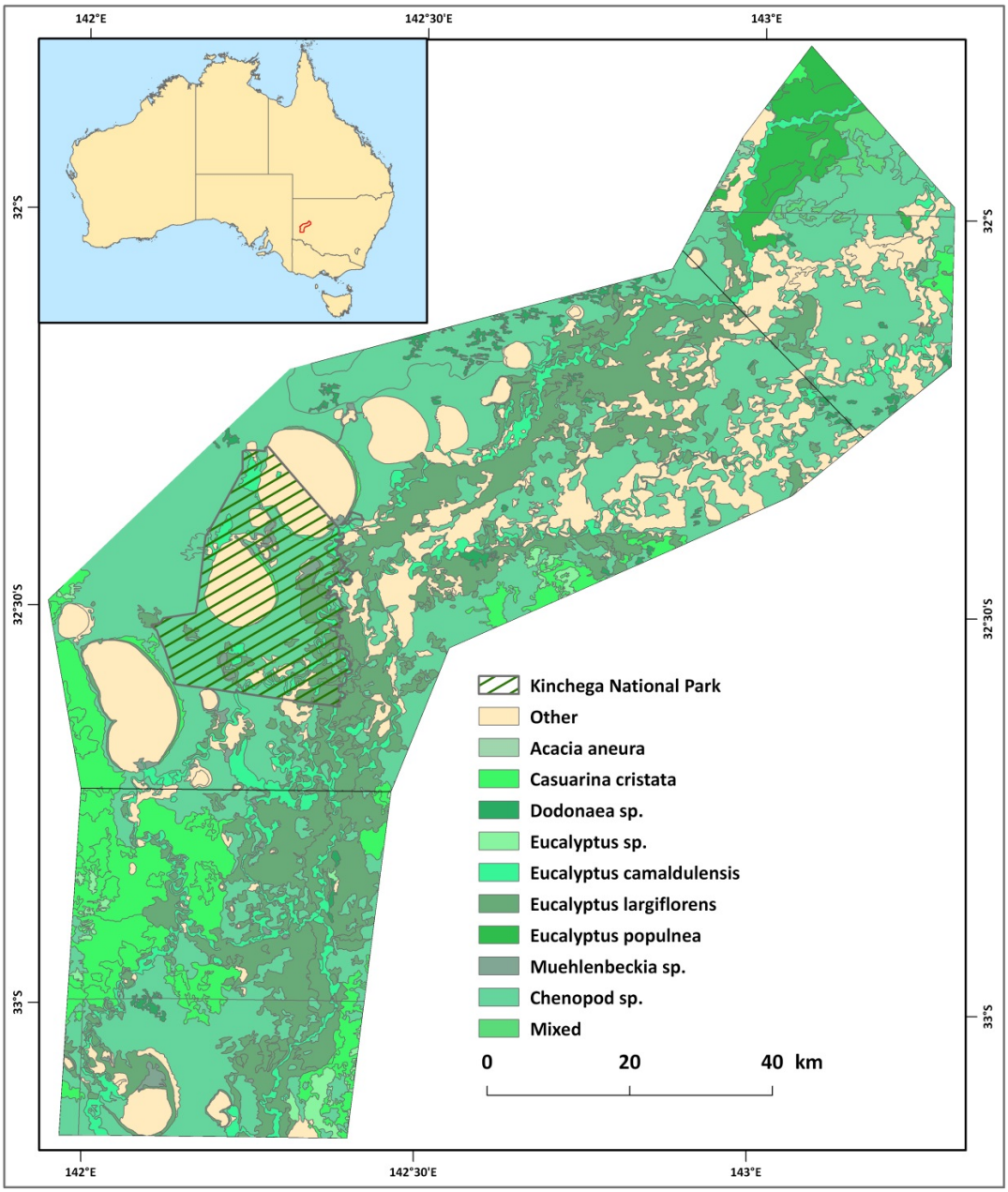

Figure 10-12. *Broken Hill MAR Project extent, indicating Kinchega National Park and pre-existing Landsat derived vegetation species mapping.*

River Red Gum (Figure 10-13) is the most widely distributed eucalypt in Australia, dominating water courses throughout the country (Cunningham *et al*., 2007). It is also one of the most loved and best recognised tree species of inland Australia (MDBC, 2003). River Red Gums grow between 25–40 m high, and are typically found along rivers, creeks and other periodically-flooded watercourses and floodplains. While they prefer heavy grey clay soils, they will grow on all soil types if given adequate water (Porteners & Ashby, 1996). River Red Gum can obtain its water from three main sources: groundwater, river flooding and rainfall (Wen *et al*., 2009). Studies in the Lower Murrumbidgee Floodplain indicated that River Red Gums require periodic inundation every 3-5 years for duration of up to 64 days to be in moderate to good condition (Wen *et al*., 2009), while other studies report a preference for every one and a half years (Doody & Overton, 2009), once every 2 years (VEAC, 2008) or as frequently as one every 7 months (Roberts & Marston, 2000).



Figure 10-13. *Photos of River Red Gum (left) and Black Box (right).*

If River Red Gums are synonymous with Australian inland water course channels, Black Box (Figure 10-13) are synonymous with Australian floodplains. Black Box grows between 10–20 m high and occurs on floodplains, river flats, depressions and dry lake margins. Black Box can withstand periodic waterlogging (Porteners & Ashby, 1996) and is drought and salt tolerant to ~55,000 EC (Doody & Overton, 2009). They prefer to be inundated every three to five years (Doody & Overton, 2009), and consequently typically grow on heavy clay soils subject to occasional flooding. Black Box can obtain its water from groundwater or a combination of groundwater and rain-derived water, including flood waters (Akeroyd *et al*., 1998).

The different preferred flood inundation regimes of River Red Gums and Black Box explains their respective locations in the floodplain; River Red Gums are located in the vicinity of permanent water or along ephemeral water courses while Black Box are located at higher floodplain elevations (Doody & Overton, 2009). River Red Gums have developed a number of adaptations that allow them to survive both drought conditions and prolonged inundation. Similarly, Black Box has also been found to survive prolonged inundation, reportedly regardless of flood length or initial tree health (Akeroyd *et al*., 1998).

10.2.6.2 Potential impacts on River Red Gum and Black Box condition

Riparian floodplain vegetation within the Murray-Darling Basin has reportedly been suffering from severe health decline for several decades (e.g. Jolly *et al*., 1993, MDBC, 2003, Cunningham *et al*., 2007). Declines can be attributed to decreased water availability due primarily to long term drought conditions and further exacerbated by river regulations and abstraction for irrigation and domestic purposes. Floodplain salinisation is also a significant contributor to dieback of native riparian vegetation (Akeroyd *et al*., 1998). Not only has mortality accelerated but tree growth rates have also declined and minimal regeneration is evident (Bacon *et al*., 1993). River Red Gums are also being replaced by less flood-dependent Black Box communities.

On inspection of AEM-derived water quality products it is apparent that vegetation within the study area is not associated with water qualities beyond recognised tolerances of River Red Gum at 30,000 EC. This suggests the volume of available water may instead be the primary driver behind vegetation decline. A study in the Macquarie River Floodplain (Steinfeild & Kingsford, 2008) found that earthworks (e.g. dams, levees, channels etc.) not only disrupted the temporal variability of floods by reducing peak flows, but also resulted in diversion of natural flows thereby isolating sections of the floodplain from fluvial processes. Similar observations have been made elsewhere in the Murray-Darling Basin (e.g. lower River Murray Floodplain, Overton *et al*., 2006). Further, river regulation has resulted in reduced extent and depth of winter flows/flooding and increased occurrence and variability of summer flows/flooding. These issues are not unique to Australian riparian and floodplain vegetation; for example a study in southern Alberta (Rood & Heinze-Milne, 1989) reported a 23-48% reduction in riparian forest over a 20 year period in response to the damming of several rivers.

The Menindee Lakes were originally a series of natural ephemerally flooded lakes however in the 1960s the NSW Government constructed the Menindee Lakes water storage scheme, by connecting the natural ephemeral lakes and the Darling River by a series of weirs, regulators, channels and levees (NOW, 2010). As a result of the works, the three major lakes (Pamamaroo, Menindee and Cawndilla) increased their storage area by approximately 6-12% (Taylor-Wood *et al*., 2001). The average period between significant inundation events doubled for the Darling Floodplain (to at least 3.5 years) as a result of water resource development. Flood volumes have also been greatly reduced such that the average annual flood volume is now less than a quarter and in some cases only a fifth of the volume under without-development conditions for floodplains (CSIRO, 2008a).

A number of studies have examined various aspects of the environmental impacts associated with the operation of the Menindee Lakes Scheme. Kingsford *et al*. (2002) stated that most of the 88,570 ha of Menindee Lakes and associated floodplain are degraded by either too much (39,244 ha) or too little (45,298 ha) flooding. Only small wetlands, filled by local rainfall, have natural hydrological patterns. The increased inundation of most major Menindee Lakes has destroyed about 13,800 ha of Lignum and 8,700 ha of Black Box ecosystems, growing on the lake floors. Auld & Denham (2001) have also analysed the depauperate lake-floor ecosystems due to inundation. Nicol (2004) examined the impact of regulation on the seed bank which provides a mechanism for plants to survive through adverse conditions and recolonise during favourable conditions. The results showed that the larger more permanently inundated lakes (Cawndilla, Menindee, Pamamaroo and Tandure) had a depauperate seed bank that was tied to the shoreline whereas the smaller upstream lakes (Malta and Bijiji), which are less impacted by regulation, had much richer and more diverse seed banks which extended from the shoreline across the lake floor. These changes have also reportedly adversely impacted water birds (e.g. Auld & Denham, 2001; Kingsford *et al*. (2002); Kingsford *et al.*, 2004; Kingsford & Porter, 2006).

While the system has been regulated to allow for controlled filling, the absence of sufficient river flows over the last 10 years have meant that the largest lakes (Menindee and Cawndilla) were last filled in 2000, prior to the 2010 floods.

Hydrological impacts of climate change in the Murray-Darling Basin remain very uncertain, however surface-water availability is expected to decline (CSIRO, 2008b). Severe droughts, like that experienced from 1997 to 2006 will become more common. With river regulation reducing the frequency of river bank-full or over-bank flows, and reduced rainfall rates during drought conditions, River Red Gums rely more heavily on groundwater to maintain function (Bacon *et al*., 1993). However exploitation of groundwater is

constrained by depth and quality of the resource. River Red Gum and Black Box have reported salinity tolerances of approximately 30,000 and 55,000 EC respectively (Doody & Overton, 2009).

Pests, over-grazing, invasive species and fire can all influence the condition of vegetation. For example the sap-sucking psyllids are one of the most devastating insect pest groups in Australia and commonly attack River Red Gums (Collett, 2001). While tree mortality seldom results from even the most severe attacks, growth can be severely affected, leading to a general decline in tree vigour. Stone (1993) reported defoliation of River Red Gums in the Murray River floodplain during 1991-92 but Farrow (1996) report River Red Gums in NSW appears to be relatively free of pysllid damage. Without a full floristic assessment of studied vegetation, it is difficult to completely rule out the influence of pest species. Pastoral operations have been in existence in this area since the 1850s. Even the area that is now Kinchega National Park was grazed prior to be being proclaimed in 1967 (Westbrooke *et al*., 2001). Grazing has played an important role in determining the present distribution and floristic composition of vegetation communities. However as this activity has been going on for such a long period of time, a specific response in vegetation condition is not expected over the period of observation. Neither River Red Gum nor Black Box requires fire to assist in the germination, establishment or reproduction. Visual inspection of the imagery (over the period of observation) specific to the area did not identify and fire scald features. Hence associated rapid regeneration was not considered to be a factor in vegetation condition.

10.2.6.3 Reported response of vegetation to changing water regimes

Previous studies have found that the response of riparian tree communities to more favourable conditions is likely to be influenced by the period of time under water stress and the duration of the improved conditions (Doody *et al*., 2009). Long periods of drought stress result in leaf biomass reduction and sapwood area decline (Hatton *et al*., 1995), reducing the ability of the trees to transport water, transpire and respond rapidly when more favourable conditions occur. Floodplain vegetation can equally be degraded from too much water (Figure 10-14; Kingsford *et al*., 2002). Flooding of woody plants has been found to induce a number of physiological disturbances, including early stomatal closure, inhibition of photosynthesis, and decreases in absorption of water and minerals (Sena Gomes & Koslowski, 1980). Subsequent changes often include alterations in root and stem morphology, reduction in root and shoot growth, and ultimate death of trees. The effects of flooding can vary widely with plant species, timing and duration of flooding. Temporal changes in understory and ground cover can also be associated with altered inundation history (Wen *et al*., 2009).

River Red Gums have developed a number of adaptations that allow them to survive both drought conditions (e.g. extensive leaf fall, Briggs & Maher, 1983; allelopathic effects, del Moral & Muller, 1970) and prolonged inundation (e.g. maintenance of oxygen supply to flooded roots through aerenchyma development, Heinrich, 1990). Physiological research into River Red Gum response to water stress (e.g. Crawford & Wilkens, 1996; Chisholm, 2001) suggests that trees retain their green colour and photosynthetic capacity even under severe conditions, manifesting this stress by changes in the internal structure of leaves and changes in chlorophyll content. This implies that once the leaves become obviously discoloured due to significant decrease in chlorophyll content, trees are severely water stressed (MDBC, 2003).

Similarly, Black Box has also been found to survive prolonged inundation, reportedly regardless of flood length or initial tree health (Akeroyd *et al*., 1998). This has been attributed to a combination of low oxygen requirements and rooting systems that are either flood tolerant or capable of varying their depth of activity in response to both water and oxygen.

Different studies undertaken across the Murray-Darling Basin suggest slightly different water regimes for optimal vegetation vigour (e.g. Sims and Thoms, 2002; Doody & Overton, 2009; Wen *et al*., 2009). This suggests that flood frequency and duration are not the only variables impacting vegetation vigour. A report by Roberts (2012) commissioned specifically for this project provided the following generalisations regarding the water regime requirements and tolerances of River Red Gum (Table 10-4) and Black Box (Table 10-5) maintenance.



Figure 10-14. *Photos of woody vegetation subject to a) too much water and b) too little water.*

Table 10-4. *General water regime specifications and tolerances for maintenance of mature River Red Gums (Roberts, 2012).*

Plant response	Frequency and Interval	Duration
Extreme (WET)	Annual flooding (or near annual) with very short recessions such that soil does not dry out and re-aerate are expected to eventually kill trees	Continuous flooding for 4 years is expected to cause death. Continuous flooding for 2-4 years is expected to be very stressful.
Stress		Repeated floods lasting 8-12 months separated by intervals that are too short and do not allow soil to crack or re-aerate (notionally 1-3 months) but maintain saturation or near to saturation are expected to cause stress: recovery is possible if dry conditions follow. Isolated events with durations of 12-24 months also expected to cause stress, but recoverable.
Vigour	About once every 1-3 year for forests; about once every 2-4 years for woodlands. Ideal interval is from 5 to 15 months	About 5-7 months for forests; about 2-4 months for woodlands. Forests (and woodlands) can tolerate longer (up to 10 months) but will retain vigour only if long duration not repeated and soil dries, cracks and re-aerates prior to next flooding: otherwise leads to stress.
Stress	Forest trees expected to show stress after 3 years with no flooding and reliance on soil water and rainfall. Woodland trees expected to show stress after 5 to 7 years with no flooding and reliance on soil water and rainfall	Repeated durations of 1-2 months, even at frequency for vigour is expected to have cumulative effect and reduce growth.
Extreme (DRY)	Complete isolation from flooding is expected to kill trees after 10 years. Lack of flooding for 5-8 years likely to cause severe stress, especially if weather pattern includes periods of high temperatures: recovery may be possible if re-flooded but is likely take years (to decades?) of favourable conditions to re-establish canopy.	

Table 10-5. *General water regime specifications and tolerances for maintenance of mature Black Box (Roberts, 2012).*

Plant response	Frequency and Interval	Duration
Extreme (WET)	Annual flooding that maintains soil in saturated condition without drying out is expected to cause death within four years.	Continuous flooding for 4 years is expected to cause death. Continuous flooding for 2-4 years is expected to be very stressful.
Stress		More than 5 months, possibly up to 18 months. Can survive 13 months continuous inundation: canopy expected to show stress, but most trees expected to recover.
Vigour	Every 3 to 7 years	About 3-6 months for vigorous. Durations of 2-3 months adequate to maintain condition unless frequency falls to once in 5-7 years.
Stress	Growth reduced if not flooded for 3-7 years (probably 3-5 years at Menindee). Expected to show canopy stress if not flooded for 7-10 years. May survive 12-16 years without flooding but condition will be poor and full recovery unlikely.	Tolerates shorter
Extreme (DRY)	May persist in absence of flooding for more than 10 years.	

10.3 METHOD SUMMARY

10.3.1 How are Vegetation Dynamics Being Assessed?

Many factors are important in understanding spatial and temporal variability in vegetation composition and distribution. In this study, vegetation structure was mapped (for a single point in time) using high resolution LiDAR data. A number of studies have similarly used LiDAR elevation data to map vegetation structure (e.g. Geerling *et al*., 2007; Suarez *et al*., 2005; Hill & Thomas, 2005). This 2009 snapshot was then used to calibrate the same classification scheme for 2009 Landsat satellite mapping. Archival Landsat mapping (1987-2011) was then used to investigate temporal trends in vegetation condition. Particular focus was made of the drought period from 2002 to 2009.

As no detailed species composition mapping existed for the study site, analysis could only be applied to structural vegetation communities (i.e. closed forest) rather than River Red Gum or Black Box. Pre-regulation vegetation distribution was investigated from 1945 aerial photography as the Landsat archive did not extend that for a back in time. Condition and distribution of vegetation was then integrated with surface water and groundwater data, hydrogeology, surface materials and geomorphology to understand the drivers behind temporal and spatial change. A brief description is provided below; see Lawrie *et al.* (2012a) for more details.

To allow for the quantitative temporal analysis of different vegetation communities, the entire study area was classified into five vegetation structural classes (Figure 10-15.; as discussed in Lawrie *et al*., 2012a):

- Closed Forest,
- Open Forest,
- Woodland,
- Open Woodland and
- Shrubs and Grasses.

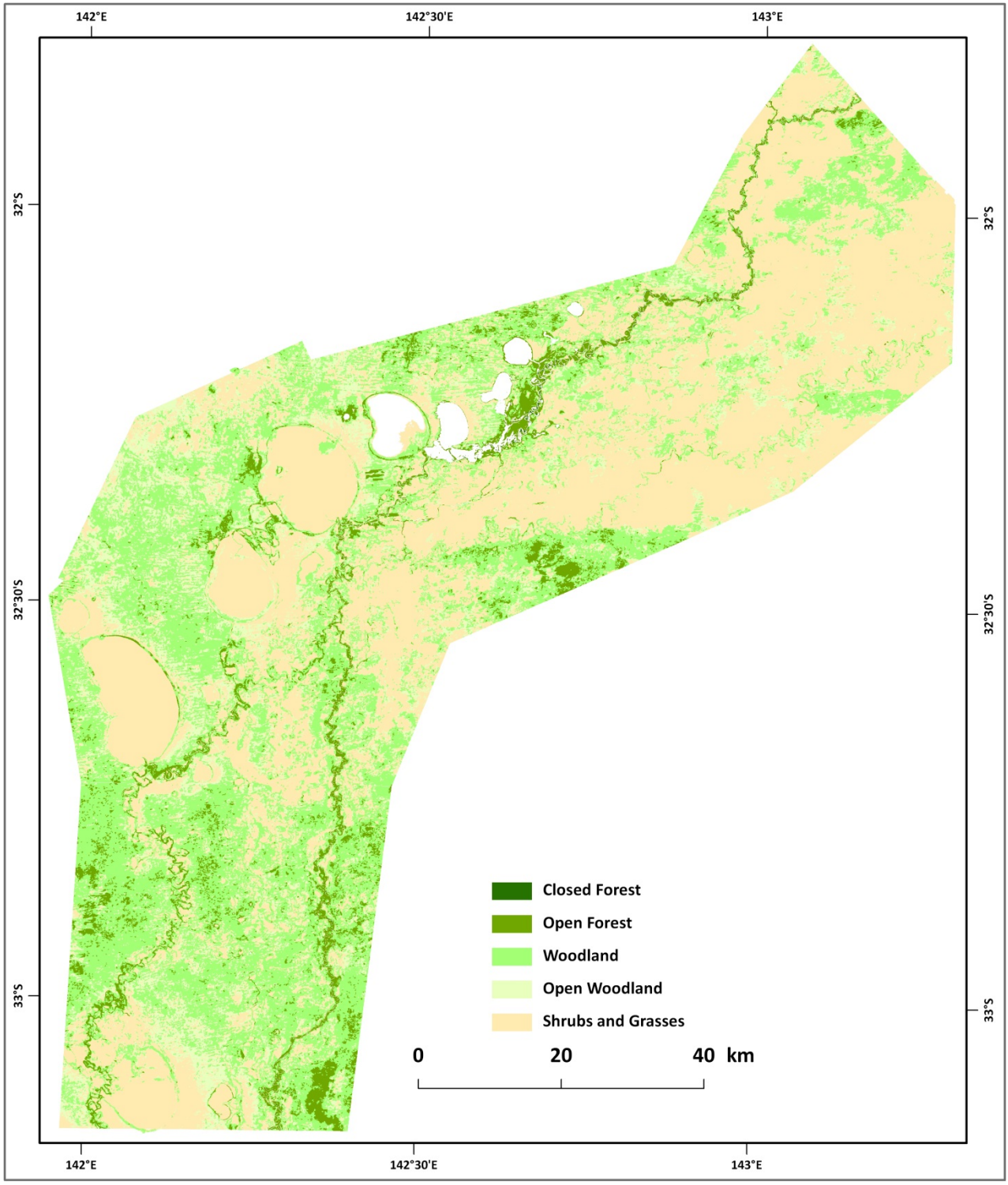

Figure 10-15. *Spatial distribution of vegetation structural classes as defined by Landsat imagery.*

There vegetation structural classes were further sub-divided based on different geomorphic characteristics (e.g. lake, floodplain, riparian zone, lake, local groundwater expression and surrounding landscape) and different water/regulation regimes (e.g. regulated lake fringing vegetation versus non-regulated lake fringing vegetation). Figure 10-16 shows the discretization of the study area into different geomorphic features.

Approximately 300 Landsat images were acquired between 1987 and 2011. A vegetation index, Normalised Difference Vegetation Index (NDVI) was applied to each image to highlight temporal and spatial changes in vegetation greenness. The discretization process allowed for the calculation of statistics (mean, minimum, maximum and standard deviation) for each unique vegetation community and for each Landsat scene (Figure 10-17). The annual minimum was then identified (for each vegetation community and for each year; Figure

10-17) as this value is more indicative of woody vegetation condition than the maximum or average. These yearly minimums can then be used to assess temporal changes in vegetation condition. For more specific details on this method, refer to Lawrie *et al*. (2012a).

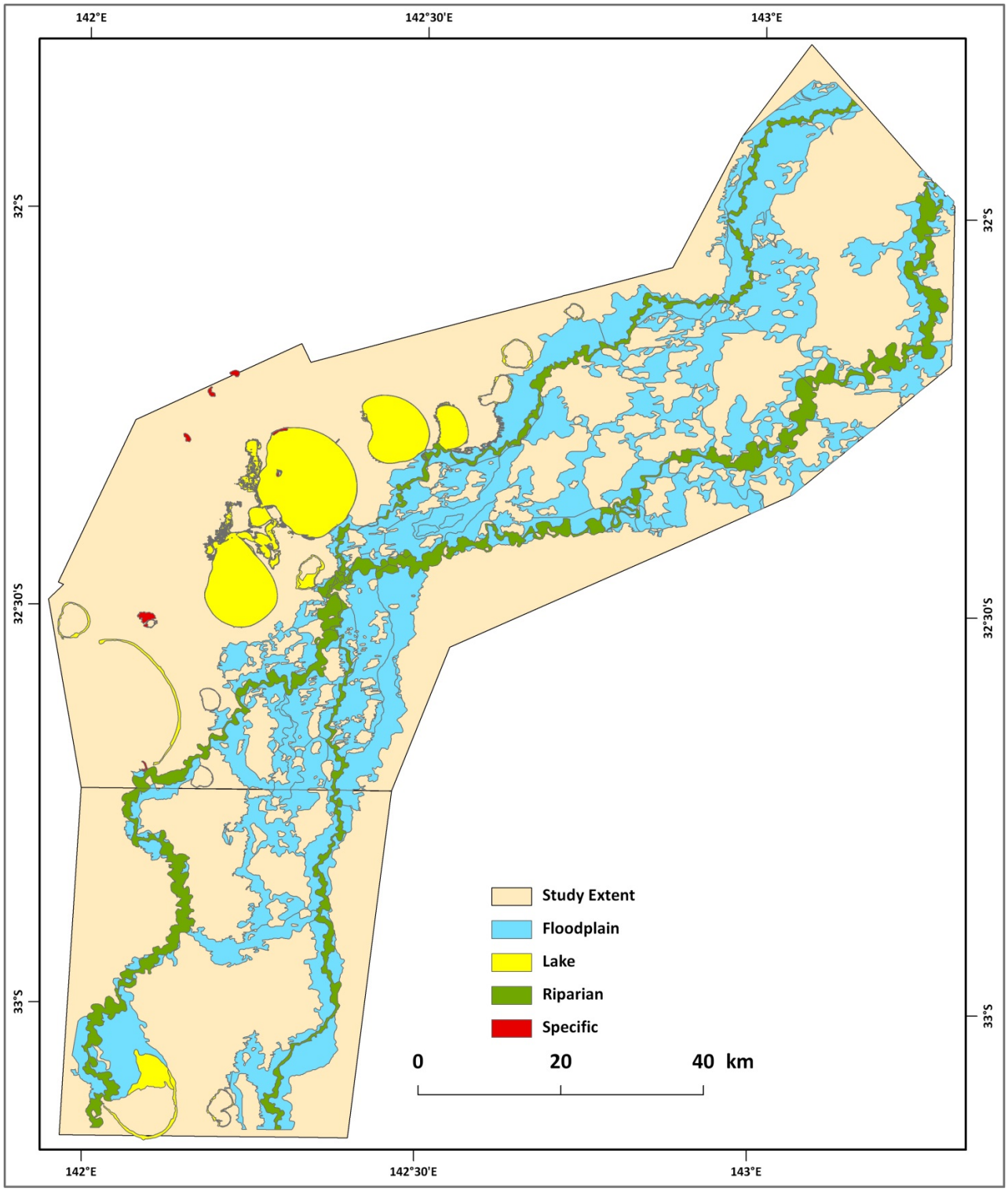

Figure 10-16. *Discretization of the study area into different geomorphic populations.*

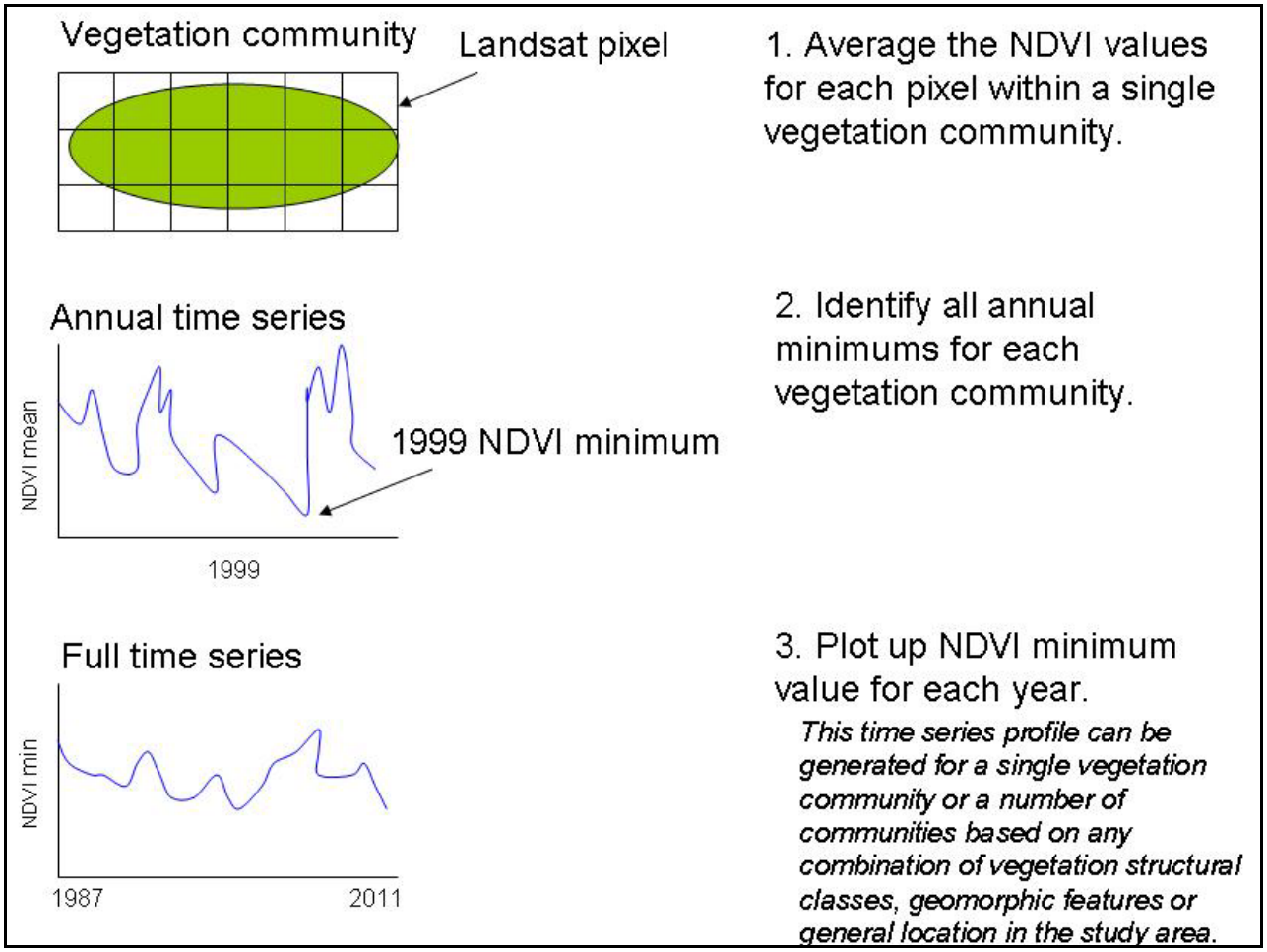

Figure 10-17. *Graphic representation of the generation and amalgamation of statistics for Landsat temporal analysis.*

10.3.2 **Specific Drought Analysis**

The basic distinction in behaviour between vegetation communities supported by groundwater compared to surface water is that groundwater dependent vegetation exhibit more consistent condition as the water resource itself is typically more static. Vegetation reliant on surface water is inherently more variable due to the variable nature of surface water processes (flows and rainfall). Three different variables were investigated: 1) condition of vegetation at the end of the drought (2009), 2) overall trend in condition from the beginning of the drought (2002 for floodplain and riparian vegetation and 2004 for lake vegetation) to the end of the drought, and 3) variability of condition throughout the drought period. These were reclassified and combined in the assessment on source water.

The overall trend and variability in vegetation condition during the drought were combined to provide an estimate of source water reliability (Table 10-6). If there was little change between 2002 (or 2004) and 2009, and little variability across the whole drought period, then source water was presumed to be high. If considerable change occurred and condition was quite variable, low source water reliability was assigned.

The condition of vegetation at the end of the drought (Table 10-7) was broken into six classes other which corresponds with vegetation below the minimum threshold for woodland vegetation; woodlands; open forest which was further divided into low condition, moderate condition and high condition; and closed forest. These classes can also be loosely related to the amount of available water; canopy density has been demonstrated to correlate with the amount of available surface and groundwater (Jones *et al*., 2008). As a consequence of this, inferred source water reliability can now be combined with inferred qualitative volume of water (Table 10-7).

These variables were integrated with hydrologic, hydrogeologic, hydrogeochemical and geophysical data to interpret spatial and temporal vegetation dynamics of woody vegetation. This included analysis of lake-fringing, riparian zone and floodplain vegetation, as well as vegetation within Kinchega National Park, and both the groundwater resource and managed aquifer recharge target sites.

Table 10-6. *Two variables a) overall trend in condition between the beginning and end of the drought and b) amount of variability in vegetation condition throughout the drought, classified and combined to provide c) an indication of source water reliability. SD indicates standard deviation.*

a)	Class	Weight Value
2009vs2002/4	<-1.5 SD	**3**
	-1.5–-0.5 SD	**2**
	-0.5–0.5 SD	**1**
	0.5–1.5 SD	**2**
	>1.5 SD	**3**

+

b)	Class	Weight Value
Variability	<=0.012	**1**
	0.013–0.017	**2**
	>0.021	**3**

=

c)	Reliability of water source
2-3	High
4	Moderate
5-6	Low

Table 10-7. *Vegetation condition at the end of the drought used as an indicator of available water volumes (qualitative) combined with water source reliability to create a matrix of water volume and reliability.*

a)	NDVI value	Vegetation Class	Volume of water	Weight value
2009 NDVI	<0.14	Other	n/a	Null
	0.14-0.19	**Woodlands**	Very low	5
	0.19-0.29	**Open forest, low condition**	Low	4
	0.29-0.39	**Open forest, moderate condition**	Moderate	3
	0.39-0.48	**Open forest, high condition**	High	2
	>0.48	**Closed forest**	Very high	1

+

b)	Reliability of water source
1	**High**
2	**Moderate**
3	**Low**

=

c)	CF	OFH	OFM	OFL	W
H	1,1	2,1	3,1	4,1	5,1
M	1,2	2,2	3,2	4,2	5,2
L	1,3	2,3	3,3	4,3	5,3

10.3.3 Interpreting Landsat Time Series Profiles

As discussed in Lawrie *et al*. (2012a), Normalised Different Vegetation Index (NDVI) was applied to the Landsat imagery to generate time series profiles of inferred vegetation condition; NDVI values range from -1 to 1 with values close to zero reflecting bare ground and negative values corresponding to water. Figure 10-18 shows a typical example of an annual Landsat NDVI minimum time series profile. There are a number of important things to note when interpreting these profiles:

- Due to the moderate resolution of Landsat (30 m pixels), reflectance values (including greenness) are likely to be generalized. Additionally, reflectance values can be more indicative of the field/ground layer, due to the low reflectivity of tree canopy relative to grass canopy (Fuller *et al*., 1997). This is particularly evident following precipitation. In the absence of detailed field data, it is unknown how the individual layers (tree layer composed of woody parts and leaves versus shrubs and bushes in the mid layer and a mixture of soil, litter, herbs and grasses in the field layer) may influence the red and near-infrared signals used to calculate NDVI. Previous studies (Fuller *et al*., 1997) have found that the tree layer appears to be a relatively important component of NDVI during the dry season when the field layer is largely senescent, accounting for 20-40 % of the satellite signal. Maximum contributions occur at the end of the rainy season. However in the inverse situation the tree layer appears to have minimal effect on landscape-scale NDVI when both layers are photosynthetically active. Consequently, increases in NDVI through time may be attributed to vegetation growth in the field layer, rather than an increase in tree canopy greenness/structure. This limitation has largely been addressed by using the annual NDVI minimum which is more indicative of dry season senescence.
- 2009 annual minimum NDVI threshold values were used to differentiate four woody vegetation structural classes – closed forest, open forest, woodland and open woodland. These thresholds are shown in the time series profiles as dashed lines of different colours depending on the vegetation class they represent. As this classification was based on the condition of vegetation at a single point in time, it is expected that NDVI values will vary through time, relative to this threshold.
- When vegetation is inundated (from lake filling or flood waters), the spectral response being detected by the Landsat satellite is a mixture of both water and vegetation. As water exhibits very low (negative) values on the NDVI scale it subsequently draws down the average NDVI for that vegetation community. Any vegetation community exhibiting below zero NDVI or known to be inundated at the time are consequently being influenced by the presence of water and cannot be used to infer condition. Hence, interpretation is largely based on the response of vegetation immediately following inundation and any previous or subsequent dry periods. When inundation is known, it is represented on the time series profiles as a shaded zone (typically blue).
- The number of images used to generate annual statistics varies. Consequently, in the years when the total number of Landsat scenes was low, NDVI values can be biased. 2003 is an example of this. Only two scenes were available for the northern half of the study site, both of which were obtained during winter. As a consequence, 2003 statistics are not included in the time series profiles. Additionally, a number of scenes during 2007 correspond with winter rain events that, although small in relation to long-term averages, were quite large for the drought period. As a consequence of this annual statistics for 2007 reflect the associated spike in vegetation condition relating to these rainfall events.

–

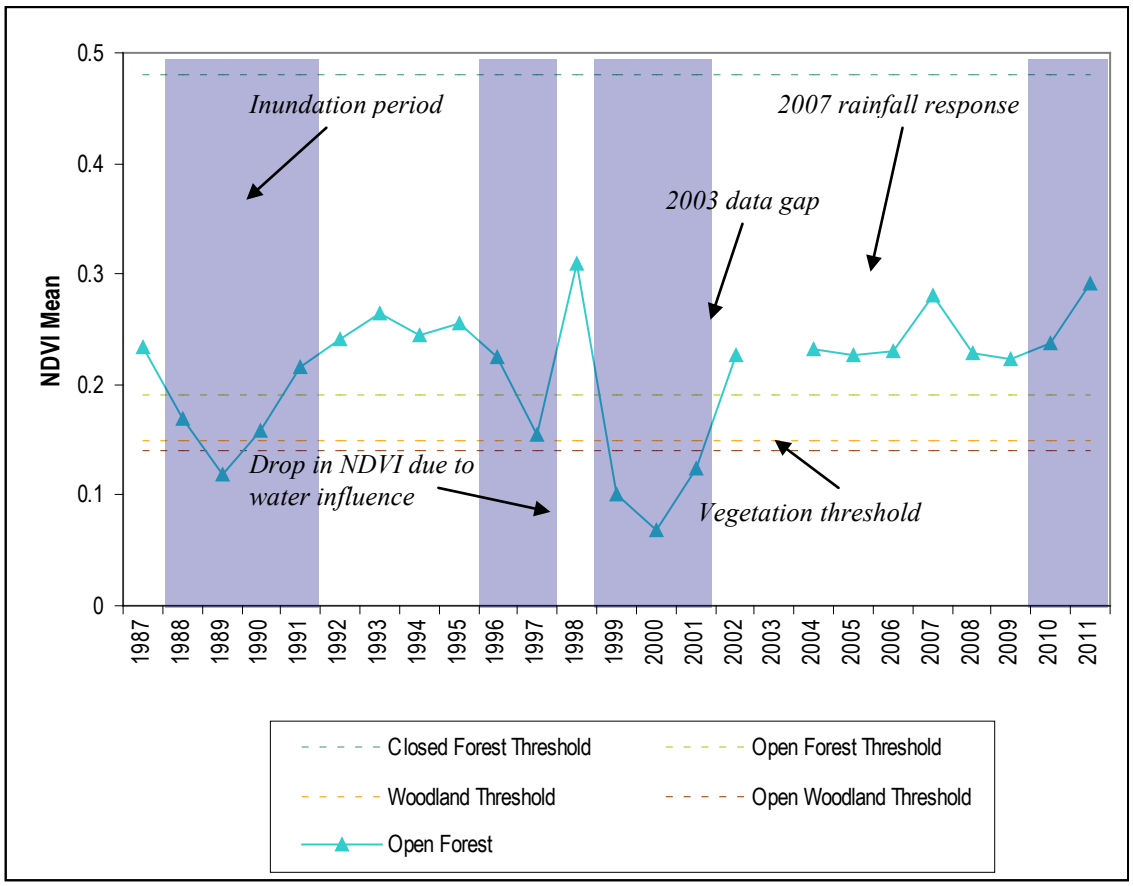

Figure 10-18. *Example of an annual Landsat time series profile.*

10.4 ANALYSIS

10.4.1 Impacts of Regulation on Menindee Lakes Woody Vegetation

10.4.1.1 Introduction

The condition of woody vegetation varies with different water regimes. River and lake regulation in the Darling Floodplain has resulted in significant hydrological and biophysical changes. To emphasis these changes, limited (but indicative) 1945 (pre-regulation) aerial photography over Lakes Pamamaroo, Menindee, Cawndilla and Tandou was compared with 2009 vegetation structural mapping. Due to time constraints, stereoscopic aerial photographic interpretation could not be completed; instead, basic visual interpretation was performed. At particular risk from management of the lakes are existing fringing vegetation communities. Historic lake-level data was used to model the extent of surface inundation resulting from three different water level conditions:

- Full Supply Level (FSL);
- Water level elevation equivalent to the 2010/11 flood maximum; and
- The highest recorded lake level in the respective lake (historic maximum).

Temporal response of vegetation within these different extents was then assessed.

Levels vary between lakes and are summarized in Table 10-8. Due to the presence of an unregulated channel between Lakes Cawndilla and Menindee, once a sufficient volume of water has flowed into Menindee, water levels at these two lakes are largely the same. The same can be said for Lakes Wetherell and Tandure. Consequently, the same water level conditions (Table 10-8) were used for both lakes.

Table 10-8. *Different water level conditions for each lake.*

	Cawndilla/Menindee	Pamamaroo	Wetherell/Tandure
FSL	59.8	60.4	61.67
2010/11 max.	60.5	61.6	62.3
Historic max.	61.4	62	62.93

The spatial extent of each different level were coupled with the lake-level time-series data discussed in Section 10.2.2 to identify which woody vegetation was subject to inundation, when, for how long and how regularly. Although four components (frequency, duration, time and depth of flooding) are generally used to describe any water regime, in this scenario neither depth nor seasonality was considered critical factors for maintenance of mature trees (Roberts, 2012). The timing, frequency and duration of inundation of different vegetation structural classes (closed forest, open forest, woodland and open woodland) was then compared with the Landsat time series analysis to better understand temporal behaviour.

While vegetation condition can be strongly influenced by surface water during wet periods, in the absence of this water resource (either during drought conditions or due to regulation), access to groundwater becomes far more important. This issue was explored in more detail for riparian, floodplain and lake-fringing vegetation. The northern lakes (Pamamaroo, Wetherell, Tandure, Bijiji, Balaka and Malta) were not included as they contained water at varying times throughout the drought which would not only result in an underestimation of vegetation condition but would also complicate the issue of source water. Because of these issues a dry period was selected from either 2002 (or 2004 in the case of the lakes as water was held in Lakes Menindee and Cawndilla prior to this) to 2009. Packers and Kangaroo Lakes may have received regulated flows during this period pumped from the Darling River for irrigation purposes. Yartla Lake is also likely to have received natural flows from the Darling River.

Three different variables were investigated: 1) condition of vegetation at the end of the drought (2009), 2) overall trend in condition from the beginning of the drought (2002 for floodplain and riparian vegetation and 2004 for lake vegetation), and 3) variability of condition throughout the drought period. These were reclassified and combined in the assessment on source water.

This section details the following:

- Basic physical parameters of the each of the key lakes in the Menindee Lakes system,
- Comparison between pre-regulation vegetation distribution based on 1945 aerial photography with current vegetation at each lake,
- Drought analysis at each lake using Landsat time series data, and
- A comparison between the different lakes.

10.4.1.2 Lake Menindee (and Lake Speculation)

Physical characteristics

Lake Menindee has uneven lake floor topography, with elevation differences of over 2 m across its floor (Figure 10-19). The lowest part of the lake occurs in the north-east quadrant near the artificial inlet regulator from Copi Hollow. Lake Menindee also has an extensive delta extending north west from the original natural inlet (current artificial outlet regulator) and a system of broad 'levees' adjacent to the lake-floor channel that connects to Lake Cawndilla. The lake floor slopes from the broad levee adjacent to the channel towards the north-eastern low point.

Under natural (pre-regulation) conditions, these topographic low points would have effectively behaved as the residual pools during flooding cycles, evaporating over time and depending on flood frequency and becoming progressively more saline. Most of the lake floor adjacent to the channel would have formed extensive mud flats when flood waters receded.

Lake Speculation is a small, deep (8.5 m) lake west of Lake Menindee. Water flows into and out of Lake Speculation via a series of naturally occurring shallow channels leading to and from Lake Menindee. Prior to the Menindee Lakes storage scheme, the lake would drain into Lake Menindee, with an expected inflow episode of about once in 20 years (Taylor-Wood *et al*., 2001). An artificial sill at 59.1 m was created between Lakes Menindee and Speculation. Thus, while Lake Menindee receiving inflows more frequently and for longer periods of time post-regulation, Lake Speculation only received inflows when the sill level is overtopped. This sill prevents water from flowing back to Lake Menindee when water levels recede.

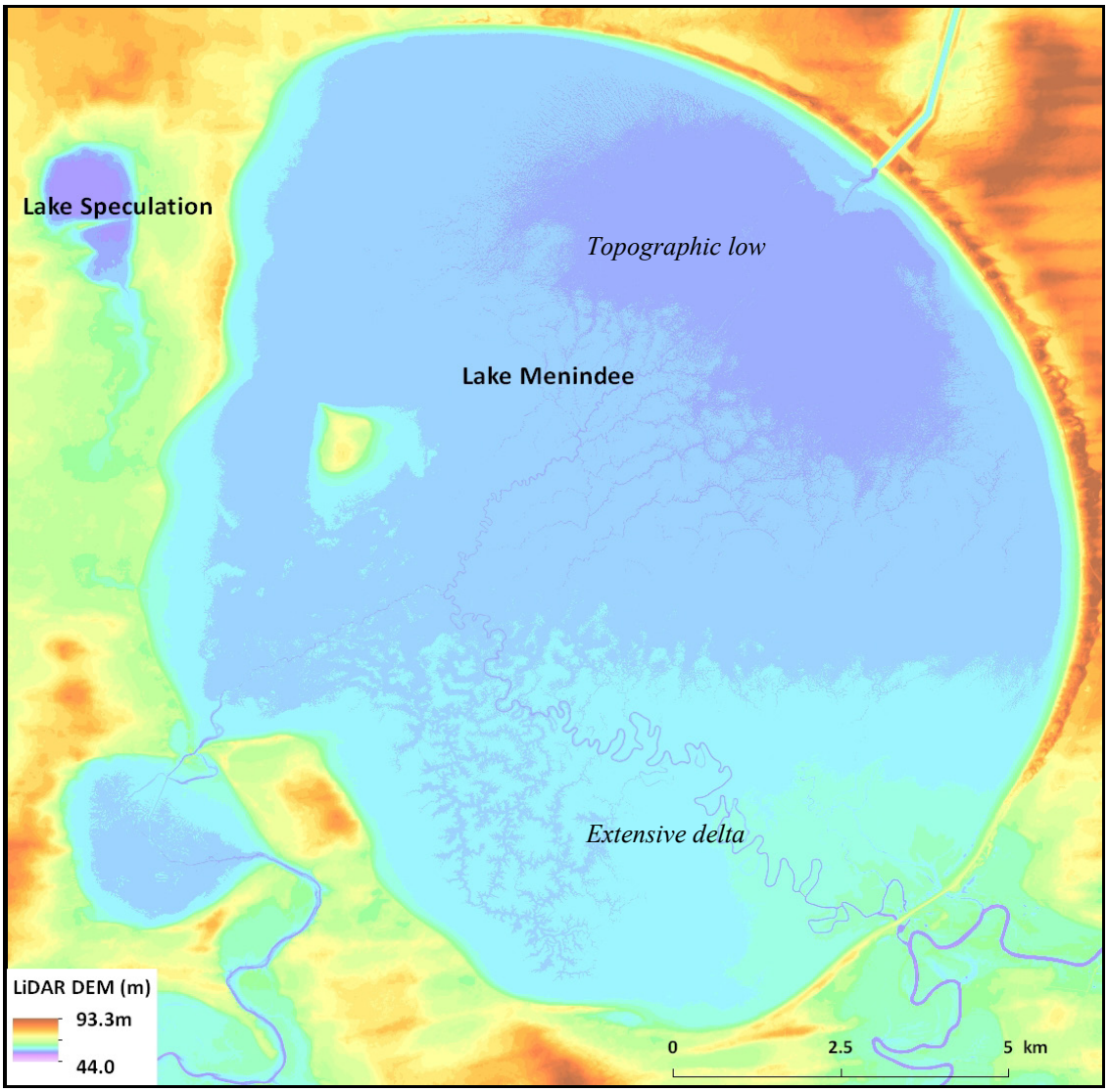

Figure 10-19. *Lake Menindee LiDAR DEM. Note the sloping lake floor topography.*

Pre-regulation vegetation (1945)

Both the low-lying lake floor and extensive delta at Lake Menindee appear to be largely devoid of woody vegetation in 1945 (Figure 10-20), possibly due to the presence of the residual (often quite saline) pools. Black Box and Lignum vegetation communities however appear to have been extensive across the rest of the lake floor which is consistent with previous reports of vegetation distribution at Lake Menindee (Kingsford *et al*., 2002). River Red Gums also appear to have been present along the main channel. Lake Speculation however has a patchy distribution of Black Box vegetation (Figure 10-20) interspersed with areas of shallow freshwater marsh and dry lake-bed herbfields/grasslands/sedgeland (Taylor-Wood *et al*., 2001).

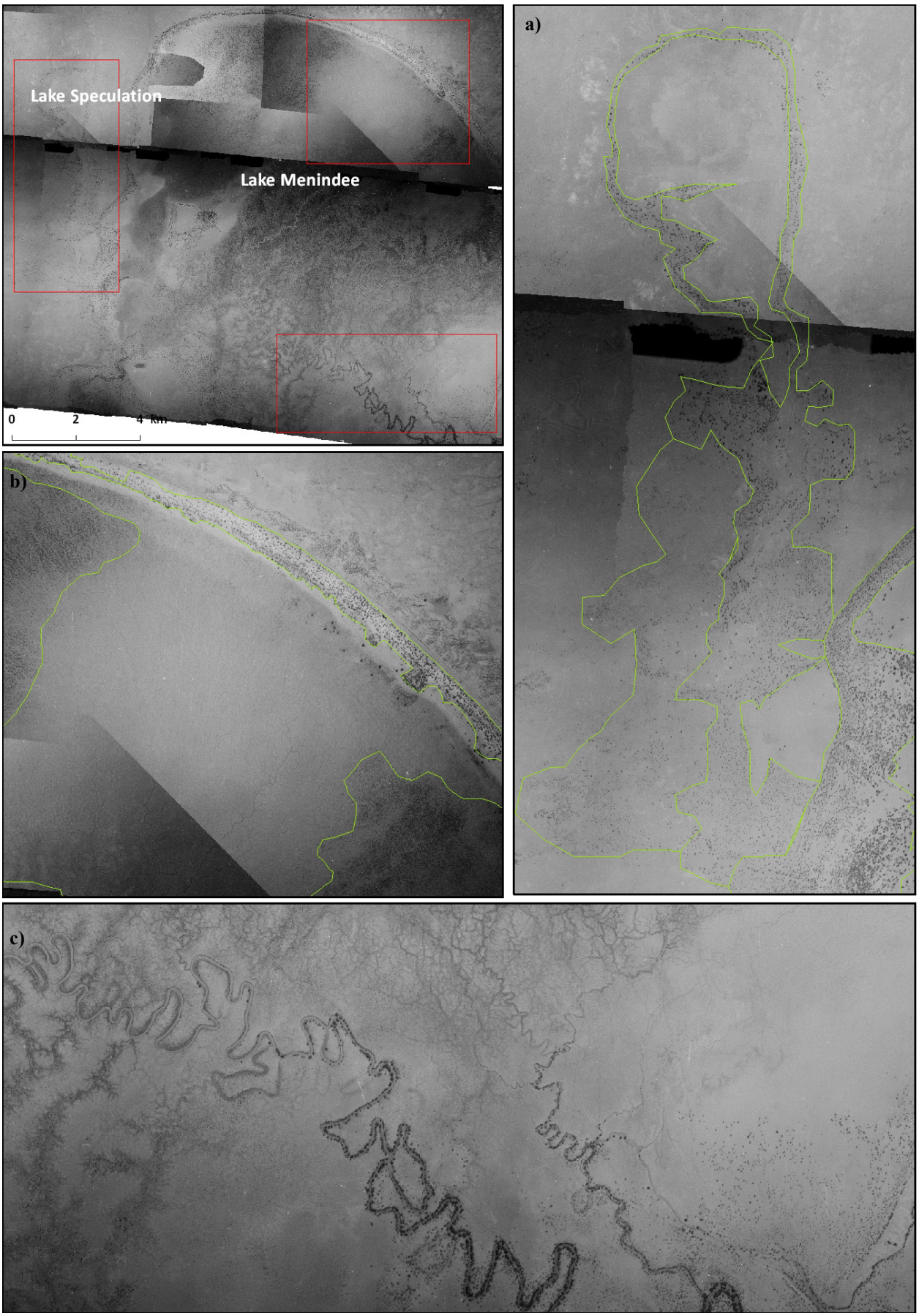

Figure 10-20. *1945 aerial photograph at Lake Menindee, including a) Lake Speculation, b) low-lying lake floor, and c) channel and delta.*

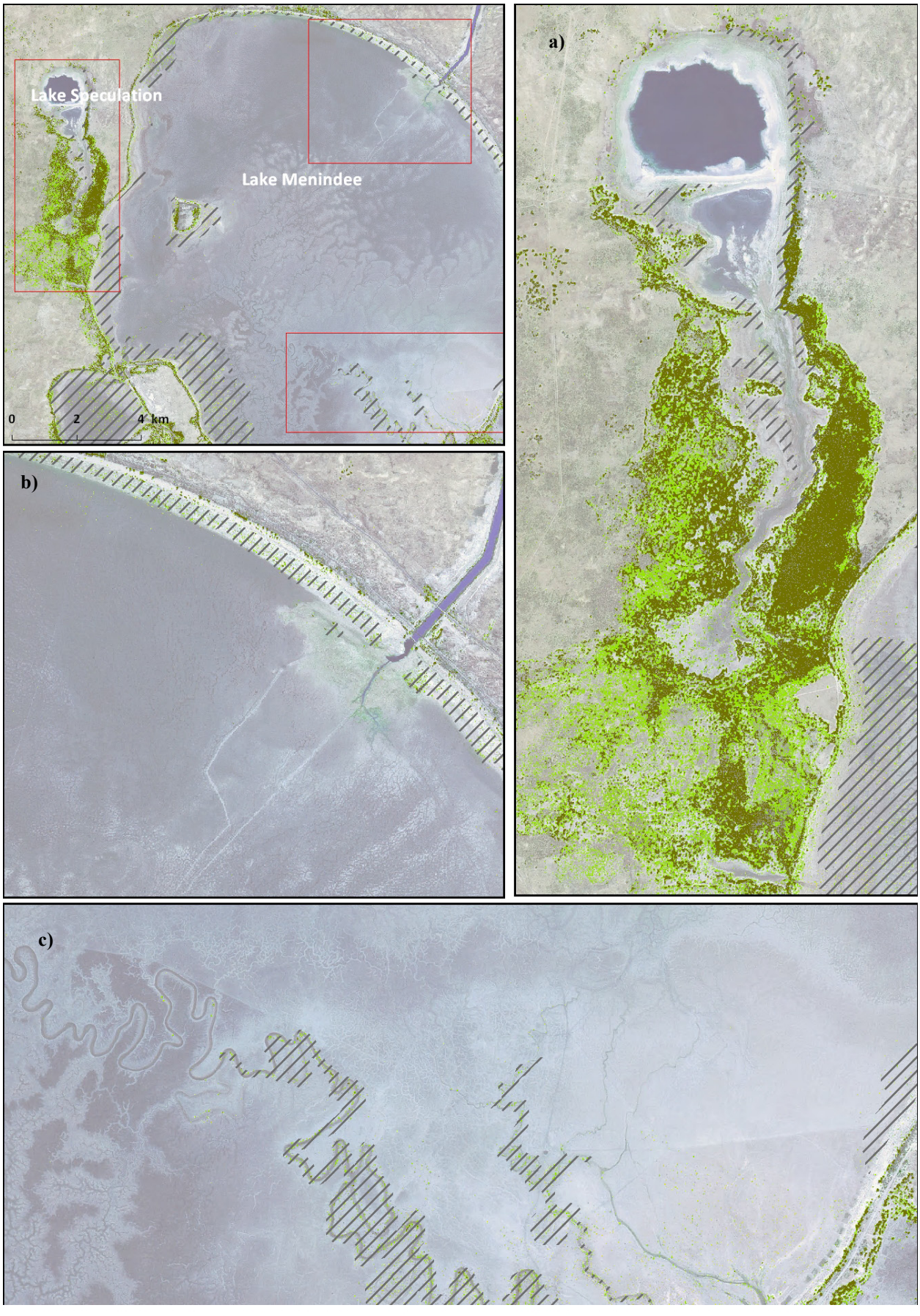

Figure 10-21. *2009 LiDAR vegetation structural mapping at Lake Menindee, including a) Lake Speculation, b) low-lying lake floor, and c) channel and delta.*

Post-regulation vegetation (2009)

By comparison, LiDAR derived vegetation structural mapping from 2009 detected very little woody vegetation on the lake floor (Figure 10-21), reflecting the impact of prolonged inundation caused by the lake regulation. Remnant vegetation, predominantly naturally lake-fringing and riparian zone vegetation, still exists (Figure 10-21). These trees appear to have been the most mature, well established and densely populated which might explain their persistence in the landscape. These trees were however reported to be dead in 2001 (Taylor-Wood *et al*., 2001). Currently existing fringing vegetation is but a remnant of pre-regulation communities, and as such is more aptly (and hereafter) referred to as 'artificially' fringing vegetation.

Drought behaviour

In 2009, Lake Menindee was artificially fringed by a combination of Black Box and River Red Gums open woodland or woodland with a small pocket of River Red Gums reportedly extending slightly onto the lake floor (Figure 10-22). A small stand of healthier fringing vegetation, exists in the northwest and western shoreline as indicated in Figure 10-22.

In general, lake floor vegetation was much more extensive in 1945 (prior to regulation) however much of this has since been killed due to prolonged inundation. Some vegetation recovery has occurred since lake levels receded in 2003, suggesting that in the absence of lake water, vegetation has access to an alternative water source. This is further confirmed by the ability of lake fringing and lake-floor vegetation to maintain, and is some cases improve condition by the end of the drought (Figure 10-23), coupled with minimal variation in condition throughout the drought (Figure 10-24).

Northern lake-fringing and lake-floor vegetation corresponds with a hole in the upper confining aquitard (Figure 10-25), resulting in inter-aquifer connectivity between the Calivil Formation aquifer and the shallow aquifer. Direct recharge processes are confirmed by hydrographic data at BHMAR23 bores (Figure 10-26). Extensive recharge via lake leakage has also resulted in a very shallow watertable (Figure 10-27). A number of smaller holes in the upper confining aquitard are present along the western shoreline of Lake Menindee (Figure 10-25). As was concluded elsewhere, maintained condition (Figure 10-23) with little variation (Figure 10-24), coupled with a shallow (~3 m) watertable (Figure 10-27), suggests vegetation fringing Lake Menindee to the west, appear to have utilised shallow groundwater resources during the drought.

The extent of lake-floor and lake-fringing vegetation is limited by regulation of Lake Menindee. As was the case with the commencement of regulation, prolonged inundation either results in severe stress to, or death of lake-floor and some lake-fringing vegetation dependent on lake-surcharge levels. In the absence of prolonged inundation, it is postulated that fringing vegetation would again expand across the lake floor in areas where the upper confining aquitard is absent and water levels are high. Current lake management practices however result in enhancement of natural shallow groundwater resources associated with lake leakage while still allowing for fringing vegetation to flourish outside of inundation events.

Black Box vegetation at Lake Speculation was also in relatively good condition in 2009, particularly those areas prone to flooding related to surcharging of Lake Menindee (Figure 10-22). Vegetation in closer proximity to Lake Speculation itself exhibited poorer condition, possibly due to salinisation of residual surface water via evaporation. When comparing open forest lake-fringing vegetation at Lake Menindee and Lake Speculation, condition during the drought was fairly similar. However, while the condition of fringing vegetation at Menindee remained constant at the conclusion of the drought, Lake Speculation open forest vegetation began to decline (Figure 10-23); this decline is most evident in vegetation to the south east of Lake Speculation. The high variability in condition throughout the drought (Figure 10-24) coupled with a declining condition (Figure 10-23) suggests vegetation is highly reliant on surface water, principally inundation, for maintenance of condition. Current lake management practices (i.e. more frequent inundation) may have thus resulted in expansion of open forest Black Box vegetation at Lake Speculation.

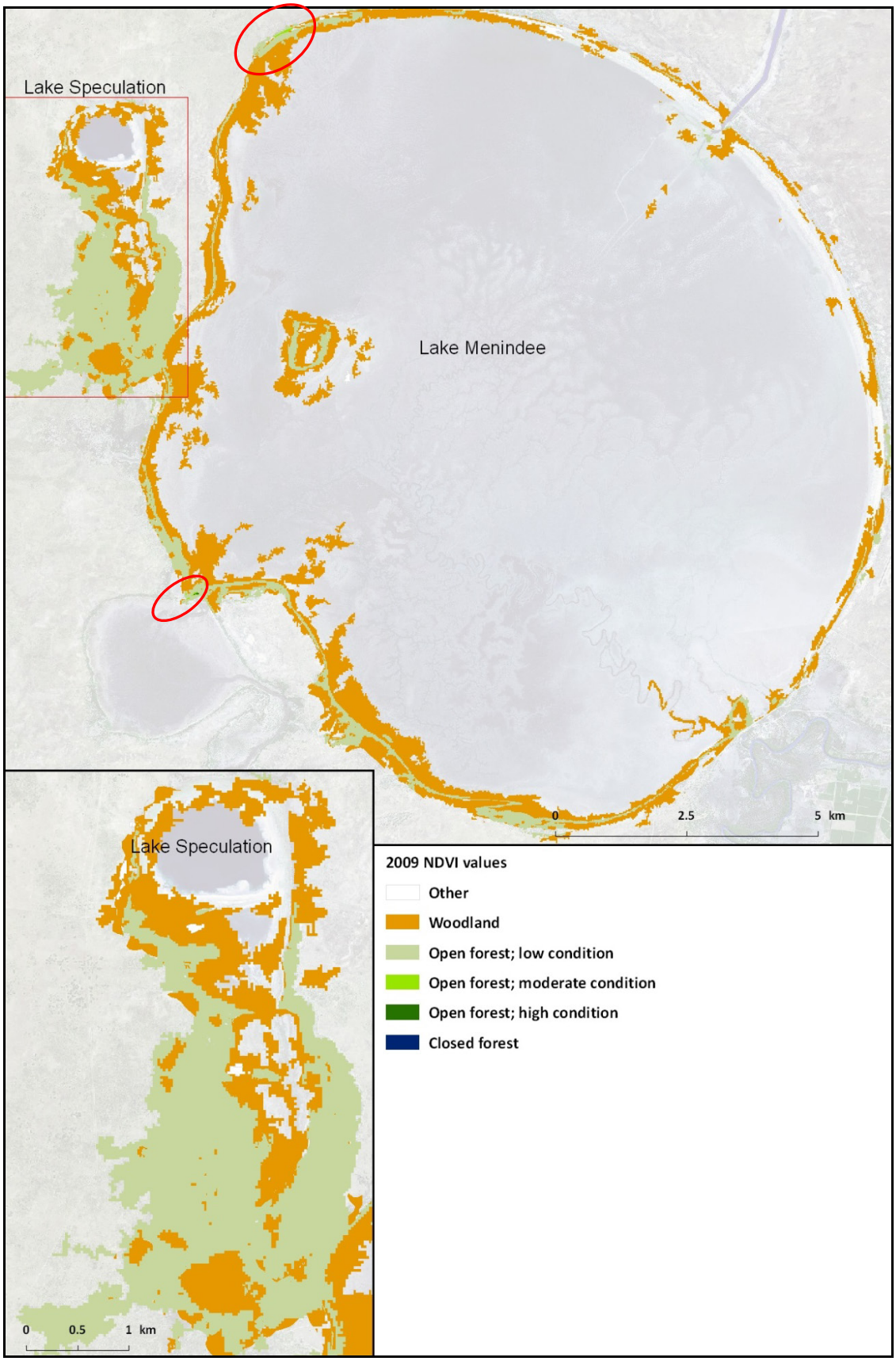

Figure 10-22. *NDVI values for lake-fringing woody vegetation in 2009. The majority of vegetation is either woodlands or open forest of low condition however two small stands of open forest of moderate condition are indicated by the red circles.*

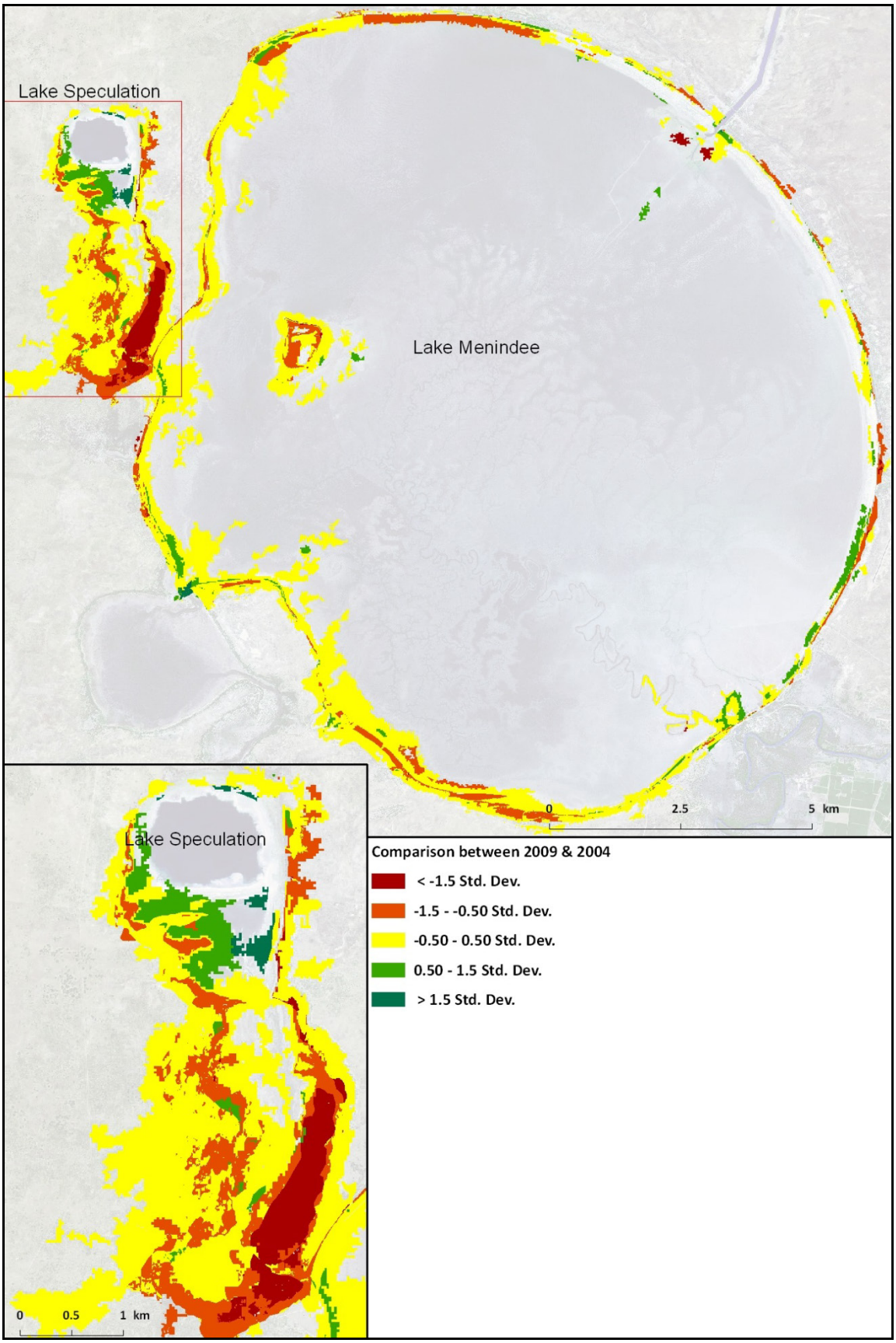

Figure 10-23. *Comparison between vegetation condition in 2009 with respect to 2004. Positive standard deviations (Std. Dev.) relate to an increase in condition with time, negative standard deviations relate to an decrease in condition with time and -0.5 to 0.5 standard deviations (shown in yellow) equate to effectively no (or minimal) change with time.*

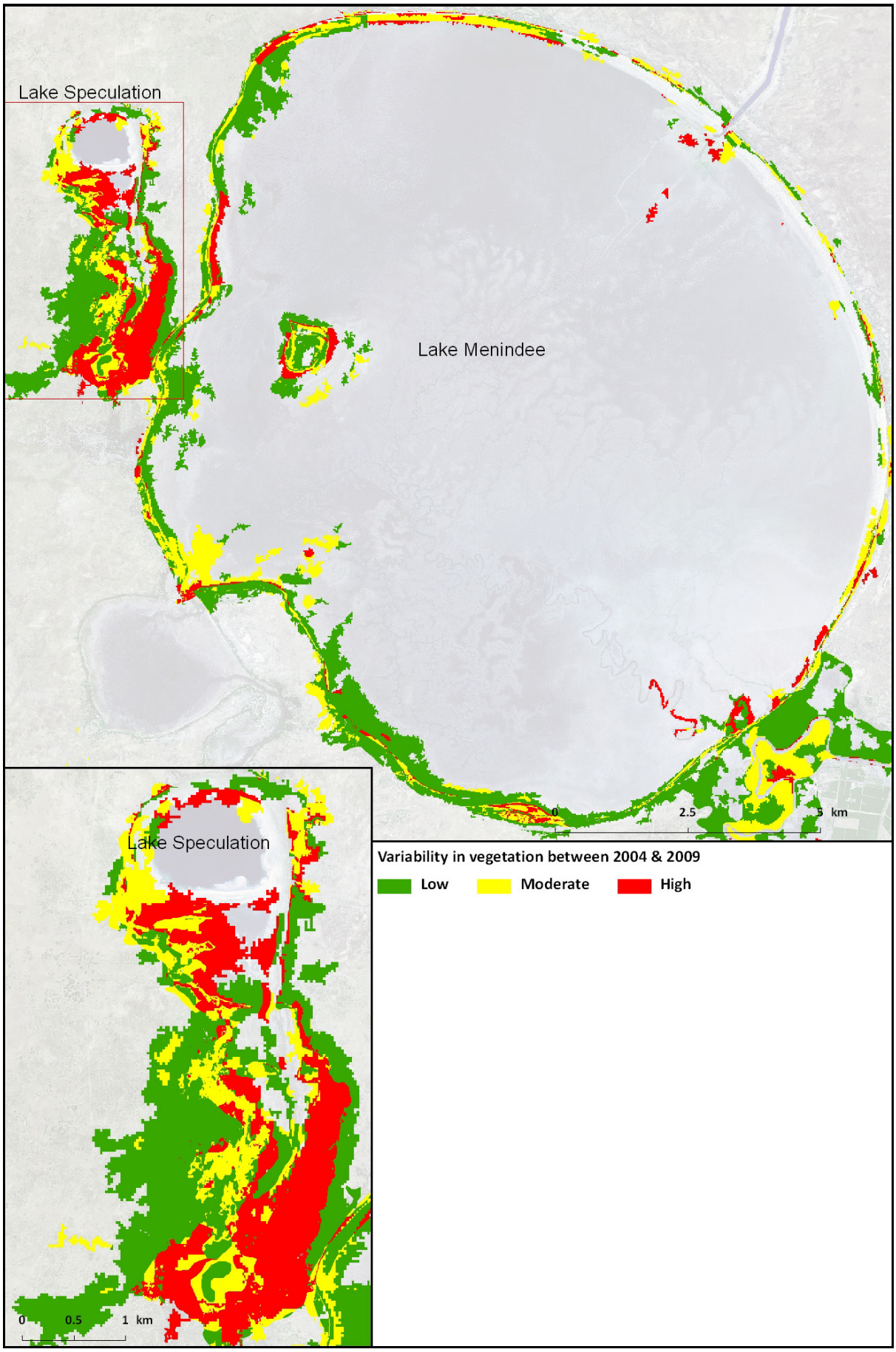

Figure 10-24. *Variability in lake-fringing vegetation condition during the drought (2004-2009).*

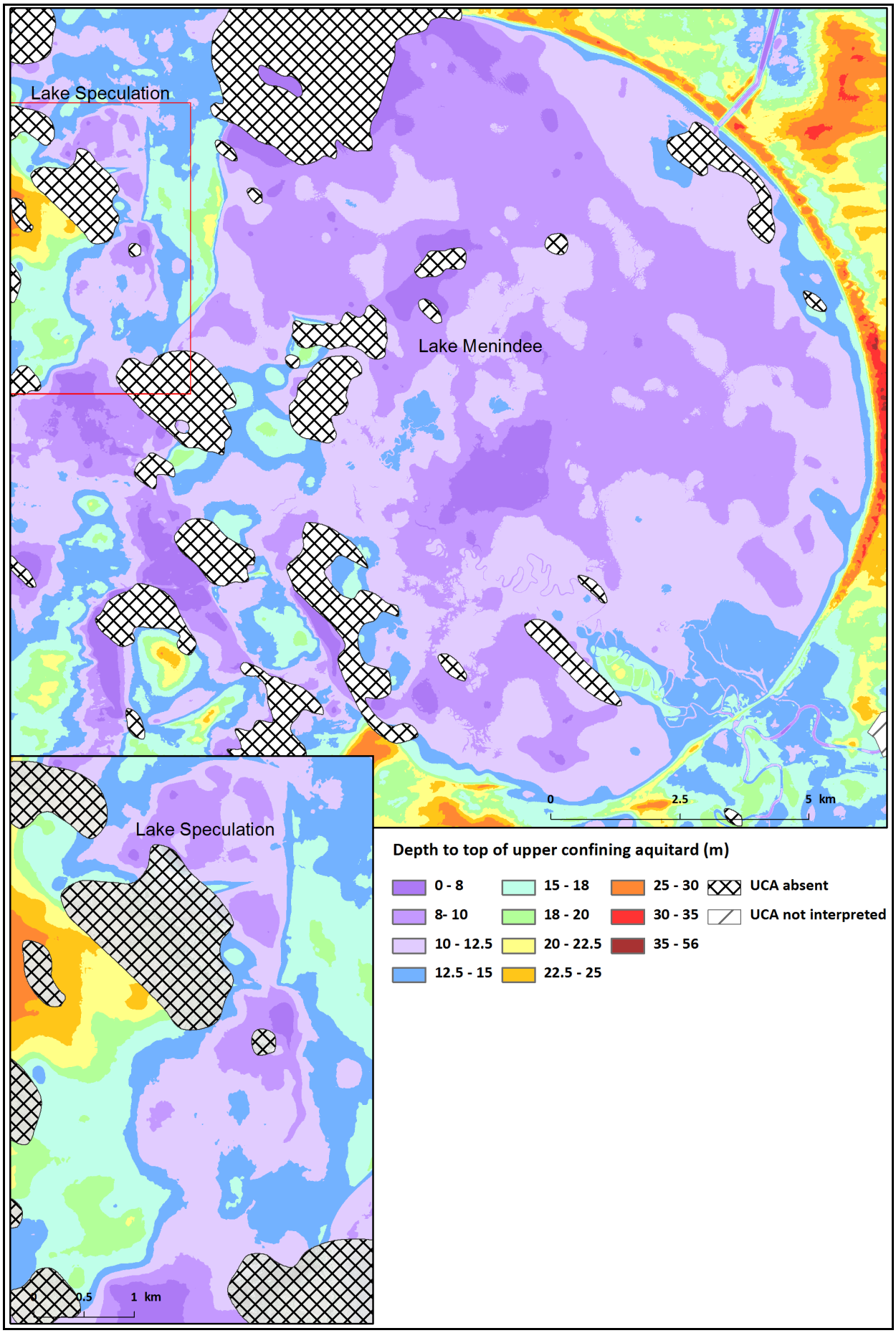

Figure 10-25. *Aquitard map, including depth to the top of the upper confining (UC) aquitard and interpreted holes.*

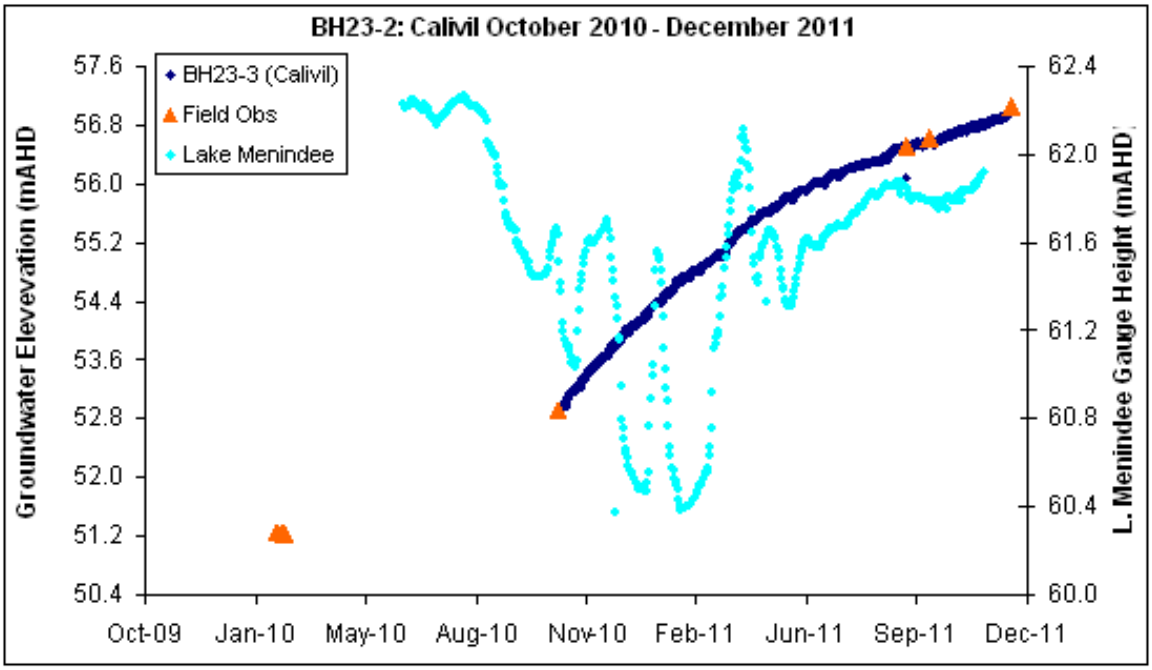

Figure 10-26. *Hydrographic response in the Calivil Formation aquifer at Lake Menindee. The dark blue crosses, labelled BH23-3 (Calivil) in the legend, are the hydrograph record from the down-hole logger (which records water-table depth at hourly intervals). The brown triangles are spot water-table measurements taken in the field. The pale blue crosses are the water level hydrograph from Lake Menindee indicating the timing and height of the flood event.*

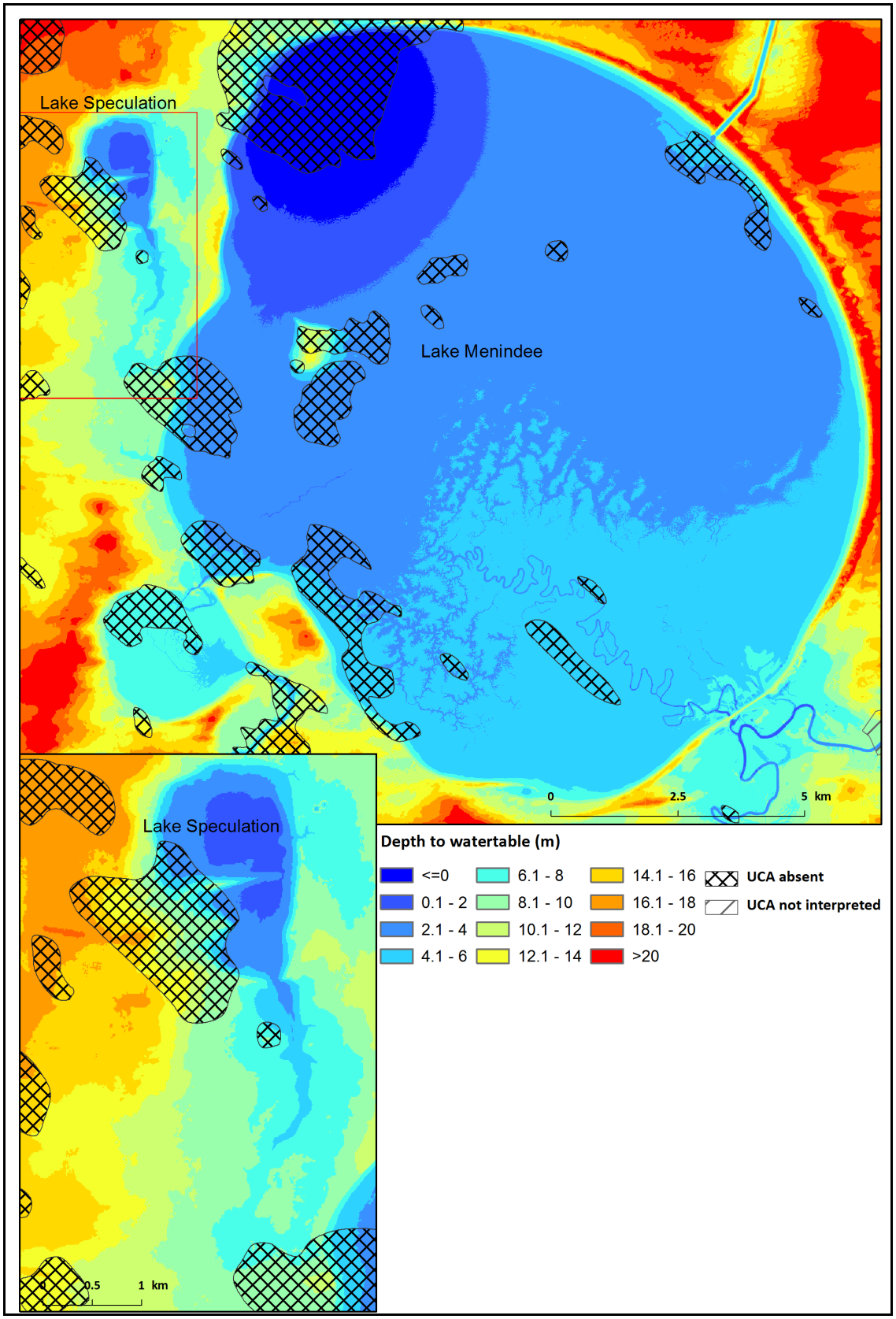

Figure 10-27. *Depth to watertable. This surface has been derived from the potentiometric surface of the surficial aquifer and topography. These values reflect the depth to which the rooting systems of vegetation must travel to encounter the watertable. Values of zero or less indicate the occurrence of groundwater discharge. Values greater than 20 m are likely to be beyond the reach of River Red Gums and Black Box in this landscape. Holes in the upper confining aquitard are also shown.*

In contrast, vegetation to the south west of Lake Speculation maintained condition between 2004 and 2009 (Figure 10-23) and showed minimal variation throughout the drought (Figure 10-24). Depth to the watertable and upper confining aquitard is slightly greater than at Lake Menindee (Figure 10-27 and Figure 10-25). A hole in the upper confining aquitard (Figure 10-25) suggests connectivity between the shallower and deeper aquifers. Vegetation may thus be able to access groundwater resources in both the shallow and deeper aquifers, potentially assisting in the maintenance of vegetation condition in the absence of other water sources.

10.4.1.3 Lake Cawndilla

Physical characteristics

Lake Cawndilla has a more regular dish-shaped lake-floor topography (Figure 10-28) and lower lake floor elevation in comparison to Lake Menindee, hence acted as a residual pool for floods into Lake Menindee. Under these conditions, the opportunity for woody vegetation to become established was limited, as reported by Taylor-Wood *et al*. (2001) and Kingsford (2000), and evidenced by the general lack of lake-floor vegetation in the 1945 aerial photography (Figure 10-30).

Pre-regulation vegetation

Unlike Lake Menindee, under natural conditions Lake Cawndilla only had a very narrow band of fringing Black Box vegetation that transitioned from an open forest community on the north-west fringe, through to isolated trees in an anti-clockwise direction around the lake (Figure 10-29). It is postulated that the relative steepness of the banks of Lake Cawndilla (Figure 10-28) in contrast to other lakes, may have limited the distribution of woodland vegetation. As already mentioned, the lake floor lacked vegetation due to the presence of residual (possibly saline) pools.

Post-regulation condition

Some of the natural lake-fringing vegetation has since been killed due to inundation. A new lake-fringe has developed and supports a narrow band of remnant Black Box vegetation more abundant on the western shoreline (Figure 10-30). Further expansion of fringing vegetation extent (even with lowered lake levels) is unlikely due to the steep lake shore.

Drought behaviour

In 2009 Lake Cawndilla was characterised by a very narrow band of fringing vegetation (Figure 10-31). With few exceptions, this vegetation community was composed of open woodland/woodland vegetation. Open forest vegetation of low condition is concentrated around Spectacle Lakes and along Cawndilla Channel that connects Lake Menindee to Lake Cawndilla (Figure 10-31). Additionally, vegetation immediately adjacent to the lake floor at Spectacle Lakes was in poorer condition in 2009, possibly due to salinisation of residual surface water. A similar spatial distribution of vegetation was observed at Lake Speculation.

When comparing 2009 (end of the drought) with 2004 (early in the drought), quite a range of trends are observed (Figure 10-32). While the fringing vegetation at Lake Cawndilla either exhibited an increase in condition or minimal change, the condition of vegetation around Spectacle Lakes significantly declined (Figure 10-32). Combined with a large amount of variability in condition throughout the drought (Figure 10-33), these trends suggest that the presence of surface water is important for the maintenance of vegetation condition.

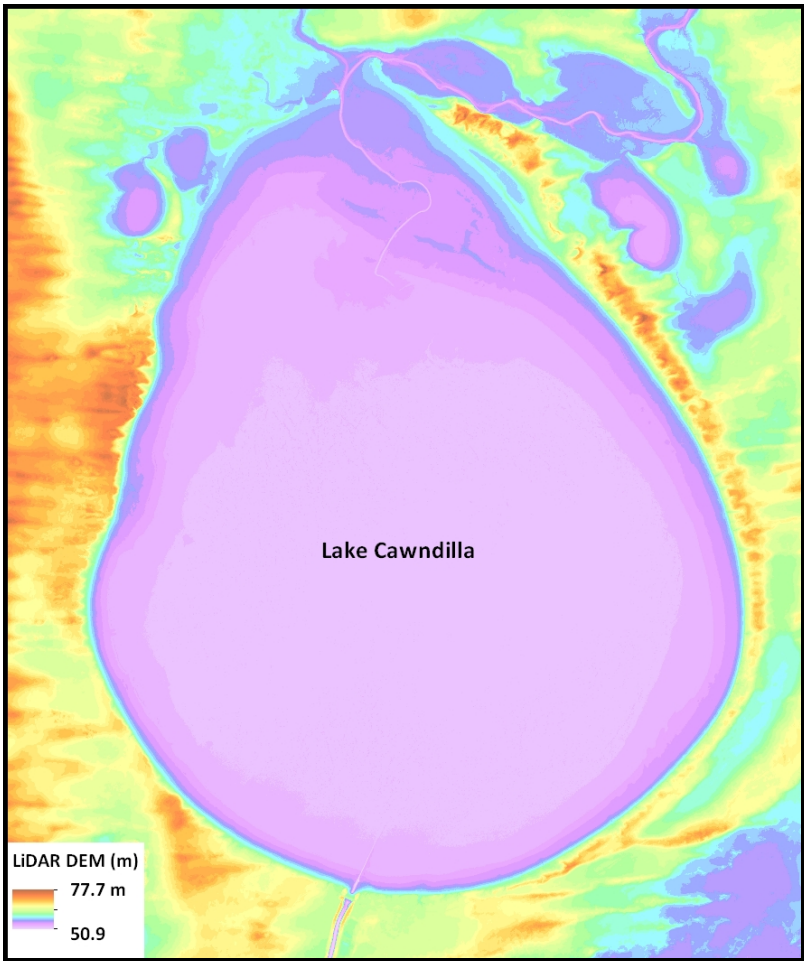

Figure 10-28. *Lake Cawndilla LiDAR DEM. Note the dish-shaped lake floor topography.*

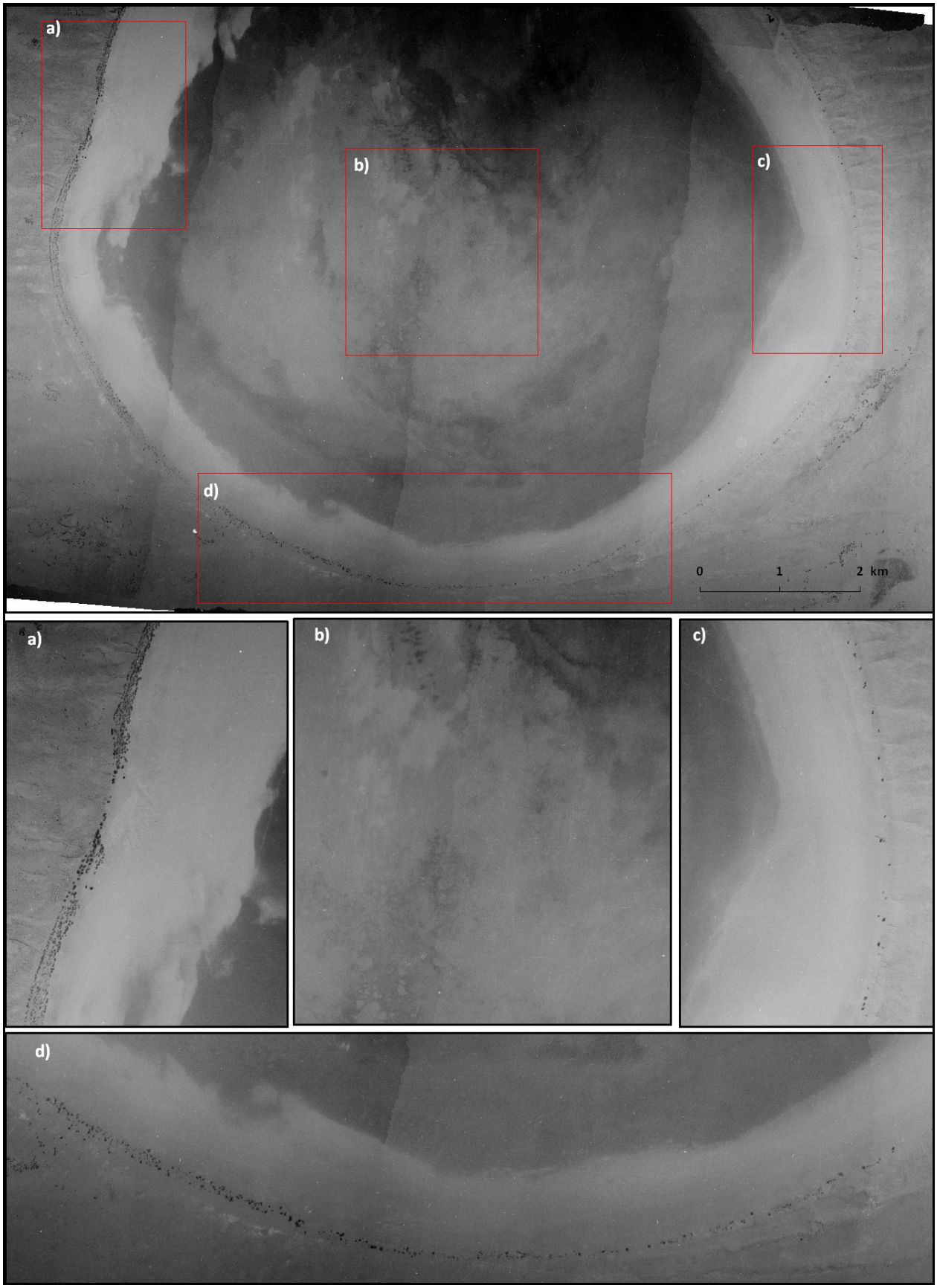

Figure 10-29. *1945 aerial photograph at Lake Cawndilla, including a) open forest, b) bare lake floor, c) woodland/open woodland and d) isolated trees.*

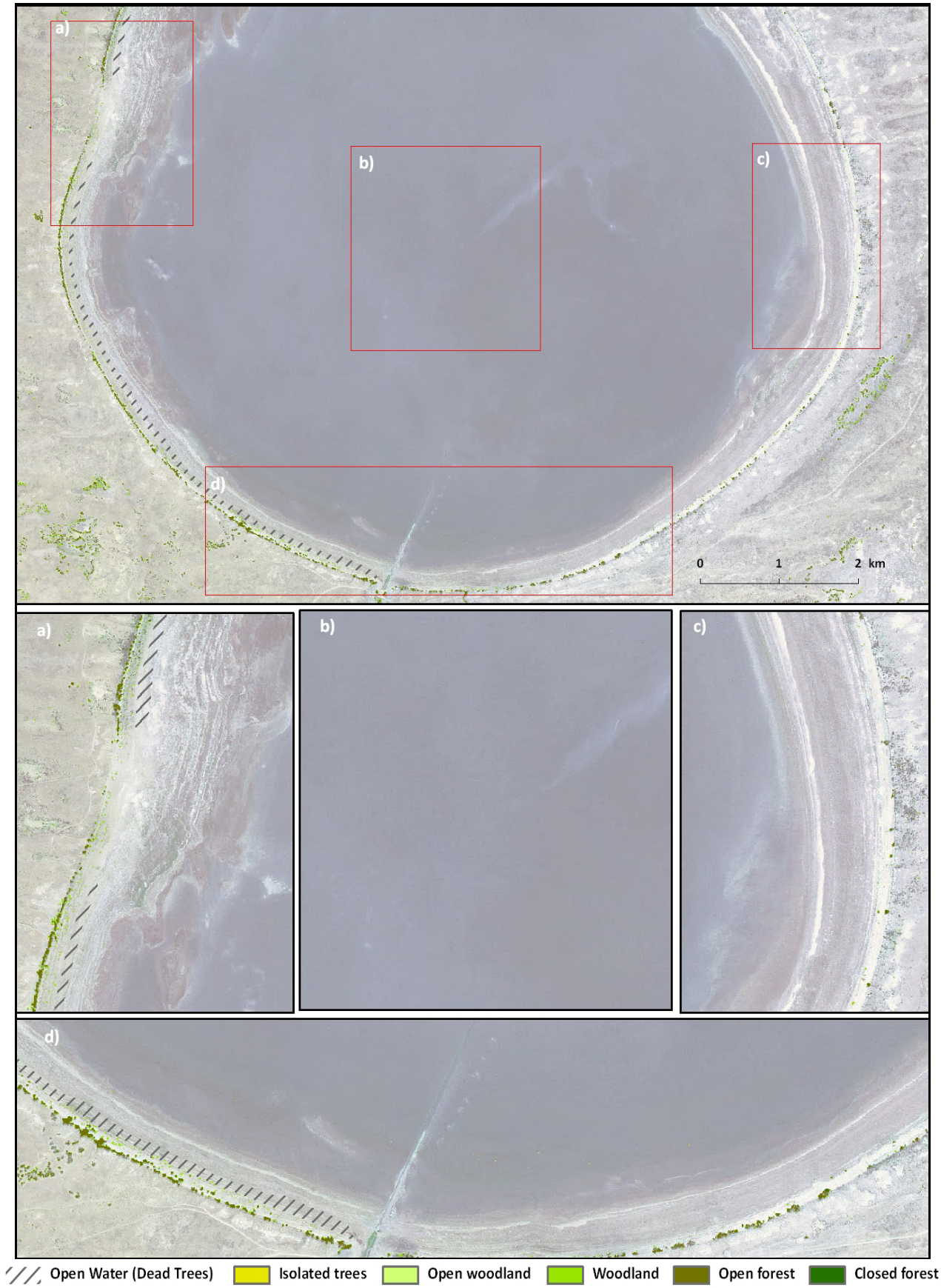

Figure 10-30. *2009 LiDAR vegetation structural mapping at Lake Cawndilla, including a) open forest, b) bare lake floor, c) woodland/open woodland and d) isolated trees.*

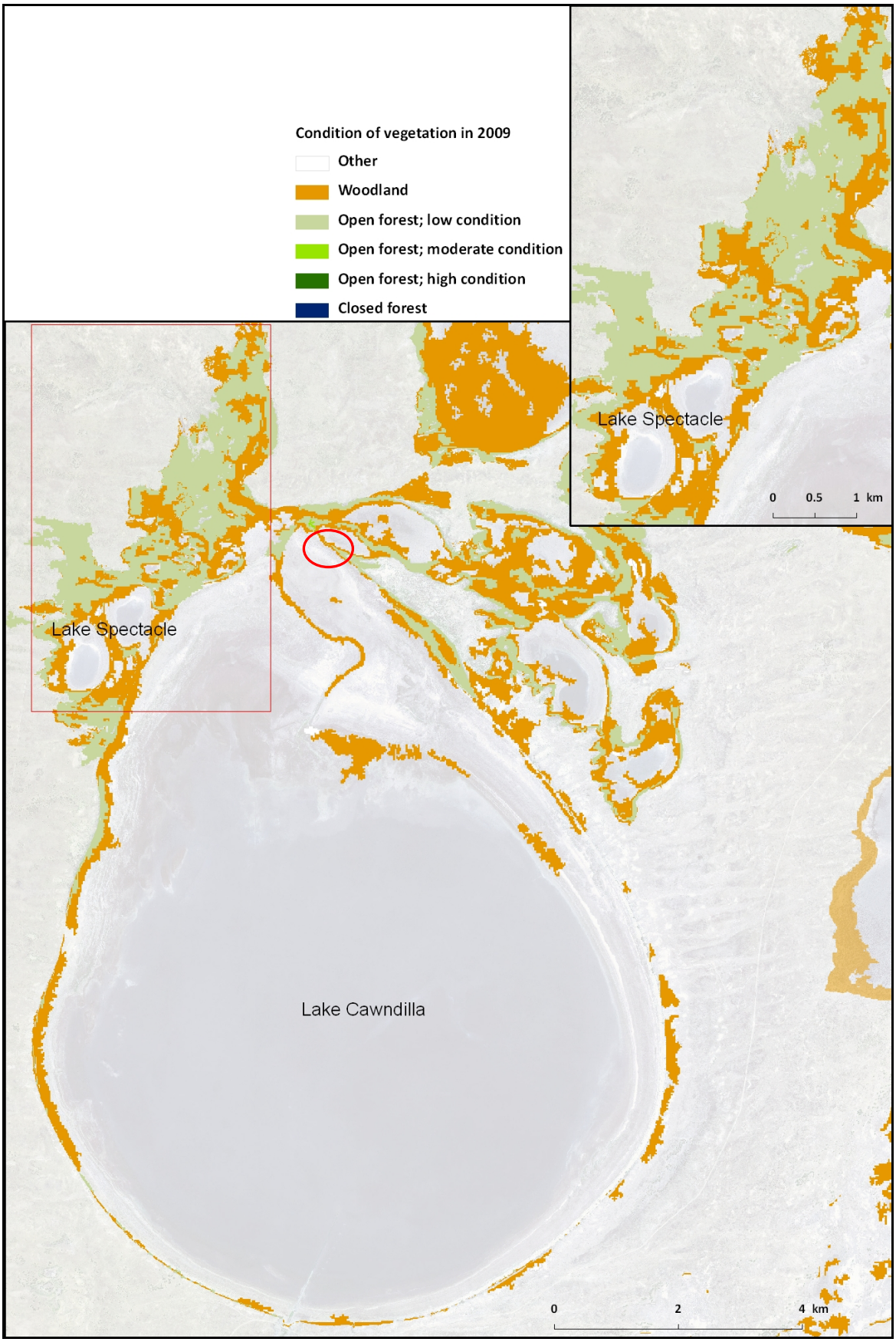

Figure 10-31. *NDVI values for lake-fringing woody vegetation in 2009. The majority of vegetation is either woodlands or open forest of low condition however two small stands of open forest of moderate condition are indicated by the red circles.*

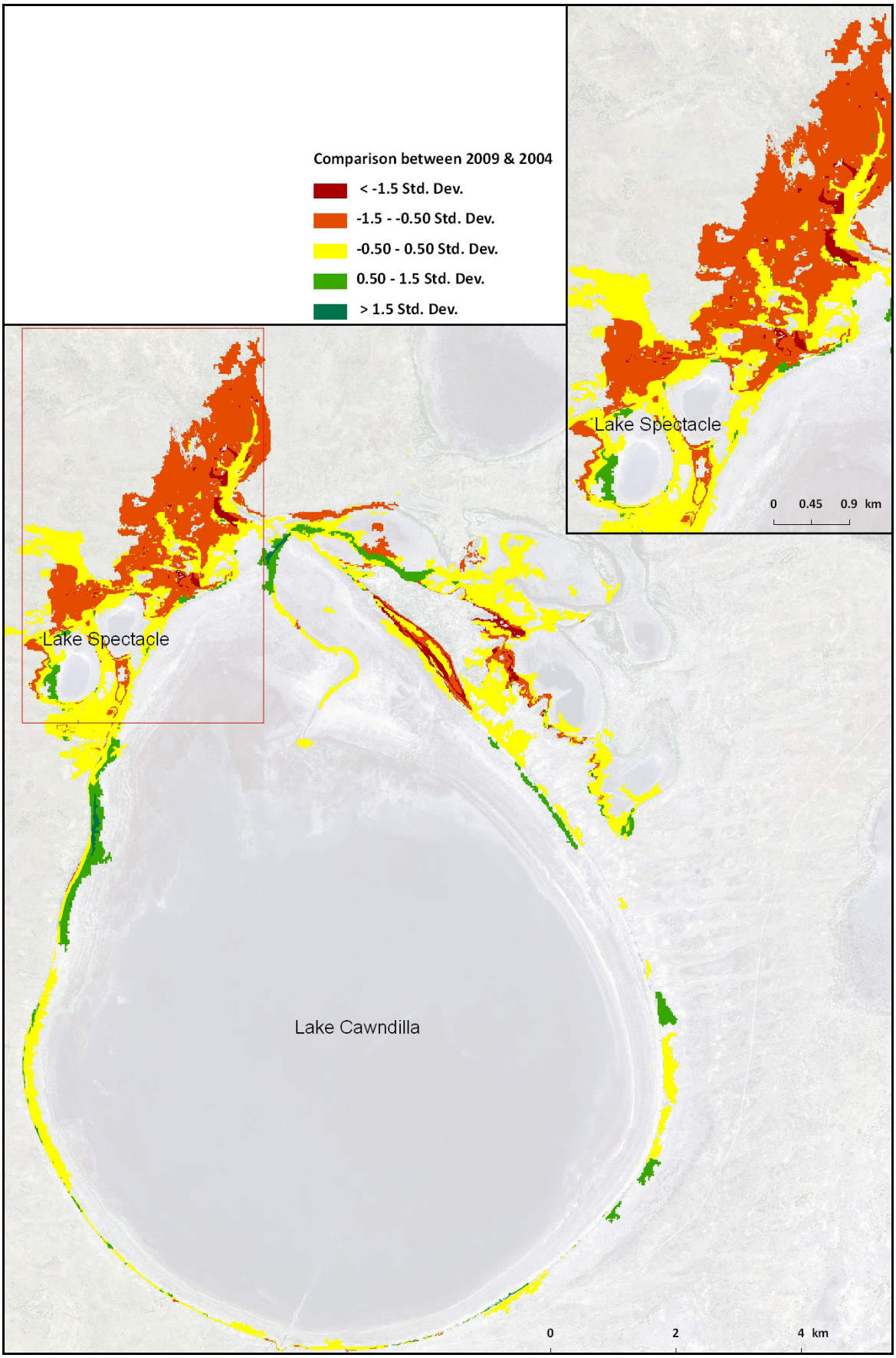

Figure 10-32. *Comparison between vegetation condition in 2009 with respect to 2004. Positive standard deviations (Std. Dev.) relate to an increase in condition with time, negative standard deviations relate to an decrease in condition with time and -0.5 to 0.5 standard deviations (shown in yellow) equate to effectively no (or minimal) change with time.*

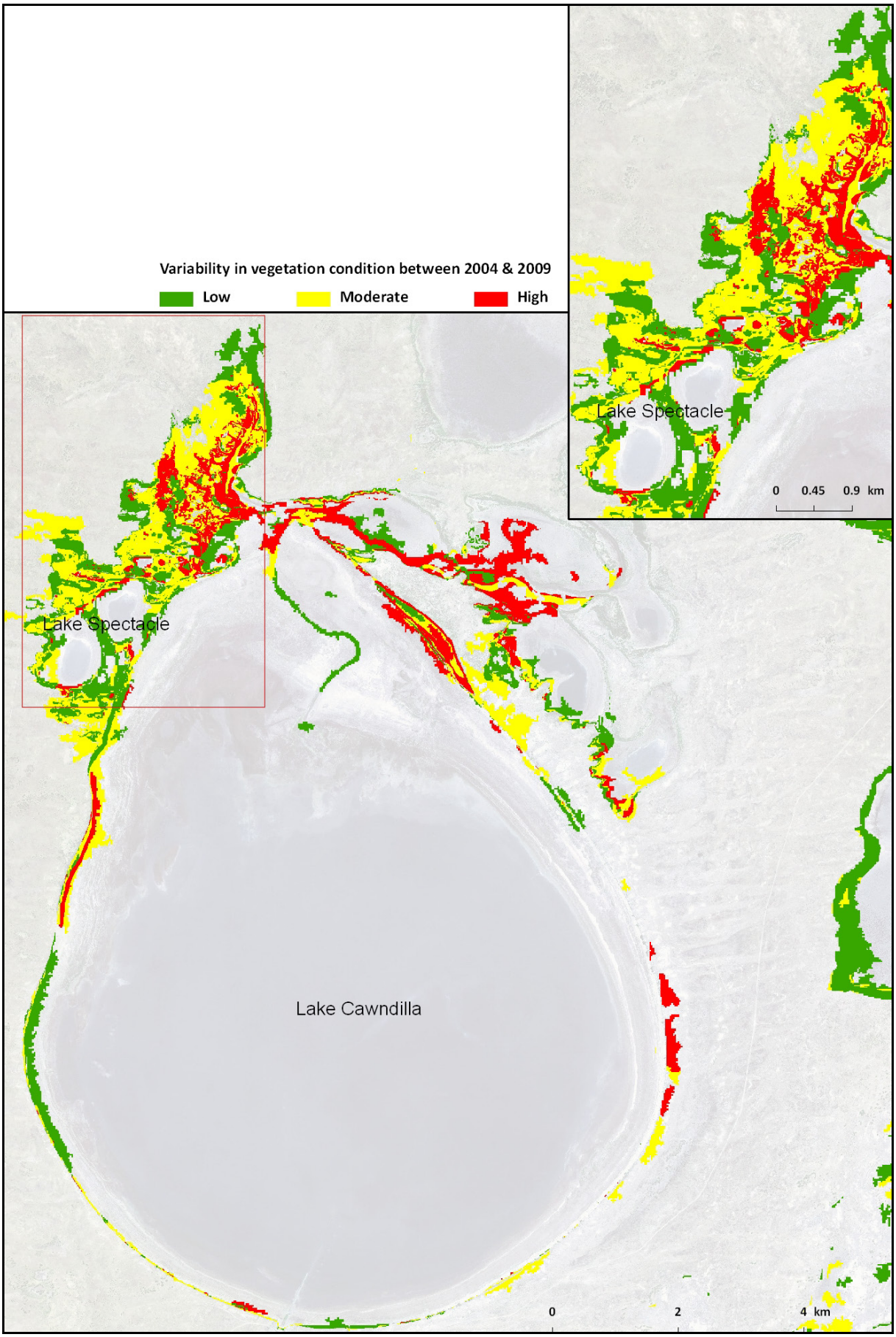

Figure 10-33. *Variability in lake-fringing vegetation condition during the drought (2004-2009).*

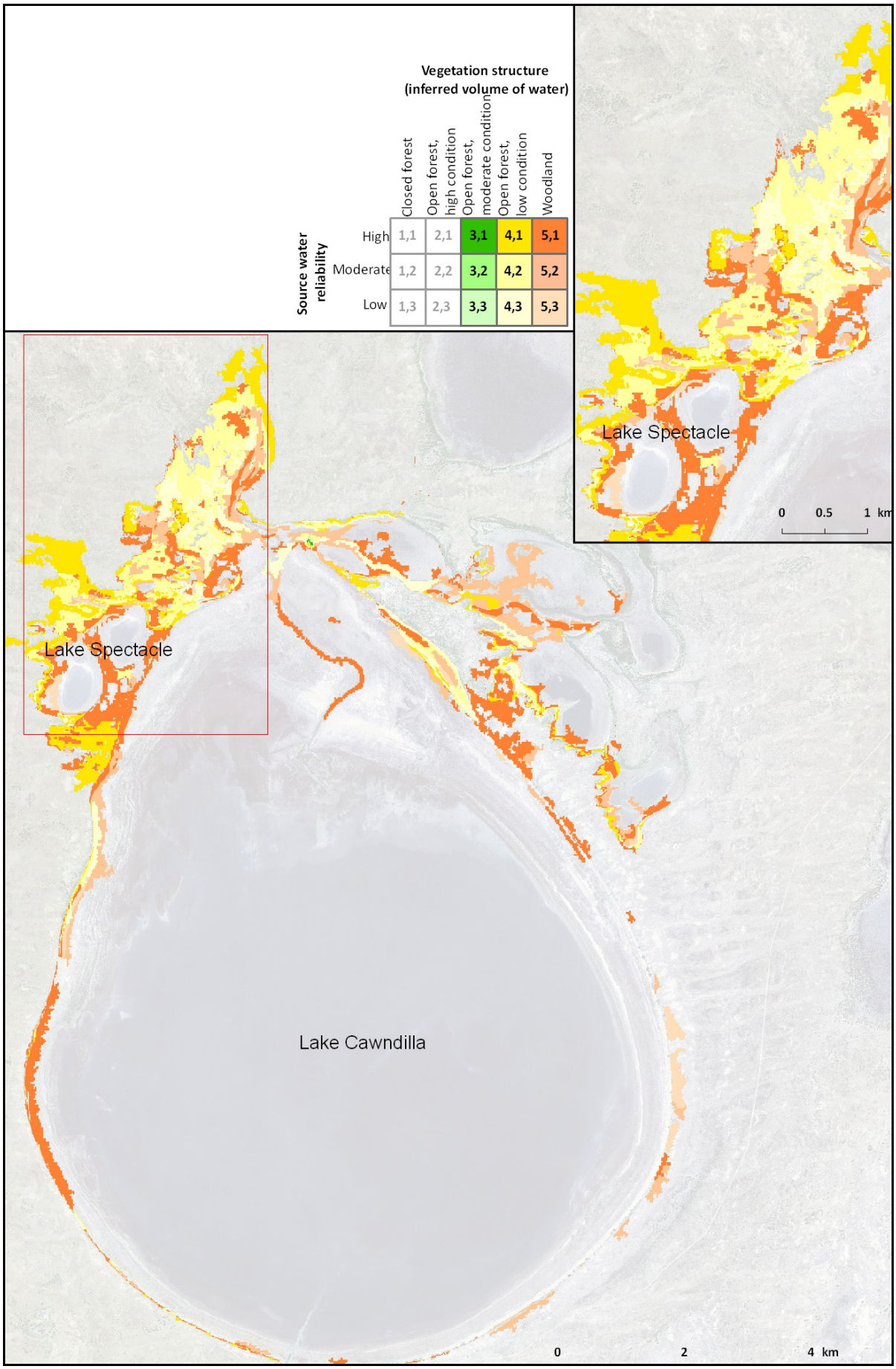

Figure 10-34. *Relative reliance of lake-fringing woody vegetation on groundwater and surface water.*

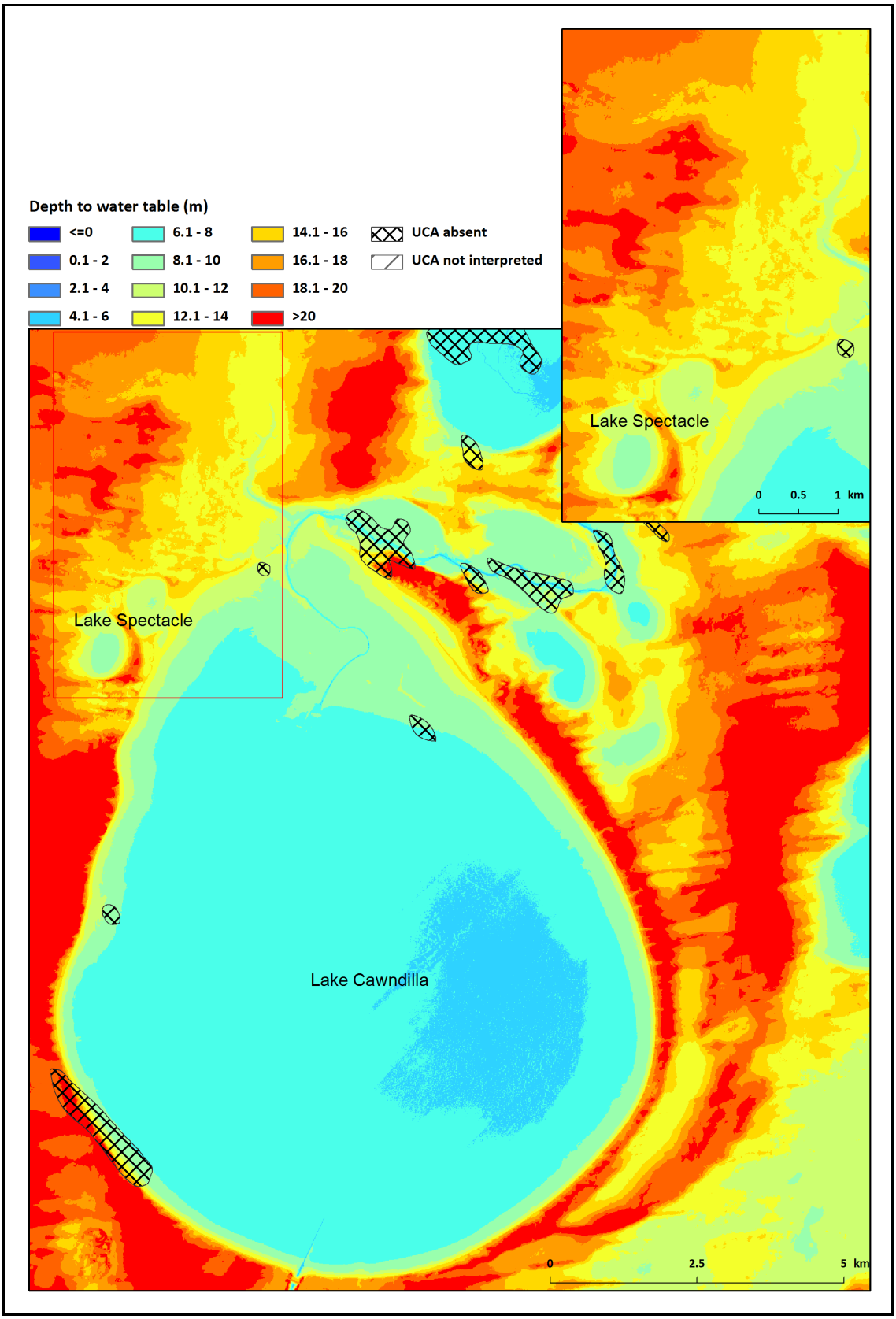

Figure 10-35. *Depth to watertable. This surface has been derived from the potentiometric surface of the surficial aquifer and topography. These values reflect the depth to which the rooting systems of vegetation must travel to encounter the watertable. Values of zero or less indicate the occurrence of groundwater discharge. Values greater than 20 m are likely to be beyond the reach of River Red Gums and Black Box in this landscape. Holes in the upper confining aquitard are also shown.*

10.4.1.4 Lake Pamamaroo

Physical characteristics

Lake Pamamaroo, under the natural pre-regulation regime had simpler lake floor topography than Lake Menindee and probably a simpler flooding regime. There is a large delta evident at the natural inlet/outlet in the south east (Figure 10-36) and box/lignum ecosystem is widespread on the lake floor (Figure 10-38). This strongly suggests that the inlet/outlet channel sill level was relatively low resulting in recession of water out of the lake after the flood peak passed.

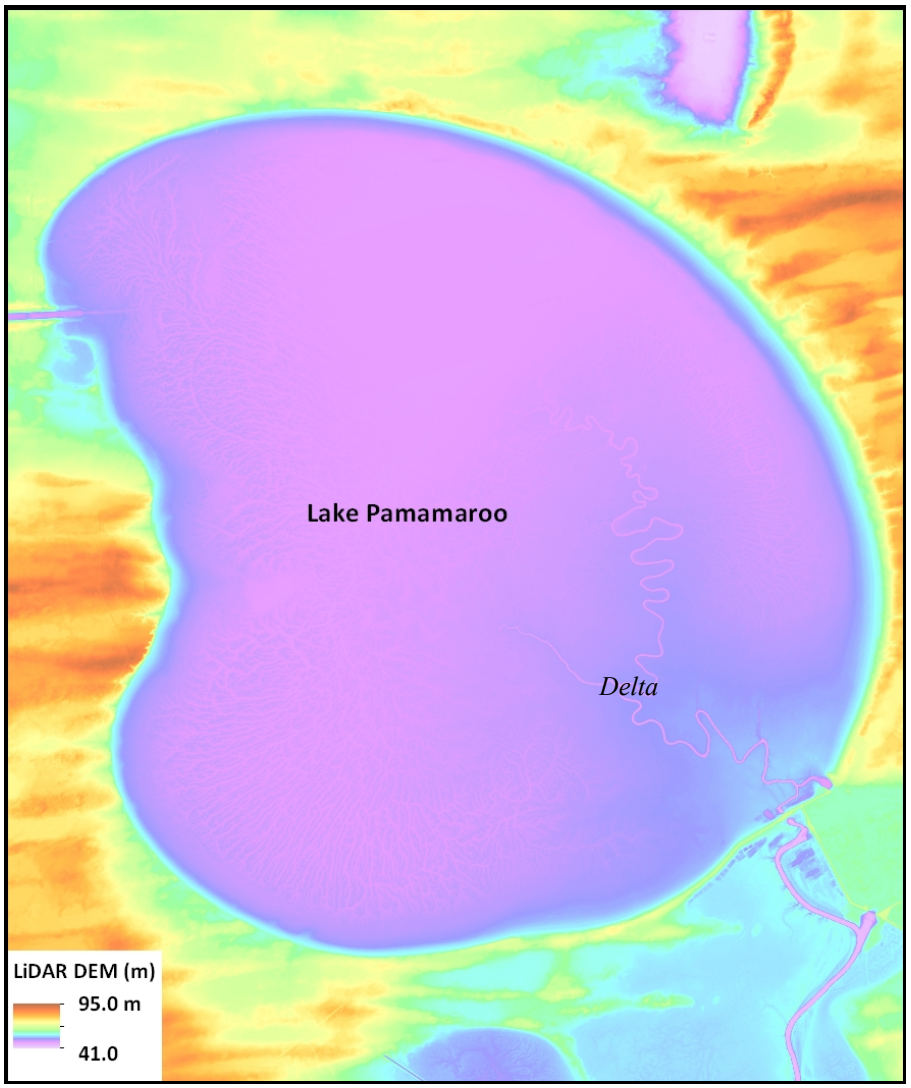

Figure 10-36. *Lake Pamamaroo LiDAR DEM. Note the delta on the lake floor where the Darling River flows into Lake Pamamaroo*

Pre-regulation vegetation

Extensive, well-established fringing woody vegetation is evident in the 1945 (pre-regulation) aerial photography as is the widespread lake-floor box/lignum ecosystem (Figure 10-38). Fringing vegetation reached a maximum width of approximately 1.5 km with several fingers of trees extending further into the lake (to approximately 3 km from the bank).

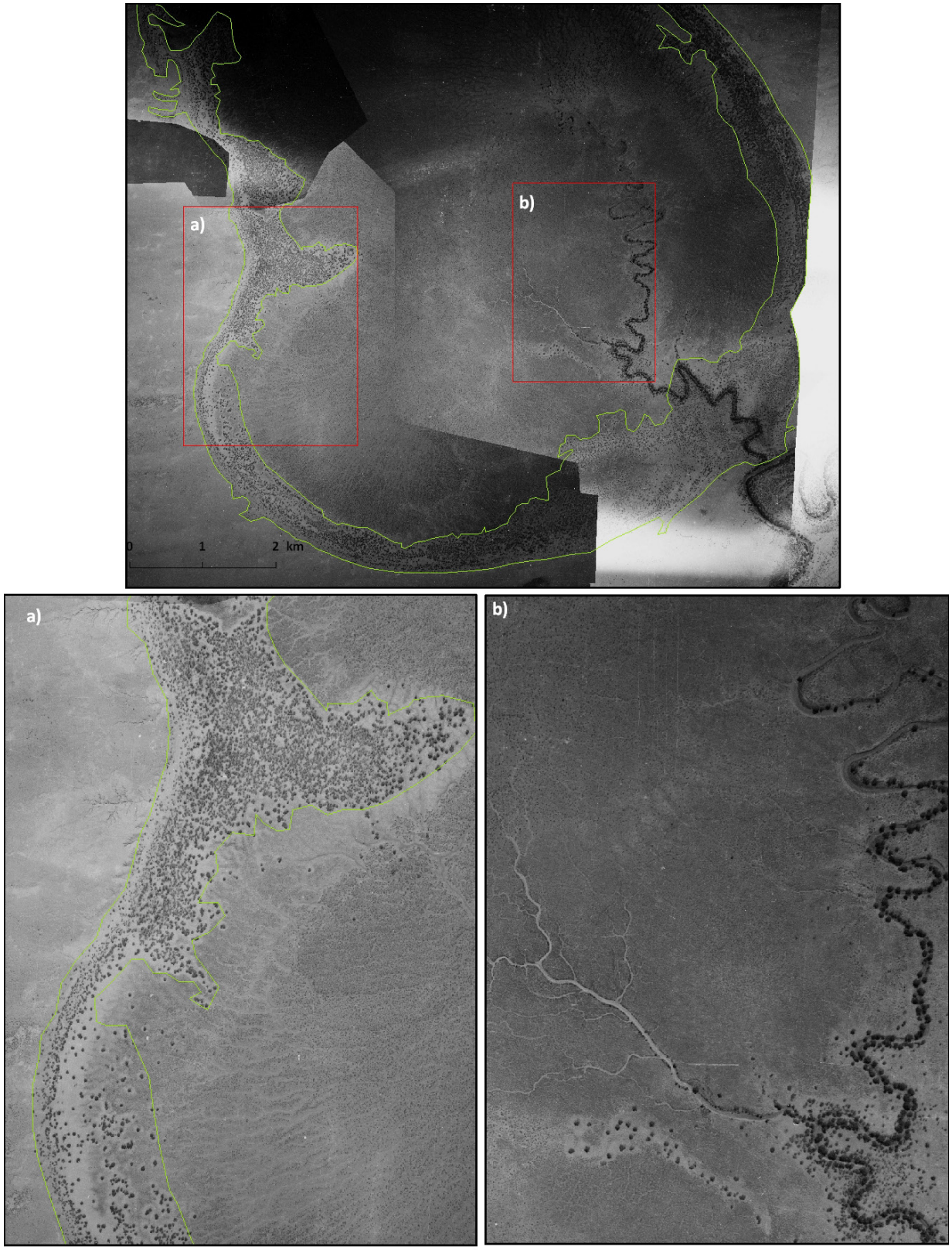

Figure 10-37. *1945 aerial photograph at Lake Menindee, including a) Lake Speculation, b) low-lying lake floor, and c) channel and delta. Green linework denotes lake-fringing vegetation.*

Post-regulation condition

Since regulation, these naturally occurring lake-fringing vegetation has been subject to (semi) permanent inundation and consequently died (Figure 10-38; Taylor-Wood *et al*., 2001). Current artificially fringing vegetation is but a remnant of pre-regulation vegetation stands and consists of a mix of both River Red Gum and Black Box (Taylor-Wood *et al*., 2001).

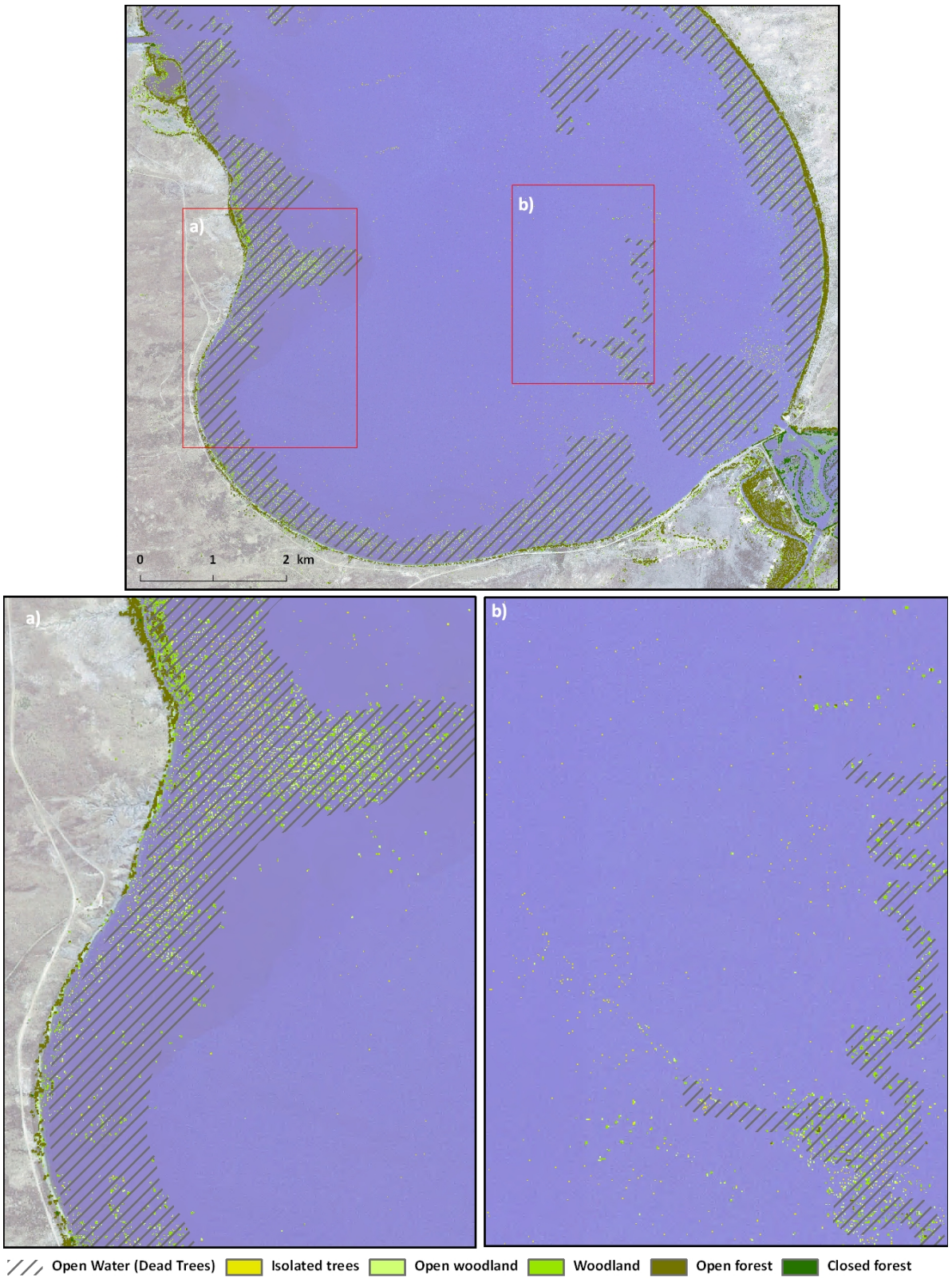

Figure 10-38. *1945 aerial photography and 2009 LiDAR vegetation structural mapping at Lake Pamamaroo, including a) dead naturally occurring fringing vegetation and remnant artificially fringing vegetation, b) isolated woody vegetation on the lake-floor including dead trees along the channel.*

Drought summary

Analysis of fringing vegetation during the drought was not possible and this lake as it was subject to inundation throughout the drought period.

10.4.1.5 Lake Wetherell (and Lake Tandure)

Physical characteristics

As part of the Menindee Lakes water storage scheme, Main Weir was constructed to control flows continuing down the Darling River and into Lake Pamamaroo. As a consequence of this infrastructure, Lake Wetherell was created by the ponding of water behind Main Weir, artificially joining (from north to south) Lakes Malta, Balaka, Bijiji and Tandure (Figure 10-39). Under normal (non-flood) conditions, Lakes Wetherell and Tandure contain water while under extreme flood conditions (e.g. 1990 flood), surface water can extent as far as Lake Malta. During drought conditions, water is typically maintained in Lakes Pamamaroo and Wetherell (and Tandure); in the event of small inflows during drought conditions, these lakes are surcharged in favour of releasing water to Lakes Menindee and Cawndilla. Consequently fresh surface water resources are constantly available for use by vegetation at both Lakes Wetherell and Tandure.

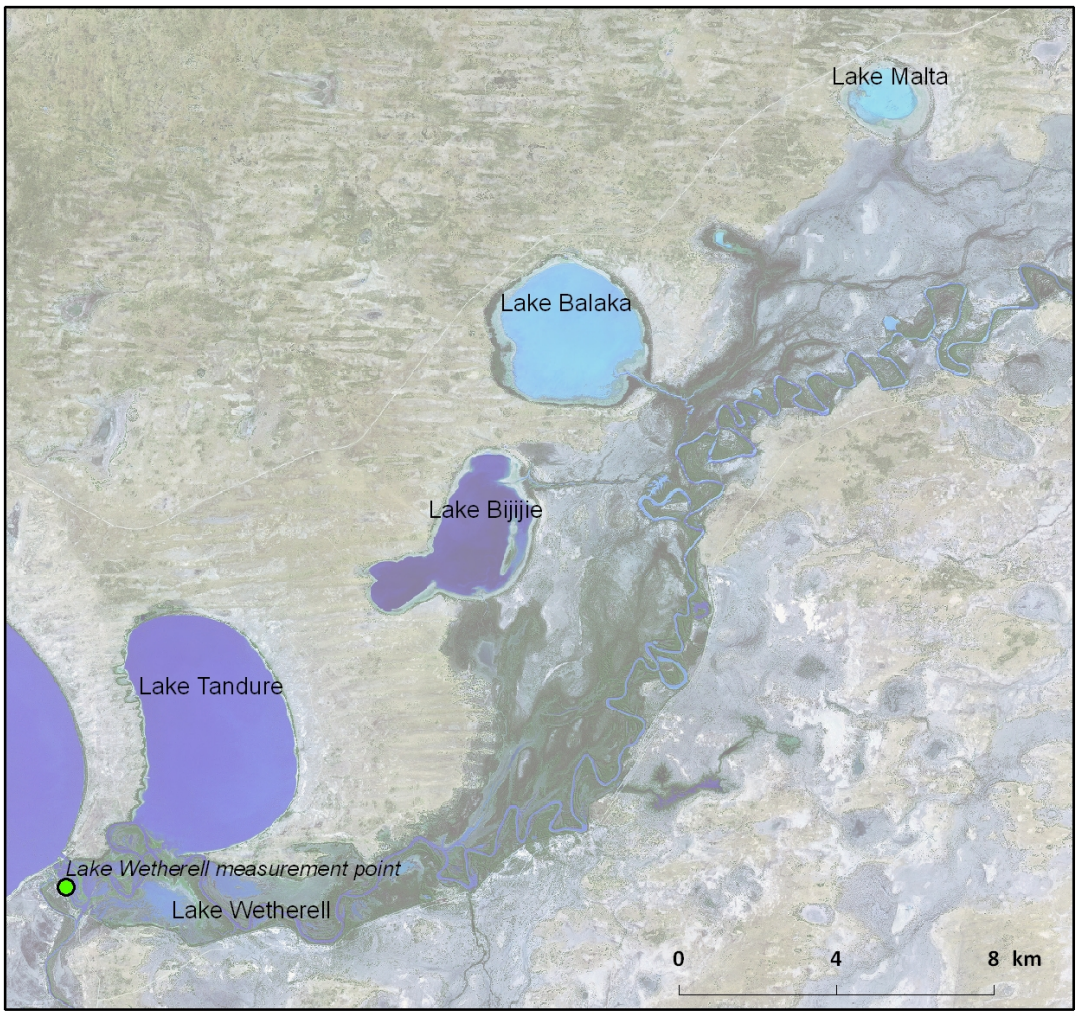

Figure 10-39. *Location of Lake Wetherell in relation to Lakes Tandure, Bijiji, Balaka and Malta, all of which can be joined during high flood events.*

Pre-regulation vegetation

No aerial photography was available for these lakes.

Post-regulation condition

Similar to Lake Pamamaroo, vegetation/habitat mapping indicates that a substantial portion of fringing/lake-floor vegetation has died at Lake Tandure due to prolonged inundation (Figure 10-40). There are also similar pockets of dead vegetation in Lake Wetherell. River Red Gums dominate the Darling River scroll plain upstream of the permanently inundated area of Lake Wetherell. Only small pockets of Black Box vegetation grow in this region, mostly located on the less frequently inundated floodplain.

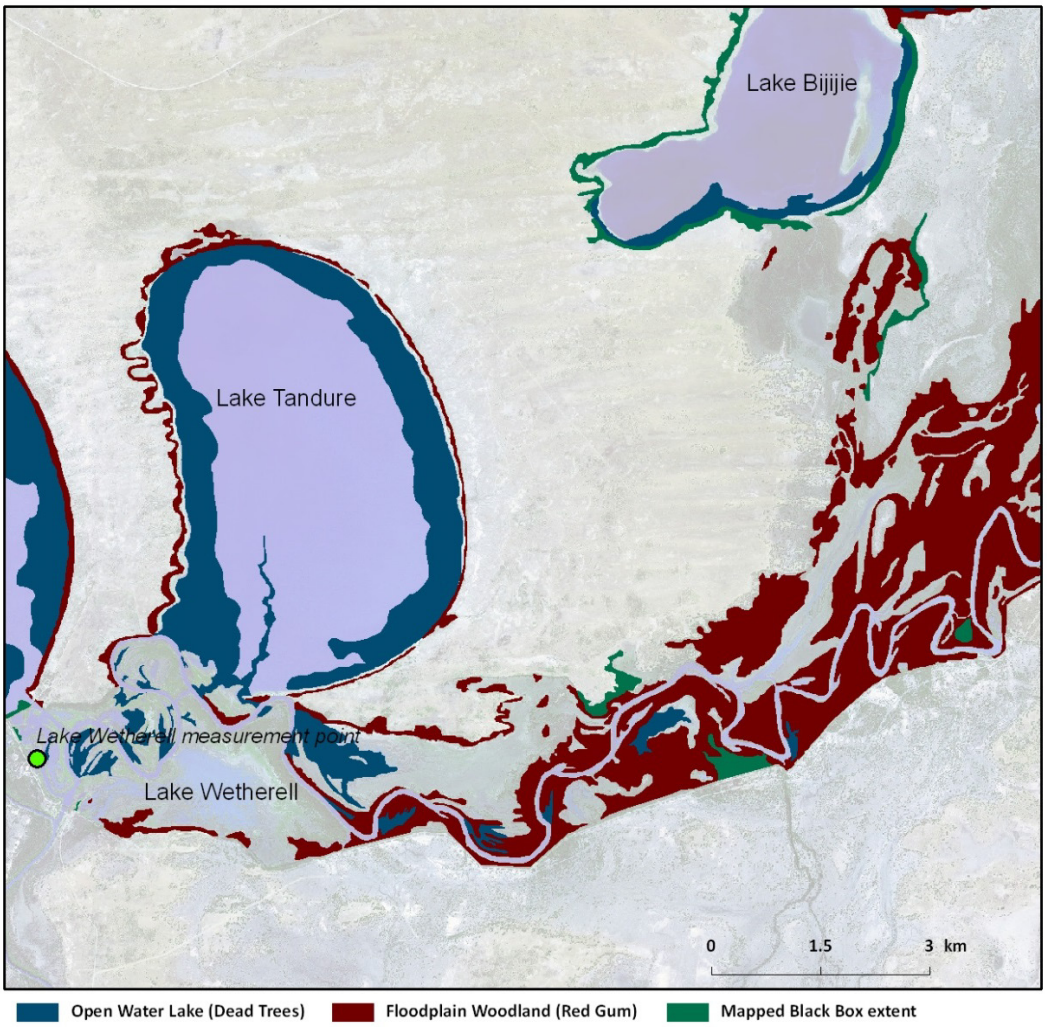

Figure 10-40. *Vegetation/habitat mapping in associated with Lakes Wetherell and Tandure (Taylor-Wood et al., 2001).*

10.4.1.6 Lake Tandou

Physical characteristics

Lake Tandou also has a relatively simple dish-shaped floor and little indication of the development of southern inlet/outlet (Figure 10-41). It seems likely that under natural conditions, the sill level in the inlet/outlet channel was relatively high suggesting inundation was not frequent but once water entered Lake Tandou, it likely remained after recession of the flood peak in the river, precluding box/lignum from all but a fringing zone.

Pre-regulation vegetation

While minimal woody vegetation appears to have grown on the lake floor in 1945, a well-established band of fringing vegetation is apparent both on the western and eastern foreshore. Vegetation is also observed to have extended onto the adjacent lunette (Figure 10-42).

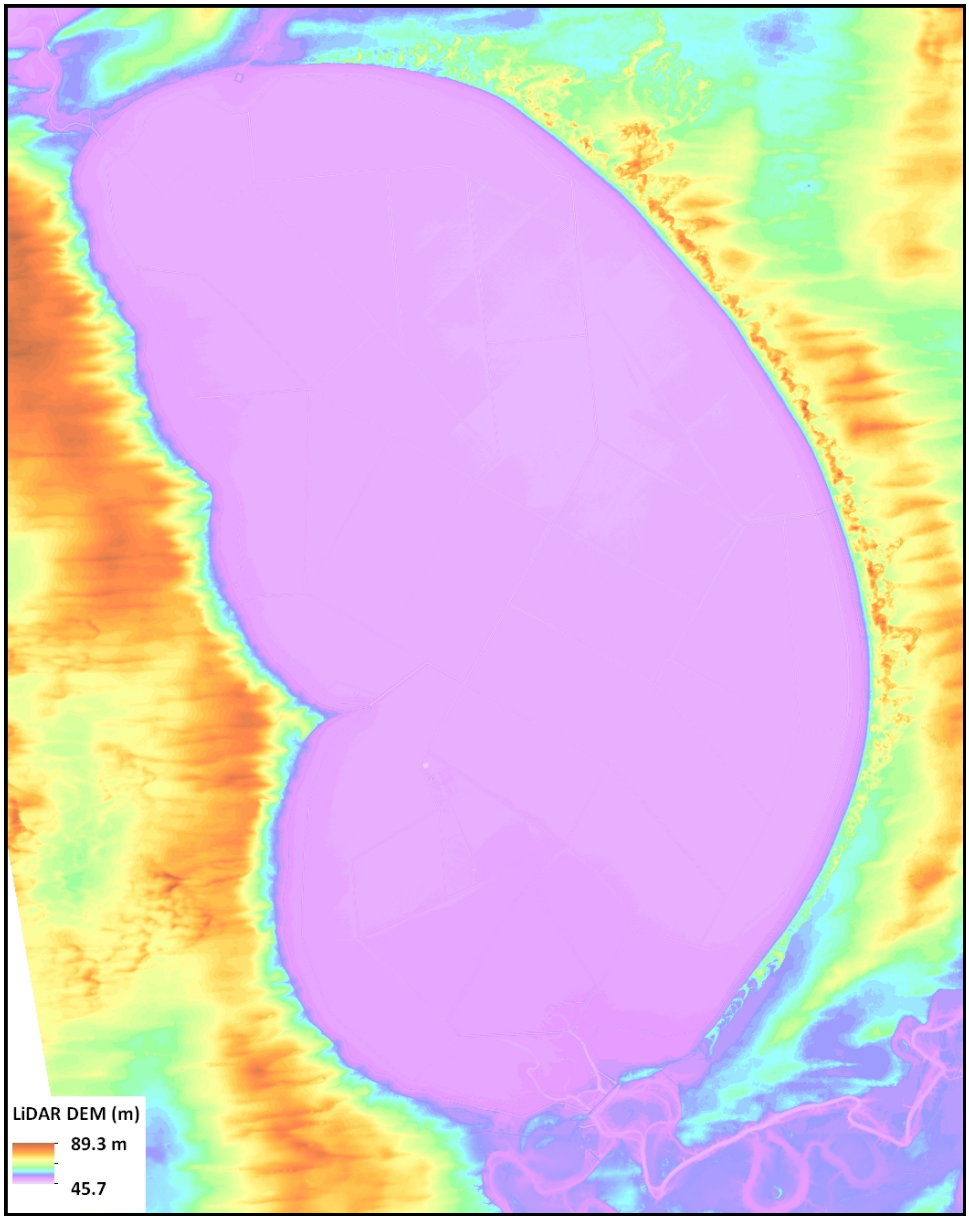

Figure 10-41. *Lake Tandou LiDAR DEM.*

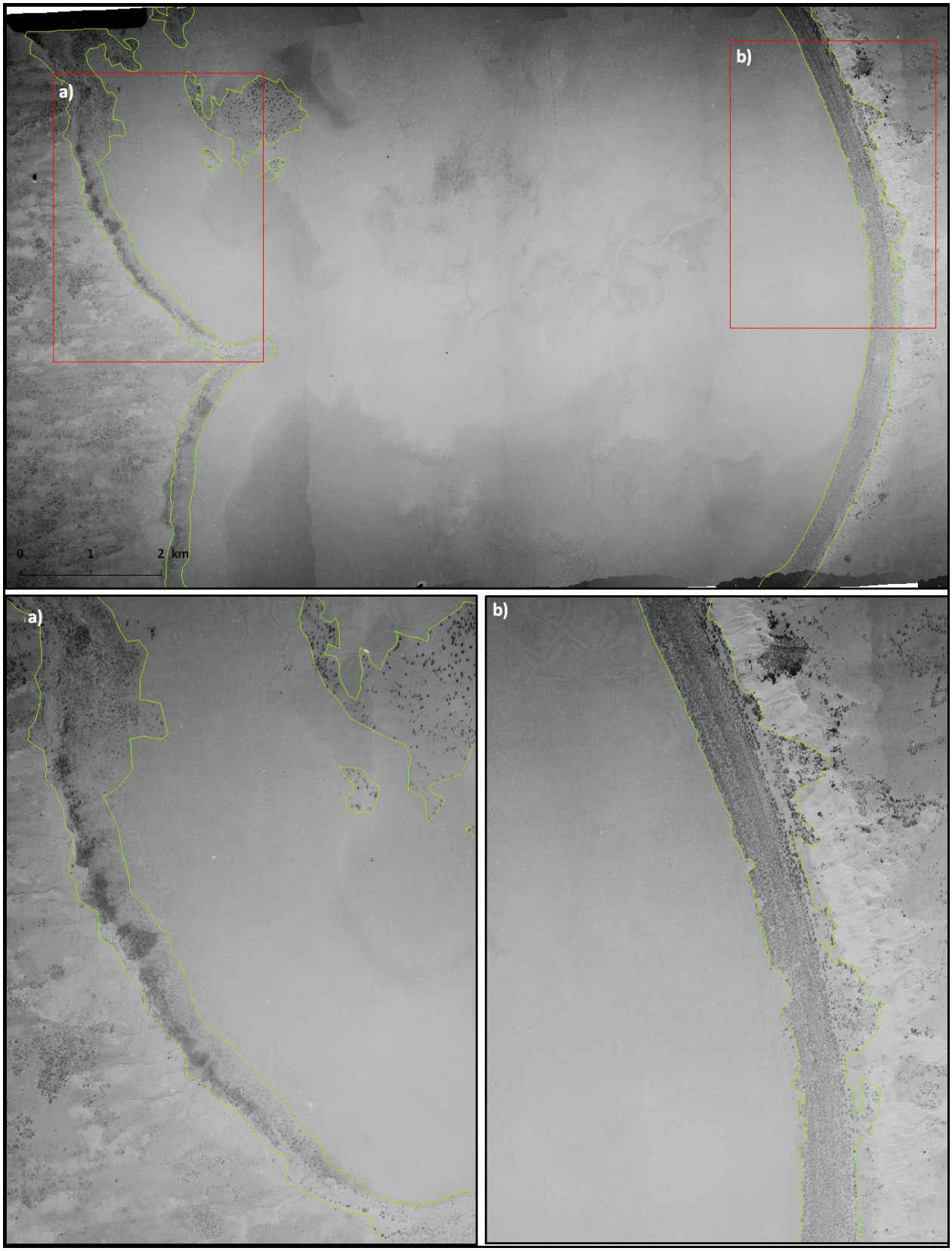

Figure 10-42. *1945 aerial photograph at Lake Tandou, including a) western and b) eastern fringing vegetation. Vegetation on the eastern side extends onto the alluvial sands while some lake-floor vegetation is present.*

Post-regulation condition

Lake Tandou was regulated by embankments and the lake floor modified by channels and levelling for irrigation in 1979. Fringing vegetation however still appears to be the same; vegetation on the western foreshore has thinned somewhat but the Black Box vegetation on the eastern fringe appears largely unchanged (Figure 10-43).

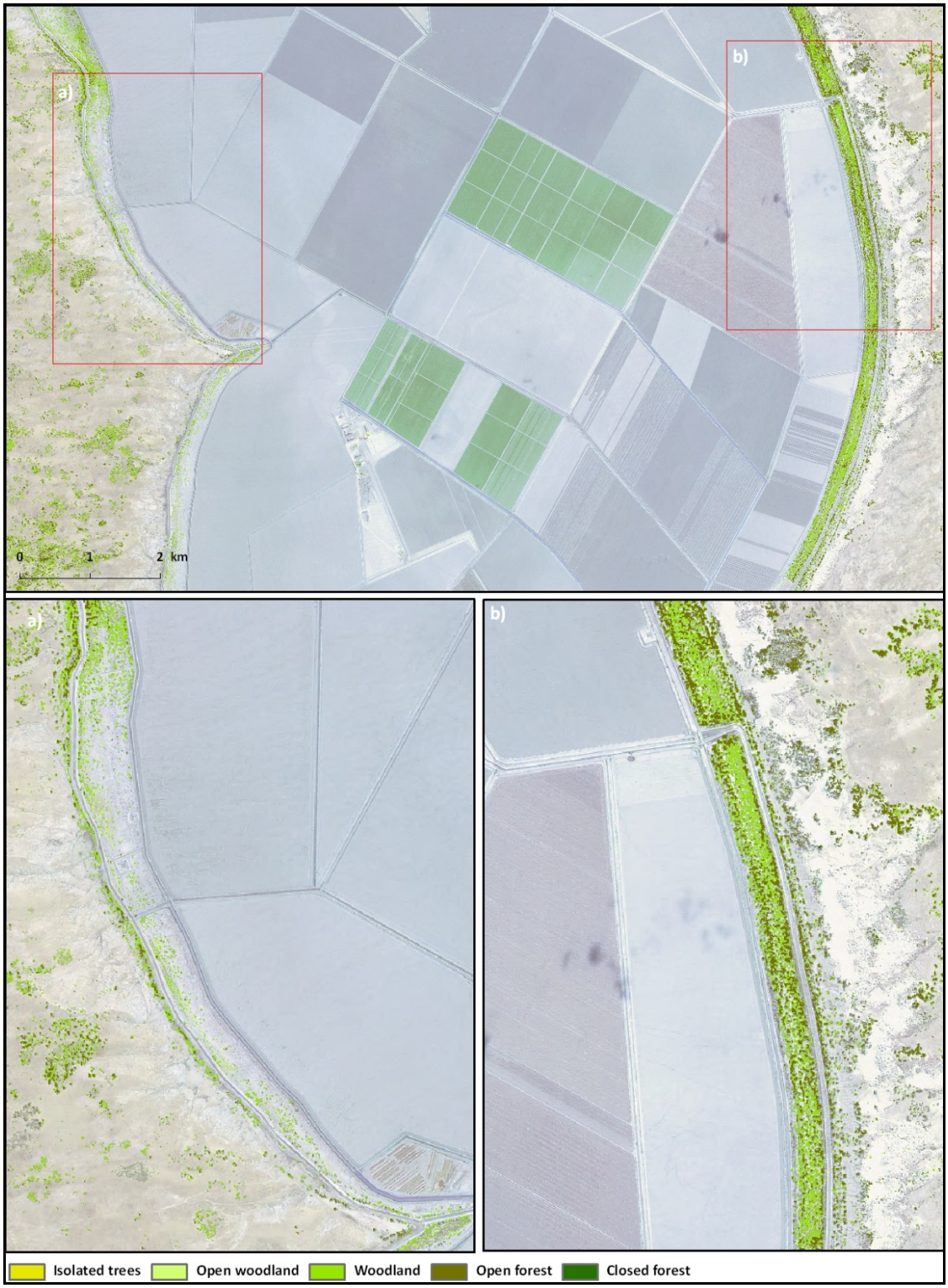

Figure 10-43. *2009 LiDAR vegetation structural mapping at Lake Tandou, including a) western and b) eastern fringing vegetation. Note the establishment of crops and pasture, and irrigation channels particular prominent on the eastern edge.*

Drought behaviour

The condition of the fringing Black Box vegetation in 2009 is shown in Figure 10-44. While patchy, vegetation condition appears to improve towards the north. There does also appear to be some sectioning of the vegetation, with better condition observed on the eastern and western edges of the fringing vegetation and poorer condition observed in the centre. This may be attributed to the channel irrigation system constructed for Lake Tandou and the possible presence of a perched water resource in the adjacent lunette to the east.

This hypothesis is supported by the 2009/2004 comparison as shown in Figure 10-45. The condition of vegetation in 2009 is either largely the same as 2004 or has declined. Areas that have declined are concentrated in the central. There are however narrow vegetation communities, mostly in the south that have declined while the vegetation immediately adjacent (both to the east and west) has maintained condition. The same patterning is seen when looking at the amount of variability in vegetation condition throughout the drought (Figure 10-46). When these datasets all come together, it is quite evident that the central section (running north south) of the Black Box community is exposed to a less reliable water source (Figure 10-47). It can thus be concluded that west of this section vegetation is accessing irrigation water from the channels, while eastward, vegetation must be utilising a groundwater resource. The northern half of the fringing vegetation does not exhibit the same patterning. Instead, vegetation exhibiting greater condition corresponds with a resistive feature as observed in the airborne electromagnetics (AEM; Figure 10-44). At 5 m below the lake floor, a linear feature is observed to correspond with the location of the irrigation channels. It is postulated that a degree of leakage occurs in association with this irrigation channel, creating a fresh soil moisture resource available to fringing vegetation. That said, the irrigation channel network is complex, and without detailed knowledge of management practices it is difficult to tease out the various drivers behind temporal changes in vegetation condition.

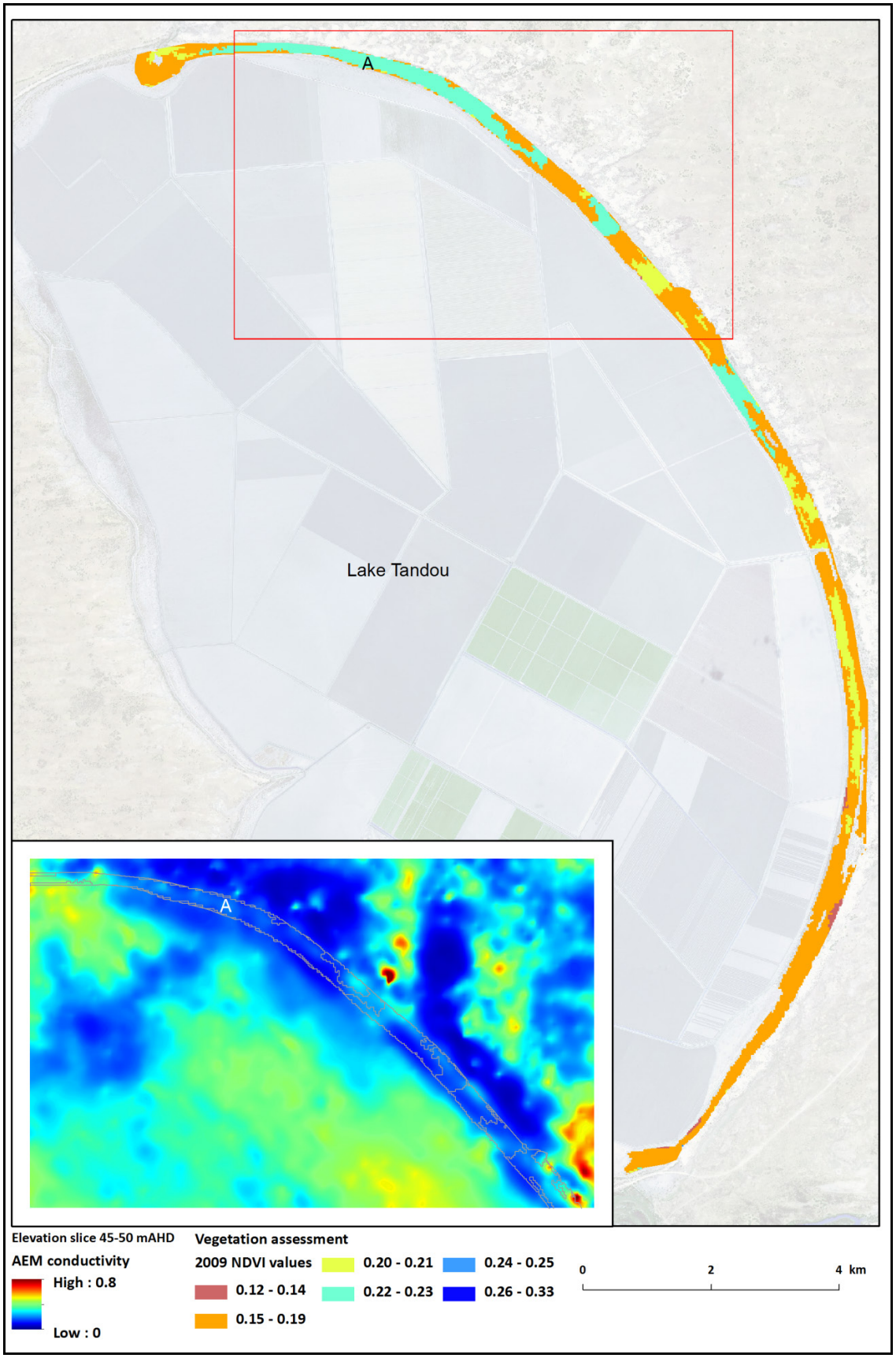

Figure 10-44. *NDVI values for lake-fringing woody vegetation in 2009. 0.14 is the threshold between shrubs and grasses and open woodland. Note the large resistive zone (A) in the inset image which corresponds with vegetation exhibiting higher NDVI values.*



Figure 10-45. *Comparison between vegetation condition in 2009 with respect to 2004. Positive standard deviations (Std. Dev.) relate to an increase in condition with time, negative standard deviations relate to an decrease in condition with time and -0.5 to 0.5 standard deviations (shown in yellow) equate to effectively no (or minimal) change with time.*

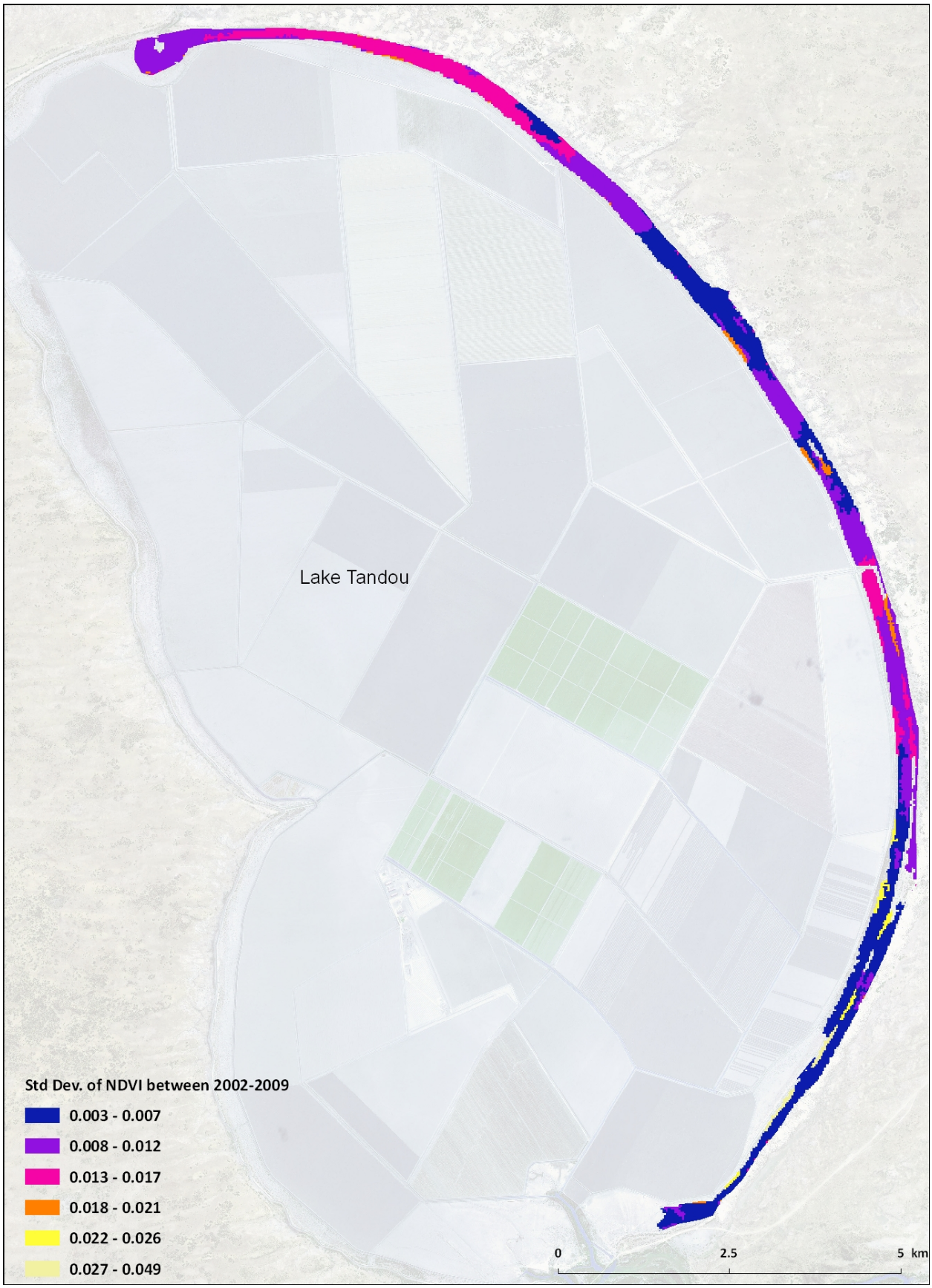

Figure 10-46. *Variability in lake-fringing vegetation condition during the drought (2004-2009).*



Figure 10-47. *Relative reliance of lake-fringing woody vegetation on groundwater and surface water.*

10.4.1.7 Comparison between lakes

Response of artificial lake-fringing vegetation to different inundation regimes

Prolonged inundation can result in the death of vegetation, as evidenced by the extensive band of dead lake-fringing vegetation now (semi) permanently inundated. Inundation can however maintain or improve the condition of vegetation if the duration and frequency are not excessive. It is suggested that in order to maintain mature River Red Gum vigour, the frequency of inundation should be once every 1–3 years (for forests) and once every 2–4 years (for woodlands), with a duration of 5–7 months, (although woodlands can tolerate infrequent longer periods of inundation), separated by 5–15 months (Roberts, 2012). Black Box prefers to be inundated once every 3–7 years for about 3–6 months (Roberts, 2012). The condition of lake-fringing vegetation at Lakes Pamamaroo, Menindee and Cawndilla was thus explored in terms of inundation history.

Three different lake level conditions were identified – Full Supply Level (FSL), maximum levels recorded for the 2010/11 flood extent and the highest level recorded for each lake (Figure 10-48). In general, the difference in water levels between FSL and maximum recorded water levels is less than 1.7 m. These slight changes in lake level do not typically result in a substantial increase due to the presence of high, steep lunettes close to the lake shoreline and also foreshore erosion processes. The exceptions to this are Lake Speculation and Spectacle Lakes. Due to their gentle gradient, both are subject to substantial increases in inundated area under the different lake level conditions (Figure 10-48).

A total of 82 km² of woody lake floor and fringing vegetation is impacted by surcharging of Lakes Menindee, Pamamaroo and Cawndilla. This includes Lake Speculation and Spectacle Lakes. FSL impacts 70% of the total area, while the 2010/11 flood maximum and highest recorded lake levels represent 11% and 19% respectively.

Time series analysis for different structural vegetation classes within each lake level condition yielded interesting results. Analysis indicates that artificially fringing woody vegetation located above the 2010/11 flood levels at Lake Pamamaroo exhibit higher condition than compared with vegetation at lower fringing levels at Lake Pamamaroo or at any location at Lakes Menindee and Cawndilla (Figure 10-49 and Figure 10-50). This vegetation has consistent access to surface water while only being inundated itself infrequently.

Lakes Menindee and Cawndilla have been subject to lower water storage levels, for shorter durations and less frequently (Figure 10-50). All zones (FSL, 2010/11 flood maximum and highest recorded levels) were subject to inundation during 1988-1991, while water levels only reached the 2010/11 maximum between 1996 and 2001. Vegetation condition during the drought (2002–2009) was appreciably worse than under relatively wet conditions (1992-1995; Figure 10-50). This suggests vegetation at Lakes Menindee and Cawndilla had access to alternative water resources during the drought. Minor fluctuations observed in Figure 10-50 between 1992 and 1995 are in response to local rainfall events. This type of response is not evident during the 2002-2009 drought period (with the exception of 2007), yet the overall trend appears constant with no apparent increase or decrease (Figure 10-50). This behaviour is thought to be indicative of access to alternative (constant) water sources, principally groundwater.

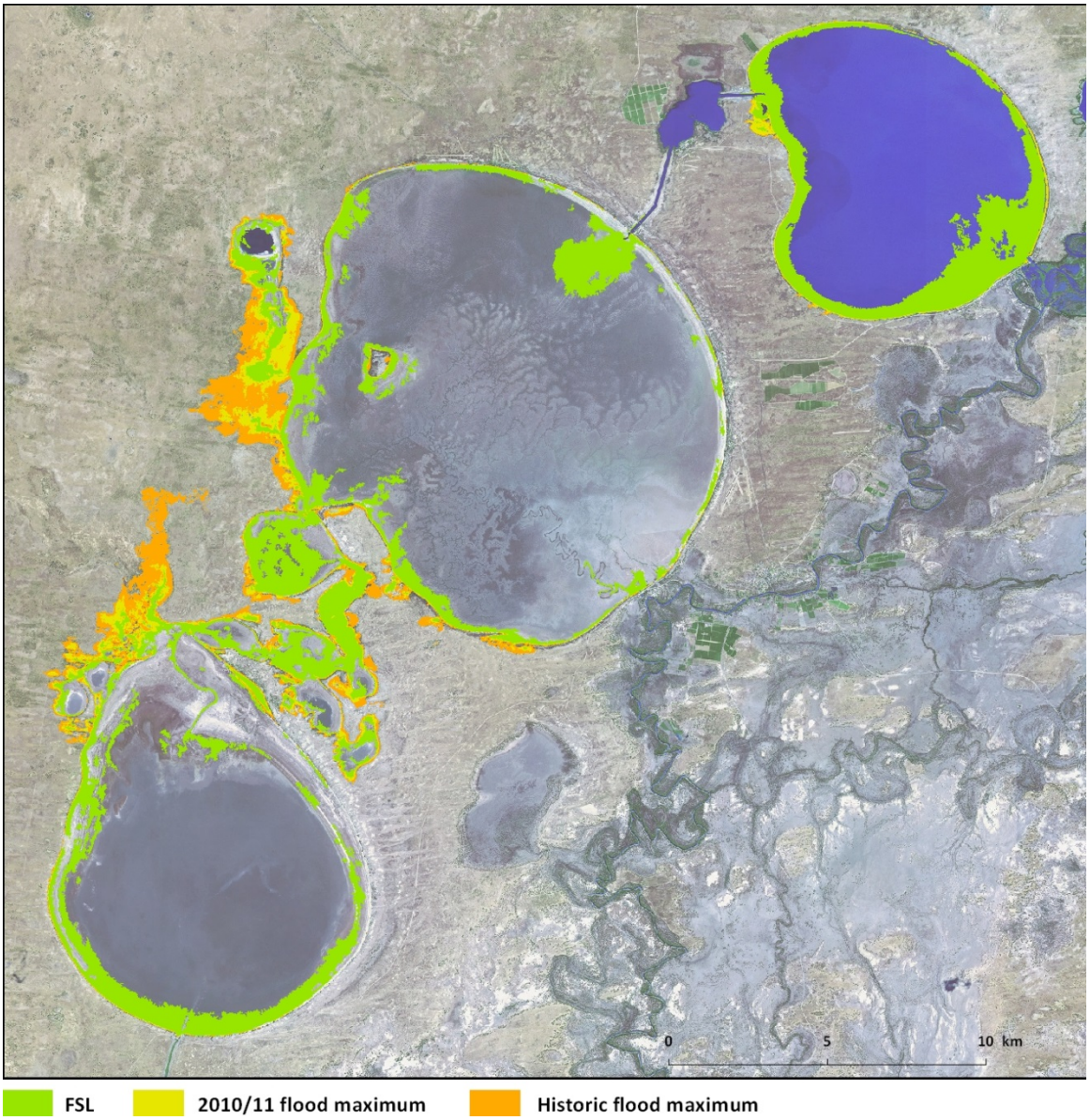

Figure 10-48. *Extent and distribution of woody vegetation within the three flood elevations – Full Supply Level (FSL), 2010/11 flood maximum, and highest recorded maximum.*

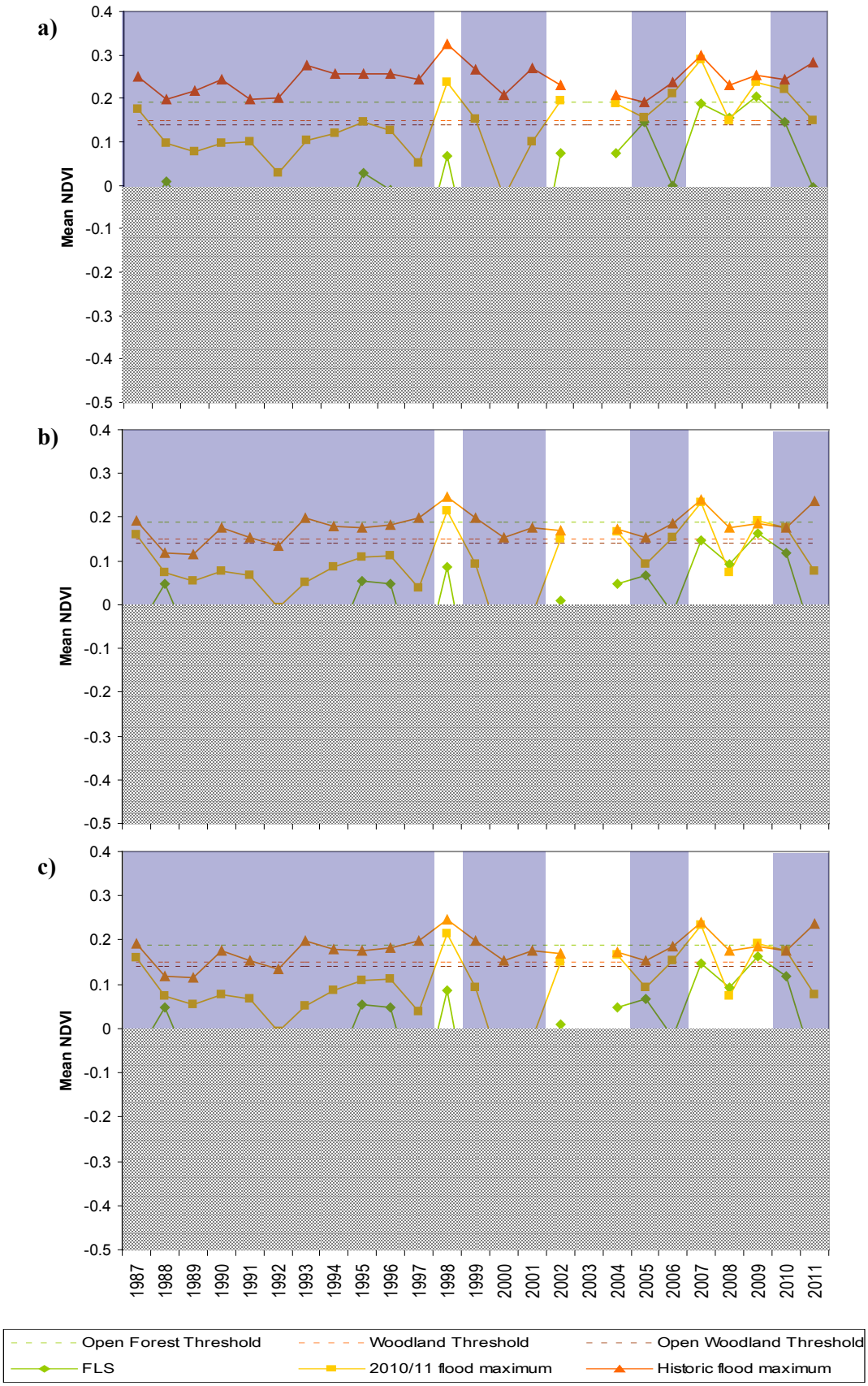

Figure 10-49. *Landsat time series analysis for a) open forest, b) woodland and c) open woodland vegetation fringing Lake Pamamaroo. Values below zero have been influenced by water. Blue shading represents FLS or greater water storage for some part of the corresponding year.*

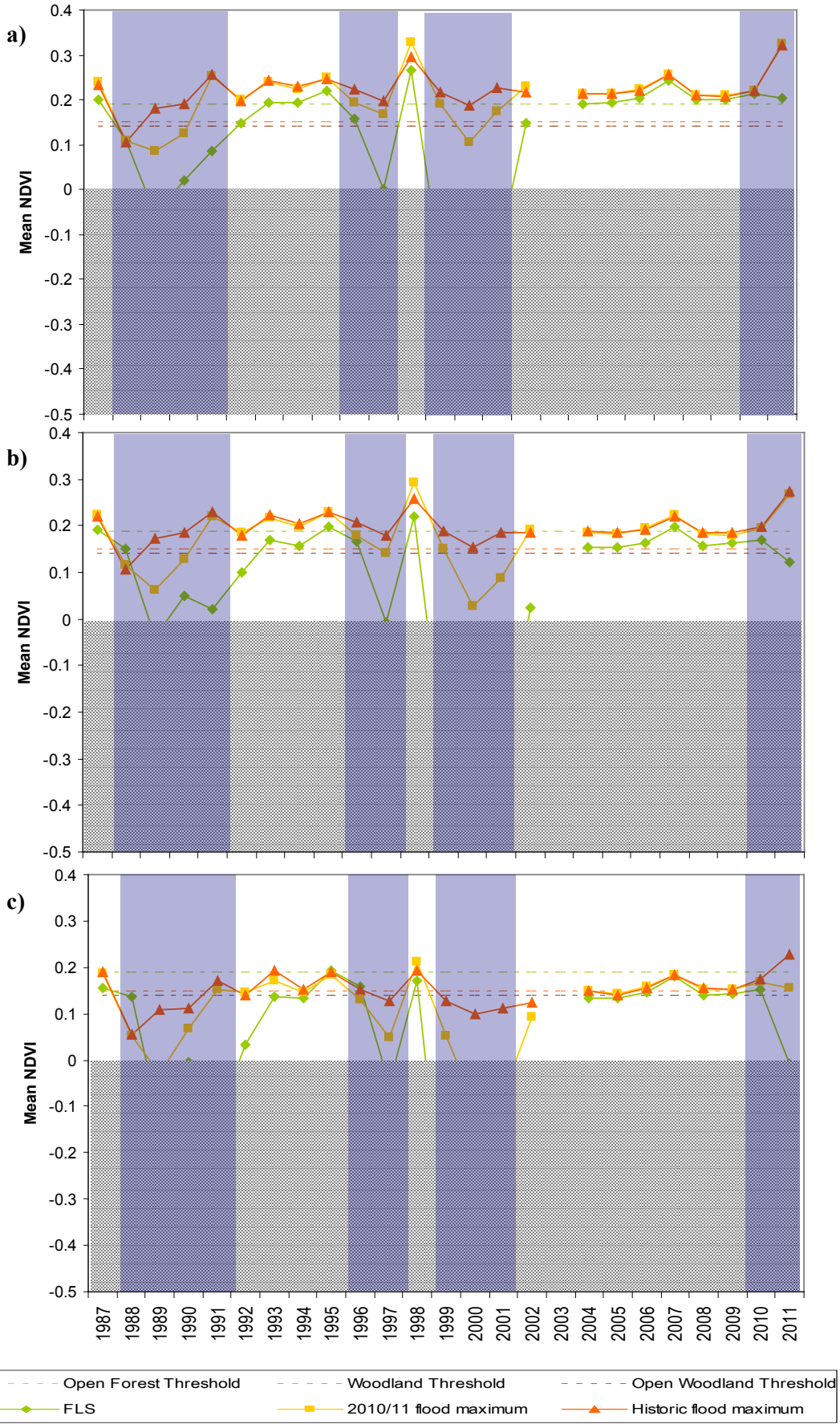

Figure 10-50. *Landsat time series analysis for a) open forest, b) woodland and c) open woodland vegetation fringing Lakes Menindee and Cawndilla. Values below zero have been influenced by water. Blue shading represents FLS or greater water storage for some part of the corresponding year.*

Black Box vegetation at Lake Speculation exhibited good condition (Figure 10-51), slightly outperforming open forest vegetation fringing Lakes Cawndilla and Menindee between 1991 and 1995 (Figure 10-52); average annual rainfall during this period was 305 mm/yr. During the drought (2002–2009; average annual rainfall of 213 mm/yr), the apparent condition of these two vegetation populations converged, showing less fluctuation in respond to rainfall events (with the exception of 2007) than the previous period (1991–1995). While the condition of open forest vegetation at Lakes Menindee and Cawndilla remained constant in 2009, the condition of Black Box at Lake Speculation began to decline. This trend was arrested with the breaking of the drought in 2010; which both vegetation populations responded strongly to. Lake Pamamaroo fringing open forest vegetation (at historic maximum) is in slightly better condition during dry periods (e.g. 2007–2009) due to the presence of abundant surface water. Similar to the fringing vegetation associated with Lakes Cawndilla and Menindee, shallow groundwater resources derived from previous flood/inundation events, may have assisted in the maintenance of vegetation condition in the absence of other water resources. These groundwater resources were likely reduced substantially by the end of the drought (and possibly unable to continue to maintain vegetation condition) due to depletion by vegetation, with no opportunity for recharge.

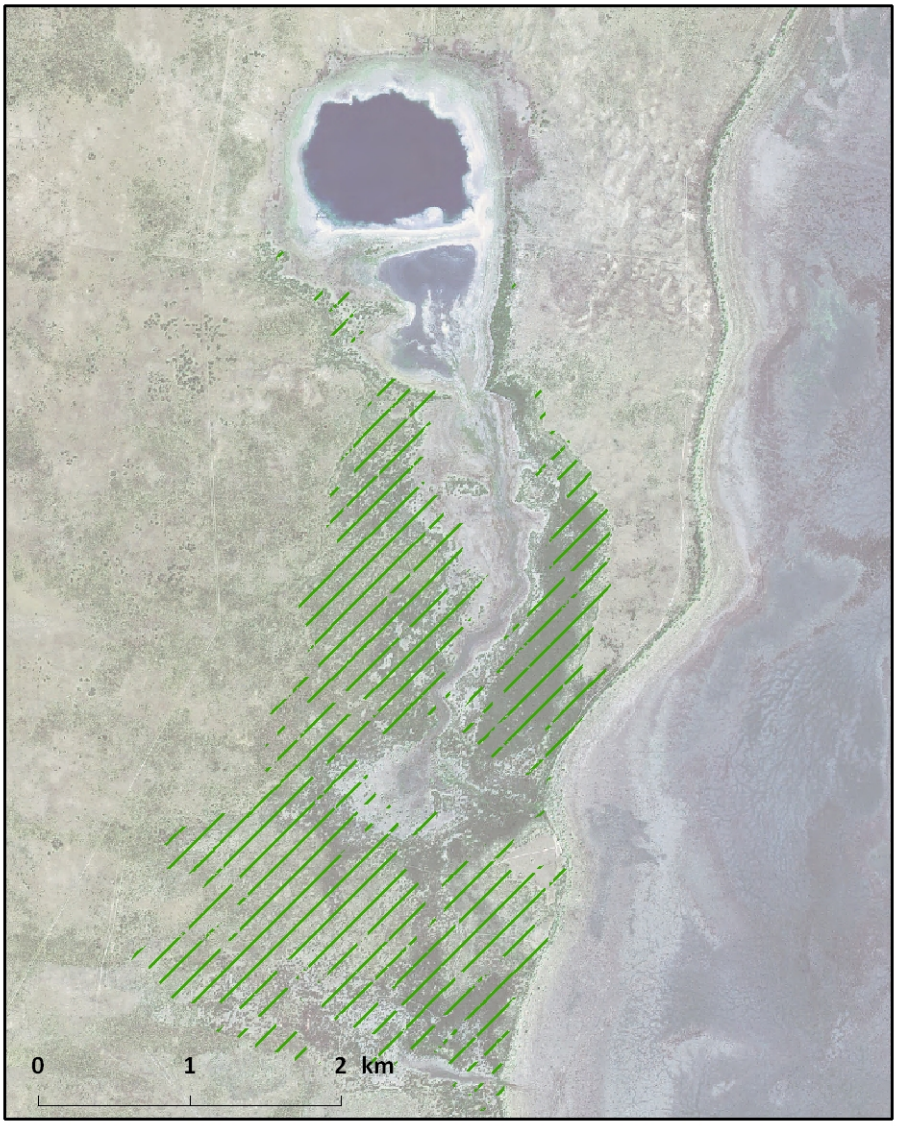

Figure 10-51. *Black Box vegetation at Lake Speculation, as shown by the green hashed region.*

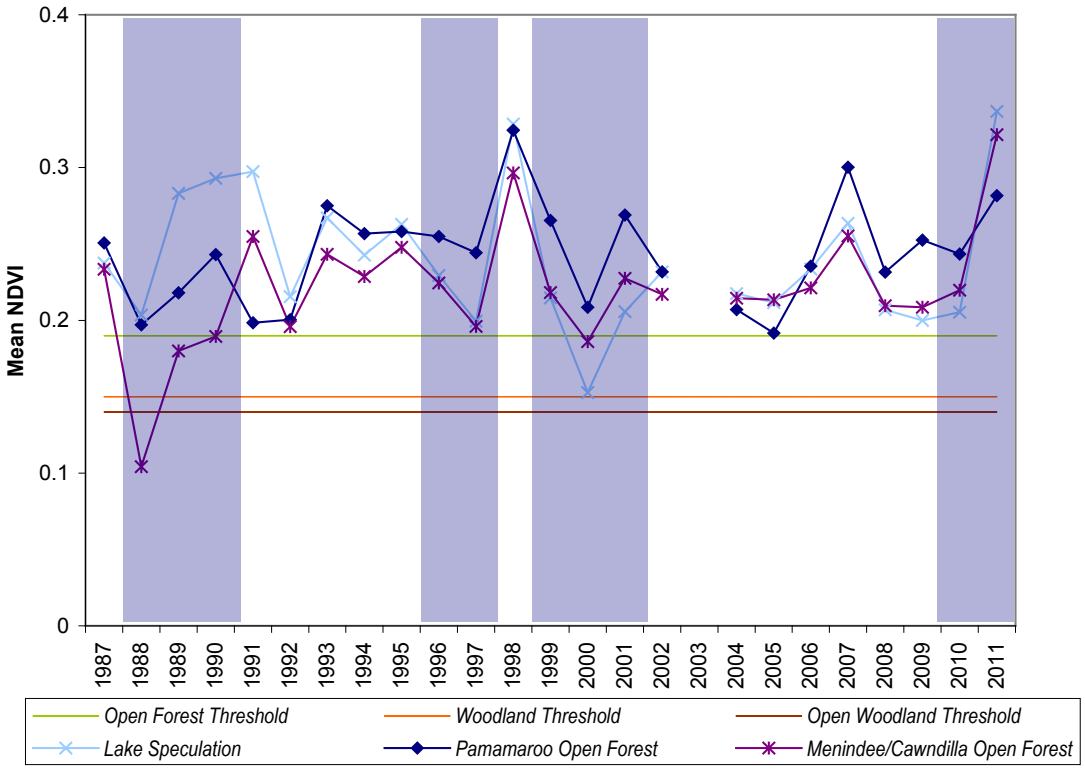

Figure 10-52. *Landsat time series analysis for Black Box and open forest vegetation fringing Lake Speculation, Menindee/Cawndilla and Pamamaroo.*

While Lake Wetherell now functions as a lake (as a consequence of regulation) rather than a floodplain, it does not have a defined lake extent and receives largely unregulated flows from the Darling River and its tributaries. Consequently the condition of woody vegetation associated with Lake Wetherell was compared against other riparian and floodplain sections in the study areas (Figure 10-53) rather than other regulated lakes. Discretization of the riparian zone and floodplain were based on differing water regimes. For example the Darling River was broken into four different sections – Upper Darling (Darling River – A), Lake Wetherell Darling (Darling River – B), Darling downstream of Lake Wetherell and upstream of Lake Menindee (Darling River – C) and Lower Darling (Darling River – D). Detailed interpretation of the floodplain and riparian zone vegetation is in Section 10.4.2.

Temporal analysis of all river/creek sections indicated a clear shift in floodplain and riparian vegetation condition at 2002, with vegetation exhibiting higher condition pre-2002. This is irrespective of vegetation structural class (e.g. open forest, woodland and open woodland) or location of the floodplain/riparian zone within the study area (Figure 10-53). The Lake Wetherell section of the Darling River (Darling River –B) is the only exception to this, with improvements in condition in all riparian vegetation classes (open forest, woodland and open woodland) and open forest floodplain vegetation post-2002 (Figure 10-53).

Vegetation communities demonstrating this improvement in condition (during the drought) are concentrated on the outer floodplain. Under wet climatic conditions, these vegetation communities were more frequently subject to longer periods of inundation due to lake management, localised rainfall and floodwaters. During the drought however, lake levels were considerably lower. Thus much of this floodplain Black Box vegetation had access to fresh surface water but without being inundated and hence improved condition under these conditions.

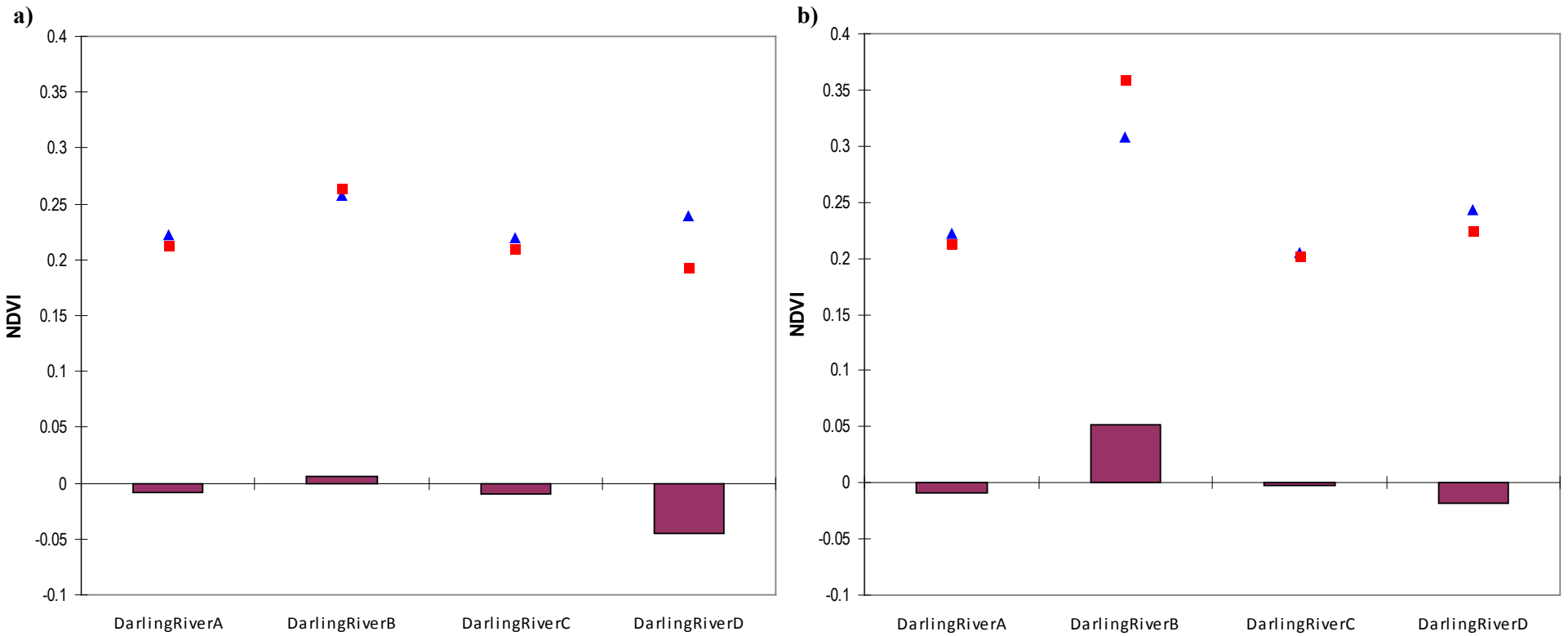

Figure 10-53. *Comparison of a) open forest floodplain, b) open forest riparian, c) woodland riparian and d) open woodland riparian vegetation condition prior to 2002 and 2002 onwards at different locations across the study area. No woodland vegetation existed occurred on Darling River D riparian zone.*

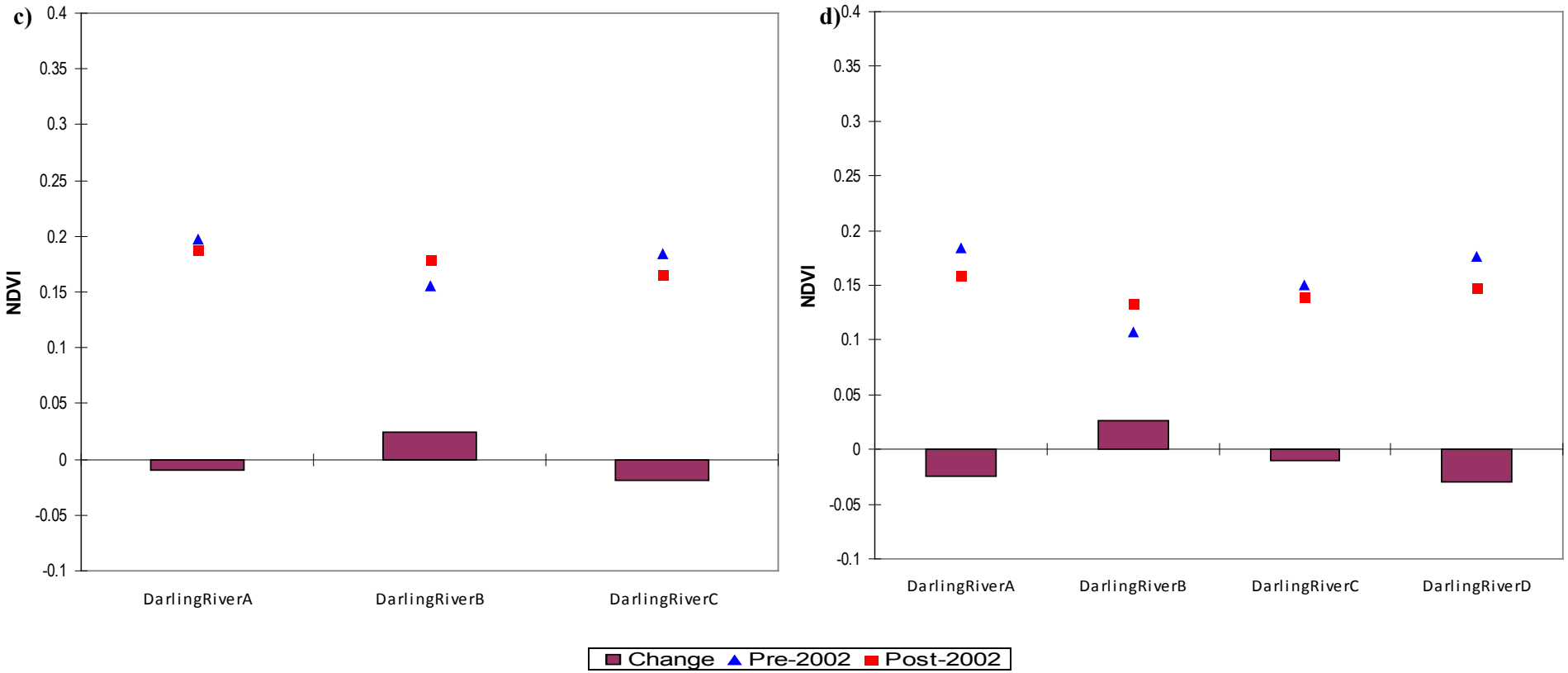

Figure 10-53. *Comparison of a) open forest floodplain, b) open forest riparian, c) woodland riparian and d) open woodland riparian vegetation condition prior to 2002 and 2002 onwards at different locations across the study area. No woodland vegetation existed occurred on Darling River D riparian zone.*

Behaviour of lake-fringing vegetation during drought conditions

In the absence of surface water resource (during drought conditions and/or due to regulation) access to groundwater may be principally responsible for supporting vegetation. While it is difficult to completely rule out other water sources, a degree of groundwater reliance can be inferred when woody vegetation maintains relatively constant condition in the absence of surface water. The recent drought (from 2002 to 2009) provided perfect conditions to assess reliance on groundwater, with minimal rainfall and very low river flow rates. Under these prolonged dry conditions, the potential of lake-fringing vegetation to access groundwater resources was explored.

All of the lakes south of Pamamaroo were investigated and discussed below. Figure 10-54 shows NDVI values of woody lake-fringing vegetation in 2009 while Figure 10-55 shows the general trends of vegetation condition between 2004 and 2009. -0.5 to 0.5 standard deviations correspond with effectively no change, while negative standard deviations indicate a decline in condition over time and positive standard deviations indicate an increase in condition. Figure 10-56 shows the variability (as indicated by standard deviation) in NDVI (or vegetation condition) throughout the drought. Small values indicate minimal change in vegetation condition throughout the drought. When coupled with minimal change from 2004 to 2009 and relatively good condition at the end of the drought (2009) source water reliability can be inferred. Figure 10-57 combines an analysis of source water reliability with vegetation condition which can also be used as an indicator of available water volumes (Jones *et al*., 2008).

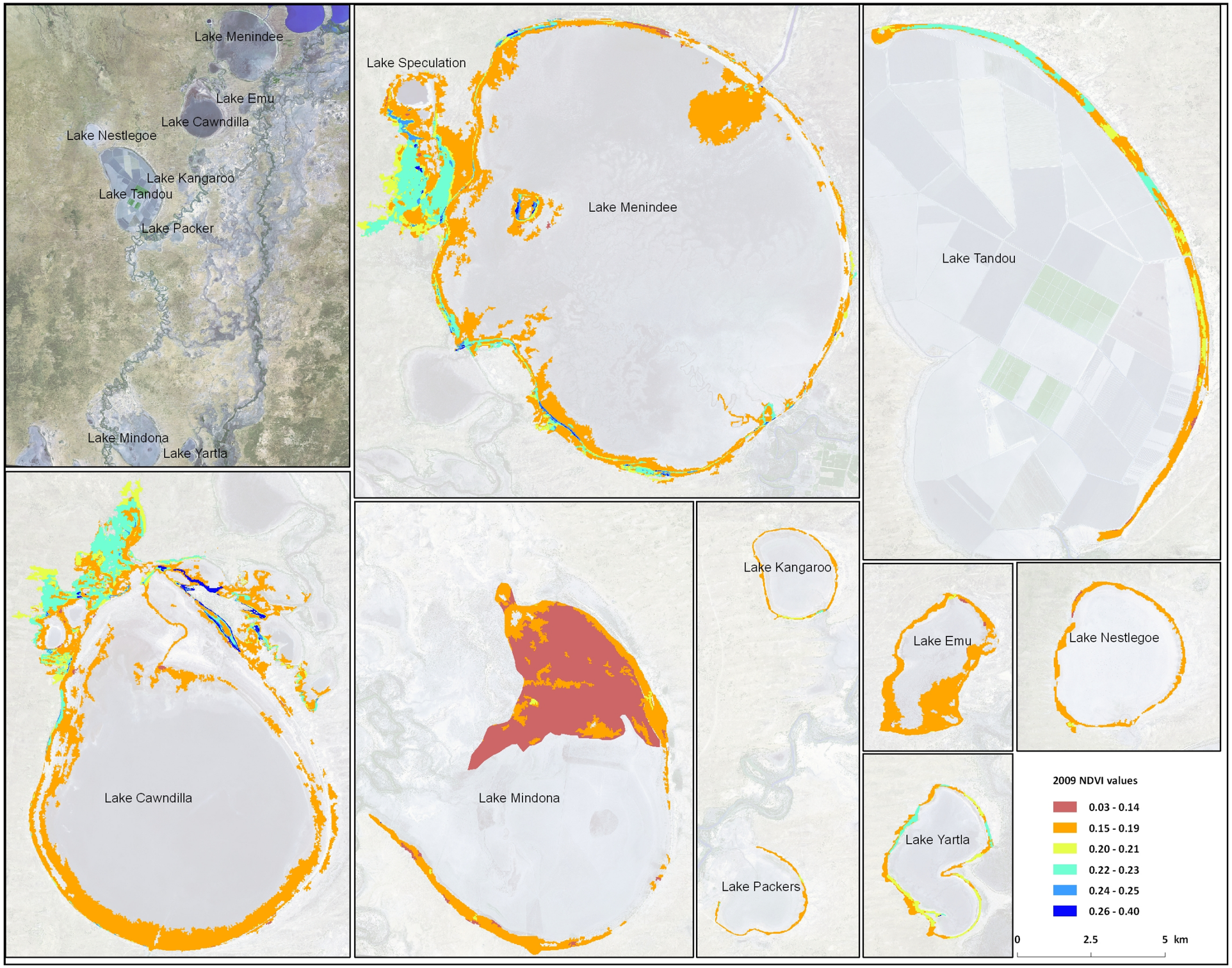

Figure 10-54. *NDVI values for lake-fringing woody vegetation in 2009. 0.14 is the threshold between shrubs and grasses and open woodland.*

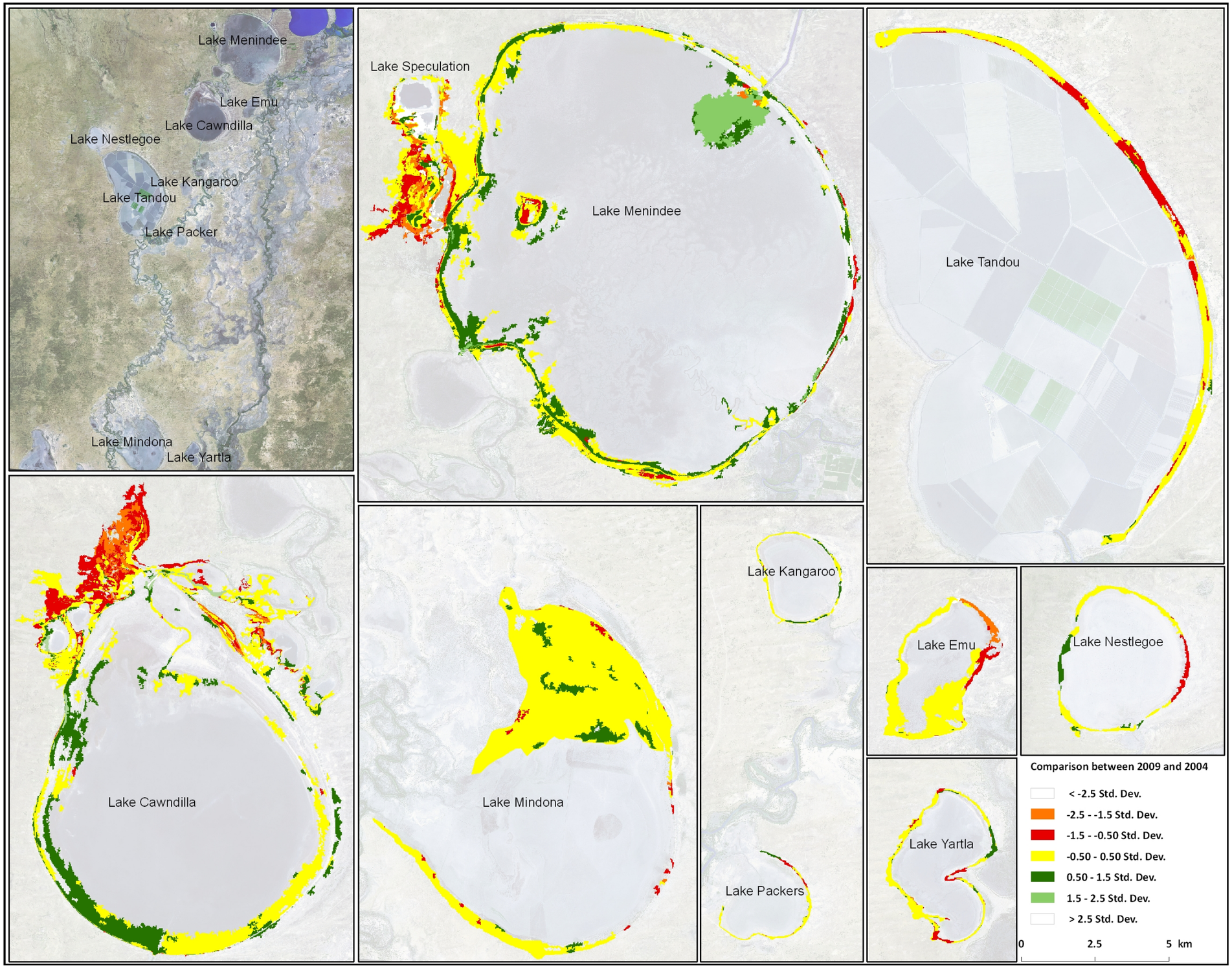

Figure 10-55. *Comparison between vegetation condition in 2009 in respect to 2004. Positive standard deviations (Std. Dev.) relate to an increase in condition with time, negative standard deviations relate to an decrease in condition with time and -0.5 to 0.5 standard deviations (shown in yellow) equate to effectively no (or minimal) change with time.*

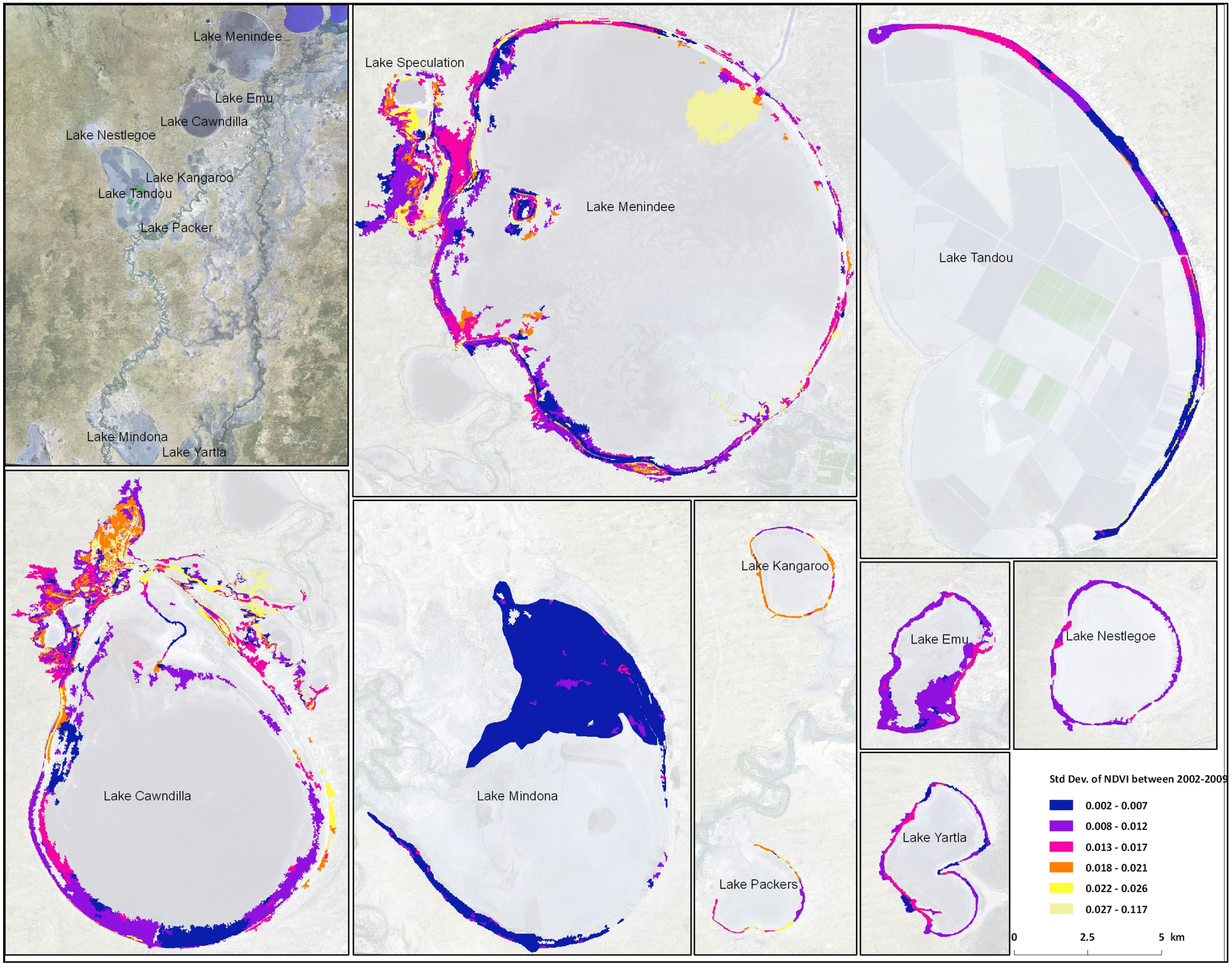

Figure 10-56. *Variability in lake-fringing vegetation condition during the drought (2004-2009).*

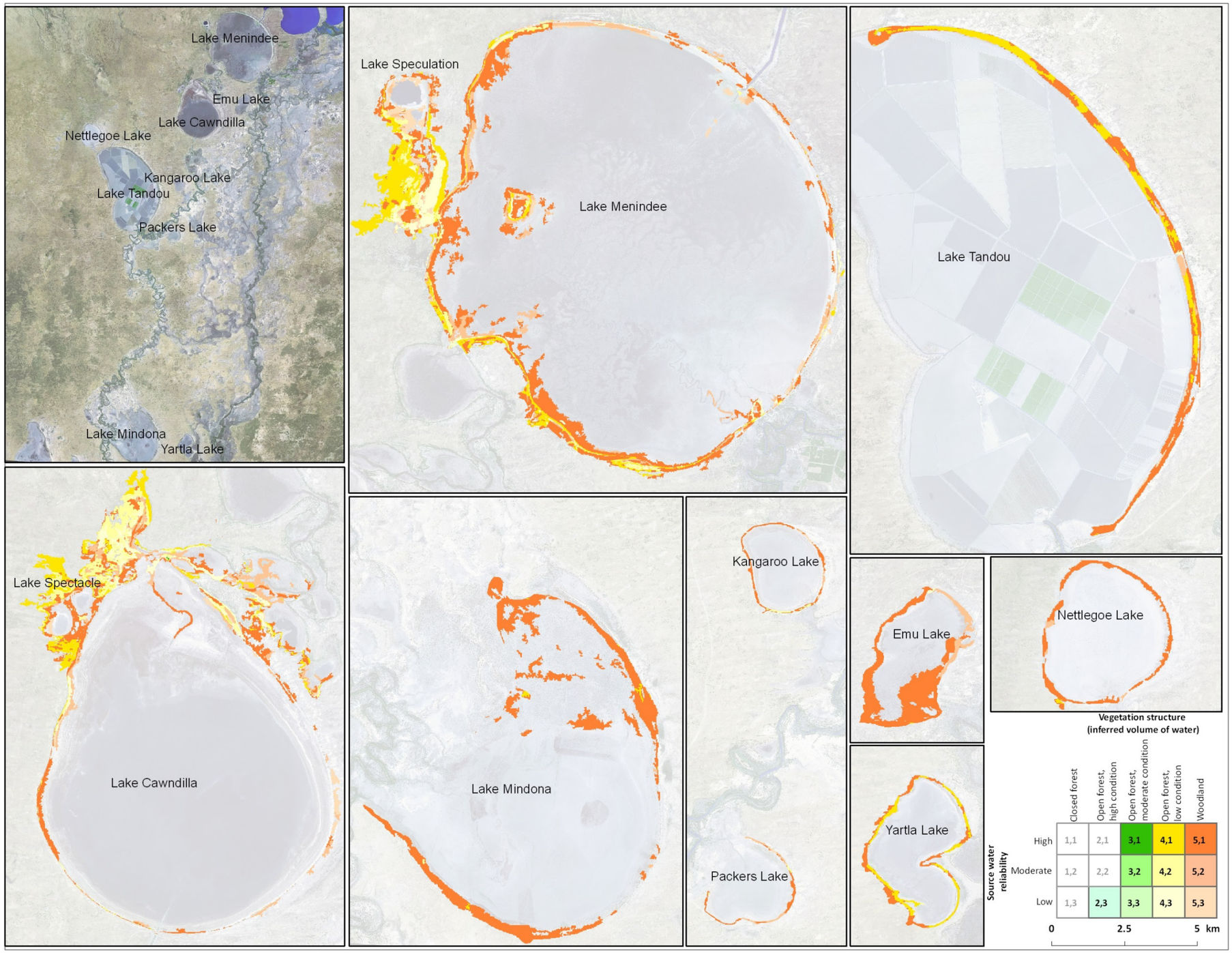

Figure 10-57. *Relative reliance of lake-fringing woody vegetation on groundwater and surface water.*

In 2009, at the end of the drought, woodland/open woodland vegetation was most commonly associated with lake-fringe (Figure 10-54). Open forest vegetation communities of low condition were however present; largely concentrated around Lake Speculation, Spectacle Lake, Lake Tandou and Yartla Lake. While the majority of lake-fringing woodland vegetation maintained condition during the drought, open forest vegetation associated with both Lake Speculation and Spectacle Lake declined (Figure 10-55), presumably reflecting declines in available water. The condition of these vegetation communities also fluctuated throughout the drought (Figure 10-56) in respond to localised rainfall events. Both communities are prone to inundation when the lakes (Cawndilla and Menindee) exceed full supply levels (Figure 10-40). Complete inundation of the area has not occurred since 1989, however smaller-scale flooding occurred in 1996/1997, 1999/2000 and 2001/2002. It is these events that result in recharge to the shallow aquifer. The higher condition observed in 2004 is likely a result of increased water availability during previous wet conditions, thus it can be concluded that inundation events similar to that in 2001/2002 are required to maintain vegetation condition at Lake Speculation and Spectacle Lakes. In the absence of surface water, condition declines.

In comparison, the open forest communities fringing Lake Menindee and Lake Tandou (Figure 10-54) maintained condition from 2004 to 2009 (Figure 10-55) and showed minimal variation throughout the drought (Figure 10-56) and thus appear to have had access to a relatively constant water source. Vegetation fringing Lake Tandou received irrigation during the drought. This, supplemented with perched water derived from channel leakage, largely maintained the condition of vegetation throughout the drought period.

Lake Menindee however received minimal flows during the drought, thus vegetation likely had access to a groundwater resource during the drought in order to sustain condition. A regional groundwater resource exists beneath Lake Menindee (refer to Lawrie *et al*., 2012c; d). This deeper aquifer is typically disconnected from shallow aquifers by the upper confining aquitard, however the aquitard is absent in the northern edge of Lake Menindee (Figure 10-25). Consequently vegetation in this area has access to a fresh, shallow groundwater resource. This resource is further enhanced by lake leakage accelerated in response to lake regulation. This is discussed in greater detail in Lawrie *et al.* (2012c). Fringing vegetation on the eastern shoreline of Lake Menindee has access to less reliable water (Figure 10-57) and these resources are thought to be quickly depleted.

Yarlta Lake connects directly (via a sill) to the Lower Darling River and likely received flows reasonably regularly throughout the drought. During the drought, Yartla Lake supported open forest communities, largely concentrated on the lake shoreline and lake floor (Figure 10-54). These communities are best placed to access any surface water inflows from the Darling River. Vegetation on the adjacent dunes exhibited poorer condition having declined since 2004 (Figure 10-55) and are presumably less able to access surface water resources. As the availability of surface water is relatively constant, vegetation condition does not vary considerably throughout the drought and can be misinterpreted as reliant on groundwater resources.

Lake Mindona which is located in close proximity to Yartla Lake exhibits very different vegetation dynamics. Much of the Black Box community exhibited condition more similar to shrubs and grasses than healthy trees (Figure 10-54). Lake Mindona is connected to the Darling Anabranch. Unlike the Lower Darling River which received constant flow during the drought, the Darling Anabranch only flowed when nominal volumes were released from Lake Cawndilla which was uncommon. In the absence of surface water, vegetation condition remained constant (Figure 10-55) and showed very little variability throughout the drought (Figure 10-56), which suggests access to groundwater resources. While Emu Lake is connected to the Darling River via Emu Creek, sill levels are such that minimal water would have entered the lake during the drought. Instead, vegetation fringing Emu Lake appears to have had access to shallow groundwater resources as well as any residual soil moisture. Nettlegoe Lake is similarly shut off from any inflows. Prior to regulation, it would have received flows from Lake Tandou, however this has not been possible since 1979. It is also unlikely to receive inflows from Charlie Stones Creek. As was the case at Lake Mindona and Emu Lake, vegetation maintained condition throughout the drought (Figure 10-55) with very little variability (Figure 10-56).

Finally, Packers and Kangaroo Lakes showed the greatest variability in condition throughout the drought (Figure 10-56). These lakes were used as short-term water storage for irrigation water either released from

Cawndilla or pumped across from the Darling River to be used at Tandou. Vegetation condition consequently reflected the variability in available water.

10.4.2 Importance of River Flow and Flooding to Vegetation Function

10.4.2.1 Introduction

The degree of vegetation response to increased water availability is reportedly more reduced following a severe and prolonged drought than during a wet year (Volcani *et al*., 2005; Doody *et al*., 2009). Vegetation in better shape is thus more able to respond to increased water availability characteristic of more favourable conditions. Flooding following a dry or stressed phase typically results in a flush of growth; if trees have been stressed, then the new foliage is largely epicormic, and canopy re-establishment may take years (Roberts, 2012). Between flood events during the intervening drying periods, salt can accumulate as tree roots extract water from the soil profile and capillary zone. During flood events, both the soil profile and groundwater can be recharged and accumulated salts flushed from tree root zones (MDBC, 2003). Salinity however does not appear to be an issue within the study area, as mapped water qualities are less than the reported salinity tolerances of River Red Gums (30,000 EC) and Black Box (55,000 EC). That said, woody vegetation within the study area is typically associated with the river/creek network and by association fresher groundwater due to recharge processes.

River Red Gums can take 2-3 months before responding to increased water availability while Black Box can take 3-5 months. River Red Gum forest tress are expected to show stress after three years with no flooding; Black Box may show similar declines. A lack of flooding for 5-8 years, combined with hot dry climatic conditions causes severe stress in River Red Gums. While recovery is possible, it may take years of favourable conditions to re-establish the tree canopy. Black Box is more drought-hardy and can survive 12-16 years without flooding (Roberts, 2012). Unsurprisingly, a relationship exists between tree health and geographical position along the river (MDBC, 2003). The bio-geophysical characteristics of a site and how river regulation and surrounding land use impact the floodplain attributes dictate the degree of environmental change being experienced by River Red Gums populations.

However stable isotope studies have found that trees adjacent to streams do not necessarily use the stream water (Dawson & Ehleringer, 1991, Smith *et al*., 1991). River Red Gum adjacent to an ephemeral stream reportedly transpired groundwater (of moderate salinity 10,000 EC) in preference to river water. Mensforth *et al.* (1994) found that River Red Gums within 15 m of the perennial stream used stream water in summer and possibly used stream water in winter, either as resident in the unsaturated zone or directly from the stream. River Red Gum trees at distances of greater than 15 m from streams used no stream water, instead used groundwater during the summer and a combination of groundwater and soil moisture derived from rainfall during the winter. Despite the high groundwater salinity (>30,000 EC), River Red Gums still used groundwater in preference to the fresh stream water within a distance of 30 m and did not cease using saline groundwater when fresh water was available at the soil surface (0.05-0.15 m).

Bacon *et al*. (1993) made similar conclusions after establishing that both distance from the channel and recent flood history significantly influenced mean leaf area. Higher mean leaf area was observed in trees within 7.5 m of the channel, although trees also appeared to be utilizing shallow groundwater and floodwaters where they were available, suggesting the effects of water supply is additive. The presence of a groundwater resource however meant trees were less reliant on floodwaters and thus less responsive in comparison to trees not accessing groundwater. Similarly, Wen *et al*. (2009) found that under highly saline environments (e.g. Chowilla Floodplain), River Red Gum trees away from the river were more dependent on floods to increase water availability by flushing accumulated salts from the unsaturated zone.

Consequently the Darling River and Darling Floodplain were divided into a series of sections or reaches that reflect the changes in river regulation, allowing for a comparison of vegetation function both spatially and temporally.

This section details the following:

- A regional overview of the various river and creek section; and
- Discussion of observed behaviour of vegetation during the drought for each river/creek section

10.4.2.2 Regional Overview

When average minimum NDVI was analysed for each vegetation structural classes (closed forest, open forest, woodland and open woodland) averaged across each river stretch, a clear drop in NDVI was consistently observed between periods pre- and post-2002, irrespective of vegetation structural class or location within the floodplain. 2001/2002 corresponded with two key hydrologic changes. Firstly, 2002 marked the beginning of the drought with reduced local rainfall and no flooding. Secondly, nominal annual (managed) releases to the Darling Anabranch ceased as of 2002. This combined with naturally dry climatic conditions ensured water scarcity for the floodplain from 2002 onwards. Consequently 1987-2001 and 2001-2010 were analysed as two separate treatment conditions: pre-2002 relating to wet conditions and 2002 onwards relating to dry conditions.

Figure 10-58 shows the average NDVI values for open forest, woodland and open woodland vegetation on the floodplain and also riparian zone, divided into river sections (as discussed in Section 10.3 and shown in Figure 10-16). Note the close correlation between the floodplain vegetation during the two different periods until Tandou Creek where NDVI values begin to diverge. This difference becomes progressively larger further downstream; river sections, listed from left to right in Figure 10-58, represent location further downstream. Without additional water input (rainfall, run-off, groundwater discharge) river flow volumes progressively decrease downstream with losses to evaporation, groundwater recharge and transpiration via vegetation. Interestingly, Weir 32, which regulates flows to the southern watercourses is located upstream of Tandou Creek, the point at which divergence is evident between vegetation greenness values experienced under wet versus dry. River flows to Darling River C are also regulated, as this section of the river is downstream of Main Weir and Lake Wetherell. Darling River C shows some variation between intervals.

The same divergence of NDVI values between treatment types is not as evident when analysing the riparian vegetation structural communities (Figure 10-58). While there does appear to be a difference between the two conditions, this difference is smaller in comparison to floodplain data. It is suggested that this divergent trend was mitigated by groundwater mounding in the shallow aquifer (Coonambidgal and Menindee Formations; refer to Figure 7-49) along the river channel, associated with previous recharge events.

Figure 10-59 is a type example hydrograph, recording water level response in the shallow aquifer with respect to river level rise. The watertable began to rise within a matter of days, indicating excellent connectivity between the river and the shallow aquifer associated with elevated flow conditions. Prior to the floodwater front, recharge was not observed in the hydrographic response suggesting it is linked to large flow events. Recharge processes are discussed in more detail in Section 9. The floodplain however appears to be too far removed from the river channel and associated groundwater mounding for vegetation condition to have been maintained over the course of the extend drought.

Darling River B is an exception, consistently showing improved vegetation condition post-regulation. Darling River B corresponds with the floodplain/riparian zone that is now Lake Wetherell. With the commencement of the drought, releases to Lakes Cawndilla and Menindee from Lakes Pamamaroo and Wetherell largely ceased in order to reduce evaporative losses. Consequently a more constant volume of water was held in the Darling River B section and thus available for vegetation, whereas prior to the drought, releases to the other lakes and downstream via Main Weir were more frequent.

More detailed analysis was carried out for each creek and river section and is discuss in this section.

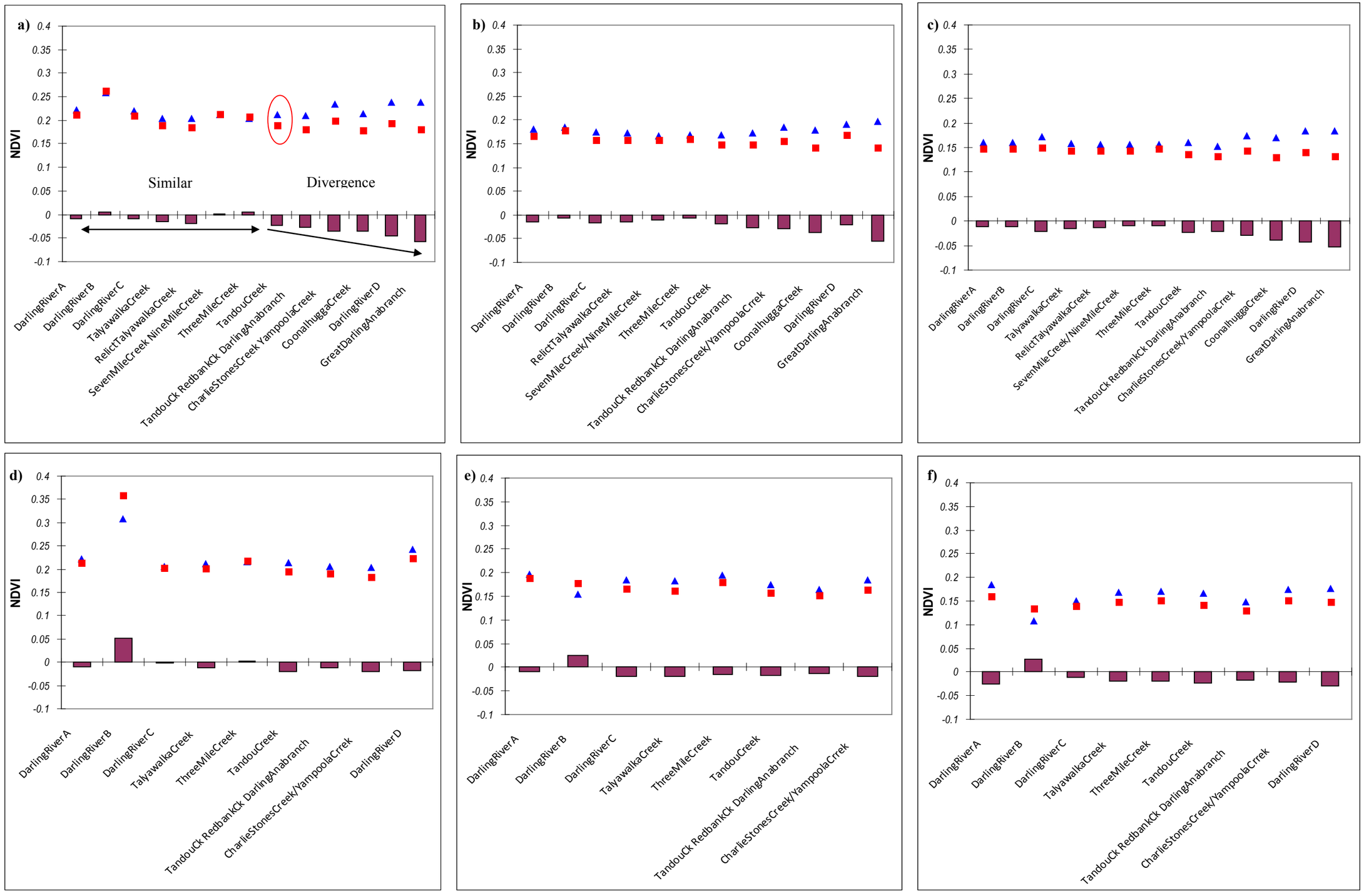

Figure 10-58. *Comparison of a) open forest floodplain, b) woodland floodplain, c) open woodland floodplain, d) open forest riparian, e) woodland riparian and f) open woodland riparian vegetation condition prior to 2002 and 2002 onwards at different locations across the study area. The divergence between pre- and post-2002 behaviour is annotated in graph a.*

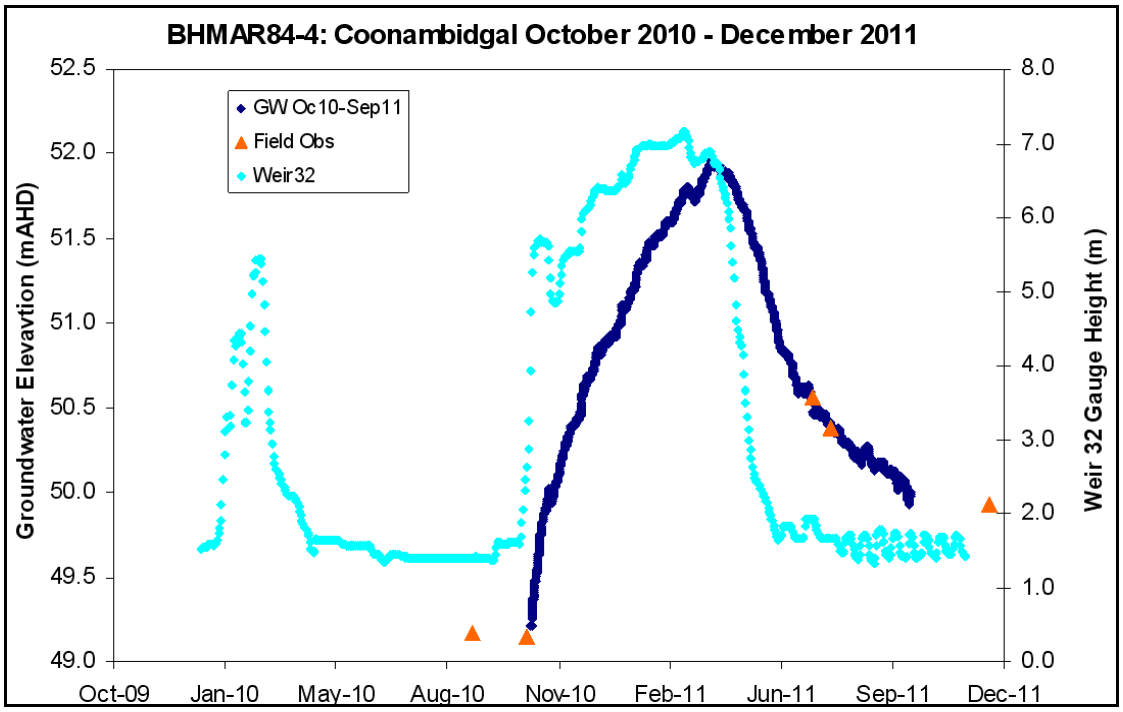

Figure 10-59. *Hydrograph data for bore BHMAR84-4, located slightly north of Weir 32 in close proximity (~600 m) to the river. Overbank flow occurs at ~5.5 m at Weir 32. Recharge to the Coonambidgal Formation began well before the river reached this level.*

Darling River

The Darling River was divided into four different sections based on varying degrees of regulation. Darling River A is the northern most section and stops at the uppermost extent of Lake Wetherell (Figure 10-60). Darling River B corresponds with Lake Wetherell and stops at the point of connection with Lake Pamamaroo (Figure 10-66). Darling River C is the section between Lake Pamamaroo and Weir 32, south of Lake Menindee (Figure 10-69). Finally Darling River D is everything south of Weir 32 (Figure 10-72). Each section of the Darling River is subject to very different water regimes. Darling River A receives largely unregulated flows but no water accumulation. Darling River B is predominantly accumulated water. Darling River C receives regulated flows when water is not being transferred to Lake Menindee via Lake Pamamaroo. Darling River D also receives regulated flows from Main Weir and Weir 32 or natural (flood) flows from Talyawalka Creek. Legislated minimum flow requirements for the lower Darling River (Darling River D) range from 200 ML/day in winter to 350 ML/day in summer.

As Darling River A is less prone to flooding, the spatial extent of vegetation is largely restricted to the riparian zone immediately adjacent to the river channel (Figure 10-60). River Red Gums dominate this position in the landscape and were in good condition (relative to other vegetation in the region) in 2009 (Figure 10-60) due to the constant supply of river water. When 2002 is compared with 2009, the condition of riparian zone vegetation largely declined. Variability in condition was also observed throughout the drought. These two factors – declining trend and high variability throughout the drought – suggest riparian zone River Red Gums at this location have a strong reliance of surface water flows and that observed flows during the drought were insufficient to maintain (pre-drought) condition.

A short section of riparian vegetation is however associated with maintained condition. This location corresponds with both a hole in the upper confining aquitard (Figure 10-62) results in connectivity between the shallow aquifer and the Calivil Formation aquifer, and groundwater mounding at depths of approximately 12–14 m over a larger area than further upstream (Figure 10-63). While similar holes are observed along this stretch of the Darling River, these do not appear to have influenced the behaviour of woody vegetation during the drought. These vegetation communities are thus interpreted to have supplemented river water with

available good quality groundwater resources during the drought in order to exhibit greater condition with respect to other vegetation communities.

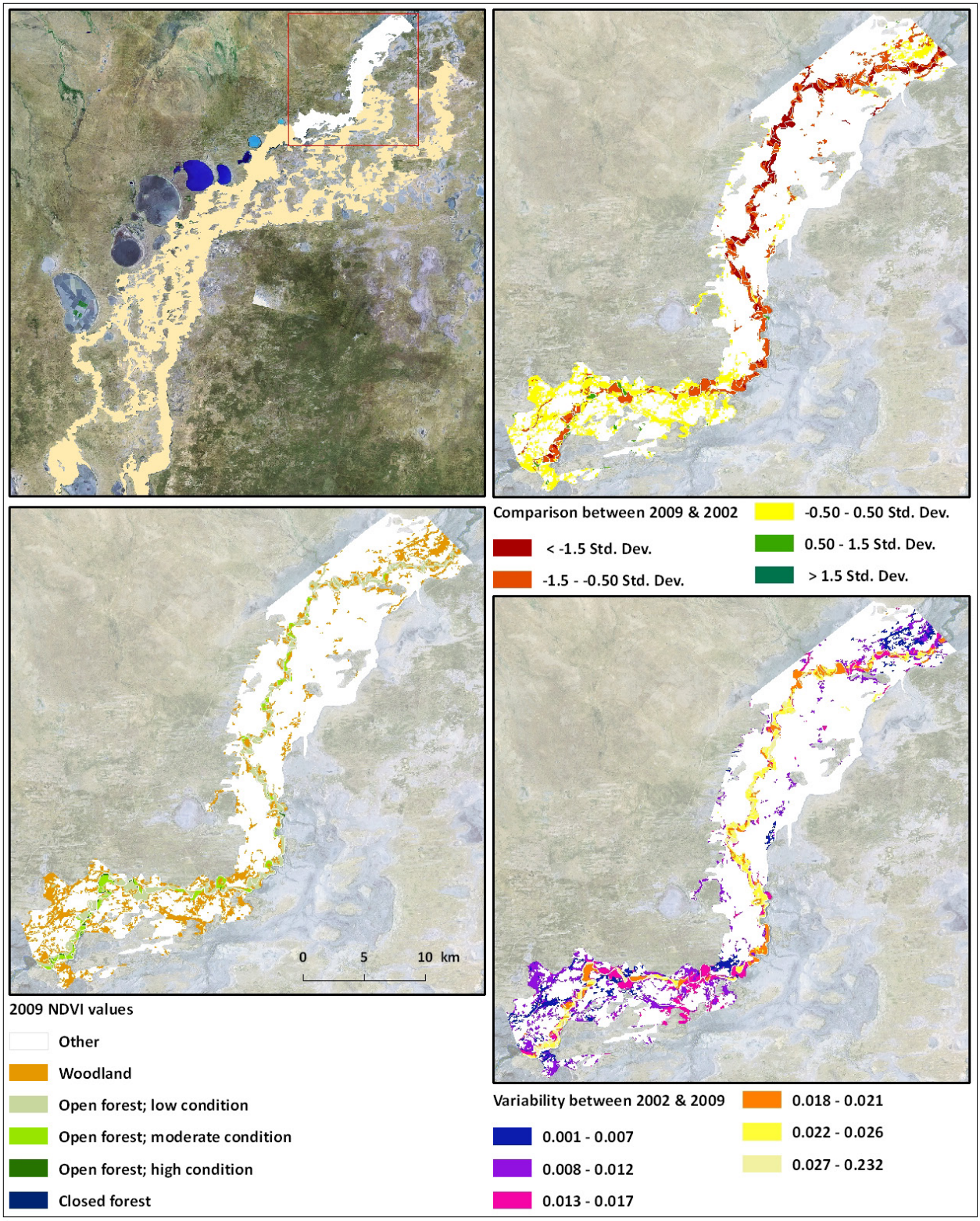

Figure 10-60. *Time series vegetation analysis for Darling River A. Analysis includes condition of vegetation in 2009, comparison between 2009 and 2002, and variability in NDVI throughout the drought (2002-2009).*

In contrast, floodplain vegetation (likely Black Box), maintained condition between 2002 and 2009 and showed minimal variation throughout the drought (Figure 10-60). This floodplain vegetation community is concentrated in the southern end of Darling River A (Figure 10-60) and is more similar to floodplain and riparian zone vegetation in Darling River B (Figure 10-66). These vegetation communities appear to have access to a reliable water source (Figure 10-61 and Figure 10-67).

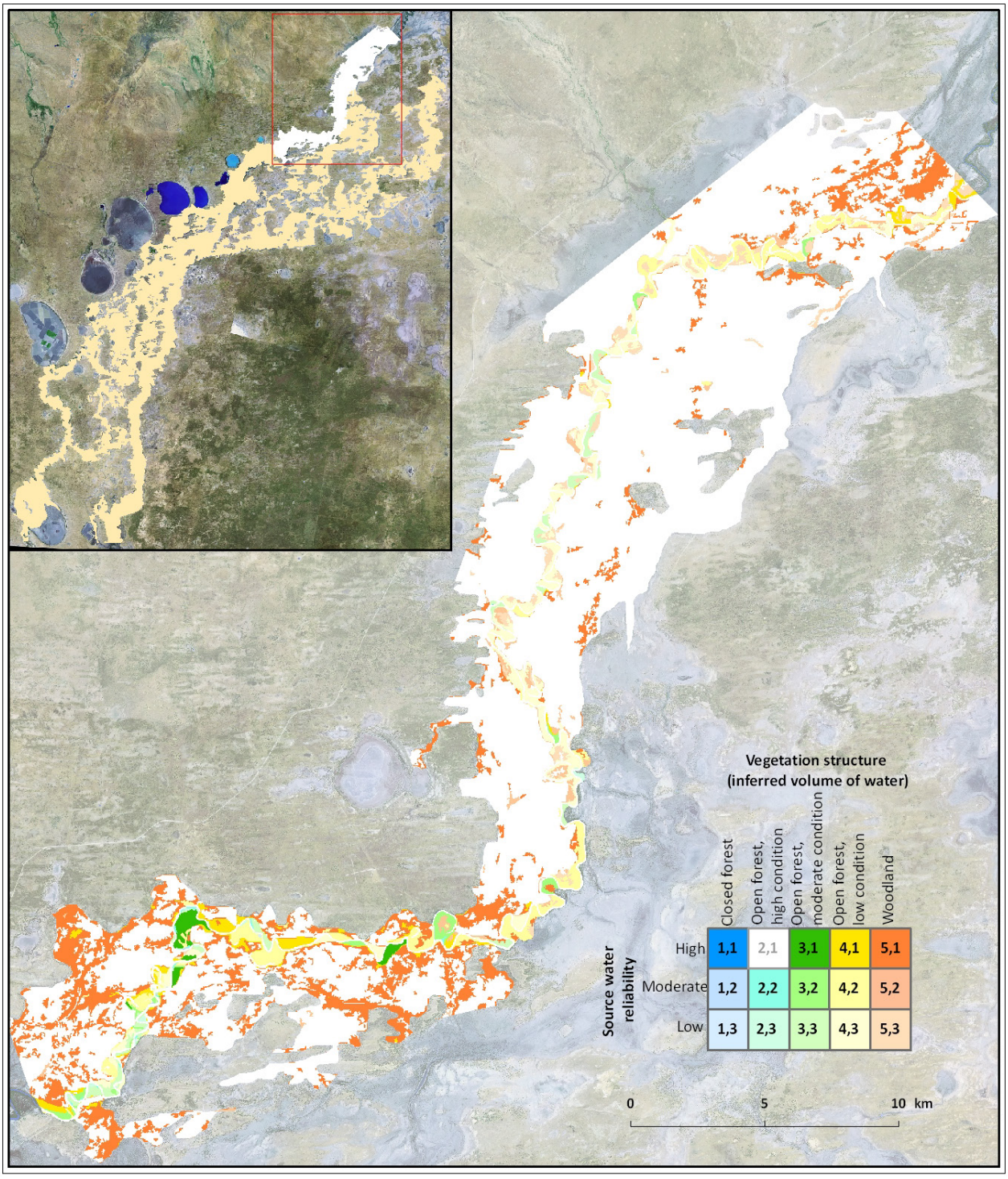

Figure 10-61. *Reliability of source water compared with vegetation condition for Darling River A.*

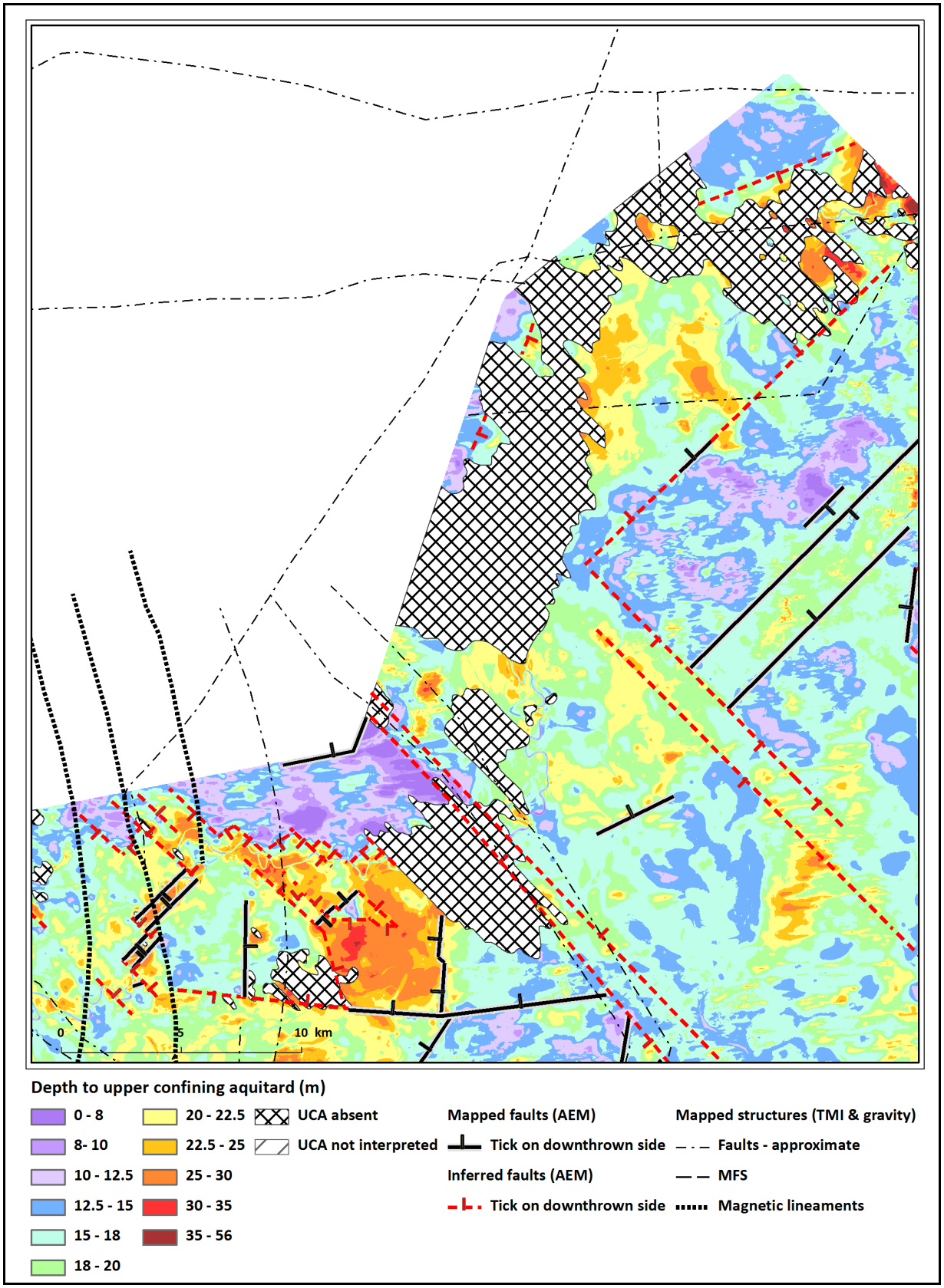

Figure 10-62. *Aquitard map, including depth to the top of the upper confining (UC) aquitard, interpreted holes, faults and lineaments.*

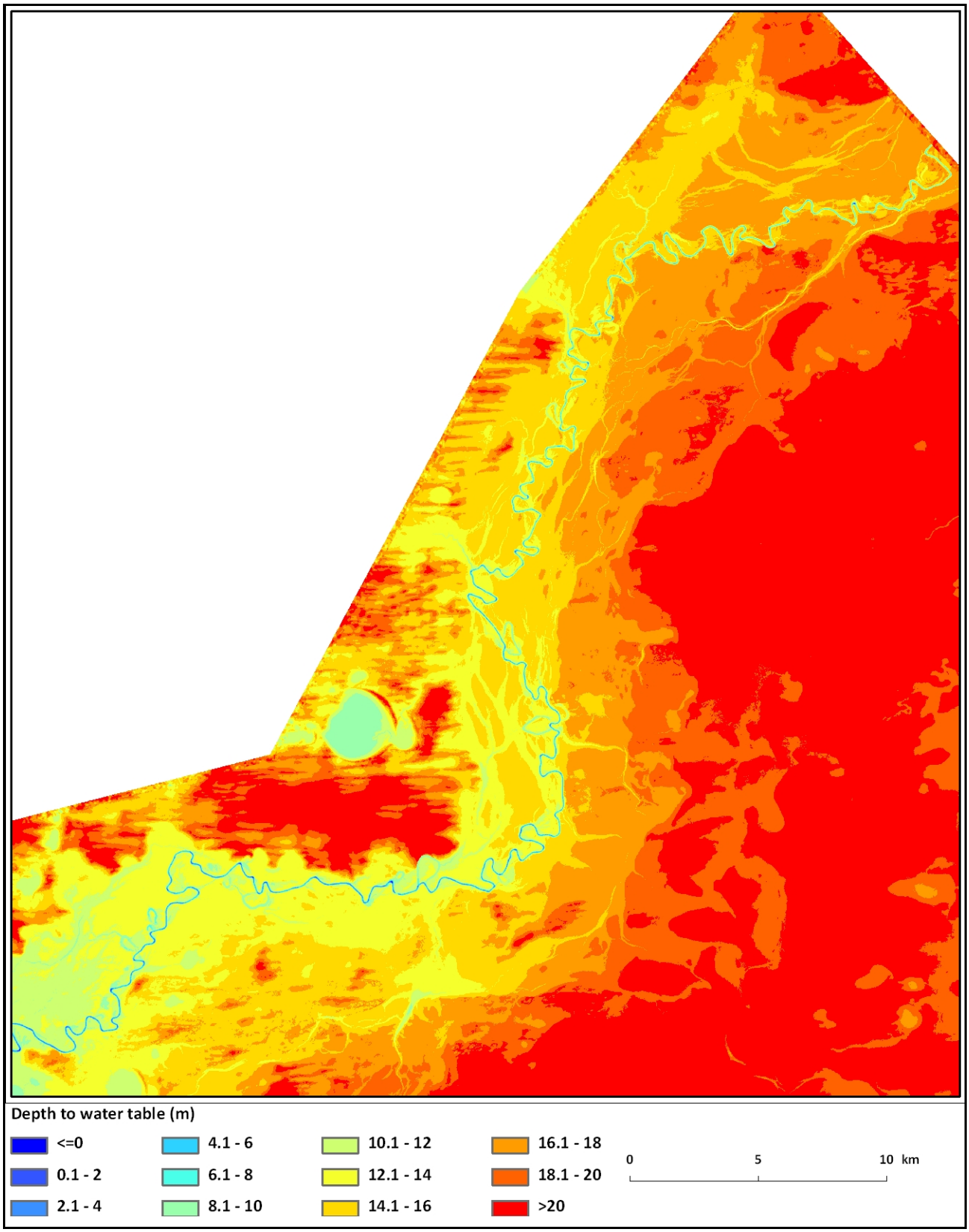

Figure 10-63. *Depth to watertable. This surface has been derived from the potentiometric surface of the surficial aquifer and topography. These values reflect the depth to which the rooting systems of vegetation must travel to encounter the watertable. Values of zero or less indicate the occurrence of groundwater discharge. Values greater than 20 m are likely to be beyond the reach of River Red Gums and Black Box in this landscape.*

Darling River B functions more like a lake than a traditional floodplain; water accumulation occurs immediately behind Lake Pamamaroo (Main Weir) and, depending on the volumes of water, can extend upstream as far as Lake Malta. It is postulated that as a consequence of prolonged surface water accumulation a shallow fresh groundwater resource has developed via recharge processes. Hydrographic data at BHMAR34 measured a response in water levels within both the shallow (Menindee Formation) and deeper (Calivil Formation) aquifers (Figure 10-64). This suggests a highly connected system made possible by holes in the upper confining aquitard (Figure 10-62). Faulting also has the potential to enhance this connectivity.

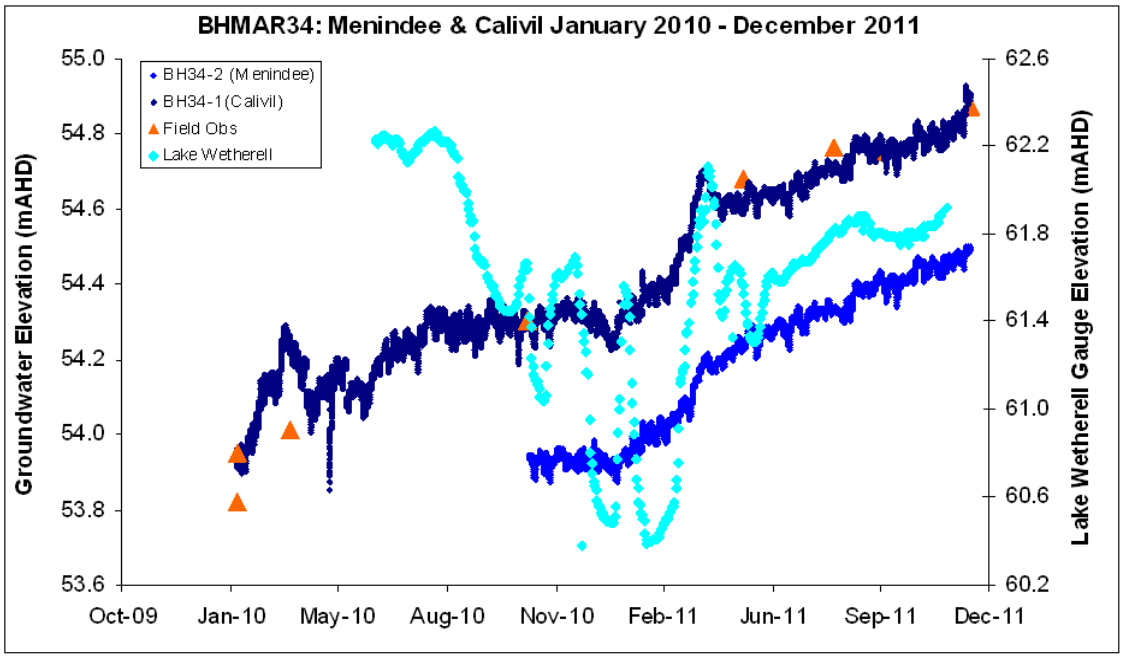

Figure 10-64. *Hydrograph data for BHMAR34 within the shallow (Menindee Formation) and Calivil Formation aquifers. Note the rapid increase in water levels mirrored in both the Menindee and Calivil Formation corresponding with high lake levels.*

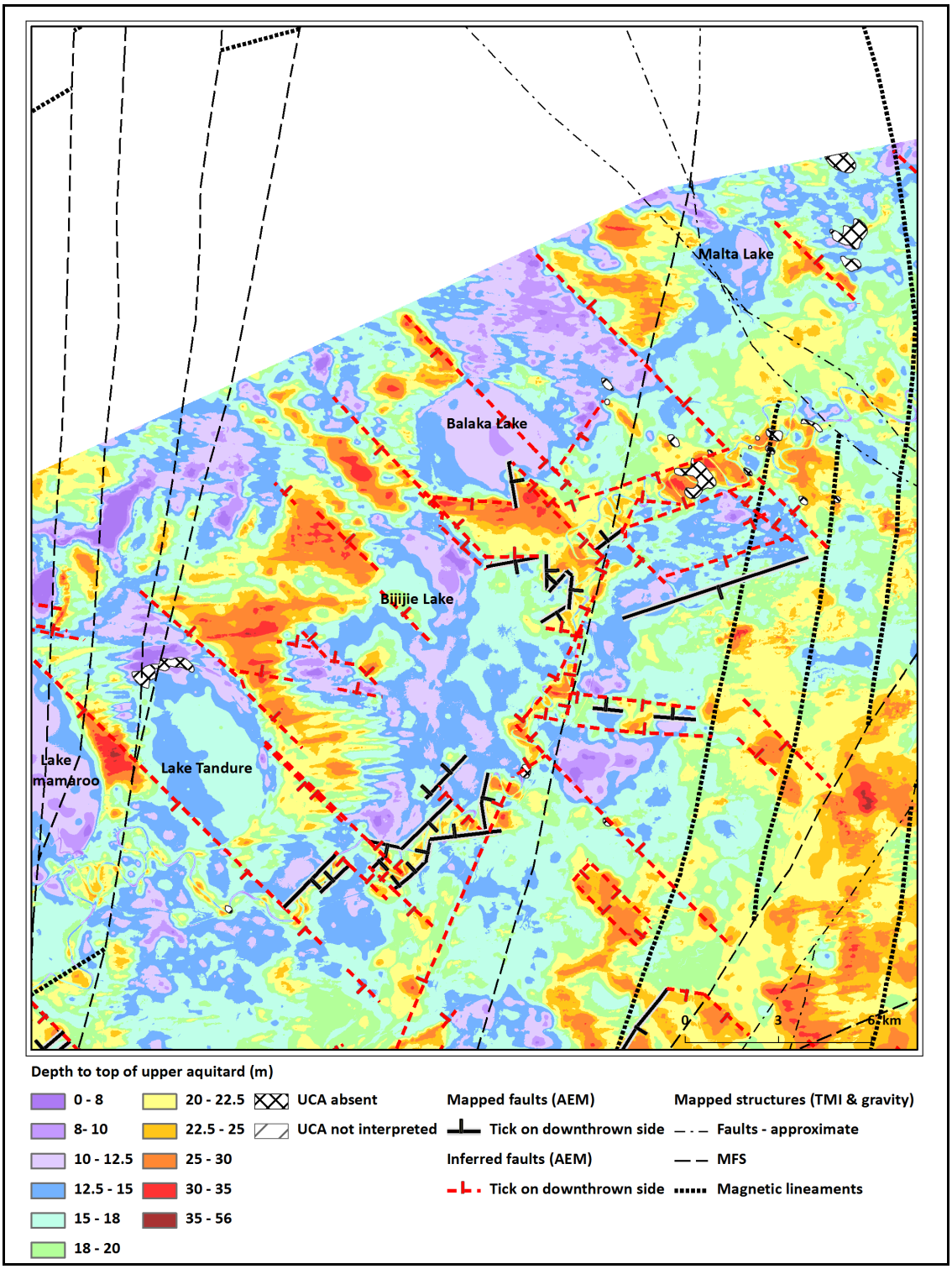

Figure 10-65. *Aquitard map, including depth to the top of the upper confining (UC) aquitard, interpreted holes, faults and lineaments.*

Vegetation is largely absent from the floodplain immediately behind Main Weir (Figure 10-66) due to permanent inundation. Further upstream, beyond where surface waters associated with Lake Wetherell routinely extend, vegetation becomes more common. Of all the river and creek sections in the entire study site, this section supports the most abundant open and closed forest vegetation communities, due to the constant availability of fresh water.

As a general rule, River Red Gum open forest located along the channel, exhibit higher NDVI values in 2009 than Black Box woodlands growing on the floodplain (Figure 10-66). In addition, there appears to be an upstream gradient of declining condition, with open forest vegetation of high condition located closer to the waters of Lake Wetherell; transitioning into open forest of low condition around Bijiji Lake; before becoming a narrow zone of open forest largely confined to the river channel (Figure 10-66). This gradient is also observed when comparing vegetation condition in 2002 to 2009 (Figure 10-66).

As the extent of Lake Wetherell is driven by the amount of water flowing down the Darling River, it can be quite variable. During the drought, inflows were relatively low. Consequently surface water did not extend as far upstream. Vegetation that had previously been inundated dried out by 2009 and improved condition (Figure 10-66). Further upstream, floodplain vegetation condition was maintained (with minimal variation throughout the drought) while riparian zone vegetation condition declined, similar to that observed along Darling River A (Figure 10-66).

Riparian zone vegetation and floodplain vegetation in close proximity to Lake Wetherell are associated with a more variable water source - river flow and lake waters respectively. Floodplain vegetation (beyond the immediate vicinity of Lake Wetherell) appears to have access to a reliable water source, specifically the shallow watertable at depth of 6–10 m (Figure 10-68). It is the presence of this resource that ensured vegetation maintained condition over the course of the drought.

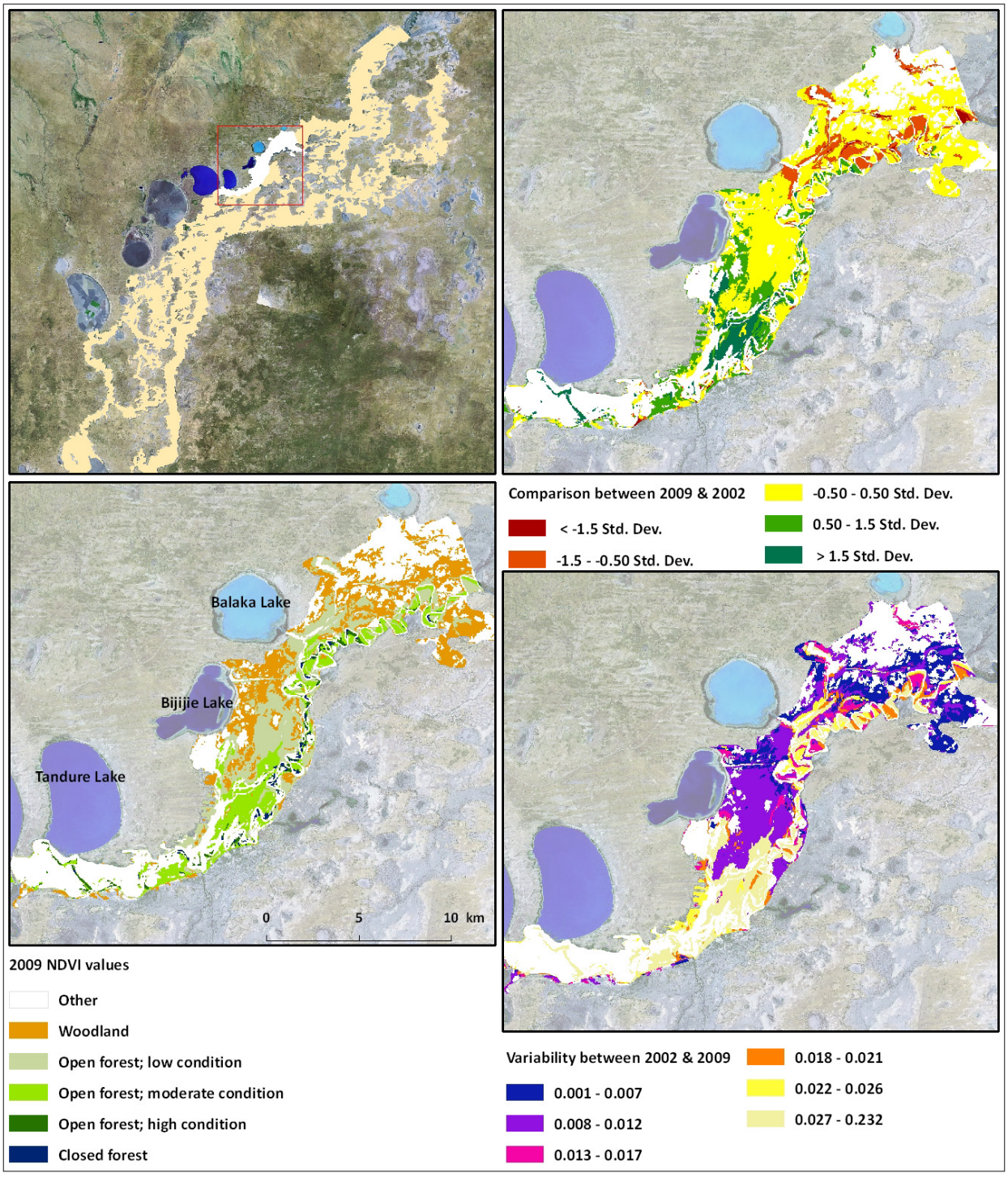

Figure 10-66. *Time series vegetation analysis for Darling River B. Analysis includes condition of vegetation in 2009, comparison between 2009 and 2002, and variability in NDVI throughout the drought (2002-2009).*

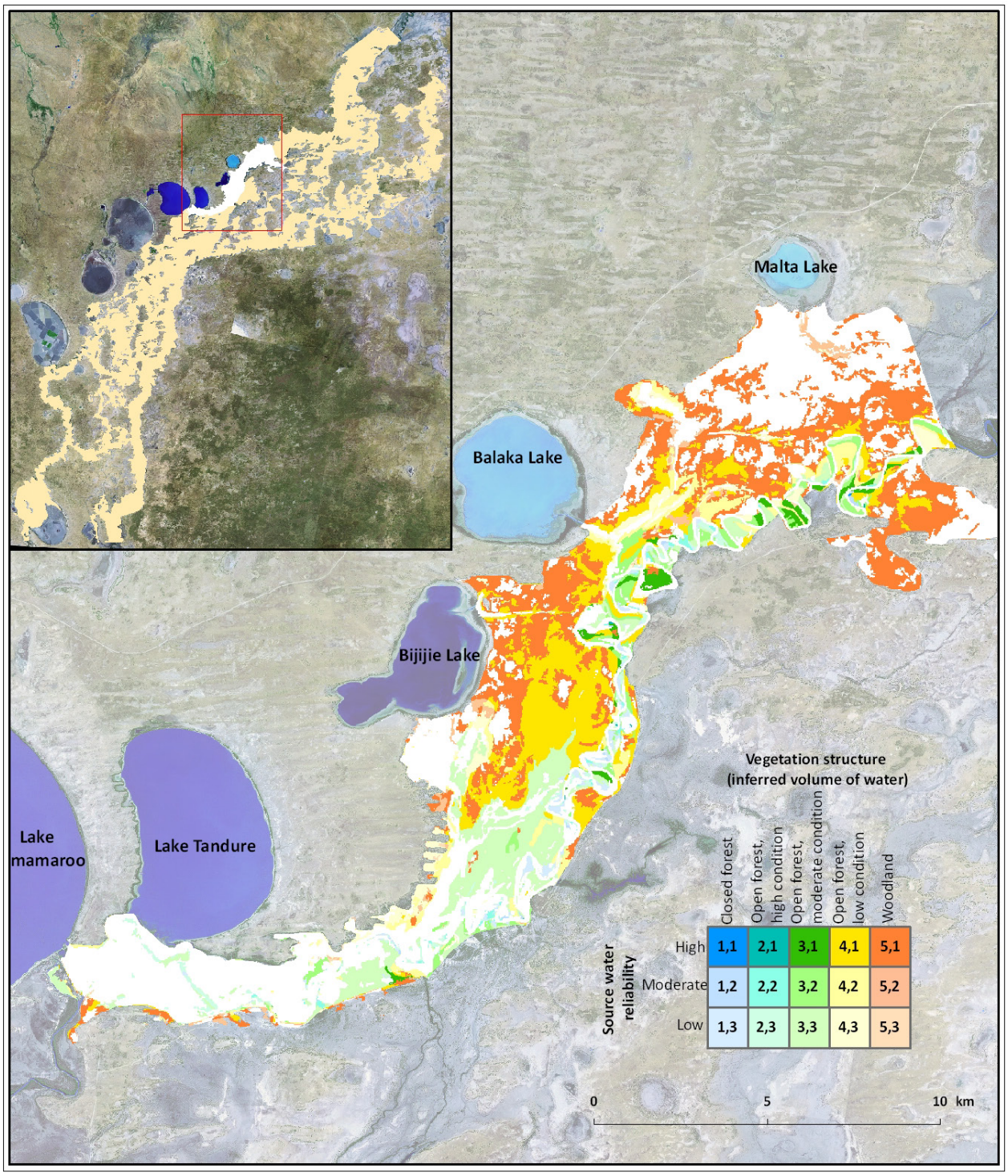

Figure 10-67. *Reliability of source water compared with vegetation condition for Darling River B.*

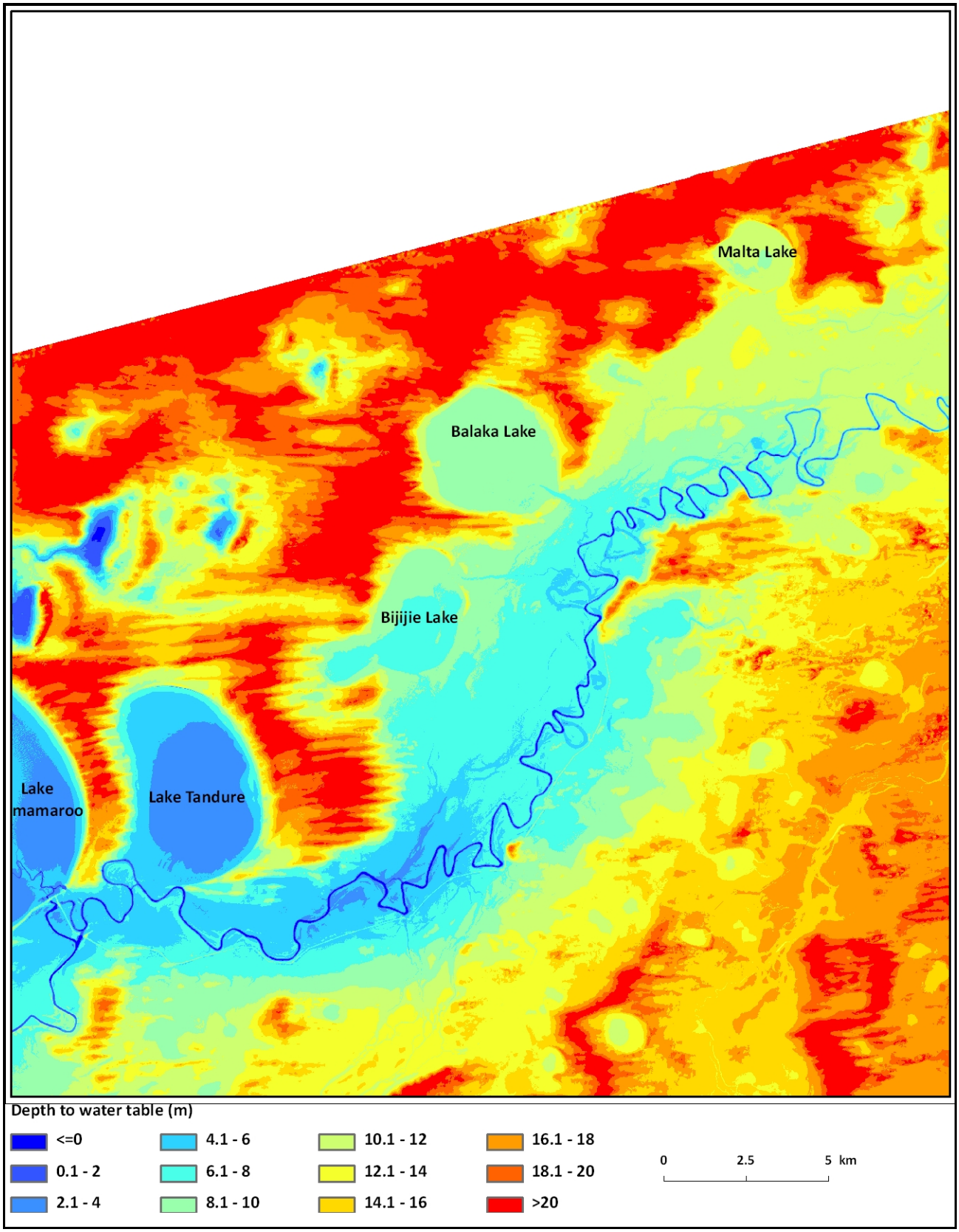

Figure 10-68. *Depth to watertable. This surface has been derived from the potentiometric surface of the surficial aquifer and topography. These values reflect the depth to which the rooting systems of vegetation must travel to encounter the watertable. Values of zero or less indicate the occurrence of groundwater discharge. Values greater than 20 m are likely to be beyond the reach of River Red Gums and Black Box in this landscape.*

Darling River C has both riparian zone and floodplain vegetation (Figure 10-69). The riparian zone River Red Gum open forest was in poorer condition (Figure 10-69) compared to that along Darling River A (Figure 10-60) and B (Figure 10-66). This appears to be a direct result of reduced river flows along this section of the Darling River. There are two means by which this section of the Darling River can receive water. Firstly via released from Main Weir directly into the Darling and secondly water released from Lake Menindee. Riparian vegetation downstream of the outlet regulator at Lake Menindee is associated with a less reliable water source than vegetation upstream of this point (Figure 10-70). This suggests that during the drought, water was more regularly released from Lake Wetherell than Lake Menindee and as a consequence, more of the associated riparian vegetation maintained condition.

Elsewhere, woodland vegetation on the floodplain appears to be supported by shallow groundwater resources at depth of 6–10 m (Figure 10-71) as indicated by their maintained condition at the conclusion of the drought and also over the course of the drought (Figure 10-69).

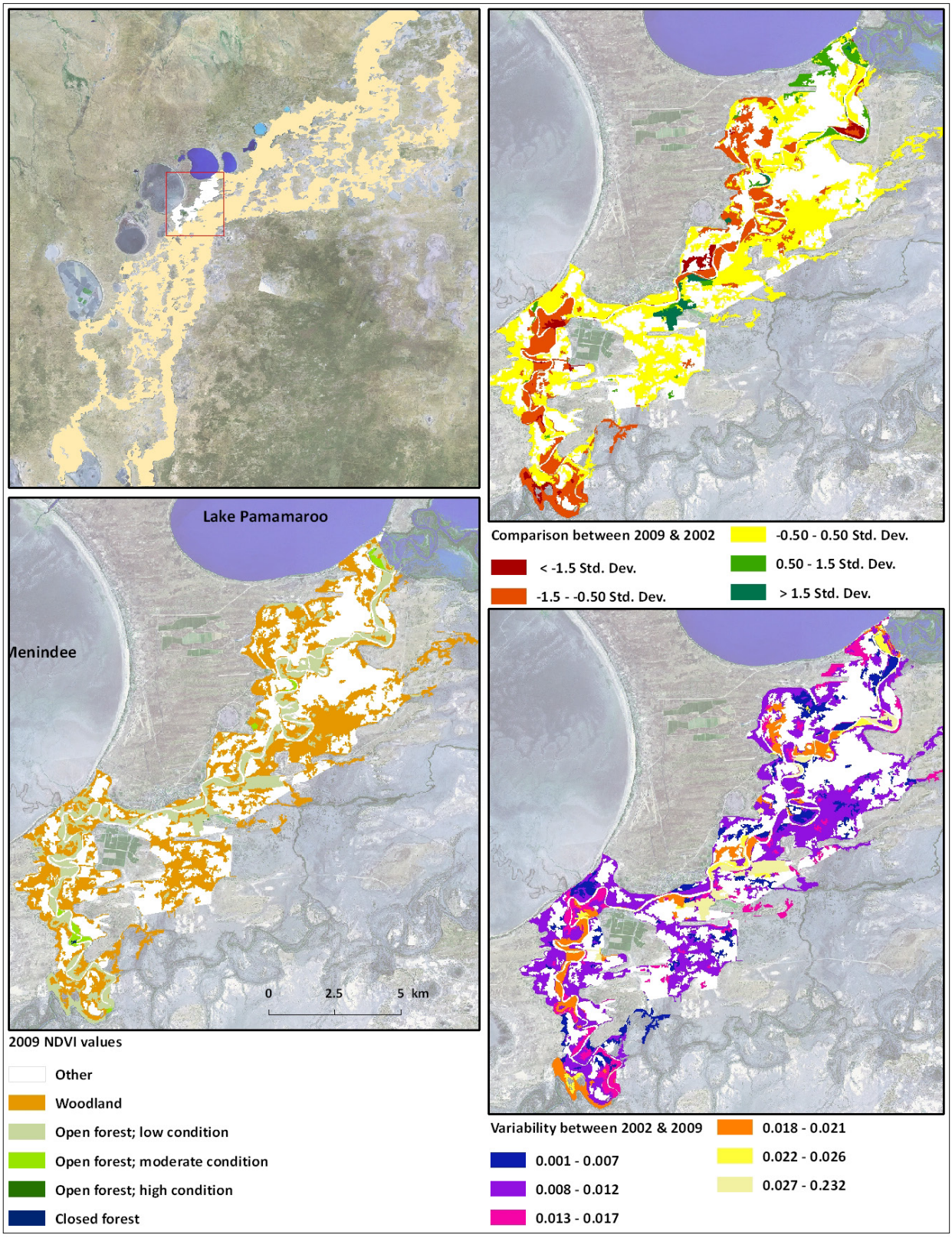

Figure 10-69. *Time series vegetation analysis for Darling River C. Analysis includes condition of vegetation in 2009, comparison between 2009 and 2002, and variability in NDVI throughout the drought (2002-2009).*

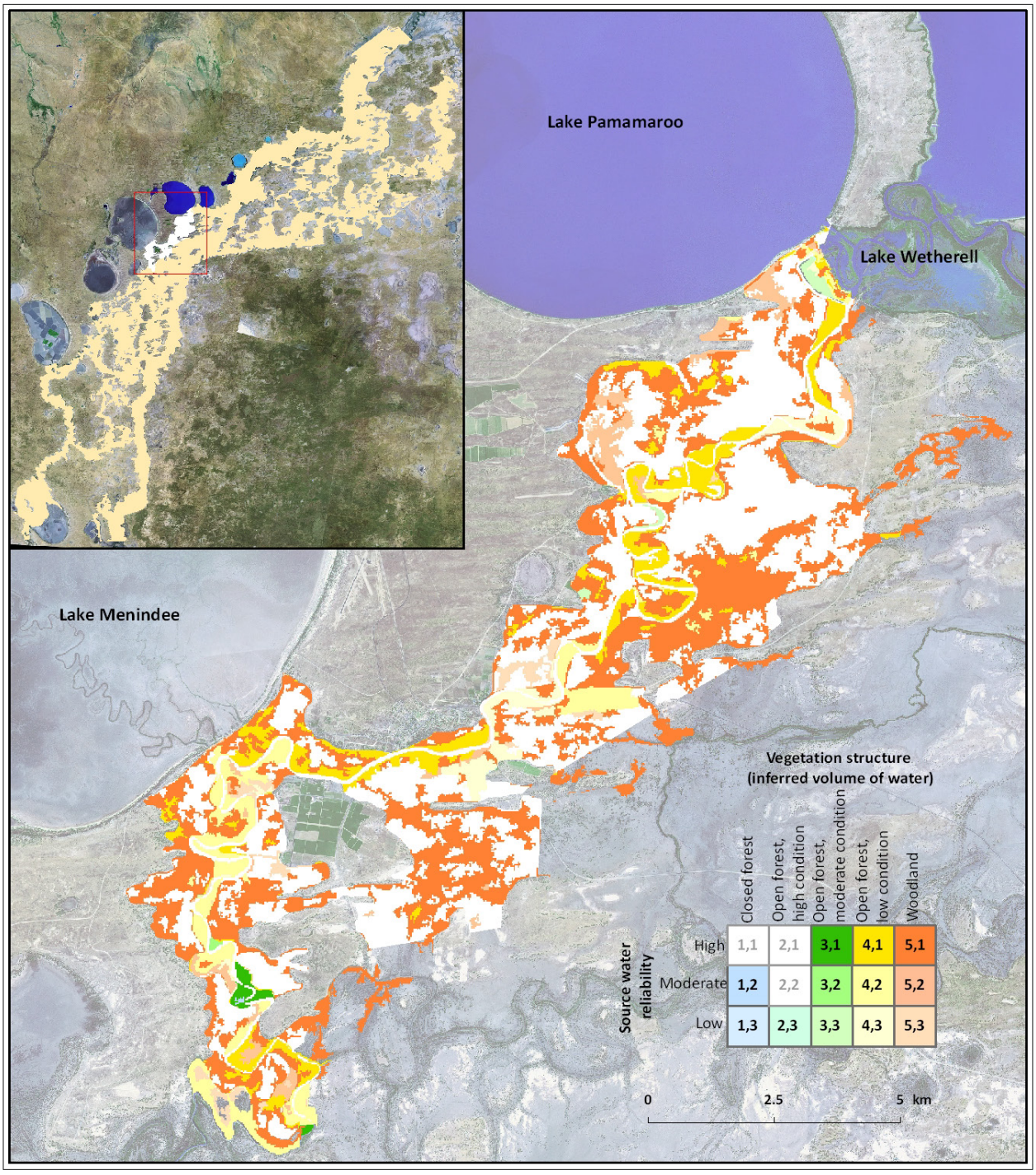

Figure 10-70. *Reliability of source water compared with vegetation condition for Darling River C.*

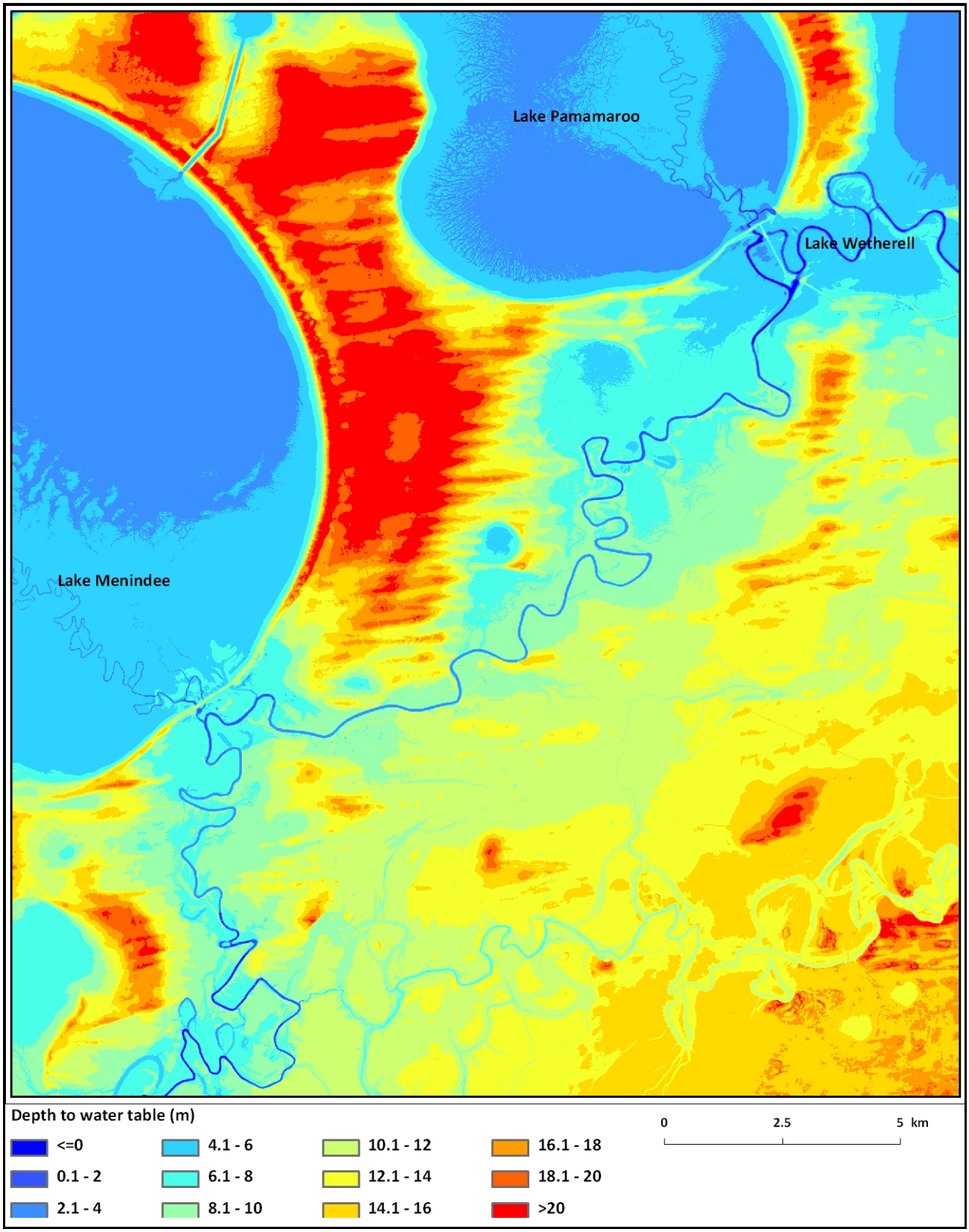

Figure 10-71. *Depth to watertable. This surface has been derived from the potentiometric surface of the surficial aquifer and topography. These values reflect the depth to which the rooting systems of vegetation must travel to encounter the watertable. Values of zero or less indicate the occurrence of groundwater discharge. Values greater than 20 m are likely to be beyond the reach of River Red Gums and Black Box in this landscape.*

Darling River D is more like Darling River A than any other section along the Darling River, in that the riparian zone vegetation is quite distinct from the floodplain vegetation, both in appearance and respond to drought conditions (Figure 10-72). The riparian zone is predominantly composed of River Red Gum open forest, with minor Black Box while the floodplain is dominated by Black Box woodland and sparse River Red Gums. The majority of Darling River D vegetation maintained condition between 2002 and 2009 however there were some isolated vegetation communities that either improved or declined (Figure 10-72). The reason for this still remains unclear.

As was the case with Darling River C, condition of riparian zone vegetation appears to be more variable (Figure 10-72), suggesting greater reliance on surface water flows. That fact that condition was maintained by the end of the drought suggests that river flows experienced during the drought were sufficient to sustain the condition of associated riparian vegetation. Floodplain vegetation condition remained more constant, suggesting access to shallow groundwater at depth of less than 12 m (Figure 10-74). Irrespective of the water source, reliability appears to be uniformly high (Figure 10-72) which has resulted in the maintained condition of both riparian and floodplain vegetation.

The presence of a number of small holes in the upper confining aquitard (Figure 10-75) indicates a degree of connectivity between the shallow and deeper (Calivil Formation) aquifers. As vegetation on the floodplain and also potentially along the river utilized the shallow groundwater resources during the drought, vegetation may also be indirectly accessing groundwater within the Calivil Formation aquifer. The target is also extensively faulted (Figure 10-75); some of these faults propagate through the upper confining aquitard and as such may result in increased connectivity between aquifers.

A large proportion of the woody vegetation interpreted to have accessed shallow groundwater resources during the drought is associated with interpreted holes in the upper confining aquitard, faults or lineaments. Consequently these vegetation communities may also be indirectly accessing Calivil Formation groundwater.

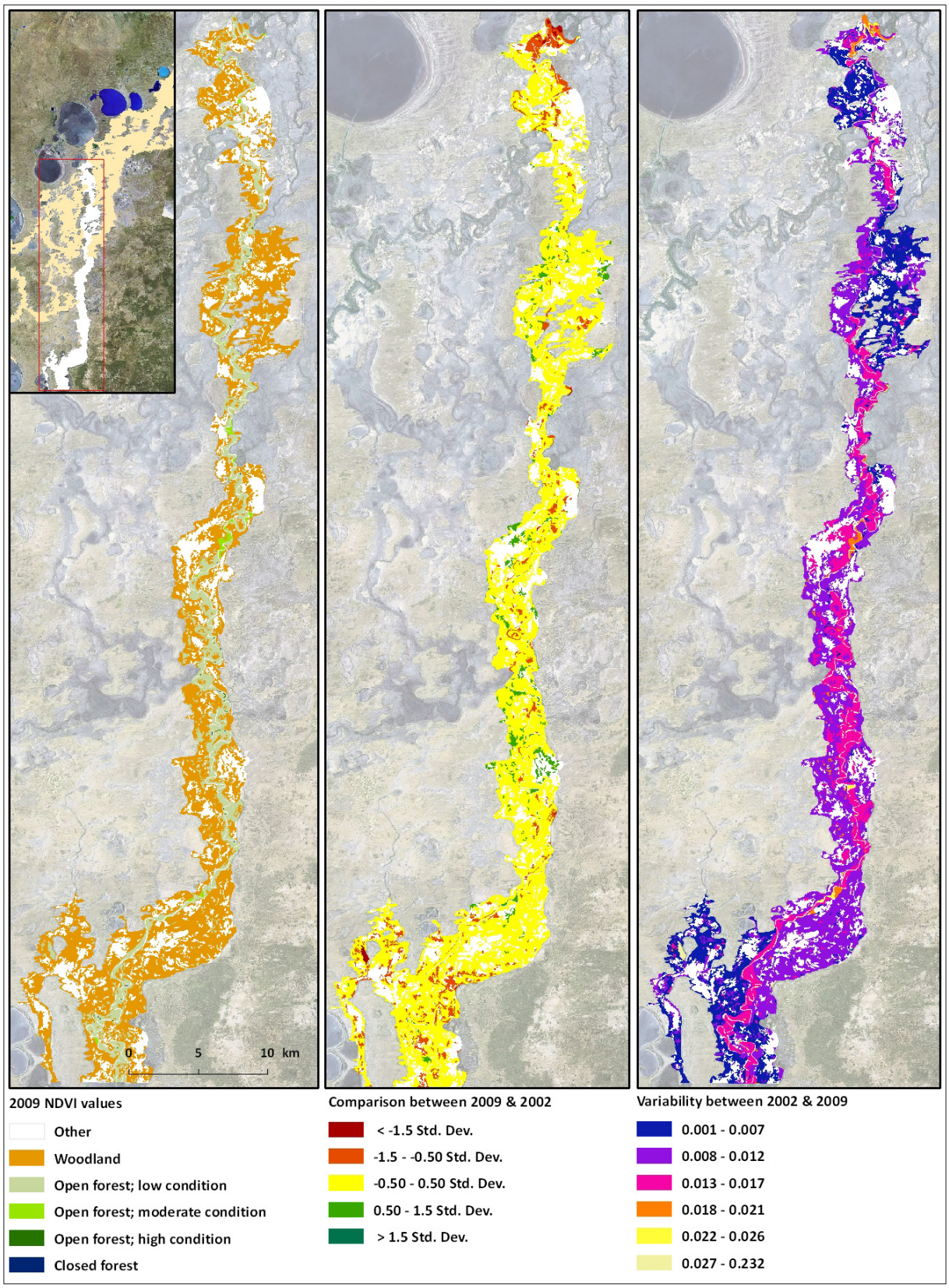

Figure 10-72. *Time series vegetation analysis for Darling River D. Analysis includes condition of vegetation in 2009, comparison between 2009 and 2002, and variability in NDVI throughout the drought (2002-2009).*

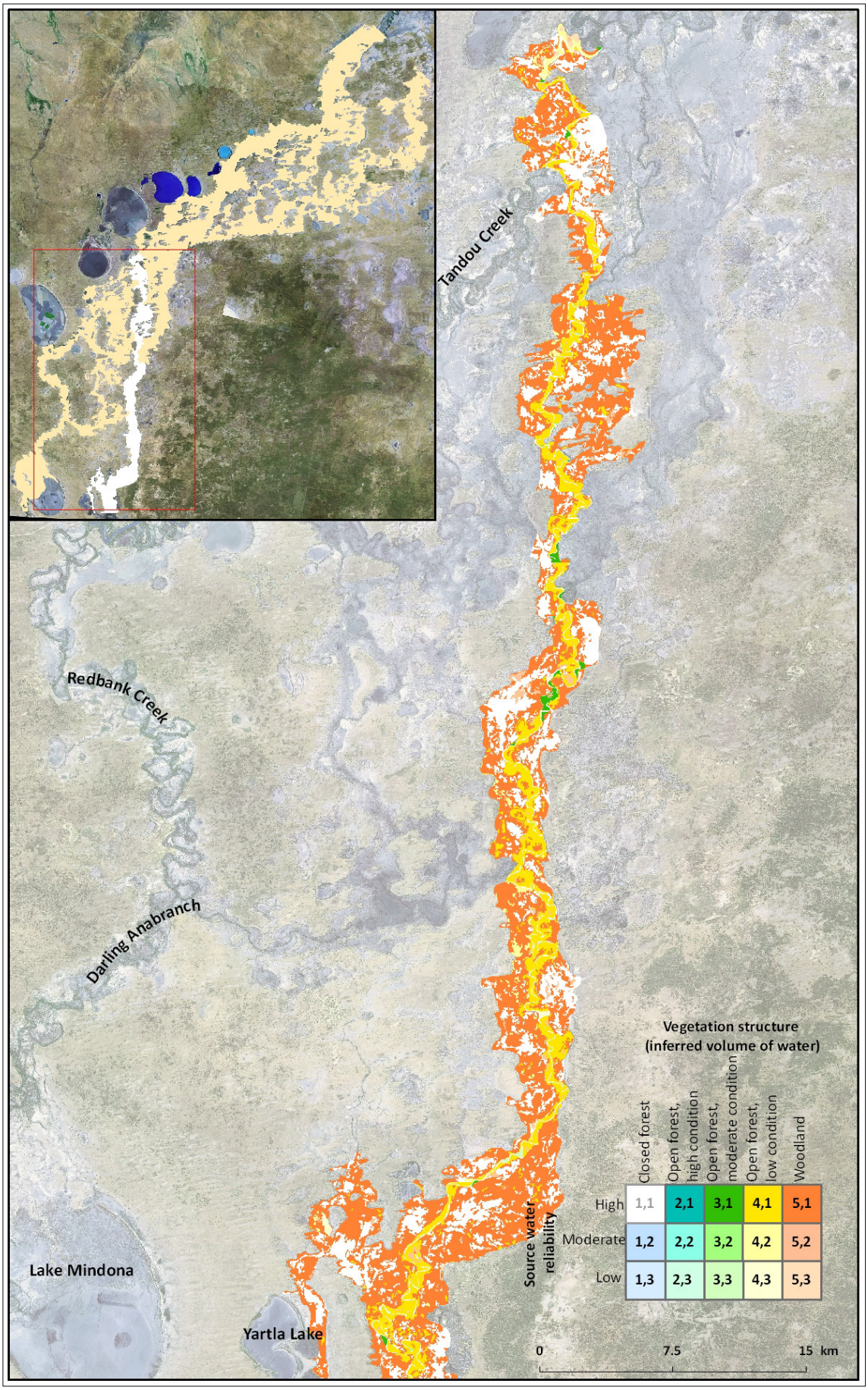

Figure 10-73. *Reliability of source water compared with vegetation condition for Darling River D.*

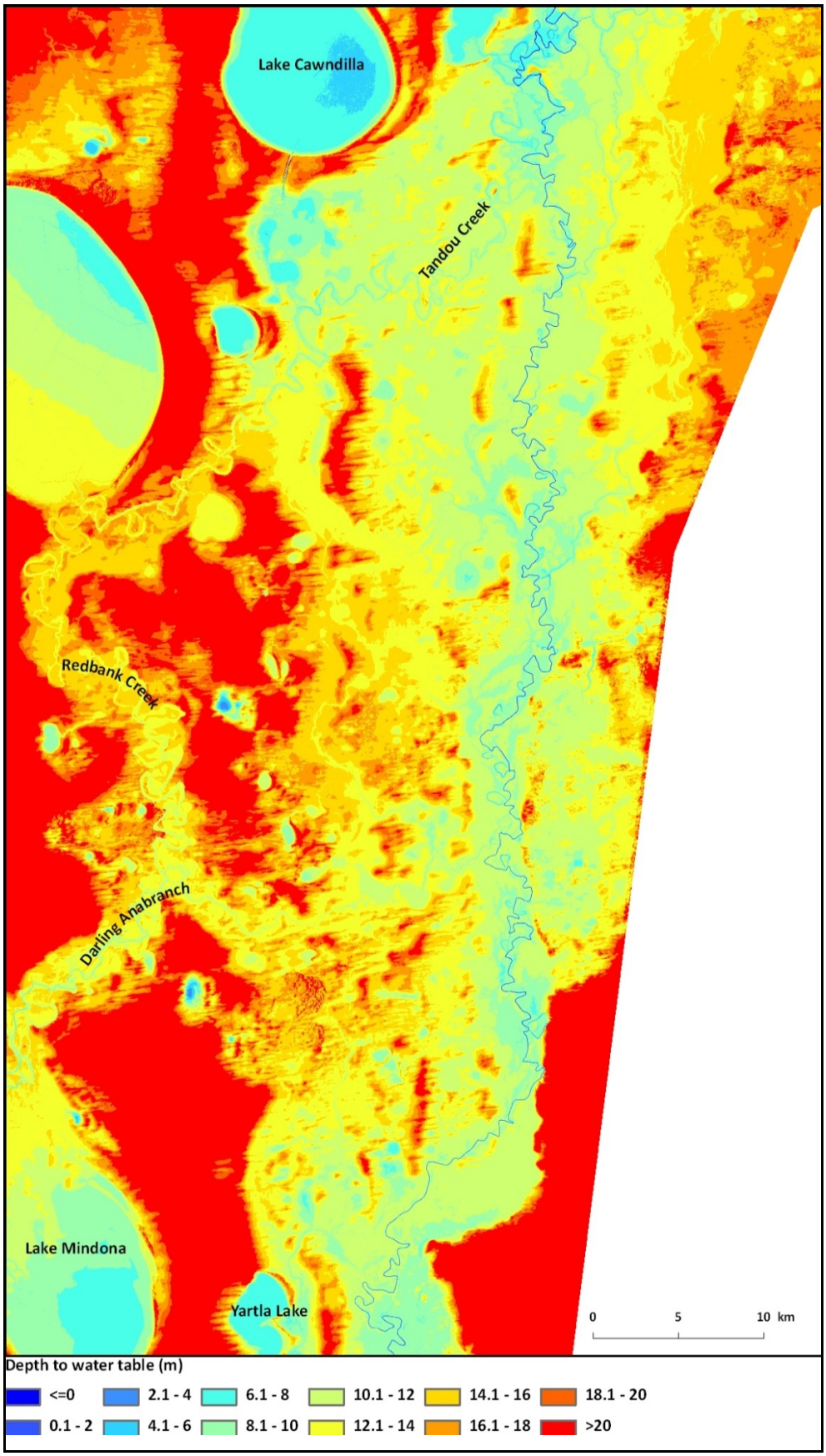

Figure 10-74. *Depth to watertable. This surface has been derived from the potentiometric surface of the surficial aquifer and topography. These values reflect the depth to which the rooting systems of vegetation must travel to encounter the water table. Values of zero or less indicate the occurrence of groundwater discharge. Values greater than 20 m are likely to be beyond the reach of River Red Gums and Black Box in this landscape.*

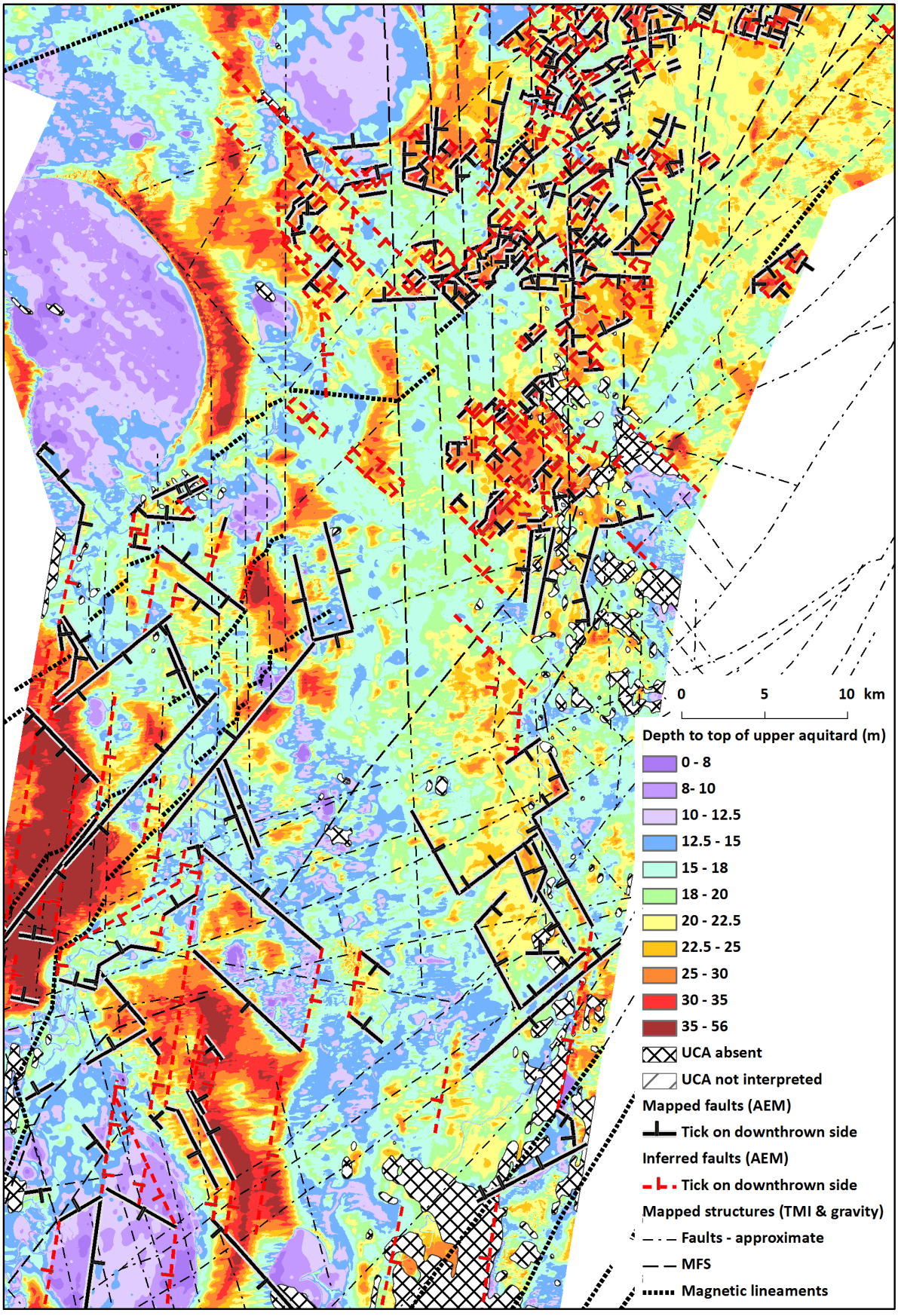

Figure 10-75. *Aquitard map, including depth to the top of the upper confining (UC) aquitard, interpreted holes, faults and lineaments.*

Talyawalka Creek (and Relict Talyawalka)

Talyawalka Creek is an ephemeral anabranch of the Darling River, diverging upstream of Wilcannia. The bottom end of Talyawalka Creek is connected to the Darling River by anastomosing channels, Yampoola Creek and Charlie Stones Creek (Withers, 1996). Talyawalka Creek only ever receives flows during high flood. Under current climatic conditions in this regulated system, the frequency of such events is low and overbank flooding only typically occurs as a consequence of particularly large events (e.g. 1990 flood). As a consequence of this, the floodplain is unable to support any vegetation and only riparian woodland vegetation grows along the creek channel (Figure 10-76).

The watertable is quite deep beneath much of Talyawalka Creek, ranging from 8–12 m beneath the channel to anywhere from 12 m in the floodplain closer to the Darling River, 16 m in central floodplain to greater than 20 m in the upstream floodplain (Figure 10-77). Saturated thickness of the shallow unconfined aquifer (Coonambidgal and Menindee Formations) varies. In some cases there the aquifer is unsaturated and instead the watertable is located within the aquitard (Blanchetown clay and upper clay-rich Calivil Formation) or the deeper semi-confined aquifer (Calivil Formation) as shown in Figure 10-78. The uppermost section of Talyawalka Creek (within the BHMAR study area) supports hardly any riparian vegetation (Figure 10-76) even though it receives the greatest amount of floodwaters during any flood event; further downstream, approximately half of the floodwaters divert down Teraweynya Creek and the Talyawalka Chain of Lakes (Withers, 1996). This upper section of the Talyawalka is subject to the deepest watertable of the whole creek, contains minimal clay in the top 5 m (Figure 10-79) to retain water in the unsaturated zone and either does not have a upper confining aquitard present or the aquitard is at considerable depth (greater than 30 m; Figure 10-80).

Under these conditions, surface water is likely to infiltrate through the soil profile directly recharging the Calivil Formation aquifer and moving laterally through the system. In the presence of the upper confining aquitard water can be held in the shallow aquifer or within the unsaturated zone as soil moisture. Due to the combination of infrequent flows down Talyawalka Creek, the limited water holding capacity of the unsaturated zone and the deep watertable, it is not surprising that little woody vegetation exists here. What vegetation is present likely utilizes soil moisture.

On the whole, riparian vegetation along Talyawalka Creek is maintained throughout the drought; there are two sections where vegetation condition showed more variability and overall declined in condition (Figure 10-76). These locations appear to loosely correspond with mapped holes in the upper confining aquitard. It is postulated that the little water available along this section of Talyawalka Creek recharges the deep watertable rather than being held within the vadose zone. This conclusion is supported by fuzzy-k mean analysis at BHMAR16-1, which reported the occurrence of vertical recharge. More details regarding recharge processes are discussed in Section 9.

The remainder of riparian vegetation associated with Talyawalka Creek appears to have maintained low condition, presumably supported by sporadic rainfall and any available soil moisture held in the unsaturated zone.

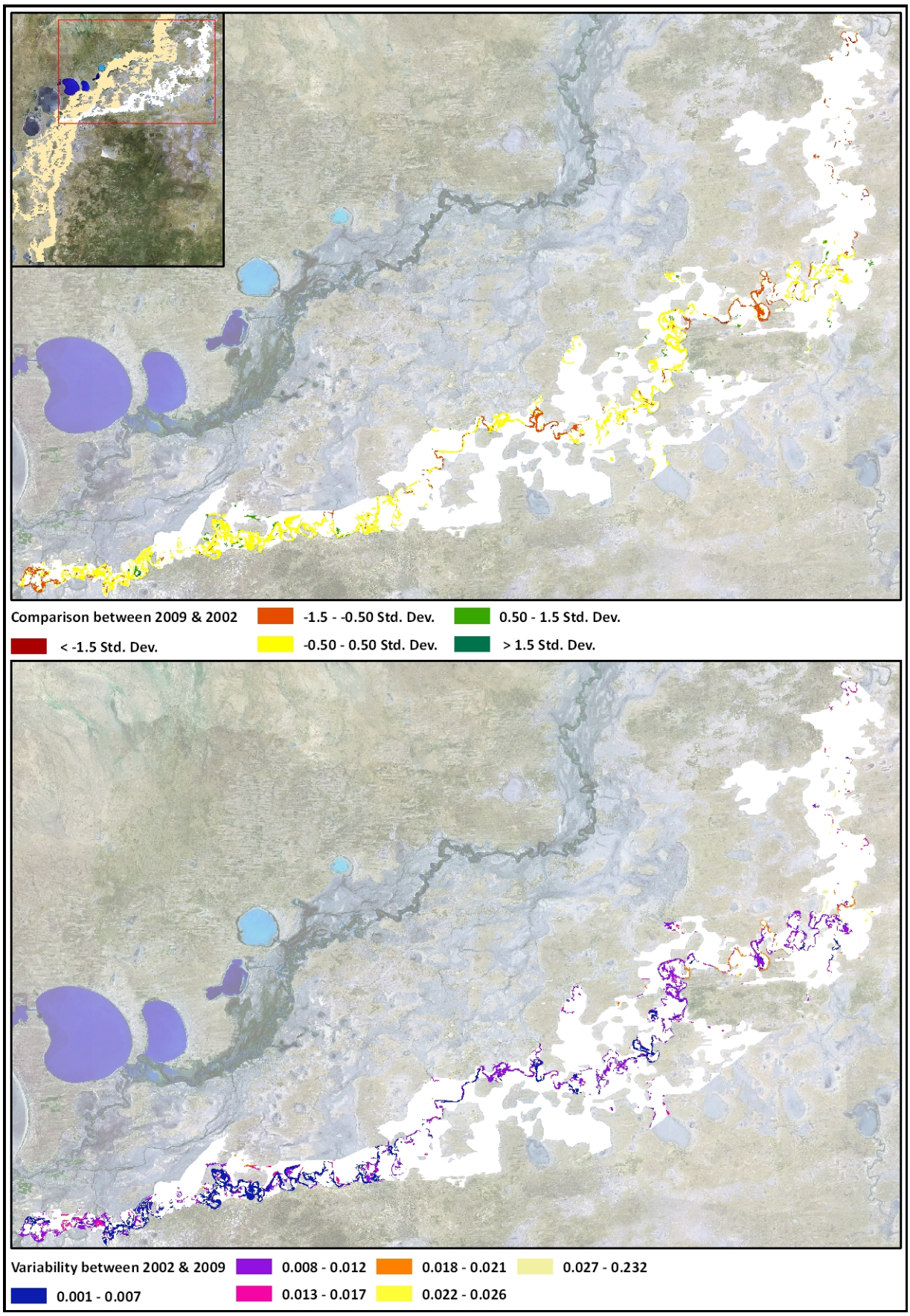

Figure 10-76. *Time series vegetation analysis for Talyawalka Creek. Analysis includes condition of vegetation in 2009, comparison between 2009 and 2002, and variability in NDVI throughout the drought (2002-2009).*

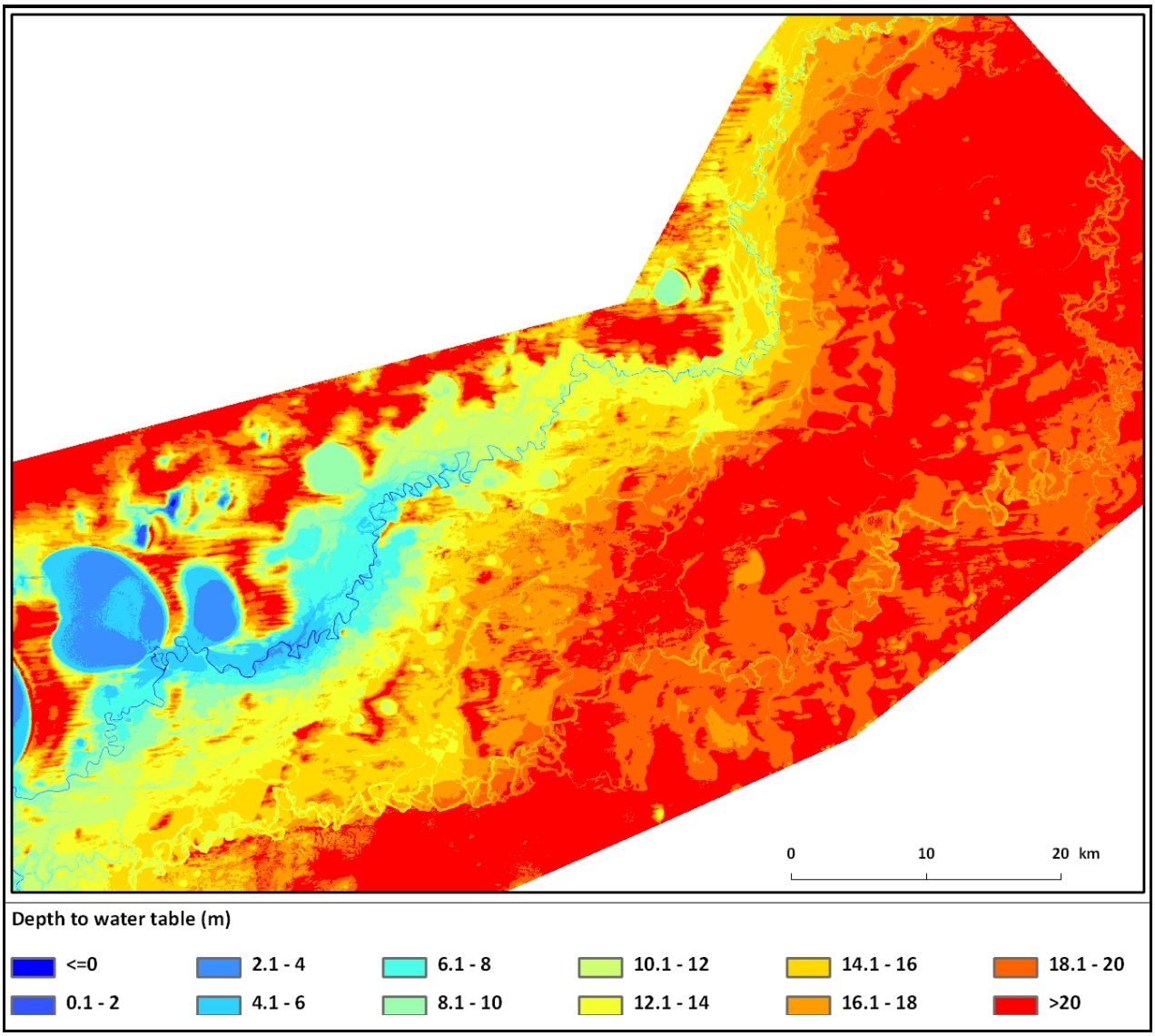

Figure 10-77. *Depth to watertable. This surface has been derived from the potentiometric surface of the surficial aquifer and topography. These values reflect the depth to which the rooting systems of vegetation must travel to encounter the water table. Values of zero or less indicate the occurrence of groundwater discharge. Values greater than 20 m are likely to be beyond the reach of River Red Gums and Black Box in this landscape.*

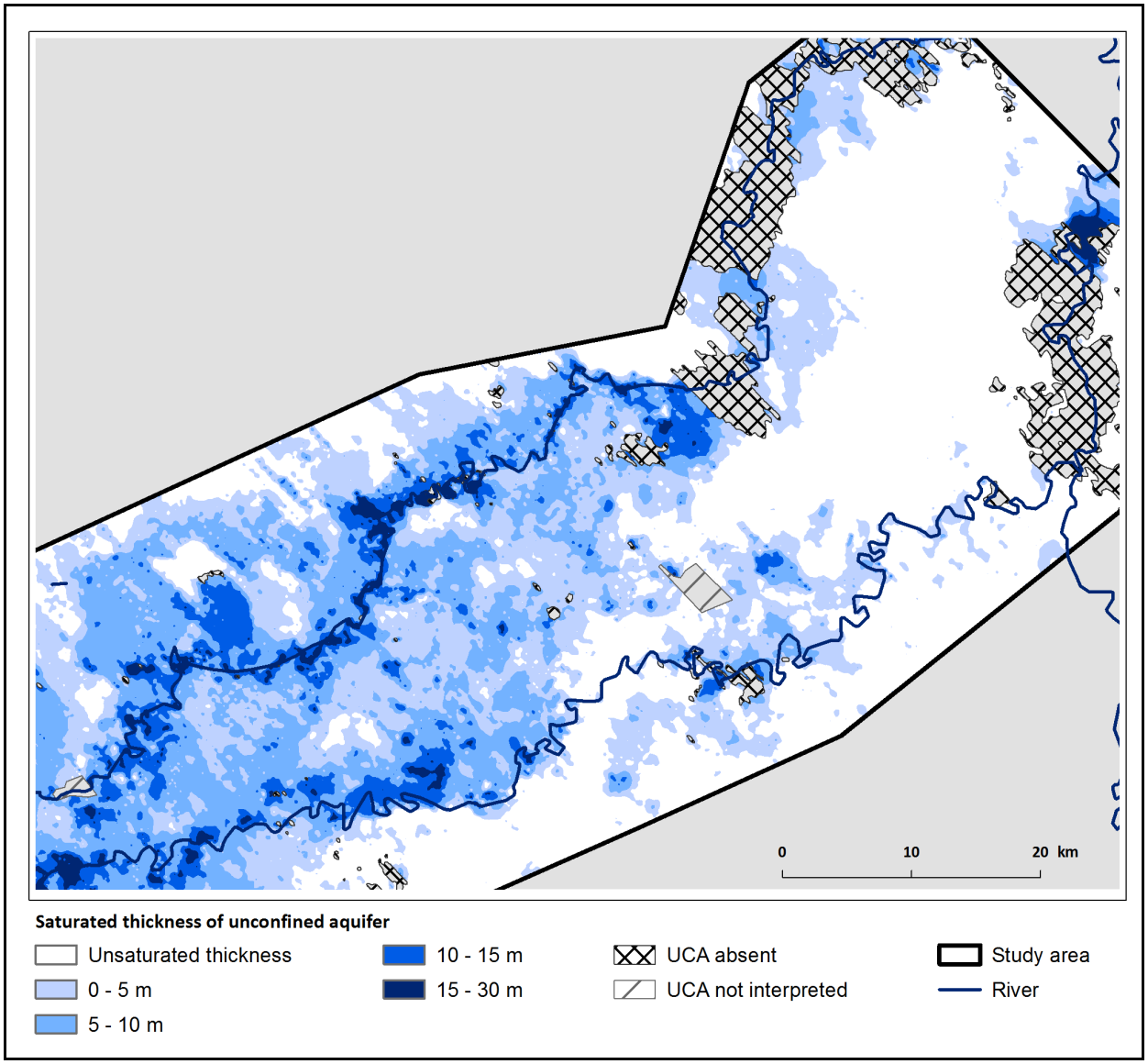

Figure 10-78. *Saturated thickness of the shallow unconfined aquifer. Note the large proportion of Menindee/Coonambidgal Formation that is unsaturated in the upper section of Talyawalka Creek. The watertable at this location is either within the upper confining aquitard or the semi-confined Calivil Formation aquifer.*

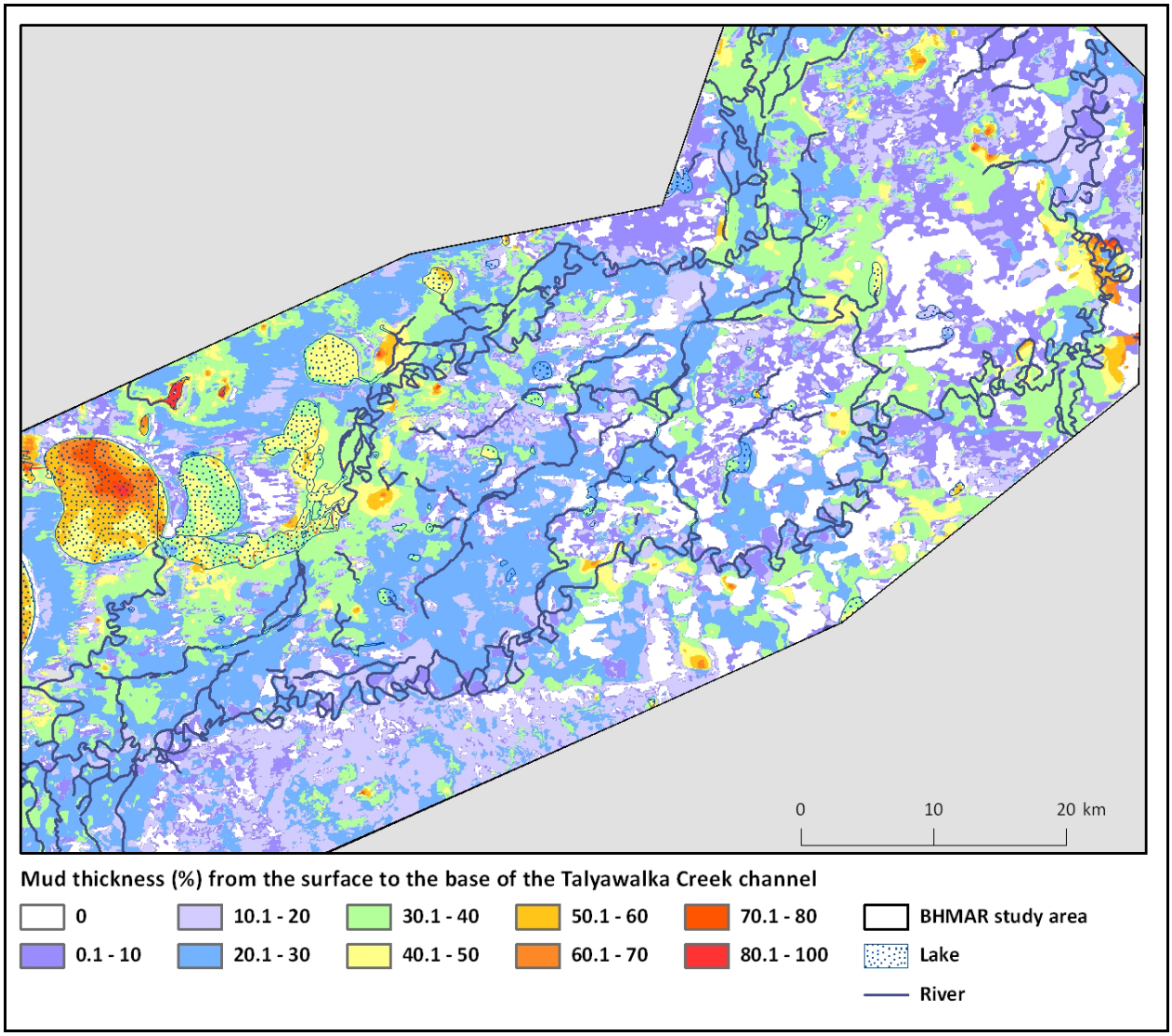

Figure 10-79. *Thickness of near-surface (mud) aquitard, represented as a percentage of the sub-surface profile extending from the surface to the base of the Talyawalka Creek channel (at 5 m depth). River linework was produced for a 1:250,000 usable scale, hence there is some discrepancy between this dataset and the near-surface aquitard mapping.*

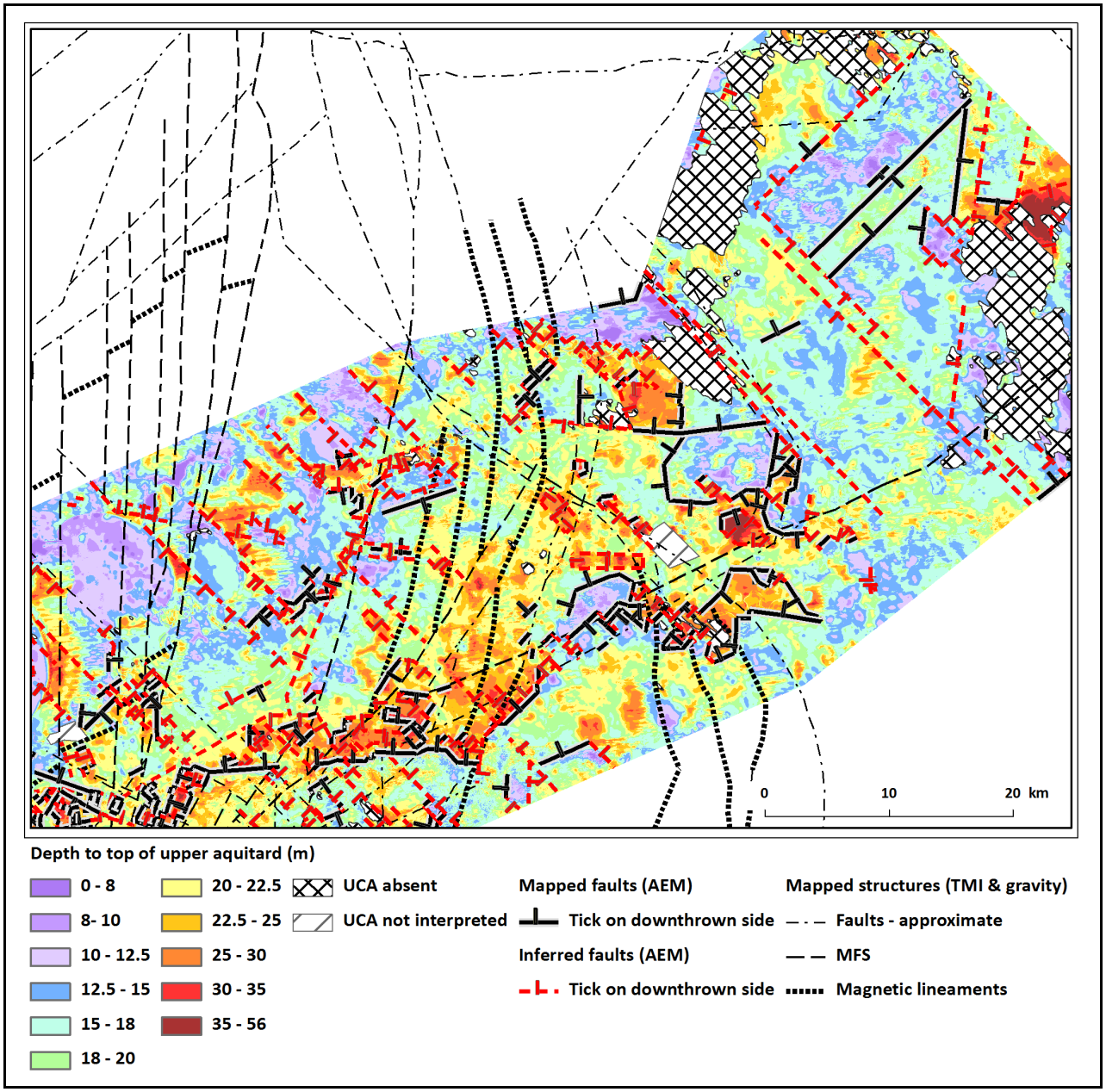

***Figure 10-80**. Aquitard map, including depth to the top of the upper confining (UC) aquitard, interpreted holes, faults and lineaments.*

Three, Seven and Nine Mile Creeks

Seven/Nine Mile Creek is completely unregulated, receiving flows only during high flood events, and as such unlikely to have received any flows during the drought period. These creeks are connected to Darling River A, Darling River B, Talyawalka Creek and Three Mile Creek. Where the creek attaches to the Darling River just upstream of Lake Wetherell, vegetation was in better condition in 2009, improved from 2002 to 2009 and showed greater variability in condition throughout the drought (Figure 10-81). This vegetation appears to have responded to a more variable and abundant supply of water (e.g. Lake Wetherell; Figure 10-82). Elsewhere Black Box woodlands are concentrated along the creek channels and typically either maintained condition or declined slightly during the course of the drought (Figure 10-81). These vegetation communities thus appeared to have had access to a reliable water source during the drought period (Figure 10-82).

There is minimal clay (20-30%) in the top 5 m (Figure 10-84) therefore minimal soil moisture is expected in the unsaturated zone. Depth to the watertable is at least 12 m and in most cases greater than 14 m (Figure

10-83). While this is towards the upper limit of reported rooting depth for sclerophyll vegetation, it is perceivable that in a water limited environment, Black Box may be capable of accessing groundwater resources at these depths.

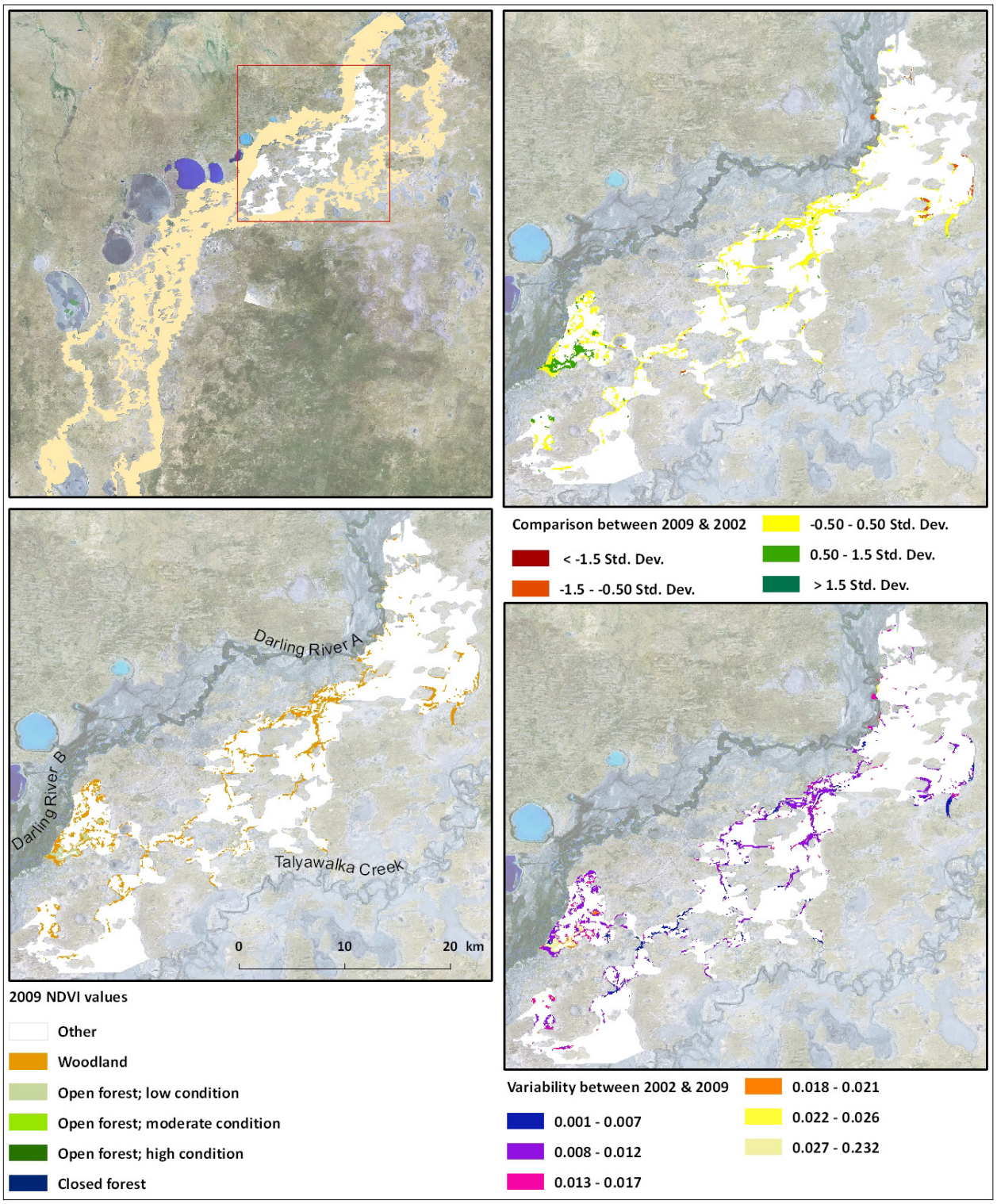

Figure 10-81. *Time series vegetation analysis for Seven and Nine Mile Creeks River A. Analysis includes condition of vegetation in 2009, comparison between 2009 and 2002, and variability in NDVI throughout the drought (2002-2009).*

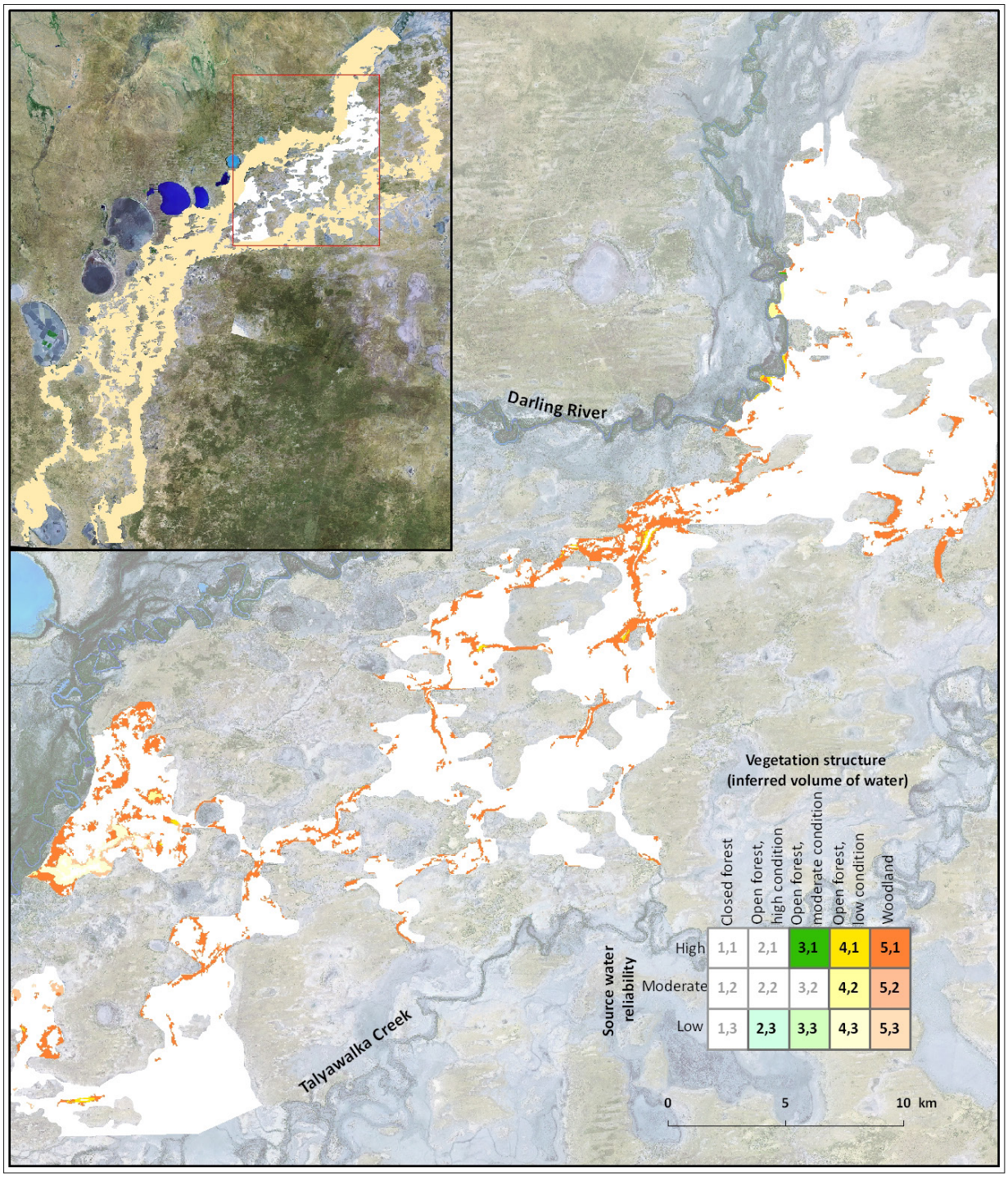

Figure 10-82. *Reliability of source water compared with vegetation condition for Darling River A.*

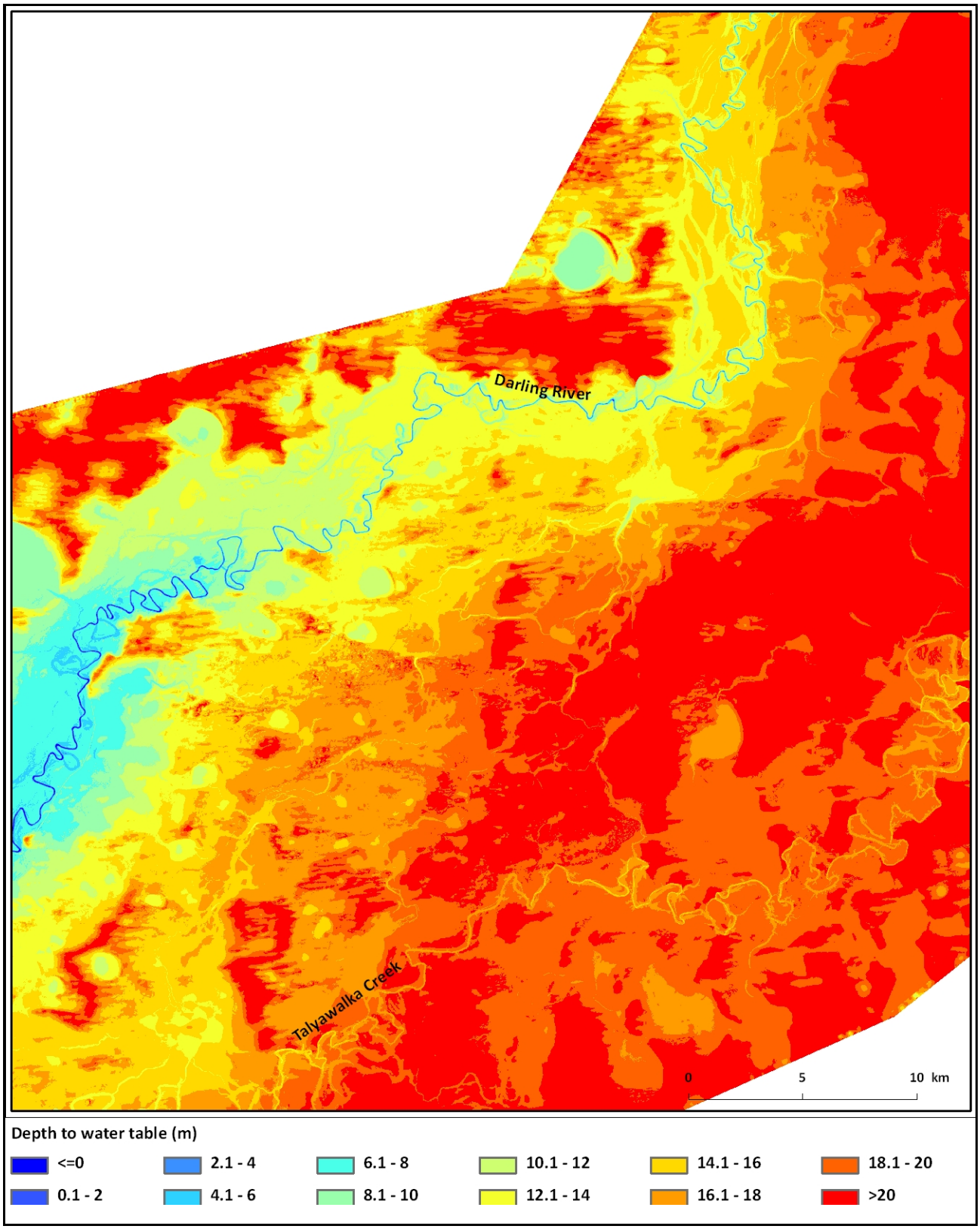

Figure 10-83. *Depth to watertable. This surface has been derived from the potentiometric surface of the surficial aquifer and topography. These values reflect the depth to which the rooting systems of vegetation must travel to encounter the water table. Values of zero or less indicate the occurrence of groundwater discharge. Values greater than 20 m are likely to be beyond the reach of River Red Gums and Black Box in this landscape.*

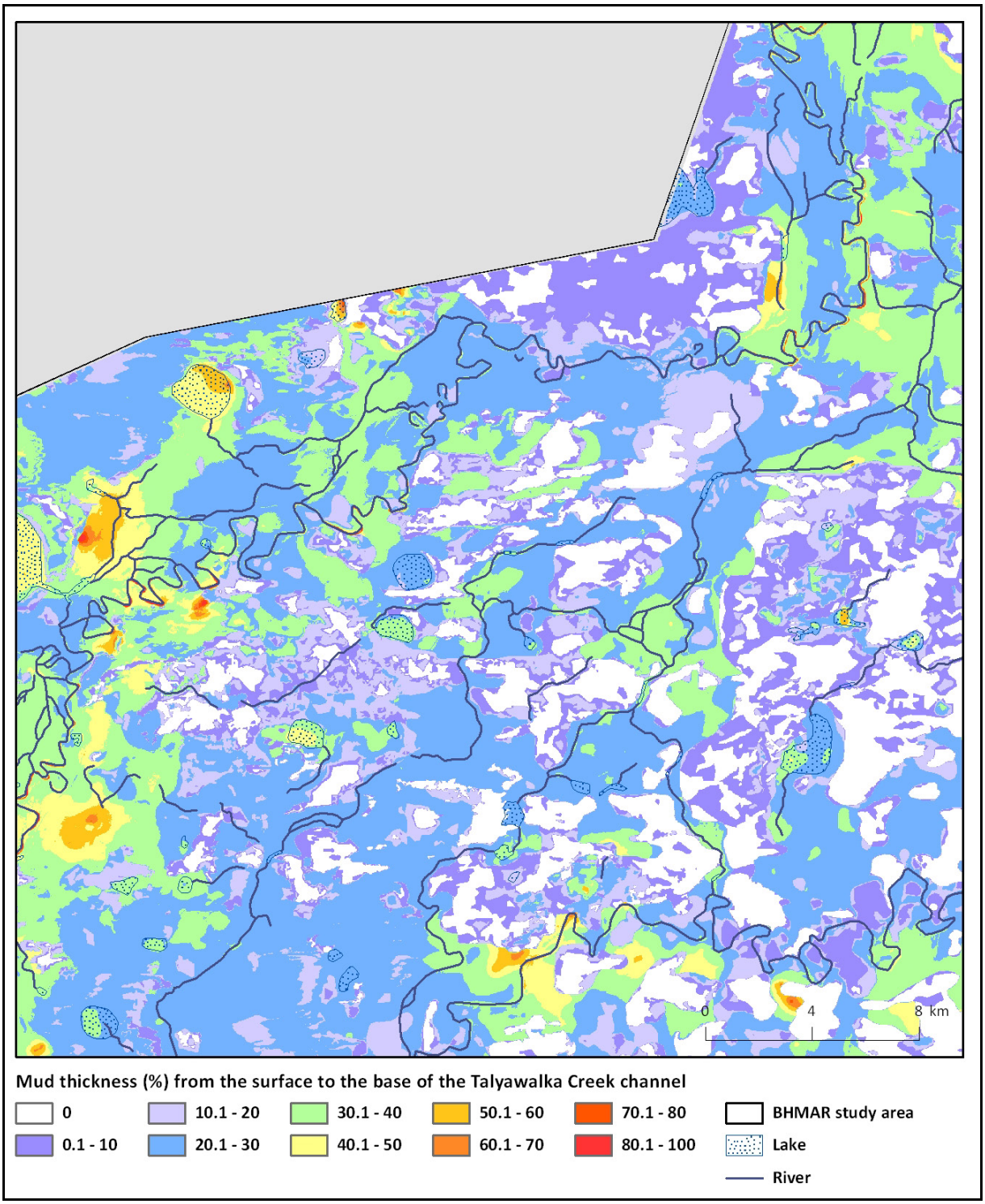

Figure 10-84. *Thickness of near-surface (mud) aquitard, represented as a percentage of the sub-surface profile extending from the surface to the base of the Talyawalka Creek channel (at 5 m depth). River linework was produced for a 1:250,000 usable scale, hence there is some discrepancy between this dataset and the near-surface aquitard mapping.*

When flood flows in the Darling River are particularly high, gates to Three Mile Creek can be opened to allow for Lake Wetherell storage water to flow through Three Mile Creek to Talyawalka Creek; an example of this was in March 1995 (Withers, 1996). As Three Mile Creek is regulated, it is more likely to have received some flows during the drought to which vegetation would have had a short-term response to. This is reflected in the slightly better condition of riparian vegetation along Three Mile Creek than Seven/Nine Mile Creeks and the greater variability in condition during the drought (Figure 10-85). Corresponding depth to

watertable is also shallower here (8–10 m; Figure 10-86) than at Seven/Nine Mile Creeks, suggesting that the shallow aquifer may be recharged in response to flows. The presence of this relatively shallow groundwater resource, in conjunction with sporadic river flows, has resulted in open forest communities being associated with Three Mile Creek and their condition being largely maintained at the conclusion of the drought (Figure 10-85).

As was the case with Seven/Nine Mile Creeks, floodplain vegetation in close proximity to Darling River B are likely to be accessing waters of Lake Wetherell and exhibit better condition with minimal variation, with respect to nearby vegetation (Figure 10-85).

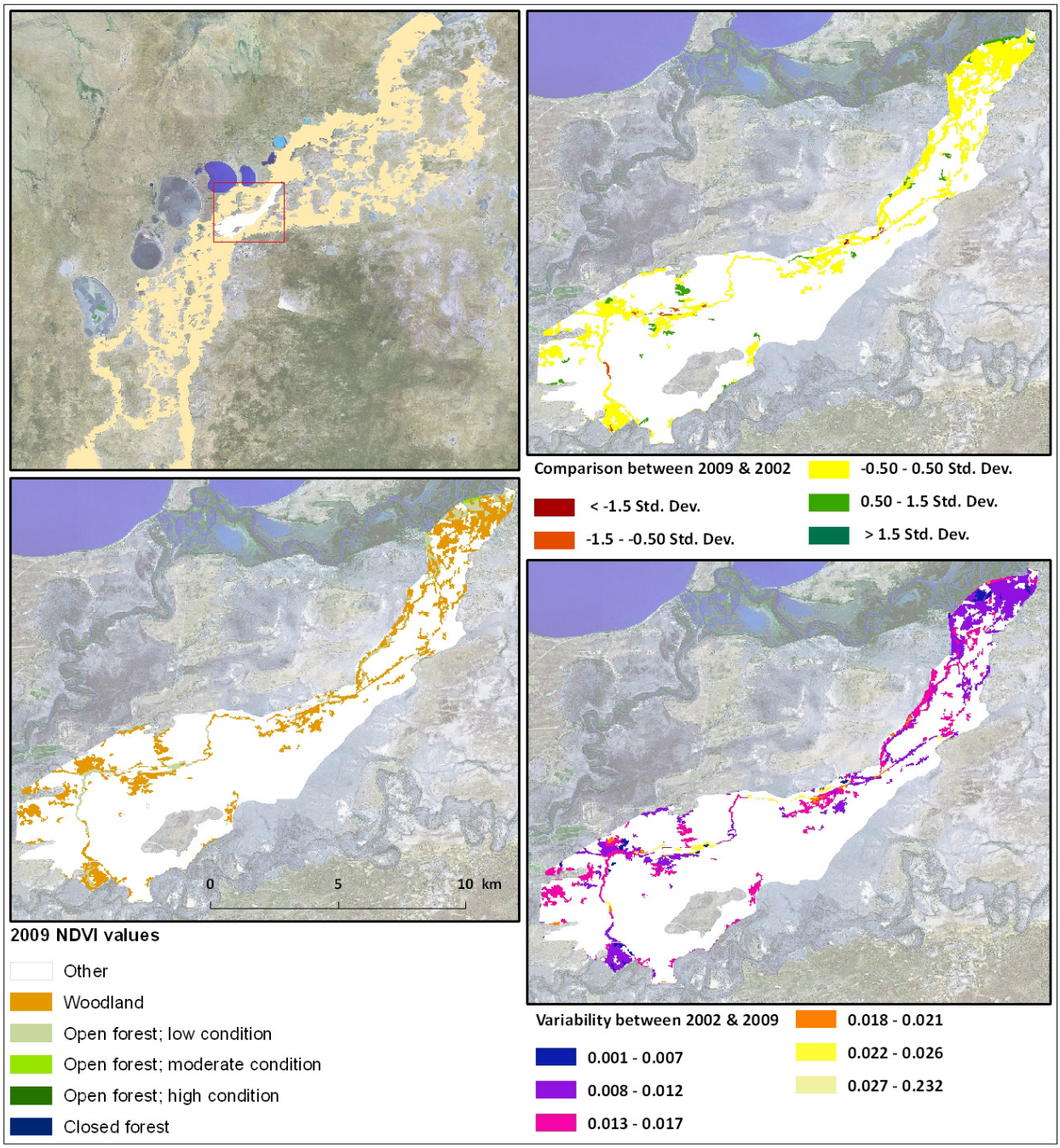

Figure 10-85. *Time series vegetation analysis for Three Mile Creek. Analysis includes condition of vegetation in 2009, comparison between 2009 and 2002, and variability in NDVI throughout the drought (2002-2009).*

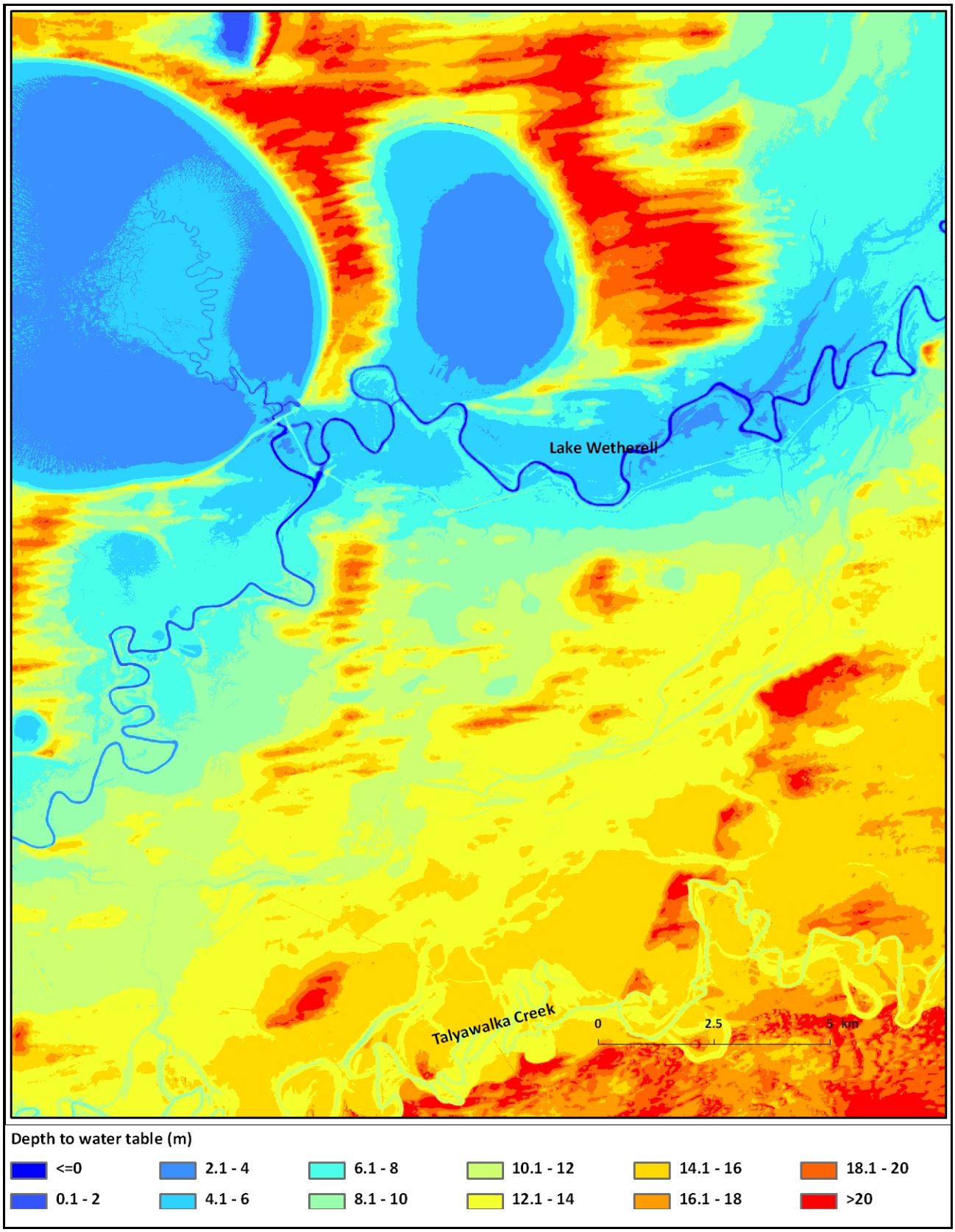

Figure 10-86. *Depth to watertable. This surface has been derived from the potentiometric surface of the surficial aquifer and topography. These values reflect the depth to which the rooting systems of vegetation must travel to encounter the water table. Values of zero or less indicate the occurrence of groundwater discharge. Values greater than 20 m are likely to be beyond the reach of River Red Gums and Black Box in this landscape.*

Tandou Creek, Redbank Creek and Darling Anabranch

The Great Anabranch of the Darling River (the Darling Anabranch) is an ancestral path of the Darling River. The Darling Anabranch is a naturally ephemeral stream which, under non-regulated conditions, would only receive inflows when flows in the Darling River reached 10,000 ML/day (Campbell & Wallace, 2009) typically every 2-3 years (Gippel & Blackham, 2002). Under regulated conditions the Darling Anabranch receives flows via the outlet at Lake Cawndilla and Tandou Creek when flows at Weir 32 exceed 10,000 ML/d and 20,000 ML/d respectively, as well as via the Great Darling Anabranch connection (Briggs & Townsend, 1993). With the completion of the Menindee Lakes storage scheme, a nominal volume of water (50,000 ML) was released annually from Lake Cawndilla to the Darling Anabranch. This occurred via Cawndilla Channel to Tandou Creek where it could be contained by a block bank and regulator at Packers Crossing. Water could then be diverted to Tandou Ltd for irrigation or passed through Packers Crossing downstream to Redbank Creek before passing to the main channel of the Darling Anabranch. Nominal flows occurred from 1961 to 2002, with a 3 year period (1992-1995) of no flow due to infrastructure issues. Tandou Creek also used to run in high floods and fill Tandou Lake which overflowed down Redbank Creek to the Darling Anabranch. Tandou Lake however was banked off for irrigation at the beginning of the 1974 flood. The three different creeks – Tandou, Redbank and Darling Anabranch – are subject to very different water regimes which are reflected in the behaviour of associated vegetation during the drought.

Tandou Creek can receive flows from three sources: 1) water from the Darling River during high floods (this did not occur during the drought period); 2) water released from Lake Cawndilla via Cawndilla Channel (there was no releases from Lake Cawndilla during the drought); and 3) water pumped across from the Darling River to supply flows to Tandou irrigation. Water was in fact pumped across from the Darling River during the drought, evident up until 2007 in Landsat surface water analysis. This resulted in a regular supply of water to Tandou Creek downstream of Cawndilla Channel. As a consequence, the behaviour of associated riparian vegetation along this section of Tandou Creek during the drought was quite different to riparian vegetation elsewhere along Tandou Creek and is interpreted as a highly reliable water source (Figure 10-88). The condition of vegetation was markedly better in 2009, overall condition improved since the beginning of the drought, and condition varied quite considerably throughout the drought (Figure 10-87). While this behaviour is most evident along the lower section of Tandou Creek, similar behaviour is also observed in open forest vegetation along Redbank Creek and further downstream along the Darling Anabranch (Figure 10-87). This suggests that a sufficient volume of surface water continued beyond Lake Tandou during the drought to support vegetation.

In contrast, vegetation upstream of this location exhibited behaviour more characteristic of a reliance on groundwater, including maintained condition with respect to the start and end of the drought and minimal variation throughout the drought (Figure 10-87). The watertable is clearly shallower is association with this stretch of Tandou creek (Figure 10-89) making shallow groundwater resources more accessible to vegetation. A similar conclusion can be made for vegetation associated with Cawndilla Channel. The shallow watertable at these two locations may be a product of lateral bank recharge during previously wet periods.

Floodplain vegetation along the Darling River also maintained condition at the end of the drought and exhibited minimal variation throughout the drought (Figure 10-87). While the watertable is deeper beneath these vegetation communities, it is still perceivably within reach of deep rooting systems, particularly around and upstream of Lake Mindona (Figure 10-89), where less variability in condition was observed (Figure 10-87). Unlike all the other river/creek sections, the section of the Darling Anabranch between the Darling River and Redbank Creek does not support any riparian zone open forest vegetation. Instead, it is dominated by woodland vegetation that largely maintained condition throughout the drought, pointing to the presence of an available groundwater resource.

The presence of small holes in the upper confining aquitard and an extensive network of faults (Figure 10-90) suggests a degree of connectivity between the shallow and deeper (Calivil Formation) aquifers which may mean groundwater dependent vegetation indirectly accesses groundwater in the Calivil Formation.

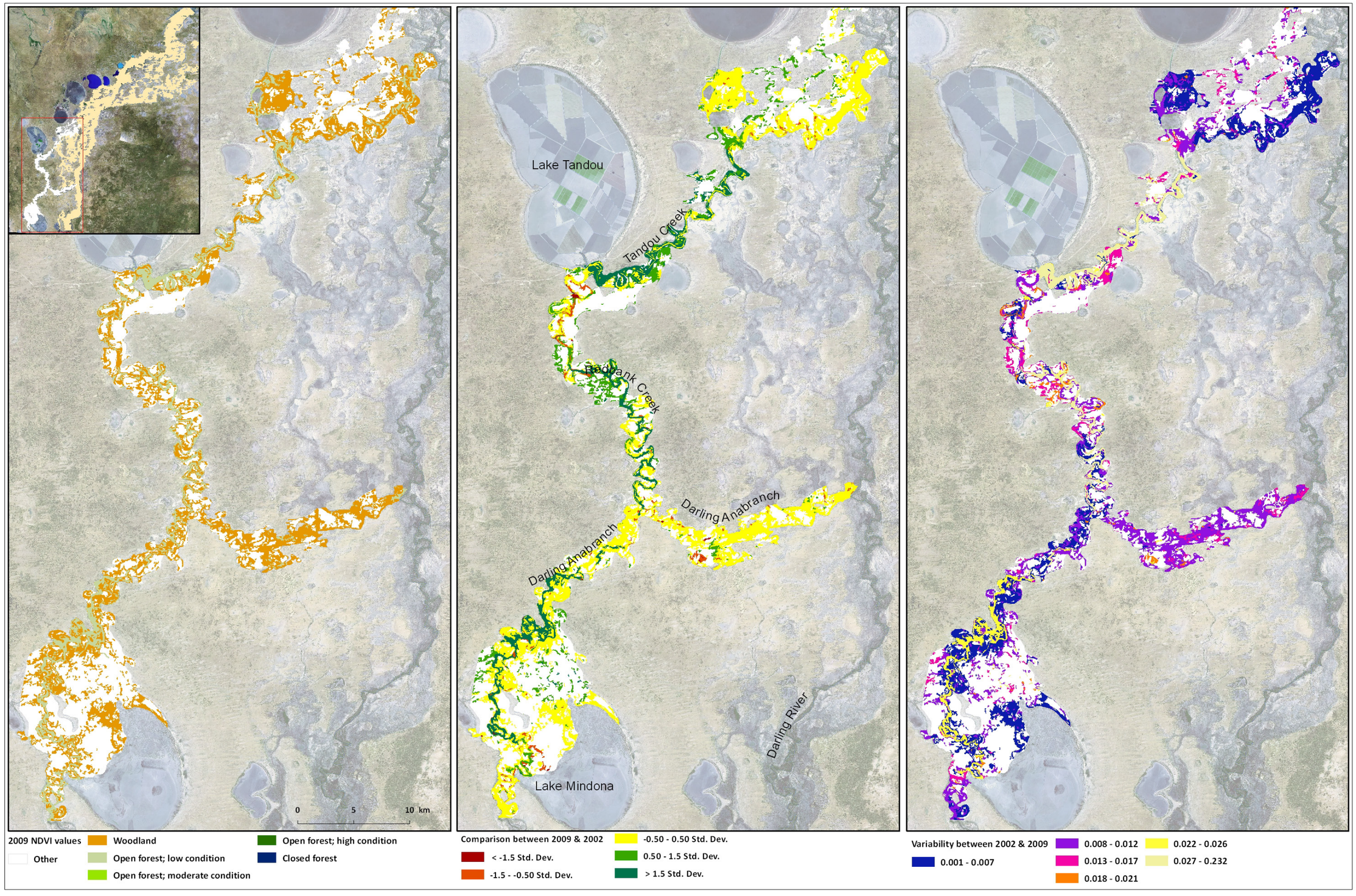

Figure 10-87. *Time series vegetation analysis for Tandou Creek, Redbank Creek and Darling Anabranch. Analysis includes condition of vegetation in 2009, comparison between 2009 and 2002, and variability in NDVI throughout the drought (2002-2009).*

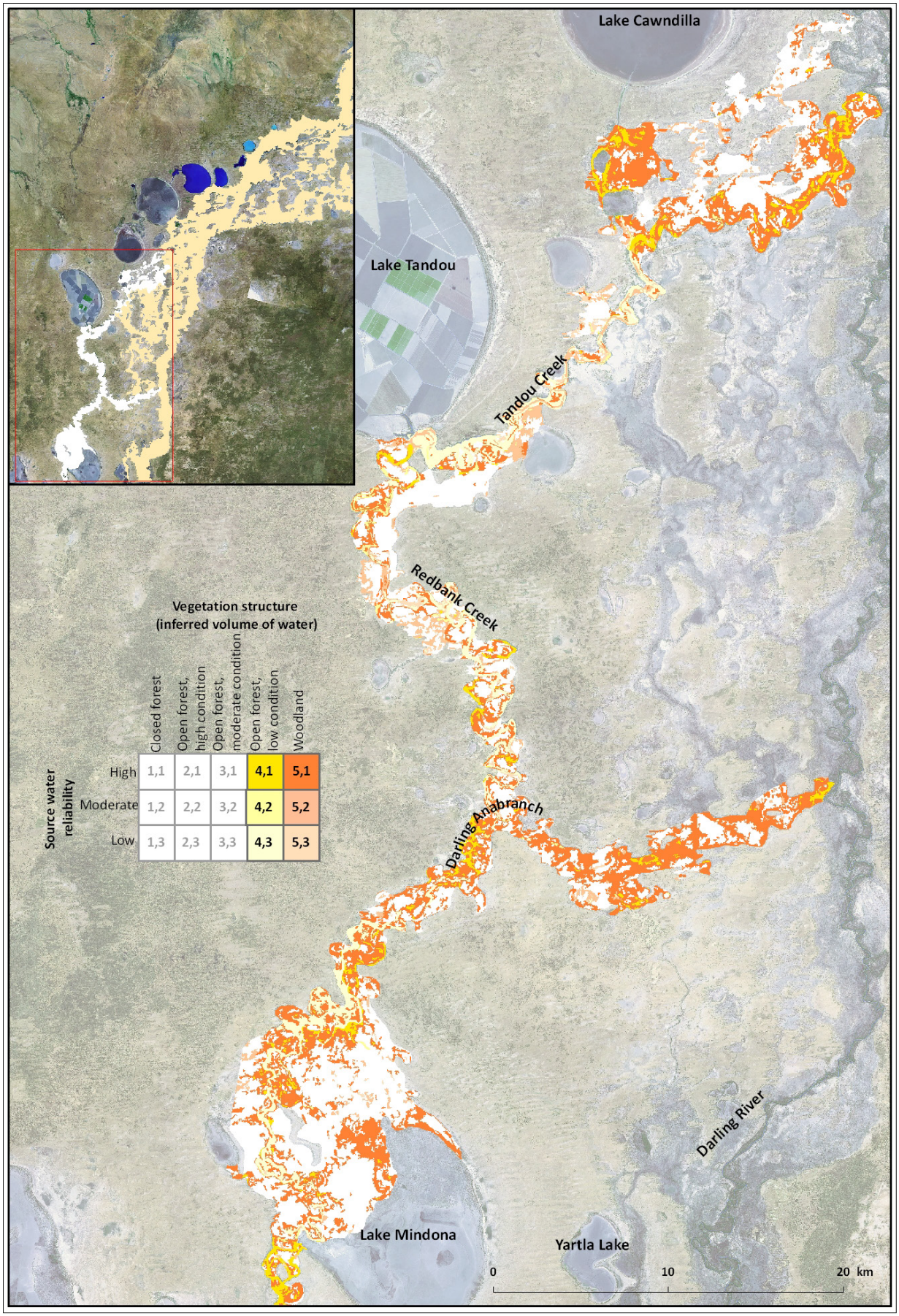

Figure 10-88. *Reliability of source water compared with vegetation condition for Tandou Creek, Redbank Creek and Darling Anabranch.*

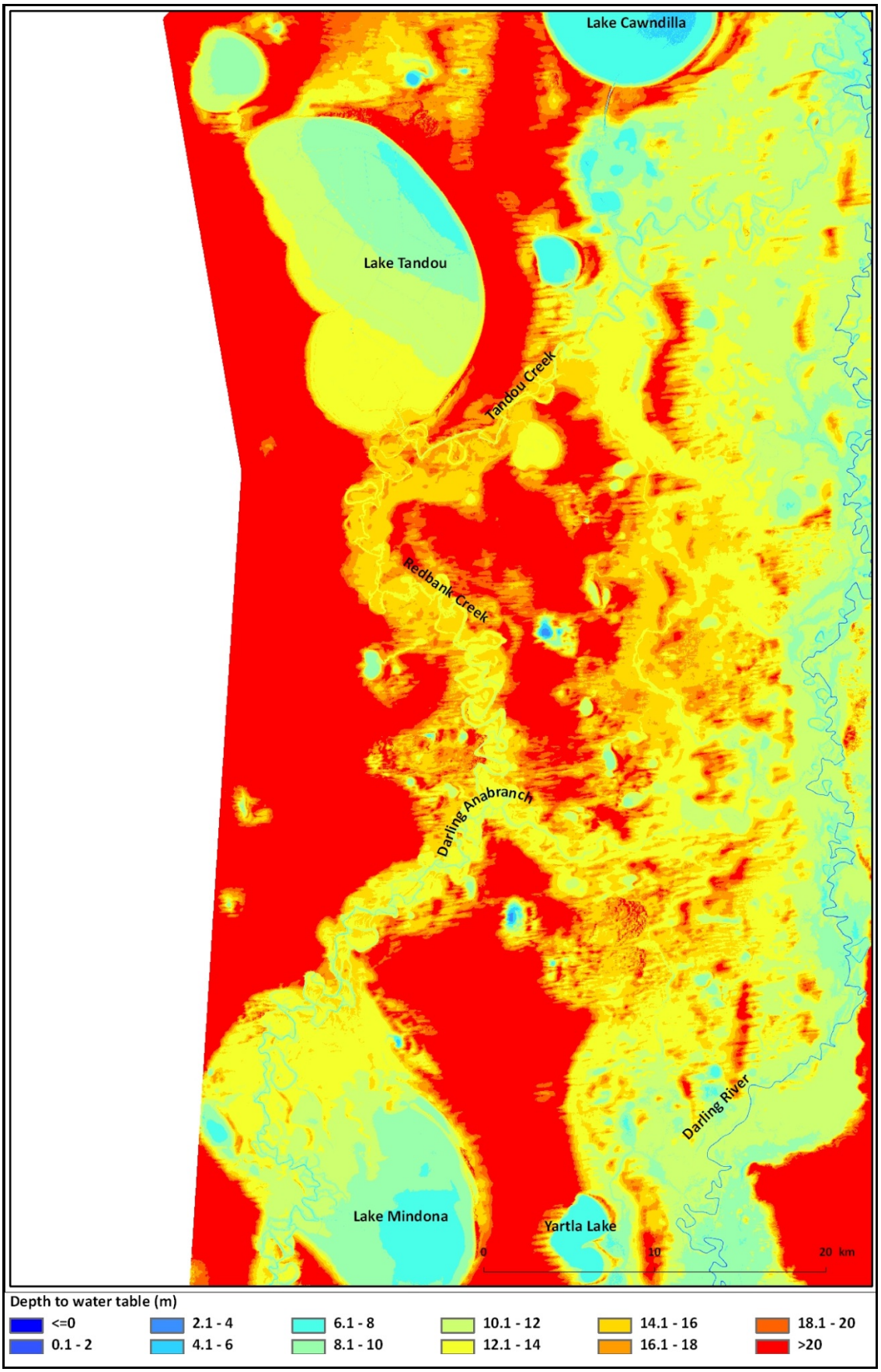

Figure 10-89. *Depth to watertable. This surface has been derived from the potentiometric surface of the surficial aquifer and topography. These values reflect the depth to which the rooting systems of vegetation must travel to encounter the water table. Values of zero or less indicate the occurrence of groundwater discharge. Values greater than 20 m are likely to be beyond the reach of River Red Gums and Black Box in this landscape.*

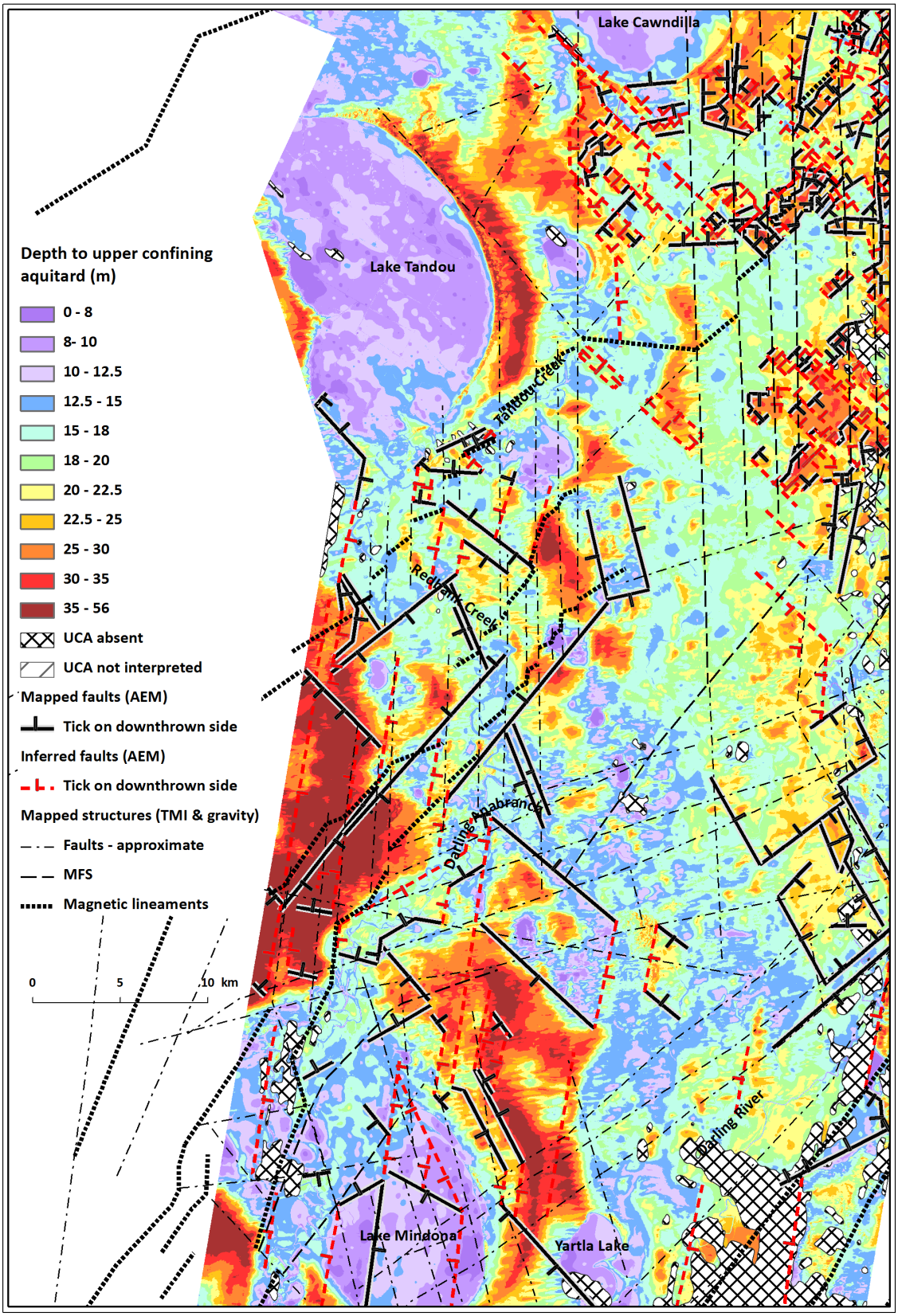

Figure 10-90. *Aquitard map, including depth to the top of the upper confining (UC) aquitard, interpreted holes, faults and lineaments.*

Charlie Stones, Yampoola and Coonalhugga Creeks

Charlie Stones Creek and Yampoola Creek are also anabranches of the Darling River and are located to the east of the Lower Darling River (Figure 10-91). There creeks only receive water during large flood events when Talyawalka Creek is flowing and substantial amounts of water flow down the Lower Darling River. Both these creeks would have been largely dry throughout the drought period thus the maintenance of woodland condition appears be the result of a reliable shallow groundwater resource (Figure 10-92) at depth of 10–14 m (Figure 10-93), likely recharged during previous flood events.

Similarly Coonalhugga Creek, located between Tandou Creek and the Lower Darling River (Figure 10-94), only receives flows during flood events. With the exception of some vegetation communities more associated with the adjacent Tandou Creek or Darling River, woodland vegetation condition is largely maintained throughout the drought even in the presence of minimal rainfall and no surface water flows. As was concluded for Charlie Stones and Yampoola Creeks, a shallow groundwater resource at less than 14 m depth (Figure 10-95) is suggested to be responsible for maintained vegetation condition (Figure 10-96).

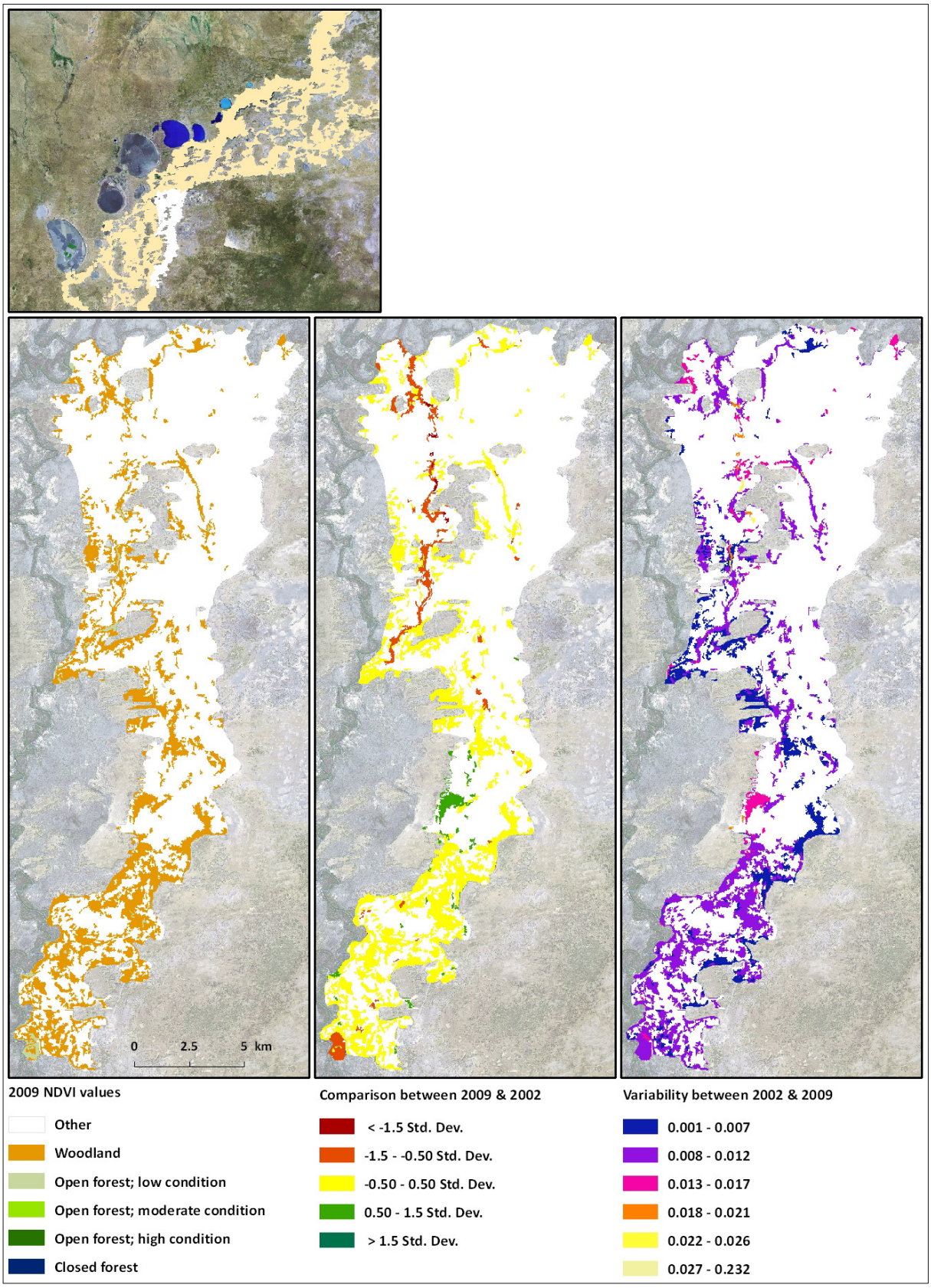

Figure 10-91. *Time series vegetation analysis for Charlie Stones Creek and Yampoola Creek. Analysis includes condition of vegetation in 2009, comparison between 2009 and 2002, and variability in NDVI throughout the drought (2002-2009).*

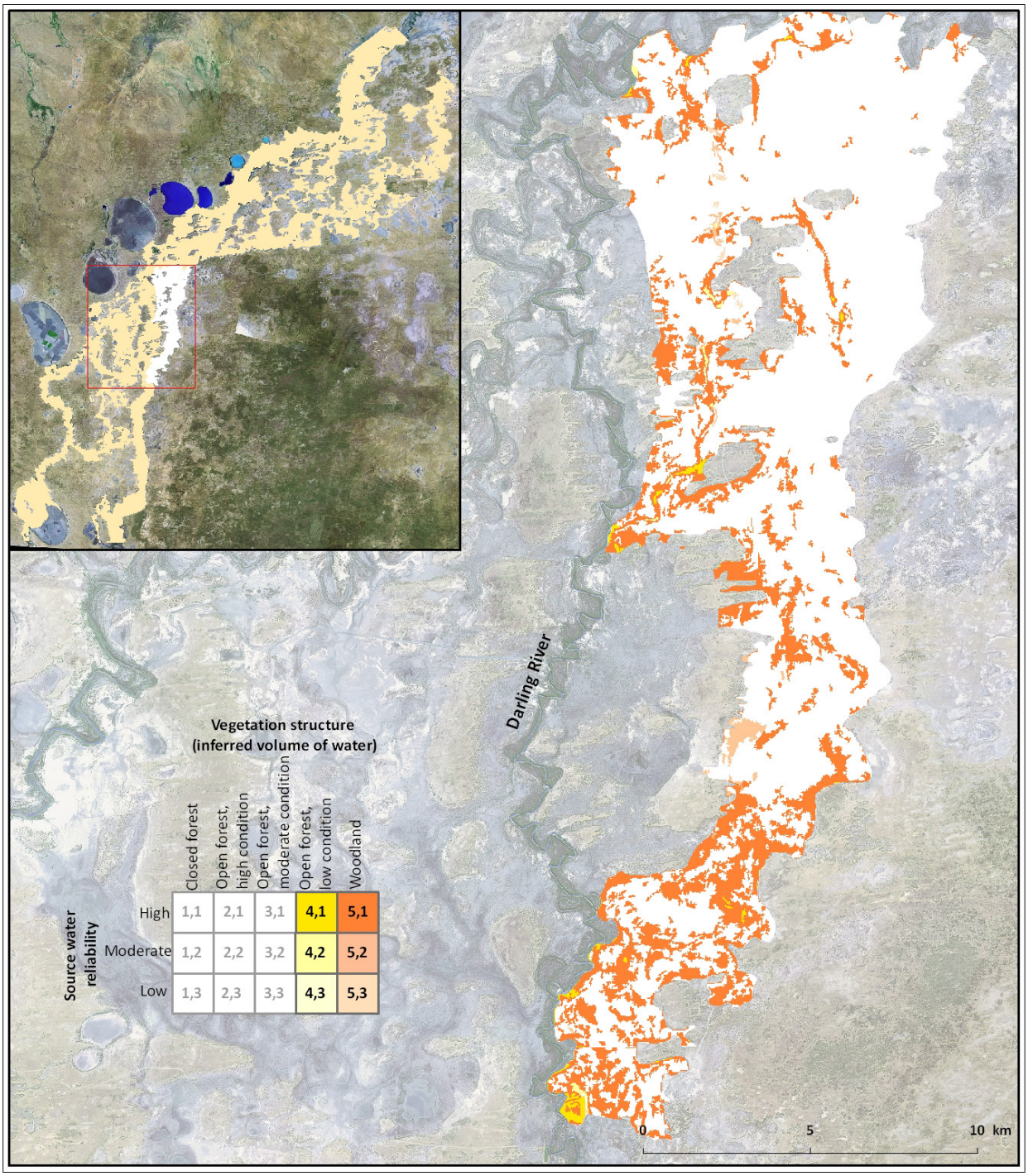

Figure 10-92. *Reliability of source water compared with vegetation condition for Charlie Stones Creek and Yampoola Creek.*

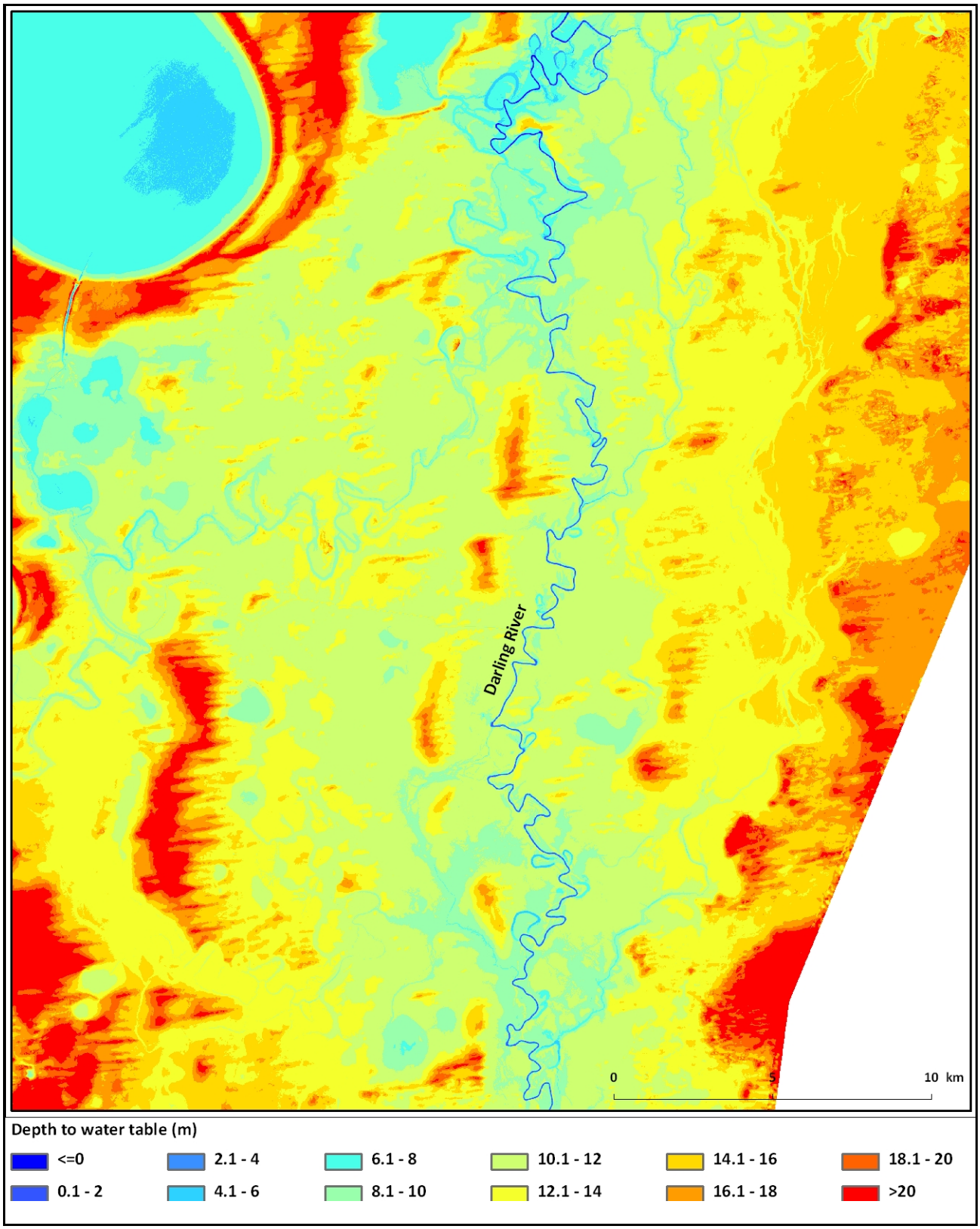

Figure 10-93. *Depth to watertable. This surface has been derived from the potentiometric surface of the surficial aquifer and topography. These values reflect the depth to which the rooting systems of vegetation must travel to encounter the water table. Values of zero or less indicate the occurrence of groundwater discharge. Values greater than 20 m are likely to be beyond the reach of River Red Gums and Black Box in this landscape.*

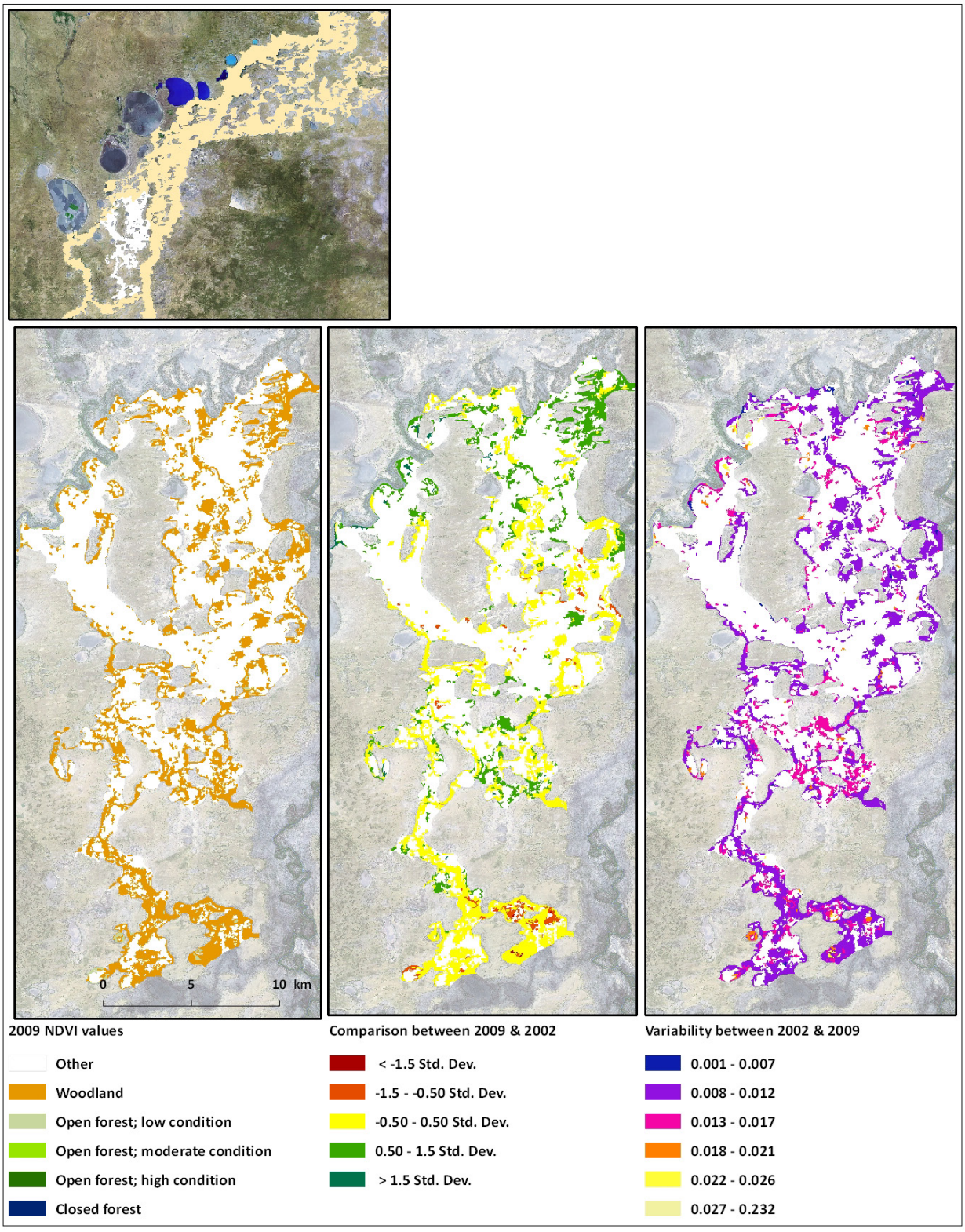

Figure 10-94. *Time series vegetation analysis for Coonalhugga Creek. Analysis includes condition of vegetation in 2009, comparison between 2009 and 2002, and variability in NDVI throughout the drought (2002-2009).*

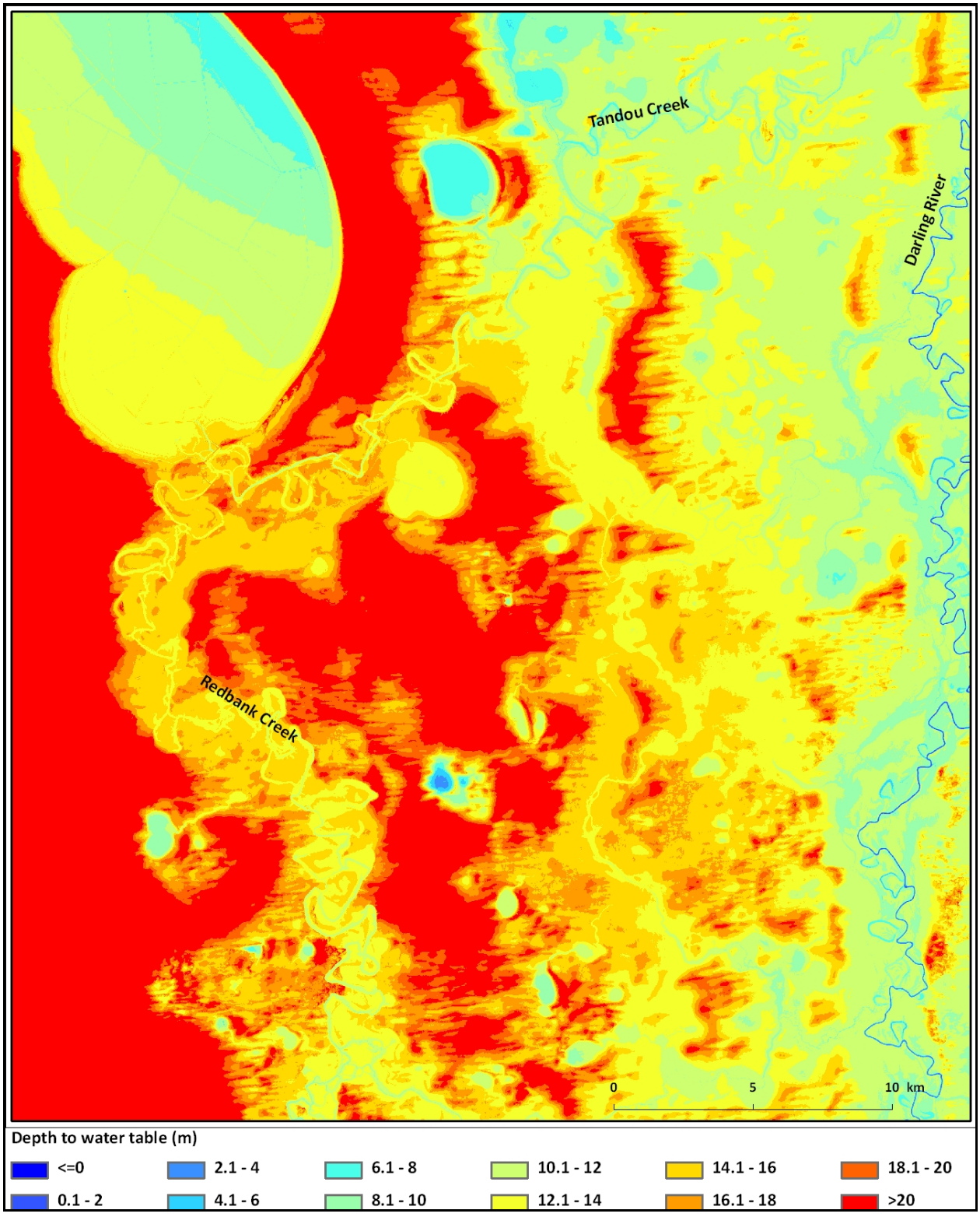

Figure 10-95. *Depth to watertable. This surface has been derived from the potentiometric surface of the surficial aquifer and topography. These values reflect the depth to which the rooting systems of vegetation must travel to encounter the water table. Values of zero or less indicate the occurrence of groundwater discharge. Values greater than 20 m are likely to be beyond the reach of River Red Gums and Black Box in this landscape.*

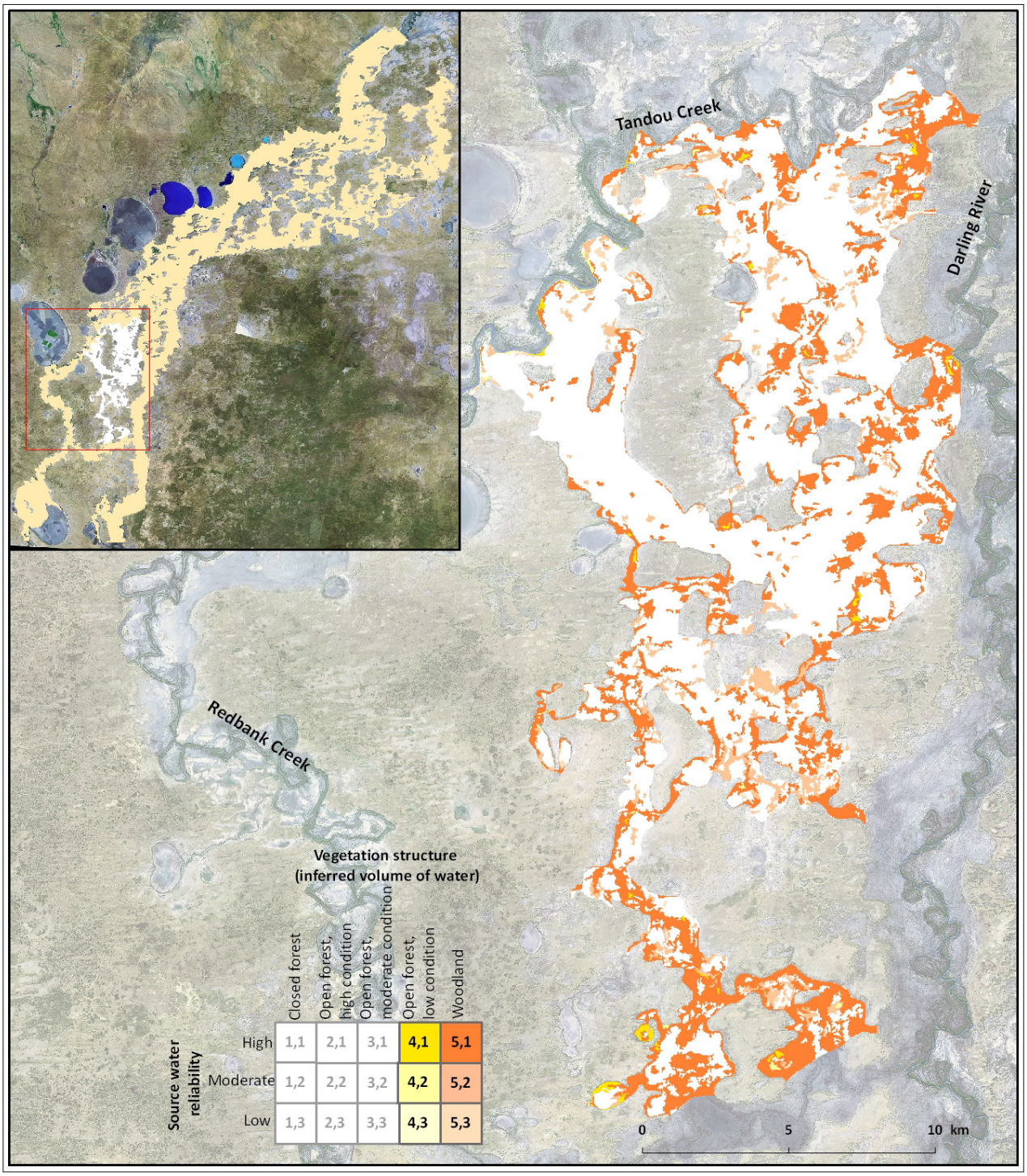

Figure 10-96. *Reliability of source water compared with vegetation condition for Coonalhugga Creek.*

10.4.3 Vulnerability of Vegetation to Potential Groundwater Extraction and MAR Schemes

10.4.3.1 Introduction

In Managed Aquifer Recharge (MAR) a water source, such as natural water from a lake or river, is used to recharge an aquifer with water under controlled conditions (Dillon *et al*., 2005; Dillon *et al*., 2009). The aquifer is used to store surplus water for later use or for environmental benefit. MAR targets are typically confined aquifers; this minimises shallow watertable fluctuations (beyond that which occurs naturally) that can have detrimental impacts on vegetation such as waterlogging, dewatering, salinisation, and acidification.

In comparison to MAR, groundwater extraction is the withdrawal of already existing groundwater resources. If the groundwater resource receives suitable recharge volumes to balance extraction, it is deemed to be sustainable. Alternatively, if more water is being extracted than what is being replaced by recharge, the groundwater resource is being 'mined'. Similar to MAR, groundwater extraction targets are typically confined aquifers, minimising lowering of the watertable and associated risks.

The two most important considerations for potential MAR and groundwater resource targets from an environmental/vegetation point of view are 1) whether vegetation is using groundwater and 2) whether the groundwater resource being utilised by vegetation is connected to the target aquifer. Fourteen groundwater resource (GWR) targets, GWR1 through to GWR14 are shown in Figure 7-23 and are discussed in detail in Lawrie *et al.* (2012d). Potential borefields have been proposed within three of these GWR targets – GWR1, GWR2 and GWR4 – which are discussed in Lawrie *et al.* (2012c). A summary is provided in below.

10.4.3.2 MAR/GWR target summary

The Darling River functions quite differently depending on the degree of river regulation. Upstream groundwater resource targets (e.g. GWR10, GWR11) are typically associated with a shallower upper confining aquitard and depth to watertable, however vegetation appear less inclined to utilize shallow groundwater resources. Instead, these vegetation communities are highly reliant on surface water resources. An exception to this is vegetation at GWR10 that corresponds directly with a hole in the upper confining aquitard. These vegetation communities appear to have supplemented existing surface water resources with available groundwater resources to maintain condition during particularly dry periods in the drought. Extracting groundwater resources at this location is likely to have detrimental impacts on these vegetation communities during periods of water stress whereas no effects are expected at GWR10.

GWR5 corresponds with Lake Wetherell. Due to the abundance and constancy of surface water both flowing down the Darling River and also held within Lake Wetherell, it is difficult to identify what, if any vegetation is solely or additionally utilizing groundwater resources. Vegetation are opportunistic thus, in the presence of a shallow, fresh groundwater resource (within the Menindee Formation), it is likely that some degree of groundwater use is occurring, particularly in association with holes in the upper confining aquitard. Should surface water become unavailable or quality decline, groundwater resources would become more important.

Downstream of Weir 32, the Darling River is heavily regulated, receiving daily flows during the drought via releases further upstream. A groundwater mound exists beneath the river channel, derived from recharge processes almost exclusively occurring during flood events. A number of holes are present in the upper confining aquitard beneath the river channel. Consequently a relatively high degree of connectivity exists between the shallow aquifer (i.e. Menindee Formation) in which the watertable is present, and the deeper aquifer (i.e. Calivil Formation). These holes facilitate vertical recharge of the Calivil Formation. Riparian vegetation at GWR3, GWR6, GWR7 and GWR8 are reliant on surface water flows, however these communities may also have utilised shallow groundwater resources during the drought. Any lowering of the watertable associated with future groundwater extraction would that have a detrimental effect on vegetation condition.

Talyawalka Creek seldom receives flows except under flood conditions. As a consequence vegetation is restricted to the channel. Where large holes in the upper confining aquitard exist (or the upper confining

aquitard is quite deep over an extensive area) riparian vegetation is very scattered and patchy, as observed at GWR9. At these locations, insufficient water is held at a depth accessible by vegetation due to the absence (or considerable depth) of the upper confining aquitard. Where small holes in the upper confining aquitard occur (e.g. GWR14), riparian vegetation is observed to decline in condition by the conclusion of the drought, again possibly as a result of water recharging the deeper Calivil Formation aquifer in preference to being accumulated as soil moisture or a shallow groundwater resource. Where the upper confining aquitard is present (e.g. GWR12), vegetation along the creek channel does maintain condition, supported by soil moisture. No impacts to vegetation are expected these groundwater resources in the event of extraction.

GWR1 incorporates a number of very different vegetation communities – riparian vegetation along the Darling River, along Cawndilla Creek and associated with the Tandou Creek element of the Talyawalka-Anabranch relict river tract; lake-fringing vegetation at Emu Lake and Lakes Menindee and Cawndilla; and floodplain vegetation. Riparian vegetation associated with the Darling River is reliant on surface water. Due to regulation, these communities received less water during the drought and as a consequence declined in condition. Riparian vegetation along Cawndilla Creek also appears to be reliant on surface water resources. Lake-fringing vegetation at Lakes Menindee and Cawndilla are influenced by the availability of lake water but in the case of Lake Menindee, vegetation is also able to access groundwater resources. The presence of holes in the upper confining aquitard on the fringes of Lake Menindee suggests associated vegetation has the capacity to exploit groundwater within the Calivil Formation. Vegetation at Emu Lake did not have access to surface water during the drought; condition was maintained due to the availability of shallow groundwater.

GWR2 is similar to GWR1 in that large holes in the upper confining aquitard have resulted in a high level of connectivity between the shallow and deeper aquifers. Lake-fringing vegetation at Lake Menindee appears to have utilized groundwater resources during the drought; made available by the combination of high watertable levels and aquifer connectivity. Vegetation at Lake Speculation in some instances is reliant on surface water and inundation and in others appears to also be accessing shallow groundwater resources. Again the presence of holes in the upper confining aquitard make it difficult to determine whether these vegetation communities are in fact utilizing water strictly contained with the shallow aquifer or a combination of water within both the shallow and deeper aquifers.

Very little woody vegetation is observed at GWR4 and GWR13. What little woody vegetation is present is unlikely to be associated with Calivil Formation groundwater. The rest of the area is dominated by rain-fed vegetation such as grasses, shrubs and acacia.

10.4.3.3 Proposed borefield summary

A portion of vegetation within all eight proposed potential borefields utilized groundwater resources during the drought. It has been demonstrated that these groundwater resources are located within the shallow aquifer and no groundwater dependent vegetation (with the exception of lake fringing vegetation at Lake Menindee GWR/MAR borefield) has the capacity to directly access groundwater within the Calivil Formation aquifer. Connection between these two aquifers may however result from holes in the upper confining aquitard or faults that propagate through the aquitard. These features are associated with groundwater dependent vegetation at Jimargil, Kinchega National Park and Larloona. Consequently, groundwater extraction from these borefields could pose a low risk to vegetation. Further investigation into the leakiness of the interpreted faults and the associated radius of influence is required when designing any borefield. Groundwater extraction at Lake Menindee poses a high risk to vegetation. Potential lowering of the watertable would detrimentally impact on lake-fringing vegetation interpreted to be utilizing shallow groundwater resources. Similarly, the development of a MAR scheme, and potential watertable rise could also have a detrimental impact on vegetation.

10.5 CONCLUSIONS

There has been much documented vegetation change during the previous 70 years. It is important to recognise that much of the vegetation throughout the region has been impacted by water management activities which have already modified the ecosystems. Consequently we are not dealing with a pristine ecosystem.

It is also important to note that there is much intra- and inter-annual variability in vegetation condition, often in response to climate variability (i.e. drought, inundation). This creates challenges in monitoring conditions throughout the region and is a source of some uncertainty. The analytical approaches used in this study have in some part attempted to minimise the influence of climate variability but this issue should not be overlooked.

10.5.1 Lake-Fringing Vegetation

Pre-regulation lake-fringing vegetation at Lakes Pamamaroo and Menindee was in much better condition and far more extensive than current lake-fringing vegetation as indicated by aerial photography in 1945. Regulation resulted in the inundation and death of considerable amounts of lake-floor and lake-fringing vegetation. Current fringing vegetation is all that remains of the much more extensive vegetation, representing the outermost extent of lake-fringing pre-regulation vegetation.

Current fringing vegetation at Lake Pamamaroo is also subject to inundation due to regular surcharging of lake levels. Vegetation more prone to prolonged inundation consistently exhibited poorer condition compared to vegetation less frequently inundated. The same can also be said for vegetation at Lake Wetherell, with the greatest condition observed in the outer floodplain where vegetation is less frequently inundation while still having access to a reliable water source. As was observed following regulation, vegetation subject to prolonged inundation exhibit poor condition and ultimately die unless the situation is reversed.

Lakes Menindee and Cawndilla have not been subject to the same degree of inundation. Unlike Lake Pamamaroo, the water regime experienced at Lakes Cawndilla and Menindee since regulation does not appear to have resulted in a decline in vegetation condition. In general, condition remained constant even during the drought period, whereas the condition of vegetation around Lake Pamamaroo fluctuates in response to localized rainfall events and inflows. The consistency observed in vegetation condition at Lake Menindee can be attributed to the presence of a shallow groundwater resource created by natural lake leakage, and connectivity (via holes in the upper confining aquitard) between this shallow resource and the deeper Calivil Formation aquifer. The spatial distribution of lake-floor vegetation in 1945 matches the location of both the hole in the upper confining aquitard and the fresh groundwater resource in the Calivil Formation, suggesting that similar lake leakage processes were occurring prior to regulation. The shallow groundwater resource is thought to have existed at this time, supporting both the lake-floor and fringing vegetation. The extent and volume of this resource is believed to have been much smaller than in modern times due to more frequent inundation under present conditions. Since regulation commenced, water has been held in Lake Menindee for years at a time, considerably enhancing natural lake leakage and increasing the extent of the resource as indicated by hydrographic data.

Vegetation at Lake Speculation has also improved since regulation. While some of this vegetation may also be exploiting the same groundwater resource available to the vegetation fringing Lake Menindee, the improved condition and increased extent of Black Box can largely be attributed to more frequent flooding resulting from higher lake levels at Lake Menindee. The same relationship can also be attributed to Spectacle Lakes north of Lake Cawndilla.

Lake regulation has had a variety of impacts on lake-fringing vegetation both positive and negative and these observed impacts need to be considered when planning any future changes to lake management practices. If lake water were to be maintained at higher levels for longer periods this is likely to detrimental impact on the condition of what little fringing vegetation remains. However, if the lakes were only filled to Full Supply Levels for shorter durations and less frequently, natural recharge via lake leakage would still occur, fringing

woody vegetation would be able to utilise both the shallow groundwater resource and lake water, without being waterlogged.

10.5.2 Riparian and Floodplain Vegetation

When looking at vegetation dynamics generalised across the whole BHMAR study area, a clear distinction has been established between behaviour of riparian and floodplain vegetation supported by a reliable/constant water source (i.e. groundwater or permanent surface water) during the drought versus vegetation that is not (i.e. variable river flows). Drought flows, particularly in the upstream unregulated river stretches, when combined with water stored in the unsaturated zone and shallow groundwater resources, appears to have been sufficient to maintain riparian vegetation condition. The same was not the case for floodplain vegetation, particularly evident along regulated river/creek stretches. In these cases increased declines in vegetation condition can be attributed to reductions in flows (due to a both drought conditions and altered surface management practices), coupled with likely depleted of soil moisture in the unsaturated zone and a lowering of the watertable.

10.6 RECOMMENDATIONS

In this study, vegetation structure was mapped (for a single point in time) using LiDAR data. This is adequate for the provision of structure and/or condition information at one point in time but does not provide a sense of how changes in hydrologic regime alter vegetation characteristics. Hence it is recommended that repeat LiDAR coverage be obtained for wet climatic conditions.

Due to the moderate resolution of Landsat (30 m pixels), reflectance values (including greenness) are likely to be generalized. Additionally, reflectance values can be more indicative of the field/ground layer, due to the low reflectivity of tree canopy relative to grass canopy. This is particularly evident following precipitation. In the absence of detailed field data, it is unknown how the individual layers may NDVI response. This uncertainty could be reduced with the collection of field observations or high resolution sensor data or aerial photography. The NDVI results could then be used to develop an understanding of patterns, trends and changes in conditions at both an overall ecosystem level as well as at the tree scale.

Finally, should the proposed groundwater management activities go ahead, the excellent baseline information discussed in this study should be paired with targeted monitoring activities, including at least some basic ‘fit-for-purpose’ field observations. Relevant field observations would go a long way towards reducing the uncertainty evident in the input data (FPC and CEM), derived products (LiDAR and Landsat vegetation structural maps, drought summary surfaces) and associated interpretation.

When looking at vegetation dynamics generalised across the whole BHMAR study area, a clear distinction has been established between behaviour of riparian and floodplain vegetation supported by a reliable/constant water source (i.e. groundwater or permanent surface water) during the drought versus vegetation that is not (i.e. variable river flows). Drought flows, particularly in the upstream unregulated river stretches, when combined with water stored in the unsaturated zone and shallow groundwater resources, appears to have been sufficient to maintain riparian vegetation condition. The same was not the case for floodplain vegetation, particularly evident along regulated river/creek stretches. In these cases increased declines in vegetation condition can be attributed to reductions in flows (due to a both drought conditions and altered surface management practices), coupled with likely depleted of soil moisture in the unsaturated zone and a lowering of the watertable.

11. BHMAR Hydrogeological Investigations- Broader Implications

11.1 EXISTING REGIONAL AND BASIN GROUNDWATER MANAGEMENT PLANS

The BHMAR study area is part of two NSW water management areas (Western and Lower Murray Darling) with the management boundary cross cutting the Darling floodplain near Menindee Lakes. The fluvial sediments of the Darling floodplain are also defined across different NSW water sharing plans for the:

- Lower Darling Alluvial Groundwater Source, defined by the fresh groundwater lens within the alluvium adjacent to the Darling River and downstream of Lake Wetherell,
- Upper Darling Alluvial Groundwater Source, incorporating the alluvial deposits associated with the Darling River upstream of Lake Wetherell to near Bourke, and
- Western Murray Porous Rock Groundwater Source, which includes the Calivil Formation, Loxton-Parilla Sands, Murray Group Limestone and Renmark Group aquifers in the Murray Geological Basin.

These Groundwater Sources have equivalent Groundwater Sustainable Diversion Limit Resource Units as defined under the *Basin Plan* for the Murray-Darling Basin (MDBA, 2012b).The groundwater management unit (GMU) boundaries for these Groundwater Sources are shown, relative to the BHMAR project area, in Figure 11-1.

11.1.1.1 Lower Darling Alluvial Groundwater Source

The *Lower Darling Alluvial Groundwater Source* is a component of the NSW *Lower Murray-Darling Unregulated and Alluvial Water Sources Water Sharing Plan* which is a 10-year State plan that commenced 30th January, 2012 (NOW, 2012a). The significance of hydraulic connectivity between the river and the shallow alluvial groundwater system is recognised in this plan. The Groundwater Source is based on fresh groundwater extending about 500 m from the Darling River, surrounded by brackish to saline regional groundwater. It incorporates shallow alluvium along and adjacent to the main Darling River stem from Tilpa to Wentworth, with the majority mapped downstream of about 100 km north of Menindee. Talyawalka and Anabranch alluvium are excluded due to the lesser recharge frequency and the absence of licensed bores.

In the plan, recharge to the near-river freshwater lenses in the shallow alluvium is interpreted to be due to leakage from Darling River flows (NOW, 2012a). Rainfall recharge is inferred to be insignificant due to low rainfall and high evaporation in the plan area. Extraction limits are based on an estimate of average annual extractions, defined as the sum of existing entitlements plus an estimate of annual water requirements for stock and domestic and native title rights. Total entitlements are 1490 ML/yr and there are currently 10 licensed extractive bores. The majority of these have a drought contingency licence where groundwater is extracted when the surface water determination for the regulated river is zero percent. Due to the issue of potential saline ingress, groundwater exceeding 3,000 µS/cm is not permitted to be extracted.

The AEM survey and drilling investigations of the BHMAR project has effectively mapped this freshening of the alluvial sequences associated with the Darling River. The project has also refined the geomorphology and near-surface geology, with the stratigraphy redefined into the Coonambidgal Formation, Menindee Formation and the Willotia beds.

11.1.1.2 Upper Darling Alluvial Groundwater Source

The *Upper Darling Alluvial Groundwater Source* is a component of the NSW *Barwon-Darling Unregulated and Alluvial Water Sources Water Sharing Plan* which is a 10-year State plan that commenced on 4th October, 2012 (NOW, 2012b). The alluvial deposits are described as being 40-50 m thick and comprised of the Narrabri, Gunnedah and Cubbaroo Formations. Perched fresh groundwater is common in the shallow Narrabri Formation, with the deeper, more significant aquifers in the Gunnedah and Cubbaroo Formations

interpreted to be mostly saline (NOW, 2012d). The aquifers are not considered to be highly connected to the Darling River, however the formations are inferred to be hydraulically connected (NOW, 2012d).

The long-term groundwater extraction limits are based on a proportion of the long-term average annual rainfall and any potential river leakage is not included in the analysis. A rainfall infiltration rate of 2% and a mean annual rainfall of 261 mm/yr were used to derive an average annual recharge of 38,838 ML/yr (NOW, 2012d). The long-term average annual extraction limit for the groundwater source is defined as 17,120 ML/yr. Groundwater is used for stock and domestic purposes as well as town water supply for Wilcannia. The majority of current extraction is from the Upper Darling salt interception scheme, designed to reduce saline groundwater discharge to the Darling River near Bourke (NOW, 2012d).

This groundwater source is hosted in the lateral equivalents to the 40-50 m sequence evident in the BHMAR study area. Therefore, as well as the Quaternary alluvials, this could include equivalents of the Calivil Formation which has been the target of BHMAR investigations.

11.1.1.3 Western Murray Porous Groundwater Source

The *Western Murray Porous Rock Groundwater Source* is part of the 10-year NSW *Murray-Darling Basin Porous Rock Groundwater Sources Water Sharing Plan* that commenced 16th January, 2012 (NOW, 2012c). The Groundwater Source incorporates the Renmark Group, Murray Group Limestone and Pliocene Sands (Calivil Formation and Loxton-Parilla) aquifers in the Murray Geological Basin. These have been assigned a low to moderate level of surface water connection, with estimated travel time in terms of movement of water between river and aquifer spanning years to decades.

The recharge calculations for all NSW Murray-Darling Basin Porous Rock Groundwater Sources were based on rainfall recharge only, so any river leakage is not included. The extraction limit is based on a proportion of recharge, calculated as a percentage of infiltration of average annual rainfall over the water source area. Table 11-1 summarises these estimates and the defined extraction limit for the Western Murray Porous Rock Groundwater Source (WMPRGS). The WMPRGS plan area reported in NOW (2012c) is up to two orders of magnitude too large compared to the mapped area (Table 11-1). However, this erroneous reported area is not reflected in the calculations of annual rainfall recharge.

Table 11-1. *Summary of the Western Murray Porous Rock Groundwater Source (NOW, 2012c).*

Area	7,301,762 km^2
Average annual rainfall	252 mm/yr
Infiltration Rate	6%
Estimated Total average annual rainfall recharge	1,103,965 ML/yr
Long term average annual extraction limit (LTAAEL)	530,486 ML/yr

11.1.1.4 Murray-Darling Basin Plan

The *Basin Plan* for the Murray-Darling Basin under the Water Act 2007 has recently been released (MDBA, 2012b). In the Basin Plan, extraction limits for a particular groundwater resource unit are defined in terms of a:

- Sustainable Diversion Limit (SDL) which is the long term average sustainable diversion limit, and a
- Baseline Diversion Limit (BDL) which is the limit of groundwater use under existing water management arrangements.

Table 11-2 summarises these proposed limits for the groundwater resource units relevant to the BHMAR project. Where numerical models are not available (as is the case for the study area), a recharge risk assessment method (RRAM) was used (CSIRO & SKM, 2010; 2011; MDBA 2012a) to derive a preliminary extraction limit (PEL). This involved:

- Using the Water Vegetation Energy and Solute (WAVES) model to determine basin-wide dryland diffuse (rainfall) recharge.
- Applying a risk matrix approach to assess risks in terms of the key environment assets, key ecosystem functions, the productive base and the key environmental outcomes. The level of uncertainty was also assessed.
- Defining a sustainability factor (SF) based on the assigned risk and uncertainty which was the proportion applied to the recharge volume to derive the PEL.

The RRAM risk matrix approach is similar in concept to the approach taken at a State level to define the NSW groundwater sharing plans for the area. River leakage is not a component of the WAVES model, so is not explicitly factored into the estimation of recharge. River leakage during flood events is acknowledged as the key recharge process for the Upper Darling Alluvium, although not explicitly incorporated into the analysis (CSIRO & SKM, 2010).

Table 11-2. *Diversion Limits for BHMAR groundwater resource units under the Basin Plan (MDBA, 2012b).*

Name	SDL ID	Category	Baseline Diversion Limit BDL (GL/yr)	Sustainable Diversion Limit SDL (GL/yr)
Lower Darling Alluvium	GS23	All groundwater	2.23	2.23
Upper Darling Alluvium	GS7	All groundwater	6.29	6.59
Western Porous Rock	GS50	All groundwater	63.1	116.6

11.2 GROUNDWATER MANAGEMENT IMPLICATIONS OF BHMAR PROJECT

Figure 11-1 places the BHMAR project area in context with the regional groundwater management units, the most significant in terms of plan area and diversion limits being the Western Murray Porous Rock Groundwater Source (WMPRGS). Figure 11-1 shows the regional mapping of groundwater salinity and aquifer yield for the Pliocene Sands, compiled as part of the Murray Basin Hydrogeological Map Series. This maps the distribution of better quality groundwater (<1500 mg/L) in the WMPRGS along a corridor associated with the Darling River, Talyawalka Creek and the Menindee Lakes. This shows the regional significance of river/lake leakage for the Pliocene Sands aquifer, as reinforced by the BHMAR study. In contrast, away from the river corridor the WMPRGS is mostly characterised by poor quality groundwater (>14,000 mg/L). There is less saline groundwater (3500-5000 mg/L) mapped near the northwest boundary of the WMPRGS (Figure 11-1). This is due to infiltration of episodic runoff from the adjacent Broken Hill Block and Scopes Range (Brodie, 1998). Overall, the regional groundwater salinity distribution (Figure 11-1) would suggest that diffuse infiltration of rainfall is a recharge mechanism that is subordinate to surface water leakage.

As discussed in Section 9.1, previous field measurements under native vegetation in this landscape indicate very low diffuse potential recharge to the unconfined aquifer, of <0.3 mm/yr or ~0.1% of average rainfall (Kennett-Smith *et al.,* 1991; Cook *et al.,* 1996). Near Pooncarie, the potential recharge rate associated with clearing and grazing was estimated at 1.5 mm/yr or 0.6% of average annual rainfall. Field data also suggest that for cleared but non-cropped areas with mean annual rainfall <250 mm/yr, potential recharge was <1 mm/yr regardless of soil type (Kennett-Smith *et al.,* 1994). These estimates from field studies are at least an order of magnitude less than that used in the WMPRGS water sharing plan (Table 11-1).

By way of comparison, potential diffuse recharge by rainfall was assessed for the BHMAR study area, by applying the chloride mass balance method using the project groundwater data (Section 9). This derived an

estimate of average rainfall recharge rate of 1.8 mm/yr, or ~0.7% of average annual rainfall. Again, this is about an order of magnitude less than the infiltration rate used for the WMPRGS (Table 11-1). It is important to note that in this application, the chloride mass balance method assumes a disconnect between surface water and groundwater, with rainfall being the only chloride source. As river/lake leakage has been inferred to be the main recharge mechanism, the underlying assumptions of this application of the chloride mass balance method do not hold and the derived recharge estimates are not valid.

From these previous recharge studies, a low diffuse recharge rate by rainfall of <1 mm/yr would be anticipated over much of the BHMAR study area and similar areas within the WMPRGS. This is based on a number of characteristics (1) the average annual rainfall between 200 and 250 mm/yr, less than the threshold of Kennett-Smith *et al*. (1994), (2) the common occurrence of fine-textured soils and near-surface aquitards that impede infiltration and (3) only limited areas of cropping which could potentially enhance rainfall accessions. Infiltration to the Calivil Formation (and Renmark) aquifers is further constrained by the extensive distribution of the overlying Blanchetown Clay aquitard, albeit structurally disrupted.

The limitations placed on diffuse rainfall recharge to the WMPRGS by factors such as the rainfall amount, the capacity for native vegetation for interception of infiltration, and the prevalence of overlying aquitards are explored further in Figure 11-2 to Figure 11-4. The regional rainfall distribution (Figure 11-2) shows that northern and western parts of the WMPRGS plan area have an average annual rainfall less than the 250 mm/yr recharge threshold of Kennett-Smith *et al*. (1994). This is the case for the BHMAR study area where diffuse rainfall recharge has been interpreted to be insignificant. Based on the factor of rainfall amount alone, Figure 11-2 can be used to extrapolate where diffuse rainfall recharge is also likely to be insignificant.

Figure 11-3 shows the regional distribution of native vegetation in the form of scattered or sparse trees. These are predominant in the southeast part of the WMPRGS plan area, where average annual rainfall is in excess of 250 mm/yr. The prevalence of such native vegetation in these areas would likely to have a significant moderating influence on potential recharge rates due to their extensive rooting depths and high water use efficiency.

Figure 11-4 shows the interpreted extent of the Blanchetown Clay (McLaren *et al*., 2011) for the WMPRGS plan area. This highlights the regional scale to which the Blanchetown Clay forms an aquitard over the Calivil Formation and Loxton-Parilla Sands of the WMPRGS. As indicated by the BHMAR project, recharge to the Pliocene Sands aquifer is localised in areas where the Blanchetown Clay has been structurally disrupted or erosionally removed, particularly in coincidence with surface water leakage. In addition to the Blanchetown Clay, there can be near-surface aquitards analogous to those mapped in the BHMAR study area that can also significantly impede downward movement of rainfall infiltration to the watertable.

These maps, combined with the previous field studies, suggest that due to the prevalence of controlling factors such as rainfall amount, native vegetation and overlying aquitards, the infiltration rate used in the WMPRGS plan (6%) is relatively high and is not necessarily uniform across the plan area. Such mapping, combined with other datasets (such as soil type, land use etc.) could be used to develop spatially distributed estimates of diffuse rainfall recharge that is validated by available field studies. Such approaches were used to develop recharge grids for input into regional steady-state groundwater flow models (Kellett, 1997; Brodie, 1998). Additional field studies would be useful to validate the recharge mapping in targeted areas (such as adjacent to the Broken Hill Block).

As indicated in Figure 11-1, the groundwater salinity of the Pliocene Sands is dominantly brackish to high saline. Hence, any potential diffuse rainfall recharge would replenish an aquifer with relatively limited beneficial uses. There are occurrences of freshwater lenses overlying the saline regional groundwater but these are thin (<5 m), localised to sandy depressions and highly sensitive to overpumping (Kellett, 1994). The regionally significant good quality water (<1500 mg/L) is limited to specific areas associated with surface water leakage. This dichotomy in groundwater quality creates a management issue, as the extraction limit is currently based on a diffuse rainfall recharge estimate aggregated over the entire management area, whilst the most beneficial resource is limited to a much smaller area. It is recommended that a zonal approach be taken that focuses on the appropriate allocations and management regime for the fresher groundwater along the near-river corridor, separate to that for the brackish to saline groundwater resource.

In summary, the BHMAR project outputs will provide a significant scientific base to support groundwater management in the region. The various project products vastly improve the mapping of aquifer architecture and hydraulic properties as well as understanding of key groundwater processes, such as recharge. For the *Lower Darling Alluvial Groundwater Source*, the BHMAR project will greatly assist with:

- Improved definition of the shallow fresh groundwater lens that defines the Groundwater Source.
- Mapping of analogous shallow fresh groundwater lenses in other parts of the Darling floodplain, such as the Talyawalka and Anabranch systems.
- Better definition of the stratigraphic, structural and hydrogeological framework of the shallow alluvial groundwater systems. For example, there is no stratigraphic definition (e.g. Coonambidgal Formation), geomorphic mapping or a nominal aquifer depth criterion in the existing NSW plan.
- Improved understanding of the magnitude and frequency of shallow groundwater recharge, associated with high-flow events in the Darling system. The current extraction limits are based on an estimate of demand, rather than the rate of groundwater replenishment.
- Improved risk assessment of the potential for ingress of saline groundwater.
- Improved understanding of the hydraulic connectivity between this shallow Groundwater Source and the deeper Pliocene aquifers of the WMPRGS.
- Improved siting of appropriate borehole monitoring.

The data and understanding of Darling floodplain hydrogeology from the BHMAR project can equally be applied to the *Upper Darling Alluvial Groundwater Source*. This includes:

- Clarification of the geomorphological and stratigraphic relationships for the fluvial aquifers (and aquitards). The NSW plan encompasses potential aquifers to depths of 50 metres, which can include lateral equivalents of the Calivil Formation target aquifer identified in the BHMAR study area. The project has also identified the Blanchetown Clay and a near-surface aquitard as being more extensive than previously mapped.
- Defining recharge (and extraction limits) based on an understanding of river leakage processes, identified as a recharge process that is dominant over diffuse rainfall recharge that is used in the plan.
- Providing criteria to aid targeting of potential zones of fresh groundwater in a data-poor region. In combination with improved hydrostratigraphy, the structural geology framework defined by the project can be used to help target field investigations.

There are also significant opportunities to take advantage of the BHMAR project outputs in any future revision of the *Western Murray Porous Rock Groundwater Source* plan, which incorporates the Calivil Formation and Renmark Group aquifers. The BHMAR outputs could be used to:

- Derive more robust estimates of recharge and therefore limits to groundwater extraction. Existing extraction limits for these aquifers, in both State and Basin plans, are based on the assumption that rainfall is the key recharge mechanism. However, the BHMAR project provides several lines of evidence that leakage from the river (and lakes) is the dominant mechanism of active recharge to the Calivil Formation. There is also evidence of fresh Calivil Formation palaeo-resources distal from the rivers and lakes that have no indicators of modern recharge by rainfall or leakage. This means that the current management paradigm for recharge being dominantly sourced from rainfall is not valid. Using a recharge volume based on an annual rainfall across the entire management area does not take into account the salinity range evident in the Calivil Formation (and Renmark Group) aquifer. There is provision for review of recharge and extraction limits during the 5th year of the NSW management plan.
- Better define the extent and geometry of the Calivil Formation aquifer, as well as the level of confinement defined by the overlying Blanchetown Clay and the potentiometric surface. The BHMAR project has identified areas with higher-yielding coarse sands hosted in palaeochannel deposits in the sequence. The overlying Blanchetown Clay and also a near-surface aquitard have

been found to be more regionally extensive than previously mapped, which would reduce the potential for diffuse rainfall recharge to the aquifer.

- Identify the beneficial uses of the Calivil Formation aquifer, particularly mapping of the zones of fresh to brackish groundwater resources. Such mapping helps target future areas of development, the siting of monitoring bores and other infrastructure, and the assessment of potential risks associated with groundwater pumping (such as ingress of saline groundwater). The BHMAR project area covers the majority of the better quality groundwater resource previously mapped within the Calivil Formation (Figure 11-1). Recognising the paucity of data supporting this previous mapping, reconnaissance AEM surveying further along the river corridor could be used to identify additional locations of enhanced river leakage and groundwater freshening in the Calivil Formation or Loxton-Parilla Sands.
- To establish a specific management regime for the better quality groundwater located near the Darling River and other surface water features. The contrast in groundwater salinity across the Groundwater Source (Figure 11-1) creates a management issue, as the current extraction limit is based on a diffuse rainfall recharge estimate aggregated over the entire management area, whilst the most beneficial resource is limited to a much smaller area. Project outputs could be used to construct groundwater flow and solute transport models to support the allocation and management regime for these fresh groundwater resources.
- Progress towards a more conjunctive management approach that recognises potential for combining the use and management of the Calivil Formation aquifer with the surface water resources of the region.

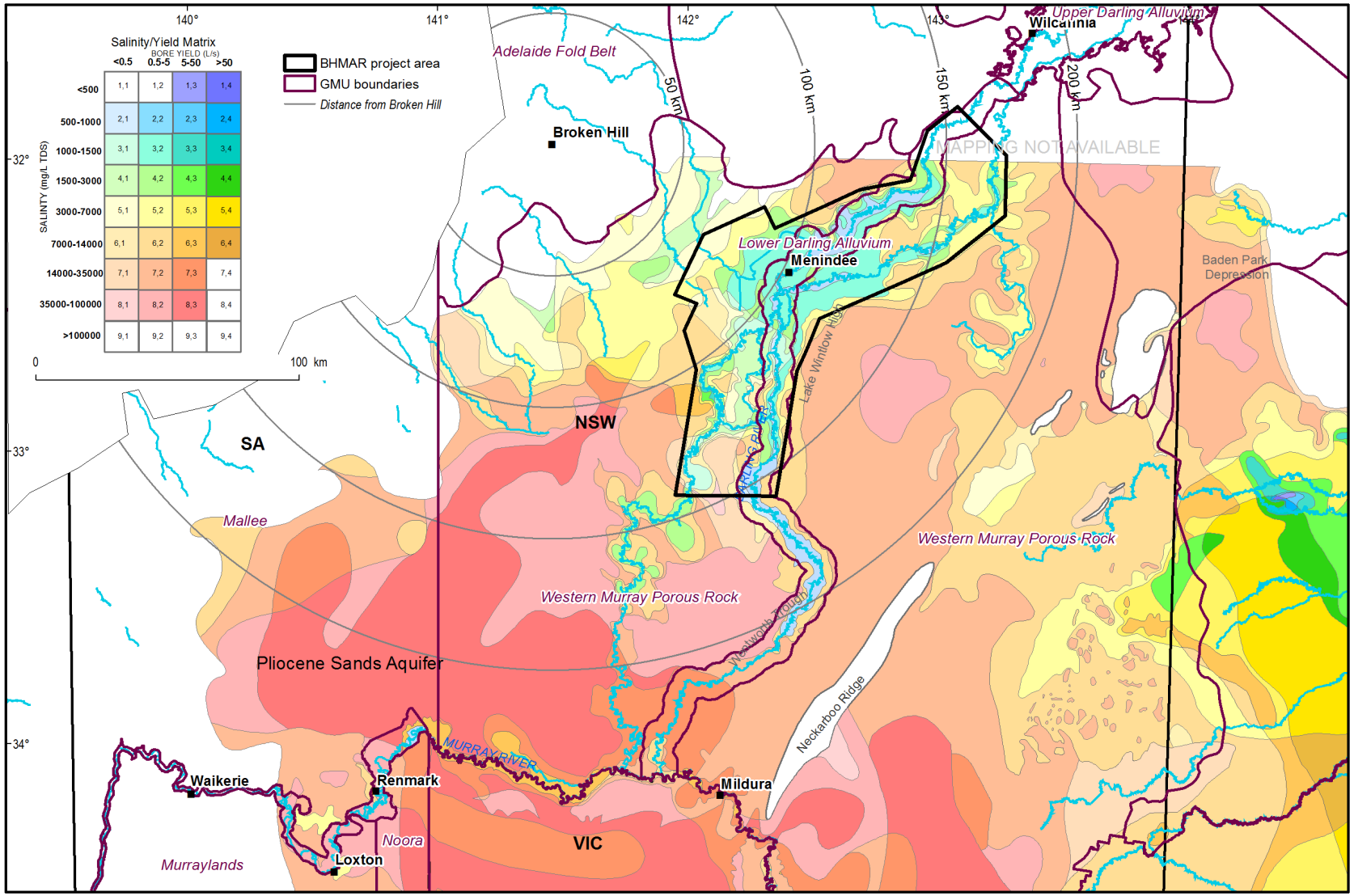

Figure 11-1. *Regional salinity-yield mapping for the Pliocene Sands (Calivil Formation and Loxton-Parilla Sands) aquifer from the 1:250,000 scale Murray Basin Hydrogeological Map Series. The BHMAR project and groundwater management unit (GMU) boundaries are also shown.*

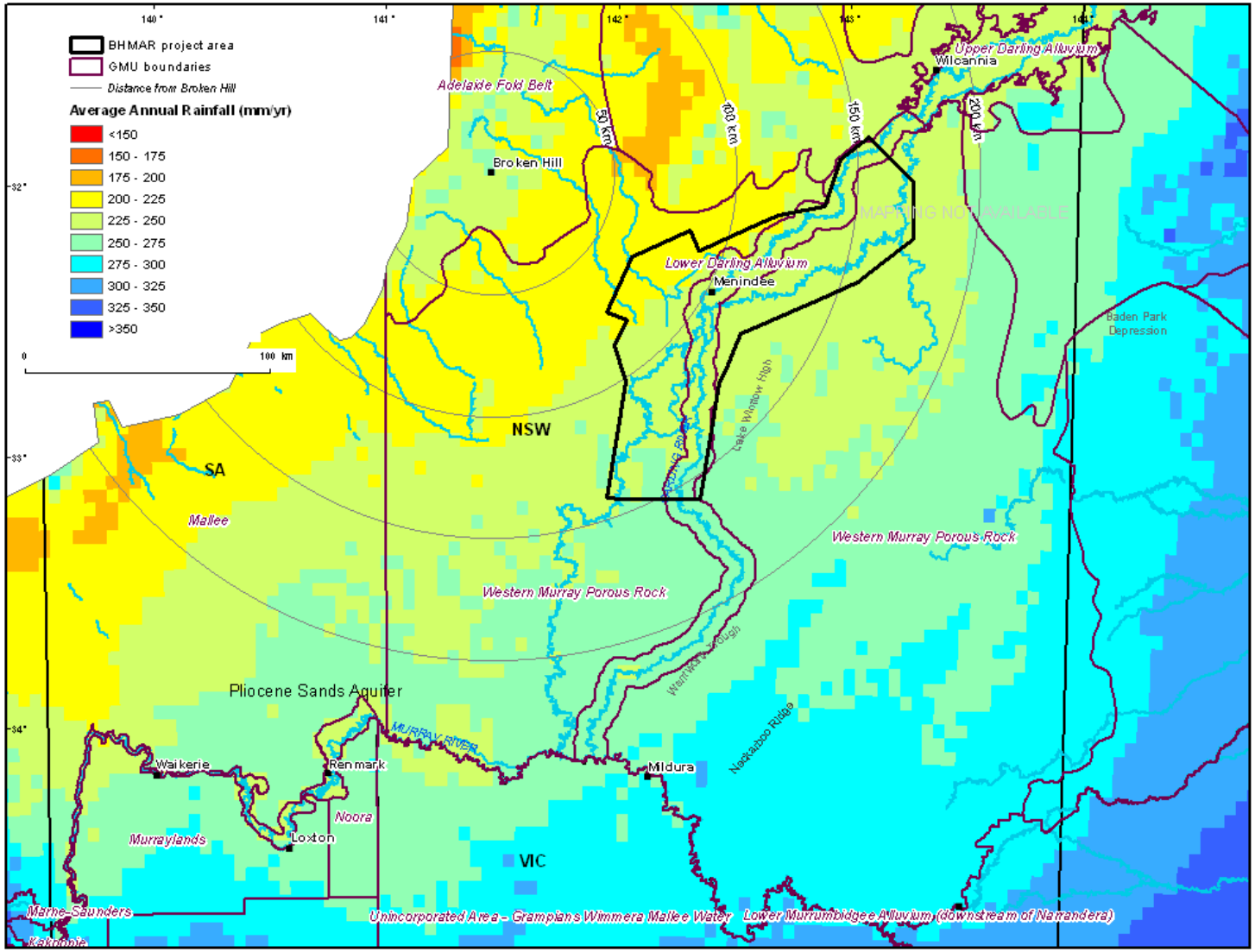

***Figure 11-2**. Regional distribution of average annual rainfall. The BHMAR project and groundwater management unit (GMU) boundaries are also shown.*

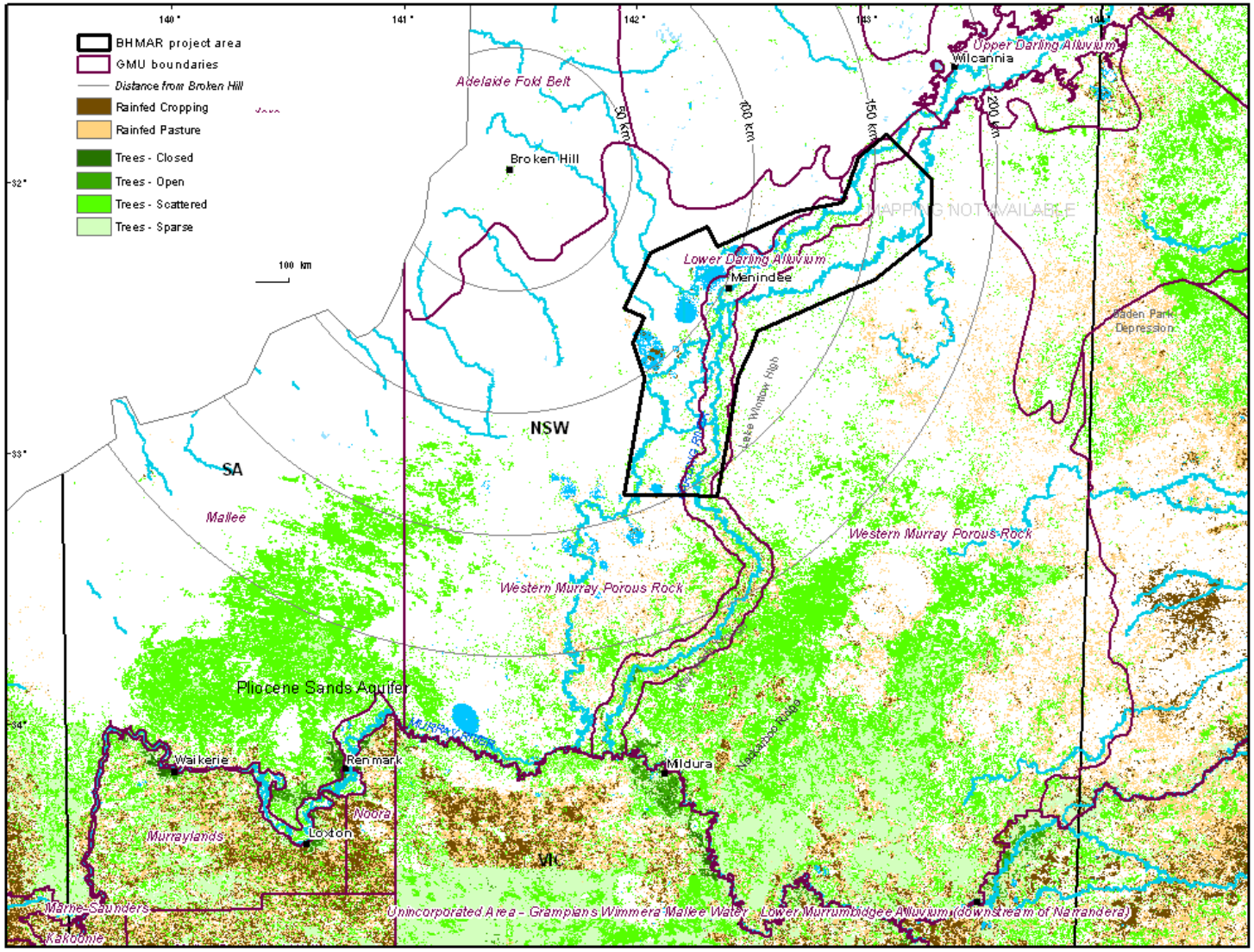

Figure 11-3. *Regional distribution of native vegetation (trees) and rainfed cropping/pasture based on MODIS time series analysis. The BHMAR project and groundwater management unit (GMU) boundaries are also shown.*

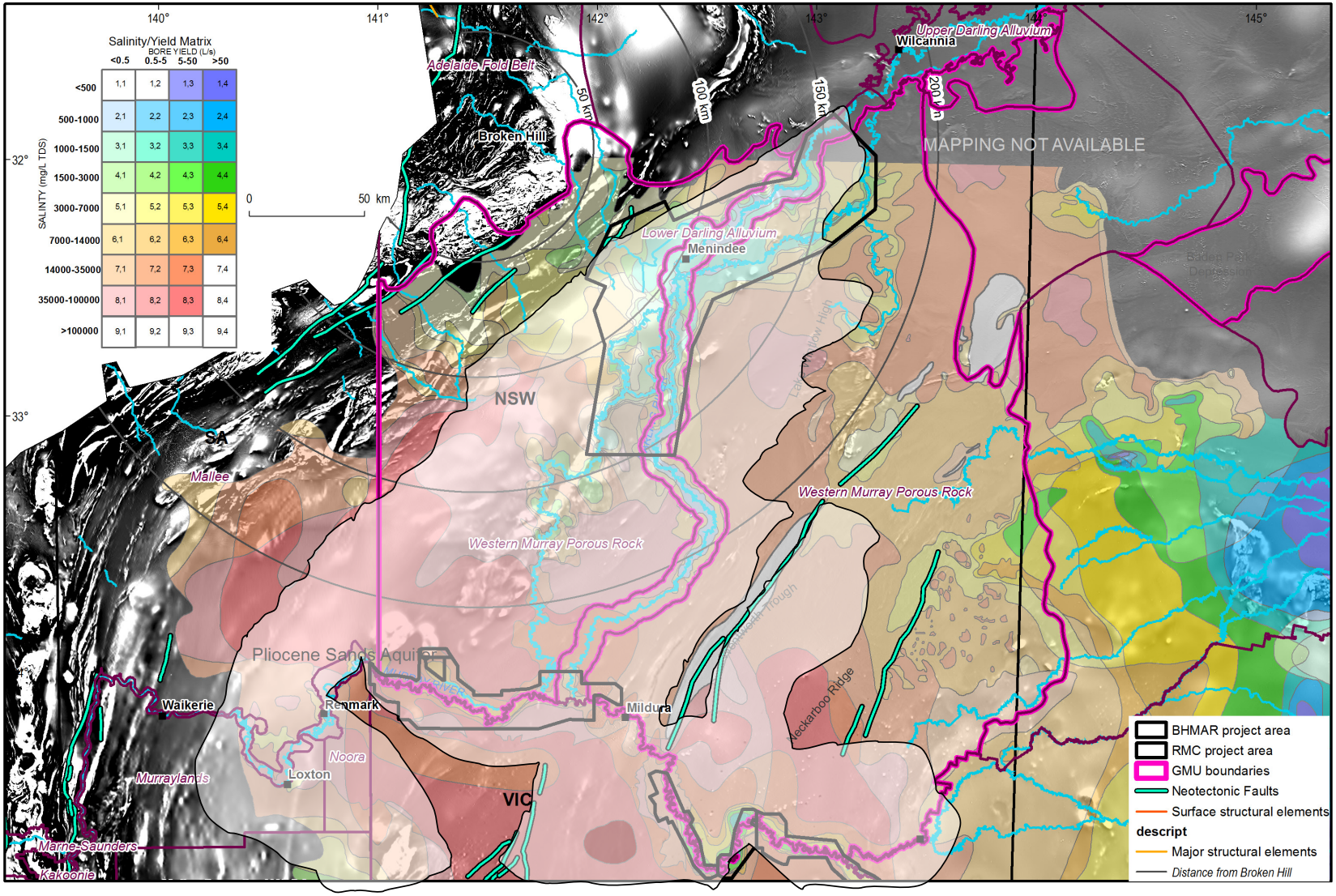

Figure 11-4. *Regional aeromagnetics overlain by salinity-yield mapping for the Pliocene Sands (Calivil Formation and Loxton-Parilla Sands) aquifer and the interpreted extent of the Blanchetown Clay (McLaren et al., 2011). The BHMAR project and groundwater management unit (GMU) boundaries are also shown.*

11.3 UPPER DARLING ALLUVIAL GROUNDWATER RESOURCE POTENTIAL

The identification of significant volumes of good quality, largely unutilised groundwater resources (Lawrie *et al*., 2012b, d) in the BHMAR study area highlights the likelihood of similar opportunities further upstream in the Darling-Barwon system, and in other data-poor river systems within the Basin. The key drivers are increasing drought security for regional communities and industries such as mining or agriculture and increasing local employment opportunities.

To this end, a rapid assessment was applied to the Upper Darling River between Bourke and Wilcannia. Current estimates of groundwater availability in this area do not account for potential recharge by river leakage. Significant generic losses from the river system have been predicted by river modelling under average conditions (CSIRO, 2008c), although the proportion attributable to leakage has not been determined due to lack of data. The BHMAR study has demonstrated that river leakage is significantly enhanced during high-flow events, so an average river budget may significantly underestimate potential transfers from the river to the shallow groundwater resource. A comparison of annual flows for specific wet years show examples of large (and unattributed) downstream reduction of flows between gauging stations, much greater than for average conditions. Recent mapping of stream-aquifer connectivity has identified medium to high losing reaches (CSIRO, 2008c).

In addition, there are a number of similarities in geomorphology, tectonics and stratigraphy between the Menindee Lakes region and the Upper Darling. Groundwater resources within the Darling Floodplain alluvium are likely to occur where recharge pathways (i.e. faults or holes in the upper confining aquitard) connect scroll-plain tracts to suitable (i.e. Calivil Formation equivalent) aquifer cells. Accordingly, groundwater investigations in the Darling upstream of Menindee should be concentrated along both coincident and separate scroll-plain tracts, in particular where the two scroll plain tracts intersect. Fundamental data acquisition is required to characterise confining aquitards, semi-confined and surficial unconfined aquifers and zones of preferential river leakage.

Understanding of the nature and extent of the groundwater resources of the Upper Darling is limited. The long-term average annual extraction rate for the Upper Darling Alluvial Groundwater Source is based on a proportion of recharge calculated as a percentage of long-term average annual rainfall. Therefore, river leakage, which has been identified as the dominant recharge process for the analogous aquifers at Menindee, is not included in the groundwater resource estimates. Current groundwater extraction is also limited. At Wilcannia, the identification of low-salinity shallow groundwater resources has enabled the establishment of water supply bores for the town. This groundwater source is linked to river leakage and considered to be significant but further investigations and monitoring is required (Woolley *et al.*, 2004).

River system modelling and monthly river reach water accounting have been undertaken for the Barwon-Darling catchment as part of the CSIRO Murray-Darling Basin Sustainable Yields project (CSIRO, 2008c). Table 11-3 summarises the results of these two approaches for the two Darling River reaches of Bourke to Louth and Louth to Wilcannia.

Table 11-3. *Water balances using river system modelling and monthly accounting approaches for two Darling River reaches (from CSIRO, 2008c).*

	Bourke to Louth			Louth to Wilcannia		
Water Balance	**Model**	**Accounts**	**Difference**	**Model**	**Accounts**	**Difference**
Gains	**GL/yr**	**GL/yr**	**GL/yr**	**GL/yr**	**GL/yr**	**GL/yr**
Main stream flows	1978	1870	108	1855	1769	86
Tributary flows	0	39	-39	0	0	0
Local inflows	0	0	0	0	0	0
Unattributed gains and noise	-	213	-213	-	154	-154
Losses	**GL/yr**	**GL/yr**	**GL/yr**	**GL/yr**	**GL/yr**	**GL/yr**
Main stem outflows	1855	1769	86	1558	1242	315
Distributary outflows	0	0	0	0	0	0
Net diversions	43	61	-19	1	1	2
River flux to groundwater	0	-	0	-	-	0
River and floodplain losses	40	95	-55	78	464	-386
Unspecified losses	39	-	39	217	-	217
Unattributed losses and noise	-	197	-197	-	215	-215

The modelling and accounting provide estimates of the river water balance on an average annual basis, including the scale of potential losses from the river system. For the Bourke to Louth reach, estimates for the total losses from the two methods used are 79 and 292 GL/yr. For the Louth to Wilcannia reach, the estimates for total river losses are 295 and 679 GL/yr. These are the losses assigned as river and floodplain losses, unspecified or unattributed losses and noise. It is important to note that a zero (or null) river leakage to groundwater has been assigned, not because that no leakage is occurring, but because groundwater exchanges were not simulated in the river model nor incorporated in the water accounting due to the lack of data.

These estimates are based on average annual conditions. Investigations at Menindee infer that river leakage to the shallow groundwater system is most apparent during high-flow events, rather than during low-flow or average river conditions. This recognises that there is huge variability in the Darling River flow regime. For example, the minimum annual discharges of the three major tributaries of the Darling (Namoi, Culgoa and Border Rivers) are all significantly below 10 % of their average annual flows, whilst their maximum annual flows are 400-800 % of average annual flows (MDBC, 2003). The relatively large but episodic flooding events drive groundwater recharge by river leakage. Hence, an average river budget may not be truly indicative of potential river transfers to the shallow groundwater resource.

To this end, a comparison was made of the annual inflows and outflows for specific wet years, for the two Darling River reaches being considered (Table 11-4). This shows the flow change over these reaches during relatively high-flow conditions as compared to average conditions. Attributing these differences is difficult as potential tributary flow gains need to be incorporated as well as distributary flow losses. For example, the Bourke to Louth reach includes potential input from flooding of the Warrego River. This is the most likely explanation for an overall gain in flow over the reach in the years 1978, 2000 and 2011. For the Louth to Wilcannia reach, outflow to the Talyawalka system during high flow needs to be considered. This also is highly variable – in 2011 this was measured as 1088 GL/yr but only 11 GL/yr in 2010. More detailed water accounting is required to better define the water balance during these wet years, but Table 11-4 indicates the potential magnitude of overall losses over these river reaches.

Table 11-4. *Comparison of Darling River main stem inflows and outflows for specific wet years.*

	Bourke to Louth			Louth to Wilcannia		
Year	**Main Stem Inflows[#] (GL/yr)**	**Main Stem Outflows (GL/yr)**	**Difference (GL/yr)**	**Main Stem Inflows (GL/yr)**	**Main Stem Outflows (GL/yr)**	**Difference (GL/yr)**
CSIRO Average Annual	1978	1855	-123	1855	1558	-297
2000	1553	1973	420	1973	1913	-60
2001	3075	2717	-358	2717	2348	-369
1996	4218	4070	-148	4070	3312	-758
1978	4506	4539	33	4539	4134	-405
2010	4901	4854	-47	4854	4390	-453
1977	5219	4506	-713	4506	4432	-74
2011	6205	6297	92	6297	4034	-1175
1983	9333	8303	-1030	8303	5433	-1096
1998	9518	4718	-4800	4718	4307	-411
1974	9743	8896	-847	8896	5491	-3405
1976	14942	14206	-736	14206	6047	-8159

As shown in Figure 11-5, mapping of surface-groundwater connectivity was also part of the assessment of water availability for the Barwon-Darling catchment (CSIRO, 2008c). This shows variability in connectivity, but importantly, the mapping of medium to high losing river reaches, particularly between Brewarrina and Bourke and a downstream section of the Louth to Wilcannia reach. The mapping is based on stream gauging and groundwater level data during low-flow conditions (e.g. in June 2006), but highlights and targets the potential for river leakage. The CSIRO (2008c) report also includes examples of borehole hydrographs showing groundwater level response to flood events, reinforcing the importance of river leakage to groundwater recharge.

In summary, the understanding of the nature and extent of groundwater resources in the Upper Darling is severely constrained by lack of baseline data. Current estimates of groundwater availability do not account for potential recharge by river leakage. Significant losses have been estimated for Upper Darling River reaches even under average conditions. The proportion of these generic losses that can be attributed to leakage to shallow aquifers has not been determined, however connectivity mapping has identified medium to high losing river reaches. Based on investigations at Menindee, the understanding and quantification of leakage processes during episodic high-flow events is a priority. It is considered likely that similarities in the hydrogeological system will also provide opportunities for MAR in the Upper Darling reaches.

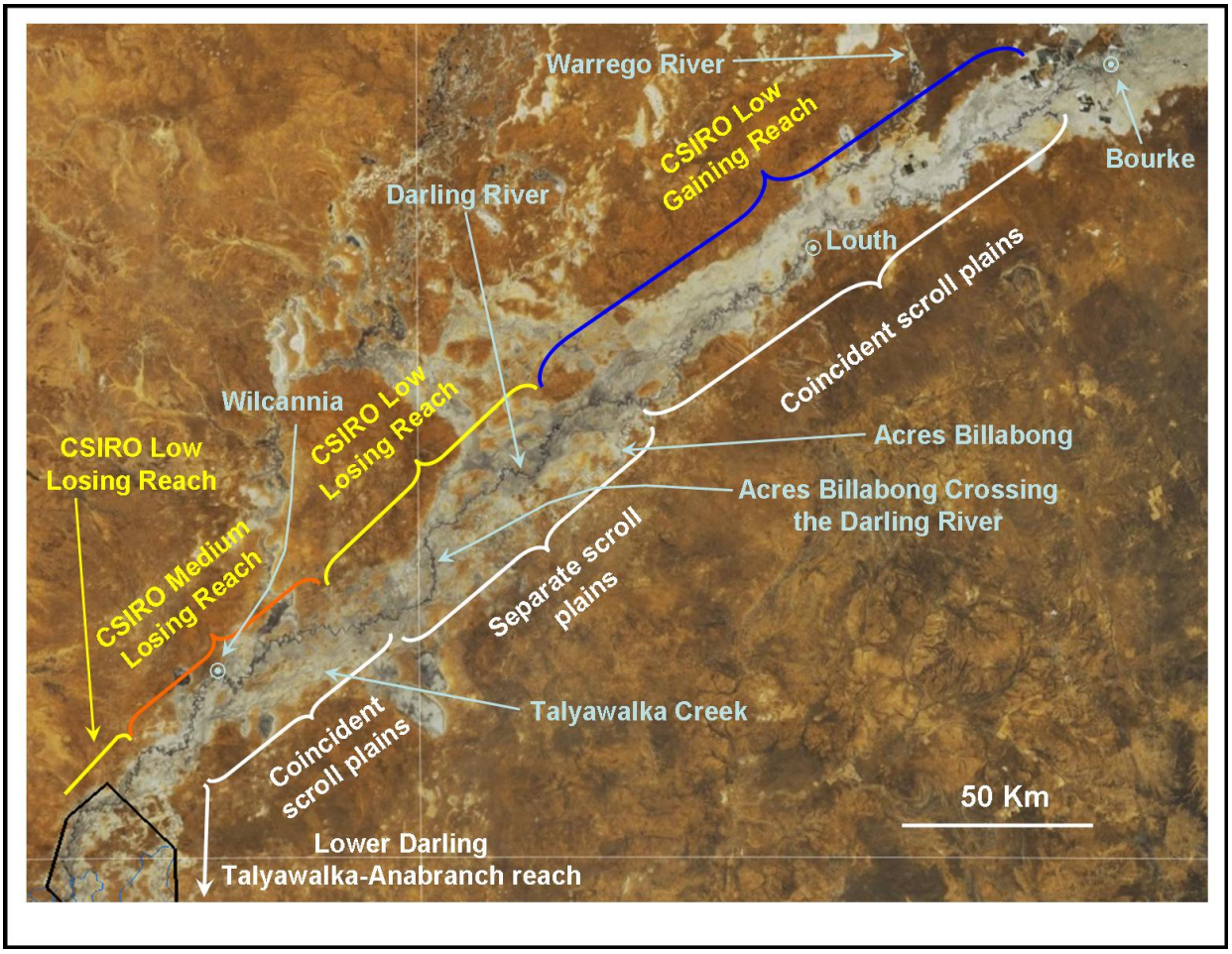

Figure 11-5. *Image showing the upper reaches of the Darling River, marked to show the gaining and losing reaches (from CSIRO, 2008c). These match consistently with major differences in floodplain morphology. Image from Google Earth.*

12. Discussion

12.1 USING AEM TO MAP MAR AND GROUNDWATER RESOURCE TARGETS

Previously, the high cost of investigations, low level of knowledge of risk, and time taken to fill hydrogeological knowledge gaps have been a deterrent to development of MAR options, especially in pioneering projects in new and/or more remote locations. In the BHMAR project, the initial scoping study concluded that despite the paucity of data, there were a number of possible MAR and groundwater resource targets in the Darling Floodplain near Menindee (Lawrie *et al.,* 2008, 2009a, b).

To meet the challenge of rapid identification and assessment of potential MAR targets and groundwater resources over a large area (7,541.5 km^2) within relatively short timeframes (18 months), it was concluded that the only cost-effective method with the ability to resolve features in this depth range was airborne electromagnetics (AEM) (Lawrie *et al*., 2009b). A review facilitated by the Australian Academy of Sciences and the Australian Academy of Technological Sciences and Engineering for the Australian Federal Government's Natural Resource Management Ministerial Council in 2004-2005 found that the only broad acre technique that could detect and resolve hydrostratigraphy and groundwater quality (salinity) in the sub-surface deeper than the root zone, particularly in the electrically conductive landscapes found in Australia, is AEM (Spies & Woodgate, 2005).

In Australia, AEM has been used effectively to map hydrostratigraphy, groundwater salinity and the salinity hazard and risk in a number of floodplain environments (Chamberlain & Wilkinson, 2004; Walker *et al*., 2004; Lawrie *et al*., 2008, 2009a, b, 2010a-c; 2012a; Munday *et al*., 2006, 2007, 2008; Palamera *et al.*, 2010), and to map salt water intrusion (Munday *et al.,* 2007; Tan *et al*., 2012). AEM surveys have also been used to detect groundwater resources within otherwise salinised landscapes (George *et al*., 1998; Reid *et al*., 2008; Edwards & McAuley *2008*; Lawrie *et al.,* 2009a, b).

The benefits from AEM surveys are maximised when these technologies are employed within multi-disciplinary, systems-based approaches to the analysis of problems and the development of customised interpretation products (Lawrie *et al*., 2000; Lawrie *et al.,* 2003a, b, 2009a, b, 2010a-c; Spies & Woodgate, 2005). Systems-based approaches incorporate an understanding of landscape evolution and scale, utilise modern investigative approaches to the conceptualisation of aquifer systems, and incorporate data on geology, water, salinity and vegetation dynamics to provide key constraints on aquifer systems (Lawrie *et al*., 2000, 2008, 2009a, 2010a-c).

Over the past five years, a staged approach to survey design combined with forward modelling studies has ensured that appropriate AEM technologies are selected to match the target objectives (Green & Munday, 2004; Lawrie, 2006; Munday *et al*., 2007, 2008d; Lawrie *et al.,* 2009a, b, 2010a-c). In Australian landscape settings AEM-based products have proven effective at providing high resolution baseline data on the spatial distribution of aquifers and aquitards as well as water quality and salt stores in shallow (<120 m) floodplain sediments (Mullen *et al*., 2007; Tan *et al*., 2005; Munday *et al*., 2006, 2007; Lawrie *et al*., 2009a, 2010a-c). However, while these datasets and information products address specific gaps in the biophysical knowledge framework, addressing salinity and land management questions usually requires an understanding of underlying biophysical processes and dynamics that often cannot reliably be determined from analysis of spatial patters of conductivity alone (Cresswell *et al*., 2007, Lawrie *et al*., 2010a).

The BHMAR AEM survey has built significantly on the principles, methodologies, experience and products developed for salinity mapping and management in Australia. In particular, the staged approach to technology selection and survey design (Lawrie *et al*., 2009a, b), and the use of a 4D systems approach to integrate complex datasets and develop a range of customised information products for use in subsequent hydrogeological and geotechnical modelling was recognised as critical to the success of the survey. The BHMAR survey would appear to be the first use of AEM methods in MAR investigation and assessment.

12.1.1 3D Mapping of Hydrostratigraphy, Structure and Groundwater Salinity

To meet the challenge of rapid identification and assessment of potential MAR targets and groundwater resources over a large area (7,541.5 km^2) within relatively short timeframes (18 months), it was concluded that the only cost-effective method with the ability to resolve key features of the hydrogeological system in the 0-150 m depth range was airborne electromagnetics (AEM) (Lawrie *et al*., 2009a, b).

In Australia's salinised landscapes, AEM has been used effectively to map hydrostratigraphy, groundwater salinity, salinity hazard and risk, and groundwater resources, in a number of floodplain environments, including the Basin. In the BHMAR study, it was necessary to select an AEM system with the capability of mapping key functional elements of the hydrogeological system critical to the success in identifying and assessing suitable MAR and groundwater resource targets. This necessitated selecting an AEM system capable of mapping heterogeneities in the hydrostratigraphy and hydrogeology, and more specifically, the:

- Thickness and extent of near-surface unconfined aquifers and aquitards that might provide recharge pathways or inhibit surface-groundwater connectivity;
- Thickness, extent and internal textural variability of Pliocene sand aquifers;
- Thickness, extent and internal variability in upper (Blanchetown Clay) and lower (upper Renmark Group) confining aquitards that 'sandwich' the Pliocene Sand aquifers;
- 3D distribution of groundwater salinity (to help define fresh and brackish groundwater resources);
- Faults that might act as discrete recharge and groundwater flow pathways;
- Zones of inter-aquifer leakage.

The use of airborne electromagnetics (AEM) for hydrogeological investigations often requires high resolution data, even for regional analysis. Optimisation of AEM data therefore requires careful consideration of AEM system suitability, calibration, validation and inversion methods.

In the BHMAR project, the helicopter-borne SkyTEM transient EM system was selected after forward modeling of system responses and comparative assessment of test line data from two systems over potential targets (Lawrie *et al*., 2009b). The SkyTEM system is a high-resolution helicopter-borne time-domain electromagnetic system, and was developed specifically for high-resolution groundwater and environmental investigations. It was developed as a rapid alternative to ground-based TEM surveying and has the advantage of delivering much higher data density and spatial area coverage.

The BHMAR survey involved acquisition of 31,834 line km of data over an area of 7,500 km^2 of the River Darling Floodplain, and was acquired by two systems over a 9-week period. Initially the geophysical data was inverted (modelled) using "Fast Approximate Inversions (FAI)" software, in order to generate data that could be viewed as flight –line sections within 48 hours of acquisition, and gridded to provide maps to guide a field investigation program. More information regarding the survey is included in Lawrie *et al*. (2012a).

The AEM data were used to target 100 sonic and rotary mud holes that were used for calibration and validation of the survey results. Subsequently, a number of different (Laterally and Spatially Constrained) inversions of the AEM data were carried out, with refinements made as additional information on vertical and lateral constraints became available. Finally, a "Wave Number Domain Approximate Inversion" procedure (Christensen, 2012; Lawrie *et al*., 2012a), with a 1D multi-layer model and constraints in 3D, was used to produce a 3D conductivity model (Lawrie *et al*., 2012a; Figure 12-1). This inversion procedure only takes days to run, enabling rapid trialling to select the most appropriate spatial constraints.

The various products derived from the AEM inversion are available in Appendix 5 (Apps *et al*., 2012b) and referred to extensively throughout Lawrie *et al*. (2012c, d). Methods pertaining to the generation of these products are also documented in detail in Lawrie *et al*. (2012a).

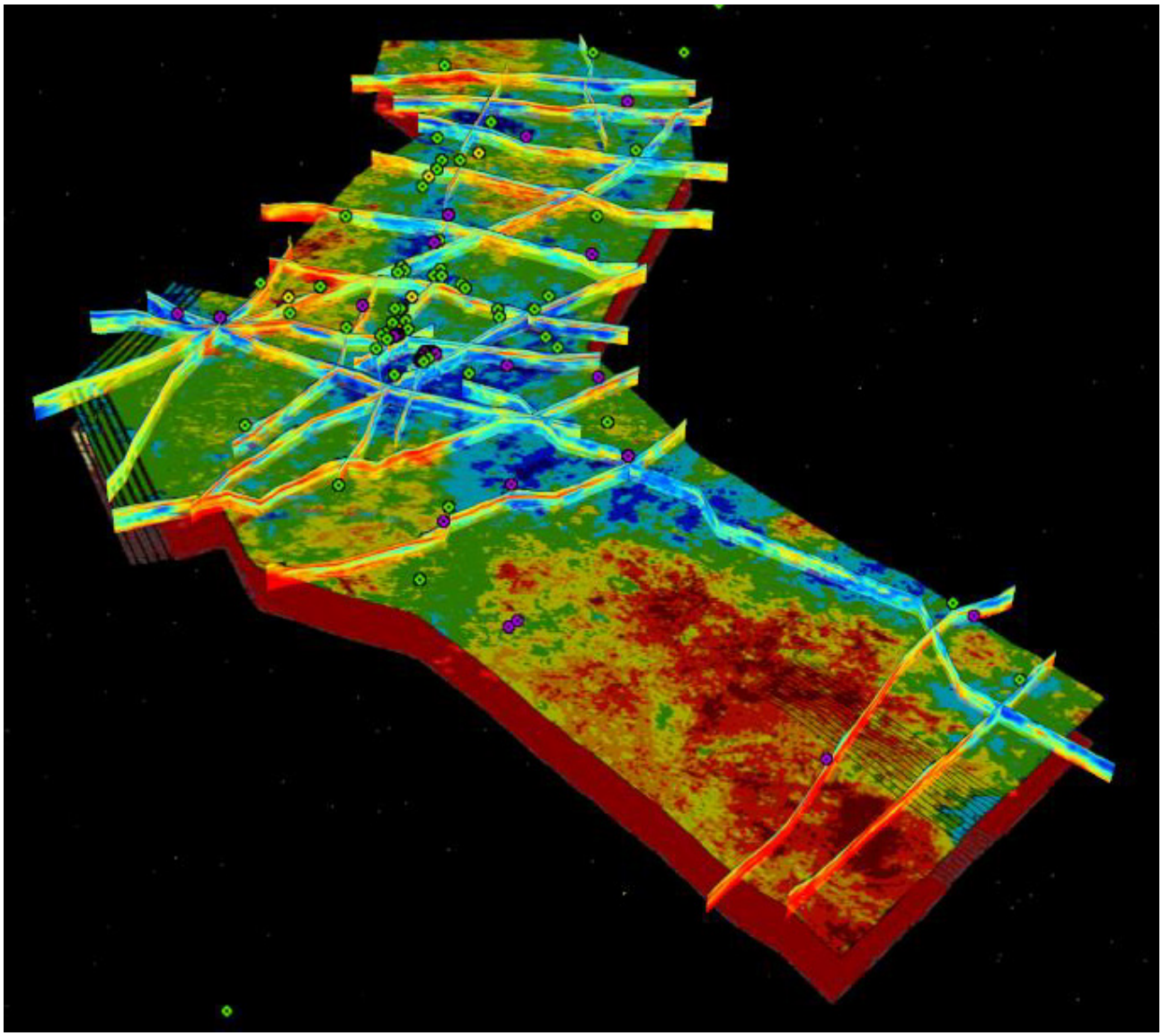

Figure 12-1. *Perspective view of AEM-derived conductivity data for the BHMAR Project study area. The figure comprises a representative conductivity depth slice and regional cross sections of the AEM data. Blue areas map low electrical conductivity in both the depth slice and cross sections. Coloured dots represent the different types of holes drilled as part of the BHMAR Project (green=sonic, cored; yellow=sonic, non-cored; purple=rotary mud)*

12.2 CHARACTERISTICS OF AUSTRALIAN RIVERS

It has been long recognised that the distinctive climate and continental evolution of Australia has led to the development of several unusual, or even unique fluvial features (Miall 1996; Miller & Gupta 1999). Many of these can be linked to the unique character of the Australian landscape as being "old, flat, and red" (Pain, 2012). Based in part on and expanded from Nanson & Tooth (2011) we can list the following characteristics of Australian rivers that stand out when compared to North American and other northern hemisphere fluvial systems.

- Prolonged tectonic stability (Ollier, 1991) resulting in low gradients, limited accommodation space, and slow alluvial accretion rates.
- Limited headwater upland erosion (Walling & Webb, 1983; Jansson, 1988).
- Extensive unconfined low gradient plains (Kernich *et al*., 2009; Page *et al*., 2009).
- Limited Quaternary glacial activity but major flow regime changes (Page *et al*., 1996; Page *et al*., 2009).
- Low sediment yields (Walling & Webb, 1983; Jansson, 1988).

- Weathering and induration of alluvium (Nanson *et al*., 2005; Lawrie *et al*., 2002)
- Drought and drought-dominated regimes (McMahon & Finlayson, 2003).
- Declining downstream discharges (Tooth & Nanson, 1995; Kemp, 2010)
- Coevolution with riparian vegetation (Bowman & Yeates, 2006; Morton *et al*., 2011).
- Extensive fluvial-aeolian interaction (Meroulis *et al*., 2007; Hesse *et al*., 2004)
- Deep weathering of sediment source areas (Ollier, 1991; Lawrie *et al*., 2002)
- Presence of unusual (in a global context) sediment types in many rivers, such as modern clay-pellet sands and Miocene fluvial oolite ironstones of the Pilbara (Nanson *et al*., 1986; Morris & Ramanaidou, 2007)
- Limited snowpack winter water storage in headwaters of most rivers apart from those with their headwaters in the Snowy Mountains or Tasmania (Hesse *et al*., 2004).
- High salinity loads derived from cyclic salts and groundwater discharge into rivers (Ruprecht & Schofield, 1991; Herczeg *et al*., 2001; Jolly *et al*., 2001)
- Scarcity of classic active alluvial fans in arid zone (Tooth, 2000). Those in the arid zone are very low gradient inland distributary systems (e.g. Kernich *et al.,* 2009); among the few active fans are coastal fan deltas (e.g. Clarke, 2004).
- Scarcity of arroyos (Tooth, 2000; Mabbutt, 1977; Thomas, 1997)
- Scarcity of badland landscapes (Tooth, 2000; Mabbutt, 1977; Thomas, 1997) despite widespread Mesozoic and Cenozoic shale deposits
- Large scale inter-annual discharge variability, twice as great as occurs in northern hemisphere rivers (Chiew & McMahon, 1993)
- Very high textural and compositional maturity of sediments (Ollier, 1991)
- Clays dominated by smectites (Gingele & De Deckker, 2004, 2005)
- Sediment sources mostly from bank erosion and reworking (Prosser *et al*., 2001)
- Strong groundwater coupling of surface flow resulting in losing and gaining river reaches (Andersen & Acworth, 2009; Herczeg *et al*., 2001; Jolly *et al*., 2001).

12.2.1 Comparing Menindee Area with Tucson Basin

The Tucson Basin in Arizona makes an interesting comparison to the stratigraphy of the Menindee area that illustrates some of the similarities and differences between Australian fluvial systems and those found elsewhere (Table 1). The overall age of the successions (Eberly & Stanley 1978, Brown & Stephenson 1991) are similar, extending from Eocene (the oldest sediments actually drilled at Menindee in this study were Miocene) through to Holocene, with ongoing sedimentation.

Scarborough & Pierce (1978) and Eberly & Stanley (1978) showed that the Tucson and other Cenozoic basins of Arizona are strike-slip basins formed by wrench faulting associated with the development of the Basin and Range province. While the tectonic style is therefore similar to that associated with the Darling fault zone at Menindee, the scale is quite different. Fault off-sets of metres to tens of metres are evident at Menindee, while those of the Tucson and other Cenozoic basins of Arizona range from hundreds of metres to kilometres. In consequence, in the Tucson Basin stratigraphic unit thicknesses and relief are greater by an order of magnitude than they are at Menindee. Rates of erosion and deposition are consequently much less at Menindee than at Tucson.

A consequence of this much lower level of tectonic activity in the Darling River and its distal location from highlands is a much greater level of textural and compositional maturity of the sediments, as shown in this report. Sands are almost exclusively quartz and the dominant mud fraction is clay. This contrasts with the Tucson Basin where the sediments are often lithic and arkosic boulder beds, sands and gravels with minor clays (Houser *et al*., 2004; Eberly & Stanley, 1978). The higher relief in the Tucson Basin results in much coarser grainsize, with coarse gravels predominating (Houser *et al*., 2004; Eberly & Stanley, 1978), in contrast with the mud- and sand-dominated sediments at Menindee. The lower level of tectonic activity in the Menindee area results in sedimentation occurring from a major through-flowing fluvial system, whereas in the Tucson Basin drainage systems are confined to individual fault basins.

Sedimentary processes in the Tucson Basin are dominated by alluvial fan and braided stream facies (Eberly & Stanley 1978). This contrasts with the Cenozoic succession at Menindee, where deposition evolved from anastomosing braided to lacustrine to meandering and sinuous across the entire project area.

With respect to the origin of salts there is a contrast also. Naiman *et al*. (2000), Gu (2005) and Adkins (2009) showed that groundwater salts in the Tucson and similar basins of Arizona were derived from both cyclic sources and from bedrock, with bedrock predominating. This contrasts with the salts of Australian rivers, which are mostly cyclic in origin (Gunn & Richardson, 1979; Chivas *et al*., 1991).

Low sedimentation rates and high salinity loads have resulted in widespread shallow and in some cases surface induration of Australian fluvial sediments. Elsewhere in Australia his has led to stream avulsion (Nanson *et al*., 2005) and relief inversion (Pain & Ollier, 1995) Such intense and rapid induration is absent from the Menindee project area, however nodular carbonate cementation is locally present in the Menindee Formation and silica and iron oxide cementation in the Calivil Formation. Where the Darling River has cut through the Menindee Formation and the Willotia beds, carbonate cementation is locally extensive through degassing CO_2 from seeping shallow groundwater. By contrast in the Tucson Basin, cementation, mostly carbonate occurs only at depths of several hundred metres and more (Houser *et al*., 2004).

Table 12-1. *Comparison between the sediments of the Tucson Basin and the Menindee project area.*

Feature	**Tucson**	**Menindee**
Age	Eocene-Holocene	Eocene-Holocene
Tectonic style	Wrench faulting	Wrench faulting
Tectonic scale	Basin scale	Local scale
Fault off-set	Metres to 10s metres	Hundreds of m to kilometres
Stratigraphic unit thickness	Kilometres	Tens to hundreds of metres
Lithologies	Gravels, sands volcanics, evaporites, minor mud	Fine to coarse sand, mud, minor gravel
Relief	Kilometres	Tens of metres
Fluvial systems	Local	Through-going
Salt sources	Rock weathering dominant	Cyclic salts dominant
Secondary induration	Low	High
Facies	Braided and alluvial fan	Anastomosing, braided, lacustrine, meandering, fixed
Sediment compositional maturity	Low	High
Sediment textural maturity	Low	High
Flow events	Winter-spring	Summer dominated

13. Conclusions

13.1 KEY SCIENTIFIC FINDINGS IN THE BHMAR STUDY AREA

1. Scientific investigations in the BHMAR project have completely revised our understanding of the age, stratigraphy and depositional mode of the Darling Floodplain surficial sediments, and the hydrostratigraphy, hydrogeology, and history of geological and landscape evolution of the Cenozoic Murray Geological Basin in the project area.
    - Details of the depositional mode, mineralogy, and characteristics of the stratigraphic units have been invaluable in guiding interpretation of the AEM data, and in characterising and evaluating the identified groundwater resources.
    - The revised 3D frameworks and details of internal geological and hydrogeological characteristics are also essential for the identification and assessment of MAR options.
    - These revisions have important implications for understanding hydrological and hydrochemical processes, and for understanding recharge and inter-aquifer leakage leading to the localisation of groundwater resources.
    - This new knowledge has practical implications for assessing groundwater resources and MAR options in the BHMAR project area, and regionally.
2. Airborne electromagnetics (AEM) and remote sensing data (LiDAR and Landsat), validated by ground and borehole geophysics, and laboratory data from a drilling program, have been used to map key functional elements of the hydrological system:
    - Surface geomorphology and the multi-layered sequence of aquitards and aquifers have been mapped at high-resolution to produce a new 3D map of the hydrostratigraphy in the top 100 m of the Lower Darling Floodplain.
    - The Blanchetown Clay occurs throughout most of the study area, providing an upper confining aquitard to key Pliocene aquifers (Calivil Formation and Loxton-Parilla Sands), and potential MAR (and groundwater extraction) options. Mapped ‘holes’ and fault offsets in the Blanchetown Clay provide potential recharge windows and inter-aquifer leakage pathways to the underlying target Pliocene aquifers.
    - The thickness, extent and salinity distribution of the Pliocene aquifers have been mapped in 3D. Multi-scale surveys combined with drilling data have revealed significant aquifer heterogeneity at regional and borefield scales. These data enabled identification of palaeochannels with favourable hydraulic properties and low salinities in the Pliocene aquifers, greatly assisting with the identification and prioritisation of groundwater resources and MAR targets.
3. There is evidence of significant Neogene-to-Present tectonics in the study area.
    - Extensive Neogene-to-Present faulting, tilting and warping of the Lower Darling Valley sediments is evident from multiple independent lines of evidence including AEM, airborne magnetic, regional gravity, seismic reflection and borehole datasets. These faults appear to be largely formed through reactivation of basement faults mapped in the underlying Darling Geological Basin.
    - The Blanchetown Clay is warped and tilted at a range of scales, and is locally sharply offset by faults with up to 20 m vertical offset. Overall, the Blanchetown Clay top surface varies in elevation by 60 m across the study area. Many of the faults controlling this deformation are reactivated basement faults mapped in magnetic, gravity and seismic datasets.
    - Neogene faults that offset the Blanchetown Clay horizon and localise inter-aquifer leakage are more numerous than surficial Neotectonic structures.
    - The palaeo-stress orientations of Neogene structures interpreted from faults mapped in the AEM data suggest a similar stress field to present day conditions, but with rotation of the maximal principal stress field within two trans-tensional strike slip fault zones (the Menindee and Talyawalka Fault Systems).

- The shallow Coonambidgal and Menindee Formation aquifers are also largely structurally controlled with deeper deposition localised in small fault-controlled trans-tensional basins (half graben and grabens).
- The target Pliocene aquifers are deposited in broad, structurally-controlled palaeovalleys.
- There is no evidence to suggest that Neogene-to-Present structures that control the Pliocene and younger sediments, had any influence on the palaeogeography or facies distribution of upper Renmark Group sediments.
- The present-day courses of Talyawalka Creek and the Darling River are largely structurally controlled, with straight-line segments and box-like drainage patterns controlled by intersecting faults mapped in LiDAR, AEM, airborne magnetic and regional gravity datasets.
    - These faults provide important recharge pathways to underlying aquifers where they intersect the river and adjacent flush zones.
    - Other evidence for neotectonics includes lake tilting (crossing shorelines); while a number of surface scarps and linear topographic highs are coincident with faults and horst blocks mapped in the underlying geology.

4. A completely new conceptual model for the Darling Floodplain hydrological system (including the Lower Darling Alluvium and Western Murray Porous Rock Groundwater Management Units) has been developed.
    - The mounding of groundwater levels near the river indicates the regional significance of losing river conditions. Groundwater chemistry and stable isotope data show that recharge is episodic and linked to high-flow flood events rather than river leakage being continuous. Critically, rapid and significant groundwater level responses were measured during flood events. Continuation of rising trends after the flood peak receded suggests that this is an actual recharge response rather than hydraulic loading, with rapid recharge facilitated by structural disruption of the aquitards.
    - Mud veneers and mineral precipitates are evident along much of the Darling River channel bank when river flows are low. During low-flow conditions these act as impediments to river leakage. During floods, high-flow velocities scour these deposits, revealing lateral-accretion surfaces in the shallow scroll-plain sediments. This scouring allows lateral bank recharge to the shallow aquifer.
    - Recharge to the underlying Pliocene aquifer occurs via erosional ‘holes’ in the confining aquitard, and in areas where vertical fault offsets enable inter-aquifer leakage through the juxtaposition of the unconfined Menindee and Coonambidgal Formation aquifers and the Pliocene aquifers. Mapped depressions in the river bed (‘cod holes’), are floored by indurated clays, and do not provide preferential connectivity to the underlying aquifer.
    - Such flow-dependent recharge has implications for groundwater assessment and management. For example, an analysis of historic river flows suggests that active recharge to the groundwater system would only occur for about 17% of the time when flow exceeds about 9,000 ML/d. Recharge would be negligible with groundwater extraction during low-flow conditions.
    - Diffuse recharge from rainfall to the Pliocene aquifers is interpreted to be insignificant, due to the combination of low average rainfall, high evaporation, minor irrigation and the presence of thick, extensive aquitards over most of the study area. This conclusion is supported by recharge estimates using the chloride mass balance approach.
5. The results of scientific investigations into MAR/groundwater options to secure Broken Hill’s water supply, are reported separately (Lawrie *et al*., 2012c). This includes the science findings associated with carrying out maximal and residual risk assessments for MAR options at a priority site (Jimargil), and three other potential borefield sites. This includes more detailed descriptions of the local geology and hydrogeology.
6. The results of scientific investigations into regional MAR/groundwater options more broadly in 14 targets across the Darling Floodplain are reported in Lawrie *et al*. (2012d). This includes a more detailed description and assessment of the geology and hydrogeology of each target.

13.2 REVISED GEOLOGICAL AND HYDROGEOLOGICAL FRAMEWORK

1. Renmark Group Sediments

   - Regionally, the Renmark Group comprises the non-marine Paleocene to Miocene sediments of the Murray Geological Basin. Deposition of the Renmark Group in the project area is controlled by the Menindee Trough, a northeast-southwest trending Paleozoic structural basin. The basal Renmark Group sequence tends to be limited to the Menindee Trough, with the upper part of the Renmark Group occurring across the whole project area. The latter is also likely to be influenced by the underlying Menindee Trough, possibly as a sag basin.
   - The upper part of the Renmark Group is a widespread non-marine succession of Miocene age in the Murray Geological Basin. Unlithified and nowhere exposed, it is a poorly understood. It is inferred from drilling to be deposited on a low-relief sedimentary plain dominated by anastomosing fixed-channel streams, flowing southward into a complex low-energy coastal plain with numerous lagoons and bays. In 90% of the BHMAR holes drilled, the upper Renmark Group is represented by fine-grained muds.
   - The upper Renmark Group sequence mostly acts as an underlying aquitard to important aquifers in the overlying Calivil Formation succession. Hydraulic connection between the Calivil Formation and Renmark Group tends to be limited, except where Renmark Group channel sands immediately underlie the Calivil Formation. In these areas there can be a distinct salinity gradient.

2. Pliocene Aquifers (Calivil Formation and Loxton-Parilla Sands)

   - The Pliocene aquifers are the main focus of investigations in this study. In the project area, the Pliocene aquifers predominantly comprise the fluvial Calivil Formation, with the shoreline and shallow marine Loxton-Parilla Sands restricted to the southernmost part of the area. Post-depositional warping, tilting and discrete offsets associated with tectonic activity have influenced the thickness, extent and preservation of the Pliocene aquifers. AEM mapping validated by drilling has enabled the lateral extents and thickness of the Pliocene aquifers to be identified.
   - Facies analysis indicates the Calivil Formation was deposited in deep braided streams across a dissected sedimentary landscape. Overall, the sequence is fining-upwards, with evidence that the rivers that deposited the Calivil Formation prograded over the Loxton-Parilla Sands. Channel fill materials comprise gravels and sands, and local fine-grained units represent abandoned channel fills and local floodplain sediments. Integration of textural and hydraulic testing data has revealed there are five hydraulic classes (coarse to very coarse sand and gravel, medium sand, fine sand, muddy sand, and mud) within the Calivil Formation. At a local scale (10s to 100s of metres), there is considerable lithological heterogeneity, however at a regional scale (km), sands and gravels are widely distributed with particularly good aquifers developed in palaeochannels and at the confluence of palaeo-river systems.
   - The Calivil Formation aquifer varies significantly in thickness (0-70 m) over the project area. This variability results from (1) in-filling of broad (structurally-controlled) palaeovalleys in an undulating palaeo-landscape, with relief of up to 40 m from valley bottoms to hill tops; and (2) post-depositional tectonic effects that include movement on discrete faults, as well as warping and tilting of the landscape. The effect of tectonic inversion along reactivated faults has been erosion and local thinning of the Calivil Formation sequence prior to deposition of the overlying lacustrine Blanchetown Clay. In some narrow fault zones, the Calivil Formation appears to have been completely eroded. Tectonic activity after deposition of the Blanchetown Clay has resulted in further warping, tilting and faulting of the Calivil Formation.
   - The lower bounding surface of the formation is marked by an erosional contact with Renmark Group sediments. There is a 10m year hiatus between deposition of the Renmark Group and the Calivil Formation. Beneath this erosional surface, the Renmark Group sediments show evidence of significant weathering, particularly where preserved on local palaeo-highs. The upper surface of the Calivil Formation is irregular, with up to 16 m of relief evident. This relief is due to the channel and bar topography in the upper Calivil Formation at the time of

inundation by Lake Bungunnia (and commencement of Blanchetown Clay deposition) combined with post Calivil Formation tectonic warping and faulting.

- The semi-confined to confined Calivil Formation aquifer is the principal target aquifer for MAR and groundwater extraction in the study area. The level of confinement of the aquifer is defined by the presence, thickness, lithology and structural integrity of the overlying Blanchetown Clay. In places, a fine-grained upper part of the Calivil Formation sequence can also act as an upper confining layer for the Calivil Formation aquifer proper. In localised areas away from the groundwater mounding associated with the modern drainage, the standing water level may locally lie beneath the upper confining aquitard, and in these areas, the Calivil Formation aquifer becomes unconfined.
- The Loxton-Parilla Sands were deposited as marginal marine and beach-barrier deposits during a major Miocene-Pliocene marine regression. In this study, drilling has demonstrated the presence of Loxton-Parilla sands in the south of the area, with stranded dunes also present about 30 km southeast of Lake Menindee. Drilling has also demonstrated that the Calivil Formation locally overlies the Loxton-Parilla Sands. In the south of the area, the latter form a good aquifer approximately 40 m thick.

3. Blanchetown Clay

   - This study has mapped the near-ubiquitous presence of relatively thin (~10 m) Blanchetown Clay deposited in palaeo-megalake Bungunnia throughout the project area. An integrated mapping approach has revealed variations in Blanchetown Clay aquitard extent and thickness, with a complex sub-surface distribution observed. Variations in the elevation of the top of the Blanchetown Clay (20-80 m AHD) are attributed mainly to tectonic activity.
   - The aquitard properties of the Blanchetown Clay are demonstrated by hydrograph responses in overlying and underlying aquifers, by wetting profiles observed in drill core, moisture data obtained from cores, nuclear magnetic resonance (NMR) and gamma logging, laboratory permeameter measurements on cores, and hydrogeochemical data. The study has also confirmed that the aquitard forms a major barrier to recharge and discharge.
   - Recharge and inter-aquifer leakage to the underlying Pliocene aquifers is localised where the Blanchetown Clay is either absent (through erosion by the Darling River system, non-deposition, or facies change to fluvial sand), and/or where fault offsets juxtapose the Menindee and Coonambidgal Formation unconfined aquifers with the Pliocene aquifers. This has resulted in previously unrecognised resources of fresh to slightly brackish water in the underlying semi-confined aquifer. Where present, the Blanchetown Clay could form an effective confining aquitard for MAR schemes.

4. Quaternary fluvial units and geomorphology, Lower Darling Valley.

   - The Lower Darling Valley is a laterally confined valley, which widens southwards into the Murray Geological Basin from a constriction at Wilcannia
   - The surficial Quaternary fluvial (river-deposited) sediments of the valley form a complex group of units which vary in their distribution, character and geomorphic expression through the BHMAR project area. Two new units, the Willotia beds and the Menindee Formation have been designated for the older fluvial units, while the previously defined Coonambidgal Formation is retained for the youngest unit.
   - All three fluvial units were deposited by active meandering lateral-migration phases apparently separated by phases of incision or channel stability, as occurs at present.
   - Over time, continued mud deposition on floodplains buried and obscured scroll-plain morphology, and soil formation and precipitation of secondary minerals such as carbonate altered the sediment character and reduced the effectiveness of the surficial aquifers.
   - The location of the active river tract has changed through time, almost certainly controlled by neotectonic structural movements.

5. Willotia beds.
    - The new term ‘Willotia beds’ is here used for a suite of river to lake sediments that are not sufficiently well known to give them full formation status. They overlie the Blanchetown Clay at higher elevations bounding the Darling Floodplain.
    - The stratigraphy and sedimentology of the unit (from project cores and cliff exposures) is similar to other surficial fluvial units and is typically 10-20 m in thickness with basal fine to coarse sands and an upper fine-grained overbank muddy facies.
    - The Willotia beds are virtually always overlain by aeolian sediments, and occur outside the Darling floodplain margins and underlie large areas of aeolian sediment within the floodplain.
    - The heavily modified overbank muds form an effective vertical infiltration barrier and precipitation of secondary minerals in the lower sand probably reduces groundwater movement.
6. Menindee Formation. The newly defined Menindee Formation replaces the former use of Shepparton Formation in the Lower Darling Valley.
    - Morphologically the Menindee Formation floodplain is highly variable and ranges from upper rarely flooded floodplain with thin patches of aeolian (wind-deposited) cover to lower floodplain with channels scoured by floods. The average thickness is about 14 m with basal fine to coarse sands (6.5 m average thickness) overlain by overbank muds (7.7 m average thickness).
    - Lateral-migration phases were active at 85 thousand years ago (ka) and >150 ka and many more phases almost certainly occurred, but have not yet been dated.
    - The overbank mud unit is widespread and is part of the near-surface aquitard, forming an effective barrier to vertical infiltration. The basal sands represent a shallow unconfined aquifer in the river corridor.
    - Secondary mineralisation in the sands, especially of carbonate, probably becomes better developed with age and reduces aquifer transmissivity. In particular, banks of the Darling River cut into Menindee Formation lower sands are often impregnated with secondary carbonate which is very likely to impede lateral infiltration.
7. Coonambidgal Formation
    - The Coonambidgal Formation consists of inactive scroll-plain tracts (river deposits with preserved traces of meander migration), formed by episodic lateral-migration phases that are incised into the Menindee Formation floodplain.
    - Four cross-cutting scroll-plain phases have been dated at 2-6 ka, 17-22 ka and 25-30 ka and 45-50 ka are designated Coonambidgal Formation Phases 1-4. Stratigraphically and sedimentologically, Coonambidgal Formation sediments are essentially identical to the Menindee Formation with an average thickness of 14 m and basal fine to coarse sands (7.3 m average thickness) overlain by overbank muds (7.5 m average thickness).
    - Morphologically, the scroll-plain meander dimensions vary, apparently due to variations in river discharge while the lateral migration phases were active. Preservation of scroll morphology becomes less distinct with increasing age.
    - As for the Menindee Formation, the overbank mud unit is widespread and is part of the near-surface aquitard, forming an effective barrier to vertical infiltration. However, secondary mineralisation in the lower sands is much less developed than the Menindee Formation and provides minimal impediment to lateral infiltration. As the Coonambidgal Formation is the youngest Quaternary fluvial unit, it is the shallow unconfined aquifer with the closest hydraulic connection with the Darling River and its anabranch channels.
8. Tectonic Activity
    - Evidence for significant Neogene-to-Present tectonic activity is evident in AEM and LiDAR data, and validated by drilling and surface mapping. The AEM data in particular reveals that the unconsolidated alluvial sediments in the study area are significantly affected by tectonic

activity, with evidence of widespread faulting, warping and regional tilting of sub-surface stratigraphy due to deformation within regional shear zones, and due to basin subsidence or margin uplift. For example, the Blanchetown Clay shows considerable modification, with up to 60 m difference in elevation largely as a result of post-depositional faulting, tilting and warping of these lacustrine deposits. Vertical fault offsets of up to 20 m are mapped at the Blanchetown Clay horizon in the AEM data.

- Faults mapped in the AEM and LiDAR datasets are coincident with faults and lineaments mapped independently in the geological basement using other geophysical datasets including regional gravity, airborne magnetics, and seismic datasets in the basement. Major faults appear to be linked to long-lived basement faults that control the location of underlying Devonian Basins.
- Reactivation of these basement faults appears to be a factor in controlling deposition of the Pliocene aquifers, the overlying Blanchetown Clay, and Pleistocene aquifers. There is evidence for tectonic inversion on several of these structures. Examples include horst structures during or post-Calivil Formation and Blanchetown Clay deposition becoming graben structures in the Pleistocene.
- Most faults do not appear to offset near-surface Pleistocene mud aquitards, with only a few more recent fault scarps evident in LiDAR data. However, the Talyawalka Creek and Darling River follow long-lived structural corridors. There is also evidence of recent tilting, with crossing shorelines observed at Lake Mindona, and a few up-warped areas observed to be associated with local landscape highs, suggesting relatively recent movement.
- Vertical offsets of the upper confining aquitard (Blanchetown Clay) up to ~20 m have been mapped, although vertical displacements are generally less than 5 m. No faults were intersected during drilling, however there is substantial indirect evidence of a link between aquifer recharge and fault distribution, with inter-aquifer leakage across faulted stratigraphic offsets postulated as a principal recharge (inter-aquifer leakage) mechanism in many of the key groundwater resource targets. In particular, fast response rates (days) observed in bore hydrographs lateral to the river are taken as evidence of hydraulic connection via discrete structures, or through inter-aquifer leakage where faults have juxtaposed the Coonambidgal Formation and Menindee Formations and the Calivil Formation.
- Overall, tectonics appears to have played a significant role in development of the sedimentary system since the Pliocene, and strongly influence groundwater flow and recharge dynamics.

13.3 SUMMARY OF GEOLOGY AND LANDSCAPE EVOLUTION

The geomorphic/geological history for the Menindee area as determined by this project can be summarised as:

1. Complex history of pre-Palaeozoic deformation and metamorphism in Proterozic basement rocks. Several E-W shear zones mapped in the Darling Geological Basin basement are reactivated in Neogene times (e.g. Talyawalka Fault System);
2. Formation of Palaeozoic-Mesozoic Basins (e.g. Menindee, Wentworth and Blantyre Troughs) as part of the Darling Geological Basin. Deposition of a thick (several km) sequence of clastic sediments within extensional fault-bounded basins is interrupted episodically by structural inversion along these structures (e.g. in Carboniferous). Several of these structures appear to have been reactivated in Neogene times;
3. Formation of the Murray Geological Basin, with deposition of Renmark Group clastic sediments by rivers flowing southward towards a shallow sea to the south of the BHMAR project area in the Palaeocene to Miocene;
4. Depositional hiatus in the Miocene with weathering and local erosion of the Renmark Group sediments;
5. In the south of the study area, deposition of marginal marine sands and shoreline dunes (Loxton-Parilla Sands) in shallow water at the northern margin of a marine basin. Pene-contemporaneous with this was deposition of fluvial Calivil Formation sediments by the palaeo-Darling River and

its tributaries in the Pliocene. The Calivil Formation sediments locally overlie the Loxton-Parilla Sands in the study area;

6. Damming of the palaeo-Murray River and its tributaries, including the palaeo-Darling River, with Blanchetown Clay deposition in palaeo-Lake Bungunnia in the Late Pliocene to Pleistocene;
7. Pliocene regression, and the drying up of Lake Bungunnia, due to a combination of lowering of the sill of the dam that initiated the lake (McLaren *et al*., 2012) and the onset of a dryer climate;
8. Continued fluvial and local lacustrine deposition, with sediment derived from the northwest (Broken Hill area) and the north (palaeo-Darling River, which passed through a gap in basement hills at Wilcannia at the edge of the Murray Basin). These Willotia bed sediments may be also partly a time equivalent of the upper part of the Blanchetown Clay deposited further south in Lake Bungunnia;
9. Incision of a trench into the Blanchetown Clay to form the modern course of the Murray River (Murray Gorge). This trench propagated headwards up the Darling Valley by nickpoint retreat, incising the Willotia beds but generally not the Blanchetown Clay in the Menindee area;
10. Deposition of fluvial sediments of the Menindee Formation and subsequently Coonambidgal Formation within the eroded trench by the Darling River and its distributaries;
11. Concurrent with 8, 9 and 10 formation of the lake basins around Menindee, with local wave erosion and shoreline deposition; and
12. Concurrent with 8, 9 and 10, deposition and preservation of aeolian sand across much of the area, particularly where not flooded and reworked in the trunk river valley.
13. There are multiple lines of evidence to show that the area has been tectonically active in the Neogene-to-present day, as evidenced by a number of scarps, lineaments, and drainage alignments that are coincident with underlying faults. There is also evidence of neotectonics from some lake tilting in the south of the project area.

As the project area sits astride the Darling Fault Lineament, a continental-scale structural feature, it is perhaps not surprising that tectonic activity has played a major role in shaping the landscape in the project area. The Darling River Lineament itself may be a much younger structure than commonly thought.

Tectonics appears to have influenced the distribution of the major Pliocene and younger aquifers and aquitards. Although the data appear to show that tectonic activity has waned significantly since the Pleistocene, with only a few structures apparent in the modern landscape, tectonics still influence the location of the major drainage elements.

13.4 NEW HYDROGEOLOGICAL CONCEPTUAL MODEL

Figure C summarises the conceptual model showing the configuration of aquifers and aquitards within the sediments of the Lower Darling Floodplain. It also shows the recharge dynamics associated with leakage from the Darling River. The importance of river (and lake) leakage in recharging the shallow unconfined aquifers and Calivil Formation target aquifer is inferred from different lines of evidence, including:

- Interpolation of groundwater salinities based on a relationship between the AEM and pore fluid chemistry showed freshening near the river and also in particular leakage sites associated with the Menindee Lakes.
- Watertable contours interpreted for the shallow aquifer show significant mounding near the Darling River and the MLS. The interpreted groundwater levels for the underlying Calivil Formation aquifer have a broadly similar pattern suggesting the influence of river leakage. The dominant hydraulic gradient near the river is downwards, reflecting greater opportunity for river leakage (rather than groundwater discharge to the river).
- The majority of shallow groundwaters have a chemistry dominated by sodium, calcium, magnesium and bicarbonate, which is similar to the Darling River samples. In contrast, local rainfall samples are more enriched in calcium and potassium, suggesting that recharge from rainfall is not as important as

river (or lake) leakage. A mixing trend is evident between the surface waters and shallow groundwaters, and the more saline and evolved Calivil Formation and Renmark Group regional groundwaters.

- The stable isotopes of water (oxygen-18 and deuterium) in rainfall, river, lake and groundwater samples show that the Darling River recharges the unconfined and semi-confined near-surface aquifers. The fresh Calivil Formation groundwaters have a stable isotope signature similar to Darling River samples collected during high flows. This would support recharge into the Calivil Formation being linked to high-flow events, rather than continual river leakage. The tight clustering of the Calivil Formation stable isotope samples suggests that recharge is relatively rapid. The contrast in the isotopic signature of the fresh Calivil Formation groundwaters and that of the shallow groundwaters, suggests that recharge to the Calivil Formation occurs near-river, rather than via infiltration through the shallow aquifer in the floodplain.
- The fresh near-river shallow groundwater typically has a modern carbon signature, further supporting river leakage under current climatic conditions as being the dominant recharge process. There is a decrease in the proportion of modern carbon as the Calivil Formation groundwaters progressively become more saline and less influenced by modern recharge.
- Data from monitoring bores screened in the unconfined, Calivil Formation and upper Renmark Group aquifers show rises in groundwater levels associated with high flow events in the Darling River. Overbank flow is not necessary for such recharge to occur. The continuation of rising trends in the Calivil Formation monitoring bores after the flood peak recedes suggests that this is an actual recharge response rather than hydraulic loading. Simple Darcian vertical infiltration cannot explain the rapid response. Faulting and vertical structural offsets of formations near the river could result in pathways for such by-pass flow.

In summary, during low-flow conditions there is no recharge as a mud veneer and also mineral precipitates along the river bed and banks act as an effective seal. Under no-flow conditions, the deep holes in the river bed can be windows to the watertable and act as critical drought refuges for the aquatic ecosystem.

During high-flow conditions, the riverbanks and bed are scoured and the mud veneer seal is removed. This allows recharge to occur predominantly by lateral bank recharge through the sandy sequences in the shallow aquifer as well as bypass flow via faulted offsets. The high river stage level facilitates lateral and downward leakage. Overbank flow is not a pre-requisite for recharge but can provide other localised recharge pathways in the floodplain. Structural features and gaps in the Blanchetown Clay confining layer provide flow paths to the Calivil Formation aquifer. During flood recession, there may be some drain-back from bank storage in the unconfined aquifers encouraging carbonate precipitation at the riverbanks. The mud veneer is also redeposited with declining river stage and flow velocities. Over time, the system returns to relatively low-flow conditions with the channel mud veneer again constraining river leakage.

13.5 BROADER SCIENTIFIC FINDINGS

1. A new, multi-scale methodology was developed to estimate groundwater quality and storage volumes, and applied to the Pliocene aquifers. This methodology is a significant improvement on previous approaches that rely upon extrapolation from limited borehole data.
    - Salinity thresholds were estimated by comparing the downhole pore fluid data with the AEM response at a borehole scale. Bulk volumes for each water quality class in a target were then calculated using these thresholds on an AEM depth slice basis, which had been mapped into textural classes. An effective porosity range for each textural class was developed by integrating borehole nuclear magnetic resonance (NMR) data and laboratory porosity data (from Lexan-encapsulated core samples). These effective porosity ranges were used to convert the depth-slice bulk volume estimates to stored groundwater volumes.
    - Sensitivity analysis revealed that there are still significant uncertainties in volume estimates using this approach. There can be order-of-magnitude differences in the volume calculations depending on the AEM technology, inversions and constraints used. Significant variations were also found when different AEM conductivity thresholds were used to map groundwater salinity. Various estimates of effective porosity were used to represent the geological heterogeneity.

- Due to this uncertainty, the groundwater storage volumes should only be considered as indicative estimates. The estimates are still useful in a relative sense, as a tool to prioritise the groundwater targets and to scope the potential aquifer storage capacity for MAR options.

2. This study has demonstrated the importance of selecting the most appropriate AEM system and optimizing the AEM inversions for generating a wide range of customized interpretation products.
   - New inversion code (WANDA) has been developed for rapid inversion of the AEM data.
   - A lateral correlation procedure was developed to correlate AEM data strictly horizontally.
   - New Fiduciary (FID)-point borehole correlation procedures were developed to assess AEM inversions.
   - Bayesian inference via a reversible jump Markov Chain Monte Carlo (RJ-McMC) inversion for selected AEM data sets provided useful (quantitative) assessment of the final inversion models.
3. A new methodology, integrating fuzzy-k means (FCM) cluster analysis with conventional hydrochemical and hydrodynamic analysis provides invaluable new insights into groundwater processes.
4. Fundamental vertical accuracy (at 95% confidence level) of the LiDAR 5 m DEM dataset was found to be 0.52 m, due to inherent inaccuracies of the methodology, insufficient ground control points and cumulative errors including the ellipsoid-geoid transformations and resampling procedures. These vertical inaccuracies need to be factored in to flood modelling, and in utilisation of LiDAR datasets as an absolute height datum. Even considering this factor, flood inundation extent mapping of the central project area has a 93% compatibility with corresponding Landsat TM 5 imagery.
5. Critical to successful completion of the study was development of a trans-disciplinary research methodology. This approach enabled the team to recognise fundamental problems in discipline approaches, helped identify critical data gaps, and led to significant innovation across discipline boundaries. This research methodology was vital in the development of the hydrogeological conceptual model that underpinned MAR assessment.
6. It is our understanding that this is the first use of AEM for MAR identification and assessment. The project has developed trans-disciplinary methodologies and workflows that provide a template for future hydrogeological investigations and MAR assessments.

14. Recommendations

BHMAR Project Area Specific Science Recommendations

1. If an alternative water supply option for Broken Hill involving MAR or groundwater extraction is pursued at the Jimargil site, then it is recommended that the following steps be taken to characterise this site from a geological and hydrogeological perspective:
   i. Additional drilling, sampling and ground geophysics is required to validate the interpretation of aquifer properties and groundwater quality, particularly in the central part of the Jimargil potential borefield target area where existing data is limited. Understanding the heterogeneity of the hydrogeological system at the borefield scale is essential for optimising borefield design.
   ii. Long-term aquifer pump tests to (1) derive key aquifer hydraulic parameters for the target Calivil Formation, (2) assess leakage between the Calivil Formation aquifer and the overlying Quaternary aquifers, including the potential impact on the shallow watertable and (3) assess the potential for ingress of more saline or lower quality groundwater into the pumped aquifer, either laterally from within the Calivil Formation or vertically, particularly from the underlying upper Renmark Group.
   iii. Construction of a borefield scale GOCAD mesh model is required to integrate hydrostratigraphic mapping and geological faults in 3D. This is essential if full use is to be made of project datasets in numerical groundwater models. This is also essential for understanding recharge, interaquifer leakage and groundwater flow paths.
   iv. Ground geophysical (electrical) surveys are recommended to characterise potential pump test sites at high resolution.
   v. It is recommended that the AEM data be re-inverted to incorporate new drilling, ground and borehole geophysical data, to maximise the value of all existing project borehole data.
   vi. Geochemical and geophysical (resistivity) monitoring of the borefield site should be undertaken in conjunction with aquifer pump tests to map any spatial changes in groundwater salinity.
   vii. In the BHMAR study, recharge to the Pliocene aquifers is dominated by episodic leakage during high river flows and via structurally controlled disruptions to the regional overlying aquitards. This results in significant variations in recharge rates in both space and time, resulting in significant challenges in terms of extrapolating point-based recharge estimates. To address this spatial and temporal variability in recharge, it is recommended that a calibrated, transient numerical groundwater flow and solute transport model be constructed. This will also help optimise borefield design and assess potential negative impacts, regardless of the option selected at the Jimargil site.
   viii. If Aquifer Storage and Recovery (ASR) is further contemplated at this site, additional science investigative and modelling steps have been outlined in Lawrie *et al*. (2012c).
2. If any of the other regional MAR/groundwater resource targets are to be developed, then a similar program to that outlined above for the Jimargil site will be required to characterise the sites from a geological and hydrogeological perspective.
   i. Currently, very few of these regional targets are characterised using more than one borehole. If groundwater extraction is to be considered at these targets, a significant additional program of drilling, sampling and analysis would be required.
   ii. Establishing baseline groundwater-level monitoring is important, particularly in the context of understanding the aquifer response to episodic flood events.
   iii. Groundwater sampling is required to better define and understand potential water-quality issues.
   iv. Tracers or isotopes (such as radiocarbon) are required to help define the extent to which modern recharge is occurring in a target.
   v. Calibrated, transient numerical groundwater flow models would be required to determine the recharge, environmental impacts and acceptable groundwater extraction limits for the individual targets for all potential development options.
   vi. It is recommended that solute transport modelling is also incorporated, considering the possibility of saline ingress.
   vii. At present, only entry-level MAR assessments have been carried out on most of the regional targets. If MAR is to be considered at any of the regional sites, then a substantive program of

scientific investigations, similar to that undertaken in Phase 3 of the BHMAR study, would be required to address issues in the maximal and residual risk assessment process.

3. Structural analysis has revealed a complex history of Neogene-to-Present tectonics in the study area. Further analysis is required to:
   i. Systematically classify faults based on the amount of vertical displacement, with a particular emphasis on identifying those faults which completely offset the confining aquitards. This is required to assess the potential for recharge and inter-aquifer leakage.
   ii. Classify faults based on their relative age of movement. This could be accomplished based on their AEM and geomorphic (and LiDAR) expression, noting subsequent erosion history. Identifying faults that have a more recent neotectonic expression in the landscape will assist with understanding recharge processes and broader evaluation of seismic risk in the area.
   iii. Trenching and age dating of potential fault scarps is recommended to conclusively demonstrate that the lineaments observed in the LiDAR data have a tectonic origin. The data obtained would also provide invaluable information on regional tectonic models and earthquake risk.
4. It is recommended that further detailed studies be undertaken at an individual target scale to integrate hydrogeochemical, geomorphic, hydrostratigraphic and structural data to map recharge, inter-aquifer leakage and groundwater flow pathways at a target scale. This would best be accomplished in 3D, using an appropriate GOCAD mesh model which could then provide a basis for numerical groundwater models.
5. It is recommended that detailed geomorphic mapping be finalised across the entire BHMAR study area. More broadly, in areas where the trend in the floodplain dictates, it is recommended that the regional digital elevation model be levelled prior to geomorphic mapping. This will then facilitate the generation of both rapid and highly detailed geomorphic mapping of the floodplain using a semi-automated contouring tool. More detailed mapping will be particularly important in regional targets where MAR involving enhanced infiltration options may be considered.
6. Recommendations relating to hydrographic monitoring and analysis include:
   i. Continue to collect time-series groundwater-level and barometric data from the existing project monitoring network. The monitoring of the groundwater response to flood events of varying magnitude is required to better quantify recharge dynamics.
   ii. Trial the installation of additional logger technologies in the monitoring bores to collect time-series data of complimentary parameters (such as groundwater electrical conductivity or temperature).
7. Recommendations with respect to the use of tracers and age dating include:
   i. Trials should be conducted into alternative groundwater age-dating techniques (such as sulfur hexafluoride SF_6) to test and extend the interpretations based on the use of carbon-14 and chlorofluorocarbon analyses.
   ii. Using chlorofluorocarbon as a tracer tool, analysis of CFC-113 is recommended in addition to the conventional analysis of CFC-11 and CFC-12. This would improve evaluation of groundwater mixing fractions between the fresh river leakage and the saline regional groundwaters.
   iii. Investigations should be carried out into the use of heat as a tracer for interactions between the river (or lakes) and the shallow unconfined aquifer. This can include the installation of infrastructure to monitor temperature in the river and also within the near-river sediments.

Broader Regional Scientific Recommendations

1. The revised understanding of the age, stratigraphy, mode of deposition and tectonic history of the Lower Darling Valley floodplain sediments has broader implications for the hydrogeology of the Western Murray Porous Rock Aquifer and Lower Darling Alluvium Groundwater Management Units (GMUs). It is recommended that further geological and hydrogeological studies be undertaken to up-date the hydrogeological conceptual models underpinning groundwater management in these two GMUs.
2. Based on the conceptual understanding of key groundwater processes from this study, it is recommended that similar scientific investigations be carried out in the Basin (and nationally), to identify other river reaches where the hydrogeological conceptual models may require up-dating based

on the new knowledge generated in the BHMAR study. This new knowledge and the datasets generated could be used to assess the potential for additional MAR options and/or groundwater resources across the Basin (and nationally). Studies should include the Upper Darling River between Bourke and Wilcannia.

3. Identification of significant Neogene tectonics (and neotectonics) in the BHMAR study area most likely has broader regional (and national) implications. It is recommended that regional studies utilising similar mapping methodologies be used to assess the extent and significant of tectonics in the Murray-Darling Basin (and Australia more generally).
    i. Reconnaissance mapping of the area covering the Western Murray Porous Rock Aquifer, utilising regional gravity, airborne magnetics and high resolution DEMs, has identified regionally significant lineaments that may play an important role in recharge and inter-aquifer leakage processes. However, further work is recommended to characterise these lineaments and assess their significance, if any, for groundwater processes.
    ii. Similar studies are required in the Basin and more broadly, prioritised to areas where connectivity between surface water and key aquifers, or where inter-aquifer leakage, has been identified as a key factor in water management.
    iii. It is also recommended that future hydrogeological and MAR studies should consider tectonic studies as an integral part of future investigations and assessments.
4. The project provides the opportunity to develop a Darling Floodplain strategic science site. The BHMAR project area is the most data-rich site in Australia from a hydrology-hydrogeology-geomorphology-neotectonics perspective. A groundwater observation network (40 bores) has been established, and sites established for the trialling of new geophysical and remote sensing technologies.
    i. It is recommended this site be recognised as a strategic science site for the trialling of a range of new geophysical, remote sensing technologies, and science methods.
    ii. More specifically, it is recommended that a number of monitoring sites (e.g. tiltmeters, microseismic monitoring stations, GNSS reference station) be established at strategic locations within this area to provide baseline stations for future technology and science trials.
    iii. It is also recommended that InSAR techniques be trialled in the BHMAR study area to assess the degree of floodplain breathing as a consequence of episodic flooding.
    iv. It is also recommended that inSAR techniques be trialled in the BHMAR study area to assess the capability of InSAR techniques for mapping watertable fluctuations in unconfined aquifers under Australian landscape conditions.

Broader Scientific Recommendations

1. The BHMAR study has demonstrated that a trans-disciplinary systems science approach, utilising modern investigative mapping, characterisation and assessment technologies, can provide substantive new insights into the hydrogeology of Australia's unique near-surface landscapes. Similar methodologies and technologies are recommended for future groundwater investigations in Australia, particularly in shallow sedimentary systems. These methods provide the integrative framework required to address the many inter-related issues encountered in assessing MAR options and groundwater extraction, particularly in hydrogeologically and hydrogeochemically complex areas.
2. Future assessments and models of surface-groundwater interaction in similar environments in the Murray-Darling Basin need to take into account possible linkages between high-volume floods and episodic recharge events. Physically based hydraulic modelling could also be undertaken to better understand the relationship between river-flow rates, groundwater-infiltration rates, sediment scouring and deposition. Based on the conceptual understanding of key groundwater processes from this study, it is recommended that a broader assessment be carried out in the Basin to identify other river reaches where additional groundwater resources may exist, and/or MAR options may provide enhanced drought security and regional-development opportunities.
3. Future assessments of groundwater quality for ASR and/or a groundwater extraction schemes in Australia need to pay particular attention to hydrogeochemical processes relating to groundwater salinity, clay dispersion and acidification, in addition to redox-sensitive trace metal processes. The hydrological (and recharging) conditions can be highly variable under the alternating drought and flood periods which are so characteristic of the hydrology in Australia. These changing conditions can

in turn affect water quality by saturation of oxidised/reduced materials via changes in aquifer watertable height and also by inter-aquifer mixing of groundwater with variable water quality.

4. Studies of Neogene-to-Recent intraplate deformation are recommended nationally to identify and characterise key structures that might play an important role in recharge and inter-aquifer leakage processes, and to refine models of present-day and neotectonic palaeostress trends and partitioning.
5. A number of recommendations are made about the use of AEM technology for the high-resolution mapping of near-surface hydrogeological systems and the identification and assessment of MAR targets:
    i. AEM data acquisition should be considered as part of any data-acquisition strategy in data-poor areas. These data can map large near-surface areas rapidly, maximising the likelihood of identifying multiple MAR targets.
    ii. The mapping and assessment of MAR targets often requires high-resolution geophysical data to resolve the complexities of the hydrogeological system. Traditional derivative analysis approaches for AEM technology selection are inadequate for assessing the ability of candidate systems to map MAR targets. A comparative analysis of candidate systems, consisting of both theoretical considerations and field studies including test lines over representative hydrostratigraphic targets is recommended.
    iii. Optimisation of AEM data for MAR investigations should also involve careful consideration of AEM data-acquisition strategy, AEM system calibration, and validation and inversion methods.
    iv. It is recommended that a phased approach to AEM data acquisition be trialled to decrease the costs of acquiring AEM data for MAR target mapping. Depending on the nature of the target and the size of the area of investigation, initial reconnaissance mapping of MAR targets could utilise wide line-spaced data to identify potential MAR targets in Australia's major river basins.
        a. As shown in this study, one risk of using this phased approach is that wide line-spacing data may identify targets that on closer inspection may not pass assessments. To minimise these risks, a swath-mapping approach, with 3-5 closely-spaced (e.g. 200 m) flight lines separated by wider line spaced data (e.g. 1-2 km), could be trialled to give more opportunity for key elements of the hydrogeological system to be mapped and assessed.
        b. It should be noted however, that for logistic reasons, it is not always possible to acquire data in phased approaches, however the potential benefits of using such an approach for MAR mapping and assessment should be investigated in future investigations.
        c. The area surveyed should be sufficient to allow for assessment of multiple targets, given the likelihood of failure of some targets on hydrogeological, economic, environmental or social factors.
        d. Depending on the hydrogeological system, it is likely that high-density line spacing and/or follow up high-resolution ground geophysics would be required to provide sufficient data to resolve the complexities of many Australian hydrogeological systems.
6. The key learnings and recommendations from applying various methods to estimate recharge are outlined below.
    i. There are many different methods for estimating groundwater recharge. Some of these provide estimates of potential recharge or deep drainage, which is the flux below the root zone that has the potential to reach the watertable over varying periods of time. Other methods focus on groundwater responses where recharge accessions have actually reached the watertable. Many of these methods apply only to the unconfined aquifer and cannot be extrapolated to estimating groundwater recharge to confined or semi-confined aquifers. An understanding of the geometry and structure of the hydrostratigraphy, including any overlying aquitards is recommended to ensure that the recharge-estimation method is appropriate.
    ii. It is important to understand the assumptions inherent in any recharge-estimation method and the implications of these on method suitability. This is important to ensure that the recharge method is appropriate to the conceptual model developed for the groundwater system. For example, the groundwater chloride mass-balance method assumes that the chloride in groundwater originates from rainfall, with no other subsurface chloride sources. It also assumes that surface-water leakage to the aquifer is absent. With river/lake leakage interpreted as the dominant recharge mechanism, these assumptions are not met for the BHMAR study area so the derived potential

recharge estimates are not valid. A verification of the underlying assumptions of the recharge method against the conceptual model is recommended in future investigations.

7. A significant number of additional recommendations that follow from the specific science methodologies used in the BHMAR project are made in Lawrie *et al*. (2012a). The reader is referred to the latter report for the details of specific science methodology recommendations.

15. References

Adkins, C.B. 2009. Evidence for compartmentalization of aquifer systems: solute and isotope geochemistry of groundwaters in the middle San Pedro basin, Arizona. Masters Thesis submitted to the Faculty of the Department of Geosciences, University of Arizona (unpublished).

ADWG. 2011. Australian Drinking Water Guidelines 2011. National Water Quality Management Strategy. National Health and Medical Research Council – Natural Resource Management Ministerial Council. http://www.nhmrc.gov.au/guidelines/publications/eh52

Akeroyd, M.D., Tyerman, S.D., Walker, G.R. & Jolly, I.D. 1998. Impact of flooding on the water use of semi-arid riparian eucalypts. Journal of Hydrology 206, 104-117.

Alcala, F.J. & Custodio, E. 2008. Using the Cl/Br ratio as a tracer to identify the origin of salinity in aquifers in Spain and Portugal. Journal of Hydrology 359, 189-207

Alexander, J., Fielding, C.R. & Jenkins, G. 1999. Plant-material deposition in the tropical Burdekin River, Australia: implications for ancient fluvial sediments. Palaeogeography, Palaeoclimatology, Palaeoecology 153, 105-125.

An, Z., Bowler, J.M., Opdyke, N.D., Macumber, P.G. & Firman, J. B. 1986. Palaeomagnetic stratigraphy of Lake Bungunnia: Plio- Pleistocene precursor of aridity in the Murray Basin, southeastern Australia. Palaeogeography, Palaeoclimatology, Palaeoecology 54, 219–239.

Andersen, M.S. & Acworth, R.I. 2009. Stream-aquifer interactions in the Maules Creek catchment, Namoi Valley, New South Wales, Australia. Hydrogeology Journal 17, 8, 2005-2021.

Anderson, M.P. 2005. Heat as a ground water tracer. Groundwater 43, 951-968.

Anderson, M.P., Aiken, J.S., Webb, E.K. & Mickelson, D.M. 1999. Sedimentology and hydrogeology of two braided stream deposits. Sedimentary Geology 129, 187–199

Appelo, C.A.J. & Postma, D. 2005. Geochemistry, groundwater and pollution. 2nd Edition. AA Balkema, Netherlands.

Apps, H.E., Clarke, J.D.A., Gow, L. & Halas, L. 2012a. BHMAR Project Appendix 8: Recharge models and data. Geoscience Australia Record 2012/17. Geocat 73824.

Apps, H.E. & Gibson, D. 2012. BHMAR Project Appendix 12: Drilling construction, location and remediation data and reports. Geoscience Australia Record 2012/17. Geocat 73824.

Apps, H.E., Halas, L., Knox, K., Cook, B., Beaudreau, D., Tan, K.P., Gibson, D., Smith, M., Lawrie, K.C., Brodie, R.S., Brodie, R.C., Abraham, J., Christensen, N.B., Gow, L., Magee, J.W. & Clarke, J.D.A. 2012b. BHMAR Project Appendix 5: AEM-based interpretation products: maps and cross-sections. Geoscience Australia Record 2012/17. Geocat 73824.

Apps, H.E. & Lawrie, K.C. 2012. BHMAR Project Appendix 11: CSIRO MAR reports. Geoscience Australia Record 2012/17. Geocat 73824.

Apps, H.E., Lawrie, K.C., Christensen, N.B., Brodie, R.C., Smith, M. & Knox, K. 2012c. BHMAR Project Appendix 4: AEM data: acquisition reports, inversion and calibration, and basic conductivity map and cross-section products. Geoscience Australia Record 2012/17. Geocat 73824.

Apps, H.E., Lawrie, K.C., Halas, L., Atkinson, I., Clarke, J.D.A., Wintle, C. & Wilson, O. 2012d. BHMAR Project Appendix 10: Ground and in-river geophysics and supporting data. Geoscience Australia Record 2012/17. Geocat 73824.

Apps, H.E., Magee, J.W. & Clarke, J.D.A. 2012e. BHMAR Project Appendix 7: Age dating (contractor reports). Geoscience Australia Record 2012/17. Geocat 73824.

Apps, H.E., Schoning, G., Tan, K.P., Clarke, J.D.A., Magee, J.W., Gibson, D., Halas, L., Gow, L. & Davies, A. 2012f. BHMAR Project Appendix 3: Borehole geophysical and geological data. Geoscience Australia Record 2012/17. Geocat 73824.

Apps, H.E., Tan, K.P. & Brodie, R.S. 2012g. BHMAR Project Appendix 13. Borehole hydraulic data (contractor reports). Geoscience Australia Record 2012/17. Geocat 73824.

Auld, T.D. & Denham, A.J. 2001. Flora conservation issues at Kinchega National Park, western NSW. Cunninghamia 7, 27-41.

Aydin, A.A. & Nur, A. 1982. Evolution of pull-apart basins and their scale independence. Tectonics, v. 1, p. 11-21.

Aydin, A. A., and Nur, A. 1985. The types and roles of stepovers in strikeslip tectonics. In: Biddle, K. T. & Christie-Blick, N. (eds). Strike-slip deformation, basin formation, and sedimentation: Society of Economic Paleontologists and Mineralogists Special Publication 37, p. 35–45.1

Bacon, P.E., Stone, C., Binns, D.L., Leslie, D.J. & Edwards, D.W. 1993. Relationships between water availability and *Eucalyptus camaldulensis* growth in a riparian forest. Journal of Hydrology 150, 541-561.

Balme, J. & Hope, J. 1990. Radiocarbon dates from midden sites in the Lower Darling River area of western New South Wales. Archaeology in Oceania 25, 85-101.

Banerjee, D., Page, K. & Lepper, K. 2002. Optical dating of palaeochannel deposits in the Riverine Plain, southeastern Australia: testing the reliability of existing luminescence dates. Radiation Protection Dosimetry 101, 327–332.

Barlow, P.M., DeSimone, L.A. & Moench, A.F. 2000. Aquifer response to stream-stage and recharge variations. II. Convolution method and applications. Journal of Hydrology 230, 211-229.

Barma, D. 2010. Hydrological assessment of water saving strategies for the Menindee Scheme and Upper Darling Basin. Darling River Water Savings Project – Final Report Part B, Barma Water Resources, Sydney, February.

Barnett, S., 1991. Renmark Hydrogeological Map (1:250 000 scale). Murray Basin Hydrogeological Map Series. Canberra, Australian Geological Survey Organisation.

Barron, O.V., Crosbie, R.S., Charles, S.P., Dawes, W.R., Ali, A., Evans, W.R., Cresswell, R., Pollock, D., Hodgson, G., Currie, D., Mpelasoka, F., Pickett, T., Aryal, S., Donn, M. & Wurcker, B. 2011. Climate change impact on groundwater resources in Australia. In: Waterlines Report. Canberra, National Water Commission.

Barrows, T.T., Stone, J.O., Fifield, L.K. & Cresswell, R.G. 2001. Late Pleistocene glaciation of the Kosciuszko Massif, Snowy Mountains, Australia. Quaternary Research 55, 179-189.

Barrows, T.T., Stone, J.O. & Fifield, L.K. 2004. Exposure ages for Pleistocene periglacial deposits in Australia. Quaternary Science Reviews 23, 697-708.

Baskaran, S., Brodie, R.S., Ransley, R. & Baker, P. 2009. Time-series measurements of stream and sediment temperature for understanding river-groundwater interactions: Border Rivers and Lower Richmond catchments, Australia. Australian Journal of Earth Sciences 56, 21-30.

Bastiaanssen, W.G.M., Menenti, M., Feddes, R.A. & Holtslag, A.A.M. 1998. A remote sensing surface energy balance algorithm for land (SEBAL) - 1. Formulation. Journal of Hydrology 212-213, 198-212.

Bedrosian, P.A., Densmore-Judy, J., Martin, P., Burgess, M., Langenheim, V. & Jachens, R. 2012. Faulting and groundwater in arid environments: Airborne electromagnetics in support of framework hydrology in the northern Mojave Desert, southern California. 22nd ASEG Conference, Brisbane, Australia. (Ext. Abs.).

Bertin, C. & Bourg, C.M. 1994. Radon-222 and chloride as natural tracers of the infiltration of river water into an alluvial aquifer in which there is significant river/groundwater mixing. Environmental Science and Technology 28, 794-798.

Bethke, C.M. & Johnson, T.M. 2008. Groundwater age and groundwater age dating. Annual Review of Earth and Planetary Sciences 36, 121-152.

Birch, W.D. (ed.) 2003. Geology of Victoria. Geological Society of Australia Special Publication 23. Geological Society of Australia (Victoria Division), 842 pp.

Bird, M.I., Ayliffe, L.K., Fifield, L.K., Cresswell, R., Turney, C.S.M., Barrows, T.T. & David, B. 1999. Radiocarbon dating of 'old' charcoal using a wet oxidation-stepped combustion procedure. Radiocarbon 41, 127-40.

Bird, M.I., Turney, C.S.M., Fifield, L.K., Jones, R., Ayliffe, L.K., Palmer, A., Cresswell, R.G. & Robertson, S. 2002. Radiocarbon analysis of the early archaeological site of Nauwalibila I, Arnhem Land, Australia: implications for sample suitability and stratigraphic integrity. Quaternary Science Reviews 21, 1061-1075.

Bish, S. & Salotti, D., 1996. Review of Groundwater Flow Around Menindee Lakes Storages - Lake Menindee to Lake Cawndilla. NSW Department of Land and Water Conservation.

Blevin, J., Pryer, L., Henley, P. & Cathro, D. 2007. Darling Basin reservoir prediction study and GIS. Project Code MR 706. Confidential report to NSW-DPI. Eraring Energy, Macquarie Generation & Delta Electricity by FROG Tech. Pty. Ltd. (Unpublished.)

Bourke, M.C. 1994. Cyclical construction and destruction of flood dominated floodplains in semiarid central Australia. In: Olive, L.J., Loughlan, R.J. & Kesby, J.A. (eds) Variability in stream erosion and sediment transport. International Association of Hydrological Sciences, Wallingford, 113-123.
Bourke, M.C. & Pickup, G. 1999. Fluvial form variability in arid central Australia, In: Miller, A. & Gupta, A. (eds) Varieties of fluvial form. Wiley, 249-271.
Bouwer, H. 2002. Artificial recharge of groundwater: hydrogeology and engineering. Hydrogeology Journal 10, 121-142.
Bowler, J.M. 1973. Clay dunes: Their occurrence, formation and environmental significance. Earth-Science Reviews 9, 315–338.
Bowler, J.M. 1978. Quaternary climate and tectonics in the evolution of the Riverine Plain, south-eastern Australia. In: Davies, J.L. & Williams, M.A.J. (eds) Landform evolution in Australasia, 70–111. Australian National University Press, Canberra.
Bowler, J.M. 1980. Quaternary chronology and palaeohydrology in the evolution of Mallee landscapes. In: Storrier, R.R. & Stannard, M.E. (eds) Aeolian landscapes in the semi-arid zone of south eastern Australia, 17-36. Australian Society of Soil Science, Riverina Branch.
Bowler, J.M. 1981. Australian salt lakes: a palaeohydrologic approach. Hydrobiologia.81-82, 431-444;
Bowler, J.M. 1983. Lunettes as indices of environmental change: a review of Australian evidence. Proceedings of the Royal Society of Victoria 95, 147-168.
Bowler, J.M. 1986. Spatial variability and hydrologic evolution of Australian lake basins: analogues for Pleistocene hydrologic change and evaporite formation. Palaeogeography, Palaeoclimatology, Palaeoecology 54, 1-4, 21-41.
Bowler, J.M. 1998. Willandra Lakes revisited: environmental framework for human occupation. Archaeology in Oceania 33, 156-168.
Bowler, J.M. & Magee, J.W. 1978. Geomorphology of the Mallee Region in semi-arid northern Victoria and western New South Wales. Proceedings of the Royal Society of Victoria 90, 5–21.
Bowler, J.M., Duller, G.A.T., Perret, N., Prescott, J. & Wyrwoll, K.H. 1998. Hydrologic changes in monsoonal climates of the last glacial cycle: Stratigraphy and luminescence dating of Lake Woods, N.T., Australia. Palaeoclimates 3, 179–207.
Bowler, J.M., Huang, Q., Chen, K., Head, J. & Yuan, B. 1986. Radiocarbon dating of playa lake hydrological changes; examples from north-western China and central Australia. Palaeogeography, Palaeoclimatology, Palaeoecology 54, 241-260.
Bowler, J. M., Gillespie, R., Johnston, H. & Bolijkovac, K. 2012. Wind v water: Glacial maximum records from the Willandra Lakes. In: Haberle, S.G. & David, B. (eds) Peopled landscapes: Archaeological and biogeographic approaches to landscapes. Terra Australis 34, ANU E Press The Australian National University, Canberra, Australia, 271-296.
Bowler, J.M., Johnston, H., Olley, J.M., Prescott, J.R., Roberts, R.G., Shawcross, W. & Spooner, N.A. 2003. New ages for human occupation and climatic change at Lake Mungo, Australia. Nature 421, 837–840.
Bowler, J.M., Kotsonis, A. &. Lawrence, C.A. 2006. Environmental evolution of the Mallee Region, western Murray Basin. Proceedings of the Royal Society of Victoria 118, 161-210.
Bowler, J.M., Stockton, E. & Walker, M.J. 1978. Quaternary stratigraphy of the Darling River near Tilpa, NSW. Proceedings of the Royal Society of Victoria 90, 79–87.
Bowler, J.M., Wyrwoll, K.H. & Lu, Y. 2001. Variations of the northwest Australian monsoon over the last 300,000 years: The paleohydrological record of the Gregory (Mulan) Lakes System. Quaternary International 83–85, 63–80.
Bowman, D. & Yeates, D. 2006. A remarkable moment in Australian biogeography. New Phytologist 170, 2, 208–212.
Bridge, J.S. & Tye, R.S. 2000. Interpreting the dimensions of ancient fluvial channel bars, channels, and channel belts from wireline-logs and cores. AAPG Bulletin 84, 8, 1205–1228.
Briggs, S.K. & Maher, M.T. 1983. Litter fall and leaf decomposition in a river red gum (*Eucalyptus camaldulensis*) swamp. Australian Journal of Botany 31, 307-316.
Briggs, S.V. & Townsend, G. 1993. Restoration and management of Nearie Lake. National Parks and Wildlife Service.
Brodie, R.S. 1994. MENINDEE Hydrogeological Map (1:250 000 scale). Murray Basin Hydrogeological Map Series. Australian Geological Survey Organisation, Canberra.
Brodie, R.S. 1998. The Lower Darling regional steady state groundwater flow model. AGSO Record 1998/19. Australian Geological Survey Organisation, Canberra.

Brown, C. M., Jackson, K. S., Lockwood, K. L. & Passmore, V. L., 1982. Source Rock Potential and Hydrocarbon Prospectivity of the Darling Basin, NSW. BMR Journal of Australian Geology and Geophysics, 7, 23-33

Brown, C.M. 1989. Structural and stratigraphic framework of groundwater occurrence and surface discharge in the Murray Basin, southeastern Australia. BMR Journal of Australian Geology and Geophysics 11, 127-146.

Brown, C.M. & Radke, B.M. 1989. Stratigraphy and sedimentology of Mid-Tertiary permeability barriers in the subsurface of the Murray Basin, southeastern Australia. BMR Journal of Australian Geology and Geophysics 11, 367- 385.

Brown, C.M. & Stephenson, A.E. 1991. Geology of the Murray Basin, south-eastern Australia. BMR Bulletin 235, 430 pp.

Brown, J.F., Wardlow, B.D., Tadesse, T., Hayes, M.J. & Reed, B.C. 2008. The Vegetation Drought Response Index (VegDRI) - a new integrated approach for monitoring drought stress in vegetation. GIScience and Remote Sensing 45, 16-46.

Browne, G.H. & Naish, T.R. 2003. Facies development and sequence architecture of a late Quaternary fluvial-marine transition, Canterbury Plains and shelf, New Zealand: implications for forced regressive deposits. Sedimentary Geology 158, 57–86.

Browne, W.R. 1945. An attempted post-Tertiary chronology of Australia. Linnaean Society of New South Wales 70, 5-24.

Brunke, M. & Gosner, T. 1997. The ecological significance of exchange processes between rivers and groundwater. Freshwater Biology 37, 1-33.

Butler, B.E. 1950. A theory of prior streams as a causal factor of soil occurrence in the Riverine Plain of southeastern Australia. Australian Journal of Agricultural Research 1, 231–252.

Butler, B.E. 1958. Depositional systems of the Riverine Plain of south-eastern Australia in relation to soils. CSIRO Soils Publication, 10. CSIRO.

Butler, B.E., Blackburn, G., Bowler, J.M., Lawrence, C.R., Newell, J.W. & Pels, S. 1973. A geomorphic map of the Riverine Plain of south-eastern Australia. Australian National University Press, Canberra, 39 pp.

Caldwell, N., de Hoog, M., Navin, J., Lawrie, K., Brodie, R.S., Apps, H. & Halas, L. 2012. Fly-through movie. Broken Hill Managed Aquifer Recharge Project, Geocat 63827.

CalPal. 2007. Cologne Radiocarbon Calibration and Paleoclimate Research Package, Online CalPal Radiocarbon Date Calibration. http://www.calpal-online.de/index.html

Campbell, C.J. & Wallace, T. 2009. The Darling Anabranch Adaptive Management Monitoring Program: Establishment of monitoring sites, field data sheets and data management protocols. A report prepared for the Lower Murray Darling Catchment Management Authority by The Murray-Darling Freshwater Research Centre.

Canadell, J., Jackson, R.B., Ehleringer, J.R., Mooney, H.A., Sala, O.E. & Schulze, E.D. 1996. Maximum rooting depth of vegetation types at the global scale. Oecologia 108, 583-95.

Cartwright, I. 2009. Using groundwater chemistry and environmental isotopes to assess the correction of ^{14}C ages in a silicate-dominate aquifer system. Journal of Hydrology 382, 174-187.

Cendón, D.I., Larsen, J.R., Jones, B.G., Nanson, G.C., Rickleman, D., Hankin, S.I., Pueyo, J.J. & Maroulis, J. 2010. Freshwater recharge into a shallow saline groundwater system, Cooper Creek floodplain, Queensland, Australia. Journal of Hydrology 392, 150–163.

Chamberlain, T. & Wilkinson, K. (eds) 2004. Salinity investigations using airborne geophysics in the Lower Balonne area, Southern Queensland. Queensland Department of Natural Resources and Mines, 257 pp.

Chen, X.Y. 1992. Lakes Menindee, Cawndilla and Victoria in western NSW: Their geomorphology, stratigraphy and shoreline erosion. NSW National Parks and Wildlife Service Report to NSW Water Resources Department, 190 pp.

Chiew, F.H.S. & McMahon, T.A. 1993. Detection of trend or change in annual flow of Australian rivers. International Journal of Climatology 13, 6, 643–653.

Chiew, F., Wang, Q.J., McConachy, F., James, R., Wright, W. & deHoedt, G. 2002. Evapotranspiration maps for Australia. Hydrology and Water Resources Symposium, Melbourne, 20-23 May, 2002, Institution of Engineers, Australia. http://www.bom.gov.au/climate/averages/climatology/evapotrans/text/evapotranspiration-paper.pdf

Childs, E.C. 1960. The nonsteady state of the water table in drained land. Journal of Geophysical Research 65, 780–782.

Chisholm, L.A. 2001. Characterisation and evaluation of moisture stress in *E. camaldulensis* using hyperspectral remote sensing. PhD thesis. University of New South Wales, Sydney.
Chivas, A.R., Andrew, A.S., Lyons, W.B., Bird, M.I. & Donnely, T.H. 1991. Isotopic constraints on the origin of salts in Australian playas. 1. Sulfur. Palaeogeography, Palaeoclimatology, Palaeoecology 84, 309-332.
Christensen, N.B. 2012. "Wave Number Domain Approximate Inversion" procedure. Aarhus University Report to Geoscience Australia. (Unpublished).
Clarke, J.D.A. 1994. Evolution of the Lefroy and Cowan palaeodrainages, Western Australia. Australian Journal of Earth Sciences 41, 55-68
Clarke, J.D.A. 2004. Fan delta geometry of the lower Burdekin river system, north Queensland. Extended abstracts, CRC LEME regolith symposium 2004, 57-61.
Clarke, J.D.A. & Riesz, A.L. 2004. Fluvial architecture of the subsurface of the Lower Balonne area, Southern Queensland, Australia. CRC LEME Open File Report 162.
Clarke, J.D.A. & Stoker, C.R. 2011. Concretions in inverted and exhumed channels near Hanksville Utah: implications for Mars. International Journal of Astrobiology 10, 161-175.
Clarke, J., Wong, V., Pain, C., Apps, H., Gibson, D., Luckman, J. & Lawrie, K. 2009. Geomorphology and surface materials: Lindsay to Wallpolla. CRC LEME Open File Report 237, Cooperative Research Centre for Landscapes, Environments and Mineral Exploration. Perth, Western Australia, 68 p.
Coetsers, M. & Walraevens, K. 2009. A new correction model for ^{14}C ages in aquifers with complex geochemistry – Application to the Neogene Aquifer, Belgium. Applied Geochemistry 24, 768-776.
Cohen, T.J., Nanson, G.C., Jansen, J.D., Jones, B.G., Jacobs, Z., Treble, P., Price, D.M., May, J-H., Smith, A.M., Ayliffe, L.K. & Hellstrom, J.C. 2011. Continental aridification and the vanishing of Australia's megalakes Geology 39, 167-170.
Cohen, T.J., Nanson, G.C., Jansen, J.D., Jones, B.G., Jacobs, Z., Larsen, J.R., May, J-H., Treble, P., Price, D.M. & Smith, A.M. 2012. Late Quaternary mega-lakes fed by the northern and southern river systems of central Australia: Varying moisture sources and increased continental aridity. Palaeogeography, Palaeoclimatology, Palaeoecology, 356-357, 89-108.
Coleman, J.M. & Prior, D.B. 1982. Deltaic environments. In: Scholle, P.A. & Spearing, D. (eds) Sandstone depositional environments. AAPG Memoir 31, 139-179.
Coleman, J.M. 1988. Dynamic changes and processes in the Mississippi River delta. Geological Society of America Bulletin 100, 999-1015.
Collett, N. 2001. Biology and control of psyllids, and the possible causes for defoliation of *Eucalyptus camaldulensis* Dehnh. (river red gum) in south-eastern Australia - a review. Australian Forestry 64, 88-95.
Cook, P.G. & Bohlke, J-K. 2000. Determining timescales for groundwater flow and transport. In: Cook, P.G & Herczeg, A.L (eds) Environmental tracers in subsurface hydrology. Kluwer.
Cook, P.G. & Walker, G.R., 1989. Groundwater recharge in south western New South Wales: A report on results of a drilling project carries out at field sites near Euston & Balranald. Centre for Research in Groundwater Processes. Report 9.
Cook, P.G., Kennett-Smith, A.K., Walker, G.R., Budd, G.R., Williams, R.M. & Anderson, R. 1996. Impact of dryland agriculture on land and river salinisation in the western lands, New South Wales. CSIRO Technical Memorandum 96.16.
Cook, P.G., Favreau, G., Dighton, J.C. & Tickell, S. 2003. Determining natural groundwater influx to a tropical river using radon, chlorofluorocarbons and ionic environmental tracers. Journal of Hydrology 277, 74-88.
Cooney, P. M. & Mantaring, A. M., 2004. Prospectivity of the Darling Basin. Preview, Journal of the Australian Society of Exploration Geophysicists, 108, 18
Country Water 2009. Annual Drinking Water Quality Report, Broken Hill and Menindee. http://www.essentialwater.com.au/asset/cms/pdf/Drinking_Water_Quality_Report_2009.pdf
Craig, H. 1961. Isotopic variations in meteoric water. Science 133, 1702-1703.
Crandall, C.A., Katz, B.G. & Hirten, J.J. 1999. Hydrochemical evidence for mixing of river water and groundwater during high-flow conditions, lower Suwannee River basin, Florida. USA. Hydrogeology Journal 7, 454-467.
Crank, J. 1956. The mathematics of diffusion. Oxford University Press, Oxford, 347 pp.
Crawford, S.A. & Wilkens, S. 1996. Ultrastructural aspects of damage to leaves of *Eucalyptus camaldulensis* by the Psyllid *Cardiaspina retator*. Micron 27, 359-66.

Cresswell, R.G., Mullen, I.C., Kingham, R., Kellett, J., Dent, D.L. & Jones, G.L. 2007. Airborne electromagnetics supporting salinity and natural resource management decisions at the field scale in Australia. International Journal of Applied Earth Observation and Geoinformation 9, 91-102.

Crosbie, R.S., Jolly, I.D., Leaney, F.W. & Petheram, C. 2010. Can the dataset of field based recharge estimations in Australia be used to predict recharge in data poor areas? Hydrology and Earth Systems Sciences 14, 2023-2038.

Crowell, J. C. 1974. Origin of late Cenozoic basins in southern California. In: Dott, R. H. & Shaver, R. H., (eds). Modern and ancient geosynclinals sedimentation: Society of Economic Palaeontologists and Mineralogists. Special Publication 19, p. 292–303.

CSIRO. 2008a. Water availability in the Murray. A report to the Australian Government from the CSIRO Murray-Darling Basin Sustainable Yields Project. 217 pp.

CSIRO. 2008b. Water availability in the Murray-Darling Basin. Summary of a report to the Australian Government from the CSIRO Murray-Darling Basin Sustainable Yield Project. CSIRO, Australia.

CSIRO. 2008c. Water availability in the Barwon-Darling. A report to the Australia Government from the CSIRO Murray-Darling Basin Sustainable Yield Project. CSIRO Australia.

CSIRO & SKM. 2010. Sustainable extraction limits derived from the Recharge Risk Assessment Method – New South Wales (Part 3). Report to the Murray-Darling Basin Authority. CSIRO Water for a Healthy Country National Research Flagship.

CSIRO & SKM. 2011. The groundwater SDL methodology for the Murray-Darling Basin Plan. Report to the Murray-Darling Basin Authority. CSIRO Water for a Healthy Country National Research Flagship.

Cunningham, S.C., MacNally, R., Read, J., Baker, P.J., White, M., Thomson, J.R. & Griffioen, P. 2009. A robust technique for mapping vegetation condition across a major river system. Ecosystems 12, 207-219.

Cunningham, S.C., MacNally, R., White, M., Read, J., Baker, P.J., Thomson, J. & Griffioen, P. 2007. Mapping the current condition of River Red Gum (*Eucalyptus camaldulensis* Dehnh.) stands along the Victorian Murray River floodplain. A report to the Northern Victorian Catchment Management Authorities and the Department of Sustainability and Environment.

Cunningham, W.D. & Mann, P. 2007. Tectonics of strike-slip restraining and releasing bends. Geol. Soc. Lond. Geol. Soc. Spec. Pub. 290, 1-12.

Cupper, M.L. 2005. Last glacial to Holocene evolution of semi-arid rangelands in south-eastern Australia. The Holocene 15, 541-553.

Cupper, M.L., 2006. Luminescence and radiocarbon chronologies of playa sedimentation in the Murray Basin, southeastern Australia. Quaternary Science Reviews 25, 2594-2607.

Cupper, M.L., Drinnan, A.N. & Thomas, I. 2000. Holocene palaeoenvironments of salt lakes in the Darling Anabranch region, south-western New South Wales, Australia. Journal of Biogeography 27, 1079-1094.

Cupper, M.L. & Duncan, J. 2006. Last glacial megafaunal death assemblage and early human occupation at Lake Menindee, southeastern Australia. Quaternary Research 66, 332-341.

Davies, N. 1953. Investigations on the soil and water relations of the river red gum forests. Final Report Murray Management Survey. Report No.R124. Forestry Commission of New South Wales, Resources Branch.

Dawson, T.E. & Ehleringer, J. R. 1991. Streamside trees that do not use stream water. Nature 350, 335-337.

De Deckker, P., Magee, J.W. & Shelley, J.M.G. 2011. Late Quaternary palaeohydrological changes in the large playa Lake Frome in central Australia, recorded from the Mg/Ca and Sr/Ca in ostracod valves and biotic remains. Journal of Arid Environments 75, 38-50.

de Hoog, M., Navin, J., Lawrie, K., Apps, H., Halas, L. & Brodie, R.S. 2012. WORLDWIND virtual globe model. Broken Hill Managed Aquifer Recharge Project, Geocat 63827.

Delin, G.N., Healy, R.W., Lorenz, D.L. & Nimmo, J.R. 2007. Comparison of local- to regional-scale estimates of ground-water recharge in Minnesota, USA. Journal of Hydrology 334, 231-249.

del Moral, R. & Muller, C.H. 1970. The allelopathic effects of *Eucalyptus camaldulensis*. American Midland Naturalist 83, 254-282.

Demko, T.M., Currie, B.S. & Nicoll, K.A. 2004. Regional paleoclimatic and stratigraphic implications of paleosols and fluvial/overbank architecture in the Morrison Formation (Upper Jurassic), Western Interior, USA. Sedimentary Geology 167, 115–135

Department of Land and Water Conservation. 1998. A review of the management of the Menindee Lakes Storage, Issues Paper.

Dillon, P., Toze, S., Pavelic, P., Vanderzalm, J., Barry, K., Ying, G-G., Kookana, R., Skjemstad, J., Nicholson, B., Miller, R., Correll, R., Prommer, H., Greskowiak, J. & Stuyfzand, P. 2005. Water quality improvements during aquifer storage and recovery at ten sites. In: UNESCO (ed.) Recharge systems for protecting and enhancing groundwater resources. Proceedings of the 5th International Symposium on Management of Aquifer Recharge (ISMAR5), Berlin, 11–16 June 2005, 85–94. http://unesdoc.unesco.org/images/0014/001492/149210e.pdf

Dillon, P., Pavelic, P., Page, D., Beringen, H. & Ward, J. 2009. Managed aquifer recharge. Waterlines Report Series No. 13, February 2009.

Doody, T.M., Holland, K.L., Benyon, R.G. & Jolly, I.D. 2009. Effect of groundwater freshening on riparian vegetation water balance. Hydrological Processes 23, 3485-3499.

Doody, T. & Overton, I. 2009. Environmental management of riparian tree health in the Murray-Darling Basin, Australia. Transactions on Ecology and the Environment 124, 197-206.

Drummond, M.A., Auch, R.F., Karstensen, K.A., Sayler, K.L., Taylor, J.L. & Loveland, T.R. 2012. Land change variability and human-environment dynamics in the United States Great Plains. Land Use Policy 29, 710-723.

Dunkerley, D.L. 2008. Bank permeability in an Australian ephemeral dry-land stream: variation with stage resulting from mud deposition and sediment clogging. Earth Surface Processes and Landforms 33, 226–243.

Edmunds, W.M. 2009. Geochemistry's vital contribution to solving water resource problems. Applied Geochemistry 24, 1058-1073.

Edwards, D. & MacAuley, S. 2008. Airborne electromagnetic surveying for answering environmental /land management questions: a case study from the Lower Macquarie Catchment, NSW, Australia. AEM 08, Helsinki, Finland. Extended Abstract 08-05, 2 pp.

Eilertsen, R.S. & Hanson, L. 2008. Morphology of river bed scours on a delta plain revealed by interferometric sonar. Geomorphology 94, 58–68.

Elberly, L.D. & Stanley, T.B. 1978. Cenozoic history and geologic history of southwestern Arizona. Geological Society of America Bulletin 89, 921-940.

Eldridge, S.R., Thorburn, P., McEwan, K.L. & Hatton, T.J. 1993. Health and structure of Eucalyptus communities on Chowilla and Monoman islands of the River Murray floodplain, South Australia. Divisional Report - CSIRO Australia, Division of Water Resources, 93.

Ellins, K.K, Roman-Mas, A. & Lee, R. 1990. Using ^{222}Rn to examine groundwater/surface discharge interaction in the Rio Grande De Manati, Puerto Rico. Journal of Hydrology 155, 319-341.

Evans, R., Murrihy, E., Bastiaanssen, W. & Molloy, R. 2009. Using satellite imagery to measure evaporation from storages- Solving the great unknown in water accounting. Irrigation and Drainage Conference 2009, Irrigation Australia Ltd, Swan Hill, Vic, Australia, 18 – 21 Oct. 2009.

Evans, W.R. & Kellett, J.R. 1989. The hydrogeology of the Murray Basin, southeastern Australia. BMR Journal of Australian Geology and Geophysics 11, 147-166.

Farrow, J. 1996. Insect pests of eucalypts on farms and in plantations. CSIRO, Collingwood, Vic.

Fenner, C. 1934. The Murray River Basin. Geographical Review 24, 79-91.

Ferguson, J. & Radke, B. M., 1992. Hydrodynamics of the Scotia, Nulla and Murquong Groundwater Discharge Complexes. Report to Murray-Darling Basin Commission. Canberra, Australian Geological Survey Organisation.

Ferguson, J., Radke, B.M., Jacobson, G., Evans, W.R., Chambers, L.A., White, I.A., Wooding, R.A., Whitford, D. & Allan, G.L. 1995: The Scotia groundwater discharge complex, Murray Basin, SE Australia. AGSO Record 1995/43. Australian Geological Survey Organisation, Canberra.

Ferguson, J., Radke, B.M., Jacobson, G., Evans, W.R., Chambers, L.A., Wooding, R.A., White, I.A., Whitford, D.J., Allan, G.L. & Grün, R. 1997. The Nulla groundwater discharge complex, Murray Basin, SE Australia. AGSO Record 1997/39. Australian Geological Survey Organisation, Canberra.

Fetter, C.W. 2001. Applied hydrogeology. 4th Edition, Prentice-Hall, New Jersey.

Fielding, C.R., Allen, J.P., Alexander, J. & Gilbing, M.R. 2009. Facies model for fluvial systems in the seasonal tropics and subtropics. Geology 37, 7, 623–626.

Finch, J. & Calver, A. 2008. Methods for the quantification of evaporation from lakes. World Meteorological Organization, Commission for Hydrology. http://nora.nerc.ac.uk/14359/1/wmoevap_271008.pdf

Firman, J.B., 1965. Late Cainozoic lacustrine deposits in the Murray Basin, South Australia. Geological Survey South Australia, Quarterly Geological Notes 16, 1-2.

Firman, J.B. 1966. Stratigraphy of the Chowilla area in the Murray Basin. Quarterly Notes of the Geological Survey of South Australia 20, 3-7.
Firman, J.B. 1969. Quaternary period. In: Parkin, L.W.(ed.) Handbook of South Australian geology. Geological Survey of South Australia, 204-233
Firman, J.B. 1973. Regional stratigraphy of surficial deposits in the Murray Basin and Gambier Embayment. Geological Survey of South Australia, Report of Investigations 39.
Fontes, J.-Ch. & Garnier, J-M. 1979. Determination of the initial ^{14}C activity of the total dissolved carbon: a review of the existing models and a new approach. Water Resources Research 15, 399–413.
Freeze, R.A. & Cherry, J.A. 1979. Groundwater. New Jersey, Prentice Hall 604 pp,
Fuller, D.O., Prince, S.D. & Astle, W.L. 1997. The influence of canopy strata on remotely sensed observations of savanna-woodlands. International Journal of Remote Sensing 18, 2985-3009.
Galloway, R.W. 1965. Late Quaternary climates in Australia. Journal of Geology 73, 603-18.
Garrett, D.R. & Hoy R.D. 1978. A study of monthly lake to pan coefficients using a numerical lake model. Institute of Engineers, Australia, Publication 78/9, 145-149.
Geerling, G.W., Labrador-Garcia, M., Clevers, J.G.P.W., Ragas, A.M.J. & Smits, A.J.M. 2007. Classification of floodplain vegetation by data fusion of spectral (CASI) and LiDAR data. International Journal of Remote Sensing 28, 4263-4284.
Gentilli, J. 1986. Climate. In: Jeans, D.N. (ed.) The natural environment – Volume 1, Australia, a geography. Sydney University Press, Sydney, 14–48.
George, R.J., Beasley, I., Gordon, D., Heislers, D., Speed, R., Brodie, R., McConnell, C. & Woodgate, P. 1998. Evaluation of airborne geophysics for catchment management. National Report to AFFA on National Airborne Geophysics Project (unpublished).
Gibling, M.R. 2006. Width and thickness of fluvial channel bodies and valley fills in the geological record: a literature compilation and classification. Journal of Sedimentary Research 76, 731–770.
Gibson, D.L. 1999. Explanatory notes for the Broken Hill and Curnamona Province 1:500 000 regolith landform maps. CRC LEME Open File Report, No.77, 59 pp.
Gibson, J.J., Sadek, M.A., Stone, D.J.M., Hughes, C.E., Hankin, S., Cendon, D.I. & Hollins, S.E. 2008. Evaporative isotope enrichment as a constraint on reach water balance along a dryland river. Isotopes in Environmental and Health Studies 44, 83-98.
Gill, E.D. 1973. Geology and geomorphology of the Murray River region between Mildura and Renmark, Australia. Memoirs of the National Museum of Victoria 34, 1–98.
Gillespie, R., Fifield, L.K., Levchenko, V. & Wells, R. 2008. New ^{14}C ages on cellulose from Diprotodon gut contents: explorations in oxidation chemistry and combustion. Radiocarbon 50, 75-81.
Gingele, F.X. & De Deckker, P. 2004. Fingerprinting Australia's rivers with clay minerals and the application for the marine record of climate change. Australian Journal of Earth Sciences 51, 339–348
Gingele, F.X. & De Deckker, P. 2005. Clay mineral, geochemical and Sr–Nd isotopic fingerprinting of sediments in the Murray–Darling fluvial system, southeast Australia. Australian Journal of Earth Sciences 52, 965 – 974.
Gingel, F.X. & De Deckker, P. 2005. Clay mineral, geochemical and Sr-Nd isotopic fingerprinting of sediments in the Murray-Darling fluvial system, southeast Australia. Australian Journal of Earth Sciences 52, 96-974.
Gippel, C.J. & Blackham, D. 2002. Review of environmental impacts of flow regulation and other water resource developments in the River Murray and Lower Darling River system. Report by Fluvial Systems Pty Ltd to Murray-Darling Basin Commission, Canberra. http://www.mdbc.gov.au/TLM/pdf/Final_Review_reg_impacts_eflow.pdf (accessed 28 Feb 2003).
Glen, R.A., Clare, A. & Spencer, R. 1996. Extrapolating the Cobar Basin Model to the regional scale: Devonian basin formation and inversion in Western NSW, Figure 2, The Cobar Mineral Field - A 1996 Perspective; AusIMM Spectrum Series no 3/96.
Gow, L., Apps, H.E., Halas, L., Tan, K.P., Lawrie, K.C., Brodie, R.S., Gibson, D., Magee, J.W., Somerville, P., Smith, M., Clarke, J.D.A., Schoning, G., Halas, V., Spulak, R., Beudreau, D., Cook, B., Knox, K., Lymburner, L., McIntyre, A., Christensen, N.B., Brodie, R.C., Abraham, J., Jaycock, J., Davies, A. & Ley-Cooper, Y. 2012a. Broken Hill Managed Aquifer Recharge Project GIS. GeoCat no. 73825.
Gow, L., Lymburner, L., Halas, L., McIntyre, A., Magee, J.W. & Beaudreau, D. 2012b. BHMAR Project Appendix 9: Remote sensing /vegetation health analysis background data and intermediate products. Geoscience Australia Record 2012/17. Geocat 73824.

Grayson, R.B., Argent, R.M., Nathan, R.J., McMahon, T.A. & Mein, R.G. 1996. Hydrological Recipes: Estimation techniques in Australian hydrology. Cooperative Research Centre for Catchment Hydrology.

Green, A.A. & Munday, T. 2004. Forward modelling airborne electromagnetic data for the Riverland, S.A. CRC LEME Open File Report 171.

Groen, J., Velstra, J. & Meesters, A.G.C.A. 2000. Salinization processes in paleowaters in coastal sediments of Suriname: Evidence from δ^{37}Cl analysis and diffusion modelling. Journal of Hydrology 234, 1-20.

Gu, A. 2005. Stable isotope geochemistry of sulfate in groundwater of southern Arizona: implications for groundwater flow, sulfate sources, and environmental significance. PhD Dissertation submitted to the Faculty of the Department of Geosciences, University of Arizona (unpublished).

Gunn, R.H. & Richardson, D.P. 1979. The nature and possible origins of soluble salts in deeply weathered landscapes of Eastern Australia. Australian Journal of Soil Research 17, 197-215.

Halas, L., Halas, V., Schoning, G., Tan, K.P., Clarke, J.D.A., Gibson, D., Somerville, P., Spulak, R., Magee, J.W., Smith, M., Smith, M., Boston, K., Brodie, R.S., Lawrie, K.C. & Apps, H.E. 2012a. BHMAR Project Appendix 1: Graphical display of borehole geological and geophysical logs and hydrogeochemical data. Geoscience Australia Record 2012/17. Geocat 73824.

Halas, L., Apps, H., Lawrie, K., Brodie, R.S. & Tan, K.P. 2012b. 3D GoCAD Model. Broken Hill Managed Aquifer Recharge Project. Geocat, 63827.

Hanneman, W.M. 2002. The Central Arizona Project. Department of Agricultural & Resource Economics, UCB, CUDARE Working Papers (University of California, Berkeley), Paper 937, 1-12.

Hansen, M.C., Roy, D.P., Lindquist, E., Adusei, B., Justice, C.O. & Altstatt, A. 2008. A method for integrating MODIS and Landsat data for systematic monitoring of forest cover and change in the Congo Basin. Remote Sensing of Environment 112, 2495-2513.

Hanson, R.L. 1991. Evapotranspiration and droughts, In: Paulson, R.W., Chase, E.B., Roberts, R.S. & Moody, D.W. (eds) National Water Summary 1988-89 Hydrologic events and floods and droughts. U.S. Geological Survey Water-Supply Paper 2375, 99-104.

Hantush, M.S. 1967. Growth and decay of groundwater mounds in response to uniform percolation. Water Resources Research 3, 227-234.

Harding, T.P. & Lowell, J.D. 1974. Structural styles, their plate tectonic habitats, and hydrocarbon traps in petroleum provinces. Bull. Am. Assoc. Petrol. Geol. 63, 1016-1058.

Harrington, G. & Cook, P. 2011. Mechanical loading and unloading of confined aquifers: implications for the assessment of long-term trends in potentiometric levels. Waterlines Report 51, National Water Commission, Canberra.

Hasiotis, S.T. 2004. Reconnaissance of Upper Jurassic Morrison Formation ichnofossils, Rocky Mountain Region, USA: paleoenvironmental, stratigraphic, and paleoclimatic significance of terrestrial and freshwater ichnocoenoses. Sedimentary Geology 167, 177–268.

Hatton, T., Moore, S. & Reece, P. 1995. Estimating stand transpiration in a *Eucalyptus populnea* woodland with the heat pulse method: measurement errors and sampling strategies. Tree Physiology 15, 219-227.

Healy, R.W. & Cook, P.G. 2002. Using groundwater levels to estimate recharge. Hydrogeology Journal 10, 1, 91-109.

Heinrich, P. 1990. The eco-physiology of riparian River Red Gum (*Eucalyptus camaldulensis*) Final Report, Australian Water Resources Advisory Council.

Herczeg, A.L., Dogramaci, S.S. & Leaney, F.W.J. 2001. Origin of dissolved salts in a large, semi-arid groundwater system: Murray Basin, Australia Marine and Freshwater Research 52, 1, 41- 52.

Hesse, P.P., Magee, J.W. & van der Kaars, S. 2004. Late Quaternary climates of the Australian arid zone: a review. Quaternary International 118-119, 87-102.

Hesse, P.P., Luly, J.G. & Magee, J.W. 2005. The beating heart: environmental history of Australia's deserts. In: Smith, M.K. & Hesse, P.P.(eds) 23 degrees S: Archaeology and environmental history of the southern deserts. National Museum of Australia Press, Canberra, 436 pp.

Hill, R.A. & Thomson, A.G. 2005. Mapping woodland species composition and structure using airborne spectral and LiDAR data. International Journal of Remote Sensing 26 3763-3779.

Hill, S.M., Eggleton, R.A. & Taylor, G. 2003. Neotectonic disruption of silicified palaeovalley systems in an intraplate, cratonic landscape: Regolith and landscape evolution of the Mulculca range-front, Broken Hill Domain, New South Wales. Australian Journal of Earth Sciences 50, 691-707.

Hillis, R.R., Sandiford, M., Reynolds, S.D. & Quigley, M.C. 2008. Present-day stresses, seismicity and Neogene-to-Recent tectonics of Australia's 'passive' margins: intraplate deformation controlled by plate boundary forces. Geol. Soc. Lond. Spec. Pub. 306, 71-90.

Hills, E.S. 1955. A contribution to the morphotectonics of Australia. Journal of the Geological Society of Australia. 3, 1, 1-15.

Hope, J.H. 1981. Prehistoric research in the lower Darling region. In: Hope, J.H. (ed.) Darling Surveys I. Occasional Papers in Prehistory 3, Department of Prehistory, Research School of Pacific Studies, Australian National University, 1-8.

Hope, J.H. 1993. Pleistocene archaeological sites in the central Murray-Darling Basin. In: Smith, M.A., Spriggs, M. & Fankhauser, B. (eds) Sahul in Review: Pleistocene archaeology in Australia, New Guinea and island Melanesia. Canberra, Australian National University, 183-196.

Hope, J.H., Dare-Edwards, A.J. & McIntyre, M.L. 1983. Middens and megafauna: Stratigraphy and dating of Lake Tandou lunette, western New South Wales. Archaeology in Oceania 18, 45-53.

Hounam, C.E. 1973. Comparison between pan and lake evaporation. Technical Note 126, World Meteorological Organization.

Houser, B.B., Peters, L., Esser, R.P., &. Gettings, M.E. 2004. Stratigraphy and tectonic history of the Tucson Basin, Pima County, Arizona, based on the Exxon State (32)-1 well. USGS Scientific Investigations Report 2004–5076.

Hoy, R.D. 1977. Pan and lake evaporation in Northern Australia. Institute of Engineers Australia, Conference Publication No 77/5, 57-61.

Hughes, C.E., Meredith, K.T., Cendon, D.I. & Hollins, S.E. 2009. Evaporative losses from the Darling River, NSW, during drought from 2002-2005. 10th Australian Environmental Hydrology Research Conference, Perth. W.A. Abstract Volume.

Ingerson, E. & Pearson Jr., F.J. 1964. Estimation of age and rate of motion of groundwater by the ^{14}C-method. In: Miyake, Y. & Koyama, T. (eds) Recent Researches in the Fields of Atmosphere, Hydrosphere and Nuclear Geochemistry, Sugawara Festival Volume, 263–283. Tokyo: Maruzen Co.

J. Harlen Glen Associates. 2001. Sahuarita lake manual. Report prepared for Rancho Sahuarita, J. Harlen Glenn Associates, June 22, 2001.

Jansson, M.B. 1988. A global survey of sediment yield. Geografiska Annaler. Series A, Physical Geography 70, 1-2, 81-98.

Jenkins, K.M. & Boulton, A.J. 2003. Connectivity in a dryland river: short-term aquatic microinvertebrate recruitment following floodplain inundation. Ecology 84 10, 2708-2723

Jensen, M.E. 2010. Estimating evaporation from water surfaces. CSU/ARS Evapotranspiration Workshop, Fort Collins, Colorado, 15 March 2010. http://ccc.atmos.colostate.edu/ET_Workshop/ET_Jensen/ET_water_surf.pdf

Jewell, C. M., 1993. Lower Darling River, Groundwater-River Level Relationships and Qualitative Indications of Environmental Flows in Rivers and Wetlands. C.M. Jewell & Associates Pty. Ltd.

Jewell, C.M.J. 2007. Options for use of the Menindee and Broken Hill aquifers. Consultants report for Country Energy. C.M Jewell & Associates Pty Ltd, Wentworth Falls.

Jolly, I.D., Walker, G.R. & Thorburn, P.J. 1993. Salt accumulation in semi-arid floodplain soils with implications for forest health. Journal of Hydrology 150, 589-614.

Jolly, I.D., Williamson, D.R., Gilfedder, M., Walker, G.R., Morton, R., Robinson, G., Jones, H., Zhang, L., Dowling, T.I., Dyce, P., Nathan, R.J., Nandakumar, N., Clarke, R. &. McNeill, V. 2001. Historical stream salinity trends and catchment salt balances in the Murray–Darling Basin, Australia. Marine and Freshwater Research 52, 1, 53 – 63

Jones, K.B., Edmonds, C.E., Slonecker, T.E., Wickham, J.D., Neale, A.C., Wade, T.G., Riitters, K.H. & Kepner, W.G. 2008. Detecting changes in riparian habitat conditions based on patterns of greenness change: A case study from the Upper San Pedro River Basin, USA. Ecological Indicators 8, 1, 89-99.

Kalbus, E., Reinstorf, F. & Schirmer, M. 2006. Measuring methods for groundwater-surface water interactions: a review. Hydrology and Earth System Sciences 10, 873-887.

Katz, B.G., Catches, J.S., Bullen, T.D. & Michel, R.L. 1998. Changes in the isotopic and chemical composition of groundwater resulting from a recharge pulse from a sinking stream. Journal of Hydrology 211, 178-207.

Kellett, J.R. 1994. MANARA Hydrogeological Map (1:250 000 scale). Murray Basin Hydrogeological Map Series. Australian Geological Survey Organisation, Canberra.

Kellett, J.R. 1997. Lachlan Fan/Ivanhoe Block steady state groundwater model: Model development, calibration, sensitivity analysis and predictions. AGSO Record 1997/29. Australian Geological Survey Organisation.
Kellett, J.R. 1989. The Ivanhoe Block – its structure, hydrogeology and effect on groundwaters of the Riverine Plain of New South Wales. BMR Journal of Australian Geology and Geophysics 11, 333-353.
Kemp, J. 2010. Downstream channel changes on a contracting, anabranching river: the Lachlan, southeastern Australia. Geomorphology 121, 231-244.
Kennett-Smith, A.K., Budd, G.R. & Walker, G.R., 1991. Groundwater recharge beneath woodlands cleared for grazing in south western New South Wales. Centre for Groundwater Studies, Report 35.
Kennett-Smith, A., Cook, P.G. & Walker, G.R., 1994. Factors affecting groundwater recharge following clearing in the south western Murray Basin. Journal of Hydrology 154, 85-105.
Kernich, A.L., Pain, C.F., Clarke, J.D.A. & Fitzpatrick, A. 2009. Geomorphology of a dryland depositional system: the lower Balonne River, southern Queensland, Australia. Australian Journal of Earth Sciences 56, S139-153.
Kingham, R., 1998. Geology of the Murray-darling Basin - Simplified Lithostratigraphic Groupings. AGSO Record 1998/21. Australian Geological Survey Organisation.
Kingsford, R.T., Jenkins, K.M. & Porter, J.L. 2002. Waterbirds and effects of river regulation on Menindee lakes of the Darling River. New South Wales National Parks and Wildlife Service, Hurstville.
Kingsford, R.T., Jenkins, K.M. & Porter, J.L. 2004. Imposed hydrological stability on lakes in arid Australia and effects on waterbirds. Ecology 85, 2478-2492.
Kingsford, R.T. & Porter, J.L. 2006. Waterbirds and wetlands across Eastern Australia. Technical report prepared for the Department of the Environment and Heritage, Canberra. http://www.deh.gov.au/soe/2006/techncial/waterbirds/index.html
Kjemarud, A.V., Schomacker, E.R. & Cross, T.A. 2008. Architecture and stratigraphy of alluvial deposits, Morrison Formation (Upper Jurassic), Utah. AAPG Bulletin 92, 1055–1076.
Kloppman, W., Negrel, P., Casanova, J., Klinge, H., Schelkes, K. & Guerrot, C. 2001. Halite dissolution derived brines in the vicinity of a Permian salt dome (N German Basin): Evidence from boron, strontium, oxygen and hydrogen isotopes. Geochimica et Cosmochimica Acta 65, 4087-4140.
Knighton, A.D. & Nanson, G.C. 2000. Waterhole form and processes in the anastomosing channel system of Cooper Creek, Australia. Geomorphology 35, 101–117.
Kohler, M.A., Nordenson, T.J. & Fox, W.E. 1955. Evaporation from pans and lakes. U.S. Department of Commerce, Weather Bureau Research Paper 38, 21 pp.
Kohler, M.A., Nordenson, T.J. & Fox, W.E. 1958. Pan and lake evaporation. In: Harbeck, G.E. Jr., Kohler, M.A., Koberg G.E., Nordenson, T.J, Fox, W.E., Garstka, W.U., Phillips, H.B., Allen, I.E., Ebert, D.J. (eds) Water Loss Investigations: Lake Mead Studies. US Geological Survey Professional Paper 298, 38-60.
Kotsonis, A. 1999. Tertiary shorelines of the western Murray Basin: weathering, sedimentology and exploration potential. In: Stuart, R. (ed.) Murray Basin Mineral Sands Conference, Extended Abstracts. Australian Institute of Geosciences Bulletin 26, 57–63.
Krasny, J. 1993. Classification of transmissivity magnitude and variation. Groundwater 31,2, 230-236.
Kutzbach, J.E. & Guetter, P.J. 1986. The influence of changing orbital parameters and surface boundary conditions on climate simulations for the past 18,000 years. Journal of Atmospheric Science 43, 1726–1759.
Lawrence, C.R. 1975. Geology, hydrodynamics and hydrochemistry of the southern Murray Basin. Geological Survey of Victoria, Memoir, 30.
Lawrie, K.C., Pain, C.F., Gibson, D.L., Munday, T.J., Wilford, J. & Jones, G. 2002. Regolith – a missing link in mapping salinity processes and predicting dryland salinity. In: Phillips, G.N. & Ely, K.S., Victoria Under Cover: Benalla 2002 Conference proceedings and field guide. CSIRO Publishing, Collingwood, Victoria.
Lawrie, K.C., Brodie, R.S., Tan, K.P., Gibson, D., Magee, J.W., Clarke, J.D.A., Halas, L., Gow, L., Somerville, P., Apps, H.E., Christensen, N.B., Brodie, R.C., Abraham, J., Smith, M., Page, D., Dillon, P., Vanderzalm, J., Miotlinski, K., Hostetler, S., Davis, A., Ley-Cooper, A.Y., Schoning, G., Barry, K. & Levett, K. 2012a. BHMAR Project: Data acquisition, processing, analysis and interpretation methods. Geoscience Australia Record 2012/11. Geocat 73819.

Lawrie, K.C., Brodie, R.S., Tan, K.P., Gibson, D., Magee, J.W., Clarke, J.D.A., Halas, L., Gow, L., Somerville, P., Apps, H.E., Smith, M., Christensen, N.B., Abraham, J., Hostetler, S. & Brodie, R.C. 2012b. BHMAR Project: Geological and hydrogeological framework and conceptual model. Geoscience Australia Record 2012/12. Geocat 73820.

Lawrie, K.C., Brodie, R.S., Dillon, P., Tan, K.P., Gibson, D., Magee, J.W., Clarke, J.D.A., Somerville, P., Gow, L., Halas, L., Apps, H.E., Page, D., Vanderzalm, J., Abraham, J., Hostetler, S., Christensen, N.B., Miotlinski, K., Brodie, R.C., Smith, M., Schoning, G., Barry, K. & Levett, K., 2012c. BHMAR Project: Assessment of conjunctive water supply options involving managed aquifer recharge options at Menindee Lakes. Geoscience Australia Record 2012/14. Geocat 73821.

Lawrie, K.C., Brodie, R.S., Tan, K.P., Somerville, P., Gibson, D., Magee, J.W., Clarke, J.D.A., Abraham, J., Gow, L., Halas, L., Apps, H.E., Hostetler, S., Christensen, N.B., Smith, M., Brodie, R.C. & Schoning, G. 2012d. BHMAR Project: Assessment of conjunctive water supply options involving groundwater extraction options at Menindee Lakes. Geoscience Australia Record 2012/15. Geocat 73822.

Lawrie, K.C., Brodie, R.S., Dillon, P., Tan, K.P., Gibson, D., Magee, J.W., Clarke, J.D.A., Somerville, P., Gow, L., Halas, L., Apps, H.E., Page, D., Vanderzalm, J., Abraham, J., Hostetler, S., Christensen, N.B., Miotlinski, K., Brodie, R.C., Smith, M., Schoning, G., Barry, K. & Levett, K. 2012e. BHMAR Project: Securing Broken Hill's water supply: Assessment of conjunctive water supply options involving managed aquifer recharge and/or groundwater extraction at Menindee Lakes- Summary Report. Geoscience Australia Record 2012/16. Geocat 73823.

Lawrie, K.C., Halas, L. & Apps, H.E. 2012f. BHMAR Project Appendix 14: LiDAR acquisition and processing contractor reports. Geoscience Australia Record 2012/16. Geocat 73824.

Lawrie, K.C., Clarke, J.D.A., Cullen, K., Brodie, R.S., Munday, T., Hatch, M., Apps, H.E., Fitzpatrick, A., Cahill, K., Lane, R., Richardson, M., Ransley, T. & English, P., 2008. Broken Hill Managed Aquifer Recharge Project, Phase 1: Progress report against the Project Plan and Project Scope. Geoscience Australia Professional Opinion 2008/06.

Lawrie, K.C., Munday, T., Clarke, J.D.A., Fitzpatrick, A., Cullen, K., Apps, H.E., Brodie, R.S., Ransley, T., Cahill, K., Lane, R., Richardson, M., English, P. & Hatch, M. 2009a. Broken Hill Managed Aquifer Recharge Project, Phase 1: Final Report. Geoscience Australia Professional Opinion 2009/03.

Lawrie, K.C., Brodie, R.C., Gibson, D., Kuske, T.J., Halas, L., Tan, K.P., Cullen, K., Brodie, R.S., Hannah, A. & Richardson, M. 2009b. Broken Hill Managed Aquifer Recharge Project, Phase 2: Report on AEM system selection. Geoscience Australia Professional Opinion 2009. (Unpublished).

Lawrie, K.C., Brodie, R.S., Dillon, P., Gibson, D., Clarke, J.D.A., Tan, K.P., Page, D., Magee, J.W., Halas, L., Vanderzalm, J., Apps, H.E., Davis, A., Ley-Cooper, A.Y., Smith, M.S., Miotlinski, K., Somerville, P., Gow, L., Boston, K., Smith, M., Barry, K. & Levett, K. 2010a. Broken Hill Managed Aquifer Recharge Project Phase 3a: Assessment of managed aquifer recharge viability at Menindee Lakes. Interim Report. Geoscience Australia Professional Opinion 2010/08, p.468.

Lawrie, K.C., Brodie, R.S., Gibson, D., Tan, K.P., Magee, J.W., Davis, A., Halas, L., Clarke, J.D.A., Ley-Cooper, A.Y., Wallace, L., Smith, M., Apps, H.E., Pain, C., Ransley, T., Gow, L., Brodie, R.C., Christensen, N.B., Cullen, K., Bastrakov, E., & Mernagh, T. 2010b. Broken Hill Managed Aquifer Recharge Project, Phase 2: Interim Report. Geoscience Australia Professional Opinion 2010/02. pp 472.

Lawrie, K.C., Tan, K.P., Clarke, J.C., Munday, T.J., Fitzpatrick, A., Brodie, R.S., Pain, C.F., Apps, H., Cullen, K., Halas, L., Kuske, T.J., Cahill, K. & Davis, A. 2010c. Utilising time domain airborne electromagnetics (AEM) to map aquifer systems and salinity hazard in the Ord Valley, Western Australia. Geoscience Australia Professional Opinion 2009, 500p. Geocat No. 69583.

Lawrie, K.C., Brodie, R.S., Dillon, P., Tan, K.P., Halas, L., Christensen, N.B., Ley-Cooper, A.Y., Davis, A., Somerville, P., Smith, M.S., Apps, H.E., Magee, J.W., Gibson, D., Clarke, J.D.A., Page, D., Vanderzalm, J., Miotlinski, K., Barry, K., Levett, K., & Gow, L. 2011. Securing Broken Hill's water supply: Assessment of groundwater extraction and conjunctive water supply options at Menindee Lakes. Geoscience Australia Professional Opinion, 2011/02, p.55.

Leaney, F.W., Crosbie, R.S., O'Grady, A., Jolly, I.D., Gow, L., Davies, P., Wilford, J. & Kilgour, P. 2011. Recharge and discharge estimation in data poor areas: Scientific reference guide. CSIRO: Water for a Healthy Country National Research Flagship.

Leckie, D.A. 2003. Modern environments of the Canterbury Plains and adjacent offshore areas, New Zealand - an analogue for ancient conglomeratic depositional systems in non-marine and coastal zone settings. Bulletin of Canadian Petroleum Geology 51, 389-425.

Lee, R.W. & Hollyday, E.F. 1993. Use of radon measurements in Carters Creek, Maury County, Tennessee, to determine location and magnitude of ground-water seepage. In: Gunderson, L.C.S. & Wanty, R.B. (eds) Field studies of radon in rocks, soils and water. CK Smoley, 237-242.
Leopold, L.B., Wolman, M.G. & Miller, J.P. 1964. Fluvial processes in geomorphology. W.H. Freeman and Co., San Francisco and London, pp 522.
Lewis, S.J., Roberts, J., Brodie, R.S., Gow, L., Kilgour, P., Ransley, T., Coram, J.E. & Sundaram, B., 2008. Assessment of groundwater resources in the Broken Hill region. Geoscience Australia Professional Opinion 2008/05, Canberra.
Li, Y-H. & Gregory, S. 1974. Diffusion of ions in sea water and in deep-sea sediments. Geochimica et Cosmochimica Acta 38, 703–714.
Linacre, E.T. 1993. Data-sparse estimation of lake evaporation, using a simplified Penman equation. Agricultural and Forest Meteorology 64, 237-256.
Linacre, E.T. 1994. Estimating U.S. Class-A pan evaporation from few climatic data. Water International 19, 5-14.
Linacre, E. & Hobbs, J.E. 1977. The Australian climatic environment. John Wiley & Sons, Brisbane, 354 pp.
Liu, J., Fu, G., Song, X., Charles, S.P., Zhang, Y., Han, D. & Wang, S. 2010. Stable isotopic compositions in Australian precipitation. Journal of Geophysical Research 115. D23307.
Lowe, L., Webb, A., Nathan, R., Etchells, T. & Malano, H. 2009. Evaporation from water supply reservoirs: An assessment of uncertainty. Journal of Hydrology 376, 261-274.
Luly, J. 2001. On the equivocal fate of late Pleistocene Callitris Vent. (*Cupressaceae*) woodlands in arid south Australia. Quaternary International 83-85, 155-168.
Lynds, R. & Hajek, E. 2006. Conceptual model for predicting mudstone dimensions in sandy braided-river reservoirs. AAPG Bulletin 90, 1273–1288.
Mabbutt, J.A. 1977. Desert landforms. Australian National University Press, Canberra.
McLean, W. & Jankowski, J. 2003. The importance of hydrochemical investigations in sustainable groundwater resource management in irrigated catchments. 28th International Hydrology and Water Resources Symposium, About Water; Symposium Proceedings. Institution of Engineers, Australia, 2003.
Macphail, M. 2013. Palynostratigraphic analysis of cuttings samples from the Type Section of the Calivil Formation in Calivil-2 and 'a representative section' in Marma-1, southern Murray Basin. Palynostratigraphic report prepared for the BHMAR Project, Groundwater Group, Geoscience Australia, 29 April 2013.
Macphail, M. 2010. Palynostratigraphic dates from sonic coreholes BHMAR Project, Lake Menindee area, Broken Hill, far western New South Wales. Palynostratigraphic report prepared 20 August 2010 for the Broken Hill Managed Aquifer Recharge Project, Geoscience Australia by Consultant Palynological Services/Morgan Palaeo Associates, 13 Walu Place, Aranda. ACT 2614.
Macphail, M. 2007. Australian palaeoclimates: Cretaceous to Tertiary - A review of palaeobotanical and related evidence to the year 2000. CRC LEME Special Volume Open File Report 151, 266 pp. http://crcleme.org.au/Pubs/OPEN%20FILE%20REPORTS/OFR%20151/OFR%20151.pdf
Macphail, M.K. 1999. Palynostratigraphy of the Murray Basin, inland southeastern Australia. Palynology 23, 199-242.
Macumber, P.G. 1973. Progress report on the groundwater survey of the Avoca & Loddon Valleys, Victoria. Department of Mines, Groundwater Investigation Program. Report, 1972, 7 pp.
Macumber, P.G. 1980. The influence of groundwater discharge on the Mallee landscape. In: Storrier, R.R. & Stannard, M.E. (eds) Aeolian landscapes in the semi-arid zone of south-eastern Australia. Australian Society of Soil Science, Inc., Riverina Branch, Wagga Wagga, Australia, 67-84.
Macumber, P.G. 1991. Interaction between groundwater and surface systems in northern Victoria. Department of Conservation and Environment, Victoria, Melbourne, Australia, 345 pp.
Magee, J.W. 1991. Late Quaternary lacustrine, groundwater, aeolian and pedogenic gypsum in the Prungle Lakes, southwestern New South Wales, Australia. Palaeogeography, Palaeoclimatology, Palaeoecology 84, 3–42.
Magee, J.W. 2007. Australian lake-level studies. In: Elias, S.A. (ed.) Encyclopedia of Quaternary Science. Elsevier, B.V.,1359-1365.
Magee, J.W., Apps, H.E. & Knox, K. 2012. BHMAR Project Appendix 15: Cultural Heritage and environmental clearance surveys. Geoscience Australia Record 2012/17. Geocat 73824.

Magee, J.W., Miller, G.H., Spooner, N.A. & Questiaux, D. 2004. Continuous 150 k.y. monsoon record from Lake Eyre, Australia: Insolation-forcing implications and unexpected Holocene failure. Geology 32, 885–888.

Maroulis, J.C., Nanson, G.C., Price, D.M. & Pietsch, T. 2007. Aeolian–fluvial interaction and climate change: source-bordering dune development over the past 100 ka on Cooper Creek, central Australia. Quaternary Science Reviews 26, 386–404.

Marshall, L.G. 1973. Fossil vertebrate faunas from the Lake Victoria region, SW New South Wales, Australia. National Museum of Victoria, Memoir 34, 35-54.

Martin, S. 2001. Aboriginal cultural heritage of the Menindee Lakes Area, Part 1: Aboriginal ties to the land. Unpublished report to the Menindee Lakes Ecologically Sustainable Development Project steering committee, NSW DLWC.

Maunsell. 2007. Darling River Water Savings Project, Part A Report. Report to NSW Department of Natural Resources and National Water Commission, 62 pp.

McJannet, D.L., Webster, I.T., Stenson, M.P. & Sherman, B.S. 2008. Estimating open water evaporation for the Murray Darling Basin. A report to the Australian Government from the CSIRO Murray-Darling Basin Sustainable Yields Project, CSIRO, Australia, 50 pp.

McLaren, S., Wallace, M.W., Pillans, B.J., Gallagher, S.J., Miranda, J.A. & Warne, M.T. 2009. Revised stratigraphy of the Blanchetown Clay, Murray Basin: age constraints on the evolution of paleo Lake Bungunnia. Australian Journal of Earth Sciences 56, 259 – 270.

McLaren, S. & Wallace, M.W. 2010. Plio-Pleistocene climate change and the onset of aridity in southeastern Australia. Global and Planetary Climate Change 71, 55-72.

McLaren, S., Wallace, M.W., Gallagher, S.J., Miranda, J.A., Holdgate, G.R., Gow, L.J., Snowball, I. & Sandgren, P. 2011. Palaeogeographic, climatic and tectonic change in southeastern Australia: the Late Neogene evolution of the Murray Basin. Quaternary Science Reviews 30, 1086-1111.

McLaren, S., Wallace, M.W. & Reynolds, T. 2012. The Late Pleistocene evolution of palaeo megalake Bungunnia, southeastern Australia: A sedimentary record of fluctuating lake dynamics, climate change and the formation of the modern Murray River. Palaeogeography, Palaeoclimatology, Palaeoecology 317–318, 114–127.

McClay, K. & Dooley, T. 1995. Analogue models of pull-apart basins. Geology 23, 8, 711-714.

McMahon, T.A. & Finlayson, B.L. 2003. Droughts and anti-droughts: the low flow hydrology of Australian rivers. Freshwater Biology 48, 1147–1160.

McWhorter, D.B. & Sunada, D.K. 1977. Ground-water hydrology and hydraulics. Water Resources Publications LLC.

MDBA. 2010a. Assessing environmental water requirements Chapter 8 – Lower Darling River System. Murray-Darling Basin Authority, Canberra.

MDBA. 2010b. Guide to the proposed plan: overview. Murray-Darling Basin Authority, Canberra.

MDBA. 2011. Proposed basin plan. Murray-Darling Basin Authority, Canberra.

MDBA. 2012a. The proposed groundwater baseline and sustainable diversion limits: methods report. MDBA publication no. 16/12. Murray-Darling Basin Authority, Canberra.

MDBA. 2012b. Basin Plan – Water Act 2007. Commonwealth of Australia, Murray-Darling Basin Authority, Canberra.

MDBC. 2003. Preliminary investigations into observed River Red Gum decline along the River Murray below Euston. Technical Report 03/03, Murray-Darling Basin Commission.

MDBC. 2007. Water Audit Monitoring Report 2005/06. Murray-Darling Basin Commission.

Meinzer, O.E. 1923. The occurrence of groundwater in the United States with a discussion of principles. US Geological Survey Water Supply Paper 489, 321 pp.

Mensforth, L.J., Thorburn, P.J., Tyerman, S.D. & Walker, G.R. 1994. Sources of water used for riparian *Eucalyptus camaldulensis* overlying highly saline groundwater. Oecoloigia 100, 21-28.

Meredith, K.T., Hollins, S.E., Hughes, C.E., Cendon, D.I., Hankin, S. & Stone, D.J.M. 2009. Temporal variation in stable isotopes (^{18}O and ^{2}H) and major ion concentrations within the Darling River between Bourke and Wilcannia due to variable flows, saline groundwater influx and evaporation. Journal of Hydrology 378, 313-324.

Meyers, J.S. & Nordenson, T.J. 1962. Evaporation from the 17 western states with a section on evaporation rates. USGS, Professional Paper 272D, 67-99.

Miall, A.D. 1996. The geology of fluvial deposits. Springer, Berlin, 582 pp.

Miller, G.H., Fogel, M.L., Magee, J.W., Gagan, M.K., Clarke, S.J. & Johnson, B.J. 2005. Ecosystem collapse in Pleistocene Australia and a human role in megafaunal extinction. Science 309, 287-290.
Miller, G.H., Magee, J.W. & Jull, A.J.T. 1997. Low-latitude glacial cooling in the Southern Hemisphere from amino-acid racemization in emu eggshells. Nature 385, 241-244.
Miller, G.H., Magee, J.W., Johnson, B.J., Fogel, M.L., Spooner, N.A, McCulloch, M.T. & Ayliffe, L.K. 1999. Pleistocene extinction of *Genyornis newtoni*: human impact on Australian megafauna. Science 283, 205-208.
Miller, G.H., Mangan, J., Pollard, D., Thompson, S., Felzer, B. & Magee, J.W. 2005. Sensitivity of the Australian Monsoon to insolation and vegetation: Implications for human impact on continental moisture balance. Geology 33, 65–68.
Miller, A.J. & Gupta, A. 1999. Varieties of fluvial form. John Wiley & Sons, Chichester, UK, 521 pp.
Miranda, J.A., Wallace, M.W. & McLaren, S., 2008. The Norwest Bend Formation: implications for the evolution of Neogene drainage in southeastern Australia. Sedimentary Geology 205, 53–66.
Moench, A.F. & Barlow, P.M. 2000. Aquifer response to stream-stage and recharge variations. I. Analytical step-response functions. Journal of Hydrology, 192-210.
Moffitt, R. S. & Weatherall, G., 2004. Assessment of bore water Geochemistry - Darling basin, New South Wales. Geological Survey Report: GS2004/328. NSW Department of Mineral Resources.
Monteith, J. 1965. Evaporation and the environment. In: 19th Symposium of the Society of Experimental Biology. Cambridge, UK Cambridge University Press, 205-234.
Moore, P. 2005. Plants of inland Australia. New Holland Publishers, Sydney.
Moore, S. 2000. Menindee Lakes Ecologically Sustainable Development Project, Business Plan. Report to the Menindee Lakes Ecologically Sustainable Development Project Steering Committee, NSW Department of Land and Water Conservation, 35 pp.
Moore, S. & Midgley, T. 2002. The Menindee Lakes Ecologically Sustainable Development Project, Unpublished report (8 Volumes) to NSW DLWC, 1962 pp.
Morris, R.C. & Ramanaidou, E.R. 2007. Genesis of the channel iron deposits (CID) of the Pilbara region, Western Australia. Australian Journal of Earth Sciences 54, 5, 733-756.
Morton, S.R., Stafford Smith, D.M., Dickman, C.R., Dunkerley, D.L., Friedel, M.H., McAllister, R.R.J., Reid, J.R.W., Roshier, D.A., Smith, M.A., Walsh, F.J., Wardle, G.M., Watson, I.W. & Westoby, M. 2011. A fresh framework for the ecology of arid Australia. Journal of Arid Environments 75, 4, 313–329.
Mullen, I.C., Wilkinson, K.E., Cresswell, R.G. & Kellett, J. 2007. Three-dimensional mapping of salt store in the Murray-Darling Basin, Australia 2. Calculating landscape salt loads from airborne electromagnetic and laboratory data. International Journal of Applied Earth Observation and Geoinformation 9, 103-115.
Mullholand, C. S. J., 1940. Geology and Underground Water Resources of the East Darling District. NSW Department of Mines.
Munday T., Fitzpatrick, A., Noble, R., Berens, V., Hatch, M. & Cahill, K. 2006. The combined use of air, ground and 'in river' electromagnetics in defining spatial processes of salinisation across ecologically important floodplain areas - Lower River Murray, SA. Regolith 2006: Consolidation and Dispersion of Ideas, Proceedings of the CRC LEME Regolith Symposium, November 2006, CRC LEME, Perth, 249-255.
Munday, T.J., Overton, I., Fitzpatrick, A., Cahill, K., Berens, V., Hatch, M. & Brodie, R.C. 2007. Spatio-temporal monitoring of floodplain environments using electromagnetic methods: a scaled approach to understanding surface water- groundwater interactions on the Chowilla floodplain, South Australia. In: 20th SAGEEP, Denver.
Naiman, Z., Quade, J. & Patchett, P. J. 2000. Isotopic evidence for eolian recycling of pedogenic carbonate and variations in carbonate dust sources throughout the southwest United States. Geochimica et Cosmochimica Acta 64, 18, 3099–3109.
Nanson, G.C., Jones, B.G., Price, D.M. & Pietsch, T.J. 2005. Rivers turned to rock: Late Quaternary alluvial induration influencing the behaviour and morphology of an anabranching river in the Australian monsoon tropics. Geomorphology 70, 398–420.
Nanson, G.C., Price, D.M. & Short, S.A. 1992. Wetting and drying of Australia over the past 300 ka. Geology 20, 791–794.
Nanson, G.C., Rust, B.R. & Taylor, G. 1986. Coexistent mud braids and anastomosing channels in an arid-zone river: Cooper Creek, central Australia. Geology 14, 175–178.

Nanson, G.C. & Tooth, S. 2011. Why are Australian rivers so unusual? Conference program and abstracts. 14th Australian & New Zealand Geomorphology Group Conference, Oamaru, New Zealand 2011, 56.
Naylor, M.A., Mandl, G. & Sipjesteijn, C.H.G. 1986. Fault geometries in basement-induced wrench faulting under different initial stress states. Journal of Structural Geology 8, 7, 737-752.
Neef, G. 2005. Devonian–Carboniferous structure at MacCullochs Range, and the recognition and tectonics of the Darling Basin Conjugate Fault System showing the switching of the directions of principal horizontal stress. Australian Journal of Earth Sciences 52, 315–326.
Neef, G. 2007. Early Devonian synorogenic alluvial fan deposits of the MacCullochs Range, western New South Wales. Australian Journal of Earth Sciences 54, 647–660.
Neef, G. 2012. Mid Silurian–Carboniferous tectonic and depositional history of the Darling Basin conjugate fault system, western New South Wales: Overview. Australian Journal of Earth Sciences 59, 91-117
Neton, M.J., Dorsch, J., Olsen, C.D. & Young, S.C. 1994. Architecture and directional scales of heterogeneity in alluvial fan aquifers. Journal of Sedimentary Research B64, 245-257.
Newman, B.D., Osenbruck, K., Aeschbach-Hertig, W., Solomon, D.K., Cook, P., Rozanski, K. & Kipfer, R. 2010. Dating of 'young' groundwaters using environmental tracers: advantages, applications and research needs. Isotopes in Environmental and Health Studies 46, 3, 259-278.
NHMRC-NRMMC. 2011. Australian Drinking Water Guidelines Paper 6. National Water Quality Management Strategy. National Health and Medical Research Council, National Resource Management Ministerial Council, Commonwealth of Australia, Canberra.
Nicol, J.M. 2004. Vegetation dynamics of the Menindee lakes with reference to the seed bank. PhD Thesis, University of Adelaide.
NOW. 2010. Management of the 2010 flood event in the Menindee Lakes System. Sydney, NSW Office of Water.
NOW. 2011. Summary report - Management of the Barwon-Darling floods of December 2010-April 2011. Sydney, NSW Office of Water.
NOW. 2012a. Water Sharing Plan for the Lower Murray-Darling Basin unregulated and alluvial water sources – Background document. NSW Office of Water.
NOW. 2012b, Draft Water Sharing Plan for the Barwon-Darling unregulated and alluvial water sources – order. NSW Office of Water.
NOW. 2012c. Water Sharing Plan for the Murray-Darling porous rock groundwater sources – Background document. NSW Office of Water.
NOW. 2012d. Water Sharing Plan for the Barwon-Darling unregulated and alluvial water sources – Background document. NSW Office of Water.
NRMMC-EPHC–NHMRC. 2008. Australian Guidelines for Water Recycling: Managing Health and Environmental Risks. Phase 2A: Augmentation of drinking water supplies. Environment Protection and Heritage Council, National Health and Medical Research Council, and Natural Resource Management Ministerial Council www.ephc.gov.au/taxonomy/term/39.
NRMMC-EPHC–NHMRC. 2009. Australian Guidelines for Water Recycling: Managing Health and Environmental Risks. Phase 2C: Managed aquifer recharge. Environment Protection and Heritage Council, National Health and Medical Research Council, and Natural Resource Management Ministerial Council www.ephc.gov.au/taxonomy/term/39.
Odeh, I.O.A. & Onus, A. 2008. Spatial analysis of soil salinity and soil structural stability in a semiarid region of New South Wales, Australia. Environmental Management 42(2), 265-278.
Ollier, C.D. 1991. Ancient landforms. Belhaven Press, London.
Omuto, C.T. 2011. A new approach for using time-series remote-sensing images to detect changes in vegetation cover and composition in drylands: a case study of eastern Kenya. International Journal of Remote Sensing 32, 6025-6045.
O'Neill, D.J. & Beckham, J. 1995. Menindee Lake Geophysical Survey. NSW Department of Land and Water Technical Services Division.
O'Sullivan, P.B., Kohn, B. & Mitchell, M.M. 1998. Phanerozoic reactivation along a fundamental Proterozoic crustal fault, the Darling River Lineament, Australia: Constraints from apatite fission track thermochronology. Earth and Planetary Science Letters, 164, 451-465.
Overton, I.C., Jolly, I.D., Slavich, P.G., Lewis, M.M. & Walker, G.R. 2006. Modelling vegetation health from the interaction of saline groundwater and flooding on the Chowilla floodplain, South Australia. Australian Journal of Botany 54, 207-220.

Page, D., Barry, K., Levett, K., Vanderzalm, J., Miotlinski, K. & Dillon, P. 2010. Broken Hill aquifer storage and recovery and infiltration laboratory column studies. CSIRO: Water for a Healthy Country National Research Flagship.
Page, K., Dare-Edwards, A., Nanson, G. & Price, D. 1994. Late Quaternary evolution of Lake Urana, New South Wales, Australia. Journal of Quaternary Science 9, 47–57.
Page, K.J., Kemp, J. & Nanson, G.C. 2009. Late Quaternary evolution of Riverine Plain paleochannels, southeastern Australia. Australian Journal of Earth Sciences 56, S1, S19-S33.
Page, K.J. & Nanson, G.C. 1996. Stratigraphic architecture resulting from Late Quaternary evolution of the Riverine Plain, southeastern Australia. Sedimentology 43, 927–945.
Page, K.J., Nanson, G.C. & Price, D. 1996. Chronology of Murrumbidgee River palaeochannels on the Riverine Plain, southeastern Australia. Journal of Quaternary Science 11, 311–326.
Pain, C.P. 2012. Old, flat and red – Australia's distinctive landscape. In: Blewett R.S. (ed.) Shaping a Nation: A Geology of Australia. Geoscience Australia and ANU E Press, Canberra, 226-275.
Pain, C.F. & Ollier, C.D. 1995. Inversion of relief—A component of landscape evolution. Geomorphology 12, 151–165.
Palamara, D., Rodriguez, V., Kellett, J. & Macaulay, S. 2010. Salt mapping in the Lower Macquarie area, Australia, using airborne electromagnetic data. Environmental Earth Sciences 61, 3, 613-623.
Pardoe, C., 2003. The Menindee Lakes: A regional archaeology. Australian Archaeology 57, 42-53.
Pardoe, C. & Martin, S. 2002 The nature and distribution of archaeology at the Menindee Lakes. Unpublished report to New South Wales Department of Land and Water Conservation.
Parrish, J.T., Peterson, F. & Turner, C.E. 2004. Jurassic "savannah" – plant taphonomy and climate of the Morrison Formation (upper Jurassic, western USA). Sedimentary Geology 167, 137–162.
Parsons, M.L. 1970. Groundwater thermal regime in a glacial complex. Water Resources Research 6, 1701-1720.
Pels, S. 1964. The present and ancestral Murray River system. Australian Geographical Studies 2, 111–119.
Penman, H.L. 1948. Natural evaporation from open water, bare soil and grass. Proceedings of the Royal Society, A193, 120-145.
Peterson, F. 1980. Sedimentology of the uranium-bearing Salt Wash Member and Tidwell Unit of the Morrison Formation in the Henry and Kaparowits Basins, Utah. Proceedings of the Henry Mountains Symposium, Utah Geological Association, 305-322.
Plummer, L.N., McConnell, J.B., Busenberg, E., Drenkard, S., Schlosser, P. & Michel, R.L. 1998a. Flow of river water into a karstic limestone aquifer 1. Tracing the young fraction in groundwater mixtures in the Upper Floridan aquifer near Valdosta, Georgia. Applied Geochemistry 13, 995-1015.
Plummer, L.N., Busenberg, E., Drenkard, S., Schlosser, P., McConnell, J.B., Michel, R.L., Ekwurzel, B. & Weppernig, R. 1998b. Flow of river water into a karstic limestone aquifer 2. Dating the young fraction in groundwater mixtures in the Upper Floridan aquifer near Valdosta, Georgia. Applied Geochemistry 13, 1017-1043.
Podger, G.M. 2010. Darling Water Savings: Options for environmental filling, CSIRO: Water for a Healthy Country National Research Flagship, CSIRO, Australia, 31 pp.
Podger, G.M. 2011. Darling water savings: Options for environmental filling. No impacts, version 2, CSIRO: Water for a Healthy Country National Research Flagship, CSIRO, Australia, 30 pp.
Porteners, M.P. & Ashby, E.M. 1996. Plants of Pooncarie and the Willandra Lakes. Sydney, Royal Botanic Gardens.
Prosser, I.P., Rutherfurd, I.D., Olley, J.M., Young, W.J., Wallbrink, P.J. & Moran, C.J. 2001. Large-scale patterns of erosion and sediment transport in river networks, with examples from Australia. Marine and Freshwater Research 52, 81–99.
Quigley, M.C., Cupper, M.L. & Sandiford, M. 2006. Quaternary faults of south-central Australia: Palaeoseismicity, slip rates and origin. Australian Journal of Earth Sciences 53, 285-301.
Radke, B.M. 1990. Sedimentology and diagenesis of the Renmark Group aquifer in Hatfield-1, Murray Basin. Groundwater Series No. 18, Bureau of Mineral Resources, Australia, Record 1990/1.
Rasmussen, W.C. & Andreasen, G.E. 1959. Hydrologic budget of the Beaverdam Creek Basin, Maryland. US Geological Survey Water Supply Paper 1472, 106 pp.
Rau, G.C., Andersen, M.S., McCallum, A.M. & Acworth, R.I. 2010. Analytical methods that use natural heat as a tracer to quantify surface water-groundwater exchange, evaluated using field temperature records. Hydrogeology Journal 18, 1093-1110.

Reid, J., Eade, R. & Kemp, T. 2009. SkyTEM final processed data: Broken Hill Managed Aquifer Recharge Project Part B. Geoforce Report to Geoscience Australia, 158 pp.
Remenda, V.H., van der Kamp, G. & Cherry, J.A. 1996. Use of vertical profiles of $\delta^{18}O$ to constrain estimates of hydraulic conductivity in a thick, unfractured aquitard. Water Resources Research 32, 2979.
Restrepo, J.D. & Sergio, A.L. 2008. Morphodynamics of the Pacific and Caribbean deltas of Colombia, South America. Journal of South American Earth Sciences 25, 1–21
Reynolds, S.D., Mildren, S.D., Hillis, R.R. & Meyer, J.J. 2006. Constraining stress magnitudes using petroleum exploration data in the Cooper-Eromanga Basins, Australia. Tectonophysics 415, 123–140.
Ritman, K.T. 1995. Structural vegetation data: a specifications manual for the Murray Darling Basin Project M305.
Roach, I.C. (ed.). 2012. The Frome airborne electromagnetic survey, South Australia: implications for energy, minerals, and regional geology. Geoscience Australia Record 2012/40.
Roberts, J. 2012. Trees and shrubs for inundation modelling at Menindee Lakes and their water regime specifications. Advisory report for Geoscience Australia.
Roberts, J. & Marston, F. 2000. Water regime of wetland and floodplain plants in the Murray-Darling Basin: A source book of ecological knowledge. CSIRO Land and Water. Technical Report 30/00. October 2000.
Roberts, J. & Marston, F. 2011. Water regime for wetland and floodplain plants: a source book for the Murray–Darling Basin. National Water Commission, Australia, Canberra, pp 170.
Robinson, J.W. & McCabe, P. J. 1997. Sandstone-body and shale-body dimensions in a braided fluvial system: Salt Wash Sandstone Member (Morrison Formation), Garfield County, Utah. American Association of Petroleum Geologists Bulletin 81, 8, 1267-1291.
Robinson, J.W. & McCabe, P. J. 1998. Evolution of a braided river system: Salt Wash Sandstone Member of the Morrison Formation (Jurassic) in southern Utah. Society of Economic Paleontologists and Mineralogists Special Publication 59, 93-107.
Rohwer, C. 1931. Evaporation from free water surfaces. US Department of Agriculture, Technical Bulletin 271, 96 pp.
Rood, S.B. & Heinze-Milne, S. 1989. Abrupt downstream forest decline following river damming in southern Alberta. Canadian Journal of Botany 67, 1744-1749.
Roy, P.S. & Whitehouse, J. 2003. Changing Pliocene sea levels and the formation of heavy minerals beach placers in the Murray Basin, Southeastern Australia. Economic Geology 98, 975-983.
Ruprecht, J.K. & Schofield, N.J. 1991. Effects of partial deforestation on hydrology and salinity in high salt storage landscapes. I. Extensive block clearing. Journal of Hydrology 129, 1–4, 19–38.
Rural Water Commission, 1991. Mildura Hydrogeological Map (1:250 000 scale). Murray Basin Hydrogeological Map Series. Canberra, Australian Geological Survey Organisation.
Sandiford, M. 2003. Neotectonics of southeastern Australia: linking the Quaternary faulting record with seismicity and in situ stress. In: Hillis, R.R. & Muller, D. (eds), Evolution and dynamics of the Australian Plate. Geological Society of Australia, Special Publication, 22, 101-113.
Sandiford, M. & Quigley, M. 2009. Topo-Oz: Insights into the various modes of intraplate deformation in the Australian continent. Tectonophysics, 474, 405-416.
Scarborough, R.B. & Pierce, H.W. 1978. Late Cenozoic basins of Arizona. New Mexico Geological Society. Guidebook, 29th Field Conference., Land of Cochise, 253-259.
Schreurs, G. 1994. Experiments on strike-slip faulting and block rotation. Geology 22, 567-570.
Schubert, J. 2002. Hydraulic aspects of riverbank filtration—field studies. Journal of Hydrology 266, 145–161.
Schumm, S.A. 1960. The shape of alluvial channels in relation to sediment type. USGS Professional Paper 252B, 17-30.
Schumm, S.A. 1977. The fluvial system. John Wiley & Sons, New York, 338 pp.
Sear, D.A., Armitage, P.D. & Dawson, F.H. 1999. Groundwater dominated rivers. Hydrological Processes 13, 255-276.
Segall, P. & Pollard, D.D. 1980. Mechanics or discontinuous faults. Journal of Geophysical Research 85, 4337-4350.
Sena Gomes, A.R. & Kozlowski, T.T. 1980. Effects of flooding on *Eucalyptus camaldulensis* and *Eucalyptus globulus* seedlings. Oecoloigia 46, 139-142.

Shulka, U.K., Singh, I.B., Sharma, M. & Sharma, S. 2001. A model of alluvial megafan sedimentation: Ganga Megafan. Sedimentary Geology 144, 243-262.
Silliman, S.E. & Booth, D.F. 1993. Analysis of time-series measurements of sediment temperature for identification of gaining vs. losing portions of Juday Creek, Indiana. Journal of Hydrology 146, 131-148.
Sims, N.C. & Thoms, M.C. 2002. What happens when flood plains wet themselves: Vegetation response to inundation on the lower Balonne flood plain. IAHS-AISH Publication - The structure, function and management Implications of fluvial sedimentary systems 276, 195-202.
Singh, M., Singh, I.B. & Müller, G. 2007. Sediment characteristics and transportation dynamics of the Ganga River. Geomorphology 86, 144–175.
Skelly, R.L., Bristow, C.S. & Ethridge, F.G. 2003. Architecture of channel-belt deposits in an aggrading shallow sandbed braided river: the lower Niobrara River, northeast Nebraska. Sedimentary Geology 158, 249–270.
SKM. 2009a. Darling River Water Savings Project - Part B, Stage 1 – Preliminary environmental issues of Part A schemes. Technical Report for the NSW Department of Water and Energy.
SKM. 2009b. Assessment of evaporation losses from the Menindee Lakes using SEBAL remote sensing technology. Report to the National Water Commission, Australia, 40 pp.
SKM. 2010. Darling River water saving project – Part B draft final report (unpublished). Report for NSW Office of Water and Department of the Environment, Heritage and the Arts.
Smith, D.G. 1986. Anastomosing river deposits, sedimentation rates, and basin subsidence, Magdalena River, northwestern Columbia, South America. Sedimentary Geology 46, 177-196.
Smith, K. & Watkins, N., 1993. Border to the Barrages - Natural resource criteria for sustainable irrigation on the River Murray. River Murray Water Resources Committee.
Smith, N.D. 1971. Transverse bars and braiding in the Lower Platte River, Nebraska. Geological Society of America Bulletin 82, 3407-3420.
Smith, S.D. Wellington, A.B., Nachlinger, J.I. & Fox, C.A. 1991. Functional responses of riparian vegetation to streamflow diversion in the eastern Sierra Nevada. Ecological Applications 1, 89-97.
Somerville, P., Brodie, R.S., Gow, L., Halas, L. & Apps, H.E. 2012. BHMAR Project Appendix 6: Hydrological, climate, hydrochemical and hydrodynamic data. Geoscience Australia Record 2012/17. Geocat 73824.
Sophocleous, M. 2002. Interactions between groundwater and surface water: the state of the science. Hydrogeology Journal 10, 52–67.
Spies, B. & Woodgate, P. 2005. Salinity mapping methods in the Australian context. Land and Water Australia, Department of the Environment and Heritage; and Agriculture Fisheries and Forestry, 236 pp. http://www.nrm.gov.au/publications/salinity-mapping
Spulak, R., Schoning, G., Halas, V., Long, R., Rousseau, J. & Clarke, J.D.A. 2012. BHMAR project Appendix 2: Core photographs. Geoscience Australia Record 2012/17. Geocat 73824.
Stannard, M. E., 1981. Irrigation Development between Wentworth and Menindee. NSW Department of Water Resources.
Steinfeld, C. & Kingsford, R.T. 2008. Floodplain development and vegetation health on the Macquarie River floodplain of the Murray–Darling Basin. University of New South Wales, Sydney.
Stephenson, A.E. 1986. Lake Bungunnia: a Plio-Pleistocene megalake in southern Australia. Palaeogeography, Palaeoclimatology, Palaeoecology 57, 2-4, 137-156.
Stevenson, J., Gillespie, R., Hope, G., Jacobsen, G., Fallon, S. & Levchenko, V. 2010. The archaic and puzzling record of Lake Xere Wapo, New Caledonia. In: Haberle, S., Stevenson, J. & Prebble, M. (eds) Altered Ecologies: fire, climate and human influence on terrestrial landscapes. Terra Australis 32, 381-393.
Stone, C. 1993. Insect pest problems of eucalypt plantations in Australia, 2: New South Wales. Australian Forestry 56, 363-369.
Suarez, B.E.S. 2004. The Sinu river delta on the northwestern Caribbean coast of Colombia: Bay infilling associated with delta development. Journal of South American Earth Sciences 16, 623–631.
Suarez, J.C., Ontiveros, C., Smith, S.D. & Snape, S. 2005. Use of airborne LiDAR and aerial photography in the estimation of individual tree heights in forestry. Computers and Geosciences 31, 253-262.
Sylvester, A.G. 1985. Strike-slip faults. Geol. Soc. America Bull. 100, 1666-1703.
Tamers, M.A. 1975. Validity of radiocarbon dates on ground water. Geophysical Surveys 2, 2, 217-239.

Tan, K.P., Clarke, J.D.A., Halas, L., Lawrie, K.C., Apps, H.E., Brodie, R.C., Costelloe, M., Sumner, J., Fell-Smith, S., Christensen, N.B., Schoning, G.L., Halas, V. & Lewis, S.J. 2012. Northern Territory Coastal Plain: Mapping seawater intrusion in coastal plain aquifers using airborne electromagnetic data. Geoscience Australia Record, 2012/41, Canberra. 218 p.

Tan, K.P., Apps, H., Halas, L., Gibson, D. & Lawrie, K. 2005. Utilizing airborne electromagnetic data to model the subsurface salt load in a catchment, Bland Basin, NSW. In: Zerger, A. & Argent, R.M. (eds) MODSIM 2005 International Congress on Modelling and Simulation. Modelling and Simulation Society of Australia and New Zealand, December 2005, 1478-1484. http://www.mssanz.org.au/modsim05/papers/ascough_1.pdf

Tate, R. 1885. Notes on the physical and geological features of the basin of the Lower Murray River. Transactions of the Royal Society of South Australia 7, 1–26.

Taylor, P.J., Walker, G.R., Hodgson, G., Hatton, T.J. & Correll, R.L. 1996. Testing of a GIS model of *Eucalyptus largiflorens* health on a semiarid, saline floodplain. Environmental Management 20, 553-564.

Taylor-Wood, E., McCormick, S., Mueck, S., Richardson, M. & Jukic, M. 2001. Report for the Menindee Lakes Ecologically Sustainable Development Project Steering Committee. Vegetation/habitat mapping of inundated areas of Menindee Lakes. Project no: 3445.

Tedford, R.H. 1967. The fossil Macropodidae from Lake Menindee, New South Wales. University of California. Publications in Geological Sciences 64, 116 pp.

Theiss Services. 2002. Topographic survey of Lake Wetherell. Report to the Menindee Lakes Ecologically Sustainable Development Project Steering Committee, NSW Department of Land and Water Conservation, 35 pp.

Thomas, D.S.G. 1997. Arid environments: their nature and extent. In: Thomas, D.S.G. (ed.) Arid zone geomorphology: Process, form and change in drylands. 2nd ed. Wiley, Chichester,. 3–12

Thoms, M.C., Sheldon, F., Roberts, J., Harris, J. & Hillman, T.J. 1996. Scientific panel assessment of environmental flows for the Barwon–Darling River. NSW Department of Land and Water Conservation, Sydney, 180 pp.

Thoms, M.C. & Sheldon, F. 2000. Water resource development and hydrological change in a large dryland river: the Barwon–Darling River, Australia. Journal of Hydrology 228, 10–21.

Thoms, M., Sheldon, F. & Crabb, P. 2004. A hydrological perspective on the Darling River. In: Breckwoldt, R., Boden, R. & Andrew, J. (eds) The Darling. Murray-Darling Basin Commission, Canberra.

Tickell, S.J. & Humphrys, W.G. 1980. Preliminary report on the hydrogeology of the Victorian part of the Riverine Plain. Geological Survey of Victoria, Report 1980/71.

Tooth, S. & Nanson, G.C. 1995. Anabranching rivers on the northern plains of arid central Australia. Geomorphology 29, 3–4, 211–233.

Tooth, S. 2000. Process, form and change in dryland rivers: a review of recent research. Earth-Science Reviews 51, 67–107.

Turney, C.S.M, Bird, M.I., Fifield, L.K., Roberts, R.G., Smith, M.A., Dortch, C.E., Grun, R., Lawson, E., Ayliffe, L.K., Miller, G.H., Dortch, J., & Cresswell, R.G. 2001a. Early human occupation at Devil's Lair, southwestern Australia 50,000 years ago. Quaternary Research 55, 3-13.

Turney, C.S.M., Haberle, S., Fink, D., Kershaw, A.P., Barbetti, M., Barrows, T.T., Black, M., Cohen, T.J., Correge, T., Hesse, P.P., Hua, Q., Johnston, R., Morgan, V., Moss, P., Nanson, G., Van Ommen, T., Rule, S., Williams, N.J., Zhao, J.-X., D'costa, D., Feng, Y-X., Gagan, M., Mooney, S. & Xia, Q. 2006. Integration of ice-core, marine and terrestrial records for the Australian Last Glacial Maximum and Termination: a contribution from the OZ INTIMATE group. Journal of Quaternary Science 21, 751–761.

Turney, C.S.M., Kershaw, A.P., Moss, P., Bird, M.I., Fifield, L.K., Cresswell, R.G., Santos, G.M., di Tada, M.L., Hausladen, P.A. & Zhou, Y. 2001b. Redating the onset of burning at Lynch's Crater (North Queensland): implications for human settlement in Australia. Journal of Quaternary Science 16, 767-771.

VEAC. 2006. River Red Gum forests investigation discussion paper. Victorian Environmental Assessment Council, Melbourne.

Vekerdy, Z. & Meijerink, A.M.J. 1998. Statistical and analytical study of the propagation of flood-induced groundwater rise in an alluvial aquifer. Journal of Hydrology 205, 112-125.

Vogel, J.C. 1966. Investigations of groundwater flow with radiocarbon. Proceedings of Symposium on Isotope Hydrology, 1966. IAEA Vienna, 355-367.

Volcani, A., Karnieli, A. & Svoray, T. 2005. The use of remote sensing and GIS for spatio-temporal analysis of the physiological state of a semi-arid forest with respect to drought years. Forest Ecology and Management 215, 239-250.
Wagenseil, H. & Samimi, C. 2007. Woody vegetation cover in Namibian savannahs: A modelling approach based on remote sensing. Erdkunde 61, 325-334.
Walker, R.G. & Cant, D.J. 1984. Sandy fluvial systems. In: Walker, R.G. (ed.) Facies Models, Second Edition, Geoscience Canada Reprint Series 1, Geological Association of Canada Publications, Toronto, Canada, 71-89.
Walker, G.R. & Cook, P.G. 1991. The importance of considering diffusion when using carbon-14 to estimate groundwater recharge to an unconfined aquifer. Journal of Hydrology 128, 41-48.
Walker, G., Cresswell, R., Munday, T. & Liddicoat, C. 2004. South Australian salinity mapping and management support project: final report (overall project summary report), South Australia. Department of Water, Land and Biodiversity Conservation. Report, DLWBC 2004/39.
Walling, D.E. & Webb, B.W. 1983. Patterns of sediment yield. In: Gregory, K. J. (ed.) Background to Palaeohydrology. Wiley, Chichester, UK, 69-100.
Webb, McKeown & Associates. 2007. State of the Darling Interim Hydrology Report. Murray-Darling Basin Commission, Canberra, MDBC Publication No. 07/07, 61 pp.
Wen, L., Ling, J., Saintilan, N. & Rogers, K. 2009. An investigation of the hydrological requirements of River Red Gum (*Eucalyptus camaldulensis*) forest: using classification and regression tree modelling. Ecohydrology 2, 143-155.
Westbrooke, M., Leversha, J. & Kerr, M. 2004. The vegetation of the Darling River. In: Breckwoldt, R., Boden, R. & Andrew, J. (eds) The Darling. Murray-Darling Basin Commission, Canberra.
White, W.N. 1932. A method of estimating groundwater supplies based on discharge by plants and evaporation from soil – results of investigations in Escalante Valley, Utah. US Geological Water Supply Paper 659, 106 pp.
Willcox, J. B., Yeates, A. N., Meixner, A. J. & Shaw, R. D., 2003. Structural Evolution and Potential Petroleum Plays in the Darling Basin: Pondie Range Trough-Mount Jack Area: Based on a Seismic Sequence Analysis. GA Record. Canberra, Geoscience Australia.
Williams, N.J., Harle, K.J., Gale, S.J. & Heijnis, H. 2006. The vegetation history of the last glacial–interglacial cycle in eastern New South Wales. Australian Journal of Quaternary Science 21, 735–750.
Williams, R. M. & Beckham, J., 1995. Stream/Aquifer Interactions Along the Lower Darling River, NSW. NSW Department of Water Resources.
Withers, M. 1994. Flooding and water conservation in the Great Anabranch of the Darling River. (Unpublished)
Withers, M. 1996. The Talyawalka Creek and associated lakes. (Unpublished)
Witter, D. 2009. Lake Bed Archaeological Survey for Menindee, Cawndilla and Pamamaroo Lakes.
Wohling, D.L., Leaney, F.W. & Crosbie, R.S. 2012. Deep drainage estimates using multiple linear regression with percent clay content and rainfall. Hydrology and Earth Systems Sciences, 16, 563-572.
Woodyer, K.D. 1978. Sediment regime of the Darling River. Proceedings of the Royal Society of Victoria 90: 139 – 147.
Woolley, D., Williams, R.M. & Varathan, S. 2004. New Water? - Groundwater supply for Wilcannia, NSW. Balancing the Basin. 9th Murray-Darling Basin Groundwater Workshop. Bendigo, Victoria, Murray-Darling Basin Commission.
Woolley, D.R. & Williams, R.M. 1978. Tertiary stratigraphy and hydrogeology of the eastern part of the Murray Basin, New South Wales. In: Storrier, R.R. & Kelly, I.D. (eds) The hydrogeology of the Riverine Plain of southeastern Australia. Australian Society of Soil Science, Riverina Branch, 45-65.
Wyrwoll, K.H. & Miller, G.H. 2001. Initiation of the Australian summer monsoon 14,000 years ago. Quaternary International 83–85, 119–128.
Young, A. & Young, R. (eds.). 2001. Soils in the Australian landscape. Oxford University Press, Melbourne.

Acknowledgements

The BHMAR Project was commissioned and managed by the Australian Government Department of Environment, Water, Heritage and the Arts (DEWHA), which subsequently became the Department of Sustainability, Environment, Water, Population and Communities (SEWPaC) and in turn the Department of the Environment. Through these changes, the project has been directed by Richard McLoughlin and Mary Harwood, and the project team would like to express their appreciation for their unwavering support. Current and former DoE staff, notably Lee Harris, Geraldine Cusack, Warren Sillick, Angela Robinson and Frank Cita are thanked for their marvellous efforts in facilitating the project, and providing clear guidance to the Geoscience Australia (GA) team.

The BHMAR project has involved a very significant data acquisition phase on a scale not undertaken on-shore by Geoscience Australia for >30 years. Moreover, the relatively short timeframes available for data acquisition challenged all involved, both within the formal Geoscience Australia project team as well as those who volunteered or were seconded from other parts of the organisation. Of course, none of these efforts would have been successful if it were not for the heroic efforts of a significant number of external participants, and it is the latter whom we wish to thank first.

External participants

The BHMAR project area is one of great cultural and environmental sensitivity. The guidance and practical assistance we received in this study from Noeline Ferguson, Coordinator at the Menindee Land Council (MLC), other Elders in the MLC, and members of the Indigenous Community is greatly appreciated. Noeline organised for members of the Indigenous community to assist with carrying out cultural and heritage assessments of field sites, and then provided staff to work in gruelling conditions, on both day and night shifts, as drilling field assistants. Dennis Sloan, Menindee Land Council Contractor, is particularly thanked for taking on so much of the workload helping with the drilling. Other MLC contractors also assisted with a range of other fieldwork activities, and their efforts are greatly commended.

Sarah Martin, Archaeologist, is thanked for providing initial introductions to the MLC and for carrying out the initial cultural heritage site assessments for the drilling. Wilfred Shawcross is also thanked for stepping in to provide additional advice and clearances on the cultural and heritage issues surrounding the drilling sites.

The drilling activities would not have taken place without the considerable efforts of two New South Wales (NSW) Agencies: the NSW Office of Water, and the NSW Land and Property Management Authority. Staff from both agencies pulled out all the stops to help us obtain the requisite licences for drilling in our tight timeframes, despite the extra workload that this produced. The assistance of Peter Winton from the NSW Office of Water in Buronga, and the team of Shaun Baker, Donna Basham and Elizabeth Burke from the NSW Land and Property Management Authority are particularly thanked for working extra time for us to obtain the clearances we required. The guidance and assistance from the local NSW and Country Energy/Water staff at Menindee is also greatly appreciated. Barry Philp is particularly thanked for his on-going willingness to assist in all practical ways.

The assistance of local landowners, too numerous to mention individually, has been critical to the success of the field program. Without their support for the project, we could not have completed the field program in the allotted timeframe. However, Sandy Crombie needs special mention. As Idleview property owner, Sandy provided accommodation in Menindee when we were working in more remote locations. Sandy has gone above and beyond the call of duty with her assistance in providing accommodation for the field parties travelling to Menindee. The Menindee Hotel and Motel are also thanked for showing great flexibility in accommodating to our evolving field program. Richard Unsworth, from the Grape Exchange provided fantastic assistance with storing the core in refrigeration containers while the core truck was in Canberra unloading. Landholders Stewart Oates and John Caskey provided land access and drilling-related earthworks and rehabilitation on their own land.

AEM data acquisition can be fraught with delays, and was recognised as a significant project risk. So it is with great pleasure that we can thank the team from Geoforce (ably supported by HeliWest), who delivered a

high quality AEM dataset in record time. We would like to thank Eric Wedepohl and the field crews and data processing team in Perth for running a very professional field operation. James Reid is particularly thanked for his technical and scientific advice to members of the project team, and for going that extra step to identify and solve issues as they arose.

It is a credit to the Boart Longyear Company that they have been able to carry out such a large sonic drilling program in a short period of time using such a relatively new technology in difficult drilling conditions. Ken Patterson and Scott Barnes are thanked for their excellent communication and flexibility in delivering this program. The efforts of the various drillers, particularly Denzel and Mike who flew in from the USA to lead the drilling teams with great skill and tenacity in completing the program in exhausting conditions. Simon Barwald and Duncan Black (formerly of Boart Longyear) provided drilling services.

Compression of various field activities into a remarkably short timeframe meant that Geoscience Australia had to enlist the assistance of geological contractors to assist with drilling activities. David Jenkins, CEO of Terrasearch, provided enormous support by supplying contractors, sometimes within 24 hours. David Tognon, Contract Geologist/Hydrogeologist worked on both the sonic rig as the onsite Geologist and on the mud rig for drilling and development of the bores. He worked tirelessly in intense conditions from mid November 2009 through to March 2010. Kevin D'Arcy, Contract Geologist worked on both the sonic rig as the onsite Geologist and the mud rig in some of the hottest weeks Menindee saw that summer, November and December 2009. They provided reliable and always friendly and professional service, and their efforts are greatly appreciated.

Congratulations go to Terry O'Shaughnessy and the rest of the Impax Group team for successfully organising and implementing the pump tests at the Jimargil site, providing such critical data for our assessments. Rod Harwood (Environmental Strategies) provided a wealth of experience in pump test operation and data interpretation. Lucy Lytton and Anne Riesz took time out from their busy schedules at the Murray-Darling Basin Authority (MDBA) to help out as on-site hydrogeologists during the pump tests as well as subsequent water sampling. It was also comforting to have the hydrogeological experience of Mark Hocking (Hocking et al) during our field activities. Steve Hostetler (FrOGTech) helped crunch the numbers in terms of pump test analysis, as well as much-needed and timely contributions in hydrochemical, hydrographic and hydrological analysis.

When one of our geophysics team went off on paternity leave, it was with great relief that first CSIRO and then Zonge Engineering stepped in to assist. Kevin Cahill is thanked for giving up the delights of a Perth office for coming once more to Menindee in the heat of summer, while Kelly Keates, Managing Director of Zonge Engineering is thanked for providing the services of the excellent Nkhil Dhyan, at such short notice to assist with our borehole geophysical logging program. Kelly Keates, Simon Mann, Anton Khrapov (Zonge Engineering and Research Organisation) provided ground geophysical investigations. David Walsh (Vista Clara), Andrew Fitzpatrick (CSIRO), Mike Hatch and Kevin Cahill assisted with downhole geophysical logging.

Safety in the field is always a top concern and it was with great relief when we discovered the services of Complete Ute and Van hire, who supplied us on short notice with safe and fully kitted vehicles in excellent condition. Customer service was A1, and a credit to Rob and Steve Harris. Andrew Pressler (West State Training and agent for Complete Ute and Van Hire) assisted with vehicle hire and other field logistics.

We would also like to acknowledge the services of Justin and Brett Green, Tolbra Earthmovers, who provided contract services for the digging of pits for the sonic drilling and also assisted in the rehabilitation of the bores. Bernard Blore as well as Brett and Justin Green carried out drilling-related earthworks and rehabilitation. Nathan White, Roadmaster, Canberra, provided/providing storage of the core in refrigeration.

Staff from Aarhus University have come to the rescue at a couple of critical points in the project to date. Niels B. Christensen is particularly thanked for a massive effort in writing new inversion software and in developing procedures for calibrating and validating the AEM inversion products. Without Niels' efforts we would not have been able to reconcile the various strands of the project and would not have been able to develop a coherent hydrogeological conceptual model. At earlier stages in the project, Aarhus University also stepped in to re-process the datasets and carry out full inversions when necessary due to unforeseen

circumstances. The efforts of Esben Auken, Camilla Sorensen, Gianluca Fiandaca and Nikoli Foghed are greatly appreciated in these tasks. Niels Christensen's contribution to the write-up of the reports is also greatly appreciated. Jared Abraham (formerly USGS, now XRI Geophysics) also guided us through the intricacies of AEM data acquisition and its interpretation. Jared was also instrumental in moving forward our first foray into NMR logging, helping us make sense of all that data. His contribution to the reports is also greatly appreciated.

Importantly, we would be remiss not to mention the efforts and advice of member of the project steering committee. Peter Dillon from CSIRO is Australia's expert in MAR, and the team greatly appreciate the time he has taken to assist the project leadership team with scientific and technical guidance, and for his strong overall support for the project. Peter and Declan Page, Joanne Vanderzalm and Konrad Miotlinski (CSIRO) are also thanked for their contributions in MAR risk assessment, geochemical interpretation and numerical modelling. Mike Williams from NSW Office of Water, is also thanked for his uncompromising advice and constant reality checks! Andy Green is thanked for giving of his precious time for advice on all matters geophysical and for his participation in Steering Committee meetings. Phil Commander and Don Woolley provided the all-important peer reviews of Interim reports, while Phil also peer reviewed the final reports. The USGS is also greatly thanked for undertaking an exhaustive peer review of the BHMAR reports. Jodie Eimers is thanked for facilitating the process, while Jim Leenhouts coordinated the review by 14 USGS staff members. Addressing the review comments added significantly to the time required to finalise the reports, however the comments greatly improved the quality of the science within the reports, and the efforts of the USGS review team are to be highly commended.

GA volunteers and secondees

Delays in commencement of the project, compounded by delays in obtaining field clearances for drilling, meant that a number of extra Geoscience Australia staff were brought in from different corners of the organisation to assist with field and laboratory activities.

Raymond DeGraaf, Marine Mechanical Manager, Petroleum and Marine Division (PMD), has gone above and beyond providing staff and his own time to go into the field for us and to drive the core truck to and from Canberra/Menindee. Ray and his team continually came through for us whenever we had a need they always provided assistance even if it meant working extra hours and harder in their own jobs so that they could help us out. Ray also assisted in sourcing a refrigerated storage container to store the core at GA.

The efforts of those listed next, were essential for assisting with delivery of the field program: Andrew Hislop (PMD) assisted with driving the core truck as well as site preparation and clearances and rehabilitation of the bores; Dave Holdway (PMD) and Andre Clive (GEMD) also drove the core truck; Craig Wintle (PMD) was also a core truck driver and also assisted with the site preparation and clearances as well as rehabilitation of the bores; Mark Sharah (PMD) and Matthew Carey (PMD) assisted with borehole rehabilitation, data logging and water sampling; Anthony Schofield (OEMD) assisted us with a shift as the day time supervising Geologist on the sonic rig; Chris Consoli (PMD) assisted us with a shift as the night time supervising Geologist on the sonic rig; Gerard Stewart (OEMD) assisted with doing a shift on the site preparation and clearances as well as rehabilitation of the bores; Pauline English (GEMD) assisted us with a shift as the day time supervising Geologist on the sonic rig. Tehani Kuske helped out in all manner of activities while on her graduate rotation.

With a critical shortage of GIS staff, Greg Scott kindly volunteered the excellent services of Danielle Beaudreau, Kristen Knox and Brad Cook, all of whom put in many hours producing map figures that appear in this and other reports. The 3D visualisation (Worldwind) and movie fly-through team of James Navin, Michael de Hoog, Neil Caldwell and Michael O'Rourke are thanked for their considerable efforts in simplifying complex datasets and portraying these in an effective manner. Laurent Ailliers is greatly thanked for constructing the GoCAD model.

The 'Official' project team

The BHMAR report write-up team is recognized in the authorship of the individual reports. Within GA, current and former BHMAR Project Team members who contributed to interim reports and activities, but are

not authors in this report include: Aaron Davis, Yusen Ley-Cooper, Michael Smith, Rebecca Norman, Anthony Pressler, Luke Wallace, Martin Smith, Katherine Boston, Pauline English, Tim Ransley, and Kristen Cullen.

Most importantly, we would like to acknowledge the efforts of Tenai Luttrell, project coordinator, who played a pivotal role in being able to find staff and contract resources when all other efforts looked forlorn. Tenai coordinated the field resources to ensure that multiple field parties had flights and/or vehicles to get them safely to their destinations, and that they had a bed to sleep in when they arrived. Tenai also assisted with arranging drilling permissions, and with managing the project's financial resources. A stellar effort, and all that while working part-time. Tenai was also assisted by Kim Forbes, Samantha Murray, and Sally Moon. Kriton Glenn is thanked for stepping in as acting project leader for a 2 month period.

In the laboratories, Stuart McEwen (PMD Laboratory Manager and Project Leader), and his team provided a very professional service, designing effective workflows that have seen a very steady flow of results to the interpretation team. Stuart also provided assistance and direction with the lab analysis and arranged the Analytical Equipment Service Agreements. Christian Thun (Laboratory Manager, PMD) provided assistance and direction with the lab analysis of cores coming into GA. He also assisted with the recruitment of various lab assistants that were required due to the extra workload. Tony Watson (PMD Laboratory) supervised laboratory analysis, provided QA/QC on laboratory analysis, and supervised equipment procurement and maintenance, training and procedure development.

Alexandra Plazinska and Janice Trafford provided assistance in relation to pore fluid samples and core samples under very tight deadlines. Kylia Wall provided laboratory analysis assistance, training and procedure development, while Amber Green, Billie Poignand, Gregory O'Connell and Mathew Brown also provided sterling service in Geoscience Australia laboratory analysis. Jonathon Rousseau, Viktoria Halas and Rick Long assisted with core sampling, assisted by Ross Spulak and Gerhard Schoning, who also greatly assisted with fieldwork. Gerhard, Ross and Victoria also greatly assisted with preparation of Strater logs and cross-sections and preparation of Report Appendices. Liz Webber and Bill Pappas (Inorganic Geochemistry Laboratory) worked on XRF, XRD and ICP analysis of Broken Hill samples.

The efforts of Robert Apps, Contracts Manager in Geoscience Australia rate a special mention. Robert brought a wealth of experience to the tendering and the management of contracts in general, and he managed to streamline processes and ensure external contracts were implemented with no fuss delay. The late Trish Yates is also remembered for her efforts in shepherding this project through the financial and contracts side of things at the commencement of this project.

Murray Richardson is thanked for his very effective management of the AEM acquisition program, while Ian Atkinson and his team are thanked for carrying out the in-river surveys. Leo Lymburner and Elexis McIntyre are thanked for their terrific contribution to the Landsat processing and interpretation.

Phil Tickle and Hamish Anderson are also thanked for managing the LiDAR acquisition program, while Hamish, Jonah Sullivan and John Dawson are thanked for their work in determining the accuracy of the LiDAR dataset. Peter Maher assisted with obtaining land owner permissions and official clearances from the Land and Property Management Authority and NSW Office of Water and coordinated the cultural and heritage clearances. Tanya Fomin (OEMD) provided advice and information in relation to a possible Seismic Survey.

John Jaycock, Tim Ransley and Ross Spulak also spent an enormous amount of time in the field assisting with the drilling and water and groundwater sampling programs, while Heike Apps is thanked for foregoing family commitments, and virtually taking up residence at Menindee for several months prior to her retirement.

Jane Coram, and Matt Hayne at an earlier stage in the project, are thanked for helping to ensure the BHMAR team had the necessary internal resources to undertake this project.

Glossary

Aeolian. Applied to landforms or sedimentary materials which are formed or transported by the action of wind.

Aeolian. Wind depositional environments.

Airborne Electromagnetic (AEM). A geophysical survey method that measures the electromagnetic properties of geological material by use of geophysical sensors carried by airplane or helicopter. Electric conductivity and magnetic susceptibility are calculated, and because these properties vary depending on the nature of the rock, water saturation, salinity and other parameters, the resultant maps are used for estimation of the nature of underground rock Formations, ground water, contamination and other geological and environmental changes.

Alluvial/alluvium. Non-marine sediments deposited by the action of water.

Anabranch. A distributary channel divergent from a main stream and either rejoining downstream or remaining separate and diminishing in size until becoming indistinct.

Anastomosing Rivers. Have multiple, relatively stable, interconnecting channels.

Aquifer. A geological formation, group of formations or part of a formation which is sufficiently porous and permeable to store, and allow the movement of groundwater. Aquifers can also be defined in terms of yielding quantities of groundwater for consumptive use or for ecosystems.

Aquifer Storage and Recovery (ASR). ASR is a type of managed aquifer recharge (MAR) that involves the injection of water into a well for storage in an aquifer and recovery from the same well. The aquifer may be confined or unconfined.

Aquifer Storage, Transport and Recovery (ASTR). ASTR is a type of managed aquifer recharge (MAR) that involves injection of water into a well for storage in an aquifer and recovery from a different well, generally to provide additional water treatment.

Aquitard. Saturated geological unit that can store large volumes of water but cannot transmit significant quantities of water to production wells. Also can be called a 'confining bed'.

Bank Filtration. In bank filtration, groundwater is extracted from a well or caisson near or under a river or lake by inducing infiltration from the surface water body, thereby improving water quality.

Basement. Bedrock that underlies the geological materials of interest.

Bioturbation. The displacement and mixing of sediment particles by plants and animals.

Biogenic Carbonate. Calcium carbonate directly precipitated by biological processes, such as shells, corals.

Bore Yield. The amount of water that can be abstracted from a bore (either by pumping or natural artesian flow) over a specific time interval. Bore yields are usually measured in litres per second (L/s).

Cenozoic. Geological Era extending from 65.5 million years ago to the present.

Clast. A rock fragment or grain resulting from the breakdown of larger rocks.

Colluvial. Gravity deposits in slope depositional environments.

Conductivity (σ). How the earth or a geological Formation conducts electricity. Conductivity is usually measured in milli-Siemens per metre (mS/m). It is the reciprocal of resistivity.

Conductor. Used to describe anything in the ground more conductive than the surrounding geological material. Conductors are most often clays, graphite, metallic mineralization or saline groundwater.

Confined Aquifer. An aquifer that is overlain and underlain by impervious layers (aquitards), and is not associated with the water table.

Conjunctive Water Use. Coordinated management of surface-water and groundwater resources.

Core/coring. Drilling method that recovers intact samples of subsurface materials.

Crevasse. A crevasse is a break in a river levee through which flood waters and sediments split out onto the floodplain, forming a crevasse-splay deposit.

Darcian Vertical Infiltration. Vertical infiltration is determined by applying Darcy's Law which describes the flow of a fluid through a porous medium.

Deflation. Erosion of sediment and resultant ground-surface lowering by wind action.

Depth of Exploration. The maximum depth at which the geophysical system can detect the target and this maximum depth depends on a variety of characteristics. This term often refers to the resolution depth of the strongest conductive target.

Devonian. Geological Period extending from 416 to 359 million years.

Discharge (Groundwater). The flow of groundwater to surface water, bores, and between aquifers or the sea.

Discharge (Stream). Amount of water flowing in the stream.

Distributary. A stream that branches off and flows away from a main stream channel. Often called an anabranch in Australia.

Drawdown. Watertable lowering.

Electrical Conductivity (EC). The ability of electrical current to pass through a substance. EC is commonly used to estimate the amount of soluble salt in solution. EC measurements can be made with a range of devices on ground and stream water, soils, and soil-paste extracts. Units of electrical conductivity are commonly given in mS/m, dS/m or μS/cm; 100 mS/m = 1 dS/m = 1000 μS/cm. Here, S is the symbol for siemens, and the prefixes d is deci (10^{-1}), c is centi (10^{-2}), m is milli (10^{-3}) and μ is micro (10^{-6}).

Electromagnetic (EM). Comprised of a time-varying electrical and magnetic field. Radio waves are common electromagnetic fields. In geophysics, an electromagnetic system is one that transmits a time-varying primary field to induce eddy currents in the ground, and then measures the secondary field emitted by those eddy currents.

Ephemeral. Watercourses (streams) that are active for only a short period of time.

Exceedance Threshold. In water quality standards it is the limit between acceptable and unacceptable amounts of a particular water component or characteristic.

Extensional Fault. A normal fault characterised by vertical movement on an inclined plane that vertically thins and horizontally extends portions of the Earth's crust. In normal faults the hanging wall (rock above the fault plane) moves downward relative to the footwall (rock below the fault plane).

Facies. Characteristics or bodies of sediments recognised by the depositional environment.

Fault Scarp. A break in slope at the earth's surface caused by relative uplift along a fault.

Ferruginised. Geological material that has gained iron following its original formation. Commonly, iron-rich groundwater solutions may precipitate iron under favourable hydrochemical conditions.

Fiducial, or fid. Timing mark on a survey record. Originally these were timing marks on a profile or film; now the term is generally used to describe 1-second timing records in digital data and on maps or profiles.

Flood-out Lakes. Lakes adjacent to a stream that fill and empty via a connecting channel or channels.

Floodplain. A low-lying area adjacent to a river or stream subjected to inundation when that stream floods. Floodplains are often sites of deposition of fine-grained sediments.

Fluvial. River depositional environment.

Footprint This is a measure of the area of sensitivity under the aircraft of an airborne geophysical system; depends on the altitude of the system, the orientation of the transmitter and receiver, the separation between the receiver and transmitter, the conductivity of the ground and the strength of the contrasting anomaly.

Fractured Rock Aquifer. Aquifers that store groundwater in the fractures, joints, bedding planes and cavities of the rock mass.

Fuzzy-k Means. A statistical cluster-analysis method.

Gamma Logging. Down-hole geophysical logging techniques that maps the gamma radiation released by naturally occurring uranium, thorium and radioactive potassium.

Gaining Stream. A stream or river-reach into which groundwater flows via the stream bed and/or banks.

Geodynamics. Dynamics of the Earth produced by large-scale processes such as plate tectonics.

Geological Basement. Rock mass below a sedimentary platform or cover; or more generally, any rock below sedimentary rocks or sedimentary basins that are metamorphic or igneous in origin.

Geophysics. The study of the Earth by quantitative physical methods, such as magnetics, electromagnetics, gamma ray spectrometry (radiometrics), seismology and gravity.

Gigalitre (GL). 1000 megalitres or 1 billion litres

Glacial-Interglacial Cycles. Earth ice-age climate cycles that have seen ice-sheets advance (glacial) and contract (interglacial) on timescales of up to 100 thousand years over the past 2.5 million years.

Global Meteoric Water Line. Worldwide average relationship between hydrogen and oxygen isotope ratios in natural terrestrial waters.

Graben. A depressed or down-thrown block bounded on at least two sides by faults.

Groundwater. Water stored below ground that saturates the pore spaces, cavities or fractures within geological material. The upper surface of this saturated zone is the water table.

Groundwater Management Unit. A hydraulically connected groundwater system that is defined and recognised by Australian State and Territory agencies for management purposes.

Groundwater Models. Simulations of groundwater flow or other groundwater characteristics. **Numerical groundwater models** use mathematical equations to simulate the hydraulics of groundwater flow processes.

Groundwater Mounding. Outward and upward expansion of the watertable caused by water injection.

Half-Graben. An asymmetric depressed or down-thrown block bounded on only one side by a fault.

Hazard. Something with the potential to cause harm. For example, salinity when above a health or other guideline threshold is considered a hazard when it has the potential to move or be moved to where it can threaten assets such as agriculture, infrastructure, water resources and biodiversity.

Head (or hydraulic head). A measurement of water pressure representing the total energy at the entrance of a piezometer. Usually measured as a water surface elevation. Differences in Head between two or more points can be used to determine the hydraulic gradient and direction of groundwater flow. Synonymous with Hydraulic Head.

Holocene. Most recent Geological Epoch extending from 12 000 years ago to the present.

Horst. A raised or up-thrown block bounded by faults or grabens, which remains stationary or is uplifted while the land has dropped on either side.

Hummocky Dunes. Low irregular dune forms.

Hydraulic Classes. Hierarchical grouping of sediments according to their hydraulic properties.

Hydraulic Conductivity (K). Hydraulic conductivity is the volume of water flowing through a 1 m^2 cross-sectional area of an aquifer under a hydraulic gradient of 1 m/1 m (100%) in a given time (usually 1 day).

Hydraulic Gradient. With regard to an aquifer, the rate of change of pressure head per unit of distance of flow at a given point and in a given direction.

Hydraulic loading. Increased head pressure due to increased water depth.

Hydrochemistry. Study of the chemical characteristics of water.

Hydrodynamics. Study of the motion of fluids, especially noncompressible fluids, under the influence of internal and external forces.

Hydrogeology. The study of geological properties of rocks, soils, and sediments as they relate to groundwater movement and storage.

Hydrogeophysics. Geophysical measurement of hydrological parameters and processes.

Hydrograph (Stream). Graphical representation showing the variation in time in the water level and/or flow in a surface water body.

Hydrograph (Bore). Graphical representation showing the variation in time in the groundwater level within a bore.

Hydrostratigraphy. The identification of mappable stratigraphic units on the basis of hydraulic properties (aquifer / aquitard).

Infiltration Basins or Ponds. Infiltration structures that are usually constructed off-stream where diverted surface water infiltrates (through an unsaturated zone) to the underlying unconfined aquifer.

Infrabasins. Bedrock sedimentary basins underlying the geological sequence of interest.

Inter-disciplinary Research. An interactive process whereby researchers work jointly, each drawing from their own discipline-specific perspective, to address a common research problem.

Inversion or Inverse Modelling. A process of converting geophysical data to an earth model; theoretical models iteratively compare the earth response to the data measured, until the model fits closely.

Isotope. A different chemical species of a chemical element with a different atomic mass. Used in hydrogeologic applications to date and understand the origin and evolution of groundwater.

Lacustrine. Lake depositional environments and deposits.

Laterally Constrained Inversion (LCI). A geophysical inversion process whereby the theoretical models are changed to fit the measured response along the direction of the flight path of an AEM survey.

Spatially Constrained Inversion (SCI). A geophysical inversion process whereby the theoretical models that are changed to fit the measured response a spatial sense (both horizontally and vertically).

Borehole-Constrained SCI (or LCI). A spatially constrained inversion whereby data from borehole conductivity logs are added to the starting SCI or LCI models.

Lateral Migration. Erosion and subsequent deposition of sand and gravel channel and bed-load by meandering rivers.

Lateral Infiltration. Horizontal movement of water from a river into its banks.

Layered Earth. A common geophysical model which assumes that the earth is horizontally layered – the physical parameters are constant to infinite distance horizontally, but change vertically.

Levees. Natural levees are raised banks adjacent to channels formed by initial rapid over-bank deposition of the coarsest suspended sediment during floods. Artificial levees are man-made flood-control embankments.

LiDAR. Light Detection And Ranging. A highly accurate topographic surveying method using an aircraft-founded laser scanner to measure variations in altitude.

Lineament. A linear feature in a landscape that expresses an underlying geological structure such as a fault.

Lithification. The process of consolidation, compaction and hardening to form rocks from sediments.

Lithology. Physical characteristics of a rock or sediment.

Local Meteoric Water Line. Relationship between hydrogen and oxygen isotope ratios in natural precipitation in a given area.

Losing Stream. A stream or river reach where the stream bed leaks surface water to an underlying aquifer.

Lunette. Elongated, crescent-moon shaped dune built up by wind on the downwind margin of a lake.

Macropore. Relatively large cavities in rock, soil or sediment; water flow is not impeded by capillarity.

Magnetic survey. Geophysical mapping of the distribution of magnetic materials in the earth. Magnetic surveys can be carried out on the ground or from aircraft (**Airborne**).

Managed Aquifer Recharge (MAR). The purposeful recharge of water to aquifers for subsequent recovery or environmental benefit.

Meanders. Tight bends in a river channel that can either be fixed or migrating.

Microfauna. Microscopic organisms.

Miocene. Geological Epoch extending from 23 to 5.3 million years ago.

Megalitre (ML). 1,000,000 litres.

Morphostratigraphic unit. A body of sediment that is identified primarily from the surface form it displays with such units including both landform and lithologic information in their definition.

Multi-disciplinary Research. A sequential process whereby researchers in different disciplines work independently, each from their own discipline-specific perspective, with a goal of eventually combining efforts to address a common research problem.

Neotectonics. Study of current or recent motions and deformations of the Earth's crust.

Nick Point. A point at which there is a sudden break of slope in the long profile of a river.

Noise. That part of a geophysical signal that is being measured that is derived internal to the equipment or from external sources deemed to be meaningless.

Nuclear Magnetic Resonance (NMR) Logging. A type of down-hole geophysical logging that uses the NMR response of the sediment to directly determine its porosity and permeability.

Numerical Dating. Assigning of an actual age in thousands or millions of years to geological materials.

Oligocene. Geological Epoch extending from 33.9 to 23 million years ago.

Optically Stimulated Luminescence (OSL). System of dating sediments that measures progressive increase in energy accumulated in crystals due to damage from natural environmental radiation.

Overbank Flow. River flow during a flood that extends beyond the channel.

Palaeo-. Prefix meaning old or ancient often now-defunct.

Palaeovalley. The preserved remnants of an ancient drainage system, now infilled with sediment and no longer forming an active surface drainage feature. Palaeovalleys can contain aquifers and have active groundwater flow systems.

Palaeochannel. Preserved remnants of the channel of an ancient fluvial system.

Paleozoic. Geological Era extending from 542 to 251 million years ago.

Palynology. The study of pollen and other resistant plant, protist, and fungi microfossils.

Pedogenesis. Modification of original deposits or rocks by soil-forming processes.

Permeability. The ability of a material, such as rock or sediment, to allow the passage of a liquid such as water. Permeable gravel and sand allow free movement of groundwater whereas impermeable clays do not and can be considered barriers to groundwater movement.

Permeameter. Instrument for measuring water infiltration rates through soil or sediment.

Piezometer. A bore used specifically to monitor water levels or hydraulic head within an aquifer.

Pleistocene. Geological Epoch extending from 2.6 million to 12 thousand years ago.

Pliocene. Geological Epoch extending from 5.3 to 2.6 million years ago.

Point Bars. Depositional areas on the inside of river meander beds where bed-load sand and gravel are deposited as the meander migrates laterally.

Porosity. A measure of the water-bearing capacity of an aquifer. Water movement depends on both the size and interconnectivity of voids.

Potentiometric Surface. A surface that represents the hypothetical level that water under pressure within a confined aquifer would rise to if tapped by a bore.

Primary field. The EM field emitted by a transmitter. This field induces eddy currents in (energizes) the conductors in the ground, which then create their own secondary fields.

Progradation. Seaward movement of a shoreline by deposition of sediment.

Pump Test. A hydrological assessment undertaken when an aquifer is 'stressed' by pumping or injecting water and noting the water drawdown (or rise) level over space and time.

Quaternary. Geological Period including the Pleistocene and the Holocene extending from 2.6 million years ago to the present.

Receiver. The signal detector of a geophysical system. This term is most often used in active geophysical systems that transmit. In AEM surveys it is most often a coil (see also transmitter).

Recharge. The entry into the saturated zone of water made available to the watertable surface, together with associated flow away from the watertable within the saturated zone.

Recovery Efficiency. The fraction or percentage of injected water that can be recovered.

Redox. Variations in chemical state between oxidation and reduction.

Regolith. The entire unconsolidated or secondarily re-cemented cover that overlies more coherent bedrock, that has been formed by weathering, erosion, transport and/or deposition of the older material.

Regression. A term used in geology, to mean the withdrawal of the sea from a large area of land.

Regularization. Regularization of the solution to the inversion of AEM data with a multi-layer model involves imposing smoothness constraints on the vertical variability of the conductivity. The smoothness constraint limits the variability of the subsurface conductivity model thus excluding models that are erratic or geologically unrealistic. When the constraints are set tightly, the model becomes smoother than when the constraints are set loosely.

Resistivity (ρ). The strength with which the earth or a geological Formation resists the flow of electricity, typically the flow induced by the primary field of the electromagnetic transmitter. Normally expressed in ohm-metres, it is the reciprocal of conductivity.

Reversible Jump Markov Chain Monte Carlo (RJ-McMC) analysis. A computational statistical technique that can assess model sampling validity even if the number of parameters in the model is unknown.

Reverse Osmosis. A filtration method that removes many types of molecules and ions from solutions (such as brackish to saline groundwater) by applying pressure to pass the solution through a selective membrane.

Riedel Shears. Characteristic sets of small faults with various orientations, which occur within the overlying cover in the early stages of strike-slip fault formation and displacement within basement rocks or where an active strike-slip zone lies within an area of continuing sedimentation.

Riparian. Of, on, or relating to the banks of a natural stream.

Risk. The likelihood that harm will occur from exposure to a hazard. For example, salinity risk is a measure of the chance that a salt hazard will cause harm to an asset at some time in the future.

Runoff. Overland flow of rainfall not absorbed by the soil. This is a major component of the water cycle and a primary agent of erosion.

Salinity Ingress. Saline groundwater entering an area previously occupied by fresh groundwater.

Salinity Up-coning. The vertical rise of saline water into a production well.

Salt Stores. Vertical and spatial distribution of soil and sediment salinity.

Saturation (water). The condition whereby water fills all available pore space in rock, sediment or soil.

Scour Channels. Floodplain channels formed by erosion, commonly relatively straight and non-depositional.

Scroll Bars. Scroll bars are sub-parallel curving ridges found on meander point bar deposit surfaces, formed by progressive migration of a meander. Scroll bars nearest the river are the youngest. Scroll bars form a scroll tract or **scroll-plain** tract along the river course.

Secondary Field. The field created by conductors in the ground, as a result of electrical currents induced by the primary field from the electromagnetic transmitter. Airborne electromagnetic systems are designed to create and measure a secondary field.

Semi-confined Aquifer. An aquifer that is partly overlain and completely underlain by impervious layers.

Signal. That component of a measurement that the user wants to see – the response from the targets, from the earth, etc. (see also noise).

Sodicity. A measure of the amount of available sodium in water or soil.

Spectrometry. Measurement across a range of energies, where amplitude and energy are defined for each measurement. In gamma-ray spectrometry, the number of gamma rays is measured for each energy window, to define the spectrum.

Spectrum. In gamma ray spectrometry, the continuous range of energy over which gamma rays are measured. In time-domain electromagnetic surveys, the spectrum is the energy of the pulse distributed across an equivalent, continuous range of frequencies.

Spring. A naturally occurring groundwater discharge feature.

Strike-slip Faulting. Where a fault surface is usually near vertical and the footwall moves laterally (either left or right) with very little vertical motion. Strike-slip fault types are defined by the direction of movement of the ground on the opposite side of the fault from an observer and those with left-lateral motion also known as *sinistral* faults and those with right-lateral motion also known as *dextral* faults.

Sub-Artesian Aquifer. An aquifer containing groundwater under pressure that rises to a level greater than that at which it is first encountered, when tapped by a bore, but does not reach the surface.

Sustainable Yield. The level of groundwater extraction measured over a specified planning timeframe that would, if exceeded, compromise key environmental assets, ecosystem functions or the productive base of the resource associated with the aquifer. Also referred to as the environmentally sustainable level of extraction.

Swale. Low point between adjacent dune crests.

Tectonics. The study of structures in the Earth's crust.

Tectonic Inversion. Reactivation of a fault in the opposite direction to its original movement.

Thalweg. The line defining the lowest points along the length of a river bed or channel.

Total Dissolved Solids (TDS). The amount of material dissolved in water (mostly inorganic salts).

Transcurrent Fault. A fault with a near-vertical surface that moves laterally with very little vertical motion. **Sinistral faults** have left-lateral motion and **dextral faults** have right-lateral motion.

Trans-disciplinary Research. An integrative process in which researchers work jointly to develop and use a shared conceptual framework that synthesizes and extends discipline-specific theories, concepts, methods, or all three to create new models and language to address a common research problem.

Transgression. A term used in geology, to mean the invasion of a large area by the sea.

Transient. Time-varying. Usually in this study used to describe a very short period pulse of electromagnetic field.

Transmissivity (T). The capacity of a rock to transmit water under pressure. Expressed as the volume of water flowing through a cross-sectional area of an aquifer that is 1 m x the aquifer thickness under a hydraulic gradient of 100% in a given amount of time (usually 1 day). Transmissivity is equal to the hydraulic conductivity (K) times the aquifer thickness.

Trans-tensional Region. An area that experiences both *extensive* and *transtensive* shear and is characterised by both extensional structures (normal faults, grabens) and strike-slip faults.

Trough. Elongated sedimentary basin where sediments accumulate.

Turbidity. Water opacity or clouding due to suspended sediment or particles.

Uni-disciplinary Research. Researchers from a single discipline work together to address a common research problem.

Up-coning. A situation where a well, located close to saline water underlying freshwater, is pumped at a rate sufficient to cause the salt water to be drawn into the well in an upward shaped cone or mound.

Unconfined Aquifer. A type of aquifer in which the upper boundary is defined by the water table. Unconfined aquifers can be recharged from infiltration of rainfall or by leakage from surface water bodies.

Vertical Aggradation or Accretion. Deposition of overbank muds on flood plains adjacent to river channels during flood events.

Vertical Infiltration. Downward movement of water from the surface into soil or sediment.

Waterlogging. Permanent wetting of the surface due to groundwater rise.

Well Clogging. Filling of sediment pores adjacent to a well due to injection of water; reduces permeability.

Wetting Profile. Moisture penetration depth in soil or sediment.